



ICAROB 2016

PROCEEDINGS OF THE 2016 INTERNATIONAL CONFERENCE ON ARTIFICIAL LIFE AND ROBOTICS

January 29-31, 2016
Okinawa Convention Center, Okinawa, JAPAN
International Meeting Series

Editor-in-Chief
Masanori Sugisaka
Editors: Yingmin Jia, Takao Ito, Ju-Jang Lee
ISBN 978-4-9908350-1-9

The 2016 International Conference on Artificial Life and Robotics (ICAROB 2016), Okinawa Convention Center, Okinawa, Japan, January 29-31, 2016

Proceedings of The 2016 International Conference on

ARTIFICIAL LIFE AND ROBOTICS

(ICAROB 2016)

January 29-31, 2016
Okinawa Convention Center, Okinawa, Japan

Editor-in-Chief: Masanori Sugisaka
Editors: Yingmin Jia, Takao Ito, Ju-Jang Lee,
ICAROB 2016 ISBN 978-4-9908350-1-9

Contents

1	Organization, etc.	1
2	Messages	9
3	Time Table	13
4	Opening Ceremony	16
5	Technical paper index	17
6	Abstracts	
6-1	PS abstracts	30
6-2	IS abstracts	31
6-3	OS abstracts	31
6-4	GS abstracts	52
7	Authors index	68
8	Conference room	75

SPONSERED BY

AROB (ALife Robotics Corporation Ltd.)



ORGANIZED BY

International Steering Committee of International Conference on Artificial Life and Robotics (ICAROB)



TECHNICAL CO-SPONSORED BY

IEEE Fukuoka Section (Japan)



IEEE Robotics and Automation Society (USA)



CO-ORGANIZED BY

Chinese Association for Artificial Intelligence (CAAI, P. R. China)



ADVISORY COMMITTEE CHAIR

Moshe Kam (New Jersey Institute of Technology, Former IEEE President, USA)

ADVISORY COMMITTEE

Fumio Harashima (Tokyo Metropolitan University, President, Japan)

Bruce Eisenstein (Drexel University, Former IEEE President, USA)

Hideki Kimura (RIKEN, Japan)

Masayoshi Tomizuka (University of California Berkeley, USA)

Moshe Kam (New Jersey Institute of Technology, Former IEEE President, USA)

Adam Grzech (Wrocław University of Technology, Poland)

Kazuyuki Aihara (The University of Tokyo, Japan)

D. J. Glyn James (Coventry University, United Kingdom)

Jeffery Johnson (The Open University, UK)

Kazuo Kyuma (Mitsubishi Electric Corporation, Japan)

Steen Rasmussen (University of Southern Denmark, Denmark)

Joshua M. Epstein (The Johns Hopkins University, USA)

Jezry Świątek (Wrocław University of Technology, Poland)

Paul Kalata (Drexel University, USA)

Paul Oh (Drexel University, USA)

Robert Fischl (Drexel University, USA)

Toshio Fukuda (Meijo University, Japan)

Kai-Tai Song (National Chiao Tung University, Taiwan)

GENERAL CHAIR

Masanori Sugisaka (Alife Robotics Corporation Ltd., Japan)

CO-GENERAL CHAIRS

Yingmin Jia (Beihang University, P. R. China)

Takao Ito (Hiroshima University, Japan)

Ju-Jang Lee (KAIST, Korea)

VICE GENERAL CHAIR

Changshui Zhang (Tinghua University, P. R. China)

Henrik H. Lund (Technical University of Denmark, Denmark)

John L. Casti (International Institute for Applied Systems Analysis, Austria)

Jangmyung Lee (Pusan National University, Korea)

Luigi Pagliarini (Technical University of Denmark, Denmark)

(Academy of Fine Arts of Macerata, Italy)

Mohd Rizon bin Mohamed Juhari (University of Sultan Zainal Abidin, Malaysia)

Yongguang Zhang (Academia Sinica, P. R. China)

PROGRAM CHAIRMAN

Makoto Sakamoto (University of Miyazaki, Japan)

SUB PROGRAM CHAIR

M. Oswald (The Vienna University of Technology, Austria)

INTERNATIONAL ORGANIZING COMMITTEE

Akira Fukuda (Kyushu University, Japan)
Eiji Hayashi (Kyushu Institute of Technology, Japan)
Hazry Desa (University of Malaysia, Perlis, Malaysia)
Hidehiko Yamamoto (Gifu University, Japan)
Hideyuki Suzuki (The University of Tokyo, Japan)
Hiroshi Kage ((Mitsubishi Electric Corporation, Japan)
Hiroshi Matsuno (Yamaguchi University, Japan)
Jiwu Wang (Beijing Jiaotong University, P. R. China)
Jovana Jovic (CNRS-AIST JRL, Japan, France)
Katsunori Shimohara (Doshisha University, Japan)
Kenichi Tanaka (Meji University, Japan)
Kenji Hashimoto (Waseda University, Japan)
Kevin Voges (Canterbury University, New Zealand)
Kohei Ohtsu (Tokyo University of Marine Science and Technology, Japan)
Kuo-Hsien Hsia (Far East University, Taiwan)
Kuo-Lan Su (National Yunlin University of Science and Technology, Taiwan)
Masahito Yamamoto (Hokkaido University, Japan)
Masao Kubo (National Defense Academy of Japan, Japan)
Masanao Obayashi (Yamaguchi University, Japan)
Masafumi Yamashita (Kyushu University, Japan)
Mehta Rajiv (New Jersey Institute of Technology, USA)
Peter Sapaty (Ukrainian Academy of Science, Ukraine)
Qu Yanbin (Harbin Institute of Technology, P. R. China)
Seiji Ishikawa (Kyushu Institute of Technology, Japan)
Takashi Kohno (LIMMS/CNRS-IIS, Institute of Industrial Science,
The University of Tokyo, Japan)
Takashi Ogata (Iwate Prefectural University)
Teruhisa Hochin (Kyoto Prefectural University, Japan)
Tetsuro Hattori (Kagawa University, Japan)
Thomas S. Ray (University of Oklahoma, USA)
Toru Yamamoto (Hiroshima University, Japan)
Victor Berdonosov (Komsomolsk-on-Amur State University of
Technology, Russia)
Yasunari Yoshitomi (Kyoto Prefectural University, Japan)

Yo Horikawa (Kagawa University, Japan)
Yoshifumi Morita (Nagoya Institute of Technology, Japan)
Yoshiro Imai (Kagawa University, Japan)
Yuichi Tanji (Kagawa University, Japan)

INTERNATIONAL PROGRAM COMMITTEE

Akira Nakamura (AIST, Japan)
Ali Selamat (University of Technology of Malaysia (UTM), Malaysia)
Arsit Boonyaprapasorn (Chulachomkloa Royal Military Academy, Thailand)
Bin Fu (Shanghai Jiaotong University, P. R. China)
Dongmei Ai (University of Science and Technology Beijing, P. R. China)
Endra Joelianto (Bandung Institute of Technology, Indonesia)
Fengzhi Dai (Tianjin University of Science & Technology, P. R. China)
Haruna Matsushita (Kagawa University)
Hidetsugu Suto (Muroran Institute of Technology, Japan)
Hiroyuki Iizuka (Osaka University, Japan)
Huailin Zhao (Shanghai Institute of Technology, P. R. China)
Hussein Abbass (University of New South Wales and ADFA, Australia)
Istvan Harmati (Budapest Institute of Technology and Economics, Hungary)
Ivan Tanev (Doshisha University, Japan)
Jiandong Zhao (Beijing Jiaotong University, P. R. China)
Jinglu Hu (Waseda University, Japan)
Joono Cheong (Korea University, Korea)
Kathryn Elizabeth Merrick (University of New South Wales and ADFA, Australia)
Kunikazu Kobayashi (Aichi Prefectural University, Japan)
Manabu Yamada (Nagoya Institute of Technology, Japan)
Masahide Ito (Aichi Prefectural University, Japan)
Malachy Eaton (University of Limerick, Ireland)
Masayoshi Kano (Chukyo University, Japan)
Masayoshi Tabuse (Kyoto Prefectural University, Japan)
Masaomi Hatakeyama (University of Zurich, Switzerland)
Norrima Mokhtar (University of Malaya, Malaysia)
Noritaka Sato (Nagoya Institute of Technology, Japan)
Palakorn Tantrakool (King Mongkut's Institute of Technology Thonburi, Thailand)
Satoshi Ikeda (The University of Miyazaki, Japan)
Sanjay S. Joshi (College of Engineering, University of California, USA)
Seong-Ik Han (Pusan National University, Korea)
Shingo Mabu (Yamaguchi University, Japan)
Shyi-Ming Chen (National Taichung University of Education, Taiwan)
Takashi Kuremoto (Yamaguchi University, Japan)
Takayoshi Yamada (Gifu University, Japan)
Taishiro Kishimoto (Keio University, Japan)
Tao Zhang (Tsinghua University, P. R. China)
Takashi Iwamoto (Mitsubishi Electric Corporation, Advanced Technology)

R&D Center, Japan)

Tetsuro Katayama (The University of Miyazaki, Japan)

Thunyaseth Sethaput (Thammasat University, Thailand)

Toshinori Nawata (Kumamoto National College of Technology, Japan)

Tsunehiro Yoshinaga (Tokuyama National College of Technology, Japan)

Weicun Zhang (University of Science and Technology Beijing, P. R. China)

Yuanyuan Shang (Capital Normal University, P. R. China)

Yueyue Fan (University of California-Davis, USA)

Young Im Cho (The University of Suwon, Korea)

LOCAL ARRANGEMENT COMMITTEE

M. Sakamoto (University of Miyazaki, Japan)

M. Sugisaka (ALife Robotics Co., Ltd., Japan)

Takao Ito (Hiroshima University, Japan)

HISTORY

The International Conference on Artificial Life and Robotics (ICAROB) resulted from the AROB-symposium whose first edition was held in 1996 and the eighteenth and last edition in 2013. The AROB symposium was annually organized by Oita University, Nippon Bunri University (NBU), and ALife Robotics Corporation Ltd., under the sponsorship of the Science and Technology Policy Bureau, the Ministry of Education, Science, Sports, and Culture (Monbusho), presently, the Ministry of Education, Culture, Sports, Science, and Technology (Monkasho), Japanese Government, Japan Society for the Promotion of Science (JSPS), the Commemorative Organization for the Japan World Exposition ('70), Air Force Office of Scientific Research, Asian Office of Aerospace Research and Development (AFOSR/AOARD), USA. I would like to express my sincere thanks to not only Monkasho (annually fund support from 1996 to 2013) but also JSPS, the Commemorative Organization for the Japan World Exposition ('70), and various other Japanese companies for their repeated support. The old symposium (this symposium has been held every year at B-Con Plaza, Beppu, Oita, Japan except in Oita, Japan (AROB 5th '00) and in Tokyo, Japan (AROB 6th '01).) was organized by the International Organizing Committee of AROB and was co-operated by the Santa Fe Institute (USA), RSJ, IEEJ, ICASE (Now ICROS) (Korea), CAAI (P. R. China), ISCIE, IEICE, IEEE (Japan Council), JARA, and SICE. The old AROB-symposium expanded much by absorbing much new knowledge and technologies into it. This history and character of the former AROB symposiums are passed on the current ICAROB conference and to this journal, International Journal of Robotics, Networking and Artificial Life (JRNAL). From now on, ALife Robotics Corporation Ltd. is in charge of management of both the conference and the journal. The future of the ICAROB is brilliant from a point of view of yielding new technologies to human society in the 21st century. This conference invites you all.

AIMS AND SCOPE

The objective of this conference is the development of new technologies for artificial life and robotics which have been recently born in Japan and are expected to be applied in various fields. This conference presents original technical papers and authoritative state-of-the-art reviews on the development of new technologies concerning robotics, networking and artificial life and, especially computer-based simulation and hardware for the twenty-first century. This conference covers a broad multidisciplinary field, including areas such as:

- Artificial intelligence & complexity
- Artificial living
- Artificial mind research
- Artificial nervous systems for robots
- Artificial sciences
- Bipedal robot
- Brain science and computing
- Chaos
- Cognitive science
- Computational Molecular biology
- Computer graphics
- Data mining
- Disasters robotics
- DNA computing
- Empirical research on network and MOT
- Environment navigation and localization
- Evolutionary computations
- Facial expression analysis, music recommendation and augmented reality
- Foundation of computation and its application
- Fuzzy control
- Genetic algorithms
- Human-welfare robotics
- Image processing
- Insect-like aero vehicles
- Intelligence in biological systems
- Intelligent control
- Management of technology
- Medical surgical robot
- Micro-machines
- Multi-agent systems
- Nano-biology
- Nano-robotics
- Networking
- Neural circuits
- Neuro-computer
- Neuromorphic Systems
- Neuroscience

- Pattern recognition
- Quantum computing
- Reinforcement learning system & genetic programming
- Robotics
- Software development support method
- System cybernetics
- Unmanned underwater vehicles
- Unmanned Aerial Systems Technologies
- Unmanned Aerial Systems designing, controls and navigation
- Unmanned Aero vehicles
- Virtual reality
- Visualization

Hardware-oriented submissions are particularly welcome. This conference will discuss new results in the field of artificial life and robotic

GENERAL SESSION TOPICS

GS1 Neuromorphic Systems (5)

GS2 Pattern Recognition & Image Processing(6)

GS3 Reinforcement Learning System & Genetic Programming(6)

GS4 Micro-Machine(4)

GS5 Multi-Agent Systems & Visualization(2)

GS6 Intelligent Control & System Cybernetics(3)

GS7 Robotics I (6)

GS8 Robotics II (5)

GS9 Robotics III(4)

GS10 Poster Sessions(5)

ORGANIZED SESSION TOPICS

OS1 Artificial Life and Quality Enhancement of Life(6)

OS2 Intelligence Control System and Artificial Life(6)

OS3 Construction Engineering and Management(6)

OS4 Construction Technology and Management(5)

OS5 Advanced Control Systems(6)

OS6 Intelligent Control(6)

OS7 Image Analysis and Content Security(5)

OS8 Image, Circuit and Control(9)

OS9 Modern approaches of MOT and Corporate Strategy(3)

OS10 Reality Mining(3)

OS11 Kansei Engineering and Application(4)

OS12 Advanced Research on Computer Science and Information Processing(4)

OS13 Automatic Generation, Creation, and Production of Narrative Contents(4)

COPYRIGHTS

Accepted papers will be published in the proceeding of The 2016 International Conference on Artificial Life and Robotics (ICAROB 2016). Some of high quality papers in the proceeding will be requested to re-submit their papers for the consideration of publication in an international journal ROBOTICS, NETWORKING AND ARTIFICIAL LIFE under agreement of both Editor-in- Chief and 3 reviewers. All correspondence related to the conference should be addressed to ICAROB Office.

ICAROB Office

ALife Robotics Corporation Ltd.

3661-8 Oaza Shimohanda, Oita 870-1112, JAPAN

TEL/FAX: +81-97-597-7760

E-MAIL:

icarob@alife-robotics.co.jp

Home Page: <http://alife-robotics.co.jp/>

MESSAGES

Masanori Sugisaka

General Chair of ICAROB



Masanori Sugisaka
General Chair

**(Professors, Open University
(UK), University of Malaysia-
Peris (Malaysia) and President
of ALife Robotics Co., Ltd.
(Japan))**

Masanori Sugisaka

It is my great honor to invite you all to The 2016 International Conference on Artificial Life and Robotics (ICAROB 2016).

This Conference is changed as the old symposium from the first (1996) to the Eighteenth (2013) annually which were organized by Oita University, Nippon Bunri University (NBU), and ALife Robotics Corporation Ltd. under the sponsorship of the Science and Technology Policy Bureau, the Ministry of Education, Science, Sports, and Culture (Monbusho), presently, the Ministry of Education, Culture, Sports, Science, and Technology (Monkasho), Japanese Government, Japan Society for the Promotion of Science (JSPS), The Commemorative Organization for the Japan World Exposition ('70), Air Force Office of Scientific Research, Asian Office of Aerospace Research and Development (AFOSR/AOARD), USA. I would like to express my sincere thanks to not only Monkasho (annually fund support from 1996 to 2013) but also JSPS, the Commemorative Organization for the Japan World Exposition ('70), Japanese companies for their repeated support.

The old symposium was organized by International Organizing Committee of AROB and was co-operated by the Santa Fe Institute (USA), RSJ, IEEJ, ICASE (Now ICROS) (Korea), CAAI (P. R. China), ISCIE, IEICE, IEEE (Japan Council), JARA, and SICE. The old AROB symposium was growing up by absorbing many new knowledge and technologies into it.

This history and character was inherited also from ICAROB 2014 (The 2014 International Conference on Artificial Life and Robotics) to now. From now on, ALife Robotics Corporation Ltd. is in charge of management. This year we have The 2016 International Conference on Artificial Life and Robotics (ICAROB 2016). The future of The ICAROB is brilliant from a point of view of yielding new technologies to human society in 21st century.

I hope that fruitful discussions and exchange of ideas between researchers during Conference (ICAROB 2016) will yield new merged technologies for happiness of human beings and, hence, will facilitate the establishment of an international joint research institute on Artificial Life and Robotics in future.

Yingmin Jia

Co-General Chair of ICAROB



Yingmin Jia
Co-General Chair
(Professor, Beihang
University,
R .P. China)



It is my great pleasure to invite you to The 2016 International Conference on Artificial Life and Robotics (ICAROB 2016), in Ginowan City, Okinawa, Japan from Jan. 29th to 31st, 2016.

ICAROB develops from the AROB that was created in 1996 by Prof. Masanori Sugisaka and celebrated her birthday of 21st years old in 1996. Doubtless, new mission and big challenges in the field of artificial life and robotics will promote ICAROB to start a new stage and attract wide interests among scientist, researchers, and engineers around the world.

For a successful meeting, many people have contributed their great efforts to ICAROB. Here, I would like to express my special thanks to all authors and speakers, and the meeting organizing team for their excellent works.

Looking forward to meeting you at ICAROB in Ginowan City, Okinawa and wishing you enjoy your stay in Japan.



Takao Ito
Co-General Chair
(Professor Hiroshima
University, Japan)

Takao Ito

Co General Chair of ICAROB

It is my great honor to invite you all to The 2016 International Conference on Artificial Life and Robotics (ICAROB 2016). This Conference is changed as the old symposium from the first (1996) to the Eighteenth I am pleased to welcome you to The 2016 International Conference on Artificial Life and Robotics in the wonderful city of Ginowan, Okinawa, Japan

The ICAROB has long history. The former organization of the ICAROB was developed under the strong leadership of the President, Professor. Masanori Sugisaka, the father of AROB. We gathered many researchers, faculty members, graduate students from all over the world, and published numerous high-quality proceedings and journals every year.

Over the years, dramatic improvements have been made in the field of artificial life and its applications. The ICAROB has becoming the unifying the exchange of scientific information on the study of man-made systems that exhibit the behavioral characteristic of natural living systems including software, hardware and/or wetware. Our conference shapes the development of artificial life, extending our empirical research beyond the territory circumscribed by life-as-we-know-it and into the domain of life-as-it-could-be. It will provide us a good place to present our new research results, good ideas, and valuable information about artificial intelligence, complex systems theories, robotics, management of technology, etc.

In order to provide an outstanding technical level for the presentations at the conference, we have invited more than 60 distinguished experts in the field of artificial life in the organizing committee and program committee. We will have 22 sessions during 3 days of conference, including 4 invited sessions.

The conference site is Okinawa Convention Center, one of the finest congress centers in Okinawa. It is situated near the center of the Ginowan city in Okinawa. You can find many fantastic scenic spots and splendid historical places in Naha city. Enjoy your stay and take your time to visit the city of Okinawa.

I am looking forward to meeting you in Okinawa during ICAROB 2016 and to sharing a most pleasant, interesting and fruitful conference



Ju-Jang Lee
Co-General Chair
(Professor, KAIST)



Ju-Jang Lee

Co-General Chair of ICAROB

The First International Conference on Artificial Life and Robotics (ICAROB) was held in Oita City, Oita, Japan from Jan. 11th to 13th, 2014. This year's Conference will be held amidst the high expectation of the increasingly important role of the new interdisciplinary paradigm of science and engineering represented by the field of artificial life and robotics that continuously attracts wide interests among scientist, researchers, and engineers around the globe.

Distinguished researchers and technologists from around the world are looking forward to attending and meeting at ICAROB. ICAROB is becoming the annual excellent forum that represents a unique opportunity for the academic and industrial communities to meet and assess the latest developments in this fast growing artificial life and robotics field. ICAROB enables them to address new challenges, share solutions, discuss research directions for the future, exchange views and ideas, view the results of applied research, present and discuss the latest development of new technologies and relevant applications.

In addition, ICAROB offers the opportunity of hearing the opinions of well-known leading experts in the field through the keynote sessions, provides the bases for regional and international collaborative research, and enables to foresee the future evolution of new scientific paradigms and theories contributed by the field of artificial life and robotics and associated research area. The twenty-first century will become the century of artificial life and intelligent machines in support of humankind and ICAROB is contributing through wide technical topics of interest that support this direction.

It is a great honor for me as a Co-General Chair of the 3rd ICAROB 2016 to welcome everyone to this important event. Also, I would like to extend my special thanks to all authors and speakers for contributing their research works, the participants, and the organizing team of the 3rd ICAROB.

I'm looking forward to meeting you at the 3rd ICAROB in Naha City, Okinawa and wishing you all the best.

1/28(Thu.) 17:30-19:30	Welcome Party(Conference Site: Farm Café TAIYO ICHIBA)
-------------------------------	---

TIME TABLE (1/29)

1/29(Fri.)	RoomB2	RoomB3	RoomB4
8:50-		Registration	
9:10-10:25	OS4 Construction Technology and Management(5) Chair: C. C. Chang Co-Chair: Y. C. Shiau	GS8 Robotics II (5) Chair: J. J. Lee	GS10 Poster Sessions (5)
10:25-11:40	Coffee break		
10:40-11:10	Opening Ceremony (RoomB2)		
11:20-12:00	Chair: T. Ito Invited Speech IS1(RoomB2) Luigi Pagliarini		
12:00-13:00	Lunch		
13:00-14:00	Chair: T. Ito Plenary Speech PS1(RoomB2) Henrik H. Lund		
14:00-14:20	Coffee break		
14:20-15:50	OS11 Kansei Engineering and Application(4) Chair: T. Hattori Co-Chair: Y. Imai	OS1 Artificial Life and Quality Enhancement of Life(6) Chair: S. H. Li Co-Chair: S. D. Wu	OS3 Construction Engineering and Management(6) Chair: Y. C. Shiau Co-Chair: Y. Y. Tsai
15:50-16:10	Coffee break		
16:10-18:10	OS2 Intelligence Control System and Artificial Life(6) Chair: K. H. Hsia Co-Chair: K. L. Su	GS1 Neuromorphic Systems(5) Chair: T. Kondo	GS4 Micro-Machine(4) Chair: J.M. Lee GS9 RoboticsⅢ(4) Chair: A. Boonyaprapasorn

TIME TEBLE (1/30)

1/30(Sat.)	RoomB2	RoomB3	RoomB4
8:50-		Registration	
9:10-10:40	GS2 Pattern recognition & image processing(6) Chair: T. Fujita	GS7 Robotics I (6) Chair: A. Yamaguchi	OS5 Advanced Control Systems(6) Chair: Y. Jia Co-Chair: F. Wang
10:40-11:00	Coffee break		
11:00-11:40	Chair: Y. Jia Invited speech IS2(RoomB2) Kaoru Sumi		
11:40-13:00	Lunch		
13:00-14:00	Chair: Y. Jia Plenary Speech PS2(RoomB2) Ju-Jang Lee		
14:00-14:20	Coffee break		
14:20-15:50	OS8 Image, Circuit and Control(6) Chair: F. Dai Co-Chair: H. Jia	OS6 Intelligent Control(6) Chair: Y. Jia Co-Chair: W. Zhang	GS5 Multi-Agent Systems & Visualization(2) Chair: S. Mabu GS6 Intelligent Control & System Cybernetics(3) Chair: M. C. Lee
15:50-16:10	Coffee break		
16:10-17:10		OS12 Advanced Research on Computer Science and Information Processing(4) Chair: T. Ito Co-Chair: M. Sakamoto	OS8 Image, Circuit and Control(3) Chair: F. Dai Co-Chair: H. Jia
18:00-20:00	Banquet: Culture Resort Festone		

TIME TABLE (1/31)

1/31(Sun.)	RoomB3	RoomB4
8:50-	Registration	
9:10-9:55	OS10 Reality Mining(3) Chair: M. Kubo Co-Chair: S. Iwanaga	OS9 Modern Approaches of MOT and Corporate Strategy(3) Chair: T. Ito Co-Chair: S. Matsuno
9:55-10:10	Coffee break	
10:10-11:25	OS13 Automatic Generation, Creation, and Production of Narrative Contents(4) Chair: T. Ogata Co-Chair: Y. Kawamura	OS7 Image Analysis and Content Security(5) Chair Y. Yoshitomi Co-Chair: M. Tabuse
11:25-13:00	Lunch	
13:00-14:30	GS3 Reinforcement Learning Systems & Genetic Programing(6) Chair: K. Kobayashi	
14:40-15:40	Farewell Party (Conference Site: Farm Café TAIYO ICHIBA)	

GS1 Neuromorphic Systems(5) GS2 Pattern Recognition & Image Processing(6) GS3 Reinforcement Learning Systems & Genetic Programing(6) GS4 Micro-Machine(4) GS5 Multi-Agent Systems & Visualization(2) GS6 Intelligent Control & System Cybernetics(3) GS7 Robotics I (6) GS8 Robotics II (5) GS9 RoboticsIII (4) GS10 Poster Sessions(5)	OS1 Artificial Life and Quality Enhancement of Life(6) OS2 Intelligence Control System and Artificial Life(6) OS3 Construction Engineering and Management(6) OS4 Construction Technology and Management(5) OS5 Advanced Control Systems(6) OS6 Intelligent Control(6) OS7 Image Analysis and Content Security(5) OS8 Image, Circuit and Control(9) OS9 Modern Approaches of MOT and Corporate Strategy(3) OS10 Reality Mining(3) OS11 Kansei Engineering and Application(4) OS12 Advanced Research on Computer Science and Information Processing(4) OS13 Automatic Generation, Creation, and Production of Narrative Contents(4)
--	---

The 2016 International Conference on ARTIFICIAL LIFE AND ROBOTICS (ICAROB 2016)

January 28 (Thursday)

17:30-19:30 **Welcome Party (Conference Site: Farm Café TAIYO ICHIBA)**

January 29 (Friday)

Room B2 10:40-11:10

Opening Ceremony

Chair: Jiwu Wang (Beijing Jiaotong University, China)

Welcome Addresses

- | | |
|---|---|
| 1. General Chairman of ICAROB | M. Sugisaka (ALife Robotics Corporation Ltd. Japan) |
| 2. Co-General Chairman of ICAROB | Y. M. Jia (Beihang University, China) |
| 3. Co-General Chairman of ICAROB | T. Ito (Hiroshima University, Japan) |
| 4. Co-General Chairman of ICAROB | J. J. Lee (KAIST, South Korea) |

January 30 (Saturday)

Banquet: Culture Resort Festone

18:00-20:00

Chair: T. Ito (Hiroshima University, Japan)

Welcome Addresses

- Prof. Yingmin Jia (Beihang University, P.R. China.)
- Prof. Jang-Myung Lee (Pusan National University, South Korea)
- Prof. Kaoru Sumi (Future University Hakodate, Japan)
- Prof. Saori Iwanaga (Japan Coast Guard Academy, Japan)

TECHNICAL PAPER INDEX

January 29 (Friday)

08:50-Registration

Room B2

9:10-10:25 OS4 Construction Technology and Management (5)

Chair: Ching-Ching Chang (Chung Hua University, Taiwan)

Co-Chair: Yan-Chyuan Shiau (Chung Hua University, Taiwan)

- OS4-1 *Study on the Promotion of Steel Slags Recycling in Taiwan*
Shu-Chen Chang, Ching-Jung Chang (Chung Hua University, Taiwan)
- OS4-2 *The Research on the Utilization of Green Building Ecological Index Group in Campus Environment – Taking of Elementary Schools at Houli District, Taichung City as Example*
Ching-Jung Chang, Yung- Feng Hsu, Chun-Hsien Chen (Chung Hua University, Taiwan)
- OS4-3 *The Assessment and Research on the Reconstruction of Enclosing Wall into Open Type in Elementary School Campus – Taking of Erlin Township, Changhua County as Example*
Ching-Jung Chang, Chia-Chen Li, I-Chen Wu (Chung Hua University, Taiwan)
- OS4-4 *The Study and Analysis on the Reuse and Transformation Strategy of Tile Kiln Space – Taking of San-He Tile Kiln as Example*
Ching-Jung Chang, Hsiao-Yu Lin, Ying-Yu Su (Chung Hua University, Taiwan)
- OS4-5 *The Research on the Influence of Economic Benefit for High-Rise Buildings Constructed by Different Excavation Method – Taking of Residence Buildings at New Taipei City as Example*
Ching-Jung Chang, Cheng-Min Yang, Hsiu-Hsiung Hsu (Chung Hua University, Taiwan)

10:40-11:10 Opening Ceremony

11:20-12:00

Chair: Takao Ito (Hiroshima University, Japan)

Invited Speech (IS1) *Redefining robot based technologies for elderly people assistance: a survey.*

^{1,2}Luigi Pagliarini, ¹Henrik Hautop Lund (¹Technical University of Denmark, Denmark, ²Academy of Fine Arts of Macerat, Italy)

13:00-14:00

Plenary Speech (PS1) *Disrupting the Industry with Play*

Henrik Hautop Lund (Technical University of Denmark, Denmark)

14:20-15:20 OS11 Kansei Engineering and Application (4)

Chair: Tetsuo Hattori (Kagawa University, Japan)

Co-Chair: Yoshiro Imai (Kagawa University, Japan)

OS11-1 *Automated Multiple-Brightness Peak Image Processing Method Using Curvature and Variance Estimation*

¹Yusuke Kawakami, ²Tetsuo Hattori, ²Yoshiro Imai, ²Kazuaki Ando, ²Yo Horikawa
(¹DynaxT Co., Ltd. ²Kagawa University, Japan)

³R. P. C. Janaka Rajapakse (³Tainan National University of the Arts, Taiwan)

OS11-2 *Histogram Matching Based on Gaussian Distribution on the HSB Color System*

¹Yusuke Kawakami, ²Tetsuo Hattori, ²Yoshiro Imai, ²Kazuaki Ando, ²Yo Horikawa
(¹DynaxT Co., Ltd. ²Kagawa University, Japan)

³R. P. C. Janaka Rajapakse (³Tainan National University of the Arts, Taiwan)

OS11-3 *Quantitative Evaluation of Flash-based Educational Visualizing Simulator*

Kei Takeichi, Yoshiro Imai, Kazuaki Ando, Yusuke Kawakami, Tetsuo Hattori
(Kagawa University, Japan)

OS11-4 *Relation between Optimal Stopping Solution and NSPR for Structural Change Point Detection Problem*

¹Tetsuo Hattori, ¹Yoshihide Koyama, ¹Yoshiro Imai, ¹Yo Horikawa, ²Hiromichi Kawano
(¹Kagawa University, ²NTT advanced technology Company Ltd, Japan)

16:10-17:40 OS2 Intelligence Control System and Artificial Life (6)

Chair: Kuo-Hsien Hsia (Far East University, Taiwan)

Co-Chair: Kuo-Lan Su (National Yunlin University of Science & Technology, Taiwan)

OS2-1 *Modified Quantum Particle Swarm Optimization for Chaos Synchronization*

Ching-I Lee, Chia-Nan Ko (Nan Kai University of Technology, Taiwan)

OS2-2 *A Simulation Model of Hall Sensor Misalignment in BLDC Motors*

Chung-Wen Hung, Chu-Lin Hsu

(National Yunlin University of Science & Technology, Taiwan)

OS2-3 *Using Multi-Target Tracking and Identification TLD Algorithm for Intelligent Mobile Robot*

Jr Hung Guo, Kuo-Hsien Hsia, Kuo-Lan Su

(National Yunlin University of Science & Technology, Taiwan)

OS2-4 *Handheld Mobile Devices for Remote Monitoring of Factory*

Bing-Gang, Jhong, Jian-Sing, Hu, Mei-Yung, Chen

(National Taiwan Normal University, Taiwan)

OS2-5 *Task Assignment and Checking Process for Pattern Reformation on a Square Grid Plane*

Kuo-Hsien Hsia¹, Bo-Yi Li², Kuo-Lan Su² (¹Far-East University, ²National Yunlin University of Science & Technology, Taiwan)

OS2-6 *The Design of a Multifunctional Acousto-Optical Device With a Mobile Power Pack*

Yi-Yu Lu, Wen-Bin Lin, Zheng-Ying Li (Far-East University, Taiwan)

Room B3

9:10-10:25 GS8 Robotics II (5)

Chair: Ju-Jang Lee (KAIST, South Korea)

GS8-1 *Visual-servo Control of 4-DOF Robot Manipulator for Sorting Moving objects*

Longtan Wang, Seon-woo Kim, Hyun-Wook Ha, Jang-Myung Lee
(Pusan National University, South Korea)

GS8-2 *Self-identification of Mental State and Self-control through Indirect Biofeedback -Indirect Representation and Placebo Effect-*

Madoka Takahara, Ivan Tanev, Katsunori Shimohara (Doshisha University, Japan)

GS8-3 *Construction of a sense of force feedback and vision for micro-objects: Recreate the response and a sense of force of objects*

Yusei Ishii, Eiji Hayashi (Kyusyu Institute of Technology, Japan)

GS8-4 *Dynamic Behavior Selection Model based on Emotional States for Conbe-I robot*

Wisanu Jitviriyaya, Jiraphan Inthiam, Eiji Hayashi (Kyushu Institute of Technology, Japan)

GS8-5 *Consideration on a Crawler Robot with Six Legs*

Toyomi Fujita, Taiga Sasaki (Tohoku Institute of Technology, Japan)

14:20-15:50 OS1 Artificial Life and Quality Enhancement of Life (6)

Chair: Shang-Hui Li (Far East University, Taiwan)

Co-Chair: Sheu-Der Wu (Cheng Shiu University, Taiwan)

OS1-1 *The development of new products of pineapple cheesecakes*

Sheu-Der Wu¹, Hung-Wen Su² (¹Cheng Shiu University, ²Far East University, Taiwan)

OS1-2 *The study on ballroom service quality to affect customer satisfaction*

Hsiu-Min Lin, Yang Wu, Jei-Fu Ho (Far East University, Taiwan)

OS1-3 *The relationship between employees' personality traits, work values and job involvement with the contribution to their companies – For the micro food service industry*

Hsiu-Chen Chung¹, Chiou-Lan Chien¹, Lung-Chi Tsai² (¹Tainan University of Technology, ²Southern Taiwan University of Science and Technology, Taiwan)

- OS1-4 *Consumer's acceptance to the new product- pineapple jam as example*
Shang-Hui Li, Jei-Fu Ho (Far East University, Taiwan)
- OS1-5 *Development of an innovative design process for green products*
Ming-Chieh Wang (Far East University, Taiwan)
- OS1-6 *Research on Nail Art 3D design with Different Materials - A Case Study of the Tang Dynasty Style*
Mei-Yin Lee, Kung-Yu Liu, Sih-Jie Guan, Jei-Fu Ho (Far East University, Taiwan, ROC)

16:10-17:25 GS1 Neuromorphic Systems (5)

Chair: Tadashi Kondo (Tokushima University, Japan)

- GS1-1 *Compensating Temperature-Dependent Characteristics of a Subthreshold-MOSFET Analog Silicon Neuron*
Ethan Green, Takashi Kohno (The University of Tokyo, Japan)
- GS1-2 *Medical image analysis of brain X-ray CT images by deep GMDH-type neural network*
Tadashi Kondo, Junji Ueno, Shoichiro Takao (Tokushima University, Japan)
- GS1-3 *Medical image diagnosis of lung cancer by deep feedback GMDH-type neural network*
Tadashi Kondo, Junji Ueno, Shoichiro Takao (Tokushima University, Japan)
- GS1-4 *Feature Linking by Synchronized Response in Chaotic Cellular Neural Network for Visual Stimulus of Moving Objects*
Akihiro Yamaguchi¹, Satoshi Arakane¹, Masao Kubo² (¹Fukuoka Institute of Technology, ²National Defense Academy of Japan, Japan)
- GS1-5 *An FPGA-based cortical and thalamic silicon neuronal network.*
Takuya Nanami, Takashi Kohno (The University of Tokyo, Japan)

Room B4

9:10-10:25 GS10 Poster Sessions (5)

- GS10-1 *Analysis of Postgraduates' Entrance Examination Scores Based on Linear Regression with Dummy Variables*
Ning Xiaojun, Huang Ruocheng, Liang Xiaoyi, Ai Dongmei
(University of Science and Technology Beijing, P.R. China)
- GS10-2 *Clinical Evaluation of UR-System 2 for Recovery of Motor Function of Plegic Upper Limb after Stroke*
¹Hirofumi Tanabe, ¹Masahiro Mitsukane, ²Norihiro Toya, ²Ryosuke Takeichi, ²Hitomi Hattori, ²Yoshifumi Morita, ³Yoshiaki Takagi, ³Norio Hasegawa (¹Shonan University of Medical Sciences, ²Nagoya Institute of Technology, ³Sanyo Machine Works, Ltd., Japan)

GS10-3 *Knee Android Model Reproducing Internal-External Rotation with Screw-Home Movement of Human Knee*

Daichi Yamauchi, Sho Takei, Noritaka Sato, Yoshifumi Morita
(Nagoya Institute of Technology, Japan)

GS10-4 *Wood Species Recognition System based on Improved Basic Grey Level Aura Matrix as feature extractor*

¹Mohd Iz'aan Paiz Zamri, ¹Anis Salwa Mohd Khairuddin, ¹Norrima Mokhtar, ²Rubiyah Yusof
(¹University of Malaya, ²Universiti Teknologi Malaysia, Malaysia)

GS10-5 *Evaluation the Performance of a New Quadrotor Model Based on the Arm's Length Variation*

Yasameen Kamil N., D. Hazry, Khairunizam Wan, Zuradzman M. Razlan
(University Malaysia Perlis, Malaysia)

14:20-15:50 OS3 Construction Engineering and Management (6)

Chair: Yan-Chyuan Shiau (Chung Hua University, Taiwan)

Co-Chair: Yi-Yin Tsai (Chung Hua University, Taiwan)

OS3-1 *Discussion on Factors Influencing the Performance of Hospital Renovation Engineering Taking one Medical Center in Taiwan as Example*

Wen-Lung Lin, Yan-Chyuan Shiau, Ting-Chi Lai, Chen-Chung Liu
(Chung Hua University, Taiwan)

OS3-2 *Discussion on Land Expropriation Compensation System*

Hung-Chi Liu, Yan-Chyuan Shiau, Yao-Shan Huang, Chen-Chung Liu
(Chung Hua University, Taiwan)

OS3-3 *Study on User Satisfaction of Pick Areas for Elementary Schools – Using Nanyang Elementary School in Taichung City as Example*

Chun-Feng Chang, Yan-Chyuan Shiau, Kuan-Yin Chen
(Chung Hua University, Taiwan)

OS3-4 *Study on User Satisfaction in Sport Site Facilities for Senior Students of Elementary Schools in Taichung City*

Pei-Ling Lin, Yan-Chyuan Shiau, Ling-Lin Chang (Chung Hua University, Taiwan)

OS3-5 *The Establishment of the Sustainability Performance Indicators for Wetland Ecological Project: Using Construction Inspection Phase as Example*

Ching-Mei Miao, Yan-Chyuan Shiau, Chen-Chung Liu, Jen-Kuo Chang
(Chung Hua University, Taiwan)

OS3-6 *Development of Type Control Guidelines for the Old Town District of Hsinchu City*

Yi-Yin Tsai (Chung Hua University, Taiwan)

16:10-18:10 GS4 Micro-Machine (4) + GS9 Robotics III(4)

GS4 Micro-Machine (4)

Chair: Jang-Myung Lee (Pusan National University, South Korea)

- GS4-1 *Applying Fuzzy Sliding Mode Control on Electrowetting on Dielectric System*
 ¹Arsit Boonyaprapasorn, ²Thavida Maneewarn, ²Eakkachai Pengwang (¹Chulachomkloa Royal Military Academy, ²King Mongkut's University of Technology Thonburi, Thailand)
- GS4-2 *Development of Micro-Permanent Magnet Synchronous Reluctance Generator for TPMS on Smart Robots*
 ¹Chun-Chieh Chang, ¹ Cheng-Tang Pan, ¹Shao-Yu Wang, ¹An-Yun Yang, ¹Gu-Xuan Lin, ²Roger Chenglung Lee, ² Ting-Hung Chung, ¹Yu-Jen Wang
 (¹National Sun Yat-sen University, ²Naroller Electronics, Taiwan)
- GS4-3 *Study of Micro-Flux-Switching Permanent-Magnet Generator for TPMS on Smart Robots*
 ¹An-Yun Yang, ¹ Cheng-Tang Pan, ¹Shao-Yu Wang, ¹Chun-Chieh Chang, ¹Gu-Xuan Lin, ²Roger Chenglung Lee, ²Ting-Hung Chung, ¹Yu-Jen Wang
 (¹National Sun Yat-sen University, ²Naroller Electronics, Taiwan)
- GS4-4 *MEMS Microrobot Controlled by Mounted Neural Networks IC with Two Types Actuators*
 Kei Iwata, Hirozumi Oku, Yuki Okane, Yohei Asano, Masaki Tatani, Yuki Ishihara, Kazuki Sugita, Satoshi Chiba, Satoko Ono, Mizuki Abe, Minami Takato, Ken Saito, Fumio Uchikoba
 (Nihon University, Japan)

GS9 Robotics III(4)

Chair: Arsit Boonyaprapasorn (Chulachomklao Royal Military Academy, Thailand)

- GS9-1 *Social Expression of Pet Robot Based on Artificial Consciousness and Biologically Inspired On-line Topological Method*
 Sakmongkon Chumkamon, Eiji Hayashi (Kyushu Institute of Technology, Japan)
- GS9-2 *Anthropomorphic robot modelling with virtual height inverted pendulum approach in Simulink: step length and period influence on walking stability*
 Ramil Khusainov, Ilya Afanasyev, Evgeni Magid (Innopolis University, Russia)
- GS9-3 *A low cost genetic algorithm based control scheme for wheelchair control in hospital environment*
 Karam Dad Kallu, Muhammad Jawad Khan, Wang Jie, Min Cheol Lee
 (Pusan National University, South Korea)
- GS9-4 *Simultaneous Localization and Mapping (SLAM) algorithm base on EKF and SPKF.*
 Zolghadr Javad, Yuanli Cai ,Yekkehfallah Majid (Xi'an Jiaotong University, P.R. China)

January 30 (Saturday)

08:50-Registration

Room B2

09:10-10:40 GS2 Pattern Recognition & Image Processing (6)

Chair: Toyomi Fujita (Tohoku Institute of Technology, Japan)

- GS2-1 *An accurate method for the extraction of structured light stripe*
Jiwu Wang¹, Yaodong Li¹, Zhijing Jian¹, Sugisaka Masanori²
(¹Beijing Jiaotong University, P.R. China) (²Alife Robotics Corporation Ltd, Japan)
- GS2-2 *Feature Acquisition From Facial Expression Image Using Convolutional Neural Networks*
Taiki Nishime, Satoshi Endo, Koji Yamada, Naruaki Toma, Yuhei Akamine
(University of The Ryukyus, Japan)
- GS2-3 *Estimating Age on Twitter Using Self-Training Semi-Supervised SVM*
Tatsuyuki Iju, Satoshi Endo, Koji Yamada, Naruaki Toma, Yuhei Akamine
(University of The Ryukyus, Japan)
- GS2-4 *Interactive musical editing system to support human errors and offer personal preferences for an automatic piano*
Kenji Tsunenari, Eiji Hayashi (Kyushu Institute of Technology, Japan)
- GS2-5 *Geometric parameters measurement of wheel tread based on line structured light*
Jiwu Wang¹, Zhijing Jian¹, Yaodong Li¹, Chao Yang¹, Sugisaka Masanori²
(¹Beijing Jiaotong University, P.R. China), (²Alife Robotics Corporation Ltd, Japan)
- GS2-6 *Study on the ORB algorithm in the application of Monocular SLAM*
Jiwu Wang¹, Shunkai Zheng¹, Masanori Sugisaka²
(¹Beijing Jiaotong University, P.R. China), (²Alife Robotics Corporation Ltd, Japan)

11:00-11:40

Chair: Yingmin Jia (Beihang University, P. R. China)

Invited Speech (IS2) Affective Human Computer Interaction

Kaoru Sumi (Future University Hakodate, Japan)

13:00-14:00

Plenary Speech (PS2) A Study on Differential Evolution Using BetaCOBL, B³R, and TPBO

So-Youn Park, **Ju-Jang Lee** (KAIST, South Korea)

14:20-15:50 OS8 Image, Circuit and Control (6)

Chair: Fengzhi Dai (Tianjin University of Science and Technology, P.R. China)

Co-Chair: Hongyan Jia (Tianjin University of Science and Technology, P.R. China)

- OS 8-1 *Image Encryption Implementation Based on fractional-order Chen System*
Hongyan Jia, Qinghe Wang (Tianjin University of Science and Technology, P.R. China)
- OS 8-2 *Mobile Camera based Motion Segmentation by Image Resizing*
Chunyu Yu (Syracuse University, USA)
- OS 8-3 *Synchronization of the fractional-order permanent magnet synchronous motor*
Xue Wei, Li Xue (Tianjin University of Science and Technology, P.R. China)
- OS 8-4 *Analog Circuit Implementation and Full State Observation of Chua's Circuit*
Hong Niu, Dongchen Tan, Yongjun Wu
(Tianjin University of Science and Technology, P.R. China)
- OS 8-5 *Research on visualizational rescue robot*
YuanLi Yue, Fengzhi Dai, Qijia Kang, Pengfei Xie
(Tianjin University of Science and Technology, P.R. China)
- OS 8-6 *Development of training instrument for upper limb muscle rehabilitation*
Qijia Kang, Fengzhi Dai, Yuanli Yue, Bo Liu, Hongtao Zhang
(Tianjin University of Science and Technology, P.R. China)

Room B3

09:10-10:40 GS7 Robotics I (6)

Chair: A. Yamaguchi (Fukuoka Institute of Technology, Japan)

- GS7-1 *Haptic system with fuzzy controller for extended control of Teleoperation mine detector wheeled robots*
Yekkehfallah Majid, Guao Yang, Yuanli Cai, Naebi Ahmad, Zolghadr Javad
(Xi'an jiaotong university, P.R. China)
- GS7-2 *Effect of System Parameters and Controlled Torque on the Dynamics of Rigid-Flexible Robotic Manipulator*
Sachindra Mahto (North Eastern Regional Institute of Science & Technology, India)
- GS7-3 *Modeling of Mobile Manipulator and Adaptive Super-Twisting Backstepping Control*
Seong Ik Han, Hyunuk Ha, Jangmyung Lee
(Pusan National University, South Korea)
- GS7-4 *Self-tuned Local Feedback Gain Based Decentralized Fault Tolerant Control of Reconfigurable Manipulators*
Bo Zhao¹, Bo Dong², Yan Li², Fumitoshi Matsuno³, Yuanchun Li²
(¹Chinese Academy of Sciences, ²Changchun University of Technology, P.R. China),
(³Kyoto University, Japan)

- GS7-5 *Study on Decentralized Integral Nested Sliding Mode Control for Constrained Reconfigurable Manipulator with Harmonic Drive Transmission*
Bo Dong¹, Zeyu Dong¹, Bo Zhao², Yan li¹, Fumitoshi Matsuno³, Yuanchun Li¹
(¹Changchun University of Technology, ²Chinese Academy of Sciences, P.R. China),
(³Kyoto University, Japan)
- GS7-6 *A Number of Mobile Manipulator Control for Moving Object by using Cooperative Control*
Deok-Su Kim, Dong-Eon Kim, Seong-Ik Han, Jang-Myung Lee
(Pusan National University, South Korea)

14:20-15:50 OS6 Intelligent Control (6)

Chair: Yingmin Jia (Beihang University, P. R. China)

Co-Chair: Weicun Zhang (University of Science and Technology, P. R. China)

- OS6-1 *Adaptive Control of Discrete-Time Systems Using Multiple Fixed and One Adaptive Identification Models*
Zhang Yuzhen, Li Qing, Zhang Weicun
(University of Science and Technology Beijing, P. R. China)
- OS6-2 *Adaptive Polynomial Regression and Its Applications to Gene Selection of Rat Liver Regeneration*
Juntao Li, Yimin Cao, Xiaoyu Wang, Cunshuan Xu (Henan Normal University, P.R. China)
- OS6-3 *Adaptive Consensus via Dynamic Output Feedback for Lipschitz Nonlinear Multi-Agent Systems*
Lin Li, Heyang Wang (University of Shanghai for Science and Technology, P.R. China)
- OS6-4 *Iterative Learning based Thrust Ripple Suppression for PMLSM*
Caixia Gao, Fuzhong Wang, Ziyi Fu (Henan Polytechnic University, P.R. China)
- OS6-5 *Adaptive Sliding Mode Control for A 2-DOF Magnetic Levitation System with Uncertain Parameters*
Meng Duan, Yingmin Jia (Beihang University, P.R. China)
- OS6-6 *Undershoot Reduction in Discrete-Time ADRC of NMP Plant by Parameters Optimization*
Tong Wu, Weicun Zhang (University of Science and Technology Beijing, P.R. China)

16:10-17:10 OS 12 Advanced Research on Computer Science and Information Processing (4)

Chair: Takao Ito (Hiroshima University, Japan)

Co-Chair: Sakamoto Makoto (University of Miyazaki, Japan)

- OS12-1 *Development of a Tool to Keep Consistency between a Model and a Source Code in Software Development Using MDA.*
Yuuki Kikkawa¹, Tetsuro Katayama¹, Yoshihiro Kita², Hisaaki Yamaba¹, Kentaro Aburada³ and Naonobu Okazaki¹ (¹University of Miyazaki, ²Tokyo University of Technology, ³Oita National College of Technology, Japan)

- OS12-2 *Necessary spaces for seven-way four-dimensional Turing machines to simulate four-dimensional one-marker automata*
Makoto Nagatomo¹, Shinnosuke Yano¹, Makoto Sakamoto¹, Satoshi Ikeda¹, Takao Ito², Tsutomu Ito², Yasuo Uchida³, Tsunehiro Yoshinaga⁴, and Hiroshi Furutani¹
(¹University of Miyazaki, ²Hiroshima University, ³Ube National College of Technology, ⁴Tokuyama College of Technology, Japan)
- OS12-3 *Analysis for 4×12 board of Othello*
Yuki Takeshita¹, Satoshi Ikeda¹, Makoto Sakamoto¹, Takao Ito²
(¹Miyazaki University, ²Hiroshima University, Japan)
- OS12-4 *A space lower-bound technique for four-dimensional alternating Turing machines*
Makoto Nagatomo¹, Shinnosuke Yano¹, Makoto Sakamoto¹, Satoshi Ikeda¹, Takao Ito², Tsutomu Ito², Yasuo Uchida³, Tsunehiro Yoshinaga⁴, and Hiroshi Furutani¹
(¹University of Miyazaki, ²Hiroshima University, ³Ube National College of Technology, ⁴Tokuyama College of Technology, Japan)

RoomB4

9:10-10:40 OS5 Advanced Control Systems (6)

Chair: Yingmin Jia (Beihang University, P.R. China)

Co-Chair: Fuzhong Wang (Henan Polytechnic University, P.R. China)

- OS5-1 *Socialized Multi-Agent System Rendezvous via Networks of Networks*
Yunzhong SONG, Ziyi FU, Fuzhong WANG (Henan Polytechnic University, P.R.China)
- OS5-2 *Global sensor selection for maneuvering target tracking in clutter*
Wenling Li, Yingmin Jia (Beihang University, P.R. China.)
- OS5-3 *Attitude/Position Estimation of Rigid-Body using Inertial and Vision Sensors*
Shihao Sun, Yingmin Jia (Beihang University, P.R. China)
- OS5-4 *Modeling and Control of a Suspended Gravity Compensation System with the Rigid-Flexible Coupling*
Jiao Jia, Yingmin Jia, Shihao Sun (Beihang University, P.R. China)
- OS5-5 *Trajectory Tracking Control for Omnidirectional Mobile Robots with Input Constraints*
Wenhao Zheng, Yingmin Jia (Beihang University, P.R. China)
- OS5-6 *Parameters Tuning Approach for Prescribed Performance Function Based Active Disturbance Rejection Control*
Wei Wei, Bo Liang, Weijun Su (Beijing Technology and Business University, P.R. China)

14:20-15:35 GS5 Multi-Agent Systems & Visualization (2) +GS6 Intelligent Control & System Cybernetics (3)

GS5 Multi-Agent Systems & Visualization (2)

Chair: Shingo Mabu (Yamaguchi University, Japan)

- GS5-1 *Moving Robots Lies and Their Minds with Degree of Confidence in a Decentralized Autonomous FMS*
Shizuka Tanaka, Hidehiko Yamamoto, Takayoshi Yamada (Gifu University, Japan)
- GS5-2 *Conquest Oriented Robot Knowing Its Own Availability*
Sho Yamauchi, Keiji Suzuki (Future University Hakodate, Japan)

GS6 Intelligent Control & System Cybernetics (3)

Chair: Min Cheol lee ((Pusan National University, South Korea)

- GS6-1 *A Consideration on Feature Extraction for Operation Skill Based on Control Engineering Approach*
Kazushige Koiwai¹, Liao Yantao¹, Toru Yamamoto¹, Takao Nanjo², Yoichiro Yamazaki², Yoshiaki Fujimoto²
(¹Hiroshima University, ²KOBELCO Construction Machinery CO., LTD., Japan)
- GS6-2 *Design of a Data-Driven Control System for a Hydraulic Excavator*
¹Takuya Kinoshita, ¹Yasuhito Oshima, ¹Kazushige Koiwai, ¹Toru Yamamoto ²Takao Nanjo, ²Yoichiro Yamazaki, ²Yoshiaki Fujimoto
(¹Hiroshima University, ²KOBELCO Construction Machinery CO., LTD, Japan)
- GS6-3 *An Optimization of Spatio-Spectral Filter Bank Design for EEG Signal Classification*
Masanao Obayashi, Takuya Geshi, Takashi Kuremoto, Shingo Mabu
(Yamaguchi University, Japan)

16:10-16:55 OS8 Image, Circuit and Control (3)

Chair: Fengzhi Dai (Tianjin University of Science and Technology, P.R. China)

Co-Chair: Hongyan Jia (Tianjin University of Science and Technology, P.R. China)

- OS 8-7 *Design and Analog Circuit Implementation of a Dynamic Feedback Control System Based on RLC Series Circuit*
Hong Niu, Yongjun Wu, Dongchen Tan (Tianjin University of Science & Technology, P.R. China)
- OS 8-8 *Maximal power point tracking technology for the solar photovoltaic battery based on model predictive control*
Xia Zhao, Huailin Zhao (Shanghai Institute of Technology, P.R. China)
- OS 8-9 *Analysis and unidirectionally coupled synchronization of a novel chaotic system*
Li Xue, Xue Wei (Tianjin University of Science and Technology, P.R. China)

January 31 (Sunday)

8:50- Registration

Room B3

9:10-9:55 OS10 Reality Mining (3)

Chair: Masao KUBO (National Defense Academy of Japan, Japan)

Co-Chair: Saori Iwanaga (Japan Coast Guard Academy, Japan)

- OS10-1 *Fast collective photographic subject detection without pixels by an assumption about a shot and its elevation angle*
Sora Tanioka, Masao Kubo, Hiroshi Sato (National Defense Academy of Japan, Japan)
- OS10-2 *Evaluation of a safety map generated from a collection of difference of Individuals*
Masao Kubo, Dang Viet-Chau, Hiroshi Sato, Akira Namatame
(National Defense Academy of Japan, Japan)
- OS10-3 *Endeavor to adopt GIS data on evacuation decision making model*
¹Saori Iwanaga, ²Akira Namatame
(¹Japan Coast Guard Academy, ²National Defense Academy of Japan, Japan)

10:10-11:10 OS13 Automatic Generation, Creation, and Production of Narrative Contents (4)

Chair: Takashi Ogata (Iwate Prefectural University, Japan)

Co-Chair: Yoji Kawamura (Kinki University, Japan)

- OS13-1 *Automatic Generation, Creativity, and Production of Narrative Contents*
Takashi Ogata (Iwate Prefectural University, Japan)
- OS13-2 *A Design Plan of a Game System including an Automatic Narrative Generation Mechanism: The Entire Structure and the World Settings*
Jumpei Ono, Takashi Ogata (Iwate Prefectural University, Japan)
- OS13-3 *A Way for using the Verb Conceptual Dictionary in an Integrated Narrative Generation System: Focusing on the use of Co-occurrence Information on the Verb Concepts*
Takashi Ogata, Jumpei Ono (Iwate Prefectural University, Japan)
- OS13-4 *A Viewing Experiment on the Effects of Advertising Story*
Yoji Kawamura (Kinki University, Japan)

13:00-14:30 GS3 Reinforcement Learning Systems & Genetic Programing (6)

Chair: Kunikazu Kobayashi (Aichi Prefectural University, Japan)

- GS3-1 *Examination of Robotic Aerospace Engines Maintenance Supported by Augmented Reality through Cloud Manufacturing*
Mosab Alrashed, Yaser Yadekar, John Ahmet Erkoyuncu, Yifan Zhao (Cranfield University, UK)

- GS3-2 *Unit Layout Design Supporting System of Cell Assembly Machine Using Two Robots by Reinforcement Learning*
Yusaku Ikai, Hidehiko Yamamoto, Takayoshi Yamada (Gifu University, Japan)
- GS3-3 *Virtual Input Parts Decision System of Job-Shop Production Line by using GA with ON / OFF Gene*
Junji Ito, Hidehiko Yamamoto, Takayoshi Yamada (Gifu University, Japan)
- GS3-4 *An Evolutionary Algorithm for Making Decision Graphs for Classification Problems*
Shingo Mabu, Masanao Obayashi, Takashi Kuremoto (Yamaguchi University, Japan)
- GS3-5 *Improvement of Computational Efficiency of UPF by Automatic Adjustment of the Number of Particles*
Kenta Hidaka, Takuo Suzuki, Kunikazu Kobayashi (Aichi Prefectural University, Japan)
- GS3-6 *Multi Objective Evolutionary Algorithms for Association Rule Mining: Advances and Challenges*
Aswini Kumar Patra (North Eastern Regional Institute of Science & Technology, India)

RoomB4

9:10-9:55 OS9 Modern Approaches of MOT and Corporate Strategy (3)

Chair: Takao Ito (Hiroshima University, Japan)

Co-Chair: Seigo Matsuno (National Institute of Technology, Ube College, Japan)

- OS9-1 *A Study on the Structural Hole of Patent Applicant Network in R&D Management*
Iori Nakaoka¹, Yousin Park², Yun-ju Chen³ (¹National Institute of Technology, Ube College, ²Prefectural University of Hiroshima, ³Shiga University, Japan)
- OS9-2 *The TCE-RBV framework for information systems outsourcing: Empirical testing using survey data in Japan*
¹Seigo Matsuno, ²Tsutomu Ito, ¹Yasuo Uchida, ³Yoshiki Mikami, ⁴Takao Ito
(¹National Institute of Technology, Ube College, ²Hino Motors, Ltd., ³Nagaoka University of Technology, ⁴Hiroshima University, Japan)
- OS9-3 *Momentum and its Implications in Corporate Management*
Tsutomu Ito¹, Takao Ito¹, Rajiv Mehta², Sakamoto Makoto³, Katsuhiko Takahashi¹, Katsumi Morikawa¹ (¹Hiroshima University, ³Miyazaki University, Japan) (²New Jersey Institute of Technology, USA)

10:10-11:25 OS7 Image Analysis and Content Security (5)

Chair: Yasunari Yoshitomi (Kyoto Prefectural University, Japan)

Co-Chair: Masayoshi Tabuse (Kyoto Prefectural University, Japan)

- OS7-1 *A Method for Secure Communication Using a Discrete Wavelet Transform for Sound Data*
Yuji Tsuda¹, Kouhei Nishimura², Haruka Oyaizu³, Yasunari Yoshitomi², Taro Asada², Masayoshi Tabuse² (¹Software Service, Inc., ²Kyoto Prefectural University, ³NHK Media Technology, Inc., Japan)
- OS7-2 *An Authentication Method Using a Discrete Wavelet Transform for a Recaptured Video*
Ren Fujii, Yasunari Yoshitomi, Taro Asada, Masayoshi Tabuse
(Kyoto Prefectural University, Japan)
- OS7-3 *A System for Facial Expression Analysis of a Person While Using Video Phone*
Taro Asada, Yasunari Yoshitomi, Ryota Kato, Masayoshi Tabuse, Jin Narumoto
(Kyoto Prefectural University, Japan)
- OS7-4 *Emotion Recognition of a Speaker Using Facial Expression Intensity of Thermal Image and Utterance Time*
Yuuki Oka¹, Yasunari Yoshitomi², Taro Asada², Masayoshi Tabuse²
(¹NTT DATA Financial Solutions Corp. ²Kyoto Prefectural University, Japan)
- OS7-5 *Estimation of Learners' Subjective Difficulty in e-Learning Using Thermal Image Processing*
Yuki Yoshimitsu, Masayoshi Tabuse (Kyoto Prefectural University, Japan)

PS abstracts

PS1 Disrupting the Industry with Play

Henrik Hautop Lund (Technical University of Denmark, Denmark)

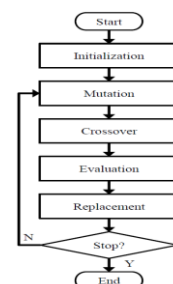
Decades of research into intelligent, playful technology and user-friendly man-machine interfaces has provided important insight into the creation of robotic systems and intelligent interactive systems which are much more user-friendly, safer and cheaper than what appeared possible merely a decade or two ago. This is significantly disrupting the industry in several market sectors. This paper describes the components of the playware and embodied artificial intelligence research that has led to disruption in the industrial robotics sector, and which points to the next disruption of the health care sector. This includes playful robotics, LEGO robots for kids, minimal robot systems, user-friendly, behavior-based, biomimetic, modular robotics and intelligent systems. The insight into these components and the use in synthesis for designing robots and intelligent systems allows anybody, anywhere, anytime to use these systems, providing an unforeseen flexibility into the sectors, which become disrupted with these systems.



PS2 A Study on Differential Evolution Using BetaCOBL, B³R, and TPBO

So-Youn Park, Ju-Jang Lee (KAIST, South Korea)

New parameters are defined to use a beta distribution without limitation and two beta utilizations to control the search magnitude of the stacte algorithm are proposed: one for adding randomness to OBL (BetaCOBL) and the other for individual distribution-oriented reproduction (B³R). BetaCOBL and B³R are developed into DE embedding BetaCOBL (BetaCODE) and two-phase B³R optimization (TPBO) respectively. The proposed algorithms are tested on various test functions and two real world applications and compared with other algorithms with respect to the performance criteria. The results indicate that the proposed algorithms outperform or perform comparatively to the comparison group especially in terms of solution accuracy and reliability.



IS abstracts

IS1 Redefining robot based technologies for elderly people assistance: a survey.

Luigi Pagliarini^{1,2}, Henrik Hautop Lund¹

(¹ Technical University of Denmark, Denmark, ² Academy of Fine Arts of Macerata, Italy)

We analyse the state of the art of hi-tech and robot based technologies in terms of Assistive Technology for all patients and, in particular, elderly people assistance and everyday activities aid. By focusing on different aspects and characteristics (such as *playfulness*, *invasiveness*, *learning-speed*, *efficiency*, *short and long-term effect*, *active vs. passive*, etc.) we show the most important existing examples, and highlight all the factors that might help researchers when developing technologies for elderly care. Decades of research have not yet declared what the optimal HMI is, in such context. Since there is an urgent need to clarify how various technologies can be a goal or an approach for preventive, rehabilitative and assistive interaction, we try to make a first step towards a redefinition of Robotics Assistive Technology.



IS2 Affective Human Computer Interaction

Kaoru Sumi (Future University Hakodate, Japan)

This talk introduces a study of spoken dialogue agent systems using emotional expressions as affective human computer interaction. The paper describes an experiment investigating the effect that the expression and words of the agent have on people, introduces a spoken agent for customer services using expressive facial expressions and a spoken agent for mental care using expressive facial expressions and positive psychology as application systems for affective human computer interaction, and presents a discussion and a conclusion.



OS abstracts

OS1 Artificial Life and Quality Enhancement of Life (6)

OS1-1 The development of new products of pineapple cheesecakes

Sheu-Der Wu¹, Hung-Wen Su² (¹Cheng Shiu University, ²Far East University, Taiwan)

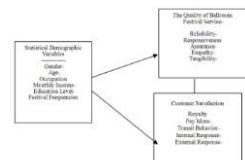
We are in view of the product - pineapple cheesecakes newly developed for this study, the questionnaire answers proposed by consumers after sensory evaluations find the most popular flavor with 27% recipe proportion of pineapple chops added. Furthermore, after pineapples are added into cheesecakes, a new flavor has emerged in cheesecakes yet reduces the oily taste without sacrificing its original flavor and nutrient value. In the experiment of formal sensory evaluation, genders, ages, occupations, incomes and purchase intention are served as factors to analyze consumers' preference to pineapple cheesecakes. Research results after investigation finds the strongest acceptability is the samples of pineapple cheesecakes added with 27% pineapple chops. The least acceptability happens to the samples of pineapple cheesecakes added with 27% pineapple jams. After analysis, it is found the overall acceptability is high but the purchase intention is low revealing a higher preference to cheesecakes added with pineapple chops.



OS1-2 The study on ballroom service quality to affect customer satisfaction

Hsiu-Min Lin , Yang Wu, Jei-Fu Ho (Far East University, Taiwan)

For hoteliers, customer expectations and the real performance of service probably existed in perceptive variance between the emphasized details and satisfaction to bring about the gaps of service quality. As such, it naturally caused customer unsatisfied with service quality to lose their patronage. As it is found from research results, service quality exerted positive influence on demographic variables. If it was available to improve the service quality and the expectations to customer satisfaction, then it was naturally available to enhance the repeated purchase intention of customers. In 10 dimensions cited in this research, after researching analysis, "tangibles" was satisfied by customers the most. If providers could keep the satisfaction always, then it was naturally available to enhance the first image in customers' mind. Additionally, "external response" scored the least and provides should improve their own service quality by focusing on the parts highly emphasized by customers. Furthermore, more emphasis should be placed on the opinions of customers to win their trust and avoid external complaint lodged by customers without losing the source of customers. The excellency or inferiority of service quality would directly affect customer satisfaction. If providers were planning for sustainable business management, excellent service quality was imperatively required. As such, it was just available to win the trust from customers under the fiercely competitive business climate with the goal of sustainable business management achievable.

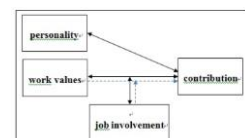


OS1-3 The relationship between employees' personality traits, work values and job involvement with the contribution to their companies – For the micro food service industry

Hsiu-Chen Chung¹, Chiou-Lan Chien¹, Lung-Chi Tsai²

(¹Tainan University of Technology, ²Southern Taiwan University of Science and Technology, Taiwan)

We The purpose of the study is to discover the influence between the employee's (for whom who works in the micro food industry) personality, work values and job involvement to the contribution and dedication. Research sample focus on the snack bar in night market, bakery stores and the micro food industries' employees or owners from Taizhong, Changhua, Yunlin, Jiayi and Tainan cities. We send 450 questionnaires, the effective questionnaires are 333, and the percentage of effective retrieve of the questionnaire is 87.63%. After using reliability analysis, correlation analysis, one-way analysis of variance (ANOVA), independent, work values and personality can forecast prediction the employee's contribution and dedication very precisely; in addition, we find out that job involvement has a very clear effects between work values and job contribution.



OS1-4 Consumer's acceptance to the new product- pineapple jam as example

Shang-Hui Li, Jei-Fu Ho (Far East University, Taiwan)

Based on the health and environmental considerations, consumers paid their more attention to the pursuit of natural ingredient. In other words, a safe and non-toxic diet is the basic consideration for the consumers. More consumers pay more attention on natural foods; they gradually change their eating habits. In recent years, many food safety events such as tainted milk, clenbuterol, poison starch, plasticizers etc. have been reported. Consumers tend to buy natural foods, less chemical additives and security food as the primary concern. This study attempts to take the natural pineapple jam as the major structure. And try to add dates and plum into pineapple jam instead of any artificial additives, and enhance the taste level. Meanwhile, different flavors could derive from the natural products according to the pineapple jam proportion of different formulations. The study expects to be able to create the pineapple jam which is not the same as made by the market products. The study selected 150 consumers of Tainan area to be tested of preferences of sensory evaluation, and SPSS 12.0 statistical software was used as the data analysis of the outcomes of the study. The result found among 123 valid questionnaires. The original flavor pineapple jam in its appearance, aroma, stiffness, acidity, sweetness and overall acceptability can be accepted by most consumers and there are significant differences with other products. Consumer also showed their strongest willingness to buy the original flavor pineapple jam and there are significant differences with other products.

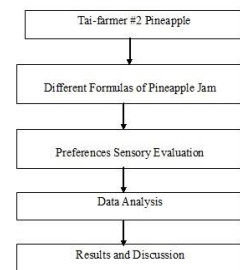
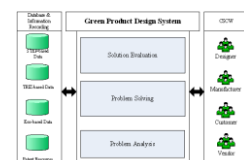


Chart 1. Pineapple Jam Test Flowchart

OS1-5 Development of an innovative design process for green products

Ming-Chieh Wang (Far East University, Taiwan)

We are Under the growing trend of environmental protection, many different eco-design methods have been proposed, at the same time, there are many TRIZ tools used to support these processes. In this study, we proposed an innovative design process for green products. This process includes three frameworks-collaborative design, innovative design environment, and the green product design system. Collaborative design framework aims to assist the designer and their upstream and downstream partners to combine their ideas by CSCW tools. The innovative design environment includes data layer, information layer, and knowledge layer, analyzed through the data exchange, information sharing and decision making during the design process. The green product design system was consists of the problem analysis, problem solving, and solution evaluation used to assist the design process with collaborative coordination and information recording. This construct integrating the design ideas, knowledge exchange, problem solving and feedback for the green product design process.



OS1-6 Research on Nail Art 3D Design with Different Materials

-- A Case Study of the Tang Dynasty Style

Mei-Yin Lee, Kung-Yu Liu, Sih-Jie Guan and Jei-Fu Ho (Far East University, Taiwan, ROC)

Women in Tang Dynasty, China (618 A.D.-907 A.D.) had concerned with beauty. They had painted color in their nails in addition to emphasis on clothing and makeup. Tang's costumes had blended the diverse characteristics of northern ethnic groups. Meanwhile a variety of engineering methods had been used such as embroidery, painting, printing, wearing gems and gemstones. Floral patterns had been appeared in large numbers in clothing, accessories and poetry. This study has tried to build the Tang Dynasty decorative painting technique or way of painting reappeared on modern nail art and to make the nail painting presents the different faces. After collecting a lot of relevant documents and experimenting many combinations of different materials, such as sculpture, super-light clay, foam paper, popsicle sticks, and Styrofoam, many hand-made stereoscopic flowers, such as peony, rose, plum etc., with painting have been made. Hence different from the past nail art, beautiful pieces of finger nail with the mood of Tang Dynasty poetry are presented. Furthermore, this study has investigated whether the stereoscopic nail art design with different materials could be promoted to the daily nail decoration to enhance the quality of life.

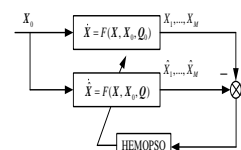


OS2 Intelligence Control System and Artificial Life (6)

OS2-1 Modified Quantum Particle Swarm Optimization for Chaos Synchronization

Ching-I Lee, Chia-Nan Ko (Nan Kai University of Technology, Taiwan)

In this study, a modified quantum-behaved particle swarm optimization (MQPSO) based on hybrid evolution (HEMQPSO) approach is proposed to synchronize chaotic systems, in which the proposed HEMQPSO algorithm combines the conceptions of genetic algorithm (GA) and adaptive annealing learning algorithm with the MQPSO algorithm to search optimal solutions. Simulation results are illustrated to verify the performance of chaos synchronization using the proposed HEMQPSO approach. From the numerical simulations and comparisons with other extant evolutionary methods in chaotic systems, the validity and superiority of the HEMQPSO approach are verified.

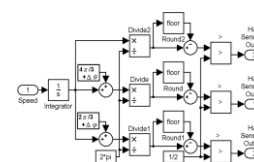


OS2-2 A Simulation Model of Hall Sensor Misalignment in BLDC Motors

Chung-Wen Hung, Chu-Lin Hsu

(National Yunlin University of Science & Technology, Taiwan)

A simulation model of Hall sensor misalignment in BLDC motors is proposed in this paper. The Hall sensor is popularly used in brushless DC motor to decide commutate and rotational speed. However, the accuracy of Hall sensor position is limited in most of BLDC motors, and it is lack of suitable simulation model for Hall Sensor installation misalignment. The details of simulation model are discussed in this paper, and simulation results are also provided to show the model workable.



OS2-3 Using Multi-Target Tracking and Identification TLD Algorithm for Intelligent Mobile Robot

Jr Hung Guo, Kuo-Hsien Hsia, Kuo-Lan Su
(National Yunlin University of Science & Technology, Taiwan)

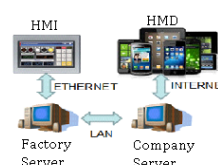
Image algorithms used herein are Tracking-Learning-Detection (TLD) and Speed UP Robust Features (SURF). TLD is used for target tracking and SURF is used to identify targets. We use zoning identification, with the use of statistical probability to strengthen the efficiency of TLD and SURF. With such a method, the efficiency of image identification and target tracking can be enhanced so that the robot can simultaneously track and identify multiple targets.



OS2-4 Handheld Mobile Devices for Remote Monitoring of Factory

Bing-Gang, Jhong, Jian-Sing, Hu, Mei-Yung, Chen
(National Taiwan Normal University, Taiwan)

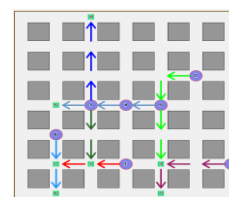
In this paper, a handheld mobile device system is presented for remote monitoring of the factory to short the downtime of machines and recovery more quickly. The human-computer interaction of the system is developed by GP-Por EX, and operates by using commercial or free distal APP combining with sign-in-website of the company. The way for the program linked can be linked with multi-way links, such as long-distance link (3G/4G or Wi-Fi wireless INTERNET), medium distance (LAN) and short distance (ETHERNET) and can be chosen in the company portal page. With supplemented Internet browser program for remote monitoring, the distal end operator or the person in charge can confirm the machine condition through the distal end of the server, port, user name and password settings. Therefore, the operational efficiency and system transparency can be improved with the handheld mobile devices for remote monitoring system.



OS2-5 Task Assignment and Checking Process for Pattern Reformation on a Square Grid Plane

Kuo-Hsien Hsia¹, Bo-Yi Li, Kuo-Lan Su
(¹Far-East University, National Yunlin University of Science & Technology, Taiwan)

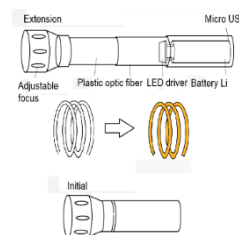
Pattern reformation problem on a grid plane is an interesting problem. Suppose there is a group of mobile robots on a square grid plane with the number of robots equaling to the number of columns/rows of the grid plane. The mobile robots are initially in a certain formation and they are commanded to change to another formation as soon as possible. Any one of them has to prevent himself from colliding with others during the moving of reformation process. In this paper, we will provide a systematic process on task assignment of route programming for the pattern reformation problem on a square grid plane. We will also provide a checking process to check if the suggested program is really good or not.



OS2-6 The Design of a Multifunctional Acousto-Optical Device With a Mobile Power Pack

Yi-Yu Lu, Wen-Bin Lin, Zheng-Ying Li (Far-East University, Taiwan)

This study presents details of a multifunctional acousto-optic warning device that recently obtained a patent in Taiwan. The device comprises three subsystems, which are RGB LEDs, warning system and mobile power pack. This device has multiple functions, including as a traffic baton, camping light, glow sticks and for women's security at night. The tube body of the device is adjustable, and can extend to 1.5 times its length. The design is both functional and practical, and it is also energy efficient due to the use of polymer optical fiber and a lithium battery. Since this device also has a USB charge and discharge function, it can also work as a mobile power pack.

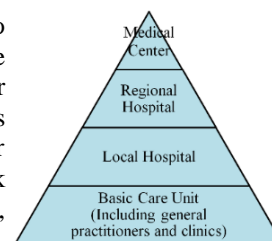


OS3 Construction Engineering and Management (6)

OS3-1 Discussion on Factors Influencing the Performance of Hospital Renovation Engineering Taking one Medical Center in Taiwan as Example

Wen-Lung Lin, Yan-Chyuan Shiau, Ting-Chi Lai, Chen-Chung Liu (Chung Hua University, Taiwan)

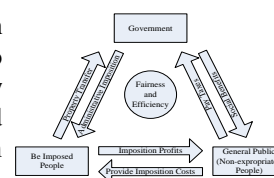
Renovation engineering is conducted to create the high-quality medical environment to meet the public's medical demands. The subjects of this study were to investigate the renovation engineering case of four hospital areas in Mackay Memorial Medical Center in Taiwan. 50 factors influencing the engineering performance were concluded in this study. The rank of each factor's influencing severity and influencing performance in four stages for hospital renovation engineering was summarized. The factors' severity rank influencing the performance in the four stages were planning and design stage, construction management stage, bidding stage and case acceptance and closing stage. The conclusions and suggestions of this study can be used as reference for future hospital renovation projects.



OS3-2 Discussion on Land Expropriation Compensation System

Hung-Chi Liu, Yan-Chyuan Shiau, Yao-Shan Huang, Chen-Chung Liu (Chung Hua University, Taiwan)

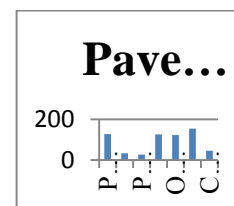
Land expropriation is a necessary means for the public construction of country. Usually some appropriate compensation was paid to imposed people. How land expropriation should be compensated in accordance with the spirit of the Constitution for governs to protect people's property rights have been explored in this study. The study results show that the public in Taiwan is rather satisfied with the current land expropriation at the land market value. "Estimation of land value by real-estate estimators" and "Compensation based on values listed on the Actual Price Registration" are much accepted by the public. It is also suggested that the existing land expropriation compensation shall adjust to meet the public wish to reduce incidences of struggles and improve administrative proficiency.



OS3-3 Study on User Satisfaction of Pick Areas for Elementary Schools – Using Nanyang Elementary School in Taichung City as Example

Chun-Feng Chang, Yan-Chyuan Shiau, Kuan-Yin Chen (Chung Hua University, Taiwan)

Most of the campus accidents happen on the way between school and home, and most of the locations are close to their homes or schools. The elementary school children have low autonomy and they are mainly picked by parents. This study has investigated the user satisfaction of pick areas for elementary schools and their improvement requirements. Questionnaire is adopted to discuss user satisfaction of the school environment. The improvement strategies for pick areas were inspected for different various backgrounds. The research results have showed that overall satisfaction ranges from general to satisfaction. Some useful suggestions are proposed. These suggestions can be served as reference for schools and educational organizations to establish an unimpeded pick area for a safe school commuting environment.



OS3-4 Study on User Satisfaction in Sport Site Facilities for Senior Students of Elementary Schools in Taichung City

Pei-Ling Lin, Yan-Chyuan Shiau, Ling-Lin Chang (Chung Hua University, Taiwan)

In Taiwan, obesity rate of children and adolescents is 26.8% and physical fitness also falls behind the neighboring Asian countries. This study has discussed senior students' actual use and satisfaction towards school sport field facilities in elementary schools of Taichung City. This study adopted questionnaire method and senior students in elementary schools of Taichung City were used as research subjects which were sampled with stratified cluster sampling method. The obtained data were analyzed by descriptive statistics, Chi-square test, T test, one-way ANOVA, and Pearson product-moment correlation. It is expected to provide reference for relevant personnel so as to provide the ideal campus sports environment.



OS3-5 The Establishment of the Sustainability Performance Indicators for Wetland Ecological Project: Using Construction Inspection Phase as Example

Ching-Mei Miao, Yan-Chyuan Shiau, Chen-Chung Liu, Jen-Kuo Chang (Chung Hua University, Taiwan)

Taiwan's government has invested considerable material, human resources and money to build many artificial by using ecological engineering methods. The critical success factors of sustainable performance indicator (SPI) were investigated in this research. A wetland water purification project of a stream in Hsinchu was used as an example in this paper. The experiment information was integrated as feedback to correct the index library. The measurement from test results verifies the SPI from sample project case in some facet is consistent with the results of current inspection system. Adopting the SPI integrated from this study can quickly detect the sustainability of the construction project and dramatically reduce labor inspection and costs. The research result can be served as reference for the sustainable development of ecological engineering achievements.



OS3-6 Development of Type Control Guidelines for the Old Town District of Hsinchu City

Yi-Yin Tsai (Chung Hua University, Taiwan)

The study employed the concept of "Building Type Control" to establish the hierarchy model and design guideline for the urban regeneration process. GIS was used to efficiently manage database and map out the building environmental features to serve as a visual reference tool. Existing building regulations and urban design policies set out by the government were reviewed to set out limitation and ultimate vision for the study district, three type control zonings were set out with type control design guidelines respectively. Results of the study can serve as a sufficient reference tool to assist design decision making in the urban regeneration process.

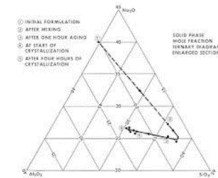


OS4 Construction Technology and Management (5)

OS4-1 Study on the Promotion of Steel Slags Recycling in Taiwan

Shu-Chen Chang, Ching-Jung Chang (Chung Hua University, Taiwan)

The fast development of global economy makes the great development of industry, causes the excess development and abuse of natural resources, and causes the resources depletion gradually. So the topic of waste reuse has already become an energy strategy paid more attention the worldwide research units and governments day by day. The construction industry uses a large amount of concrete, and its basic materials are the fine and coarse aggregates and cement, which are taken from sandstone mining and limestone calcining, and they will be exploited excessively and destroy the environment. This study tries to use the industrial waste to replace the aggregates and cement in concrete, and use them suitably in accordance with their different properties.



OS4-2 The Research on the Utilization of Green Building Ecological Index Group in Campus Environment – Taking of Elementary Schools at Houli District, Taichung City as Example

Ching-Jung Chang, Yung- Feng Hsu, Chun-Hsien Chen (Chung Hua University, Taiwan)

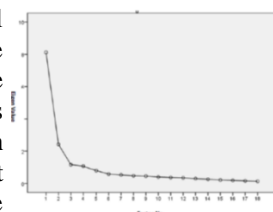
Due to overexploitation of the earth, the mankind causes the phenomena such as the climate anomaly, ozone layer depletion, forest disappearance, species extinction, ocean pollution, debris flow, global warming and sea level rise etc. Therefore every country in the world begins to launch the comprehensive environmental protection action of earth. This research took elementary schools at Houli District, Taichung City as study subjects, based on “Green Building Assessment Manual” announced by official authority, and conducted “ecological index group” assessment. Through field investigation, analyzed and compared three assessment indices of “biodiversity”, “greening amount” and “base water preservation”, and provided recommendation of improvement, in order to raise the ecological environment of campus. It is hoped there should have appropriate contribution for the planning of similar school or environment in the future.



OS4-3 The Assessment and Research on the Reconstruction of Enclosing Wall into Open Type in Elementary School Campus – Taking of Erlin Township, Changhua County as Example

Ching-Jung Chang, Chia-Chen Li, I-Chen Wu (Chung Hua University, Taiwan)

In recent years, Taiwan government has pursued the open campus by reconstructing the enclosing wall of campus into the friendly fence or dismantling the enclosing wall directly, let the community residents participate in the school space together. So the government subsidizes the funds and encourages the school to reconstruct or remove the enclosing wall. Because the change for the type and height of enclosing wall, the teachers and parents have the doubt for the security of students in the campus. This research conducted the regional investigation for the school teachers, students and parents against the friendly fence and security opinion of open campus. It hopes to provide the reference for the reconstruction and design of enclosing wall in Elementary School campus by the government authority in the future.



OS4-4 The Study and Analysis on the Reuse and Transformation Strategy of Tile Kiln Space – Taking of San-He Tile Kiln as Example

Ching-Jung Chang, Hsiao-Yu Lin, Ying-Yu Su (Chung Hua University, Taiwan)

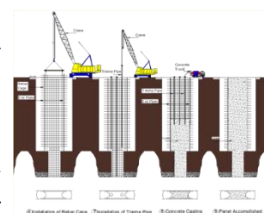
Because the new technology was introduced and the abundant use of concrete and steel products, the tile kiln industry was declined gradually in Taiwan. This paper attempts to review a successful case of kiln space reuse that has good culture assets preservation and combines cultural and creative industry. This research selects San-He Tile Kiln as the study subject. The questionnaire for investigating the visitors on different requirement was designed through interviewing the kiln owners and experts in advance and collating the interview information systematically. The Principal Component Analysis simplified the questionnaire variables to become the aspects of appeal. This research hopes to provide the operation reference to the civilian tile kiln owners or the other related space reuse sector.



OS4-5 The Research on the Influence of Economic Benefit for High-Rise Buildings Constructed by Different Excavation Method – Taking of Residence Buildings at New Taipei City as Example

Ching-Jung Chang, Cheng-Min Yang, Hsiu-Hsiung Hsu (Chung Hua University, Taiwan)

Every domestic big construction company hunted the land for development aggressively, in order to get the priority of obtaining the profit. The selection of excavation method has great relative relationship on the construction speed of structure, influence of adjacent building, acquisition of use license and delivery of house. This research adopted diverse excavation methods used by the constructor to analyze the advantage and disadvantage, construction period difference, and construction cost prediction etc. Finally, the results are compiled and contrasted to verify the relative relationship of excavation method on the difference of construction period, and cost etc. The purpose of this research is expected to provide the developer to select suitable excavation method effectively to reach the highest benefit of delivering the finished house.

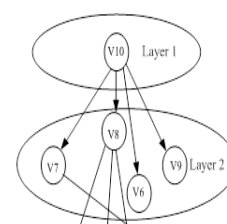


OS5 Advanced Control Systems (6)

OS5-1 Socialized Multi-Agent System Rendezvous via Networks of Networks

Yunzhong Song, Ziyi Fu, Fuzhong Wang (Henan Polytechnic University, P.R. China)

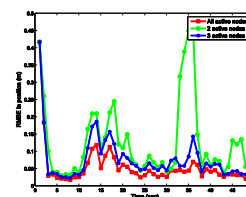
Networks of networks paradigm was introduced to explore rendezvous problems of leader-follower multi-agent system, where rendezvous actors were categorized into target object, leader agents, informed follower agents and isolated follower agents, respectively. Three humanized system inspired strategies were investigated. Results demonstrated that democracy strategy could fulfill rendezvous task in expenses with a long convergent time and autarchy democracy could come to targeted object quickly with risk of failing in rendezvous, while mixed strategy cared about both of convergent speed and utmost task, would take autarchy strategy when connections were available for follower agents, while democracy rules had to be used if the connections were not possible.



OS5-2 Global sensor selection for maneuvering target tracking in clutter

Wenling Li, Yingmin Jia (Beihang University, P.R. China.)

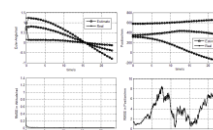
In this paper, we consider the problem of sensor selection for maneuvering target tracking in clutter. By utilizing the global knowledge of all sensors locations, a cost function that minimizes the expected filtered mean square localization error is developed to select a given number of active sensors. As the cost function is derived based on the decentralized structure, we investigate how to derive the decentralized fusion formula by applying EKF and PDA technique so that the clutter information can be combined into the cost function. By minimizing the cost function, a sensor selection scheme is proposed based on the 'add one sensor node at a time' strategy. Simulations are provided to illustrate the effectiveness of the proposed approach.



OS5-3 Attitude/Position Estimation of Rigid-Body using Inertial and Vision Sensors

Shihao Sun, Yingmin Jia (Beihang University, P.R. China)

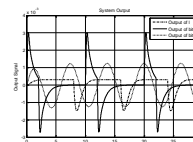
This paper is concerned with the attitude and position estimation of a rigid-body using inertial and vision sensors. By employing the Newton-Euler method, a kinematic model is developed for the rigid-body by treating the inertial measurements as inputs. Based on the coordinate transformation, a nonlinear visual observation model is proposed by using the image coordinates of feature points as observations. Then the unscented Kalman filter (UKF) is utilized to estimate the attitude and position recursively. Simulation results are provided to show the effectiveness of the proposed algorithm.



OS5-4 Modeling and Control of a Suspended Gravity Compensation System with the Rigid-Flexible Coupling

Jiao Jia, Yingmin Jia, Shihao Sun (Beihang University, P.R. China)

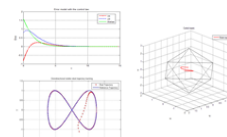
In this paper, the suspension gravity compensation system (SGCS) is modeled and the corresponding controller is designed. The system is a servo platform consisting of three sub-systems by which a micro-gravity environment can be established. The system model is deduced based on Lagrange equation. The system state variables are classified in two parts based on their physical meaning and the model dimensions are reduced on the classification. A PID controller is designed based on the feedback linearization. The simulation results show the effectiveness of the proposed method.



OS5-5 Trajectory Tracking Control for Omnidirectional Mobile Robots with Input Constraints

Wenhao Zheng, Yingmin Jia (Beihang University, P.R. China)

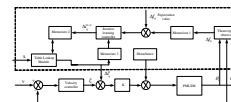
In this paper, a trajectory tracking controller based on kinematics for omnidirectional mobile robots with input constraints is presented. The tracking error model with the control law is proved to be global asymptotic stability by Lyapunov stability theory. The input limits can be described as an octahedron in three-dimensional space, so that a spatial vector analysis method is proposed to design time-varying feedback parameters to limit robot inputs. Simulation results show the feasibility and effectiveness of the control strategy.



OS6-4 Iterative Learning based Thrust Ripple Suppression for PMLSM

Caixia Gao, Fuzhong Wang, Ziyi Fu (Henan Polytechnic University, P.R. China)

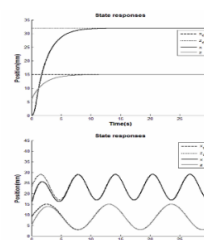
To solve problem of thrust ripple of multi-segment primary Permanent Magnet Linear Synchronous Motor (PMLSM), a control strategy combining fuzzy PID, which was based on velocity regulation and iterative learning algorithm, which was based on current compensation was proposed to deal with thrust ripple in advance. Through investigation of thrust ripple of PMLSM, mapping relationship between thrust ripple and motor critical parameters has been established, then thrust ripple suppression model for multi-segment primary Permanent Magnet Linear Synchronous Motor was available, and control law can be made possible. Results show that, thrust ripple was less than 1% under different position; strong suppression of thrust ripple caused by periodic disturbance could also be inhibited.



OS6-5 Adaptive Sliding Mode Control for A 2-DOF Magnetic Levitation System with Uncertain Parameters

Meng Duan, Yingmin Jia (Beihang University, P.R. China)

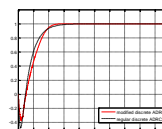
This paper investigates the stability control for a 2 degrees of freedom magnetic levitation system with both parameters uncertainty and external disturbance. This system includes one magnet and two coils, the magnet which levitated by two coils can only move through x-axis and z-axis. The electromagnetic forces between the magnet and coils are obtained by numerical calculation that brings uncertain parameter of input to the system dynamical model. To this end, an adaptive sliding mode controller is proposed. The system stability and robustness are proved by the Lyapunov stability theory. Simulation results are presented to verify the effectiveness of the proposed control strategy.



OS6-6 Undershoot Reduction in Discrete-Time ADRC of NMP Plant by Parameters Optimization

Tong Wu, Weicun Zhang (University of Science and Technology Beijing, P.R. China)

Undershoot phenomena caused by unstable zeros of non-minimum-phase (NMP) plant is difficult to deal with in active disturbance rejection control (ADRC). This paper proposes a new method to reduce undershoot by optimizing the controller parameters of discrete-time ADRC system. Simulation results are given to verify the effectiveness of the proposed scheme.

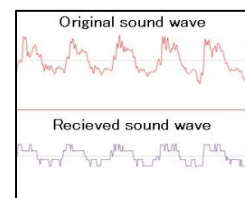


OS7 Image Analysis and Content Security (5)

OS7-1 A Method for Secure Communication Using a Discrete Wavelet Transform for Sound Data

Yuji Tsuda¹, Kouhei Nishimura², Haruka Oyaizu³, Yasunari Yoshitomi², Taro Asada², Masayoshi Tabuse²
(¹Software Service, Inc., ²Kyoto Prefectural University, ³NHK Media Technology Inc., Japan)

We developed a method for secure communication using a discrete wavelet transform for sound data. Two users must have one piece of music before communicating each other. The music is beforehand transformed into a code using the scaling coefficients obtained from a discrete wavelet transform. The sound data are transformed into another code using the same method as that for the music. The information on the difference between these two codes is sent from one user to the other. The user can produce the sound similar to the original sound using an inverse discrete wavelet transform with the code made from the music, the information on the difference between these two codes, and values of zero for all wavelet coefficients. The voice produced by the proposed method was audible.



OS7-2 An Authentication Method Using a Discrete Wavelet Transform for a Recaptured Video

Ren Fujii, Yasunari Yoshitomi, Taro Asada, Masayoshi Tabuse (Kyoto Prefectural University, Japan)

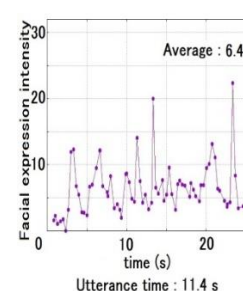
Recently, several digital watermarking techniques have been proposed for hiding data in the frequency domain of moving image files to protect their copyrights. In this study, we developed an authentication method for a recaptured video by using the previously proposed method using a discrete wavelet transform for a static image and a method for selecting several frames in the moving image. In contrast to digital watermarking, no additional information is inserted into the original moving image by the newly proposed method. The experimental results show that the proposed method has a good performance for authentication.



OS7-3 A System for Facial Expression Analysis of a Person While Using Video Phone

Taro Asada, Yasunari Yoshitomi, Ryota Kato, Masayoshi Tabuse, Jin Narumoto
(Kyoto Prefectural University, Japan)

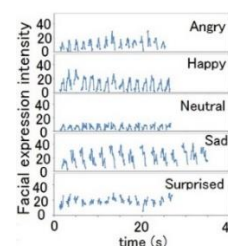
We developed a wireless local area network system, consisting of two personal computers and one router, where a module for analyzing facial expressions of a person while speaking with another person using a phone video is equipped in a personal computer in front of a subject and is controlled by an operator using another personal computer in the system. In the module, a function for determining the reference frame and locally searching the mouth-part area with the most appropriate position for each frame to be analyzed is contained. The video saved in the personal computer in front of the subject is analyzed using image processing software (OpenCV) and the previously proposed feature parameter (facial expression intensity), which is measured for the mouth-part area. The experimental result shows the usefulness of the proposed system.



OS7-4 Emotion Recognition of a Speaker Using Facial Expression Intensity of Thermal Image and Utterance Time

Yuuki Oka¹, Yasunari Yoshitomi², Taro Asada², Masayoshi Tabuse²
(¹NTT DATA Financial Solutions Corp., ²Kyoto Prefectural University, Japan)

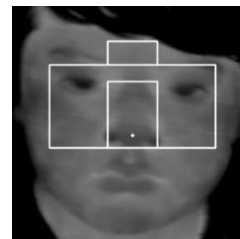
We previously proposed a method for recognizing human emotion. A video is analyzed by thermal image processing and the feature parameter of facial expression, which is extracted in the area of the mouth and jaw. The facial expression intensity, defined as the norm of the difference vector between the feature vector of the neutral facial expression and that of the observed one, is measured. The standardized mean value of facial expression intensity for a major cluster, and the standardized mean value of time at utterance for a major cluster are used for recognizing human emotion. In this study, the emotions of one subject were discriminable with 76.5% accuracy in speaking each of 23 kinds of utterances with exhibiting each of the five intentional emotions of "angry," "happy," "neutral," "sad," and "surprised."



OS7-5 Estimation of Learners' Subjective Difficulty in e-Learning Using Thermal Image Processing

Yuki Yoshimitsu, Masayoshi Tabuse (Kyoto Prefectural Univ., Japan)

In recent years, e-learning has been utilized as a learning system in many schools. In a conventional class, a teacher teaches learners face-to-face, so that a teacher observes facial expressions and posture change of learners and estimates learners' subjective difficulty of the lecture. On the other hand, e-learning is usually utilized in the self-study. A learner learns a teaching material using a computer by oneself, so that a teacher can't observe the state of the learner. It is difficult for a teacher to estimate learners' subjective difficulty. Therefore, we propose a learners' subjective difficulty estimation system. This system captures the face of a learner in e-learning with a thermal camera. It extracts the face region, measures the temperature changes of the nose region and the forehead region of the learner, and estimates the subjective difficulty of the learner based on the temperature changes.

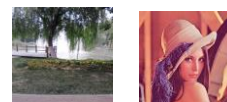


OS8 Image, Circuit and Control (9)

OS 8-1 Image Encryption Implementation Based on fractional-order Chen System

Hongyan Jia, Qinghe Wang (Tianjin University of Science and Technology, P.R. China)

In this paper, based on the fractional-order Chen system, a kind of double encryption algorithm method is adopted to realize the image encryption. The method mainly refers to the transformation of the pixel position and the transformation of pixel value. The effectiveness of the double encryption method is verified by encryption and decryption of a typical image. The experimental results show that this method not only has the ideal effect of image encryption and decryption, but also possesses a better guarantee on the image security. That is, this encryption method is practical and feasible.



OS 8-2 Mobile Camera based Motion Segmentation by Image Resizing

Chunyu Yu (Syracuse University, USA)

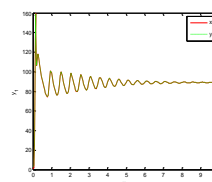
The need of detecting moving object like human and vehicle by mobile camera is increasing in commerce and industry. In this paper, an image-resize methodology which can abstract motion segmentation and detect moving object from moving background is proposed. First, edges images are computed. Then movement vector between frame images are computed and the relative background motion is compensated. By adjusting the parameters of resize algorithm, human liked object or vehicle liked object can be segmented separately and the segmentation can be used for further detection. Experiments have been performed under three different environments for human detection and vehicle detection.



OS 8-3 Synchronization of the fractional-order permanent magnet synchronous motor

Xue Wei, Li Xue (Tianjin University of Science and Technology, P.R. China)

In this paper, the synchronization of the fractional-order permanent magnet synchronous motor is investigated. The presented control scheme is simple and flexible, and it is suitable both for design and for implementation in practice. According to the stability theory of fractional-order linear system, adopting the linearization by feedback method, a nonlinear feedback controller to implement the synchronization of the drive system and the response system is designed. The numerical simulation results coincide with that of theoretical analysis, which can further demonstrate the feasibility and effectiveness of the proposed synchronization scheme.

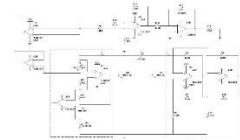


Variation of x_1 and y_1

OS 8-4 Analog Circuit Implementation and Full State Observation of Chua's Circuit

Hong Niu, Dongchen Tan, Yongjun Wu
(Tianjin University of Science and Technology, P.R. China)

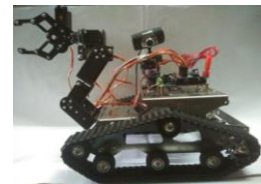
In this paper, an inductance simulator and a nonlinear resistor, which are constructed by operational amplifiers and resistors, are applied to complete the analog circuit implementation of Chua's circuit as well as improve the accuracy of circuit parameters. For the observation of all variables, the state variable z , which represents the product of the linear resistance and the inductor current in Chua's circuit, should be observed even if it is not an actual measurable physical quantity. It is found that z can be obtained via scaling of the voltage of the resistor in the inductance simulator. The real chaotic curves generated from the analog Chua's circuit are displayed on the oscilloscope clearly and correctly.



OS 8-5 Research on visualizational rescue robot

YuanLi Yue, Fengzhi Dai, Qijia Kang, Pengfei Xie
(Tianjin University of Science and Technology, P.R. China)

Aimed at the shortcomings of the low efficiency and the limitation of the search and rescue robot, this paper presents a visualizational search and rescue robot based on Arduino platform. The infrared detector for searching human body is used to detect life, and the camera can transmit the information back to the mobile phone or computer terminal in real-time. The track wheel improves the capability of shuttle and over obstacle, and can easily cope with complex terrain. The mounded manipulator can complete many missions, such as clean up the road block and deliver essential supplies to small space. It can replace humans to carry out the task into the dangerous environment and search-and-rescue person into the confined space.



OS 8-6 Development of training instrument for upper limb muscle rehabilitation

Qijia Kang, Fengzhi Dai, Yuanli Yue, Bo Liu, Hongtao Zhang
(Tianjin University of Science and Technology, P.R. China)

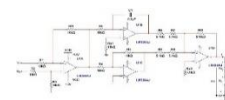
This equipment can work in multiple degrees. By the single joint and composite motion, it imitates human upper limb movement. Composite motion can be multiple degrees of freedom, so that the equipment can fit with the physiological structure of human body well. Upper limb strength can be recovered efficiently and the muscle contraction can also be well preserved as expected. Obtaining vibration module, it enhances the effect of recovering. Wireless transceiver module makes the wireless monitoring and data wireless transmission be a feasible way. It is connected with the computer, and the recover information of patients could be gathered, analyzed and recorded in computer as well. Data can also be transmitted by the internet, so as to offer the recover information to medical institution.



OS 8-7 Design and Analog Circuit Implementation of a Dynamic Feedback Control System Based on RLC Series Circuit

Hong Niu, Yongjun Wu, Dongchen Tan (Tianjin University of Science and Technology,)

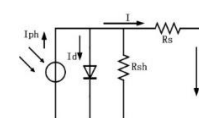
The purpose of this paper is to verify that a dynamic feedback control system can be realized by a simple small analog circuit. A normal RLC series circuit, which is an electrical two-order circuit only consisting of one resistor, one inductor and one capacitor, is taken as the controlled object, and the voltage of the capacitor is taken as the output of the system. The engineering design method of regulator in DC drive control system is applied to design the dynamic feedback compensator, so that the output of the system can track the given input, and the system is stabilized and has expected performance. The simulation results of the theoretical model and the corresponding results of the real analog circuit implementation are given in the paper to illustrate that the circuit can accomplish the tracking function of dynamic feedback control system.



OS 8-8 Maximal power point tracking technology for the solar photovoltaic battery based on model predictive control

Xia Zhao, Huailin Zhao (Shanghai Institute of Technology, P.R. China)

The solar photovoltaic battery is a new type of renewable distributed energy. Its output power is directly affected by light intensity and the temperature, and its voltage-current characteristic has the obvious nonlinear feature. In order to improve the energy conversion efficiency of the photovoltaic system, it's very significant to study the effective control algorithm's realization on the maximal power point tracking (MPPT) control. A new MPPT technology based on model predictive control (MPC) is proposed. The proposed method is developed to control the output current of a boost converter in order to extract the maximal solar power from the photovoltaic panel.



OS 8-9 Analysis and unidirectionally coupled synchronization of a novel chaotic system

Li Xue, Xue Wei (Tianjin University of Science and Technology, P.R. China)

In this paper, a new three-dimensional autonomous chaotic system is proposed. By means of theoretical analysis and numerical simulation, some basic dynamical properties, such as equilibrium points, fractal dimension, Lyapunov exponent spectrum and chaotic dynamical behaviors of the new chaotic system are investigated. The obtained results show clearly that this system is a new chaotic system. Furthermore, based on Lyapunov stability theory of the system, we observe unidirectionally coupled synchronization of the new three-dimensional chaotic system through designing the appropriate coupling coefficient. Results of numerical simulation illustrate the effectiveness of the presented synchronization scheme.

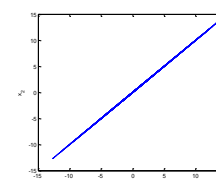


Fig.curve of state variable
(x_1, y_1)

OS9 Modern approaches of MOT and Corporate Strategy (3)

OS9-1 A Study on the Structural Hole of Patent Applicant Network in R&D Management

¹Iori Nakaoka, ²Yousin Park, ³Yun-ju Chen (¹National Institute of Technology, Ube College, ²Prefectural University of Hiroshima, ³Shiga University, Japan)

The arrangement of R&D staff refers to the issue of the linkage between structural holes in a network (Burt, 2003). In order to examine the linkages between multiple R&D projects in a company, we use the patent information as the index of R&D capability and examine our propositions by social network analysis. In this paper we focus on top-shared companies in Japanese cosmetics industry, and suppose that these companies keep their market shares due to their smoothly changes of business fields to cope with the threat of new entrants from other industries. The analysis in this paper include: 1) calculate the betweenness centrality, and create heat-maps to visualize the change of the betweenness centrality, 2) examine the structure hole.

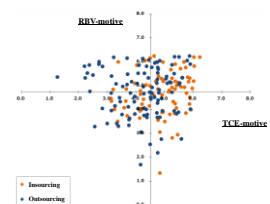


OS9-2 The TCE-RBV framework for information systems outsourcing: Empirical testing using survey data in Japan

Seigo Matsuno¹, Tsutomu Ito², Yasuo Uchida¹, Y. Mikami³, Takao Ito⁴

(¹National Institute of Technology, Ube College, ²Hino Motors, Ltd., ³Nagaoka University of Technology, ⁴Hiroshima University, Japan)

This paper investigates the factors that influence the motives of make-or-buy decisions on information systems from the viewpoints of Transaction Cost Economics (TCE) and the Resource-based View (RBV). Using our original questionnaire survey data carried out in 2007 targeting Japanese firms, we analyze the relationships between the recognition related to the role of their information systems and the pattern of their make-or-buy decisions. As a result, we make it clear that there are two cases in which TCE-motive and RBV-motive are complement or contradict with each other. And in latter case, TCE-motive tends to dominate over RBV-motive. Finally, The implications for theory and practice are discussed.



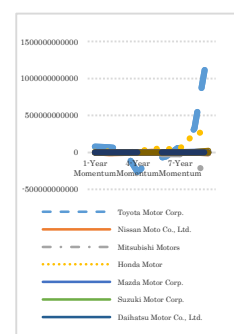
OS9-3 Momentum and its Implications in Corporate Management

Tsutomu Ito¹, Takao Ito¹, Rajiv Mehta², Sakamoto Makoto³, Katsuhiko Takahashi¹, Katsumi Morikawa¹

(¹Hiroshima University ³Miyazaki University, Japan)

(²New Jersey Institute of Technology, USA)

In contrasting conventional theses with current strategic theories, discussions on momentum, an important concepts, have been sparse, although in the context of current management strategies the pivotal nature of momentum recently has been operationalized and discussed in research on marketing, and finance. The current manuscript reviews the literature associated with corporate strategy, and proposes a new approach of acceleration to measure momentum based on limited cycle theory. Thus, this research manuscript makes a contribution to extant thought by: (1) Defining momentum, (2) Discussing the nature of the relationship between momentum to its external environment, and company scale, 3) Ascertaining the momentum period, and 4) Proposing a four-cell model composed of momentum and company scales for judging a firm position. Additionally, the relationship between momentum and the impact of the 2007-2008 financial crises is addressed. Based on the findings, the study limitations are identified and directions for further research are suggested.

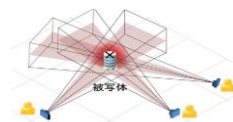


OS10 Reality Mining (3)

OS10-1 Fast collective photographic subject detection without pixels by an assumption about a shot and its elevation angle

Sora Tanioka, Masao Kubo, Hiroshi Sato
(National Defense Academy of Japan, Japan)

In this paper, we propose a collective intelligence to discover photographic subjects without pixel information. A collection of information about shooting, for example, EXIF, Geotag, and Tiff which is automatically attached into a digital photograph is only used for this detection. So far we have to use a large number of such the not-pixel information for this task because the original model of taking a photo is not efficient. In this paper, we estimate the improvement of the performance to discover subject if there is a relation between a shot and its elevation angle of the camera.



OS10-2 Evaluation of a safety map generated from a collection of difference of Individuals

Masao Kubo, Dang Viet-Chau, Hiroshi Sato, Akira Namatame
(National Defense Academy of Japan, Japan)

In this paper, we propose a collective intelligence approach to generate safety maps of road environment from a collection of logs of vehicle behavior recorded by drivers' smartphone. Usually a general collective intelligence uses the average of the data and it is difficult to apply it for complex problems. This paper proposes a reasonable method for generation of safety maps to evaluate the difference of the behavior. The accuracy of the map is evaluated by official accident record



OS10-3 Endeavor to adopt GIS data on evacuation decision making model

¹Saori Iwanaga, ²Akira Namatame
(¹Japan Coast Guard Academy, ²National Defense Academy of Japan, Japan)

By Multi Agent Simulation: MAS, we focused on contagion of evacuation decision making on real map assuming that not all people evacuate at the time of disaster. Then, we found that for contagion of evacuation decision making, local neighborhood is needed and connection of sub network is needed. But, there we faced on difficulty of obtaining realistic population data on map, because Census Bureau data consists of not position data but numbers and properties. In this paper, we attempt to use geographic information system GIS data and population data, then we simulate of population with heterogeneous agents and their decision making.



OS11 Kansei Engineering and Application (4)

OS11-1 Automated Multiple-Brightness Peak Image Processing Method Using Curvature and Variance Estimation

¹Yusuke Kawakami, ²Tetsuo Hattori, ²Yoshiro Imai, ²Kazuaki Ando, ²Yo Horikawa (¹DynaxT Co., Ltd., ²Kagawa University, Japan) ³R. P. C. Janaka Rajapakse (³Tainan National University of the Arts, Taiwan)

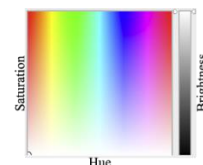
This paper describes the improvement method for the image which have multiple-brightness peak using Histogram Matching based on the Gaussian Distribution (HMGD). The previous papers, we have illustrated that the HMGD is an automated image processing method for improve feeling impression better, through the comparative investigation results of feeling impression among the original image, Histogram Equalization image, and HMGD image. However, the multiple-brightness peak images have been hard to improve using the previous HMGD. In this paper, we propose the processing method of HMGD to correspond image which have multiple-brightness peak, using curvature computation and variance estimation.



OS11-2 Histogram Matching Based on Gaussian Distribution on the HSB Color System

¹Yusuke Kawakami, ²Tetsuo Hattori, ²Yoshiro Imai, ²Kazuaki Ando, ²Yo Horikawa (¹DynaxT Co., Ltd., ²Kagawa University, Japan) ³R. P. C. Janaka Rajapakse (³Tainan National University of the Arts, Taiwan)

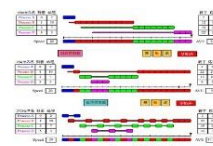
This paper proposes Histogram Matching based on Gaussian Distribution (HMGD) processing on the HSB color system which is close to the human visual property. In the previous paper, we have proposed HMGD processing on the brightness axis which is calculated from RGB color system. And we have considered that HSB color system is more suitable for HMGD processing, because it contains brightness axis. In this paper, we describe how to transform the color image from RGB color system into HSB color system first. Second, we describe that the principal of HMGD on this color system. And then, we also explain how to re-transform HSB color system to RGB color system.



OS11-3 Quantitative Evaluation of Flash-based Educational Visualizing Simulator

Kei Takeichi, Yoshiro Imai, Kazuaki Ando, Yusuke Kawakami, Tetsuo Hattori
(Kagawa University, Japan)

A Flash-based simulator of CPU scheduling has been developed and utilized for educational visualization in the class of university lecture. We have designed and implemented it with Flash-based scripting language in order to execute it as a stand-alone application as well as in various browsing environment such as Microsoft IE, Google Chrome and/or FireFox (Mozilla). Based on questionnaire for our simulator in the lecture, its quantitative evaluation has been carried out by means of statistical analysis. Our report describes overview of our Flash-based simulator and the results of the above quantitative evaluation.



OS11-4 Relation between Optimal Stopping Solution and NSPR for Structural Change Point Detection Problem

Tetsuo Hattori, Yoshihide Koyama, Yoshiro Imai, Yo Horikawa, Hiromichi Kawano¹
(Kagawa University, ¹NTT advanced technology Company Ltd, Japan)

Previously, we have proposed a novel method using New Sequential Probability Ratio (NSPR) for the structural change point detection (SCPD) of ongoing time series data instead of using SPRT (Sequential Probability Ratio Test). Moreover, we have formulated the SCPD problem in time series data as an Optimal Stopping one using the concept of DP (Dynamic Programming) and also have shown the solution theorem in the form of Inequality. In this paper, we discuss the relation between the solution of Optimal Stopping and NSPR for the SCPD Problem.

Optimal Solution

$$a < (A + a) \cdot P(\bar{S}_n | S^{n-1})$$

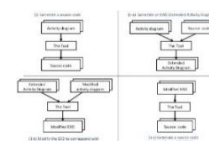
$$NSPR = \frac{P(H_1 | S^n)}{P(H_0 | S^n)} < \frac{\left(\frac{A}{A+a}\right) - R}{R_c - \left(\frac{A}{A+a}\right)}$$

OS12 Advanced Research on Computer Science and Information Processing (4)

OS12-1 Development of a Tool to Keep Consistency between a Model and a Source Code in Software Development Using MDA.

Yuuki Kikkawa¹, Tetsuro Katayama¹, Yoshihiro Kita², Hisaaki Yamaba¹, Kentaro Aburada³,
Naonobu Okazaki¹ (¹University of Miyazaki, ²Tokyo University of Technology,
³Oita National College of Technology, Japan)

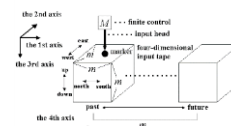
This study improves efficiency of software development using MDA. This paper develops the tool that keeps consistency between a model and a source code in software development using MDA. The tool has two functions: (i) Generating a source code and (ii) Keeping consistency between a model and a source code. Inputs of (ii) are an unmodified activity diagram, the modified activity diagram, and the source code including the detail specification. An output of (ii) is a source code which is consistent with the modified activity diagram and includes the detail specification. In executing (ii), the tool generates EAD (Extended Activity Diagram) as intermediate data.



OS12-2 Necessary spaces for seven-way four-dimensional Turing machines to simulate four-dimensional one-marker automata

Makoto Nagatomo¹, Shinnosuke Yano¹, Makoto Sakamoto¹, Satoshi Ikeda¹, Takao Ito²,
Tsutomu Ito², Yasuo Uchida³, Tsunehiro Yoshinaga⁴, Hiroshi Furutani¹ (¹University of Miyazaki,
²Hiroshima University, ³Ube National College of Technology, ⁴Tokuyama College of Technology, Japan)

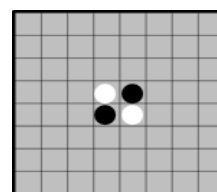
We think that recently, due to the advances in many application areas such as motion image processing, computer animation, and so on, it is very useful for analyzing computational complexity of multi-dimensional information processing to explicate the properties of four-dimensional automata, i.e., three-dimensional automata with the time axis. As far as we know, there is no investigation about four-dimensional automata. Then, in 2002, we first introduced four-dimensional finite automata in the world. In 2003, we investigated four-dimensional alternating Turing machines. In 2015, we show the sufficient spaces for four-dimensional Turing machines to simulate four-dimensional one-marker automata. In this paper, we continue the investigations, and deal with the necessary spaces for four-dimensional Turing machines to simulate four-dimensional one-marker automata.



OS12-3 Analysis for 4×12 board of Othello

Yuki Takeshita¹, Satoshi Ikeda¹, Makoto Sakamoto¹, Takao Ito²
(¹Miyazaki University, ²Hiroshima University, Japan)

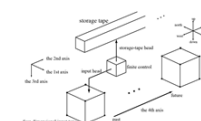
More than 20 years has passed since J. Feinstein (1993) found that a perfect play on 6×6 board of Othello gives a 16-20 win for the second player. A computer Othello surpasses a much more human now. However, standard 8×8 board remain unsolved. In our previous paper, we were able to obtain the perfect plays on 6×6 board and 4×10 board. In this paper, we challenge the unsolved problem of 4×12 board by dividing it into about 150 small problem.



OS12-4 A space lower-bound technique for four-dimensional alternating Turing machines

Makoto Nagatomo¹, Shinnosuke Yano¹, Makoto Sakamoto¹, Satoshi Ikeda¹, Takao Ito²,
Tsutomu Ito², Yasuo Uchida³, Tsunehiro Yoshinaga⁴, Hiroshi Furutani¹ (¹University of Miyazaki,
²Hiroshima University, ³Ube National College of Technology, ⁴Tokuyama College of Technology, Japan)

Alternating Turing machines were introduced in 1981 as a generalization of nondeterministic Turing machines and as a mechanism to model parallel computation. On the other hand, we have no enough techniques which we can show that some concrete four-dimensional language is not accepted by any space-bounded four-dimensional alternating Turing machines. The main purpose of this paper is to present a technique which we can show that some four-dimensional language is not accepted by any space-bounded four-dimensional alternating Turing machines. Concretely speaking, we show that the set of all four-dimensional input tapes over $\{0,1\}$, which each top half part is equal to each bottom half part, is not accepted by any $L(m)$ space-bounded four-dimensional alternating Turing machines for any function $L(m)$ smaller than $\log m$.

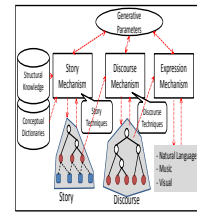


OS 13 Automatic Generation, Creation, and Production of Narrative Contents (4)

OS13-1 Automatic Generation, Creativity, and Production of Narrative Contents

Takashi Ogata (Iwate Prefectural University, Japan)

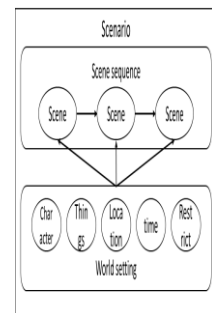
According to the concept of this organized session, in this presentation, we will consider the study of automatic narrative or story generation as a research field of artificial intelligence in the following levels: generation, creation, and production. At first, we study the technologies of narrative or story generation systems based on mainly artificial intelligence and cognitive science. Next, the artistic and aesthetic problems of narrative creation are considered in the relationships with the technologies and systems of narrative generation. Further, issues toward organizational or social narrative production are presented. These survey and discussion will be done based on some topics in this session relating to a game and advertising systems and our integrated narrative generation system.



OS13-2 A Design Plan of a Game System including an Automatic Narrative Generation Mechanism: The Entire Structure and the World Settings

Jumpei Ono, Takashi Ogata (Iwate Prefectural University, Japan)

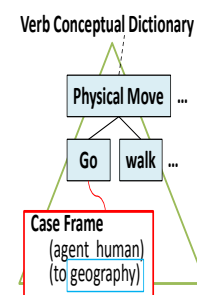
We present a plan of a narrative generation system based on a scenario generation method in tabletop role-playing games (TRPGs). It uses an integrated narrative generation system (INGS) that synthesizes various narrative generation mechanisms. A TRPG is an analog game in which one or more player (PL) play each role as characters in a framework of narrative by the game master (GM). A PL promotes the development of scenes, and, as a result, a narrative is completed. In particular, we concentrate on the “world setting” that has a role of rules or constricts in narrative and consists of components defined by its rule and the stage setting of the narrative. In the ordinary use, a GM sets a basic world setting to guide generation through the interaction between PLs. We consider preliminarily prepared scripts corresponding to various world settings in addition to the detailed mechanism for the use it.



OS13-3 A Way for using the Verb Conceptual Dictionary in an Integrated Narrative Generation System: Focusing on the use of Co-occurrence Information on the Verb Concepts

Takashi Ogata, Jumpei Ono (Iwate Prefectural University, Japan)

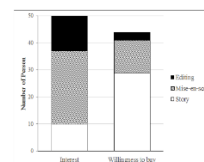
This paper presents a way for selecting verb concepts based on the analysis of co-occurrence information of verb words in the data of modern Japanese novels (“Aozora Bunko”). The proposed method will be incorporated into some mechanisms in an integrated narrative generation system (INGS) that synthesizes various mechanisms for narrative generation that we have been developing. We show an overview of INGS, in particular the mechanism relating to the proposed method in this paper. In the verb conceptual dictionary, as verb concepts of a variety of difficulty or understandability are mixed, the objective in this paper is to adjust the usage by using co-occurrence information on verb concepts. Our hypothesis is that the original concepts of co-occurrence and the resulted concepts have a proportional relation. We will investigate it by incorporating the mechanism into the INGS.



OS13-4 A Viewing Experiment on the Effects of Advertising Story

Yoji Kawamura (Kinki University, Japan)

This research lays out the conception and functions of developed Commercial Film Production Support System (CFPSS). The research then explains the results of a viewing experiment that utilized CFPSS. In this experiment where commercial films of beer were utilized, the following findings were obtained: in inducing interest, the evaluation of image type of advertising story is high; in stimulating willingness to buy, the evaluation of provider type is high; and mise-en-scène or editing attracts interest and the advertising story associated with product function and the supporting production and distribution stimulates willingness to buy. These findings gradually clarify the following creative know-how of the creator; to attract consumer interests by focusing on the stories of consumer situations in case consumers do not aware or understand their products or services; to arouse their willingness to buy by focusing on the products and stories of their acceptance and effects in case consumers have a certain level of understanding and interests in products or services.



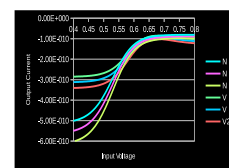
GS abstracts

GS1 Neuromorphic Systems (5)

GS1-1 Compensating Temperature-Dependent Characteristics of a Subthreshold-MOSFET Analog Silicon Neuron

Ethan Green, Takashi Kohno (The University of Tokyo, Japan)

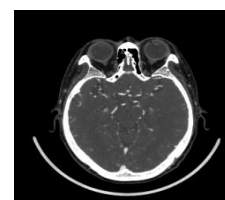
Analog silicon neurons are neuro-mimetic VLSI (very-large-scale-integrated) circuits that replicate the electrophysiological behavior of animal nerve tissue. These circuits send and receive spike trains in continuous time and require minimal power. This research focuses on the temperature sensitivity of a subthreshold-MOSFET silicon neuron. Subthreshold operation of CMOS transistors allows for low power consumption and desirable current-voltage characteristics, but is also drastically sensitive to temperature changes. This critical issue must be addressed before these circuits can be implemented into massive networks to develop future technologies, which could include neuromorphic computers, artificial brains, brain-machine-interfaces, and ultra-low power computing platforms.



GS1-2 Medical image analysis of brain X-ray CT images by deep GMDH-type neural network

Tadashi Kondo, Junji Ueno, Shoichiro Takao (Tokushima University, Japan)

In this study, the deep Group Method of Data Handling (GMDH)-type neural network is applied to medical image analysis of brain X-ray CT images. The deep GMDH-type neural network algorithm can automatically organize the deep neural network architecture which has many hidden layers, using the heuristic self-organization method which is a type of evolutionary computations. This algorithm is applied to the medical image analysis of brain X-ray CT images. The deep neural network is automatically organized from brain X-ray CT images and recognizes and extracts the brain, bone and blood vessels regions in the brain images.



GS1-3 Medical image diagnosis of lung cancer by deep feedback GMDH-type neural network

Tadashi Kondo, Junji Ueno, Shoichiro Takao (Tokushima University, Japan)

The deep feedback Group Method of Data Handling (GMDH)-type neural network is applied to the medical image diagnosis of lung cancer. The deep feedback GMDH-type neural network has feedback loops and the complexity of the neural network architecture is increased by feedback loop calculations. Each feedback loop is constructed with the three layers which are the input, hidden and output layers. This deep feedback GMDH-type neural network is applied to the medical image diagnosis of lung cancer and the deep neural network which can recognize and extract the lung cancer and blood vessel regions, is automatically organized from the chest X-ray CT images.



GS1-4 Feature Linking by Synchronized Response in Chaotic Cellular Neural Network for Visual Stimulus of Moving Objects

Akihiro Yamaguchi¹, Satoshi Arakane¹, Masao Kubo²

(¹Fukuoka Institute of Technology, ²National Defense Academy of Japan, Japan)

A feature linking mechanism by the synchronized response of neural assemblies was studied for the chaotic cellular neural network (Chaotic-CNN). The Chaotic-CNN consists of chaotic spike response neurons that show the chaotic inter-spike-interval dynamics. In our scheme of feature linking, the features of the target objects are linked by the synchronized spike responses that are characterized by the temporal chaotic pattern of spike sequence. In this paper, we analyzed the synchronized spike responses that invoked by the visual stimulus of moving bars. As a result, neural assemblies have higher correlation for the visual stimulus of moving two bars with the same direction (Fig.1 (a)) than the opposite direction (Fig.1 (b)). Then we discussed a possibility of feature linking by the chaotic synchronized response in the view point of neural coding.

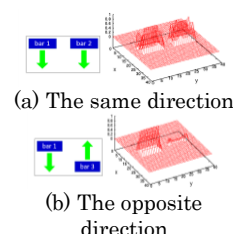
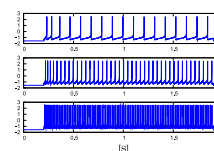


Fig.1 Correlation of neural assemblies

GS1-5 An FPGA-based cortical and thalamic silicon neuronal network.

Takuya Nanami, Takashi Kohno (The University of Tokyo, Japan)

A DSSN model is a neuron model which is designed to be implemented efficiently by digital arithmetic circuit. In our previous study, we expanded this model to support the neuronal activities of cortical and thalamic neurons. They are regular spiking, fast spiking, intrinsically bursting and low-threshold spike. In this paper, we report our implementation of the expanded DSSN model and kinetic-model-based silicon synapses on a Xilinx / Spartan -6 LX45 FPGA. Here, synaptic efficacy was stored in block RAMs. The DSP modules integrated on the FPGA chip were utilized to facilitate efficiency in implementation of multiplication in the DSSN model.



GS2 Pattern Recognition & Image Processing (6)

GS2-1 An accurate method for the extraction of structured light stripe

Jiwu Wang¹, Yaodong Li¹, Zhijing Jian¹, Sugisaka Masanori²

(¹Beijing Jiaotong University, P.R. China), (²Alife Robotics Corporation Ltd, Japan)

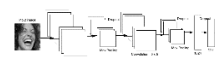
In order to obtain the highest measurement accuracy in the On-line measurement of rail profile with a line structured light based on machine vision, the extraction of structured light stripe is a necessary step. An accurate extraction method is proposed for the structural light stripe extraction in practical applications. The noise in the captured image can be removed with region segmentation method. The structured light stripe is separated and extracted accurately based on the characteristics of the structure light stripe in the binary image. The method was verified in laboratory conditions. Experiment results show that the method can effectively solve the problem of real-time and accurate extraction of structured light stripe.



GS2-2 Feature Acquisition From Facial Expression Image Using Convolutional Neural Networks

Taiki Nishime, Satoshi Endo, Koji Yamada, Naruaki Toma, Yuhei Akamine
(University of The Ryukyus, Japan)

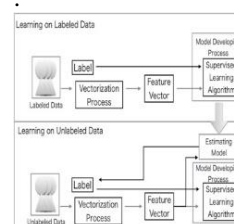
In this study, we carried out the emotion acquisition from facial expression image using a Deep Neural Networks(DNN). Emotions we focused on are "happiness", "sadness", "surprise", "anger", "disgust", "fear" and "neutral". By using Convolutional Neural Networks(CNN) approaches, we have obtained an average emotion recognition score of 58%; two emotions (happiness, surprise) recognition score was about 70%. This result was the same tendency as preliminary experiment of human recognition. From CNN model after training, specific unit were confirmed to be learning the feature about happiness. The results corroborate that CNNs work effectively for learning facial expression about happiness, surprise representations.



GS2-3 Estimating Age on Twitter Using Self-Training Semi-Supervised SVM

Tatsuyuki Iju, Satoshi Endo, Koji Yamada, Naruaki Toma, Yuhei Akamine
(University of The Ryukyus, Japan)

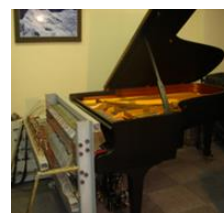
Most recent researches for estimating Twitter user's latent attributes are concerned with making attribute estimator from only user tweets with one's profile known, that is, ground truth data. However, it tends to be high cost to collect enough amount of ground truth data to provide estimator. In our study, we employ SVM with self-training, with words in tweets used as features, in order to reduce the cost of collecting data. We carry out some parameter surveys to investigate how these parameters affect performance of classifier. We utilize predict-probability of LIBSVM package as a threshold to determine which of unlabeled users to be labeled during self-training. At last, we evaluate the classifier for parameters which are found to be the best on parameter surveys.



GS2-4 Interactive musical editing system to support human errors and offer personal preferences for an automatic piano

Kenji Tsunenari, Eiji Hayashi (Kyushu Institute of Technology, Japan)

Recently, electronic musical instruments are achieving progress for development of electronics and seen everywhere. However, their sound quality and ambience are inferior to real musical instruments. Therefore, we developed automatic piano by using grand piano. Pre-edit is needed to play music in the manner of a live pianist. In the case of piano music, there are often 1000 or more notes in the score of even a short piece of music, requiring that an editor spend a huge amount of time to accurately simulate the emotionally expressive performance of a highly skilled pianist. Therefore, we have developed an interactive musical editing system that utilizes a database to edit music more efficiently.



GS2-5 Geometric parameters measurement of wheel tread based on line structured light

Jiwu Wang¹, Zhijing Jian¹, Yaodong Li¹, Chao Yang¹, Sugisaka Masanori²
(¹Beijing Jiaotong University, China), (²Alife Robotics Corporation Ltd, Japan)

The positioning precision is important in the processing of geometric parameters measurement technology of wheel tread. In this paper, a new method with no-contact measurement based on line structured light is given to solve this problem. Here traditional mechanical locating method is used as a rough reference. Moreover, some digital image processing techniques are developed for each of the key dimensions of measurement. According to the feature points (particularly, the key points that have not been worn) and lines extracted effectively on the wheel tread, precise positioning is realized. In this paper, the experiments show that the proposed method is feasible and excellent to design and implement non-contact measurement of the wheel tread, wheel flange thickness and rim width. It also ensures the accuracy of positioning and analyses the factors of measurement error.



GS2-6 Study on the ORB algorithm in the application of Monocular SLAM

Jiwu Wang¹, Shunkai Zheng¹, Masanori Sugisaka²
(¹Beijing Jiaotong University, P.R. China) (²Alife Robotics Corporation Ltd, Japan)

In view of reducing the accumulative error, we perform loop closing (detection + correction) based on PTAM in our Monocular SLAM. As this method relies on extracting natural environment features, we chose ORB algorithm as the feature extraction and matching. We demonstrate that ORB features have enough recognition power to enable place recognition from severe viewpoint change and they are so fast to extract and match (without needing multi-threading or GPU acceleration) that enable real time accurate tracking and mapping. Through outdoor scene experiment, we validate the algorithm performance.

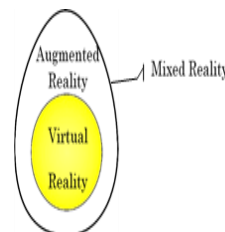


GS3 Reinforcement Learning System & Genetic Programing (5)

GS3-1 Examination of Robotic Aerospace Engines Maintenance Supported by Augmented Reality through Cloud Manufacturing

Mosab Alrashed, Yaser Yadekar, John Ahmet Erkoyuncu, Yifan Zhao (Cranfield University, UK)

This Paper aims to develop a demonstration using a mobile device to apply augmented reality to allow remote maintenance activities. This research was focused primarily on the aerospace industry studies as there was a research gap as there are few relevant researches in the manufacturing field and accepted industry needs. The targets were achieved by developing and designing controls in the engineering steps to create the optimum conditions for augmented reality. The design process pursued in four stages: first, research the current practice of using augmented reality remotely in manufacturing maintenance; second, classify maintenance remote assisting problems and weakness in augmented reality; third, design and develop software and hardware, depending on the case study for a prototype solution to remote maintenance enhanced by the augmented reality that can be demonstrated and tested; finally, validate the developed software and demonstration using industrial experts and authentic reports.



GS3-2 Unit Layout Design Supporting System of Cell Assembly Machine Using Two Robots by Reinforcement Learning

Yusaku Ikai, Hidehiko Yamamoto, Takayoshi Yamada (Gifu University, Japan)

In this study, we explain the development of Design Supporting System for Cell Assembly Machine System (CAMS) which systemize the decision of the unit layout that compose the assembly machine using two robots. CAMS uses Profit Sharing which is one of the Reinforcement Learning methods, determining each units layout. Profit Sharing is performed by the following flow: (1) The units layout is determined by Roulette Selection, (2) The one cycle work time of the robot is calculated to evaluate the unit layout, (3) If the evaluation is good, the units layout is given rewards. Efficient units layout is decided by the number of regulation times repeating the flow 1-3. We apply CAMS to assembly of the Differential which is automotive parts to verify its validity.



GS3-3 Virtual Input Parts Decision System of Job-Shop Production Line by using GA with ON / OFF Gene

Junji Ito, Hidehiko Yamamoto, Takayoshi Yamada (Gifu University, Japan)

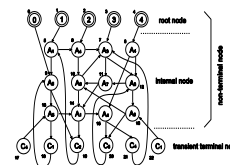
We propose the simulator to decide the best parts input order. We call this simulator as Virtual Input Parts Decision by ON/OFF Genes (VIPDOG). VIPDOG has 2 configuration systems as follows: 1) The parts order decision system to indicate the parts input and processing orders of a job shop production line. 2) The virtual production system that performs the visualization of the working environments acquired by VIPDOG. The virtual production system can check what will happen in the future and some experienced engineers can discuss the problems to solve them.



GS3-4 An Evolutionary Algorithm for Making Decision Graphs for Classification Problems

Shingo Mabu, Masanao Obayashi, Takashi Kuremoto (Yamaguchi University, Japan)

Classification is one of the major research in pattern recognition and a large number of methods have been proposed such as decision trees, neural networks (NNs), support vector machines (SVMs). In order to easily understand and analyze the reason of the classification results, decision trees are useful comparing to NNs and SVMs although these methods have shown distinguished classification abilities. In this paper, to enhance the classification ability of decision trees, a new evolutionary algorithm for creating decision graphs is proposed, where multi-root nodes, unique genetic operators and majority voting mechanism based on Maximum a posteriori are introduced. In the performance evaluation, it is clarified that the proposed method shows better classification ability than decision trees.

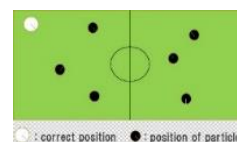


GS3-5 Improvement of Computational Efficiency of UPF by Automatic Adjustment of the Number of Particles

Kenta Hidaka, Takuo Suzuki, Kunikazu Kobayashi (Aichi Prefectural University, Japan)

In RoboCup Standard Platform League (SPL), the method using unscented particle filter (UPF) has been proposed for self-localization.

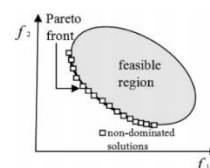
The UPF resolves a problem of particle filter (PF) which cannot be sampled appropriately when the likelihood is too high or low. It is also applicable to the kidnapping problem. The filter can estimate the precise position if the number of particles is large enough but the computational cost may also increase in proportion to the number of particles. In the present paper, we propose an automatic adjustment method for the number of particles in UPF using the variance of distances between the position of a particle and the average position of all the particles and the absolute error between the position of a particle and the correct position of robot. Through computer simulations, we confirmed the improvement of computational efficiency of UPF.



GS3-6 Multi Objective Evolutionary Algorithms for Association Rule Mining: Advances and Challenges

Aswini Kumar Patra (North Eastern Regional Institute of Science & Technology, India)

Association rule mining, one of the most important and well researched techniques of data mining. The challenge, posed by most of the association rule mining methods, is the amount of time consumed for generating frequent items sets. To overcome this evolutionary algorithms have been used widely. Moreover, apart from support and confidence, there are many other metrics available to measure the quality of association rules. That is the reason why multi-objective approach plays a crucial role. Therefore, two methodologies namely, multi-objective and evolutionary algorithms as a combination proved to be a preferred choice. Though numerous works have been proposed for mining association rules, use of multi-objective evolutionary algorithms are still in its infancy stage. This paper explores the challenges and advances that has been made in this regard in terms of nature of algorithm, encoding mechanism, objective functions and operators.

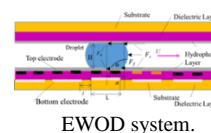


GS4 Micro-Machine (4)+GS9 Robotics III (4)

GS4-1 Applying Fuzzy Sliding Mode Control on Electrowetting on Dielectric System

¹Arsit Boonyaprapasorn, ²Thavida Maneewarn, ²Eakkachai Pengwang (¹Chulachomklao Royal Military Academy, ²King Mongkut's University of Technology Thonburi, Thailand)

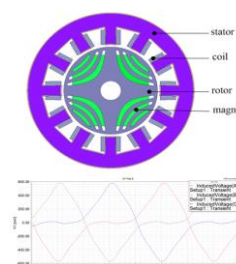
In Lab-on-a-chip (LOC) devices, an electrowetting on dielectric (EWOD) method can be performed to create, cut, mix, and transport droplets. Moreover, the micro assembly process of micro parts can be manipulated by the EWOD system. High accuracy of droplet motion in both applications is required. Based on the simplified model, the feedback control such as sliding mode control can be applied so that the droplet motion can achieve a high accuracy performance under disturbances. However, the sliding mode control often has chattering problem. Thus, in this study, the fuzzy sliding mode control was applied to manipulate the droplet in the EWOD system. The study was conducted via simulation in MATLAB environment. The result showed that the proposed control method could provide an accurate motion control with lower chattering compared to that of classical sliding mode control.



GS4-2 Development of Micro-Permanent Magnet Synchronous Reluctance Generator for TPMS on Smart Robots

¹Chun-Chieh Chang, ¹Cheng-Tang Pan, ¹Shao-Yu Wang, ¹An-Yun Yang, ¹Gu-Xuan Lin, ²Roger Chenglung Lee, ²Ting-Hung Chung, ¹Yu-Jen Wang (¹National Sun Yat-sen University, ²Naroller Electronics, Taiwan)

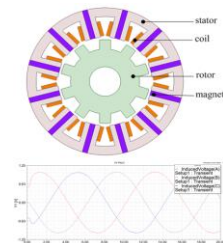
Synchronous Reluctance Generator (SynRG) is a high-functioning and robust motor with simple structure and low cost. In this study, the rotor was embedded magnet and developed with a miniature size of permanent magnet generators, which can be applied to the tire pressure monitoring system (TPMS) on the smart robots. The SynRG was studied for voltage producing to achieve sufficient power for TPMS. The experiment focuses on the specific winding distribution, such as distributed winding or concentrated winding, and the number of stator slots per phase. On the other hand, the structural design of the generator focuses on the magnet configuration, the rotor structure, and working air gap to optimize the parameters. In addition, the generator was considered with a different rotational speeds and the rotor resistances. High power output, stable voltage waveform, and torque ripple were analyzed to determine the generator. In the selection of the magnetic materials, ferrite magnet was selected which has the advantage of lower-cost. Finite element method (FEM) is used to simulate the magnetic properties of the generator. The optimized design of SynRG in this study was centralized distribution of windings, ratio 12/4 of the slot and pole, 500-1200 rpm of the rotation speed and 5 mm of lamination thickness, 50 mm of outer diameter of the stator. The results indicate that the generating capacity of 2.3 V can be achieved.



GS4-3 Study of Micro-Flux-Switching Permanent-Magnet Generator for TPMS on Smart Robots

¹An-Yun Yang, ¹Cheng-Tang Pan, ¹Shao-Yu Wang, ¹Chun-Chieh Chang, ¹Gu-Xuan Lin, ²Roger Chenglung Lee, ²Ting-Hung Chung, ¹Yu-Jen Wang (¹National Sun Yat-sen University, ²Naroller Electronics, Taiwan)

Flux-Switching Permanent-Magnet Generator (FSPMG) is of high flux density and high efficiency due to its double salient structures. This study presents a micro FSPMG which can be applied to tire pressure monitoring system (TPMS) on the smart robots. To design a micro FSPMG, we tested the slot-pole ratio to find out an optimal voltage output. This steady rotation generator with high generating capacity and low torque ripple was obtained by optimizing the design of air gap, arc ratio and salient ratio with different rotation speeds. In this paper, we used finite element method (FEM) to simulate the magnetic properties of generator and the voltage output. The magnetic material used in this study was ferrite magnet which has the advantage of lower-cost. The design of FSPMG in this study was ratio 12/10 of the slot and pole, 500-1200 rpm of the rotation speed and 5 mm of lamination thickness, 50 mm of outer diameter of the stator. The results indicate that the generating capacity achieves to 3.4 V where the air gap is the main factor to affect this generator.



GS4-4 MEMS Microrobot Controlled by Mounted Neural Networks IC with Two Types Actuators

Kei Iwata, Hirozumi Oku, Yuki Okane, Yohei Asano, Masaki Tatani, Yuki Ishihara, Kazuki Sugita, Satoshi Chiba, Satoko Ono, Mizuki Abe, Minami Takato, Ken Saito, Fumio Uchikoba (Nihon University, Japan)

We report the hexapod microrobot controlled by the hardware neural networks. MEMS (Micro Electro Mechanical System) was used for fabrication of the microrobot. Hexapod walking of microrobots that mimics such motion of ants is realized by link mechanisms. Actuators of the robots can be classified as piezoelectric (PZT) type and shape memory alloy (SMA) type. The rotation of PZT actuator is generated by the impact head attached to the piezoelectric element. On the other hand, rotation of SMA actuator is generated by shrinkage of SMA from four directions. The microrobots are controlled by the bare chip IC of hardware neural networks. As the result, PZT type microrobot was realized the walking motion by bare chip IC. Moreover, SMA type microrobot could be systemsral networks. The walking speed was 2.4mm / min and the step width was 0.083mm.

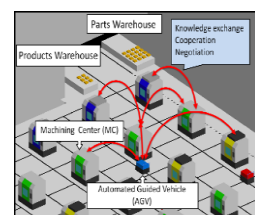


GS5 Multi-Agents Systems & Visualization

GS5-1 Moving Robots Lies and Their Minds with Degree of Confidence in a Decentralized Autonomous FMS

Shizuka Tanaka, Hidehiko Yamamoto, Takayoshi Yamada (Gifu University, Japan)

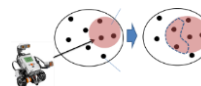
An autonomous decentralized FMS needs to control the entire factory and avoid the route interference of automated guided vehicles (AGVs). To solve this problem, we inserted an arrogant mind and a modest mind into AGVs. Also, in an autonomous decentralized FMS, it is assumed that the information provided by agents is always correct. However, incorrect information can sometimes be sent as a result of machine failures in a real factory. In this study, we define and find this incorrect information as a "lie" of AGV. We propose the method of finding lies and sending the lie information to the AGVs. We also propose a degree of confidence to control the AGV's moving. The result of simulation has shown the number of production was increased. Therefore, it is useful to control behavior by finding AGV's lies and using the degree of confidence.



GS5-2 Conquest Oriented Robot Knowing Its Own Availability

Sho Yamauchi, Keiji Suzuki (Future University Hakodate, Japan)

Robot is designed for achieving specific task. However, robot is able to do much more things than it is expected by its own hardware. If both human and robot become to be able to know the things robot can do in the place, robot become to deal with variable tasks that are not expected. In this paper, concept of conquest oriented robot is proposed to know its availability systematically and autonomously. Conquest action for the robot that knows its own availability is defined and the thing that conquest oriented robot do is to know, increase and maintain things it can do. Algorithm of conquest oriented robot and its experimental result in simulation field for the first step is shown.



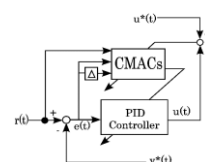
GS6 Intelligent Control & System Cybernetics

GS6-1 A Consideration on Feature Extraction for Operation Skill Based on Control Engineering Approach

Kazushige Koiwai¹, Liao Yantao¹, Toru Yamamoto¹,
Takao Nanjo², Yoichiro Yamazaki², Yoshiaki Fujimoto²

(¹Hiroshima University, ²KOBELCO Construction Machinery CO., LTD., Japan)

Technologies of automation or manpower-saving are innovated in production fields. However, there are many industrial equipments to need human operation, i.e. construction site. The human-skill optimized by professionals exists in those fields. However, the transfer of skills is not processing in leading countries because of decreasing or aging of professionals. Therefore the quantification of the human-skill is required to transfer those skills. In this study, the human-skill is considered as a kind of controller. It consists of CMAC-PID that is learned by using system outputs and control inputs of operators. CMACs calculate PID parameters, and human-skill is evaluated by trajectories of parameters. As an example, the comparison of operator skills for an excavator will be performed.

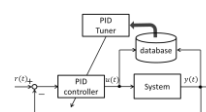


GS6-2 Design of a Data-Driven Control System for a Hydraulic Excavator

Takuya Kinoshita¹, Yasuhito Oshima¹, Kazushige Koiwai¹, Toru Yamamoto¹,
Takao Nanjo², Yoichiro Yamazaki², Yoshiaki Fujimoto²

(¹Hiroshima University, ²KOBELCO Construction Machinery CO., LTD, Japan)

PID control schemes have been widely used in most industrial systems. However, most systems have nonlinearity and it is difficult to achieve the desired control performance by using fixed PID parameters. The hydraulic excavators have nonlinearity, therefore it is difficult to maintain the desired control performance. In order to overcome such a problem, data-driven PID control scheme based on database has been proposed. Moreover, data-driven scheme has a learning method in off-line by using the closed-loop data. In this paper, data-driven control scheme is applied to a hydraulic excavator in order to get desired control performance. The effectiveness of the proposed scheme is numerically verified by using a simulation example.



GS6-3 An Optimization of Spatio-Spectral Filter Bank Design for EEG Signal Classification

Masanao Obayashi, Takuya Geshi, Takashi Kuremoto, Shingo Mabuchi (Yamaguchi University, Japan)

Recently, studies on brain computer interface (BCI) which enables us to operate electronic devices directly using electroencephalogram: EEG signal have been actively done. From knowledge of brain science, in order to distinguish the EEG signals accurately, it plays important role to make an appropriate combination of both optimal selection of EEG sensors and filter bank, due to theory of localization of brain function. From this point of view, Bayesian Spatio Spectral Filter Optimization (BSSFO) has been already proposed. However, the method still has room for improvement in constructing optimal combination mentioned above. We intend to improve BSSFO from the point of them, that is, a modification of a part of the optimization algorithm.



The classification procedure of EEG signal in this paper

GS7 Robotics I

GS7-1 Haptic system with fuzzy controller for extended control of Teleoperation mine detector wheeled robots

Yekkehfallah Majid, Guao Yang, Yuanli Cai, Naebi Ahmad, Zolghadr Javad
(Xi'an jiaotong university, P.R. China)

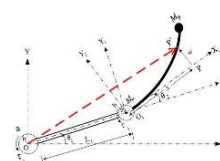
This paper proposes an approach of haptic system and fuzzy logic controller with implementation on teleoperation deminer robot, in order to reduce operator's error through fusion of fuzzy logic controller and haptic system, this approach provides vibrotactile feedback and speed controller corresponding to mine detector sensor and arm status system which are used in robot. This method can uses in all area of teleoperation robotic but we implemented on deminer wheeled robot and for illustrating results of this work we also implemented on MATLAB fuzzy toolbox.



GS7-2 Effect of System Parameters and Controlled Torque on the Dynamics of Rigid-Flexible Robotic Manipulator

Sachindra Mahto (North Eastern Regional Institute of Science & Technology, India)

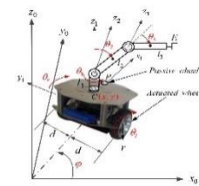
There are several advantages of the flexible robotic system with respect to its counter-part convention system. Conventional robotic systems are heavy and bulky with poor payload to weight ratio; and most of energy is used to overcome the inertia of the system in the engineering applications. As there is significant static deflection due to the loads, it is very difficult to have high position accuracy of the robotic system. Therefore, sometimes some of the links of the conventional robotic system are replaced by the flexible link to have the advantages of the lightweight system. Rigid-flexible robotics systems are the compromise in between of these two systems. Since, one of the link is flexible, its behaviour is highly nonlinear and complex in nature. The dynamics of this system highly depends upon various system parameters viz., length and mass of the links, joint motor mass, payload, hub inertias, etc. A comparative study is also done for different input torque profiles along with the controlled input torques. Results of the comparative study for the effect of variation of the system parameters are very interesting technically.



GS7-3 Modeling of Mobile Manipulator and Adaptive Super-Twisting Backstepping Control

Seong Ik Han, Hyunuk Ha, Jangmyung Lee (Pusan National University, South Korea)

A mobile manipulator with three wheels and three DOF links is modeled by using Euler-Lagrange method and vector orientated constraint conditions. In this modeling process, the conventional complex nonholonomic constraint transformation need not be considered in mobile robot system and then much simpler dynamic model can be obtained. Next, the super-twisting sliding mode control is combined with nonlinear backstepping control to obtain the systematic nonlinear controller design, fast response speed, and improved robustness to uncertainty due to dynamic coupling and disturbance. Simulation and experiment were carried out to prove the effectiveness of the proposed control methodology.



GS7-4 Self-tuned Local Feedback Gain Based Decentralized Fault Tolerant Control of Reconfigurable Manipulators

Bo Zhao¹, Bo Dong², Yan Li², Fumitoshi Matsuno³, Yuanchun Li² (¹Chinese Academy of Sciences, ²Changchun University of Technology, P.R. China, ³Kyoto University, Japan)

This paper investigates the decentralized fault tolerant control (DFTC) scheme based on self-tuned local feedback gain to against partial loss of actuator effectiveness of reconfigurable manipulators. Consider the entire system as a set of interconnected subsystems due to its modularity property, the decentralized control method is proposed by employing two neural networks for the fault-free system. For the subsystem in related failure, the self-tuned local feedback gain is added to the proposed decentralized control method to guarantee the control performance. Finally, a simulation example is provided to demonstrate the effectiveness of the present DFTC scheme.

Fig.1 shows the excellent trajectory tracking performance is derived though the reconfigurable manipulator suffers to actuator failure after $t=4s$. The main contributions of this method are: i) The FTC structure is simple since it is no need to be redesigned in the presence of partial loss of actuator effectiveness; ii) The actuator fault can be handled in its local subsystem, it implies that the performance degradation of the faulty subsystem cannot affect the fault-free subsystems.

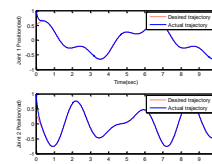


Fig.1 Joint tracking curves with DFTC

GS7-5 Study on Decentralized Integral Nested Sliding Mode Control for Constrained Reconfigurable Manipulator with Harmonic Drive Transmission

Bo Dong¹, Zeyu Dong¹, Bo Zhao², Yan li¹, Fumitoshi Matsuno³ and Yuanchun Li¹ (¹Changchun University of Technology, ²Chinese Academy of Sciences, P.R. China, ³Kyoto University, Japan)

This paper addresses the problems of trajectory tracking control of a constrained reconfigurable manipulator with harmonic drive transmission under a decentralized integral nested sliding mode control (INSMC) method, and a high-performance control is achieved without using force/torque sensor. The dynamic model of the constrained reconfigurable manipulator is formulated with a nonlinear harmonic drive model. Based on only local dynamic information of each module, a decentralized integral nested sliding mode control method is proposed to reduce the chattering effect of the controller and compensating the model uncertainties. Finally, simulations are performed for a constrained 2-DOF reconfigurable manipulator to study the effectiveness of the proposed method. Fig. 1 shown that the desired trajectory of robot end-effector can be tracked accurately under the proposed INSMC method.

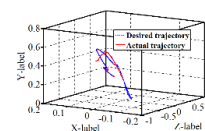
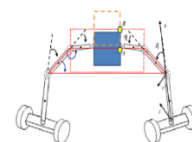


Fig. 1 Trajectory tracking curves of robot end-effector

GS7-6 A Number of Mobile Manipulator Control for Moving Object by using Cooperative Control

Deok-Su Kim, Dong-Eon Kim, Seong-Ik Han, Jang-Myung Lee
(Pusan National University, South Korea)

This paper proposes a method of cooperative control of a three mobile manipulator for moving an object. These robots go to desired position independently by using encoder data and inverse kinematics and after arriving in the position, they grasp and lift the object. For the carrying operation, the lifting operation is implemented by using the manipulator mounted on the top of the mobile robots cooperatively. In this system, master-slave mode is used for finding each position of robots and for coordinating among the robots. During the moving operation, a trajectory planning has been kept constantly. The real cooperative carrying motions are implemented to check the possibility of the master-slave mode control based on the mobile manipulator's kinematics



GS8 Robotics II

GS8-1 Visual-servo Control of 4-DOF Robot Manipulator for Sorting Moving objects

Longtan Wang, Seon-Woo Kim, Hyun-Wook Ha, Jang-Myung Lee
(Pusan National University, South Korea)

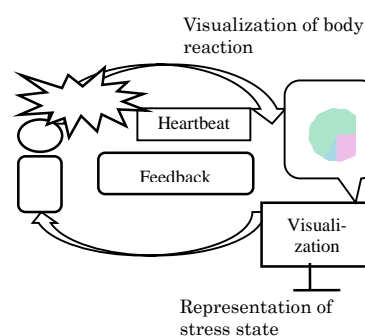
This paper considers the problem of estimating position and determining class of objects on the moving conveyor belt. A 2D camera is utilized to capture the image of moving objects. The control system directly integrates visual data into the servoing process. Objects are recognized by using SURF(Speeded-Up Robust Features) key point detector and FLANN(Fast Library for Approximate Nearest Neighbor) based matcher. Then Rotating calipers algorithm is adopted to estimate the centroid position and orientation of the objects. The proposed system is able to control the robot so that it can approach the desired position and grab the specific object. Experimental result demonstrates that the approach is efficient and reliable



GS8-2 Self-identification of Mental State and Self-control through Indirect Biofeedback -Indirect Representation and Placebo Effect-

Madoka Takahara, Ivan Tanev, Katsunori Shimohara
(Doshisha University, Japan)

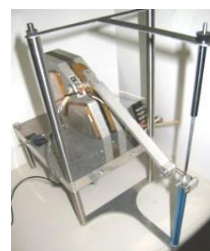
This paper describes a possible new scheme for a user with mental health problems to identify his/her own mental state and control it, not by visiting specialists passively, but by proactively confronting his/her symptoms. For that purpose, the scheme should provide the user with the ability not only to externalize and objectify his or her mental state but also for the user him/herself to control their physiological state. So we propose an indirect biofeedback system that represents physiological information with colors and shapes, and enables the user to grasp his/her inner state and to proactively change and control it through methods of breathing. These methods facilitate the user to control their autonomic nervous system by themselves. Here, we discuss indirect representation and placebo effect.



GS8-3 Construction of a sense of force feedback and vision for micro-objects: Recreate the response and a sense of force of objects

Yusei Ishii, Eiji Hayashi (Kyusyu Institute of Technology, Japan)

Technologies that can accurately perform minute work are now being sought for medical treatment and in the field of manufacturing semiconductors. Such minute work is improved by using micromanipulators, but their operation is difficult because the operator has no sense of force; he or she relies only on sight through a microscope. As a result, a person skilled in the use of this technology is needed for all minute work. For the efficiency of minute work, we used a haptic device and amplified the force feedback from a minute sample.



GS8-4 Dynamic Behavior Selection Model based on Emotional States for Conbe-I robot

Wisanu Jitviriyia, Jiraphan Inthiam, Eiji Hayashi (Kyushu Institute of Technology, Japan)

Currently, the rapid development of non-industrial robots that are designed with artificial intelligence (AI) method to improve the robotics system is to have them imitate human thinking and behavior. Therefore, our works have been focused on studying and investigating the application of brain-inspired technology for developing the conscious behavior robot (Conbe-I). We created the hierarchical structure model, which is called “Consciousness-Based Architecture: CBA” module, but it has limitation in managing and selecting the behavior that only depends on the increase and decrease in the motivation’s level. Consequently, in this paper, we would like to introduce the dynamic behavior selection model based on emotional states, which develops by Self-organizing map learning and Markovian model in order to define the relationship between the behavioral selection and emotional expression model. We confirm the effectiveness of the proposed system with the experimental results.



GS8-5 Consideration on a Crawler Robot with Six Legs

Toyomi Fujita, Taiga Sasaki (Tohoku Institute of Technology, Japan)

In this study, we consider development of a crawler-type mobile robot which is equipped with six legs at its body. This type of robot may have possibilities of both high mobility on rough terrain and working ability with handling such as carrying an object and removing small obstacles in its movement by using the legs as manipulation arms. This paper presents mechanisms and characteristics of this type of robot and some possible hybrid motions in which crawler and legs are used. Several simulations are also performed based on statics to analyze necessary torques for joint of the legs in the motions.

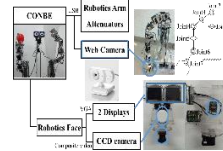


GS9 RoboticsIII

GS9-1 Social Expression of Pet Robot Based on Artificial Consciousness and Biologically Inspired On-line Topological Method

Sakmongkon Chumkamon, Eiji Hayashi (Kyushu Institute of Technology, Japan)

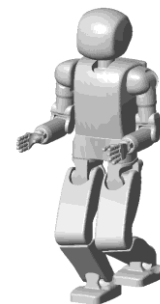
Toward robot becoming friend, the social and natural behavior of the robot is the most needed function for emerging future realistic human-like robot. This paper proposes the topological consciousness based on a pet robot using the artificial neurotransmitter and motivation. Since, the significant is a cross-creature communication to friendly companionship. This system focuses on three points. The first, the organization of the behavior and emotion model regarding the phylogenetic. The second, the robot empathy from human expression. The third, the social interaction by robot expression using biologically inspired topological on-line method for encouragement by its own emotion and the human expression. We believe the artificial consciousness based on complexity level and the robot social expression enhance the user affinity by the demonstration.



GS9-2 Anthropomorphic robot modelling with virtual height inverted pendulum approach in Simulink: step length and period influence on walking stability.

Ramil Khusainov, Ilya Afanasyev, Evgeni Magid (Innopolis University, Russia)

Humanoid stable walking is a complex task due the high number of degrees of freedom, system nonlinearity and relatively small size of robot footprint. Biped robots tend to fall down as walking speed increases or when the terrain conditions change. This paper presents dynamically stable walking modelling of Russian humanoid AR-601M in Simulink environment with virtual height inverted pendulum model, an effective and simple trajectory generation method based on inverted pendulum model (IPM). This algorithm adjusts height of the center of mass in IPM model to reduce ZMP error and guarantees stable locomotion up to some critical speed. We investigate influence of the step length and step period on walking stability. Maximum torque values in leg joints are estimated in order to verify if such trajectories are attainable by robot motors. We demonstrate that the robot model is capable to achieve significant walking speeds on flat surfaces using this method.



GS9-3 A low cost genetic algorithm based control scheme for wheelchair control in hospital environment

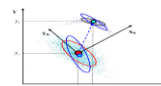
Karam Dad Kallu, Muhammad Jawad Khan, Wang Jie, Min Cheol lee
(Pusan National University, South Korea)

In this paper, a control strategy to operate a wheelchair in a hospital is proposed to assist patients. The strategy is tested using a mobile robot, that is navigated in a hospital using line following. The mobile robot was operated using both genetic algorithm and A* algorithm for a thorough comparison of the control scheme. The comparison of the results revealed that genetic algorithm is a better solution in controlling the wheelchair in a hospital environment.



GS9-4 Simultaneous Localization and Mapping (SLAM) algorithm base on EKF and SPKF. Zolghadr Javad, Yuanli Cai ,Yekkehfallah Majid (Xi'an Jiaotong University, P.R. China)

Simultaneous Localization and Mapping (SLAM) is the problem in which a sensor-enabled mobile robot incrementally builds a map for an unknown environment, while localizing itself within this map. The Kalman Filter's linearized error propagation can result in big errors and instability in the SLAM problem. One approach to reduce this situation is using of iteration in Extended Kalman Filter (EKF) and Sigma Point Kalman Filter (SPKF). We will show that the recapitulate versions of kalman filters can improve the estimation accuracy and robustness of these filters beside of linear error propagation. Simulation results are presented to validate this improvement of state estimate convergence through repetitive linearization of the nonlinear model in EKF and SPKF for SLAM algorithms. Results of this evaluation are introduced by computer simulations and verified by offline implementation of the SLAM algorithm on mobile robot in MRL Robotic Lab. Index Terms— Extended Kalman Filter, Sigma Point Kalman Filter, SLAM, instability, Mobile Robot, Nonlinear Estimation.



GS10 Poster Sessions (5)

GS10-1 Analysis of Postgraduates' Entrance Examination Scores Based on Linear Regression with Dummy Variables

Ning Xiaojun, Huang Ruocheng, Liang Xiaoyi, Ai Dongmei
(University of Science and Technology Beijing, P.R. China)

Research on the main factors influencing the students' score is a very important part of the student achievement evaluation system. Several factors that have a significant influence on postgraduates' entrance examination score including enrollment category, university category, age, gender, fresh graduate were studied by ANOVA in this paper. Quantitative analysis of the correlation between the discrete variables and admission scores were performed by linear regression with dummy variables and 85% confidence prediction interval of postgraduates' admission scores were obtained. Data support is provided by these results for graduate school enrollment work.

$$\begin{cases} X_{ij} = \mu + \alpha_i + \varepsilon_{ij}, & j = 1, \dots, n_i, i = 1, \dots, r \\ \varepsilon_{ij} \sim N(0, \sigma^2), i.i.d. \\ \sum_{i=1}^r n_i \alpha_i = 0 \end{cases}$$

GS10-2 Clinical Evaluation of UR-System 2 for Recovery of Motor Function of Plegic Upper Limb after Stroke

¹Hirofumi Tanabe, ¹Masahiro Mitsukane, ²Norihiro Toya, ²Ryosuke Takeichi, ²Hitomi Hattori, ²Yoshifumi Morita, ³Yoshiaki Takagi, ³Norio Hasegawa (¹Shonan University of Medical Sciences, ²Nagoya Institute of Technology, ³Sanyo Machine Works, Ltd., Japan)

We developed a new training system UR-System 2 for restoring motor function of the upper limb after stroke in patients with hemiplegia. And then, we conducted clinical evaluation of the therapeutic effect of training with the UR-System 2 in six patients. The UR-System uses Proprioceptive Neuromuscular Facilitation (PNF) to promote muscle strength. In this training, elbow flexion and extension of the supinated forearm were repeated 250 times. As a result of the training, active ranges of motion of elbow extension and supination of the forearm improved after training. Moreover, the modified Ashworth scores for elbow extension and supination of the forearm increased, indicating improvement of spastic paralysis. These results show the immediate therapeutic effect of training with the UR-System 2 for restoring the motor function of the upper limb.



GS10-3 Knee Android Model Reproducing Internal-External Rotation with Screw-Home Movement of Human Knee

Daichi Yamauchi, Sho Takei, Noritaka Sato, Yoshifumi Morita (Nagoya Institute of Technology, Japan)

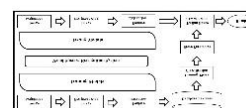
It has been reported that the internal-external rotation during knee extension in human can be classified into three types. In our previous study, we proposed a knee android model (Knee-AM) consisting of a tibia model, a femur model and nylon-cords imitating the ligaments. We found that the Knee-AM can reproduce one type. This paper proposed a Knee-AM that can reproduce another type. This type, to which most of human knee motion belongs, has external rotation occurring at the end of extension, called the screw-home movement (SHM). This type were realized by changing the lengths and the fixing points of the nylon-cords. Moreover, when the anterior cruciate ligament (ACL) was removed from the Knee-AM to imitate ligament injury, the SHM did not occur during extension. The results showed the ACL played an important role for the SHM.



GS10-4 Wood Species Recognition System based on Improved Basic Grey Level Aura Matrix as feature extractor

¹Mohd Iz'aa Paiz Zamri, ¹Anis Salwa Mohd Khairuddin, ¹Norrima Mokhtar, ²Rubiyah Yusof
(¹University of Malaya, ²Universiti Teknologi Malaysia, Malaysia)

An automated wood species recognition system is designed to perform wood inspection at custom checkpoints in order to avoid illegal logging. The system that includes image acquisition, feature extraction and classification is able to classify the 52 wood species. There are 100 images taken from the each wood species is then divided into training and testing samples for classification. In order to differentiate the wood species precisely, an effective feature extractor is necessary to extract the most distinguished features from the wood surface. In this research, an Improved Basic Grey Level Aura Matrix (I-BGLAM) technique is proposed to extract 136 features from the wood image. The technique has smaller feature dimension and is rotational invariant due to the considered significant feature extract from the wood image. Support vector machine (SVM) is used to classify the wood species. The proposed system shows good classification accuracy compared to previous works.



GS10-5 Evaluation the Performance of a New Quadrotor Model Based on the Arm's Length Variation

Yasameen Kamil N., D. Hazry, Khairunizam Wan, Zuradzman M. Razlan
(University Malaysia perlis, Malaysia)

The field of UAV has exceptional level of growth; in addition it is predictable to be one of the most prevalent fields of development and research in future. The unmanned aerial vehicle (UAV)- quadrotor widely used as a service robotic in several field. This paper presents a new design of this miniature aerial vehicle in altitude and attitude movements, based on varying the arm's length of quadrotor instead of varying the speed of motors to obtain a rotation around each axes. The length of arms varying are achieved by fixing a stepper motor in each arm of quadrotor to increase or decrease the length of these arms according to controller command for attitude movement. The controller commands are accomplished by designing a PID controller with specific parameters to maintain the stability of the quadrotor in the flight path. A MATLAB software code used to evaluate the simulation results and demonstrate the ability of the proposed design to perform a mission.

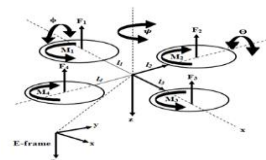


Fig.1 Quadrotor structure

AUTHORS INDEX

Notation of session name

PS: Plenary Session IS: Invited Session, OS: Organized Session, GS: General Session,

Note: 33/90 = (page no. in Technical Paper Index) / (page no. in Abstracts)

[A]				Chang	Jen-Kuo	OS3-5	21/37
Abe	Mizuki	GS4-4	22/59	Chang	Ling-Lin	OS3-4	21/37
Aburada	Kentaro	OS12-1	25/49	Chang	Shu-Chen	OS4-1	17/38
Afanasyev	Ilya	GS9-2	22/65	Chen	Chun-Hsien	OS4-2	17/38
Ai	Dongmei	GS10-1	20/66	Chen	Kuan-Yin	OS3-3	21/37
Akamine	Yuhei	GS2-2	23/54	Chen	Mei-Yung	OS2-4	18/35
		GS2-3	23/54	Chen	Yun-ju	OS9-1	29/47
Alrashed	Mosab	GS3-1	28/56	Chiba	Satohiro	GS4-4	22/59
Ando	Kazuaki	OS11-1	18/48	Chien	Chiou-Lan	OS1-3	19/32
		OS11-2	18/49	Chumkamon	Sakmongkon	GS9-1	22/65
		OS11-3	18/49	Chung	Hsiu-Chen	OS1-3	19/32
Arakane	Satoshi	GS1-4	20/53	Chung	Ting-Hung	GS4-2	22/58
Asada	Taro	OS7-1	30/42			GS4-3	22/59
		OS7-2	30/43				
		OS7-3	30/43	[D]			
		OS7-4	30/43	Dai	Fengzhi	OS8-5	24/45
Asano	Yohei	GS4-4	22/59			OS8-6	24/45
				Dang	Viet-Chau	OS10-2	28/48
[B]				Desa	Hazry	GS10-5	21/67
Boonyaprapasorn	Arsit	GS4-1	22/58	Dong	Bo	GS7-4	24/62
						GS7-5	25/62
[C]				Dong	Zeyu	GS7-5	25/62
Cao	Yimin	OS6-2	25/41	Duan	Meng	OS6-5	25/42
Chang	Ching-Jung	OS4-1	17/38	[E]			
		OS4-2	17/38	Endo	Satoshi	GS2-2	23/54
		OS4-3	17/38			GS2-3	23/54
		OS4-4	17/39	Erkoyuncu	John Ahmet	GS3-1	28/56
		OS4-5	17/39				
Chang	Chun-Chieh	GS4-2	22/58	[F]			
		GS4-3	22/59	Fu	Ziyi	OS5-1	26/39
Chang	Chun-Feng	OS3-3	21/37				

Fu	Ziyi	OS6-4	25/42			OS11-4	18/49
Fuji	Ren	OS7-2	30/43	Hsia	Kuo-Hsien	OS2-3	18/35
Fujimoto	Yoshiaki	GS6-1	27/60			OS2-5	19/35
		GS6-2	27/60	Hsu	Chu-Lin	OS2-2	18/34
Fujita	Toyomi	GS8-5	19/64	Hsu	Hsiu-Hsiung	OS4-5	17/39
Furutani	Hiroshi	OS12-2	26/50	Hsu	Yung- Feng	OS4-2	17/38
		OS12-4	26/50	Hu	Jian-Sing	OS2-4	18/35
				Huang	Ruocheng	GS10-1	20/66
				Huang	Yao-Shan	OS3-2	21/36
[G]							
Gao	Caixia	OS6-4	25/42	Hung	Chung-Wen	OS2-2	18/34
Geshi	Takuya	GS6-3	27/61				
Green	Ethan	GS1-1	20/52		[I]		
Guan	Sih-Jie	OS1-6	20/34	Iju	Tatsuyuki	GS2-3	23/54
Guao	Yang	GS7-1	24/61	Ikai	Yusaku	GS3-2	29/56
Guo	Jr Hung	OS2-3	18/35	Ikeda	Satoshi	OS12-2	26/50
						OS12-3	26/50
						OS12-4	26/50
[H]							
Ha	Hyunuk	GS7-3	24/62	Imai	Yoshiro	OS11-1	18/48
Ha	Hyun-Wook	GS8-1	19/63			OS11-2	18/49
Han	Seong Ik	GS7-3	24/62			OS11-3	18/49
		GS7-6	25/63			OS11-4	18/49
Hasegawa	Norio	GS10-2	20/66	Inthiam	Jiraphan	GS8-4	19/64
Hattori	Hitomi	GS10-2	20/66	Ishihara	Yuki	GS4-4	22/59
Hattori	Tetsuo	OS11-1	18/48	Ishii	Yusei	GS8-3	19/64
		OS11-2	18/49	Ito	Junji	GS3-3	29/56
		OS11-3	18/49	Ito	Takao	OS9-2	29/47
		OS11-4	18/49			OS9-3	29/47
Hayashi	Eiji	GS2-4	23/55			OS12-2	26/50
		GS8-3	19/64			OS12-3	26/50
		GS8-4	19/64			OS12-4	26/50
		GS9-1	22/65	Ito	Tsutomu	OS9-2	29/47
Hidaka	Kenta	GS3-5	29/57			OS9-3	29/47
Ho	Je-Fu	OS1-2	19/32			OS12-2	26/50
		OS1-4	20/33			OS12-4	26/50
		OS1-6	20/34	Iwanaga	Saori	OS10-3	28/48
Horikawa	Yo	OS11-1	18/48	Iwata	Kei	GS4-4	22/59
		OS11-2	18/49				

[J]							
				Kobayashi	Kunikazu	GS3-5	29/57
Jhong	Bing-Gang	OS2-4	18/35	Kohno	Takashi	GS1-1	20/52
Jia	Hongyan	OS8-1	24/44			GS1-5	20/53
Jia	Jiao	OS5-4	26/40	Koiwai	Kazushige	GS6-1	27/60
Jia	Yingmin	OS5-2	26/40			GS6-2	27/60
		OS5-3	26/40	Kondo	Tadashi	GS1-2	20/52
		OS5-4	26/40			GS1-3	20/53
		OS5-5	26/40	Koyama	Yoshihide	OS11-4	18/49
		OS6-5	25/42	Kubo	Masao	OS10-1	28/48
Jian	Zhijing	GS2-1	23/54			OS10-2	28/48
Jian		GS2-5	23/55			GS1-4	20/53
Jie	Wang	GS9-3	22/65	Kuremoto	Takashi	GS3-4	29/57
Jitviriya	Wisanu	GS8-4	19/64			GS6-3	27/61
[K]				[L]			
Kallu	Karam Dad	GS9-3	22/65	Lai	Ting-Chi	OS3-1	21/36
Kang	Qijia	OS8-5	24/45	Lee	Ching-I	OS2-1	18/34
		OS8-6	24/45	Lee	Jangmyung	GS7-3	24/62
Katayama	Tetsuro	OS12-1	25/49			GS7-6	25/63
Kato	Ryota	OS7-3	30/43			GS8-1	19/63
Kawakami	Yusuke	OS11-1	18/48	Lee	Ju-Jang	PS2	23/30
		OS11-2	18/49	Lee	Mei-Yin	OS1-6	20/34
		OS11-3	18/49	lee	Min Cheol	GS9-3	22/65
Kawamura	Yoji	OS13-4	28/52	Lee	Roger	GS4-2	22/58
Kawano	Hiromichi	OS11-4	18/49		Chenglung		
Khairuddin,	Anis Salwa	GS10-4	21/67			GS4-3	22/59
	Mohd			Li	Bo-Yi	OS2-5	19/35
Khan	Muhammad	GS9-3	22/65	Li	Chia-Chen	OS4-3	17/38
	Jawad			Li	Juntao	OS6-2	25/41
Khusainov	Ramil	GS9-2	22/65	Li	Lin	OS6-3	25/41
Kikkawa	Yuuki	OS12-1	25/49	Li	Qing	OS6-1	25/41
Kim	Deok-Su	GS7-6	25/63	Li	Shang-Hui	OS1-4	20/33
Kim	Dong-Eon	GS7-6	25/63	Li	Wenling	OS5-2	26/40
Kim	Seon-Woo	GS8-1	19/63	Li	Yaodong	GS2-1	23/54
Kinoshita	Takuya	GS6-2	27/60			GS2-5	23/55
Kita	Yoshihiro	OS12-1	25/49	Li	Yan	GS7-4	24/62
Ko	Chia-Nan	OS2-1	18/34			GS7-5	25/62

Li	Yuanchun	GS7-4	24/62	Mokhtar	Norrima	GS10-4	21/67
		GS7-5	25/62	Morikawa	Katsumi	OS9-3	29/47
Li	Zheng-Ying	OS2-6	19/36	Morita	Yoshifumi	GS10-2	20/66
Liang	Xiaoyi	GS10-1	20/66			GS10-3	21/67
Liang	Bo	OS5-6	26/41				
Lin	Gu-Xuan	GS4-2	22/58	[N]			
		GS4-3	22/59	N.	Yasameen	GS10-5	21/67
Lin	Hsiao-Yu	OS4-4	17/39		Kamil		
Lin	Hsiu-Min	OS1-2	19/32	Naebi	Ahmad	GS7-1	24/61
Lin	Pei-Ling	OS3-4	21/37	Nagatomo	Makoto	OS12-2	26/50
Lin	Wen-Bin	OS2-6	19/36			OS12-4	26/50
Lin	Wen-Lung	OS3-1	21/36	Nakaoka	Iori	OS9-1	29/47
Liu	Bo	OS8-6	24/45	Namatame	Akira	OS10-2	28/48
Liu	Chen-Chung	OS3-1	21/36			OS10-3	28/48
		OS3-2	21/36	Nanami	Takuya	GS1-5	20/53
		OS3-5	21/37	Nanjo	Takao	GS6-1	27/60
Liu	Hung-Chi	OS3-2	21/36			GS6-2	27/60
Liu	Kung-Yu	OS1-6	20/34	Narumoto	Jin	OS7-3	30/43
Lu	Yi-Yu	OS2-6	19/36	Ning	Xiaojun	GS10-1	20/66
Lund	Henrik	PS1	17/30	Nishime	Taiki	GS2-2	23/54
	Hautop			Nishimura	Kouhei	OS7-1	30/42
		IS1	17/31	Niu	Hong	OS8-4	24/45
						OS8-7	27/46
[M]							
M.Razlan	Zuradzman	GS10-5	21/67	[O]			
Mabu	Shingo	GS3-4	29/57	Obayashi	Masanao	GS3-4	29/57
		GS6-3	27/61			GS6-3	27/61
Magid	Evgeni	GS9-2	22/65	Ogata	Takashi	OS13-1	28/51
Mahto	Sachindra	GS7-2	24/61			OS13-2	28/51
Maneewarn	Thavida	GS4-1	22/58			OS13-3	28/51
Matsuno	Fumitoshi	GS7-4	24/62	Oka	Yuuki	OS7-4	30/43
		GS7-5	25/62	Okane	Yuki	GS4-4	22/59
Matsuno	Seigo	OS9-2	29/47	Okazaki	Naonobu	OS12-1	25/49
Mehta	Rajiv	OS9-3	29/47	Oku	Hirozumi	GS4-4	22/59
Miao	Ching-Mei	OS3-5	21/37	Ono	Jumpei	OS13-2	28/51
Mikami	Y.	OS9-2	29/47			OS13-3	28/51
Mitsukane	Masahiro	GS10-2	20/66	Ono	Satoko	GS4-4	22/59

Oshima	Yasuhito	GS6-2	27/60			OS2-5	19/35
Oyaizu	Haruka	OS7-1	30/42	Su	Weijun	OS5-6	26/41
				Su	Ying-Yu	OS4-4	17/39
[P]				Sugisaka	Masanori	GS2-1	23/54
Pagliarini	Luigi	IS1	17/31			GS2-5	23/55
Pan	Cheng-Tang	GS4-2	22/58			GS2-6	23/55
		GS4-3	22/59	Sugita	Kazuki	GS4-4	22/59
Park	So-Youn	PS2	23/30	Sumi	Kaoru	IS-2	23/31
Park	Yousin	OS9-1	29/47	Sun	Shihao	OS5-3	26/40
Patra	Aswini	GS3-6	29/57			OS5-4	26/40
	Kumar			Suzuki	Keiji	GS5-2	27/60
Pengwang	Eakkachai	GS4-1	22/58	Suzuki	Takuo	GS3-5	29/57
[R]				[T]			
Rajapakse	R. P. C.	OS11-1	18/48	Tabuse	Masayoshi	OS7-1	30/42
	Janaka					OS7-2	30/43
		OS11-2	18/49			OS7-3	30/43
						OS7-4	30/43
						OS7-5	30/44
[S]							
Saito	Ken	GS4-4	22/59	Takagi	Yoshiaki	GS10-2	20/66
Sasaki	Taiga	GS8-5	19/64	Takahara	Madoka	GS8-2	19/63
Sakamoto	Makoto	OS9-3	29/47	Takahashi	Katsuhiko	OS9-3	29/47
		OS12-2	26/50	Takao	Shoichiro	GS1-2	20/52
		OS12-3	26/50			GS1-3	20/53
		OS12-4	26/50	Takato	Minami	GS4-4	22/59
Sato	Hiroshi	OS10-1	28/48	Takei	Sho	GS10-3	21/67
		OS10-2	28/48	Takeichi	Kei	OS11-3	18/49
Sato	Noritaka	GS10-3	21/67	Takeichi,	Ryosuke	GS10-2	20/66
Shiau	Yan-Chyuan	OS3-1	21/36	Takeshita	Yuki	OS12-3	26/50
		OS3-2	21/36	Tan	Dongchen	OS8-4	24/45
		OS3-3	21/37			OS8-7	27/46
		OS3-4	21/37	Tanabe	Hirofumi	GS10-2	20/66
		OS3-5	21/37	Tanaka	Shizuka	GS5-1	27/59
Shimohara	Katsunori	GS8-2	19/63	Tanev	Ivan	GS8-2	19/63
Song	Yunzhong	OS5-1	26/39	Tanioka	Sora	OS10-1	28/48
Su	Hung-Wen	OS1-1	19/31	Tatani	Masaki	GS4-4	22/59
Su	Kuo-Lan	OS2-3	18/35	Toma	Naruaki	GS2-2	23/54

Toma	Naruaki	GS2-3	23/54	Wu	Yang	OS1-2	19/32
Toya	Norihiro	GS10-2	20/66	Wu	Yongjun	OS8-4	24/45
Tsai	Lung-Chi	OS1-3	19/32			OS8-7	27/46
Tsai	Yi-Yin	OS3-6	21/37				
Tsuda	Yuji	OS7-1	30/42	[X]			
Tsunenari	Kenji	GS2-4	23/55	Xie	Pengfei	OS8-5	24/45
				Xu	Cunshuan	OS6-2	25/41
[U]				Xue	Li	OS8-3	24/44
Uchida	Yasuo	OS9-2	29/47			OS8-9	27/46
		OS12-2	26/50				
		OS12-4	26/50	[Y]			
Uchikoba	Fumio	GS4-4	22/59	Yadekar	Yaser	GS3-1	28/56
Ueno	Junji	GS1-2	20/52	Yamaba	Hisaaki	OS12-1	25/49
		GS1-3	20/53	Yamada	Koji	GS2-2	23/54
						GS2-3	23/54
[W]				Yamada	Takayoshi	GS3-2	29/56
Wan	Khairunizam	GS10-5	21/67			GS3-3	29/56
Wang	Fuzhong	OS5-1	26/39			GS5-1	27/59
		OS6-4	25/42	Yamaguchi	Akihiro	GS1-4	20/53
Wang	Jiwu	GS2-1	23/54	Yamamoto	Hidehiko	GS3-2	29/56
		GS2-5	23/55			GS3-3	29/56
		GS2-6	23/55			GS5-1	27/59
Wang	Longtan	GS8-1	19/63	Yamamoto	Toru	GS6-1	27/60
Wang	Heyang	OS6-3	25/41			GS6-2	27/60
Wang	Ming-Chieh	OS1-5	20/33	Yamauchi	Daichi	GS10-3	21/67
Wang	Qinghe	OS8-1	24/44	Yamauchi	Sho	GS5-2	27/60
Wang	Shao-Yu	GS4-2	22/58	Yamazaki	Yoichiro	GS6-1	27/60
		GS4-3	22/59			GS6-2	27/60
Wei	Wei	OS5-6	26/41	Yang	An-Yun	GS4-2	22/58
Wang	Xiaoyu	OS6-2	25/41			GS4-3	22/59
Wang	Yu-Jen	GS4-2	22/58	Yang	Chao	GS2-5	23/55
		GS4-3	22/59	Yang	Cheng-Min	OS4-5	17/39
Wei	Xue	OS8-3	24/44	Yano	Shinnosuke	OS12-2	26/50
		OS8-9	27/46			OS12-4	26/50
Wu	I-Chen	OS4-3	17/38	Yantao	Liao	GS6-1	27/60
Wu	Sheu-Der	OS1-1	19/31	Yekkehfallah	Majid	GS7-1	24/61
Wu	Tong	OS6-6	25/42			GS9-4	22/66

Yoshimitsu	Yuki	OS7-5	30/44
Yoshinaga	Tsunehiro	OS12-2	26/50
		OS12-4	26/50
Yoshitomi	Yasunari	OS7-1	30/42
		OS7-2	30/43
		OS7-3	30/43
		OS7-4	30/43
Yu	Chunyu	OS8-2	24/44
Yuanli	Cai	GS7-1	24/61
		GS9-4	22/66
Yue	YuanLi	OS8-5	24/45
		OS8-6	24/45
Yusof	Rubiyah	GS10-4	21/67

[Z]

Zamri	Mohd Iz'aan	GS10-4	21/67
	Paiz		
Zhao	Bo	GS7-4	24/62
		GS7-5	25/62
Zhao	Yifan	GS3-1	28/56
Zhang	Hongtao	OS8-6	24/45
Zhang	Weicun	OS6-1	25/41
		OS6-6	25/42
Zhang	Yuzhen	OS6-1	25/41
Zheng	Shunkai	GS2-6	23/55
Zheng	Wenhao	OS5-5	26/40
Zhao	Xia	OS8-8	27/46
Zhao	Huailin	OS8-8	27/46
Zolghadr	Javad	GS7-1	24/61
		GS9-4	22/66

Conference Building B



Select the meeting facility best suited to your needs

Conference Room B1, which may be arranged to seat 226 people in a theater-style setting, can readily serve as a venue for seminars or lectures. There are also six smaller meeting rooms with theater seating for between 49 and 112 people. These rooms are available for a broad panorama of uses, such as academic meetings, business forums or cultural exchange events. Moreover, food and beverage are permitted in all of these areas. With a break room and green room available for event sponsors, these facilities provide the perfect location for small parties and other such events.



Partible conference hall B1



Conference hall B3 and B4 combined



Conference hall B5 and B7 combined

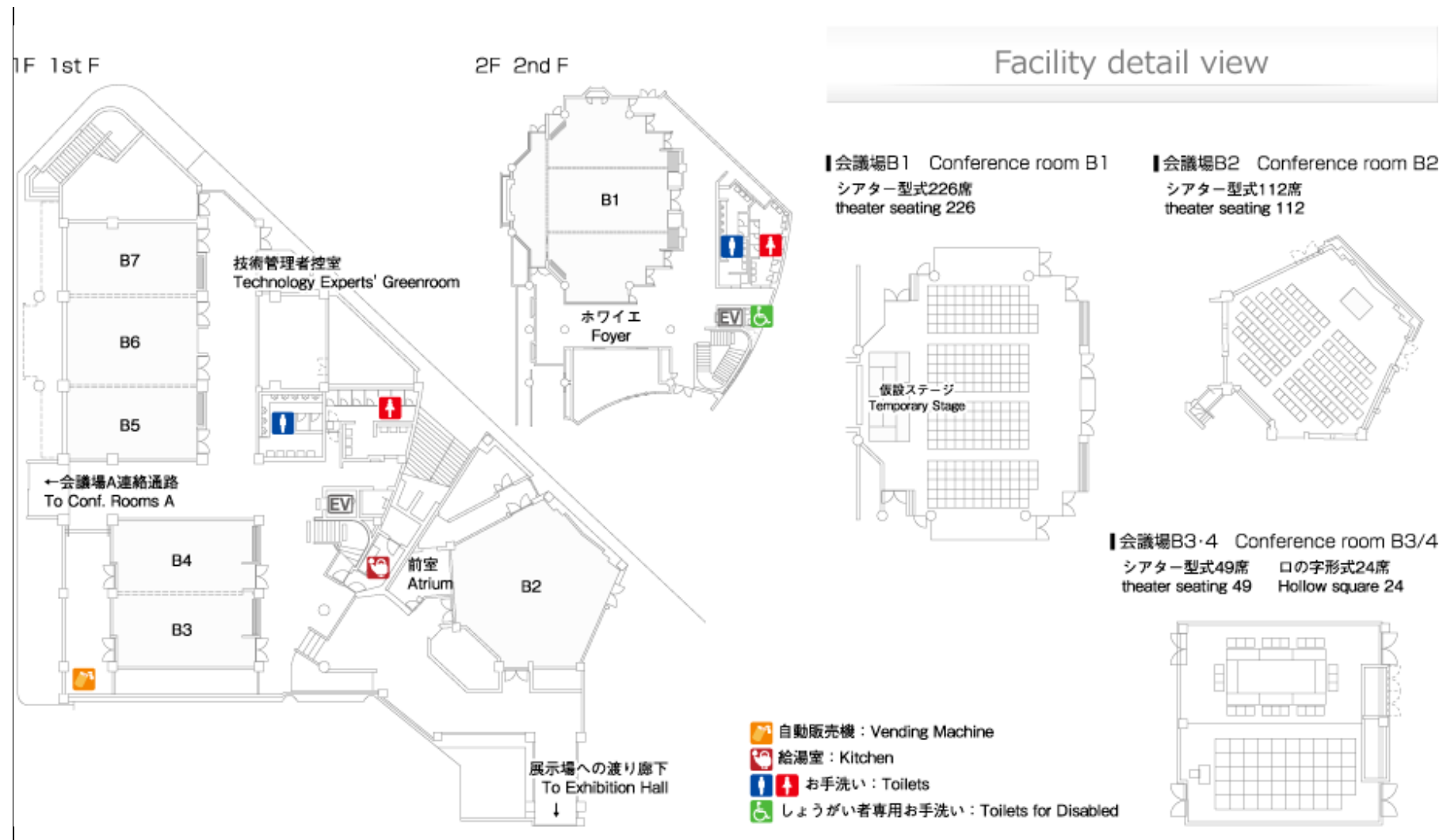


Interpretation service booth equipped

Conference hall B2



Conference hall (single use)



Study on the Promotion of Steel Slags Recycling in Taiwan

Shu-Chen Chang ,Ching-Jung Chang*

Department of Construction Management, Chung Hua University

707, Sec.2, WuFu Rd., Hsinchu, Taiwan 30012, R.O.C.

*E-mail: jg104@mail.jges.ntpc.edu.tw, *cjchang@chu.edu.tw*

Abstract

The constant development and abuse of natural resources have led to shortage, which also causes many countries to pay attention to waste recycling issues and promote concepts in resource sustainable recycling, in order to reduce the depletion of natural resources. The current development trend in waste recycling has gradually shifted from single use in cradle to grave to the sustainable recycling in cradle to cradle (C2C), using resource recycling to achieve the economic concept of sustainable management.

Key words: Waste-to-Resource, Electric Arc Furnace Steelmaking Slag, Oxidative Slag, Reductive Slag

1. Introduction

Iron & steel are the foundation of industrial development. The construction engineering, transportation and commercial machines & tools are all closely related to the iron/steel industries. How to dispose and utilize the waste generated along with the manufacturing process shall be carefully faced and considered. Slag is the waste generated during the smelting of iron & steel. According to the different production approach, it can be categorized into: 1. The waste generated in the Blast Furnace during the iron smelting process is called 『Blast Furnace Slag』. Under the high temperature, the blast furnace slag is still the liquid stage. Along with the different temperature dropping and cooling process, it will generate 『Air-cooled Blast Furnace Slag』 and 『Water-quenched Blast Furnace Slag』 separately. 2. Steelmaking process. It can be categorized into the 『Convertor』 steelmaking of integrated steelmaking plant and the 『Electric Arc

Furnace』 steelmaking of non-integrated steelmaking plant. Since the manufacturing process of convertor steelmaking is smelted all the way to iron and then smelted to steel, therefore, it is called the integrated steelmaking plant. The slag generated during the steelmaking process is called 『Basic Oxygen Furnace Slag』. 3. As to the Electric Arc Furnace (EAF) : steelmaking of non-integrated steelmaking plant, the main raw materials used for steelmaking are the recycling scrapped iron and steel. The slag generated during the steelmaking process can also be categorized into the 『Electric Arc Furnace Oxidative Slag』 of front-end process and 『Electric Arc Furnace Reductive Slag』 of back-end process. [1, 2]

The operation of electric arc furnace smelting recycling system in Taiwan has already well completed. The main sources of scrapped iron and steel used for steelmaking are: general household scrapped steel, scrap and defective products generated during the plant manufacturing

process, rebar from demolition of plants and houses, scrapped steel from obsoleted vessels, machinery and cars/motorcycles etc. According to the smelting process, the slag of EAF can be categorized into EAF oxidative slag (hereinafter referred to as oxidative slag) and EAF reductive slag (hereinafter referred to as reductive slag) two major items. The EAF steelmaking plants in Taiwan produce around 10-million metric tons (MT) of crude steel annually and generate around 1.4-million MT of oxidative slag and 0.4-million MT of reductive slag simultaneously [3].

This study integrates the resource promoting strategy of EAF steelmaking slag and brings together the relevant technologies as the reference for promoting the slag-to-resource of EAF steelmakers.

2. Analysis & Discussion

The Taiwan government has regulated the management of related generating sources, storage, recycling, removal, disposal, reutilization and flow with respect to the general waste and industrial waste, and considered in sequence to reduce the waste generation, reuse, recycling and utilization, energy recovery and proper disposal, clearly defined the environment-friendly specification to promote the material recycling and reutilization.

2.1. Related Status of Reutilizing Waste & Construction Industries in Taiwan

In Taiwan, the wastes were categorized into the general waste and industrial waste. The general waste refers to the solid or liquid waste generated from the household or non-industry; the industrial waste refers to the waste generated from the industrial institutions. The total amount of waste was around 25.35-million MT in 2012, in which, the general waste was around 7.4039-million MT (holding 29.21%) and the industrial waste was around 17.95-million MT (holding 70.79%) [4]. The reutilizing key of waste should have the features of high and stable demand (5), and the market demand shall be greater than the generation volume of waste to facilitate the reutilization of waste resources and reduce the stacked space of waste and the amount of waste.

The aggregates are the most important bulk material for construction engineering. The material demand is high

and stable which is the best way of option for promoting recycling material to the industry promoted. To proceed the better implementing approach for reutilization introduction of waste-to-resource, its indexes of assessing feasibility include the elimination of demanding amount, applied technology, process equipment, locality, product value, restriction of acts and specifications six items, shown as Table 1.

Even Taiwan has already permitted the import of sand and gravel, however, the main source still depends on the nature sand and gravel obtained from the local rivers. Due to the rising of environmental consciousness, the concept for maintaining natural landscape, the weak concept of quarrying industry to the mining environment and preventing various disasters, etc., that cause the imbalance of supply and demand, and even trigger the price escalation of aggregates which becomes the major potential concern of construction industries. Therefore, the development of aggregates supply source shall be coordinated with the demand, adopt the diversified supply source development and reutilization to achieve the target of sustainable development.

The promotional approach for waste reutilization is to proclaim the appropriate ways of using material through the environmental protection department; incorporate the recycling material items and using specification & proportion in the engineering guidelines through the engineering application end to induce the market channels of construction resource recycling. Most of the waste generated from the industrial manufacturing may suitable for using in the civil engineering including the properties of hardness and anti-wear which is suitable for using as the aggregate; with the hydration property and large internal friction angle which is suitable for using as the ground material or the ground improvement material; if the chemical composition contains FeO, CaO, SiO₂ etc., it may use as the cement additive; in addition, if the chemical composition contains the fertilizing elements of CaO, SiO₂, MgO, FeO etc., it is suitable for using as the agricultural compost material. Accumulate the resource material suitable for the aggregate material produced yearly in Taiwan, and assess the constructions with large demand of aggregate material, and then utilize the

strategy approach that will be able to link the reutilization of waste to the construction adequately.

Table 1 Waste-to-Resource Introducing Engineering Reusing Feasibility Assessment [1]

Item	Assessment Criteria	Description of Benefits
1	Eliminate Demanding Amount	High Demand and stable market.
2	Applied Technology	Mature technology and able to ensure quality.
3	Process Equipment	No need additional investment of high technology or complicated equipment to avoid increasing cost.
4	Locality	Nearby use to lower transportation cost.
5	Product Value	Shall exceed disposal cost.
6	Restriction of Acts & Specifications	Shall comply with reuse purpose act, CNS national standards, construction outlines and the related operating specification standards.

2.2. Construction Application Market Analysis of EAF Steelmaking Slag

The direct reutilization pathways of oxidative slag are road subgrade layer, asphalt pavement, non-structural concrete respectively (such as Controlled Low Strength Material, CLSM) [6]. The annual demand of road subgrade layer is around 1.5-million MT, the asphalt pavement is around 12-million MT, however, the recycling of reclaimed asphalt pavement has already up to 40%. The annual demand of CLSM is around 2.2-million MT, the market demand is far beyond the generating amount of oxidative slag waste and has already reached the reutilizing effect of waste resource. The annual generating amount of reductive slag is around 0.4-million MT. The reutilizing pathway of reductive slag is distinguished by if the stabilization is to be applied, mainly used for the cement material without requiring the stabilizing treatment and stabilizing the expansion of slag. The reutilizing pathways and relative total demand of EAF slag are shown as Table 2.

2.3. Resource Technology Assessment of EAF Steelmaking Slag

(1) Promoting Pathway of EAF Steelmaking Slag

Taiwan has already accumulated quite rich research with respect to the reutilization study of EAF slag including the cement material, asphalt concrete aggregate, CLSM aggregate material, basic layer of pavement construction or bottom level aggregate material etc. Under the restriction of Waste Reuse Types of Soil Pollution Control Standards and Industries issued by Taiwan government, the reutilizing amount of EAF slag was limited and could not be effectively promote.

Table 2 Resource Market Analysis of Taiwan EAF Steelmaking Slag [1]

Dividing Mode		Feasible Pathway	Annual Demand (10-Thousand MT)	Aggregate/Material (10-Thousand MT)	Introduce to Restriction Assessment
Oxidative Slag 【0.7-million MT, the statistics of year 2013 is 1.4-million MT】	Same as water-quenched blast furnace slag, directly introduce to reutilizing purpose	1.Road Subgrade Layer	150	150	Newly built road, decreased year by year
		2.Asphalt Pavement	1,200	1,000	Reclaimed material already up to 40%
		3.Non-structural Concrete (CLSM or cement products)	220	165	Other waste resources have elimination demand as well
		4. Carboundum	Less demand elimination		Less demand elimination
		5. Other reutilizing approaches			
Reductive Slag 【0.4-million MT, the statistics of year 2013 is 0.4-million MT】	Stabilization is not required	1.Cement	1,200	1,920 (Raw material)	1.Able to add raw material 10% 2.Transportatio n cost is high
		2.Melt down process	Reduce reductive slag 20 ~ 40%		Application Technology has not skillful
	Stabilization is required	1.CLSM	220	165	Other waste resources have elimination demand as well
		2. Other reutilizing approaches (such as Mainland China steel slag cement, Southeast reutilization etc.)			Disposal & transporting finished product are to be assessed

In addition, the industry lacks of knowledge about the non-toxic steelmaking slag and the hazardous steelmaking ash collection, blended handling and improper disposal results the trouble to the domestic steel/iron industries as well.

Therefore, for the promotion of slag reutilization shall be able to overcome the corroded situation created by the expansion property of slag and the metallic iron remained on the surface, other than through the stabilization treatment and strengthening the magnetic separation efficiency, shall be further promoted through the planning of selecting the applicable construction purpose to avoid further negative perception caused to the slag from the public.

The types of slag produced in Taiwan include the basic oxygen furnace slag, oxidative slag and reductive

slag. After completing the assessment in accordance with the material properties and applicable construction purposes, the reutilization of EFA slag is mainly selected the asphalt concrete pavement with coverage and CLSM backfill material, additional assessment is implemented to use as the additive for cement raw mix.

(2) Technology Research for Oxidative Slag

The Los Angeles abrasion rate and soundness of EAF oxidative slag are equivalent to the general natural gravel, however, the specific gravity is higher than the natural gravel due to higher iron content. The water absorption is greater than the natural gravel due to more porosity of slag itself. However, the results of running water quality standard, radiation dose test and toxicity dissolution test have all complied with the current specification values, and will not cause any hazard to the environment. Therefore, it can be considered as the general industrial waste and reutilized for the application of road pavement.

(3) Technology Research for Reductive Slag

The main ingredients of reductive slag are categorized into 3 parts (1) active ingredient (2) oxidized metal and (3) other materials. The active gradient is mainly SiO_2 and CaO , and its gradient is similar to the cement raw mix, however, itself contains free calcium oxide which results its instable characteristics. Therefore, the reductive slag is used as the cement raw mix, and place in the rotary kiln with high kilning temperature to lower its instability in order to ensure its stability and practicality.

3. Assessment & Discussion

Construction industries, the promotional pathways would be mainly locked on the road subgrade layer, asphalt pavement, CLSM and cement additive. The strategy is to provide the complete technical data and promote the implementation of verification system in order. For the part of build-up technology, the stage is to proceed from the asphalt concrete pavement of oxidative slag and cement raw mix of reductive slag two aspects.

As to the assessment aspect of applying the original slag to the cement raw mix, since its chemical contents are similar to the cement raw mix, and after replacing partial cement raw mix in accordance with the different

content of reductive slag, and proceeding the thermomechanical analysis (TMA) test in accordance with the different cement proportion, the impact change to the burning temperature of rotary kiln becomes less after adding the reductive slag to the cement raw mix, it proves the feasibility of replacing partial cement raw mix.

4. Conclusion

- (I). The annual capacity of EAF steelmaking slag was almost fixed, propose the appropriate reutilization source and transparentize the elimination flow, and cooperate with the government policy toward the direction of diversified reutilization in order to develop the pathway.
- (II). The product of oxidative slag has the features of high stability, low silt content, low abrasion rate and good soundness, to improvement of stabilization and the main promotional purposes shall be locked on the asphalt pavement, road subgrade layer and non-structural concrete.
- (III). The implementation concept of waste resource recycling management, it will be handled and processed by each industry competent authority based on the announced related acts; the engineering unit is responsible for maintaining the on-site quality. If the prescribed use restrictions are followed, it may indicate that resource product has no doubt about the impact to the environmental aspect.

5. References

- 1.H. Motz; J. Geiseler, Products of Steel Slag an Opportunity to Save Natural Resources, Waste Management, 21(3), 2001, pp. 285-293.
- 2.Geiseler, J. (1996). Use of Steel Works Slag in Europe. Waste Management, 16(1-3), pp. 59-63.
- 3.Taiwan Construction Research Institute, 「Slag Reutilization Program Feasibility Assessment and Promotional Strategy Plan」. Taiwan Steel & Iron Industries Association (2013).
- 4.Taiwan Steel & Iron Industries Association 50th Anniversary Special Issue, 「Coping Strategy of Reutilizing Taiwan Steelmaking Slag at Current Stage」, Taiwan Steel & Iron Industries Association (2013).
- 5.Taiwan Construction Research Institute, 「Road Construction Application Effects Assessment Plan of EFA Oxidative Slag」, Taiwan Steel & Iron Industries Association (2014).

6. Taiwan Construction Research Institute, 「 Feasibility Assessment Plan of Applying EFA Reductive Slag to Cement Material」 , Tung Ho Steel Enterprise Corp. (2014)

The Research on the Utilization of Green Building Ecological Index Group in Campus Environment – Taking of Elementary Schools at Houli District, Taichung City as Example

Ching-Jung Chang*, Yung- Feng Hsu, Chun-Hsien Chen

Department of Construction Management, Chung Hua University

707, WuFu Rd., Sec. 2, Hsinchu 30012, Taiwan

*E-mail: *cjchang@chu.edu.tw, jg129@mail.jges.ntpc.edu.tw, cindy4066@yahoo.com.tw*

Abstract

The elementary school is the most basic educational site, and the spatial characteristics of school building have relative large area of outdoor space. If the ecological education can be promoted from the campus, it will not be able to improve the overall environmental ecology, but also able to root the ecological education from the lowest base. The paper research takes the field survey at the elementary school and analysis the relevant affecting factors. It hopes to provide appropriate reference contribution to planner or government in the future.

Key words: Green Building, Ecological Index Group, Elementary School Campus, Ecological Quality, Sustainable Campus

1. Introduction

Due to the over-exploitation to Earth and dramatic increase in energy consumption that cause the concentration of CO₂ increased year by year, and result the environmental imbalance phenomena of Earth warming, abnormal climate, ozone depletion, forests gradually disappeared and debris flow etc. [1]. Taiwan government incorporated the「Green Building」into 「Urban-Rural Sustainable Development Policy」 as the implementation priority in the year of 1996, and fully promotes the green building policy, in March 2004.

Facing the crisis of Earth environment, the promotion and education of sustainable development are the foundations for resolving the problem [3]. The school ecology is the most important part in the urban-rural

ecological environment, school has large area space, if it can be converted into the quality ecological environment that will be great help to the urban-rural ecological green network, ecological conservation and even the national ecological education [2,7].

This article takes the campus of five elementary schools located in Houli District, aims at the Ecological Index Group, most closely to the campus outdoor space including biodiversity, greenery, Soil Water Content 3 indexes to perform assessment and research. It is expected to enhance the environmental quality of elementary school campus in that district and city, and provide the basic analysis data for the reference of follow-on researchers and planning units.

2. Literature

The trend of thought for green building started at the two times of energy crisis in 1970s, due to the panic

from the oil crisis, the energy-saving design was raised in the construction industry. In recent decade, under the environmental crisis of Earth warming and climate abnormal change, the earth environmental design and green building concept of life cycle assessment, CO₂ reduction, biodiversity design have been further developed [4]. The green building is the concept of pursuing the environment sustainable design, it is called as ecology building Japan; European countries call as 「Ecological Building」 and 「Sustainable Building」, United States, Canada also call as 「Green Building」, it is the general call of ecology, environmental protection, sustainable, ecology building [5,6].

In the year of 1990, British Building Research Establishment (BRE) brought the first assessment system for green building i.e. BREEAM which affected the follow-on assessment method e.g. LEED of United States in the year of 1996, GBTool of Canada in the year of 1998 etc. Taiwan established the green building evaluation system of EEWB in the year of 1999 which is the 4th green building assessment system in the world [5]. Up to the year of 2011, there are 26 countries formerly owned the green building assessment system in the world shown as Fig. 1, there are 89 countries already established or under preparation for organizing the green building related associations.



Fig. 1. Countries with Assessment System [5]

In Taiwan, it formulated green building assessment manual in 1999, and it has been revised for many times until 2012 to establish EEWB (Ecology, Energy Saving, Waste Reduction & Health) assessment indexes. The index of WVEH includes 1. Ecology: biodiversity, greenery, soil water content three indexes 2. Energy Saving: the daily energy saving index, 3. Waste Reduction: waste reduction and CO₂ reduction 4. Health: indoor environment, water resource, improvement of sewage waste, totally there are 9 indexes [5].

3. Research Method

This research is assessed in accordance with the ecological assessment items and standards stated in the 「Green Building Assessment Manual」 issued by Taiwan Construction & Planning Agency, take the biodiversity, greenery and soil water content index.

3.1 Assessment Mode of Biodiversity Index

The biodiversity index is the base of biological habitat and biological exchange, the base scale shall be over 1 hectare and then be applicable to assess by this index. According to biodiversity index BD, its value shall be greater than the baseline value of biodiversity index BD_c, and the score of biodiversity index system RS1 shall comply with $0.0 \leq RS1 \leq 9.0$, its relative formula is as follows Eq.1~2:

$$BD = \sum_{i=1}^n Xi, i=1,2,3,...,23 \quad \dots\dots\dots (1)$$

$$RS1 = 18.75 \times \frac{BD - BD_c}{BD_c} + 1.5, 0 \leq RS1 \leq 9 \quad \dots (2)$$

BD : Biodiversity Index Calculation Value

Xi : Sub-score, $i=1, 2, 3, \dots, 23$

RS1 : Biodiversity Index System Score, $0.0 \leq RS1 \leq 9.0$

BD_c : Baseline Value of Biodiversity Index

3.2 Assessment Mode of Greenery Index

The greenery index takes the plant photosynthesis as the assessment baseline, configure the 40 years of CO₂ fixed volume as the conversion baseline of greening benefit, the calculation value of greenery index TCO₂ is calculated from the total CO₂ fixed volume of all plants in the base, the system score of its greenery index RS2 i.e. converted from its index calculation value TCO₂ and greenery index baseline value TCO_{2c}, the score of greenery system RS2 shall comply with the limit of $0.0 \leq RS2 \leq 9.0$, its relative calculation formula is as follows Eq.3~5:

$$TCO_2 = \left(\sum_{i=1}^n (Gi \times Ai) \right) \times \alpha \quad \dots\dots\dots (3)$$

$$A' = (A_0 - A_p) \times (1 - r), A' \geq 0.15 \times A_0 \quad \dots (4)$$

$$RS2 = 6.81 \times \left(\frac{TCO_2 - TCO_{2c}}{TCO_{2c}} \right) + 1.5, 0 \leq RS2 \leq 9 \quad \dots (5)$$

Gi : Unit Area of Certain Planting Species CO₂ Fixed

Volume (kg/m²)
 A_i : Planting Area Baseline
 A' : Minimum Green Area (m²)
 α : Ecological Greening Correction coefficient
 A_o : Base Area (m²) i.e. 「School Land Area」 of this research.
 A_p : Unable to greening area (m²)
 r : Legal Floor Area Ratio

3.3 Assessment Mode of Soil Water Content

The assessment of soil water content index is categorized into the common soil water content design and special soil water content design two items, the calculation value of soil water content λ is the relative ratio between the nature land soil water content prior to development Q_0 and the land soil water content after development Q' , base λ_c is the baseline of land soil water index. The larger λ value indicates that the performance of soil water content is better, otherwise the worse. When its value is 1.0, it indicates that the land development activities have no damage to the function of soil water content of the original nature bare land. The system score of soil water content RS3, conversion from the design value of soil water content

λ and baseline value λ_c , its system score must have the limit of $0.0 \leq RS3 \leq 9.0$, its relative calculation formula is as follows Eq.6~8:

$$\lambda = \sum_{i=1}^n Q_i / A_o \cdot f \cdot t \quad \dots\dots\dots (6)$$

$$\lambda_c = 0.5 \times (1.0 - r) \quad \dots\dots\dots (7)$$

$$RS3 = 4 \times \left(\frac{\lambda - \lambda_c}{\lambda_c} \right) + 1.5, 0 \leq RS3 \leq 9 \quad \dots\dots (8)$$

RS3 : System Score of Soil Water Content Index
 λ : Calculation Value of Soil Water Content Index
 λ_c : Baseline Value of Soil Water Content Index
 Q_i : Soil Water Content Volume of Various Kind of Soil Water Content Design (m³)
 A_o : Total Base Area (m³)
 r : Legal Floor Area Ratio
 f : Base Final Infiltration Rate (m/s)
 t : Maximum Rain Delay (s)

4. Case Survey Results & Analysis

The basic data of this research scope are shown as Table 1, the Houli elementary school has the highest floor are ratio, up to 33.5%, the floor area ratio of other four schools are very similar, all less than 15%.

Table1 List of Basic Data of Elementary Schools in Houli District

School Name	School LandArea _{m2}	Building Area m2	Floor Area Ratio %	Numbers of Students	Density of Student m2 /person	Built Year of School
Tai'an	22402	2408.825	10.75	167	134.1	1946
Hoili	19374.92	6490.28	33.50	707	27.4	1946
Neipu	30812	3414.8	11.08	1484	20.8	1904
Qixing	11592	1562	13.47	279	41.5	1958
Yuhing	12912	1622.89	12.57	262	49.3	1964

4.1 Status Analysis of Biodiversity Index

The biodiversity index assessment result of relative survey data are shown as Table 2 i.e., the calculation results of biodiversity index assessment studied by this article. From the Table 2, only the ratio of biodiversity index (BD/BDc) of Tai'an elementary school was 1.12 since its relative smaller floor area ratio and larger green area, it indicates that the biodiversity part shall be further enhanced.

4.2 Status Analysis of Greenery Index

As summarize from the data of each elementary school in Houli District, the calculation results of greenery index are shown as Table 3. From the Table 3 got the greenery and greening baseline value (TCO₂/ TCO_{2c}) of 5 elementary schools are all greater than 1, it meet the baseline. It indicates that the greenery implementation status of elementary schools in Houli District is quite well.

Table 2 Calculation Results of Biodiversity Index Assessment

Primary Category	Minor Category	Design Item	Tai'an Elementary School	Hoili Elementary School	Neipu Elementary School	Qixing Elementary School	Yuhing Elementary School
	Total (BD)		56	43.3	15.6	18.3	21.9
	Baseline Vale (BDc)		50	50	50	50	50
	BD/BDc		1.12	0.87	0.31	0.37	0.44
	Qualification Rate				20%		

Table 3 Statistical Table of Greenery

School Name	School Land Area m2	Sports Field m2	TCO2	TCO2c	TCO2/ TCO2c	Qualification Rate	System Score RS2
Tai'an	22402	3,084	5,256,643	3,622,125	1.45	100%	4.57
Hoili	19375	3,240	5,120,505	3,025,313	1.69		6.22
Neipu	30812	10,451	5,928,899	3,817,688	1.55		5.27
Qixing	11592	3,428	3,233,848	1,530,750	2.11		9
Yuhing	12912	3,193	4,796,559	1,822,378	2.63		9

4.3 Status Analysis of Soil Water Content

The soil water content are shown as Table4. From Table 4, the index value and soil water content baseline value ($\lambda / \lambda c$) is greater than 1 for Tai'an & Hoili

elementary schools and Neipu, Qixing & Yuhing elementary schools are all lower than 1. It did not meet the baseline due to the insufficient green area, the main water conservation of soil water content mainly comes from the green area.

Table 4 Statistical Table of Soil Water Content Index

School Name	School Land Area m2	Green Area m2	λ	λc	$\lambda / \lambda c$	Qualification Rate	System Score RS3
Tai'an	22402	13,984	0.64	0.5	1.28	40%	2.64
Hoili	19375	8,645	0.5		1		1.5
Neipu	30812	4,189	0.48		0.96		1.33
Qixing	11592	2,580	0.23		0.47		0
Yuhing	12912	3,227	0.34		0.67		0.19
Ecological Index Group Total Score		27	10.96	7.72	6.6	9	9.19

5. Conclusion & Recommendation

The qualification rate of greenery is up to 100%, biodiversity and soil water content are 20% and 40% respectively, consolidate the reasons as follows:

1. Poor planning for the bio-friendly environment, the pavement common uses excess of asphalt or concrete, causes the poor hydrophilic property of land.
2. The green area is the important role of campus ecological environment, only with sufficient green area plus the complete biological environment and perfect lawn or using pavement with good permeability will then be able to achieve the 「 qualitative 」 and 「 quantitative 」 baseline of greening.
3. The water biological habitat is the richest place for biological gathering and exchange. The sports field

is the mandatory facility for elementary school, excessively high proportion will cause the green area relatively reduced, and how to give balance for both will be very important issue while planning the campus.

4. Increase the species of trees in campus, species diversification, it will then have variety of creatures inhabit, breed, change the cement revetment and pool bottom to the masonry revetment with more ecological and natural soil as the pool bottom to create the ecological waters space for providing habitat.

Reference Literatures

1. Chen Chun-Hsien, 「 The Research on the Utilization of Green Building Ecological Index Group in Campus Environment – Taking of Elementary Schools at Houli District, Taichung City as Example 」, Master Thesis, Department of

Construction Management, Chung Hua University, Hsinchu 2014.

2. Lin Xian-De, 「Ecology and Energy Conservation Planning for Sustainable School」, Chan's Arch-Publishing Co., Ltd, 2004.
3. Wang Xi-Zhi, 「Greening」 & 「Soil Water Content」 in 「Green Building」 Evaluation Index Applications at Middle/Elementary School Campus - Taking Hsinchu City as example」, Master Thesis, Graduate School, Department of Building & Urban Planning, Feng Chia University, Taichung, 2002.
4. Lin Xian-De, 「Green Building」, Chan's Arch-Publishing Co., Ltd, 2006.
5. Architecture and Building Research Institute, Ministry of the Interior, 「Green Building Evaluation Manual – Basic Version」, 2015.
6. Yang Yi-jeng, 「An Evaluation Research of Green Building Ecological Indicator Group of Zhang Hua County Primary School」, Master Thesis, Graduate School, Department of Architecture, Feng Chia University, Taichung, 2009.
7. Tang Zhi-Min, 「School Buildings and Campus Planning」, Wu-Nan Book Inc., 2006.

The Assessment and Research on the Reconstruction of Enclosing Wall into Open Type in Elementary School Campus – Taking of Erlin Township, Changhua County as Example

Ching-Jung Chang, Chia-Chen Li, I-Chen Wu

Department of Construction Management, Chung Hua University

707, WuFu Rd., Sec. 2, Hsinchu 30012, Taiwan

E-mail: cjchang@chu.edu.tw, jg216@mail.jges.ntpc.edu.tw, iciness26@yahoo.com.tw

Abstract

The purpose of enclosing wall is to demarcate, segment field and blocking of school. The Taiwan government encourages schools to perform the enclosing wall to become the open type campus with friendly affinity. The change of enclosing wall caused concern from the teachers and parents. This paper article takes the elementary school at Changhua as the research objects, made field investigation, collecting data and interviewing by experts, design the questionnaire and made analysis to explore the reaction. It hopes to provide as the reference for the design of elementary school.

Key words: One-Way Analysis of Variance (ANOVA), Open Type Enclosing Wall, Enclosing Form, Design Questionnaire, Factor Analysis

1. Introduction

In the early 2000s, most of the school enclosing wall were the solid wall made by concrete or bricks, towering with the barrier and protective function, and the shape feature was monotonous, the wall surface lacked of aesthetic feeling. Usually, the school building focuses on the schoolhouses and sports facilities used as the activity spots and educational environment for teachers/students. The school enclosing wall always separates the campus from the surrounding environment area, and just like forming an enclosed space [1]. After 921 earthquake occurred in the year of 1999, there were many school buildings and schoolhouses collapsed and ruinous, there were many school campus near the disaster area facing the reconstruction. It coincided with the open education, green school and campus open concepts promoted by Taiwan government [2]. That promoted the open type

campus without walls idea and hoped to bring the cohesion between school environment and community closer.

The reconstruction plan causes doubt from the parents with respect to the security level of school children, i.e. if the open type enclosing wall is applicable for different schools which shall be the part to be discussed. This paper takes part of elementary school campus located at Chung Hua, Taiwan as the research objects, it is expected to explore the recognition of teachers and parents with respect to the reconstructed open type enclosing wall, and the status, problems faced and solution of the schools. The research collected the related literatures, questionnaire, expert interview and made statics analysis, and provide the result to the government departments as the design reference for

planning the reconstruction of campus enclosing wall in the future.

2. Literatures

The main functions of building enclosing wall are interval, demarcation, segmenting field, defining scope and uses as the construction of barrier, the function of school enclosing wall is to segment the space between the inside and outside of school environment. It has the functions of anti-strong wind, dust and noise isolation, it also has the effect of security and blocking plus the function of aesthetic appearance and education [1, 3]. Currently, there are many European countries adopted open styling for schoolhouses and open space design for classrooms, and lower the enclosing wall or without walls. It indicates that the school construction planning toward to the development trend of open style [4].

In the early 2000s in Taiwan, most of the school enclosing wall were the solid wall made by concrete or bricks, towering with the barrier and protective function, however, the form was monotonous, wall surface lacked of aesthetic feeling. The government prompted to the idea of campus without wall promoted by Ministry of Education that is gradually push to expand, it expects to demolish the old enclosing wall structured by cement or barbed wire, and replace by the greening planting or are design products to achieve the school opening and increase community interaction.

The campus enclosing wall can be categorized by its different aspects of function, height, materials, shapes, features, performance and visual penetration, greening/beautify degree etc. [5, 6], this article categorizes the forms of enclosing wall as follows:

1. Close Type Enclosing Wall: Height is over 140cm, with solid wall, no visual penetration, shown as Fig. 1.1~1.2.

- (1) Traditional Solid Enclosing Wall: Most of them are made by concrete or bricks, with solid wall.
- (2) Color Painting, Collage Wall: Add color painted patterns or mosaics collage on the solid wall.

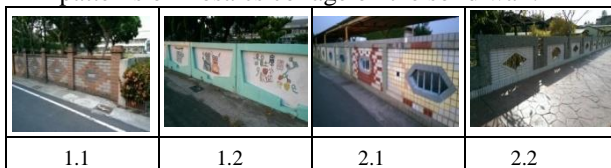


Fig. 1. Close Type

Fig. 2. Semi-open Type

2. Semi-open Type Enclosing Wall: Height is over

140cm, solid wall with partial hollow treatment, the visual penetration is higher than the closed enclosing wall, enhance the visual penetration but still able to keep the privacy, shown as Fig. 2.1~2.2.

3. Open Type Enclosing Wall: Height is lower than 120cm, good visual penetration, most of them have the beautiful styling, but due to the height is lowered, barrier and blocking are lower, also able to achieve the purpose of natural monitor, comply with Newman's Defensible Space theory [7]. The open type enclosing wall is categorized as follows, shown as Fig. 3.1~3.5:

- (1) Barrier Type Enclosing Wall: Full hollow or partial hollow, high visual penetration, lower the height decrease the protective, easy to create the climbing opportunity from the schoolchildren or outsiders.
- (2) Green Hedge: Low shrubs or flower stands, constructed with plant material, high visual penetration, but easy create the problems of crossing by the outsiders or maintenance & Management.
- (3) Dwarf Type Enclosing Wall: Lower the original wall height, most of them are below 80cm, high visual penetration, width and height are suitable for pedestrian sitting and resting, poor protective and blocking function.
- (4) Hybrid Type Enclosing Wall: Wall combined with more than two different forms or material, consolidate the advantages of multiple forms or material, good visual penetration and beautiful styling.
- (5) No Enclosing Wall Form: Demolish solid wall, adopt full-open design, highest visual penetration, poor protective and blocking function.

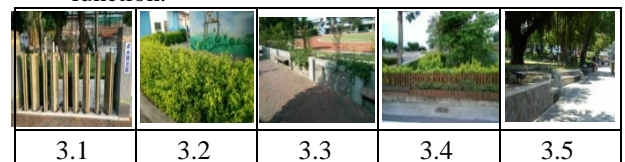


Fig.3. Open Type

3. Research Method

This research adopts the literature exploration, environmental status survey, expert interview and questionnaire, through the statistical analysis on the

questionnaire results, use ANOVA to inspect the differences of various different opinions from the teachers and parents, simplify the questionnaire opinion variables to the demand dimensions through the principle component analysis, and able to briefly and concisely express the user demands [8].

The questionnaire objects are the teachers and parents of elementary schools where the campus enclosing wall has been reconstructed to the open type, through the approach of questionnaire survey to understand the recognition and satisfaction of questionnaire objects with respect to the reconstruction of open type enclosing wall in the campus. Questionnaire adopts five-level of Likert scale, survey scene first, collect data and after interviewing by experts, design the pretest questionnaire items, adopt the closed questionnaire which will allow the participants answering fully in accordance with the options provided by the researcher, item design are all 18 items for both teachers and parents questionnaire. First start with pretest questionnaire, randomly issue 120 copies in the research area, After performing the statistical analysis, test its reliability and validity analysis, and then determine based on the test results, and re-establish the formal questionnaire items.

This research takes the questionnaire results performing the descriptive statistics, ANOVA and factor analysis to analyze and compare the objects with different background, and their views to reconstruct the campus enclosing wall to the open type enclosing wall. ANOVA inspects the opinion differences between the different identities, ages, principle component analysis simplifies the questionnaire variables to demand dimensions. When perform the principle component analysis, the test of KMO and Bartlett shall be performed, it is applicable for performing the principle component analysis when KMO value is over 0.8; the larger value acquired by Bartlett sphericity test, the more suitable for analysis.

After determining the data suitable for the principle component analysis, select suitable factor dimensions in accordance with the eigenvalue, select eigenvalue large than 1 or the factor selecting point when the slope of scree plot starts to downward, the factor with small eigenvalue does not have the explained variable difference which can be discarded, and the selected cumulative explained variance percent shall reach 70%. The principle component analysis is to show the

correlation between the measurement variable and extracted component through the eigenvalue, if the difference of component loading is not too large, the rotation may be used to change the factor loading of each component, after the rotation, the variance of new component become the largest, this research uses the Varimax rotation.

4. Research Results & Analysis

The total formal questionnaire for the teacher portion are 155 copies, valid questionnaire are 137 copies, the parents portion are 210 copies, valid questionnaire are 163 copies. Take the questionnaire results performing the descriptive statistics, one-way analysis of variance and principle component analysis. The descriptive statistics and ANOVA analyze and compare the objects with different background, and the view difference with respect to the campus enclosing wall reconstructed to the open type enclosing wall.

The principle component analysis simplifies the questionnaire variables, after analyzing the questionnaire, select the one with eigenvalue large than 1, its referred scree plot is shown as Fig. 4, simply to 4 dimensions, namely as 「Reconstruction Effectiveness」, 「Visual Perception」, 「Safety Sense」, 「Environmental Facility」.

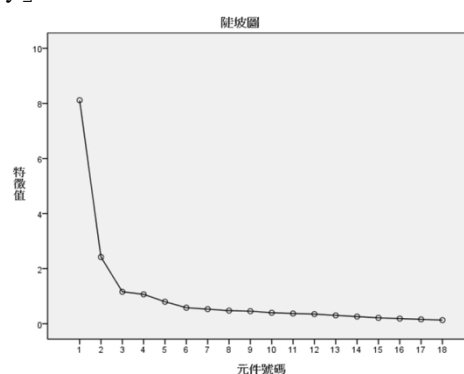


Fig. 4. Scree Plot

Analysis Results:

1. As found out from the survey results, teachers and parents have higher recognition to the perception of open type enclosing wall, and the recognition of parents is generally higher than teachers.
2. As to the part of invasion by outsiders, easy climbing by schoolchildren, both parents and teachers also recognize, it indicates that even the open type enclosing wall has enhanced the visual penetration and slightly enhanced

the security, however, due to the wall height is lowered, form is changed, there is still doubt on the teachers and parents mind with respect to the safety.

3. As to the selection of favorite enclosing wall form, collage enclosing wall receives the highest number of votes (shown as Fig. 1.2), the next one is the hollow enclosing wall (shown as Fig. 2), hybrid enclosing wall (shown as Fig. 3.4), it indicates that the teachers and parents recognize the various functional performance of open type enclosing wall, however, as viewing from the security of schoolchildren, the enclosing wall with traditional height, blocking, visual beautify and variability of color painting, collage wall and hollow wall is more favorable by the interviewee. In addition, although the height of hybrid enclosing wall is lowered, however, due to coordinate with planting, it has the plus effect to the overall campus greening which is also favorable by the teachers.

5. Conclusion

This research inspects the perception of reconstructing the campus to the open type enclosing wall as viewing from the teachers and parents angle through the questionnaire and expert interview, inspect by the statistical analysis and simplify the opinion trend dimensions of questionnaire items by factor analysis. This is able to distinguish the opinion difference of different identity in details, and also understand the common demands, the research results may provide as the reference for the follow-on planning and researchers, the research conclusions are described as follows:

1. After reconstructing to the open type enclosing wall, the overall response of teachers and students is good, however, due to the wall height is lowered, the blocking is more weak, easy to cause insecurity, therefore, the location of enclosing wall, circumstance of surrounding roads, community customs, environment conditions shall be considered when the reconstruction is selected, if the planting is collocated, then the geology, climate, monsoon, human impact factors shall be considered.
2. After reconstructing to the open type enclosing wall, even the school security event does not increase, but there are circumstances of taking shortcut to step cross the open type enclosing wall by the outsiders, the school shall reinforce the dissuasion and propaganda; the schoolchildren will also depend on

the school to construct the concept and education.

3. Although the teachers and parents recognize the various functional performance of open type enclosing wall, but viewing from the security of schoolchildren, the enclosing wall with traditional height, blocking, visual beautify and variability of color painting, collage wall and hollow wall is more favorable by the interviewee. In addition, although the height of hybrid enclosing wall is lowered, however, due to coordinate with planting, it has the plus effect to the overall campus greening which is also favorable by the teachers.

This research takes the suburban schools as the research scope, due to the environmental factor, part of schools have reservation about the open type enclosing wall, the research results may not applicable for the metropolitan areas. Therefore, the follow-on researchers may focus on the metropolitan areas proceeding research and exploration to propose recommendation for the reconstruction of enclosing wall with different city attributes.

Reference

1. Wu I-ChenWu, 「The Assessment and Research on the Reconstruction of Enclosing Wall into Open Type in Elementary School Campus - Taking of Erlin Township, Changhua County as Example」, Master Thesis, Department of Construction Management, Chung Hua University, Hsinchu 2014.
2. Li Mei-Huei, 「A Research of Campus Rebuilding Planning of Primary School in Nan-Tou after Ji-Ji Earthquake」, Master Thesis, Graduate School, Department of Spatial Design, National Yunlin University of Science & Technology, Yunlin, 2003.
3. Chen Mi-Tao, 「Exploration of Certain Practical Problems on School Buildings」, Journal of Education Research, pp2-7, 1997.
4. Tang Zhi-Min, 「School Buildings and Campus Planning」, Wu-Nan Book Inc., 1992.
5. Fan Yin-Jo, 「A Research on the Interaction between Campus Wall Reform in Elementary Schools and Security Identification Among Teachers and Students : Tainan City」 Master Thesis, Graduate School, Department of Architecture, National Cheng Kung University, Tainan, 2010.
6. Yu Zheng-Lu, 「City Environment Creation: Landscape & Environmental Facilities Design」, Garden City, 2004.
7. Newman Oscar, Defensible Space, New York : Macmillan Publishing Co.,Inc,1973.
8. Chen Shun-Yu, Multivariate Analysis, Huatai Bookstore, Taipei City, 2005.

The Study and Analysis on the Reuse and Transformation Strategy of Tile Kiln Space – Taking of San-He Tile Kiln as Example

Ching-Jung Chang, Hsiao-Yu Lin, Ying-Yu Su

Department of Construction Management, Chung Hua University

707, WuFu Rd., Sec. 2, Hsinchu 30012, Taiwan

E-mail: cjchang@chu.edu.tw, jg333@mail.jges.ntpc.edu.tw, btofi@ms41.hinet.net

Abstract

Due to the reduction of brick demand, Taiwan traditional brick kiln is declined gradually. The policy for preservation of local cultural and spatial utilization, it is successfully transformed the traditional kiln into the business model. This research selects San-He tile kiln as the case study, through the interview with the kiln owner, experts, and tourists, and made the questionnaire to perform the statistical analysis to find out the common demand and expectation of business model. It could provide the analysis to the kiln owner as the reference for operational strategy.

Key words: Brick Kiln, Spatial Reuse, One-Way Analysis of Variance (ANOVA), Factor Analysis

1. Foreword

During the year of 1895 and 1945, Taiwan traditional brick kiln, due to the public construction and proceeding the large-scale urban planning, the demand of red brick was significantly increased, that caused the brick kiln industry entering into the industrialization and possessed different types and forms of old kiln plants. However, after the year of 1970, due to the introduction of new technology and change of building mode, extensive use of concrete and rebar plus steel reinforced, that caused the brick kiln industry declined gradually. Most of the brick kiln industry requires the vast space, when the industrial recession would cause idled or abandoned. This paper tries to explore the declined traditional brick kiln plant and consolidate

culture & creation, tourism and preservation viewpoint of cultural assets, make detailed case study to the spatial reuse of kiln industry.

The reuse of abandoned industrial culture assets is the important strategy to strengthen industrial culture preservation, if the cultural assets preservation and spatial reuse are able to combine with the local cultural memory, it will definitely generate multiplying effect. This research selects San-He tile kiln, in Kaohsiung City, since the kiln owner recognizes the importance of industrial and cultural assets preservation, preserves the old kiln plant and utilizes the landscape with local cultural memory, successfully reuses the vacant space and transforms into the business model of cultural & creative industry, successfully continues the old kiln plant and activates the business industry.

This research goes through the advanced interview with the kiln owner, experts, local tourists, after organizing the interview information systematically, then design the questionnaire, makes the investigation with focusing on the different demanding for the business model of brick kiln industry from the tourists. From the view point of experts, artists and tourists to verify the analysis results, provide the different level of thinking to the civil owners with respect to the preservation and reuse strategy.

2. Literatures

After the industrial revolution in 18th century, the industry was rapidly developed, however, followed the industrial transformation in 20th century which caused part of the traditional industries declined, started in the year of 1960, European and America enthusiastic research the topics of industrial archaeology, industrial assets preservation and reuse, industrial culture tourism, becomes the city planning and development trend [1]. Taiwan government started to promote the industrial culture assets regeneration project in the year of 2006, supports the industries to evaluate the cultural assets by themselves, the concept and actions of industrial culture assets reuse are gradually valued [2]. It created many sightseeing landscapes such as railways/station, docks & warehouses, rice granary, old plant areas of Taiwan Sugar Corporation, traditional brick & tile kilns., these vacant space were reused and combined with the creative industries successfully develop as the new tourism landscapes.

The vacant space may be the abandoned public quarters, administrative offices, military facilities, religious facilities, educational facilities. It may also be the 「Dissimilation Space」 during the connecting process of new metropolitan space, especially the transportation facilities. The historical buildings shall have the continuation and regeneration value, it shall contain the historical facts, culture and emotion, and the major consideration of historical facts is the features of original style. The cultural value is the special group perception or behavior action, and the emotional value is the support exists in the memory and spirit. The expected regeneration value of historical buildings includes use, economics and education, the major consideration of abandoned space reutilize is the new function of building, and the economic value is the basic source of continuous survival, and the educational value is to inherit the historical culture [3].

The basic theory and technology of monument preservation and historical space preservation/reuse are close, if the value of preserved object is not high in terms of science, memorial or other academic value, and has less relationship with historical event or person but only presents the architectural style, settlement context, or localism, make flexible use of the historical space preservation is the effective method not only able to preserve the monument but also able to protect the rights of residents [4].

For Taiwan experience, the vacant space is not only a new space utilize mode or concept, but also the handling memories of city sentimental [5]. In the form of city space with the rapid development of real estate, lack of an emotion link with the emotional memories to land, consequently, form a kind of the 「New/Old Street Bloc Mode」 to segment the significant urban space [6]. After many years of experience in promoting the reuse of vacant space by the government and scholars, most of the vacant space in these years have the aesthetics and tourism effect; create very unique spatial reuse culture.

3. Research Method & Application

This article takes the methods of literature review, questionnaire survey and expert interview, organize the questionnaire data, use the independent sample T test/inspect the independent samples or group of two unrelated groups to determine if the average at a certain variable reaches the significant difference. Use one-way analysis of variance (ANOVA) to understand if there is significant difference between the questionnaire data with various different conditions, if the significant difference exists, then proceed the post hoc comparisons with Scheffe method [7], simplify the questionnaire opinion variable to the constructs through the principle component analysis, explore the strategy of reuse brick/tile kiln space and the satisfactory condition of kiln industry business model from the tourists.

This paper research surveys scene first, collect data and after interviewing by experts, design the pretest questionnaire items, adopt the closed questionnaire which will allow the participants answering fully in accordance with the options provided by the researcher. The questionnaire adopts five-level of Likert scale, after performing the statistical analysis to the pretest questionnaire, proceed the items, validity and reliability analysis inspection, and then determine based on the test results, and re-establish the formal questionnaire

items, and issue the questionnaire at San-He tile kiln, let the tourists personally fill the questionnaire.

This research uses T test to analyze the different gender (male, female) with regard to if there is significant difference between the satisfactory degree variables of the various reuse and transformation strategy. The one-way analysis of variance (ANOVA) analyzes if there is significant difference between the variables of different tourist background and the variables of satisfactory degree and the various reuse and transformation strategy. The main purpose of principle component analysis is to simplify the questionnaire variables, simplify the designed variables to factor constructs. Before performing the principle component analysis, the statistics test of KMO and Bartlett shall be performed, it is applicable for performing the principle component analysis when KMO value is over 0.8; the larger value acquired by Bartlett sphericity test, the more suitable for analysis.

After determining the data suitable for the principle component analysis, select suitable factor constructs in accordance with the eigenvalue, select eigenvalue large than 1 or the factor selecting point when the slope of scree plot starts to downward, the factor with small eigenvalue does not have the explained variable difference which can be discarded, and the selected cumulative explained variance percent shall reach 70%. The principle component analysis is to show the correlation between the measurement variable and extracted component through the eigenvalue, if the difference of component loading is not too large, the rotation may be used to change the factor loading of

each component, after the rotation, the variance of new component become the largest, this research uses the Varimax rotation.

4. Research Results & Analysis

This case locates at San-He tile kiln, Kaohsiung City, after the tile kiln industry of Kaohsiung area declined, only San-He tile kiln continues the production. In 2004, it was registered by the government as the historical building and able to continue the traditional tile kiln culture, and forms the monument preservation district together with the surrounding the Kaohsiung-Pingtung old iron bridge and water intake station.

This research issues 350 copies of questionnaire, retrieves 331 copies, screen the answering, if there is missing item, the questionnaire is invalid, therefore, invalid questionnaire has 11 copies, valid questionnaire has 320 copies, the retrieving rate of valid sample is 91.43%. After the formal questionnaire items through the validity analysis, KMO =0.929, it indicates that it is applicable for proceeding the principle component analysis [6.7]. After processing through the principle component analysis and the maximum variance rotation, its component eigenvalues are shown as Table 1, take the components with eigenvalue large than 1 and simplify to 4 dimensions, 4 main components are named respectively as 1.Cultural creation marketing 2.Environmental space planning. 3. Service quality. 4. Willing for re-visit.

Table 1. After Varimax Rotation

Factor	Eigenvalue	Explained Variance %	Accumulated Variance %
Factor 1	4.874	24.368	24.368
Factor 2	4.026	20.131	44.499
Factor 3	3.144	15.719	60.219
Factor 4	1.999	9.994	70.213

Use the principle component analysis to integrate the data and perform the statistical result analysis, obtain the common needs tendency and expectation of kiln industry business model from the tourists and categorize into 4 dimensions: 1. Cultural creation marketing dimension. 2. Environmental space planning 3.Service quality 4.Visit willing. After analyzing the questionnaire, interview with the experts, cultural & creative dealers, art workers for cross-comparison, the

business ideas of kiln owner, tourist view are close to the cultural & creative dealers, this is able to verify that this reuse of brick/tile kiln space and transformation strategy is a successful case.

5. Conclusion

This article explores the historical meaning of brick/tile kiln industrial culture assets in Taiwan,

according to the results of literature review, personal experience of participating the visiting activity in the brick/tile kiln, questionnaire survey and expert interview, organize and analyze/investigate the satisfactory degree of brick-tile kiln reuse strategy from the tourists. Data integration, statistical analysis, result analysis, reduce questionnaire variables, simplify to obtain the common needs tendency and expectation of kiln industry business model from the tourists, categorize into 4 major dimensions, add with expert interview, interview with the operator of brick-tile kiln, cultural & creative dealers, art workers for comparison, verify that this reuse of brick/tile kiln space and transformation is a successful business strategy.

The summarized research conclusions are described as follows:

- i. Diversified business model of San-He tile kiln: Operate the traditional making of brick/tile in parallel with the cultural & creative merchandises, and link with Kaohsiung-Pingtung old iron bridge landscape, old kiln culture combines with leisure tourism, provide the feasible strategy for the old industry and spatial reuse.
- ii. San-He tile kiln takes the traditional craft combined with the young craftsmen, participant the craft design exhibition regularly, establish diversified marketing channels, cultural & creative products adopting together with LOGO recognition, establish the new thinking with both of product practicality and artistry.
- iii. San-He tile kiln is able to coordinate with the overall community creation, cultivates the local new craftsmen, explore the pass, present and future of kiln industry from the history, geography, culture, economy, arts etc., in order to extend education to help the next generation paying more attention to the preservation of traditional technology & culture.
- iv. The overall environment, Exhibits and exhibition space of brick/tile kiln allow the visitors enjoying cultural and spiritual relaxation, cultural products and art space environment, attract the re-visit willing of tourists.

As shown from the research survey, San-He tile kiln shall combine with the government entity power in the aspect of environmental space planning, improve the tourism road signs and marks, and the river sewage water in front of its entrance, and then be able to completely enhance the comfortable level of overall environment.

Reference Literatures

1. Su Ying-Yu, 「An Exploration and Analysis of the Space Reutilization and Transformation Strategies of Brick and Tile Kilns -San-He Tile Kiln as an Example」, Master Thesis, Department of Construction Management, Chung Hua University, Hsinchu 2013.
2. Huang Hai-Ming, "Promote the Reuse of Vacant Space Operating Reference Manual", Ministry of Culture of the Republic of China, Taipei, 2003.
3. Chen, Ching-Tju, 「A Study of Application the idea of Environmental Symbiosis to the Regeneration of Historical Buildings - A case study of the Red-House of West Gate Market in Taipei」, Master Thesis, Graduate Institute of Architecture & Urban Design, Chinese Culture University, 2000.
4. Xue Qin, "Change of Taiwan Historical Space from Preservation to Re-use", Graduate School, Cultural Assets, Chung Yuan Christian University, 2001.
5. Xiao Li-Hong, Huang Rui-Mao Edited, 「Creative Programming in Reuse of Space : An International Perspective」, Ministry of Culture of the Republic of China, Taipei, 2002.
6. Chen Shun-Yu Writing, 「Multivariate analysis Third Edition」, Huatai Bookstore.
7. Wu Ming-Long Writing, 「SPSS Statistics Application Learning Practice」, Yi Xi Books.
8. Sun Yan-Ling, Ho Yuan, Li Yang-Xu, Writing, 「Learning SPSS Statistical Analysis from Examples」, DrMaster Press Co., Ltd.

The Research on the Influence of Economic Benefit for High-Rise Buildings Constructed by Different Excavation Method – Taking of Residence Buildings at New Taipei City as Example

Ching-Jung Chang¹, Cheng-Min Yang², Hsiu-Hsiung Hsu³

Department of Construction Management, Chung Hua University

707, WuFu Rd., Sec. 2, Hsinchu 30012, Taiwan

E-mail: cjchang@chu.edu.tw¹, m10316009@chu.edu.tw², andy@mail.cylee.com³

Abstract

The application of engineering technology could influence the cost and progress, and the excavation method for the infrastructure might cause significant difference of construction planning and cost. This research studies the construction time and cost efficiency for various infrastructure excavation methods. Based on the designed case, carry on the evaluation of construction time, construction price, and performance in accordance with different excavation method. It could provide the developer to select the best method at the initial design and planning stage, in order to obtain the highest benefit.

Keywords: Top-down Construction, up-up Construction, the high-rise buildings, the diaphragm wall

1. Introduction

In the metropolis, there is limited land with the overcrowding in Taiwan, so the building land was difficult to get in the downtown. Because of overcrowding, convenient traffic and life function, it caused the expensive land costs [1]. The developer always expected the project could achieve the high benefit and satisfy the parking requirement, which was the trend for high-rise buildings and deeper infrastructure excavation in the metropolis. This paper tried to study the performance of deep excavation method on construction time and cost efficiency.

The construction industry is changed from the constructor into the project administrator gradually, to ensure the execution life cycle of project can be controlled in a predictable range [2]. If the same scale and type of project is implemented by different construction method, there will be a significant difference for the cost efficiency. There is unique

property and different management method for various construction projects, so the risk management of construction project are higher than other industries.

From the data of government, this paper first reviews development trend of the domestic real estate in recent ten years as fig.1, in order to understand the prosperous fluctuation situation of construction industry. The prosperity pulse of construction industry is closely to the domestic and international economic boom. This paper uses the excavation methods commonly used for high-rise buildings, as bottom-up, top-down and up-up construction, to evaluate the construction time and cost efficiency. An actual project was studied to assess and compare in order to get the most favorable construction time and cost efficiency to the developer.

2. Literature

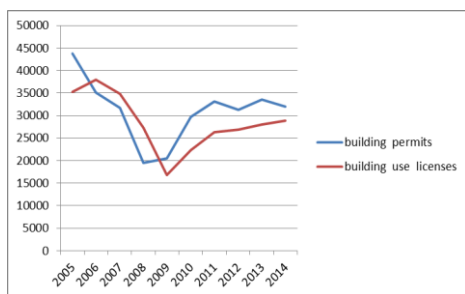
In Taiwan, the construction industry was integrated the planning, automation, financial administration and risk management instead of the previous labor intensive. The

selection for the method of construction project has close relationship with the cost. The price of material, the different technique, equipment, personnel and schedule might cause direct or indirect influence.

The land developers always follow the market trend and expect to construct the building by faster and economic way. If the infrastructure of high-rise buildings took the tradition excavation and supported it might be increase duration due to the topographical, weather factors or space limited and poor management [3]. For the mention reasons, the innovative research, expert and scholar develop Top-Down Method and Up-Up construction method to overcome the dilemma [4].

The quantities of building permits and building usage licenses showed in Fig.1, issued by Taiwan Government from 2005 to 2015, reveal the information that the constructor could make the investment opportunity by following the wave band peak of house market [5].

Fig. 1 Construction permit and usage permit issued by Taiwan Government



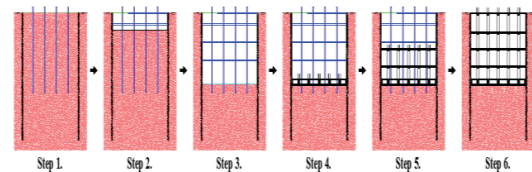
2.1 Excavation Method

Because of the fast development of economy and construction in the 1970s, the high-rise buildings were built gradually at urban area in Taiwan. Most of the excavation of infrastructure used the Bottom-Up construction method. Because of the space limited for working requirement and duration reduce, the contractor used the new technology by the Top-Down construction method. This method could construct both the Superstructure and infrastructure simultaneously after completing the ground floor, which would get the result of shortening construction time. The Up-Up method was even developed subsequently, the various methods were used with different project and building condition.

2.1.1 Bottom-Up Method

The Bottom-Up construction method normally followed the procedure 1. making the diaphragm wall 2. complete piling works 3. king post work 4. excavation 5. horizontal supports. After finishing the mat foundation, the basement structure was constructed from the bottom of the basement to the top floor.. The construction procedures are shown in Fig. 2. [7]

Fig. 2 The construction sequence of Bottom-Up Method

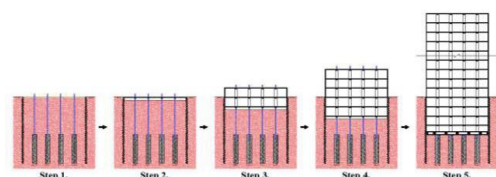


Most of the building project adopted the Bottom-Up construction method, because the construction procedure is simple, suitable for general medium-scale buildings without special construction time requirement etc., all regard this method as the prior choice.

2.1.2 Top-Down Method

First to construct the diaphragm wall and the bore-pile foundation with Steel stanchion place, afterwards completed the ground floor to be transition floor. This method could construct both the Superstructure / infrastructure at the same time after completing the transition floor. During the excavation, the building structure would become the horizontal supports, and the completed bore-pile foundation with steel stanchion place work as the vertical support. Because of the Superstructure / infrastructure could construct simultaneously, which would arrive the target to shorten the construction duration. The infrastructure construction for the building constructed from top to bottom, so the construction method was known as the Top-Down. Its construction procedures are shown in Fig. 3. [7]

Fig.3 The construction sequence of Top-Down Method



The Top-Down method constructed both the Superstructure and infrastructure at the same time, which could effectively shorten construction duration and avoid the neighboring building security during the construction period [6]. This construction method required with complicated technology and might meet more unexpected risk, so this method was suitable for large-scale building with space limited and tight schedule requirements.

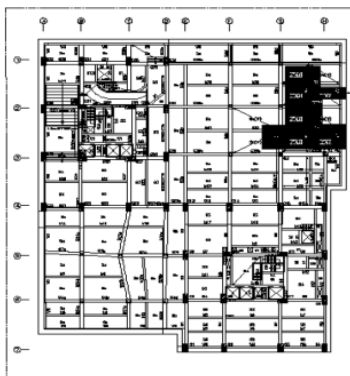
2.1.3 Up-Up Method

For the target to shorten the project duration, the contractor always expected to construct both the Superstructure and infrastructure at the same time. They modified the top-down method and developed the up-up construction method, whose procedure as 1. the diaphragm wall 2. piling work 3. king post work 4. excavation and support 5. Repeat the step 5 and finished the mat foundation 6. construct the Superstructure structure from 1st floor up 7. construct the infrastructure structure from mat foundation up to ground floor. The infrastructure structure excavation and each layer of excavation support and finish, and after finishing in lower structural raft base, can carry on the first floor edition and construct at once. The UP-Up construction method constructed both the Superstructure and infrastructure simultaneously.

3. Case Study

The case was the high-rise building in New Taipei City. Its plane drawing of building is shown in Fig. 4.

Fig. 4 The Plan of the case study building



3.1 Difference Analysis for Excavation Method to Construction Time, Cost

Because the construction complicated, difficult degree and construction condition, the various method were with different duration and construction cost. This case on the initial planning stage, the planner made analysis by the Bottom-Up, Top-Down, and Up-Up construction method to evaluate the benefit on duration and cost. The owner finally adopted the Top-Down Method through the research before the construction.

To consider the geological condition with liquefaction reaction, the building project designed the deep foundation with boring-pile which prevent the effect of liquefaction of soil. All of the three construction method designed in same condition with boring-pile.

The various construction method was exhaustive planned and made analysis, the infrastructure could be completed in 209 days by Top-Down Method. The Bottom-Up method took 380days and the Up-Up method took 254 days relatively. If the Top-Down method acted as a benchmark, the Bottom-Up method took more 171 days and the Up-Up method needs more 45 days. The cost estimations were NT\$ 50,142,815, 30,939,065 and 40,706,905 for the Top-Down, the Bottom-Up and the Up-Up method relatively. If the Top-Down method acted as a benchmark, the Bottom-Up method took 1.52 times and the Up-Up method needs 1.23 times.

4. Conclusion

The infrastructure was constructed by the Top-Down Method to get 171 and 45 days less compared with the Bottom-Up and the Up-Up Method respectively. The construction cost of Top-Down Method was 1.52 times of Bottom-Up Method and 1.23 times of Up-Up Method. Although the construction cost of Top-Down Method was most expensive, it created more value and benefit than the other two methods due to the construction duration saved. The overall benefit can be summed up as follows:

1. As for higher construction cost of Top-Down Method, because upon excavating, the steel columns have to be used as the support, the PC has to be used at every floor, the consumption of forms is higher, and the non-shrink cement has to be used at the joint of piles.

The high construction cost can be compensated by the short construction time.

2. As for shorter construction time of Top-Down Method, because after the end of story change, the upper part structure and underpart structure can be constructed at the same time. When the construction time and urban space are limited, the largest benefit can be developed.
3. Only the benefit of construction time and construction cost of the project is studied in this case. The next research goal will focus on the interest effect of construction time and the expedient analysis.

5. References

1. Shu, H. H., "Study on the Influence of Excavation Methods to the Construction Cost and Time of High-Rise Buildings - Taking of Residence Buildings at Xinzhuang District of New Taipei City as Example", Master Thesis, Department of Construction Management, Chung Hwa University, June 2013.
2. Shen, S. C., "Investigation of Hidden Costs for Building Construction – A Case Study of Top-down Construction Building Projects", Master Thesis, Department of Civil Engineering, National Central University, June 2008.
3. Huang, W. L., "Construction Build to Use Wall-type Foundation and Other Manner Results to Analyze Research", Master Thesis, Department of Civil Engineering, National Central University, November 2008.
4. Paek, J. H., and Ock, J. H. (1996), "Innovative Building Construction Technique: Modified Up/Down Method", *J. Constr. Engrg. and Mgmt.*, ASCE, 122(2), 141–146.
5. Lee, H. S., and Lee, J. Y. (1999), "Nonshored Formwork System for Top-Down Construction", *J. Constr. Engrg. and Mgmt.*, ASCE, 125(6), 392–399.
6. Wu, C. H., "Investigations of the Variations of Unit Prices and Cost-down Methods", Master Thesis, Department of Civil Engineering, National Chiao Tung University, 2005.
7. Chang, C., J. Hsu, H., H., and Lee, C., H., "Evaluation of the Construction Cost and Time for Different Excavation Methods on High-Rise Buildings", the Nineteenth International Symposium on Artificial Life and Robotics 2014, Beppu, Japan, Jan. 22-24, 2014

Redefining robot based technologies for elderly people assistance: a survey

Luigi Pagliarini^{1,2} Henrik Hautop Lund¹

¹Center for Playware, Technical University of Denmark, Building 326, 2800 Kgs. Lyngby, Denmark

²Academy of Fine Arts of Macerata, Via Berardi, 6, 405111 Macerata, Italy

E-mail: luigipagliarini@gmail.com
www.playware.elektro.dtu.dk

Abstract

We analyse the state of the art of hi-tech and robot based technologies in terms of Assistive Technology for all patients and, in particular, elderly people assistance and everyday activities aid. We focus on different aspects and characteristics of these tools, such as *playfulness, invasiveness, learning-speed, efficiency, short and long-term effect, active vs. passive, etc.* We do so by showing the most important existing examples, and by taking into account all the possible factors that might help researchers when thinking of developing appropriate technologies for elderly care, as well as, for their relative assistance personnel. Indeed, while in rehabilitation robotics, a major role is played by the human-machine interface (HMI) used to gather the patient's intent from biological signals, and convert them into control signals for the robotic artefacts, surprisingly, decades of research have not yet declared what the optimal HMI is in this context [1]. Further, there is an urgent need to clarify how various technologies can be a goal or an approach for preventive, rehabilitative and assistive interaction. Therefore, we try to make a first step towards a redefinition of Robotics Assistive Technology.

Keywords: Assistive Technology, Robotics, Prevention, Rehabilitation, Healing, Production.

1. Introduction

Quite recently, a new field has emerged from both private and public research that has been denominated Assistive Technology. In few cases such research reaches the final state, and releases specific Assistive Technology Products. As matter of fact, Assistive Technology seems to be a generic definition [2] that aims at covering technologies, services, apparatus, products as well as systems mostly used by disadvantaged people, like disabled and elderly ones. The aim is to increase those people's quality of life by helping them reaching the best possible autonomy either in social or private life. In other words, it means giving them the chance to recuperate their impaired or weakened skills, both motor and cognitive ones so that they can execute tasks, which might have become too difficult or too dangerous to them.

Therefore, the definition of assistive technologies relies on the classification of either social or medical models of disability. This is an important point that tends to distinguish ludic productions from assistive technologies themselves. Although, this is surely a good way to look at Assistive Technology, along this paper we will try to enrich such a vision by including in the set of Assistive Technology Products tools that might work at a *prevention* level, a level that from our point of view is still one of the most desirable ones.

Normally, the definition of assistive technology products, as described by Hersh [3], can be classified in at least five "flexible" categories, such as:

- *Mainstream Products* (i.e. general population products that are available everywhere);

© The 2016 International Conference on Artificial Life and Robotics (ICAROB 2016), Jan. 29-31, Okinawa Convention Center, Okinawa, Japan

- *Universal Design Products* (i.e. products that are conceived to be used by the largest possible group of users) ;
- *Assistive Products* (i.e. designed to remove barriers for elderly and disabled people);
- *Rehabilitation Products* (i.e. products designed to restore functions in elderly and disable people);
- *Medical Products* (i.e. products designed to support a range of health care practices and promote healing).

It is to be noticed that the difference between assistive and rehabilitative products stand in the fact that the assistive products modify the people interaction with the environment by removing the “obstacles” in some way, while the rehabilitative ones are meant to directly re-enable persons, in order to overcome their “limitations”.

Once such a product is released, there are a number of different ways of classifying evaluation and evaluation methods (e.g. evaluation can be purely evaluative or diagnostic). By generalising a categorisation inherited from human computer interaction [4], assistive products gives at least four classes:

- *Analytical methods*: specialists manipulate system models to predict performance.
- *User reports*: users work with representations or their memories of particular products. (i.e. interviews and questionnaires, etc.).
- *Specialist reports*: human factors specialists or other professionals assess real products, prototypes or simulations.
- *Observational methods*: real users assess real products, prototypes or simulations.

Considering the pragmatic of productions, it has been proven that there are factors that are most important in product success and product screening decisions, as well as factors that influence decisions on whether or not to discontinue a product. They are somehow crucial in understanding the effective value of a product and they include [5, 6, 7, 8]:

- Product advantages and expected market reaction;
- Expected financial potential, including market share, sales and market growth and expected profitability;
- The implications for the firm's financial, physical and human resources;
- Fit to current business, organisation, technology, marketing and managerial skills;
- The potential or availability of new products and alternative opportunities, as well as the product range policy.

In this perspective, we will here report some examples of Assistive Technology Products based on Robotics and will compare them to both review the state of the art in such fields’ intersection, and to try to underline how it fits with the general standards of Assistive Technology.

2. Assistive Technology - Examples

The first examples of Assistive Technology Product we present are the HONDA Walking Assist Device and its Cyberdyne precursor HAL (Fig. 1). They both represent the classical Assistive Technology devices designed to remove barriers for elderly and disabled people, and that help users to support bodyweight to reduce the load on the user's legs while walking, going up and down stairs, and in a semi-crouching position.

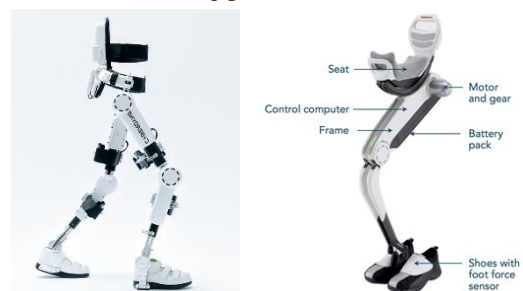


Fig. 1. Cyberdyne HAL, and HONDA’s Walking Assist Device

Both HAL and Walking Assist are examples of an efficient production that is professionally evaluated throughout specialist reports. They both fit their firm’s current business, organisation, technology, marketing and managerial skills and financial potential, including a big potential market share. In other words, in their assistive niche, they represent the perfect product and

product design, although they almost exclusively act in the no-rehabilitation zone.

On the same line are the Assistive Robotic Manipulator, as InMotion's Arm, Wrist, Hand and Exoskeletal Arm Robot produced by the Interactive Motion Technologies. These technologies should help patients with Stroke, Cerebral Palsy, Traumatic Brain Injury, Spinal Cord Injuries, Multiple Sclerosis, and Parkinsons to add a level of independence to their lives. These products are evaluated either by the patients and the specialists are well tested and seem to be promising for Assistive Technology Clinical practice, at least.

Further, there are a long number of productions oriented towards becoming caregiver robots. Amongst them, the RIBA (or Robear) developed by researchers at RIKEN and Tokai Rubber Industries (TRI) is the most advanced example. It is in between an Assistive and a Medical Product since besides removing barriers, it is meant to take care of patients, substituting some nursery functions. Besides those, there are other fields of research, like for



Fig. 2. The RIBA Robot lifting a patient.

example Socially Assistive Robotics - see "The Robotics Primer" [9] for further information - which are currently trying to develop robot-assisted therapies for children with autism spectrum disorders, stroke and traumatic brain injury, and individuals with Alzheimer's Disease and other forms of dementia. But, despite of the fact that the field seems to be promising and important, and with some good indications from the Paro robot by Shibata, there is not an effective Assistive Products outcome, yet.

On the contrary, on the side of what we will here call *Active Assistive Robotics* the production can be considered much more concrete. One example could be RoboCoach, developed by Yaacob Ibrahim at the Ngee Ann Polytechnic, that coaches the elderly in performing 15 types of arm exercise each week, recognizing a human voice that tells it to start the workout.



Fig. 3. RoboCoach.

Vice versa, on the Rehabilitative Robotics Products side there seems to be a quite fruitful production that results in an enlarging number of companies specialized on different branches of artefacts. *AlterG Inc.*, that makes anti-gravity treadmills and bionic legs for athletic training and physical therapy. *Ekso Bionics*, that makes robotic exoskeletons providing gait training and neurorehabilitation by extending the individual's strength and also helping the therapist to work with their patients. *Hocoma*, that provides spine evaluation devices that enables computer-assisted analysis and display of the spine's shape and mobility, or robotic gait orthosis in which the patient's legs are guided to a pre-programmed physiological gait pattern on the treadmill. *Bioextreme*, specialized in robotics rehabilitation innovative Error Enhancement treatment for patients. *Intead Technologies* and *Kinestesica*, specialized in neuromotoric disorders. A very interesting approach is the one from the *Kinetic Muscles* that is merging digital gaming, robotic, and telemedicine technologies with the most up-to-date discoveries in neurorehabilitation science to provide solutions that are practical and clinically effective for engaging post-stroke rehabilitation. *MediTouch*, that produces wearable motion capture devices and dedicated rehabilitation software that allow patients with upper and/or lower extremity movement dysfunction to practice intensive virtual functional task training. *SynTouch* that makes the only sensor technology in the world that endows robots with the ability to replicate the human sense of touch, or *TouchBionics* provider of world-leading prosthetic technologies and supporting services. Besides them, the technologies realized by *Kinova*, *Rehab-Robotics*, *Reha-Stim*, *YouRehab* and the above mentioned *Interactive Motion Technologies* are very interesting.

All of them work with patients suffering from partial spinal cord injuries, strokes, multiple sclerosis, traumatic brain injuries, cerebral palsy, Parkinson's disease: generally speaking with nervous system injuries and patients with minimal forearm strength and problems in standing and walking. Some of these have a mainly *passive* approach while other push a *proactive* exercising. Amongst these last ones a few are also targeting *playfulness* as a philosophy. They also differ as level of Human-Machine Interface (HMI) *invasiveness*, although in different cases appropriate and engaging HMI design to be the only effective way.

On the *Robotics Medical Products* side, there is a large production. Medical apparatus, especially in surgery, are day-by-day moving towards a robotics-based practice. As, for example, Magnetic Microbots, a group of tiny robots used in various operations, such as removing plaque from a patient's arteries or helping with ocular conditions and disease screenings. In short, robotic advancements are used to better the day-to-day lives of patients, helping them eat (e.g. Bestic Arm), or helping a patient regain her ability to walk (e.g. Toyota's Healthcare Assistants). Obviously, robotics is a very attractive industry since within the hospitals, a robot's work can fulfil the full-time work of one or more employees (e.g. Aethon TUG) and outside of them caregivers use robots to enhance telemedicine and care for those restricted to their homes (e.g. Vasteras Giraff) or, surprisingly enough, in the open (e.g. Anybots). Some of them are playful and non-invasive ones, as those used to enhance the therapy of developmentally disabled children between 5 and 12 years old (e.g. CosmoBot).

On the Mainstream and Universal Design Products side there is a large number of contributions which mainly focus their attention on fitting products in the ecological system of humans. Therefore the products try to be portable, fit in the apartment or outside homes trying to follow the scheme of the "walk up and use" design philosophy, to be scalable, to allow user to initiate interaction, to provide different choices for any given task, to provide multiple and multimodal output and feedback, to provide mutable functionality and to target the largest number of people and contexts. See [10] for further information.

Good examples can be considered the iRobot products, the Toyota's i-REAL, the Universal Robots products, and many other products for the toys and gaming industry (e.g. WowWee) or, sometimes, those that are specifically

targeted for the assistive technology market (e.g. Cyberdyne).

3. Moto tiles

In this context, we present our *Moto tiles*, robot tiles that light up when you touch them and that are mostly used to improve the balance of the elderly, and strengthen their muscles and endurance with a high grade of efficiency, as it has been demonstrated by scientific tests [11, 12]. Despite of their specific Medical Technology target and rehabilitative application, Moto tiles use can be easily translated in quite different contexts since they fulfil almost all of the typical criteria of the Universal Design Products. Their use is easy to learn. They are multimodal and can easily adapt to any kind situation, either indoor or outdoor, since they are very portable, reconfigurable and well fit to any context and user's age. Therefore, they might be used either as gaming or educational platform. More than that, they show their best when combining playfulness with fitness, rehab or educational exercises, all together. Besides, if compared with the mainstream assistive technology or medical technology products, they show their peculiarity in being a mostly "active" tool. Indeed, the software platform they use promotes users' motor and/or cognitive activation at the best and tends to adapt to the rate of users' responses in a fairly adaptive way.



Fig. 4. Moto tiles – an example of an *active* tool for prevention and rehabilitation (www.mototiles.com).

Furthermore, they represent a rather unique example of Assistive Technology Robotics applied to "*prevention*", a "medical zone" which is rarely considered within the field and that, on the contrary, might represent one of the most important fields of robotics applications, in the future.

In other words, the Moto tiles might represent, by themselves, a new dimension of how to apply robotics within an Assistive Technology context, by promoting

the idea of cure as “prevention” and therefore by stressing the “activation” at its best. The Moto tiles also show how, by focusing on such a direction, Assistive Technology can reach important results in either short or long term effects.

4. Discussion and Conclusion

In this paper we discussed the most important general principles of Assistive Technologies and, in particular, analysed the state of the art Robotics Assistive Technologies. At a first sight, it seems that much is to be done and that despite of decades of research, both the optimal HMI in this context is still to be understood and the borders of such a field is to be defined. We also reported the most successful examples of market and science industries trying to underline differences amongst what is to be considered a good or a bad example of production. By doing that we also highlighted the different application fields and how production itself is moving within them, by providing possible solutions under different circumstances.

In this context, we presented the Moto tiles robotic system as an innovative example on how to approach Assistive Technology, by opening new fields of application and new approaches to users’ attitude. Indeed, in our opinion, it is important to continuously change the philosophy by which we approach robotics (i.e. either as research and as an applicative field of production), trying to find new technological and behavioural scenarios that better fit to users’ need of easily understanding and use of technology in assistive, rehabilitative, and preventive robotics. We believe that, ideally, as already happened in telecommunication technologies, user and patient oriented robotic technologies must get simpler, adaptable, and enlarge the range of action as much as possible.

References

1. http://journal.frontiersin.org/article/10.3389/fnbot.2014.00024/full?utm_source=newsletter&utm_medium=email&utm_campaign=Robotics_and_AI-w49-2015
2. M.A. Hersh, and M.A. Johnson. Assistive technology for visually impaired and blind people. (Springer Verlag. 978-1-84628-866-1. 2008)
3. M.A. Hersh. 2010. The Design and Evaluation of Assistive Technology Products and Devices Part 2: Evaluation of Assistive Products. In: JH Stone, M Blouin, editors. International Encyclopedia of Rehabilitation.
4. A. Whitefield, Wilson F, Dowell J. 1991. A framework for human factors evaluation. Behaviour and Information Technology 10(1):65-79.
5. G. J. Avlonitis 1993. Project Dropstrat: what factors do managers consider in deciding whether to drop a project. European Journal of Marketing 27(4):35-57.
6. Brentani de U. 1986. Do firms need a custom-designed new product screening model. Journal of Product Innovation Management 3:108-119.
7. J. R. Schmidt, Sarangee, KR, Montoya MM. 2009. Exploring new product development project review practices. Journal of Product Innovation Management 26:520-535.
8. X. M. Song, Parry ME. 1996. What separates Japanese new product winners from losers. Journal of Product Innovation Management 13:422-439.
9. <https://mitpress.mit.edu/books/robotics-primer>
10. <http://repository.cmu.edu/cgi/viewcontent.cgi?article=1044&context=hcii>
11. H. H. Lund, Modular Robotics for Playful Physiotherapy, in Proceedings of IEEE International Conference on Rehabilitation Robotics (IEEE Press, 571-575, 2009)
12. H. H. Lund, and J. D. Jessen, Effects of short-term training of community-dwelling elderly with modular interactive tiles. *GAMES FOR HEALTH: Research, Development, and Clinical Applications*, 3(5), 277-283, 2014.

Disrupting the Industry with Play

Henrik Hautop Lund

Center for Playware, Technical University of Denmark, Building 326, 2800 Kgs. Lyngby, Denmark

E-mail: hhl@playware.dtu.dk

www.playware.elektro.dtu.dk

Abstract

Decades of research into intelligent, playful technology and user-friendly man-machine interfaces has provided important insight into the creation of robotic systems and intelligent interactive systems which are much more user-friendly, safer and cheaper than what appeared possible merely a decade or two ago. This is significantly disrupting the industry in several market sectors. This paper describes the components of the playware and embodied artificial intelligence research that has led to disruption in the industrial robotics sector, and which points to the next disruption of the health care sector. This includes playful robotics, LEGO robots for kids, minimal robot systems, user-friendly, behavior-based, biomimetic, modular robotics and intelligent systems. The insight into these components and the use in synthesis for designing robots and intelligent systems allows anybody, anywhere, anytime to use these systems, providing an unforeseen flexibility into the sectors, which become disrupted with these systems.

Keywords: Playware, user-friendly, modular robots, playful robotics and intelligent systems.

1. Introduction

Over the last half century, most robots have been characterized by being large, squared, metallic and hard objects, which are controlled by fairly complicated control software to the novice user. This led to large robots, for instance employed in the heavy industries in car factories, shipyards, etc. installed by highly skilled engineers. These robots were automatic in the sense that they were self-regulating, but did not make the laws that their regulatory activities seek to satisfy. These laws were given to the robot, or built into the robot. They were done so by engineers with years of training, and experience with control theory and practice. In many cases, the large, squared, metallic and hard robots were kept in a cage to perform their actions in order to screen away human beings for security reason, since being hit by one of the large robots could be deadly to a human being.

Since these industrial robots had their clear place in automating the industry, it became standard to develop and utilize such robots with this approach, and most researchers and roboticists would adhere to this standard.

Nevertheless, decades of research into intelligent, playful technology and user-friendly man-machine interfaces has provided important insight into the creation of robotic systems and intelligent interactive systems which are much more *user-friendly*, *safer* and *cheaper* than what appeared possible merely a decade or two ago, and this is now disrupting the industry.

2. Play and playful robotics

The basis of such disruption of the industry is the quest to create truly user-friendly robotic systems. Since the 1990's, with a bottom-up approach, we have investigated how to create minimal robot systems that are playful to interact with, in order to develop technological systems

that anybody can interact with. Play is important, since play is a free and voluntary activity that we do for no other purpose than play itself [1]. We play for the enjoyment. So installing play in the interaction can lead to people interacting with the system out of their own free will and enjoyment. Further, when in play, people performs an ontological shift according to Gadamer [2], and almost become another representation of themselves when they forget about time and place. In such a state of being, i.e. in a play dynamics, people can often perform more than they would normally do [3].

The first playful robot systems were in the form of Khepera miniature robots and LEGO robot prototypes, before we started the collaboration with LEGO on the development of LEGO Mindstorms robots. The development of these robotic systems in the 1990's facilitated the development and practical experimentation of modern artificial intelligence with artificial life experiments, evolutionary robotics, user-guided evolutionary robotics, and user-guided behavior-based robotics.



Fig. 2. A robot orchestra that we developed for the LEGO Mindstorms promotion tour in Europe in late 1990's.

Despite of the core research effort in these embodied artificial intelligence themes, all experiments had the underlying focus of creating robotic and interactive systems that anybody – even young children – could interact with and understand within minutes. This focus on the user and understandable interaction for anybody within minutes distinguished the research and development from the traditional robot, automation, and control research.

© The 2016 International Conference on Artificial Life and Robotics (ICAROB 2016), Jan. 29-31, Okinawa Convention Center, Okinawa, Japan

The experiments resulted in an understanding of how minimal robot systems can result in task-fullfilling behavior guided by the user in different ways. One example is the development of *user-guided behavior-based systems*, in which the engineer develops the primitive behavior modules, and the end-user is allowed to combine the primitive behaviors to coordinate these into the overall behavior of the robotic system. Since the engineer performs the difficult task of handling the details (e.g. reading, interpretation and classification of sensory signals; and complicated motor commands) in the design and debugging of the primitive behaviors, the end-user can work on the higher abstraction level of combining these primitive behaviors with no need of knowledge of the (more complicated) low-level details. This approach of creating user-friendly robot control for any user with user-guided behavior-based systems was developed and verified on LEGO Mindstorms robots for RoboCup Junior [4], for the LEGO Mindstorm Europe launch tour with a robotic orchestra, robot fashion show, and robot art show, for the RoboCup Humanoids Freestyle World Champion 2002 [5]. Further, it became the basis for the development of *user-friendly modular robotic systems* such as the I-Blocks [6], in which each of the primitive behaviors is a module, and the user is allowed to physical build with the modules to create the overall robotic system. Further, this became the inspiration to create other user-friendly modular robotic systems such as the music cubes, MusicTiles MagicCubes, modular interactive tiles [7], and Moto tiles (www.mototiles.com).

3. Disrupting the Industrial Robot Sector

Based on these studies of playful robotics as user-friendly interfaces, our students during a decade went on to form the Universal Robots company to create an industrial robot arm, which should be light-weight, safe, and easily programmable by anybody.

Indeed, the founder of Universal Robots, Esben Østergaard reports that “in the mid 90's, we built robots with pure ferocity. It culminated in 1998 when we won the football World Cup for robots, which was seen by 50 million people. Football robots could be programmed by children without any technical knowledge, and if children can learn to program robots, then all people can learn it.

This approach was one of the fundamental values of our company Universal Robots. We found out that Danish food companies needed to be able to adapt quickly. It was absolutely impossible to do that with the existing robots. So we built a robotic arm that could be reprogrammed easily and without specialist knowledge, and the idea turned out to be pretty good.” [8]



Fig. 2. One of the Universal Robots industrial robot arms.

Indeed, Universal Robots created such robotic arms, which suddenly made it feasible for SMEs to invest in robots and automation, since the SMEs could afford the robot arm and could easily adapt the robot arm to new processes. This disrupted the industrial robot industry, the Universal Robots company was sold for 285 million USD to Teradyne, and most other robot companies had to follow up to create similar light-weight, safe and user-friendly robotic arms. A good example is Rodney Brooks’ Rethink Robotics company and their Baxter robot. Like the Universal Robots company did, also Rethink Robotics tries to develop user-friendly robots that anybody can control by allowing the factory worker to grab the robot arm and show the robot what to do by moving it around while the robot learns what to perform and with which objects.



Fig. 3. Robots from Rethink Robotics and Universal Robots.

Further, crowdfunding sites such as Kickstarter are seeing several projects funded to build low-cost table-top robotic arms for personal use, e.g. for the maker movement and light manufacturing.

In our case, the lessons learned were that long-term focus on play and user-friendliness can lead to disruption of an industrial sector such as the industrial robot sector, where the growth now is characterized by the development and sales of such low-cost, user-friendly robots. The development of such robots was based upon the extensive knowledge gained in playful robotics, LEGO robots for kids, minimal robot systems, user-friendly, behavior-based, biomimetic, modular robotics and intelligent systems.

4. Disrupting the Health Sector

One of the next sectors to experience a similar disruption may be the health sector. In many areas of the health sector, patient compliance to the treatment is important. This is the case in prevention and rehabilitation, for instance, in which the subject is asked to perform a certain series of actions at regular intervals. But unfortunately compliance to the protocol is often low, due to little intrinsic motivation to perform those actions that may be viewed as tedious and repetitive.

Also here, play and playware may disrupt the sector by providing new technological opportunities that radically changes the way such practices in prevention and rehabilitation is performed. Play as a free and voluntary activity, which is performed for the personal enjoyment, may result in highly motivated patients, if the technology can mediate such playful engagement. At the same time, it may be possible to observe the *collateral effects of play* in the form of quantifiable health effects that exceeds the effects measured with traditional health intervention methods [9].

Therefore, we developed modular playware in the form of the modular interactive tiles called Moto tiles (www.mototiles.com). The Moto tiles activates the user to perform playful interaction with play and games on the tiles that light up in different colors and registers when users step on them. The Moto tiles are connected to a

tablet with the ANT+ radio protocol. On the tablet, the user can select between numerous games that challenge both the physical and cognitive abilities of the user. Further, the tablet shows the score in each games, shows statistics for the user, and make automatic documentation of effect.

Scientific studies of effect among community-dwelling elderly who perform group play on the modular tiles once per week show highly statistical significant effect on functional abilities of the elderly. Especially, the balancing abilities of the elderly (avg. 83 years of age) increase by more than 60% after merely 13 training sessions [10]. Also, all other measured functional abilities (strength, mobility, agility, and endurance of the elderly) improved with statistical significant effect.

Qualitative studies suggest that the high health effect from playing with the Moto tiles arises from the fact that the Moto tiles act as a play force, which pushes the participants into a play-dynamics, in which they forget about time and place, and thereby perform more than they would normally do. In play, they may forget about their fears of falling and forget about their perceived physical and cognitive limitations.



Fig. 4. The Moto tiles and the tablet interface.

With such quantifiable health effect results of play, we believe that playware technology may disrupt certain areas of the health sector. Already, the Moto tiles are used in the health sector for the benefit of cardiac patients, stroke patients, elderly citizens at risk of falling, dementia patients, children with cerebral palsy, and in special schools in three continents. As is the case with the disruptive technology for the industrial robot sector, also this disruptive technology for the health sector is based

on the possibility for the end-user to easily adapt to different tasks and practices, e.g. for different kinds of patients.

5. Discussion and Conclusion

The developments of disruptive technologies are based on the Playware ABC concept. The Playware ABC concept focusses on the development of technology to be used by anybody, anywhere, anytime based on building bodies and brains, and thereby facilitating that users can construct, combine and create. Indeed, the possibility for anybody to create new interactions with the systems seem to provide new opportunities, as is showcased in the industrial robot sector and health sector. At the same time, the concept leads to solutions that are cheaper, safer and more flexible than previous solutions in the sectors.

Acknowledgements

The author would like to thank colleagues at the Center for Playware, Technical University of Denmark.

References

1. J. Huizinga, *Homo Ludens*. (1938) (Homo Ludens. Beacon Press 1971).
2. H.-G. Gadamer, *Truth and Method*. (Crossroad, New York, 1989)
3. C. Jessen and H. H. Lund. On play forces, play dynamics, and playware. Unpublished manuscript.
4. H. H. Lund and L. Pagliarini, LEGO Mindstorms Robot Soccer. In *Proceedings of RoboCup'98, LNAI 1604*, (Springer-Verlag, Heidelberg, 1999).
5. H. H. Lund and L. Pagliarini, Modular behavior-based control for team humanoids. *Advanced Robotics*, 18(7), 659–676, 2004
6. H. H. Lund, Intelligent Artefacts. In Sugisaka and Tanaka (Eds.), *Proc. of 8th International Symposium on Artificial Life and Robotics* (Oita: ISAROB, 2003).
7. H. H. Lund, Modular Robotics for Playful Physiotherapy, in *Proceedings of IEEE International Conference on Rehabilitation Robotics* (IEEE Press, 571-575, 2009)
8. Børsen newspaper (In Danish), 22-09-2015.
9. H. H. Lund, Play for the Elderly - Effect Studies of Playful Technology, In *Human Aspects of IT for the Aged Population. Design for Everyday Life*. (LNCS Vol. 9194, pp 500-511, Springer-Verlag, 2015)
10. H. H. Lund, and J. D. Jessen, Effects of short-term training of community-dwelling elderly with modular interactive tiles. *GAMES FOR HEALTH: Research, Development, and Clinical Applications*, 3(5), 277-283, 2014.

Automated Multiple-Brightness Peak Image Processing Method Using Curvature and Variance Estimation

Yusuke Kawakami

*DynaxT Co., Ltd., 2217-6 Hayashi
Takamatsu City, Kagawa 761-0301, Japan*

Tetsuo Hattori, Yoshiro Imai, Yo Horikawa

*Kagawa University, 2217-20 Hayashi
Takamatsu City, Kagawa 761-0396, Japan*

R. P. C. Janaka Rajapakse

*Tainan National University of the Arts, 66 Daci
Guantian District, Tainan 72045, Taiwan*

E-mail: riverjp2002@gmail.com, {hattori, imai, horikawa}@eng.kagawa-u.ac.jp, janakaraja@gmail.com

Abstract

This paper describes the improvement method for the image which have multiple-brightness peak using Histogram Matching based on Gaussian Distribution (HMGD). The previous papers, we have illustrated that the HMGD is an automated image processing method for improve feeling impression better, through the comparative investigation results of feeling impression among the original image, Histogram Equalization image, and HMGD image. However, the multiple-brightness peak images have been hard to improve using the previous HMGD. In this paper, we propose the processing method of HMGD to correspond image which have multiple-brightness peak, using curvature computation and variance estimation.

Keywords: Image processing, Curvature, Variance estimation, Histogram matching, HMGD

1. Introduction

These days, automated image processing for enhancement of color images has been more familiar to us, for example, Digital Signage, Smart Phone, etc ¹⁻³.

In the previous paper, we have presented that the Histogram Matching based on Gaussian Distribution (HMGD) processing is one of the automated image arrangement method using Elastic Transformation ⁴⁻⁵ based on the brightness axis. And through the comparative investigation, we have illustrated that HMGD processing could improve feeling (or Kansei) impression better than original image⁶.

In this paper, we present the improvement HMGD processing method for multiple-brightness peak image using curvature computation and variance estimation of image histogram. We explain the principle of HMGD, and we also explain peak detection and variance

estimation of histogram. Last, we illustrate the results of the HMGD processing for multiple-brightness peak image through the experimentation.

2. Principle

2.1. Histogram Matching based on Gaussian Distribution

In the section, we explain the principle of HMGD processing.

Fig. 1 shows the conceptual image of HMGD. Let $f(x)$ and $h(y)$ be two probabilistic density functions (PDF) on real variables x and y , respectively. The PDF is corresponding to histogram of image brightness level which is discretely defined.

In addition, let $y=\phi(x)$ be a continuous and monotonic increase function corresponding to cumulative histogram

of image brightness level between variables x and y ⁷⁻⁹. And let $y=\phi(x)$ be defined by Eq. (1).

$$y = \phi(x) = L \int_0^x f(x) dx. \quad (1)$$

At first, we have to expand brightness level of original image histogram and convert into uniform distribution histogram, because we aim to match Gaussian distribution. From Eq. (1) and Fig. 1, we can derive Eq. (2) and (3).

$$f(x) = h(y)\phi'(x) = h(y)Lf(x). \quad (2)$$

$$h(y) = \frac{1}{L}. \quad (3)$$

We understand the histogram of original image $f(x)$ becomes uniform distribution $h(y)$ by Eq. (3). This means that brightness level of original image $f(x)$ is expanded to $h(y)$.

Then, let $Gauss(z)$ and $\gamma(z)$ be the function that is defined by Eq. (4) and (5), respectively.

$$Gauss(z) = \frac{1}{\sqrt{2\pi\sigma^2}} \exp\left(-\frac{(z-\mu)^2}{2\sigma^2}\right). \quad (4)$$

$$\begin{aligned} y = \gamma(z) &= L \int_0^z Gauss(z) dz \\ &= \frac{1}{\sqrt{2\pi\sigma^2}} \int_0^z \exp\left(-\frac{(z-\mu)^2}{2\sigma^2}\right) dz. \end{aligned} \quad (5)$$

Here, Fig.1 shows the relationship between $y=\phi(x)$ and $y=\gamma(z)$. So we can be obtained following Eq. (6).

$$L \int_0^x f(x) dx = \frac{L}{\sqrt{2\pi\sigma^2}} \int_0^z \exp\left(-\frac{(z-\mu)^2}{2\sigma^2}\right) dz. \quad (6)$$

And we can derive Eq. (7) from differential of Eq. (6).

$$\frac{d}{dx} L \int_0^x f(x) dx = \frac{d}{dz} \frac{L}{\sqrt{2\pi\sigma^2}} \int_0^z \exp\left(-\frac{(z-\mu)^2}{2\sigma^2}\right) dz. \quad (7)$$

If we perform Eq. (7),

$$L\phi'(x) = L\gamma'(z), \quad f(x) = Gauss(z). \quad (8)$$

That is, we understand that $f(x)$ becomes Gaussian distribution $Gauss(z)$ when we take the transform function as (1) and (5). Thus, HMGD processing is the function which defined by cumulative histogram

transformation the original histogram into Gaussian histogram⁹.

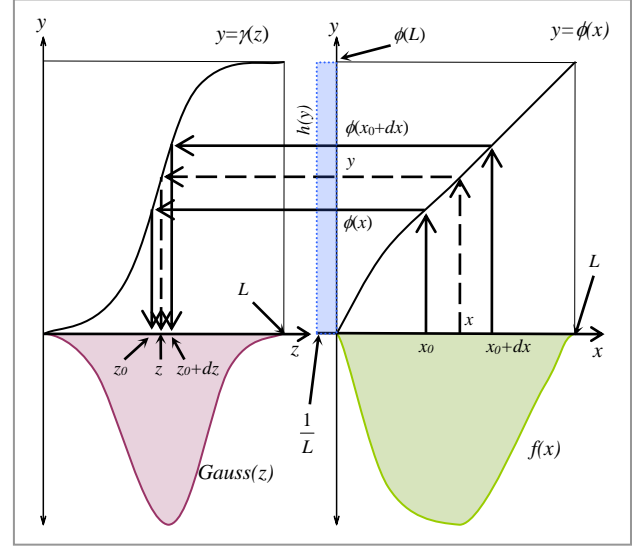


Fig. 1. Conceptual image of HMGD^{6,9}.

2.2. Peak Detection of Histogram

The HMGD processing method for multiple-brightness peak image need to calculate transforms function for each brightness peak of histogram. And the solution to detect it is curvature computation of the histogram.

Let y be a function with respect to x , the definition curvature R is given by Eq. (9)⁶⁻⁹.

$$R = \frac{d^2 y}{dx^2} \left(1 + \left(\frac{dy}{dx} \right)^2 \right)^{-\frac{3}{2}}. \quad (9)$$

Let $g(x)$ and K be Gaussian distribution function and a coefficient which is defined by following equation, respectively.

$$\begin{aligned} g(x) &= \frac{K}{\sqrt{2\pi\sigma^2}} \exp\left(-\frac{(x-a)^2}{2\sigma^2}\right), \\ \frac{K}{\sqrt{2\pi\sigma^2}} \int_0^L \exp\left(-\frac{(u-a)^2}{2\sigma^2}\right) du &= 1. \end{aligned} \quad (10)$$

Next, let $y=f(x)$ be a function representing the cumulative histogram which is represented Eq. (11). That is, dy/dx and d^2y/dx^2 be described as Eq. (12) and (13), respectively. From Eq. (12) and (13), we obtain the approximation of curvature R as Eq. (14).

$$f(x) = \int_0^x g(u) du = \frac{K}{\sqrt{2\pi\sigma^2}} \int_0^x \exp\left(-\frac{(u-a)^2}{2\sigma^2}\right) du. \quad (11)$$

$$\frac{dy}{dx} = g(x) \frac{K}{\sqrt{2\pi\sigma^2}} \exp\left(-\frac{(u-a)^2}{2\sigma^2}\right). \quad (12)$$

$$\frac{d^2y}{dx^2} = \frac{dg(x)}{dx} = \frac{(a-x)}{\sigma^2} g(x) \quad (13)$$

$$R = \frac{\frac{(a-x)}{\sigma^2} g(x)}{\left(1 + g(x)^2\right)^{\frac{3}{2}}} \approx \frac{(a-x)}{\sigma^2} g(x). \quad (14)$$

From Eq. (14), we understand that the curvature R varies the sign according to the value of x ⁹. That is, if $x < a \rightarrow R > 0$ (downward convex shape), and if $x > a \rightarrow R < 0$ (upward convex shape).

2.3. Variance Estimation

In this section, we propose how to optimize the shape of the reference histogram, which is used in the HMGD processing method for multiple-brightness peak image. Fig. 2 shows the conceptual image of the original image histogram which is variance σ^2 and average a . From Eq. (10), let $g(a)$ be a Gauss density function with variance σ^2 at average a .

$$g(a) = \frac{K}{\sqrt{2\pi\sigma^2}}. \quad (14)$$

Using Eq. (14), we can describe $g(a \pm \sqrt{2}\sigma)$ and its curvature as Eq. (15) and (16), respectively.

$$g(a \pm \sqrt{2}\sigma) = \frac{K}{\sigma\sqrt{2\pi}} \exp\left(-\frac{(a \pm \sqrt{2}\sigma - a)^2}{2\sigma^2}\right) = g(x) e^{\mp 1}. \quad (15)$$

$$R(a \pm \sqrt{2}\sigma) = \frac{(a - (a \pm \sqrt{2}\sigma))}{\sigma^2} g(a \pm \sqrt{2}\sigma) \left(1 + g(a \pm \sqrt{2}\sigma)^2\right)^{\frac{3}{2}}. \quad (16)$$

From Eq. (15), we can derive Eq. (17) and (18).

$$\begin{aligned} R(a \pm \sqrt{2}\sigma) &= \left(\mp \frac{\sqrt{2}}{\sigma^2}\right) g(a \pm \sqrt{2}\sigma) \left(1 + g(a \pm \sqrt{2}\sigma)^2\right)^{\frac{3}{2}} \\ &= \left(\mp \frac{\sqrt{2}}{\sigma^2}\right) \frac{g(a)}{e^{\left(1 + g(a \pm \sqrt{2}\sigma)^2\right)^{\frac{3}{2}}}} \equiv \left(\mp \frac{\sqrt{2}}{\sigma^2}\right) H. \end{aligned} \quad (17)$$

$$H = \frac{g(a)}{e^{\left(1 + g(a \pm \sqrt{2}\sigma)^2\right)^{\frac{3}{2}}}}. \quad (18)$$

Then, we understand that we can obtain reference histogram variance σ^2 from Eq. (17). For example, let $v = \sqrt{2}\sigma$ be the distance from average a ,

$$R(a-v) - R(a+v) = \frac{2\sqrt{2}}{\sigma} H = \frac{4}{v} H, \quad \sigma^2 = \frac{v^2}{2}. \quad (19)$$

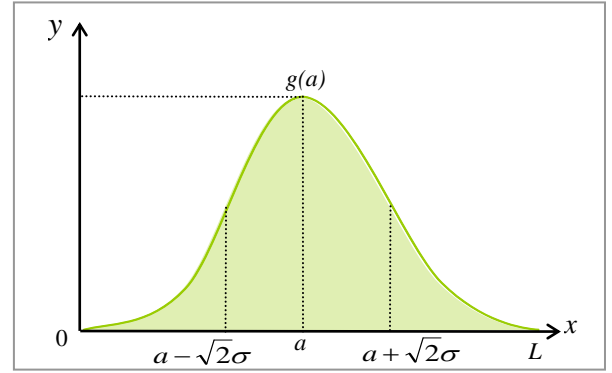


Fig. 2. Conceptual image of the original image histogram⁸.

3. HMGD Processing for Multiple-Brightness Peak

In the previous chapter, we have described about the principle for HMGD processing for multiple-brightness peak. In this section, we propose the concrete process of it.

- (i) Detect the brightness-peak values x_m ($m=1, \dots, n$) of original image histogram.
- (ii) Perform variance estimation and generate the reference histogram for brightness-peak value x_m .
- (iii) Perform HMGD processing and make an image i_m which has histogram h_m .
- (iv) Proceed to (v) if original image has no brightness-peak value. Otherwise, set the brightness-peak value to x_{m+1} and return to (ii).
- (v) Calculate the average of the HMGD processed image I_a using Eq. (20).

$$I_a = \frac{1}{n} \sum_{m=1}^n i_m \quad (20)$$

- (vi) Output the processed image I_a .

4. Experimentation

Fig. 3(a) shows the example of results for HMGD and HMGD-MBP for multiple-brightness peak (HMGD-MBP). And Fig. 3(b) and Fig. 3(c) show the corresponding histogram and cumulative histogram, respectively. In this case, we understand that HMGD-MBP processing image is enhancing contrast naturally than HMGD processing image. And in the HMGD-MBP image, the edges in the mountain (located left below of image) become clear and detailed.

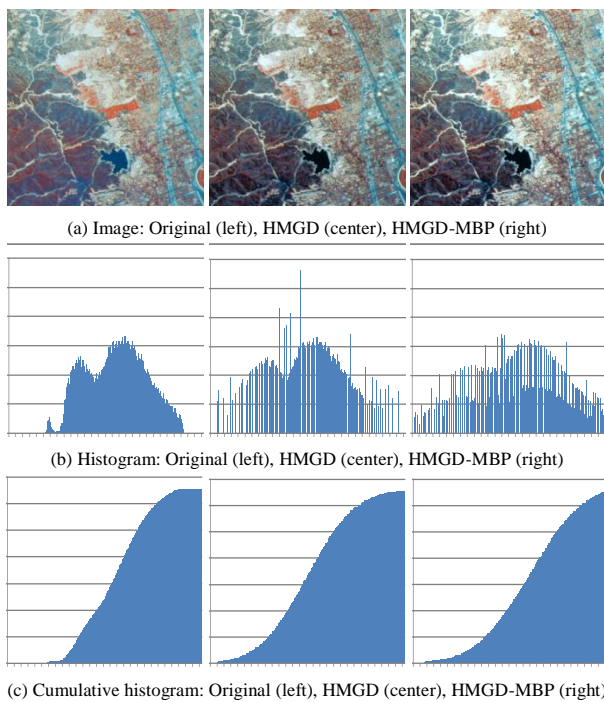


Fig. 3. Example of results (HMGD, HMGD-MBP, and the corresponding histograms).

5. Conclusion

In this paper we have aimed improvement automated processing for multiple-brightness peak image, we have proposed “Histogram Matching based on Gaussian Distribution for multiple-brightness peak (HMGD-MBP)”.

As for the concrete processing method, we have used curvature computation and variance estimation for detecting brightness peaks and optimizing the shape of the reference histogram. Then we have taken an average of HMGD processed images.

From the experimentation results, HMGD-MBP processing image is enhancing contrast naturally and the edges of image becomes clear and detailed. That is, we consider that the HMGD-MBP processing method is useful than previous HMGD.

References

1. R. C. Gonzalez and R. E. Woods, *Digital Image Processing* (Addison-Wesley Publishing Company, 1993).
2. B. Jahne, *Digital Image Processing --Concepts, Algorithms, and Scientific Applications-- 4th edition* (Springer, 1995).
3. E. S. Umbaugh, *Computer Vision and Image Processing: A Practical Approach Using CVIP tools* (Prentice Hall PTR, 1998).
4. W. Burger and J. M. Burge, *Principles of Digital Image Processing: Fundamental Techniques* (Springer 2009).
5. T. Izumi, T. Hattori, S. Sugimono, and T. Takashima, Color Image Arrangement Using Elastic Transform on Principal Component Axis (in Japanese), *Journal of Japan Society of Kansei Engineering* 8(3) (2009) 667-674.
6. Y. Kawakami, T. Hattori, D. Kutsuna, H. Matsushita, Y. Imai, H. Kawano, R.P.C. Janaka Rajapakse, Automated Color Image Arrangement Method Based on Histogram Matching - Investigation of Kansei impression between HE and HMGD -, *International Journal of Affective Engineering* 14(2) (2015) ISSN 2187-5413, 85-93.
7. Y. Kawakami, T. Hattori, Y. Imai, H. Matsushita, H. Kawano, R. P. C. Janaka Rajapakse, Kansei Impression and Automated Color Image Arrangement Method and Kansei Impression, *Journal of Robotics, Networking and Artificial Life* 1(1) (2014) ISSN 2352-6386, 60-67.
8. Y. Kawakami, T. Hattori, Y. Imai, H. Matsushita, H. Kawano, and R. P. C. Janaka Rajapakse, Automated Color Image Arrangement Method Using Curvature Computation in Histogram Matching, in *Proceedings of International Conference on Artificial Life and Robotics* (ICAROB 2015) (Oita, Japan, 2015) ISBN 978-4-9902880-9-9, pp. 272-277.
9. Y. Kawakami, T. Hattori, Y. Imai, Y. Horikawa, H. Matsushita, R. P. C. Janaka Rajapakse, Automated Color Image Arrangement Method for Multiple-Peak Image, in *Proceedings of The Second International Conference on Computer Science, Computer Engineering, & Social Media* (Lodz, Poland, 2015), ISBN 978-1-4799-1789-1, pp. 27-30.

Histogram Matching Based on Gaussian Distribution on the HSB Color System

Yusuke Kawakami

*DynaxT Co., Ltd., 2271-6 Hayashi
Takamatsu City, Kagawa 761-0113, Japan*

Tetsuo Hattori, Yoshiro Imai, Yo Horikawa

*Kagawa University, 2217-20 Hayashi
Takamatsu City, Kagawa 761-0113, Japan*

R. P. C. Janaka Rajapakse

*Tainan National University of the Arts, 66 Daci
Guantian District, Tainan 72045, Taiwan*

E-mail: riverjp2002@gmail.com, {hattori, imai, horikawa}@eng.kagawa-u.ac.jp, janakaraja@gmail.com

Abstract

This paper proposes Histogram Matching based on Gaussian Distribution (HMGD) processing on the HSB color system which is close to the human visual property. In the previous paper, we have proposed HMGD processing on the brightness axis which is calculated from RGB color system. And we have considered that HSB color system is more suitable for HMGD processing, because it contains brightness axis. In this paper, we describe how to transform the color image from RGB color system into HSB color system first. Second, we describe that the principal of HMGD on this color system. And then, we also explain how to re-transform HSB color system to RGB color system.

Keywords: Histogram matching, RGB, HSB, Image processing, HMGD

1. Introduction

Recently, the automated image arrangement has become more familiar to us¹⁻³. For example, if we take a photo using Digital Camera or Smartphone, these devices will process which aimed to improve feeling impression from raw taken one. And the method of image processing is in the research stage.

In the previous papers, we have proposed histogram Matching based on Gaussian Distribution (HMGD), as the automated image processing which is one of the elastic transform. This HMGD has been the processing on the brightness axis which is calculated from RGB color system.

As for the method of improvement the feeling (or Kansei) impression, we have apply curvature computation for

detect multiple-brightness peak of image. Also, we have applied variance estimation to optimize for reference histogram which is used HMGD. Through these improvements, HMGD processing works well not only single-brightness peak image but also multiple-brightness peak image.

However, we have considered that HSB color system^{4, 5} is more suitable for HMGD processing, because HSB color system is more close to visual feature of human.

In this paper, we describe about HSB color system first. Next, we illustrate principle of transform the color image from RGB color system into HSB color system. Then, we propose the principle of HMGD on this color system. Last, we also propose the method of HMGD on the HSB color system.

2. Principle

2.1. HSB color system

HSB (or HSV) color system is the color system due to Hue, Saturation and Brightness, as shown in Fig. 1. This color space has been proposed from A. R. Smith, the author of Ref. 5 published in 1978.

Hue means the primary color and it is the angular dimension⁵ starting at the red primary at 0°. And green primary and blue primary is located at 120° and 240°, respectively, and then primary color become red at 360°. Next, saturation is corresponding to the clearness of color. This means that the high saturation color is close to primary, and the low saturation color is close to achromatic.

Then, brightness is corresponding to brightness of color. This means that the high brightness color is bright color, and the low brightness color is close to black.

That is, HSB color system is the most common cylindrical-coordinate representations of points in a RGB color system.

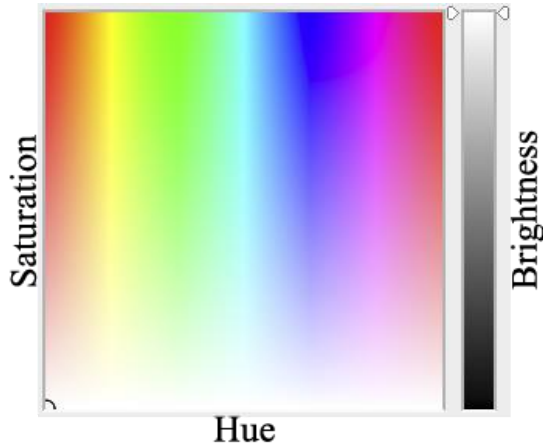


Fig. 1. Conceptual image of HSB color space

interconversion between RGB color system and HSB color system in this section.

2.2.1. Color system conversion from RGB to HSB

Let b_{\max} and V be the maximum value of RGB color system in one pixel and the brightness value on HSB color system in one pixel, respectively. And, let H and S be the hue value and saturation value. Then, V is defined by Eq. (1).

$$V = b_{\max}. \quad (1)$$

If $b_{\max} = 0$, let H and S is defined by Eq. (2).

$$H = 0, \quad S = 0. \quad (2)$$

And let be b_{\min} the minimum value of RGB color system in one pixel, S is defined by Eq. (3).

$$S = 255 \times \frac{b_{\max} - b_{\min}}{b_{\max}}. \quad (3)$$

From Eq. (1) ~ (3), we understand that we can derive saturation (S) and brightness (V) of HSB color system. And, let R , G , and B be defined red, green, and blue value of RGB color system, we can derive the H by Eq. (4).

$$\begin{cases} H = 60 \times \left(\frac{B - G}{b_{\max} - b_{\min}} \right). & (b_{\max} = R) \\ H = 60 \times \left(\frac{R - B}{b_{\max} - b_{\min}} \right) + 120. & (b_{\max} = G) \\ H = 60 \times \left(\frac{G - R}{b_{\max} - b_{\min}} \right) + 240. & (b_{\max} = B) \end{cases} \quad (4)$$

In Eq. (4), H may be taken negative value H' . If H is H' , we have to correct by following Eq. (5) because H is defined 0° ~ 359°.

$$H = H' + 360. \quad (5)$$

2.2. Color system conversion

In the previous section, we have described the principle of HSB color system. So, we describe the principle of

2.2.2. Color system conversion from HSB to RGB

Let R , G , and B be defined red, green, and blue value of RGB color system, respectively. And let H , S , and V be defined hue, saturation, and brightness value of HSB color system, respectively. If we take into account of definition of HSV color space, $S=0$ must be black color by Eq. (6).

$$R = 0, G = 0, B = 0. \quad (S = 0) \quad (6)$$

And here, let H_F , I , J , K , and L be defined following equations.

$$H_F = \lfloor H/60 \rfloor \quad (7)$$

$$I = (H/60) - H_F \quad (8)$$

$$J = V \left(1 - \frac{S}{255} \right), \quad K = V \left(1 - \frac{S}{255} F \right), \quad L = V \left(1 - \frac{S}{255} (1 - F) \right). \quad (9)$$

From Eq. (7) ~ (9), conversion equation of R , G , and B is derived by Eq. (10) and (11).

$$\begin{cases} H_F = 0 \Rightarrow R = V, G = L, B = J. \\ H_F = 1 \Rightarrow R = K, G = V, B = J. \\ H_F = 2 \Rightarrow R = J, G = V, B = L. \end{cases} \quad (10)$$

$$\begin{cases} H_F = 3 \Rightarrow R = J, G = K, B = V. \\ H_F = 4 \Rightarrow R = L, G = J, B = V. \\ H_F = 5 \Rightarrow R = V, G = J, B = K. \end{cases} \quad (11)$$

2.3. Histogram Matching based on Gaussian Distribution

In this section, we describe the principle of Histogram Matching based on Gaussian Distribution (HMGD).

HMGD is one of a kind of automated image arrangement method based on the Elastic Transformation^{6, 7}.

Fig. 2 shows the conceptual image of HMGD. Let $f(x)$ and $h(y)$ be two probabilistic density functions (PDF) on real variables x and y , respectively. PDF is corresponding to the brightness value histogram of HSB color system. And, we define the relationship between x and y by Eq. (12).

$$y = \phi(x) = L \int_0^x f(x) dx. \quad (12)$$

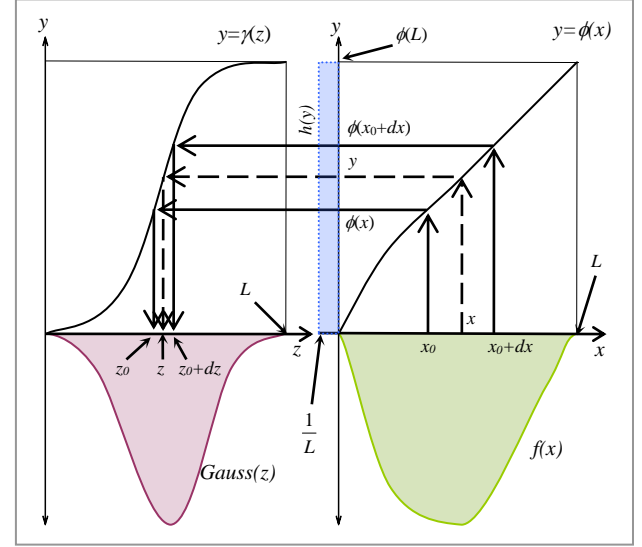


Fig. 2. Conceptual of Histogram matching based on Gaussian Distribution (HMGD)⁸⁻¹⁰.

By Eq. (12), we define that $\phi(x)$ means the cumulative histogram of $f(x)$.

First, we transform from original histogram $f(x)$ into uniform distribution histogram $h(y)$ because we need to expand brightness value for histogram matching. We can derive Eq. (13) and (14) from Eq. (12) and Fig. 2.

$$f(x) = h(y) \phi'(x) = h(y) L f(x). \quad (13)$$

$$h(y) = \frac{1}{L}. \quad (14)$$

Then, let $Gauss(z)$ and $\gamma(z)$ be the function that is defined by Eq. (15) and (16), respectively. And we obtain Eq. (17) from the relationship between $y = \phi(x)$ and $y = \gamma(z)$ as shown in Fig. 2.

$$Gauss(z) = \frac{1}{\sqrt{2\pi\sigma^2}} \exp\left(-\frac{(z-\mu)^2}{2\sigma^2}\right). \quad (15)$$

$$y = \gamma(z) = L \int_0^z Gauss(z) dz. \quad (16)$$

$$L \int_0^x f(x) dx = \frac{L}{\sqrt{2\pi\sigma^2}} \int_0^z \exp\left(-\frac{(z-\mu)^2}{2\sigma^2}\right) dz. \quad (17)$$

So, we can derive Eq. (18) and (19) from differential of Eq. (17).

$$L \int_0^x f(x) dx = \frac{L}{\sqrt{2\pi\sigma^2}} \int_0^z \exp\left(-\frac{(z-\mu)^2}{2\sigma^2}\right) dz. \quad (18)$$

$$L\phi'(x) = L\gamma'(z), \quad f(x) = \text{Gauss}(z). \quad (19)$$

That is, we understand that we can match the original histogram $f(x)$ to Gaussian distribution histogram $\text{Gauss}(z)$.

3. Method of HMGD on the HSB Color System

In the previous chapter, we described the principle of HSB color system, its conversion, and HMGD. In this chapter, we propose the method of HMGD on the HSB color system.

- (i) Load original image.
- (ii) Perform color system conversion from RGB to HSB.
- (iii) Perform HMGD on the brightness axis of HSB color system.
- (iv) Perform color system conversion from HSB to RGB.
- (v) Output processed image.

4. Conclusion

In this paper, we have proposed about Histogram Matching Based on Gaussian Distribution (HMGD) on the HSB color system, and we have described principles of color conversion and HMGD.

As the proposed method, we have performed color system conversion and HMGD on the brightness axis of HSB color system image. And then, we have performed re-conversion of color system as the post processing.

For the further study, we have to validate investigation feeling (or Kansei) impression evaluation through the questionnaire survey, for the review proposed method for effectiveness. Also we have to review the proposed method for effectiveness.

References

1. R. C. Gonzalez and R. E. Woods, Digital Image Processing (Addison-Wesley Publishing Company, 1993).
2. B. Jahne, Digital Image Processing --Concepts, Algorithms, and Scientific Applications-- 4th edition (Springer, 1995).
3. E. S. Umbaugh, *Computer Vision and Image Processing: A Practical Approach Using CVIP tools* (Prentice Hall PTR, 1998).
4. S. Matsushashi, K. Fujimoto, O. Nakamura, T. Minami, A Proposal of the Modified HSV Colour System Suitable for Human Face Extraction (in Japanese), *Journal of Television* **49**(6) (1995) 787-797.
5. A. R. Smith, Color Gamut Transform Pairs, in *Computer Graphics* **12**(3), (1978), 12-19.
6. W. Burger and J. M. Burge, *Principles of Digital Image Processing: Fundamental Techniques* (Springer, 2009).
7. T. Izumi, T. Hattori, S. Sugimono, and T. Takashima, Color Image Arrangement Using Elastic Transform on Principal Component Axis (in Japanese), *Journal of Japan Society of Kansei Engineering* **8**(3) (2009) 667-674.
8. Y. Kawakami, T. Hattori, D. Kutsuna, H. Matsushita, Y. Imai, H. Kawano, and R.P.C. Janaka Rajapakse, Automated Color Image Arrangement Method Based on Histogram Matching - Investigation of Kansei impression between HE and HMGD -, *International Journal of Affective Engineering*, ISSN 2187-5413, **14**(2) (2015) 85-93.
9. Y. Kawakami, T. Hattori, Y. Imai, H. Matsushita, H. Kawano, and R. P. C. Janaka Rajapakse, Automated Color Image Arrangement Method Using Curvature Computation in Histogram Matching, in *Proceedings of International Conference on Artificial Life and Robotics (ICAROB 2015)* (Oita, Japan, 2015) ISBN 978-4-9902880-9-9, pp. 272-277.
10. Y. Kawakami, T. Hattori, Y. Imai, Y. Horikawa, H. Matsushita, R. P. C. Janaka Rajapakse, Automated Color Image Arrangement Method for Multiple-Peak Image, in *Proceedings of The Second International Conference on Computer Science, Computer Engineering, & Social Media* (Lodz, Poland, 2015), ISBN 978-1-4799-1789-1, pp. 27-30.

Quantitative Evaluation of Flash-based Educational Visualizing Simulator

Kei Takeichi, Yoshiro Imai, Kazuaki Ando, Tetsuo Hattori

Kagawa University, 2217-20 Hayashi

Takamatsu City, Kagawa 761-0113, Japan

E-mail: {hattori, imai, ando}@eng.kagawa-u.ac.jp

Yusuke Kawakami

DynaxT Co., Ltd., 2271-6 Hayashi

Takamatsu City, Kagawa 761-0113, Japan

E-mail: riverjp2002@gmail.com

Abstract

A Flash-based simulator of CPU scheduling has been developed and utilized for educational visualization in the class of university lecture. We have designed and implemented it with Flash-based scripting language in order to execute it as a stand-alone application as well as in various browsing environment such as Microsoft IE, Google Chrome and/or FireFox (Mozilla). Based on questionnaire for our simulator in the lecture, its quantitative evaluation has been carried out by means of statistical analysis. Our report describes overview of our Flash-based simulator and the results of the above quantitative evaluation.

Keywords: Educational visualization, Questionnaire-based Evaluation, Statistical analysis

1. Introduction

As a matter of course, software system covers many important areas from fundamentals to applications. This time, we focus on Operating System, and particularly CPU scheduling algorithm. It must be cover several kinds of themes that students should understand during their school days. A simple algorithm, namely FCFS (First Come and First Served) is very natural so that it is one the most fundamental strategies to decide its priority for users, clients, processes/tasks and so on. Priority based algorithm is another candidate to determine the order of execution. It is very significant idea to choose a suitable item around potentially selected targets. It means which

is better, or which is optimal of them. SPTF (Shortest Processing Time First) is to be chosen as one of the priority-based algorithms in this study. In other view point, RR (Round Robin) is evaluated as a policy of algorithm to realize equality of opportunity around the targets. It is a little complicated but very useful strategy to choose item with equal opportunities.

In order to teach students these above algorithms efficiently, we had better utilize some suitable educational tool to visualize their behavior and results for specific conditions^{1,2}. A visual simulator is one of the useful solutions to provide educational tool(s) for students who wants to understand such theme of information processing education in an efficient and

© The 2016 International Conference on Artificial Life and Robotics (ICAROB 2016), Jan. 29-31, Okinawa Convention Center, Okinawa, Japan

effective manner³. In this study, we have developed some useful educational tools to demonstrate practical CPU scheduling algorithm(s) and provide visual understanding for students in an effective way.

2. Overview of Visualizing Simulator

In a lecture of Operating System of our university, most important algorithms of CPU scheduling are FCFS, SPTF, and RR, we think. They are very trivial but sometimes very useful in the real operating systems. So we have employed these above algorithms as fundamental procedures to decide CPU scheduling in our visualizing simulator. The above three procedure based on FCFS, SPTF and RR are as follows;

(1) FCFS is very much simple, but clearly well-defined strategy to decide next candidate to be performed, just like First-In First-Out(FIFO queue). This algorithm is sometimes the target to be compared with other algorithm(s). And moreover, a result applied by this algorithm will be not so worse than other ones derived from complicated algorithm(s).

(2) SPTF is one of the most famous priority-based assigning/allocating algorithm. Whenever every event happens, namely conditions have changed, it must be investigated which candidate has the best priority at that time. So we had better call this algorithm Shortest Remaining Processing Time First (SRPTF), because we must consider not the total processing time but remaining processing one in order to decide which candidate has the best priority at that time or later.

(3) RR is a typical non-priority based algorithm in order to provide 'equality of opportunity' which can realize taking turns at it. This algorithm can retrieve candidates which are waiting for service and select/assign one of them who wait for the longest time or longer than others. It is a little complicated for beginners to understand details of RR-based procedure and/or develop a kind of corresponding programs. And we may sometimes meet its results with not suitable performance for specific applications. But equality of opportunity is very important for several users to receive their necessary services.

3. Quantitative Evaluation

This section presents quantitative evaluation of our visualizing simulator. As one of the quantitative evaluation for our CPU scheduling simulator, at first, we compare the execution time of simulation of native Flash player with ones on the below three major browsers. The result is summarized in the following Table 1.

Table 1. Comparison of Execution Time(s) between Different Environments.

Host Application	Execution Time
Flash Player (Ver.10) Stand alone	32.25 (sec.)
MS-Internet Explorer 11.0.9600	28.95 (sec.)
Mozilla FireFox 35.0.1	35.19 (sec.)
Google Chrome 40.0.2214.11 m	93.61 (sec.)

As another quantitative evaluation for our simulator, secondly, we have carried out questionnaire in the classroom lecture of Operating System in our university after using our simulator. The questionnaire includes following six questions;

Q#1 Is it easy to utilize this simulator? (yes: 2, neutral:1, no:0)

Q#2 Is it effective to learn CPU scheduling algorithm with this visualizing simulator? (yes: 2, neutral:1, no:0)

Q#3 Do you understand CPU scheduling algorithm more suitably with this simulator? (yes: 2, neutral:1, no:0)

Q#4 Are you interesting in CPU scheduling algorithm by means of this simulator? (yes: 2, neutral:1, no:0)

Q#5 Are you interesting in other themes of Operating System after usage of this simulator? (yes: 2, neutral:1, no:0)

Q#6 Do you need to utilize another type of simulator in order to learn Operating System? (yes: 2, neutral:1, no:0)

Our questionnaire described before can obtain just 20 answers from students of the class because of carrying out on a voluntary basis, although we used to have the class for Operating System with 40 students or more. The result of such a questionnaire is summarized in Table 2. Q#1 has 17 numbers of answer "yes" per 20 students (i.e. 85%), Q#2 has 18 numbers of answer "yes" per 20 students (i.e. 90%) and Q#3 has 12 numbers of answer "yes" per 20 students (i.e. 60%). From the questionnaire, many students do feel easy to utilize our CPU scheduling

simulator and consider to be effective for learning CPU scheduling algorithm by means of using our simulator. And majority, namely six out of ten, of replying students understand CPU scheduling algorithm more suitably with this simulator.

Table 2. Result of Questionnaire about our Simulator.

Student	Q#1	Q#2	Q#3	Q#4	Q#5	Q#6
S01	2	2	2	1	1	2
S02	2	2	1	1	1	2
S03	1	1	0	2	1	2
S04	2	2	2	1	2	2
S05	2	2	1	1	1	1
S06	2	2	2	1	1	2
S07	2	2	1	1	1	2
S08	2	2	2	1	1	2
S09	2	2	2	1	1	1
S10	2	2	2	1	1	2
S11	2	2	1	1	1	2
S12	2	2	2	1	1	1
S13	1	2	1	1	1	2
S14	2	1	2	1	1	2
S15	2	2	2	2	1	2
S16	2	2	1	1	1	2
S17	2	2	1	2	1	2
S18	2	2	2	2	2	2
S19	2	2	2	1	1	2
S20	1	2	2	2	2	2

At the same time, however, Q#4 has just 5 numbers of answer "yes" per 20 students (i.e. 25%) and Q#5 has only 3 numbers of answer "yes" per 20 students (i.e. 15%). In order to perform test of independence among Q#1, Q#2 and Q#3, we will demonstrate to calculate " χ^2 test of goodness-of-fit" for relation between results from Q#1 and Q#2 as well as one for Q#1 and Q#3, respectively. Relation between results from Q#1 and Q#2 is expressed in the left-hand of Table 3, while relation for Q#1 and Q#3 is done in the right-hand. The former has 2 x 2 table-items and the latter has 2 x 3 ones.

Table 3. Relation between Results from Q#1 and Q#2 (left-hand) & from Q#1 and Q#3 (right-hand).

		Q#2			Q#3		
		yes	neutral	no	yes	neutral	no
Q#1	yes	16	1		11	6	0
	neutral	2	1		1	1	1
	no						

Based on Table 3, a two-way contingency table for Q#1 and Q#2 can be introduced, which is shown in Table 4, while another two-way contingency table for Q#1 and Q#3 can be also done, which is shown in Table 5.

Table 4. Two-way Contingency Table for Q#1 and Q#2.

		Q#2		SUM _R
		yes	neutral	
Q#1	yes	16(18*17/20)	1(2*17/20)	17
	neutral	2(18*3/20)	1(2*3/20)	3
SUM _C		18	2	20

χ^2 : goodness-of-fit statistic for Table 4 can be calculated in the following expression (Eq-1);

$$\chi^2 = \sum_{i=1}^2 \sum_{j=1}^2 \left\{ (y_{ij} - \frac{sum_R * sum_C}{Total})^2 / \frac{sum_R * sum_C}{Total} \right\}$$

$$= \{16 - (18 * 17 / 20)\}^2 / (18 * 17 / 20) + \dots$$

$$+ \{1 - (2 * 3 / 20)\}^2 / (2 * 3 / 20) = 2.135 \quad (\text{Eq-1})$$

As described in expression (Eq-1), degree of freedom for Table 4 is $\nu = (2-1) \times (2-1) = 1$. So we can have $\chi^2_{\alpha=0.05(\nu=1)} = 3.8415$ from the χ^2 distribution table. "Statistical independence" between results from Q#1 and Q#2 can be confirmed so that users of our simulator not only consider it to be easy to utilize but also recognize effectiveness to learn CPU scheduling algorithm with it respectively and independently.

Table 5. Two-way Contingency Table for Q#1 and Q#3.

		Q#3			SUM _R
		yes	neutral	no	
Q#1	yes	11(12*17/20)	6(7*17/20)	0(1*17/20)	17
	neutral	1(12*3/20)	1(7*3/20)	1(1*3/20)	3
SUM _C		12	7	1	20

Just like the same way, χ^2 : goodness-of-fit statistic for Table 4 can be calculated in the following expression (Eq-2);

$$\chi^2 = \sum_{i=1}^2 \sum_{j=1}^2 \left\{ \left(y_{ij} - \frac{\text{sum}_R * \text{sum}_C}{\text{Total}} \right)^2 / \frac{\text{sum}_R * \text{sum}_C}{\text{Total}} \right\}$$

$$= \{11 - (12 * 17 / 20)\}^2 / (12 * 17 / 20) + \dots$$

$$+ \{1 - (1 * 3 / 20)\}^2 / (1 * 3 / 20) = 0.1365 \quad (\text{Eq-2})$$

As described in expression (Eq-2), degree of freedom for Table 5 is $\nu = (2-1) \times (3-1) = 2$. So we can have $\chi^2_{\alpha=0.05(\nu=2)} = 5.9915$ from the χ^2 distribution table. "Statistical independence" between results from Q#1 and Q#3 can be confirmed so that users of our simulator not only consider it to be easy to utilize but also understand CPU scheduling algorithm more suitably with our simulator respectively and independently.

In other words, both of results from Q#1 and Q#2 are not only very good scores, namely 85% of the former's answers are "yes" and 90% of the latter's answers are "yes", but also the two scores are statistically independent each other, namely there is no reason that one scores can become good because another scores are good. And major part (i.e. 60%) of users, whose answers from Q#3 are "yes", understand CPU scheduling algorithm more suitably by means of our simulator independently from its operability.

4. Conclusion

The paper describes an Adobe-Flash based educational visualizing simulator for students to learn CPU scheduling algorithm graphically and practically. Our Flash-based simulator can execute on the major Web browsers such as Microsoft Internet Explorer, Mozilla FireFox and Google Chrome and provide efficient explanation for students of lecture "Operating System".

As quantitative evaluation for our simulator, we have carried out questionnaire for the students using the simulator and apply statistical analysis for the results of the questionnaire. We can obtain and confirm a good results from the above performance through analysis.

Namely,

(1) It can be confirmed that users of our simulator not only consider it to be easy to utilize but also recognize effectiveness to learn CPU scheduling algorithm with our visualizing simulator respectively and independently.

(2) It can be confirmed that users of our simulator not only consider it to be easy to utilize but also understand

CPU scheduling algorithm more suitably with our simulator respectively and independently.

References

1. Sarjoughian, H., Yu Chen, Burger, K. : A component-based visual simulator for MIPS32 processors. Proceedings of 38th Annual Conference on Frontiers in Education (FIE 2008), pp. F3B-9 – F3B-14 (October 2008)..
2. Kabir, M.T., Bari, M.T., Haque, A.L. : ViSiMIPS: Visual simulator of MIPS32 pipelined processor. Proceedings of 6th International Conference on Computer Science & Education (ICCSE2011), pp. 788 – 793 (August 2011).
3. Imai, Y., Tomita, S., Niimi, H., Kitamura, T. : Web-Based Computer Visual Simulator. Technology Enhanced Learning (IFIP International Federation for Information Processing), Volume 171, pp 111–120 (Summer 2005).
4. Lee, K.-C., Lee, J. : Programming physics softwares in Flash. Computer Physics Communications, Volume 177, Issues 1-2, pp 195–198 (July 2007).
5. Stodulka, P., Privitzer, P., Kofranek, J., Tribula, M., Vacek, O. : Development of WEB accessible medical educational simulators. Proceedings of 6th EUROSIM Congress on Modelling and Simulation, 6 pages (September 2007).
6. Imai, Y., Takeichi, K. : Development and Evaluation of Adobe Flash based CPU Scheduling Simulator Executable on Major Multiple Web Browsers. Proceedings of 2015 IEEE International Conference on Intelligent Networking and Collaborative Systems (INCoS-2015, Tamkang University, Taipei, TAIWAN (RoC)), pp.149–155 (September 2015).

Relation between Optimal Stopping Solution and NSPR for Structural Change Point Detection Problem

Tetsuo Hattori

*Kagawa University, 2217-20 Hayashi Cho
Takamatsu City, Kagawa 761-0396, Japan*

Yoshihide Koyama, Yusuke Kawakami, Yoshiro Imai, Yo Horikawa

*Kagawa University, 2217-20 Hayashi Cho
Takamatsu City, Kagawa 761-0396, Japan*

Hiromichi Kawano

*NTT advanced technology Company Ltd, Mitaka, Tokyo, Japan
E-mail: {hattori, imai, horikawa}@eng.kagawa-u.ac.jp, hiromichi.kawano@ntt-at.co.jp*

Abstract

Previously, we have proposed a novel method using New Sequential Probability Ratio (NSPR) for the structural change point detection (SCPD) of ongoing time series data instead of using SPRT (Sequential Probability Ratio Test). Moreover, we have formulated the SCPD problem in time series data as an Optimal Stopping one using the concept of DP (Dynamic Programming) and also have shown the solution theorem in the form of Inequality. In this paper, we discuss the relation between the solution of Optimal Stopping and NSPR for the SCPD Problem.

Keywords: Image processing, Curvature, Variance estimation, Histogram matching, HMGD

1. Introduction

For ongoing time series analysis, three stages are considered: prediction model construction, structural change detection (and/or disparity detection between the model and observing data), and renewal of prediction model. Above all, it is important to detect the change point as quickly and also correctly as possible. Especially in the second stage, in order to renew the accurate prediction model as soon as possible after the detection.

As the structural change detection, or change point detection (CPD), some methods have been proposed¹⁻⁴. The standard well known method is Chow Test that is used in econometrics². It does a statistical test by setting

the hypothesis that the change has occurred at time t for all of data obtained so far.

Meanwhile, we have previously formulated the structural change detection method in time series as an Optimal Stopping Problem with an action cost, using the concept of DP (Dynamic Programming)⁵⁻⁶. Moreover for the change point detection problem, we have proposed a model introduced SPRT (Sequential Probability Ratio Test) as a New Sequential Probability Ratio (NSPR) test method⁷⁻⁸.

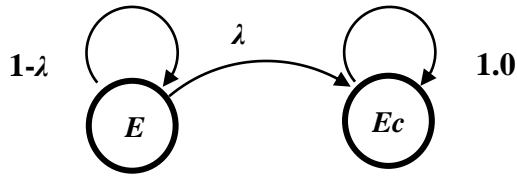
In this paper, we present that there is a relation between the NSPR and the optimal solution theorem for CPD that dealt as an Optimal Stopping Problem and describe it concretely.

2. Definitions and Equations

2.1. Structural Change Model⁵⁻⁶

We assume that the structural change is Poisson occurrence of average λ , and that, once the change has occurred during the observing period, the structure does not go back to the previous one. The reason why we set such a model is that we focus on the detection of the first structural change in the sequential processing (or sequential test). The concept of the structural change model is shown in Fig. 1.

Moreover, we introduce a more detailed model. Let R be the probability of the failing when the structure is unchanged. Let Rc be the probability of the failing when the structure change occurred. We consider that Rc is greater than R , i.e., $Rc > R$. The detailed model for the State Ec and E are illustrated as similar probabilistic finite state automats in Fig.2 and Fig.3, respectively.



Ec : State that the structural change occurred.
 E : State that the structure is unchanged.
 λ : Probability of the structural change occurrence.
(Poisson Process.)

Fig.1. Structural change model.

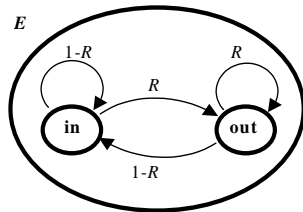


Fig.2. Internal model of the State E .

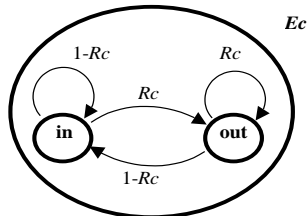


Fig.3. Internal model of the State Ec .

2.2. Optimal Stopping Formulation and its Solution Theorem⁵⁻⁶

Let the cost(n) be $a \cdot n$ as a linear function for n , where a is the loss caused by the failing in one time. And for simplicity, let T and A denote the Total_cost and cost (A), respectively. Then, the evaluation function is denoted as the following equation (1).

$$T = A + a \cdot n \quad (1)$$

We recursively define a function $ET(n, N)$ to obtain the optimum number of times n that minimizes the expectation value of the evaluation function of Equation (3), using the concept of DP (Dynamic Programming). Let N be the optimum number. Let the function $EC(n, N)$ be the expectation value of the evaluation function at the time when the failing has occurred in continuing n times, where n is less than or equal to N , i.e., $0 \leq n \leq N$.

Thus the function is recursively defined as follows.

$$(\text{if } n = N) \quad ET(n, N) = A + a \cdot N \quad (2)$$

$$(\text{if } n < N) \quad ET(n, N) = P(\bar{S}_{n+1} | S^n) \cdot a \cdot n + (1 - P(\bar{S}_{n+1} | S^n)) ET(n+1, N) \quad (3)$$

where S^n means the state of failing in continuing n times, \bar{S}_{n+1} the state of hitting at the $(n+1)$ th observed data, and $P(\bar{S}_{n+1} | S^n)$ means the conditional probability that the state \bar{S}_{n+1} occurs after the state S^n .

The first term in the right-hand side (RHS) of the equation (3) indicates the expectation value of the evaluation function at the time when hitting happens at the $(n+1)$ th data after the continuing n times failing. The second term in the RHS of the equation (3) indicates the expectation value of the evaluation function for the time when failing happens at the $(n+1)$ th data after continuing n times failing.

Then, from the definition of the function $ET(n, N)$, the goal is to find the N that minimizes $ET(0, N)$, because the N is the same as n that minimizes the expectation value of the evaluation function of (1).

[Optimal Solution Theorem (OST)]

The N that minimizes $ET(0, N)$ is given as the largest number n that satisfies the following Inequality (4).

$$a < (A + a) \cdot P(\bar{S}_n | S^{n-1}) \quad (4)$$

where the number $N+1$ can also be the optimum one that minimizes $ET(0, N)$, i.e., $ET(0, N) = ET(0, N+1)$, only if

$$a = (A + a) \cdot P(\bar{S}_{N+1} | S^N)$$

2.3. New Sequential Probability Ratio (NSPR) Based on Structural Change Model⁷⁻⁸

Let $a_1 a_2, \dots, a_i, \dots, a_n$ $a_i \in \{\text{IN}, \text{OUT}\}$ be a string (or symbol sequence) obtained from the observed data.

Let θ_i and $\tilde{\theta}_i$ be the conditional probability that outputs the observed data (or above symbol sequence, $C_n = a_1 a_2 \dots a_n$ in the state S_0 and S_1 , respectively. That is, it means that $\theta_i \in \{R, 1-R\}$ and $\tilde{\theta}_i \in \{R_c, 1-R_c\}$, respectively.

And let $P(a_1 \dots a_n, H_0)$ and $P(a_1 \dots a_n, H_1)$ be the joint probability of the symbol sequence C_n happens with the event H_0 (the structural change is not occurred) and H_1 (the change is occurred), respectively.

Then, the following equations hold.

$$\begin{aligned} P(a_1 \dots a_n, H_0) &= P(C_n, H_0) \\ &= (1-\lambda)^n \theta_1 \dots \theta_n = (1-\lambda)^n \prod_{i=1}^n \theta_i \end{aligned} \quad (5)$$

$$\begin{aligned} P(a_1 \dots a_n, H_1) &= P(C_n, H_1) \\ &= \lambda \prod_{i=1}^n \tilde{\theta}_i + ((1-\lambda)\theta_1)(\lambda \prod_{i=2}^n \tilde{\theta}_i) \\ &\quad + ((1-\lambda)^2 \theta_1 \theta_2)(\lambda \prod_{i=3}^n \tilde{\theta}_i) + \dots \\ &= \sum_{k=1}^n ((1-\lambda)^{k-1} \cdot \prod_{j=0}^{k-1} \theta_j)(\lambda \prod_{i=k}^n \tilde{\theta}_i) \end{aligned} \quad (6)$$

New Sequential Probability Ratio (NSPR) Λ_n that we propose is represented using the aforementioned equations as following Eq.(7).

$$\begin{aligned} \text{NSPR } \Lambda_n &= \frac{P(H_1 | a_1 \dots a_n)}{P(H_0 | a_1 \dots a_n)} = \frac{P(H_1 | C_n)}{P(H_0 | C_n)} = \frac{P(C_n, H_1)}{P(C_n, H_0)} \\ &= \frac{\sum_{k=1}^n ((1-\lambda)^{k-1} \cdot \prod_{j=0}^{k-1} \theta_j)(\lambda \prod_{i=k}^n \tilde{\theta}_i)}{(1-\lambda)^n \prod_{i=1}^n \theta_i} \end{aligned} \quad (7)$$

If the NSPR is greater than 1.0, we can regard that the structural change has been occurred before the present time.

3. Relation between NSPR and OST

We show the relations using the probability in the Optimal Solution Theorem, considering $R_c \gg R$.

$$\begin{aligned} P(\bar{S}_{n+1} | S^n) &= (1-R)(1-P(E_{cn} | S^n)) + (1-R_c)P(E_{cn} | S^n) \\ &= (1-R) - P(E_{cn} | S^n)(R_c - R) \end{aligned} \quad (8)$$

Therefore, we have

$$P(E_{cn} | S^n) = \frac{(1-R) - P(\bar{S}_{n+1} | S^n)}{(R_c - R)} \quad (9)$$

Similarly,

$$P(E | S^n) = \frac{P(\bar{S}_{n+1} | S^n) - (1-R_c)}{(R_c - R)} \quad (10)$$

Since

$$P(E_{cn} | S^n) = P(H_1 | S^n) \text{ and } P(E | S^n) = P(H_0 | S^n)$$

we have

$$\text{NSPR } \Lambda_n = \frac{P(H_1 | S^n)}{P(H_0 | S^n)} = \frac{(1-R) - P(\bar{S}_{n+1} | S^n)}{P(\bar{S}_{n+1} | S^n) - (1-R_c)} \quad (11)$$

Since $P(\bar{S}_{n+1} | S^n)$ is a monotonous decreasing function with respect to n , NSPR becomes an increasing one. From the OST, the optimal N is the maximum n that satisfies (4), so the N is the the maximum n that satisfies the following Inequality (12).

$$\text{NSPR } \Lambda_n = \frac{P(H_1 | S^n)}{P(H_0 | S^n)} < \Theta \equiv \frac{\left(\frac{A}{A+a}\right) - R}{R_c - \left(\frac{A}{A+a}\right)} \quad (12)$$

If $R = 0.05$, $R_c = 0.9$, $A = 10$, $a = 1$, $\Theta = 21.5$.

Meanwhile, since NSPR is a probability ratio, NSPR makes unnecessary the restriction condition of n times continuous failures (or “OUT”) in the Optimal Stopping Formulation.

4. Conclusion

We have described the relation between New Sequential Probability Ratio (NSPR) method and the Optimal Solution Theorem for CPD that dealt as an Optimal Stopping Problem. From this relation, we can use NSPR as well in the case where we have to consider some constraints with respect to loss cost.

References

1. R.Jana and S.Dey, Change detection in Teletraffic Models, *IEEE Trans. Signal Processing*, vol.48, No.3, pp.846-853, 2000.
2. Chow,G.C., Tests of Equality Between Sets of Coefficients in Two Linear Regressions, *Econometrica*, Vol.28, No.3, pp.591-605, 1960.
3. S.MacDougall, A.K. Nandi and R.Chapman, Multisolution and hybrid Bayesian algorithms for automatic detection of change points, *Proc. of IEEE Visual Image Signal Processing*, vol.145, No.4, pp.280-286, 1998.
4. E.S.Page, Continuous inspection schemes, *Biometrika*, Vol.41, pp.100-115, 1954.
5. Tetsuo Hattori, Katsunori Takeda, Izumi Tetsuya, Hiromichi Kawano, "Early Structural Change Detection as an Optimal Stopping Problem (I) --- Formulation Using Dynamic Programming with Action Cost ----", *Proc. of the 15th International Symposium on Artificial Life and Robotics (AROB15th'10)*, ISBN 978-4-9902880-4-4, pp.763-766, 2010.
6. Hiromichi Kawano, Tetsuo Hattori, Katsunori Takeda, Izumi Tetsuya, "Early Structural Change Detection as an Optimal Stopping Problem (II) --- Solution Theorem and its Proof Using Reduction to Absurdity ----", *Proc. of the 15th International Symposium on Artificial Life and Robotics (AROB15th'10)*, ISBN 978-4-9902880-4-4, pp.767-772, 2010.
7. Yoshihide Koyama, Tetsuo Hattori, Hiromichi Kawano, "Model Introduced SPRT for Structural Change Detection of Time Series (I)", *Journal of Robotics, Networks and Artificial Life* (ISSN: 2352-6386), Vol.1, No.1, pp.55-60 (Atlantis Press, Jun. 2014)
8. Yoshihide Koyama, Tetsuo Hattori, Katsunori Takeda, Hiromichi Kawano, "Model Introduced SPRT for Structural Change Detection of Time Series (II)", *Journal of Robotics, Networks and Artificial Life* (ISSN: 2352-6386), Vol.1, No.3, pp.237-243 (Atlantis Press, Dec. 2014)

Modified Quantum Particle Swarm Optimization for Chaos Synchronization

Chia-Nan Ko

*Department of Automation Engineering, Nan Kai University of Technology
t105@nkut.edu.tw*

Ching-I Lee

*Department of Automation Engineering, Nan Kai University of Technology
lcy@nkut.edu.tw*

Abstract

In this study, a modified quantum-behaved particle swarm optimization (MQPSO) based on hybrid evolution (HEMQPSO) approach is proposed to synchronize chaotic systems, in which the proposed HEMQPSO algorithm combines the conceptions of genetic algorithm (GA) and adaptive annealing learning algorithm with the MQPSO algorithm to search optimal solutions. Simulation results are illustrated to verify the performance of chaos synchronization using the proposed HEMQPSO approach. From the numerical simulations and comparisons with other extant evolutionary methods in chaotic systems, the validity and superiority of the HEMQPSO approach are verified.

Keywords: Quantum-behaved particle swarm optimization, Chaotic system, Genetic algorithm, Chaos synchronization, Hybrid evolution.

1. Introduction

A chaotic system is a nonlinear deterministic system that has some special features of sensitive dependence on initial conditions and unstable bounded trajectories in the phase space. Synchronization in chaotic dynamic systems attains much interest among scientists from various fields. Applications in chaotic systems synchronization are very significant in nonlinear fields. Recently, some researchers have paid much attention to identification and synchronization of chaotic systems.¹⁻³ Due to their characteristics sensitivity to initial conditions, chaotic systems are not easy to synchronize. Recently, some

researchers have endeavored to improve the synchronization of chaotic time series.⁴⁻⁸ In this article, we propose a scheme to synchronize Chen system and Genesio system with known parameters.⁶

Although the original PSO algorithm possesses the ability of high convergent speed, easily falling in some local optima is its fatal defect. Many researchers^{9,10} have presented revised PSO algorithms and obtained good results. Another improvement on traditional PSO algorithm is quantum-behaved particle swarm optimization (QPSO).¹¹⁻¹⁴ However, in QPSO, particles fall into local optimal state in multimode optimization

problems and cannot find any better state, the QPSO algorithm will take on the premature phenomenon.

To overcome the premature phenomenon in QPSO, a modified quantum-behaved particle swarm optimization (MQPSO) based on hybrid evolution (HEMQPSO) algorithm is proposed to synchronize chaotic systems will be proposed to perform the synchronization of chaotic systems in this study. In HEMQPSO, the significant improvement is that the evolutionary algorithm combines the concept of mutation algorithm in GA and adaptive annealing learning similar to SA with QPSO to achieve global search and defeat premature phenomenon in searching optimal solutions. From the illustrated results for three chaotic dynamical systems, the synchronization performance of the proposed HEMQPSO approach is demonstrated.

2. Modified Quantum Particle Swarm Optimization

In the PSO algorithm, each particle keeps trajectory of its coordinates in the problem space. The coordinate of each particle is related to its own best position (local best position) and the global best position achieved so far. The trajectories of particles are updated according to the following equations:

$$v_i(k+1) = w \cdot v_i(k) + c_1 \cdot r_1(p_i^l - p_i) + c_2 \cdot r_2(p^g - p_i), i = 1, 2, \dots, n, \quad (1)$$

$$p_i(k+1) = p_i(k) + v_i(k+1), i = 1, 2, \dots, n, \quad (2)$$

where n denotes the number of particles in a population; $p_i(k)$ and $v_i(k)$ are position and velocity of the i th particle at generation k in n -dimensional search space; p_i^l and p^g are the best position of the i th particle and the global best position; w is the inertia weight; c_1 and c_2 are cognitive and social constriction coefficients, respectively; r_1 and r_2 are random numbers between 0 and 1.

From the view of classical dynamics, to avoid explosion and guarantee convergence, particles must be bounded and fly in an attractive potential field. Clerc and Kennedy¹³ have proved that if these coefficients are properly defined, the particle's position p_i will converge

to the center of potential field, $pf^c = [pf_1^c, pf_2^c, \dots, pf_n^c]$, and is defined as:

$$pf_i^c = \frac{(c_1 \cdot r_1 \cdot p_i^l + c_2 \cdot r_2 \cdot p^g)}{(c_1 \cdot r_1 + c_2 \cdot r_2)}, i = 1, 2, \dots, n. \quad (3)$$

Inspired by the behavior that particles move in a bounded state and preserve the global search ability, Sun et al.¹⁵ proposed the QPSO algorithm. In the QPSO model, particles move in a quantum multi-dimensional space, the state of particles is usually depicted by a normalized wave function. That is, a single particle with m mass is subjected to the influence of a potential field in quantum space and the wave function of this particle is governed by the Schrödinger equation.¹² The solution of time-independent Schrödinger equation for this system in one dimensional space can be expressed as¹²:

$$p_i = pf_i^c \pm \frac{L}{2} \cdot \ln\left(\frac{1}{\lambda}\right), \quad (4)$$

where λ is a random number uniformly distributed on $[0, 1]$ and L is the characteristic length of delta potential well (called "Creativity" of particles) which specifies the search scope of a particle. In order to improve performance, Sun et al.¹⁵ employ a mainstream thought point to evaluate the parameter. The mainstream thought point and can be expressed as the following forms:

$$mbest = \left[\sum_{i=1}^n \frac{p_{i,1}}{n}, \sum_{i=1}^n \frac{p_{i,2}}{n}, \dots, \sum_{i=1}^n \frac{p_{i,n}}{n} \right], i = 1, 2, \dots, n, \quad (5)$$

$$L = 2 \cdot \beta |mbest - p_i|, \quad (6)$$

where β is a creative coefficient which is used to adjust the convergence speed of an individual particle and the performance of this algorithm.

Firstly, in order to achieve global searching, β should be set to a large number at the beginning. Then the parameter β is adjusted decreasingly. The decreasing rate of β can be linear, but nonlinear revision according to the convergence of optimization process is more reasonable. The creative coefficient β with adaptive annealing learning mechanism according to the change rate of optimal estimation has the form:

$$\beta = \beta_{\max} - \Delta\beta \cdot (\Delta fit)^{\gamma}, \quad (7)$$

$$\Delta fit = |p^g - p_i^l|, \quad (8)$$

where $\Delta\beta$ is step length of β , Δfit is the change rate of optimal estimation so far. The mechanism of adaptive annealing learning can overcome the stagnation problem to accelerate the convergent speed. Another improvement

of the HEMQPSO is elitist reproduction. The mutation mechanism is usually used for keeping diversity and avoiding premature.

3. Problem Formulation

This section presents two chaos systems of Chen system and Genesio system to synchronize their behavior. The dynamic equation of Genesio system is given by

$$\begin{cases} \dot{\hat{x}}_1 = \hat{x}_2, \\ \dot{\hat{x}}_2 = \hat{x}_3, \\ \dot{\hat{x}}_3 = r_1 \hat{x}_1 + r_2 \hat{x}_2 + r_3 \hat{x}_3 + \hat{x}_1^2, \end{cases} \quad (9)$$

where $\hat{x}_1, \hat{x}_2, \hat{x}_3$, are state variables, $r_1 = -6$, $r_2 = -2.92$, $r_3 = -1.2$, for the chaotic system (9). Chen system is described by

$$\begin{cases} \dot{x}_1 = q_1(x_2 - x_1), \\ \dot{x}_2 = (q_2 - q_1)x_1 + q_2x_2 - x_1x_3, \\ \dot{x}_3 = x_1x_2 - q_3x_3, \end{cases} \quad (10)$$

when $q_1 = 35$, $q_2 = 28$, $q_3 = 3$, the system (10) is chaotic.

4. Simulation Results

Consider that Genesio system (9) is the drive system and the controlled Chen system (11) is the response system. The synchronization behavior between Chen system and Genesio system using active control is observed.

$$\begin{cases} \dot{x}_1 = q_1(x_2 - x_1) + u_1, \\ \dot{x}_2 = (q_2 - q_1)x_1 + q_2x_2 - x_1x_3 + u_2, \\ \dot{x}_3 = x_1x_2 - q_3x_3 + u_3, \end{cases} \quad (11)$$

Three control functions u_1, u_2, u_3 , are introduced in system (11), in order to determine the control functions to realize synchronization between systems (9) and (11), we subtract (9) from (11) and get the deviation of errors system can be expressed as

$$\begin{cases} \dot{e}_1 = -q_1e_1, \\ \dot{e}_2 = -q_2e_2, \\ \dot{e}_3 = -q_3e_3, \end{cases} \quad (12)$$

where $e_1 = x_1 - \hat{x}_1$, $e_2 = x_2 - \hat{x}_2$, $e_3 = x_3 - \hat{x}_3$, The error system (12) is asymptotically stable by linear control theory.⁶

The sampling time is equal to 0.005 and the number of states is set as 200 for three simulated examples. The

initial values of the drive and response systems are $\hat{x}_1(0) = -1$, $\hat{x}_2(0) = 0$, $\hat{x}_3(0) = 1$, $x_1(0) = -5$, $x_2(0) = 10$, $x_3(0) = 5$, respectively. In HEMQPSO, the parameters, β_{\max} and γ in Eq. (7), are set as 0.5 and 0.5. Comparisons of HEQPSO¹⁶ and HEMQPSO are shown in Figs. 1 and 2, respectively, in which the superiority of the proposed HEMQPSO is verified.

5. Conclusions

This paper presents the proposed HEMQPSO to synchronize chaotic systems. The evolutionary algorithm can overcome the stagnation in searching global solutions for synchronizing two chaotic systems. From the simulation results, we can conclude that the proposed HEMQPSO method has good performance for chaos synchronization. The future work is to apply HEMQPSO for investigating more complex chaotic systems.

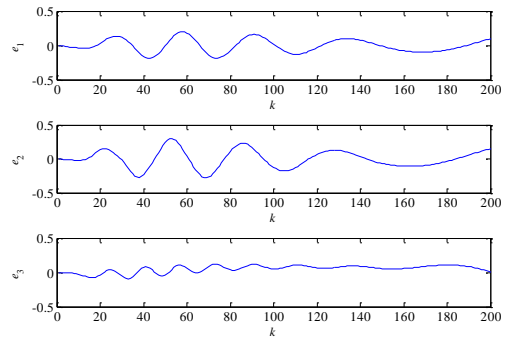


Fig. 1. Synchronization errors between Chen and Genesio systems via active control with HEQPSO.

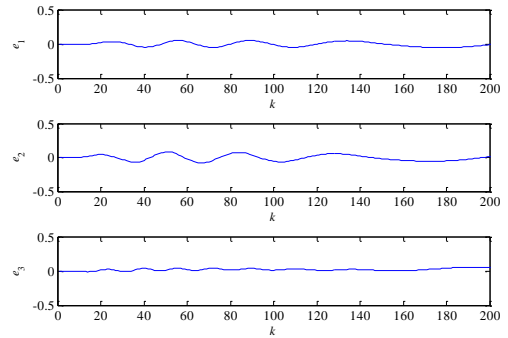


Fig. 2. Synchronization errors between Chen and Genesio systems via active control with HEMQPSO.

Acknowledgements

This work was supported in part by the Ministry of Science and Technology, R.O.C., under grants MOST 104-2221-E-252-004.

References

1. J. H. Kim, C. W. Park, E. Kim, and M. Park, Fuzzy adaptive synchronization of uncertain chaotic systems, *Physics Letters A* **334** (2005) 295-305.
2. J. P. Yeh, Identifying chaotic systems using a fuzzy model coupled with a linear plant, *Chaos, Solitons and Fractals* **32** (2007) 1178-1187.
3. H. Modares, A. Alf, and M. M. Fateh, Parameter identification of chaotic dynamic systems through an improved particle swarm optimization, *Expert Systems with Applications* **37** (2010) 3714-3720.
4. C. H. Lee, F. Y. Chang, and C. M. Lin, An efficient interval type-2 fuzzy CMAC for chaos time-series prediction and synchronization, *IEEE Transactions on Cybernetics* **44**(3) (2014) 329-341.
5. M. P. Aghababa and A. Heydari, Chaos synchronization between two different chaotic systems with uncertainties, external disturbance, unknown parameters and input nonlinearities, *Applied Mathematical Modeling* **36** (2012) 1639-1652.
6. X. Y. Wu, Z. H. Guan, Z. P. Wu, T. Li, Chaos synchronization between Chen system and Genesio system, *Physics Letters A* **364** (2007) 484-487.
7. A. S. Hegazi, E. Ahmed, and A. E. Matouk, On chaos control and synchronization of the commensurate fractional order Liu system, *Communications in Nonlinear Science and Numerical Simulation* **18**(5) (2013) 1193-1202.
8. Y. H. Deng, H. P. Hu, N. X. Xiong, W. Xiong, and L. F. Liu, A general hybrid model for chaos robust synchronization and degradation reduction, *Information Sciences* **305** (2015) 146-164.
9. A. Ratnaweera, S. K. Halgamuge, and H. C. Watson, Self-organizing hierarchical particle swarm optimizer with time-varying acceleration coefficients, *IEEE Transactions on Evolutionary Computation* **8** (2004) 240-255.
10. P. J. Chuang and C. P. Wu, Employing PSO to enhance RSS rang-base node localization for wireless sensor networks, *Journal of Information Science and Engineering* **27** (2011) 1597-1611.
11. L. S. Coelho and P. G. Alotto, Global optimization of electromagnetic devices using an exponential quantum-behaved particle swarm optimizer, *IEEE Transactions on Magnetism* **44** (2008) 1074-1077.
12. Y. Fu, M. Ding, and C. Zhou, Phase angle-encoded and quantum-behaved particle swarm optimization applied to three-dimensional route planning for UAV, *IEEE Transactions on Systems, Man and Cybernetics, Part A: Systems and Humans* **42** (2012) 511-526.
13. M. Clerc and J. Kennedy, The particle swarm: explosion, stability, and convergence in a multidimensional complex space, *IEEE Transactions on Evolutionary Computation* **1** (2002) 68-73.
14. S. M. Mikki and A. A. Kishk, Quantum Particle Swarm Optimization for Electromagnetics, *IEEE Transactions on Antennas and Propagation* **54** (2006) 2764-2775.
15. J. Sun, B. Feng, and W.B. Xu, Particle swarm optimization with particles having quantum behavior, *In: Proceedings of IEEE Congress on Evolutionary Computation*, 2004. pp. 325-331.
16. C. N. Ko, Y. M. Jau, and J. T. Jeng, Parameter Estimation of Chaotic Dynamical Systems Using Quantum-behaved Particle Swarm Optimization Based on Hybrid Evolution, *Journal of Information Science and Engineering* **31**(2) (2015) 675-689.

A Simulation Model of Hall Sensor Misalignment in BLDC Motors

Chung-Wen Hung

*Department of Electrical Engineering, National Yunlin University of Science & Technology,
123, Sec. 3, University Road, Douliou, Yunlin, 64002, Taiwan*

Chu-Lin Hsu

*Department of Electrical Engineering, National Yunlin University of Science & Technology,
123, Sec. 3, University Road, Douliou, Yunlin, 64002, Taiwan
E-mail: wenhung@yuntech.edu.tw, B10100061@yuntech.edu.tw
www.yuntech.edu.tw*

Abstract

A simulation model of Hall sensor misalignment in BLDC motors is proposed in this paper. The Hall sensor is popularly used in brushless DC motor to decide commutate and rotational speed. However, the accuracy of Hall sensor position is limited in most of BLDC motors, and it is lack of suitable simulation model for Hall Sensor installation misalignment. The details of simulation model are discussed in this paper, and simulation results are also provided to show the model is workable.

Keywords: simulation model, BLDC motor, Hall sensor, misalignment.

1. Introduction

BLDC motors are popularly used nowadays due to its high power density, low maintenance requirement, and easy control. Most BLDC motors have Hall sensors which are used to decide commutation timing and estimate rotational speed. However, it is impossible to install Hall sensors in accurate position without error. This misalignment effect will cause torque ripple due to wrong commutation timing and incorrect speed feedback.

This phenomenon is highlighted in some studies and these papers tried to propose solution. [1] proposed a Hall-effect-sensor-based position observer to mitigate torque ripple in permanent-magnet synchronous machines, and the hardware and simulation validation showed the proposed algorithm is workable. [2] proposed an auxiliary circuit for BLDC motors, to reject the Hall sensor signal noise and capture time interval. The circuit is built in field programmable gate array, FPGA, and the experimental results show the circuit works as expecting. This work could be a good

reference for BLDC motor control integrated circuit. However, those two studies didn't discuss any simulation. [3] focused on commutation behavior situation of BLDC motor, and proposed a simulation model in MATLAB. [4] presented an efficient simulation model for variable sampling system, which is caused by low resolution effect of Hall sensors. However, it is a lack of simulation model for the Hall sensor position misalignment.

2. The Simulation Method

To simulate the Hall sensors in BLDC motors, the rotation information, distance, is necessary. It is used to decide the hall sensor signals. The most of BLDC motor simulation models only provide the rotational speed output, so an integrator will be used to perform the rotation distance. As shown in Fig. 1, to simplify explanation, the pole pair number is set to 1; H_x indicates Hall sensor whether x is a, b or c. When the BLDC motor rotational angle arrives 0 or π radians, means the point O reaches origin or H_a , the output of Hall sensor A will change due to the change of magnetic

field direction. The detail is presented in Fig. 2. If without reverse, the output of the integrator is monotony increasing. However, only the angular information within 0 to 2π is used, so the remainder divided by 2π is useful for the decision of Hall sensor signal. Similarly, when point rotates $5\pi/3$ or $2\pi/3$ radians, the output of the Hall sensor B will change. Again, Hall sensor C will change at $\pi/3$ and $4\pi/3$ radians.

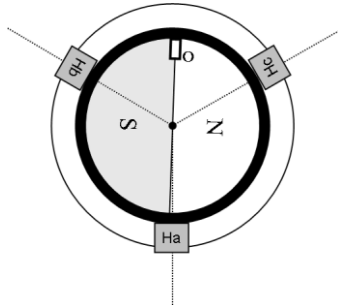


Fig. 1. Diagram of Hall-sensor and relative rotor positions

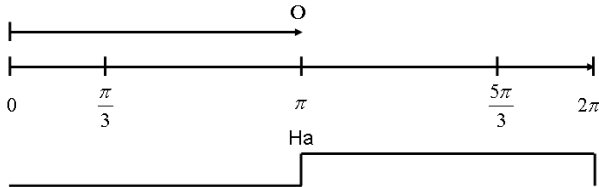


Fig. 2. The relationship between Rotation angle and Hall sensor output

3. The Proposed Simulation Model

As discussed in the previous section, an integrator is used to integrate rotational speed to rotational distance, which is equivalent to rotational angle; a remainder block is built to calculate rotational angle within 0 to 2π . This block comprises a divider, a rounder, and an adder. A relational operator is applied to decide Hall sensor signal. The simulation model is shown in Fig. 3. Note, to simplify the calculation, the output of the remainder block is ratio of 2π , and the second input of the relational operator is changed to $1/2$ from π . The other relational operator could be skipped, because remainder function will change the output to zero when divisible. However, the output of Hall Sensor B is positive, when rotational angle is larger than $5\pi/3$ or less than $2\pi/3$. And again, Hall Sensor C output high when larger than $\pi/3$ and less than $4\pi/6$. The details are shown in Fig. 4,

and described as (1)-(3). Here, % indicates remainder operator and θ presents the integrated rotational angle.

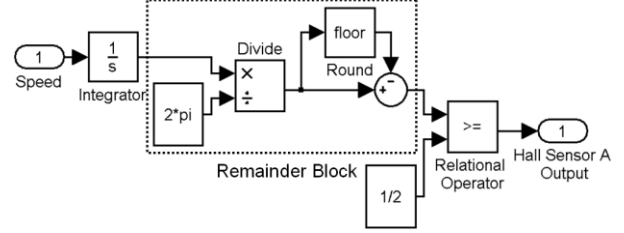


Fig. 3. Simulation model of Hall-sensor

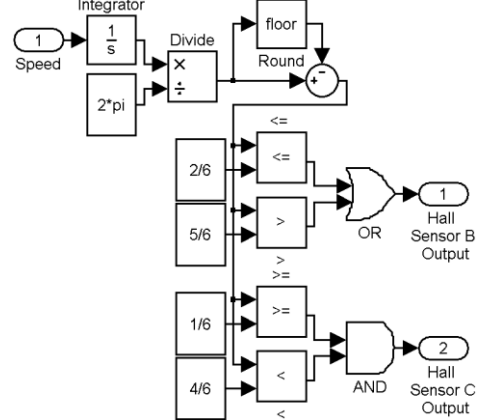
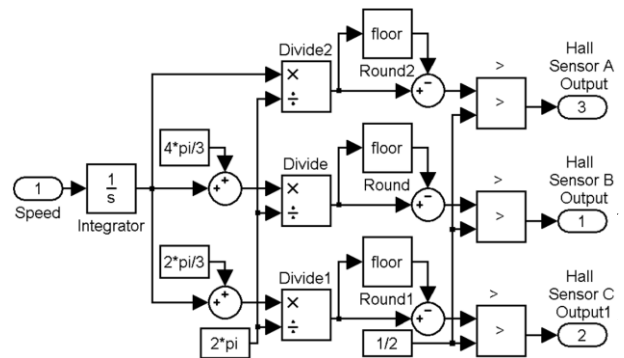


Fig. 4. Simulation model of Hall-sensor B and C

Hall _A (θ) = 0,	if ($\theta \% 2\pi$) < π	(1)
= 1,	if ($\theta \% 2\pi$) $\geq \pi$	
Hall _B (θ) = 1,	if ($\theta \% 2\pi$) $\leq 2\pi/3$, or ($\theta \% 2\pi$) > $5\pi/3$	(2)
= 0,	o. w.	
Hall _C (θ) = 1,	if ($\theta \% 2\pi$) $\geq \pi/3$, and ($\theta \% 2\pi$) < $4\pi/3$	(3)
= 0,	o. w.	



However, an equivalent operation could be performed with adding an angle shifter to the integrator output. For the Hall sensor B, the output is high till the point O runs to $2\pi/3$, and then keep in low before it runs to $5\pi/3$. If $4\pi/3$ is added into to the integrator output, the

summation will be fed into the remainder block and relational operator block, which are the same as Hall channel A. The outputs will be equivalent to the previous model. Similarly, a $4\pi/3$ shifter performs the same effect for channel C. The calculation requirement may not be less than previous one. However, it is simpler and easier to understand. Moreover, it implies an advance what will be introduced in next section.

In most BLDC motor, the accuracy of hall sensor installation is limited, as presented in Fig. 6. The hall sensor may not be installed in correct position, it will cause wrong interval of HALL sensor signal. A novel simulation model is proposed to simulate this misalignment effect, and the position error is added to the two relational operators in Fig. 4. As shown in Fig. 7, the Hall sensor B channel is modified, and it can work well to reflect the misalignment effect.

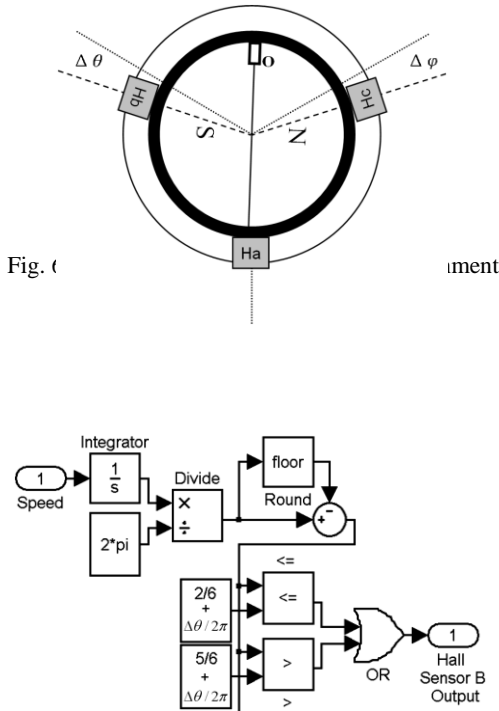


Fig.7. Misalignment simulation model of Hall-sensor B

However, misalignment effect could be simulated easier, if the previous equivalent simulation model is selected. Because rotor and Hall sensor are symmetric, only one

shifter which is used to add position error is needed, as shown in Fig. 8. It is more intuitive and can avoid missing the other relational operator in Fig. 7. Note that, an extra shifter could be added into channel A if there is any position error for the Hall sensor A.

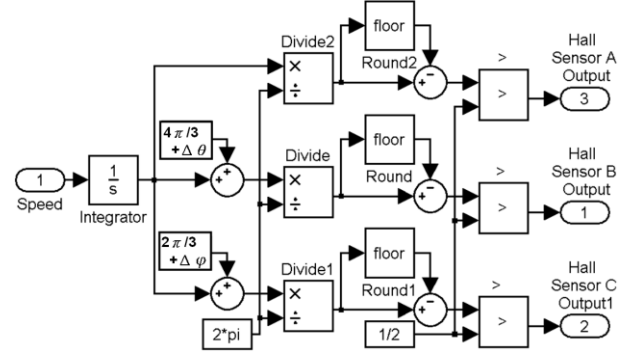


Fig. 8. Equivalent misalignment simulation model

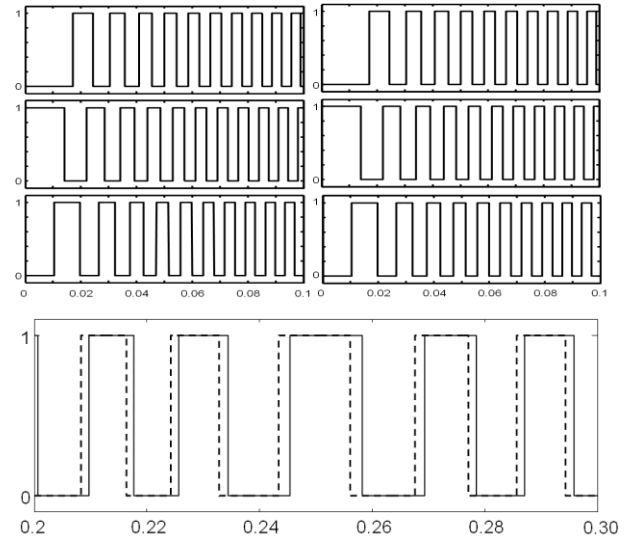


Fig. 10. Simulation result of Hall sensor B with misalignment

5. Simulation Results

To verify the proposed simulation model work well, the proposed model is add to the BLEDM DEMO model in Matlab Simulink. The input of the proposed model is the BLDC motor speed, and the output is Hall sensor output. Fig. 9 presents the Hall sensor signal comparison between the Matlab Simulink demonstrational and proposed models without misalignment. It shows that the two outputs of Hall

sensors are the same. Next, to show the misalignment effect, the proposed misalignment model is used to replace, and the channel B result is shown in Fig. 10. Obviously, the proposed simulation model could simulate the misalignment effect well.

6. Conclusion

A Simulation Model of Hall Sensor Misalignment in BLDC Motors is proposed in this paper. For most BLDC motors, it is very difficult and expensive to install Hall sensors in correct position accurately. And it will cause torque ripple and wrong speed feedback. The proposed model could simulate exactly this misalignment effect, and it can provide a good simulation reference to engineers for designs of BLDC motor controllers.

Acknowledgements

This work is partially supported by the Ministry of Science and Technology, ROC, under contract No. NSC 103-2622-E-224-056 and 104-2221-E-224-012.

References

1. P. B. Beccue, S. D. Pekarek, B. J. Deken, and A. C. Koenig, Compensation for Asymmetries and Misalignment in a Hall-Effect Position Observer Used in PMSM Torque-Ripple Control, *IEEE Transactions On Industry Applications*, Vol. 43, NO. 2, MARCH/APRIL 2007, pp. 560-570.
2. C.-W. Hung and J.-H. Chen, A Hall Sensor Auxiliary Circuit with Noise Rejection and Time Interval Capture Functions for BLDC Motors, *Sensor Letters*, Vol. 10, 2012, pp. 1178–1184.
3. B. Tibor, V. Fedák, and F. Ďurovský, Modeling and Simulation of the BLDC Motor in MATLAB GUI, in *Proc. 2011 IEEE International Symposium on Industrial Electronics (ISIE)*, 27-30 June 2011 pp.1403-1407
4. C.-W. Hung, C.-T. Lin and C.-W. Liu, An Efficient Simulation Technique for the Variable Sampling Effect of BLDG Motor Applications, in *Proc.33rd Annual Conference of the IEEE Industrial Electronics Society*, Nov. 5-8, 2007 (Taipei, Taiwan, 2007), pp. 1175 - 1179

Using Multi-Target Tracking and Identification TLD Algorithm for Intelligent Mobile Robot

Jr-Hung Guo

*Department of Electrical Engineering, National Chin-Yi University Of Technology, No.57, Sec. 2, Zhongshan Rd.,
Taiping Dist., Taichung 41170, Taiwan*

Kuo-Hsien Hsia*

Department of Electrical Engineering, Far East University, No.49, Chung Hua Rd., Hsin-Shih. 74448 Tainan, Taiwan

Kuo-Lan Su

*Department of Electrical Engineering, National Yunlin University of Science & Technology, 123 University Road,
Section 3, Douliou, Yunlin 64002, Taiwan*

E-mail: g9710801@yuntech.edu.tw, khhsia@cc.feu.edu.tw, sukl@yuntech.edu.tw*

Abstract

Image algorithms used herein are Tracking-Learning-Detection (TLD) and Speed UP Robust Features (SURF). TLD is used for target tracking and SURF is used for identifying targets. We use zoning identification, with the use of statistical probability to strengthen the efficiency of TLD and SURF. With such a method, the efficiency of image identification and target tracking can be enhanced so that the robot can simultaneously track and identify multiple targets.

Keywords: multi-target tracking, TLD, SURF, image identification, mobile robot.

1. Introduction

Image recognition and tracking technology are important issues on robotics research. Fabian et al. [1] used Microsoft Kinect and Simulink for instant object tracking. Marković et al. [2] used omnidirectional camera on a mobile robot to track and follow objects. Huang et al. [3] used the SURF algorithm to make the robot have the ability to follow the object. As can be seen from previous studies, image recognition and tracking technology usually require dedicated imaging equipment or complex algorithms. But this will cause an increase in the cost of mobile robot, or reduce the efficiency of the mobile robot. Therefore, how to enhance the efficiency of the mobile robot on image identification and tracking is the main research purpose of this paper.

The image tracking algorithm that we use is TLD [4] which was developed by Zdenek Kalal, University of Surrey, Czech. The TLD algorithm used for tracking single-target for a long time. In this paper we extend the TLD algorithm to multi-target tracking based on the original single-target tracking. But this algorithm cannot identify the tracked target. The TLD framework improves the tracking performance by combining a detector and an optical-flow tracker. Since this algorithm is based on optical flow, the accuracy of TLD cannot be high. So we use Speed UP Robust Features (SURF) to assist the targets identification and as an auxiliary for TLD algorithm to track the targets.

SURF is based on the scale-invariant feature transform Scale-invariant feature transform (SIFT) to identify the object. Although SURF operation is relatively light to the SIFT, it will still affect the effectiveness of the mobile robot. Therefore, in this paper, the image is divided into some separate regions. Each region is detected in turn. Supplemented with the statistics and probability, it can assist TLD on tracking. The target tracking and identification process with SURF and TLD is shown in Fig. 1. The relevant algorithms will be explained in the next section.

2. Algorithms

2.1. TLD

TLD technology is divided into three parts. They are the tracker, the learning process and the detector. Tracker and detector operate in parallel in TLD. Both the tracking and detecting results will feed into the learning process. The new model after learning is feedback to the tracker and detector resulting in a real-time updating. The overall process ensures that even if the target appearance changes, the target can still be tracked. The architecture of TLD tracking is shown in Fig. 2.

TLD's tracker estimates the motion of the target using the Lucas-Kanada [6] [7] optical flow, which is a frame to frame tracking method. However, the precision of the optical flow tracking is not high, thus it often results in a tracking failure. The detector records the history of target locations and surface information, called learning, and will re-detect while tracking failure.

P-N learning [9] is a very important part of tracking in TLD. Here P is Positive Constraint, also known as P-expert or growing event, and N is Negative Constraint, also known as N-expert or pruning event. In practice, P-experts as well as N-experts will have a certain bias, but the study of Zdenek Kalal found that, although there is an error, under certain conditions, the error is acceptable, and performance testing module will therefore be improved. The P-N learning consists of four parts:

- (i) A classifier for learning;
- (ii) A training sample set;
- (iii) Supervised learning;
- (iv) P-N experts: to generate positive and negative samples in the learning process;

The relationship between these parts is shown in Fig. 3.

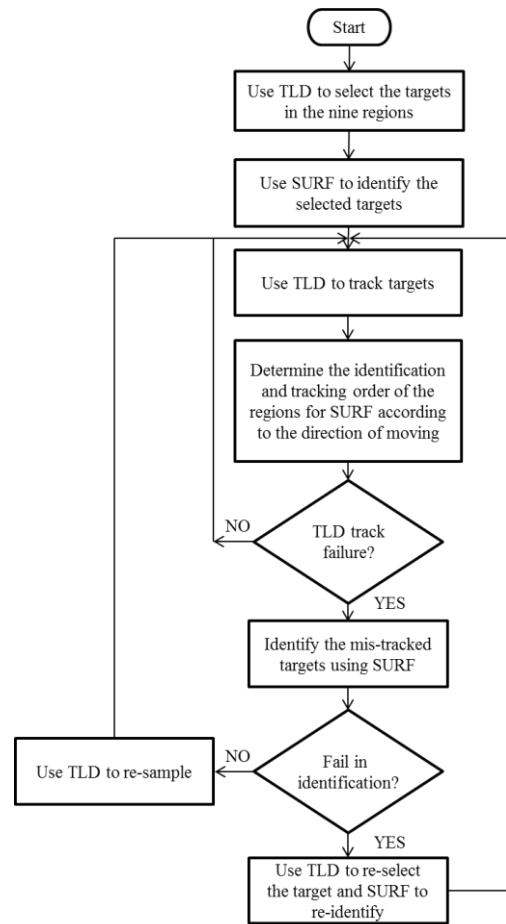


Fig. 1. Target tracking and identification process with SURF and TLD.



Fig. 2. TLD tracking architecture [4].

The “random forest” classifier, which can instantly update and forecast, is used in the detector [4, 6]. The information for the feature detector is generated by random forests 2bitBP (2 bit binary pattern). The gradient orientation information of a specific area will be

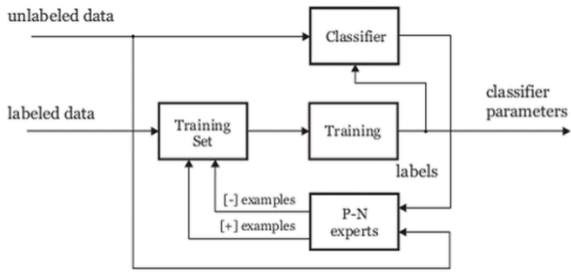


Fig. 3. TLD learning architecture [8].

converted into encoded output. 2bitBP is similar to harr-like feature which includes the feature type and the corresponding characteristic values. Therefore, when using nFeat type to express the object, each Fern is a Quad tree because of the 2bitBP characteristics.

TLD tracking module is based on the Median Flow tracker method. This method is performed on a frame. Select some pixels as the feature points in the previous frame and then find the corresponding positions in the current frame by the feature values. Then sort the displacements of these features pixels and find the median of these displacements. Finally let the pixels less than 50% of the median as the next feature pixels. Since this approach assumes that the tracked object is in the frame, it will fail once the object is out of the frame or obscured. The SURF will be used for confirmation at that time. Once it is confirmed, the new tracking target will be selected by the TLD.

2.2. SURF

SURF is a technology for image recognition and tracking based on SIFT. The main difference is that SIFT uses DoG (Difference-of-Gaussians) image, and SURF uses the determinant of a Hessian matrix to approximate the image. The Hessian matrix of a pixel in an image can be defined as [5]:

$$H(f(x, y)) = \begin{bmatrix} \frac{\partial^2 f}{\partial x^2} & \frac{\partial^2 f}{\partial x \partial y} \\ \frac{\partial^2 f}{\partial x \partial y} & \frac{\partial^2 f}{\partial y^2} \end{bmatrix} \quad (1)$$

The determinant of H is:

$$\det(H) = \frac{\partial^2 f}{\partial x^2} \frac{\partial^2 f}{\partial y^2} - \left(\frac{\partial^2 f}{\partial x \partial y} \right)^2 \quad (2)$$

The sign of the determinant value can be used to classify the point and to determine the point is an extreme point or not. In the SURF algorithm, the function value $f(x, y)$ is replaced by the image pixel $I(x, y)$, and a second-order standard Gaussian function is chosen as a filter. Then elements of H matrix can be obtained by convolution and second-order partial derivatives as following:

$$H(x, y, \sigma) = \begin{bmatrix} L_{xx}(x, y, \sigma) & L_{xy}(x, y, \sigma) \\ L_{xy}(x, y, \sigma) & L_{yy}(x, y, \sigma) \end{bmatrix} \quad (3)$$

$$L(x, y, \sigma) = G(x, y, \sigma) * I(x, y) \quad (4)$$

where

$$G(x, y, \sigma) = \frac{1}{2\pi\sigma^2} e^{-(x^2+y^2)/2\sigma^2} \quad (5)$$

and σ is the scale. The determinant of the H matrix of each pixel of the image can be obtained. Hence each point can be classified. For the ease of application, Herbert Bay proposed to replace the L by an approximation [9]. The discriminant of H matrix can be expressed as:

$$G(t) = \frac{\partial^2 g(t)}{\partial x^2} \quad (6)$$

Finally, what we want is a transformed image of the original image, because we have to look for the feature points on the transformed image and then reflect it onto the original image. And this is constituted by the approximate determinant of the Hessian matrix of each pixel with the approximate determinant defined by:

$$\det(H_{approx}) = D_{xx}D_{yy} - (0.9D_{xy})^2 \quad (7)$$

Since SURF process the pixels at the image for Hessian matrix processing simultaneously on both X and Y directions, its efficiency is better than SIFT. But it still requires a large amount of computation. So we take the solution as follows:

- (i) Identify region by region to reduce the amount of pixel processing. Because the entire image is divided into nine regions for TLD tracking, SURF will therefore use the same area for identification and tracking.
- (ii) Determine the identification sequence according to the orientation. Since the orientation of the robot can be known, we design the scanning sequence following the orientation of the robot, as shown in

Fig. 4. The central region is of higher priority, then the upper and lower regions. With this strategy, the target tracking for the mobile robot can be of higher efficiency.

3. Experimental Results

A Microsoft's LifeCam Cinema was used in our experiments. Because of its large aperture and high-resolution, images with better quality can be obtained. For the image tracking and identification system, the entire image was cut into nine regions, and TLD was applied to have the tracked object, and then SURF was used for identification. The CPU of the computer for the experiment is INTEL I5-3470 with 8G memory, and the system was developed by EMGUCV 2.4 and Microsoft Visual Studio VB2010. The experimental results are shown in Fig. 5. The red box marks the tracking target of TLD, and the blue box marks the SURF tracking and identification results with the identification result of SURF marked at the upper right corner.

4. Conclusion

The TLD and SURF algorithms are successfully combined in this paper so that the robot's vision system can track and identify the targets. The entire image is divided into nine regions, in order to reduce the loading on image processing, and to enhance the efficiency of tracking and identification. You used a mid-level webcam in this paper resulting a lower image quality and higher failure rate in tracking and identification. High-level camera and CUDA (Compute Unified Device Architecture) can increase the quality of image and efficiency of image processing. Thus this algorithm can be used in a more complex environment. We believe that the algorithm can be widely used in robot systems in the near future.

Acknowledgements

This work was partially supported by National Science Council of Taiwan. (NSC 104-2221-E-224 -015 -).

References

1. J. Fabian, T. Young, J.C. Peyton Jones, and G.M. Clayton, Integrating the Microsoft Kinect with Simulink: Real-time object tracking example, *IEEE/ASME Transactions on Mechatronics*, 19(1) (2014) 249-257.

© The 2016 International Conference on Artificial Life and Robotics (ICAROB 2016), Jan. 29-31, Okinawa Convention Center, Okinawa, Japan

3	5	8	6	2	7	8	5	3
1	2	7	4	1	5	7	2	1
4	6	9	8	3	9	9	6	4
(a) turn left			(b) forward			(c) turn right		

Fig. 4. Robot orientation relationship with SURF scanning order.



Fig. 5. Tracking and identification result by TLD and SURF.

2. I. Marković, F. Chaumette and I. Petrović, Moving object detection, tracking and following using an omnidirectional camera on a mobile robot, *2014 IEEE Int. Conf. Robotics and Automation (ICRA)* (Hong Kong, China, 2014), pp. 5630-5635.
3. P.T. Huang, C.Y. Li, C.C. Hsu, and C.M. Hong, Object following based on SURF for mobile robots, *2012 IEEE 1st Global Conf. Consumer Electronics (GCCE)* (Tokyo, Japan, 2012), pp. 382-386.
4. Z. Kalal, K. Mikolajczyk, and J. Matas, Tracking-learning-detection, *IEEE Trans. on Pattern Analysis and Machine Intelligence*, 34(7) (2012) 1409-1422.
5. C. Evans, *Notes on the OpenSURF library*, (University of Bristol, Tech. Rep. CSTR-09-001, January, 2009).
6. B.D. Lucas, *Generalized image matching by the method of differences*, (doctoral dissertation, tech. report, Robotics Institute, Carnegie Mellon University, 1984).
7. B.D. Lucas, and T. Kanade, An iterative image registration technique with an application to stereo vision, in *Proceedings of the 7th Int. Joint Conf. Artificial Intelligence (IJCAI)* (1981) 674-679.
8. Z. Kalal, J. Matas, and K. Mikolajczyk, P-N learning: Bootstrapping binary classifiers by structural constraints, *2010 IEEE Conf. Computer Vision and Pattern Recognition (CVPR)* (San Francisco, CA, 2010) 49-56.
9. H. Bay, A. Ess, T. Tuytelaars, and L. Van Gool, SURF: Speeded Up Robust Features, *Computer Vision and Image Understanding (CVIU)*, 110(3) (2008) 346-359.

Handheld Mobile Devices for Remote Monitoring of Factory

Bing-Gang, Jhong

*Department of Mechatronic Engineering, National Taiwan Normal University,
162 Section 1 Heping E. Rd., Taipei City 106, Taiwan*

Jian-Sing, Hu; Mei-Yung, Chen

*Department of Mechatronic Engineering, National Taiwan Normal University,
162 Section 1 Heping E. Rd., Taipei City 106, Taiwan
E-mail: Jhong.bing.gang@gmail.com, cmy@ntnu.edu.com.tw
www3.ntnu.edu.tw*

Abstract

In this paper, a handheld mobile device system is presented for remote monitoring of the factory to short the downtime of machines and recovery more quickly. The human–computer interaction of the system is developed by GP-Por EX, and operates by using commercial or free distal APP combining with sign-in-website of the company. The way for the program connected can be connected with multi-way links, such as long-distance link (3G/4G or Wi-Fi wireless INTERNET), medium distance (LAN) and short distance (ETHERNET) and can be chosen in the company portal page. With supplemented Internet browser program for remote monitoring, the distal end operator or the person in charge can confirm the machine condition through the distal end of the server, port, user name and password settings. Therefore, the operational efficiency and system transparency can be improved with the handheld mobile devices for remote monitoring system.

Keywords: Human Machine Interface, Remote monitoring, GP-Por EX, GP-Viewer EX.

1. Introduction

Human Machine Interface, often used with touch panel, is a control equipment connecting with human and machines. Because of within CPU, memories and connect interface units, it can connect to other hardware, such as PLC, PID controller and servo controller, so that theirs information can be shown on the screens for the operators to understand the state of machines. Developed by different companies and different purposes, HMI may have different functions.

In early stage, the aim of developing HMI is only for simplifying the control interface, reducing the risk of design, and increasing the modification of electrical

panel design. As technology advances, HMI now is not the button-only panel, but with logic control,

Multi-machine interconnected communication. Therefore, due to its versatility, wide adaptation, high reliability and other advantage, HMI has widely used in the automated machine equipment control to propose high quality automated machine service.

The inner workings of monitoring and abnormal maintenance both need engineering staff to maintenance in site in the past, which is time-consuming and effortless. If we can use the network function, and with the internet and wireless network, the dream of remote monitoring may become true [1-2]. For our case as example, due to the technology limit for the early construction of the

factory, only few machines can be connected to internet. However, thanking for the continuous evolution of network technology, now we can use the free APP with handheld devices to connect to the program of company entrance, build the HMI by GP-Por EX software for coordination, so that all the automation equipment have the abilities of remote monitoring.

The different HMIs are used in different location. 3G/4G and Wi-Fi is for where is far away from factory. Therefore, if the data of company entry, such as server IP, port, user name and password are known and already preset, then we can achieve remote monitoring to get the information about the states of automation equipment in the factory.

This paper is organized as follows. The methodology is proposed in Section 2. Section 3 presents experiment results. Finally, some conclusions are summarized in Section 4.

2. The Main Text

2.1. HMI Monitoring program

Our HMI program is developed by GP-Por EX software, and import the network components form the communication software named GP-Viewer EX. With connecting to the server of factory, GP-Viewer EX will read the HMI after running, and check this link is Connect or not. If the link is correct, all the state of automation equipment will be shown on the screen by switching the screen. However, if the link is not correct, this program will try to do malfunction reset to recover its production. The screen of monitor program is shown in fig. 2.

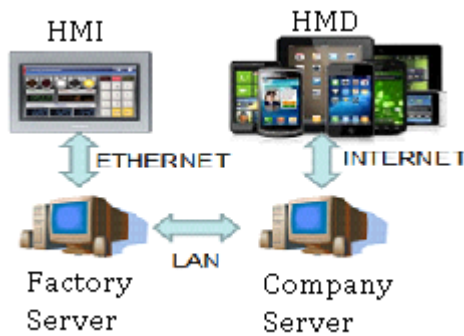


Fig. 1. The diagram of communication equipment

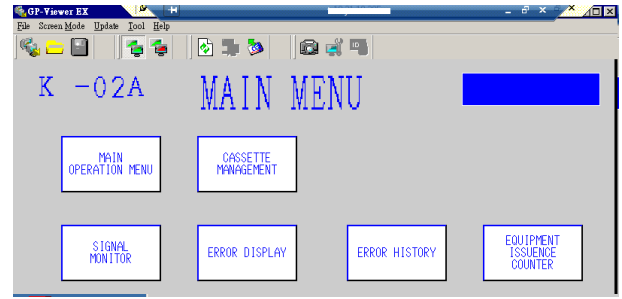


Fig. 2. The main window of monitoring program

2.2. Automation equipment malfunction reset

To describe reset process in detail, we propose the diagram of malfunction reset in fig. 3.

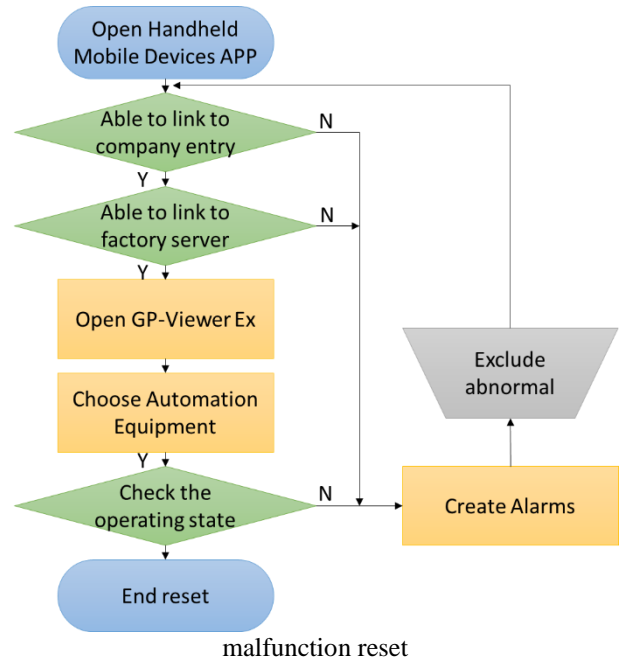


Fig. 3. The diagram of abnormal reset

2.3. The choosing of monitoring HMI

Porface company has developed many HMI. With different developing targets, their types are also different, and the connecting ways need to be used are different, too. Therefore, it is necessary to choose the types of HMI at the program beginning, so that this program can make correct choice for different type. For our monitoring program, it can work for the series of GT3000 and series of GT4000.

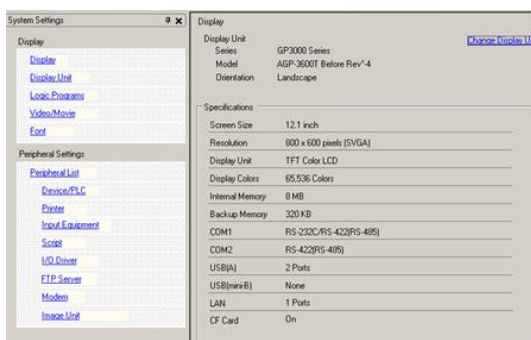


Fig. 4. The illustration of system setting

2.4. The handheld mobile devices and the communication interface

The handheld mobile devices APP requests the connecting data, including server IP, port, user name and password, shown in fig. 5. The select settings of communication interface of HMI against the ETHERTER internet is shown in fig. 6. With the correct setting IP, network number and station number shown in fig. 7, and all correct data in fig. 5 and fig. 6. The connecting between GP-Viewer EX program and HMI could be successfully.

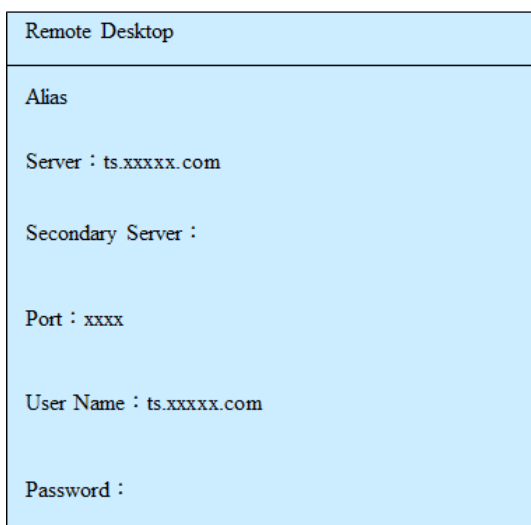


Fig. 5. The communication preferences page of handheld mobile devices

2.5. The connect between monitor APP and HMI

In the handheld mobile devices monitor APP, the interface connecting to HMI needs through the company

© The 2016 International Conference on Artificial Life and Robotics (ICAROB 2016), Jan. 29-31, Okinawa Convention Center, Okinawa, Japan

entry and the network of factory. Finally, the interface uses the communication software to connect the functions proposed from GP-Viewer EX, so that all the states of automation equipment appear in the software window at handheld mobile devices shown in fig. 8, or at PC shown in fig. 9. If the link is successful, it will return a running normally message and able to observe all the states of automation equipment. Otherwise, it will stop the foregoing actions.

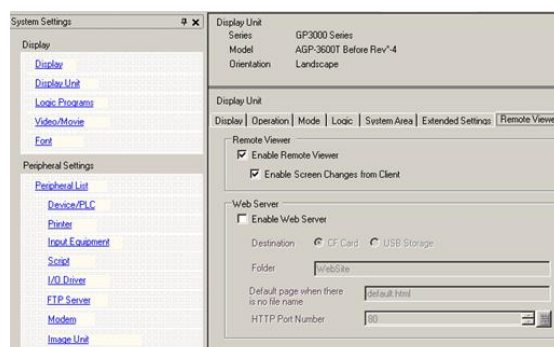


Fig. 6. The communication preferences page of HMI

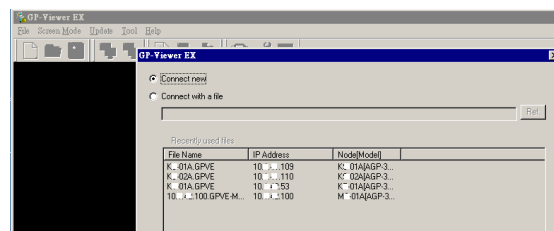


Fig. 7. The communication page of GP-Viewer EX

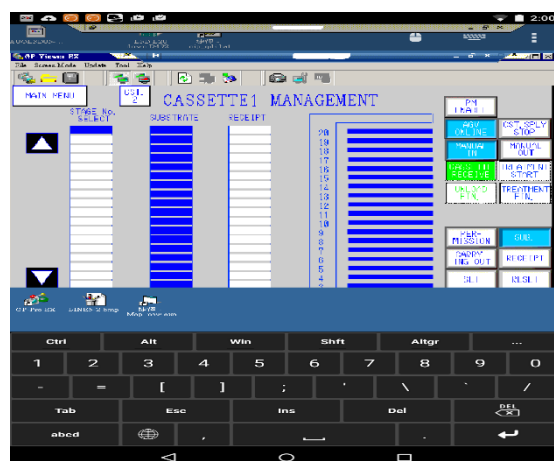


Fig. 8. The monitor program at handheld mobile devices

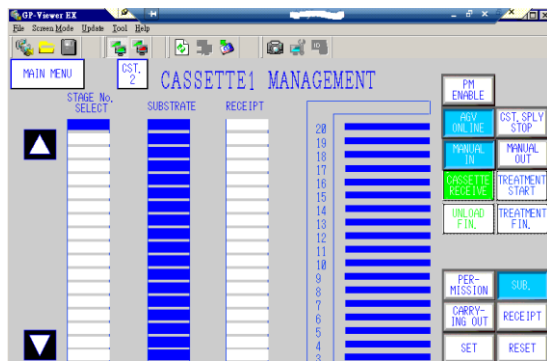


Fig. 9. The monitor program at PC

2.6. Exception Handling by HMI

When the online staff or equipment engineer find there are some errors which can't be solved, and the major engineer is also not in the factory at the same time, then he/she will start the remote monitoring program from his/her handheld mobile devices, and get the alarm by the HMI screen. With this information, the major engineer can try to analysis which parts are going wrong and do abnormal reset, so that the production equipment can recover to the normal state as soon as possible.

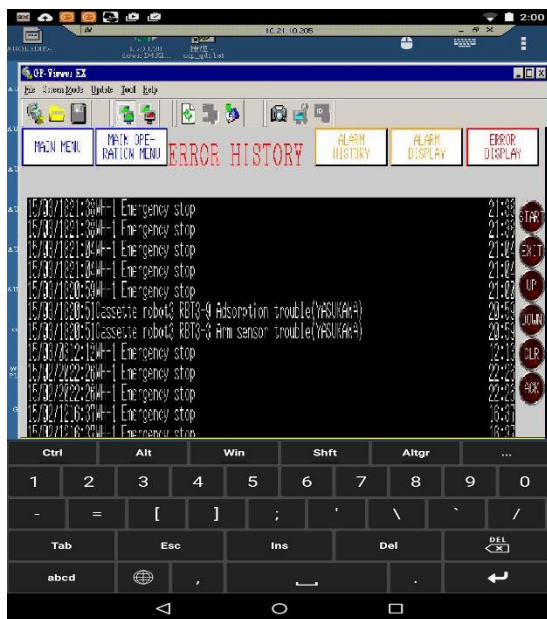


Fig. 10. The monitor program when get alarms

3. Experiment Results

In our research, we use the tablet Nexus II with 2X RDP APP as our handheld mobile devices for remote monitoring. In the local part, we use the server PC with GP-Viewer EX software to get the information of HMI through intranet. This server PC also connects to the entry of company. The handheld mobile devices are more popularize now, and the bandwidth of mobile network is larger and larger, so the location can be for grasping the operating of factory is not limited at established place. We test the time cost of start-up with different connection ways, including Wi-Fi, 3G and 4G. The result is given in Table 1, and can learn that the time cost will be shorter with larger download speed.

Table 1. The cost time with different connection mode.

Mode	Update	Download	Cost time
3G	1.12 Mb/s	9.15Mb/s	120s
4G	17.86Mb/s	21.23Mb/s	96s
Wi-Fi	2.78Mb/s	25.18Mb/s	90s

4. Conclusion

In this paper, we develop a handheld mobile device program using mobile internet through the entrance of company to the HMI of automated production equipment for remote monitoring. In the beginning, because of the firewall of server PC, we need to find some method, such as VNC, to connect the server PC. However, it will cause significant delays and only with the monitor screen and unable to fulfil the requirements of remote monitoring. Therefore, we change our research to replace the HMI of equipment with independent development of connection systems to accomplish mission.

References

1. Kusunoki, K., A CORBA-based remote monitoring system for factory automation, *International Symposium on Object-Oriented Real-time Distributed Computing*(Kyoto, Japan, 1998), pp. 396–402.
2. Xiaolan Xie et al., A Factory Remote Monitoring System Based on Pervasive Environment, *International Conference on Pervasive Computing and Applications*(Birmingham, UK, 2007), pp. 647–651.
3. Sharp Electric, Sharp Programmable Controller User Manual, Sharp Electric (1997).
4. Sharp Electric, Sharp Human Machine Interface User Manual, Sharp Electric (1997).

Task Assignment and Route Programming for Pattern Reformation on Grid Plane

Kuo-Hsien Hsia

*Department of Electrical Engineering, Far East University
No.49, Zhonghua Rd., Xinshi Dist., Tainan City 74448, Taiwan (R.O.C.)*

Bo-Yi Li

*Graduate School of Engineering Science & Technology (Doctoral Program)
National Yunlin University of Science & Technology
No. 123, University Road, Section 3, Douliou, Yunlin 64002, Taiwan (R.O.C.)*

Kuo-Lan Su

*Department of Electrical Engineering, National Yunlin University of Science & Technology
No. 123, University Road, Section 3, Douliou, Yunlin 64002, Taiwan (R.O.C.)
E-mail: khhsia@cc.feu.edu.tw, g9910813@yuntech.edu.tw, sukl@yuntech.edu.tw
www.feu.edu.tw*

Abstract

Pattern reformation problem on a grid plane is an interesting problem. Suppose there is a group of mobile robots on a square grid plane with the number of robots equaling to the number of columns/rows of the grid plane. The mobile robots are commanded to change to another formation as soon as possible. Any one of them has to prevent himself from colliding with other mobile robots during the moving of reformation process. In this paper, we will provide a systematic process on task assignment of route programming for the pattern reformation problem on a square grid plane. We will also provide a checking process to check if the suggested program is really good or not.

Keywords: Task assignment, pattern reformation, grid plane.

1. Introduction

There are mainly two category of programming problem: one is maximization problem and the other one is minimization problem. Minimum cost and minimum time are two of the most commonly used criterion of the minimization problem. Usually, the objective function of a minimum time problem is the sum of the spent time. However, for a problem that people start their works in cooperation at the same time and they want to complete the works as soon as possible, the objective function should be the maximum of the spent time. Pattern reformation problem is one of these problems.

2. Problem Formulation

Suppose there are some mobile robots placed on a square grid plane and forming certain pattern. The number of the mobile robots are the same as the rows of the square grid plane. There may or may not be obstacles on the grid plane. The mobile robots are commanded to reform another pattern in the shortest time and they can only move along the rows or the columns of the grid plane. This is definitely a minimum-time programming problem. Figure 1 is an example for six mobile robots on a 6x6 grid plane where the black squares form the target pattern, i.e. the 6 mobile robots are commanded to form the new pattern designated by the circles.

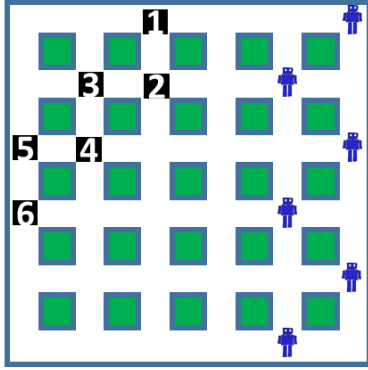


Fig. 1. Example of 6 mobile-robots on a 6x6 grid plane with the black squares forming the target formation.

There are two sub-problems that have to be considered for solving this problem. The first one is the task-assignment problem that each mobile robot's destination has to be determined for the minimum time requirement. The second one is the route programming problem that how each mobile robot should move to the target position in the shortest time without colliding with any other one mobile robot once the task assignment is completed. While dealing with the second sub-problem, it is possible to return to the first sub-problem because of the route conflict of any two mobile robots and one of them should wait for a step or detour to a further routing.

3. Algorithm for Task Assignment with Verification

Let each mobile robot has its ID and each target is also assigned an ID for convenience. The grid points on the grid plane are numbered sequentially with column majored from up to down and from left to right. For example, the grid point on the cross of the i^{th} row and j^{th} column on a 6x6 grid plane is numbered as $(j-1) \times 6 + i$. With these information, we can form a distance matrix with the row number represents the robot ID and the column number represents the destination ID. The element at row i and column j represents the steps needed for the mobile robot i to the destination j . This matrix can be determined by the diffusion method [1-2].

For the case of Fig. 1, suppose the robots are numbered from top to bottom as 1 to 6. By diffusion method, the distance matrix is:

	D1	D2	D3	D4	D5	D6
R1	3	4	5	6	7	8
R2	3	2	3	4	5	6
$\Delta =$ R3	5	4	5	4	5	6
R4	5	4	5	4	5	4
R5	7	6	7	6	7	6
R6	7	6	7	6	7	6

After the initial formation and target formation are determined, one can do the task assignment process. We have developed two algorithms for task assignment process [3-4]. The algorithm in [3] is simple but cannot guarantee the obtained result being with shortest time. When there is 0's in the distance matrix, the assignment result will often be wrong. Hence we developed a new algorithm, which is more complex but with better result, in [4]. However, there is still no mathematical proof for the optimality. Hence, in this paper, we develop a new task assignment algorithm, with which we believe that the shortest time can be guaranteed, as in the following.

- Step 1: Use the algorithm in [3] or [4] to determine the first assignment for the original distance matrix, Δ_1 . Determine the necessary moving time t_1 for the reformation.
- Step 2: Replace the elements greater than or equal to t_1 of the distance matrix by a sufficiently large number Z , e.g. 999. This forms the 2nd distance matrix.
- Step 3: Use the Hungarian algorithm [5] to check the minimum working time T_2 for the 2nd distance matrix Δ_2 . If $T_2 \geq Z$, then the obtained task assignment is the optimal one, else add 1 to the indices of Δ and t , and go to Step 1.

Because the Hungarian algorithm is a well-known method for solving minimum-cost task assignment problem, and the sufficiently large number Z is much larger than the required time for the task, the check can guarantee that there is no better alternative for the task assignment. Hence, each mobile robot will have its destination to form the overall new pattern.

There is one thing that should be noticed. The optimal task assignment is not unique. But one cannot find any other assignment way that will have a shorter time to complete the task.

After the target position determined, there may be more than one possible route to the target position. Refer to Fig.

2, both Routes 1 and 2 for Robot 1 are of distance 3. If both robots choose the dashed route, then they will collide after one step. If anyone of them waits a step to prevent the collision, then the task will be delayed for 1 unit of time. If any one and only one of them chooses the solid route, then there will be no collision and the task will be completed on time.

4. Experimental Results

Consider the example shown in Fig. 1. This means that the distance matrix is as equation (1).

$$\Delta_1 = \begin{bmatrix} 3 & 4 & 5 & 6 & 7 & 8 \\ 3 & 2 & 3 & 4 & 5 & 6 \\ 5 & 4 & 5 & 4 & 5 & 6 \\ 5 & 4 & 5 & 4 & 5 & 4 \\ 7 & 6 & 7 & 6 & 7 & 6 \\ 7 & 6 & 7 & 6 & 7 & 6 \end{bmatrix} \quad (1)$$

Use the algorithm in [3] to solve this task assignment problem and we will have:

Robot 1 → Destination 1, Robot 2 → Destination 3
 Robot 3 → Destination 5, Robot 4 → Destination 2
 Robot 5 → Destination 4, Robot 6 → Destination 6

The required shortest time t_1 for the pattern reformation is 6. Replace the elements greater than or equal to 6 of the Δ_1 by 99, and we have the second distance matrix as:

$$\Delta_2 = \begin{bmatrix} 3 & 4 & 5 & 99 & 99 & 99 \\ 3 & 2 & 3 & 4 & 5 & 99 \\ 5 & 4 & 5 & 4 & 5 & 99 \\ 5 & 4 & 5 & 4 & 5 & 4 \\ 99 & 99 & 99 & 99 & 99 & 99 \\ 99 & 99 & 99 & 99 & 99 & 99 \end{bmatrix} \quad (2)$$

Applying the Hungarian Algorithm on Δ_2 , we have the minimum cost for this problem is 211 which is much more large than 99. Thus the obtained task assignment result is the best one. And the routes for the pattern reformation are shown in Fig. 3.

For this problem, there is another assignment way that will result in the same time 6 for the pattern reformation. This way is:

Robot 1 → Destination 1, Robot 2 → Destination 2
 Robot 3 → Destination 5, Robot 4 → Destination 3
 Robot 5 → Destination 6, Robot 6 → Destination 4

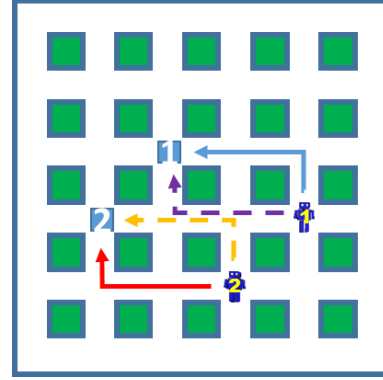


Fig. 2. Route select on route programming.

Consider another example shown in Fig. 4. There are 7 mobile robots on a 7x7 grid plane. The target positions are prescribed. The distance equation is:

$$\Delta_1 = \begin{bmatrix} 1 & 2 & 1 & 6 & 4 & 3 & 2 \\ 6 & 5 & 4 & 5 & 5 & 8 & 7 \\ 2 & 5 & 4 & 3 & 1 & 4 & 3 \\ 3 & 4 & 3 & 4 & 2 & 5 & 4 \\ 4 & 3 & 2 & 5 & 3 & 6 & 5 \\ 2 & 5 & 4 & 5 & 1 & 2 & 1 \\ 4 & 3 & 2 & 9 & 7 & 6 & 5 \end{bmatrix} \quad (3)$$

Use the algorithm in [3] to solve this task assignment problem and we will have:

Robot 1 → Destination 7, Robot 2 → Destination 4
 Robot 3 → Destination 5, Robot 4 → Destination 1
 Robot 5 → Destination 2, Robot 6 → Destination 6
 Robot 7 → Destination 3

The required shortest time t_1 for the pattern reformation is 5. Replace the elements greater than or equal to 5 of the Δ_1 by 99, and we have the second distance matrix as:

$$\Delta_2 = \begin{bmatrix} 1 & 2 & 1 & 99 & 4 & 3 & 2 \\ 99 & 99 & 4 & 99 & 99 & 99 & 99 \\ 2 & 99 & 4 & 3 & 1 & 4 & 3 \\ 3 & 4 & 3 & 4 & 2 & 99 & 4 \\ 4 & 3 & 2 & 99 & 3 & 99 & 99 \\ 2 & 99 & 4 & 99 & 1 & 2 & 1 \\ 4 & 3 & 2 & 99 & 99 & 99 & 99 \end{bmatrix} \quad (4)$$

Applying the Hungarian Algorithm on (4), we have the minimum cost for this problem is 20 which is less than 99. Thus we have to use the algorithm in [3] to solve (4) and we will have:

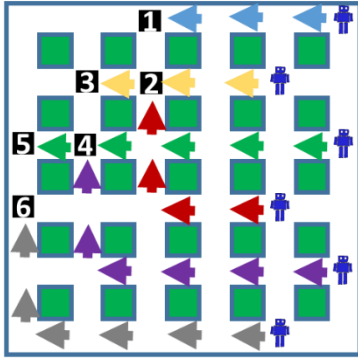


Fig. 3. Programmed routes for Example of Fig.1.

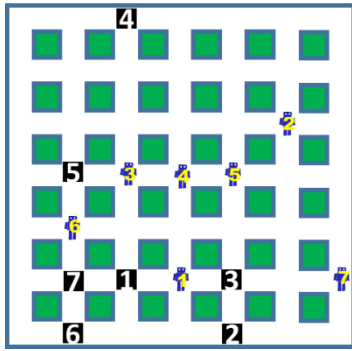


Fig. 4. Example of 7 mobile-robots on a 7x7 grid plane with the squares forming the target formation.

Robot 1 → Destination 7, Robot 2 → Destination 3
 Robot 3 → Destination 4, Robot 4 → Destination 1
 Robot 5 → Destination 5, Robot 6 → Destination 6
 Robot 7 → Destination 2

The required shortest time t_1 for the pattern reformation is 4. Replace the elements greater than or equal to 4 of the Δ_1 by 99, and we have the third distance matrix as:

$$\Delta_3 = \begin{bmatrix} 1 & 2 & 1 & 99 & 99 & 3 & 2 \\ 99 & 99 & 99 & 99 & 99 & 99 & 99 \\ 2 & 99 & 99 & 3 & 1 & 99 & 3 \\ 3 & 99 & 3 & 99 & 2 & 99 & 4 \\ 99 & 3 & 2 & 99 & 3 & 99 & 99 \\ 2 & 99 & 99 & 99 & 1 & 2 & 1 \\ 99 & 3 & 2 & 99 & 99 & 99 & 99 \end{bmatrix} \quad (5)$$

Applying the Hungarian Algorithm on (5), we have the minimum cost for this problem is 114 which is greater than 99. Thus we can feel free that the shortest time for

© The 2016 International Conference on Artificial Life and Robotics (ICAROB 2016), Jan. 29-31, Okinawa Convention Center, Okinawa, Japan

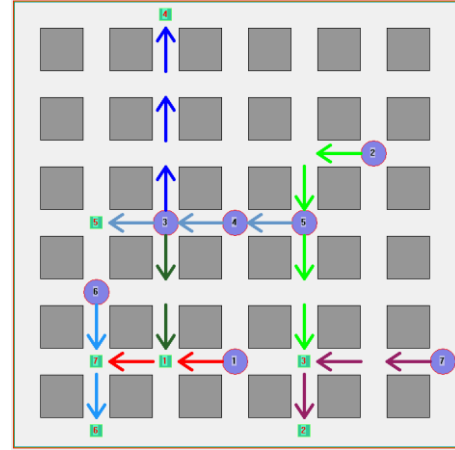


Fig. 5. Programmed routes for Example of Fig.4.

the task has been obtained. The programmed route in shown in Fig. 5.

5. Conclusions

In this paper, we developed a new algorithm, which combines our early developed algorithm with the Hungarian algorithm, to guarantee the task assignment result to be the best one. Since the Hungarian algorithm has been well applied on minimum cost programming problem, we believe that the proposed algorithm in this paper can be well applied on any size of grid plane.

References

1. E. W. Dijkstra, A note on two problems in connexion with graphs, *Numerische Mathematik*, **1** (1959) 269-271.
2. T. H. Cormen, C. E. Leiserson, R. L. Rivest and C. Stein, Section 24.3: Dijkstra's algorithm in *Introduction to Algorithms, Third ed.*, (MIT Press and McGraw-Hill, 2009) pp. 658-663.
3. K.H. Hsia, B.Y. Li and K.L. Su, Task assignment on pattern reformation for multiple mobile robots, *The nineteenth Int. Symp. on Artificial Life and Robotics 2014 (AROB 19th 2014)* (Beppu, Japan, 2014), pp.438-441.
4. K.H. Hsia, B.Y. Li and K.L. Su (2015). Task assignment on grid plane for multiple mobile robots, *Tenth Int. Conf. on Innovative Computing, Information and Control (ICICIC2015)* (Dalian, China, 2015), p.193.
5. H.W. Kuhn, Variants of the Hungarian method for assignment problems, *Naval Research Logistics Quarterly*, **3** (1956) 253-258.

The Design of a Multifunctional Acousto-Optic Device with a Mobile Power Pack

Yi-Yu Lu and Zheng-Ying Li

*Department of Electrical Engineering, Far-East University
No. 49, Zhonghua Rd., Xinshi Dist., Tainan City, 74448, Taiwan
E-mail: yiyulu@cc.feu.edu.tw, marspopopo431@gmail.com*

Wen-Bin Lin

*Department of Optoelectronic Engineering, Far-East University
No. 49, Zhonghua Rd., Xinshi Dist., Tainan City, 74448, Taiwan*

Abstract

The new designed acousto-optic device has adjustable, it is 1.5 times to extend its length. Fitting plastic optical fiber into transparent tube, the path of light can be increased and the light area will be enlarged. The device can present different color mode of light with RGB and high light LEDs as the light source. Adding the USB charge and discharge function into the device, make it has the function of mobile power pack.

Keywords: Multifunction, acousto-optic warning device, mobile power pack.

1. Introduction

Traffic batons plays an important role in policemen daily works. Their accoutrements also need a flashlight and whistle when on duty, and thus this study aimed to integrate these into one device. This work thus presents the design of a single apparatus with the functions of a glow stick, warning system and camping light in the form of an acousto-optic warning device. The multifunctional acousto-optic device with a mobile power pack will be introduced for the demand of amusement and convenient consideration.

A typical flashlight is constructed from a light bulb and focusing mirrors, and over the last twenty years light emitting diodes (LEDs) have been applied on more lighting devices, as they can reduce electricity consumption and have a long lifecycle. Flashlight manufacturers are also facing the product innovation and orientation problem and how to improve the applications

and extend the product life-cycle. Moreover, since smartphones can also work as flashlights, the flashlight industry is facing a crisis of falling sales. Further investigate the destruction of mobile phone innovation, just like the original online music under carrier service arise, causing the collapse of the traditional record industry is facing the same crisis [1]. Today, the mobile phone also undermine innovation in many industries began to face a crisis of survival. Flashlight if not actively seek to change, they may face the fate of being eliminated.

This study thus presents the design of a multifunctional acousto-optic warning device with a mobile power pack using plastic optical fiber [2]. Since the late 1990s, high performance plastic optical fiber based on perfluorinated polymers began to appear on the marketplace [3-4], but it has not yet been used in flashlights. Plastic optical fiber has the advantage of bending easily and not breaking, and its falling price means that it is now used for medical and recreational purposes. The advantages of the area of the

light guide path increasing are implemented for this acousto-optic device design.

Conventional flashlights usually project light in only one direction only, and while this enables of directivity and concentration, the relation between the light source and direction of sight is unclear, and thus people may be unsure of the location of the light source [5]. This is an issue that could be improved.

2. Materials and methods

The device includes five major parts: (1) adjustable focus, (2) plastic optical fiber, (3) LED driver, (4) battery, and (5) micro USB power pack. The structure of multifunction acousto-optic warning device is depicted in Fig. 1.

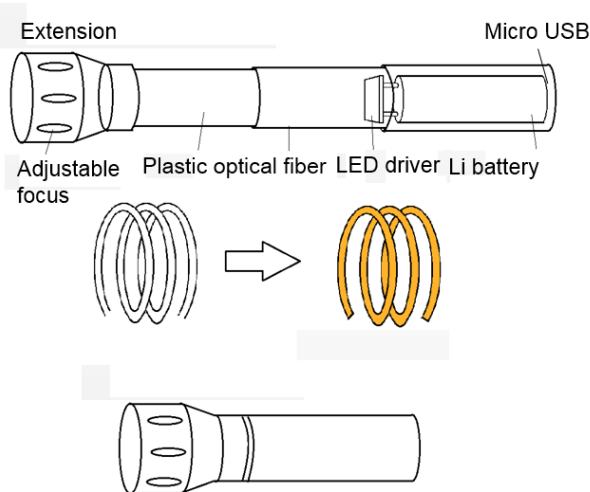


Figure 1. The multifunctional acousto-optic warning device.

2.1. Hardware

The basic circuit of the microcontroller unit (MCU) is shown in Fig. 2. The related program is written in Keil C.

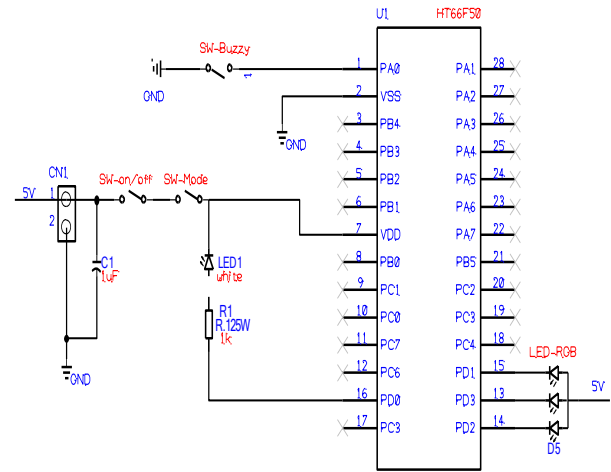


FIGURE 2. MCU circuit

A 555 Oscillator is a type of relaxation oscillator for generating stabilized square wave output waveforms of either a fixed frequency of up to 500 kHz or of varying duty cycles from 50 to 100%. The OP amplifier 741 is used to increase the volume. The warning function circuit is shown in Fig. 3.

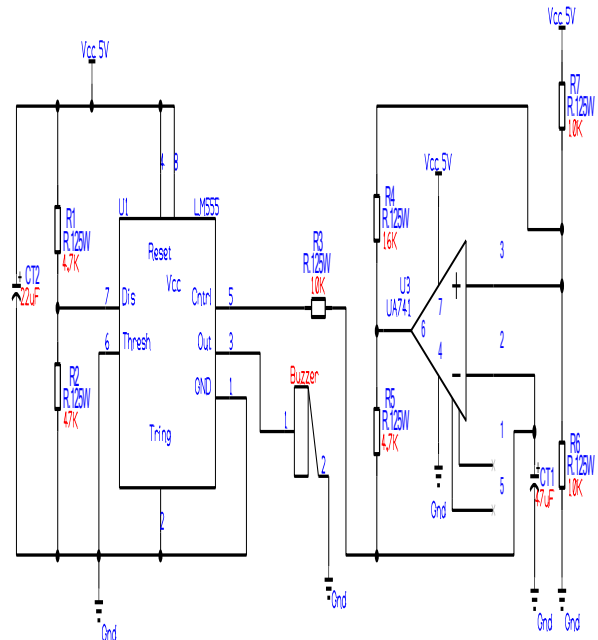


FIGURE 3. The warning function circuit

2.2. USB power pack

The USB boost and buck module are shown in Figs. 4 and 5.



FIGURE 4. USB boost module



FIGURE 5. USB buck module

2.3. Software

The flowchart and interrupt subroutine for the acoustooptical warning device are depicted in Fig. 6.

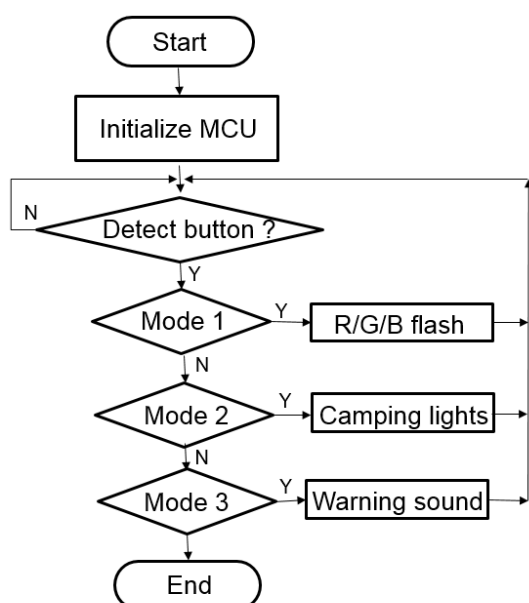


Figure 6. Flowchart for acoustooptical warning device

3. Results and Discussion

The device comprises three subsystems which are RGB LED, warning system and mobile power pack. Be able to give consideration to people's recreation and demand of amusement at the same time, an acousto-optic warning device with multifunction was designed. The transparent tube used in the device contains a plastic optical fiber, which is not currently seen in any similar product. The tube can increase the light guide and improve the luminous area. The device uses both RGB LEDs and high-brightness white LEDs as dual light sources, thus enabling different patterns of light and color, so the device is both functional and usable. The flashlight can be extended to 1.5 times its length, increasing the light guide and the illuminated area. In addition, the use of a USB charge and discharge function from lithium battery means that this device can also work as a mobile power pack.

The body of the flashlight is flexible, and it is convenient for use at night and for directing traffic. It combines a flashlight and a baton, and can be used when camping and to make warning sounds. On the other hands, it introduced the design of polymer optical fiber and lithium battery for energy-conservation and increasing efficiency consideration. Further, since it includes RGB LEDs, it can be used as a glow stick in concerts. The LEDs can make the light cover the whole flashlight via the optical fiber. The flashlight has an additional micro USB charging socket. The multi-functional design is the goal of various products now. This design has already been patented as a multi audible warning device at the Intellectual Property Office of Taiwan on September 21, 2014. Images of different colors of flash lighting are shown in Fig. 7.

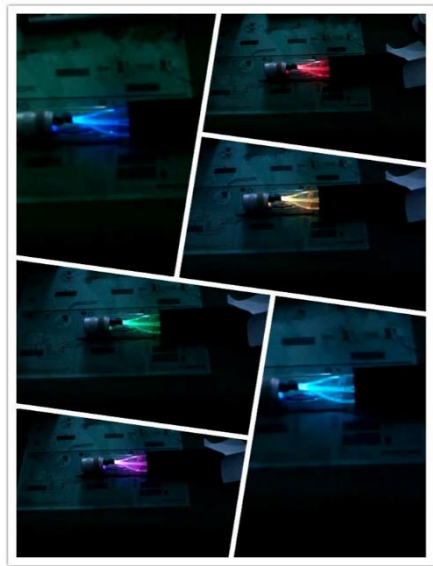


FIGURE 7. Photos of different colors of flash lighting

4. Conclusions

The design have functionality and practicability concurrently. The concept of a multifunctional acousto-optic warning device is introduced in this work. A multifunction acousto-optic warning device has obtained our country's new patent for this study. There are multifunction in this device which are as the traffic baton, camping light, glowing sticks in the concert and using for women's security at night, etc. The new designed acousto-optic device has adjustable, it is 1.5 times to extend its length. The advantage of this device is that when the body is exposed outside the transparent tube, the LED light source can diffuse along the light guide, and thus the lamp body can be projected in one direction, and so achieve the effect of centralized lighting. The structure also has the effect of concentrated and omnidirectional diffusion of light.

Acknowledgements

This work was in part supported by the Ministry of Science and Technology, Taiwan, Republic of China, under the research grants 104-2815-C-269-018-E.

References

1. Industrial technology, vol. 283, no. 5, pp. 4-7, 2015.
2. C. M. Okonkwo, E. Tangdionga, H. Yang, D. Visani, S. Loquai, R. Kruglov, B. Charbonnier, M. Ouzzif, I. Greiss, O. Ziemann, R. Gaudino and A. M. J. Koonen, "Recent results from the eu pof-plus project: multi-gigabit transmission over 1 mm core diameter plastic optical fibers," vol. 29., no.2., pp. 186–193, 2011.
3. S. Randel and C. Bunge, "Spectrally efficient polymer optical fiber transmission," Coherent Optical Communications, Subsystems and Systems, Proc. of SPIE, vol. 7960, 2011.
4. F. Beguin and E. Frackowiak ed., "Supercapacitors: Materials, Systems and Applications," New Jersey: Wiley, pp. 515, 2013.
5. J. Zubia and J. Arrue, "Plastic optical fibers: an introduction to their technological processes and applications," Optical Fiber Technology, vol. 7, pp. 101-140 2001.

Visual-servo Control of 4-DOF Robot Manipulator for Sorting Moving objects

Longtan Wang

*Dep. of Electronic Eng., Pusan National University, Jangjeon-dong, Geumjeong-gu
Busan, 609-735, Republic of Korea*

Seon-Woo Kim

*Dep. of Electronic Eng., Pusan National University, Jangjeon-dong, Geumjeong-gu
Busan, 609-735, Republic of Korea*

Hyun-Wook Ha

*Dep. of Electronic Eng., Pusan National University, Jangjeon-dong, Geumjeong-gu
Busan, 609-735, Republic of Korea*

Jang-Myung Lee

*Dep. of Electronic Eng., Pusan National University, Jangjeon-dong, Geumjeong-gu
Busan, 609-735, Republic of Korea*

*E-mail: longtan7379@pusan.ac.kr, seonwoo7379@pusan.ac.kr, hyunuk.ha@gmail.com, jmlee@pusan.ac.kr
www.pusan.ac.kr*

Abstract

This paper considers the problem of estimating position and determining class of objects on the moving conveyor belt. A 2D camera is utilized to capture the image of moving objects. The control system directly integrates visual data into the servoing process. Objects are recognized by firstly removing the background using adaptive thresholding algorithm, then find objects outer contours and determine the size and shape by topological structure analysis tracking boards, then Rotating calipers algorithm is adopted to estimate the centroid position and orientation of the objects. Finally control the robot manipulator pick different moving objects to different position. The proposed system is able to control the robot so that it can approach the desired position and grab the specific object.

Keywords: Robot; Adaptive thresholding; Topological Structure Analysis; Rotating calipers

1. Introduction

Sorting objects on the moving conveyor belt by robot is an essential part in a production line [1]. Despite many methods to sort the objects, vision based robot may be one of the most favored one in terms of the cost and efficiency.

However different kinds of objects holds different features, classify them often needs different algorithms. For a sorting system, if the sorting objects changes, the segmentation algorithm always need be altered. The past research mostly devoted to segment and recognize objects by surface features. For example, when sorting the transparent or reflective objects, the surface features changes as the illumination changes, typical vision

algorithms first extract the features of the surface and then compare it with the database to determine the class of it. So recognizing them by using feature related algorithms becomes a difficult job.

In this paper a sorting system with objects holds different size is addressed. As mentioned above, the surface appearance of the object is easily affected by the illumination, which makes it difficult to extract features and thus segment them becomes impossible. Instead of segment them by surface feature, we propose a way to segment and recognize objects by its size.

2. Develop Environment

As shown in Fig. 1. the robot system consists of a 4-DOF manipulator and a finger like gripper, a tablet PC, a conveyor belt, a Basler industry camera with ring light, which is installed on top of conveyor belt and in front of robot operation area.



Fig. 1. Experiment environment

As shown in Fig. 2. once the object appears in the view of the camera. The vision system will begin to find all the outer contours and thus get each shape. This way we will get the size of each object in the view. After that, the system will continue to compute its current position and orientation. According to information got from vision system, the PC will figure out a suitable strategy of motion planning and control the robot sorting objects.

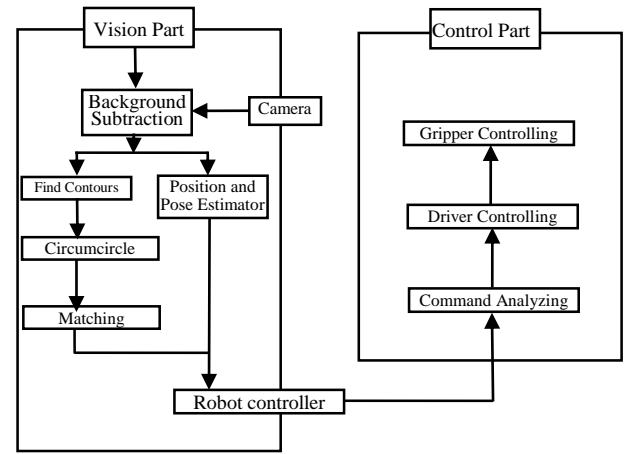


Fig. 2. System architecture

3. System Operation

The system Operation is make up of several main steps, each step is an essential part.

3.1. Background Subtraction

Background subtraction is a very important procedure for of many vision based applications. Background model is a relatively static model and its modeling is at heart of any background subtraction algorithm. Due to its flat and monochrome surface, consider the conveyor belt as a time invariant background, and it is sensitive to the illumination. Apply the background subtraction process in order to eliminate noise and correct uneven illumination. Also can determine whether the objects have come in view of camera. If so, the vision system will save the image for further processing. If not, the vision system will continue monitoring the conveyor belt.

Adaptive thresholding [2] is a form of thresholding that takes into account spatial variations in illumination. Due to the video stream, we have to maintain real-time performance, which means the less iteration times the better. A simple and fast adaptive thresholding technique is adopted. The first step is to get the integral image.

$$I(x,y) = f(x,y) + I(x-1,y) + I(x,y-1) - I(x-1,y-1) \quad (1)$$

Eq. (1) shows the process of integral image. To compute the integral image, we store at each location,

$I(x,y)$, the sum of all $f(x,y)$ terms to the left and above the pixel (x,y) . This is accomplished in linear time using the following equation for each pixel (taking into account the border cases).

Fig. 3. shows adaptive thresholding effects, which decrease the influence of uneven illumination.

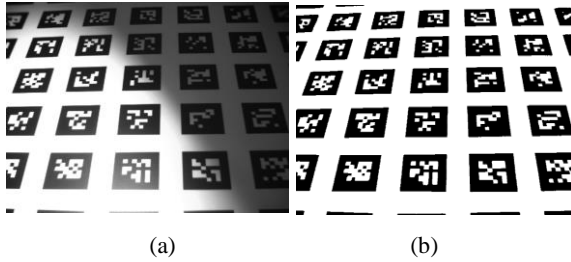


Fig. 3. (a) Original image, (b) After adaptive thresholding

3.2. Find Contours

After removing background, we need to find the contours by using topological structural analysis [3]. This step is the used for finding all the objects appeared in view of the camera. Each outer contour represents an object.

Find the contours by border following using topological structural analysis. Since the outer borders and the hole borders have a one-to-one correspondence to the connected components of 1-pixels and to the holes, respectively, the topological structural analysis by

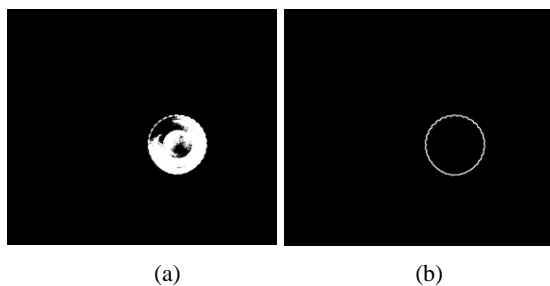


Fig. 4. (a) Origin binary image; (b) Contour of object

border following yields a representation of a binary image, from which one can extract some sort of features without reconstructing the image. As shown in Fig. 4. The shape can be recognized

3.3. Position and Orientation Estimation

In order to get the centroid position of an object, what we need we have to know firstly is its shape. Assume that the centroid is the center of its minimum bounding rectangle(NBR), which means this rotated rectangle is the smallest one that enclosing the object in the image. While the pose is represented by the angle this rectangle has rotated. What we need is to find its minimum bounding rectangle.

We adopt Rotating calipers algorithm [4] which is a well-known algorithm for finding the minimum rectangle [5]. As shown in Fig. 5.

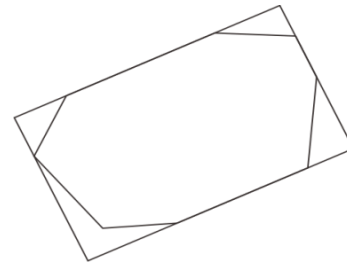


Fig. 5. Minimum bounding rectangle

3.4. Motion Planning and Control

The control strategy is assigned based on information got from vision part. The manipulator and gripper will work together to move the object to specified area [6][7].

4. Experiment Result

We design an experiment which will test the result of the recognizing effects and real-time performance.

In this experiment, different kinds of objects are placed in order continually. The robot will recognize their kinds and place different kinds of objects to different places.

In this experiment the camera continues capturing gray-level image at 500*690 resolution. The camera capture images in real-time and each frame of the image will be checked to find and recognizing the objects. Then the robot manipulator will grab the object and place each to a specified area. Fig. 6. shows the experiment process. Different kind of object will be recognized.

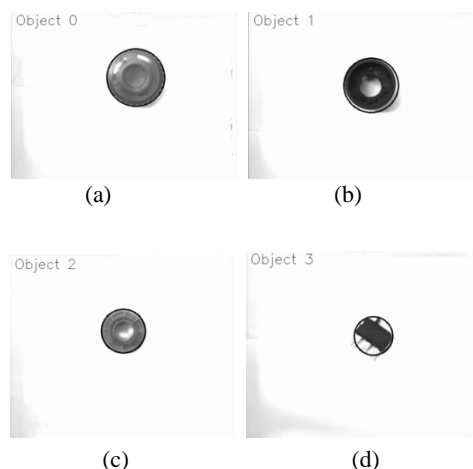


Fig. 6. Experiment results. (a) Object 0; (b) Object 1; (c) Object 3; (d) Object 4

5. Conclusion

This paper proposes a design of robust recognizing and grasping objects in real time. High robustness has been demonstrated in recognizing featureless objects. The adaptive thresholding algorithm and topological structure analysis are used in recognizing objects, while rotating calipers algorithm is applied to estimate the centroid position and orientation of the objects. A path planning scheme is thus yielded based on the information gotten from vision system. Experimental results illustrate the good efficiency performance.

Acknowledgements

This research was supported by the MOTIE (Ministry of Trade, Industry & Energy), Korea, under the Industry Convergence Liaison Robotics Creative Graduates Education Program supervised by the KIAT (N0001126).

This work was supported by the National Research Foundation of Korea(NRF) Grant funded by the Korean Government(MSIP) (NRF-2013R1A1A2021174).

References

1. Ik Sang Shin, et al. "Conveyor visual tracking using robot vision." *Proceedings of 2006 Florida Conference on Recent Advances in Robotics*, (2006) 1-5.
2. Derek Bradley, Gerhard Roth. "Adaptive thresholding using the integral image." *Journal of graphics, gpu, and game tools* 12.2 (2007) 13-21.

3. Suzuki, Satoshi. "Topological structural analysis of digitized binary images by border following." *Computer Vision, Graphics, and Image Processing* 30.1 (1985) 32-46.
4. Toussaint, Godfried T. "Solving geometric problems with the rotating calipers." *Proc. IEEE Melecon*, Vol. 83, (1983).
5. D. Chaudhuri, A. Samal. "A simple method for fitting of bounding rectangle to closed regions." *Pattern recognition* 40.7 (2007) 1981-1989.
6. Hyun Woo Kim, Hu Chen, Jang Myung Lee, "Path planning of 5-DOF manipulator." *Advanced Intelligent Mechatronics (AIM)*, (2014) 877-881.
7. Dirk Buchholz, et al. "Combining visual and inertial features for efficient grasping and bin-picking." *Robotics and Automation (ICRA)*, 2014 *IEEE International Conference on. IEEE*, (2014).

Self-identification of Mental State and Self-control through Indirect Biofeedback

--- Indirect Representation and Placebo Effect ---

Madoka Takahara, Jilin Huang, Ivan Tanev, Katsunori Shimohara
Graduate School of Science and Engineering, Doshisha University,
1-3 Tatara-miyako-dani, Kyotanabe, Kyoto, 610-0321 Japan
E-mail:{takahara2012, jhuang2014, itanev, kshimoha}@sil.doshisha.ac.jp

Abstract

This paper describes a possible new scheme for a user with mental health problems to identify his/her own mental state and control it. For that purpose, we propose an indirect biofeedback system which represents physiological information with color and shape, and enables the user to grasp his/her inner state and to proactively change and control it through methods of breathing. Those methods facilitate the user to self-control the autonomic nervous system. Here, we discuss indirect representation and placebo effect.

Keywords: Indirect biofeedback, Autonomic nervous system, Breathing, Placebo effect, Indirect representation.

1. Introduction

The number of people with stress and mental problems has been gradually increasing in Japan. However, their situation is often not improved by consultation with specialists in psychiatry or psychosomatic medicine.¹ We hypothesize that consulting such specialists is not very effective because it is merely a passive experience.² We believe that if the patient is instead asked to approach the symptoms of their disease in a voluntary and proactive way, the treatment is more likely to succeed. In order to elicit proactive behavior from the client, he or she must become aware of their current mental condition. The client can then act appropriately to maintain his/her self-control. A device or mechanism is needed to externalize the internal state of the client, while establishing a sense of unity between the external device and him/herself.

Here, we propose an indirect biofeedback system that helps the client to be self-aware of his/her current mental condition by monitoring a device with visual features that vary according to the client's heartbeat. That is, the device not only externalizes the mental state of the self but also keeps a sense of unity with the self. We also investigate how effectively clients could control their mental condition through breathing techniques such as abdominal and costal breathing.

We would ultimately like to determine whether it is possible for individuals to learn to easily and automatically identify their own internal state and control it through breathing.

2. Biofeedback for Identifying the Self and Self-control

2.1. Concept

It has already been reported that individuals can, to some extent, control their autonomic nervous system (ANS) using biofeedback. Specifically the report claims that individuals can use biofeedback to produce useful improvements in their physiological functions, such as decreases in anxiety symptoms and physical disorders.³ Biofeedback systems are generally used at medical institutions and seen as medical treatments to be executed under a medical doctor's direct supervision. Acquired physiological data are usually represented numerically and/or as waveforms. Such systems are not designed to be used by ordinary clients on a daily basis.

In the research reported here, we aim to provide a system by which ordinary users can identify their physiological state and exercise self-control on a daily basis. For that

purpose, we propose an indirect feedback enables users to understand their internal state intuitively with a user-friendly representation of physiological data.

In addition, in this research, we employ breathing techniques as a means of exercising self-control over internal state, since this is the only known means by which individuals can control their ANS.

2.2. Acquisition of information on balance of autonomic nervous system from heartbeat fluctuation

In this research, we estimate the balance of the autonomic nervous system (ANS) by analyzing the frequency of heartbeat fluctuation. Heartbeat fluctuation can be measured simply and non-invasively, and a frequency analysis of heartbeat fluctuation gives us an index of stress manifesting itself by way of the influence of the ANS on the heart. It is well known that heartbeat can be changed by regulatory control by the nervous and endocrine systems, as well as by physical position and movement. ANS works autonomously and regulates itself automatically. Unlike motor nerves, we cannot control it intentionally. The ANS consists of the sympathetic nervous system (SNS) and the parasympathetic nervous system (PNS). The SNS mainly activates and tenses the body; for example, when we have sweaty palms and a racing heart. The activation of the SNS constricts blood vessels and increases heart rate. As a result, blood pressure goes up, and blood flow to peripheral areas is increased. On the other hand, the PNS activates the internal organs, and puts the body into a resting state.

This research is focused on the proposition that we can keep our body and mind in good condition by intentionally controlling the ANS and by that means recover its proper balance. The relationship between the ANS and heartbeat fluctuation is as follows:

- The low frequency (LF) component of heartbeat fluctuation is observed when SNS and PNS are activated
- The high frequency (HF) component of heartbeat fluctuation is observed when the PNS is more active than the SNS, and this state is reflected in breath fluctuation.

2.3. Indirect biofeedback

Fig. 1 shows the configuration of the proposed system in this research.

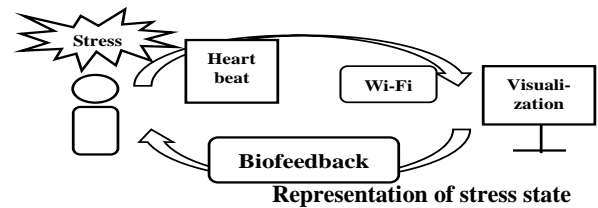


Fig. 1. System configuration

Physiological information is acquired through a heartbeat sensor pasted on a user's chest, and heartbeat fluctuations are used as the basis for generating a biofeedback signal. To generate this signal, heartbeat fluctuation is analyzed. A measure of the balance of the SNS and PNS within the ANS is calculated and displayed to the user as changes in the color and shape of a circle. Fig. 2 shows an example of the indirect biofeedback representation which we propose here.

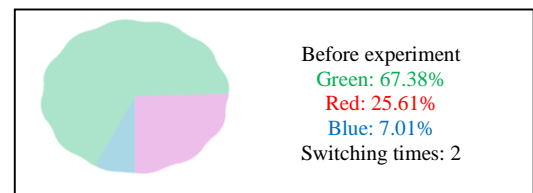


Fig. 2. Example of Indirect Biofeedback Representation

We designed the indirect biofeedback display as follows:

- Feedback was provided via a circular display that can assume one of three colors. Red was used to indicate active situations with SNS superiority. Green shows mood-stabilizing situations. Blue shows depressive situations with PNS superiority
- The shape of the display can vary from a circle to a flattened ellipse, depending on the rate of switching from a SNS to a PNS dominated condition. This is inferred from heart rate fluctuation.
- If the switching rate is high, the user's mental condition is not stable. At such times the display becomes more strongly elliptical.

3. Experiments and Results

3.1. Self-identification of mental state and self-control: indirect biofeedback

We conducted 4 different types of experiments with human participants by the proposed system. In each experiment, there were 2 different loads of stress and 2 different ways of breathing with 16 study participants. The results indicate that study participants could properly control their inner states after the loads of stress, since they are healthy.⁴

According to the results of the subjective evaluation (via the questionnaire), some participants said they were able to relax by using the proposed biofeedback system. On the other hand, the results of objective evaluation indicate that there were no significant differences in the inner state of the participants before and after the experiments.

In this study, objective experimental results did not indicate an improvement in the study participants' physiological condition due to the use of biofeedback. However, the participants reported that they felt more relaxed. We think the discrepancy between the subjective and objective results indicates that the proposed system causes a placebo effect. Here we define a placebo effect as reporting feeling relaxed regardless of the actual objective experimental results. And some of the participants wanted to see the balance of physiological information displayed as a graph rather than a circle.

3.2. Effects of fake biofeedback: Placebo effect

3.2.1. Experiments

We conducted an additional experiment in which the participants evaluated both real and fake biofeedback. In the fake biofeedback, the user evaluated the data provided by another healthy participant.

We designed this experiment as follows. The participant should use the following 2 kinds of systems;

- *1: Real biofeedback system
- *2: Fake biofeedback system

In the real feedback system, the participant gets his/her own biological information. On the hand, in the fake feedback system, the participant gets another healthy participant's biological information as the feedback. The participant is asked to use abdominal breathing as the stress control techniques.

3.2.2. Subjective evaluation

In a subjective evaluation, 17 out of 23 participants judged the real biofeedback to reflect their mental state better than the fake biofeedback.

3.2.3. Objective evaluation

As an objective evaluation, after the participants self-controlled using both real and fake biofeedback, we compared the effectiveness of the real and fake biofeedback in increasing of the green area that represents the balanced situation between SNS and PNS. The result is illustrated in Fig. 3.

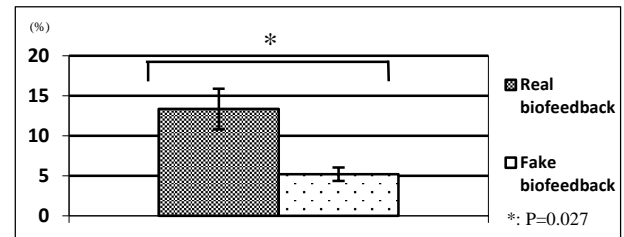


Fig. 3. T-test Results of Placebo Effect
(i.e. Increase of the good balance of ANS)

As shown in Fig.3, the real biofeedback was significantly better at producing a balanced situation in ANS than was the fake biofeedback. Some participants doubted the behavior of the fake biofeedback readout because it changed even when they were not feeling anything. The participants felt that the real biofeedback reflected their mental states more closely.

3.3. Comparison with existing methods of biofeedback

3.3.1. Experiments

We additionally conducted an experiment comparing the proposed indirect biofeedback display with a conventional direct biofeedback display with waveform representation.

We designed this experiment as follows. The participant should use the following 2 kinds of systems;

- *1: Indirect feedback system
- *2: Direct feedback system

In the indirect feedback system, the participants get their own biological information as a form of circular representation proposed in this study. On the other hand, in the direct feedback system, the participants get their own biological information with waveform representation. The participant is asked to use abdominal breathing as a stress control technique.

3.3.2. Subjective evaluation

Twenty out of 23 study participants reported, in a subjective evaluation, that the indirect biofeedback display was better than the direct one.

3.2.3. Objective evaluation

As an objective evaluation, we compared the ability of participants using the circle image and a conventional waveform display to achieve a good balance of their ANS. The result is illustrated in Fig. 4, which shows that the indirect feedback system was much more effective than

the direct one. The result ($p=0.04$) was significant by the T-test with $p<0.05$.

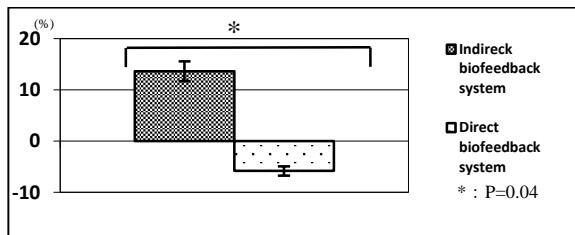


Fig. 4. T-test Results of the Experiment about Representation (i.e. Increase of the good balance of ANS)

Some possible reasons for this result are:

- Direct Biofeedback
 - 1) It might be difficult for the subjects to grasp their inner state during the given time.
 - 2) The waveform image sometimes seemed to cause negative reactions response in the subjects through straight expressions.
 - 3) The direct feedback causes the participants to have stress with certain amount of tense or irritated and thereby reduce their level of ANS balance.
- Indirect Biofeedback
 - 1) The subjects can easily grasp their inner state through expressions easy to understand.
 - 2) The circular image and easily understandable expressions do not cause negative reactions which may occur in Direct Biofeedback to the participants.

Thus, we conclude that users can control themselves more easily using the proposed indirect biofeedback than the direct biofeedback common to existing biofeedback systems.

4. Discussion

In the experiment on the Placebo effect, most of the participants doubted the fake feedback image. Even if the participants see the green area increase on the display, it is usually hard for them to believe that the data reflect their own mental state.

From the comparative experiment on representation of feedback information, the participants preferred the circular representation proposed here to the previous means of representation, namely, waveform representation.

5. Conclusion

In this research, we developed an indirect biofeedback system. This system externalizes and objectifies the

user's physiological state for the purpose of allowing the user to self-control their inner state.

The indirect biofeedback, which we have introduced here allows the user to keep a sense of unity between a device that externalizes the internal state of the self, and the user him/herself. For that purpose, we designed the system so that the circle represents the user him/herself. We evaluated the measured data as well as the questionnaire results carried out after the experiments. The results indicate that study participants could properly control their inner states after the loads of stress, since they are healthy.

Moreover, we conducted the additional two experiments on the Placebo effect and on representation of biological information. In the experiment on the Placebo effect, when a participant has the fake information, we couldn't confirm any Placebo effect, however, when the participant has the real information, we could confirm the Placebo effect.

In the comparative experiment on representation of biological information, we could confirm that the indirect biofeedback is much better than the direct one.

References

1. About medical plan (mental disease), (2015.Available:) http://www.mhlw.go.jp/seisakunitsuite/bunya/kenkou_iryau/iryau/iryau_keikaku/dl/shiryou_a-3.pdf
2. Keiji Hoshikawa, Religions and Others --- Study on Language and Reality---,(SHUNJUSHA Tokyo, 2011)
3. Taishi Aoyama and Mieko Osuga, Breath inducing system for relaxation,(*Japanese Society of Biofeedback Research*,33(2006), pp.61-62.
4. Madoka Takahara et al, Self-identification of mentality and self-control through indirect biofeedback, *Int. Conf. on Electronics and Software Science*, (2015), pp.377-380.

Construction of a micro sense of force feedback and vision for micro-objects: development of a haptic device

Yusei Ishii

*Graduate School of Computer Science
and System Engineering
Kyushu Institute of Technology
680-4, Iizuka City, Fukuoka, Japan, 820-8502
ishii@mmcs.mse.kyutech.ac.jp*

Eiji Hayashi

*Department of Mechanical Information
Science and Technology
Kyushu Institute of Technology
680-4, Iizuka City, Fukuoka, Japan, 820-8502
haya@mmcs.mse.kyutech.ac.jp*

Abstract

The purpose of this research was to develop a combined sense system that uses both force feedback and visual feedback to determine the shape of the microscopic features of a sample. We constructed a haptic device that gives a sense of that force to the operator when touching the sample. We recreated touch of salmon roe as one of minute samples this time.

Keywords: force feedback, haptic interface, simulation.

1. Introduction

Technologies that can accurately perform minute work are now being sought for medical treatment and in the field of manufacturing semiconductors. Such minute work is improved by using micromanipulators, but their operation is difficult because the operator has no sense of force; he or she relies only on sight through a microscope. As a result, a person skilled in the use of this technology is needed for all minute work. The efficiency of minute work would be improved if the operator were able to have a sense of force while using a manipulator.

Here we describe the development of a more efficient system for minute operations. Our aim was to develop a system using not only the sense of sight through a microscope but also a sense of force from the

manipulator. For this fundamental research, a system was created to assess the reaction force when a minute sample was touched. A cantilever was used to touch the sample, and the reaction force was obtained from the degree to which the sample bent. In addition, we used a haptic device and amplified the force feedback from a minute sample of a virtual object.

2. System Structure

The system structure is shown in Fig. 1. This system consists of a microscope with an automatic x-y stage, a piezo stage, a feedback stage controller to control the x-y stage, a piezo stage controller, a haptic device for transmitting force feedback, a cantilever, and a PC via which the user can control and operate these components. The sample was fixed on the x-y stage by an injector and a holding pipette. When the cantilever,

which was fixed to the piezo stage, touched the sample, the operator could maintain the cantilever's position by obtaining the value of the reaction force through the interface. The resolution of the piezo stage is 1 nm.

Fig. 2 provides a diagram of the haptic device. It consists primarily of a rotor, a laser, and a position-sensitive device (PSD). We installed a coil on the rotor with a polarity magnet, which generated electromagnetic induction by an electric current and a magnetic force. The angle of the rotor can be measured

by the laser and the PSD. The rotor was able to follow any input waveform.

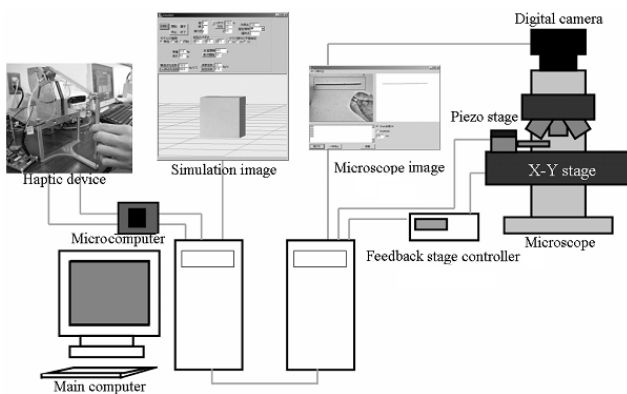


Fig.1. Photograph of the system structure.

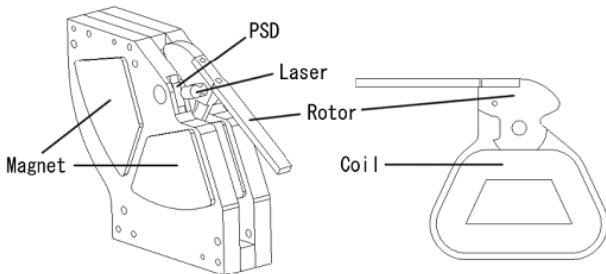


Fig.2. Diagram of the haptic device.

The actuator is controlled by a servomechanism on the actuator. The system driving the actuator therefore consisted of four actuators: a microcomputer, an inputting AD/DA port, an outputting microcomputer, and a PC outputting order value. The system controls the actuator during each part of the process. Fig. 3 shows the structure of the haptic device.

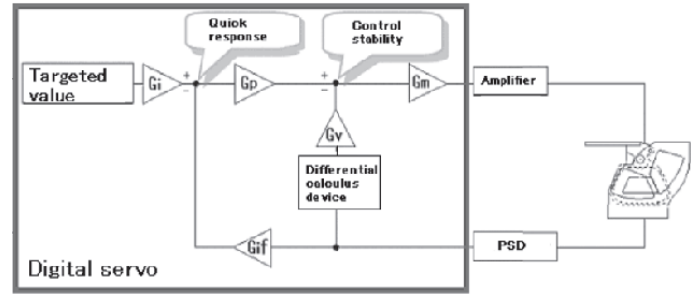


Fig.3. Structure of the haptic device.

The actuator, whose actions are governed by the PD control, is operated through a digital differential calculus device. A transfer function for the quadratic function system shown in Fig. 4 is provided for the actuator servo system. The role of each parameter of the control system is to adjust the total offset to a master in G_i/G_{if} , to regulate the item viscosity/resonance point in G_p/G_v , and to regulate the total gain in G_m .

Table 1 provides a list of the control parameters of the servomechanism system.

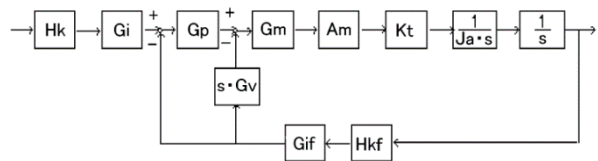


Fig.4. Block diagram of the servomechanism system.

3. Measuring the reaction force

The reaction force was used to calculate the force applied by the minute object. In this experiment, we touched the minute object with the cantilever, and the reaction force was obtained based on the degree of bend of the cantilever. The environment of the experiment is shown in Figs. 5. Based on this experiment, we were able to determine the reaction force applied by the minute object.

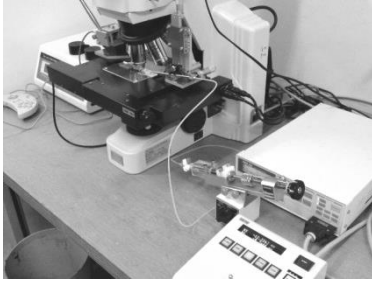


Fig.5. Environment of the experiment.

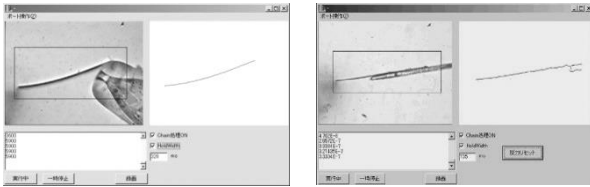


Fig.6. The cantilever moving

Left of the figure 6 shows the cantilever touching the tip of the holding pipette. Right of the figure 6 shows the experiment that measures the reaction force of the downy hair. The image-processing speed of the cantilever was improved by the tracking process. The bend of the cantilever is assumed to be linear-elastic so that Hooke's law may be applied. The restoring force, F , of the bend of the cantilever is given by

$$F = kx \quad (1)$$

where x is the compression distance from the equilibrium position, and k is the spring constant.

4. Deforming the sample in simulation

In this study, we attempted to build a working system using a microscope, a haptic device, and a simulation. A fundamental element was simulating the deformation of a minute object. Figure 7 shows the graphical user interface (GUI) of the simulator. A graphic tool was created using OpenGL to draw the object and to choose the shape of the sample, for instance, a cube or sphere. The dynamic model of the sample consisted of a spring-mass array of mass points in both the vertical and horizontal directions. An example of the arrangement of mass points is shown in Fig. 8. When a force was

applied at a mass point, the simulation calculated the speed of all mass points that had been affected. The image was renewed after every ten calculations.

We defined a spring as having a size but no weight, and a mass point as having a size, a weight, and a rigid body. An arbitrary mass object can be placed on a spring on a bitmap (Fig. 9). In addition, a sample can be seen from various viewpoints, and the deformation of the sample, which is impossible to observe by microscope, can be checked. The shape of this object can be either a cube or a sphere, and any point may be selected as a fixed point or an operating point.

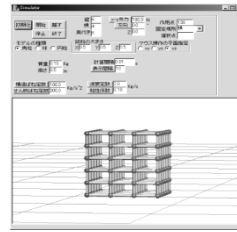


Fig.7. Simulator.

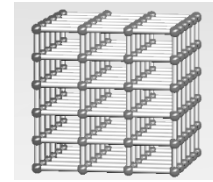


Fig.8. Arrangement of mass points

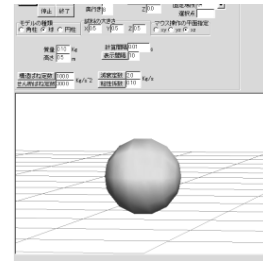


Fig.9. Placing an arbitrary object on a bitmap.

5. Characteristic measurements and a reappearance experiment for an object

Dynamic characteristics of the object were measured and then recreated using the haptic device. The object used this time was salmon roe. We measured response of salmon roe and showed the displacement of its surface a figure. Fig. 10 shows the response of the salmon roe.

Salmon roe is 6 millimeters in diameter and we cannot precisely feel the sense of touch. Hence values in the

figure are multiplied by 68 so that human can feel the sense of salmon roe's touch. Fig. 11 shows that response of the salmon roe and haptic device. Table1 shows the frequency, constant of spring, and damping coefficient in each ectopic focus.

In this experiment, there was a tendency for a touch feeling close to that of real and big salmon roe to be created when characteristic was recreated.

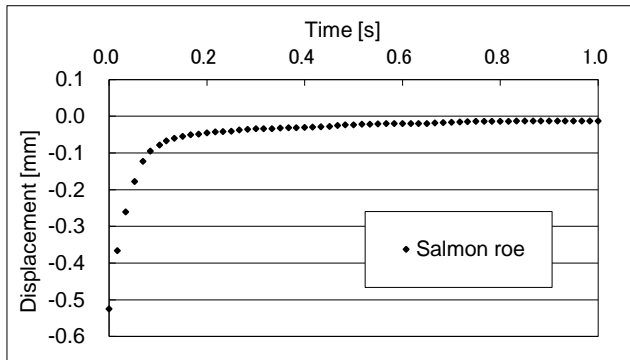


Fig.10. Time response of Salmon roe

Table1. Haptic device parameter of dynamic characteristic

Displacement [mm]	Frequency [Hz]	Spring constant [N/mm]	Damping ratio
0~6	6	0.072	2.6
6~35	6	0.072	1.0

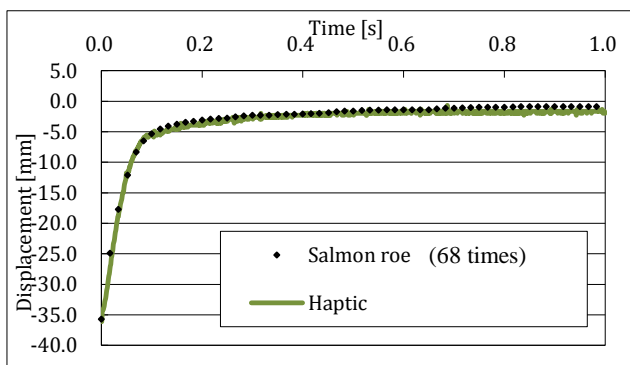


Fig.11. Time response of Salmon roe and Haptic device

6. Conclusion

In the present study the characteristics of salmon roe were measured and recreated, the evaluations also were carried out with regard to response and sense of force using a haptic device. The characteristics of various objects will be measured in the future, and the characteristics should recreate.

Future research should focus on building a system that allows a reaction force to be detected and shown more precisely. Such a system would make it possible to test smaller samples.

7. Acknowledgement

This research was partially supported by the Ministry of Education, Science, Sports and Culture, Grant-in-Aid for Scientific Research, 2012.

8. References

1. T.DOMOTO (2012) Construction of a sense of force feedback and vision for micro-objects: Recreate the response and a sense of force of objects. Kyushu Institute of Technology. Proceedings of the 15th International Symposium on Artificial Life and Robotics, Beppu, Oita, Japan, 2012

Dynamic Behavior Selection Model based on Emotional States for Conbe-I robot

Wisanu Jitviriya and Jiraphan Inthiam

*Computer Science and Systems Engineering, Kyushu Institute of Technology.
680-4, Kawazu, Iizuka, Fukuoka, 820-8502, Japan.
wisanu@mmcs.mse.kyutech.ac.jp, jiraphan@mmcs.mse.kyutech.ac.jp*

Eiji Hayashi

*Mechanical Information Science and Technology, Kyushu Institute of Technology.
680-4, Kawazu, Iizuka, Fukuoka, 820-8502, Japan.
haya@mse.kyutech.ac.jp*

Abstract

Currently, the rapid development of non-industrial robots that are designed with artificial intelligence (AI) methods to improve the robotics system is to have them imitate human thinking and behavior. Therefore, our works have focused on studying and investigating the application of brain-inspired technology for developing the conscious behavior robot (Conbe-I). We created the hierarchical structure model, which is called “Consciousness-Based Architecture: CBA” module, but it has limitation in managing and selecting the behavior that only depends on the increase and decrease of the motivation levels. Consequently, in this paper, we would like to introduce the dynamic behavior selection model based on emotional states, which develops by Self-organizing map learning and Markov model in order to define the relationship between the behavioral selection and emotional expression model. We confirm the effectiveness of the proposed system with the experimental results.

Keywords: Behavior selection model, Self-organizing map (SOM) learning, Markovian model.

1. Introduction

Nowadays, the focus of research of service robots is a development of the robots that are able to express emotions, imitate human thinking and change their behavior based on variety surrounding environment. However, development of these robots that are still a huge challenge when they have interaction with humans. Therefore, Hayashi laboratory’s works [1]-[2] have focused on studying and investigating the application of brain-inspired technology by developing the robots with a hierarchical structure module based on Tran Duc Thoa’s research [3]. This model is called “Consciousness-Bead Architecture (CBA)” model which relates between consciousness field and behavior group.

But the conventional (CBA) model has limitation in managing and selecting the behavior that only depends on the increase and decrease of the motivation levels. For a truly effective of the robotic system, the robots should not only perform the behavior, but also express the appropriate emotional state. Thus, the general objective of this research, we would like to introduce the proposed system, which can autonomously select the suitable behavior based on transition of emotional states.

Our paper is organized as follows: Chapter 2 explains the autonomous behavior selection system which has three processes. In Chapter 3, our results are shown how our robot can choose behavior depending on its emotional states. In the final section we conclude the paper and describe our future works.

2. Autonomous Behavior Selection System

In this paper, we would like to propose the behavior selection model which autonomously selects and performs the suitable action based on variation of emotional expression. The proposed system has three major processes as described below.

2.1. Computation dopamine and robot's motivation

2.1.1. Determination of occurring dopamine model

The Conbe-I robot uses only the acquired images from the CCD camera and web camera for operating the actions and emotional expression in recognition process. The robot is not usable the other sensors (tactile sensor or laser range finder sensor). Thus, the robot can evaluate the rough position of the target object by only using the image processing. The system may simplify the acquired images by dividing into four color groups: green, blue, flesh-color and the other colors. With the simplification, the sequential recognition process has the reduced image size, the changed color model of image from RGB method to HSV method, the labeling process based on the color of visual information and the calculation of the position of the target object. Then, the visual information (the color, shape, size, labeling and distance of the target object) is used to calculate and form the naturally occurring dopamine waveform [4]. The computation of the typical pattern of dopamine model is explained. The dopamine waveform can be evaluated and divided into rise and fall portions. The rising part and falling part are created by the 2nd order and 1st system equations as shown in Eq. (1) and Eq. (2) respectively, where the input variable $x(t)$ is an accelerator of dopamine, the output variable $y(t)$ is a naturally dopamine, ζ is damping factor, ω_n is the natural frequency and T_c is time constant.

$$y''(t) + 2\zeta\omega_n y'(t) + \omega_n^2 y(t) = \omega_n^2 x(t) \quad (1)$$

$$T_c y'(t) + y(t) = x(t) \quad (2)$$

2.1.2. Calculation of the robot's motivation

Since the computation of the naturally occurring dopamine as described above, the sum of positive and negative dopamine values that is used as the input

variable for calculating the robot's motivation. The motivation waveform can estimate by the 2nd order system of differential equation as expressed by Eq. (3).

$$Motivation''(t) + 2\zeta\omega_n Motivation'(t) + \omega_n^2 Motivation(t) = \omega_n^2 Total_dopamine(t) \quad (3)$$

2.2. Classification emotions and behaviors based on Self-organizing map (SOM) learning

After recognition process, the robot's motivation and the visual information are used to define as the input parameters of the Self-Organizing Map (SOM) learning in order to generate the behavior and emotion maps. The robot is set the nine behaviors and six emotions. To classify and select the most appropriate behavior and emotion correspond to the surrounding environment. The results of the SOM learning the will be verified.

2.2.1. SOM algorithm

The Self-Organizing Map is a neural network architecture which is proposed by T. Kohonen [5]. It is well known as an effective pattern classifier that is an unsupervised learning method. The SOM method can provide topologically preserved mapping from high-dimensional input data to a low - dimensional array based on competitive learning. The procedure of the basic SOM learning can explain by the following steps:

Step 1: Each node must to be initialized with weight value based on setting the small standardized random value.

Step 2: Calculate and find the minimum Euclidean distance that is called "winner node or best matching unit (BMU)".

Step 3: After finding the BMU, the weight vectors of the BMU, and its topological neighbors are moved closer to the input vector. The new weight vectors are updated by Eq. (4), where t is the training step index is, $\eta(t)$ is the learning rate, and $h_{j,c}(t)$ defines as the neighborhood kernel function around the winner nodes.

$$w_j(t+1) = w_j(t) + \eta(t)h_{j,c}(t)[x - w_j(t)] \quad (4)$$

Step 4: The training step increases to $t+1$. Steps 2 to 4 are repeated with decreasing the width of the neighborhood function.

2.2.2. Formation of behavior and emotion maps

In order to verify the SOM learning, the motivation value, the slope of robot's motivation, the pixels of colors (green, blue and flesh colors) are defined as the input data for testing. For example, if the robot recognizes the green object, which is near the robot's hand. The testing data are the motivation flag = 1 (positive level), the motivation value = 0.45, the slope of robot's motivation = 0.003, the motivation waveform is a positive slope = 1, the green pixels = 0.6, the blue pixels = 0.02 and the flesh-color pixels = 0.2. During the SOM learning process, we have not only considering the changing position of the winner nodes in behavior and emotion maps, but also observe the evolution of the form of both maps as shown in Fig.1 and Fig.2. The blue cells showed on behavior and emotion maps that were the winner nodes of each behavior and emotion pattern. The green cells represented as the response action according the testing input data. Therefore, in this situation, the robot should perform the action as "Approach", and express the emotion as "Happiness" at the same time. Because, the green object is a favorite object, thus it tries to possess the target object.

2.3. Behavior selection based on Emotional States

The last process is the behavioral-emotional selection process, which is modeled based on a Markov model [6]. The Markov model is memoryless property that means the next state will be changed based on a transition rule and depends only on the current state.

In this study, the Emotional Markovian model that consists of the six nodes representing the basic emotion states. The arrows are the probabilities of getting out of the states. The next emotional state can determine by Eq. (5), where, A is the emotional state transition matrix.

$$Emotion_{k+1} = A \cdot Emotion_k \quad (5)$$

All elements of the emotional state transition matrix can be updated by the affective factors, which calculates by averaging the sum of the weights of individual group of behavior and emotional patterns in SOM learning process. In addition, the behavior selection module is based on its emotional expression, thus the behavior state will be selected by the emotional state that can estimate with Eq. (6), here, C denotes as the behavioral state transition matrix.

© The 2016 International Conference on Artificial Life and Robotics (ICAROB 2016), Jan. 29-31, Okinawa Convention Center, Okinawa, Japan

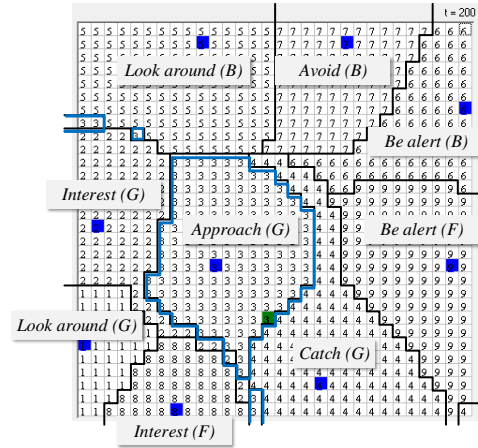


Fig.1 Behavior map

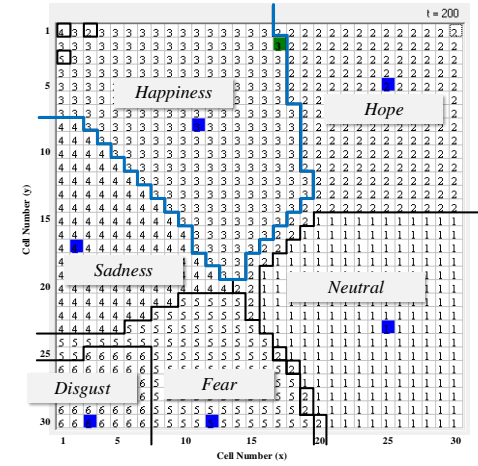


Fig.2 Emotion map

$$Behavior_{k+1} = C \cdot Emotion_{k+1} \quad (6)$$

All element values in the behavioral state transition matrix ($C_{behavior/emotion}$) can be modified later based on the behavioral and affective factors.

3. Experimental results

The intelligent behavioral-emotional selection system was tested and evaluated, that confirmed its effectiveness in the surrounding environment.

The robot was verified its behavior and emotional expression when it recognized the favorite object (green object) and disliked object (blue object) in a realistic environment. Throughout the task period (T1-T8), the robot was able to act the appropriate behaviors and emotional expressions as illustrated in Fig.3. After the

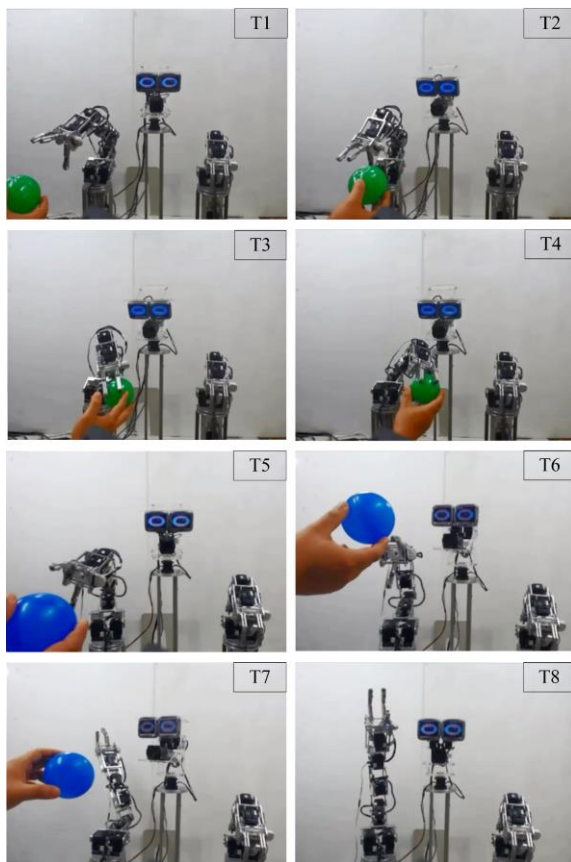


Fig.3 Behavioral and emotional selections at period T1-T8

robot was started. The robot selected “Look around” and “Interest (Flesh)” actions when it recognized the flesh-color. At T1, the robot was able to capture the favorite object, thus the robot’s motivation increased and the robot performed the behavior between “Look around” and “Interest”, the robot also express emotion as “Neutral”. From T2-T3, the robot performed the actions as “Interest” and “Approach” meanwhile it expressed “Hope” and “Happiness” emotions. Then, the blue object was presented in order to decrease the robot’s motivation. At T5, the motivation model achieved in the negative level, during periods T5-T6, the robot felt unhappiness when it confronted the disliked object, the robot expressed “Sadness” and “Fear” emotions meanwhile it performed the action as “Look around” and “Alertness”. After that (T6-T7), the blue object was moved closer to the robot, it felt dislike this situation, thus it performed “Avoidance” behavior and express “Disgust” emotion. Moreover, during period T6-T8, the robot expressed

“Hope” emotion, when it did not see the disliked object or the robot’s motivation increased to the positive level.

4. Conclusions

In this paper, the overview of the proposed system that consists of the recognition process, cognitive process and behavioral-emotional selection process. The system is executed by the Conbe-I robot in the realistic environment. All experimental results confirm the effectiveness of the proposed system such as the system can classify and generate the behavior and emotion maps based on the SOM learning method in the cognitive process, and the robot can suppress and change all emotional states based on the Markov model. In addition the robot can perform its behavior based on updating the emotional transition state. For the future work, we would like to combine the other neurotransmitters (noradrenaline and serotonin models) into the dopamine model in order to generate the dynamic emotional expression model.

References

1. N. Goto and E. Hayashi, “Design of Robotic Behavior that imitates animal consciousness,” *Journal of Artificial Life Robotics*, vol. 12, pp. 97-101, 2008.
2. E. Hayashi, T. Yamasaki, and K. Kuroki, “Autonomous Behavior System Combing Motivation and Consciousness Using Dopamine,” *Proc. of 8th Int. IEEE Symposium on Computational Intelligence in Robotics and Automation (CIRA 2009)*, pp. 126-131, 2009.
3. T. D. Thao, D. J. Herman, and D.V. Morano, *Phenomenology and dialectical materialism (Boston Studies in the Philosophy of Science)*, D. Reidel Pub., 1986
4. H. Kimura, “A trial to analyze the effect of an atypical antipsychotic medicine, risperidone on the release of dopamine in the central nervous system,” *J. of Aichi Medical University Association*, vol. 33, no. 1, pp. 21-27, 2005.
5. T. Kohonen, “Self-organized formation of topologically correct feature map,” *J. Biological Cybernetics*, vol. 43, pp. 56-69, 1982.
6. K. Koji, and B. Martin, “Towards an emotion core based on a Hidden Markov Model,” *Proc. of 13th IEEE International Workshop on Robot and Human Interactive Communication*, Sep. 20-22, Kurashiki, Okayama, Japan, pp. 119-124, 2004.

Consideration on a Crawler Robot with Six Legs

Toyomi Fujita and TIGA Sasaki

Department of Electronics and Intelligent Systems, Tohoku Institute of Technology,
Sendai, 982-8577, Japan

E-mail: t-fujita@tohotech.ac.jp

www.eis.tohotech.ac.jp/study/labs/fujita/FUJITALAB

Abstract

In this study, we consider development of a crawler-type mobile robot which is equipped with six legs at its body. This type of robot may have possibilities of both high mobility on rough terrain and working ability with handling such as carrying an object and removing small obstacles in its movement by using the legs as manipulation arms. This paper presents mechanisms and characteristics of this type of robot and some possible hybrid motions in which crawlers and legs are used. A running motion over a large gap by this type of robot is also considered as a typical hybrid motion with crawlers and legs. Necessary joint-torques of the legs in the motion are also analyzed in a computer simulation.

Keywords: Crawler-type mobile robot, legged robot, hybrid motion, handling task with locomotion, running motion over a gap

1. Introduction

With the recent spate of disasters in the world, the need for robots which can perform rescue activities in a disaster area has been growing. Such rescue-purpose robots should not only move to obtain information but also complete handling tasks by themselves in their working area. Therefore, the robot that has a hybrid mechanism with crawlers and robotic arms is useful because it can perform tasks for manipulation. In fact, some literatures describe that hybrid systems have capabilities of not only locomotion but also performance of work such as handling task.¹

However, conventional types of robot which has the hybrid mechanism have not been satisfied with both of movement and working ability very much. For example, in leg-wheel hybrid systems, many types such as Roller-Walker² and ATHLETE³ have a wheel at the end of each leg, so these are not suitable due to limitation of the handling task. In case of the mobile robots with leg-

crawler hybrid system, even though it has an advanced locomotion ability⁴, the mechanism in which a leg itself drives as a crawler^{5, 6} may not be suitable for our aim with respect to capability of handling task. A crawler-type robot with four legs presented by Hirose et al.⁷ have not been considered on handling tasks very much because movement mechanisms and how to obtain information from the surrounding environment have been mainly focused on. On the other hand, some leg-crawler hybrid robots are considered on some handling work. For instance, HELIOS IX⁸ is equipped with a manipulator for rescue operations. However, the type of task and the size of target object are restricted because of its single arm.

We thus consider another type of hybrid mobile robot with crawlers and six legs which are used as manipulators. Basically, in order to achieve stable static walking, six or more legs are necessary.⁹ Even though the increase of the number of legs brings the decrease of mobility due to heavy weight and energy consumption,

we consider the robot which has six legs is appropriate to the leg-crawler hybrid mobile robot with respect to both locomotion and working abilities.

This paper describes the structure and mechanism of devised crawler-type mobile robot which has six legs. Some possible hybrid motions by crawlers and legs are considered as an advantage of this type of robot. A computer simulation is also performed based on statics to analyze necessary joint-torques of the legs in the running motion over a gap.

2. Crawler-type Mobile Robot with Six Legs

2.1. Overview

We have devised a crawler-type mobile robot which has six legs. Fig. 1 shows an overview of the robot. The robot consists of two crawlers and six legs. Three legs are mounted on the left or right side of robot body. Each leg has 4-DOF mechanism and can be used as a manipulator.

This mechanism enables the robot to have high mobility such as running over a large gap by using front and rear legs to support the robot body appropriately, climbing a steep slope by assisting the crawler movement using legs, and so on. In addition to the high mobility, this type of robot is able to perform some useful tasks at a disaster area by acting the legs as manipulators. For example, the robot will be able to remove a small obstacle such as stone on the pathway of the robot in its movement using one leg, carry a large object to destination using multiple legs, get into a large rubble with supporting or removing it using multiple legs and retrieve a target object using the other legs, and so on. Fig. 2 shows a typical example of motion indicating an advantage of the robot; running over a large gap, which normal type of robot is not able to perform, by four legs with carrying a box by two legs.

2.2. Crawler Mechanisms

Two crawlers are attached at both sides of the robot body. Each crawler can be made by a belt with attachments and pulleys. One pulley which is at the most front or rear side can act as a driving pulley by connecting a DC motor. The other pulleys then act as idling pulley. A rotary encoder is also attached to a pulley for the control of crawler movement. The two

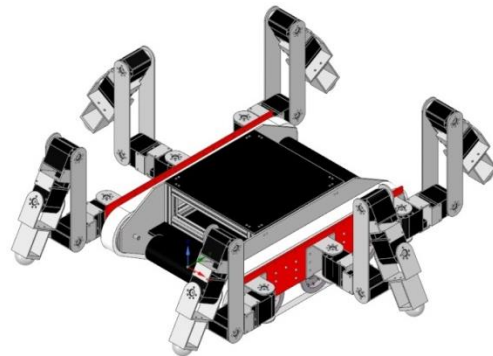


Fig. 1. Overview of crawler-type mobile robot with six legs.

driving pulleys for the left and right crawlers should be located diagonally to balance the body such that the right crawler has a driving pulley at the rear side and the left crawler has it at the front side. Symmetric location of the motors and encoders will enable the robot to run straight stably.

2.3. Leg Mechanisms

Fig. 3 shows the mechanism of devised leg. The leg has four joints: two yaw joints (J_1, J_4) and two roll joints (J_2, J_3). This mechanism enables the robot to perform a walking motion using each leg as 3-DOF mechanism by fixing the angle of J_4 . On the other hand, the joint J_4 will be used when the robot performs a manipulation task such as carrying an object. Servo motors will be able to be used as joint actuators. These can be selected based on a statics analysis of necessary torques in hybrid locomotion such as running over a gap, which will be presented later.

3. Consideration of Hybrid Running Over Gap

We consider a running over a long gap as a hybrid motion by crawlers and legs with carrying a box by the robot as shown in Fig. 2. If the robot doesn't have nor use legs, the robot will fall in the gap when the center of gravity of main body goes out of the edge of the gap. In this case, however, the presented crawler-type robot is able to use front and rear legs so that the robot prevents falling. Specifically, the robot can ground the tips of front legs on the opposite edge before the center of gravity of the robot come to just above the edge of the gap, continue movement by the crawlers with the

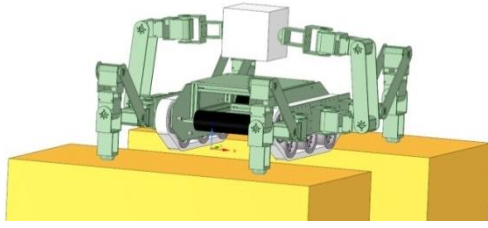


Fig. 2. Running over a large gap with carrying a box by crawler-type mobile robot with six legs.

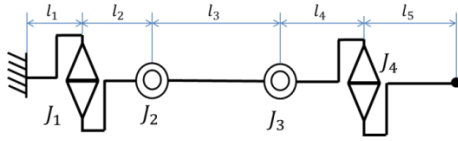


Fig. 3. Mechanism of a leg.

support of the front tips, touch the tips of rear legs at a little behind the edge before the robot body completely comes above the gap, then get across the gap by supporting the body by four legs. When the front part of body touches the ground at the opposite side of the edge, the robot can release the tips of front legs from the ground, then continue running by the crawlers with the support of the rear tips. When the center of gravity of the body comes above the opposite edge of the gap, the robot can release the rear tips and return to normal locomotion using crawlers only. In this motion, the robot doesn't have to use the fourth joint J_4 for each leg so that it acts as 3 DOF.

Let us suppose that the height of ground between the gap is same and the robot moves slowly. The models in this motion in the side view are shown in Fig. 4. We can divide the motion into three states: (a) *front leg auxiliary supporting*, (b) *front and rear legs supporting*, and (c) *rear leg auxiliary supporting*.

In the state of *front leg auxiliary supporting*, the distance between the edge of the gap and the center of gravity of the robot, L , meets $0 \leq L \leq B_h$ where B_h is the length between the center of gravity and the rear end of the body of the robot. In this state, the balance of moment around the edge point of the gap gives

$$Lmg = L_1 F_{zf} \quad (1)$$

where m is the mass of the robot, g is the acceleration of gravity, L_1 is the horizontal distance between the edge

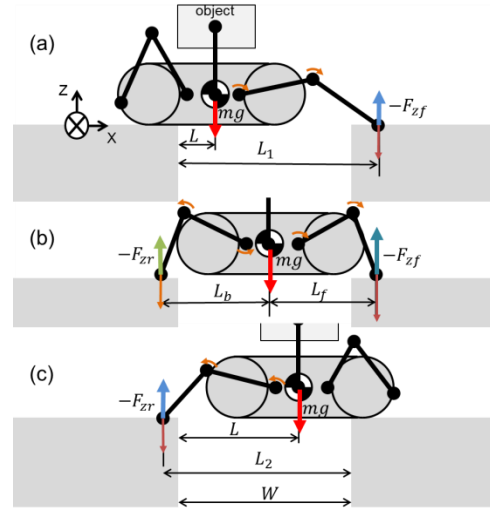


Fig. 4. Models in the motion of running over a gap (a): front leg auxiliary supporting (b): front and rear legs supporting (c): rear leg auxiliary supporting.

of the gap and the contact point of the front tip, and F_{zf} is the vertical component of the force to be generated at the front tip, so reaction force $-F_{zf}$ are acted to the contacting point of the tip.

In the state of *front and rear legs supporting*, because of supporting by four legs, the balances of moment around the both contact points of front and rear tips should be considered. The balance of moment around the rear tip gives

$$F_{zf}(L_r + L_f) = L_b mg, \quad (2)$$

and the balance of moment around the front tip gives

$$F_{zf}(L_r + L_f) = L_f mg \quad (3)$$

where L_f and L_r are the horizontal distances between the center of gravity of the robot and the front and rear contact points respectively, and F_{zf} is the vertical component of the force at the rear tip.

In the state of *rear leg auxiliary supporting*, it meets $(W - B_h) \leq L \leq W$ where W is the horizontal distance of the gap. In this state, the balance of moment around the opposite edge point of the gap gives

$$(W - L)mg = L_2 F_{zf} \quad (4)$$

where F_{zf} is the vertical component of the force at the rear tip and L_2 is the horizontal distance between the front edge of the gap and the contact point of the rear tip.

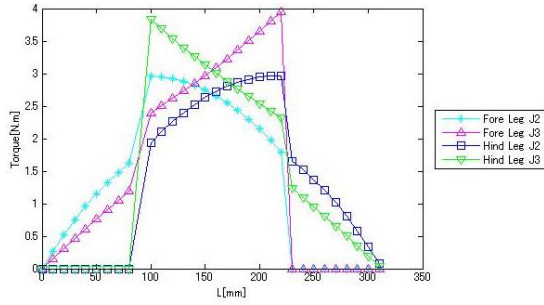


Fig. 5. Joint torques for the front and rear legs in the motion of running over a large gap.

From Eqs. (1)-(4), we can obtain necessary forces at the tips of the front and rear legs, then compute necessary torques for the joints J_1 , J_2 , and J_3 of each leg, $\boldsymbol{\tau} = (\tau_1, \tau_2, \tau_3)^T$ based on statics by

$$\boldsymbol{\tau} = \mathbf{J}^T \mathbf{F} \quad (5)$$

where \mathbf{J} is Jacobian corresponding to the tip position at each time, and $\mathbf{F} = (F_x, F_y, F_z, \tau_x, \tau_y, \tau_z)^T$ is a vector which consists of x, y, z components of the force, F_x, F_y, F_z , and moments around x, y, z axis, τ_x, τ_y, τ_z generated at the tip position.

Fig. 5 shows the computational result of the joint torques for the front and rear legs to L . In this case, we supposed that the distance between the bases of front and rear legs is 150 mm, the lengths of five links of each leg shown in Fig. 3 are $l_1 = 45$, $l_2 = 42$, $l_3 = 150$, $l_4 = 68$, and $l_5 = 95$ mm. $W = 312$ mm was also assumed as the distance of the gap. In the result, $0 \leq L \leq 90$ shows the state of *front leg auxiliary supporting*, $90 \leq L \leq 226$ shows the state of *front and rear legs supporting*, and $226 \leq L \leq 312$ shows the state of *rear leg auxiliary supporting*. For each state, F_{xf} or F_{xr} was applied to F_z , and 0 was given the other components of \mathbf{F} in Eq. (5). The torque of the first joint is not shown because it was always zero.

From this result, we can select appropriate joint motors which are enough for performing this motion; their maximum torques should be equal to 4 Nm at least.

4. Conclusions

In this study, we have considered development of a crawler-type mobile robot which has six legs. Because each leg can be used as a manipulator, the robot is able

to perform variety of tasks as well as high mobility. For future work, we plan to develop this type of robot and perform hybrid locomotion and working motions with legs and crawlers.

Acknowledgements

This work was supported by the Ring Ring Project of the JKA Foundation.

References

1. Bruzzone, L., and Quaglia, G., 2012. "Review article: locomotion systems for ground mobile robots in unstructured environments". *Mechanical Sciences*, 3(2), pp. 49–62.
2. Hirose, S., and Takeuchi, H., 1996. "Study on roller-walk (basic characteristics and its control)". In *Proceedings, 1996 IEEE International Conference on Robotics and Automation*, 1996, Vol. 4, pp. 3265–3270.
3. Wilcox, B. H., Litwin, T., Biesiadecki, J., Matthews, J., Heverly, M., Morrison, J., Townsend, J., Ahmad, N., Sirota, A., and Cooper, B., 2007. "Athlete: A cargo handling and manipulation robot for the moon". *Journal of Field Robotics*, 24(5), pp. 421–434.
4. Gao, X., Li, K., and Gao, J., 2009. "A Mobile Robot Platform with Double Angle-Changeable Tracks". *Advanced Robotics*, 23, pp. 1085–1102.
5. Michaud, F., Letourneau, D., Arseneault, M., Bergeron, Y., Cadrin, R., Gagnon, F., Legault, M.-A., Millette, M., Pare, J.-F., Tremblay, M.-C., et al., 2005. "Multimodal locomotion robotic platform using leg-track-wheel articulations". *Autonomous Robots*, 18(2), pp. 137–156.
6. Yokota, S., Kawabata, K., Blazevic, P., and Kobayashi, H., 2006. "Control law for rough terrain robot with leg-type crawler". In *Mechatronics and Automation, Proceedings of the 2006 IEEE International Conference on*, IEEE, pp. 417–422.
7. Hirose, S., Hodoshima, R., Fukumura, Y., and Amano, H., 2010. "Development of Track-changeable Quadruped Walking Robot TITAN X –Design of Leg Driving Mechanism and Basic Experiment–". In *IEEE/RSJ International Conference on Intelligent Robots and Systems (IROS)*, pp. 3340–3345.
8. Guarnieri, M., Takao, I., Debenest, P. C., Takita, K., Fukushima, E. F., and Hirose, S., 2008. "HELIOS IX Tracked Vehicle for Urban Search and Rescue Operations: Mechanical Design and First Tests". In *2008 IEEE/RSJ International Conference on Intelligent Robots and Systems*, pp. 1612–1617.
9. Siegwart, R., Nourbakhsh, I. R., and Scaramuzza, D., 2011. *Introduction to autonomous mobile robots*. MIT press.

The development of new products of pineapple cheesecakes

Sheu-Der Wu

*Department of Food and Beverage Management , Cheng Shiu University, No. 840, Chengcing Road, Niasong Dist.,
Kaohsiung City 83347, Taiwan (ROC)
E-mail: ws8245@yahoo.com.tw*

Hung-Wen Su

*Department of Food and Beverage Management, Far East University
No.49, Zhonghua Rd., Xinshi Dist., Tainan City 74448, Taiwan (R.O.C.)*

Abstract

In view of the product - pineapple cheesecakes newly developed for this study, the questionnaire answers proposed by consumers after sensory evaluations find the most popular flavor with 27% recipe proportion of pineapple chops added. Furthermore, after pineapples are added into cheesecakes, a new flavor has emerged in cheesecakes yet reduces the oily taste without sacrificing its original flavor and nutrient value. In the experiment of formal sensory evaluation, genders, ages, occupations, incomes and purchase intention are served as factors to analyze consumers' preference to pineapple cheesecakes. Research results after investigation finds the strongest acceptability is the samples of pineapple cheesecakes added with 27% pineapple chops. The least acceptability happens to the samples of pineapple cheesecakes added with 27% pineapple jams. After analysis, it is found the overall acceptability is high but the purchase intention is low revealing a higher preference to cheesecakes added with pineapple chops.

Keywords: Pineapple, Cheesecakes, Sensory evaluations..

1. Introduction

Nowadays, because people prefer to chase after innovative and novel products. Currently, there are few products of pineapple cheesecakes available on the markets. Because Kuanmiao, a town in southern Taiwan, is rich in pineapples with its agricultural yields of famous Diamond Pineapples (Tainon Number 17) throughout the year. Compared with the pineapples originated from tropical regions, our pineapples raised in the subtropical hilly regions are merited with the appropriate proportion of sweetness against acidity due to the remarkable temperature differences between days and nights in summer. Our pineapples combined with highly distinctive sweetness and acidity can intertexture a stunning flavor in mouths [1].

The science of Chinese Medicine proposes pineapples are featured with sweet yet sour flavors. It can stop thirst and facilitate digestion after eating with its major healing effect of deficient stomach secretion, frequent thirst, indigestion, appetite loss and diarrhea [2]. Because pineapples are featured with aforesaid effect, affordable prices and easy availability, this study focuses on the raw material of pineapples to develop new products and also takes people's purchase intention into consideration. The pineapples are further combined with the cheesecakes with a higher preference to explore consumers' preference for this kind of product.

2. The Review of Scientific Literatures

Pineapples (*Ananas comosus*) are a kind of evergreen perennial trees with its English name of the pineapple and the Chinese aliases like Buoluo and Huangli.

The Nutrients of Pineapples :

In view of the nutrients of pineapples, the pulps of pineapples are abundant in nutrients. Every 100g of pineapple pulp contain 52 calories, 87g of water, 0.9g of protein, 0.2g of fat, 11.6g of carbohydrate, 1.4g of fibers and 0.3g of ash [3].

Pineapple pulps containable bromelain with the effect like those of papain or pepsin available to decompose protein and facilitate digestion. Fruits contain a large volume of sugars (such as glucose, fructose, sucrose) and organic acids (Most ingredients are citric and others like malic acid and tartaric acid, etc.) available to eliminate fatigue. There are also some inorganic components such as iron, magnesium, potassium, sodium, calcium, phosphorus. Furthermore, pineapple fruits can also exert the effect of relieving heat, diureses, detoxification and stopping thirst [3] [4].

3. Research Method & Goal

(1) The Design of Questionnaires

Questionnaire design can be divided into two major parts. In previously prepared experimental products, the Control Group - Product B is added with pineapple chops and pineapple jams and divided into 3 different kinds of food stuffs for scoring evaluation analysis. Among them, 2 kinds of cheesecake recipes containing pineapple chops and pineapple jams with higher popularity are further analyzed available for formal sensory evaluation.

(2) Formal Sensory Evaluation:

This study continues referring to the recipe results adopted from commercial cooking books and sets Recipe A as a control group. Thereafter, two better flavors of the Group C with pineapple chops and the Group D with pineapple jams after screened from experimental preparation are further added with the recipes of the Control Group and the Group B with pineapple juice for 7-point scoring evaluation. Also, every asking item is clearly described convenient for

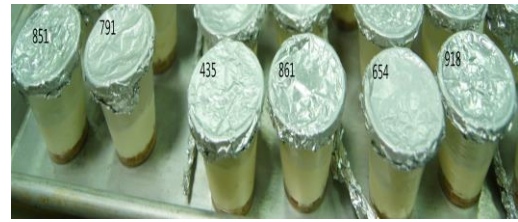


Fig. 1. Pineapple cheesecakes are combined with different content proportions for experimental tests.

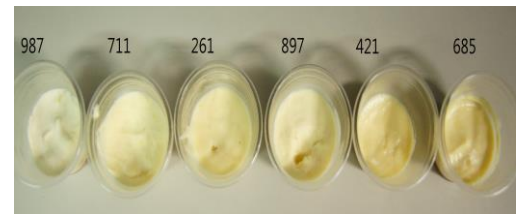


Fig. 2. Illustrates the finished products of pineapple cheesecakes made from different content proportions prepared for formal tests.

respondents to answer. In the 7-point scoring evaluation, 7 points mean the strongest flavor or preference and 1 point means the weakest flavor or preference. In view of the tests of sensory evaluation, "1" means "dislike very much"; "4" means "accept reluctantly"; "7" means "like very much". Meanwhile, to understand if the basic information of respondents will affect their own preference and acceptability to pineapple cheesecakes.

4. Production & Analysis

(1) Evaluation Method

The Methods for Experimental Preparation:

By referring to the cheesecake recipes adopted from commercial cooking books, a group of food stuffs combined with Recipe A and B is viewed as the control group and further improved as the group C and D with two best recipes selected. Cream cheese, whipped cream, gelatin powder, sugar, yogurt and lemon juice are served as raw materials with 3 different mixture proportions of Recipe C and D ready for formal sensory scoring evaluation few days later. The experiment is randomly conducted on 15 people passing through new urban regions for blind sensory evaluation.

Blind Test: Every sampling doze weighs 25g. During tests, respondents are not aware of food contents and pineapple weight. Figure 1 illustrates the finished

products of pineapple cheesecakes combined with different content proportions for experimental tests.

Formal Sensory Evaluation: The sampling recipes for formal sensory evaluation are exactly the same as those previously prepared for experiments, but new random codes are marked. Figure 2 illustrates the finished products of pineapple cheesecakes made from different content proportions prepared for formal tests.

(2) The Analysis of Demographic Variables of Formal Sensory Evaluation

Experimental respondents are those consumers on new urban regions with the frequency analysis focusing on their genders, ages, occupations, incomes and purchase intention .

In gender survey, there are 62 females occupying 59.6% and 42 males occupying 40.4%. In age survey, the ages of respondents include 32 respondents aging below 20 (inclusive) occupying 30.8%, 30 respondents aging 21~25 (inclusive) occupying 28.8%. About income survey, there are 48 respondents with incomes below 20,000 NTDs (inclusive) occupying 46.2%, 31 respondents earning 20,001~30,000 NTDs occupying 29.8%. In occupation, there are 20 respondents with their occupations separately in academic, agricultural and industrial fields occupying 19.2%, 21 respondents in the commercial field occupying 20.2%, 43 students occupying 41.3% and 20 unemployed or retired respondents occupying 19.2%. About purchase intention : In this survey, there are 84 respondents with purchase intention occupying 80.8%.

The Variance Analysis of purchase intention : This study is operated with the Independent Sample T-test to explore and analyze if there is any remarkable difference happening to purchase intention against different recipe proportions added to pineapple cheesecakes. Results are shown as Table 1. It is found there is no remarkable difference happening to the purchase intention from those of different occupations. Among them, no matter if there is any purchase intention, respondents show highly similar degrees in acceptability.

However, respondents show stronger purchase intention to sample 711 and 897 wherein sample 897 receives stronger preference. It means consumers feel more enjoyable in chewing acceptability. Some consumers

show higher preference to cheesecakes without any additive fruit granule.

Table 1 reveals the ANOVA variance analysis of pineapple cheesecakes with different recipe proportions felt by those of different occupations

Question Item	Purchase Intention	Count	Average	S.D.	F-test	Significance
987 Overall Acceptability	Yes	84	4.70	1.487	1.213	.273
	No	20	4.80	1.704		
711 Overall Acceptability	Yes	84	4.87	1.412	2.305	.132
	No	20	5.20	1.105		
261 Overall Acceptability	Yes	84	4.71	1.393	.002	.965
	No	20	5.30	1.302		
897 Overall Acceptability	Yes	84	5.02	1.388	.671	.415
	No	20	5.55	1.191		
421 Overall Acceptability	Yes	84	4.64	1.580	.753	.387
	No	20	4.90	1.373		
685 Overall Acceptability	Yes	84	4.56	1.524	1.435	.234
	No	20	5.15	1.226		

5. Conclusion & Prospect

In view of the product - pineapple cheesecakes newly developed for this study, the questionnaire answers proposed by consumers after sensory evaluations find the most popular flavor with 27% recipe proportion of pineapple chops added. Furthermore, after pineapples are added into cheesecakes, a new flavor has emerged in cheesecakes yet reduces the oily taste without sacrificing its original flavor and nutrient value.

In the experiment of formal sensory evaluation, genders, ages, occupations, incomes and purchase intention are served as factors to analyze consumers' preference to pineapple cheesecakes. Research results after investigation finds the strongest acceptability is the samples of pineapple cheesecakes added with 27% pineapple chops. The least acceptability happens to the samples of pineapple cheesecakes added with 27% pineapple jams. After analysis, it is found the overall acceptability is high but the purchase intention is low revealing a higher preference to cheesecakes added with pineapple chops.

We assume not everyone like the product of pineapple cheesecakes. However, in view of overall flavors, the product is acceptable but no purchase intention shows. Also, respondents show no remarkable feeling to the

acidity of pineapple cheesecakes proposed in this study. Furthermore, the sweetness after sugaring making the acidity of pineapple vaguer also affects respondents' preference to samples with research results influenced. Because of the limitation of research fund, it is hoped in the future, the vague acidity of pineapple cheesecakes after the sugaring of pineapple chops and jams can be improved. Additionally, purchase intention can be further investigated to continuously find out the product of pineapple cheesecakes with the best preference from consumers to improve product diversities.

Reference

1. Taiwan Fruit Exports (2012/4/29)
http://trade.coa.gov.tw/index_b.jsp.
2. Gao, Kai-Ping (2009) Herbal Healing Science, China: The Chemical Industry Publisher.
3. The Department of Health (2011/05/06)
http://www.doh.gov.tw/cht2006/index_populace.asp.
4. Kang, Pei-Ci (2007) The Study on the R&D of Pineapple High-fiber Bread and its Quality. The Master's Degree Disseminate of the Graduate Institute of Applied Science, Tainan Science and Technology University, Tainan City, Unpublished Article.

The Study on Ballroom Service Quality to Affect Customer Satisfaction

Hsiu-Min Lin *

*Department of Food and Beverage Management, Far East University
No.49, Zhonghua Rd., Xinshi Dist., Tainan City 74448, Taiwan (R.O.C.)
E-mail: linhsiumin@cc.feu.edu.tw*

Yang Wu

*Department of Food and Beverage Management, Far East University
No.49, Zhonghua Rd., Xinshi Dist., Tainan City 74448, Taiwan (R.O.C.)*

Jei-Fu Ho

*Department of Food and Beverage Management, Far East University
No.49, Zhonghua Rd., Xinshi Dist., Tainan City 74448, Taiwan (R.O.C.)*

Abstract

For hoteliers, customer expectations and the real performance of service probably existed in perceptive variance between the emphasized details and satisfaction to bring about the gaps of service quality. As such, it naturally caused customer unsatisfied with service quality to lose their patronage. As it is found from research results, service quality exerted positive influence on demographic variables. If it was available to improve the service quality and the expectations to customer satisfaction, then it was naturally available to enhance the repeated purchase intention of customers. In 10 dimensions cited in this research, after researching analysis, "tangibles" was satisfied by customers the most. If providers could keep the satisfaction always, then it was naturally available to enhance the first image in customers' mind. Additionally, "external response" scored the least and provides should improve their own service quality by focusing on the parts highly emphasized by customers. Furthermore, more emphasis should be placed on the opinions of customers to win their trust and avoid external complaint lodged by customers without losing the source of customers. The excellency or inferiority of service quality would directly affect customer satisfaction. If providers were planning for sustainable business management, excellent service quality was imperatively required. As such, it was just available to win the trust from customers under the fiercely competitive business climate with the goal of sustainable business management achievable..

Keywords: Ballroom, Customer Satisfaction, Service Quality

1. Introduction

Ballroom incomes occupied from 40% to 80% of the total revenue of a restaurant department roughly with its undoubted importance. It was quite a critical income source. Ballroom visitors were all the potential customers of restaurants and excellent ballroom festival service would be certainly the most powerful marketing tool to gain such potential interest [1]. Joining a wonderful ballroom service would be an impressive occasion in mind to add the frequencies of repeated visit

in the future and even enhance the intention to hold a ballroom festival event [2].

2. Literature Review

There were various combinations and types of festival service available with the markets mainly focusing on the events held by associations, commercial organizations and social groups. An ordinary association was normally composed of members less than one hundred. The annual meetings and other campaigns held by such associations were mostly combined with meals and meetings together

wherein it also included rest time and the service of providing coffee and snacks, cocktail parties and formal festivals.

As for service quality, service quality meant the quality of service and products provided by service industries in customers' mind, a comparison between the quality expected by customers and the quality practically experienced by customers [3]. Service was not only a kind of intangible products but also a kind of virtual stuffs without fixed standards and models. It did not only mean products themselves but also emphasize the intangible service quality available for customers. As [4] supposed, the excellency of service quality depended on the comparison between the expectations to service and product quality and the quality practically experienced by customers. If the service and product quality practically experienced by customers was beyond expectations, then customers showed higher satisfaction with a positive perception of better service quality and vice versa.

The firstly proposed the concept of customer satisfaction and health contended on a certain occasion, timing or setting, in view of the perceive status after customers sacrificed the cost and obtained the reward through purchasing products, whenever perceived reward was higher than sacrificed cost, the satisfaction was arisen[5]. As Parsuraman, Zeithaml, and Berry contended, there were 5 kinds of service gaps existing in service processes and interfering service experience[6]. The said 5 kinds of service gaps were respectively service positioning, service explanation, service delivery, service communication and service delivery. In this research, further based on the research data proposed by [6], the "natures of service quality" were summarized as research goals. etc. In this study, the preferences evaluation was used to research the consumers' taste.

3. Research Methods

3.1. 3.1. Research Structure

In this research, the research structure was summarized in accordance with research motivations, goals and scientific literatures by using statistical demographic variables to analyze and understand the variance of customer satisfaction among various levels of customers.

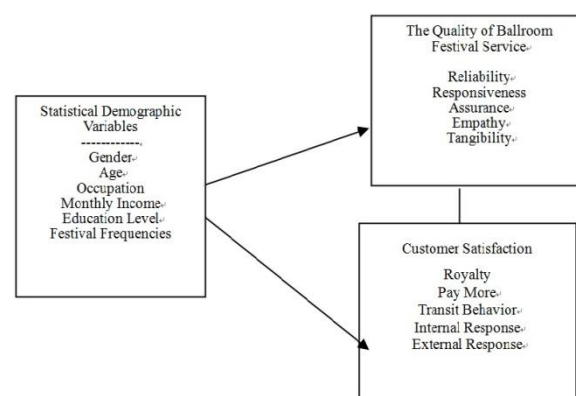


Figure 1, The Map of Research Structure

3.2. 3.2. The Operational Definitions of Research Variables

The researching dimensions adopted the SERVQUAL Scales modified by Parasuraman (1985) by focusing on service quality as a basis. Also, the correction was made in accordance with the natures of occupations to serve as the questionnaires to test service quality. The scoring measurements were conducted in accordance with the Likert 5-Point Scale available for respondent evaluation wherein "1" meant very much disagree; "2" meant disagree; "3" meant fair; "4" meant agree and "5" meant very much agree. Higher scores meant higher satisfaction.

3.3. 3.3. Questionnaire Design

Based on contents and structure, this research could be divided into two major parts with every part respectively described as below questionnaire contents: The statistical demographic variables were divided into 6 dimensions in accordance with the demands of this research including genders, ages, occupations, education levels and consumption frequencies.

4. The Analysis of Research Results

This research was meant to explore the customer satisfaction against the service quality provided by hotels. In this article chapter, the valid questionnaire replies

were retrieved for data processing and analyzing with the SPSS 18 Suite Application as a kit. Research results were respectively explained on the basis of customer basic information including the analysis on the evaluated results of satisfaction, customer genus against service quality and the influence on customer satisfaction. This chapter was divided into 3 sections with Section 1 to describe the analysis of formal questionnaire surveys, Section 2 to describe the analysis on basic information further subdivided into two parts, namely service quality and customer satisfaction for detailed explication and Section 3 to describe the Independent Sample T-test. In respect of independent sample T-test, It could be known from tested results the significant two-tailed P-value (0.049) of different genders against the dimension of external response was below 0.05. It indicated the customers of different genders caused significant variance in the dimension of external response meaning the customers of different genders showed their special preference or detest to the average of the dimension of external response. For the customers of different genders, all the values against other dimensions were above 0.05 and it indicated the customers of different genders showed no special preference or detest.

5. Conclusion and Suggestion

5.1. Research Conclusion

Female customers showed a lower average rated at 3.64 in the dimension of external response. It indicated female customers respectively showed different opinions to the dimension of external response wherein the item - "If I was unsatisfied with the service of a hotel, I would lodge a complaint to external organizations." scored the least. It indicated female customers the service provided by hotels could not fulfill their demands.

The customers aging above 50 (inclusive) showed a lower average rated at 3.50 in the dimension of reliability. It indicated the customers at theses ages respectively showed different opinions to the dimension of reliability wherein the item - "If service givers could answer questions appropriately?" scored the least.

The customers with self-employed occupations showed a lower average rated at 2.99 in the dimension of "pay more", It indicated the customers with self-employed occupations respectively showed different opinions to the

dimension of "pay more" wherein the item - "I would still patronize this hotel repeatedly even if the prices were raised!" scored the least. It indicated the customers with self-employed occupations contended the service provided by hotels could not fulfill their special demands. The customers with monthly incomes within 25,001~35,000 NTDs showed a lower average rated at 3.31 in the dimension of transit. It indicated the customers with such monthly incomes respectively showed different opinions to the dimension of transit wherein the item - "The first priority was based on the transportation convenience!" scored the least. It indicated the customers with monthly incomes within 25,001~35,000 contended the service provided by hotels could not fulfill their special demands.

The customers with festival frequencies within 1~2 times annually showed a lower average rated at 3.60 in the empathy dimension. It indicated the customers with such monthly incomes respectively showed different opinions to the empathy dimension wherein the item - "I would ask for extraordinary service from the service givers!" scored the least. It indicated the customers with festival frequencies within 1~2 times annually contended the service provided by hotels could not fulfill their special demands.

5.2. Suggestion

A company should enhance its own education and training projects for their employees and allow employees to aggressively ask about customers' opinions after meals. It is available to understand and solve problems immediately.

A company should introduce novel and excellent facilities to replace the old ones and allow customers with the entirely novel atmosphere.

It is available to serve customers with customary service to fulfill their special demands and consolidate customer royalty with admirable words of mouth won (such as special menu, music bands and small giveaways etc.).

A company can hold irregular favorable deduction events, charity campaigns and advertisement to promote the uniqueness quite different from other competitors, availably allowing customers with totally different experience.

A company can provide employees with some training courses to fulfill their professionalism and knowledge. It

is available to enhance the responsiveness of employees when facing various problems and improve employees' self-confidence.

References

1. Ministry Y. X. Zhang, The Dissatisfaction at the 1st Restaurant Management Symposium., (The Foundation of Chinese Dietary Culture. Taipei, Taiwan 1996).
2. S. W. Xu, *The Management of Ballroom Festival Service: Theories & Practical Affairs.*(The Yang-Chih Book Co Ltd. Taipei, Taiwan 2005)
3. F. J. Su, *The Management & Practical Affairs of Hospitality Service.* (The Yang-Chih Book Co Ltd. Taipei, Taiwan 2008).
4. P. G. Klaus, Quality Epiphenomenon: The Conceptual Understanding of Wuality in Face-to-Face Service Encounters. In J. Czepial, M. Solomon, and C. Surprenant, eds. *The Service Encounter.* (Lexington, KY: Lexington Books, 17-33. 1985).
5. R. N. Cardozo, An Experimental Study of Customer Effort, Expectation, and Satisfaction. *Journal of Marketing Research*, 2(3)(1965), pp. 244-249.
6. A. Parsuraman, V. A. Zeithaml, and L. L. Berry. A Conceptual Model of Service Quality and Its Implications for Future Research. *Journal of Marketing* . 49 (1985), pp.44-50.

The Relationship between Employees' Personality Traits, Work Values and Job Involvement with the Contribution to their Companies – For the Micro Food Service Industry

Hsiu-Chen Chung

*Department of Food and Beverage Services, Tainan University of Technology,
No.529, Zhongzheng Rd., Yongkang District, Tainan City 71002, Taiwan (ROC)*

Chiou-Lan Chien*

*Department of Food and Beverage Services, Tainan University of Technology,
No.529, Zhongzheng Rd., Yongkang District, Tainan City 71002, Taiwan (ROC)
E-mail: t10156@mail.tut.edu.tw*

Lung-Chi Tsai

*Department of Leisure, Recreation, and Tourism Management, Southern Taiwan University of Science and Technology,
No.1, Nan-Tai Street, Yongkang District, Tainan City 71005, Taiwan (ROC)*

Abstract

The purpose of the study is to discover the influence between the employee's (for whom who works in the micro food industry) personality, work values and job involvement to the contribution and dedication. Research sample focus on the snack bar in night market, bakery stores and the micro food industries' employees or owners from Taizhong, Changhua, Yunlin, Jiayi and Tainan cities. We send 450 questionnaires, the effective questionnaires are 333, and the percentage of effective retrieve of the questionnaire is 87.63%. After using reliability analysis, correlation analysis, one-way analysis of variance (ANOVA), independent, work values and personality can forecast prediction the employee's contribution and dedication very precisely; in addition, we find out that job involvement has a very clear effects between work values and job contribution.

Keywords: personality, work values, job involvement, contribution.

1. Introduction

Micro-Enterprise is an easier way of starting a personal-owning business due to the relative low market entrance. In Taiwan, it only costs five hundred thousand New Taiwanese Dollars to start an eating house [1], and therefore most of the people make livings on Micro-Enterprise, which is important and irreplaceable to social development [2]. Staff is the most important resource of an enterprise [3], only by choosing and keeping key staff long can an enterprise increase its competitive advantage [4]. Researchers pointed out that the personal values, personality traits, and the job involvement of staff

would affect individual performance and efficiency on work [5] [6] [7]. A staff's high job involvement, satisfaction, spontaneous professional proactive behavior with passion, and low intention of turnover refer to a high employee engagement, and therefore leveling up the efficiency of an enterprise [8] [9] [10].

This study aimed to discuss how the personality traits, personal work values, and job involvement of staff affect the employee engagement, and hope to offer advices to the Micro Food Service Industry runners on staff election and keep-on.

2. Study Purpose

The study was focused on investigating: 1) The effect of personal backgrounds on personality traits, work values, job involvement and employee engagement of individual staff. 2) The relationships among personality traits, work values, job involvement of staff and employee engagement. 3) The effect of personality traits, work values, job involvement of staff on its employee engagement. 4) The mediation of job involvement on work values and employee engagement.

3. Research Methods

The study applied convenience sampling from employers and staff in eating houses, small restaurants, combinative bakery, and food stands in the night markets in Taichung, Changhua, Yunlin, Chiayi, and Tainan. 450 designed questionnaires were released and 380 of them were returned, with the valid response rate of 87.63%. All data were analyzed with statistical software SPSS 12.0 for frequency distribution, mean, standard deviation, non-paired t-test, one-way ANOVA, Pearson's correlation coefficient, and regression for further discussions.

The questionnaire with high reliability was designed including the following scales. Personality traits scale applied for the study was adopted from Work Locus of Control Scale [11], including internal and external facets. And the items on the scale were condensed from 16 into 5 for the study. Originally there were 15 items in personal traits variable scale, and this study only concerned the 7 items of external facet, with total scale $\alpha = .892$. Items of work values scale including instrumental value and objective value evaluation parts were designed according to Wu [12] [13] [14]. These 17 items have a total scale of $\alpha = .905$, with $\alpha = .915$ and $\alpha = .877$ on instrumental value and objective value facet, respectively. Job involvement scale including 13 high-involvement items were designed according to Kanungo [15], and Lodahl & Kejner [16], with total scale of $\alpha = .902$. 15 items of employee engagement scale including vitality, concentrating, and professional effectiveness parts were designed according to Lee, Lain, & Chen (1999) [17], and Schaufeli, Salanova, Gonzalez-Roma, & Bakker [18] (2002). In this part, the total scale $\alpha = .916$,

vitality facet $\alpha = .841$, concentrating facet $\alpha = .803$, and professional effectiveness facet $\alpha = .901$.

4. Results and discussions

4.1. Descriptive statistics

1) For personality traits facet, the significant others for promotion, and the luck of having a good job are highly valued by employees involved in micro catering and beverage businesses.

2) For work value facet, participants regarded good interaction relationships, the improvement and learning experiences the job could provide, and the increasing opportunities of promotion due to learning hard as important factors.

3) For job involvement facet, high-involvement participants regarded assuming responsibility as an important factor.

4) For employee engagement facet, most of the participants regarded professional ability as the most important factor.

4.2. Correlation coefficient analysis

There were no significant correlation of personality traits and employee engagement ($r = -.027$). Work value and job involvement are significantly positive correlated to employee engagement, with $r = .707$ and $.734$, respectively. The results suggested that if participants of micro catering and beverage enterprises have more positive attitudes, involving more in their jobs, and have higher instrumental and objective values, their vitality, concentrating and professional effectiveness are higher, and the same as their employee engagement.

4.3. ANOVA

1) There were significant differences on external personality traits among different age groups.

2) There were significant differences on position and job grade among external personality traits, job involvement (high involvement), and employee engagement (professional effectiveness).

3) There were significant differences on external personality traits, objective value, and employee engagement (concentrating and professional

effectiveness) among participant groups with different years of working experience and different.

4) Experienced participants have higher job involvement and vitality than non-experienced ones.

5) There were significant differences on job involvement (high involvement) among participant groups with different years of working experience related to catering and beverage businesses.

6) The objective value of male was higher than female.

7) There were significant differences on job grade among external personality traits, objective value, high job involvement, concentrating, and professional effectiveness.

4.4. Regression analysis

1) The more the participants think highly of job involvement and job value, the more employee engagement they contribute, and jobs involvement affects employee engagement more than job value.

2) The more the participants think highly of high job involvement, objective value, and instrumental value, the more employee engagement, concentrating, and professional effectiveness they contribute. Among those, high job involvement affects employee engagement and concentrating facet the most, and objective value affects professional effectiveness the most.

3) The more the participants think highly of high job involvement and objective value, the more vitality they performed, and high job involvement affects vitality the most. The more the participants think highly of high job involvement, objective value, and instrumental value, the larger the concentrating sub-facet is, and high job involvement affects the most on concentrating sub-facet.

4) The more the participants think highly of high job involvement, objective value, and instrumental value, the larger the professional effectiveness sub-facet is, and objective value affects the most on it.

4.5. Mediation

1) The affects of work value toward employee engagement is partially mediated by job involvement.

2) The affects of objective value and instrumental value toward employee engagement are both partially mediated by job involvement.

3) The affects of objective value and instrumental value toward vitality facet, concentrating facet, and professional effectiveness facet are all partially mediated by job involvement.

5. Conclusions and suggestions

5.1. Conclusions

1) Staff with external personality traits hope to get a better job with significant others and luck, and this is extremely different from the career expectations of staff with high working passion, be willing of facing challenges, and sticking on one's place on catering and beverage business.

2) Once the staff confirm that they can have high individual achievements for the future in a company or an enterprise, they are more likely to involve themselves in their work.

3) Staff with high involvement is staff whom is passionate to their jobs with vitality, and also thinks highly on the SOP and their working efficiency.

4) Although external personality traits has negative effects on employee engagement and professional effectiveness, the study found that to the supervisors, the most important thing are that staff can be familiar with their job content and working progress, and finish their individual missions conscientiously and effectively.

5) Understanding the items staff are willing to devoted to, e.g. accomplishment, interests, and chances of learning thins, would help increasing the work value to the staff, and therefore increase staff's passion, vitality, responsibility, and working efficiency.

6) Among variables related with individuals, age, position, job grade, and years of working experience have significant effects on external personality traits, but have no significant effects on work value. Position, job grade, related working experience, and years of working experience related to catering and beverage business have significant effects on job involvement. Position, job grade, and related years of working experience have significant effects on employee engagement and professional effectiveness. Job grade and related years of working experience have significant effects on concentrating, while related working experience has significant effects on vitality.

5.2. Suggestions

- 1) Elect and apply staff with internal personality traits as the staff.
- 2) Build a fair managing system on working efficiency evaluation and promotion to help building a positive social interaction of the entire enterprise.
- 3) Build a reasonable and transparent celery managing system to lower the intention of staff turnover.
- 4) Build an encouragement system that fits the culture of the enterprise to make staff to be more willing to devote to the enterprise.

Table 1. The verification of research hypotheses.

Hypothesis	Result
1) Individual background has significant effects on personality traits, work value, job involvement, and employee engagement.	Partially accepted
2) Personality traits, work value, and job involvement are significantly positive correlated to employee engagement.	Partially accepted
3) Personality traits, work value, and job involvement have significant positive effects on employee engagement.	Partially accepted
4) Work value and employee engagement are mediated by job involvement.	Accepted

References

1. MINISTRY of LABOR, A Case Study of a Micro-Enterprise Program (MINISTRY of LABOR, Taipei, 2014).
2. Z. K. Zheng, May the Micro-Entrepreneurs Springing up all over the Place (Common Wealth Magazine, Taipei, 2014).
3. Z. X. Chen, Small and Medium Enterprise Management of Sharing (Reinvent Corporates Values and Strategies, Taipei, 2007).
4. L. R. Rui, How to Retain on the Key Talents (Workforce Development Agency, Taipei, 2005).
5. S. P. Robbins, Essentials of Organizational Behavior (New Jersey: Prentice Hall, 1992).
6. B. Scheider, W. H. Macey, K. M. Barbera, & N. Martin, Driving customer satisfaction and financial success through employee engagement, *People & Strategy*. **32**(2) (2009) 22-27.
7. W. S. Huang and S. P. Shen, A study of the relationship among work values, job involvement, and teaching efficacy of junior high school teachers in Kaohsiung city, *Association for Curriculum and Instructio*. **15**(4) (2012) 161-188.
8. M. Buckingham, and C. Coffman, First, Break all the rules. (New York: Simon & Schuster, 1999).
9. S. Sonnentag, Recovery, work engagement, and proactive behavior: A new look at the interface between nonwork and work. *Journal of Applied Psychology*, **88**(3) (2003) 518-528.
10. W. B. Schaufeli, and A. B. Bakker, Job demands, job resources, and their relationship with burnout and engagement: A multi-sample study, *Journal of Organizational Behavior*. **25** (2004) 293-315.
11. P. E. Spector, Development of the work locus of control scale, *Journal of Occupational Psychology*. **61** (1988) 335-340.
12. T. H. Wu, The Study of the Construction of the Sales Work Value Scale (National Youth Commission, Taipei, 1996).
13. I. C. Huang, and P. W. Huang, The relation between practical training values and job involvement: A study of college students majoring in Tourism, Leisure, Recreation, and Hospitality, *Journal of Tourism Studies*. **10**(1) (2003) 63-79.
14. S. H. Lin, and K. C. Hung, The study on the view of value toward work of the students who major in business administration and related departments of vocational colleges, *Journal of International Esthetic Science*. **5**(2) (2008) 177-214.
15. R. N. Kanungo, Measurement of job and work involvement, *Journal of Applied Psychology*, **67**(3), (1982) 341-349.
16. Lodahl, T. M., and M. Kejner, The definition and measurement of Jjob involvement, *Journal of Applied Psychology*, **49**(1), (1965) 24-33.
17. Y. D. Lee, J. W. Lain, & C. Y. Chen, A study on the measurement of productivity for White-Collar employees: A case of electronic industry in Taiwan. *The Chinese Military Academy Journal*. (1999) 345-361.
18. W. B. Schaufeli, M. Salanova, V. Gonzalez-Roma, & A. Bakker, The measurement of engagement and burnout: A two sample confirmatory factor analytic approach. *Journal of Happiness Studies*, **3**(1) (2002) 71-92.

Consumer's Acceptance to The New Product- Pineapple Jam as Example

Shang-Hui Li*

*Department of Food and Beverage Management, Far East University
No.49, Zhonghua Rd., Xinshi Dist., Tainan City 74448, Taiwan (R.O.C.)
E-mail:a0956358700@gmail.com*

Jei-Fu Ho

*Department of Food and Beverage Management, Far East University
No.49, Zhonghua Rd., Xinshi Dist., Tainan City 74448, Taiwan (R.O.C.)*

Abstract

Based on the health and environmental considerations, consumers paid their more attention to the pursuit of natural ingredient. In other words, a safe and non-toxic diet is the basic consideration for the consumers. More consumers pay more attention on natural foods; they gradually change their eating habits. In recent years, many food safety events such as tainted milk, clenbuterol, poison starch, plasticizers etc. have been reported. Consumers tend to buy natural foods, less chemical additives and security food as the primary concern. This study attempts to take the natural pineapple jam as the major structure. And try to add dates and plum into pineapple jam instead of any artificial additives, and enhance the taste level. Meanwhile, different flavors could derive from the natural products according to the pineapple jam proportion of different formulations. The study expects to be able to create the pineapple jam which is not the same as made by the market products. The study selected 150 consumers of Tainan area to be tested of preferences of sensory evaluation, and SPSS 12.0 statistical software was used as the data analysis of the outcomes of the study. The result found among 123 valid questionnaires. The original flavor pineapple jam in its appearance, aroma, stiffness, acidity, sweetness and overall acceptability can be accepted by most consumers and there are significant differences with other products. Consumer also showed their strongest willingness to buy the original flavor pineapple jam and there are significant differences with other products.

Keywords: Pineapple, Pineapple Jam, Sensory Evaluation.

1. Introduction

Pineapple is low in calories, rich in vitamin C, B₁ and E, also with minerals, dietary fiber, water etc., it is widely used in health food and fruit juice [1]. However, the media often reported that pineapple could be sold out cheaply, destroyed directly or to be used as a plant fertilizer during in season period. Because fresh fruit is very difficult to save, it is necessary through using fruit processing to continue its value. Pineapple jam, a commercial commodity, is the other way to keep its "life".

In this study, the innovative pineapple jam was as the research theme to discuss the acceptance and purchase intention of consumers on different types of pineapple jams.

2. Literature Review

Pineapple is a kind of tropical fruit originated to the Amazon River. Presumably, it was introduced to Taiwan in 1664, or Emperor Kangxi, Qing Dynasty, from southern China. Current pineapple cultivars in Taiwan can be divided into local, foreign and hybrid species [1].

Codex Alimentarius Commission, CODEX, regulated only solidified or sticky products which have more than 65% sugar could be defined as "fruit jam". However, the liquid sugar and cooked sauce was taken as a jam in Japan marketing, even the sugar content was reduced to about 40 percent [2]. 50% - 65% sugar content of the jam could be acceptable for most of Taiwan consumers [3].

"Purchase intention" is an attempt to buy product possibilities [4]. The information resources will create the different opinions and preferences to consumers, thereby affecting their purchase intention [5]. In 1988, proposed to measure the purchase intention by perceived value such as possible purchase, want to purchase, consider to purchasing etc[6]. The study results of Wu and Peng in 2010 showed that the attitude to the brand will affect the purchase intention of consumers [7].

Institute of Food Technologists, U.S. defined sensory evaluation named in line with the basic human capacity for food or something of the sense of taste, smell, etc. Also, to obtain a correct conclusion of systematic knowledge through the scientific booting, measured, analyzed and judged the test done [8].

There are many kinds of sensory evaluation methods to be used. To select the appropriate method in accordance with the purpose of the test, then the results make sense [9]. In 2003, pointed out that consumer preferences referred to test scores of palatability [10]. However, the high or low score was not directly related to the actual strength of a certain taste. Hobby of tasting referred to appearance, flavor and overall acceptability, etc. In this study, the preferences evaluation was used to research the consumers' taste.

3. Research Methods

Kuanmiao-planted "Tai-farmer #2" pineapples were taken as the research object, because it contains less water, making jam time can be shortened and easy to obtain.

The study process was shown as in Fig. 1.

In this study, two preliminary tests were conducted in order to find a better formula for an official test. Original pineapple jam, date-added pineapple jam, plum-added pineapple jam and on the market pineapple jam were the

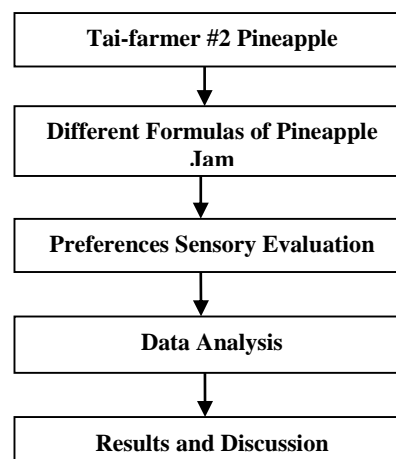


Fig. 1. Pineapple Jam Test Flowchart

official test samples. Then, preferences sensory evaluation test was conducted. A "five-point" score was used. "5" represents "very much like or very dark"; "1" represents "did not like very much or too light". Repeatevaluation was acceptable. The difference of evaluation results was analyzed by SPSS 12.0.

4. Data Analysis

In this study, 150 convenience samples were collected from Tainan City residents to fill up the sensory evaluation survey, 150 questionnaires were distributed, and a total recovery of 123 valid questionnaires, 81%, while 27 were for invalid questionnaires, 17%.

Regarding the gender, male respondents accounted for 49.59% and 50.40% for female. Respondents of 21 to 30 years old were at most (36.58%). 48.78% received the higher education majority. 72.35% respondents considered that they always put their attention on the issue of processed food safety.

Preferences analysis results of pineapple jam were shown in Table 1. The analysis result on the difference of

Table 1. Preferences analysis results of pineapple jam

Item	Sample	Number	Average	Standard deviation	F test	Distinctiveness
Appearance	254	123	2.71 ^a ±1.233	35.317	0.000***	
	396	123	4.05 ^c ±1.047			
	642	123	2.74 ^a ±1.240			
	875	123	3.07 ^b ±1.146			
Aroma	254	123	2.89 ^a ±1.144	16.430	0.000***	
	396	123	3.63 ^b ±1.141			
	642	123	2.91 ^a ±1.138			
	875	123	2.68 ^a ±1.081			
Stiffness	254	123	3.14 ^b ±1.019	10.221	0.000***	
	396	123	3.70 ^c ±0.949			
	642	123	3.14 ^b ±1.019			
	875	123	3.05 ^a ±1.144			
Acidity	254	123	2.98 ^b ±1.127	15.458	0.000***	
	396	123	3.53 ^c ±0.969			
	642	123	2.99 ^b ±1.149			
	875	123	2.61 ^a ±1.013			
Sweetness	254	123	3.10 ^a ±1.190	13.968	0.000***	
	396	123	3.76 ^b ±1.066			
	642	123	3.08 ^a ±1.178			
	875	123	2.89 ^a ±1.065			
Overall Acceptance	254	123	3.15 ^b ±1.248	20.710	0.000***	
	396	123	3.84 ^c ±1.074			
	642	123	3.11 ^b ±1.248			
	875	123	2.63 ^a ±1.266			
Purchase Intention	254	123	3.03 ^b ±1.152	19.883	0.000***	
	396	123	3.69 ^c ±1.174			
	642	123	3.05 ^b ±1.156			
	875	123	2.54 ^a ±1.160			

Note 1 : * $p < 0.1$, ** $p < 0.01$, *** $p < 0.001$

Note 2 : 396 = pineapple + apple + sugar + lemon; 254 = pineapple + apple + sugar + lemon + dates;
642 = pineapple + apple + sugar + lemon juice + plum; 875 = on the market jam

appearance preferences degree showed that the original flavor pineapple jam can be accepted by most respondents (396, average 4.05). The plum-added pineapple jam was followed by (642, average 2.74) and there was a significant difference ($P < 0.000$ ***) between them.

As for aroma analysis, the analysis result on the difference of aroma showed that the original flavor pineapple jam can be accepted by most respondents (396, average 3.63) and there were a significant difference ($P < 0.000$ ***) with the other three products ($P < 0.000$ ***). The original flavor pineapple jam can also be accepted by most respondents (396) in stiffness, acidity and sweetness.

Concerning the overall acceptance, the differences analysis showed that the original flavor pineapple jam can be accepted by most respondents (396, average 3.84), the on the market pineapple jam (875, average 2.63) was the minimum, and there were significant difference ($P < 0.000$ ***)).

Finally, concerning the purchase intention, the analysis result on the difference of purchase intention showed that on the market pineapple jam (875, average 2.54) and dates-added pineapple jam (254, average 3.03) can't be accepted by most respondents. The plum-added pineapple jam was followed by (642, average 3.05). However, the original flavor pineapple jam can be accepted by most respondents (396, average 3.69) and

there were a significant difference ($P < 0.000$ ***) amid them.

5. Conclusion and Suggestion

The finding results showed that the consumers had the highest preference on the appearance of original flavor pineapple jam. It might be that consumers preferred the original color of jam. Both the colors of plum-added and date-added jams were too dark, but, the contents of “on the market” pineapple jam was too little. The study suggested that the manufacturers should be noted the color and contents of pineapple jam.

The consumers had the highest overall acceptance on the original flavor pineapple jam. It might be that consumers considered that no any inference or other ingredients on pineapple jam would bring less health burden. The study suggested that the manufacturers should be noted with no added artificial additives or starch while making pineapple jam, although the shelf life is shorter, but will give less effect to health.

The study found only Tainan area consumers showed the strongest purchase intention to buy the original flavor of pineapple jam. The study suggested that manufacturers could be pay their attention on its differences with the other jams for their future market strategy such as the idea of safety and no artificial additives etc., or some free samples for tryout at the super market, so that consumers can experience the delicious pineapple jam directly.

References

1. Ministry of Health and Welfare, Taiwan (2015). *Taiwan Area Food Nutrition Database*. Download from <https://consumer.fda.gov.tw/FoodAnalysis/ingredients.htm?nodeID=640>. August 14, 2015.
2. A. Shimosako. *The Magic of Jam*. (Candied Fruits and Wiping, SauceUnited Culture, Taipei 2012).
3. J. L. Yi, *Best quality Jam*. (Apple House Publishing Co., Taipei, Taiwan 2011).
4. W. B. Dodds, K. B. Monroe and D. Grewal, The effects of price, brand, and store information on buyer's product evaluations. *Journal of Marketing Research*, 28(3) (1991) pp. 307-319.
5. Y. Liebermann and A. Flint-Goor, Message strategy by product-classtype: A matching model. *International Journal of Marketing Research*, 13 (1996) pp. 237-249.
6. V. A. Zeithaml, Consumer Perceptions of price, quality, and value: A means-end model and synthesis of evidence. *Journal of Marketing*, 52 (1998) pp. 2-22
7. S. I. Wu and P. K. Da, The Effect of Consumers to Airlines' Brand Awareness, Perceived Quality and Perceived Value on Brand Attitude and Purchase Intentions. *Chinese Management Review*. 13(2) (2010) pp. 1-17.
8. G. Jellinek, *Sensory evaluation of food*. VCH Publishers. (Florida. U. S. A. 1985).
9. Q. S. Lin and R. Y. Ye, *Application and Practice of Sensory Evaluation*. (Rui Yu Publishing Co., Pingtung. Taiwan, 2013).
10. S. Ou, Andi M, *Food Sensory Evaluation and Practice*. (Wagner Publishing. Taipei, Taiwan 2003).

Development of An Innovative Design Process for Green Products

Ming-Chieh, Wang

*Department of Food and Beverage Management, Far East University, No.49, Chung Hua Rd.,
Hsin-Shih, Tainan County 744, Tainan, Taiwan
E-mail:wang10071009@yahoo.com.tw*

Abstract

Under the growing trend of environmental protection, many different eco-design methods have been proposed, at the same time, there are many TRIZ tools used to support these processes. In this study, we proposed an innovative design process for green products. This process includes three frameworks-collaborative design, innovative design environment, and the green product design system. Collaborative design framework aims to assist the designer and their upstream and downstream partners to combine their ideas by CSCW tools. The innovative design environment includes data layer, information layer, and knowledge layer, analyzed through the data exchange, information sharing and decision making during the design process. The green product design system was consists of the problem analysis, problem solving, and solution evaluation used to assist the design process with collaborative coordination and information recording. This construct integrating the design ideas, knowledge exchange, problem solving and feedback for the green product design process.

Keywords: col laborative design, innovative design environment, green product design system

1. Introduction

Under the growing trend of environmental protection, many different eco-design methods have been proposed. In various fields, researchers all do their efforts to create new products to fit the new global standard. Many advanced countries even listed Green Design Rules as the first priority in government policy. In the past, products have been designed without consideration of the impact on environment. Traditional factors considered in the product design process are function, quality, cost, and safety. Now, it is imperative to consider the environmental impact of products throughout their life cycle. At the end of the traditional instruction or regulations only focused on manufacturing process. However, the adverse effects on the environment may occur in the life cycle stages, such as the recycling, distribution, and any kind of material collected. Therefore, companies need to analyze and evaluate the influence from product's entire life cycle, in

order to focus on the core issues, and solve the problem effectively.

In recent years, many eco-design methods have been proposed [1] and many innovative tools and methods were used to eco-design process[2]. [3]. But how to analyze the design problem and how to evaluate the design result are seldom explored in previous researches. For that reason, how to construct an integrated method to solve green design problems would be the key point. In this study, some design tools such as the TRIZ tools [4], computer supported cooperative work tools collaborative design concept and knowledge management environment creation were used to construct innovative green product design system.

2. Literature Review

2.1 TRIZ

TRIZ was a theory developed by Genrich Altshaller in Russia, who had analyzed over 400,000 patents to

© The 2016 International Conference on Artificial Life and Robotics (ICAROB 2016), Jan. 29-31, Okinawa Convention Center, Okinawa, Japan

construct the contradiction matrix and 40 inventive principles [5]. TRIZ was based on the patents and used for system analyzed and problems solved through inventive principles. TRIZ was a complex system including Inventive Principles, Contradiction Matrix, Ideal Final Result (IFR), S-Fields, Function Analysis, Separation Principles, Subversion Analysis, Trimming, etc. Among these tools, the contradiction matrix along with 40 inventive principles is the most famous tool. TRIZ also can be seen as a symbol of a set of tools, a method, a way of thinking and a philosophy [6]. Altshaller analyzed thousands of patents and identified the same fundamental problems and found solutions. TRIZ was a tool with knowledge and experiences of the world's best inventive concept for design engineers to handle these conflict conditions during the innovative design problem solving process [7]. The most important parts of TRIZ was the contradictions, through analyzed large amount of patents' problems and solutions, the ideas were created to solve the problems. In the field of science, TRIZ was an innovative tool providing a systematic process to confirm and solve problem, many scholars have proposed some new contradiction matrices in their researches. A hierarchical view of TRIZ was shown in Fig. 1.

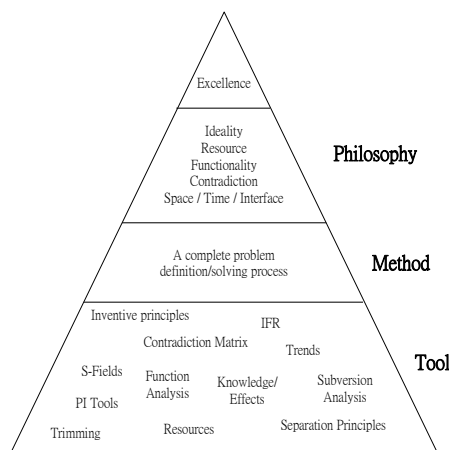
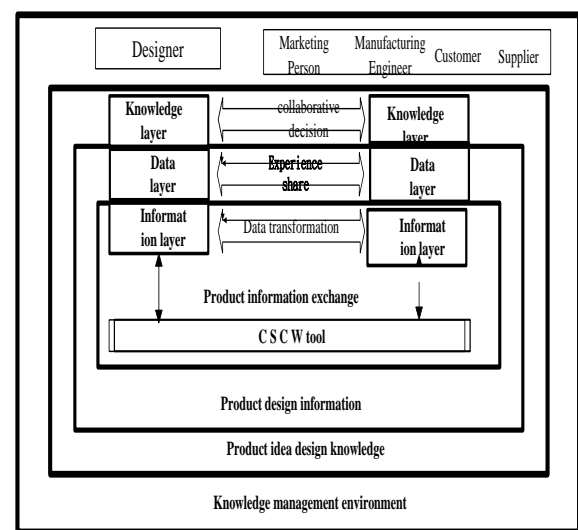


Fig. 1. Hierarchical view of TRIZ

2.2 Green design

Product design concerning environmental impacts has many expressions that include ecological design,

environmental design, environmentally conscious design, environmentally responsible design, sustainable design, green design , etc. The purpose of green design was to decrease the environmental impact during the product life cycle: raw materials, preliminary design, detailed design, manufacturing, assembly, packaging and transportation, use, and disposal [8]. Liu & Chen (2001) combined engineering parameters in TRIZ method with the 7 Eco-Efficiency Elements put forth by the World Business Council for Sustainable Development (WBCSD), allowing designers discovered the engineering parameters needed [9]. Micheline and



Razzoli proposed a model including three types of innovations, product-innovation, function-innovation and method-innovation [10]. Horváth presented that the eco-design research was used to investigate the concepts of corrective products, to reduce the environmental humiliation, and ameliorative products, and to cope with the environmental effects [11]. Dewulf and Duflou discussed how to integrate different levels into the business operations, and proposed a concept of the 3-layered framework for eco-design [12]. Trappey, Chen, Hsiao, and Lin proposed an integrated green product design methods and system. Though there are many researches try to develop a systematic method in order to design products complying with natural and economic needs [13].

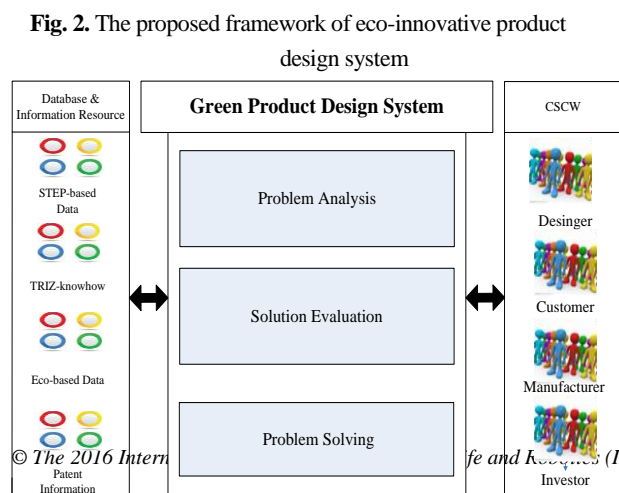
3. Framework and methodology

In this paper, a framework and its related product design process for eco-innovative product design were proposed and shown in Fig. 1. and Fig. 2.

The design environment framework for green innovative product was proposed and shown in Fig. 1. In this framework includes three layers: data layer, information layer, and knowledge layer, which deal with the collaborative (products) detail design, idea design and activities of knowledge management. Products data exchange provided by data layer, it also used for data standard exchange. Information layer provided information sharing with products design. Knowledge layer can provide experience and knowledge to make right decision. Therefore, if green design and innovative design could be integrated in knowledge layer, it could be efficiency to develop products for highly value.

In Fig. 2, a green product design system was proposed and shown. At left side, collaborative design knowledge includes general product design knowledge, TRIZ innovative principles, green design guidelines and regulations. At right side, design team includes designer, customer, Manufacturer and vendor. The CSCW tool can support the collaborative tools and method for members located on different places. Design Team could share or exchange information through the CSCW tools immediately. At the top, green design process and knowledge management includes: product design and develop process, knowledge exchange and collaborative design information system development.

Fig. 1. Design environment framework



4. Conclusions

In recent years, in order to fulfill end user demands and environmental awareness, TRIZ and eco-design concept get more attention of the academy and industry. The most important contribution of this paper is to propose an innovative design process for green products. This process includes three frameworks-collaborative design, innovative design environment, and the green product design system. Collaborative design framework aims to assist the designer and their upstream and downstream partners to merge ideas by CSCW tools. This eco-innovative product design system was consist of data flow from designer, consumer, manufacturer... to transport, collect and feedback during the life-circle, then it also could be used for data exchange, information sharing and collaborative decision-making through CSCW. The collaborative design in this model consists of three layers: data layer, information layer, and knowledge layer, which corresponding to different level from lower-higher in the design process. The lower layer could support higher layer, higher layer provided lower design with directives and regulations to avoid form the wrong decision-making or the unsuitable design, then delayed the products entered to the market and production costs increasing.

This innovative product design system was based on knowledge management construct illustrated a new collaborative model to create green products. Since many research aimed to green design and innovative design, but very less study focused on collaborative design within knowledge management. In the future we will try to build the prototype of knowledge management for the green product design.

5. References

1. A. J. Gottberg Morris, S. Pollard, C. Mark-Herbert, and M. Cook, Producer Responsibility, Waste Minimisation and the WEEE Directive: Case Studies in Eco-Design from The European Lighting Sector, *Science of the Total Environment*, 359 (2006) pp. 38-56.
2. D. Pujari, Eco-Innovation and New Product Development: Understanding the Influences on Market Performance, *Journal of Technovation*, 26 (2006) pp. 76-85.
3. M. T Smith, Eco-Innovation and Market Transformation, *J. Sustainable Product Design*, 1(1999) pp. 147-161.

Life and Resources (ICAROB 2016), Jan. 29-31, Okinawa Convention Center, Okinawa, Japan

4. J. L. Chen and C. C. Liu, Green Innovation Design of Products by TRIZ Inventive Principles and Green Evolution Rules, *Int. Conf. CIRP Design Seminar*, (Hong Kong, China, 2002) , pp.16-18,.
5. G. Ashuller, *Suddenly the Inventor Appeared –TRIZ the theory of Inventive Problem Solving*(Worcester, Technical Innovation Center, MA, 1996).
6. D. Mann, *Hands-On Systematic Innovation*. (Creax Press, IEPER, 2002) .
7. S. d. Savransky, *Engineering of creativity*. (Boca Raton, CRC Press, FL, 2000)
8. E. Jones and D. Harrison, Investigating the use of TRIZ in Eco- innovation, *The TRIZ Journal*, (<http://www.triz-journal.com/>, 2000).
9. C-C Liu, J.L Chen, Development of product green innovation design method. Proceedings of Eco-design, in *Proc. 2nd Int. Conf. Symposium on Environmentally Conscious Design and Inverse Manufacturing*.(Tokyo, Japan, 2001), pp.168-173.
10. Michelini R.C. and R.P. Razzoli, Product-Service Eco-design: Knowledge-based Infrastructures, *Journal of Cleaner Production*, 12 (2004) pp. 415-428.
11. I. Horváth, A Treatise on Order in Engineering Design Research, *Journal of Research in Engineering Design*, 15 (2004) pp. 155-181.
12. W. Dewulf and J.R. Duflou, *Product Engineering*. (Springer science, Business Media, USA,2005).
13. A. J. C. Trappey, M. Y. Chen, D. W. Hsiao, and G. Y. P. Lin, The Green Product Eco-design Approach and System Complying with Energy Using Products (EuP) Directive, *Global Perspective for Competitive Enterprise, Economy and Ecology*(Springer, London, 2008).

Research on Nail Art 3D Design with Different Materials -- A Case Study of the Tang Dynasty Style

Mei-Yin Lee*

*Department of Cosmetic Application and Management
Department of Innovative Design and Entrepreneurship Management
Far East University
No.49, Zhonghua Rd., Xinshi Dist., Tainan City 74448, Taiwan (R.O.C.)
E-mail:mey.lee@msa.hinet.net*

Kung-Yu Liu, Sih-Jie Guan

*Department of Cosmetic Application and Management, Far East University
No. 49, Zhonghua Road, Xinshi District, Tainan City, 74448, Taiwan (R.O.C)*

Jei-Fu Ho

*Department of Food and Beverage Management, Far East University
No. 49, Zhonghua Road, Xinshi District, Tainan City, 74448, Taiwan (R.O.C)*

Abstract

Women in Tang Dynasty, China (618 A.D.-907 A.D.) had concerned with beauty. They had painted color in their nails in addition to emphasis on clothing and makeup. Tang's costumes had blended the diverse characteristics of northern ethnic groups. Meanwhile a variety of engineering methods had been used such as embroidery, painting, printing, wearing gems and gemstones. Floral patterns had been appeared in large numbers in clothing, accessories and poetry. This study has tried to build the Tang Dynasty decorative painting technique or way of painting reappeared on modern nail art and to make the nail painting presents the different faces. After collecting a lot of relevant documents and experimenting many combinations of different materials, such as sculpture, super-light clay, foam paper, popsicle sticks, and Styrofoam, many hand-made stereoscopic flowers, such as peony, rose, plum etc., with painting have been made. Hence different from the past nail art, beautiful pieces of finger nail with the mood of Tang Dynasty poetry are presented. Furthermore, this study has investigated whether the stereoscopic nail art design with different materials could be promoted to the daily nail decoration to enhance the quality of life.

Keywords: Nail art, sculpture, different materials, Tang Dynasty poetry.

1. Introduction

Nail painting has gradually swept in Taiwan in recent years. The continuous painted modeling has been innovated. Especially, the city women are looking forward to having a beautiful painting color on their nail. Meanwhile, they hope to make changes in their nails with the different materials.

In this study, 3D sculpture techniques were used with different materials and the Tang Dynasty poetry mood on nail painting techniques. Finally, painted nail sheets different from past works are presented.

This paper is organized as follows. Section 2 states a brief literature review. In Section 3, the creative elements and analyses, and the creative inspiration are described.

Section 4 shows some nail creative works. Finally, some conclusions and recommendations are made in Section 5.

2. Literature Review

The nail art was used in ancient times. [1] Women in ancient Egypt used red nail polish and got the color from henna, which was a plant used to color hair and nails. [2] Some documents showed that the ancient Egyptian had dyed their nails golden. Also, they had refined the bronze oil from insect secretions as the nail dying. Nails paintings had begun to legalize in 1830s. In 1916, the decorative nail polish was begun to use. About 3,000 B.C., some Chinese documents showed that bees wax, proteins and gelatin had been used as nail polish [3].

Pigment in nail polish had been successfully introduced and have been started to commercialization in 1950s to 1960s. Women around the world regardless of class had begun a crush on nail polish. Subsequently, the chemical engineer had invented the silk nails and crystal nails, such invention of artificial acrylic nails had helped the nails become more slender and beautiful.

Nail cosmetic, art nails, crystal nail and painting nail have been developed rapidly by the end of 20th century. Nowadays, with a pair of gorgeous nail hands are indispensable for many fashion women [4]. The nail manicurist and the related industries have been risen by the popularity of the nail art. The professional nail manicurist must undergo a rigorous training with hand, foot care, nail and other aspects of professional knowledge providing multivariate and higher quality nail services.

In 21st century, nail painting arts have made huge progress due to the different new technologies. They are painting nails, bright crystal nails, French-style crystal nails, 3D crystal nails, phototherapy nails, watery nails, nail inkjet, 3D sculpture nails, and so on. These new nail arts keep the consumers' eyes greatly feasted on [5]. There are many kinds of commonly used nail painting techniques, e.g., painting, sponge rubbings, stack heap color dying, crystal nails and sculpture painting and others [4-7].

In this study, 3D stereoscopic sculpture painted was used for the creation of nail arts. For 3D stereoscopic sculpture, different colors of nail sculpting powder are painted on a nail piece resulting in a three-dimensional effect like oil painting.

Poetry, one of the Chinese great culture, is the most widespread literature in Tang Dynasty (618 A.D.-907 A.D.) particularly. There were many elaborate floral works in Tang poetries. There were many elaborate floral works in Tang poetries such as Yuxi Liu (poet, 772 A.D.-842 A.D.), he referred to the "lotus and peony" in his poem of "Peony Viewing"; The other one, Pian Gao (General, 821 A.D.- 887 A.D.) in his famous poem "A Summer's Day in a Hill Garden", he described as "Green trees, greener shades, and the summer's day is long. Fine buildings studied their own reflections in the pond. The crystal curtains stir when a light breeze descends. A bed of roses permeates the garden with their scents".

In this study, a three-dimensional relief patterns called "Flourishing" and "Fragrant Yard" were created under the base of the above-mentioned two poems combining 3D technology with different materials and nail painted sculpture. There were many elaborate floral works in Tang poetries such as Yuxi Liu, he referred to the "lotus and peony" in his poem of "Peony Viewing"; The other one, Pian Gao in his famous poem "A Summer's Day in a Hill Garden", he described as "Green trees, greener shades, and the summer's day is long. Fine buildings studied their own reflections in the pond. The crystal curtains stir when a light breeze descends. A bed of roses permeates the garden with their scents".

3. Creative Design

3.1. Creative elements and analyses

In general, sculpture powder is used for creating patterns for a 3D sculpture nail. In this study, we use multi-materials, including super light clay, sculpture powder, and foam paper, and auxiliary tools including glass drilling, oil-paper umbrella, paints, nail glue, artificial grass, thin wire, scissors, luminescent nail polish and crystal monomer, for the series of creation works.

3.2. Creative inspiration

The creative inspiration comes from some kinds of flowers with good imagery in China. Peony, known as the "king of flowers" in China, has a lofty status Aromatic. In Chinese people's minds, other flowers are never attainable like the on the prominent of prestige and the status of honor. Lotus, being lightness finds, always gives the feeling of pure and noble. Multiflora rose, often

Pen Drawing	3D with different materials painting
Peony	Peony combined by different materials
	
Lotus and peony	Sculpture lotus, leaves and lotus
	
Tang Woman and Rendezvous	Sculpture Tang Woman
	
Rose	Roses designed by different materials
	
The design draft of "Fragrant Yard"	The design patterns by different materials
	

Fig. 1. The creative design and actual creation

densely forested and full of branches and quite brilliant when flowering, is loved by poet and general people in China.

© The 2016 International Conference on Artificial Life and Robotics (ICAROB 2016), Jan. 29-31, Okinawa Convention Center, Okinawa, Japan

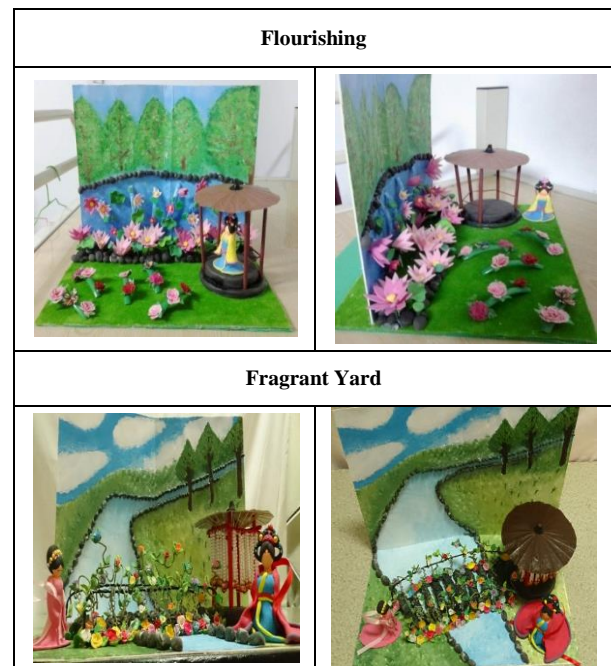


Fig. 2. The Completed "Flourishing" and "Fragrant Yard"

4. Nail Creative Works

All kinds of creative ideas and characters of flowers, garden exhibited. The creative design and actual creation were shown as Figure 1. The design idea of the first work "Flourishing" is a scenery of poem "lotus and peony" by Yuxi Liu. A woman of the Tang Dynasty standing next to a gazebo with grace and elegance along the lotus and peony, fully presents the brilliant flourishing Tang Dynasty. The design idea of the second work "Fragrant Yard" is also a mood emulation of Tang's poem. In a quiet courtyard in the mountains, the only things are trees and the reflections in the pond. When the breeze blows, the curtain sways gently and the aroma of multiflora roses is also spread to everywhere of the yard. The Completed "Flourishing" and "Fragrant Yard" are shown as Figure 2.

5. Conclusion and Recommendation

In this study, 3D sculpture techniques were used with the different materials. Meanwhile, flowers and background mood of Tang poetry were reflected on nail painting techniques. Finally, to express the innovative nail painting works.

This study expects to promote the 3D different materials and innovative nails design to the daily nail decoration. To provide more choices for anyone who love nail creation or nail design, to enhance the taste and quality of life.

References

1. Wikipedia, Nail art, https://en.wikipedia.org/wiki/Nail_art, retrieved Nov. 30, 2015.
2. Alyssa1, The BEST Guidelines to Makeup and Nail polish!, http://www.teenink.com/hot_topics/all/article/334907/The-BEST-Guidelines-to-Makeup-and-Nail-polish/, retrieved Nov. 30, 2015.
3. H.D. Peng (Translator), *History of Beauty*, U. Eco ed. (Linking Publishing, Taipei, Taiwan, 2006) (in Chinese)
4. H.S. Zhan and X.J. Chen, *Nail Art* (New Wun Ching Developmental Publishing, Taipei, Taiwan, 2005) (in Chinese)
5. E.F. Hsiao, Study on the vocational high school students' preference for nail design techniques, *J. Aesthetics and Visual Arts*. **3** (2011) 1-14. (in Chinese)
6. C.C. Cheng, C. C. 2011. Application of Artificial Nail to the Creation of Accessories. *Unpublished thesis of Institute of Applied Design, Shu-Te University* (Shu-Te University, Kaohsiung, Taiwan 2011). (in Chinese)
7. H. Tsai 2011. Study on Painting Techniques and Design of Nail Art. *Unpublished thesis of Institute of Applied Design, Shu-Te University* (Shu-Te University, Kaohsiung, Taiwan 2011). (in Chinese)

Compensating Temperature-Dependent Characteristics of a Subthreshold-MOSFET Analog Silicon Neuron

Ethan Green

Department of Electrical Engineering and Information Systems, The University of Tokyo, 4-6-1 Komaba, Meguro-ku, Tokyo, 153-8505, Japan

Takashi Kohno

Institute of Industrial Science, The University of Tokyo, 4-6-1 Komaba, Meguro-ku, Tokyo, 153-8505, Japan

*E-mail: green@sat.t.u-tokyo.ac.jp, kohno@sat.t.u-tokyo.ac.jp
www.u-tokyo.ac.jp*

Abstract

Analog silicon neurons are neuro-mimetic VLSI (very-large-scale-integrated) circuits that replicate the electrophysiological behavior of animal nerve tissue. This research focuses on the temperature sensitivity of a subthreshold-MOSFET analog silicon neuron. Subthreshold operation of CMOS transistors allows for low power consumption, but is also drastically sensitive to temperature changes. This critical issue must be addressed before these circuits can be implemented into massive networks to develop future neuromorphic technologies.

Keywords: neuromorphic engineering, analog VLSI, silicon neurons

1. Introduction

The field of neuromorphic engineering seeks to design circuits that mimic the electrophysiological behavior and network structure of neurons to create biologically-inspired or neuromimetic technology that can perform calculations in ways fundamentally different from traditional digital computers. Motivations for research in this field include developing brain-like computers and bio-silico hybrid systems for medical devices.

Analog silicon neurons are electronic circuits that exploit the characteristics of transistors to mimic how nerve cells control membrane potential. These circuits operate in continuous time, can replicate a variety of spike shapes and spiking behavior, and require low power^{1,2,3,4}. They are expected to be a promising tool to construct neuromorphic systems. However, many technical challenges must be addressed before these circuits can be implemented in large-scale networks. A possible method to solve a key issue, temperature sensitivity, is to actively tune the circuit parameters depending on temperature. We report our approach in which appropriate parameter sets for several

temperatures are found and parameter sets for intermediary temperatures are obtained by interpolation.

2. Circuit Description

The circuit used in this research (Fig. 1) is an ultra-low power VLSI silicon neuron based on qualitative neuronal modeling¹, which seeks to use judicious approximation and mathematical understanding⁵ to convert the model of membrane potential to equations with fewer variables that are more suitable for circuit implementation. In the model for this circuit, variable v represents membrane potential and variable n represents abstracted ionic activity. The value of each variable is calculated by subtracting the voltage over each capacitor from V_{dd} (1.0V). These two variables control the output currents of transconductance circuit components $f_x(v)$, $g_x(v)$ ($x=v, n$), and $r(n)$ that charge and discharge capacitors attached to the v -block and n -block within the circuit. This circuit was shown to support the dynamical behaviors of Class I and II neurons in the Hodgkin's classification⁶. The system equations of this model are as follows:

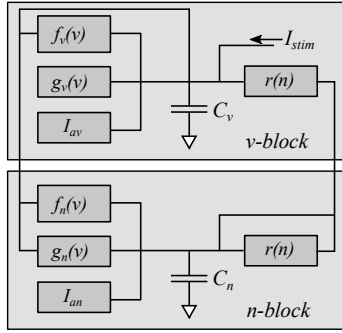


Fig. 1. Circuit block diagram of the silicon neuron circuit.

$$C_v \frac{dv}{dt} = f_v(v) - g_v(v) + I_{av} - r(n) + I_{stim} \quad (1)$$

$$C_n \frac{dv}{dt} = f_n(v) - g_n(v) + I_{an} - r(n) \quad (2)$$

I_{stim} is an external stimulus current, and I_{av} and I_{an} are constant currents. The current-voltage characteristics of the $f_x(v)$, $g_x(v)$ ($x=v,n$), and $r(n)$ components are expressed by the following sigmoidal relationships:

$$f_x(v) = M_x / (1 + \exp(-\frac{\kappa}{U_T}(v - \delta_x))) \quad (3)$$

$$g_x(v) = I_0 \sqrt{\exp(\frac{\kappa}{U_T} \theta_x) / (1 + \exp(-\frac{\kappa}{U_T}(v - \theta_x)))} \quad (4)$$

$$r(n) = I_0 \sqrt{\exp(\frac{\kappa}{U_T} \theta_r) / (1 + \exp(-\frac{\kappa}{U_T}(v - \theta_r)))} \quad (5)$$

I_0 is the PMOS transistor off-current, U_T is the thermal voltage (~ 26 mV at room temperature), and κ is the capacitive coupling ratio. Parameters M_x , θ_x , δ_x ($x=v,n$), and θ_r can be tuned by bias voltages applied to the circuit. All transistors are operated in the subthreshold regime. Figure 2 (a) shows a differential pair attached to a current mirror used for $f_v(v)$ and $f_n(v)$. Figure 2 (b) shows the circuit used for $g_v(v)$, $g_n(v)$, and $r(n)$. This circuit is a cascoded transistor with source degeneration and a detached bulk voltage.

This silicon neuron circuit includes a nullcline-drawing function which assists in the diagramming of a phase plane to evaluate the circuit's dynamical structure. For example, a sigmoidally shaped n -nullcline and cubic-shaped v -nullcline that cross at 3 distinct points yields Class I behavior in the Hodgkin's classification

© The 2016 International Conference on Artificial Life and Robotics (ICAROB 2016), Jan. 29-31, Okinawa Convention Center, Okinawa, Japan

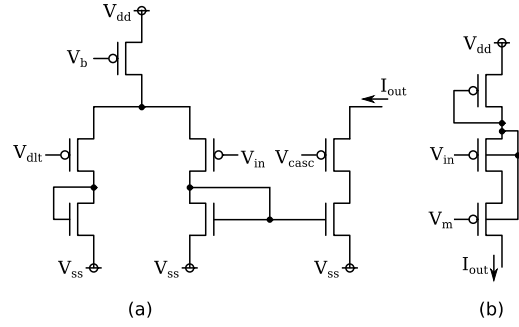
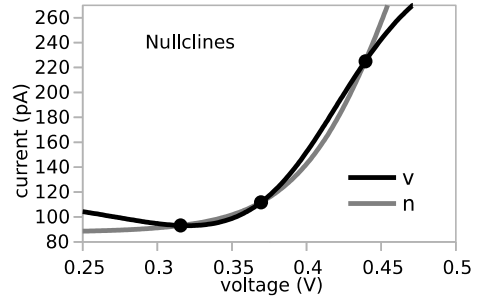

 Fig. 2. Circuit components. (a) $f_v(v)$ and $f_n(v)$, (b) $g_v(v)$, $g_n(v)$, and $r(n)$.


Fig. 3. Nullclines in Class I mode.

(Fig. 3). The points are characterized mathematically through analysis with nonlinear dynamics⁵.

The temperature sensitivity of this circuit originates in the intrinsic temperature sensitivity of MOSFETs in the subthreshold regime. Figure 4 illustrates periodic spiking behavior in the Class I mode in response to a 4 pA sustained stimulus over a narrow range of temperatures from 25 to 26.5°C. The stimulus begins at 0.2 seconds. As can be seen from the figure, the spiking frequency varies by temperature, and ceases at 26.5°C.

3. Parameter Compensation by Interpolation

In this work, we suppose a temperature sensitivity management algorithm in which the parameter voltages applied to the circuit are adjusted depending on the temperature. Such an algorithm will be used by simple on-chip components to control circuit parameters, thus complementing the low-power characteristics of the circuit. We examined an approach to finding appropriate parameter sets for each temperature which maintain the important characteristics of a neuron: spike frequency in

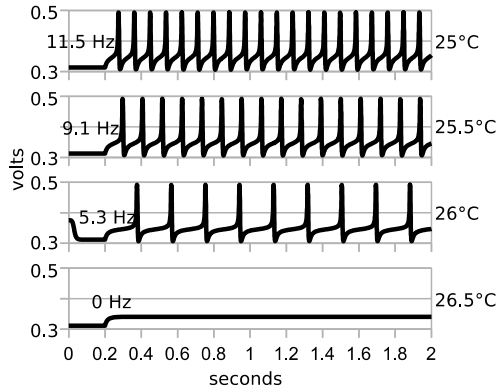


Fig. 4. Periodic spiking at different temperatures.

response to sustained stimuli and the threshold pulse stimulus for spike generation.

First, circuit behavior was analyzed at 27°C and these results were considered the benchmark for operation at other temperatures. The data recorded included frequency response to 5 pA and 10 pA sustained stimuli, and the threshold current I_{th} of a pulse stimulus (500μs pulse width) required to generate an action potential. The v and n -nullclines were also plotted. Next, the circuit was simulated at 17, 22, 32, and 37°C. Selected circuit parameters were tuned to generate behavior that most closely matched the 27°C benchmark. The nullcline-drawing function was used extensively, with the conjecture that similarly shaped nullclines lead to similar circuit behavior. Finally, the tuned parameter sets were input into a script which interpolates functions from these data points and returns circuit parameter sets for any intermediary temperature. This procedure was performed with the Class I setting simulated by the Spectre circuit simulator.

4. Simulation Results

4.1. Simple approach

We selected 5 significant circuit parameters because exploring high-dimensional parameter space is inefficient. The tail current of the $f_n(v)$ component, the bias voltages of the $g_v(v)$ and $r(n)$ components, and the constant current sources I_{av} and I_{an} were tuned with all other circuit parameters held constant. The $g_n(v)$ component was turned off. Table 1 shows the best parameter sets which most closely replicated the

benchmark behavior at each temperature. The bottom 3 rows of the table show the circuit behavior at each temperature. The script was then used to generate parameter sets for all intermediary temperatures in 0.5°C steps from 17 to 37°C. Parameters were rounded to the nearest 0.5 mV. These 42 parameter sets were then simulated with Spectre in their corresponding temperatures. The "simple" column in Table 2 summarizes the results. "Average % change" refers to the average percent difference from the benchmark behavior. Firing frequencies were relatively close to the benchmark behavior, with the exception of the 5 pA stimulus at 29°C which failed to fire. The threshold current showed a downward trend with higher values above 200 pA at lower temperatures and lower values around 140 pA at higher temperatures.

Table 1. Parameter sets with corresponding circuit behavior using the simple approach

Temperature (°C)	17	22	27	32	37
gv_Vm (mV)	388	417	432	443	449.5
fn_Vb (mV)	257	248	237	231	219
Iav_Vin (mV)	434	450	461	468.5	473.5
Ian_Vin (mV)	420	449.5	464.5	475	481.5
rn_Vm (mV)	480.5	462.5	445	430	415
I_{th} (pA)	201	185	178.5	164	147
5 pA response (Hz)	16.3	15.8	15.1	15.7	18.5
10 pA response (Hz)	39	38.8	36.2	38.7	39.4

Table 2. Analysis of interpolation results

	simple	full
5 pA stim average freq. (Hz)	15.8	11.9
5 pA stim average % change	5.2	-9.3
5 pA stim frequency range (Hz)	3.7–27.1	2.4–26.1
10 pA stim average freq. (Hz)	38.7	35.5
10 pA stim average % change	6.8	-0.6
10 pA stim freq. range (Hz)	34.6–43.2	26.8–40.4
Average threshold current I_{th} (pA)	172	185.4
Average I_{th} % change	-3.6	-0.1
I_{th} range (pA)	115.5–216	131–303.5

Table 3. Parameter sets with corresponding circuit behavior using the full-parameter approach

Temperature (°C)	17	22	27	32	37
fv_Vb (mV)	256.5	248.5	238	230	219
fv_Vdlt (mV)	567	571	580	588	596
gv_Vm (mV)	464	451	432	420	398
fn_Vb (mV)	255	246	237	228.5	219
fn_Vdlt (mV)	517	520	520	521	524
Iav_Vin (mV)	437	452	461	469	472
gn_Vm (mV)	220	178.5	156	132.5	113
Ian_Vin (mV)	395	445.5	461	473	479
rn_Vm (mV)	480.5	463.5	445	427	413
I_{th} (pA)	250	191	186	169	145
5 pA response (Hz)	13.3	17.1	13.2	13.2	13.2
10 pA response (Hz)	32.7	36.5	35.7	36.0	38.6

4.2. Full-parameter approach

A second approach augments the strategy used above by incorporating all the influential circuit parameters including the tail current and offset voltage of $f_v(v)$, the offset voltage of $f_n(v)$, and the bias voltage of $g_n(v)$. First, each of the circuit components were simulated individually and circuit parameters were sought that maintained I - V characteristics over a range of temperatures. These parameters were then used as a starting point for tuning the entire circuit at different temperatures. Focus was placed on matching the nullclines as closely as possible. Through analysis of the individual components, it was discovered that the $g_v(v)$, and $g_n(v)$ components experience a temperature induced offset, which can be compensated for by tuning the offset voltages of the $f_v(v)$ and $f_n(v)$ components.

The parameters for the pillar temperatures are listed in Table 3. Those for the intermediary temperatures in the range 17–37°C in 0.5°C steps were determined in the same way as in the previous approach. The "full" column in Table 2 shows the results of the Spectre simulations. I_{th} showed a downward trend and the firing frequencies were relatively close to the benchmark, but the 5 pA sustained stimulus failed to induce periodic spiking at 17.5–21°, 29.5°, 34.5°, 35.5°, and 36.5°C. While the temperature compensation with this approach was less effective, nullclines that more accurately matched the benchmark were obtained, suggesting that future modifications may yield better results.

5. Discussion

The above results can be improved by setting the interpolation script to return parameters rounded to the nearest 0.1 mV, but this accuracy would be difficult to replicate with real-world circuits because of thermal noise and other restrictions including the limited precision of bias voltage generator circuits.

The relative success of the simple approach suggests that limiting the available parameters leads to a smoother progression of values over a range of temperatures, allowing more success in intermediary steps. The full-parameter approach in contrast offered too much fine tuning capability. At a given temperature, some parameters were tuned more aggressively than others, depending on which yielded the most desirable behavior. This is a potential cause of the problems in the intermediary steps. Using a meta-heuristic algorithm to obtain the pillar parameter sets may solve this problem.

Acknowledgements

This study was supported by JST PRESTO and VLSI Design and Education Centre (VDEC) at the University of Tokyo with collaboration from Cadence Corporation.

References

1. T. Kohno and K. Aihara, "A Qualitative-Modeling-Based Low-Power Silicon Nerve Membrane," *Electronics, Circuits, and Systems (ICECS)*, IEEE, pp. 199-202, December, 2014.
2. S. Liu, et al., *Analog VLSI: Circuits and Principles*, MIT Press, 2002.
3. E. Chicca, F. Stefanini, C. Bartolozzi, and G. Indiveri, "Neuromorphic electronic circuits for building autonomous cognitive systems," *Proceedings of the IEEE*, 102, 9, pp. 1367-1388, 2014.
4. S. Brink, S. Nease, and P. Hasler, "Computing with networks of spiking neurons on a biophysically motivated floating-gate based neuromorphic integrated circuit," *Neural Networks*, 45, pp. 39-49, 2013.
5. J. Rinzel and B. Ermentrout, "Analysis of Neural Excitability and Oscillations," *Methods in Neuronal Modeling*, Massachusetts Institute of Technology, pp. 251-291, 1998.
6. A. Hodgkin, "The local electric changes associated with repetitive action in a non-medullated axon," *The Journal of Physiology*, 107, 2, pp. 165-181, March, 1948.

Medical Image Analysis of Brain X-ray CT Images By Deep GMDH-Type Neural Network

Tadashi Kondo[†]

*Graduate School of Health Sciences, Tokushima University
3-18-15 Kuramoto-cho Tokushima 770-8509 Japan
Email: [†]kondomedsci@gmail.com*

Junji Ueno

*Graduate School of Health Sciences, Tokushima University
3-18-15 Kuramoto-cho Tokushima 770-8509 Japan*

Shoichiro Takao

*Graduate School of Health Sciences, Tokushima University
3-18-15 Kuramoto-cho Tokushima 770-8509 Japan*

Abstract

The deep Group Method of Data Handling (GMDH)-type neural network is applied to the medical image analysis of brain X-ray CT image. In this algorithm, the deep neural network architectures which have many hidden layers and fit the complexity of the nonlinear systems, are automatically organized using the heuristic self-organization method so as to minimize the prediction error criterion defined as Akaike's Information Criterion (AIC) or Prediction Sum of Squares (PSS). The learning algorithm is the principal component-regression analysis and the accurate and stable predicted values are obtained. The recognition results show that the deep GMDH-type neural network algorithm is useful for the medical image analysis of brain X-ray CT images.

Keywords: Deep neural networks, GMDH, Medical image recognition, Evolutionary computation

1. Introduction

The deep GMDH-type neural network algorithms were proposed in our early works^{1,2} and can automatically organize the neural network architectures using heuristic self-organization method³ which is a type of the evolutionary computation. In this study, deep GMDH-type neural network algorithm¹ is applied to the medical image analysis of brain X-ray CT images. The learning calculations of the weights is the principal component-regression analysis and the accurate and stable predicted values are obtained. In this GMDH-type neural network, two type neurons such as the sigmoid function neuron and the polynomial neuron are used to organize the deep neural network and very complex

nonlinear systems can be identified using this deep GMDH-type neural network. In our previous work², we have applied the deep multilayered GMDH-type neural network to the medical image recognition of brain and blood vessels. The brain and blood vessel regions are recognized and extracted accurately. In this study, the deep logistic GMDH-type neural network algorithm is applied to the medical image analysis of brain X-ray CT images and the skull and the blood vessels in the brain are recognized and extracted. The recognition results are compared with those obtained using the conventional neural networks trained using the back propagation algorithm and it is shown that this deep neural network is accurate and useful for the medical image analysis of the brain X-ray CT image.

© The 2016 International Conference on Artificial Life and Robotics (ICAROB 2016), Jan. 29-31, Okinawa, Japan

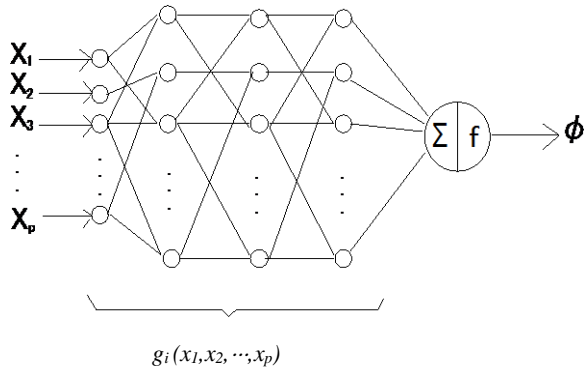
2. Deep GMDH-type neural network¹

The GMDH-type neural network architecture is shown in Fig.1. Here, nonlinear function g_i is described by the following Kolmogorov-Gabor polynomial:

$$g_i(x_1, x_2, \dots, x_p) = a_0 + \sum_i a_i x_i + \sum_{i,j} a_{ij} x_i x_j + \dots \quad (1)$$

This nonlinear function is automatically organized by using the polynomial neurons. The architecture of the GMDH-type neural network is automatically organized using the heuristic self-organization and is produced as follows:

In the GMDH-type neural network, the original data are not separated into training and test sets because AIC⁴ or PSS⁵ can be used as the test errors.



Σ : (Nonlinear function)

$$z_k = \Sigma w_i g_i(x_1, x_2, \dots, x_p)$$

f : (Nonlinear function)

$$\phi = 1/(1 + \exp(-z_k))$$

Fig.1 Architecture of the deep GMDH-type neural network

2.1 The first layer

$$u_j = x_j \quad (j=1, 2, \dots, p) \quad (2)$$

where x_j ($j=1, 2, \dots, p$) are the input variables of the system, and p is the number of input variables.

2.2 The second layer

All combinations of two variables (u_i, u_j) are generated. For each combination, the neuron architecture is described by the following equations:

Σ : (Nonlinear function)

$$z_k = w_1 u_i + w_2 u_j + w_3 u_i u_j + w_4 u_i^2 + w_5 u_j^2 - w_0 \theta_l \quad (3)$$

f : (Linear function)

$$y_k = z_k \quad (4)$$

where $\theta_l = 1$ and w_i ($i=0, 1, 2, \dots, 5$) are weights between

the first and second layer. The weights w_i ($i=0, 1, 2, \dots, 5$) are estimated by using the principal component-regression analysis. This procedure is as follows:

First, the values of z_k are calculated using the following equation:

$$z_k = \log_e(\phi'/(1-\phi')) \quad (5)$$

where ϕ' is the normalized output variable. Then the weights w_i ($i=0, 1, 2, \dots, 5$) are estimated by using the principal component-regression analysis.

[Principal component-regression analysis]

In the GMDH-type neural network, the multicollinearity is generated in the function Σ of the neurons because heuristic self-organization method is used. In this study, the function Σ is calculated using the principal component-regression analysis.

In the case of Eq.(3), orthogonal vector \underline{v} is calculated.

$$\underline{v} = C \cdot \underline{u} \quad (6)$$

Here,

$$\underline{v} = (v_1, v_2, \dots, v_5)$$

$$\underline{u} = (u_i, u_j, u_i u_j, u_i^2, u_j^2)$$

\underline{v} is orthonormal vectors and C is orthonormal matrix. C is calculated using the following eigenvalue equation.

$$R \cdot C = C \cdot \Lambda \quad (7)$$

Here, R is a correlation matrix. Then, variable z_k is calculated using orthogonal regression analysis.

$$z_k = \underline{w}^T \cdot \underline{v}$$

$$= w_1 v_1 + w_2 v_2 + \dots + w_5 v_5 \quad (8)$$

Using the principal component-regression analysis, variable z_k in the function Σ is calculated without multicollinearity. In (8), useful orthogonal variables v_i ($i=1, 2, \dots, 5$) are selected using AIC or PSS.

From these generated neurons, L neurons which minimize AIC⁴ or PSS⁵ values are selected. The output values (y_k) of L selected neurons are set to the input values of the neurons in the third layer.

2.3 The third and succeeding layers

In the third and succeeding layers, the same computation of the second layer is iterated until AIC or PSS values of L neurons are not decreased. When the iterative computation is terminated, the following calculation of the output layer is carried out.

2.4 The output layer

In the output layer, the output values of the neural

network are calculated from z_k as follows:

$$y_k = 1/(1+\exp(-z_k)) \quad (9)$$

So, in the output layer, the neuron architecture becomes as follows:

Σ : (Nonlinear function)

$$z_k = \sum w_i g_i(x_1, x_2, \dots, x_p) \quad (10)$$

f : (Nonlinear function)

$$\phi = 1/(1+\exp(-z_k)) \quad (11)$$

The complete neural network architecture is produced by selected neurons in each layer.

In this algorithm, the principal component-regression analysis is used for the learning calculation of the neural network and the accurate and stable prediction values are obtained. The structural parameters such as the number of layers, the number of neurons in hidden layers and useful input variables are automatically selected to minimize prediction error criterion defined as AIC or PSS. The GMDH-type neural network is organized with two types of neurons which are the sigmoid function neuron and the polynomial neuron and this neural network can identify very complex nonlinear system.

3. Application to the medical image analysis of brain X-ray CT images.

In this study, the regions of the skull and the blood vessels in the brain were recognized and extracted automatically. Multi-detector row CT (MDCT) images of the brain are used in this study.

3.1 Extraction of the skull regions

An brain MDCT image shown in Fig.2 was used for organizing the deep GMDH-type neural network. The statistics of the image densities and x and y coordinates in the neighboring regions, the $N \times N$ pixel regions, were used as the image features. The neural networks were organized when the values of N were from 3 to 10. When N was equal to 3, the neural network architecture had the smallest recognition error. Fig.3 shows the variation of PSS values in each layer. The PSS values were decreased gradually through the layers and small PSS value was obtained in the seventh layer. The deep GMDH-type neural network output the skull image (Fig.4) and the post-processing analysis of the output

skull image was carried out. Fig.5 shows the output image after the post-processing. The output image after the post-processing was overlapped to the original image (Fig.2) as shown in Fig.6. The recognized skull region are very accurate. The skull region was extracted from the original image as shown in Fig.7. These image processing were carried out for all slices by the organized deep GMDH-type neural network and the 3-dimensional skull image was generated as shown in Fig.8. A conventional neural network trained using the back propagation algorithm was applied to the same recognition problem. The output images, when the numbers of neurons in the hidden layer (m) are 5, 7 and 9, are shown in Fig.9. These images contain more regions which are not part of the skull.

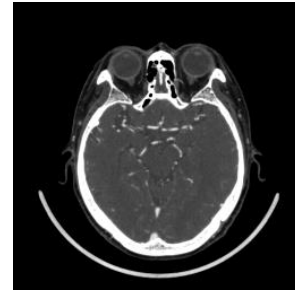


Fig. 2 Original image of the brain

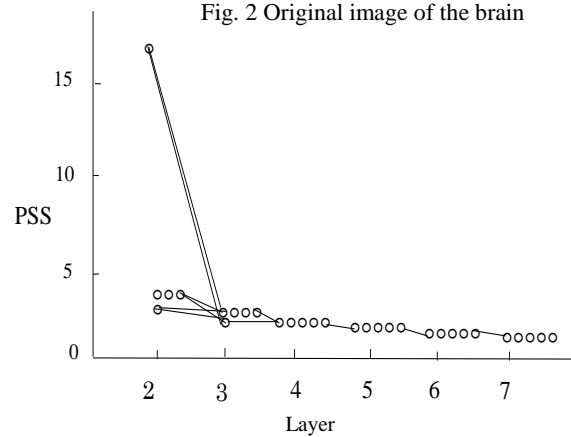


Fig. 3 Variation of PSS values in each layer (1)

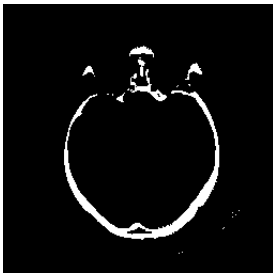


Fig. 4 Output image(1)

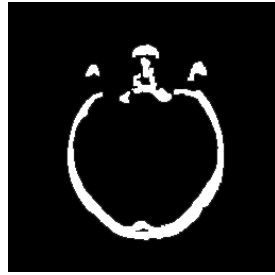


Fig. 5 Output image after the post processing



Fig.6 Overlapped image(1)

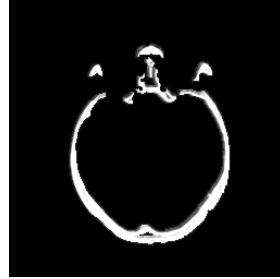


Fig.7 Extracted image (1)

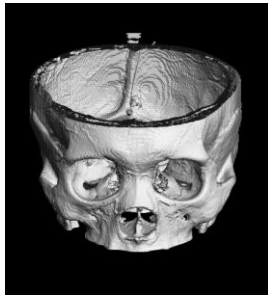
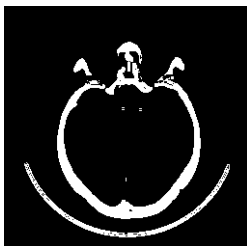
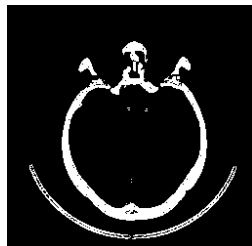


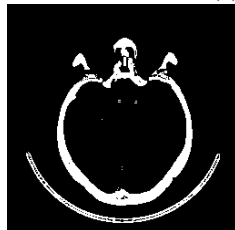
Fig.8 The 3-dimensional skull image



(a) $m=5$



(b) $m=7$



(c) $m=9$

Fig.9 Output images of the conventional neural network (1)

© The 2016 International Conference on Artificial Life and Robotics (ICAROB 2016), Jan. 29-31, Okinawa, Japan

3.2 Extraction of the blood vessel regions

Another deep GMDH-type neural network was organized and applied to the recognition of the blood vessel regions in the brain using the MDCT image shown in Fig.10 which is extracted from the original image in Fig.2. Fig.11 shows the variation of PSS values in each layer. Very small PSS values were obtained in the seventh layer. The deep GMDH-type neural network output the blood vessel image as shown in Fig.12. The output image after the post-processing (Fig.13) was overlapped as shown in Fig.14. The recognized blood vessel regions were very accurate. The blood vessel regions were extracted from the original image as shown in Fig.15. A conventional neural network trained using the back propagation algorithm was applied and the output images, when the numbers of neurons in the hidden layer (m) are 5, 7 and 9, are shown in Fig.17. These images contained many noise compared with the output image of the deep GMDH-type neural network which is shown in Fig.12.

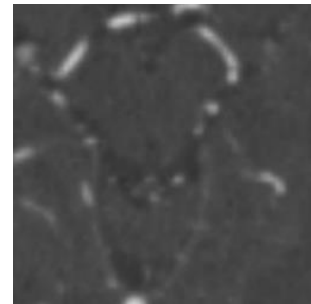


Fig.10 Original image of blood vessels

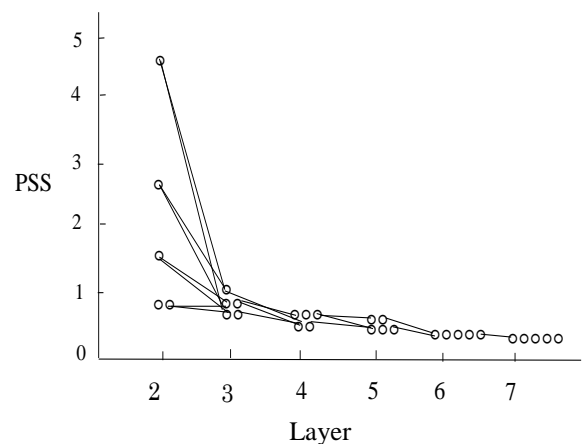


Fig. 11 Variation of PSS values in each layer (2)



Fig.12 Output image (2)

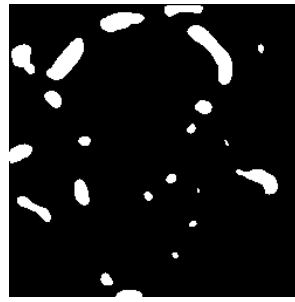


Fig.13 Output image after the post-processing (2)

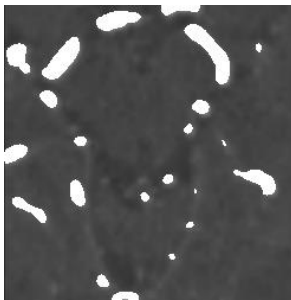


Fig.14 Overlapped (2)

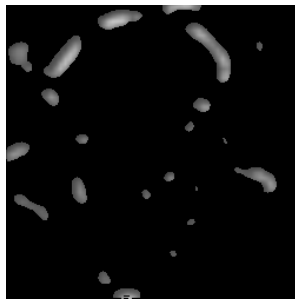


Fig.15 Extracted image (2)

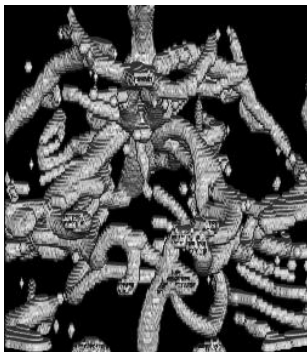


Fig.16 The 3-dimensional blood vessel image



(a) $m=5$



(b) $m=7$



(c) $m=9$

Fig.17 Output images of the conventional neural network (2)

4. Conclusions

In this paper, the deep GMDH-type neural network algorithm using principal component-regression analysis was applied to the medical image analysis of the brain X-ray CT image, and these results were compared with those of the conventional sigmoid function neural network.

Acknowledgment

This work was supported by (JSPS) KAKENHI 26420421.

References

1. T. Kondo, J. Ueno and S. Takao, Logistic GMDH-type neural network using principal component-regression analysis and its application to medical image diagnosis of lung cancer, *Artificial Life and Robotics* **20**(2)(2015) 137-144.
2. T. Kondo, J. Ueno and S. Takao, Deep multi-layered GMDH-type neural network using principal component-regression analysis and its application to medical image recognition of brain and blood vessels, *Proceedings of the twentieth international symposium on artificial life and robotics* (2015) pp.92-95.
3. S. J. Farlow ed., *Self-organizing methods in modeling, GMDH-type algorithm*, New York: Marcel Dekker Inc., 1984.
4. H. Akaike, A new look at the statistical model identification, *IEEE Trans. Automatic Control*, **AC-19**, (6) (1974) 716-723.
5. H. Tamura, T. Kondo, Heuristics free group method of data handling algorithm of generating optimum partial polynomials with application to air pollution prediction, *Int. J. System Sci.* **11** (9) (1980) 1095-1111.

Medical Image Diagnosis of Lung Cancer by Deep Feedback GMDH-Type Neural Network

Tadashi Kondo[†]

*Graduate School of Health Sciences, Tokushima University
3-18-15 Kuramoto-cho Tokushima 770-8509 Japan
Email: [†]kondomedsci@gmail.com*

Junji Ueno

*Graduate School of Health Sciences, Tokushima University
3-18-15 Kuramoto-cho Tokushima 770-8509 Japan*

Shoichiro Takao

*Graduate School of Health Sciences, Tokushima University
3-18-15 Kuramoto-cho Tokushima 770-8509 Japan*

Abstract

The deep feedback Group Method of Data Handling (GMDH)-type neural network is applied to the medical image diagnosis of lung cancer. The deep feedback GMDH-type neural network can identify very complex nonlinear systems using heuristic self-organization method which is a type of evolutionary computation. The deep neural network architectures are organized so as to minimize the prediction error criterion defined as Akaike's Information Criterion (AIC) or Prediction Sum of Squares (PSS). In this algorithm, the principal component-regression analysis is used for the learning calculation of the neural network. It is shown that the deep feedback GMDH-type neural network algorithm is useful for the medical image diagnosis of lung cancer because deep neural network architectures are automatically organized using only input and output data.

Keywords: Deep neural networks, GMDH, Medical image recognition, Evolutionary computation

1. Introduction

The deep GMDH-type neural network algorithms were proposed in our early works¹⁻³ and can automatically organize the neural network architectures using heuristic self-organization method⁴ which is a type of the evolutionary computation. In this study, deep feedback GMDH-type neural network algorithm¹ is applied to the medical image diagnosis of lung cancer. The learning calculations of the weights is the principal component-regression analysis. In previous our work², we applied the logistic GMDH-type neural network to the medical image diagnosis of lung cancer. First, the lung regions were recognized by the logistic GMDH-

type neural network and these lung regions were extracted and then the lung cancer regions were extracted using the image post processing of the extracted lung regions. In another previous our work³, we applied the hybrid feedback GMDH-type neural network to medical image diagnosis of liver cancer. The liver cancer regions were recognized and extracted using the same image processing using the hybrid feedback GMDH-type neural network.

In this paper, we apply the deep feedback GMDH-type neural network and the lung cancer regions are recognized directly using the deep feedback GMDH-type neural network and the lung cancer regions are extracted accurately. The recognition results shows that

© The 2016 International Conference on Artificial Life and Robotics (ICAROB 2016), Jan. 29-31, Okinawa, Japan

the deep feedback GMDH-type neural network can recognize the lung cancer regions directly and extract accurately.

2. Deep feedback GMDH-type neural network¹

The architecture of the deep feedback GMDH-type neural network used in this paper has a feedback loop as shown in Fig.1.

2.1 First loop calculation

First, all data are set to the training data. Then the architecture of the input layer is organized.

2.1.1 Input layer

$$u_j = x_j \quad (j=1,2,\dots,p) \quad (1)$$

where x_j ($j=1,2,\dots,p$) are the input variables of the system, and p is the number of input variables.

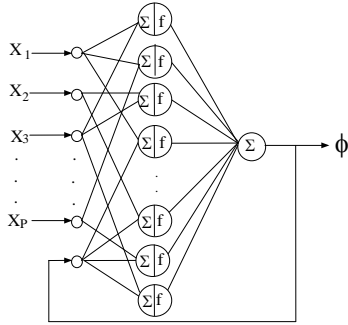


Fig.1 Architecture of the deep feedback GMDH-type neural network

2.1.2 Hidden layer

All combinations of the r input variables are generated. For each combination, three types of neuron architectures which are the sigmoid function neuron, the radial basis function (RBF) neuron and the polynomial neuron, are generated and L neurons which minimize AIC⁵ and PSS⁶ value are selected for each type of neuron architectures.

(1) Sigmoid function neural network

1) The first type neuron

Σ : (Nonlinear function)

$$z_k = w_1 u_i + w_2 u_j + w_3 u_i u_j + w_4 u_i^2 + w_5 u_j^2 - w_0 \theta_l \quad (2)$$

f : (Nonlinear function)

$$y_k = \frac{1}{1 + e^{(-z_k)}} \quad (3)$$

2) The second type neuron

Σ : (Linear function)

$$z_k = w_1 u_i + w_2 u_j + w_3 u_i u_j + \dots + w_r u_r - w_0 \theta_l \quad (r < p) \quad (4)$$

f : (Nonlinear function)

$$y_k = \frac{1}{1 + e^{(-z_k)}} \quad (5)$$

(2) Radial basis function neural network

1) The first type neuron

Σ : (Nonlinear function)

$$z_k = w_1 u_i + w_2 u_j + w_3 u_i u_j + w_4 u_i^2 + w_5 u_j^2 - w_0 \theta_l \quad (6)$$

f : (Nonlinear function)

$$y_k = e^{(-z_k^2)} \quad (7)$$

2) The second type neuron

Σ : (Linear function)

$$z_k = w_1 u_i + w_2 u_j + w_3 u_i u_j + \dots + w_r u_r - w_0 \theta_l \quad (r < p) \quad (8)$$

f : (Nonlinear function)

$$y_k = e^{(-z_k^2)} \quad (9)$$

(3) Polynomial neural network

1) The first type neuron

Σ : (Nonlinear function)

$$z_k = w_1 u_i + w_2 u_j + w_3 u_i u_j + w_4 u_i^2 + w_5 u_j^2 - w_0 \theta_l \quad (10)$$

f : (Linear function)

$$y_k = z_k \quad (11)$$

2) The second type neuron

Σ : (Linear function)

$$z_k = w_1 u_i + w_2 u_j + w_3 u_i u_j + \dots + w_r u_r - w_0 \theta_l \quad (r < p) \quad (12)$$

f : (Linear function)

$$y_k = z_k \quad (13)$$

Here, $\theta_l = 1$ and w_i ($i=0,1,2,\dots,5$) and w_i ($i=0,1,2,\dots,r$) are weights between the input and hidden layer. Weights w_i ($i=0,1,2,\dots$) in each neural network architecture are estimated by the principal component-regression analysis.

[Estimation procedure of weight w_i]

First, values of z_k^{**} are calculated for each neural network architecture as follows.

a) Sigmoid function neural network

$$z_k^{**} = \log_e \left(\frac{\phi'}{1 - \phi'} \right) \quad (14)$$

b) RBF neural network

$$z_k^{**} = \sqrt{-\log_e \phi'} \quad (15)$$

c) Polynomial neural network

$$z_k^{**} = \phi \quad (16)$$

where ϕ is an output variable and ϕ' is the normalized output variable whose values are between 0 and 1.

[Principal component-regression analysis]

Multi-collinearity is generated in the function Σ of the neurons. In this study, the function Σ is calculated using the principal component-regression analysis.

In the case of Eq.(2), orthogonal vector \underline{v} is calculated .

$$\underline{v} = C \cdot \underline{u} \quad (17)$$

Here, $\underline{v}=(v_1, v_2, \dots, v_5)$, $\underline{u}=(u_i u_j, u_i u_j^2, u_j^2)$

\underline{v} is orthonormal vectors and C is orthonormal matrix. C is calculated using the following eigenvalue equation.

$$R \cdot C = C \cdot \Lambda \quad (18)$$

Here, R is a correlation matrix. Then, variable z_k is calculated using orthogonal regression analysis.

$$z_k = \underline{w}^T \cdot \underline{v} \\ = w_1 v_1 + w_2 v_2 + \dots + w_5 v_5 \quad (19)$$

Using the principal component-regression analysis, variable z_k in the function Σ is calculated without multi-collinearity. In (19), useful orthogonal variables $v_i(i=1,2,\dots,5)$ are selected using AIC⁵ or PSS⁶ criterion.

L neurons having the smallest AIC or PSS values are selected for three types of neuron architectures. The output variables y_k of L selected neurons for three types of neuron architectures are set to the input variables of the neurons in the output layer.

2.1.3 Output layer

For three types of neural network, the outputs y_k of the neurons in the hidden layer are combined by the following linear function.

$$\phi^* = \alpha_0 + \sum_{k=1}^L \alpha_k y_k \quad (20)$$

Here, L is the number of combinations of the input variables and y_k is the intermediate variables. Eq. (20) is calculated for three types of neural network architectures. The neural network architecture which has smallest AIC or PSS value is selected. Then, the estimated output values ϕ^* which is selected in the output layer is used as the feedback value.

2.2 Second and subsequent loop calculations

First, the estimated output value ϕ^* is combined with the input variables x and all combinations between the estimated output value ϕ^* and the input variables x are generated. The same calculation as the first feedback loop is iterated. When AIC or PSS value of the linear function in (20) is not decreased, the loop calculation is terminated and the complete neural network architecture

is organized by the L selected neurons in each feedback loop.

3. Application to the medical image diagnosis of lung cancer

In this study, the lung cancer regions were automatically recognized using the deep feedback GMDH-type neural network and these regions were extracted. Multi-detector row CT (MDCT) images of the lung were used in this study.

3.1 Results of the medical image recognition by the deep feedback GMDH-type neural network

The MDCT image shown in Fig.3 which was extracted from the MDCT image in Fig.2, was used for organizing the neural network. x and y coordinates and the statistics of the image densities in the neighboring regions of the $N \times N$ pixels at the positions of the learning points are used as the input variables of the neural network. Only five input variables which are the mean, the standard deviation, the variance and x and y coordinates were automatically selected as useful input variables. The output value of the neural network is zero or one. When $N \times N$ pixel region is contained in the lung cancer and blood vessel regions, the neural network set the pixel value at the center of the $N \times N$ pixel region to one and this pixel is shown as the white point. The neural networks were organized when the values of N were from 3 to 10. It was determined that when N was equal to 3, the neural network architecture had the smallest recognition error. Five useful neurons were selected in each hidden layer. Fig.4 shows the PSS values of the three types of neurons in the second layer. The RBF neural network architecture was selected by the deep GMDH-type neural network algorithm. Fig.5 shows the variation of PSS values in each layer. PSS values decreased gradually and very small PSS values were obtained at the seventh layer. The lung cancer and blood vessel regions were recognized by using the organized neural network and was extracted automatically. Fig.6 shows the output image of the deep feedback GMDH-type neural network. This output image was processed by the post-processing analysis. In the post-processing, the small isolated regions were

eliminated and the outlines of the lung cancer regions were expanded outside by $N/2$ pixels. Fig.7 shows the output image after this processing. In order to check the matching between the original image and the output image of the neural network, the output image was overlapped on the original image in Fig.3. The overlapped image is shown in Fig.8. From Fig.8, we can see that the output image was very accurate. Fig.9 shows the extracted lung cancer image. These image processing were carried out for all slices by the organized deep feedback GMDH-type neural network and the 3-dimensional lung cancer image was generated as shown in Fig.10.

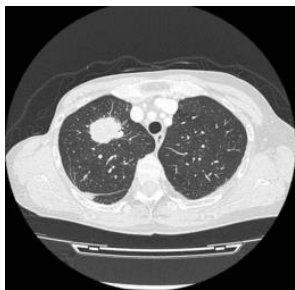


Fig.2 Original image

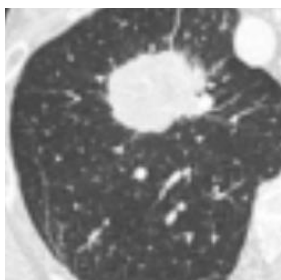


Fig.3 Original image extracted from Fig.2

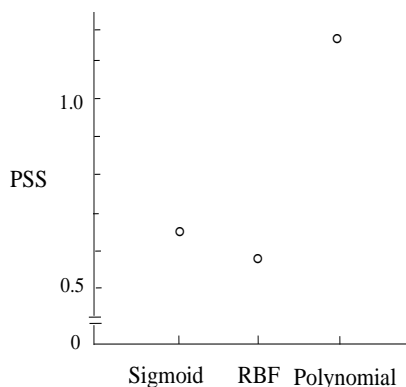


Fig. 4 PSS values of three types of neurons

© The 2016 International Conference on Artificial Life and Robotics (ICAROB 2016), Jan. 29-31, Okinawa, Japan

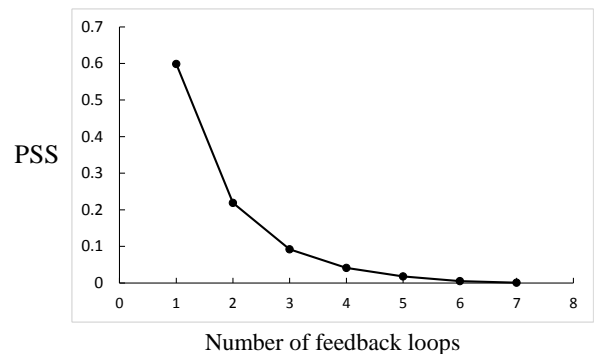


Fig. 5 Variation of PSS value in each layer



Fig. 6 Output image



Fig.7 Output image after the post processing

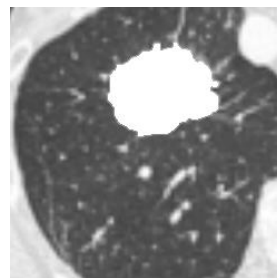


Fig. 8 Overlapped image



Fig. 9 Extracted image



Fig.10 The 3-dimensional image of lung cancer

3.2 Extraction by the conventional neural network using sigmoid function.

A conventional neural network trained using the back propagation algorithm was applied to the same recognition problem. The learning calculations of the weights were iterated changing structural parameters such as the number of neurons in the hidden layer and the initial values of the weights. The output images, when the numbers of neurons in the hidden layer (m) are 5, 7 and 9, are shown in Fig.11. These images contain more regions which are not part of the lung cancer and blood vessel regions, and the outlines of the lung cancer are not extracted with required clarity compared with the output images obtained using the deep feedback GMDH-type neural network algorithm, which are shown in Fig.6.

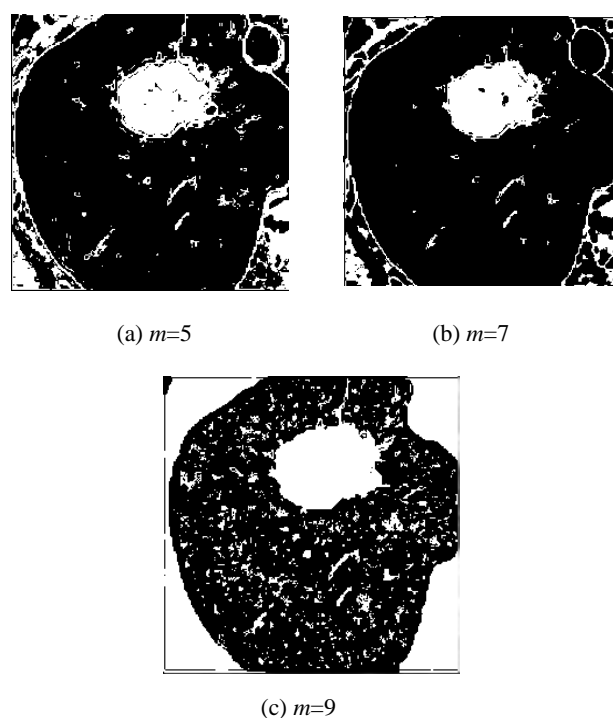


Fig. 11 Output images of the conventional sigmoid function neural network

4. Conclusions

In this paper, the deep feedback GMDH-type neural network algorithm was applied to the medical image

recognition of lung cancer regions and the results were compared with those of the conventional sigmoid function neural network trained using the back propagation algorithm. It was shown that the deep feedback GMDH-type neural network algorithm was a useful method for the medical image diagnosis of the lung cancer because the deep feedback neural network architecture is automatically organized so as to minimize the prediction error criterion defined as AIC or PSS.

Acknowledgment

This work was supported by (JSPS) KAKENHI 26420421.

References

1. T. Kondo, J. Ueno and S. Takao, Deep feedback GMDH-type neural network using principal component-regression analysis and its application to medical image recognition of abdominal multi-organs, *Journal of Robotics, Networking and Artificial Life* **2**(2)(2015) 94-99.
2. T. Kondo, J. Ueno and S. Takao, Logistic GMDH-type neural network using principal component-regression analysis and its application to medical image diagnosis of lung cancer, *Artificial Life and Robotics* **20**(2)(2015) 137-144.
3. T. Kondo, J. Ueno and S. Takao, Medical image diagnosis of liver cancer by hybrid feedback GMDH-type neural network using principal component-regression analysis, *Artificial Life and Robotics* **20**(2)(2015) 145-151.
4. S. J. Farlow ed., *Self-organizing methods in modeling, GMDH-type algorithm*, New York: Marcel Dekker Inc., 1984.
5. H. Akaike, A new look at the statistical model identification, *IEEE Trans. Automatic Control* **AC-19** (6) (1974) 716-723.
6. H. Tamura, T. Kondo, Heuristics free group method of data handling algorithm of generating optimum partial polynomials with application to air pollution prediction, *Int. J. System Sci.* **11** (9) (1980) 1095-1111.

© The 2016 International Conference on Artificial Life and Robotics (ICAROB 2016), Jan. 29-31, Okinawa, Japan

Feature Linking by Synchronized Response in Chaotic Cellular Neural Network for Visual Stimulus of Moving Objects

Akihiro Yamaguchi *, Satoshi Arakane

*Department of Information and Systems Engineering, Fukuoka Institute of Technology,
3-30-1 Wajiro-higashi, Higashi-ku, Fukuoka, 811-0116, JAPAN*

Masao Kubo

*Department of Computer Science, National Defense Academy of Japan,
1-10-20 Hashirimizu, Yokosuka, Kanagawa, 239-8686, JAPAN*

*E-mail: *aki@fit.ac.jp*

Abstract

A feature linking mechanism by the synchronized response of neural assemblies was studied for the chaotic cellular neural network (Chaotic-CNN). The Chaotic-CNN consists of chaotic spike response neurons that show the chaotic inter-spike-interval dynamics. In our scheme of feature linking, the features of the target objects are linked by the synchronized spike responses that are characterized by the temporal chaotic pattern of spike sequence. In this paper, we analyzed the synchronized spike responses that invoked by the visual stimulus of moving bars. As a result, neural assemblies have higher correlation for the visual stimulus of moving two bars in the same direction than the opposite direction. Then we discussed a possibility of feature linking by the chaotic synchronized response in the view point of neural coding.

Keywords: chaotic synchronization, neural coding, spike response model, feature linking

1. Introduction

For the brain system, feature linking is one of the principal functions to realize the recognition of visual objects. From the physiological experiments, the correlated firing among neurons is regarded as a candidate of the mechanism of such feature linking^{1,2}. In the neural coding scheme using the synchronization of neurons, the feature linking information is represented by the synchronized firing among the corresponding neurons such that the features detected by neurons are linked if their firing pattern are synchronized.

On the other hand, the chaotic system is well known for its complex behavior. Comparing with the periodic spike pattern, the chaotic spike pattern is expected to have an advantage for the variety of represented

information. Therefore, there is a possibility to increase the performance of information representation by using a chaotic synchronization of spike responses^{3,4}.

In the view point of neural coding, authors have studied the formation of the chaotic cell assemblies in the chaotic cellular neural network (Chaotic-CNN) that is a two dimensional coupled network of chaotic neurons⁵⁻⁷. The chaotic neuron is modeled by the chaotic spike response model (Chaotic-SRM) that is an extended SRM to show chaotic inter-spike interval by adding the background sinusoidal oscillation⁵⁻⁷.

In our previous study, chaotic cell assemblies were formed in the Chaotic-CNN for the visual stimulus when the stationary image was inputted^{6,7}. In this research, we analyze the formation of chaotic cell assemblies for the

visual stimulus of moving objects and the feature linking property of them.

2. Chaotic Cellular Neural Network

The Chaotic-CNN is defined as a two dimensional coupled system of the Chaotic-SRM⁵⁻⁷. In the following, the definition of the neuron model and the network is described, respectively.

2.1 Neuron Model

As a neuron model, we use the Chaotic-SRM that is an extended spike response model (SRM). The spike response model (SRM) was introduced by Gerstner and Kistler⁸. The definition of Chaotic-SRM is as follows.

The membrane potential $u(t)$ of the neuron at the time t is defined as

$$u(t) = u_{rest} + \eta(t - t^*) + \beta, \quad (1)$$

where u_{rest} , t^* , and β denote the resting potential, the last firing time, and the external input, respectively. The kernel function η is defined as

$$\eta(t - t^*) = -\eta_{init} \exp\left(\frac{t - t^*}{\tau_{\eta_0}}\right) \Theta(t - t^*), \quad (2)$$

where τ_{η_0} is the time constant of the spike response, and Θ is a step function such that $\Theta(s)$ is 1 for $s \geq 0$ and 0 for the other values.

In this model, when the membrane potential exceeds the threshold value θ , the neuron is firing and the membrane potential is reset by the update of the last firing time t^* . The term $-\eta_{init}$ is an initial value of the kernel function η after firing.

We extended the original SRM to show the chaotic response by adding a background sinusoidal oscillation in the same way as the bifurcating neuron⁹ and the chaotic pulse coupled neural network⁴. In our model, the background oscillation is added to the term η_{init} such that

$$\eta_{init} = \eta_0 - A_{\eta_0} \sin(2\pi\omega_{\eta_0} t^* + \phi), \quad (3)$$

where A_{η_0} , ω_{η_0} , and ϕ denote the amplitude, the frequency, and the phase shift of the background oscillation, and η_0 is constant. The Chaotic-SRM shows various chaotic behaviors depending on the parameters A_{η_0} and β .

2.2 Definition of Network

In the Chaotic-CNN, each neuron is located in the $N \times M$ lattice and connected to neighbors. Let $n_{x,y}$ be a neuron located at the position (x, y) where $x \in \{0, 1, \dots, N-1\}$

and $y \in \{0, 1, \dots, M-1\}$. The membrane potential $u_{x,y}$ of the neuron $n_{x,y}$ is defined as

$$u_{x,y}(t) = u_{rest} + \eta(t - t_{x,y}^*) + \beta_{x,y} + \xi \times \sum_{n_{x',y'} \in B(x,y;r)} o_{x',y'}(t) \quad (4)$$

where u_{rest} , $t_{x,y}^*$, $\beta_{x,y}$, ξ and $B(x, y)$ denote the resting potential, the last firing time, the external input, the coupling weight, and the set of connected neurons, respectively. A set of connected neurons is defined as

$$B(x, y; r) = \{n_{x',y'} \mid (x', y') \neq (x, y), \max(|x - x'|, |y - y'|) \leq r, 0 \leq x' \leq N-1, 0 \leq y' \leq M-1\}. \quad (5)$$

The function $o_{x',y'}$ is the output from the connected neuron $n_{x',y'}$ and it is also defined as

$$o_{x',y'}(t) = \sum_{t_{x',y'}^{(k)} < t_{x',y'}^* + \Delta\epsilon < t} \epsilon(t - t_{x',y'}^{(k)} - \Delta\epsilon) \quad (6)$$

where $t_{x',y'}^{(k)}$ denotes the k -th firing time of the neuron $n_{x',y'}$ and $\Delta\epsilon$ is the time delay of synaptic connection. The kernel function ϵ describes the response of the synaptic connection. The definition of the kernel function ϵ is

$$\epsilon(s) = \frac{s}{\tau_\epsilon} \exp\left(-\frac{s}{\tau_\epsilon}\right) \Theta(s), \quad (7)$$

where τ_ϵ is the time constant of the synaptic connection.

2.3 Gradient Field of Phase Shift

In this research, to emphasize the synchronized response in one direction, a gradient field of the phase shift is introduced in Eq.(3). The gradient field of the phase shift is defined as,

$$\phi_{x,y}(\alpha) = D(\cos(\alpha)x + \sin(\alpha)y) \bmod 2\pi, \quad (8)$$

where D is the constant of gradient and α is the direction of gradient. Therefore $\phi_{x,y}$ is the same value in the orthogonal direction of α in the Chaotic-CNN.

3. Numerical Analysis of Coupled two Neurons

As a preliminary numerical experiment, we examined the synchronizing property of the coupled two neurons that corresponds to the Chaotic-CNN 2×1 . In this case, the neuron $n_{0,0}$ and $n_{1,0}$ are coupled to each other. In the numerical simulation, the parameter values of the Chaotic-SRM are set as follows: $u_{rest} = -70$ mv, $\theta =$

-35 mv , $\eta_0 = 55$, $\tau_\eta = 10$, $\omega_{\eta_0} = \frac{0.75}{2\pi}$, $A_{\eta_0} = 10.9$, $\tau_\varepsilon = 1.5$ and $\Delta\varepsilon = 0.1$. The external input is chosen as $\beta_{0,0} = \beta_{1,0} = 52.5$ such that the single neuron exhibits chaotic spike response.

As an index of the synchronization, the cross-correlation between two spike sequences is analyzed. Let $S_{x,y}$ be a set of the firing times of the neuron $n_{x,y}$. The cross-correlation between $S_{x,y}$ and $S_{x',y'}$ is defined as

$$CC(S_{x,y}, S_{x',y'}; \Delta t) = \#(\{t_{x,y}^{(k)} \in S_{x,y} | \exists t_{x',y'}^{(l)} \in S_{x',y'}, |t_{x,y}^{(k)} - t_{x',y'}^{(l)} - \Delta t| \leq \Delta s\}) / \#(S_{x,y}) \quad (9)$$

where $\#(X)$ denotes the number of elements of X , and Δs is the time resolution of the coincident firing. In this research, Δs is set to 0.5 ms. The auto-correlation is also defined as $AC(S_{x,y}; \Delta t) = CC(S_{x,y}, S_{x,y}; \Delta t)$. In the

case of $\Delta t = 0$, the cross-correlation $CC(S_{x,y}, S_{x',y'}; 0)$ corresponds to the ratio of synchronized spikes.

We simulated these coupled two neurons and calculated the cross-correlation $CC(S_{0,0}, S_{1,0}; 0)$ for generated spike sequences. Results are shown in Fig. 1 and Fig. 2. Fig. 1 shows the dependency of the cross-correlation to the coupling weight ξ . In the case that the phase shift is equivalent for two neurons ($\phi_{0,0} = \phi_{1,0}$), the complete synchronization such that $CC(S_{0,0}, S_{1,0}; 0) \simeq 1$ is achieved as increasing the coupling weight ξ . Fig. 2 shows the dependency of the cross-correlation to the difference of phase shifts ($\phi_{1,0} - \phi_{0,0}$). The cross-correlation exhibits a selective preference for the case that the difference of phase shifts is 0. In this research, we apply this selective preference of coupled system to the feature linking.

4. Numerical Experiment

4.1 Experimental Model

In order to examine the feature linking property by the synchronized response, we construct the simulation model of the Chaotic-CNN 40×40 and the motion picture of moving two bars is inputted as visual stimulus like the physiological experiments of cat visual cortex¹. In this research, we also make two motion patterns. One is the moving two bars in the same direction (Fig. 3(a)) and the other is in the opposite direction (Fig. 3(b)).

The image of bar is represented by a rectangle of 5×12 pixels. The velocity of bar is 0.07 pixels /msec. The external input $\beta_{x,y}$ is 52.5 for the neurons inputted the image of the rectangle and 0 for the others. The parameter of the connection r is 2. The gradient field of the phase shift is set as $D = 0.353$ and $\alpha = 0$.

4.2 Cross-correlation analysis

Numerical simulations are performed for the spike responses during 1,000 ms. Then, the cross-correlation is calculated for the neuron $n_{20,10}$ and the others. The neuron $n_{20,10}$ locates at the center of the way of the bar 1 in Fig. 3.

The cross-correlation for the moving two bar in the same direction (Fig. 3(a)) is shown in Fig. 4(a). Fig. 4(a) shows the formation of neural assemblies in which neurons are synchronized. Furthermore, the neural assembly corresponds to the bar 1 has high cross-correlation with the assembly of the bar 2. On the other hand, the cross-correlation for the moving two bar in the opposite direction (Fig. 3(b)) is shown in Fig. 4(b). Although Fig. 4(b) also shows the formation of neural

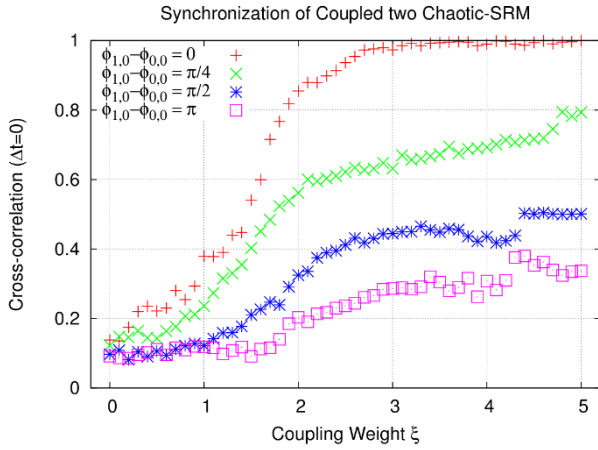


Fig. 1. The cross-correlation vs. the coupling weight ξ for the coupled two neurons.

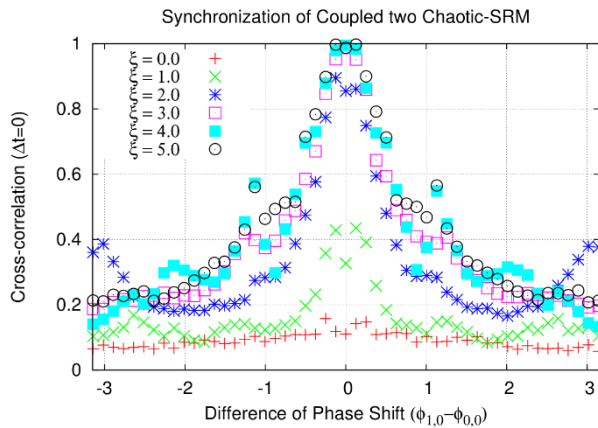


Fig. 2. The cross-correlation vs. the difference of the phase shift ($\phi_{1,0} - \phi_{0,0}$) for the coupled two neurons.

assembly, the cross-correlation between the assembly of the bar 1 and the bar 3 is low.

5. Discussions

For the visual stimulus of moving objects, the formation of neural assemblies were observed in the Chaotic-CNN.

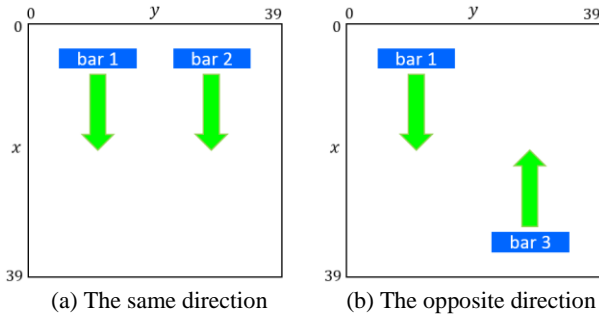


Fig. 3. Visual stimuli for the numerical experiment. The motion of moving two bars in the same direction (a) and the opposite direction (b).

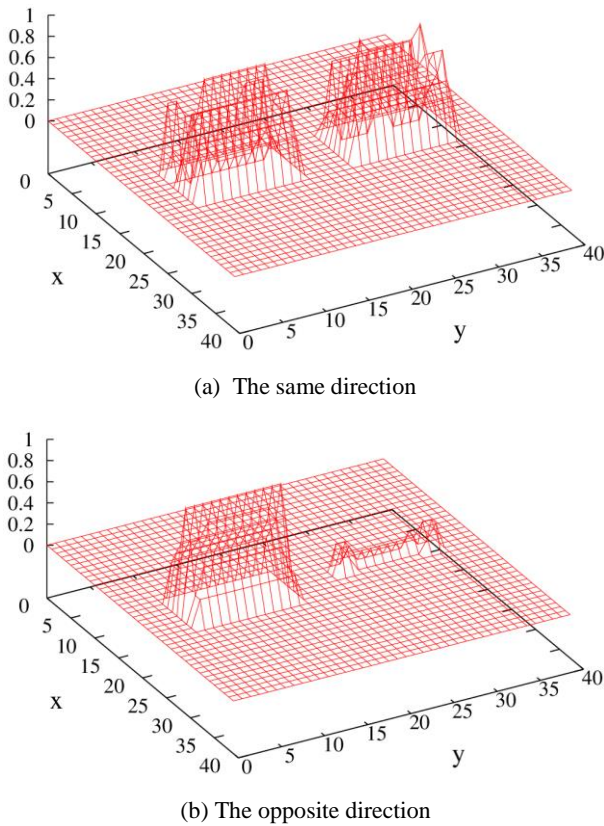


Fig. 4. The cross-correlation between the neuron $n_{20,10}$ and the others when the visual stimuli as shown in Fig. 3 were inputted.

© The 2016 International Conference on Artificial Life and Robotics (ICAROB 2016), Jan. 29-31, Okinawa Convention Center, Okinawa, Japan

By the cross-correlation analysis, the invoked neural assemblies have high correlation for the moving objects in the same direction and low correlation for the opposite direction. These results indicate a possibility of the feature linking by the synchronized spike responses in the Chaotic-CNN in terms of the cross-correlation. In our model, this linking property might be achieved by the preference for the difference of phase shifts mentioned in Sec. 3. Analysis of the dynamics of invoked spike sequences along the moving assembly and the application to the real image are our future works.

Acknowledgements

This work was supported by JSPS KAKENHI Grant Numbers 24650120.

References

1. Gray, C.M., Koenig, P., Engel, A. K., and Singer, W., Oscillatory responses in cat visual cortex exhibit inter-columnar synchronization which reflects global stimulus properties, *Nature*, 338, pp.334-337, 1989.
2. Eckhorn, R., Reitboeck, H.J., Arndt, M., Dicke, P., Feature linking via stimulus-evoked oscillations: experimental results from cat visual cortex and functional implications from a network model, *International Joint Conference on Neural Networks*, pp 723-730, 1989.
3. Yamaguchi, A., Okumura, N., Chaki, H., and Wada, M., Chaotic synchronized cluster in the network of spike response neurons, *IEICE Tech. Rep.*, Vol.99, No.685, NC99-119, pp. 15-20, Mar. 2000 (in Japanese).
4. Yamaguti, Y., Ishimura, K., and Wada M., Chaotic synchronized assembly in Pulse Coupled Neural Networks, *IEICE Tech. Rep.*, Vol.101, No.615, NC2001-98, pp.127-134, Jan. 2002 (in Japanese).
5. Yamaguchi, A., On a chaotic synchronization of one-way coupled two spike response neurons, *Fukuoka Institute of Technology Reports of Computer Science Laboratory*, Vol.24, pp.1-6, 2013 (in Japanese).
6. Yamaguchi, A., On an information coding using localized synchronization in the two dimensional coupled system of chaotic spike response neurons, *Fukuoka Institute of Technology Reports of Computer Science Laboratory*, Vol.25, pp.1-6, 2014 (in Japanese).
7. Fujiwara, M., Yamaguchi, A., and Kubo M., Synchronized Response to Grayscale Image Inputs in Chaotic Cellular Neural Network, *Journal of Robotics, Networking and Artificial Life*, Vol.2, No.1, pp.26-29, 2016.
8. Gerstner, W., and Kistler, W., *Spiking Neuron Models: Single Neurons Populations Plasticity*, Cambridge University Press, 2002.
9. Lee G., and Farhat, N.H., The Bifurcating Neuron Network 1, *Neural Networks*, Vol. 14, pp.115-131, 2001.

An FPGA-based cortical and thalamic silicon neuronal network

Takuya Nanami

*School of Engineering, The University of Tokyo
Tokyo, Japan*

Takashi Kohno

*Institute of Industrial Science, The University of Tokyo
Tokyo, Japan*

Abstract

A DSSN model is a neuron model which is designed to be implemented efficiently by digital arithmetic circuit. In our previous study, we expanded this model to support the neuronal activities of several cortical and thalamic neurons; Regular spiking, fast spiking, intrinsically bursting and low-threshold spike. In this paper, we report our implementation of this expanded DSSN model and a kinetic-model-based silicon synapse on an FPGA device. Here, synaptic efficacy was stored in block RAMs, and external connection was realized based on a bus that conform to the address event representation. We simulated our circuit by the Xilinx Vivado design suit.

Keywords: silicon neuronal network, neuron model, FPGA, cortex, thalamus.

1. Introduction

Silicon neuronal networks can simulate neuronal activity with low power consumption and in high speed. They are thought to be a promising way to realize an extremely large-scale network comparable to the human brain in future. The Field-Programmable Gate Array (FPGA) devices are commonly used for silicon neuronal networks because they can implement user-designed circuits with low cost. Many silicon neuronal networks on an FPGA can run at a higher speed than the biological real-time [1][2]. For example, a fully-connected 1024-neuron network that is 100 times the real-time speed has been implemented on a single Virtex-5 FPGA [3]. Thomas et al. adopted the Izhikevich (IZH) model that can simulate various types of neuronal activities with their corresponding parameter sets. Li et al. [4] constructed an auto-associative memory with 256 fully connected digital spiking silicon neuron (DSSN) models on an FPGA. The DSSN model [5] is an qualitative neuronal model designed for efficient implementation by efficiently in a digital arithmetic circuit. This model is a non-I&F-based model and can realize several neuronal activities including Class I and II in the Hodgkin's classification [6]. This model can reproduce the gradient response in Class II neurons [7], because it does not abbreviate the calculation of the spiking process. Due to a trade-off between the reproducibility of neuronal activity and

computational efficiency, diversified neuronal models are used in silicon neuronal networks. For example, the ionic-conductance models can reproduce a neuronal activity accurately but consumes excessive computational resources in large-scale implementations. On the other hand, neuronal models that approximate a spiking process by resetting of the state variables (integrate-and-fire (I&F) -based models), such as the LIF, exponential I&F model[], adaptive exponential I&F model[8] and IZH models, can be implemented at low computational cost. However, it has reduced reproducibility of complex neuronal activities. For instance, these models assume fixed maximum membrane potentials during the spike process, whereas these potentials are non-uniform in the nervous system.

In our previous research [9], we expanded the DSSN model to cover cortical and thalamic neuron classes, including regular spiking (RS), fast spiking (FS), low-threshold spike (LTS) and intrinsically bursting (IB). We confirmed that the model behaves in the same way as the ionic-conductance model [10] in response to various magnitude of step input in each neuron classes.

In this paper, we designed digital arithmetic circuit for the DSSN model on an FPGA. We simulated our circuit on Xilinx Vivado design suit. The remainder of this paper is organized as follows. Section 2 introduces our neuron model and details of its implementation. The simulation

result is shown in Section 3. Section 4 summarizes the work and suggests ideas for future.

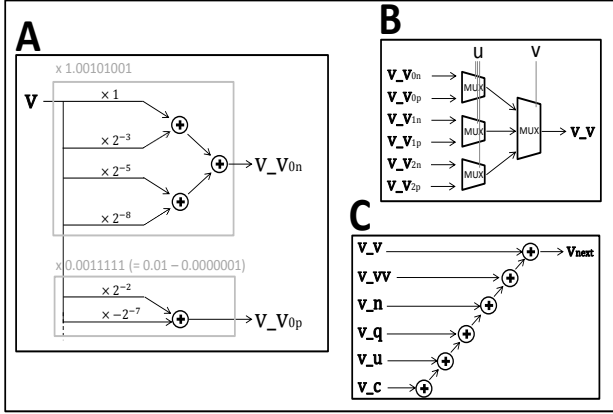


Fig. 1 Block diagram of the v -circuit. Symbols \times , $+$ and MUX mean a multiplier, adder, multiplexer, respectively. (A) Multiplication realized by shift operation and adder. (B) Add operation of the differential equation of v . (C) Correct v_{ij} are chosen by multiplexer depending on v and u .

2. Methods

2.1 DSSN model

The DSSN model is a qualitative neuronal model. It is designed so that diverse neuronal activities with fixed point Euler method. Given appropriate parameter sets, this model can reproduce various neuron classes including regular spiking (RS), fast spiking (FS), intrinsically bursting (IB), and low-threshold spike (LTS). The model is given by

$$\frac{dv}{dt} = \frac{\phi(u)}{\tau} (f(v) - n - q + I_0 + I_{stim}),$$

$$\frac{dn}{dt} = \frac{1}{\tau} (g(v) - n),$$

$$\frac{dq}{dt} = \frac{\varepsilon}{\tau} (h(v) - q),$$

$$\frac{du}{dt} = \frac{\varepsilon_1}{\tau} (v - v_0 - au),$$

$$\phi(u) = \begin{cases} \phi_0 & (u < r_{u0}) \\ \phi_1 & (r_{u0} < u < r_{u1}) \\ \phi_2 & (r_{u1} < u), \end{cases}$$

$$f(v) \equiv \begin{cases} a_{fn}(v - b_{fn})^2 + c_{fn} & (v < 0) \\ a_{fp}(v - b_{fp})^2 + c_{fp} & (v \geq 0), \end{cases}$$

$$g(v) \equiv \begin{cases} a_{gn}(v - b_{gn})^2 + c_{gn} & (v < r_g) \\ a_{gp}(v - b_{gp})^2 + c_{gp} & (v \geq r_g), \end{cases}$$

$$h(v) \equiv \begin{cases} a_{hn}(v - b_{hn})^2 + c_{hn} & (v < r_h) \\ a_{hp}(v - b_{hp})^2 + c_{hp} & (v \geq r_h), \end{cases}$$

where v denotes the membrane potential, and n and q are

© The 2016 International Conference on Artificial Life and Robotics (ICAROB 2016), Jan. 29-31, Okinawa Convention Center, Okinawa, Japan

the fast and slow variables, respectively, that abstractly

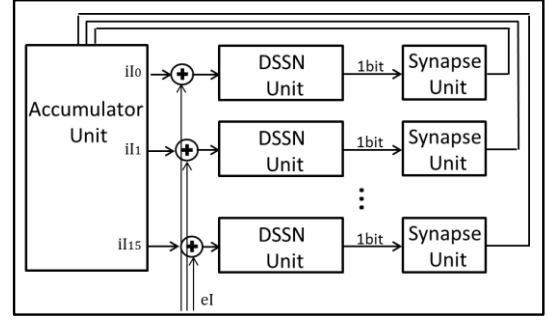


Fig. 2 The architecture of 16 fully-connected network. The network is composed of 16 DSSN, 16 silicon synapse, and an accumulator unit

describe the activity of the ion channels. The slow variable q controls the slow dynamics of the neuronal activity and has a key role to realize spike-frequency adaptation and burst firing. Variable u is the slowest that modifies the structure of the fast subsystem comprising v and n . If sustained stimulus to the fast subsystem is taken as a bifurcation parameter, a saddle-node bifurcation is observed in the RS, FS, and LTS modes, and a homoclinic - loop bifurcation in the IB mode. The parameter I_0 is a bias constant and I_{stim} represents the input stimulus. The other parameters determine the dynamical properties of the model. All of the variables and constants in this qualitative model are purely abstracted and have no dimension.

The model is solved by the Euler's method ($\Delta t = 0.0001$). We developed differential equations for efficient implementation. The equations of the circuit for calculation of v are

$$v_{next} = v_{vv} + v_{vn} + v_{vq} + v_{vI} + v_{vc},$$

$$v_{vv_{ij}} = v^2 \cdot (\Delta t \cdot a_{fj} \cdot \phi_i / \tau),$$

$$v_{v_{ij}} = v \cdot (\Delta t \cdot b_{fj} \cdot a_{fj} \cdot \phi_i / \tau + 1),$$

$$v_{n_{ij}} = n \cdot (-\Delta t \cdot \phi_i / \tau),$$

$$v_{q_{ij}} = q \cdot (-\Delta t \cdot \phi_i / \tau),$$

$$v_{I_{ij}} = I_{stim} \cdot (\Delta t \cdot \phi_i / \tau),$$

$$v_{c_{ij}} = \Delta t \cdot (b_{gj} \cdot b_{gj} \cdot a_{gj} + c_{gj}) / \tau,$$

$$v_x = \begin{cases} v_{x_{0n}} & \text{when } u < r_{u0} \text{ and } v > 0, \\ v_{x_{0p}} & \text{when } r_{u0} < u < r_{u1} \text{ and } v > 0, \\ v_{x_{1n}} & \text{when } r_{u1} < u \text{ and } v > 0, \\ v_{x_{1p}} & \text{when } u < r_{u0} \text{ and } v > 1, \\ v_{x_{2n}} & \text{when } r_{u0} < u < r_{u1} \text{ and } v > 1, \\ v_{x_{2p}} & \text{when } r_{u1} < u \text{ and } v > 1, \end{cases}$$

for $x = vv, v, n, q, I$, and c .

where, i denotes 0, 1, or 2 and j denotes n or p . In these,

equations, we can calculate a product of parameters in advance and store it as a constant value. The

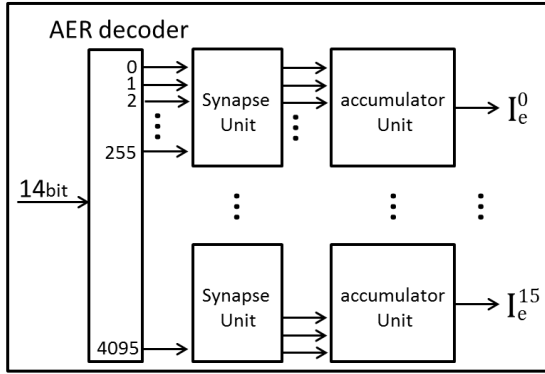


Fig. 3 The architecture of external connection. This module has 16 silicon synapse units and 16 accumulator units and an AER decoder.

multiplication of a variable and a parameter is realized by shifters and adders (Fig.1(A)). To reduce the number of adders, coefficient was approximated by the sum of 2^{-x} ; x denotes arbitrary integer number. Multiplier circuit is used once in an Euler's method's step for calculation of v^2 . v_{ij} are screened by the multiplexer depending on the value of v and u (Fig. 1(C)). We constructed n -circuit and q -circuit in the same way. The DSSN unit consumes 1 multiplier and 4 multiplexers. The numbers of adders are 35, 33, 60, and 88 for RS, FS, LTS, and IB classes.

We adopted the silicon synapse circuit in [4] based on the kinetic synapse model [11]. The equations are given by

$$\frac{dI_s}{dt} = \begin{cases} \alpha(1 - I_s) & ([T] = 1) \\ -\beta I_s & ([T] = 0) \end{cases}$$

where, I_s represent the post-synaptic current and the value of $[T]$ is 1 when the membrane potential of the presynaptic neuron is over the threshold (0). This silicon synapse unit costs 1 multiplexer and 2 adders, and it requires 2 clocks by a step.

2.2 Circuit architecture

Our circuit is composed of 16 fully-connected neurons and external input from an address event representation (AER)-based stimulus receiver module. The fully-connected neuronal network consumes 16 DSSN and 16 silicon synapse units and an accumulator unit comprising 1 multiplier and 1 adder and an 18kb block random access memory that stores synaptic weights (Fig. 2). The synapse units calculate postsynaptic input depending on the 1-bit signal that denotes whether the membrane potential v of the pre-synaptic DSSN is over the threshold or not. The accumulator unit calculates weighted sum of the post-synaptic input. The I_{stim} is calculated as follows.

$$I_{stim}^i = c_0 \sum_{j=1}^{16} w_{ij} I_s^j + I_e^i$$

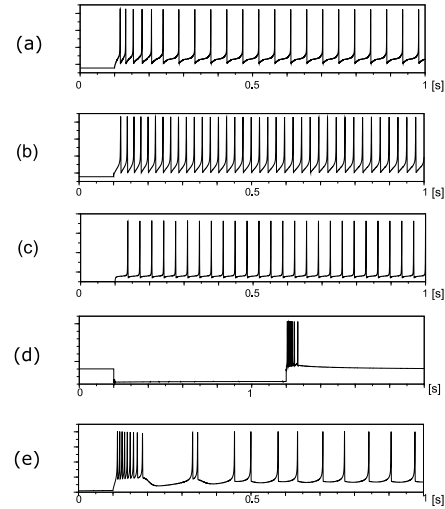


Fig. 4 Waveforms generated by the DSSN unit of RS (a), FS (b), LTS (c, d), IB (e). Excitable step inputs rise at $t = 0.1$ (a-c,e). inhibitory step inputs are provided from $t = 0.2$ to $t = 1.0$ (d).

where i and j are the indices of the post- and pre-synaptic neurons respectively, and I_e^i denotes an external input to the i th neuron, respectively. The parameter c_0 is a coefficient to scale I_{stim} into an appropriate range.

The units for the external connection is composed of 16 silicon synapse units and 16 accumulator units and an AER decoder (Fig.3). AER decoder receives 14-bit input signal by a clock. First 12-bit of input signal specifies an address of 4096 synapses by AER decoder. Next 1-bit represents rising or trailing of the pulse input, and the value of the bit is stored in the register corresponding to the specified address. Therefore, we can assigne input pulse having an arbitrary length. Last 1-bit is an enable signal.

Synaptic weights are loaded from the 16 18kb block random acces memory. A synapse unit updates 256 post-synaptic current depending on the decoded input signal at each Δt step, and the accumulator unit calculates an weighted sum of the post-synaptic inputs.

$$I_e^i = c_1 \sum_{k=1}^{256} w_{ik} I_s^k$$

where i and k are the indices of the neurons and synapses, respectively. The parameter c_1 is a coefficient to scale I_e^i into an appropriate range.

In our system, a Δt step corresponds to 1024 clocks, and 1024 input signals are acceptable by 1 step. The DSSN unit require 10000 steps to simulate a second, and it runs 10 times faster than real-time under the assumtuion that a clock correspond to 10 ns. We represent all variables and synaptic weights using 18-bit signed fixed point with 14-bit fractions.

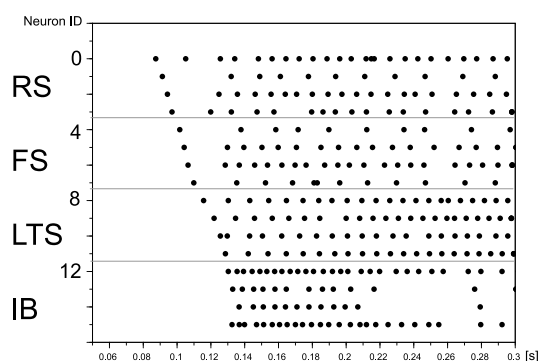


Fig.5 Raster plots of the spikes in the network. Neurons are RS (Neuron ID = 0-3), FS (4-7), LTS (8-11), IB (12-15).

3. Result

Here, we show the waveforms generated by the DSSN unit in response to external stimulus inputs. Figure 4(a) shows the waveform of the RS class that is a most typical neuron class in the cortex. A characteristic behavior of this class is spike-frequency adaptation; that is, the spike frequency decreases over time in response to a constant stimulation input. On the other hand, FS neurons fire with almost constant frequency (Fig.4(b)). LTS neurons exhibit periodic firing in reaction to excitable input stimulus (Fig.4(c)) and generate a burst firing just after the termination of a sufficient hyperpolarizing stimulus (Fig.4(d)). IB neurons generate the bursting at the onset of a stimulus, then continue to spiking (Fig. 4(e)).

Figure 5 shows raster plots of the spikes in the network. We applied 12-bit signal correspond to each neuron by rotation and evoked spike, and additional spikes were evoked by the inner connection. Synaptic weights were assigned randomly.

4. Conclusion

In this paper, we constructed digital circuit of the DSSN model that supports four cortical and thalamic neuron classes. The implemented circuit could generate activities qualitatively comparable to the ionic-conductance model for each neuron class. It consumed only 1 multiplier for calculation of an Euler's Method's step, which is an expensive module in an FPGA. We confirmed the behavior of a network of 16 fully-connected DSSNs that can receive stimuli via 4096 synapses. Each synapse is controlled by 12-bit input signal through an AER decoder.

Our previous study implemented the DSSN model that supports the Class I and Class II in the Hodgkin's classification. We expect the circuit constructed in this work will be a basis for digital silicon neuronal networks that can support a wide variety of neuronal activities more elaborately than the I&F-based circuits.

In future works, we will implement the DSSN model that supports the square-wave bursting and elliptic

bursting which were already realized by software simulation. Larger-scale network will also be pursued.

5. Acknowledgement

This work was supported by JSPS Grant-in-Aid for scientific Exploratory Research Number 25240045.

6. Reference

1. R. K. Weinstein and R. H. Lee. Architectures for high-performance fpga implementations of neural models. *J. Neural Eng.*, 3(1):21–34, 2006.
2. M. J. Pearson, A. G. Pipe, B. Mitchinson, K. Gurney, C. Melhuish, I. Gilhespy, and M. Nibouche. Implementing spiking neural networks for real-time signal-processing and control applications: A model-validated fpga approach. *IEEE Transactions on Neural Networks*, 18(5):1472–1487, 2007.
3. D. B. Thomas and W. Luk. Fpga accelerated simulation of biologically plausible spiking neural networks. In K. L. Pocek and D. A. Buell, editors, *FCCM*, pages 45–52. IEEE Computer Society, 2009.
4. J. Li, Y. Katori, and T. Kohno. An fpga-based silicon neuronal network with selectable excitability silicon neurons. *Frontiers in neuroscience*, 6(183), 2012.
5. T. Kohno and K. Aihara. Digital spiking silicon neuron: Concept and behaviors in gj-coupled network. *Proceedings of International Symposium on Artificial Life and Robotics 2007*, 2007.
6. A. L. Hodgkin. The local electric changes associated with repetitive action in a non-medullated axon. *The Journal of physiology*, 107(2):165–181, Mar. 1948.
7. X.-J. Wang and J. Rinzel. Oscillatory and bursting properties of neurons. In M. A. Arbib, editor, *The Handbook of Brain Theory and Neural Networks*, pages 835–840. MIT Press, MA, 2nd edition, 2003.
8. R. Brette and W. Gerstner. Adaptive Exponential Integrate-and-Fire Model as an Effective Description of Neuronal Activity. *J. Neurophysiol.*, 94:3637–3642, 2005.
9. T. Nanami and T. Kohno. Simple cortical and thalamic neuron models for digital arithmetic circuit implementation. In preparation.
10. M. Pospischil, M. Toledo-Rodriguez, C. Monier, Z. Piwkowska, T. Bal, Y. Fregnac, H. Markram, and A. Destexhe. Minimal hodgkin-huxley type models for different classes of cortical and thalamic neurons. *Biological Cybernetics*, 99(4-5):427–441, 2008.
11. Alain Destexhe, Zachary F. Mainen, and Terrence J. Sejnowski. *Kinetic Models of Synaptic Transmission*. in: *Methods in Neuronal Modeling*, Edited by Koch, C. and Segev, I. (2nd Edition) MIT Press, Cambridge, 1998.

Analyses of Postgraduates' Entrance Examination Scores Based on Linear Regression with Dummy Variables

Ning Xiaojun,

Graduate School, University of Science and Technology Beijing, Beijing, China

Huang Ruocheng, Liang Xiaoyi, Ai Dongmei*

School of Mathematics and Physics, University of Science and Technology Beijing, Beijing, China

*corresponding author :Ai Dongmei, E-mail: aidongmei@ustb.edu.cn

Abstract

Detecting the main factors influencing the students' score is an important part of the student evaluation system. Several factors that have significant influence on postgraduates' entrance examination scores including enrollment category, university category, age, gender, fresh graduate were studied by ANOVA in this paper. Quantitative analysis of the correlation between the discrete variables and postgraduates' entrance examination scores were performed by linear regression with dummy variables and 85% confidence prediction interval of postgraduates' entrance examination scores were obtained. Data support were provided by these results for graduate school enrollment work.

Keywords: Postgraduates' Score; ANOVA; Dummy Variables; Linear Regression

1. Introduction

A digital campus information management system is being promoted in universities recently. Especially, complete postgraduate information management systems are being used by graduate school in universities [1]. Thus, a large number of postgraduates' data have formed valuable information resources. However, these data are only used for simple query and statistics at present, and its inherent information was not properly mined and utilized [2].

In this paper, enrollment information of postgraduates within three years was extracted and analyzed by ANOVA and stepwise regression analysis with dummy variable, in order to explore the factors that affect the postgraduates' entrance examination scores and measure the quality of enrollment postgraduates. The attribute variables (e.g. gender, university category) were analyzed using ANOVA in order to judge if they have a significant impact on the postgraduates' entrance examination scores. Those significant attribute variables were then applied in stepwise regression and obtained regression equations. Prediction interval with 85% confidence of postgraduates' entrance examination scores were obtained and the forecasted scores for each college were compared.

2. Method

2.1 Analysis of Variance

The attribute variable which has a significant impact on the postgraduates' entrance examination scores were selected using one-way ANOVA. Let a factor (attribute variable) A with r levels: A_1, A_2, \dots, A_r , collecting data X_{ij} by n times observation under A level, where $j = 1, 2, \dots, n_i$, $i = 1, 2, \dots, r$. Let μ be the grand mean of all the samples, α_i is the significance level, ε_{ij} is the random error, and then comes the following ANOVA models [3]:

$$\begin{cases} X_{ij} = \mu + \alpha_i + \varepsilon_{ij}, & j = 1, \dots, n_i, i = 1, \dots, r \\ \varepsilon_{ij} \sim N(0, \sigma^2), & i.i.d. \\ \sum_{i=1}^r n_i \alpha_i = 0 \end{cases}$$

whose null hypothesis is $H_0: \alpha_1 = \alpha_2 = \dots = \alpha_r$. Then its test statistic can be constructed base on the Sum of Squares of Deviation: $F(r-1, n-r)$. If the null hypothesis is rejected, it shows that there are significant differences in different levels. The variance homogeneity assumption of variance analysis can be tested by Bartlette's test or Levene's test [4]

2.2 Stepwise Regression with Dummy Variables

The quantitative relation between each attribute variable and postgraduates' entrance examination scores can be analyzed using stepwise regression with dummy variables.

The basic idea of linear regression is as follows: let

$Y = X\beta + \varepsilon$, where X is independent variables, Y is

dependent variables, β is the vector of regression

3 Data analysis

3.1 Analyses of Admission Scores by ANOVA

The data are from the postgraduate registration and enrollment information database of a university for three years, which totally consist of 5384 records. 29 variable attributes are included, such as admission college, test method and test scores after the raw data are merged and standardized. The universities where postgraduates got bachelor degree were divided into seven major categories, include 985 project university, 211 project university with graduate school, 211 project university without graduate school, key university, ordinary university, secondary college and this university, which in total has seven attribute variables.

The relationship between the five factors of gender (with 2 attribute values of Male and Female respectively), admission category (with 4 attribute values of Directional training, Non Directional training, Self-fund Training, Training respectively), register age groups (with 3 attribute values of less than 22 years old, between the ages of 22 and 25, over 25 years olds respectively), this year's graduates (with 2 attribute values of Yes and No respectively), graduate university (with 7 attribute values shown above respectively) and the postgraduates' entrance examination scores were analyzed by ANOVA. If the postgraduates' entrance examination scores show significant differences under the different values of one attribute variable, then this variable is an important factor to influence the postgraduates' entrance examination scores.

Each factor's homogeneity of variance was tested by Bartlett test function in R, while the one-way ANOVA

for postgraduates' entrance examination scores by aov function. The result showed that admission category, graduate university and register age groups are the important factors to influence the postgraduates' entrance examination scores, while gender is not a significant factor. Take admission category as an example. Its ANOVA result is shown in Table 1, where the p-value is 0.0005, which indicates that there are significant difference among distinct admission category values. The significant differences among values of admission category can be shown in Fig. 1.

Table 1 ANOVA for admission category

Source	F.D.	Sum of Sq.	p-value
Admission Category	3	11.8574	0.0005
Error	7	1.1616	

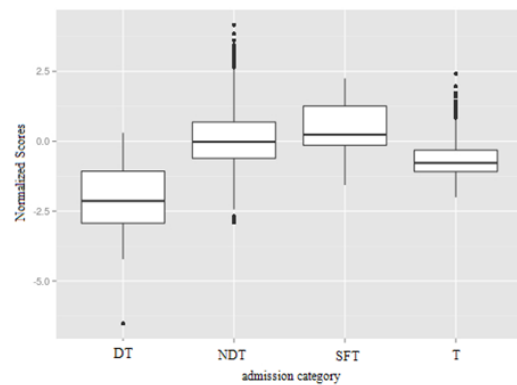


Fig. 1 normalized scores of admission category

3.2 Analyses of Admission Scores by Regression

The quantitative relationship between the postgraduates' entrance examination scores and the above three significant attribute variables was analyzed through regression analysis in this paper. We established an effective regression equation of independent variables with statistical significance by a stepwise regression method based on AIC information entropy. As an example of introducing dummy variables for a discrete attribute variable, let one's postgraduate admission score is Y which could take three different values, and thus

three dummy variables could be introduced for register age groups as follows:

$$C_{1i} = \begin{cases} 1 & 22-25 \text{ years old} \\ 0 & \text{otherwise} \end{cases}$$

$$C_{2i} = \begin{cases} 1 & \text{less than 22 years old} \\ 0 & \text{otherwise} \end{cases}$$

$$C_{3i} = \begin{cases} 1 & \text{over 25 years old} \\ 0 & \text{otherwise} \end{cases}$$

Likewise, four dummy variables of D were introduced for admission category, and seven dummy variables of E were introduced for graduate university, so the regression equation could be represented as

$$Y_i = \beta_0 + \beta_1 C_{1i} + \dots + \beta_3 C_{3i} + \beta_4 D_{1i} + \dots + \beta_7 D_{4i} + \beta_8 E_{1i} + \dots + \beta_7 E_{7i} + \varepsilon_i$$

which contains 14 regression variables, and totally 15 regression coefficients to be determined. We extracted postgraduates' data of different department of graduate school, then analyzed these independent variables by a stepwise regression method based on AIC information entropy [9] respectively. The results from the School of Metallurgical and Ecological Engineering are shown in Table 2. As for postgraduate students in this School, the p-values of attribute variables except 985 project university are all less than 0.05, which shows these attribute variables are significant factors to influence the postgraduates' entrance examination scores of postgraduates. And the obtained regression results for each school can be used to predict their students' scores, and the result are shown in Fig. 2, from which it can be seen that the School of Foreign Language, Computer and Community, Economy and Management and Humanity and Law have much higher predictions.

Table 2 Results of independent variables by a stepwise regression method

	estimated	Standard error	t-value	p-value
β_0	396.469	6.094	65.057	< 2e-16
985 project university	10.479	6.173	1.698	0.090
this university	13.116	4.571	2.869	0.004
211 university without graduate school	16.558	5.722	2.894	0.004
key university	16.681	4.927	3.386	0.001
ordinary university	11.789	4.323	2.727	0.007
Non Directional	10.946	3.353	3.265	0.001
less than 22 years old	15.903	5.663	2.808	0.005
between the ages of 22 and 25	11.683	4.055	2.881	0.004

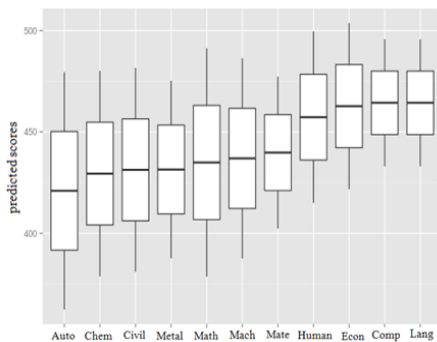


Fig. 2 Predicted scores from regression results

4. Conclusion

Enrollment data of postgraduates of one university are processed by ANOVA and stepwise regression analysis with dummy variable in this paper. A wealth of information was revealed, which can be important guide to cultivation for postgraduates.

Analyzing the factors affecting the postgraduates' entrance examination scores of postgraduates and prediction of the postgraduates' entrance examination scores of postgraduates, can provide a more scientific basis for the development of the graduate school and achievement clarifying objectives and scientific work.

Acknowledgements

This paper is supported by The Postgraduate Education and Development Grant of University of Science and Technology Beijing.

References

1. Hu Quintai, Zheng kai, Lin Nanhui (2014), Transformation: From "Digital Campus" to " Intelligent Campus". China Audio Visual Education (1): 35-39.
2. Zhang Junchao (2014), Institutional Research and University Management in the Age of Big Data. Researches in Higher Education of Engineering (1): 023.
3. Chen Xiru (2009), Advanced Mathematical Statistics. University of Science and Technology China Press.
4. Marozzi, Marco (2011), Levene type tests for the ratio of two scales. Journal of Statistical Computation and Simulation 81 (7): 815-826.
5. He Xiaoqun, Liu Wenqing (2007), Applied Regression Analysis. Renmin University of China Press.
6. Fang Kaitai (1989), Practical Multivariate Statistical Analysis. East China Normal University Press.
7. Spiegelhalter, David J., et al (2014), The deviance information criterion: 12 years on. Journal of the Royal Statistical Society: Series B (Statistical Methodology) 76(3): 485-493.
8. Kleinbaum, et al (2014), Applied regression analysis and other multivariable methods. Cengage Learning.
9. Chowdry, Haroon, et al (2013), Widening participation in higher education: analysis using linked administrative data. Journal of the Royal Statistical Society: Series A (Statistics in Society), 176 (2): 431-457.

Clinical Evaluation of UR-System 2 for Recovery of Motor Function of Plegic Upper Limb after Stroke

Hirofumi Tanabe, Masahiro Mitsukane

*Department of Health Sciences, Shonan University of Medical Sciences
16-48 Kamishinano, Totsuka-ku, Yokohama, Kanagawa 244-0806, Japan
E-mail: hirofumi.tanabe@sums.ac.jp*

Norihiro Toya, Ryosuke Takeichi, Hitomi Hattori, Yoshifumi Morita

*Nagoya Institute of Technology
Gokiso-cho, Showa-ku, Nagoya, Aichi 466-8555, Japan*

Yoshiaki Takagi, Norio Hasegawa

*Sanyo Machine Works, Ltd.
1 Oka, Okimura, Kitanagoya-shi, Aichi 481-8540, Japan*

Abstract

We developed a new training system UR-System 2 for restoring motor function of the upper limb after stroke in patients with hemiplegia. And then, we conducted clinical evaluation of the therapeutic effect of training with the UR-System 2 in six patients. The UR-System uses Proprioceptive Neuromuscular Facilitation (PNF) to promote muscle strength. The results show the immediate therapeutic effect of training with the UR-System 2 for restoring the motor function of the upper limb.

Keywords: Rehabilitation, Training system, Hemiplegic stroke patient, Clinical evaluation, PNF

1. Introduction

The synergy movement pattern often seen in hemiplegic patients after stroke is one of the factors inhibiting improvement of motor function. According to the Brunnstrom recovery stages of hemiplegia, elbow flexion, pronation/supination of the forearm, wrist flexion, and finger flexion occur abnormally and simultaneously in hemiplegic patients during the early stage of recovery; this is called the synergy movement pattern. In the recovery stage, a patient gradually evolves from a synergy movement pattern, and will be able to extend the elbow, supinate the forearm, and extend the wrist and fingers¹. Proprioceptive Neuromuscular Facilitation (PNF) is an effective therapy facilitating recovery from

spastic paralysis^{2, 3}. Since this repetitive technique is performed manually, the therapist's physical workload is considerable. Therefore, we are developing a training system for recovery of normal movement isolated from synergy movement patterns by facilitating contraction of elbow extension and forearm supination muscles.

In our previous work⁴, we developed a training system (UR-System: Useful and Ultimate Rehabilitation System) for recovery of motor function of the upper limb after stroke in patients with hemiplegia. This system uses PNF to promote muscle strength. Clinical evaluation of the therapeutic effect of training with the UR-System was performed in eight patients for two weeks. Active ranges of motion (A-ROMs) of elbow extension and forearm supination improved after training with the UR-System.

Moreover, the modified Ashworth scale (MAS) scores⁵ for elbow extension and forearm supination increased. This means that spastic paralysis was reduced. This shows the effectiveness of training with the UR-System for recovery of motor function of the upper limb.

However, the following problems persist. Since the UR-System was not equipped with sensors that can measure the movement of the paralyzed forearm and the force/torque exerted by the forearm, the therapeutic effect was not evaluated in detail (Problem I). It was difficult for therapists to adjust the parameters of the rubber belt to facilitate elbow extension suitable for the patient's condition (Problem II).

In order to solve these problems this study developed a new training system, the UR-System 2. We evaluated the immediate therapeutic effect of recovery of motor function by training with the UR-System 2.

2. UR-System 2

To solve Problem I, we introduced sensors on the brace. To solve Problem II, we developed an elbow-pushing arm on the brace in place of the rubber belt to facilitate elbow extension. Moreover, since the previous UR-System was over-engineered, we reconsidered the specifications, and developed the UR-System 2. As a result, the number of parts, weight of the mechanical system, and total cost decreased.

The UR-System 2 is a force display system with one degree of freedom. The system consists of a mechanical system and a controller. The mechanical system consists of a training arm, a powder brake (SINFONIA TECHNOLOGY CO., LTD., PRB-2.5H), and a brace. The brace was used to secure the patient's forearm to the training system. The patient moves the training arm independently. The powder brake generates a resistance force during training. Four different resistance patterns, i.e., step, slope, wall, and constant modes, were installed in the controller. The length of the training arm can be altered within the range of 0.60-0.89 m. The maximum resistance is 49 N when the length of the training arm is 0.75 m.

The brace has three degrees of freedom, allowing rolling, yawing, and pitching motions of the fixing plate. The rolling motion can be switched between free motion and fixed motion with a double nut. When the UR-

System 2 is used in training, the rolling motion is fixed, but is allowed when evaluating the therapeutic effect. The brace is equipped with three potentiometers (ALPS ELECTRIC CO. LTD., RDC803001A) and a 6-axis force sensor (Leptrino Co. Ltd., PFS055YA251A6). The potentiometers measure roll, yaw, and pitch angles of the fixing plate of the brace. The 6-axis force sensor measures the force and torque between the forearm and the fixing plate. An elbow-pushing arm is installed on the fixing plate to facilitate elbow extension. As the patient moves the forearm forward, the elbow-pushing arm pushes the elbow to facilitate contraction of a deltoid muscle. The elbow-pushing arm is rigid and does not bend to the external force. The contact portion of the elbow-passing arm to the deltoid muscle is made by harder cushion. When the forearm is fixed to the brace, the portions of the forearm near the wrist and the elbow are fixed with a non-expandable bandage and an expandable bandage, respectively. Therefore, the portion of the forearm near the elbow can leave the brace due to the extensibility of the expandable bandage. Moreover, the patient can extend his/her elbow fully in spite of the existence of the elbow pushing arm. If a non-expandable bandage is not used, the patient cannot extend his/her elbow fully.

Because this system is not equipped with motors, it is extremely safe and economical. It should be noted that the system is used only for active exercise training.

The UR-System 2 was equipped with various functions. The resistance display function allows therapists to perform various types of resistance training by changing the arm length and the resistance level. The touch panel parameter setting function allows the parameters of the resistance patterns to be easily set by pushing buttons on the touch panel display. The parameters consist of the magnitudes and positions of the resistance patterns. The magnitudes are selected from among twenty-five levels. The positions are determined by moving the training arm to the desired position. This function provides good visibility and easy operability for the therapist.

The resistance to the movement of the forearm and compression of the elbow are expected to facilitate elbow extension. These concepts are based on facilitation elements, namely resistance to movement, compression arthrodesis, passive movement, and manual contact in

PNF techniques. Therefore, the patient is expected to extend the elbow joint fully. Moreover, pronation and supination of the forearm, wrist flexion, and finger flexion are not permitted during elbow extension and flexion, because the forearm is fixed on the fixing plate of the brace, preventing a synergy movement pattern from occurring. Therefore, isolated movement should be facilitated by using the UR-System 2.

3. Clinical Evaluation of Therapeutic Effect

3.1. Method

We evaluated six patients who satisfied the following conditions:

- 1) The subject had a hemiplegic upper limb after a stroke.
- 2) More than one year had passed since stroke onset.
- 3) The subject did not have pain in training with the UR-System 2.
- 4) The Brunnstrom Stage was IV or V.

The post-stroke durations were 10 years in Subject A, 12 in Subject B, two in Subject C, four in Subject D, one and one-half in Subject E, and five in Subject F. We obtained written consent from all patients.

We used two training protocols for a comparative study. One employed training without PNF-facilitating elements, namely resistance and compression arthrodesis, and was referred to as Control-training. The other employed training with PNF-facilitating elements, and was referred to as PNF-training. PNF-training was performed at least three days after Control-training.

The patient performed repeated training for elbow flexion and extension with the paralyzed forearm in the supinated position. Repeated training was performed 50 times per set for five sets. The rest time between sets was 5 minutes.

The therapeutic effects of training with the UR-System 2 were assessed using the MAS and the A-ROM test before and after training, and were compared with those of Control-training and PNF-training.

3.2. Results and discussion

All subjects completed two types of training with the UR-System 2. Table 1 presents the summary of scores for outcome measures. Table 1 shows that the A-ROMs and MAS score in PNF-Training increased significantly after training. Figures 2-4 show the A-ROMs and MAS score

were improved greatly in PNF-Training as compared with Control-training. Thus, isolated movement was facilitated by PNF-training with the UR-System 2. The immediate effect of restoring motor function in PNF-training was excellent as compared with Control-training. Moreover, it is noteworthy that motor function was restored even in Patients A and B, who had stroke episodes more than ten years prior to training. Consequently, training with the UR-System 2 can immediately improve motor function of the upper limb after stroke in patients with hemiplegia.

Since the therapeutic effect shown in this study is immediate, we will investigate this effect after daily continuous PNF-training. Moreover, the workload of therapists will decrease because the system can be used for independent training for recovery of motor function.

4. Conclusion

The immediate therapeutic effect of PNF-training with the UR-System 2 was shown from the results of the clinical evaluation. PNF-training with the system can immediately improve motor function of the hemiplegic upper limb.

In a future study, we will confirm the therapeutic effect after daily continuous PNF-training with the system 2 for a larger number of subjects, and develop a training method for recovery of motor function of the shoulder and lower extremities of hemiplegic patients by modifying the UR-System 2.

References

1. I. Safaz, B. Ylmaz, E. Yaşar, R. Alaca, Brunnstrom recovery stage and motricity index for the evaluation of upper extremity in stroke: Analysis for correlation and responsiveness, *Int. J. Rehabilitation Res.*, **32**(3) (2009), pp. 228-231.
2. J. Stein, R. Harvey, C. Winstein, G. Wittenberg, R. Zorowitz, Stroke recovery and rehabilitation, *Demos Medical Publishing*, (NY,2008).
3. K. B. Hindle, T. J. Whitcomb, W. O. Briggs, J. Hong, Proprioceptive neuromuscular facilitation (PNF): Its mechanisms and effects on range of motion and muscular function, *J. Hum. Kinet.*, **31** (2012), pp. 105-113.
4. Y. Morita, N. Sato, H. Ukai, H. Tanabe, T. Nagao, R. Tanemura, Y. Takagi, Y. Aoki, Clinical evaluation of training system for recovery of motor function after stroke in patients with hemiplegia, *Proc. of the 2nd Int. Conf. on NeuroRehabilitation (ICNR2014)* (2014), pp. 83-92.

© The 2016 International Conference on Artificial Life and Robotics (ICAROB 2016), Jan. 29-31, Okinawa Convention Center, Okinawa, Japan

5. Ashworth B, Preliminary trial of carisoprodal in multiple sclerosis, *Practitioner*, **192** (1964), pp.540-542.

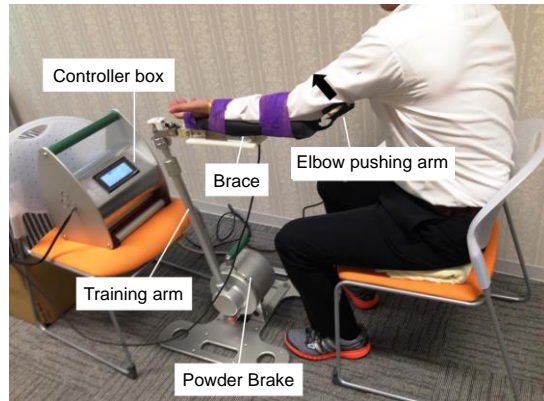


Fig. 1. UR-System 2.

Table 1. Summary of scores for outcome measures
(Control: Control-training, PNF: PNF-training,
Pre: Before training, Post: After training,
Diff: Difference between the results before and after training,
Positive difference values mean improvement.)

(a) A-ROM of elbow extension.

Subject	Control			PNF		
	Pre	Post	Diff.	Pre	Post	Diff.
A	-20	-15	+5	-20	-5	+15
B	-15	-25	-10	-15	-5	+10
C	-25	-25	+0	-25	-10	+15
D	-20	-15	+5	-20	0	+20
E	-20	-15	+5	-20	-10	+10
F	-30	-15	+5	-30	-5	+25

(b) A-ROM of supination of forearm.

Subject	Control			PNF		
	Pre	Post	Diff.	Pre	Post	Diff.
A	65	75	+10	65	90	+25
B	40	55	+15	40	70	+30
C	55	60	+5	55	65	+10
D	35	45	+10	35	55	+20
E	40	65	+25	40	70	+30
F	65	75	+10	65	90	+25

(c) MAS Score of elbow flexor group.

Subject	Control			PNF		
	Pre	Post	Diff.	Pre	Post	Diff.
A	4	4	0	4	5	+1
B	4	4	0	4	5	+1
C	3	4	+1	3	4	+1
D	3	3	0	3	4	+1
E	3	4	+1	3	4	+1
F	3	3	0	3	4	+1

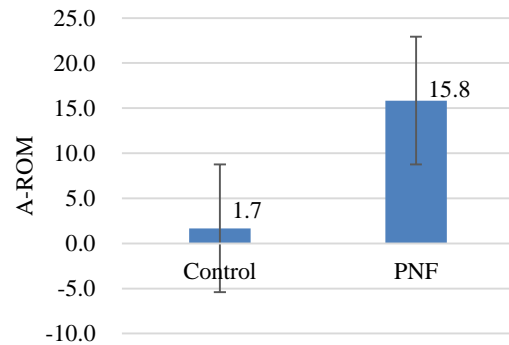


Fig. 2. Improvement of A-ROM of elbow extension.

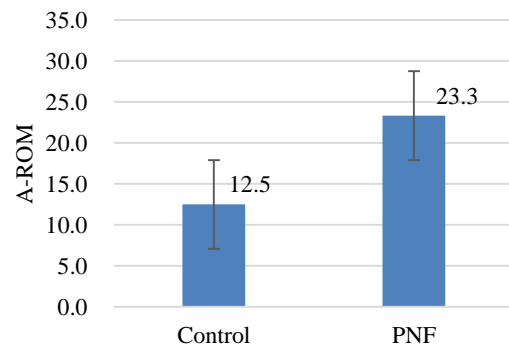


Fig. 3. Improvement of A-ROM of supination of forearm.

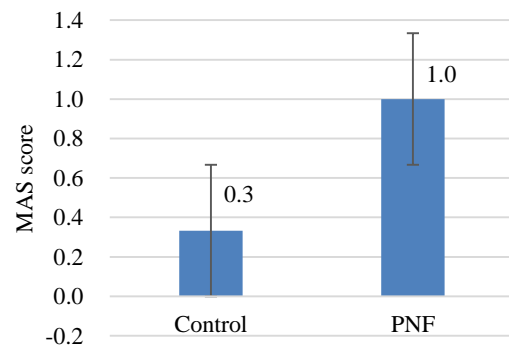


Fig. 4. Improvement of MAS Score of elbow flexor group.

Knee Android Model Reproducing Internal-External Rotation with Screw-Home Movement of Human Knee

Daichi Yamauchi, Sho Takei, Noritaka Sato, Yoshifumi Morita

Department of Computer Science and Engineering, Nagoya Institute of Technology,

Gokiso-cho, Showa-ku, Nagoya, Aichi 466-8555, Japan

E-mail: d.yamauchi.170@nitech.ac.jp

Abstract

This paper proposed a knee android model (Knee-AM) that can reproduce the internal-external rotation with screw-home movement (SHM) of the human knee. This rotation of the Knee-AM was realized by changing the number, the lengths and the fixing points of the nylon-cords of our previous Knee-AM. Moreover, when the anterior cruciate ligament (ACL) was removed from the Knee-AM to imitate ligament injury, the SHM did not occur during knee extension. The results showed the ACL played an important role for the SHM.

Keywords: Android model, Knee model, Human knee joint, Screw-home movement, Joint mechanism.

1. Introduction

Recently, time of rehabilitation treatment is restricted from increasing the number of patients with an increase in the elderly. From the background, efficiency and effective treatments are social needs in rehabilitation field. As a solution for the needs, we had proposed a knee android model (Knee-AM) for supporting a treatment planning¹.

An android model of a human joint was developed to improve medical technology in the field of rehabilitation². Android models are anatomical models composed of the minimum number of parts required for reproduction of human movement. They can reproduce the three elements of movement (“slide”, “roll” and “leave”) that occur between two articulating bones. Sanaka² found that the kinematic mechanisms of an android model of the index finger had some different properties than those of the actual movement of the index finger. The rehabilitation based on this theory has contributed to the improvement on the range of motion reduced after tenorrhaphy. The study above confirmed that applying

the kinematic mechanisms obtained from the use of android models is beneficial to medical treatment.

It has been reported that the internal-external (IE) rotation during knee extension in human can be classified into three types³. The three types were called “External rotation type”, “Internal rotation at the end type” and “Internal rotation type”, respectively. In our previous study, we proposed a Knee-AM consisting of a tibial model, a femoral model and 10 nylon-cords imitating the ligaments. The IE rotation of the Knee-AM was similar to those of internal rotation at the end type. This type was not majority and often occurred in the human who had a joint laxity³.

In this paper, we aimed to propose a Knee-AM which can reproduce the IE rotation of external rotation type. Since most of human knee motion belongs to the IE rotation of external rotation type, reproduction of the IE rotation of this type in the knee-AM was important for expanded utilization of the Knee-AM. Additionally, since this type had external rotation occurring at the end of extension, what is referred to as the screw-home movement (SHM), we investigated mechanism for causing the SHM using the Knee-AM. Furthermore, we

also aimed to gain some knowledges of a ligament injury from simulating the ligament injury in the Knee-AM.

2. Knee Android Model (Knee-AM)

The Knee-AM is shown in Fig. 1. The Knee-AM imitated the right knee joint and consisted of a tibial model, a femoral model and five nylon-cords. In order to make the Knee-AM extend automatically, we used a drive unit.

2.1. Bone models

We used the same bone models as those in our previous study¹. The tibial and the femoral models, imitating the tibia and the femur, were made with a 3D printer out of a smooth nylon-based material. The femoral model was cut near the knee joint to about one-fifth of its full length. An aluminum rod was attached to the cut surface along the long-axis of the femoral model to fix the femoral model to the drive unit. A light weight square plate (length of side: 150 mm) also was attached on the tibial model for attachment of measuring makers.

2.2. Nylon-cords

We attached five inextensible nylon-cords to imitate the ligaments of the knee on the basis of the motion and the anatomy of the human knee⁴ as shown in Fig. 2. The nylon-cords were attached to the bone models by copper nails. When measuring the lengths of the nylon-cords, we measured the lengths between the centers of two copper nail heads. The correspondences of the five nylon-cords to the ligaments of human knee and these lengths were shown in Table 1. From our previous Knee-AM¹, we reduced the number of nylon-cords to investigate knee motion in the simple structure, and also we rearranged

the positions and the lengths of nylon-cords to reproduce human knee motion precisely.

The tibial collateral ligament (TCL) was imitated by one nylon-cord (Cord T). One end of Cord T was attached near the center of medial femoral condyle (MFC) so that Cord T did not become a loose when the flexion angle was from 90° to 0°. The other end was attached on the posterior of the insert part of the pes anserinus.

The fibular collateral ligament (FCL) was imitated by one nylon-cord (Cord F). One end of Cord F was also attached near the center of lateral femoral condyle (LFC) so that Cord F did not become a loose when the flexion angle was from 90° to 0°. The actual other end is attached on the fibular head. However, since the Knee-AM did not include the fibular model, the other end was attached on the insert part of the posterior ligament of the fibular head.

The anterior cruciate ligament (ACL) was imitated by two nylon-cords (Cords A1 and A2, collectively referred to as Cord A). The reason why Cord A was 2 was that the ACL and the PCL consisted of many fibers having different lengths⁴. One end of Cord A1 was attached on the distal posterior of the LFC. The other end was attached near the insert part of the medial meniscus. Similarly, one end of Cord A2 was attached on the proximal posterior of the LFC. The other end was attached on the 9 mm medial posterior from the end of Cord A1 on the tibial model.

The posterior cruciate ligament (PCL) was imitated by one nylon-cord (Cord P). In order to reproduce the motion between 90° of flexion angle and full extension, we imitated the PCL, which tighten in flexion position⁴, with one nylon-cord. One end of Cord P was attached on the distal anterior of the MFC. The other end was attached on the center posterior of the tibial plateau.

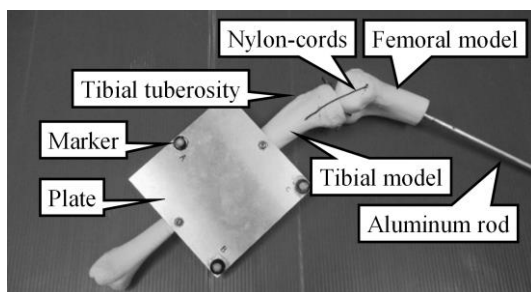


Fig. 1. Knee android model (Knee-AM)

Table 1. Correspondences of five nylon-cords to ligaments of human knee and these lengths (TCL: Tibial collateral ligament, FCL: Fibular collateral ligament, ACL: Anterior cruciate ligament, PCL: Posterior cruciate ligament)

Name of cord	Ligament	Length [mm]
Cord T	TCL	58.5
Cord F	FCL	39.3
Cord A1	ACL	34.2
Cord A2	ACL	37.3
Cord P	PCL	31.1

2.3. Drive unit

The drive unit and the Knee-AM are shown in Fig. 3. The drive unit was composed of a motor, a reel fixed on the motor shaft, a pulley, a wire and a frame. The drive unit extended the joint of the Knee-AM by pulling a wire connected to the tibial tuberosity. The wire was run through the pulleys and wound onto the reel. The motor was placed above the long-axis of the femoral model, so that the horizontal angle of the wire with respect to the long-axis of the femoral model was 0° . The pulley were placed in the position corresponding the human patella at full extension. The femoral model was fixed on the frame by clamping the aluminum rod and the proximal part of the femoral model. This fixing method was improved from that of our previous study¹ to fix the Knee-AM on the drive unit firmly.

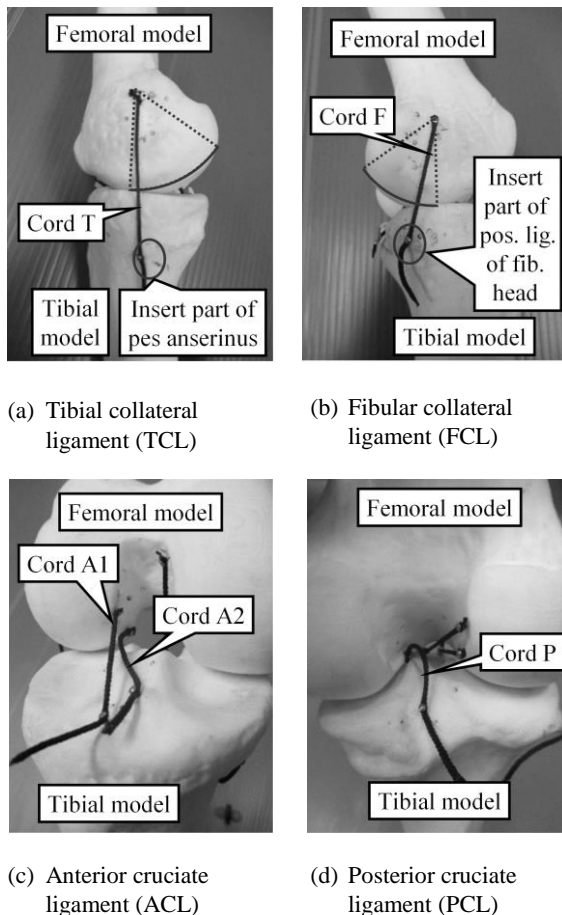


Fig. 2. Nylon-cords imitating ligaments of human

3. Experiment

We conducted two experiments to confirm the utility of the Knee-AM. In the experiments, we measured the motions of the bone models with a motion capture system VICON (Vicon Movement Systems Ltd.) and calculated flexion angle and IE rotation angle by using the same calculation methods as our previous study¹.

3.1. Experiment method

Firstly, we tested the reproducibility of the Knee-AM for the IE rotation of the human knee. In this test, the Knee-AM was extended from 90° of extension angle to full extension by the drive unit. To evaluate the reproducibility, we compared the IE rotation of Knee-AM with that of human knee.

Secondly, we investigated the knee motion of an ACL injury by using the Knee-AM. In this simulation, Cords A1 and A2 were removed as the shown in Fig. 4. The Knee-AM simulating an ACL injury is referred to as the injured Knee-AM. The experimental procedure was the same as that of the first experiment.

The measured data included small vibration caused by a mechanical resonance of the Knee-AM. In order to eliminate it, we used the low-pass filter with 5Hz of cutoff frequency.

3.2. Result

The IE rotations of the Knee-AM and the injured Knee-AM are shown in Fig. 5. In order to compare the IE rotations of two types of Knee-AMs to those of the

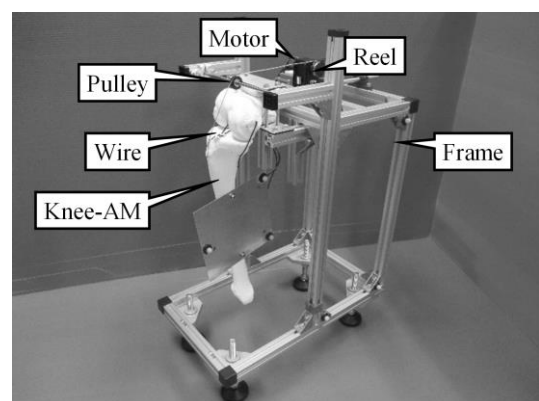


Fig. 3. Drive unit and Knee-AM

human knees, we used the human knee movement data obtained from Ref. 3.

In this graph, the horizontal axis is the flexion angle, with extension denoted in the positive direction. The vertical axis is the IE rotation angle, with internal rotation denoted in the positive direction, and rotation angle is set to be zero at -90° of flexion angle. The markers show each maximum absolute value of rotation angle between -90° and 0° of flexion angle.

Ishii et al.³ classified IE rotation of the thirty subjects into three types. “Type 1”, was external rotation occurring at the end of extension, namely Screw-Home Movement (SHM) occurring. “Type 2”, was external rotation occurring at the beginning of extension, and internal rotation occurring in the second half of extension. “Type 3”, was internal rotation occurring over the entire extension.

In the Knee-AM, the round marker is in group of the Type 1, and SHM occurred. Therefore, the Knee-AM can reproduce the IE rotation with the SHM of the human knee. On the other hand, in the injured Knee-AM, the round marker is in group of the Type 1, though the SHM did not occur. Consequently, ACL was a necessary component for occurrence of the SHM.

3.3. Discussion

We considered the mechanism for causing the SHM. Compared in Fig. 5, the two waveforms of the Knee-AM and the injured Knee-AM show different movements between -20° and 0° of flexion angle. Accordingly, it was assumed that Cord A started to tighten from -20° and that the SHM was caused by Cord A.

In order to clarify the mechanism for causing the SHM, we observed the motions of the lateral and the

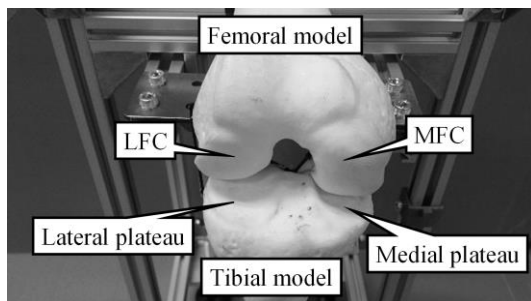


Fig. 4. Injured Knee-AM

medial plateaus with respect to the femoral model and the tensions of the nylon-cords of the two types of Knee-AMs. The motions of the lateral and the medial plateaus and tensions of the nylon-cords investigated by observation are shown in Table 2. In the case of the Knee-AM, Cords T, F and P were weakly stretched at -90° of flexion angle. When the Knee-AM started to extend, the lateral and the medial plateaus started to slide toward anterior, the tension of Cord T increased until the full extension, and Cord P became loose. Around -20° of flexion angle, Cord A started to tighten, and the lateral plateau ceased to slide and began to roll. In contrast, the medial plateau kept sliding toward anterior. That difference of the motions of the lateral and the medial plateaus causes SHM⁴. Additionally, Cord F tightened with the roll of the lateral plateau. At the full extension, Cords T, F and A strongly tightened, and the tibial model became fixed state on the femoral model. This means that the phenomenon which the knee was locked occurred in the Knee-AM.

The motion of the Knee-AM mentioned above was in agreement with that in Ref. 4 in the following points:

- (i) the lateral plateau rolls larger than the medial plateau,
- (ii) the TCL and the FCL tighten during extension,
- (iii) the ACL tighten at extended position, and the PCL tighten at flexed position.

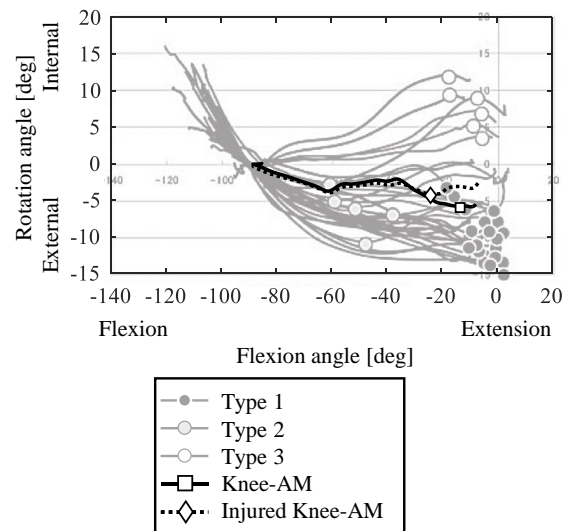


Fig. 5. Comparison of internal-external rotations during extension of Knee-AM and thirty human subjects³.

This agreement implies that the knowledge gained using the Knee-AM is valid.

On the other hand, in the case of the injured Knee-AM, the motion of lateral plateau and the tension of Cord F were different from those of the Knee-AM between -20° and 0° of flexion angle. The lateral plateau continued sliding toward anterior until the full extension, and Cord F did not strongly tighten. Thereby, the SHM did not occur, and the tibial model did not become fixed state on the femoral model at the full extension. This means that the phenomenon which the knee was locked did not occur in the injured Knee-AM.

Table 2. Time chart of tension of nylon-cords and motion of medial and lateral plateaus (WT: Weakly Tight, T: Tight, ST, Strongly Tight, L: Loose, S: Slide, R: Roll)

(a) Knee-AM

Flexion angle [$^\circ$]	-90	-20	0
Tension of Cord T	WT ↗	T ↗	ST
Tension of Cord F	WT →	WT ↗	ST
Tension of Cord A	L →	L ↗	ST
Tension of Cord P	WT ↘	L →	L
Motion of medial plateau	S	S	S
Motion of lateral plateau	S	S	R

(b) Injured Knee-AM

Flexion angle [$^\circ$]	-90	-20	0
Tension of Cord T	WT ↗	T ↗	T
Tension of Cord F	WT →	WT →	WT
Tension of Cord A		None	
Tension of Cord P	WT ↘	L →	L
Motion of medial plateau	S	S	S
Motion of lateral plateau	S	S	S

4. Conclusion

In this paper, we proposed a Knee-AM which can reproduce the IE rotation of external rotation type by rearranging the nylon-cords of our previous Knee-AM. From our investigation of the mechanism for causing the SHM by using the Knee-AM, we found that the roll of the lateral plateau tighten Cord F and that strong tightening of Cords T, F and A fixed the tibial model on the femoral model. In addition, from our simulation results of the ACL injury in the Knee-AM, we found that the lack of the ACL did not make the SHM and the locking phenomenon.

For future studies, we will investigate some roles of other ligaments by some experiments. We also plan to discuss our finding with medical personnel in regard to medical treatments, the improvement of medical technology, and other applications of the Knee-AM.

References

1. D. Yamauchi, N. Sato and Y. Morita, An Experimental Study on the Relationship between the Components and Movement of the Human Knee Using an Android Model - Measurement of Internal-External Rotation and Anterior-Posterior Tibial Translation -, in *Procs. of Int. Conf. on Control, Automation and Systems 2015* (BEXCO, Busan, 2015), pp. 811-815.
2. K. Sanaka, Android with biological structure for supporting medical technology, in *Tokai-Section Joint Conference on Electrical, Electronics, and Related Engineering* (Shizuoka Univ., Hamamatsu, 2013), S2-5. (in Japanese)
3. S. Ishii and S. Yamamoto, Kinematic Analysis of Screw Home Motion with Active Knee Extension in the Non-Weight Bearing Position, in *Rigakuryoho Kagaku*, **23**(1) (2008), pp. 11-16. (in Japanese)
4. I. A. Kapandji and E. Shiota (transl.), *Physiology of the Joints: Volume 2 Lower Limb*, 6th edn. (Ishiyaku Publishers, Inc., Tokyo, 2010), pp. 108-129. (in Japanese)

Wood Species Recognition System based on Improved Basic Grey Level Aura Matrix as feature extractor

¹Mohd Iz' aan Paiz Zamri, ¹Anis Salwa Mohd Khairuddin, ¹Norrima Mokhtar, ²Rubiyah Yusof

¹Department of Electrical Engineering, Faculty of Engineering, University of Malaya, 50603 Kuala Lumpur, Malaysia

²Malaysia Japan International Institute of Technology, Universiti Teknologi Malaysia, Kuala Lumpur Malaysia
E-mails: izanpaiz@gmail.com, anissalwa@um.edu.my

www.um.edu.my, www.fk.um.edu.my, www.mjiit.utm.my

Abstract

An automated wood species recognition system is designed to perform wood inspection at custom checkpoints in order to avoid illegal logging. The system that includes image acquisition, feature extraction and classification is able to classify the 52 wood species. There are 100 images taken from the each wood species is then divided into training and testing samples for classification. In order to differentiate the wood species precisely, an effective feature extractor is necessary to extract the most distinguished features from the wood surface. In this research, an Improved Basic Grey Level Aura Matrix (I-BGLAM) technique is proposed to extract 136 features from the wood image. The technique has smaller feature dimension and is rotational invariant due to the considered significant feature extract from the wood image. Support vector machine (SVM) is used to classify the wood species. The proposed system shows good classification accuracy compared to previous works.

Keywords: image classification, wood texture, wood species, support vector machine, pattern recognition.

1. Introduction

Traditional wood identification system which is based solely on human expertise is not practical nowadays. Several automatic wood species recognition have been developed based on spectral analysis and image analysis. The wood species identification based on the spectrum analysis involves a lot of time, money and specialists as shown in the previous research¹⁻⁶. In addition, the technique is not suitable to be applied in real life applications by non-experts and is more practical to do it in the laboratory rather than in the field. On the other hand, the image-based processing provides a simpler method in classifying the wood species. The method involves only the inspection of a cross section of the

wood surface that can be determined by human naked eye with the aid of magnifying lens. Refs. 7 and 8 develop an automatic tropical wood species recognition system to classify 20 wood species and 10 wood species respectively. In both works, Grey Level Co-occurrence Matrix (GLCM) is used as the feature extractor to extract the features from the wood texture. After the database is increased to 52 wood species the accuracy dropped to 50% indicating that the GLCM in the previous work is inadequate for large wood database. This is due to the unvaried nature of macroscopic anatomy image of the wood, but it contains a visual texture - variation of intensities which form certain repeated arrangements⁹.

© The 2016 International Conference on Artificial Life and Robotics (ICAROB 2016), Jan. 29-31, Okinawa Convention Center, Okinawa,, Japan

In order to improve the performance of the wood species recognition system, a reliable and precise feature extractor is needed. To correctly extract the wood features from the wood texture and overcome the limitations of GLCM, a new feature extractor, Improved Basic Grey Level Aura Matrix (I-BGLAM) is proposed. Support Vector Machine (SVM) is used as classifier to classify the wood species based on the feature extracted from the I-BGLAM. Several phases which consist of image acquisition, feature extraction and classification are proposed as the design of the automated wood recognition system.

2. Proposed Methodologies

The proposed wood identification system based on image analysis consists of several parts: image acquisition, feature extraction and classification. The illustration of the proposed system is shown in the Fig. 1.

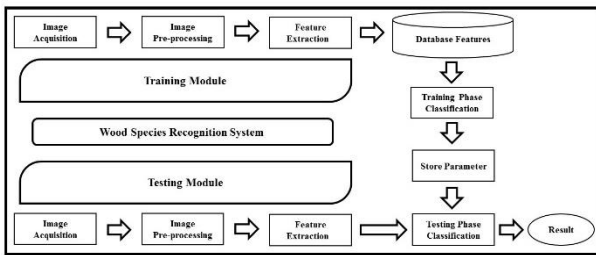


Fig. 1. Proposed wood identification system

2.1. Image acquisition

In image acquisition stage, images of wood surface are captured by a specially designed portable camera. The portable camera has 10 times magnification, which is the same specification as the magnifier used in manual wood identification process. The size of each image is 768×576 pixels.

The wood images are pre-processed using homomorphic filters to enhance the image presentation. Homomorphic filtering uses a linear filter to do a non-linear mapping to a different domain and later it is mapped back to the original domain. This algorithm reduces all unwanted illumination and reflectance on the image. Image brightness is also normalized, thus enhancing the contrast of the image. The algorithm of

homomorphic filtering is explained in more detail in Ref. 10.

2.2. I-BGLAM feature extractor

In order to overcome the limitations of the conventional BGLAM technique, an improved BGLAM feature extractor is proposed. Basically, the improved BGLAM feature extractor is rotational invariant and the size of feature dimension is reduced by considering only the discriminative features. Besides that, I-BGLAM features are directly calculated from the grey level mapping of images which overcome the limitations of GLCM.

This is done by creating a new characteristic vector which combine of the occurrence of 00 together, the occurrences of 01 and 10 together and the occurrences of 11 together.

$$[6 \text{ } 6 \text{ } 4 \text{ } 4 \mid 3 \text{ } 8 \text{ } 3 \text{ } 2 \mid 6 \text{ } 6 \text{ } 3 \text{ } 5 \mid 6 \text{ } 3 \text{ } 3 \text{ } 4] \Rightarrow [21 \text{ } 36 \text{ } 15]$$

For example,

$$6 + 3 + 6 + 6 = 21, 4 + 2 + 5 + 4 = 15 \text{ and } 6 + 4 + 8 + 3 + 6 + 3 + 3 + 3 = 3$$

This is how a 32 feature vector BGLAM becomes a 3 feature vector invariant to image rotation. The number of I-BGLAM features depends only on the grey level segmentation as shown in Eq. (1):

$$N_f = \frac{GL \times (GL + 1)}{2} \quad (1)$$

Where N_f is the number of features and GL represents grey level.

Consequently, the number of features becomes less at the same time. In this research, the numbers of grey level experimented is 2, 4, 8, 16. Finally, a grey level of 16, which gives 136 features is chosen for the final experiment because it gives the highest classification accuracy compared to other grey levels.

2.3. Classification

The classification process is performed by training a classifier model that works by differentiating features of the class of observed collected data. Support Vector Machine (SVM) is a useful tool as a learning algorithm

in analyzing and recognizing data. Previous works in Refs. 11-17 shows that the implementation of SVM classifier result to high classification rate.

3. Results and Discussion

The experiment was conducted by using 90 training samples and 10 test samples for each wood species and is repeated for 30 iterations. From the result obtained (Table 1), the classification accuracy for training samples for all set showed 100% in accuracy. The computed training accuracy showed that SVM is able to train the training model and identify the trained data in training samples database accurately. The classifier managed to classify the test samples with an average accuracy of 99.84 ± 0.23 % for 52 wood species.

Table 1. Average classification accuracy

Set	Classification accuracy (%)
Train	100
Test	99.84 ± 0.23

The proposed system showed an increment in test accuracy compared to the previous works done shown in the Table 2.

Table 2. Previous works on wood species recognition system based on image texture

Ref.	No of species (No of samples)	Texture feature (No of features)	Classification accuracy (%)
7	20 (1949)	GLCM (20)	95.00
17	7(101)	Image segmentation (5)	93.00
18	5 (250)	GLCM (20)	72.00
19	11 (347)	GLCM (24), Color (18)	82.00
20	22 (1270)	GLCM (24), Color (18)	80.80
21	25(1250)	GLCM (124)	68.40
22	10 (1000)	GLCM (3)	95.00
23	25 (500)	GLCM (44)	92.60
24	20 (2010)	Gabor filters-GLCM (200)	91.00

25	30 (3000)	Gabor filters-GLCM (200), Gabor filters (80),GLCM(20)	90.33
----	-----------	---	-------

4. Conclusion

The classification of features extracted from I-BGLAM using SVM classifier shows an improvement in the classification accuracy compared to previous proposed systems. The features extracted from the wood species using I-BGLAM as feature extractor are more distinct, thus improved the accuracy of the wood recognition system. In future, an advance wood recognition system is needed to overcome the size of wood database and able to differentiate the wood species that contain more likely features with each other. A robust feature extractor that capable to extract the most discriminant features from the wood texture is the aim for development in future.

Acknowledgements

The authors would like to thank Malaysian Ministry of Higher Education (MOHE) and University of Malaya for funding this research through High Impact Research Grant (UM.C/HIR/MOHE/ENG/16) and BKP Grant (BK047-204). The authors also would like to thank Forest Research Institute of Malaysia (FRIM) for providing us with the wood samples. The first author would like to thank to Ministry of Higher Education (MOHE) for awarded him MyMaster scholarship.

References

1. Fuentealba, C., et al. *Wood products identification by internal characteristics readings*. in *Industrial Technology, 2004. IEEE ICIT'04. 2004 IEEE International Conference on*. 2004. IEEE.
2. Choffel, D. *Automation of wood mechanical grading: coupling of vision and microwave devices*. in *Photonics East'99*. 1999. International Society for Optics and Photonics.
3. Piuri, V. and F. Scotti, *Design of an automatic wood types classification system by using fluorescence spectra*. Systems, Man, and Cybernetics, Part C: Applications and Reviews, IEEE Transactions on, 2010. 40(3): p. 358-366.

4. Baas, P., E. Wheeler, and M. Chase, *Dicotyledonous wood anatomy and the APG system of angiosperm classification*. Botanical Journal of the Linnean Society, 2000. 134(1-2): p. 3-17.
5. Rojas, J., et al., *Wood species identification using stress-wave analysis in the audible range*. Applied Acoustics, 2011. 72(12): p. 934-942.
6. Puttonen, E., et al., *Tree species classification from fused active hyperspectral reflectance and LIDAR measurements*. Forest Ecology and Management, 2010. 260(10): p. 1843-1852.
7. Khalid, M., et al., *Design of an intelligent wood species recognition system*. International Journal of Simulation System, Science and Technology, 2008. 9(3): p. 9-19.
8. Bremananth, R., B. Nithya, and R. Saipriya. *Wood species recognition using GLCM and correlation*. in *Advances in Recent Technologies in Communication and Computing, 2009. ARTCom'09. International Conference on*. 2009. IEEE.
9. Petrou, M. and P.G. Sevilla, *Image Processing. Texture: Dealing with Texture*. 2006, Wiley John and Sons.
10. Gonzalez, R.C. and R.E. Woods, *Digital image processing 3rd edition*. 2007, Prentice Hall.
11. Martins, J., et al., *A database for automatic classification of forest species*. Machine Vision and Applications, 2013. 24(3): p. 567-578.
12. Martins, J., et al., *Forest species recognition based on dynamic classifier selection and dissimilarity feature vector representation*. Machine Vision and Applications, 2015. 26(2-3): p. 279-293.
13. Paula Filho, P.L., et al., *Forest species recognition using macroscopic images*. Machine Vision and Applications, 2014. 25(4): p. 1019-1031.
14. Yadav, A.R., et al., *Multiresolution local binary pattern variants based texture feature extraction techniques for efficient classification of microscopic images of hardwood species*. Applied Soft Computing, 2015. 32: p. 101-112.
15. Hji, W., et al., *Wood recognition using image texture features*. PloS one, 2013. 8(10): p. e76101.
16. Turhan, K. and B. Serdar, *Support vector machines in wood identification: the case of three Salix species from Turkey*. Turk J Agric For, 2013. 37: p. 249-256.
17. Mallik, A., et al., *Classification of wood micrographs by image segmentation*. Chemometrics and intelligent laboratory systems, 2011. 107(2): p. 351-362.
18. Tou, J.Y., P.Y. Lau, and Y.H. Tay. *Computer vision-based wood recognition system*. in *Proceedings of International Workshop on Advanced Image Technology*. 2007. Citeseer.
19. de Paula Filho, P.L., L.S. Oliveira, and A.S. Britto Jr. *A database for forest species recognition*. in *Proceedings of the XXII Brazilian Symposium on Computer Graphics and Image Processing*. 2009.
20. Filho, P.L.P., et al. *Forest Species Recognition Using Color-Based Features*. in *Pattern Recognition (ICPR), 2010 20th International Conference on*. 2010.
21. Hasan, A.F., et al., *Application of Binary Particle Swarm Optimization in Automatic Classification of Wood Species using Gray Level Co-Occurrence Matrix and K-Nearest Neighbor*. Int. J. Sci. Eng. Res, 2013. 4: p. 50-55.
22. Mohan, S., K. Venkatachalapathy, and P. Sudhakar, *An Intelligent Recognition System For Identification Of Wood Species*. Journal of Computer Science, 2014. 10(7): p. 1231-1237.
23. Yadav, A.R., et al. *Classification of hardwood species using ann classifier*. in *Computer Vision, Pattern Recognition, Image Processing and Graphics (NCVPRIPG), 2013 Fourth National Conference on*. 2013. IEEE.
24. Yusof, R., N.R. Rosli, and M. Khalid. *Tropical wood species recognition based on Gabor filter*. in *Image and Signal Processing, 2009. CISP'09. 2nd International Congress on*. 2009. IEEE.
25. Yusof, R., N.R. Rosli, and M. Khalid. *Using gabor filters as image multiplier for tropical wood species recognition system*. in *Computer Modelling and Simulation (UKSim), 2010 12th International Conference on*. 2010. IEEE.

Evaluation the Performance of a New Quadrotor Model Based on the Arm's Length Variation

Yasameen Kamil N.¹, D. Hazry², Khairunizam Wan³, Zuradzman M.Razlan⁴

^{1,2,3,4} *School of Mechatronic Engineering, University Malaysia Perlis (uniMAP)
026000Arau, Perlis, Malaysia*

^{1,2,3,4} *Centre of Excellence for Unmanned Aerial System (COEUAS), University Malaysia Perlis (uniMAP)
01000Kangar, Perlis, Malaysia*

E-mail: ¹moonom2002@gmail.com, ²hazry@unimap.edu.my, ³khairunizam@unimap.edu.my

Abstract

The field of UAV has exceptional level of growth; in addition it is predictable to be one of the most prevalent fields of development and research in future. The unmanned aerial vehicle (UAV)- quadrotor widely used as a service robotic in several fields. This paper presents a new design of this miniature aerial vehicle in altitude and attitude movements, based on varying the arm's length of quadrotor instead of varying the speed of motors to obtain a rotation around each axes. The length of arms varying are achieved by fixing a stepper motor in each arm of quadrotor to increase or decrease the length of these arms according to controller command for attitude movement. The controller commands are accomplished by designing a PID controller with specific parameters to maintain the stability of the quadrotor in the flight path. A MATLAB software code used to evaluate the simulation results and demonstrate the ability of the proposed design to perform a mission.

Keywords: arm's length; PID controller; quadrotor, trajectory tracking, UAV.

1. Introduction

The autonomous miniature aerial vehicle has attracted the interest of researchers and represents a challenge in the world of Unmanned Aerial Vehicle (UAV) from few years ago. One of the UAV is the quadrotor, which has an endless list of applications in civil, military and commercial. Therefore, the quadrotor included the tasks of search rescue, fire monitoring in the forest, the inspection in contaminated with nuclear radiation areas, where human pilot not desirable to be there. The quadrotor is underactuated nonlinear system [1]. It has exceptional advantage over helicopter and other multi-rotor aerial vehicle according to its simple mechanical arrangement, weight, size, minimum cost and without any risk to human life [2], and it has the ability to

payload. Major disadvantage in quadrotor is the consumption of energy [1] this means the lower endurance for life time.

The conventional quadrotor structure comprises of four motors which are arranged such that two motors rotate counter clockwise in frontal and rear, and other two motors in the lateral rotate clockwise. This arrangement of motors achieves stability in hover and the total momentum of the system equiponderant [3]. Many methods have been proposed to develop the quadrotor model and validation. In [4], the structure of quadrotor was comprised of four propellers, three of them were horizontally placed to control the roll and pitch whereas the fourth was vertically placed to control the yaw rotation. . But the authors conclude that the dynamic model was difficult to derive and cannot get

©The 2016 International Conference on Artificial Life and Robotics (ICAROB 2016), Jan. 29-31, Okinawa Convention Center, Okinawa, Japan

the accurate model. In [5], a new design for quadrotor was presented by tilting propellers to solve the problem of under- actuated system. In which the normally fixed propellers are permitted to tend about the body axes of quadrotor.

Another papers adopted the controller design to achieve the stability of quadrotor. In [1] the altitude and yaw channel are controlled by using PD controller and backstepping based on PID are used to control the attitude. In [6] the PID controller is used for developing the stability of pitch, roll, yaw and altitude of the vehicle. Unfortunately, the system contains some transient overshoot because of disturbance and some other reasons like some certain of mechanical parameter and simplification of the controller. . In [7], the position and altitude of quadrotor are controlled by using PID controller in the condition of wind gust and conclude that the controller worked effectively under this condition. In [8], the PID based on feedback linearization combined with block control technique are used for controlling the position of quadrotor. This technique mathematically complex may have some fault in the mathematical model leads to a fault in the design, and the performance of the system is slow.

In this paper, a new model for quadrotor attitude is proposed based on varying the length of arms to generate variable torque without altering the motors' speed. This torque has the ability to rotate the attitude angles of quadrotor to the desired orientations and keeping quadrotor balance. Varying the arms' length have been done by using stepper motor in each arm to increase or decrease the length of arm depending on controller command. The PID controller is used to control the altitude, attitude, and position movements for stabilization requirement of quadrotor.

The rest of the paper is arranged as, section 2 shows the conventional quadrotor design, section 3 the proposed quadrotor design, section 4 presents the dynamic model of quadrotor, section 5 presents the control strategy which include the altitude, attitude, and position controller algorithm, section 6 included the simulation results and finally, section 7 included the conclusion.

2. Conventional Quadrotor Design

The conventional quadrotor consist of four motors fixed on the end of a cross frame and motors speed are

controlled to produce a lift force [3]. Quadrotor is under-actuated nonlinear system with four input forces and six output motions. Each motor produces torque and force, the collection of all motors are produced the main thrust, the pitch torque, the roll torque and the yaw torques. The force generated from each motor f_i is proportional to the square of the angular velocity ω^2 , such that $f_i=k(\omega_i)^2$, where $k > 0$ and constant.

Finally, the front motor (m_1) and the rear motor (m_3) rotate counter clockwise (C.C.W). The right motor (m_2) and the left (m_4)are rotated clockwise (C.W). This arrangement in motors' rotation is to maintain balance [2]. The transitional and rotational movements of conventional quadrotor are illustrated clearly in [9].

3. Proposed Quadrotor Design

The quadrotor faces many problems, the main problem is the consumption energy during flight and maneuverability due to varying the speed of four motor. Where, at least the speed of one motor must be increased to perform rotational movements, this mean lower endurance time. Herein, for roll rotational movement about the x-axis, the arms length related to lateral motors; one of them must be increased and another must be decreases as shown in Fig.1(c) and (d). The other two motors in frontal and rear must be fixed at the same length while the speed of four motors will be fixed. In the same manner, to achieve the pitch rotational movement about the y-axis, but the arms' lengths related to frontal and rear motors must be varying, whereas the arms lengths related to lateral motors must be fixed as shown in Fig.1 (a) and (b).

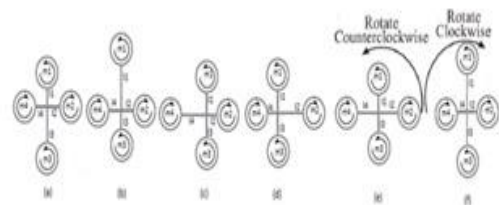


Fig. 1. Quadrotor's motion due to the proposed design

The yaw rotational movement achieved by increasing the arm's length of two motors and decreasing the arm's length of two other motors with fixed the speed of the

four motors. When the propeller rotate (C.W) then it is generates a torque in (C.C.W). The quadrotor rotates in the direction of the greater torque as shown in Fig.1(e). This approach done by using stepper motor fixed in each arm which produces stepping rotation, the arm's length varying due to the stepping rotate of the stepper motors, when the stepper motor rotate (C.C.W) the arm's length increased and when the stepper motor rotate (C.W) the arm's length decreased [10].

The stepper motor fixed inside the fixed arm at a specific distance, the sliding arm is connected with the rotate shaft of the stepper motor. Therefore, when the stepper motor controlled to produce step rotate in C.W the sliding arm is sliding out of the fixed arm to increase the quadrotor total arm, if the stepper motor shaft rotate C.C.W the sliding arm is sliding inside the fixed arm and the total arm length will decrease.

Consequently, the increasing and decreasing in the arms length implemented according to the Eq.(1) and Eq.(2). The arms that increased will have maximum length and the arms that decreased will have the minimum length as illustrated in [10]

$$(l_f + l_m + L) + \Delta d. (l_f + l_m) = \text{maximum length} \quad (1)$$

$$(l_f + l_m + L) - \Delta d. (l_f + l_m) = \text{minimum length} \quad (2)$$

Where l_f is the fixed arm, l_m is the diameter of the motor, $(L + l_f + l_m)$ represent the normal arm, L is specific length to ensure the freely movement in sliding arm, Δd the rate of change in the sliding arm

4. Dynamic Model of Quadrotor

The motion of any rigid body in space can be represented by rotational and translational motions [3]. Quadrotor is nonlinear system with (6_DOF) and only four inputs which are motor speed, 3-translational and 3-rotational motion as shown in Fig 2.

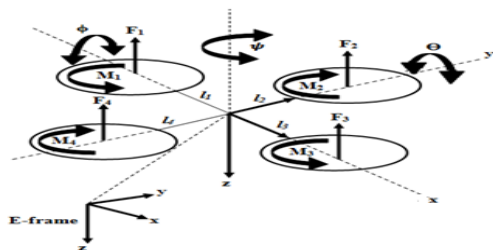


Fig. 2. Quadrotor coordination

The thrust force and control torque which acting on the quadrotor body is generated by the propellers rotation. The dynamic equations of quadrotor in the body frame are extracted from Newton- Euler form as in [8].

$$\begin{aligned} m \ddot{x} &= u_1 (\sin \phi \sin \psi + \cos \phi \sin \theta \cos \psi) - k_1 \dot{x} \\ m \ddot{y} &= u_1 (-\sin \phi \cos \psi + \cos \phi \sin \theta \sin \psi) - k_2 \dot{y} \\ m \ddot{z} &= u_1 (\cos \phi \cos \theta) - mg - k_3 \dot{z} \\ I_x \ddot{\phi} &= (I_y - I_z) \dot{\theta} \dot{\psi} + u_2 - k_4 \dot{\phi} \\ I_y \ddot{\theta} &= (I_z - I_x) \dot{\phi} \dot{\psi} + u_3 - k_5 \dot{\theta} \\ I_z \ddot{\psi} &= (I_x - I_y) \dot{\phi} \dot{\theta} + u_4 - k_6 \dot{\psi} \end{aligned} \quad (3)$$

Where m represents the body mass of quadrotor, $I = \text{diag}(I_x, I_y, I_z)$ represents the moment of inertia, x represents the linear position, the input vectors to the conventional quadrotor are defined as in [7]

$$\left. \begin{aligned} u_1 &= b(\omega_1^2 + \omega_2^2 + \omega_3^2 + \omega_4^2) \\ u_2 &= b.l(\omega_3^2 - \omega_1^2) \\ u_3 &= b.l(\omega_4^2 - \omega_2^2) \\ u_4 &= d(\omega_2^2 + \omega_4^2 - \omega_1^2 - \omega_3^2) \end{aligned} \right\} \quad (4)$$

Where u_1, u_2, u_3 , and u_4 are representing the input vectors to the quadrotor system, b represents the thrust coefficient, d represents the drag coefficient. According to the assumptions are mentioned in [11].

The quadrotor proposed design depends on varying the arms' lengths of motors and fixing the angular velocity. Therefore, the same thrust and drag coefficients from all motors are obtained; this means $(b_1=b_2=b_3=b_4)$, $(d_1=d_2=d_3=d_4)$. The change in the arms length produces variable torque around the aircraft center of mass. Thus, the induced torque is oriented the quadrotor to the desired attitude even the rotors speed are fixed to be constant. The total torques influential on the conventional quadrotor rotation are expressed as in [12] whereas in the proposed design will be derived as in [10]. Then the input vectors will be expressed as:

$$\left. \begin{aligned} u_1 &= b(\omega_1^2 + \omega_2^2 + \omega_3^2 + \omega_4^2) \\ u_2 &= b.\omega^2(-l_2 + l_4) \\ u_3 &= b.\omega^2(-l_1 + l_3) \\ u_4 &= d.\omega^2(-l_1 - l_3 + l_2 + l_4) \end{aligned} \right\} \quad (5)$$

Where l_i represents the arms length related to each motor.

5. Control Strategy

The quadrotor requires a stable and robust controller during the maneuverability and flight path [7]. In this paper a PID controller is applied in altitude, attitude and position.

The parameters of PID are adjusted to a specific value to reach steady state system. The equation of PID defined mathematically [7] as

$$u(t) = k_p e(t) + k_i \int e(t)dt + k_d \frac{de(t)}{dt} \quad (6)$$

where k_p , k_i , k_d are the proportional, integral, and the derivative gain respectively [6], $e(t)$ is the error signal which is the difference between the desired value and the measured value

5.1. Altitude controller algorithm

The quadrotor must be at desired value from the ground to maintain this distance the altitude controller is used [7]. Therefore, the quadrotor lift force must be greater than its weight and the earth's gravity to keep the quadrotor at hovering and take-off. This can be done by working on quadrotor z-axis from Eq.(3) and made x and y axis constant.

$$\ddot{z} = g - (\cos\theta \cos\phi) \frac{u_1}{m} \quad (7)$$

In the above equation, θ and ϕ must be 0 for hovering [13] and by solving the differential equation to obtain the value of z. The error signal in altitude is $e_z = z_{ref} - z$, where, z_{ref} is the desired and z is measured output this applied in Eq. (6) to obtain the PID controller equation.

5.2. Attitude controller Algorithm

Quadrotor attitude controlled the angles of orientation pitch, roll, and yaw. In this paper we present only the yaw angle and only choose yaw differential equation from Eq. (3).

$$\ddot{\psi} = \frac{u_4}{I_z} - \frac{k_6}{I_z} \dot{\psi} \quad (8)$$

By solving the differential equation can obtain ψ as the output value, so the control design for the error signal will be: $e_\psi = \psi_{ref} - \psi$ Where ψ_{ref} the desired value and ψ is the measured output signal. This applied in Eq.(6) to get the PID controller equation. At the same manner, other attitude angle (e.g Roll and itch) can be derived.

5.3 Position controller algorithm

This controller responsible for movement in x and y-axis, this movement achieved by rolling or pitching the quadrotor, the x and y equation are considered from Eq. (3) to achieve these movements.

$$\left. \begin{aligned} \ddot{x} &= -\frac{u_1}{m} (\sin\phi \sin\psi + \cos\phi \sin\theta \cos\psi) \\ \ddot{y} &= \frac{u_1}{m} (\sin\phi \cos\psi - \cos\phi \sin\theta \sin\psi) \end{aligned} \right\} \quad (9)$$

Assume a small angle for pitching and rolling [11]. The error signal to position controller will be

$$\begin{aligned} e_x &= x_d - x \\ e_y &= y_d - y \end{aligned} \quad (10)$$

Then, apply Eq. (10) in Eq. (6) to get the controller input which applied in Eq. (9)

6. Simulation results

The physical parameter used in simulated the result are the same used in [6]: $m = 2$ kg, $g = 9.81$ m/s², $I_x = I_y = 1:25$ Ns²/rad, $I_z = 2:5$ Ns²/rad, $K_1 = K_2 = K_3 = 0:01$, Ns/m, $K_4 = K_5 = K_6 = 0:012$ Ns/rad. While the chosen of the appropriate arms length as in table 1.

Table.1 Arm's length variation parameter

l_f	l_m	L (cm)	Δd	Maximum length(cm)	Minimum
-------	-------	--------	------------	--------------------	---------

(cm)	(cm)				length(cm)
17.5	2.5	5	0.25	30	20

The result shown in Fig.3 presents the performance of quadrotor and demonstrates the trajectory tracking. The path tracking include the take-off and landing of quadrotor and the way point that the quadrotor tracked are illustrated in the Fig.3.

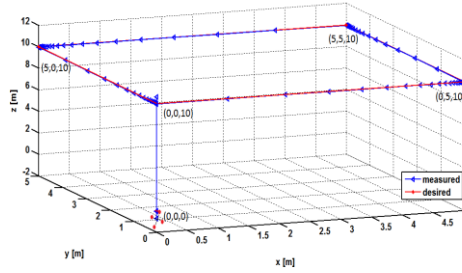


Fig.3. The path followed by quadrotor

Fig. 4 illustrated the altitude and hovering position by applying PID controller while Fig. 5 and Fig. 6 illustrated the x-position and the pitch angle respectively, when the quadrotor oriented to the desired x-position, the pitch angle change its state due to this orientation. In the same manner, Fig. 7 illustrated the y-position and Fig. 8 demonstrated the roll angle which changes its state due to y-position.

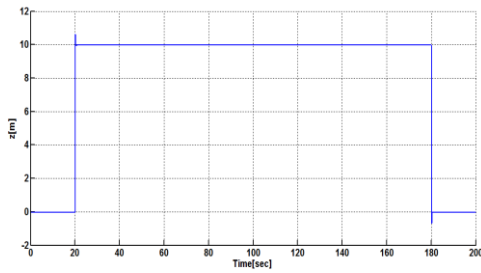


Fig.4 the z-position

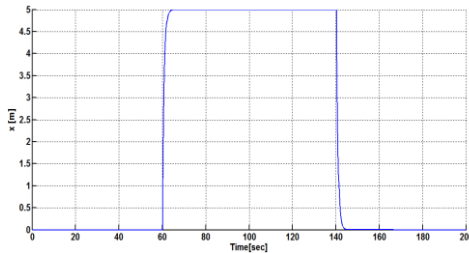


Fig.5. The x-axis position

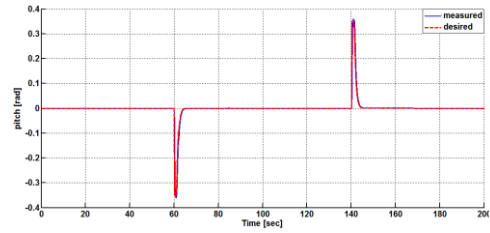


Fig. 6. The pitch angle

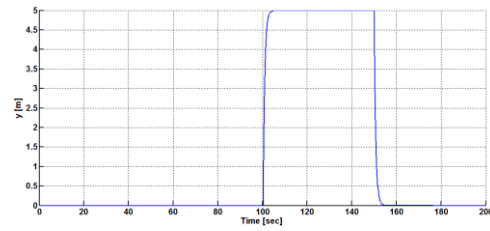


Fig. 7. The y-position

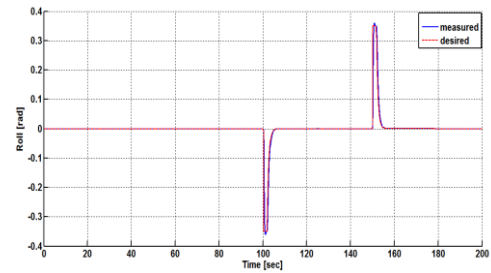


Fig. 8. The roll angle

7. Conclusion

In this paper, a new design of quadrotor is proposed depends on varying the arms length instead of varying the motors speed for performing the maneuverability. The PID controller is used in altitude, attitude, and position movements to control the stability of the system. The mathematical model of the proposed design is modeled. The simulation results evaluated the effectiveness of the proposed design with control strategy to improve the system performance.

References

1. A. Azzam and X. Wang, "Quad rotor arial robot dynamic modeling and configuration stabilization," in *Informatics in Control, Automation and Robotics (CAR), 2010 2nd*
2. A. R. Patel, M. A. Patel, and D. R. Vyas, "Modeling and analysis of quadrotor using sliding mode control," in

Robotics (ICAROB 2016), Jan. 29-31, Okinawa Convention Center, Okinawa, Japan

- System Theory (SSST)*, 2012 44th Southeastern Symposium on, 2012, pp. 111-114.
3. L. R. G. Carrillo, A. E. D. López, R. Lozano, and C. Pégard, "Modeling the Quad-Rotor Mini-Rotorcraft," in *Quad Rotorcraft Control*, ed: Springer, 2013, pp. 23-34.
 4. J. Wu, H. Peng, and Q. Chen, "RBF-ARX model-based modeling and control of quadrotor," in *Control Applications (CCA)*, 2010 IEEE International Conference on, 2010, pp. 1731-1736.
 5. M. Ryll, H. H. Bulthoff, and P. R. Giordano, "A Novel Overactuated Quadrotor Unmanned Aerial Vehicle: Modeling, Control, and Experimental Validation," *Control Systems Technology, IEEE Transactions on*, vol. 23, pp. 540-556, 2015.
 6. A. L. Salih, M. Moghavvemi, H. A. Mohamed, and K. S. Gaeid, "Modelling and PID controller design for a quadrotor unmanned air vehicle," in *Automation Quality and Testing Robotics (AQTR)*, 2010 IEEE International Conference on, 2010, pp. 1-5.
 - LENGTH VARIATION," *Journal of Theoretical & Applied Information Technology*, vol. 79, 2015.
 11. A. Nagaty, S. Saeedi, C. Thibault, M. Seto, and H. Li, "Control and navigation framework for quadrotor helicopters," *Journal of Intelligent & Robotic Systems*, vol. 70, pp. 1-12, 2013.
 12. A. A. Mian and W. Daobo, "Modeling and backstepping-based nonlinear control strategy for a 6 DOF quadrotor helicopter," *Chinese Journal of Aeronautics*, vol. 21, pp. 261-268, 2008.
 13. M. H. Tanveer, D. Hazry, S. F. Ahmed, M. K. Joyo, and F. A. Warsi, "Design of overall Stabilized controller for Quad-rotor."
 7. M. K. Joyo, D. Hazry, S. Faiz Ahmed, M. H. Tanveer, F. Warsi, and A. Hussain, "Altitude and horizontal motion control of quadrotor UAV in the presence of air turbulence," in *Systems, Process & Control (ICSPC)*, 2013 IEEE Conference on, 2013, pp. 16-20.
 8. H. K. Kim, T. T. Nguyen, S. J. Oh, and S. B. Kim, "Position Control of a Small Scale Quadrotor Using Block Feedback Linearization Control," in *AETA 2013: Recent Advances in Electrical Engineering and Related Sciences*, ed: Springer, 2014, pp. 525-534.
 9. R. Cavalcante Sa, A. L. C. De Araujo, A. T. Varela, and D. A. Barreto, "Construction and PID Control for Stability of an Unmanned Aerial Vehicle of the Type Quadrotor," in *Robotics Symposium and Competition (LARS/LARC)*, 2013 Latin American, 2013, pp. 95-99.
 10. Y. KAMIL N, D. HAZRY, K. WAN, and Z. M. RAZLAN, "TRAJECTORY TRACKING BASED ON ARM'S

Discussion on Factors Influencing the Performance of Hospital Renovation Engineering - Taking one Medical Center in Taiwan as Example

Wen-Lung Lin, Yan-Chyuan Shiau*, Ting-Chi Lai and Chen-Chung Liu

Department of Construction Management, Chung Hua University

707, WuFu Rd., Sec. 2, Hsinchu 30012, Taiwan

E-mail: E10216015@chu.edu.tw; *ycshiau@ms22.hinet.net; E10416007@chu.edu.tw; E10416003@chu.edu.tw

Abstract

The subjects of this study were to investigate the renovation engineering case of four hospital areas in Mackay Memorial Medical Center in Taiwan. The rank of each factor's influencing severity and influencing performance in four stages for hospital renovation engineering was summarized. The factors' severity rank influencing the performance in the four stages were planning and design stage, construction management stage, bidding stage and case acceptance and closing stage. The conclusions and suggestions of this study can be used as reference for future hospital renovation projects.

Keywords: Hospital Building, Hospital Refurbishment Projects, Likert Scale, Questionnaire

1. Introduction

1.1. Background

A hospital building is a complex integration of versatile professional disciplines; in addition to general building facilities, the scope includes a steady supply of medical gas (A.V.O) system, fast gas transfer system, safety protection for radiation therapy and nuclear medicine, provision of highly clean air quality of hospital quality (for the OR, supply room, burn center and laboratory), steady medical power supply, safe and clean water supply for the kidney dialysis room, negative pressure ward and positive pressure ward, IT equipment room, medical wastewater treatment plant, movement stream lines of clean objects and contaminated objects, security facilities of psychiatric wards; all the tasks, from refurbishment proposal, planning and design, tender invitation and awarding, construction management, acceptance inspection and case closure, to development of operation procedures, are included in this domain. Therefore, refurbishment of hospital facilities concerns a management science that combines complexity and professionalism.

1.2. Health care classification in Taiwan

National health insurance in Taiwan classifies medical care institutes into 4 levels (Fig. 1): Medical Centers of the regional level, regional hospitals of the regional level, local hospitals of the local level and basic health care units of locality level [2].

2. Hospital Refurbishment Project

2.1. Planning and precautions in hospital constructions

A hospital is highly professional and widely encompassing medical care installation that takes care of birth, aging, illness and death. There are delivery rooms, nurseries, labs, mortuaries, ORs, out-patient and emergency clinics, kitchens, canteens, post office, bank, barber shop, beauty parlor, sewage treatment plant, incinerator, etc., it is like a small community that requires collaboration of various professionals for achieving its perfection. The Public Construction Commission (PCC) of the Executive Yuan requires that when an entity undergoes a project of public

hospital or health center, reference must be made to “Operation Handbook for Public Buildings of Government Entities” [3] promulgated by PCC, in combination with compliance to medical care requirements, for enhancing engineering quality of the public medical care institutes. PCC has also set forth precautions for carrying out construction projects of public medical care institutes.

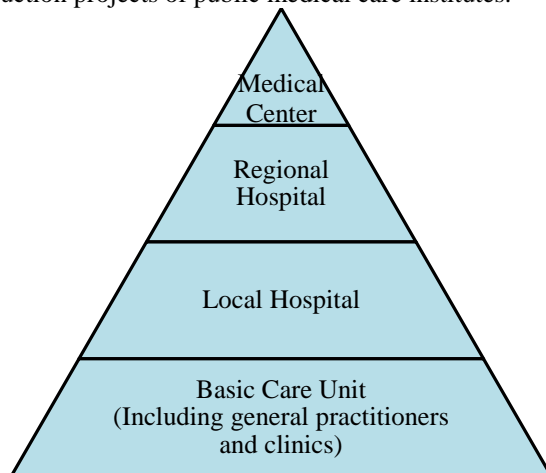


Figure1 Classification of Health Care Institutions

2.2. A study on the current status of hospital construction management

Hospitals have the most complicated spatial functionalities of all types of constructions. Via reference docu-

ments, theories, and years of personal experience in practicing design and supervision of hospital refurbishments, the author discusses critical constructional phases that affect the refurbishment, aiming to improve the quality of hospital refurbishments. The study compiles and proposes 38 performance affecting factors that may affect the refurbishment. Performance affecting factors are screened via interview and questionnaire given to 8 experts including a supervisor, auditor, labor safety officer, architect, contractor, etc., who have participated in constructions.

3. Investigation and Analysis Against Performance Affecting Factors

The study takes the refurbishment projects of a medical center in Taiwan as case study subject. Four stages of construction life cycle are concluded as Planning and Design, Tender Invitation and Awarding, Construction Management, and Acceptance Inspection or Case Closure. Performance Affecting Factors of Interview results are shown in Tables 1 to 4.

Table 1. Performance Affecting Factors at Planning and Design Stage

No.	Performance Affecting Factor	Expert								Total
		1	2	3	4	5	6	7	8	
A1	Unclear investigation of function requirements of the user unit (such as power system, air-conditioning system, etc.)	✓	✓	✓	✓	✓	✓	✓	✓	8
A2	Only CAD plotted drawings of the refurbished area are provided without actual survey of the site.	✓	✓	✓	✓	✓	✓		✓	7
A3	The user unit cannot fully comprehend the design drawing, and no sufficient communication has been made.	✓	✓	✓	✓		✓		✓	6
A4	Dimensions and space for handling movement of medical care facilities are not sufficiently considered in the planning.	✓	✓	✓	✓		✓		✓	6
A5	Drawings are not plotted for integration (such as architecture system, E&M System, air-conditioning system, gas transfer system, etc.).	✓	✓	✓	✓		✓	✓	✓	7
A6	Elevators are not located based on classified transfer of contaminated objects, wastes and relevant recycling resources.	✓	✓	✓	✓		✓		✓	6
A7	Poor design of soundproof materials of special clinic rooms or inspection units, affecting examination results (e.g., hearing examination, language therapy, consultation room).	✓	✓	✓	✓		✓		✓	6
A8	UPS system for medical care facilities not isolated from that for IT system, therefore causing interferences.	✓	✓	✓	✓		✓		✓	6
A9	Space for maintenance access of facilities not considered.		✓	✓	✓		✓		✓	5
A10	Improper material design and poor material quality causing maintenance difficulties.	✓	✓	✓	✓		✓	✓	✓	7
A11	No integrated planning given for treatment plant and space for infective wastewater and general wastewater.	✓	✓	✓	✓		✓		✓	6
Number of pros for inclusion		10	11	11	11	2	11	3	11	

Table 2 Performance Affecting Factors at Tender Invitation and Awarding Stage

No.	Performance Affecting Factor	Expert								Total
		1	2	3	4	5	6	7	8	
B1	Drawings of tender invitation document not fully cross-checked.	✓	✓	✓	✓		✓	✓	✓	7
B2	Improper definition of supplier qualification.	✓	✓	✓	✓	✓	✓	✓	✓	8
B3	Tenderer qualification not fully ratified prior to tender open.	✓	✓	✓	✓		✓		✓	6
B4	Inconsistencies in tender documents, drawings and specifications.	✓	✓	✓	✓		✓		✓	6
B5	Unclear inspection standards for work items, materials and facilities in tender documents.	✓	✓	✓	✓		✓		✓	6
B6	Irrational construction period.	✓	✓	✓	✓		✓		✓	6
B7	Improper price for work items.	✓	✓	✓	✓		✓		✓	6
	Number of pros for inclusion	7	7	7	7	1	7	2	7	

Table 3 Performance Affecting Factors at Construction Management Stage

No.	Performance Affecting Factor	Expert								Total
		1	2	3	4	5	6	7	8	
C1	Improper quality supervision of the project executive entity.	✓	✓	✓	✓		✓	✓	✓	7
C2	Lack of experience of outsourced supervisor; lack of experience in supervising medical care constructions.	✓	✓	✓	✓	✓	✓	✓	✓	8
C3	Supervising unit fails to implement construction review plan and quality plan.	✓	✓	✓	✓		✓		✓	6
C4	Contractor autonomous inspection not fully implemented.	✓	✓		✓	✓	✓		✓	6
C5	Contractor defect follow-up and remedial/preventive measures not fully implemented.	✓	✓	✓	✓	✓	✓		✓	7
C6	Review and plotting of pipeline systems not carried out prior to construction, resulting in disordered pipelines that affect spatial usage of the hospital.	✓	✓	✓	✓	✓	✓	✓	✓	8
C7	Pipelines are not identified with color code and flow direction.	✓	✓	✓	✓		✓		✓	6
C8	Air-conditioning ducts not sealed, resulting in contamination inside the duct.	✓	✓	✓	✓		✓		✓	6
C9	Emergency plugs not color coded for discriminating from general ones.	✓	✓	✓	✓		✓		✓	6
C10	Pipelines go through internal walls in the ceiling of isolated ward, damaging air-tightness of the isolated ward.	✓	✓	✓	✓		✓		✓	6
C11	Proper sealant not provided at openings where pipeline goes across fire zones.	✓	✓	✓	✓		✓		✓	6
C12	Improper location or lack of cleaning openings and vents of sewers and drainage pipelines.	✓	✓	✓	✓		✓		✓	6
C13	Insufficient firefighting facilities on the construction site.	✓	✓	✓	✓		✓		✓	6
C14	Excessive number of supporting suppliers resulting in interfacing difficulties that affect general completion date of the project.	✓	✓	✓	✓	✓	✓		✓	7
C15	Slow design change process that severely affects construction progress.	✓	✓	✓	✓	✓	✓		✓	7
C16	Failure to control critical path operation resulting in lag of construction progress and lacking an effective countermeasure.	✓	✓	✓	✓		✓	✓	✓	7
	Number of pros for inclusion	16	16	15	16	6	16	4	16	

Table 4 Performance Affecting Factors at Acceptance Inspection or Case Closure Stage

No.	Performance Affecting Factor	Expert								Total
		1	2	3	4	5	6	7	8	
D1	Failure to set up SOPs for functional test run, tests, random tests, etc.	✓	✓	✓	✓		✓	✓	✓	7
D2	Failure to provide equipment training for the hospital ADM and medical care staff.	✓	✓	✓	✓		✓		✓	6
D3	Failure to perform an integrated system test.	✓	✓	✓	✓		✓	✓	✓	7
D4	Excessive improvement deadline for acceptance inspection.	✓	✓	✓	✓	✓	✓	✓	✓	8
	Number of pros for inclusion	4	4	4	4	1	4	3	4	

4. Results

Analysis of Expert Opinion Survey is carried out mainly by using a questionnaire based on 5-point Likert Scale with the above construction Performance Affecting Factors identified by experts. Experts curve and ranking of

Performance Affecting Factors are developed for hospital refurbishment projects. The study summarizes interview and questionnaire results against 4 hospital locations as shown in Table 5. The study also compiles frequent defects seen in the refurbishing works and concludes construction Performance Affecting Factors and improve-

ment suggestions for providing valued references to practices of clients.

Table 5. Statistics of severities of Performance Affecting Factors in respective stages.

Study Subject	Stage 1	Stage 2	Stage 3	Stage 4
Taipei General Hospital	4	3	2	1
Tamsui Branch	2	1	4	3
Taitong Branch	4	3	2	1
Hsinchu Branch	4	1	3	2
Total	14	8	11	7

5. Conclusions

Via review of reference documents, study of actual construction cases, questionnaires, and integration of expert opinions, the study compiles problems in the current execution of refurbishment as follows:

- After discussing with user units at the planning and design stage, drawings have not been fully verified, resulting in confusion in the acceptance inspection, or awkwardness of modification or re-do. Respective systems were not integrated during system design, resulting in construction difficulties and subsequently design changes.
- Tender information was only available at the hospital website and bulletin boards within the hospital, suppliers were unable to acquire information from other resources, resulting in insufficient number of tenderers, which in turn resulted in failure of tender and prolonged time for contracting.
- The person-in-charge failed to demand exact compliance to specifications, such as materials not submitted for approval prior to construction, failure to implement inspection procedures at respective stages, etc.
- Excessive deadline for improving defects.

After analyzing properties of respective hospital areas and problems encountered during for carrying out works, the most severe Performance Affecting Factors at respective stages are as follows:

- Planning and Design Stage: Poor communication with relevant units, differences in demands and design, unclear investigation of function requirements of the user unit (such as power system, air-conditioning system, etc.).
- Tender Invitation and Awarding Stage: Inconsistencies in tender documents, drawings and specifications.

tions. Lack of price analysis against singular work items.

- Construction Management Stage: Contractor autonomous inspection not fully implemented. Insufficient quality supervision of the implementation entity.
- Acceptance Inspection or Case Closure Stage: Excessive improvement deadline for acceptance inspection. Failure to abide by SOPs for functional test run, tests, random tests, etc.
- Severity Ranking of Performance Affecting Factors of these 4 stages is: Tender Invitation and Awarding Stage, Construction Management Stage, Tender Invitation and Awarding Stage, and Acceptance Inspection or Case Closure Stage.

Comprehensive suggestions proposed by the study addressing the above problems are as follows:

- Strengthen communication skills of the staff at the Planning and Design Stage. Suggest setting up a communication platform for the execution unit and user unit, members of which include medical care personnel, first-line operators and heads of units. Special considerations must be given to movement streamline of the medical care, medical care facilities, and subjects requiring the service, so as to avoid differences during the acceptance inspection, and to prevent from affecting quality of medical care services.
- Tender of project must be carried out more openly with more channels. Suggest that a contractor database be established to ensure number of participating contractors and that a contractor assessment system be established for quality enhancement.
- Explicit construction specifications must be set forth at the Construction Management Stage. Suggest that the person in charge of the project demand construction quality based on contractual requirements, and that a construction inspection team must be organized.
- Set up SOPs for Acceptance Inspection.

6. References

1. Likert, R. A Technique for the Measurement of Attitudes, *Archives of Psychology*, 140, (1932) 1–55.
2. 2015 statistics of medical care institutes, Ministry of Health and Welfare, website <http://r.search.yahoo.com>.
3. Operation Handbook for Public Buildings of Government Entities, PCC, the Executive Yuan, <https://www.pcc.gov.tw>

Discussion on Land Expropriation Compensation System

Hung-Chi Liu, Yan-Chyuan Shiau*, Yao-Shan Huang and Chen-Chung Liu

Department of Construction Management, Chung Hua University

707, WuFu Rd., Sec. 2, Hsinchu, 30012, Taiwan

E-mail: E10216020@chu.edu.tw; *ycshiau@ms22.hinet.net; grace624252@gmail.com; E10416007@chu.edu.tw

Abstract

Land expropriation is a necessary means for the public construction of country. The study results show that the public in Taiwan is rather satisfied with the current land expropriation at the land market value. "Estimation of land value by real-estate estimators" and "Compensation based on values listed on the Actual Price Registration" are much accepted by the public. It is also suggested that the existing land expropriation compensation shall adjust to meet the public wish to reduce incidences of struggles and improve administrative proficiency.

Keywords: Land Expropriation Compensation, Real-estate Estimators, Compensation Standards, Construction Improvements

1. Introduction

1.1 Background

Since almost all resources of human living depend on land supply, land expropriation is often necessary in each country for the need of public works. Land expropriation contains four major elements, namely public interest, legal process, compliance to necessity and need of compensation. In case of small expropriation facing extensive resistances and conflicts, the reasons behind include public suspicion of owners' rights ignored during expropriation and mostly importantly, dissatisfaction against amount of compensation from expropriation. In order to achieve smooth expropriation that balances public and private interests, it is important to discuss from method of compensation system for expropriation, where expert's opinions are referred to draft more suitable method of land expropriation that addresses difficulties faced under current execution of

land expropriation, so mutual benefits can be obtained between the government and citizens.

1.2 Motive and Purpose of Research

Due to its compulsory nature and difficulty on defining the compensation standard, land expropriation is often criticized and opposed by landowners. Should disputes arise from compensation on land expropriation and further cause conflicts between the government and its people, the social cost is often much greater than the expense of compensation on expropriation. According to revision on Article 30 of the Land Expropriation Act in 2012[1], the method of compensation has changed from original context of "extra proportion of announced current land value upon expropriation as additional compensation" to "compensation according to current market value upon land expropriation." One of the prerequisites of land expropriation is realizing public interests; when damage to citizens' rights becomes necessary, reasonable measures shall be taken to minimize such

loss. The purpose of this research includes the following:

- Compile literature to discuss unreasonable systems and phenomenon during the operation of land expropriation.
- Use questionnaires to investigate satisfaction from the owners of land expropriated against compensation system based on current market value of expropriation.
- With reference to foreign study on compensation of expropriation, domestic experts' suggestions on compensation of expropriation are compiled for finding an improved strategy that suits the status in Taiwan.

2. Discussion on current compensation system for land expropriation in Taiwan

The content of relevant regulations to land expropriation in Taiwan was mostly duplicated from the Land Acquisition Act in Japan. To address the need of social and economic development during the period from 1980 to 1990, the government made massive investments to commence major public works and actively acquired lands needed. Since the development of relevant public facilities induced significant boost of land price at then, great difference occurred between current land price announced and market price, which caused reluctant acceptance by landowners towards compensation of expropriation. Furthermore, inconsistent compensation standard on expropriation triggered citizen opposition, which not only affected the progress of land acquisition for public works, but also caused conflicts between citizens and the government. After revision of relevant regulation in Taiwan in 2011, the compensation standard in Land Expropriation Act followed requirements under Article 30: "The value of expropriated land shall be compensated based on its current market value. The value of land reserved for public facilities in the urban planning area shall be compensated based on the average market value of its adjoining lands not reserved for public facilities. The market value referred to in the preceding paragraph shall be forwarded by the municipal or county (city) competent authority to the Land Evaluation Committee for determination." According to requirements under the Land Expropriation Act and actual situation, items qualified for compensation upon expropriation of land or land improvements include: (1) Compensation for land value; (2) compensation for construction improvements or agri-

cultural improvements; (3) compensation for paid land improvements on improved farm land that is deemed legal with possession of building license yet works terminated; (4) compensation for loss from legitimate business; (5) relocation fees. Relevant parties of land expropriation include the government (applicant), landowner and general public (see Fig. 1). Among them, the general public pays taxes to the government. The government sets budget for expropriation listed and releases compensation to the landowner that transfers property to the government and thus completes the public construction with feedback of mutual benefits to general public's use. The relationship among these three parties is closely related and inseparable.

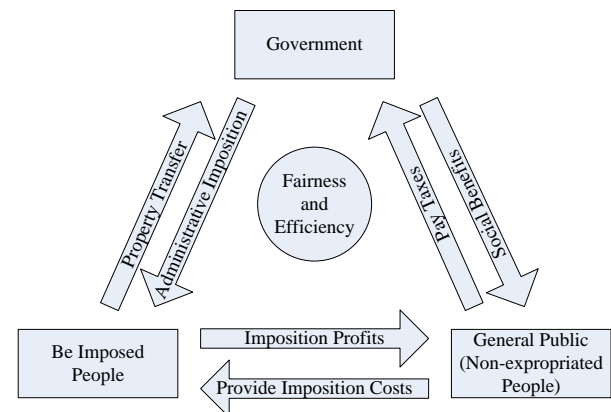


Fig. 1. Relationship among the three parties in compensation for land expropriation

3. Various compensation standards

The compensation standards for land expropriation include the following:

3.1 Compensation for land value

For land expropriated, compensation shall match current market price upon expropriation. Should an inconsistency between area reported for expropriation and area actually used after land expropriation, correction shall be implemented according to actual situation and compensation for land value of increase area will be calculated with compensation standard counted 15 days from expiration of correction notice. (Article 5, Subject and collection rules of compensation for expropriation on land or land improvements)

3.2 Compensation for construction improvements or agricultural improvements

Land improvements can be divided into construction improvements and agricultural improvements. The former include buildings or construction works attached to the land; the latter include improved crops, plants and irrigation works attached to the land. The compensation for expropriation on land improvements is assessed by authorities from the Special Municipality or County (City) together with relevant agency [2]. For agricultural improvements such as fruit trees, tea trees, bamboos, flowers / trees for viewing, trees for afforestation and other crops, the Government of Special Municipality or County shall base on “Assessment criterion of compensation for expropriation on agricultural improvements” issued by the Ministry of Interior and refer to actual local status and latest data announced by the agricultural authorities to set its own basis of assessment of compensation for expropriation on agricultural improvements, which is then submitted to the Standard Land Value Determination Committee for reassessment [3].

3.3 Compensation for land improvement

- Improvements on building foundations include leveling or excavation, water and soil maintenance, piping, earth retaining work, trench excavation and road construction.
- Improvements on farmland includes earthworks, water and soil maintenance, soil improvements, as well as constructing farm roads, irrigation works, wind breaks, sand breaks and embankments.
- Improvements for other land developments.

Damages arise from the cessation or down-scaling of trading due to expropriation shall be compensated. The relevant terminologies are defined as follows:

- “Legal business” means entity that lawfully acquired relevant license needed for operation and carried out proper trades.
- “Cessation of trade” means the termination of trading activity due to full expropriation on the land or land improvements for trading.
- “Down-scaling of trade” means reduction of original trading size due to partial expropriation on the land or land improvements for trading.

3.4 Compensation for loss from business

The above-mentioned area of trading is limited to area of land or land improvements registered or applied for trading, and excluding the non-operational parts. Should the main structure or facilities of operation be expropriated, where the remaining parts cannot continue to operate, compensation shall be provided as per requirements under Point 3) mentioned above (Point 4, Compensation criterion for business loss from land and land improvements expropriated)

3.5 Relocation fees

Upon expropriation of land or land improvements, relation fees shall be dispensed for any of the following situations (Paragraph 1, Article 34 of Land Expropriation Act).

3.6 Compensation for tenanted farmland

In case the compulsorily purchased land is tenanted farmland, Article 11 of the Equalization of Land Rights Act stipulates that the government shall compensate the lessee for the expenses he has incurred in making land improvement as well as for any crops not yet harvested. In addition, the lessor shall pay to the lessee one third of the compensated land price after a deduction for land value increment tax through the government.

3.7 Compensation for loss from adjoining land

In case the use of expropriated land affects the adjoining land and causes an inability in its original use or reduction of original performance, the owner of such adjoining land is entitled to request appropriate compensation from the land applicant. The amount of compensation shall not exceed the land value reduced due to the use of expropriated land. The regulations on relevant executions include Article 216 of Land Law, Tai-Nei-Di-Zi Letter no. 8886374 dated 1999/7/27 and Tai-Nei-Di-Zi Letter no. 8911895 dated 2000/9/5 from the Ministry of Interior.

3.8 Compensation for superficies

Rules governing the compensation for superficies shall be prescribed jointly by the central competent authority in charge of the relevant industry and the Central Com-

petent Authority. At present, the Ministry of Transportation and Communications, Ministry of Economic Affairs and Ministry of National Defense together with the Ministry of Interior have followed the above regulations and set the "Rules governing the compensation for transportation / water / defense undertakings passing through the private lands from above or underneath" (Paragraph 1 and 4, Article 57, Land Expropriation Act). Furthermore, Article 19 of the Mass Rapid Transit Act stipulates that the construction of a mass rapid transit system may pass through, over or under any government or privately owned land or any improvement on the land under work necessity.

3.9 Compensation for requisition

Compensation for the use of land shall be calculated starting from the date of public announcement of requisition and paid to the landowners or the holders of superficies, servitude of real property, agricultural right, right of permanent tenancy or the right of cultivation in one lump sum within 15 days after the expiration of the public announcement period. (Paragraph 5, Article 58, Land Expropriation Act).

4. Conclusions

Since 1st September 2012, the land expropriation policy in Taiwan has been implemented according to compensation with market price, where public benefit and necessity are in place. However, both acquirers and landowner think improvements are still needed for the land expropriation system. The conclusions are as follows:

- On topic of unreasonable compensation for expropriation

In order to comply with budget of the current year, the assessment units would make assumptions and portion of citizens would perceive this as the government controlling prices, which further lead to difference between market price recognized by the citizens and the market price assessed by the governmental unit, hence the extensive difference on the standard of price assessment between government expropriating land from the citizen and vice versa. When changing into national land with greater use, the citizens deem that price shall be calculated according to the value after development.

- Citizens showed satisfaction towards compensation at market price for land expropriation

The analysis from statistics showed that, after adding 40% of compensation on top of publicly announced current value for land expropriation, the percentage of very satisfied and satisfied citizens was greater than unsatisfied and very unsatisfied citizens. This means that government's change provides further protection of citizens' properties and reduces resentment towards expropriation, so public works can proceed smoothly. In the case of real estate valuation, it was found out-source commissioning received greater satisfaction, where citizens showed lack of trust when the government carried out its own assessment on market price for compensation.

- Improvement on strategy of compensation for expropriation

It is recommended to increase real estate valuation, where cases processed by out-sourced evaluators can be reviewed by land valuers in public sectors. Since compensation for expropriation falls under enforcement, citizens may build up a grudge easily and file appeals; thus responsibilities shall be defined precisely. The results from statistical analysis show that citizens believe the compensation for land expropriation has not reached the principle of full compensation. Therefore, such compensation shall elevate from appropriate compensation to full compensation, where economic and non-economic loss suffered by landowners can be included within compensation for expropriation.

References

1. Land Expropriation Act, Department of Land Administration, Ministry of Interior (2012)
2. Department of Land Administration, Ministry of Interior (2011), "Assessment criterion on compensation for expropriated construction improvements", URL: <http://www.land.moi.gov.tw/law/chhtml/lawmain1.asp>
3. Department of Land Administration, Ministry of Interior (2011), "Assessment criterion on compensation for expropriated agricultural improvements", URL: <http://www.land.moi.gov.tw/law/pda/lawappend.asp?lid=3132>

Study on User Satisfaction of Pick Areas for Elementary Schools – Using Nanyang Elementary School in Taichung City as Example

Chun-Feng Chang, Yan-Chyuan Shiau* and Kuan-Yin Chen

Department of Construction Management, Chung Hua University

707, WuFu Rd., Sec. 2, Hsinchu, 30012, Taiwan

E-mail: E10316003@chu.edu.tw; *ycshiau@ms22.hinet.net; jac32455@gmail.com

Abstract

This study has investigated the user satisfaction of pick areas for elementary schools and their improvement requirements. Questionnaire is adopted to discuss user satisfaction of the school environment. The improvement strategies for pick areas were inspected for different various backgrounds. The research results have showed that overall satisfaction ranges from general to satisfaction. Some useful suggestions are proposed. These suggestions can be served as reference for schools and educational organizations to establish an unimpeded pick area for a safe school commuting environment.

Keywords: Commuting Environment, Pick-up/Drop-off Area, Walkways, Satisfaction, Improvement needs

1. Introduction

1.1 Background

According to statistics from the Ministry of Health and Welfare in 2010, data showed that among campus accidents in elementary schools, the percentage of deaths from traffic accidents ranked top and reached more than one-third of total accidents. Most of the traffic accidents involved students occurred on the way to or from schools and mostly happened near students' home or school [1]. Over recent years, government institutions at various levels have actively promoted improvement on overall commuting environment to school by providing safe and comfortable commuting environment, as well as encouraging cooperation between communities and schools, which shall gradually integrates surrounding commuting environment to schools, and further achieves a perfectly smooth and safe commuting environment to school [2].

1.2 Purpose of Research

Based on the above-mentioned problems and situations, the purpose of this research includes the following:

- Discuss the satisfaction and improvement needs from parents of students in elementary schools towards current situation of commuting environment to school and pick-up/drop-off area.
- Analyze the difference between satisfaction from parents of students in elementary schools with different backgrounds towards current situation of commuting environment to school and pick-up/drop-off area.
- Discuss the difference between improvement needs from parents of students in elementary schools with different backgrounds towards current situation of commuting environment to school and pick-up/drop-off area, as well as providing relevant suggestions about establishment or improvement for commuting environment to school pick-up/drop-off area.

1.3 Definition of commuting environment to school and pick-up/drop-off area

The commuting environment to school mainly includes six fundamental areas: (1) Pedestrian walkways around the campus (i.e., walkways to school); (2) traffic safety facilities including pedestrian crossings and traffic sig-

© The 2016 International Conference on Artificial Life and Robotics (ICAROB 2016), Jan. 29-31, Okinawa Conventional Center, Okinawa, Japan

nals; (3) pick-up/drop-off block for parents; (4) pedestrian walkways, land bridges and underpasses from school to residential communities; (5) passages from school gates to campus buildings; (6) various functional facilities and landscapes with visual effects along above-mentioned passages. The pick-up/drop-off area refers to the region consisting of traffic safety facilities such as pedestrian walkways around the campus, pedestrian crossings and traffic signals, as well as pick-up/drop-off block for parents within the commuting environment to school. [3]

2. Investigation on Research Base

Nanyang Elementary School is located on Nanyang Road, Fengyuan District, Taichung City as a central school in township format with numerous stores and dense population nearby. According to information provided by education notification system of the Education Bureau of Taichung City [4]: In 2014, Nanyang Elementary School had a total of 102 classes with 2,905 students, which made it the largest school with most students among 228 public elementary schools in Taichung City. The main gate sits right next to Nanyang Road, the main road towards the City with Ziqiang Street on the east side, Tongan Street on the north side and Huiyang Street on the west side. The school is surrounded by roads that form a 4-way intersection at each corner. There are 6 gates in total, where 3 gates serve as entries and exits for students arriving and leaving the school. Investigation was made on traffic safety facilities at 4 intersections around Nanyang Elementary School and its 3 gates.

3. Results of Research

3.1 Analysis on profile of participants

This research took parents escorting students to and from Nanyang Elementary School in Taichung City as the participants, where questionnaires were used to understand their satisfaction towards the current status of the commuting environment to school and pick-up/drop-off area. In the "Gender" category under parents of students in elementary schools sampled for investigation, the majority were 453 females at 71.3 %. In the "Age" category under parents of students in elementary schools sampled for investigation, the majority were 373 parents between

40-49 years old at 58.7%. In the "Education level" category under parents of students in elementary schools sampled for investigation, the majority were 303 parents with college degree at 47.7 %. In the "Occupation" category under parents of students in elementary schools sampled for investigation, the majority were 170 parents in service industry at 26.8 %. In the "Average monthly income" category under parents of students in elementary schools sampled for investigation, the majority were 290 parents with NTD 20k-40k at 45.7%. In the "pick-up/drop-off method" category under parents of students in elementary schools sampled for investigation, the majority were 352 parents using motorcycles at 55.4.7%. In the "Most often used gate" category under parents of students in elementary schools sampled for investigation, the majority were 298 parents using the main gate (Nanyang Road) at 46.9%.

3.2 Analysis on satisfaction towards status of commuting environment to school and pick-up/drop-off area

The commuting environment to school and pick-up/drop-off area includes three items: the walkways to school, pick-up/drop-off block for parents and traffic safety facilities. In this research, the 5-point Likert Scale was used for measurements and answering. Analysis was done with descriptive statistics such as mean and standard deviation to show the difference of satisfaction between each question. The resultant statistics are as follows:

- The item with the greatest satisfaction from parents of students in elementary schools to "walkways to school" was the "adequate width". The item with the greatest satisfaction to "pick-up/drop-off block for parents" was "adequate control time". The item with the greatest satisfaction to "traffic safety facilities" was "proper execution adopted by the school on non-material control measures".
- The top three items with the greatest satisfaction from parents of students in elementary schools to current status of commuting environment to school and pick-up/drop-off area were "proper execution adopted by the school on non-material control measures", "adequate establishment of pedestrian crossings on surrounding roads" and "adequate width of walkways to school".

- The overall satisfaction from parents of students in elementary schools to current status of commuting environment to school and pick-up/drop-off area was between normal and satisfied. The item with the greatest satisfaction was "traffic safety facilities" followed by "walkways to school" and then "pick-up/drop-off block for parents".

3.3 Differential analysis of satisfaction towards the current status of item with different backgrounds

The objective of this section is to discuss the difference between satisfaction from parents of students in elementary schools with different backgrounds (including gender, age, education level, occupation, average monthly income, pick-up/drop-off method and the most often used gate) towards commuting environment to school and pick-up/drop-off area. In this research, independent sample T test and One-Way ANOVA were adopted for analysis. The background acts as the independent variable and satisfaction to commuting environment to school and pick-up/drop-off area as dependent variable. Should distinctive difference be achieved, the Scheff Method can be used afterwards to compare and verify the difference. Based on results of satisfaction from research investigation, the following three conclusions can be summarized:

- For parents of students in elementary schools with different gender, age, education level, occupation, average monthly income and pick-up/drop-off method towards commuting environment to school and pick-up/drop-off area, there is no distinctive difference in satisfaction between "walkways to school", "pick-up/drop-off block for parents" and "traffic safety facilities", as well as the "overall satisfaction".
- For parents of students in elementary schools using different gate towards commuting environment to school and pick-up/drop-off area, there is no distinctive difference in satisfaction to "pick-up/drop-off block for parents"; but distinctive difference does appear in satisfaction to "walkways to school" and "traffic safety facilities", as well as the "overall satisfaction".
- For satisfaction from parents of students in elementary schools to "traffic safety facilities", the main gate receives the greatest satisfaction, which is followed by the back gate, and then the east gate. In terms of satisfaction towards "walkways to school" and "overall satisfaction", the main gate receives greater satisfaction than the east gate.

3.4 Analysis on improvement needs for commuting environment to school and pick-up/drop-off area

The objective of this section is to discuss improvement needs from parents of students in elementary schools with different backgrounds (including gender, age, education level, occupation, average monthly income, pick-up/drop-off method and the most often used gate) towards the current situation of commuting environment to school and pick-up/drop-off area, which covers items such as walkways to school, pick-up/drop-off block for parents, traffic safety facilities. Descriptive statistics was used for analysis, where the number of items for improvement needs were represented with frequency distribution and percentage, as well as ranking the improvement needs according to magnitude of percentage (Fig. 1 to Fig. 3).

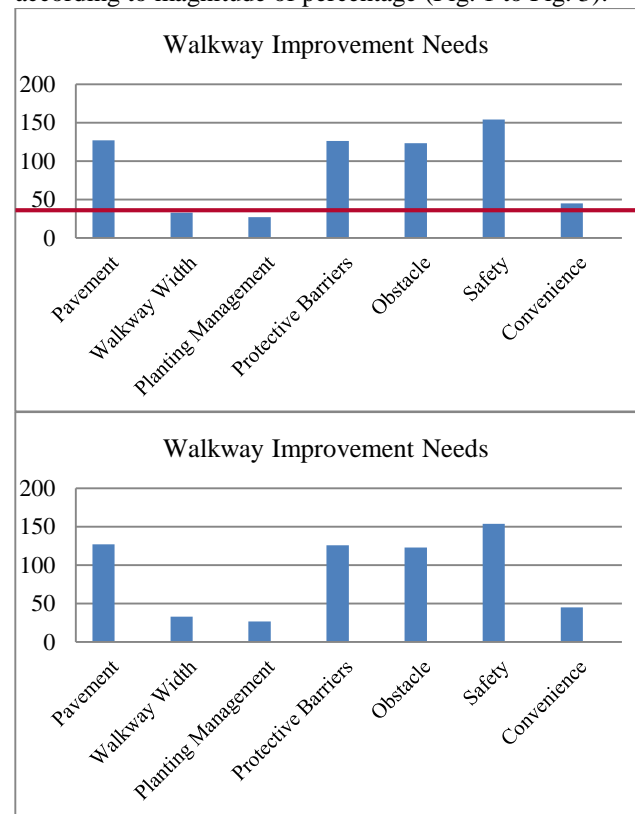


Figure 1 Analysis on improvement needs for walkways to school

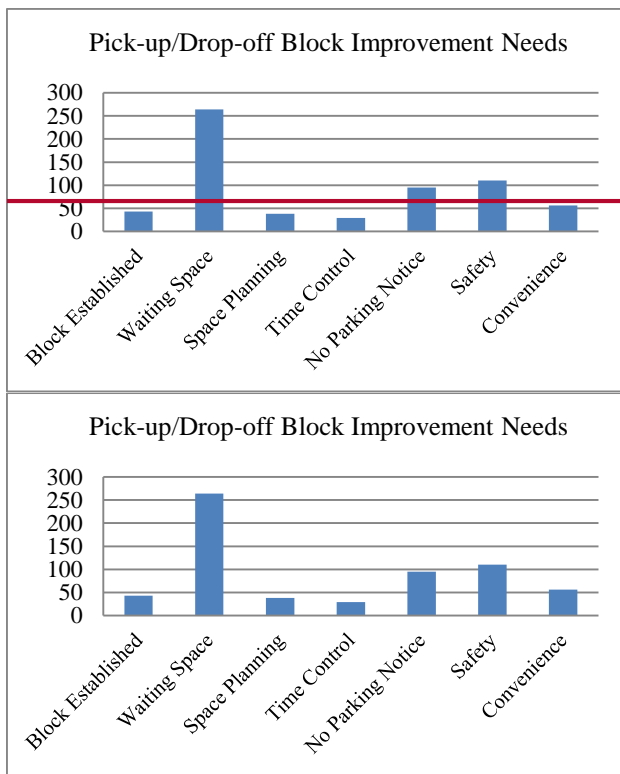


Figure 2 Analysis on improvement needs for pick-up/drop-off block for parents

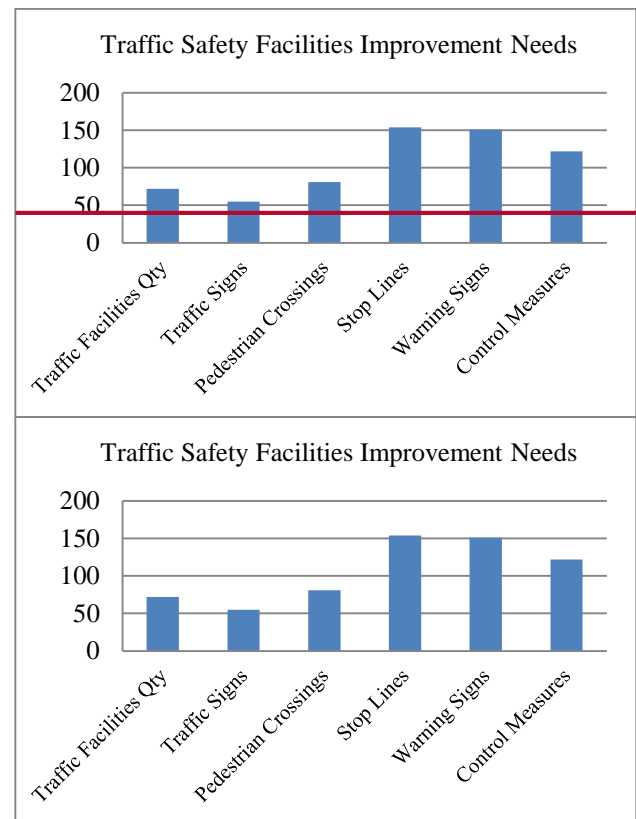


Figure 3 Analysis on improvement needs for traffic safety facilities

4. Conclusions and Suggestions

4.1 Conclusions

Based on the investigation of this research, the analysis on data of satisfaction from parents of students in elementary schools towards the current status of commuting environment to school and pick-up/drop-off area reveals the following:

- The overall satisfaction from parents of students in elementary schools towards the current status of commuting environment to school and pick-up/drop-off area is between normal and satisfied. The satisfaction on individual items ranks from "traffic safety facilities", "walkways to school" to "pick-up/drop-off block for parents".
- The satisfaction from parents of students in elementary schools towards the current status of commuting environment to school and pick-up/drop-off area does not show distinctive difference because of difference

in gender, age, education level, occupation, average monthly income and pick-up/drop-off method.

- For improvement needs from parents of students in elementary schools towards commuting environment to school and pick-up/drop-off area, the "walkways to school" shows the greatest needs for "high safety"; the "pick-up/drop-off block for parents" shows the greatest needs for "sufficient waiting space" and the "traffic safety facilities" shows the greatest needs for "clear and adequate marking of stop lines along surrounding roads".
- The suggestions made by parents of students in elementary schools for establishing perfect commuting environment to school and pick-up/drop-off area are ranked from "control time of vehicle passing, implement separate access for pedestrians and vehicles, enhance executions of penalties to illegal parking", "ask traffic police to assist with traffic guidance", "hire experts to provide suggestions of improvements" and "provide sufficient funds for improvements".

4.2 Suggestions

Based on the investigation and results of this research, the following suggestions are proposed for improvements on commuting environment to school and pick-up/drop-off area:

- Suggestions for commuting environment to school and pick-up/drop-off area
 - (i) Enhance maintenance and management of walkways to school
 - (ii) Increase waiting space in pick-up/drop-off block for parents
 - (iii) Enhance maintenance and repair of traffic safety facilities
- Suggestions for education authorities
 - (i) Hire experts in planning of commuting environment to design a suitable improvement program, as well as providing schools with sufficient funds to establish a perfectly safe commuting environment to school and pick-up/drop-off area.
 - (ii) Re-plan the school districts to reduce problems such as insufficient pick-up/drop-off space and traffic chaos in commuting environment to school due to excessive number of students.

6. References

1. P. J. Wang, Y. C. Wu, The safe way to school, *Journal of Healthy Cities*, Vol. 4, Page 46-51, 2006.
2. Y. J. Wang, A study on the degree of satisfaction of school walkways for elementary school students in Yulin County, Master's Thesis for the master's program of leisure environment management, Department of Tourism Management, Nanhua University, Chia-Yi, 2013.
3. C. A. Hsiao, A study on the safety and satisfaction of pick-up area at primary school of Taoyuan City, Master's Thesis for the master's program under the Department of Architecture, Fengchia University, Taichung, 2011.
4. Website of Education Bureau, Taichung City Government, <http://www.tc.edu.tw/school/student>.

Study on User Satisfaction in Sport Site Facilities for Senior Students of Elementary Schools in Taichung City

Pei-Ling Lin, Yan-Chyuan Shiau* and Ling-Lin Chang

Department of Construction Management, Chung Hua University

707, WuFu Rd., Sec. 2, Hsinchu, 30012, Taiwan

E-mail: E10316007@chu.edu.tw; *ycshiau@ms22.hinet.net; lin88@sish.ntpc.edu.tw

Abstract

This study has discussed senior students' actual use and satisfaction towards school sport field facilities in elementary schools of Taichung City. This study adopted questionnaire method and senior students in elementary schools of Taichung City were used as research subjects which were sampled with stratified cluster sampling method. The obtained data were analyzed by descriptive statistics, Chi-square test, T test, one-way ANOVA, and Pearson product-moment correlation. It is expected to provide reference for relevant personnel so as to provide the ideal campus sports environment.

Keywords: School Sports Site Facilities, Use Condition, User Satisfaction, Requirements for Improvement

1. Introduction

1.1 Background

Over recent years, many countries have tried to increase the amount of student physical activities in order to enhance general nation competitiveness. Article 1 of the "National Sports Act" stipulates that: "The implementation of national sports serves to strengthen the physical fitness of citizens, nurture national morals, expound ethnic spirit and fulfill the lives of the general public." [1] Good attitudes and habits towards sports shall be cultivated from childhood as stipulated in Article 6 of the "National Sports Act": "Schools at the high school levels and under and the first three years of five-year colleges should provide time slots for the daily participation of sports activities, aside from sports classes, with weekly participation of over one hundred and fifty minutes, while students are on school premises."

1.2 Motive and Purpose

According to the report from the International Obesity Task Force (IOTF), the obesity rate of children and

teenagers between the ages of 6 to 18 in Taiwan ranked the highest in Asia with 26.8%. In 2007, the Ministry of Education (MoE) took statistics on the height of students between Grade 4 and 6 from 2004 to 2006. The average student height showed negative growth for 2 consecutive years. Based on MoE's statistics in 2006, the physical fitness of students in domestic junior high schools and elementary schools fell behind neighboring countries in Asia, namely China, Japan and Korea [2]. If the learning results of our next generation are affected by poor physical fitness and health, we will lose international competitiveness and future of the nation in long term [3].

In order to encourage students' motivation and interest in sports and cultivate the habit of regular sports, as well as consolidating ability and attitude of life-time participation in physical activities, the MoE proposed the "Get Active Quick Project" in 2007, where students were expected to exercise a minimum of 30 minutes per day and 210 minutes per week, so interest in sports could be developed. This research targeted on senior students of public elementary schools in Taichung City for discussion on use condition of school sports site

facilities, user satisfaction and requirements for improvement, so adequate suggestions could be made to the education authorities and administration unit in schools. Base on the above-mentioned background and motive, the objectives of this research are as follow:

- Discussion on the perception of senior students of public elementary schools in Taichung City towards the use condition of school sports site facilities and user satisfaction.
- Discussion on variables of different student background against difference between use condition and user satisfaction towards sports site facilities, as well as the degree of relevance between the two.
- Provide relevant suggestions on school sports site facilities for senior students of public elementary schools in Taichung City.

2. Design and Implementation

Based on the background and purpose, this article designed the structure of the research, where credible questionnaires were edited as a tool of investigation and objective data were collected through sampling. The data acquired were analyzed at the final stage and the current status of the research was revealed. The research structure is shown in Fig. 1. There are a total of three sections in the Chapter, namely tools, participants, data processing and analysis.

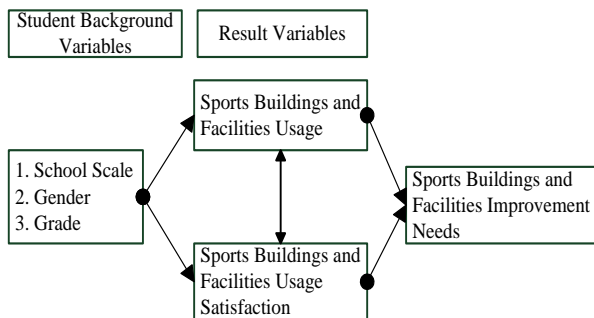


Fig. 1. The research structure of the study.

2.1 Tools

The tools used for this research were the “Questionnaire on use condition and user satisfaction from senior students of elementary schools in Taichung City towards school sports site facilities” edited by the researcher himself. The process of editing and content of questionnaire are described as follows:

● Questionnaire Editing

The “Questionnaire on use condition and user satisfaction from senior students of elementary schools in Taichung City towards school sports site facilities” used as a tool for this research selected topics from past questionnaires that implemented investigations on sports site facilities. Reference was also made to domestic regulations and literature of relevant research on school sports site facilities, where the draft of questionnaire was compiled according to the current state of sports site facilities and features of elementary schools in Taichung City.

● Content of Questionnaire

The questionnaire for this research mainly consisted of two parts with basic information in Part 1 and questions in Part 2. The relevant contents are described as follows:

(i) Basic information

These included name of the school, size of the school, gender and grade.

(ii) Questions in questionnaire

- Investigation on use condition of school sports site facilities (16 questions in total)
- Investigation on user satisfaction for school sports site facilities (23 questions in total)
- Investigation on requirements for improvement of school sports site facilities (4 questions in total)

2.2 Participants

● Specimen Population

In this research, senior students of public elementary schools in Taichung City acted as the specimen population. According to statistics taken by the Education Bureau of Taichung City, there are a total of 229 public elementary schools in Taichung City excluding one school in the process of preparation for enrollment and not yet operational. Among these schools, there are 2,190 classes (Grade 5 and 6) and 54,620 students (both male and female) in total [4].

● Specimen Selection

This research adopted the stratified cluster sampling method, which divided the elementary schools in Taichung City into four groups based on the number of general classes: below 20 classes, between 21~40 classes, between 41~60 classes and above 60 classes. The schools with classes below 20 were categorized as small schools and a total of 104 classes were counted.

The schools with classes between 41~60 were categorized as large schools and a total of 37 classes were counted. The schools with classes above 60 were categorized as jumbo schools and a total of 15 classes were counted. Table 1 shows the size grouping of the public elementary schools over each administrative district in Taichung City. 3 schools were randomly selected from the small, medium, large and jumbo schools respectively to a total of 12 schools, where 2 classes from senior grades of each school were randomly selected to a total of 24 classes and 560 students for completion of the questionnaires. This research issued 560 questionnaires in total, and 18 were not collected, which means a collection of 542 questionnaires with 539 effective questionnaires counted. 542 students were actually counted as participants to the investigation with the effective rate of collection at 96%

Table 1. Statistics on size grouping of public elementary schools over each administrative district in Taichung City [4]

Group District	below 20 classes	21-40 classes	41-60 classes	above 60 classes
East	2	3	1	0
South	0	1	3	0
West	1	2	1	0
North	0	6	0	1
Central	0	1	0	0
Beitun	2	10	3	1
Xitun	4	5	3	1
Nantun	1	4	2	3
Fengyuan	3	3	2	2
Houli	4	1	2	0
Shengang	0	4	1	0
Daya	2	4	1	1
Tanzi	1	2	2	1
Waipu	4	2	0	0
Qingshui	7	3	0	1
Wuqi	3	2	1	0
Dajia	6	2	2	0
Shalu	4	0	2	1
Daan	4	0	0	0
Longjing	3	3	1	0
Dadu	4	3	0	0
Wuri	5	2	1	0
Dongshi	9	1	0	0
Shigang	2	0	0	0
Xinshe	7	1	0	0
Heping	8	0	0	1
Dali	3	2	6	1
Wufeng	9	0	1	0
Taiping	6	6	2	1
Total	104	73	37	15

2.3 Data Processing and Analysis

In this research, invalid questionnaires with incomplete answers above 50% or careless answers (all answers were ticked) were eliminated first. Coding and registration were then implemented, where various data processing and analysis were carried out with the statistic software “IBM SPSS Statistics 22”. Each question was analyzed with discriminant analysis and item analysis, and internal consistency was acquired with Cronbach α . No statistics and analysis were made to partial data that was lost but defined with SPSS missing value. For background variables and school sports site facilities, the use condition, user satisfaction and requirements for improvement underwent descriptive statistics and analysis. Chi-Square Test was used to see if there were distinctive differences in background variable on senior students of elementary schools upon differential analysis on use condition of school sports site facilities. T-Test and One-way ANOVA were used to see if there were distinctive differences in background variable on senior students of elementary schools upon differential analysis on use condition of school sports site facilities. Finally, Pearson product-moment correlation coefficients [5] were used in statistics and analysis on relevance between use condition and user satisfaction.

3. Results from Research

Based on the results from data analysis and discovery of the research, conclusions acquired from the research can be compiled as follows:

- Use condition of senior students of elementary schools on school sports site facilities
 - (i) Use condition
 - (a) 61.1% of senior students of elementary schools knew about the rules and notes related to the school sports site facilities. 85.7% knew that outdoor facilities such as “outdoor ballpark”, “athletic field” and “playground” opened after school hours.
 - (b) 90.5% of senior students of elementary schools had the habit of using the school sports site facilities. Among them, 36.3% used the facilities “after school hours”; 32.6% used the facilities “during sports classes or club activities”. 40.0% of the senior students of elementary schools exercised

with school sports site facilities “less than 30 minutes” every time and 39.8% were between “30 minutes~1 hour”.

- (c) 44.8% of senior students of elementary schools usually used the school sports site facilities together with classmates or club members; 55.7% “played with a group” and 36.6% “played with 2~3 classmates”.
- (d) The top 3 school sports site facilities that senior students of elementary schools wished to have in future were “swimming pool”, “rock climbing field” and “table tennis court” in sequence.
- Differences in different student background on use condition of school sports site facilities
 - (i) In terms of school size: There were distinctive differences in senior students of elementary schools on “recognition on rules of school sports site facilities”, “average duration of every use”, “the sports facilities mostly used by PE teachers” and “willingness on re-use”.
 - (ii) In terms of gender: There were distinctive differences in senior students of elementary schools on “average frequency of use per week”, “average duration of every use”, “number of companions during sports”, “frequency of use during lesson breaks”, “level of fun” and “willingness on re-use”.
 - (iii) In terms of grade: There were distinctive differences in senior students of elementary schools on “average frequency of use per week” and “frequency of use during lesson breaks”.
- Requirements for improvement on school sports site facilities
 - (i) A. For outdoor facilities (athletic field, outdoor ball court, and playground): too far from classrooms, weather influence, crowded with excessive number of people, insufficient space, and insufficient quantity.
 - (ii) B. For indoor facilities (gymnasium or sports field with roof): too far from classrooms and insufficient space, insecurity due to insufficient number of people, insufficient lights and facilities closed.

4. Conclusions

In order to improve user satisfaction from senior students of elementary schools on school sports site facilities, which further encourages willingness and fun in

sports, few suggestions are proposed to the education authorities and school administrative units:

- As learned from school data provided by the Education Bureau, Taichung City, the total rate of establishment on gymnasiums for public elementary school in Taichung City was 48% (110 gymnasiums /229 schools) [6]. Since the rate of establishment on small or medium size of gymnasiums or sports ground with roof is still below the total rate of establishment, priority funds must be issued to increase number of indoor facilities including gymnasiums or sports ground with roof.
- Regardless of sports classes or hours after school, all senior students of elementary schools were fond of ball sports; but the willingness and results were often affected by insufficient number of ball courts and weather. Therefore, a sufficient number of indoor and outdoor ball courts must be provided to meet such needs. As more idle classrooms will be available due to declining birthrate, these facilities can be renovated into simple sports classrooms to reduce the influence of inclement weather on sports.
- Regarding the rate of using school sports site facilities by senior students in elementary schools, boys were higher than girls. Therefore, different needs generated from gender differences must be considered during the planning stage of school sports site facilities, where facilities more suitable for girls are provided, so the willingness of usage can be enhanced.

5. References

1. National Sports Act, Legislative Yuan, 2013.
2. C. W. Chang, New prescription for sports learning, Parenting Magazine, Vol. 28, 2011.
3. W. C. Hsu, Relevant study on social support and sports attitude towards elementary student sports in Hsinchu City, Master Thesis, Department of Physical Education, National Hsinchu University of Education, Hsinchu, 2007.
4. Education Bureau, Taichung City, School data at all levels, enquired on November 26, 2014.
5. M. L. Wu, Practical SPSS statistics and applications: Questionnaire analysis and application statistics, Yixi Publisher, New Taipei City, 2000.
6. J. W. Huppertz, J. A. Sidney & H. E. Richard, An application of equity theory to buyer-seller exchange situations, *Journal of Marketing Research*, 15, (1978) pp. 250-260.

The Establishment of the Sustainability Performance Indicators for Wetland Ecological Project: Using Construction Inspection Phase as Example

Ching-Mei Miao

Department of Civil Engineering, Chung Hua University, 707, WuFu Rd., Sec. 2, HsinChu 30012, Taiwan

Yan-Chyuan Shiau*, Chen-Chung Liu and Jen-Kuo Chang

Department of Construction Management, Chung Hua University, 707, WuFu Rd., Sec. 2, HsinChu 30012, Taiwan

E-mail: miaomei589@hotmail.com; *ycshiau@ms22.hinet.net; E10416003@chu.edu.tw; e10416014@chu.edu.tw

Abstract

The critical success factors of sustainable performance indicator (SPI) were investigated in this research. A wetland water purification project of a stream in Hsinchu was used as an example in this paper. The experiment information was integrated as feedback to correct the index library. The measurement from test results verifies the SPI from sample project case in some facet is consistent with the results of current inspection system. The research result can be served as reference for the sustainable development of ecological engineering achievements.

Keywords: SPI, Wetland, Sustainable Development, Ecological Engineering.

1. Introduction

1.1 Background

Over the past years, the Taiwanese Government has invested tremendous amount of resources, manpower and funds to build many artificial wetlands all over Taiwan with ecological engineering, and the results proved that water quality was in fact improved. However, numerous failures of artificial wetlands with ecological engineering still occur from time to time. After investigation, it was found that the stage of acceptance inspection was crucial to determine the success and remedy of the project as a whole. However, the problem of unsustainability during the stage of acceptance inspection has never been taken seriously. Instead of implementing project planning, design, construction and maintenance with sustainable thinking as a whole, the conventional approach of linear thinking still exists in the managerial concepts. With additional factors such as reduction of human resources by the government

over recent years and the lowest bid of public works awarded, the engineering sustainability could not be realized effectively. Should the techniques in construction management and performance-based contracts be adjusted and improved, they could be used to solve the problem of engineering unsustainability [1].

1.2 Sustainable performance target

In order to study and draft sustainable performance target of artificial wetland work, relevant domestic and foreign policies on sustainable use of water resources need to be collected and analyzed. The sustainable performance in this research is based on environmental, social and economic aspects that are capable of performing self-repair and reaching a balanced state [2]. The environmental aspect refers to harmless continuity of all species and the environment; the social aspect refers to fair treatment and continuity to all species, and the economical aspect refers to an economy with reasonable, balanced and sustainable benefits.

2. SPI for Ecological Engineering of Wetlands

2.1 Establishment of SPIM

The SPIM (Sustainable Performance Indicators Method) is a measure of judgment integrated within level 3 quality control process of public works to determine compliance of sustainable performance [3]. The method is objective, clear and measurable with precise measuring process, threshold value, featured indicators of relative response time as well as properties such as preliminary indicator, process indicator, result indicator and driving indicator. Instead of a general scoring method of sustainable indicator evaluation mode, this research is based on procedures of SPI establishment and referred to suggestions provided by experts to construct the SPIM used during acceptance inspection on ecological engineering of artificial wetlands, which implements inspection operation according to inspection control chart of sustainable performance on ecological engineering of artificial wetlands and continuously sends back the results for rectification of SPI database.

2.2 Inspection and control of SPI

During the stage of acceptance inspection, this research implemented inspection and payment control on the standard of contractual service. In a contract with sustainable performance format, the official process contains a monthly report where each pricing with precise results receives payment; the unofficial process contains inspections on the standard of contractual service carried out randomly, weekly and upon receipt of a complaint, where SPI acts as the basis of inspection control and payment to ensure performance of work and routine services. Penalty or reduction in payment will be implemented should failure of compliance occur, and in case of severe violation, payment will be stopped or the contract terminated. Accordingly, the contractor needs to reach a minimum threshold value of service standard under the SPI contract, or additional penalties will be executed [4].

3. Actual Verification

3.1 Case introduction

In this research, a specific artificial wetland work in Hsinchu City, Taiwan was taken as the example. In this project, living sewage was discharged into specific

streams after initial purification, entered into the wetlands via directed channels for further purification, and then discharged into a large river. The work content included the main structure (inclusive of pond and tank slope), riverbanks, alleyways and access roads in the work area. Clay crystallization was adopted to construct impervious layer of the tank base and slope; a gabion wall was applied for riverbanks; the protective fences, platforms and boardwalks were built with environmental friendly wood/plastic composites where earth excavation and backfilling provided balance and the surface was paved with re-generated asphalt.

3.2 Results of actual verification

From September to October 2014, this research carried out actual verification on SPI items completed for the water purification works on a specific artificial wetland in Hsinchu City. The inspection results recorded after measurements are shown in Table 1 and 2. The results of the SPI inspection in this case were not ideal since out of the 23 items of sectional inspection indicators according to the work progress, 14 items did not comply with the inspection indicator and a result rate of non-compliance at 61%, which exceeded the inspection determination standard of 40%. Therefore, this chosen case was an “unsustainable wholeness of work”. From inspection and construction results, it was found that the contractor did not have concepts of sustainable work and construction, yet still blamed the design unit for the poor work results, hence the contractor showed incapability in agility and flexible construction. Based on results of SPI actual verification on the case and compared to current public works audited, the work performance was marked B on September 4, 2014, which proved that results of SPI inspection on certain phases under this research were authentic.

4. Conclusions

The description of major achievement from this research includes the following:

- Compile and propose objectives of sustainable artificial wetlands with ecological engineering and key factors of success.
- Compile and propose SPIM at stage of acceptance inspection of sustainable artificial wetlands with ecological engineering.

- Provide operational experience of verified case on artificial wetlands with ecological engineering.
SPI at stage of acceptance inspection of sustainable



Table 1 Summary of SPI test results over water purification work on artificial wetlands along river in Hsinchu City

Indicator No.	SPI	Description of compliance failure	Test results
SP01	Area of foundation subsidence	8m ² and 3.5m ² of subsidence per spot with total area of subsidence >11.5m ²	2 spots in total
SP02	Area of slope collapse at pond / riverbank	1.6m ² and 1.2m ² of collapse	4 spots in total
SP03	Pothole	Pothole at diameter of 28cm and depth of 12cm over foundation surface	1 spot in total
SP04	Monetary value converted from local material acquisition	Monetary value converted from local material acquisition > 20% of total materials purchased	-
SP05	Amount of water flow in pond (leak amount)	Multiple collapses and holes in pond	16 spots in total
SP06	Water contamination in pond	Odor of water inlet & discharge, temperature, turbidity, pH value, electric conductivity, BOD ₅ , TSS, Cl ⁻ , NO ₂ ⁻ →NO ₃ ⁻ , NH ₄ ⁺ , TKN, TP	-
SP07	Site cleanness	Plastic bottles were found all over the site and reinforcement abandoned by the ecological pool	5 spots in total
SP08	Toxicity measured from construction materials	Level of toxicity measured was ≤ legal specification. There shall be no toxic substance in the pond at all due to hazard of contamination.	-
SP09	Area of construction interference around the site	The moving path of construction machinery passed through the work area and riverbeds to collect local river stones at ecologically sensitive area.	3 spots in total
SP10	Proportion of ecological engineering area	For the ecological engineering work of stone laying by the pond, concrete was used as adhesive between rocks, which severely affected living environment of species in the pond.	2 spots in total
SP11	Planting timing and survival rate on the wetland	The area of plant survival over the wetland was 20%, 30%	3 spots in total
SP12	Proportion of ecological experts from engineering industry	The ratio of ecological experts from engineering industry /total number of construction personnel was >80% (most personnel and administrators have ecological expertise)	-
SP13	Number of air pollution incidence reported	Average number of incidence /Month was ≤ 1	1 case in total
SP14	Number of complaint on construction noise	Average number of incidence /Month was ≤ 2. The noise to surrounding areas should be reduced.	-
SP15	Number of citizen complaints or reports	Average number of incidence /Month was ≤ 3	-
SP16	Proportion of overall expense on accident prevention, reduction and damage for the river and riverbanks	1. Inferior construction quality was found on river diversion and stone revetment at impacting side of the site. The height and number of layers constructed was insufficient. 2. Inferior construction quality was found on stone revetment to riverbanks. The height and number of layers constructed for stone revetment at impacting side was insufficient.	2 spots in total
SP17	Proportion of expense on safety of site and surrounding areas, as well as accident prevention facilities and measures	There were no safety fences erected by the site and surrounding areas for separation. No safety fences were erected by personnel near the pond during construction and the personnel were not wearing safety protections.	3 spots in total
SP18	Proportion of expense on preserving historical remains	Expense on preserving historical remains was ≥ 1.5 times of valuating historical remains	-
SP19	Employment ratio between minority labors and general labors	Number of minority employees / general employees on site (monthly average) was ≥ 30%	-
SP20	Loose chipping	Broken and chipped finish of fences by wooden boardwalks were covered up with industrial tape. Concrete pieces chipped off from superstructure of the water intake well.	2 spots in total
SP21	Bulged or sunken pavement	The wooden floor of observatory platform bulged to height of 2.1cm and the pavement with bricks from environmental regeneration was sunken to depth of 1.8cm.	8 spots in total
SP22	Percentage of local labors over foreign labors	Local laborers was 5%	Sep. & Oct.
SP23	Proportion on amount of material procurement locally	The amount of material procurement locally /amount of material procurement remotely was ≥ 6 times	-

Table 2 Results of SPI site test over water purification work on artificial wetlands along river in Hsinchu City

SPI	Description of inconsistency to standard required	Method of site measurement	Duration of improvement
-----	---	----------------------------	-------------------------

© The 2016 International Conference on Artificial Life and Robotics (ICAROB 2016), Jan. 29-31, Okinawa Conventional Center, Okinawa, Japan

Area of pond /river slope collapse	Area of collapse at 1.6m2	Roller tape	Repair completed within 3 days
Pictures from inspection			
			

Through case study, this research implemented actual operation, testing and application to verify applicability of SPI at stage of acceptance inspection of sustainable artificial wetlands with ecological engineering, as well as whether the case of verification provides sustainable performance. The results obtained are described as follows:

- It is verified that this research can be operated practically.
- Through SPI of this research, the sustainable performance of site works can be tested at speed and convenience with simple tools, which extensively reduces funds spent on manpower and experiments.
- The results prove that certain phases and indicators of this research are consistent with status of level I/II QC (Quality Control) check and audit results on public works.
- The SPI inspection from this research has indeed driven contractors to think of more innovative methods of work performance and realizing establishment of sustainable work gradually.
- Compared to conventional inspection, the sustainable performance inspection carried out through SPI of this research can effectively test whether there is sustainable performance on the project or not.
- For SPI inspection implemented per current work progress on the case actually tested, the standard requested, method and tools of measurements, as well as responsive allowable tolerance or TOR (Time of Reaction) set out by the indicator items tested are all adequate in practical operation of testing.

- It is feasible and effective for verification done with indicator method that integrates work procedures with sustainable performance, which realizes the mode of sustainable work at stage of acceptance inspection of work for artificial wetlands with ecological engineering.
- For subsequent research, it is recommended to provide SPI that are more diversified and suitable, where a relevant SPI study can be commenced particularly on type, functions required and construction method of artificial wetlands.

5. References

1. S. L. Liao, Establishment of sustainable indicator system, evaluation and method of comment on water and soil resources (I, II), Presentation of NSC Project Reports No. NSC-88-2621-Z-008-004, Taipei, 1999-2000
2. M. Munasinghe, Environmental economics and sustainable development, World Bank Publications, 1993.
3. H. K. Ku, A study on establishing evaluation criterion for sustainable public works, Doctoral Dissertation, Graduate Institute of Civil Engineering, National Central University, 2010.
4. C. Labuschagne and A. C. Brent, Sustainable Project Life Cycle Management: Aligning project management methodologies with the principles of sustainable development, 2004.

Development of Type Control Guidelines for the Old Town District of Hsinchu City

Yi-Yin Tsai

Department of Architecture and Urban Planning, Chung Hua University, No. 707, Sec. 2, Wufu Rd., Hsinchu, Taiwan

E-mail: yiyint@gmail.com

www.chu.edu.tw

Abstract

The concept of “Building Type Control” was employed to establish hierarchical design guidelines for the urban regeneration process. GIS was used to manage and map environmental database as visual reference tool. Existing building regulations and urban design policies were reviewed to set out limitation and development vision for the study district, type control zones were set out with control design guidelines respectively to serve as a sufficient reference tool to assist design decision making in the urban regeneration process.

Keywords: Type Control, Design Guideline, Urban Regeneration, Urban Design

1. Introduction

Addressing urban regeneration in an old town district of a compact urban city is a complex task, which involves consideration of many interconnected issues. Consequently, the subject of urban regeneration or sustainable urban development with regard to the existing building fabric requires a systematic controlling hierarchies and urban design guidelines to be employed more sufficiently in the design process in fulfilling the vision and requirements of future urban development.

1.1. Research Subject

This research selected the old town district of Hsinchu City to be the research subject. Documentation of the subject background data was carried out first with on-site interviews to collect basic information of the research area's existing condition. Through

understanding the historical development of the site, the cultural landscape features and changes over years; it was clear that a set of sufficient design guidelines or regulations is necessary to ensure the quality of urban environment through the development process. The study attempts to employ the concept of “type control” to formulate a set of rules in regulating features of each individual building, as well as the overall appearance of building streetscape. The concept of “typology” was used to identify the development types of various building district to set the zoning types initially. The type control design guidelines were set out accordingly.

2. Method

2.1. Typology

According to the Oxford Advanced Learners Dictionary of Current English, the word “Typology” is explained as to distinguish between different types of

© The 2016 International Conference on Artificial Life and Robotics (ICAROB 2016), Jan. 29-31, Okinawa Conventional Center, Okinawa, Japan

type system [1]. In the field of architectural discourse, in terms of typology, it is defined as a way of understanding and thinking. In the eighteenth century, building typology is recognized as the method of a continuous and uniform system for the classification process for architectural building. According to M. Bandini [2], the concept of typology can be summarized as three aspects: the first one to be the method of city reading which emphasizes the integrated nature of the city and explore the morphology of city with the building types; the second aspect is concerned with the cultural perspective represented by G. Argan which addresses urban typology as a method consists of various city architectural styles; the third aspect, directed by Quatremere de Quincy and represented by O. M. Ungers and others, defines typology as the production tool and production theory of architecture.

In terms of research, Johnson and Christensen [3] defined this concept as a classification system that split something into a number of different types or kinds. Grix [4] refers to the concept as dividing the study objects into many types, where the attributes of each of the type are mutually exclusive to each other but together as a exhaustive system. Since one type only requires one property; typology can be used in a variety of variables under various circumstances. In typology, a special order can be derived based on the research purpose and the research phenomena, and this order is able to set limitation on the methods of data interpretation. Thus, a hierarchical type control design guidelines could be set out for the regeneration process.

2.2. GIS Data Input

Employing the type model structure developed through literature review, GIS software was used to construct the façade feature database to illustrate the existing building condition of the study subject. Different colors were used to represent different “sub-type” or “sub-type item” of the data information. An example of the GIS mapping of a sub-type feature is shown in Figure 1.

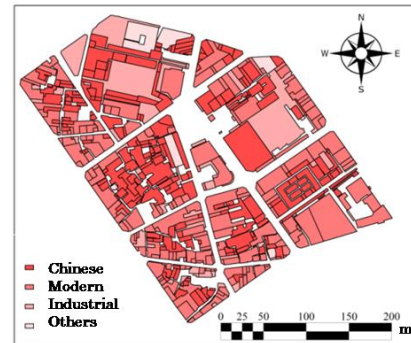


Figure 1. GIS mapping of the “Style” sub-type feature under the “Basic Element” sub-type of the existing building fabric condition of the study subject.

2.3. Policy Review

Existing government regulation and policy addressing topic of urban regeneration was first reviewed and summarized to formulate the development vision for the research subject in constructing the type control guidelines. Both the land-use zoning control regulations, and the urban design regulations of the three major city in Taiwan, the Hsinchu City, the Taichung City and the Tainan City, were reviewed to understand the basic control regulation each city used in regulating and controlling the appearance of building design in different urban district in order to establish a set of type control guideline for various urban district.

3. Result

3.1. Type Control Guidelines

The old town district of Hsinchu City serves as the urban development center of the city, it hosts most of the daily activities of the local people as well as the major tourist attractions. It has a mixture of historical and modern buildings, as well as a mixture of residential, commercial, civic, religious and governmental building functions. Thus, four type control zones were set out as following:

(1) District I: Urban Commercial & Historical Fringe Zone.

District I is the fringe of the historical street zone and the newly urban commercial development area. The

district is closed to the main urban activity traffic road and serves as a landmark for the newly developed area. Creating new city image and connecting pedestrian activities are the key considerations for setting up control guidelines for the district.

(2) District II: Historical Street Zone.

This district is a historical street control zone; the old buildings were set to be preserved and maintained according to its original historical appearance. The main control guidelines were set to emphasize on the building envelope and façade appearance type controls.

(3) District III: Art & Culture Activity Zone.

District III is designated to be the art and culture activity control zone within the old town area of Hsinchu City as the cultural art museum is located at the center of the district. Since the cultural art museum has just been listed as the City's historical building, and the museum was designed to host modern exhibition; the district was set to consider both the idea of historical preservation as well as future modern developments.

(4) District IV: Monumental & Local Business Zone.

Type IV district is classified as monumental and local business zone due to several important existing buildings within the periphery area; including the main religious temple, the Cheng Huang Temple, the city's central vegetable market, and the traditional shopping center which are all in need to be refurbished and preserved under city's urban renewal project. The local restaurant business is also very active within this district, which serves as important tourist attraction and local food cultural identity. Design guidelines for this district were set to target at preservation and maintenance of the local identity and the sense of place.

4. Conclusions

This research established a systematic type control guidelines with the concept of typology to integrate city's urban development plan with local building regulations. The results could serve as a future reference for Hsinchu City government as design guidelines for specific regional planning policy to maintain the characteristic of local building style in the process of urban regeneration. In addition, the urban environmental analysis of this research could serve as a reference for future researches in the field of environmental

management when dealing with both historical and modern urban district.

Table 1. Type Control Guidelines for District I-IV

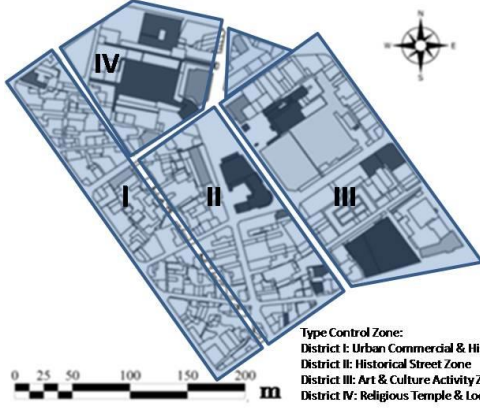
Four Type Control Zones				
 <p>Type Control Zone: District I: Urban Commercial & Historical Fringe Zone District II: Historical Street Zone District III: Art & Culture Activity Zone District IV: Religious Temple & Local Business Zone</p>				
Main Type	Sub-Type / Type Item		District	Control Guidelines
Envelope & Volume	Basic Elements	Style	I	Western style with local material.
			II	Traditional Chinese arcade style.
			III	Modern style
			IV	Traditional Chinese monumental style
	Geom etry and Shape		I III	No limitation, but maintain the overall sense of volume of the streetscape.
			II	Arch style arcade with straight line distributed on the building elevation.
			IV	Building shapes shall consider the Taiwanese traditional temple style.
	Geometry Vocabulary	Buildi ng Base	I II III IV	Building's ground level shall reserve pedestrian space. Encourage the usage of different materials, wall treatments and volume variations.
		Rooft op	I II III IV	Rooftop machinery and equipment should be sheltered and should use similar material as building itself with appropriate design.

Table 1. (Continued)

Envelope & Volume	Geometry Vocabulary	Elevation	I II III IV	Balcony or extruded parts of the building shall not exceed the building line and shall not exceed more than 50 cm of the external walls.
		Color & Material	I	Building's front façade color could be and distinctive. Building identity and harmony of the overall streetscape should be emphasized.
			II	Building's front façade color should mainly be brick red or stone gray. Building materials should have a traditional material texture appearance, or use facade tile, clear-finished brick, pebble stones or other similar materials.
			III	Building's main façade material shall consider its permanence and suitability to the local climate conditions.
			IV	The building volume color shall primarily be silvery white, light gray or other light color tones. Composition of various color tones and shades could be used.
	Composition Style	Opening Ratio	I II III IV	30-60%
		Function	I II	Residential and commercial mixed use.
			III IV	Commercial use
		Configuration	I II III IV	Align with the street.
Building Height & Skyline	Appearance		I II	Uniform skyline with proper setback arcade area.
			III	High-rise building with landmark image.
			IV	Mix of building heights with local recognition.
	Landmark		I	Street corners.
			II IV	Local temple.
			III	Local civic building.

Setback & Building Line	Length Ratio		I	Arcade’s ground level should align with the sidewalk, in the case of no sidewalk, it should be 10-20 cm higher than the traffic road with no stairs and 1/40 slope ratio.
	Area Ratio		II III IV	Setback arcade without overhead coverage should incorporate appropriate plantation and greenery Pedestrian sidewalk width shall not be less than 2.5 m. Arcade height shall not be less than 3 m. Building façade facing street less than 7 m should setback at least 0.5m from the building line.
Exterior Attachment	Advertisement	Size	I	Vertical length shall not be more than 6 m.
		Color	II	Harmony with the front elevation.
		Location	III	The lower part should not be less than 3m from the ground.
			IV	
		Style	I	Front-facing style.
	IV			
		II	Side-facing style.	
III				
Canopy		I	Rain coverage and sun shading should not be less than 6 m.	
Additional Equipment		II	Should not be placed on the front façade.	
		III		
		IV		

5. Acknowledgment

The author would like to thank The Ministry of Science and Technology of Taiwan financially supporting this research under the Contract No. NSC 102-2410-H-216-010.

References

1. A. S. Hornby, S. Wehmeier, Oxford advanced learner's dictionary of current English. Oxford: Oxford University Press, 2000.
2. B. Micha, Typology as a Form of Convention, AA Files, 6, pp. 73-82, 1984.
3. B. Johnson, and L. Christensen, Educational research, Thousand Oaks, CA: Sage, 3rd ed., 2008.
4. J. Grix, The foundations of research, 2008.

Applying Fuzzy Sliding Mode Control on Electrowetting on Dielectric System

Arsit Boonyaprapasorn

*Department of Mechanical Engineering, Chulachomklao Royal Military Academy,
Nakhon-Nayok, 26001, Thailand*

Eakkachai Pengwang

*Institute of Field Robotics (FIBO), King Mongkut's University of Technology Thonburi
Bangkok, 10140, Thailand*

Thavida Maneewarn

*Institute of Field Robotics (FIBO), King Mongkut's University of Technology Thonburi
Bangkok, 10140, Thailand*

*E-mail: urarl.urarl9@gmail.com, eakkachai@fibo.kmutt.ac.th, praew@fibo.kmutt.ac.th
www.crma.ac.th*

Abstract

In Lab-on-a-chip (LOC) devices, an electrowetting on dielectric (EWOD) method can be performed to create, cut, mix, and transport droplets. Moreover, the micro assembly process of micro parts can be manipulated by the EWOD system. High accuracy of droplet motion in both applications is required. Based on the simplified model, the feedback control such as sliding mode control can be applied so that the droplet motion can achieve a high accuracy performance under disturbances. However, the sliding mode control often has chattering problem. Thus, in this study, the fuzzy sliding mode control was applied to manipulate the droplet in the EWOD system. The study was conducted via simulation in MATLAB environment. The result showed that the proposed control method could provide an accurate motion control with lower chattering compared to that of classical sliding mode control.

Keywords: Electrowetting on Dielectric (EWOD), Digital microfluidic system, Sliding mode control, Fuzzy logic.

1. Introduction

The electrowetting on dielectric (EWOD) systems have drawn interests from engineers and scientists especially in two main applications; Lab-on-a-chip and micro assembly including micro robots and micro conveyors. The principle of the EWOD systems can be explained by utilizing the change in interfacial tension induced from the electrical voltage^{1,2}. The droplet that is applied by the electrical voltage will have variation in geometries from the change in contact angle^{1,2}. This allows the droplet to move by the pressure difference

generated inside the droplet as shown in Fig.1^{1,2}. This phenomena is able to support the required operations in Lab-on-a-chip such as mixing, creating, cutting, and transporting^{1,2}. Many of applications in Lab-on-a-chip can be seen from Refs. 1-5. Recently, some interesting EWOD systems have been presented, for example, Shen et al.⁶ developed the digital micro fluidic system with micro heater for the single-nucleotide polymorphism (SNPs) detection. Lai et al.⁷ proposed biomedical detection using EWOD system with multi electrode dot array architecture (MEDA). Moreover, transporting the small particle or a part using the droplet as a carrier can

© The 2016 International Conference on Artificial Life and Robotics (ICAROB 2016), Jan. 29-31, Okinawa Convention Center, Okinawa, Japan

be implemented by EWOD principle^{8,9}. This application also includes using EWOD as a micro actuator¹⁰⁻¹².

Another related area is the feedback control applying on EWOD system such as previous works in Refs. 13-18. For example, Shih et al.¹⁸ employed the feedback control for the movement of the droplet in the EWOD system. According to Bhattacharjee and Najjara^{13,14}, the droplet motion and operations in the EWOD system can be improved by applying feedback control. The possibility of using feedback control for EWOD system was also presented in Ref. 14.

Among various choices of control laws, the sliding mode control (SMC) has been applied to achieve the accuracy of the droplet motion in EWOD system^{15,16}. The principle and capability of the control method can be found from the Refs. 19-21. However, one of the main drawbacks of this control method is the chattering issue¹⁹⁻²³. In order to reduce this effect, the fuzzy logic can be combined with the sliding mode control as presented in Refs. 21-23. Therefore, the main focus of this study was to apply the fuzzy sliding mode control (FSMC) to the EWOD system. The control system was simulated to demonstrate the performance of the droplet motion control. Also, the simulation results of the FSMC method were compared to those of SMC method to evaluate the capability to reduce the chattering phenomena.

This paper is organized in following sections. The mathematical model of the EWOD system is presented in section 2. The controller design is demonstrated in section 3. In section 4, the simulation results and discussions are provided. Finally, the conclusion of the study is stated in section 5.

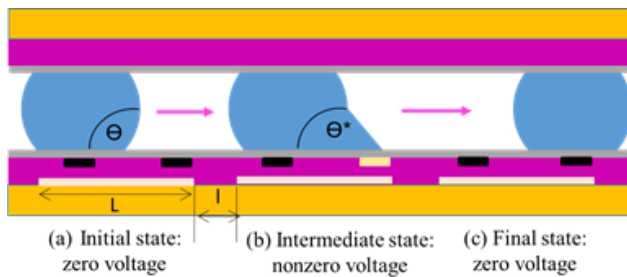


Fig. 1. Droplet movement via applying electrical field^{1,17}.

2. Mathematical Model of EWOD System

2.1. Equation of motion

The motion of the micro droplet in the EWOD system can be modeled as the one degree of freedom lumped mass model based on the Newton's law. The model is explained by previous researchers in Refs. 13-14 and 24-26. In this work, this mathematical model is used in the design procedures of this motion control.

For a mathematical model of EWOD system, the droplet is considered as the moving rigid body under the summation of driving force, threshold of driving forces, and resistive forces as shown in Fig. 2. Thus, the mathematical model describing the behavior of the droplet motion can be expressed in (1)^{13,14,24-26}.

$$m \frac{d^2x}{dt^2} = F_{dr} - F_{thresh} - F_d - F_c - F_f \quad (1)$$

where the displacement and the mass of the droplet are represented by x and m respectively. The driving force (F_{dr}) is the electrical force induced from the applied voltage and the corresponding threshold (F_{thresh}) is the minimum force needed to move the droplet from the rest^{1,13,14,24-27}. The terms F_d , F_f , and F_c represent resistive forces. These forces are listed and denoted as follows: (i) F_d is the shear force acting on the droplet on top and bottom of the droplet^{1,13,14,24-26}. (ii) F_f is the drag force acting on the droplet from the filler fluid^{13,14,24-26}. (iii) F_c is the contact line friction force acting at the contact line on the top and bottom of the droplet^{13,14,24-26}. The resistive forces can be expressed in terms of velocity of droplet ($U = \dot{x}$), fluid properties, and geometries of the droplet as shown in (2) and (3). The geometric properties of droplet related to the resistive forces are explained in the following content. (i) the radius of the droplet on the hydrophobic layer is assumed to be 5% overlapping with the length of the electrode^{13,14} and denoted by a ^{1,13,14}, and (ii) the gap between the bottom plate and the top plate, defining the height of the droplet^{13,14}, is denoted by H . Relevant fluid properties are the viscosity of the droplet and the coefficient of contact line of friction. These are represented by μ_d and ζ , respectively^{13,14,24-26}.

$$F_d = \left(\frac{6\mu_d U}{H} \right) (2\pi a^2) \quad (2)$$

$$F_c = \zeta U^n (4\pi a) \quad (3)$$

The exponent term (n) is in the range from 0 to 2^{13,14,24-26}.

According to Ref. 24, in the case of using air as a filler fluid, the drag force (F_f) can be neglected. Readers can obtain more details of all forces in Eq. (1) – (3) from Refs. 1, 13, 14, and 24-27.

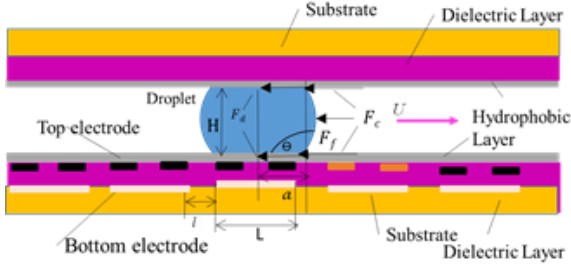


Fig 2. Moving droplet in EWOD system^{13,14,17}.

2.2. State space representation

In order to design the control law, the state space representing the EWOD system needed to be formulated. The state variables in this system are the displacement (x) and velocity (\dot{x}) of the droplet. Thus, the state vector of the system is defined as $\underline{x} = [x_1 \ x_2]^T = [x \ \dot{x}]$ ¹⁵⁻¹⁷, the state space representation can be formulated as (4)¹⁵⁻¹⁷.

$$\left. \begin{aligned} \dot{x}_1 &= x_2 \\ \dot{x}_2 &= f(\underline{x}, t) + g(\underline{x}, t)u(t) + d(t) \\ y &= x_1 \end{aligned} \right\} \quad (4)$$

where $g(\underline{x}, t) = \frac{1}{m}$

and $f(\underline{x}, t) = \frac{1}{m} \left[-\left(\frac{6\mu_d x_2}{H} \right) (2\pi a^2) - \zeta x_2^n (4\pi a) \right]$.

$u(t)$ is a control input representing F_{dr} and y is the output. The bounded disturbance signal is denoted as $d(t)$ and $\|d(t)\| \leq M$ for $M > 0$ ^{15,16,21}.

3. Fuzzy Sliding Mode Controller Design

The fuzzy sliding mode control (FSMC) based on an equivalent control is employed to achieve the accuracy of motion droplet in EWOD. Physically, the droplet is controlled to move from one electrode to the next one accurately along the desired periodic reference signal

(x_r) under the fuzzy sliding mode control. The diagram of control can be shown in Fig. 3.

The controller design consists of two parts. The design of sliding mode controller based on an equivalent control is in section 3.1. In section 3.2, the fuzzy rules are defined for further investigations.

3.1. Sliding mode control

The concept of sliding mode control based on an equivalent control is based on Refs. 19-23. The procedure of sliding mode controller based on the equivalent control (from Refs. 19 and 21-23) are presented below. In this approach, the control input u is defined as shown in (5)^{19,21-23}.

$$u = u_{eq} + u_{sw} \quad (5)$$

where u_{eq} is an equivalent control and u_{sw} is a switching control.

The corresponding sliding surface^{22, 23} or switching function²¹ (s) can be expressed in term of tracking error as in (6)^{19,21-23}.

$$s(\underline{x}, t) = c_1 e + c_2 \dot{e} \quad (6)$$

where $e = x_r - x_1$ and $\dot{e} = \dot{x}_r - \dot{x}_2$. The derivative of surface function is calculated as (7)^{19,21-23}.

$$\begin{aligned} \dot{s}(\underline{x}, t) &= c_1 \dot{e} + c_2 \ddot{e} \\ &= c_1 \dot{e} + (\ddot{x}_r - \ddot{x}_2) \end{aligned}$$

$$\dot{s}(\underline{x}, t) = c_1 \dot{e} + (-f(\underline{x}, t) - g(\underline{x}, t)u(t) + \ddot{x}_r) \quad (7)$$

When $d(t) = 0$, the equivalent control (u_{eq}) is determined by solving for $u(t)$ in (7) such that $\dot{s}(\underline{x}, t) = 0$ ^{19,21-23}.

$$c_1 \dot{e} + (-f(\underline{x}, t) - g(\underline{x}, t)u(t) + \ddot{x}_r) = 0$$

$$u_{eq} = \frac{1}{g(\underline{x}, t)} (c_1 \dot{e} + \ddot{x}_r - f(\underline{x}, t)) \quad (8)$$

In order to handle with the bounded disturbance $d(t)$, the switching control (u_{sw}) is designed below.

The Lyapunov function can be selected in the term of sliding surface (s) as (9)^{19,21-23}.

$$V = \frac{1}{2} s^2 \quad (9)$$

and the derivative is calculated as (10)^{19,21-23}

$$\dot{V} = s\dot{s} \quad (10)$$

The control u_{sw} is defined as (11)^{19,21-23}.

$$u_{sw} = \frac{1}{g(\underline{x}, t)} K \operatorname{sgn}(s) \quad (11)$$

where $K = \eta + M$, $\eta > 0$ ^{19,21-23}.

The stability of the method is proved as follows. Based on the control input in (8) and (11), it can be shown that $\dot{V} = s\dot{s} \leq 0$ ^{19,21-23} as below.

$$\begin{aligned}\dot{V} = s\dot{s}(x,t) &= s[c_1\dot{e} - f(x,t) - g(x,t)\left(\frac{1}{g(x,t)}(c_1e + \ddot{x}_r\right. \\ &\quad \left.- f(x,t)) + \frac{1}{g(x,t)}K \operatorname{sgn}(s) + \ddot{x}_r - d(t)\right] \\ &= s[-K \operatorname{sgn}(s) - d(t)] \\ &= -s(M + \eta) \operatorname{sgn}(s) - sd(t) = -\eta|s| \leq 0.\end{aligned}\quad (12)$$

It is noted that the stability is satisfied by the control input (5) as $\dot{V} \leq 0$ ^{19,21-23}. According to $f(x,t)$ and $g(x,t)$ in (4), the control EWOD system can track the reference signal accurately.

3.2. Fuzzy rules

In order to reduce the chattering problem caused by switching control (u_{sw}), the fuzzy rules is used to assign the value of switching gain (μ). This switching gain is depended on the magnitude of the disturbance^{21,23}. When $\mu=1$ in the case of SMC method, the control input in (5) becomes (13) for the case of FSMC^{21,23}.

$$u = u_{eq} + \mu u_{sw} \quad (13)$$

In the fuzzy system, μ is a fuzzy output derived from the switching function input (s). The range of μ and s are defined to be from -1 to 1²¹. The fuzzy rules are defined for the sliding mode control in (14) as presented in Ref. 21.

$$\left. \begin{array}{l} \text{If } s = 0, \text{ then } \mu = 0 \\ \text{If } s < 0, \text{ then } \mu > 0 \\ \text{If } s > 0, \text{ then } \mu > 0 \end{array} \right\} \quad (14)$$

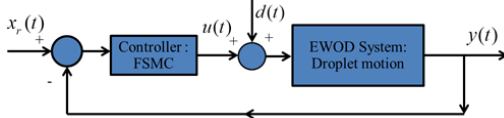


Fig 3. The Fuzzy sliding mode control applying on EWOD system^{15,16}.

4. Simulation Results and Discussions

The simulation was performed in MATLAB environment to evaluate the feasibility of fuzzy sliding mode control (FSMC) based on an equivalent control for the droplet motion in EWOD system. In addition, the chattering in the control input was considered. Thus, the simulation results of both FSMC and SMC methods were compared especially the chattering in the control

inputs. In simulation, the Runge-Kutta method was used for integration from initial time ($t=0$ s) to final time ($t=0.5$ s) with the sampling time (0.00001 s).

4.1. Simulation example

The simulation example of the EWOD system has two groups of parameters; the fluid properties and the geometry of the component of EWOD system. All necessary parameters with numerical values are summarized in this section. The dimensions of the EWOD system are as follows. First, the gap of the top and bottom surfaces was $H=300 \times 10^{-6}$ m^{13,14}. Second, the length electrode and the gap between them were $L=1600 \times 10^{-6}$ m and $l=70 \times 10^{-6}$ m as Ref. 28. The fluid properties used in simulation were as follows: (i) density of the droplet was $\rho_d = 998$ kg/m³²⁹, (ii) the contact angle of the droplet on the hydrophobic surface was $\theta=110^\circ$ ²⁴, (iii) coefficient of contact line friction was $\zeta=0.08$ Ns/m²²⁴, (iv) the radius of the droplet, $a=8.8 \times 10^{-4}$ m, defined under the overlap condition as $a=0.5L+0.05L$ ^{13,14}, and (v) the value of an exponent term was $n=2$. After the primary parameters were defined, the mass of the droplet (m) was 7.7863×10^{-7} kg, that was calculated from ρ_d and a ¹. The value of threshold force was assumed as $F_{thresh}=8 \times 10^{-6}$ N²⁴. The disturbance signal was assumed to be the Gaussian function as (15)²¹.

$$d(t) = Ae^{-\frac{(t-m_d)^2}{2s_d^2}} \quad (15)$$

where $A=3000 \times 10^{-6}$, $m_d=0.15$, and $s_d=0.02$. Most of the numerical values in this simulation were used before in our previous work¹⁵⁻¹⁷. Assuming that droplet was at rest at the initial time, the initial condition for the state variables in this simulation was defined as $x_1(0)=0$ m and $x_2(0)=0$ m/s¹⁵⁻¹⁶.

4.2. Sinusoidal reference signal

The sinusoidal function was the reference signal representing the periodic motion of the droplet travelling between two adjacent electrodes as a mixing process in Lab-on-a-chip^{1,2,15}.

$$x_r(t) = (L+l)\sin(\omega t) \quad (16)$$

The amplitude of the signal is a distance between two adjacent electrodes, including the gap between two electrodes¹⁵. The frequency of the signal was assumed to be $\omega=20\pi$ rad/s.

4.3. Control parameter

The control parameters consisted of constant terms in (6) and (11), which were selected as $c_1 = 50$, $c_2 = 1$ and $K = 15.6$. The parameter μ in (13) is defined by fuzzy rules. The membership function of the fuzzy system corresponding to μ and s are shown in Fig. 3(a) and 3(b) respectively. The terms of N , Z , and P are negative, zero, and positive values for s and μ in fuzzy rules²¹. Moreover, a centroid of area method was used in defuzzification.

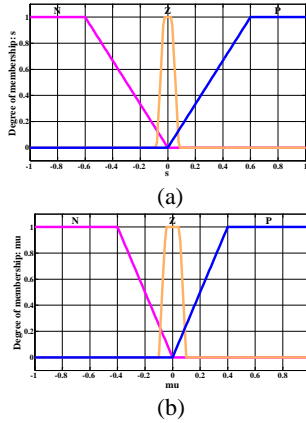


Fig. 3. Fuzzy's Rule: (a) membership function for s (b) membership function for μ .

4.4. Results of simulation example

The displacements of the droplet, tracking errors, and control inputs corresponding to the FSMC and SMC method based on an equivalent control are shown in Fig. 4(a) and 4(b) respectively. In Fig. 4, when employing the FSMC method, the control system could track the sinusoidal reference signal accurately as the SMC method. However, the tracking error of the FSMC method converges to zero slower than that of the SMC method. Additionally, the chattering in the control input of the FSMC method was less than that of the SMC method as shown clearly in Fig. 5.

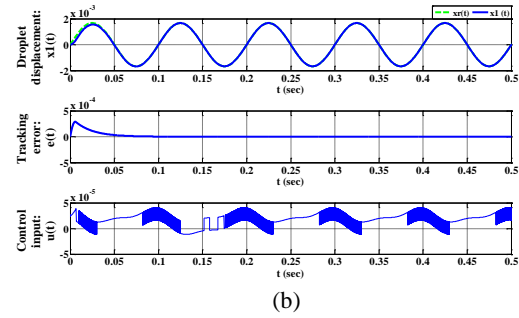
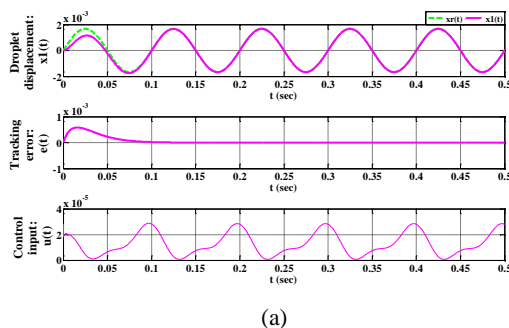


Fig. 4. The displacement, tracking errors, and control inputs; (a) Fuzzy sliding mode control (b) Sliding mode control.

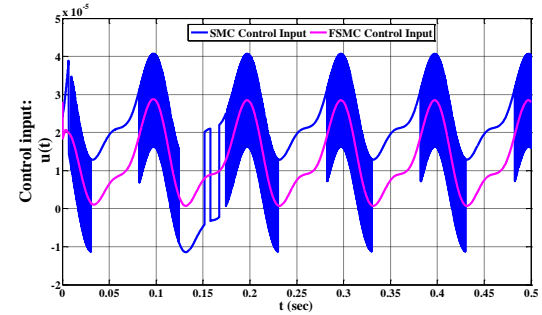


Fig. 5. Control input signal of FSMC (Pink) and SMC (Blue) methods.

5. Conclusions

This study illustrated that the FSMC method could provide a good accuracy in tracking the periodical signal under the disturbance. Thus, the droplet in the EWOD system was able to track the periodic signal accurately by using the FSMC method under the disturbance signal with lower chattering compared to that of the SMC method. The reduction of the chattering was important for this method, especially in the implementation of practical control system. Therefore, the fuzzy sliding mode control based on an equivalent control was successfully applied for the micro droplet motion in this EWOD.

6. References

1. J. Berthier, *Microdrops and Digital Microfluidics* (William Andrew, Norwich New York, 2008).
2. S. K. Cho, H. Moon and C. J. Kim, Creating, transporting, cutting, and merging liquid droplets by electrowetting-based actuation for digital microfluidic circuits, *Journal of Microelectromechanical Systems*. **12**(1), February 2003, pp. 70-80.
3. V. Srinivasan, V. K. Pamula, M. G. Pollack and R. B. Fair, Clinical diagnostics on human whole blood, plasma, serum, urine, saliva, sweat, and tears on a digital microfluidic platform, in *Proceedings of the 7th*

- International Conference on Miniaturized Chemical and Biochemical Analysis Systems*, Squaw Valley, California, U.S.A., October 5-8, 2003, pp. 1287-1290.
4. C. Rivet, H. Lee, A. Hirsch, S. Hamilton and H. Lu, Microfluidics for medical diagnostics and biosensor, *Chemical Engineering Science* **66** (2011), pp. 1490-1507.
5. H. C. Lin, Y. J. Liu and D. J. Yao, DNA ligation using coplanar electrodes electro-wetting-on-dielectric (EWOD) device, in *Proceedings of the 2009 4th IEEE International Conference on Nano/Micro Engineering and Molecular Systems (NEMS 2009)*, Shenzhen, January 5-8, 2009, pp. 358-389.
6. H-H. Shen, T-Y. Su, H-Y. Chang and D.-J. Yao, SNP detection based on temperature-controllable EWOD digital micro fluidics system, in *Proceedings of the 2012 IEEE Nanotechnology Material and Device Conference*, Hawaii, U.S.A., October 16-19, 2012, pp. 92-95.
7. K. Y.-T. Lai, Y. T. Yang and C. Y. Lee, An intelligent digital microfluidic processor for biochemical detection, *Journal of Signal Processing System* (2015) **78**, pp. 85-93.
8. T. Braun, K. F. Becker, M. Koch, E. Jung, J. Lienemann, J. G. Korvink, R. Kahle, J. Bauer, R. Aschenbrenner and H. Reichl, Contactless Component Handling on PCB using EWOD principles, in *Proceedings of 2008 10th Electronics Packaging Technology Conference, 2008 (EPTC 2008)*, Singapore, December 9-12, 2008, pp. 186-192.
9. E. Schaler, M. Tellers, A. Gerratt, I. Penskiy and S. Bergbreiter, Toward fluidic microrobots using electrowetting, in *Proceedings of 2012 IEEE International Conference on Robotics and Automation (ICRA)*, Saint Paul, MN, U.S.A., May 14-18, 2013, pp. 3461-3466.
10. I. Moon and J. Kim, Using EWOD (electrowetting-on-dielectric) actuation in a micro conveyor system, *Sensor and Actuators A: Physical*, **130-131** (2006), pp. 537-544.
11. W. Satoh, H. Hosono, K. Morimoto and H. Suzuki, Micro analysis system with an integrated microfluidic system based on electrowetting, in *Proceedings of the fourth IEEE Conference on Sensors (IEEE SENSORS 2005)*, Irvine, CA, U.S.A., October 30-November 3, 2005, pp. 37-40.
12. A. Takei, N. Binh-Khiem, E. Iwase, K. Matsumoto and I. Shimoyama, Liquid motor driven by electrowetting, in *Proceedings of IEEE 21st Conference on Micro Electro Mechanical Systems, (MEMS 2008)*, Tucson, Arizona, U.S.A., January 13-17, 2008, pp. 42-45.
13. B. Bhattacharjee and H. Najjaran, Simulation of droplet position control in digital microfluidic systems, *Journal of Dynamic Systems, Measurement, and Control* **132**(1) (2010), pp. 014501-1-014501-3.
14. B. Bhattacharjee and H. Najjaran, Droplet position control in digital microfluidic systems, *Biomed Microdevices* **12** (2010), pp. 115-124.
15. A. Boonyaprapasorn and T. Sethaput, Design of sliding mode controller for droplet position in EWOD microfluidic system, in *Proceedings of the 2015 International Conference on Artificial Life and Robotics (ICAROB 2015)*, Oita, Japan, January 10-12, 2015, pp. 17-21.
16. A. Boonyaprapasorn, E. Pengwang, T. Maneewarn, P. Sa Ngiamsunthorn, C. Pongsomboon, W. Wechsathol and R. Silapunt, Backstepping and backstepping sliding mode controller for droplet position in electrowetting on dielectric system, in *Proceedings of 2015 15th International Conference on Control, Automation and Systems (ICCAS 2015)*, Bexco Busan, Korea, October 13-15, 2015, pp. 1457-1462.
17. A. Boonyaprapasorn, T. Maneewarn and E. Pengwang, Position control of droplet in electrowetting on dielectric system using feedback linearization, in *Proceedings of The 6th TSME International Conference on Mechanical Engineering*, Regent Cha-Am Beach Resort, Petchburi, Thailand, December 16-18, 2015, (accepted September 15th, 2015).
18. S. C. C. Shih, R. Fobel, P. Kumar and A. R. Wheeler, A feedback control system for high-fidelity digital microfluidics, in *Proceedings of 14th International Conference on Miniaturized Systems for Chemistry and Life Sciences*, Groningen, The Netherland, October 3-7, 2010, pp. 2032-2034.
19. J.-J. E. Slotine and W. Li, *Applied Nonlinear Control* (Prentice Hall, New Jersey, 1991).
20. V. I. Utkin, *Sliding Modes in Control and Optimization* (Springer-Verlag, Berlin Heidelberg, 1992).
21. J. Liu and X. Wang, *Advanced Sliding Mode Control for Mechanical Systems*, (Tsinghua University Press, Beijing, and Springer-Verlag, Berlin Heidelberg, 2011).
22. C. C. Kung and C. C. Liao, Fuzzy-sliding mode controller design for tracking control of nonlinear system, in *Proceedings of the American Control Conference*, 1994, **1**, Baltimore, Maryland, U.S.A., June 29th–July 1st, 1994, pp. 180-184.
23. J.-Y., Chen, Expert SMC-based fuzzy control with genetic algorithms, *Journal of The Franklin Institute* **336** (1999), pp. 589-610.
24. H. Oprins, B. Vandevelde and M. Baelmans, Modeling and control of electrowetting induced droplet motion, *Micromachines* **3** (2012), pp. 150-167.
25. V. Bahadur and S. V. Gaimella, An energy-based model for electrowetting-induced droplet actuation, *Journal of Micromechanics and Microengineering* **16** (2006), pp. 1494-1503.
26. H. Ren, R. B. Fair, M. G., Pollack and E. J. Shaughnessy, Dynamics of electro-wetting droplet transport, *Sensor and Actuators B*, **87** (2002), pp. 201-206.
27. J. Berthier, P. Dubois, P. Clementz, P. Claustre, C. Peponet and Y. Fouillet, Actuation potential and capillary forces in electrowetting based microsystem, *Sensor and Actuators A* **134** (2007), pp. 471-479.
28. C. Phongsomboon, Mobility control of a droplet on top of a flat plate, M.S. thesis, Dept. Mechanical Engineering, King Mongkut's University of Technology Thonburi, Bangkok, Thailand, 2012 (in Thai).
29. R. W. Fox, P. J. Pritchard and A. T. McDonald, *Introduction to Fluid Mechanics 7th edition* (John Wiley and Sons, Hoboken, NJ, 2010).

Development of Micro-Permanent Magnet Synchronous Reluctance Generator for TPMS on Smart Robots

Chun-Chieh Chang, Cheng-Tang Pan, Shao-Yu Wang, An-Yun Yang, Gu-Xuan Lin, Yu-Jen Wang
National Sun Yat-sen University, Kaohsiung, 80424, Taiwan
panct@mail.nsysu.edu.tw

Roger Chenglung Lee, Ting-Hung Chung
Naroller Electronics, Kaohsiung, 80424, Taiwan
335i2007@gmail.com

Abstract

Synchronous Reluctance Generator (SynRG) is a stability and robust motor with simple structure and low cost. In this paper, the SynRG which embedded magnet was used in tire pressure monitoring system (TPMS). The slot-pole ratio was analyzed to obtain greater generating capacity, minimize cogging torque and torque ripple. A wide selection of surface permanent magnet generator (SPMG) was compare with PM-SynRG. The results show that the generating capacity of PM-SynRG was more than 3 V with high degree of stability in the operation.

Keywords: Magnet synchronous reluctance generator, Tire pressure monitoring system

1. Introduction

Synchronous reluctance generators (SynRG) have been widely used in industries such as energy, integration - starter generator (ISG), and wind turbines [1-3]. In general, an optimization characteristics of SynRG are defined as the maximum induced voltage, the minimum cogging torque, the maximum efficiency, and the maximum power factor. There are many studies on SynRG in a wind turbine power generating system [4-7]. SynRG has a robust and low price due to its simple rotor structures. In addition, SynRG is applies to variable speed operation, because of its low noise. In the most popular hybrid electric vehicle (HEV), there are many studies of SynRG to replace permanent magnet generator (PMG) [8,9]. The permanent magnet synchronous reluctance generator (PM-SynRG) was applied to micro-generator due to low cost, high efficiency and stability. Especially in the smaller size of the generator, a large torque ripple easily leads to the obstruction of rotation.

In this paper, the PM-SynRG which embedded magnet was used in tire pressure monitoring system (TPMS). It has a stable generating capacity and robust

structure. In the experiment, a wide selection of surface permanent magnet generator (SPMG) was compare with PM-SynRG to confirm the performance. Figure 1 shows the schematic of the winding structure and the rotor structures. There are plenty of magnet materials where the selection of magnet material needs to be considered carefully. The NdFeBr was selected because of the magnet undesired demagnetization [10]. The ratio of the slot and pole and the winding distribution were also analyzed in this paper. In addition to a larger amount of power, the cogging torque and torque ripple was concerned.

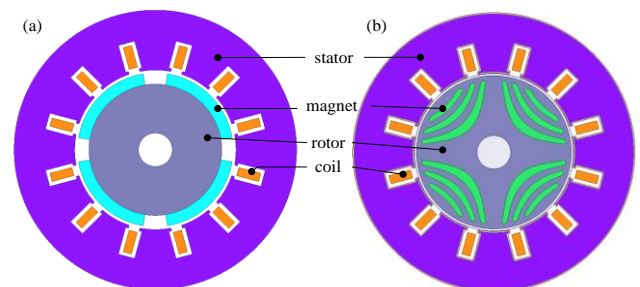


Figure 1 Schematic diagram of (a) SPMG and (b) PM-SynRG

2. Experimental Methods

2.1 Design specifications

Finite element method (FEM) was used for the magnetic circuit analysis, including the B-EMF, B-EMF waveform, torque, and torque ripple. In the structural design, as shown in table 1, the number of coils was considered to the size of generator, and the 400 turns was calculated. An air gap between the rotor and the stator was set at 0.55 mm, and rotational speed is 500 rpm.

The critical properties of permanent magnets for permanent magnet generators are high BH energy. The commercial magnet, Nd₂Fe₁₄B, have coercive force approaching 890 (kA/m). To operate the PMG with permanently excited PM poles at variable power factors is concerned.

Table 1 Specification List

Item(Unit)	Value	
Type of machines	SPMG	SynRG
Stator poles numbers	12, 24	
Rotor poles numbers	4, 8, 10	
Stator outer radius(mm)	50	
Stator inner radius(mm)	28.6	
Airgap length(mm)	0.55	
Axial length(mm)	5	
Turns per coil	400	
Magnet remanence(T)	1.23	
Coercive force of PM(kA/m)	890	
Rated speed(rpm)	500	
Load Resistance(ohm)	100	

2.2 Permanent magnet synchronous machine

The equations for the permanent magnet synchronous machine in the d-q-components were shown below [11],

$$\mu_{sd} = R_s i_{sq} - \omega_{el} L_d i_{sd} \quad (1)$$

$$\mu_{sq} = R_s i_{sq} + \omega_{el} L_d i_{sd} + \omega_{el} \phi_m \quad (2)$$

where μ_{sd} and μ_{sq} are the stator voltage in d and q axis, R_s is the armature phase resistance, ω_{el} is the electrical speed, L_d is the d-axis inductance, L_q is the q-axis inductance, i_{sd} and i_{sq} are the stator current in d and q

axis respectively and ϕ_m is the flux linkage originating from the magnets.

The torque is formed as

$$T = \frac{3}{2} P [\phi_m i_{sq} + (L_d - L_q) i_{sq} i_{sd}] \quad (3)$$

where p is the number of pole pairs.

2.3 Winding design

There are a lot of feasible combinations of stator and rotor pole numbers in multiphase PM machines, viz.,

$$N_s = k_{1m}, k_1 = 1, 2, \dots \quad (4)$$

$$N_r = N_s \pm k_2, k_2 = 1, 2, \dots \quad (5)$$

where N_s and N_r are the number of stator and rotor poles, respectively, and m is the number of phases. k_1 is an integer number when m is an even number, but k_1 should be an even number when m is an odd number, since the number of stator poles must be even, which is different from the conventional fractional-slot PM machines [12].

2.3.1 Calculation of the span θ_s of per slot is

$$\theta = \frac{N_p \times 180^\circ}{N_s} \quad (6)$$

2.3.2 Calculation of the phase offset 120° E that the required number of slots (K_0) is

$$K_o = \frac{120^\circ + q \times 360^\circ}{\theta_s} \quad (7)$$

Where $q = 1, 2, \dots, (N_p/2 - 1)$, Phase offset of slot pitch K_0 . When unable to find a suitable integer K_0 , that means that the selected number of poles and stator slots feasible combination, and to be re-selected.

The 120° means that each of phase is a gap of 120° degrees; $q \times 360^\circ / \theta_s$ means to find in all phases of a coil, and it could sense the same voltage waveform in a cross slot pitch

2.3.3 Select the number of slots spans of coil S^*

$$S^* = \max[\text{fix}(\frac{180}{\theta_s})] \quad (8)$$

The fix (.) is the maximum of two numbers in the integer part. All the slots are numbered along the direction of rotation of the generator.

2.4 Calculation of the torque ripple

Back electromotive force (B-EMF) waveform was analyzed above. When the generator was rotated, the torque was produced. The torque ripple was calculated in each of slot, poles of combination as defined in (9):

$$T_{rip}(\%) = \frac{T_{max} - T_{min}}{T_{avg}} \times 100\% \quad (9)$$

where T_{max} is the maximum torque, T_{min} is the torque minimum, and T_{avg} is average torque.

3. Simulation Analysis

FEM was used for the magnetic circuit analysis, including the B-EMF, B-EMF waveform, torque, and torque ripple.

3.1 Analysis of Back Electromotive Force(B-EMF)

Figure 2 shows that the generating capacity of SPMG is greater than PM-SynRG, because the flux of the SPMG was no obstacle in rotor. In the study, when the number of poles was increased gradually, the generating capacity of PM-SynRG was decreased; when the number of poles gradually was increased, the generating capacity of SPMG was increased. On the other hand, the number of slots was increased, generating capacity of PM-SynRG are also increased. The result above in the poles 10 poles, the 12 and 24 slots generating capacity were almost the same. When the number of slots of SPMG is increased to 24 slots, power generating capacity is not significantly increased. Figure 3 shows a B-EMF waveform diagram, B-EMF waveform was observed to exhibit a concave or flat shape of the peak, when the number of slots with pole number is less. The reason was that when the number of slots and poles was small, each slot of each phase coil which induced B-EMF was different. When all are combined, B-EMF will form a non-sinusoidal shape. Generator was stabilized and enhanced the efficiency of the operation due to the output is close to the sine wave. Although the generating capacity of PM-SynRG is

smaller than SPMG, the generating capacity of micro generators was reached that more than 3 V.

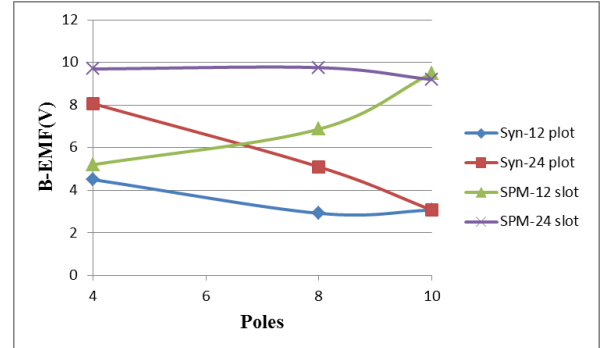


Figure 2 B-EMF of comparison of two types of generators

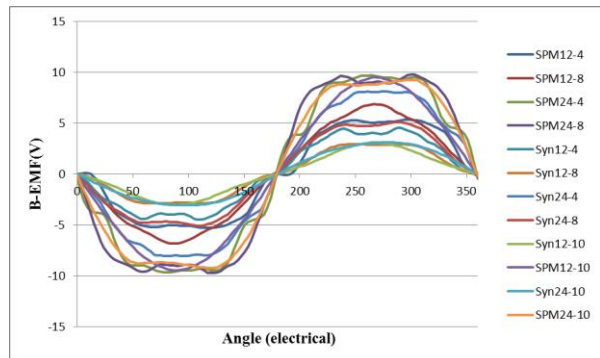


Figure 3 B-EMF waveform of comparison of two types of generators

3.2 Torque Analysis

Figure 4 shows that SPMG torque magnitudes were larger than the PM-SynRG and the gap was even greater with the increase of the number of poles. The reason was the structure of PM-SynRG had a high degree of stability during operation. The torque magnitudes of PM-SynRG were gradually reduced with the increase of the number of poles; the torque magnitudes of SPMG were gradually increased with the increase of the number of poles. Figure 5 shows a waveform diagram of torque and it was found that SPMG torque ripple was greater than the PM-SynRG. Both torque ripples were smaller with the increase of the number of slots and poles. From the above analysis, torque and torque ripple of PM-SynRG were less than SPMG. In particular, the generating capacity was less than 4V and the trend increasingly obvious.

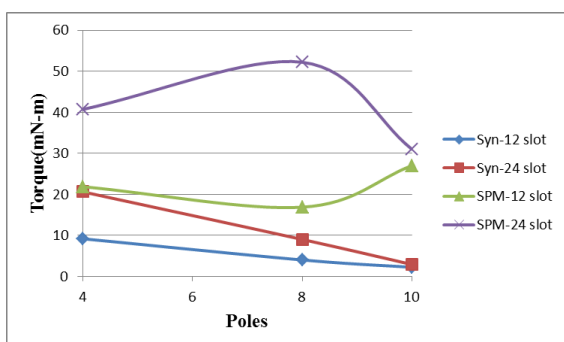


Figure 4 Torque of comparison of two types of generators

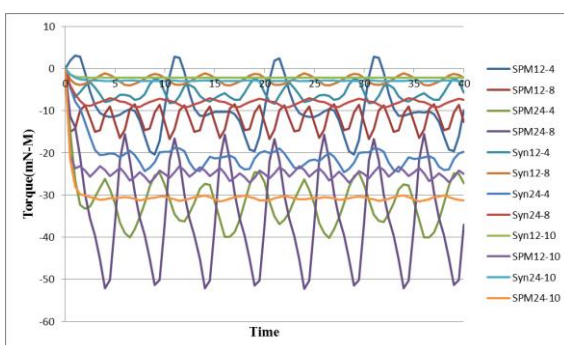


Figure 5 Torque ripple of comparison of two types of generators

4. Conclusions

In the paper, the PM-SynRG was applied to the TPMS to achieve a stable and robust power generating structure. The ratios of slot-pole number were analyzed to obtain greater power generating capacity and decrease cogging torque and torque ripple. The results show that generating capacity of PM-SynRG was more than 3 V. In the torque magnitude and torque ripple, PM-SynRG was less about 3 times than SPMG with high stability. For micro tire pressure detectors required performance, PM-SynRG was achieved the requirement for generating capacity and has a high degree of stability in the operation.

References

1. S. Tokunaga, K. Kesamaru. "FEM simulation of novel small wind turbine generating system with synchronous reluctance generator", *Electrical Machines and Systems (ICEMS)*, 2011.
2. M.A. Rahman, "Advances of Interior Permanent Magnet (IPM) Wind Generators", *Electrical Machines and Systems*, 2008, pp. 2228 - 2233.

3. Erko Lepa and Aleksander Kilk, *Analysis and Prototyping of a Low-Speed Small Scale Permanent Magnet Generator for Wind Power Applications*, *Electric Power Quality and Supply Reliability Conference (PQ)*, 2012.
4. S. Morimoto, H. Kato, M. Sanada and Y. Takeda, "Output Maximization Control for Wind Generating System with Interior Permanent Magnet Synchronous Generator", *Proceedings of IEEE - IAS Annual Meeting*, Tampa, FL, October 4-8, 2006, pp. 503-510.
5. S. Morimoto, H. Nakayama, M. Sanada and Y. Takeda, "Sensorless Output Maximization Control for Variable-Speed Wind Generating System using IPMSG", *IEEE Transactions on Industry Applications*, Vol. 41, No. 1, 2005, pp. 60-67.
6. Dept. of Electr. & Comput. Eng., Texas A&M Univ., College Station, TX, "Maximum output power control of permanent magnet-assisted synchronous reluctance generator", *ICEM*, 2008.
7. Urase, K., Tokyo, Kiyota, K., Sugimoto, H., Chiba, Design of a Switched Reluctance Generator Competitive with the IPM Generator in Hybrid Electrical Vehicles, *Electrical Machines and Systems (ICEMS)*, 2012.
8. Poopak Roshanfekr, Sonja Lundmark, Torbjörn Thiringer, and Mikael Alatalo, "A Synchronous Reluctance Generator for a Wind Application- Compared with an Interior Mounted Permanent Magnet Synchronous Generator", *Power Electronics, Machines and Drives (PEMD)*, 2014.
9. Dept. of Electr. & Comput. Eng., Texas A&M Univ., College Station, TX, "Optimal design and comparison of stator winding configurations in permanent magnet assisted synchronous reluctance generator", *Conference: Electric Machines and Drives Conference*, 2009.
10. M. Katter, "Angular Dependence of Demagnetization Stability of Sintered Nd-Fe-B Magnets," *IEEE Transactions on Magnetics*, Vol. 41, 2005, pp. 3853-3855.
11. J. T. Chen, and Z. Q. Zhu, "Winding configurations and optimal stator and rotor pole combination of flux-switching PM brushless AC machines," *IEEE Trans. Energy Conversion*, vol. 25, no. 2, 2010, pp. 293-302.
12. D. Ishak, Z. Q. Zhu, and D. Howe, "Comparison of PM brushless motors, with either all or alternative wound teeth," *IEEE Trans. Energy Convers.*, vol. 21, no. 1, 2006, pp. 95-103.

Study of Micro-Flux-Switching Permanent-Magnet Generator for TPMS on Smart Robots

An-Yun Yang, Cheng-Tang Pan, Shao-Yu Wang, Chun-Chieh Chang, Gu-Xuan Lin, Yu-Jen Wang
Department of Mechanical and Electromechanical Engineering, National Sun Yat-sen University,
No. 70, Lienhai Rd., Kaohsiung 80424, Taiwan
panct@mail.nsysu.edu.tw

Roger Chenglung Lee, Ting-Hung Chung
Naroller Electronics, Kaohsiung, 80424, Taiwan
335i2007@gmail.com

Abstract

Flux-Switching Permanent-Magnet Generator (FSPMG) with high flux density and high efficiency was designed due to its double salient structures. This study presents a micro FSPMG which was applied to tire pressure monitoring system (TPMS) on the smart robots. In this paper, finite element method (FEM) was utilized to simulate the magnetic properties of generator and then the flux and voltage output was obtained. The magnetic material used in this study was ferrite magnet which has the advantage of lower-cost.

Keywords: Generator, Flux-Switching, Tire pressure monitoring system, Finite element method.

1. Introduction

In automotive and aerospace fields, high efficiency machines are necessary nowadays. The axial field permanent magnet (PM) machine was concerned [1-3]. However, when the rotor temperature raise, the magnets inside the rotor on the conventional PM machine is irreversible demagnetize and mechanical damage. In 1995, the flux-switching PM (FSPM) machine was first proposed [4]. The feature of FSPM was that magnets in the stator with double salient structure were able to avoid the problem above [5]. FSPM machines are also high torque density with appropriate control [6-11]. The FSPM machines tend to investigate on FSPM motors so far, only few study mention about FSPM generator (FSPMG). In this study, finite element method (FEM) was utilized to simulate two types of FSPM generators properties and compared with the surface permanent magnet (SPM). Meanwhile, the FSPM generators apply

on tire pressure monitoring system (TPMS) with stable electromotive force (EMF) was discussed.

2. Design of generator

2.1. Steps of winding design

There are many combinations of slot-pole ratio, feasible winding poles formula was shown in Eq. (1) and (2) [12].

$$N_s = k_1 m \quad (1)$$

$$N_r = N_s \pm k_2 \quad (2)$$

Where N_s is slots of stator, N_r is poles of rotor, m is phase number.

If the motor is multi-teeth, feasible winding poles formula was shown in Eq. (3) and (4) [13].

$$N_r = 2N_s \pm 1 \quad (3)$$

$$N_r = N_s(2n - 1) \pm 1 \quad (4)$$

The FEM was used to analyze a three-phase FSPMG. The schematic of 12/10-pole FSPMG with a doubly-salient structure and 6/17-pole FSPMG with multi teeth were shown in Fig. 1.

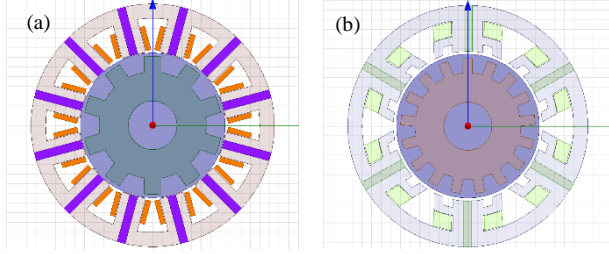


Fig. 1. (a)The structure of 12/10-pole FSPM generator
(b) The structure of 6/17-pole FSPM generator

Calculation of the span in every slot, the slot of phase offset and the slot numbers of span were shown in Eq. (5), (6) and (7) [14].

$$\theta_s = \frac{N_p}{N_s} \quad (5)$$

$$K_0 = \frac{120^\circ + q \times 360^\circ}{\theta_s} \quad (6)$$

$$S^* = \max\left[\text{fix}\left(\frac{180}{\theta_s}\right), 1\right] \quad (7)$$

Where the θ_s and the K_0 are all integer.

2.2. Winding Factor

Eq. (8) was calculated the winding factor [15],

$$K_d = \frac{\sin\left(\frac{Qva}{2}\right)}{Q\sin\left(\frac{va}{2}\right)} \quad (8)$$

where Q is the number of EMF vectors per phase, α is the angle between two adjacent vectors, and v is the order of harmonic. Stator slots, rotor poles and the number of phases can decide winding factor.

The winding factors of the FSPM machines with different combination of stator pole and rotor pole numbers cause different results. Table 1 shows the designs specifications including traditional SPM, FSPM and multi-teeth FSPM.

Table 1. FSPM, multi-teeth FSPM and SPM specification

Type of machines	FSPM	multi-teeth FSPM	SPM
Slot-pole ratio	12/10	6/17	12/10
Stator outer radius	25mm		
Stator inner radius	15mm		
Airgap length	0.58 mm	0.13mm	0.5 mm
Turns per coil	400		
Rated speed	500rpm		
Resistance	100 ohm		
Magnet magnitude	-253000 A/m		

3. Results and Discussion

The equivalent circuit of the generator was shown in Fig. 2. The circuit was including inductance and resistance with 100 ohm. The inductance was regarded as input.

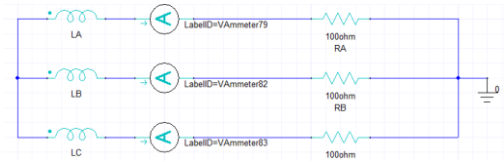


Fig. 2. The equivalent circuit

3.1. Flux distributions in FSPM, multi-teeth FSPM and SPM

Three generators were investigated by FEM. The flux distributions were shown in Fig. 3. From the flux distribution, the density of flux in the stator back-iron is lower than that in the stator teeth due to leakage flux.

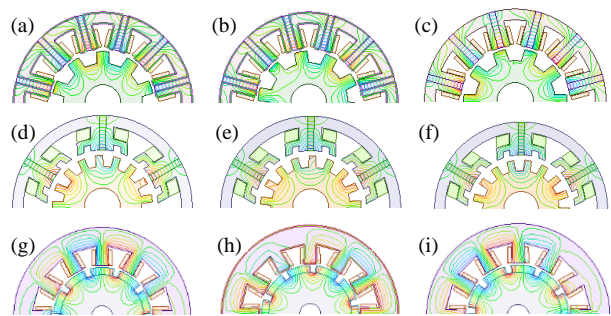


Fig. 3 (a)-(c) FSPM flux distributions from 0 s to 0.01s

(d)-(f) multi-teeth FSPM flux distributions from 0s to 0.01s, (g)-(i) SPM flux distributions from 0s to 0.01s

3.2. Flux-linkage in FSPM, multi-teeth FSPM and SPM

Fig. 4 show that three generators flux-linkage were almost sinusoidal. The FSPM is between ± 0.0121 Wb, the multi-teeth FSPM is between ± 0.0006 Wb and the SPM is between ± 0.0096 Wb

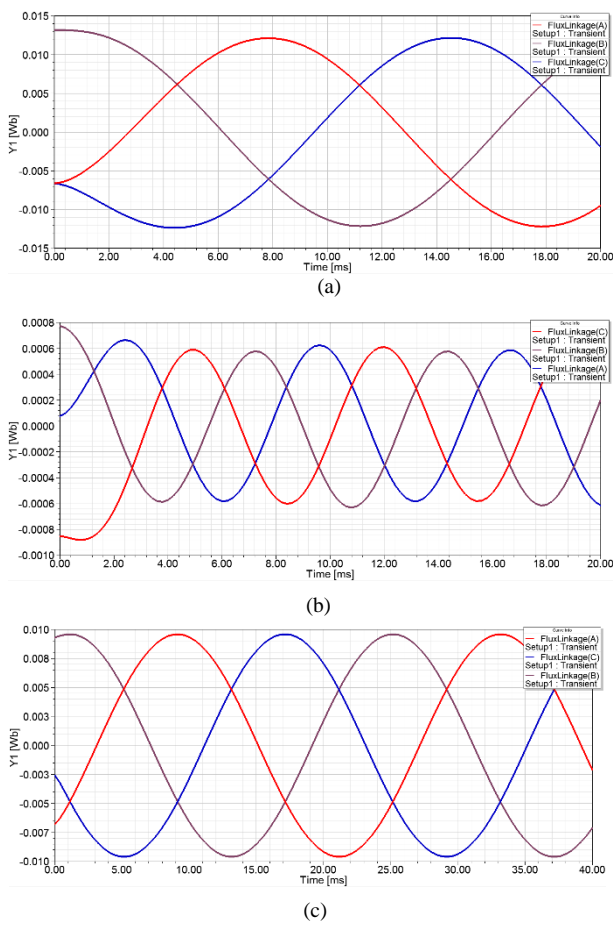


Fig. 4 The flux-linkage of (a) FSPM generator, (b) multi-teeth FSPM generator and (c) SPM generator.

3.3. EMF in FSPM, multi-teeth FSPM and SPM

Fig. 5 shows the EMF of three generators were almost sinusoidal. The FSPM is between ± 3.6 V, the multi-teeth FSPM is between ± 0.58 V and the SPM is between ± 2.5 V.

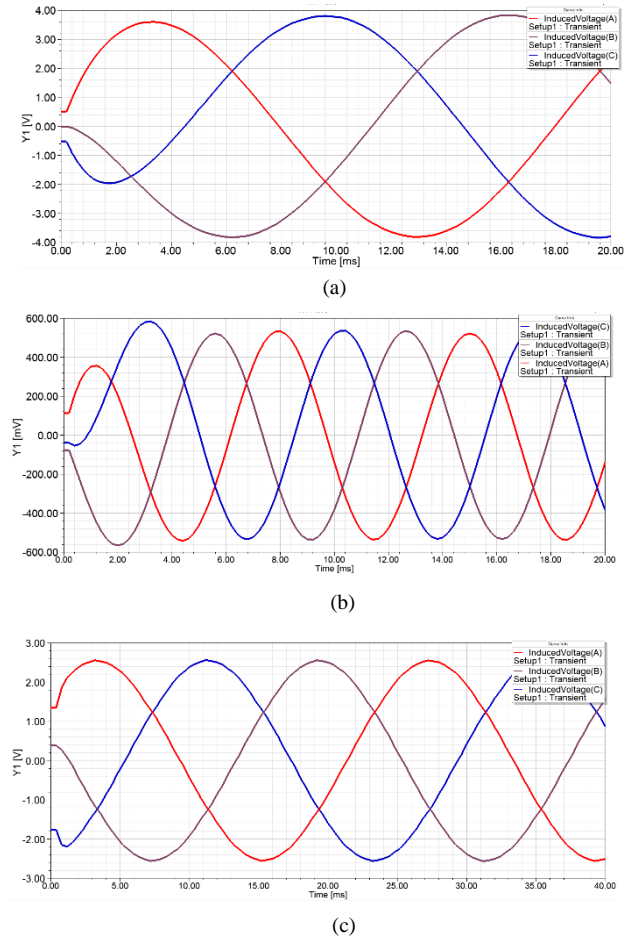
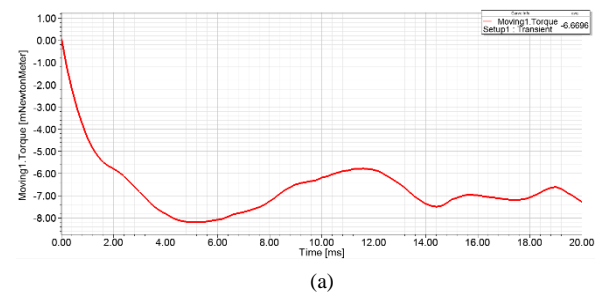


Fig. 5 The EMF of (a) FSPM generator, (b) multi-teeth FSPM generator and (c) SPM generator.

3.4. Torque in FSPM, multi-teeth FSPM and SPM

Fig. 6 shows the torque of three generators. After 6ms, the torque of FSPM is about -7 mN-m and the SPM is about -1.79 mN-m. The average torque multi-teeth FSPM is about -53.7 N-m.



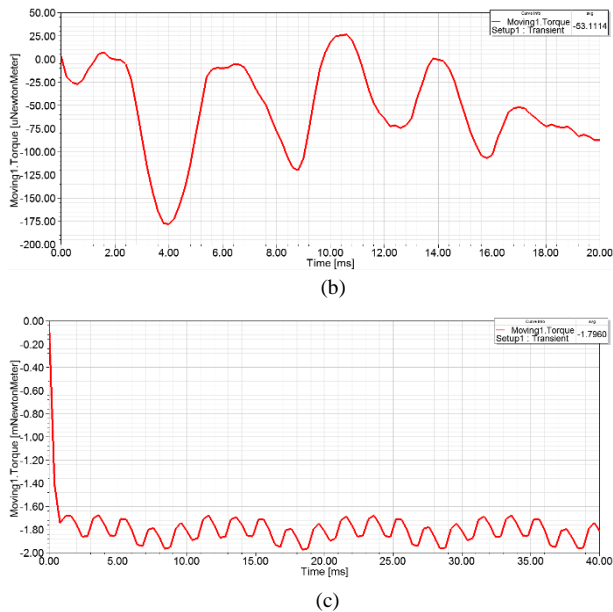


Fig. 6 The torque of (a) FSPM generator, (b) multi-teeth FSPM generator and (c) SPM generator.

4. Conclusion

A FSPM generator was proposed because of better power generation than traditional SPM. The ripple of FSPM is larger than SPM when generator, stable operation. Due to the Magnetic circuit of FSPM is complicated, it still can be improved by structure design. The power generation of FSPM is up to 3.6V. It was improved about 44% than traditional SPM. Also the frequency of EMF in FSPM is higher than SPM, it means the FSPM can save more energy than SPM in the same time. In multi-teeth FSPM, the ripple is obvious at first, but it was tended to be stable after 18 ms.

5. References

1. Y. Chen, P. Pillay, and A. Khan, "PM wind generator topologies," *IEEE Trans. Ind. Appl.*, vol. 41, no. 6, pp. 1619–1626, 2005.
2. A. Parviainen, J. Pyrhönen, and P. Konthanen, "Axial flux permanent magnet generator with concentrated wind power applications," in *IEEE Int. Conf. Electric Machines Drives*, San Antonio, TX, USA, 2005, pp. 1187–1191.
3. S. Huang, J. Luo, F. Leonardi, and T. A. Lipo, "A comparison of power density for axial flux machines based on general purpose sizing equations," *IEEE Trans. Energy Convers.*, vol. 14, no. 2, pp. 185–192, 1999.
4. S. E. Rauch and L. J. Johnson, "Design principles of the flux switch alternator," *AIEE Trans.*, vol. 74, no. 3, pp. 1261–1268, 1955.
5. E. Hoang, A. H. Ben-Ahmed, and J. Lucidarme, "Switching flux permanent magnet polyphased synchronous machines," in *Proc. 7th Eur. Conf. Power Electron and Applicat*, 1997, vol. 3, pp. 903–303.
6. E. Hoang, A. H. Ben-Ahmed, and J. Lucidarme, "Switching flux permanent magnet polyphased synchronous machines," in *Proc. 7th Eur. Conf. Power Electron. and Applicat*, 1997, vol. 3, pp. 903–303.
7. H. Wei, C. Ming, Z. Q. Zhu, and D. Howe, "Study on static characteristics of novel flux-switching doubly salient PM machine," in *Proc. CSEE*, 2006, vol. 26, no. 13, pp. 129–134.
8. Z. Q. Zhu, Y. Pang, and D. Howe, "Analysis of electromagnetic performance of flux-switching permanent magnet machines by non-linear adaptive lumped parameter magnetic circuit model," *IEEE Trans. Magn.*, vol. 41, no. 11, pp. 4277–4287, 2005.
9. W. Hua, M. Cheng, and G. Zhang, "A novel hybrid excitation fluxswitching motor for hybrid vehicles," *IEEE Trans. Magn.*, vol. 45, no.10, pp. 4728–4731, Oct. 2009.
10. W. Hua, M. Cheng, Z. Q. Zhu, and D. Howe, "Analysis and optimization of back-EMF waveform of a flux-switching permanent magnet motor," *IEEE Trans. Energy Convers.*, vol. 23, no. 3, pp. 727–733, Sep. 2008.
11. J. T. Chen, Z. Q. Zhu, and D. Howe, "Stator and rotor pole combinations for multi-tooth flux-switching permanent-magnet brushless ac machines," *IEEE Trans. Magn.*, vol. 44, no. 12, pp. 4659–4667, Dec. 2008.
12. Z. Q. Zhu, and J. T. Chen, "Advanced flux-switching permanent magnet brushless machines," *IEEE Trans. Magn.*, vol. 46, no. 6, pp. 1447–1453, Jun. 2010.
13. Z. Q. Zhu, J. T. Chen, Y. Pang, D. Howe, S. Iwasaki, and R. Deodhar, "Analysis of a novel multi-tooth flux-switching PM brushless AC machine for high torque direct-drive applications," *IEEE Trans. Magn.*, vol. 44, no. 11, pp. 4313–431, Nov. 2008.
14. R. L. Owen, Z. Q. Zhu, A. S. Thomas, G. W. Jewell, and D. Howe, "Fault-tolerant flux-switching permanent magnet brushless AC machines," *IEEE Trans. Ind. Appl.*, vol. 45, no. 6, pp. 1971–1981, Oct. 2009.
15. N. Bianchi, M. D. Pr'e, L. Alberti, and E. Fornasiero, *Theory and Design of Fractional-Slot PM Machines*. Padova, Italy: CLEUP, 2007.

MEMS Microrobot Controlled by Mounted Neural Networks IC with Two Types Actuators

Kei Iwata, Hirozumi Oku, Yuki Okane, Yohei Asano, Masaki Tatani, Yuki Ishihara, Kazuki Sugita,
Graduate school of Precision Machinery Engineering College of Science and Technology, Nihon University,
7-24-1, Narashinodai, Funabashi, Chiba, 274-8501, Japan

Satohiro Chiba, Satoko Ono, Mizuki Abe, Minami Takato, Ken Saito, Fumio Uchikoba
Department of Precision Machinery Engineering College of Science and Technology, Nihon University,
7-24-1, Narashinodai, Funabashi, Chiba, 274-8501, Japan
E-mail: takato@eme.cst.nihon-u.ac.jp, kensaito@eme.cst.nihon-u.ac.jp, uchikoba@eme.cst.nihon-u.ac.jp

Abstract

We report the hexapod microrobot controlled by the bare chip IC of hardware neural networks. MEMS technology is used for fabrication of the microrobot. Actuators of the robots are used lead zirconium titanate (PZT) and shape memory alloy (SMA). As the result, PZT type is realized the walking motion by bare chip IC. Moreover, SMA type can be succeeded the hexapod walking locomotion with mounted bare chip IC. The walking speed is 2.4mm / min and the step width was 0.083mm.

Keywords: Microrobot, Artificial Neural network, MEMS, PZT, SMA.

1. Introduction

Insects have small sophisticated motion mechanisms controlled by flexible brain neural networks. Therefore, fully understanding how insects move is among the ultimate goals of microrobotic studie.

Many researches that mimic the flexible motion mechanism of insects have been reported¹. Especially, walking is a typical movement mechanism of insects. The robot mimicking walking mechanism by using legs has been reported². However, most cases of them are large body compared with the insects. Realization of the small walking mechanism as large as the insect is difficult in conventional process. Therefore, the demand for Micro Electro Mechanical system (MEMS) technology that can create miniature components with high degrees of accuracy is increasing². In addition, the big feature of the insects is flexible thinking circuit.

The robots that introduce the model of the neural network as the control system are reported³. However, the small size robot controlled by neural networks is rare. Therefore, robots that are perfectly mimicked the insects have not been realized.

Previously, we reported on an insect-type MEMS microrobot that fits within 5-mm-cubed driven by a pulsed hardware neural network (P-HNN)⁴. However, the P-HNN circuit, which was constructed from discrete components, was found to be too big to be mounted on the microrobot. We then developed a P-HNN integrated circuit (IC) using a bare chip IC and peripheral amplifying circuits, but the resulting control system was still too big⁵. To solve the problem, the bare chip IC for SMA-type microrobot was newly developed⁶.

In this paper, we report on the development of insect-type microrobots controlled by bare chip IC of artificial neural network. Actuators of the microrobots are used piezoelectric element composed of lead zirconium titanate (PZT) and artificial muscle wire composed of

shape memory alloy (SMA). The bare chip ICs for each type of microrobot were newly developed.

2. Mechanism

Insect-type microrobot has hexapod legs like insects and falls within 5-mm-cubic. The designs of the two-type microrobot are shown in figure 1. The components of the microrobot are the frame, rotary actuator, and the link mechanisms. PZT and SMA are easy to downsize because the material itself has the function of the actuator. Almost all of the robot's parts are fabricated from silicon wafer using MEMS machining technology.

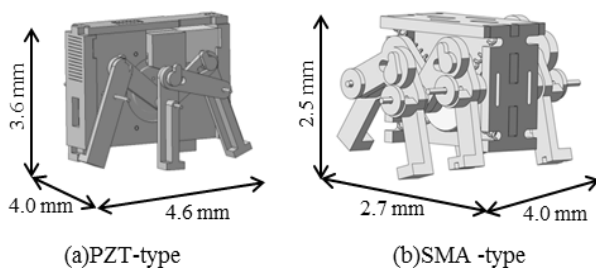


Fig. 1. Microrobot designs.

2.1. PZT-type microrobot

The PZT distorts by applying a voltage. In this study, a multilayer piezoelectric element composed of PZT is used for driving low voltage. The PZT has advantage of low electricity consumption and fast response time. However, it is difficult to use PZT as direct driven actuator because of small displacement. Therefore, the impact mechanism is adopted for the actuator of the microrobot. The design of the PZT-type actuator, which has side, end, and height dimensions of 1.0, 4.4, and 3.2 mm, respectively, is shown in figure 2. The displacements of a multilayer piezoelectric element are 110nm at applied 6V. The impact head is attached to the PZT and adjusted to contact to the impact head. The PZT impacts the rotor to generate rotary motion.

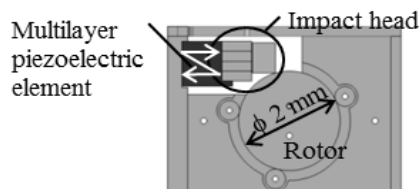


Fig. 2. Mechanism of the PZT-type rotary actuator.

2.2. SMA-type microrobot

SMA which shrinks at high temperatures and expands at low temperatures is used for the rotary actuator. The SMA displacement can be changed by applying electrical energy to create heat. We used 0.05 mm diameter wire to create the SMA with a standard coil diameter of 0.2 mm. A standard drive current from 50 to 120 mA was used, and a maximum kinetic displacement of 50 % of the original length was achieved. Figure 3 shows the design of SMA-type rotary actuator.

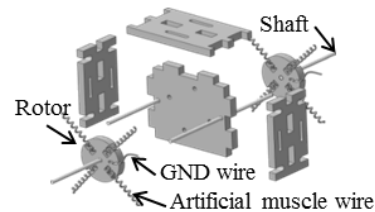


Fig. 3. Mechanism of the SMA -type actuator.

Four SMAs and a ground (GND) wire are connected to the rotor parts. Rotational motion of the actuator is generated by passing an electric current through the SMA in rotation.

2.3. Walking mechanism

Insects perform a stable hexapod walking by grounding the three legs. In this paper, link mechanisms are adopted by realizing hexapod walking like insects. Rotary motion of the actuator is converted into walking motion by link mechanisms via a shaft shown in figure 4. The locomotion pattern uses a 180° phase shift on each side.

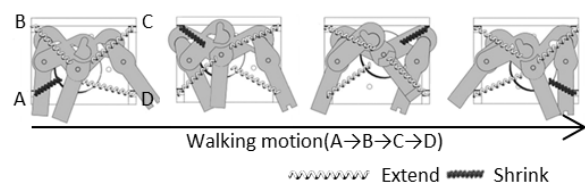


Fig. 4. Walking mechanism of the microrobot.

3. Control system

Insects function by using the neural networks in their own brains. In this study, we mimic those neural circuits

using an analog system that allows the microrobot to function in an insect-like manner.

3.1 Cell body model

The PZT-type microrobot is controlled by the cell body model shown in figure 6. The cell body model has refractory period, analog characteristic of the output pulse and time varying negative resistance characteristic. Driving frequencies of the PZT-type microrobot is 25 kHz. The amplifier circuit is added to obtain the output voltage 20V.

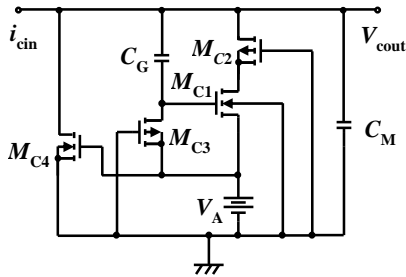


Fig. 6. Cell body model circuit diagram.

3.2 CPG model

It is well known that locomotion rhythms of living organisms are generated by central pattern generator (CPG). The SMA -type microrobot is controlled by the CPG model. CPG model can be formed by inhibitory synaptic connection of four neurons shown in Figure 7.

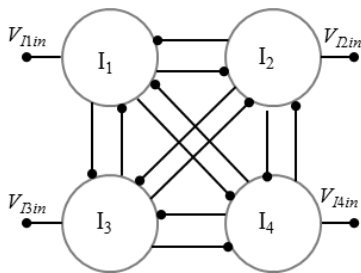


Fig. 7. Artificial neuron circuit connection diagram.

Figure 8 shows the circuit diagram of the neuron composed the cell body model and inhibitory synaptic model. The inhibitory synaptic model has spatiotemporal summation characteristics similar to living organisms. This sums the pulse waveforms outputted by other bonded cell body models.

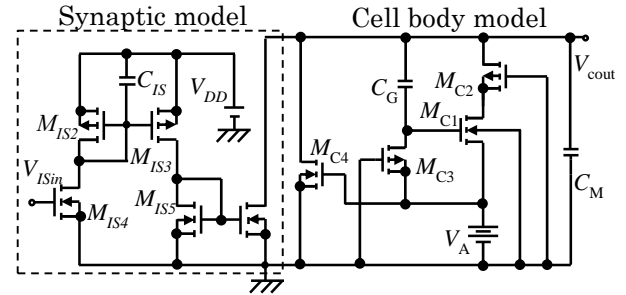


Fig. 8. Circuit diagram of the neuron.

4. Results

The bare chip IC of the neural network made it possible for the control system to be mounted on the microrobot. Figure 9 shows the fabricated microrobot mounted the bare chip IC. The side, the end, and height dimensions of the fabricated PZT-type microrobot were 4.0, 4.6, and 3.6 mm, respectively. The weight of the robot was 0.04 g. The length and the width dimensions of the control circuit were 2.0, 3.0mm, respectively. The side, the end, and height dimensions of the SMA-type microrobot were 4.0, 2.7, and 2.5 mm, respectively. The weight of the robot was 0.02 g. The length, width, and weight of the control circuit were 4.0mm, 4.0mm, and 0.059g, respectively.

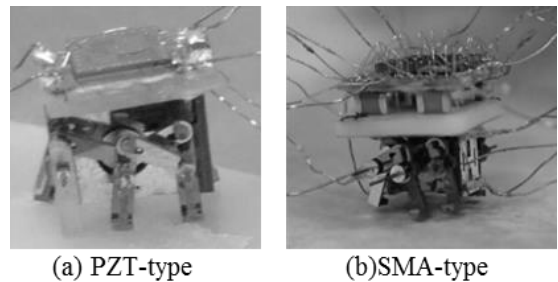


Fig. 9. Fabricated microrobot mounted control system. (a) PZT-type (b) Artificial muscle wire-type.

PZT-type microrobot could generate the walking motion by the bare chip IC. However, the robot could not achieve locomotion by itself. Because, the bare chip IC is insufficient of the output voltage for moving legs. However, the bare chip IC for the PZT-type microrobot

could drive the rotary actuator. Figure 10 shows the rotary motion of 1 s intervals.

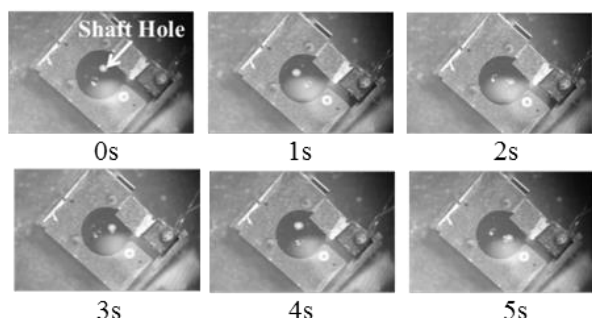


Fig. 10. Rotational motion of PZT-type actuator.

On the other hand, hexapod walking locomotion of the SMA-type microrobot, as shown in figure 11, was successfully achieved. The walking speed was 2.4 mm/min and the step size was 0.083 mm. Power source of the control circuit is externally connected.

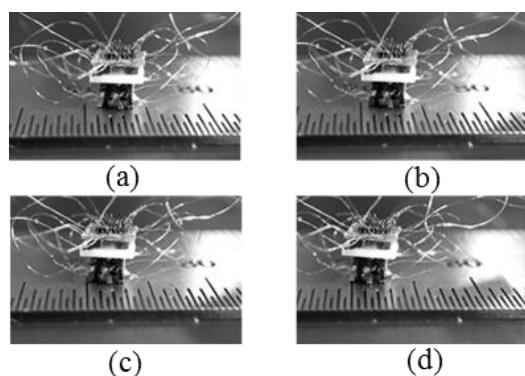


Fig. 11 Walking locomotion of the microrobot controlled by the bare chip IC. The figure show microrobot transitions at 10 s intervals.

5. Conclusion

In this paper, control system of the neural network was mounted the fabricated insect-type microrobot. It was possible to reduce a control system within a 4mm square by using a bare chip IC. In the PZT-type microrobot, the bare chip IC could actuate the rotary actuator. Moreover, hexapod walking locomotion of the SMA-type microrobot was achieved. The walking speed was 2.4 mm/min and the step size was 0.083 mm. The only external wire connections to the microrobot are to the power source.

Acknowledgements

The MEMS microrobot fabrication was supported by the Research Center for Micro Functional Devices, Nihon University. This study was supported by Nihon University College of Science and Technology Project Research and JSPS KAKENHI (25420226). We appreciate the above support. The very large scale integration (VLSI) chip used in this study was fabricated by Digital Technology, Inc. This work was supported by the VLSI Design and Education Center (VDEC) of the University of Tokyo in collaboration with Synopsys, Inc., Cadence Design Systems, Inc. and Mentor Graphics, Inc.

References

1. A. T. Baisch, P. S. Sreetharan and R. J. Wood, Biologically-inspired locomotion of a 2g hexapod robot, in *Proc. 2010 Int. Conf. on Intelligent Robots and systems*, (Taipei, Republic of China, 2010), pp. 5360-5365.
2. B. R. Donald, C. G. Levey, C. D. McGray, I. Paprotny and D. Rus, An Untethered, Electrostatic, Globally Controllable MEMS Micro-Robot, *J. Microelectromechanical Systems*. 15(1) (2006) 1-15.
3. S. A. Vukosavljev, D. Kukolj, I. Papp and B. Markoski, Mobile robot control using combined neuralfuzzy and neural network, in *Proc. 2011 12th Int. Symp. on Computational Intelligence and Informatics*, (Budapest, Hungary, 2011), pp. 351-356
4. M. Takato, M. Tatani, J. Tanida, S. Yamasaki, K. Saito, F. Uchikoba, Piezo Impact Type MEMS Rotary Actuator and Application to Millimeter Size AI Controlled Robot, in *Proc. 2013 Int. Ultrasonic Symp.*, (Prague, Czech Republic, 2013), pp. 5360-5365.
5. K. Saito, Y. Sekine, M. Takato and F. Uchikoba, MEMS Microrobot with Pulse-Type Hardware Neural Networks Integrated Circuit, in *Handbook of Research on Advancements in Robotics and Mechatronics*, (Engineering Science Reference, Hershey PA, 2015), pp. 18-35.
6. K. Saito, Y. Ishihara, K. Sugita, Y. Okane, H. Oku, Y. Asano, K. Iwata, M. Tatani, M. Takato, Y. Sekine and F. Uchikoba, Artificial Neural Circuit Integration for MEMS Microrobot System, in *Proc. 2015 Int. Conf. Advanced Intelligent Mechatronics*, (Busan, Korea, 2015), pp. 1055-1060.

Social Expression of Pet Robot Based on Artificial Consciousness and Biologically Inspired On-line Topological Method

Sakmongkon Chumkamon and Eiji Hayashi

Department of Mechanical Information Science and Technology, Kyushu Institute of Technology

680-4 Kawazu, Iizuka, Fukuoka, Japan, 820-5202

Tel: +819 0 9499 2408

E-mail: s.chumkamon.jp@ieee.org, haya@mse.kyutech.ac.jp

Abstract

The social robot becomes important to the future world of pervasive computing, where the robot currently facilitates our life. The social behavior and natural action of the robot is one of the most needed function for emerging future realistic human-like robot. Our paper proposes the artificial topological consciousness based on a pet robot using the artificial neurotransmitter and motivation. Since, the significant is cross-creature communication to friendly companionship. This system focuses on three points. The first, the organization of the behavior and emotion model regarding the phylogenetic. The second, the method of the robot that can have empathy with user expression. The third, how the robot can socially perform its expression to human using biologically inspired topological on-line method for encouragement or being delighted by its own emotion and the human expression. We believe the artificial consciousness based on complexity level and the robot social expression enhance the user affinity by the experiment.

Keywords: Consciousness-Based Architecture, Cross-Creature Communication, EQ.

1. Introduction

The personal robot in the boom of the robot market recent years, the long-standing goal of the robotics research is the autonomous behavior, having artificial cognitive and make a human delighted without the conflict. The complexity of the natural behavior, perception systems, empathy, sympathy and a cognitive stream of the robot that exists and cooperate with human is the challenge to archive the personal robot. The personal robot also improves living better for elderly people or a child by being a friend or companionship. The crucial ability of these robots to naturally interaction learn form and accordingly cooperate with human.

The traditional robot stands aloof slightly from utilizing nature cognitive process of the organism with the robot. Accordingly, the behavior and mentation of robot would not have a strategy of intrinsic movement and capability of communication with human. Due to the robot does not

have an affinity therefore it is needed to having empathy skill and need its comprehensible expression in order to human understands robot feeling as Fig 1.

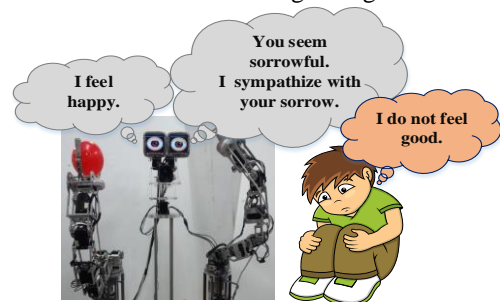


Fig. 1. The proposed concept of the companionship robot based on the social-emotional intelligence.

We have been striving to investigate and develop the personal robot and the related know-how deliberated with the biologically inspired consciousness, the social

intelligence (SI) and perception system in order to serve the organism-like consciousness and social-emotional intelligence (SEI) of personal robot come along the natural behavior and affinity [1]. In this paper, we develop conscious behavior robot named by “CONBE”. This robot includes two manipulators and one face respecting to semi-humanoid. In this paper, we propose the system of consciously behavior robot along with SI using topological adaptive resonance theory (TopoART) [2] as shown in Fig 2. The system implements concerning to organism behavior and emotion by phylogenetic illustrated by consciousness based architecture (CBA). Because of this concept, that significantly enable the robot self-awareness, which emerge naturally social interaction with human, and being a companion technically. The major contributions are the cross emotion expression from the robot toward human and cross facial emotion expression comprehension. Moreover, the robot’s expression would interact with user by deliberation of robot emotion and user’s emotional expression based on SI likes human being in society. Like human way, given example, when you are happy, however, your friends around you, they are feeling sad from some manner, and then you cannot express your actual emotion as happy. Therefore, you might sometimes express neutral or pretend to be sad as sympathy way.

2. Configuration of Conscious Behavior Robot

In this research, we contribute human-robot interaction based on the upper humanoid-like CONBE robot. It is to develop the artificial consciousness. For the proposed of enhancing the natural behavior in friendly way. The hardware of element of CONBE robot consists of two manipulators and one head as shown in Fig 1.

In the robot construction, the arms were assembled as seven degrees of freedom (DOF) included gripper. Due to the determination of angle for each joint of actuator, it is complicated to move to the target position. We then divided the seven DOF arm relating to human arm, where each part represent to be a shoulder, an elbow, a wrist and a finger. In the section of head robot, that was constructed by two DOF actuators for rotating in left-right and up-down where was equipped with a web camera and two displays. For the vision system, the camera is embedded

into the head and each hand for animal world. The robot can express the eyes by two display as shown in Fig. 1.

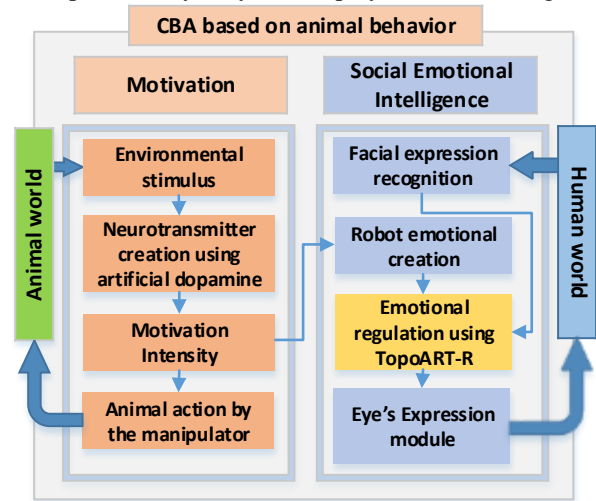


Fig. 2. The overview of the proposed methodology.

3. Robot Biologically Inspired Consciousness with Emotional Intelligence

3.1. Animal behavior and emotion of the robot

We developed the system to mimic the biological consciousness embodied to a robot. The system is composed of the animal world perception that represented by the color of interested object, which includes like-red, most favorite green and dislike-blue. For the emotion system, the artificial dopamine is used to induce the emotional motivation and behavior. There is the separated dopamine divided by each object. Each dopamine also performs a long-term memory as a robot experience in behavior process. For the creation of motivation, the intensity is calculated with the total dopamine. Therefore, The system could naturally perform the creature-like motivation. The waveform pattern is calculated using a second-order of linear differential discretized by Runge-Kutta method [3].

3.2. Emotional Intelligence

EQ is the ability to identify, use, understand and manage emotion in positive way in the society of human. EQ encompasses self-awareness, self-management, social awareness and relationship management. Therefore, EQ skill is important for the companion robot to cross-communicate between robot and human and maintain the

relationship among human. Moreover, in sociality, when the robot exists with the human, it has to consider on the etiquette in a society. Therefore, the robot is needed to have EQ skill.

3.2.1 Facial expression recognition (FER)

To archive the ability of EQ, the robot is needed to comprehend the social emotion from user or that means the social awareness in EQ. In this paper, FER system composed of the facial feature extraction by the constrained local model (CLM), and emotional expression classification by Hidden Markov Model (HMM) to process FER [4]. Afterward, the output of FER will feed to emotional intelligence regulation system to consider the proper SI expression to user.

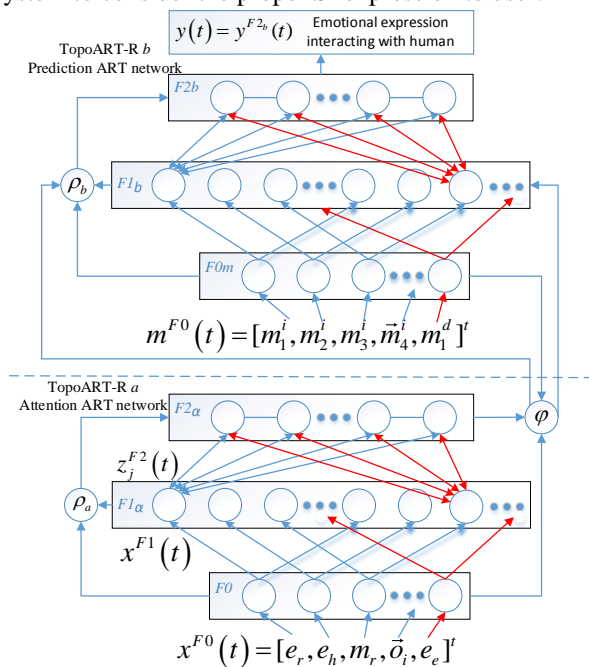


Fig. 3. The SI using TopoART-R.

3.2.2 SI regulation using TopoART-R

Because the Adaptive Resonance theory (ART) is closely related to the cognitive and neural theory of the brain instinct learning categorizing recognition and prediction and the topology relates among consciousness process, expectation, attention, resonance, and synchronization between unsupervised and supervised learning [5]. Because the real world information is dynamic and variant, this system also needs the on-line incremental

method to carry out the stable learning and fast therefore we decide to utilize the enhanced ART view by TopoART [2]. TopoART is the fast-online learning and stable, which improve the ART by using the topology learning with addition sub-network in different level of detail. Therefore, this method is more suitable for real-world information.

For the robot SI topology is shown in the Fig 3. x^{F0} represents to input data which encompass the robot emotional parameter e_r , human emotional parameter e_h , motivation value of robot m_r , object parameter vector from the robot perception system o_i and emotional expression (for training) e_e . $y(t)$ denote to the social-emotional expression depend on the user expression and robot's emotion as shown in Fig. 3.

3.2.3 Robot's eye expression for social interaction

Robot eye is the major medium for interaction. The expression includes the emotion of surprise, pleasure or happiness, hope, neutral, fear, sadness, disgust and anger. The eyes were implemented, as the 3D virtual eye regarding human's eye along with the nature expression where the eye's expression is shown in Fig. 4.

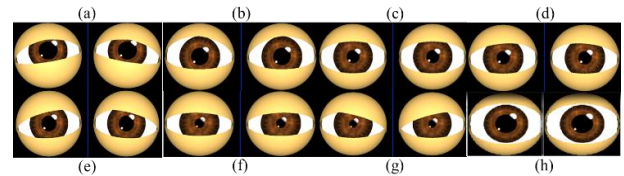


Fig. 4. The robot eye's expression a) pleasure b) hope c) neutral d) fear e) sadness f) disgust g) anger h) surprise.

4. Experimental Results

In this section, we demonstrate the robot behavior, emotion generation and social expression with human by the robot face. The experimental configuration is based on the CONBE robot, which is set the height approximated by human height. For the SI interaction, we firstly extract the facial feature parameter using CLM to predict the emotion expression by HMM. Afterward, the human emotion and robot emotion are used to consider the suitable social expression using the TopoART. The emotional expression is deliberated with the emotional sharing between human and robot, which the expression is acceptable, and not let human unsatisfied. The top of Fig. 5 shows each parameter for the experiment the

emotional motivation based on the neurotransmitter dopamine of each object, which is recognized by overtime. The bottom is observed the robot's emotion, human's emotion and the expression throughout the task period. Fig. 6 shows the capture images of FER and the robot's expression on each time from T0 to T5.

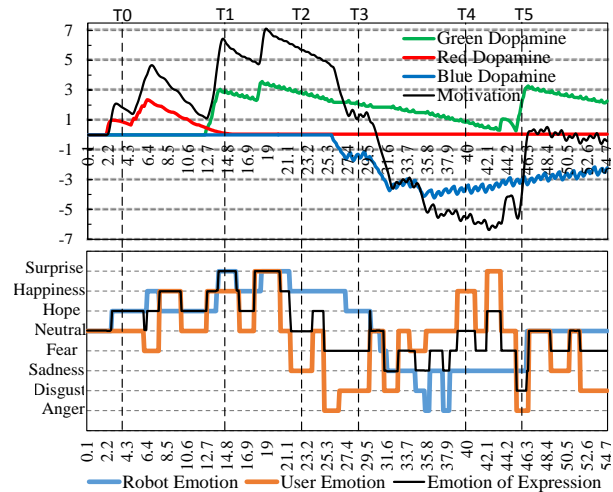


Fig. 5. The robot's motivation and emotional expression

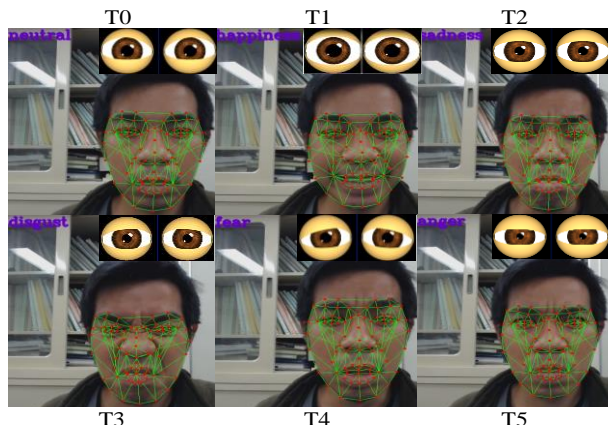


Fig.6 Robot eye's expression and human's expression.

When robot starts, it feels neutral and expresses neutral according to the motivation, when the favorite red object is recognized the motivation increased. On T0, the robot feels hope according to increased motivation and human expresses neutral, then it expresses hope due to encouraging human feeling. On T1, robot feels surprised because the most favorite green is recognized suddenly and human expresses hope then robot expresses surprise. On T2, robot is happy but human expresses sad then robot expresses neutral and masks its happiness because

of SI. On T3, robot is hope but human disgust robot then expresses fear. On T4 robot is sad but human is happy, the robot then expresses neutral and mask its sadness due to SI. On T5, robot is sad and human is angry then robot expresses disgust due to the emotion sharing.

5. Conclusion

As the demonstration and the proposed system, the CONBE robot with the emotional intelligence by sharing the emotion from the user could enhance the capability of the human affinity, which is strongly important for personal robot. For our further inspiration, we also expect this system can emerge the social ability to the creature animal due to recent research from the remote animal control [6] which the research proof the nearly future we can connect and control the animal brain. Consequently, if we embed this artificial social emotion intelligence to the animal in near future the animal might communicate with EQ skill likes human that should make the natural cross-communication creature between animal and human.

References

1. S. Chumkamon and E. Hayashi, 'ConBe robot: The development of self-perception and expression in face-to-face interaction', 2014 Joint 7th International Conference on Soft Computing and Intelligent Systems (SCIS) and 15th International Symposium on Advanced Intelligent Systems (ISIS), 2014.
2. M. Tscherepanow, 'An Extended TopoART Network for the Stable On-line Learning of Regression Functions', Neural Information Processing, pp. 562-571, 2011.
3. S.Chumkamon, K.Masato, and E.Hayashi. "Facial Expression of Social Interaction Based on Emotional Motivation of Animal Robot" In IEEE International Conference on Systems, Man, and Cybernetics, pp. 185-190, 2015.
4. S. Chumkamon and E. Hayashi, 'Facial expression recognition using constrained local models and Hidden Markov models with consciousness-based architecture', Proceedings of the 2013 IEEE/SICE International Symposium on System Integration, 2013.
5. S. Grossberg, 'Adaptive Resonance Theory: How a brain learns to consciously attend, learn, and recognize a changing world', Neural Networks, vol. 37, pp. 1-47, 2013.
6. S. Talwar, S. Xu, E. Hawley, S. Weiss, K. Moxon and J. Chapin, 'Behavioural neuroscience: Rat navigation guided by remote control', Nature, vol. 417, no. 6884, pp. 37-38, 2002.

Anthropomorphic robot modelling with virtual height inverted pendulum approach in Simulink: step length and robot height influence on walking stability.

Ramil Khusainov, Ilya Afanasyev and Evgeni Magid

Intelligent Robotic Systems Laboratory, Innopolis University, Russian Federation

E-mail: {r.khusainov, i.afanasyev, e.magid}@innopolis.ru

<http://university.innopolis.ru/en/research/robotics/lirs/>

Abstract

Humanoid stable walking is a complex task due to the high number of degrees of freedom, system nonlinearity and relatively small size of robot footprint. Biped robots tend to fall down as walking speed increases or when the terrain conditions change. This paper presents dynamically stable walking modelling of Russian humanoid AR-601M in Simulink environment with virtual height inverted pendulum model (VHIPM), an effective and simple trajectory generation method based on inverted pendulum model (IPM). This algorithm adjusts height of the center of mass in IPM model to reduce ZMP error and guarantees stable locomotion up to some critical speed. We investigate influence of the step length and step period on walking stability. Maximum torque values in leg joints are estimated in order to verify if such trajectories are attainable by robot motors. We demonstrate that the robot model is capable to achieve significant walking speeds on flat surfaces using this method.

Keywords: bipedal robot, dynamic stability, Simulink, AR-601M robot

1. Introduction

Humanoid robot design and locomotion are currently among of the most exciting and challenging research topics in robotics. Over the last decades, a number of successful approaches for stable bipedal robot walking have been developed.¹ The multi-functionality and high flexibility of anthropomorphic design, abilities of a humanoid robot to replace a human in various practical operations and human-robot interaction scenarios provide good motivation for such research activities.

To ensure walking stability, the majority of modern humanoid robots employ analytical methods, which are based on locomotion dynamics and usually apply some particular stability constraints. One of the most common stability constraints is the Zero Moment Point (ZMP).² In order to simplify equations deriving, ZMP criteria could be applied for walking reference trajectory generation together with a simplified robot model, such as Linear Inverted Pendulum Model (LIPM).³ However, LIPM

model does not consider full body dynamics. This causes ZMP errors, which may become critical for a given walking speed. To deal with this problem, the authors in Ref. 4 suggested a novel simplified robot model which was called a Virtual Height Inverted Pendulum Model (VHIPM): the authors experimentally demonstrated⁴ that the ZMP error could be significantly reduced by varying the height of Center of Mass (CoM) in LIPM model.

This paper suggests the VHIPM application for modeling of Russian anthropomorphic robot AR-601M in MATLAB/Simulink environment. We find maximal speed of AR-601M stable walking and next calculate torques in the robot joints to provide such locomotion. The rest of the paper is organized as following. Section 2 presents the robot and its Simulink model. Section 3 describes the process of walking trajectory generation, followed by simulation results within Section 4. Finally, we conclude in Section 5.

2. The Biped Model

We have constructed 41 degrees of freedom (DoF) model of AR-601M robot; however, only 12 joints (6 DoF in each pedipulator) are active during the robot locomotion. Three joint axes are in the hip, two joints are at the ankle and one in the knee. Mass and size parameters of the robot pedipulators are given in Table 1. Total mass of the robot is 65 kg. Figure 1 demonstrates the robot simulation in MATLAB/Simulink environment.

Table 1. Mass and size parameters of the pedipulators.

Link	Size parameters (mm)	Mass (kg)
Thigh	Length : 280	7.5
Shank	Length : 280	6.9
Foot	L×W×H: 254×160×106	3.2

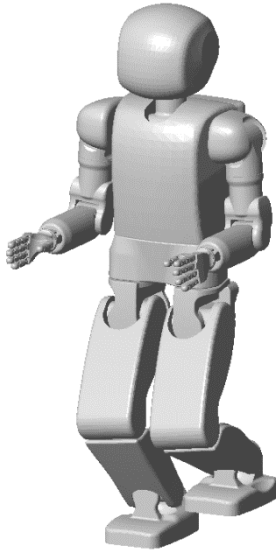


Fig. 1. A snapshot from animation window in MATLAB/Simulink environment

Complete 3-D simulation of multibody dynamics was performed using variable step period implicit solver (ODE 23t*) of MATLAB SimMechanics Toolbox. We modelled the robot feet ground contact with nonlinear spring-damper method⁵, where normal and friction forces are calculated according to Eq. (1) – Eq. (2) respectively:

$$F_n = k_n z + b_n \dot{z} \quad (1)$$

$$F_t = b_t \dot{z}, \quad F_t \leq \mu F_n \quad (2)$$

where k_n , b_n , b_t and μ are contact force parameters. The details of the contact model can be found in Ref. 6 which presents the previous work of the authors.

3. Walking Trajectory Generation

Robot locomotion could be considered as a repetition of a single step motion⁷. We calculated walking trajectory under the following assumptions, which are widely applied in experimental approaches for biped walking⁸:

- (i) The swing foot is parallel to the ground
- (ii) The upper body is always kept upright
- (iii) CoM of the robot model is moving at the constant height
- (iv) The swing foot is moving in a cycloid trajectory and its coordinates can be described with the following equations:

$$y(t) = -S \cos\left(\frac{\pi t}{T}\right) \quad (3)$$

$$z(t) = 0.5H \left(1 - \cos\left(\frac{2\pi t}{T}\right)\right) \quad (4)$$

$$x(t) = x_0 \quad (5)$$

where S is a single step length, H is a step height, T is a step period, x_0 is a distance between two feet in x direction. In Ref. 4 authors showed that equations for CoM trajectory can be expressed as:

$$\ddot{x}_{CoM} - \frac{g}{\alpha z_{CoM}} x_{CoM} = 0 \quad (6)$$

$$\ddot{y}_{CoM} - \frac{g}{\beta z_{CoM}} y_{CoM} = 0 \quad (7)$$

where coefficients α and β are found experimentally to reduce ZMP error. Therefore, we have following trajectories for CoM point of the robot:

$$x(t) = C_1 e^{-w_1 t} + C_2 e^{w_1 t}, \quad w_1 = \sqrt{\frac{g}{\alpha z_{CoM}}} \quad (8)$$

$$y(t) = D_1 e^{-w_2 t} + D_2 e^{w_2 t}, \quad w_2 = \sqrt{\frac{g}{\beta z_{CoM}}} \quad (9)$$

where C_1 , C_2 , D_1 and D_2 coefficients are found from initial and final values of CoM coordinates. After we define translational and rotational coordinates for the body and the swing foot, the joint angle trajectories are obtained from inverse kinematics problem solution.

Such trajectory assumes that robot has initial velocity. To move robot from resting state we first calculate

trajectory with a short step length and then gradually increase it (to maximal value) until ZMP errors become critical and the robot falls down.

4. Simulation Results

This section considers a walking trajectory which is described with the listed in Table 2 parameters.

Table 2. Simulation parameters

Parameter	Value
Step height	0.1 m
Step period	0.5 sec
CoM height	0.75 m
Step length	0.1 m – max. value

First, we estimated maximal speed of the robot model that could be achieved using LIPM method. We define robot's walking trial as "stable" if the robot successfully executes a sequence of 100 steps. After each stable walking trial we increase step length by 0.05 m and verify robot's walking again. The process of step increase was repeated until the robot failed to execute a successful stable walking trial.

Simulations demonstrated that maximum step length at which the robot could perform stable walking is 0.95 m, which corresponds to 0.95 m/s walking speed. CoM forward velocity value is shown in Fig 2.

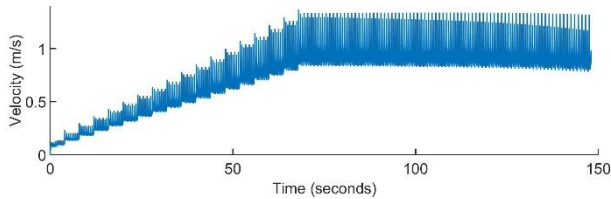


Fig. 2. Robot velocity in LIPM method

Figures 3-4 demonstrate ZMP coordinates for a step of 0.95 m length. Support foot center corresponds to (0,0) coordinate. According to the calculated values, we have approximately 2.5 cm error for X coordinate and 10 cm error for Y coordinate just after a single step.

Next, we vary α and β coefficients in Eq. (6) and (7) around 1 in order to minimize ZMP errors. Figures 5-6 show the dependence of maximal error of ZMP coordinate on α for x-coordinate and on β for y-coordinate. It was empirically detected that for

x-coordinate optimal value of coefficient α is equal to 1, for y-coordinate optimal β should lie within [0.7, 0.8] interval. Walking simulation with these coefficients showed that such optimization of trajectories allows to increase maximal step length from 0.95 m to 1.1 m and to achieve a maximal speed of 1.1 m/s accordingly while keeping stable walking for at least 100 sequential steps.

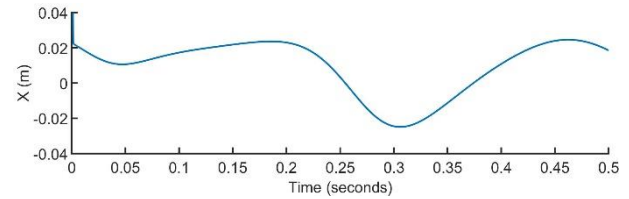


Fig. 3. ZMP x coordinate

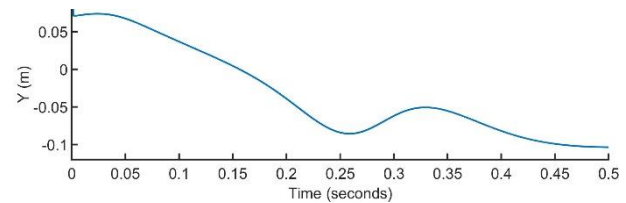


Fig. 4. ZMP y coordinate

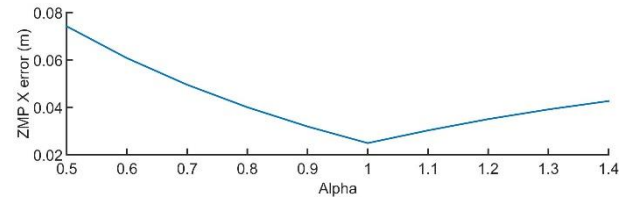


Fig. 5. Dependence of ZMP x coordinate error on alpha

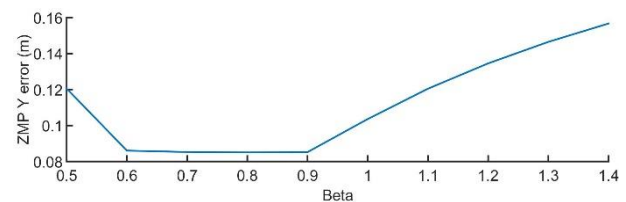


Fig. 6. Dependence of ZMP y coordinate error on beta

Finally, we estimated the peak torque value in ankle and knee joints that the robot motors should generate in order to afford the robot locomotion according to the calculated trajectory. Figures 7 and 8 show the calculated torque values for the ankle and the knee joints respectively.

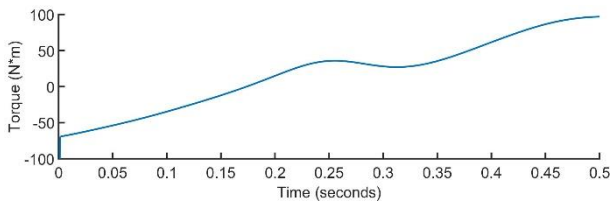


Fig. 7. Torque value in ankle joint

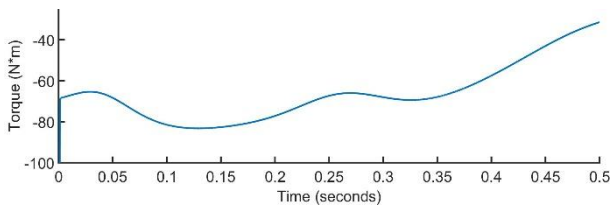


Fig. 8. Torque value in knee joint

The maximal value is approximately 100 N*m for the ankle and 80 N*m for the knee joint. With regard to the technical specifications of real AR601-M robot, its motors can generate maximal values of 50 N*m for the knee and 20 N*m for the ankle joint. Unfortunately, this means that such high maximal speeds could not be achieved for the real robot. Therefore, we are limited to use trajectories with lower maximum speed, which are dynamically stable according to simulations.

5. Conclusions

This paper presents a biped walking robot AR601-M trajectory reference generation algorithm based on ZMP approach with Linear Inverted Pendulum Model (LIPM) and Virtual Height Inverted Pendulum Model (VHIPM) methods. Simulations in MATLAB/Simulink environment indicated significantly better performance of VHIPM method when compared with LIPM method. We investigated in depth the influence of the step length and step period on walking stability. In general, proper coefficients selection with a help of simulation for each particular robot model affords to achieve maximal walking speed for stable locomotion. The resulting torque values in the knee and the ankle joints could be calculated for such maximal walking speed and next verified against the technical capabilities of the real robot joint motors. Unfortunately, in our case the maximal speed of stable locomotion that was successfully demonstrated in the flat surface walking simulation turned out to be unfeasible for AR601-M robot due to the

limited capabilities of its joint motors. However, the knowledge of the theoretically possible speed within a simulation and the robot motors specifications give a good hint for the real achievable speed. As a part of our future work, we are going to implement the presented in this paper algorithms on AR601-M robot and verify that it could perform stable locomotion and achieve the calculated through simulations peak walking speed.

6. Acknowledgements

This research has been supported by Russian Ministry of Education and Science as a part of "Scientific and Technological Research and Development Program of Russian Federation for 2014-2020 years" (agreement 14.609.21.0004, research grant ID RFMEFI60914X0004) and by "Android Technics" company, the industrial partner of the research.

References

1. J. Wright, I. Jordanov, Intelligent approaches in locomotion, in *International Joint Conference on Neural networks*, pp. 1-8, 2012.
2. M. Vukobratovich, B. Borovac, Zero-moment point - thirty five years of its life, in *International Journal of Humanoid Robotics*, vol. 01, pp.157-173, 2004.
3. S. Kajita, F. Kahehiro, K. Kaneko, K. Fujiwara, K. Harada, K. Yokoi, H. Hirukawa, Biped walking pattern generation using preview control of the zero-moment-point, in *Proceedings of IEEE International Conference on Robotics and Automation*, vol.2, pp. 1620 - 1626, 2003.
4. T. Ha, C.-H. Choi, An effective trajectory generation method for bipedal walking in *Journal of Robotics and Autonomous Systems*, vol.55(10), pp.795-810, 2007.
5. K.H Hunt., F.R.E. Crossley, Coefficient of restitution interpreted as damping in vibroimpact in *ASME Journal of Applied Mechanics*, vol.42(2), pp.440-445, 1975.
6. R. Khusainov, I. Shimchik, I. Afanasyev, E. Magid, Toward a human-like locomotion: Modelling dynamically stable locomotion of an anthropomorphic robot in Simulink environment, in *12th International Conference on Informatics in Control, Automation and Robotics*, vol.2, pp. 141-148, 2015.
7. J. Denk, G. Schmidt, Synthesis of walking primitive databases for biped robots in 3-D environments, in *IEEE International Conference on Robotics and Automation*, vol.1, pp.1343-1349, 2003.
8. A. Yonemura, Y. Nakajima, A.R. Hirakawa, A. Kawamura, Experimental approach for the biped walking robot MARI-1, in *6th International Workshop on Advanced Motion Control*, pp.548-553, 2000.

A low cost genetic algorithm based control scheme for wheelchair control in hospital environment

Karam Dad

Department of Mechanical Engineering, Pusan National University, 635-4Jangjeon 2 dong, Geumjeong-gu, Busan, 609-735, South Korea

Muhammad Jawad Khan

Department of Mechanical Engineering, Pusan National University, 635-4Jangjeon 2 dong, Geumjeong-gu, Busan, 609-735, South Korea

Wang Jie

Department of Mechanical Engineering, Pusan National University, 635-4Jangjeon 2 dong, Geumjeong-gu, Busan, 609-735, South Korea

Min Cheol Lee

School of Mechanical Engineering, Pusan National University, 635-4Jangjeon 2 dong, Geumjeong-gu, Busan, 609-735, South Korea

E-mail: karam@pusan.ac.kr, mclee@pusan.ac.kr

Abstract

In this paper, a control strategy to operate a wheelchair in a hospital is proposed to assist patients. The strategy is tested using a mobile robot that is navigated in a hospital using line following scheme. The mobile robot is operated using both genetic algorithm and A* algorithm for a thorough comparison of the control scheme. The comparison of the results revealed that genetic algorithm is a better solution in controlling the wheelchair in a hospital environment.

Keywords: Wheelchair, Patients, Mobile Robot, Genetic Algorithm, A* Algorithm.

1. Introduction

Automated wheel chairs are characterized as mobile robots due to the involvement of motion planning and control schemes [1]. The automation schemes in wheel chairs are sub-divided into two major parts i.e. (i) control schemes and (ii) navigational schemes [2]. Both are used in interpretation of human gestures for assistance via control through sensors. The navigational schemes are further sub divided into offline and online schemes [3], where the offline algorithms plan the course of actions before starting the path, while online algorithms plan the path of the robot while executing the path. Control schemes provide the disturbances which are encountered due to the irregularities in the environment [4]. This

paper proposes an offline scheme for navigation of the automated wheel chair.

2. Proposed Methodology

The main emphasis of this research is the implementation of path planning algorithms on a real time robot. Several strategies are involved in developing a real-time path following mechanism. The components used in this research are given below:

- BeInMotion® SDK Motor Control Kit
- Accelerometer
- Arduino UNO

A brief description of the methodology used for implementation of the optimal path planning in a static

environment is given in this section. This methodology is divided into three significant parts:

- Optimal Path Planning for known environment
- Communication of optimum path to the Mobile Robot
- Evaluation of optimal path tracking by the Mobile

2.1. Optimal Path Planning for known environment

Optimal path planning algorithm convergence cost is higher than the ordinary algorithms; therefore Field programmable Gate Arrays (FPGA's) are generally used for implementing these algorithms, as they possess comparatively more computational power than microcontrollers [5]. But the use of an FPGA for optimal path evaluation disturbs the scalability process of the methodology. For example, consider a case where we want to change the path planning algorithm. In that case a retransform of new path planning algorithm for the FPGA may require extensive amount of work. As this research emphasis on creating a scalable method which can be used with different path planning algorithms, therefore, a more generalized approach is proposed. As the environment is completely static the path is, therefore, to be evaluated offline. It may be more advantageous if the path is preplanned and then the coordinates are fed to the mobile robot controller. For this a control scheme to evaluate the optimal path beforehand using computer is proposed. The details are given in the next section.

2.2. Communication of optimum path to the mobile robot

Once the optimum path is planned the new path coordinates are to be communicated to the Mobile Robot for further processing. Parallel communication may require many lines and is not generally preferred while communicating with the PC is done through serial communication.

2.3. Evaluation of optimal path tracking by the mobile robot

The Mobile Robot receives the path points from the PC and starts path execution command it follows the desired path and passes through each path point. In order to localize the mobile robot in the given environment data

from two sensors, accelerometer and rotary encoders, is received and evaluated [6]. The mobile robot is first turned to the direction of next path point and then it travels the desired distance in a straight line. To force the Mobile Robot to follow a straight path Proportional Integral and Derivative (PID) control is proposed. The Mobile Robot stops when the designated distance in that direction is travelled and then turns to the next path point and repeats the process. The sensors inform that the planned distance has been travelled.

3. Implementation of Proposed Methodology

The proposed methodology is shown in the Figure 1. Flow Chart for Proposed Methodology as a flow chart which is implemented in three parts as following:

- Optimal Path Evaluation Mechanism
- Data Transfer Mechanism
- Path Following Mechanism

3.1. Optimal Path evaluation mechanism

This station performs the function of evaluating the optimal path from the desired algorithm. It consists of a PC only. In this research the optimal path has been found from Genetic Algorithm and A* algorithm but as it has been already discussed that the methodology is scalable so any other path planning algorithm can be used to find the optimum path. The Genetic Algorithm and A* algorithm takes the input environment and generates the path points of the optimum path. The station saves these path point coordinates for future operations.

3.2. Data transfer mechanism

This station performs the function of data transfer between the PC and the mobile robot. The path points which were evaluated in the first step are serially transferred to the mobile robot through this mechanism.

3.3. Path following mechanism

The path following mechanism includes motion of the robot from starting to the end point along the given path following the fed points on the path. This consists of both forward and turning of the robot along the path until arrives to the goal point [7].

4. Path Planning

The algorithms used for static environments in this study are following:

- A* Algorithm
- Genetic Algorithm

4.1. A* Algorithm

A* Algorithm finds the most cost efficient path starting from initial node to one of the destination nodes, given there are one or more destination nodes. As A* always prefers a path with the lowest expected total cost which could be distance or time or any other parameter, while keeping an already sorted priority line up of path segments that could be alternately used along the way [8]. Two functions combine to make the cost function, both of which are as follow

- Cost Function of Past Path, this is the cost between starting and current node and is generally represented by $g(x)$
- Cost Function of Future Path, this is a permissible "heuristic approximation" of the cost from current position to the destination and is represented by $h(x)$.

Each node is evaluated by adding the heuristic function $h(x)$ and $g(x)$ i.e. the cost of reaching the present node being evaluated from the start node.

$$F(x) = g(x) + h(x) \quad (1)$$

4.2. Genetic Algorithm

Genetic algorithm is based on the principle of genetics and natural selection. It comes under the class of meta-heuristic techniques which are based on the general experiences [9]. It works on the principle of survival of the fittest. In search space it searches the optimal points intelligently by using statistical evolutionary methods. Evolutionary methods are based on natural selection where the fittest chromosomes survive, reproduce and mutate so that the resulting chromosomes in successive generations are increasingly competitive. This natural selection process is coded mathematically to generate an initial population of chromosomes and use selection procedures to converge to an optimal configuration [10]. The computation can proceed in parallel rather than in series thus resulting in high computational speed-ups. A detailed pseudo-code for the GAs are as follows:

- Define GA parameters
- Generate initial population

© The 2016 International Conference on Artificial Life and Robotics (ICAROB 2016), Jan. 29-31, Okinawa Convention Center, Okinawa, Japan

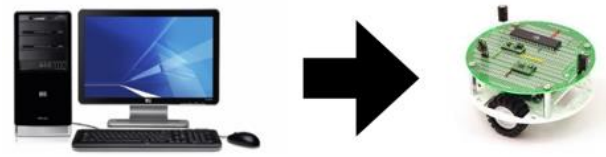


Fig. 1. Implementation Block diagram of Proposed Methodology

- Decode chromosomes
- Evaluate fitness of each chromosome
- Select mates for reproduction
- Carry out reproduction
- Carry out mutation
- Check for convergence
- If not converged go to step (iii)
- Print converged solution

GA's work on the principle of survival of the fittest. This means all the good points which give maximum value for the objective function are permissible to continue in the next generation and the points which does not give maximum values for the objective function are thrown away from our calculations. GAs maximizes a given objective function, so it is necessary to convert a minimization problem into maximization problem before applying the technique of GA. Fitness function is defined as follows:

$$F(n) = f(n) \quad \text{for a problem of maximization} \quad (2)$$

$$F(n) = 1/(1+f(n)) \quad \text{for a problem of minimization} \quad (3)$$

Equation (2) is used for the maximization of the problem whereas equation (3) is used to minimize the cost function. In path planning application, path distance is used to evaluate the fitness value of each chromosome. If the distance to the goal or path length of a certain chromosome is small, the chromosome is better than the other chromosomes in the current generation. The fitness function for path length can be defined as.

$$F_t(n) = 1/d(n) \quad (4)$$

Whereas $d(n)$ defines the path length for the specific chromosome.

5. Experiments

Experiment were tested in a mobile robot instead of a wheelchair since a automatic wheel chair is an

autonomous mobile robot that is used for the transportation of patients in a hospital.

5.1. Testing Procedure

First the offline navigational algorithm is run on a computer. The computer computes the optimum path and evaluates the path points for that particular path. It then serially transmits the coordinates to a host controller (Arduino UNO in this case) mounted on the mobile robot. The Arduino UNO board communicates with both the accelerometer and the computer. Firstly, it receives the coordinates from the computer and transmits it to the FPGA mounted on the mobile robot one by one. Secondly it acquires the acceleration values continuously from the accelerometer, applies Simpson's rule for double integration of the acceleration and acquires the distance covered and then transmits it to the Altera Cyclone IV E FPGA mounted on the mobile robot [11]. The Altera Cyclone IV E FPGA communicates with the Altera UNO board to get both the data from accelerometer and computer. It further evaluates the data acquired from the IR sensors mounted on the mobile robot base to apply the proportional integral derivative (PID) control which ensures that the mobile robot moves in a straight line. The IR sensors are also used for the computation of distance covered. The effective distance covered is the result of multiplication of the readings of distance covered from both sensors (accelerometer and IR sensor) with their respective weights and adding them.

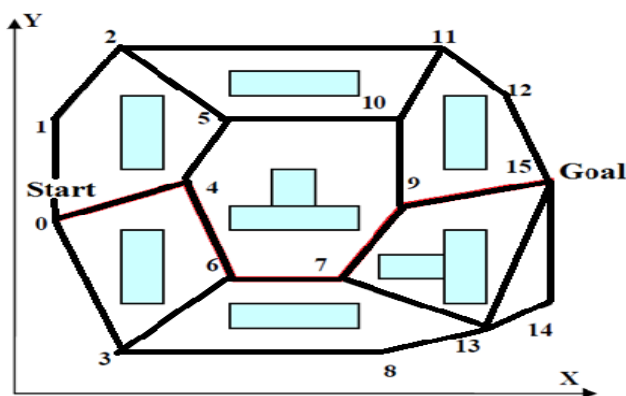


Fig. 2. Test Environment Designed

5.2. Tests Designed

The test for the mobile robot consisted of a sample which is given in Figure 2. The black lines present the linkages possible while blue boxes represent the obstacles. The start and stop points are also mentioned by "Start" and "Goal" respectively. Starting point is 0 and the goal point is 15. Each point is defined as the change in direction. There are many paths to reach the goal

6. Results and Discussion

The main objective of the research was the navigation of a Mobile Robot (BeInMotion Motor Control Kit) based upon the optimal path provided by an offline path planning algorithm.

6.1. Implementation of Optimized Solution

For the implementation of the path the environment under test was practically created. The created environment is shown in Figure 3. Figure shows the robot in given environment while navigating through the obstacles it starts from 0 and reaches to goal point 15 according to path generated by genetic algorithm. It first starts from 0 and reaches point 15 following the path created by points 0,4,6,7,9,15 respectively. Robot moves in two steps firstly it calculates the turning angle and then it moves forward and reaches desired point and this process is repeated for every movement from point to point.

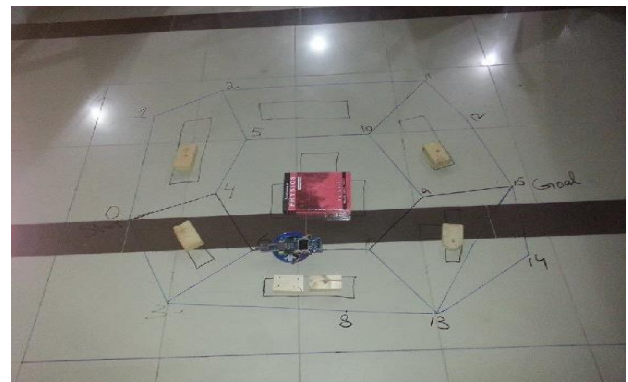


Fig. 3. Implemented Environment details

The computed path was implemented on the Mobile robot and with the help of genetic algorithm we achieved less errors and increased accuracy with each trial. The average percentage error observed from the implementation of genetic algorithm was 1.54% which can be easily reduced further by using better quality

navigational sensors. By improving the quality of the sensors, more importantly the accelerometer we can achieve greater accuracy

7. Conclusion

The results show that this technique can be used for transporting patients from one place to another in a hospital within a controlled environment where the destination point has been loaded. The result were satisfactory and can further be improved by use of a control scheme alongside the presented scheme.

Acknowledgements

This section should come before the References. Funding information may also be included here.

References

1. J. Borenstein, B. Everett, and L. Feng. Navigating Mobile Robots: Systems and Techniques. A. K. Peters, 1996.
 2. Borenstein J., Koren Y., "Tele-Autonomous Guidance for Mobile Robots," IEEE Tran. System, Man, and Cybernetics, Special Issue on Unmanned Systems and Vehicles, December, pp. 1437-1443. 1990,
 3. J. Czyzowicz , E. Kranakis , D. Krizanc , L. Narayanan , and J. Opatrny, Optimal online and offline algorithms for robot-assisted restoration of barrier coverage, arXiv: 1410.6726v1 [cs.DS] 24 oct 2014
 4. Mnif, F. & Touati, F. , An Adaptive Control Scheme for Nonholonomic Mobile Robot with Parametric Uncertainty, pp. 059 - 063, International Journal of Advanced Robotic Systems, Volume 2, Number1 (2005), ISSN 1729-8806
 5. Shilpa Kale and S. S. Shriramwar, FPGA-based Controller for a Mobile Robot, (IJCSIS) International Journal of Computer Science and Information Security, Vol. 3, No. 1, 2009
 6. J. Borenstein, H. R. Everett, L. Feng: Where Am I? Sensors and Methods for Mobile Robot Positioning, University of Michigan, Michigan 1996.
 7. Karam Dad Kallu, Muhammad Usman Rafique and Dr Zafar Ullah Koreshi, Development of a path following autonomously navigating mobile robot with parallel processing using FPGA, 1st International Young Engineers Convention (IYEC-2014) on April 18-20, 2014
 8. Delling, D. and Sanders, P. and Schultes, D. and Wagner, D., *Engineering route planning algorithm* (Algorithm of large and complex networks, 2009).
 9. Peter E. Hart, Nils J. Nilsson and Bertram Raphael, "A Formal Basis for the Heuristic Determination of Minimum Cost Paths," IEEE Transactions on Systems Science and Cybernetics, pp. 100-107, July. 1968.
 10. Eiben, A. E. et al., *Genetic algorithm with multi-parents recombination* (PPSN III: Proceedings of the International conference on Evolutionary computation. The Third conference on parallel problem solving from nature, 1994).
 11. <http://www.arrownac.com/solutions/beinmotion/>
- © The 2016 International Conference on Artificial Life and Robotics (ICAROB 2016), Jan. 29-31, Okinawa Convention Center, Okinawa, Japan

Simultaneous Localization and Mapping (SLAM) algorithm base on EKF and SPKF.

ZolghadrJavad, Yuanli Cai, Yekkehfallah Majid

School of electronic and information engineering, Xi'an Jiaotong University, Xi'an 710049, China
e-mail addresses: Javad.zolghadr@gmail.com, ylicai@mail.xjtu.edu.cn, Majid.fallah@mail.xjtu.edu.cn,

Abstract

Simultaneous Localization and Mapping (SLAM) is the problem in which a sensor-enabled mobile robot incrementally builds a map for an unknown environment, while localizing itself within this map. The Kalman Filter's linearized error propagation can result in big errors and instability in the SLAM problem. One approach to reduce this situation is using of iteration in Extended Kalman Filter (EKF) and Sigma Point Kalman Filter (SPKF). We will show that the recapitulate versions of kalman filters can improve the estimation accuracy and robustness of these filters beside of linear error propagation. Simulation results are presented to validate this improvement of state estimate convergence through repetitive linearization of the nonlinear model in EKF and SPKF for SLAM algorithms. Results of this evaluation are introduced by computer simulations and verified by offline implementation of the SLAM algorithm on mobile robot in MRL Robotic Lab.

Keywords: Extended Kalman Filter, Sigma Point Kalman Filter, SLAM, instability, Mobile Robot, Nonlinear Estimation.

1. Introduction

Simulation Localization and Mapping (SLAM) has the problem of incrementally building a spatial consistent map from noisy sensor data gathered by a robot and tracking robot pose with the built map[1][2]. In the past decade, the SLAM related research has received an increasing and extensive attention in theory and application level. Due to the mutual dependence of robot pose and the map, the noise of robot pose arise the uncertainty of map estimation and vice versa. Therefore, this problem requires a solution in a high dimensional space.

Numerous method have been used to address the SLAM problem, an overview of which is presented in [3],[4]. One of the most popular approaches to the SLAM problem are the extended Kalman filter (EKF-SLAM). The effectiveness of the EKF approach lies on the fact that it holds a fully correlated posterior over feature maps and vehicle poses [3]. Due to the inherent non-linearity of the SLAM problem, it applies the Kalman filter framework to nonlinear Gaussian systems, by employing the first-order Taylor expansion to approximate the non-liner models. However, this approximation treatment often introduces large errors in the estimate of the states and can lead filter to divergence [5]. These serious drawbacks have been

confirmed in [4],[6],[7] with carefully designated experiments. Another serious potential drawback of EKF-SLAM is the derivation of the jacobian matrices, which is really a bothersome process.

Some researchers applied these new extensions of the Kalman filters family called Sigma Point Kalman Filters (SPKF) to solve the SLAM problem [8],[9]. In spite of superiority of the SPKF over the EKF, We will study the future of SPKF over EKF.

In this paper, we want to investigate SLAM with SPKF and show this method robustness. The rest of the paper is structured as follows. Section II summarizes the EKF based SLAM. The we will briefly describe the SPKF based SLAM in section III. In section, IV the formulation of the EKF and SPKF approaches with their iterated versions in section V. Section VI concludes the paper.

2. EKF SOLUTION FOR THE SLAM

In this section we summarize the basic EKF SLAM equations to point out the steps in which linearized approximations are introduced. We subsequently analyze their influence in the consistency of the solution obtained. In the standard EKF-based approach to SLAM,

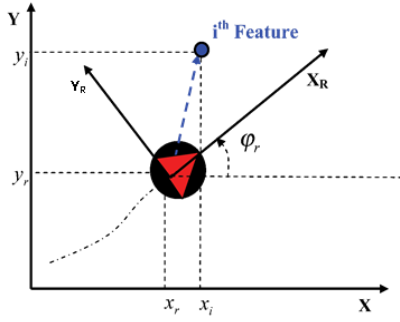


Fig.1. Robot Position

The Extended Kalman Filter estimates the mean and covariance of the posterior probability distribution function (PDF) of the random state variable X . Let $\hat{X}^+(k)$ denote the mean of the posterior PDF at time k . The corresponding covariance matrix of the posterior distribution is $B^+(k)$. The process model for vehicle and features can be written as:

$$\begin{bmatrix} X_v(k+1) \\ X_m(k+1) \end{bmatrix} = \begin{bmatrix} f_v(X_v(k), u(k+1)) \\ X_m(k) \end{bmatrix} + \begin{bmatrix} v(k+1) \\ 0 \end{bmatrix} \quad (1)$$

Where f_v is the motion model of the Robot, $u(k)$ is control input and $v(k)$ represents process noise that is zero mean white with covariance $Q(k)$. The EKF fuses the odometry measurements with a sequence of observations from the external sensors with the following observation model:

$$z(k) = h(X(k)) + w(k) \quad (2)$$

$w(k)$ is zero mean white observation noise with the covariance matrix $R(k)$. Four fundamental stages of the EKF based SLAM are briefly written as follows:

I. Prediction

$$\begin{aligned} X^-(k+1) &= f(X^+(k), u(k+1)), \\ \hat{z}^-(k+1) &= h(X^-(k+1)), \\ B^-(k+1) &= \nabla_x f(k) \cdot B^+(k) \cdot \nabla_x f^T(k) + Q(k). \end{aligned} \quad (3)$$

II. Observation

$$v(k+1) = z_i(k+1) - \hat{z}_i^-(k+1) \quad (4)$$

Moreover, corresponding matrix:

$$S(k+1) = \nabla_x h \cdot B^-(k+1) \cdot \nabla_x h^T + R(k+1). \quad (5)$$

III. Update

Poster distribution's covariance can be same as follows:

$$\begin{aligned} X^+(k+1) &= X^-(k+1) + W(k+1) \cdot v(k+1) \\ B^+(k+1) &= B^-(k+1) - W \cdot S(k+1) \cdot W^T \end{aligned} \quad (6)$$

Kalman gain:

$$W(k+1) = B^-(k+1) \cdot \nabla_x h^T \cdot S^{-1}(k+1) \quad (7)$$

IV. Consolidation

After new feature is calculated, estimation must shown at last part of consolded state vector:

$$X_i^+(k+1) = g_i(X_v^-(k), z(k)). \quad (8)$$

g_i = convert function for polar observation $z(k)$ to a global Cartesian feature location.

3. SPKF SOLUTION FOR SLAM

Mathematic framework of SPKF Based Slam will discuss in this section, in section 2 in this paper assumptions made for SLAM problem, we define a new consolidation state vector that include the original state vector $X(k)$ and process noise. Block diagonal matrix of $B(k)$ and process noise covariance matrix $Q(k)$ is new covariance matrix:

$$X_k^a = [X_k \ V_k]^T, \quad B_k^a = \begin{bmatrix} B_k & 0 \\ 0 & Q_k \end{bmatrix} \quad (9)$$

Sigma point at the time k will be:

$$\chi^{a+} = [\chi_0^+, \chi_i^+ + \gamma \sqrt{B_k^a}, \chi_i^+ - \gamma \sqrt{B_k^a}] \quad (10)$$

γ is a scaling parameter that controls the spread of sigma point around the mean. We can use cholesky factorization for calculate more efficient the covariance matrix square root. According to [10],[11] these sigma points pass through the process model and transformed sigma points will be calculated:

$$\chi_i^{x+}(k+1) = f(\chi_i^{x+}(k), u(k), \chi_i^{v+}(k)), \quad (11)$$

For the original consolidation state vector the $\chi_i^{x+}(k)$ is sigma points set and $\chi_i^{v+}(k)$ is sigma point set for process noise. The associated covariance matrix and predicted state estimate can be computed as follows:

$$\begin{aligned}\bar{\chi}_{k+1} &= \sum_{i=0}^{2N} w_i^m \chi_{i,k+1}^{x-} \\ B_{k+1}^- &= \sum_{i=0}^{2N} \sum_{j=0}^{2N} w_{ij}^c (\chi_{i,k+1}^{x-}) (\chi_{j,k+1}^{x-})^T \quad (12)\end{aligned}$$

The transformed sigma points pass through the measurement model and samples of predicted are:

$$Z_i^-(k+1) = h(\chi_i^{x-}(k+1)) \quad (13)$$

Corresponding covariance matrices and predicted measurement can obtain:

$$Z_{k+1}^- = \sum_{i=0}^{2N} w_i^m Z_{i,k+1}^- \quad (14)$$

Cross covariance matrix between state and measurement

B_{ZZ}^- and covariance matrix and measurement error with assuming correct data are:

$$B^-(k+1) = \sum_{i=0}^{2N} w_i \{ \chi_i^{AUG+}(k+1) - \hat{X}^-(k+1) \} \{ \chi_i^{AUG+}(k+1) - \hat{X}^-(k+1) \}^T$$

$$v_{k+1} = z_{k+1} - z_{i,k+1}^-$$

$$B_{ZZ,k+1}^- = R + \sum_{i=0}^{2N} \sum_{j=0}^{2N} w_{ij}^c (z_{i,k+1}^-) (z_{j,k+1}^-)^T$$

$$B_{XZ,k+1}^- = R + \sum_{i=0}^{2N} \sum_{j=0}^{2N} w_{ij}^c (\chi_{i,k+1}^{x-}) (z_{j,k+1}^-)^T \quad (15)$$

With observation noise additively the update state estimate and corresponding covariance matrix can be computed:

$$\begin{aligned}X_{k+1}^+ &= X_{k+1}^- + K_{k+1} \cdot v_{k+1}, \\ B_{k+1}^+ &= B_{k+1}^- - K_{k+1} \cdot B_{ZZ,k+1}^- \cdot K_{k+1}^T \quad (16)\end{aligned}$$

Kalam gain will be:

$$K_{k+1} = B_{XZ,k+1}^- \cdot [B_{ZZ,k+1}^-]^{-1} \quad (17)$$

After Z_{k+1} detected the consolidation process easily performed with the following equations:

$$\begin{aligned}P_{k+1}^{AUG} &= \begin{bmatrix} P_{k+1}^- & 0 \\ 0 & R_{k+1} \end{bmatrix} \\ X_{k+1}^{AUG+} &= g_i(X_{i,k+1}^{AUG}), \\ X_{k+1}^+ &= \sum_{i=0}^{2N} w_i^m \chi_{i,k+1}^{AUG+} \\ B_{k+1}^+ &= \sum_{i=0}^{2N} \sum_{j=0}^{2N} w_{ij}^c (X_{i,k+1}^{AUG+}) \cdot (X_{j,k+1}^{AUG+})^T \quad (18)\end{aligned}$$

In above equations, the parameters w_i^m and w_{ij}^c are scalar positive valued weights.

In following, we illustrated our results which we implemented on MATLAB:

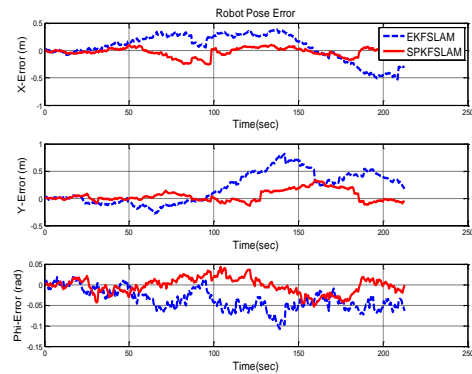


Fig.2. Comparison of vehicle pose estimate errors for EKF (Blue line) vs.SPKF (Red)

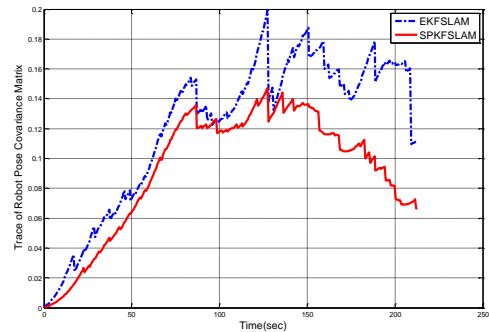


Fig. 3.State Covariance of Robot for KLF and SPKF

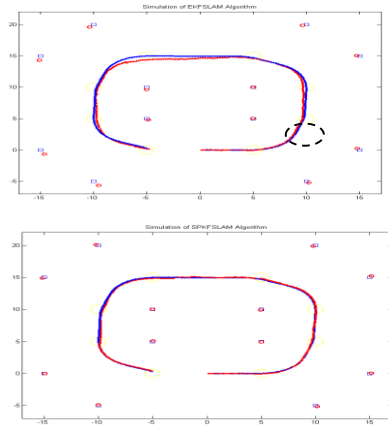


Fig.4. Comparing Robot position with EKF and SPKF

Mean Square Error (MSE)	$X_R \text{ state}$	$y_R \text{ state}$	$\phi_R \text{ state}$
EKF-SLAM	0/622	0/1180	0/002
SPKF-SLAM	0/0077	0/0120	0/0003

Table 1. Comparing the Mean Square errors for EKF and SPKF

4.CONCLUSION

In this paper, we investigated the EKF and SPKF frameworks to improve the estimation accuracy in simultaneous localization and mapping. All of simulation results consistently verified better performance and more accurate states estimate of the SPKF than EKF approaches. After Comparing the Errors and the Position vector of the Robot with two different optimizations, SPKF had significant better result than EKF.

REFERENCES

- [1] W.H. Durrant, T. Bailey. Simultaneous localization and mapping: Part I. *IEEE Robotics and Automation Magazine*, 2006, 13(2): 99–110.
- [2] T. Bailey, W.H. Durrant. Simultaneous localization and mapping: Part II. *IEEE Robotics and Automation Magazine*, 2006, 13(3): 108–117.
- [3] H.Durrant-Whyte and T. Bailey. "Simultaneous localization and mapping: Part 1", *IEEE Trans. on Robotics and Automation*, 13(2): 99-108, 2006.
- [4] T.Bailey and H. Durrant-Whyte. "Simultaneous localization and mapping:Part II", *IEEE Trans. on Robotics and Automation*, 13(3): 108-117,2006.
- [5] Y. Bar-Shalom, X. Rong Li, and T. Kirubarajan. *Estimation with Applications to Tracking and Navigation*. Wiley InterScience, 2001.
- [6] S. Julier and J. K. Uhlmann."A counter example to the theory of simultaneous localization and map building", in *Proc. IEEE Int. Conf. Robot.Autom.*, 2001, pp. 4238-4243.
- [7] S. Huang and G. Dissanayake. "Convergence and consistency analysis forextended Kalman filter based SLAM", *IEEE Transactions on Robotics and Automation*, 23(5): 1036-1049, 2007.
- [8] J. Andrade-Cetto, T. Vidal-Calleja, and A. Sanfeliu. "Unscented transformation of vehicle states in SLAM." In *Proc. of the 2005 IEEE Int. Conf. on Robotics and Automation*, pages 324-329, Barcelona, Spain, April 2005
- [9] R. Martinez-Cantin, J. A. Castellanos. "Unscented SLAM for largescale outdoor environments." In *Proc. of the 2005 IEEE Int. Conf. on Intelligent Robots and Systems*, pages 3427-3432, Aug. 2005.
- [10] Simon J. Julier, and Jeffery K. Uhlmann. "A New Extension of the Kalman Filter to Nonlinear Systems." In *The Proceedings of AeroSense: The 11th International Symposium on Aerospace/Defense Sensing, Simulation and Controls, Multi Sensor Fusion, Tracking and Resource Management II*, SPIE, 1997.
- [11] R. van der Merwe. "Sigma-Point Kalman Filters for Probabilistic Inference in Dynamic State-Space Models." PhD thesis, OGI School of Science & Engineering, Oregon Health & Science University, April 2004
- [12] Won-Seok Choi, Jeong-Gwan Kang, and Se-Young Oh, *Member, IEEE* Measurement Noise Estimator Assisted Extended Kalman Filter for SLAM Problem, 2009 St. Louis, USA

An accurate method for the extraction of structured light stripe

Jiwu Wang

*School of Mechanical, Electronic and Control Engineering, Beijing Jiaotong University
Beijing 100044, China*

Yaodong Li, Zhijing Jian

*School of Mechanical, Electronic and Control Engineering, Beijing Jiaotong University
Beijing 100044, China*

Masanori Sugisaka

*Alife Robotics Corporation Ltd, Japan and Open University, United Kingdom
E-mail: jwwang@bjtu.edu.cn; ms@alife-robotics.co.jp*

Abstract

In order to obtain the highest measurement accuracy in the On-line measurement of rail profile with a line structured light based on machine vision, the extraction of structured light stripe is a necessary step. An accurate extraction method is proposed for the structural light stripe extraction in practical applications. The noise in the captured image can be removed with region segmentation method. The structured light stripe is separated and extracted accurately based on the characteristics of the structure light stripe in the binary image. The method was verified in laboratory conditions. Experiment results show that the method can effectively solve the problem of real-time and accurate extraction of structured light stripe.

Keywords: Structured light; region segmentation; light stripe

1. Introduction

The On-line measurement of rail profile with a line structured light based on machine vision need collect and manipulate the captured image to obtain the structured light stripe. The structured light stripe stands for the measured rail profile. By comparing the extracted contour lines with the standard rail profile, the on-line measurement of the rail profile can be accomplished. In order to ensure the accuracy of measurement, the accurate extraction of structured light stripe becomes very important. The traditional method¹ includes the threshold method and the extreme value method. Those are simple, but low precision. In light of the above problems, an accurate method for the extraction of structured light stripe is proposed. The noise in the captured image can be removed with region segmentation method. According to the characteristics of the structure light stripe, the target is extracted from

the specified region, so as to achieve the accurate extraction of structural light stripe.

2. Measurement principle

Two image acquisition devices A and B are arranged on the upper and lower sides of the rail, as shown in Fig.1. The image acquisition device is composed of a line structured light emitter and an industrial camera. Because of the projection relationship, the stripe of the light can represent the rail profile. So the outline dimension of the rail can be calculated by the collection and analysis of the line structured light stripe.

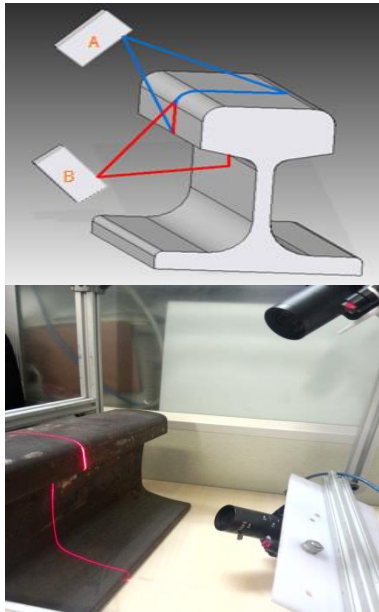


Fig.1.Measurement method

3.1 Regional intelligent segmentation

First of all, the line structure light contour line is collected, shown in Fig.2. And then binarization is shown in Fig.2. The calibration of the connected region of the image is carried out, and the result is to separate the discontinuous regions². Since the characteristics of the spot is obvious, it can be easily removed. Only the line structured light contour lines and a small part of the noise was left, as shown in Fig.3.

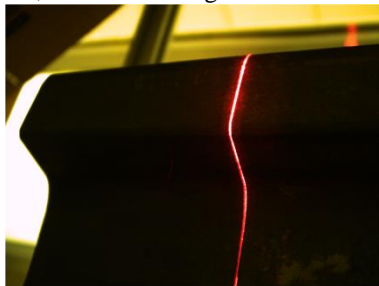


Fig.2. Structured light profile

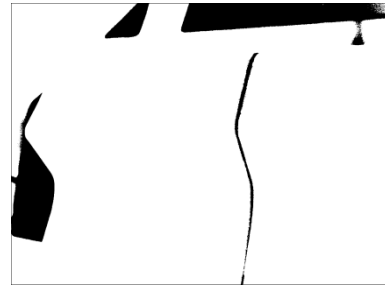


Fig.3.Binary image

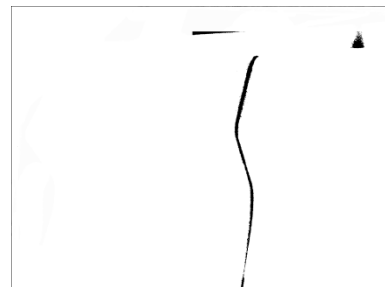


Fig.4. remove the noise

3.2 Identifying Geometric Feature

Illumination conditions and mirror reflection and other factors affecting the contour extraction of line structured light. In order to eliminate these effects, the structural light area is studied as a whole object. It can be used to directly extract the light area of the line structure by pattern recognition technology. In this area, the outer boundary and inner boundary of the line structure light contour are calculated. By analyzing the characteristics of the shape, the size of the structure and the luminance gradient of the binary image, we can determine the position of the structure light stripe. Through continuous scanning of the structured light stripe of along the X direction and the Y direction coordinate values in ascending order, structured light stripe of the outer boundary and inner boundary can be accurately extracted. Because of the method is completely combined with the imaging characteristics of the structured light on the rail tracks surface which can reduce the extraction of target range and reduce the influence of interferences, thus improving the reliability of line structured light contour extraction, stability and accuracy.

3. Analysis

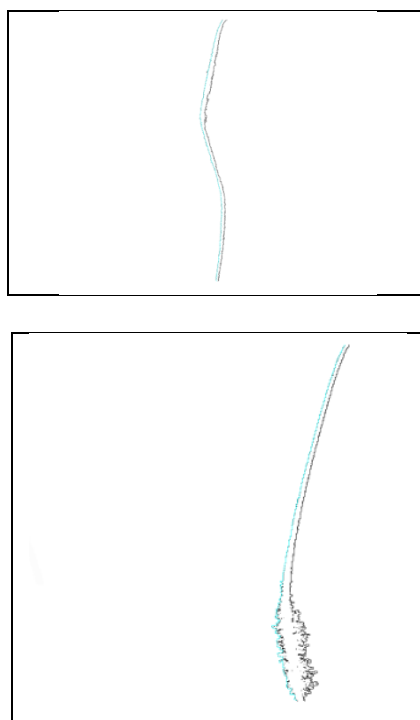


Fig.5. Fringe extraction results

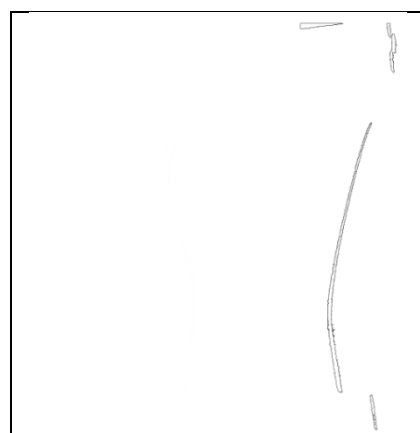


Fig.6. Edge detection operator

Line structured light stripe extraction results are shown in Fig.5. The accurate extraction of line structured light can be achieved by using region segmentation and geometrical feature recognition technology. The outer edges and inner edges of two structured light stripes are extracted respectively as shown in the Fig.5. It can be seen that the extraction of the stripe is continuous and

stable. By comparing with common edge detection operator such as Roberts operator, Canny operator, Sobel operator, the common edge detection operator has no pertinence in the binary image and can't effectively remove the noise in the image. And the result is a closed circle which can't distinguish the inner and outer edges, as shown in Fig.6. The method used in this paper can effectively eliminate the noise according to the geometrical features of the stripe and can extract the edge and the outer edge respectively. The inner boundary or outer boundary is used as the extraction result. The extraction result is used to measure the rail profile³.

4. Conclusions

By using the method of region segmentation and geometric feature extraction, the line structured light stripe can be extracted. Compared with the traditional edge detection operator, it can effectively eliminate the interference of the noise, and can extract the edge and the outer edge of the structured light stripe. It effectively solves the problem of real-time extraction of structured light stripe, which is convenient for the following contour matching.

References

1. Qiucheng Sun and Renyun Liu, An extraction method of laser stripe centre based on Legendre moment, *International Journal for Light and Electron Optics*, Volume 127, Issue 2, January 2016, Pages 912–915.
2. Qiucheng Sun and Jian Chen, A robust method to extract a laser stripe centre based on grey level moment, *Optics and Lasers in Engineering*, Volume 67, April 2015, Pages 122–127.
3. J. Cheng, S.G. Zheng, X.Y. Wu, Structured light-based shape measurement system, *Signal Process*, 93 (6) (2013), pp. 1435–1444.

Feature Acquisition From Facial Expression Image Using Convolutional Neural Networks

Taiki Nishime

*Graduate school of Information Engineering, University of Ryukyus
Nishihara, Okinawa, Japan*

Satoshi Endo, Koji Yamada, Naruaki Toma, Yuhei Akamine

*School of Information Engineering, University of Ryukyus
Nishihara, Okinawa, Japan
taiki_one@eva.ie.u-ryukyu.ac.jp, endo@ie.u-ryukyu.ac.jp, koji@ie.u-ryukyu.ac.jp
tnal@ie.u-ryukyu.ac.jp, yuhei@ie.u-ryukyu.ac.jp*

Abstract

In this study, we carried out the facial expression recognition from facial expression dataset using Convolutional Neural Networks (CNN). In addition, we analyzed intermediate outputs of CNN. As a result, we have obtained a emotion recognition score of about 58%; two emotions (Happiness, Surprise) recognition score was about 70%. We also confirmed that specific unit of intermediate layer have learned the feature about Happiness. This paper details these experiments and investigations regarding the influence of CNN learning from facial expression.

Keywords: facial expression recognition, convolutional neural networks, deep learning, feature learning

1. Introduction

Facial expression recognition is important to non verbal communications among the people. Now, opportunities to communicate using either voice or text is increasing because of developing mobile phones and Internets. Thus, it is considered that communication method via some devises has increased than face to face communication. “UNMASKING THE FACE” by Paul Ekman and W.V. Friesen [1] described that facial expressions have a closely connection with the emotions. For this reason, It is natural to think that we can recognized your happiness if you smiling. Mainstream approaches in facial expression recognition use Facial Action Coding System (FACS) labels. FACS was designed to help facial expression recognition

with resolve each expression into several Action Units (AUs). FACS labels approaches need to learn from FACS manual and test. As of now, FACS label can only be given by experts or trained individuals. As a results, not everybody using easily FACS labels to facial expression recognition.

The previous studies on facial expression recognition can be classified into two categories: FACS based method [2] or feature learning method [3]. In FACS based method, they first extracted feature from AUs, then they recognized facial expression from facial images using a these extracted feature and Support Vector Machine. In contrast to feature learning method [3], recognized facial expression using Convolutional Neural Networks (CNN) [4].

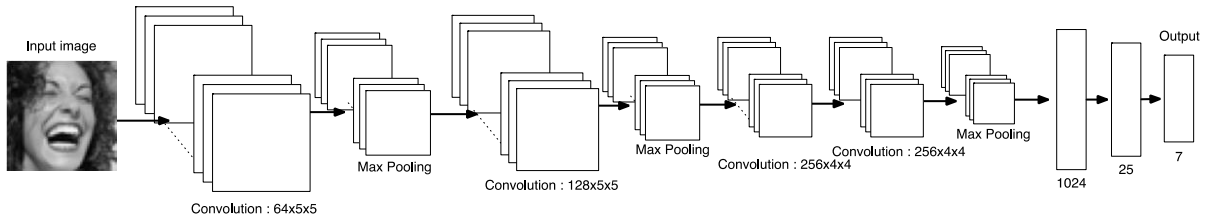


Fig 1. CNN structure: consist of three convolutional layers, three pooling layers, two fully connected layers, and output layer

But, this study is not discussed in CNN model that has finished learning, and there was no argument about learning the feature of CNN.

In this study, firstly, we carried out facial expression recognition using CNN. In addition, we analyze the intermediate outputs of CNN that obtained from facial expression images.

2. Convolutional Neural Networks

Convolutional Neural Networks is a type of feed-forward artificial neural networks that consist of convolutional layers, pooling layers, fully connected layers and output layer. Convolutional layers compute product-sum of image and weight. Pooling layers compute the max value of a particular feature over a region of the image. These convolutional layer and pooling layer were repeated for every such layer. Fully connected layers applied at the end of or after repeated each layer. Fully connected layers is the same as regular multilayer perceptron. By propagating these each layer, CNN was feature extracted from input images.

3. Experiments

3.1. FER-2013 Dataset

We have selected Facial Expression Recognition 2013 (FER-2013) dataset [6]. FER-2013 was created by Pierre Luc Carrier. This dataset was created using the Google image search API to search for images of faces that match a set of 184 emotion-related keywords like “blissful”, “enraged” etc. Each images included dataset is cropped around a face, and cropped images were then resized to 48x48 pixels and converted to grayscale. Table. 1. present the details of the dataset. Facial expression We focused on are Angry(An), Disgust(Di), Fear(Fe), Happiness(Ha), Sadness(Sa), Surprise(Su) and Neutral(Ne).

	An	Di	Fe	Ha	Sa	Su	Ne	Total
Training	3993	436	4096	7212	4828	3171	4692	28698
Test	466	56	496	895	653	415	607	3588

Table 1. Detail of FER-2013 dataset

© The 2016 International Conference on Artificial Life and Robotics (ICAROB 2016), Jan. 29-31, Okinawa Convention Center, Okinawa, Japan

3.2. Preprocessing

We preprocess the data using Global Contrast Normalization (GCN) and ZCA whitening [5]. In GCN, subtract by mean and divide by dispersion for each dataset images. By GCN preprocessing, if the value range of the input is normalized from -2 to 2, and can be aligned to that range, even if there is a different axis scales. Natural image is characterized by strong correlation with neighboring pixels. ZCA whitening has function to erase such correlation.

3.3. CNN settings

Fig 1. shows CNN model that used in this experiment. Arrows in Fig 1. show weights, and number of under each boxes show unit number. The number of input units setting to same as number of input image pixels. The number of output unit setting to same as number facial expression classes. As the facial expression recognition result, using the maximum value in output layer units.

3.4. Result

The results of this experiments shown in Table. 2. We have obtained an recognition score 57.02%; Happiness and Surprise facial expression recognition score was about 70%. In contrast, Fear, Sad and Neutral score was below 52%. Also these recognitions from only image data is seemed to be difficult. We have obtained an Disgust recognition score 0% because of Disgust data was less then other facial expression data.

	An	Di	Fe	Ha	Sa	Su	Ne
An	45.92	0	11.58	7.51	21.45	2.57	10.94
Di	37.5	0	14.28	5.35	25	1.78	16.07
Fe	10.08	0	37.9	5.84	26.2	7.25	12.7
Ha	4.24	0	2.79	76.2	6.92	2.23	7.59
Sa	10.71	0	13.32	7.65	51.14	1.68	15.46
Su	3.85	0	11.32	4.09	3.37	72.04	5.3
Ne	7.9	0	7.9	8.56	23.39	1.64	50.57

Table 2. Confusion matrix of facial expression recognition

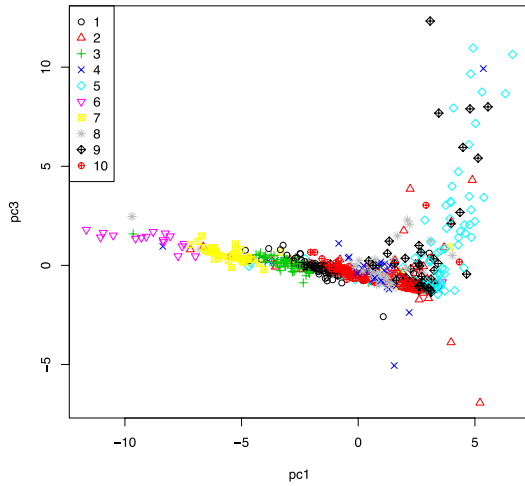


Fig 2. Visualized the 25-dimensional intermediate output of recognized Happiness. The 25-dimensional output was compressed to 2-dimension output by Principal Components Analysis. Plotting first and third principal components. 48.959% is contribution rate, it is show that 48.959% information remained by PCA. Labeled by k-means.

3.5. Analyzing the intermediate outputs

As mentioned before, CNN was extracted feature at each layers, and these result of feature extraction was influence on the recognition. Thus, it seems that recognition accuracy is higher, feature extraction is better result. From this reason, we focused on Happiness, and analyzing the intermediate output values. By this analyzing, we reveal that extracted feature from Happiness data.

In this experiment, there are image that recognized 682 Happiness images in 895 labeled images. We are focused on the Happiness images and intermediate output values previous layer for the output layer. Result of compressed intermediate output to two dimension is shown in Fig 2. From Fig 2, It can be seen that some clusters are overlapped with each other like cluster 1 and cluster 10, but independent cluster like clusters 5 and cluster 6 is also exists. As a result, we investigated the difference in the distinguishable clusters 5 and cluster 6, we examine the extracted features from the result of this investigation. Examination method is simple, we checked that whether the intermediate outputs connoting a pattern.

All of 25 units intermediate output of cluster 5 and cluster 6 are shown in Fig 3, and also examples of image and intermediate outputs include in cluster 5 and cluster 6 are shown in Fig 4. As a results, It can be seen that the intermediate outputs of cluster 6 was bigger than cluster 5. As

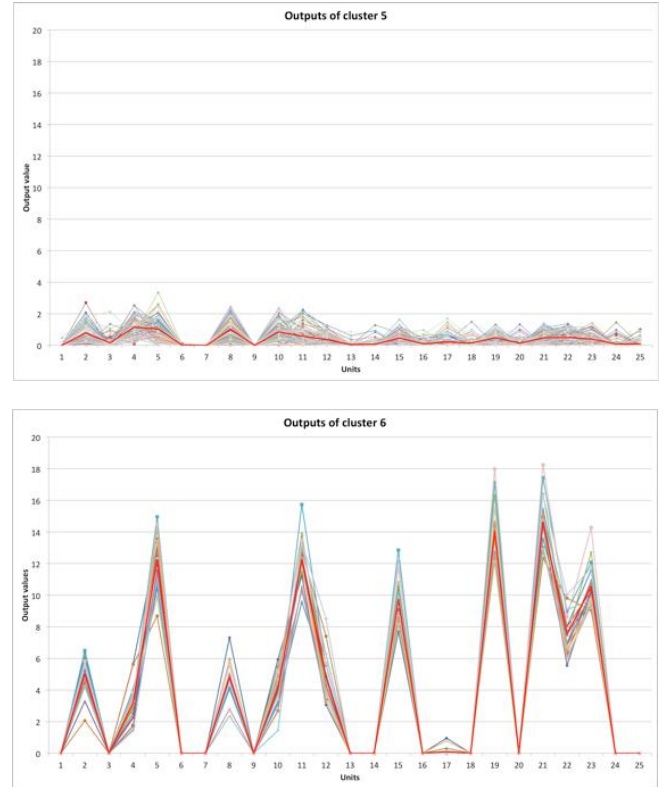


Fig 3. Intermediate outputs of all 25 units. Upper line graph is shown intermediate output of cluster 5, lower line graph is shown intermediate output of cluster 6. Red bold line is average value of 25 units. Other lines represent one input reconstructed Happiness facial image.

far as we have confirmed detail of outputs in cluster 6, all data was Happiness face, and is commonly mouth was open, as shown in Fig 4. On the other hand, cluster 5 included Happiness face both opened mouth and closed mouth. Most of cluster 5 data was Happiness face with closed mouth. We focus on the intermediate output of each unit in data of cluster 6 (Fig 3), for example, it can be seen that the output value of 21th unit is large. Also in Fig 4, the Happiness face with opened mouth and closed mouth were difference in 21th unit output value. In Fig 4, it is selected some example from cluster 5 and cluster 6. It was also observed that this result of 21th unit output value was the same tendency as Happiness face with opened mouth in other cluster. In these results, the 21th unit output have closure connected in shape of mouth open. We conclude that

CNN have learned the feature of facial expression about mouth.

3.6. Future work

In this paper, We carried out the emotion recognition from facial expression image using a CNN. As a result, we have obtained an average emotion recognition score of 58%; two emotions (Happiness, Surprise) recognition score was about 70%. From the result of the analyzing intermediate outputs of CNN, we confirmed specific intermediate outputs was likely to be reflected in shape of mouth. In this experiments, though using the simple method that analyze the intermediate outputs pattern, it is considered to effective method that analyzing the extracted feature from input data. In the future work, we will try to analyze larger intermediate outputs than in this experiment. And we revealed that method of feature extracted of deep layer.

References

- [1] Paul Ekman, W.V. Frisen, “UNMASKING THE FACE” (1975)
- [2] Hiroki NOMIYA, Teruhisa HOCHIN, “Facial Expression Recognition using Feature Extraction based on Estimation of Useful Features” (2011)
- [3] VICTOR-EMIL NEAGOE, ANDREI-PETRU BRAR, NICUSEBE, PAUL ROBITU, “A Deep Learning Approach for Subject Independent Emotion Recognition from Facial Expressions”, Recent Advances in Image, Audio and Signal Processing, pp.93-98 (2013)
- [4] “Convolutional Neural Networks (LeNet) – DeepLearning 0.1 documentation”, LISA Lab. (2013)
- [5] Alex Krizhevsky, “Learning Multiple Layers of Features from Tiny Images”, 2009.
- [6] Goodfellow, Ian J, .et al. “Challenges in Representation Learning: A report on three machine learning contest” Neural Information Processing. Springer Berlin Heidelberg, 2013.

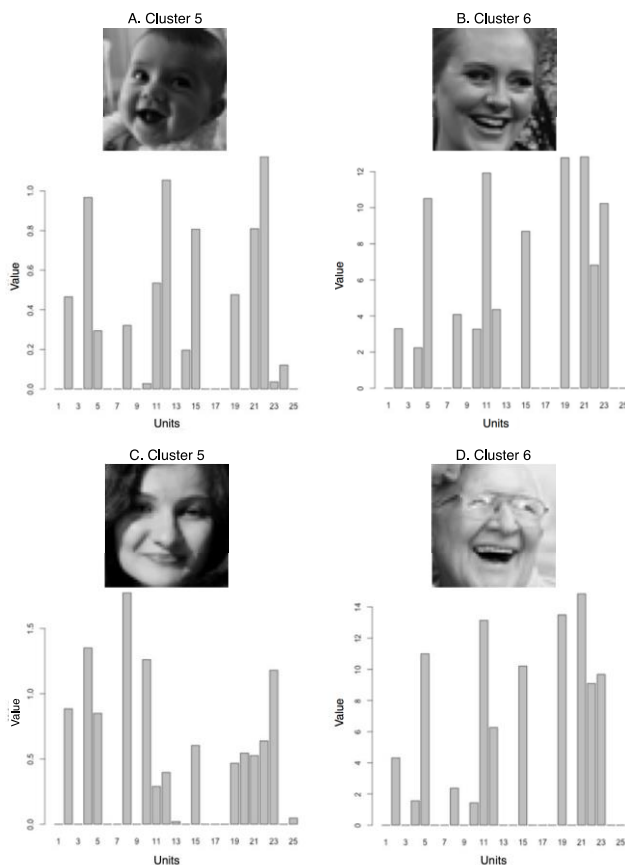


Fig 4. Example of All of 25 units intermediate output of cluster 5 and 6.

Estimating Age on Twitter Using Self-Training Semi-Supervised SVM

Tatsuyuki Iju

*Graduate School of Information Engineering, University of the Ryukyus
1 Senbaru, Nishihara-cho, Nakagami-gun, Okinawa, Japan*

Satoshi Endo, Koji Yamada Naruaki Toma, Yuhei Akamine

*School of Information Engineering, University of the Ryukyus
1 Senbaru, Nishihara-cho, Nakagami-gun, Okinawa, Japan
E-mail: k148582@ie.u-ryukyu.ac.jp Endo@ie.u-ryukyu.ac.jp
<http://www.u-ryukyu.ac.jp/en/>*

Abstract

The estimation methods for Twitter user's attributes typically require a vast amount of labeled data. Therefore, an efficient way is to tag the unlabeled data and add it to the set. We applied the self-training SVM as a semi-supervised method for age estimation and introduced Plat scaling as the unlabeled data selection criterion in the self-training process. We show how the performance of the self-training SVM varies when the amount of training data and the selection criterion values are changed.

Keywords: Twitter, Age, Semi-supervised learning, Self-training, SVM, Plat scaling

1. Introduction

Nowadays, the use of Twitter as a social activity sensor has become popular trendy. Although it is more efficient to consider attribute differences such as user age and gender for analysis, users rarely share their personal information to the public. Therefore, a variety of methods for estimating Twitter user's attributes has been studied[1][2][3]. However, these methods require a vast amount of labeled data. Since collecting labeled data is typically a high cost work, the estimation method is efficient when unlabeled data is labeled and used as additional data. We investigate a method for building classifier by using self-training SVM, which is a combination of semi-supervised method, self-training and SVM. In this study, we formulate age estimation as a binary classification problem where user is labeled as under 30 or over 30. The method for user vectorization is simple bag-of-words model and all the tweets treated as data were Japanese tweets. In section 2, we describe self-training SVMs. In section3, we describe the

experiments and present and analyze the results. Finally, we describe our findings and the extension of this work.

2. Self-training SVM algorithm

We describe about the method of building our classifier by using a self-training SVM. Self-training is a simple semi-supervised learning algorithm, with examples of applications started by Scudder[4]. The standard approach for self-training is as follows.

- i. By Using underlying learning algorithm, train a classifier from the labeled data set.
- ii. Label a part of the unlabeled data set according to the classifier, and retrain it, with the newly labeled data as an additional training set.

We construct our classifier for Twitter user's age estimation by using a self-training SVM, in which the underlying learning algorithm is SVM. Furthermore, we introduce Plat scaling as a criterion for selecting users appropriately from the unlabeled set in order to be

labeled. It is expected that poor quality data is filtered out by that criterion. Plat scaling[5] is a method used for modeling a function that returns posterior probability $P(Age|X)$ in which user X is in the Age class, according to classifier's decision function.

The steps of the self-training SVM algorithm where sample set $\{X_i, i = 1, \dots, N_I\}$ and sample set $\{X_u, u = 1, \dots, N_U\}$ belongs to training set F_I and unlabeled set F_U , respectively.

- i. Using F_I , we train a SVM and obtain probability $P(Age_l|X_u) \in \{P(Age_l|X_u), l = 1, \dots, N_A\}$ that sample X_u belongs to Age_l by Plat scaling.
- ii. Define F_{u^*} containing all X_u with at least one of the $P(Age_l|X_u) \geq threshold$. Furthermore, Define sample in F_{u^*} as X_{u^*} .
- iii. Define new F_I as $F_I = F_I + F_{u^*}$. The label of X_{u^*} is predicted as the Age_l for which $P(Age_l|X_{u^*})$ is highest. Furthermore, Define new F_U as $F_U = F_U - F_{u^*}$.
- iv. Repeat i. ~ iii. until F_{u^*} cannot be defined.

performance with the test set. Additionally, in order to provide the baselines for these classifiers, we built other classifiers by using normal SVM for each of four training set arrays and measured their performance the same way, we did for the self-training SVM ones. The performance measurement was done by the five-fold cross validation. The number of users in the test set was 480 and the number of users in the unlabeled set was 1200. In addition, the number of users from under 30 and over 30 classes were balanced in both the training and test sets. The way for user vectorization was simple bag-of-words model, at the time of classifier training and user's age prediction. Prior to proceeding the experiments, it was necessary to set hyper parameters of SVM and features in a bag-of-words representation. Therefore, we performed a grid-search, set the kernel and cost parameters of SVM as linear and 1000 respectively. As for the features, we set the 158 top-ranked words by χ^2 score which appeared in user tweets from the training set.

3.2. Results

Table 1: Results for the normal SVM

	Number of the users in training set					
	76		256		376	
Age class	Under 30	Over 30	Under 30	Over 30	Under 30	Over 30
Precision	0.613	0.792	0.638	0.825	0.647	0.834
Recall	0.882	0.441	0.896	0.492	0.898	0.509
F measure	0.723	0.563	0.745	0.616	0.752	0.632
Mean F measure	0.643		0.680		0.692	

3. Experiments

3.1. Experimental contents and settings

We defined age as two classes, under 30 and over 30. This definition is the same as Rao's research[1]. we carried out some experiments in order to evaluate the performance of the Self-training SVM for the Twitter user's age estimation. By using self-training SVM, we built a classifier for each of the nine training set arrays (three sets of different number of users containing 76, 256 and 376 with three possible selection criterions of 0.5, 0.7 and 0.9 respectively). Then, we measure the classifier's

Table2: Results for the training set with 76 number of users

	Unlabeled data selection criterion					
	0.5		0.7		0.9	
Age class	Under 30	Over 30	Under 30	Over 30	Under 30	Over 30
Precision	0.614	0.792	0.610	0.793	0.625	0.791
Recall	0.882	0.442	0.888	0.430	0.901	0.473
F measure	0.723	0.563	0.722	0.554	0.728	0.590
Mean F measure	0.643		0.639		0.659	

Table3: Results for the training set with 256 number of users

	Unlabeled data selection criterion					
	0.5		0.7		0.9	
Age class	Under 30	Over 30	Under 30	Over 30	Under 30	Over 30
Precision	0.638	0.825	0.630	0.818	0.645	0.808
Recall	0.896	0.492	0.895	0.473	0.876	0.512
F measure	0.745	0.616	0.739	0.599	0.742	0.629
Mean F measure	0.680		0.669		0.686	

Table4: Results for the training set with 376 number of users

	Unlabeled data selection criterion					
	0.5		0.7		0.9	
Age class	Under 30	Over 30	Under 30	Over 30	Under 30	Over 30
Precision	0.647	0.834	0.649	0.825	0.657	0.829
Recall	0.898	0.510	0.891	0.516	0.890	0.534
F measure	0.752	0.632	0.750	0.634	0.756	0.650
Mean F measure	0.692		0.692		0.703	

First, we describe about the results for the normal SVMs. Table 1 shows the performance of the normal SVM classifiers. From Table 1, we can assure that the classifiers can improve their performance as the size of the set is increased, at least when the size of the given training set is in the 76 to 376 range. According to this result, as well as for self-training SVM, it is expected that performance can be improved by utilizing unlabeled set with the training set size within the same range size. Additionally, regardless of the training set size, it was observed that precision is high and recall is low for the under 30 class and, oppositely the precision is low and recall is high for the over 30 class. F measure was better for the under 30 class than for over 30 one. It is, basically,

that the under 30 class user was easier to predict than the over 30 class one. As for the results about self-training SVM, Table 2, 3, 4, and correspond to the prediction results from classifiers built from 76, 256 and 376 users training sets, respectively. The classifier with the highest improvement from baseline was the one with 76 users training set with a selection criterion of 0.9 (improvement was 0.032 point for the over30 class recall). Classifier from the 376 users with a selection criterion of 0.9 was the second highest (improvement was 0.025 point for the over 30 class recall). Although the recall improvement for over 30 class is remarkable, precision for the over 30 class and both precision and recall for the under 30 class subtly improve or diminish as the mean F measure

Table 5: Results for the training set 76 number of users (labeling)

	Unlabeled data selection criterion					
	0.5		0.7		0.9	
Age class	Under 30	Over 30	Under 30	Over 30	Under 30	Over 30
Precision	0.621		0.722	0.699	0.752	0.705
Recall	1.0	0	0.890	0.425	0.90	0.440
F measure	0.766		0.796	0.524	0.820	0.537
Mean F measure			0.660		0.678	
Labeling rate	1.0		0.97		0.83	

merely improves. Table 5 shows the labeling accuracy for the 76 users set self-training and ratio of the labeled set for all the unlabeled set. Precision, F and mean F measures for the over 30 class were not defined, because the entire unlabeled set is filtered and eventually labeled as the under 30 class. We could observe better labeling accuracy for higher selection criterions and, in contrast, for bigger selection criterions the amount of labeled data from the unlabeled set is reduced. However, as indicated by Table 2 through Table 4, performance was better for a selection criterion of 0.5 than 0.7 for all of classifiers excluding the 376 users training set, although performance for a selection criterion of 0.9 was best for all classifiers. This result is inconsistent with the fact that the labeling error is more frequent for selection criterion of 0.5 than 0.7 as indicated in Table 5. For that reason, it is implicated that users are easier to predict if selected from a self-training process with a selection criterion of 0.7 than a 0.5 one, since the classifier with a selection criterion of 0.7 is more strongly affected by labeling error than a 0.5 one. In addition, it is inferable that, for a selection criterion of 0.9, the labeling error rate is so small that the classifier achieves in improving its performance.

4. Conclusions

In order to evaluate self-training SVM for Twitter user's age estimation, we construct a classifier by for each of the twelve training set arrays of (three sets of different users containing 76, 256 and 376 with three possible selection criterion of 0.5, 0.7 and 0.9 respectively). Then we evaluate the performance of the classifiers with test set. As a result, in the recall for the over 30 class, it was observed a 0.032 and 0.025 point of improvement from

baseline for training set with a size of 76 and 376 respectively with a selection criterion of 0.9. For future works, we will investigate the relation between the selection criterion and performance of self-training SVM as well as explore the way to improve them.

References

1. Rao, Delip, et al. "Classifying latent user attributes in twitter." *Proceedings of the 2nd international workshop on Search and mining user-generated contents*. ACM, 2010.
2. Burger, John D., et al. "Discriminating gender on Twitter." *Proceedings of the Conference on Empirical Methods in Natural Language Processing*. Association for Computational Linguistics, 2011.
3. Pennacchiotti, Marco, and Ana-Maria Popescu. "Democrats, republicans and starbucks aficionados: user classification in twitter." *Proceedings of the 17th ACM SIGKDD international conference on Knowledge discovery and data mining*. ACM, 2011.
4. Scudder, Henry J. "Probability of error of some adaptive pattern-recognition machines." *Information Theory, IEEE Transactions on* 11.3 (1965): 363-371.
5. Platt, John. "Probabilistic outputs for support vector machines and comparisons to regularized likelihood methods." *Advances in large margin classifiers* 10.3 (1999): 61-74.

Interactive Musical Editing System to Support Human Errors and Offer Personal Preference for an Automatic Piano

Kenji Tsunenari

*Department of Mechanical Information Science and Technology, Kyushu Institute of Technology
680-4, Kawazu, Iizuka-City, Fukuoka, 820-8502, Japan
Email: ktsune@mmcs.mse.kyutech.ac.jp*

Eiji Hayashi

*Department of Mechanical Information Science and Technology, Kyushu Institute of Technology
680-4, Kawazu, Iizuka-City, Fukuoka, 820-8502, Japan
E-mail: haya@mmcs.mse.kyutech.ac.jp*

Abstract

We have developed a system that allows a piano to perform automatically. In order to play music in the manner of a live pianist, we must add expression to the piano's performance. In the case of music, there are often 1,000 or more notes in the score, requiring that an editor spend a huge amount of time to edit. Therefore, we have developed an interactive musical editing system that utilizes a database to edit music more efficiently.

Keywords: Automatic Piano, Knowledge Database, Computer Music, Music Interface

1. Introduction

We have developed a system that allows a piano to perform automatically. In this system, 90 actuators have been installed on the keys and pedals of a grand piano. These actuators execute key strokes and pedal movements to govern the piano's performance. (See Fig.1)

In order to develop an automatic piano that plays music in the manner of a live pianist, we have to add expression to the piano's performance. Essentially, variations in tempo, dynamics, and so on are needed in order to arrange the respective tones in a desired way.

Moreover, in the case of piano music, there will often be 1000 or more notes in the score of even a short piece of music, and the editor must spend a huge amount of time to accurately simulate an actual emotionally expressive performance that a highly skilled pianist could give.

Moreover, a highly skilled pianist is able to play an unfamiliar piece of music by sight, even if the performance is not completely in accord with an intended specific musical interpretation. Current computing systems cannot perform a new piece of music by sight, and thus they cannot simulate a human pianist's musical expression. Therefore, we have developed an interactive musical editing system that

utilizes a database in order to edit music more efficiently¹.

In a current research, MIDI data regarding the performances of highly skilled pianists has been analyzed in order to observe the stylistic tendencies of their performances. The results showed that phrases having similar patterns in the same composition were performed in the similar style.

We developed a system that searches for similar phrases throughout a musical score and infers the style of the performance. Here, we proposed a method using Dynamic Programming (DP) matching as a way to search for similar phrases. In our interactive musical editing system, we have created the Score Database which contains information regarding a musical score. This database contains a field called “Note Value,” in which data indicates the type of note--e.g., a quarter note, a triplet, and so on. This system converts notes into character strings using the “Note Value” data.



Fig.1. The automatic piano.

In addition, the system computes DP matching using the character strings and calculates the degree of disagreement between these strings. It uses an index to judge the resemblance between the strings. For its method of inferring performance expression, it uses the best alignment for DP matching, which enables it to express the best correspondence between notes. In order to edit music more efficiently, we must consider dynamic marking, beat and so on and we created database contains them. We developed an inferring

process with regards to similar phrases using the best alignment and database.

In this paper, we describe the results of searching for similar phrases using DP matching and inferring for them using DP matching and database.

2. Searching for Similar Phrases

As a result of the analysis, it was found that phrases of the same pattern existing in the same tune are performed in a similar expression. This time, we used DP matching to search for similar phrases.

DP matching is a technique used widely in the field of speech recognition, bioinformatics and so on. It has a feature that can calculate the similarity between two words that are different in a number of characters from each other.

In Fig.2, the route of minimum cost in each point is taken, and the route with the lowest cost is assumed finally to be the optimal path. The cost at that time is defined as the distance between patterns. In this system, this distance is handled as a threshold to judge whether the phrases are similar to each other.

For example, if the cost moves up or to the right, then it is increased by 1. If it moves to the upper right, then it does not increase. Also, if the characters do not correspond in each point, then the cost is increased by 5.

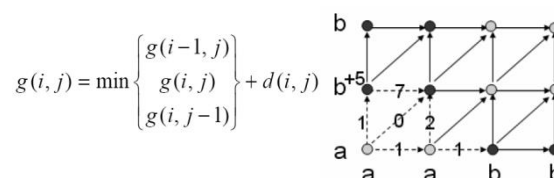


Fig.2. DP Matching

3. Musical Editing Support System

3.1. System Architecture

The structure of the system is shown in Fig.3, The user edits music via the user's interface on a computer display. The user can also access a database that has musical grammar, the user's preferences, and so on. As a result, edition work is reduced and efficient editing becomes possible.

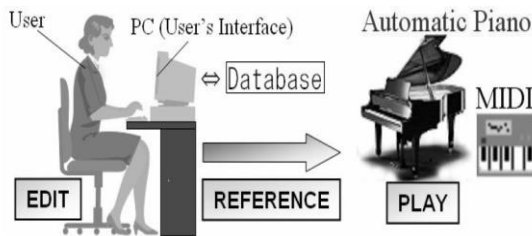


Fig.3. Structure of the editing system

3.2. Format of Performance Information

The automatic piano that we have developed uses a music data structure that is similar to MIDI. We defined performance information, dividing it into two categories: the notes and the pedals. The note information is comprised of the six parameters involved in producing a tone: “Key” (note), “Velo” (velocity), “Gate”, “Step”, “Bar” and “Time”. “Velo” is the dynamics, given by the value of 1-127. “Gate” is the duration of the note in milliseconds. “Step” is the interval of time between notes, and it also exhibits tempo. “Bar” is the vertical line placed on the staff to divide the music into measures.

The pedal information is comprised of four parameters: “Key” (indicating the kind of pedal: “Damper” or “Shifting”), “Velo” (the pedaling quantity), “Time” (the duration for which the pedal is applied), and “Bar”.

3.3. Editing Support Process with Database

Our system can automatically apply a rough performance expression using Musical Rules Database and Score Database. (See Fig.4)

In addition, the system has Preference Database, which stores the editing characteristic of the user.



Fig.4. Automatic translation with database

3.3.1 Musical Rules Database

This database contains the architecture of musical grammar necessary to interpret symbols in musical notation. It is composed of five tables containing “Dynamics marks”, “Articulation marks”, “Symbol of Changing Dynamics or Changing Tempo” (symbol that affects the speed of a note or the increase or decrease of the volume), “Time signature”, and “Tempo marks”. Analyzing a music symbol according to its usage allows efficient information processing by the system.

3.3.2 Score Database

This database has symbols including time signatures, notes, rests and so on in standard musical notation. Symbols were pulled together in order of bars, and bar symbols were arranged in a time series. Performance expression in itself is only information such as pitch, strength, and length and concerns only the enumeration of a sound. Because the identification of each sound is difficult, editing of the performance expression is difficult. By adding the Score Database’s information to performance expression, we can connect each note to its enumeration. In doing so, it becomes easy to edit each phrase. This database consists of three tables, the “Element table” (showing the position of the note and the composition of the chord), the “Symbol table” (showing the position of the music symbol) and the “Same table” (showing the position of the repetition of the phrase). The Element table contains the field “Note Value”. Data in this field indicates the type of note, e.g., a quarter note, a triplet, and so on. “Note Value” is expressed by three hexadecimal numbers, which are

shown in Fig.5.

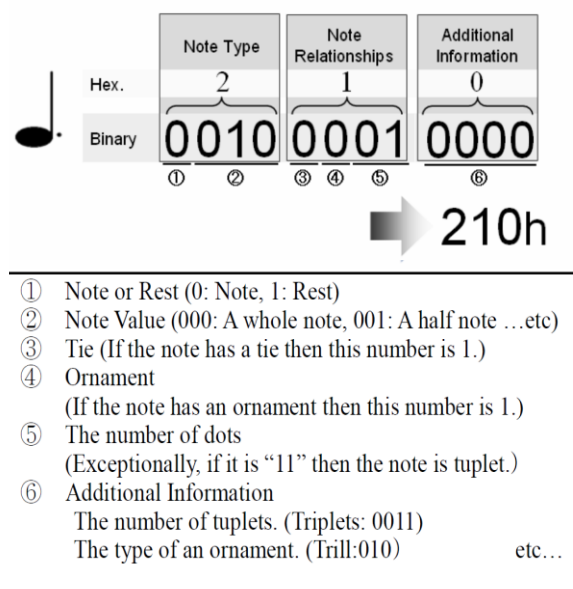


Fig.5. Note Value

3.4. Beat Database

We created Beat Database to edit music more efficiently. Beat Database is stored data which is Gerhard Oppitz's performance of beat expression. Using it, only step is inferred to change tempo.

4. Inferring Result

In Fig.6a is an input phrase used to search similar phrase for comparative experiments. Fig.6b is searched similar phrase. It is inferred two methods and results are outputted. First method, similar phrase is inferred, not to use Beat Database. The second method, Beat Database is used. The two results and data that performed by pianist in the similar phrase are compared to confirm improvement of the result.

The results of the experiment are shown Table1 and Fig.7. The results provide three values: the "Existing result" which don't use Beat Database, the "New result" which use Beat Database and the "Oppitz data" which is the actual emotional expression in a performance by a Oppitz in the similar phrase. "No." means note number. "No.1" means the first note in the phrases. We have consistently found that the emotional expression represented by the "New result" resembles

the "Oppitz Data" more than it resembles the "Existing result"

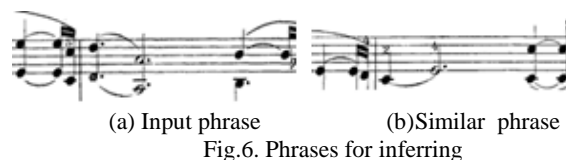


Fig.6. Phrases for inferring

Table 1. Results of inference

No.	StepRate		
	Existing result	New result	Oppitz data
1	1.0000	0.8962	0.7596
2	1.2115	1.2115	1.2981
3	1.1648	0.9184	0.8240
4	1.0440	0.9144	0.6992
5	1.1500	0.9712	0.6923

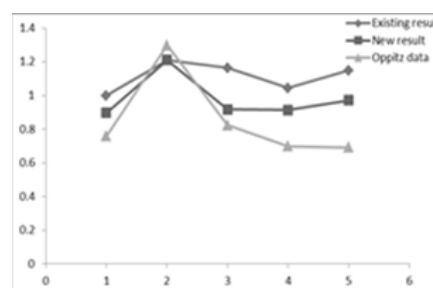


Fig.7. Results of inference

5. Conclusion

We developed an interactive musical editing system to edit music more efficiently. This system is composed of a "Searching system" and an "Inferring system". The Inferring system infers the emotional expression in a performance of similar phrases by referring to the databases automatically, greatly reducing the time needed for editing. Moreover, the interactive musical editing system provides edited phrases that resemble the "Pianist Data," which are the actual emotional expressions in a performance by a skilled human pianist.

References

1. E. Hayashi et al, *Behavior of piano-action in a grand piano.I*, Journal of acoustical Society of America, Vol.105, pp.3534-3544, 1999.

Geometric parameters measurement of wheel tread based on line structured light

Jiwu Wang

School of Mechanical, Electronic and Control Engineering, Beijing Jiaotong University, China

Zhijing Jian, Yaodong Li

School of Mechanical, Electronic and Control Engineering, Beijing Jiaotong University, China

Masanori Sugisaka

Alife Robotics Corporation Ltd, Japan and Open University, United Kingdom

*E-mail: jwwang@bjtu.edu.cn; ms@alife-robotics.co.jp
www.bjtu.edu.cn*

Abstract

The positioning precision is important in the processing of geometric parameters measurement technology of wheel tread. In this paper, a new method with no-contact measurement based on line structured light is given to solve this problem. Here traditional mechanical locating method is used as a rough reference. Moreover, some digital image processing techniques are developed for each of the key dimensions of measurement. According to the feature points (particularly, the key points that have not been worn) and lines extracted effectively on the wheel tread, precise positioning is realized. In this paper, the experiments show that the proposed method is feasible to implement non-contact measurement of the wheel tread, wheel flange thickness and rim width. It also ensures the accuracy of positioning and analyses the factors of measurement error.

Keywords: no-contact measurement, line structured light, wheelset tread, image segmentation

1. Introduction

With the rapid development of rail traffic, the issues of train safety are becoming increasingly prominent. A railway wheelset, which is indispensable and the most important component, bears all the static and dynamic load from the vehicle. Since it directly contacts with the rail, gradually and inescapably, the wheelset is worn down by the interactions between wheel and rail, which cause the undermining of critical dimensions. Moreover, the safety and operation quality are seriously affected. Hence, it is necessary to measure geometric parameters of train wheelset tread periodically^[1].

At present, the wheelset detection method can be roughly divided into the contact and non-contact measurement. The traditional methods still depend on the special mechanic tools like artificial calipers. Albeit its simple principle, there are the problem of high labor intensity, low efficiency and low accuracy^[2]. With the development of science and technology, non-contact measurement appears and is widely applied.

In this paper, the experimental model is established and the method with no-contact measurement is adopted which is based on line structure light. The problem, led by the precision of positioning between laser device and wheelset, is attempted to solve. The geometric

© The 2016 International Conference on Artificial Life and Robotics (ICAROB 2016), Jan. 29-31, Okinawa Convention Center, Okinawa, Japan

parameters, measured by using CCD to grab images and processing them with visual C++ and OpenCV, are flange height, flange width and wheel diameter.

2. Experimental principle

This part, the definition of wheelset's parameters and experimental principle are intuitively introduced.

2.1. Definition of wheelset's parameters

It is necessary to illuminate the definition of wheelset's parameters.

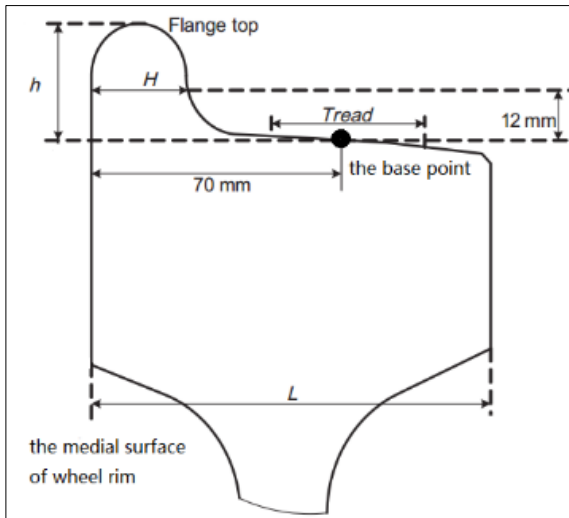


Fig. 1. the critical parameters

Fig. 1 shows the critical parameters of wheelset. the left is the medial surface of wheel rim (ostensibly, it is a line in the image). There is a point on the tread and the distance is 70mm to the medial surface of wheel rim, and it is customarily called the base point. Tread is the contacting area between wheelset and railway. Flange base line is the horizontal line 12mm above the base point. Flange thickness H is the horizontal thickness along flange base line. Flange height h is the height between flange base line and flange top. Rim width L is the distance between the medial surface and the lateral surface of wheelset^[3].

Fig. 2 shows the rolling circle passing the base point on the tread. Wheel diameter D is the average diameter of rolling circle. In this paper, the key parameters H , h and D , are mainly concerned.

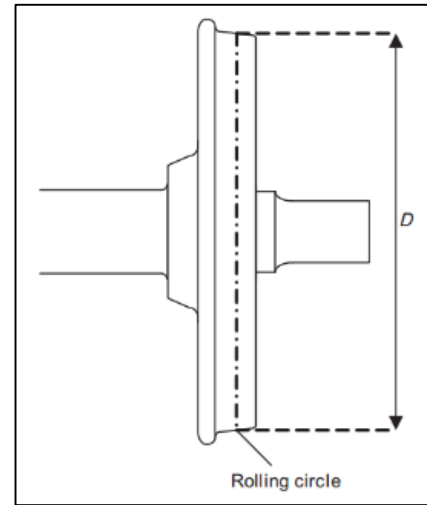


Fig. 2. one wheel of wheelset

2.2. Experimental system and principle

Fig. 3 shows the experimental device. The camera A and the camera C are used to positioning and the camera B is used to grab images of tread. Lasers and cameras are relatively fixed and calibrated.

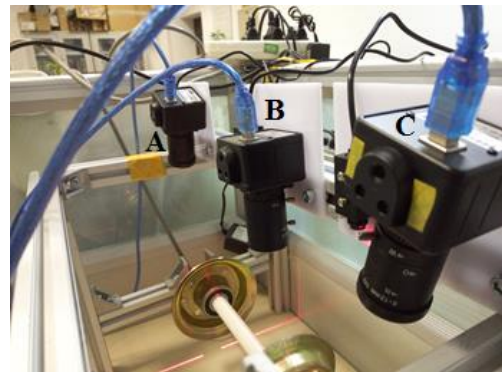


Fig. 3. The experimental device

The traditional method based on mechanism is regarded as slow and subjective to a great extent in the practical measurement. In order to ensure the light plane perpendicular to the tread, the more accurate method is proposed.

The geometric parameters of wheel tread are measured through laser scanning method in which linear light source is projected on the surface of work piece^[4]. Laser vertical incidence and vertical imaging is applied to the measuring system.

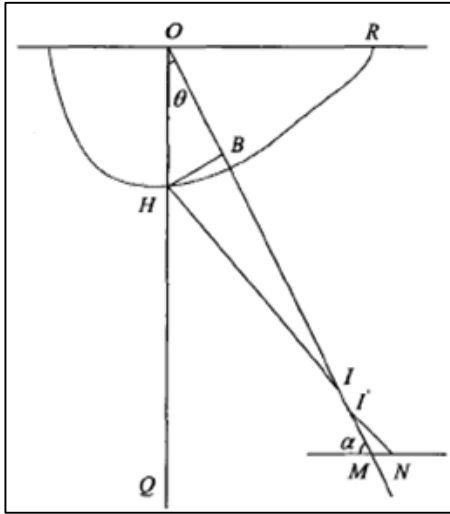


Fig.4. triangulation measurement

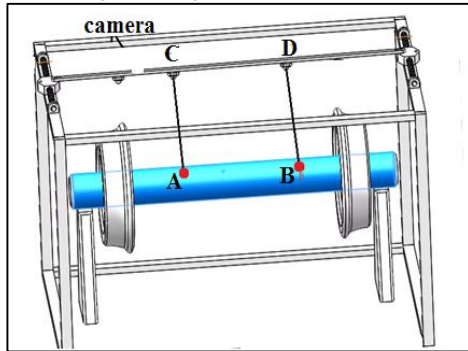


Fig.5. Diagram of positioning

According to Fig.4, θ is the angle between QO and PO, the height of point H on the work piece can be calculated as follows formula:

$$OH = \frac{(OI - f)\Delta \sin \alpha}{f \sin \theta + \Delta \sin \alpha \cos \theta}$$

In the above formula, f is the focal distance. The point on the surface of measured objects a three-dimensional coordinate reflected in the CCD's image plane, which presents as two-dimensional image, so the three-dimensional coordinates can be reconstructed by using the optical coordinate.

As Fig.5 shows, when the light is perpendicular to the axis, the distance between the highest point of axis and the optical center of camera can be obtained. If the distance AC is equal to BD, it can ensure two axes parallel. Besides, when AC or BD is minimum, the positioning is realized. Then we can use image processing to easily get the geometric parameters of wheelset. we assume that the distance between the optical

center of camera and the center of axis is h_1 , and to the base point is h_2 , so the wheel diameter D , as Fig.2 shows, can be got:

$$D = 2(h_1 - h_2)$$

The flange width H and flange height h can be obtained after image processing. The key to implement the measurement as follows:

- 1) the collocation of the cameras and the linear structured light source.
- 2) calibration method
- 3) the extraction accuracy of light stripe.

3. Image processing

As Fig.6 shows, there are lots of noises. In order to remove noises, image segmentation is adopted. The principle of image segmentation is to separate out regions of an image corresponding to objects which we want to analyze. In this paper, this separation is based on the variation of intensity between the object pixels and the background pixels. To differentiate the pixels, we are interested in from the rest (which will be eventually rejected), we perform a comparison of each pixel intensity value with respect to a threshold.

Filtering is perhaps the most fundamental operation of image processing and computer vision. In the broadest sense of the term "filtering", the value of the filtered image at a given location is a function of the values of the input image in a small neighborhood of the same location. In the practical processing, sometimes, the filters do not only dissolve the noise, but also smooth away the edges. To avoid this, at certain extent at least, the bilateral filter is recommended. In an analogous way as the Gaussian filter, the bilateral filter also considers the neighboring pixels with weights assigned to each of them. These weights have two components, the first of which is the same weighting used by the Gaussian filter. The second component takes into account the difference in intensity between the neighboring pixels and the evaluated one.

Finally, the processing result is showed in the Fig.7. As it shows, image segmentation works well and bilateral filter makes a great contribution. Then, according to the result, we can get what we want to.

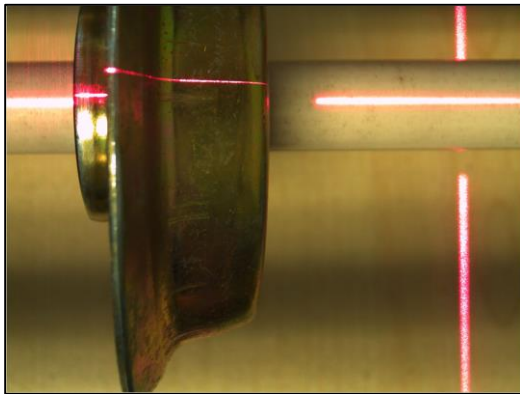


Fig.6. Wheel tread images: The initial image from camera.

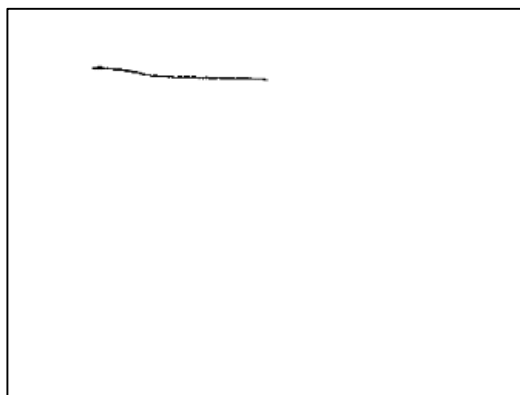


Fig.7. Wheel tread images after pre-processing

4. Error Analysis

In the process of measuring the wheel geometry parameters, the measurement precision is influenced by many factors. Usually, sensor position error, light angle error, the extraction accuracy of line structure light stripe, and so on.

All in all, errors include systematic errors and random errors. System error can be obtained by the structure parameters of the measurement accurate system calibration. Besides, it can be eliminated with the comparison between stand wheelset and measured result. Random error is mainly caused by laser sensor measurement error and the extracted line structured light stripe center, which can't be completely eliminated.

For the running heads for the authors names, please apply the following rules:

5. Conclusions

The method based on line structured light with no-contact measurement is proposed. Some digital image processing techniques, such as image segmentation and bilateral filter which not only dissolve the noise, but also reserve the edges, are used to position and measure. The error also is analyzed in order to get higher accuracy.

Eventually, the experiments show that the proposed method turn out to be feasible to implement non-contact measurement of the wheel tread, wheel flange thickness and rim width.

References

1. Xing Z, Chen Y, Wang X, et al. Online detection system for wheel-set size of rail vehicle based on 2D laser displacement sensors[J]. *Optik - International Journal for Light and Electron Optics*, 2016,127(4):1695-1702.
2. Zhang W, Zhang Y, Li J, et al. The defects recognition of wheel tread based on linear CCD[C]// *Nondestructive Evaluation/Testing (FENDT)*, 2014 IEEE Far East Forum on. IEEE, 2014:302-307.[Z].
3. YP Luom,LI Xue lei,F Wang,Y Yang. Measurement of wheel tread parameters with linear structured light[J].*JOURNAL OF RAILWAY SCIENCE AND ENGINEERING*,2005,2(3):75-77.DOI:10.3969/j.issn.1672-7029.2005.03.014. [Z].
4. Gomez E, Giménez J G, Alonso A. Method for the reduction of measurement errors associated to the wheel rotation in railway dynamometric wheelsets[J]. *MECH SYST SIGNAL PR*, 2011,25(8):3062-3077.

Study on the ORB algorithm in the application of Monocular SLAM

Jiwu Wang¹

*School of Mechanical, Electronic and Control Engineering, Beijing Jiaotong University
Beijing 100044, China¹*

Shunkai Zheng¹

*School of Mechanical, Electronic and Control Engineering, Beijing Jiaotong University
Beijing 100044, China¹*

Sugisaka Masanori²

*Alife Robotics Corporation Ltd, Japan and Open University, United Kingdom²
E-mail: jwwang@bjtu.edu.cn¹; ms@alife-robotics.co.jp²*

Abstract

In view of reducing the accumulative error, we perform loop closing based on PTAM in our Monocular SLAM. As this method relies on extracting natural environment features, we chose ORB algorithm as the feature extraction and matching. We demonstrate that ORB features have enough recognition power to enable place recognition from severe viewpoint change and they are so fast to extract and match (without needing multi-threading or GPU acceleration) that enable real time accurate tracking and mapping. Through outdoor scene experiment, we validate the algorithm performance.

Keywords: SLAM; ORB; Monocular Vision; Loop closing

1. Introduction

Monocular SLAM has been developed from the initial filtering approaches to the most modern key frame-based SLAM systems. The key frame-based SLAM system is more useful and accurate in the large environment. One of the most representative keyframe-based systems is Parallel Tracking and Mapping, PTAM¹. The map points of PTAM correspond to FAST corners matched by patch correlation. This makes the points only useful for tracking but not for place recognition. In fact PTAM does not detect large loops, and the relocalization is based on the correlation of low resolution thumbnails of the keyframes, yielding a low invariance to viewpoint.

Using just one camera is a more complex problem because the depth of observed features in the image is

unknown and multi view geometry is necessary to solve the problem. Stereo and RGB-D cameras have a range in which they can recover the depth but in certain situations such as sunny day in the outdoor they are not practical and monocular techniques are still necessary.

In this work we focus on ORB and loop closing, two open problems that are essential for real SLAM applications.

ORB features are oriented multi-scale FAST corners with a 256 bits descriptor associated². As binary features, they are extremely fast to compute and match, while they are highly invariant to viewpoint. This allows matching them from wide baselines, boosting the accuracy of BA.

Loop closing is the task of detecting when a robot is

Revisiting a previously mapped area, in order to correct the error accumulated in the robot trajectory during exploration³. So, how to determine whether a new frame in the image sequence has occurred? One is based on the robot's position, which is adjacent to the previous position; the two is the appearance of the image, which is similar to the previous key frame. In this paper, we choose the last one.

2. System Overview

The system is composed of three main tasks: tracking, local mapping and loop closing that run in parallel in a multi-core machine

Fig 1 shows a scheme of the different building blocks of the system

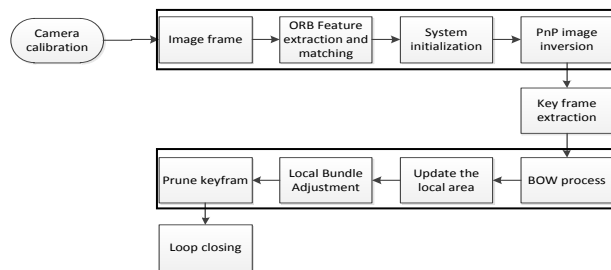


Fig.1. System Overview

2.1. Tracking

The map initialization is performed finding a planar scenes or an essential matrix from two near frames in an automatic process. Once an initial map exists, the tracking estimates the camera pose with every incoming frame. Next we describe each step of the tracking

2.1.1 ORB extraction and tracking

The first step is to extract ORB features in the frame. At first a scale image pyramid is computed and FAST key points are detected at each level, then only a subset of these key points will be described. If tracking was successful in the last frame, the tracking tries to get a first estimation of the camera pose from the last frame. Each ORB from the last frame, which has a map point associated, searches a match in the current frame in a small area around its previous position.

In the large scale environment, feature extraction and matching are influenced by Gaussian blur, rotation,

scaling, illumination and processing speed. Therefore design the following experiment to compare the ORB features extraction performance.

1. Generating and matching method of test data:

Taking image sequence Fig2 as original image that photoed in Beijing Jiaotong University mechanical building Z706



Fig2 Left: original frame Right: next frame of original frame

Then using the affine transformation of the specified argument and mathematical model including Gaussian blur, rotation, scaling, illumination for Right frame to generate the sequences, Analog cameras in the complex scene pictures taken in the process of moving, close to the performance of the real data

2. Correct judgment of matching points:

Use RANSAC find out the Homography Matrix between the generated sequences and original frame, then the sequences frame of the feature points projection to original frame, calculate the size of the projection error, if less than the threshold value of set (this experiment using threshold for 2), argues that the point is the right match, otherwise it is a false matching points. The relation between the calculated is:

$$ratioMatch = \frac{correctMatch}{Match} \times 100\% \quad (2-1)$$

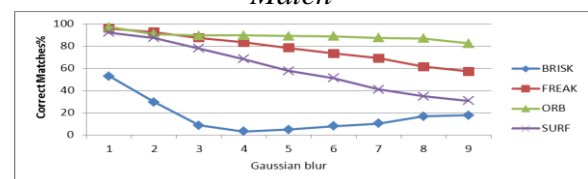


Fig3 Gaussian blur

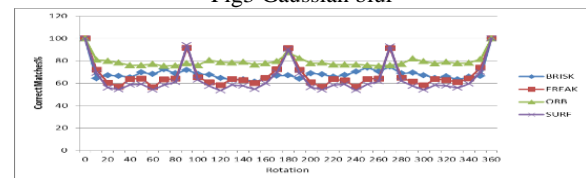


Fig4 Rotation Angle (0-360, per 20)

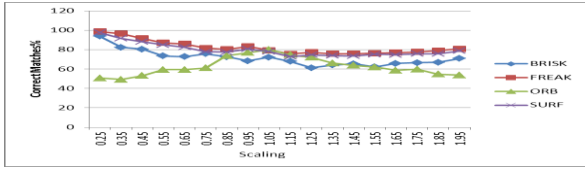


Fig5 Scaling (0.25-1.95 per 0.1)

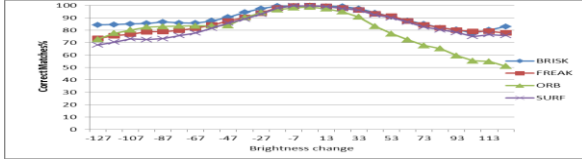


Fig6 Additional brightness values

Tab1 Processing time

Algorithm	Average time per Frame(MS)	Average time Per Key point(MS)
BRISK	58.3473	0.201757
FREAK	845.55	0.282354
ORB	132.27	0.267296
SURF	2244.56	0.61098

Fig 3 show that the feature matching performance of ORB under the condition of fuzzy is the best, it can greatly improve the stability of the algorithm; Fig4 show that ORB is the most stable for rotation .Fig 5and Fig6 show that the several feature extraction algorithms are similar to the change of the scale and brightness in a certain range.

Tab1 show that extracting all the feature points of the whole image, the speed of ORB is the fastest and 17 times faster than SURF, for every feature point of the image, ORB is 3 times faster than SURF which is the slowest.

The above results and analysis show that the excellent performance of the ORB feature extraction algorithm. We demonstrate that ORB features have enough recognition power to enable place recognition from severe viewpoint change and they are so fast to extract and match (without needing multi-threading or GPU acceleration) that enable real time accurate tracking and mapping.

2.2. Loop Closing

Fig7 is a loop closing detection of visual SLAM based on the bag-of-words .A node in the map corresponding to the position of the robot, represented by 1 - 7, each node with a key frame scene at the location of the image description. The main idea of the

bag-of-words model is to extract features from the image, the feature clustering (K-means) to the vocabulary tree, get the image of the visual word description vector, then calculate the similarity between the image and the matching strategy, complete closed-loop detection.

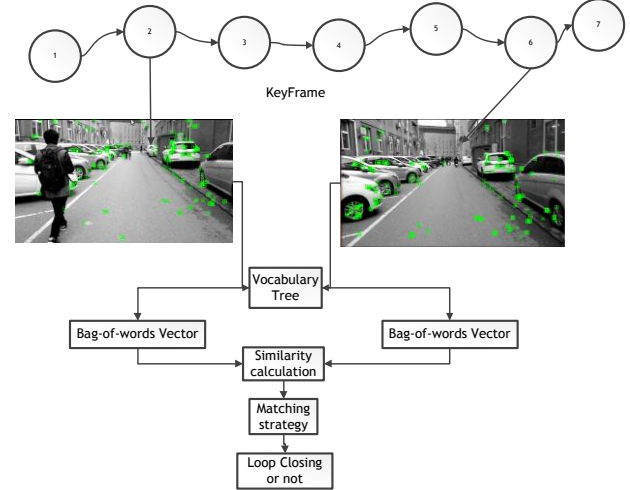


Fig7 loop closing detection based on bag-of-words model

TF-IDF (Frequency Inverse Document Frequency Term) model is used to evaluate the similarity of images. The similarity between two bag of words vectors v_1 and v_2 can be described as ⁴:

$$s(v_1, v_2) = 1 - \frac{1}{2} \left| \frac{v_1}{|v_1|} - \frac{v_2}{|v_2|} \right| \quad (2-1)$$

The loop closing thread takes K_t , the last key frame processed by the local mapping, and tries to detect and close loops. The steps are next described.

- At first we compute the similarity between the bag of words vector of K_t and all its neighbors $\{K_c\}$ in the covisibility graph and retain the lowest score S_{\min} ;
- In the DBoW2 database which save all the key frames to find the key frames whose score is not less than S_{\min} , the key frames is $\{K_s\}$, $\{K_s\}$ cannot include the $\{K_c\}$;
- By step 2 to find the key frame K_{t-1} associated with $\{K_{s-1}\}$, and the key frame K_{t-2} associated with $\{K_{s-2}\}$, if there is a key frame K_p in the

$\{K_s\}$ and similar to the key frame in the $\{K_{s-1}\}$ and $\{K_{s-2}\}$ in the covisibility graph, take K_p as a candidate key frame;

- If K_t and K_p is supported by enough inliers, the loop with K_t is accepted.

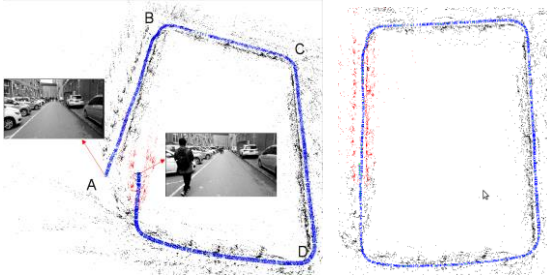


Fig8 Use loop closing to modify the map (Laboratory in Beijing Jiaotong University)

3. Experiment and Conclusion

3.1. Experiment on public data sets

The odometry benchmark from the KITTI dataset⁵ contains sequences from a car driven around a residential area with accurate ground truth from GPS and a Velodyne laser scanner. This is a very challenging dataset for monocular vision due to fast rotations, areas with lot of foliage, which make more difficult data association, and relatively high car speed, being the sequences recorded at 10 fps.

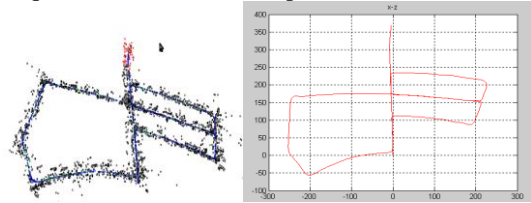


Fig9 Left: points and key frame trajectory Right: map after scale change

Tab2 Results of the KITTI dataset

Sequence	Dimension ($m \times m$)	KFs	RMSE (m)
KITTI 05	478x425	850	8.23

The result of Sequences 05 of the KITTI dataset is shown as Tab2: The RMSE of this experiment is 8.23m.

© The 2016 International Conference on Artificial Life and Robotics (ICAROB 2016), Jan. 29-31, Okinawa Convention Center, Okinawa, Japan

3.2. Experiment on our Machine building

Experiments on the image sequences generated by the road of Mechanical Laboratory of Beijing Jiaotong University, The actual map is as follows:



Fig10 the map of Mechanical Laboratory

The walking path is ABCDA, get the real map by scale transformation and the comparison between the two map:

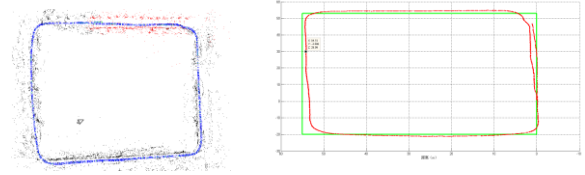


Fig11 Left: Generated map of points and key frame Right: the comparison between the two map

From the above results, the results are more accurate. In the process of the experiment, the characteristics of the corner are easy to be lost, and the error of the distance is inevitable estimated. In the future, we focus on solving the robustness of the map initialization and the processing that easy to lost at the corner.

References

1. G. Klein and D. Murray. Parallel tracking and mapping for small AR workspaces. In International Symposium on Mixed and Augmented Reality (ISMAR), 2007...
2. E. Rublee, V. Rabaud, K. Konolige, and G. Bradski. ORB: an efficient alternative to SIFT or SURF. In IEEE International Conference on Computer Vision (ICCV), 2011
3. B. Williams, M. Cummins, J. Neira, P. Newman, I. Reid, and J. D. Tard'os, "A comparison of loop closing techniques in monocular SLAM," Robotics and Autonomous Systems, vol. 57, no. 12, pp. 1188–1197, 2009.
4. R. Mur-Artal and J. D. Tard'os, "Fast relocalisation and loop closing in keyframe-based SLAM," in IEEE International Conference on Robotics and Automation (ICRA), Hong Kong, China, June 2014, pp. 846–853.
5. A. Geiger, P. Lenz, C. Stiller, and R. Urtasun, "Vision meets robotics: The KITTI dataset," The International Journal of Robotics Research, vol. 32, no. 11, pp. 1231–1237, 2013.

Affective Human Computer Interaction

Kaoru Sumi

*Future University Hakodate,
Hakodate, Hokkaido, Japan*

E-mail: kaoru.sumi@acm.org

Abstract

This paper introduces a study of spoken dialogue agent systems using emotional expressions as affective human computer interaction. The paper describes an experiment investigating the effect that the expression and words of the agent have on people, introduces a spoken agent for customer services using expressive facial expressions and a spoken agent for mental care using expressive facial expressions and positive psychology as application systems for affective human computer interaction, and presents a discussion and a conclusion.

Keywords: Affective computing, facial expression, human computer interaction

1. Introduction

According to Media Equation [1], people treat computers, television, and new media as real people and places, thereby making the users uncomfortable if an agent behaves in a disagreeable manner. In the field of persuasion technology research [2] it is said that if a user recognizes the presence of something in a computer, he or she will respond to it according to the normal social rules. However, there are still many things that we do not know about how an agent's response affects a user during their interaction.

In the development of intelligent systems, it is important to consider how best a feeling of affinity with the system and show the presence of the system that has human-like intelligent functions such as recommendation or persuasion. Therefore, evaluating the interpersonal impressions conveyed by agents is very important.

Our research group has developed intelligent dialogue system that proactively interacts with a user according to the user's circumstances. As a first step, we examined how to react with the user under several emotional situations through the experiment.

We performed an experiment to evaluate how the facial expressions of an agent and the words used by the agent affected users during agent-user interaction.

In the past, ELIZA [3] was developed to imitate a Rogerian psychotherapist, and was an early example of primitive natural language processing. SimCoach [4] is a spoken dialogue agent system used in the mental care of returned soldiers. It displays a speaking counselor agent and analyses the psychology of the user using a question and answer technique.

The paper describes an experiment investigating the effect that the expression and words of the agent have on people, introduces a spoken agent for customer services using expressive facial expressions and a

spoken agent for mental care using expressive facial expressions and positive psychology[5][6] as application systems for affective human computer interactions, presents a discussion and a conclusion.

2. Experiment investigating impressions and behavior change caused by replies from the agent

We conducted an experiment to examine how the impression that the user gets from the agent's answer is affected by the combination of facial and word expressions. It was intended to clarify the impression that the agent gave the user by answering when interacting with the user in an emotion-arousing scenario.

We chose six kinds of feelings. From the total of 216 combinations, covering multiple feelings that the user felt (6 patterns) and the facial expressions for the agent's interaction with the user (6 patterns) and word expressions used by the agent (6 patterns), we selected 96 patterns in this experiment. These covered 16 patterns in each feeling: empathetic words and consistent facial expressions, nonempathetic words and consistent facial expressions, word consistent and facial inconsistent, and word inconsistent and facial consistent. This is because the conditions of nonempathetic and both inconsistent word and facial expressions are nonsensical in normal communication. This is the condition where the word and facial expressions are inconsistent, which is the condition for double bind communication, but it can be considered as either word or facial being empathetic to the user. The case of nonempathetic condition and inconsistent word and facial expressions can be considered as pathological.

A total of 1236 people, 568 male and 668 female (AV. 38.0, SD 11.5), were assigned 96 contents. More than ten users were assigned to each content [7].

As a result, people are easy to be persuaded when the agent was favorable impression. This result is very natural; however, the combination of favorable was different from our prediction. First, we predicted that words and facial expressions reflected on the emotions aroused by the scenario would lead to the most favorable impression, so we set these data as the control group. In fact, there were more favorable impressions than those obtained for the control group.

For example, the words and facial expressions were "joy" when the user's emotion was "joy" for the control group. It is very interesting that when the user's emotion was "joy", the agent's words for "joy" with facial expressions of "surprise", "sadness", or "fright" were most favorable. On the other hand, when the user's emotion was "fright", the agent's words for "fright" with facial expressions of "disgust" or "sadness" were the most favorable.

These facial expressions were recognized as the emotion conveyed by the words and were more empathetic and somewhat meaningful emotions. For example, when the user's emotion was "joy", the agent's words of "joy" with facial expressions of "surprise" or "fright" might have been recognized as the agent being exaggeratedly surprised at the "joy" scenario. When the user's emotion was "joy", the agent's words of "joy" with facial expressions of "sadness" might have been recognized as the agent being highly pleased from the heart at the "joy" scenario. When the user's emotion was "fright", the agent's words of "fright" with facial expressions of "sadness" might have been recognized as the agent grieving deeply at the user's "fright" scenario. When the user's emotion was "fright", the agent's words of "fright" with facial expressions of "disgust" might have been recognized as the agent feeling deep hate at the user's "fright" scenario.

Through these observations, we concluded that there is a rule for facial expressions: in a certain scenario, synchronizing foreseen emotion of the user caused by the situation will make a favorable impression. For example, when the user has the emotion of "joy", he/she wants someone to be surprised or highly pleased. Then, showing surprised or highly pleased face expression make the user feels favorable impression. When the user has the emotion of "fright", he/she wants someone to grieve deeply or disgust. Then, showing grieved or disgust face expression make the user feels favorable impression.

Users want the agent to ooze synchronized their foreseen emotion by hearing the news instead of simply showing synchronized reaction according to emotion at present time.

3. A Spoken Agent System for Learning Customer Services

As an application system for affective human computer interaction, this first spoken agent system consists of a 3D spoken agent display system, a speech recognition system, a speech synthesis system, a dialogue control system and a facial expression recognition system. This system is for providing educational training in hospitality through dialogue with a spoken agent. This system focuses on the Japanese style of service-mindedness, which is typified by paying attention to individual customers [8][9].

The 3D spoken agent display system displays a 3D spoken agent, which can show the facial expressions of “smile”, “laugh”, “anger”, “sadness”, “disgust”, “fright”, and “surprise”. The system superimposes the mouth shapes of the vowels onto each facial expression, lip-synching with the sounds. Fluid movement of the facial expressions and lip-synching is made possible using Microsoft XNA morphing technology. Our system uses Google speech API as the speech recognition system, and AITalk as the Japanese speech synthesis system. As a dialogue control system, we revised Artificial Intelligence Markup Language (AIML [10]) which is based on Extensible Markup Language (XML) to use the Japanese language. Using templates, we can express a dialogue freely.

```
<pattern>* tell me your name *</pattern>
```

```
<template>My name is Ayaka</template>
```

For example, if there is a question “Tell me your name?” from a user, then the system answers, “My name is Ayaka,” in this case. The important pattern here is “*tell me your name*”, so the system can answer the sentence “Please tell me your name” or “Could you tell me your name?” because these sentences include the phrase “tell me your name.” When we analyze Japanese language, we have to add spaces between words because there are no spaces in Japanese sentences. We use MeCab, which is a fast and customizable Japanese morphological analyzer, to add spaces between words. As the facial expression recognition system, this system uses the facial recognition application of brain wave measuring equipment called “Emotive EPOC”. It recognizes the intensity of facial expressions digitally.

Using our system, a user can talk to the spoken agent, and the spoken agent teaches the user how to interact with customers. The spoken agent is displayed on the screen and sometimes the system displays lines in a scene which the user should practice, along with an appropriate facial expression. The system judges whether the user has spoken the lines appropriately by comparing them with the speech recognition system using AIML templates. The system judges whether the user’s facial expression is appropriate or not by comparing it with the facial expression recognition system.

4. A Spoken Agent System for Mental Care using Expressive Facial Expressions and Positive Psychology

We developed a spoken agent system for mental care of hikikomori (a Japanese term to refer to the phenomenon of reclusive adolescents or young adults who withdraw from social life) persons improving previous system (Figure 1). An increasing number of people are in need of mental care, because associated social issues include problems of bullying in schools, mental disability and hikikomori or social withdrawal of young people, suicide of young people, people being pressured to quit work in middle age, and PTSD (posttraumatic stress disorder) of the victim. According to the result of the experiment of first spoken agent system, it was revealed we must improve interface of the system, especially for

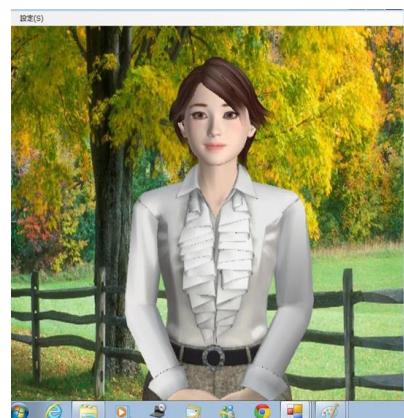


Figure 1. A spoken agent system for mental care

the attachment of Emotiv. We improved a spoken agent system. The system consists of a 3D spoken agent display system, a dialogue control system, Japanese word spacing system, a speech recognition system, a speech synthesis system, and a facial/gesture expression recognition system. The improved points are as follows.

1) KINECT sensor recognizes a user's facial expressions and gestures, 2) An agent displays gestures, 3) The facial expression/gestures can be controlled in intensity digitally, 4) An agent can be controlled its size, direction and position, 5) A background of the system is changeable, and 6) An agent blinks its eyes.

Interactive talks using gestures are enabled by recognizing a user's motion from the skeleton using a KINECT sensor. In addition, a simple facial expression is enabled by recognition of a user's face using KINECT sensor without an Emotiv. The system can be switched between a KINECT and/or an Emotiv. An agent displays gestures of "nodding", "nodding no", "waving her hand", "bowing her head" and "bowing her head deeply". An agent can be controlled its size (full body/ upper body/ face or parentage of full body), direction and position. The background of the system can be changed using the dialogue editor. The agent blinks its eyes for making the agent more human. Because, according to the experiment, there are many comments that the agent should blink its eyes.

In addition, this system offers the function of answering positively when a user speaks negatively, for creating a positive mood. This system answers with positive words to a user's negative words using Negapo Dictionary [11], which is a dictionary for translate negative words to positive words. Such counseling is provided in a field of positive psychology. For example, such as follows is talked.

The agent: How was your day? The user: I went to my university.

The agent: What kind of thing happened?

The user: I get frustrated because only a friend might be good.

The agent: I felt sorry for you. (Facial expression is "Sad") I think you should be able to make the feeling of frustrated with a motivation. (Positive words from Negapo Dic.)

5. Discussion

Even if a partner is not a human being, we are persuaded by an agent with superficial information such as facial expressions or words. Media Equation [1] and Persuasive Technology [2] researches reveal the same.

From the result of the first experiment in section 2, facial expressions and words are very important because people are easy to be persuaded when the agent was favorable impression. It is thought that an agent can make in-depth contact with the user by foreseeing the user's emotion and empathizing with the user.

Using the results, we have developed spoken agent systems for learning customer services and mental care using expressive facial expressions. These are working well as the system for an agent as an instructor or a guidance counselor using affective human interfaces.

According to the interviews, users felt the brain wave measuring equipment and the speech recognition and synthesis system were novelties, and the system's specialty was that its use was facilitated through dialogues and it was highly motivating. The brain wave measuring equipment and the speech recognition and synthesis system used in our system were highly motivating; however the subjects were divided over their use, and some felt them to be awkward to use. Some of them made comments on the speech recognition system such as "It was difficult to recognize words", "It was difficult", etc. Consideration should be given to improving the system's ease of use by developing or using a speech recognition system of greater accuracy. Also, regarding the brain wave measuring equipment, some made comments on it such as "It was hard to wear" and "It was painful", so it could be considered that it was not easy to accept. Consideration should be given to improving the human interface, including using image processing and the headset concurrently.

According to the interviews we must improve the interface of the system, especially for the attachment of the brain wave measuring equipment. Then we developed next version of the system for mental care of hikikomori social withdrawal persons or using KINECT,

which recognizes the facial expression/gestures of the user.

I think this system is helpful for mental care of hikikomori social withdrawal persons if it can be used easily in house. Because even hikikomori or social withdrawal persons are at home and stay in front of a computer most of the time. I think that supporting these people by a personal computer is a key to solution.

Study of a spoken dialogue agent system needs to be investigated further including emotions, technology and design domains. Our research group is going to advance our own studies of a spoken agent system using superficial information in the future.

6. Conclusion

This paper introduces an experiment and the spoken agent system developed according to the results. We evaluated the first version of the system and revised. Even if a partner is not a human being, we are perceived by an agent with superficial information such as facial expressions or words.

7. Acknowledgements

This work was supported in part by JSPS KAKENHI Grant-in-Aid for Scientific Research on Innovative Areas Numbers 22118503.

References

1. Reeves, Byron and Clifford Nass The Media Equation: How People Treat Computers, Television, and New Media Like Real People and Places, Cambridge University Press, 1996.
2. B.J.Fogg: Persuasive Technology –Using Computers to Change What We Think and Do-, Elsevier, 2003.
3. Weizenbaum, Joseph: "ELIZA—A Computer Program For the Study of Natural Language Communication Between Man And Machine", Communications of the ACM 9 (1): 36–45, (January 1966).
4. A. Rizzo, K. Sagae, E. Forbell, J. Kim, B. Lange, J. G. Buckwalter, J. Williams, T. D. Parsons, P. Kenny, David Traum, J. Difede, B. O. Rothbaum: SimCoach: an intelligent virtual human system for providing healthcare information and support, The Interservice/Industry Training, Simulation & Education Conference (IITSEC), 2011.
5. Christopher Peterson : A Primer in Positive Psychology , Oxford University Press;
6. Martin E. P. Seligman: Using the New Positive Psychology to Realize Your Potential for Lasting Fulfillment, Atria Books (2004)
7. Kaoru Sumi and Mizue Nagata: Evaluating a Virtual Agent as Persuasive Technology, Psychology of Persuasion, Janos Csapó and Andor Magyar eds., Nova Science Publishers.2010.
8. Kaoru Sumi, Ryuji Ebata: A Character Agent System for Promoting Service-Minded Communication, Intelligent Virtual Agents, Lecture Notes in Computer Science, LNAI8108, pp.438, Springer (2013.8).
9. Kaoru Sumi, Ryuji Ebata: Human Agent Interaction for Learning Service-Minded Communication, iHAI2013, 1st international conference on Human-Agent Interaction, (2013.8).
10. AIML: <http://www.alicebot.org/documentation/>
11. Negapo Dictionary, Syufuno-Tomo-Sya (2012). In Japanese.

A Study on Differential Evolution Using BetaCOBL, B³R, and TPBO

Prof. Ju-Jang Lee, Dept. of Electrical Engineering
Korea Advanced Institute of Science and Technology

Contents

- › Introduction
- › Background
- › Proposed beta utilization
- › Application
- › Conclusion

Introduction

- › Evolutionary algorithm
 - › Mimic biological evolution in nature
 - › Not require any prior knowledge about the problem
 - › Start with a randomly distributed population and updates the population by reproducing offspring with unique operators
 - › Genetic algorithm (GA), evolutionary strategy (ES), evolutionary programming (EP), estimation of distribution algorithm (EDA), differential evolution (DE)

Introduction

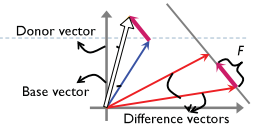
- › Opposition-based learning (OBL)
 - › Estimates and counter estimates are considered simultaneously to accelerate the search or learning process
 - › The probability that the opposite point is closer to the solution is higher than probability of a second random guess
- › A randomness is added to the algorithm
 - › Accelerate the search process
 - › Make the algorithm robust
 - › Escape the local optima
 - › Gaussian, Cauchy, and uniform distributions are most widely used

Introduction

- › A beta distribution
 - › Advantages
 - › Has a bounded input domain
 - › Has various shapes depending on the parameter values
- › Beta distribution + OBL
 - › Control degree of opposition with various shapes
- › Beta distribution + Reproduction
 - › Offspring reproduction on a bounded search space

Background

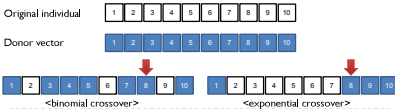
- › DE
 - › Parent selection
 - › Base vector
 - › Difference vector
 - › Mutation
 - › Donor vector: perturb a base vector using a difference between difference vectors



- Rand/1 $v_{ij}(t) = x_{r1j}(t) + F(x_{r2j}(t) - x_{r3j}(t))$
- Rand/2 $v_{ij}(t) = x_{r1j}(t) + F(x_{r2j}(t) - x_{r3j}(t)) + F(x_{r4j}(t) - x_{r5j}(t))$
- Best/1 $v_{ij}(t) = x_{bestj}(t) + F(x_{r1j}(t) - x_{r2j}(t))$
- Best/2 $v_{ij}(t) = x_{bestj}(t) + F(x_{r1j}(t) - x_{r2j}(t)) + F(x_{r3j}(t) - x_{r4j}(t))$
- Current-to-best/1 $v_{ij}(t) = x_{r1j}(t) + K(x_{bestj}(t) - x_{r1j}(t)) + F(x_{r2j}(t) - x_{r3j}(t))$
- Current-to-rand/1 $v_{ij}(t) = x_{r1j}(t) + K(x_{r1j}(t) - x_{r2j}(t)) + F(x_{r3j}(t) - x_{r4j}(t))$

Background

- › DE-cont'd
 - › Crossover
 - › Trial vector: mix an original with its donor vector
 - Binomial $u_{ij}(t) = \begin{cases} v_{ij}(t), & \text{if } \text{rand}(0,1) \leq CR \text{ or } j = j_{\text{rand}} \\ x_{ij}(t), & \text{otherwise.} \end{cases}$
 - Exponential $u_{ij}(t) = \begin{cases} v_{ij}(t), & \text{if } j = [n]_D, (n+1)_D, \dots, (n+L-1)_D \\ x_{ij}(t), & \text{otherwise.} \end{cases}$



Background

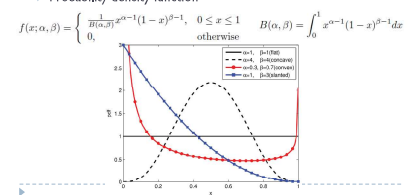
- › DE-cont'd
 - › Entire procedure

Algorithm 2 DE

 - 1: Initialize population
 - 2: while (Termination condition meets) do
 - 3: for all individuals in population do
 - 4: Select parents
 - 5: Generate a donor vector
 - 6: Mix the donor with the original individual to get a trial vector
 - 7: Evaluate the trial vector
 - 8: If The trial is better then
 - 9: Replace the original with the trial
 - 10: end if
 - 11: end for
 - 12: end while

Background

- › Beta distribution
 - › Parameterized by two parameters α, β
 - › Probability density function



Background

► Beta distribution-cont'd

► Mean

$$\text{mean} = \frac{\alpha}{\alpha + \beta}$$

► Mode

$$\text{mode} = \frac{\alpha - 1}{\alpha + \beta - 2}$$

► Variance

$$\text{variance} = \frac{\alpha\beta}{(\alpha + \beta)^2(\alpha + \beta + 1)}$$

Background

► OBL

► Opposite number

$$\tilde{x} = a + b - x$$

► Opposite point

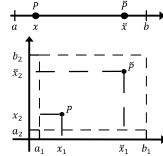
$$P(x_1, x_2, \dots, x_D)$$

$$\tilde{P}(\tilde{x}_1, \tilde{x}_2, \dots, \tilde{x}_D)$$

$$\tilde{x}_j = a_j + b_j - x_j$$

► OBL

The learning continues with x if $g(f(x)) \geq g(f(\tilde{x}))$; otherwise, it continues with \tilde{x} .



Proposed beta distribution utilization

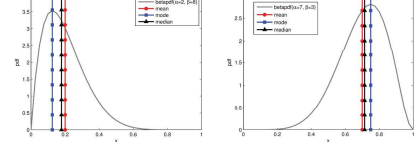
► Beta distribution using peak and spread

► Difference between mean, mode, and median

Mean: the sum of all values divided by the number of values (cardinality)

Mode: the most frequent value

Median: the middle value which separates the upper half and the lower half



Proposed beta distribution utilization

► Beta distribution using peak and spread-cont'd

► Parameter calculation from peak and spread

► New parameters: peak and spread

$$\alpha = \text{spread} \cdot \text{peak} \quad \text{when } \text{mode} < 0.5$$

$$\beta = \text{spread} \quad \text{when } \text{mode} \geq 0.5$$

given mode and spread

$$\text{peak} = \frac{(\text{spread} - 2)\text{mode} + 1}{\text{spread}(1 - \text{mode})} \quad \text{peak} = \frac{2 - \text{spread}}{\text{spread} - 1} + \frac{\text{spread} - 1}{\text{spread} \cdot \text{mode}}$$

Proposed beta distribution utilization

Theorem 1. If $\text{spread} < 1$, then $\alpha < 1$ and $\beta < 1$

If $\text{spread} > 1$, then $\alpha > 1$ and $\beta > 1$

When $\text{mode} < 0.5$, the value of peak for given spread can be rearranged as follows:

$$\text{peak} = \frac{1 - 2\text{mode}}{(1 - \text{mode})\text{spread}} + \frac{\text{mode}}{1 - \text{mode}} \quad (4.4)$$

Because $\text{mode} < 0.5$, the value of peak depending on spread is monotonically decreasing when $\text{spread} \in [0, \infty)$, so $\text{peak} > 0$ when $\text{spread} \in [0, \infty)$.

If peak is subtracted from $1/\text{spread}$, the result can be expressed as follows:

$$\frac{1}{\text{spread}} - \text{peak} = \frac{\text{mode}(\text{spread} - 1)}{(\text{mode} - 1)\text{spread}} \quad (4.5)$$

In Eqs. (4.4) and (4.5), $\text{mode}/(\text{mode} - 1)$ is always negative, whereas $(\text{spread} - 1)/\text{spread}$ is negative when $\text{spread} \in [0, 1]$ and positive when $\text{spread} \in [1, \infty)$. Hence, peak is always smaller than $1/\text{spread}$ when $\text{spread} \in [0, 1]$ and greater than $1/\text{spread}$ when $\text{spread} \in [1, \infty)$. Therefore, the parameter $\alpha (= \text{spread} \cdot \text{peak})$ is always smaller than 1 when $\text{spread} \in [0, 1]$ and greater than 1 when $\text{spread} \in [1, \infty)$. Furthermore, the parameter $\beta (= \text{spread})$ follows the same pattern.

Proposed beta distribution utilization

Similarly, when $\text{mode} \geq 0.5$, the value of peak for given spread can be rearranged as follows:

$$\text{peak} = \frac{1 - \text{mode}}{\text{mode} \cdot \text{spread}} + \frac{2\text{mode} - 1}{\text{mode} \cdot \text{spread}} \quad (4.6)$$

Because $\text{mode} \geq 0.5$, the value of peak depending on spread is monotonically decreasing when $\text{spread} \in [0, \infty)$, so $\text{peak} > 0$ when $\text{spread} \in [0, \infty)$.

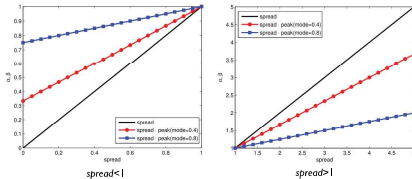
If peak is subtracted from $1/\text{spread}$, the result can be expressed as follows:

$$\frac{1}{\text{spread}} - \text{peak} = \frac{(\text{mode} - 1)(\text{spread} - 1)}{\text{mode} \cdot \text{spread}} \quad (4.7)$$

In Eqs. (4.6) and (4.7), $(\text{mode} - 1)/\text{mode}$ is always negative, whereas $(\text{spread} - 1)/\text{spread}$ is negative when $\text{spread} \in [0, 1]$ and positive when $\text{spread} \in [1, \infty)$. Hence, peak is always smaller than $1/\text{spread}$ when $\text{spread} \in [0, 1]$ and greater than $1/\text{spread}$ when $\text{spread} \in [1, \infty)$. Therefore, the parameter $\beta (= \text{spread} \cdot \text{peak})$ is always smaller than 1 when $\text{spread} \in [0, 1]$ and greater than 1 when $\text{spread} \in [1, \infty)$. Furthermore, the parameter $\alpha (= \text{spread})$ follows the same pattern.

Proposed beta distribution utilization

► Beta distribution using peak and spread

► α and β calculated

Proposed beta distribution utilization

► Existing OBLs

► Stochastic calculation using a uniform distribution

All of the dimensions are changed to the opposite values together

The best individuals among the original individuals and their opposites are passed on to the next generation

► BetaCOBL: OBL using a beta distribution with changes in partial dimensions and selection scheme

► Stochastic calculation using a beta distribution

A subset of dimensions are changed to the opposite values together

► Selection scheme switching

Proposed beta distribution utilization

► BetaCOBL-cont'd

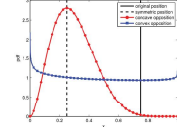
► Definition of opposition degree

► Strong degree: concave opposition

Using a beta distribution with concave shape

► Weak degree: convex opposition

Using a beta distribution with convex shape

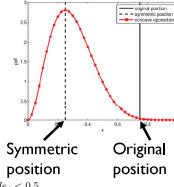


Proposed beta distribution utilization

► BetaCOBL-cont'd

► Concave opposition

$$\begin{aligned} \tilde{x}_{i,j}(t) &= a_j + (b_j - a_j) \cdot \text{Beta}(\alpha_j, \beta_j) \\ \alpha_j &= \begin{cases} \text{spread}_j \cdot \text{peak}_j, & \text{if } \text{mode}_j < 0.5 \\ \text{spread}_j, & \text{otherwise} \end{cases} \\ \beta_j &= \begin{cases} \text{spread}_j, & \text{if } \text{mode}_j < 0.5 \\ \text{spread}_j \cdot \text{peak}_j, & \text{otherwise} \end{cases} \\ \text{mode}_j &= \frac{(a_j + b_j - x_{i,j}(t)) - a_j}{b_j - a_j} \\ \text{spread}_j &= \left(\frac{1}{\sqrt{\text{normDiv}}} \right)^{\max(N(1,0.5),0)} \\ \text{peak}_j &= \begin{cases} \frac{(\text{spread}_j - 2)\text{mode}_j + 1}{\text{spread}_j(1 - \text{mode}_j)}, & \text{if } \text{mode}_j < 0.5 \\ \frac{2 - \text{spread}_j}{\text{spread}_j} + \frac{\text{spread}_j - 1}{\text{spread}_j \cdot \text{mode}_j}, & \text{otherwise} \end{cases} \end{aligned}$$

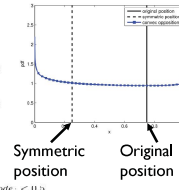


Proposed beta distribution utilization

► BetaCOBL-cont'd

► Concave opposition

$$\begin{aligned} \tilde{x}_{i,j}(t) &= a_j + (b_j - a_j) \cdot \text{Beta}(\alpha_j, \beta_j) \\ \alpha_j &= \begin{cases} \text{spread}_j \cdot \text{peak}_j, & \text{if } \text{mode}_j < 0.5 \\ \text{spread}_j, & \text{otherwise} \end{cases} \\ \beta_j &= \begin{cases} \text{spread}_j, & \text{if } \text{mode}_j < 0.5 \\ \text{spread}_j \cdot \text{peak}_j, & \text{otherwise} \end{cases} \\ \text{mode}_j &= \frac{x_{i,j}(t) - a_j}{b_j - a_j} \\ \text{spread}_j &= 0.1\sqrt{\text{normDiv}} + 0.9 \\ \text{peak}_j &= \begin{cases} \frac{(\text{spread}_j - 2)\text{mode}_j + 1}{\text{spread}_j(1 - \text{mode}_j)}, & \text{if } \text{mode}_j < 0.5 \\ \frac{2 - \text{spread}_j}{\text{spread}_j} + \frac{\text{spread}_j - 1}{\text{spread}_j \cdot \text{mode}_j}, & \text{otherwise} \end{cases} \end{aligned}$$



Proposed beta distribution utilization

► BetaCOBL-cont'd

► Normalized diversity

$$\begin{aligned} \text{normDiv} &= \frac{1}{NP} \sum_{i=1}^{NP} CD(x_i, POP) \\ CD(x_i, POP) &= \min_{c \in POP, x_i \neq c} d(c, x_i) \\ d(c, x_i) &= \sqrt{\frac{1}{D} \sum_{j=1}^D \left(\frac{x_{i,j} - c_j}{b_j - a_j} \right)^2} \end{aligned}$$

Proposed beta distribution utilization

► BetaCOBL-cont'd

► Partial dimensional change

► Opposite point calculation as DE mutation

$$\tilde{x}_{i,j}(t) = a_j + b_j - x_{i,j}(t) = a_j + F(b_j - x_{i,j}(t)) \quad F = 1$$

► Mix original individual and opposite point using crossover

- Effect of crossover rate
- Low crossover rate is beneficial for separable functions
- High crossover rate is beneficial for non-separable functions

► Generate two opposite point calculations with both low and high crossover rates

► Selection switching

- If diversity is high (μ^+ A) selection in ES
- The best individuals from the original population and its opposite are picked up
- If diversity is low (μ^+ A) selection in ES
- The worst half of the original individuals are replaced by their opposites one-to-one

Proposed beta distribution utilization

► BetaCOBL-cont'd

► Entire procedure

```

Algorithm 3 BetaCOBL
1: Calculate Diversity
2: If Diversity is high then
3:   for all individuals in population do
4:     Calculate a full dimensional convex or concave opposite point
5:     Mix the full dimensional opposite with the original individual to get partial dimensional opposite point candidates
6:     Evaluate the opposite point candidates
7:   end for
8:   Choose the best individuals from the original and opposite populations
9: else
10:  Sort individuals according to fitness value
11:  for the worst half individuals in population do
12:    Calculate a full dimensional convex or concave opposite point
13:    Mix the full dimensional opposite with the original individual to get partial dimensional opposite point candidates
14:    Evaluate the opposite point candidates
15:    Replace the original with the better candidate
16:  end for
17: end if

```

Proposed beta distribution utilization

► BetaCODE: DE embedding BetaCOBL

► Entire procedure

```

Algorithm 4 BetaCODE
1: Initialize population
2: BetaCOBL
3: while (Termination condition meets) do
4:   if rand(0,1) < JF then
5:     BetaCOBL
6:   else
7:     for all individuals in population do
8:       Select parents
9:       Generate a donor vector
10:      Mix the donor with the original individual to get a trial vector
11:      Evaluate the trial vector
12:      If The trial is better then
13:        Replace the original with the trial
14:      end if
15:    end for
16:  end while
17: end while

```

Proposed beta distribution utilization

► Existing bare bones reproductions

- Using Gaussian, Cauchy, and polynomial distributions
- Using a beta distribution with mean and standard deviation

► B³R: beta distribution-based bare bones reproduction

- Using a beta distribution
- suffer from out-of-range phenomenon
- Using a beta distribution with mode and spread

Proposed beta distribution utilization

► B³R

► Candidate generation using a beta distribution with mode and spread

$$\begin{aligned} v_{i,j}(t) &= a_j + (b_j - a_j) \cdot \text{Beta}(\alpha_j, \beta_j) \\ (\alpha_j, \beta_j) &= \begin{cases} (\text{spread}_j \cdot \text{peak}_j, \text{spread}_j), & \text{if } \text{mode}_j < 0.5 \\ (\text{spread}_j, \text{spread}_j \cdot \text{peak}_j), & \text{if } \text{mode}_j \geq 0.5 \end{cases} \\ \text{peak}_j &= \begin{cases} \frac{(\text{spread}_j - 2)\text{mode}_j + 1}{\text{spread}_j(1 - \text{mode}_j)}, & \text{if } 0 \leq \text{mode}_j < 0.5 \\ \frac{2 - \text{spread}_j}{\text{spread}_j} + \frac{\text{spread}_j - 1}{\text{spread}_j \cdot \text{mode}_j}, & \text{if } 0.5 \leq \text{mode}_j \leq 1 \end{cases} \end{aligned}$$

$$\begin{aligned} \text{mode}_j &= \frac{x_{r1,j}(t) - a_j}{b_j - a_j} \quad \text{dist}_j = \frac{|x_{r2,j}(t) - x_{r3,j}(t)|}{b_j - a_j} \\ \text{spread}_j &= \left(\frac{1}{\text{dist}_j} \right)^{\max(2+N(0,0.5),0)} \end{aligned}$$

Proposed beta distribution utilization

► B³R-cont'd

- Crossover
- Exponential crossover $CR_i(t) = \text{Beta}(5, 2.71)$
- Self-adaptive scheme in crossover rate

► TPBO: two-phase B³R optimization

- Exploration-oriented strategy
 - B³R
 - Exploitation-oriented strategy
 - DE/Current-to-best/2 with self-adaptation F
- $$v_i(t) = x_i(t) + \text{rand}() \cdot (f_{best}(t) - x_i(t)) + F_i(t)(x_{r1}(t) - x_{r2}(t)) + F_i(t)(x_{r3}(t) - x_{r4}(t))$$
- $$F_i(t+1) = \begin{cases} N(0.5, 0.1), & \text{if } f(x_i(t)) < f(v_i(t)) \text{ and } \text{rand}() < 0.1 \\ F_i(t), & \text{otherwise} \end{cases}$$

Proposed beta distribution utilization

► TPBO-cont'd

► Entire procedure

```

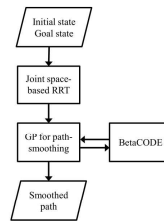
Algorithm 5 TPBO
1: Initialize population
2: while (Termination condition meets) do
3:   for all individuals in population do
4:     if First phase then
5:       BSR
6:     else
7:       if rand() < MR then
8:         BSR
9:       else
10:        DE/Current-to-best/2 reproduction
11:      end if
12:    end if
13:    Evaluate the offspring
14:    if The offspring is better then
15:      Replace the original with the offspring
16:    end if
17:  end for
18: end while

```

Application

► Path smoothing algorithms using Gaussian process (GP)

- Consider the scattering in the path generated by RRT as noise
- The scattering can be removed by GP regression
- Hyperparameters of GP is optimized by BetaCODE



Application

► Path smoothing algorithms using GP

► Simulation setup

- GP
 - Diagonal squared exponential covariance function
 - Gaussian likelihood function
- Performance metric
 - Fitness function
 - Sum of the negative log marginal likelihood
 - The number of successful runs
 - The smoothed path using the GP is regarded as successful if the initial and goal positions of the smoothed path are not far away from those of the original path
- Compared algorithm
 - BetaCODE
 - DE/Best/1/Bn (DEB)
 - Conjugate gradient method (CG)

Application

► Path smoothing algorithms using GP-cont'd

- Result
- Fitness function

BetaCODE		DEB		CG	
Mean	SD	Mean	SD	Mean	SD
-1305.83	8.03	-1301.78	11.56	749.69	1469.29

i	Algorithm	Average ranking	$z = R_0 - R_i /SE$	Unadjusted p-value	Holm APV
2	CG	3.0000	26.500	0	0
1	DEB	1.6760	5.5656	2.6124E-08	2.6124E-08
0	BetaCODE	1.3240	-	-	-

Application

► Path smoothing algorithms using GP-cont'd

- Result-cont'd
- The number of successful runs

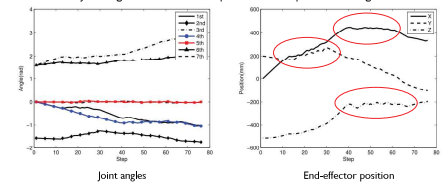
BetaCODE	DEB	CG
25	25	2

Application

► Path smoothing algorithms using GP-cont'd

► Result-cont'd

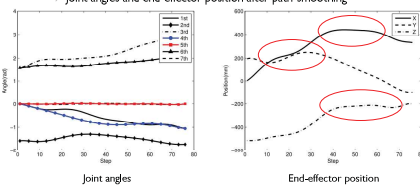
- Joint angles and end-effector position before path-smoothing



Application

► Path smoothing algorithms using GP-cont'd

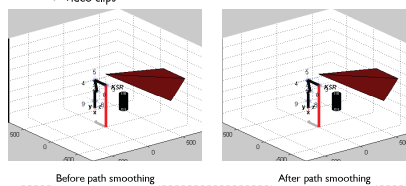
- Result-cont'd
- Joint angles and end-effector position after path-smoothing



Application

► Path smoothing algorithms using GP-cont'd

- Result-cont'd
- Video clips



Application

► Bipedal walking of a humanoid robot

- Vertical center of mass (COM) motion
- Single 3-D linear inverted pendulum model (3DUPM)

$$\begin{aligned}
 \mathbf{T}_{gr} + \mathbf{r}_{COM} \times \mathbf{F}_{gr} &= \frac{d}{dt} (\mathbf{r}_{COM} \times \mathbf{L}) \\
 \begin{bmatrix} \ddot{y} - \frac{g}{Z_c} y \\ \ddot{x} - \frac{g}{Z_c} x \end{bmatrix} &= \begin{bmatrix} -\frac{r_y}{m Z_c} \\ \frac{r_x}{m Z_c} \end{bmatrix} \\
 \mathbf{T}_{gr} - \mathbf{r}_{ZMP} \times \mathbf{F}_{gr} &= [0 \ 0 \ M_z]^T \\
 \begin{bmatrix} \ddot{y} - \frac{g}{Z_c} y \\ \ddot{x} - \frac{g}{Z_c} x \end{bmatrix} &= -\frac{g}{Z_c} \begin{bmatrix} y_{ZMP} \\ x_{ZMP} \end{bmatrix}
 \end{aligned}$$

Application

► Bipedal walking of a humanoid robot-cont'd

► Amplified sinusoidal function

$$f(t) = k_s \sin \left(\omega \left(t - \frac{\pi(\gamma-1)}{2\omega(\gamma+1)} \right) \right) + \sin \left(\frac{\pi(\gamma-1)}{2(\gamma+1)} \right)$$

$$\omega = \frac{2\pi}{T_{lfr} + T_{rfr}}, \gamma = \frac{T_{lfr}}{T_{rfr}}$$

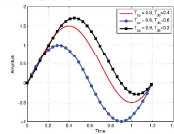
► Feedback from the GRF

$$feed = k_f |F_l + F_r - mg|$$

► Proposed vertical COM trajectory

$$z = Z_c + z_{sf}$$

$$z_{sf} = (k_s + feed) \sin \left(\omega \left(t - \frac{\pi(\gamma-1)}{2\omega(\gamma+1)} \right) \right) + \sin \left(\frac{\pi(\gamma-1)}{2(\gamma+1)} \right)$$



Application

► Bipedal walking of a humanoid robot-cont'd

► Simulation setup

► Performance metric

□ Fitness function

$$fitness(k_s, k_f) = W_s |F_l + F_r - mg| + W_e |x_c - x_{ZMP}| + W_g |y_c - y_{ZMP}| + P$$

► Compared algorithm

□ TPBO (k_s and k_f)

□ SDE (k_s and k_f)

□ TPBO(k_s only)

Application

► Bipedal walking of a humanoid robot-cont'd

► Result

► Fitness function

TPBO(k_s, k_f)		SDE(k_s, k_f)		TPBO(k_s only)		No movement
Mean	SD	Mean	SD	Mean	SD	
25693.82	1.69	25694.69	2.16	25695.25	0.04	25806.11

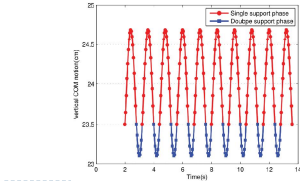
i	Algorithm	Average ranking	$z = R_0 - R_i /SE$	Unadjusted p-value	Holm APV
2	TPBO(k_s only)	2.6000	4.3134	1.6080E-05	3.2160E-05
1	SDE(k_s, k_f)	2.0200	2.2627	2.3652E-02	2.3652E-02
0	TPBO(k_s, k_f)	1.3800	-	-	-

Application

► Bipedal walking of a humanoid robot-cont'd

► Result-cont'd

► Vertical COM motion generate by the optimized sinusoidal function

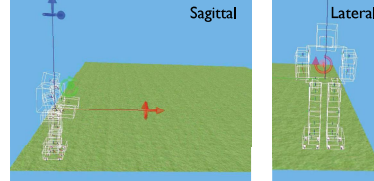


Application

► Bipedal walking of a humanoid robot-cont'd

► Result-cont'd

► Video clips



Conclusion

► New parameter definition for a beta distribution

► peak and spread

► Shape variation without limitation

► BetaCODE

► Control degree of opposition using a beta distribution

► Selection switching based on population diversity

► Partial dimensional change

► TPBO

► Bounded reproduction strategy using beta distribution

► Hybridization with DE/Current-to-best/2

Thank you for your attention



Image Encryption Implementation Based on Fractional-order Chen System

Hongyan Jia

*Department of Automation, Tianjin University of Science and Technology,
1038 Daguananlu Road, Hexi District, Tianjin 300222, PR China*

Qinghe Wang

*Department of Automation, Tianjin University of Science and Technology,
1038 Daguananlu Road, Hexi District, Tianjin 300222, PR China*

E-mail: jiahhy@tust.edu.cn

www.tust.edu.cn

Abstract

In this paper, based on the fractional-order Chen system, a kind of double encryption algorithm method is adopted to realize the image encryption. The method mainly refers to the transformation of the pixel position and the transformation of pixel value. The effectiveness of the double encryption method is verified by encryption and decryption of some typical images. The experimental results show that this method not only has the ideal effect of image encryption and decryption, but also possesses a better guarantee on the image security. That is, this encryption method is practical and feasible.

Keywords: fractional-order; Chen system; pixel; image encryption

1. Introduction

With the rapid development of information technology, the issue on network information security has attracted more and more attention in recent years. Especially for images, a kind of important information carrier, it would be very necessary to store and transmit with a high degree of security [1]. Therefore, image encryption technology has increasingly become one of research focus in the field of information security [2].

Image encryption technology is an effective method to protect the transmission of digital images [3]. So far, many kinds of image encryption technology have been reported, such as text encryption technology [4], quad-tree image encryption technology [5], chaotic encryption technology [6], and image encryption technology based on DNA [7], and so on. As one of Image encryption technology, chaotic encryption technology has increasingly highlighted its advantage because of the development of chaos theory.

In this paper, a kind of double encryption algorithm is adopted to realize the image encryption. The

algorithm will be achieved as follows. Step 1, encrypts the image by transforming the pixel position; Step 2, encrypts the image by transforming the pixel value; Step 3, decrypts the image by corresponding inverse transformation. All these transform are done by utilizing chaotic sequence from fractional-order Chen system. That is, a three-dimension chaotic sequence is firstly obtained by analyzing and computing fractional-order Chen system. Then any one of the three sequences can be selected as a position transform sequence in step 1, and subsequently all the three sequences will be selected as value transform sequences in step 2. And thus some encryption sequences for an image are gained by utilizing these chaotic sequences. Next, based on the corresponding inverse transformation, the image will be also decrypted by these chaotic sequences. At last, this encryption method is verified to be valid by encrypting and decrypting some images. All the experimental results show this method is effective and practical.

2. Fractional-order Chen system

The fractional-order Chen system is described as follows:

$$\begin{cases} \frac{d^\alpha x}{dt^\alpha} = a(y - x) \\ \frac{d^\alpha y}{dt^\alpha} = (c - a)x - xz + cy \\ \frac{d^\alpha z}{dt^\alpha} = xy - bz \end{cases} \quad (1)$$

where system parameters $a, b, c \in \mathbb{R}$, $0 < \alpha < 1$ refer to the fractional order. When fixing $\alpha = 0.9$, $a = 35$, $b = 3$, $c = 28$, the system will show a typical chaotic attractor. Under the above conditions, setting an initial value of the system, a three-dimension chaotic sequence can be obtained when utilizing four-order Runge-Kutta algorithm to solve the system. Here, system parameters, the fractional order, and initial value are all used as keys.

3. Image Encryption Algorithm

3.1 Pixel position scrambling

In this paper, the sequence x in three-dimension chaotic sequence is used as the pixel position transform sequence. The sequence x is firstly sorted by ascending order. Generally speaking, the image matrix stored in computer includes three components, R component, G component and B component. These components are all $m \times n$ matrix. Therefore, in order to complete encryption operation, R component, G component and B component of the image matrix need to be converted into one-dimension array, R-value, G-value and B-value, respectively. Then, the sort operations for R-value are carried out by using the sorted sequence x , and subsequently scrambling encrypted image for R component can be obtained. With the same method, the scrambling encrypted image for G component or B component can also be obtained.

3.2 Pixel value transform

Although the length of chaotic sequence can be selected to be same as each component of the image, every value of chaotic sequence is not consistent with the image storage value. In general, the storage value of image is an integer between 0 and 255. So it is necessary for the chaotic sequences used in encryption to carry out numerical transformation such as numerical expansion and limitation domain. After completing the

corresponding transformation, the value results of chaotic sequences are consistent with those of the image. Then the numerical encryption algorithm using XOR is used to encrypt the pixel value after image scrambling. And thus three components of the encrypted image can be obtained. Finally, three components of the encrypted image is combined together, and getting the encrypted image information.

4. Experimental Results

This paper selects two color images named Lena and Xuexiao as the research object. The size of image Lena is 512×512 , and the size of image Xuexiao is 256×256 . The experiments have been done by MATLAB 2012, with the initial values of state variables being (0.1, 0.2, 0.3). The image of Lena and its three component diagrams of R, G, B are shown in Fig.1 (a), (b), (c), and (d), respectively. The encrypted images of tricolor component after the pixel scrambling operation are shown in Fig.2 (a), (b), and (c), respectively. The encrypted image of Lena after pixel scrambling and the encrypted image of Lena after pixel value transform are given in Fig.3(a) and (b), respectively. The decrypted images of Lena are shown in Fig.4 (a), (b), and (c), respectively. The encrypted image of Xuexiao and the decrypted image of Xuexiao are shown in Fig.5 and Fig.6, respectively. The experimental results show that the encrypted image is completely different from the original image, while the decrypted image and the original image are identical. It shows that the encryption method is practical and effective, and has good encryption effect.

5. Performance Analysis

5.1 Histogram analysis

Generally speaking, histogram can clearly reflect the distribution of the quality characteristics of the image [8], so it is convenient for people to correctly evaluate the overall quality condition of image. Here because the histogram of Lena image is same as one of Xuexiao image, the histogram of Lena image is selected to illustrate the pixel distribution at each color of the image. Histograms for R components, G components, and B components, before and after encryption of Lena are shown in Fig.7 (a), (b), and (c), respectively. It can be seen that the distribution of the encrypted histogram

is very uniform, which indicates that the ability to resist statistical attack for the encryption method is good.



Fig.1 Image Lena and its three component diagrams

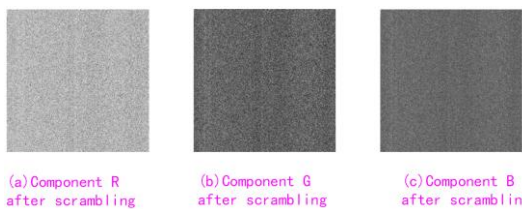


Fig.2 The encrypted images of tricolor component after the pixel scrambling operation

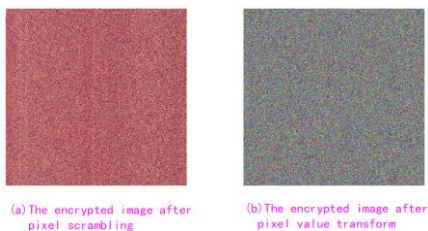


Fig.3 The encrypted image of Lena

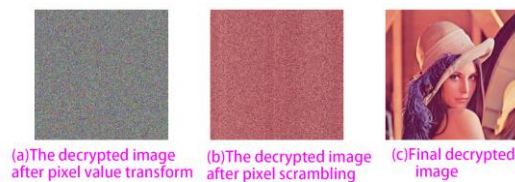


Fig.4 The decrypted image of Lena

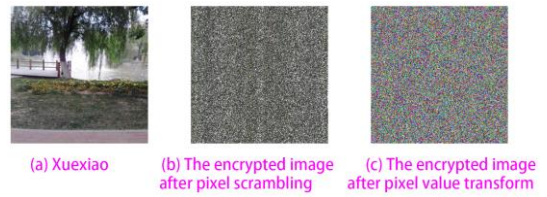


Fig.5 The encrypted image of Xuexiao

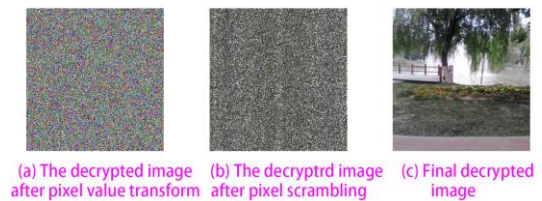


Fig.6 The decrypted image of Xuexiao

5.2 Correlation analysis

In this paper, the correlation coefficient among adjacent pixels of the image is shown in Table 1. As can be seen from the table, the correlation coefficient of the original image is close to one, which indicates that the adjacent pixels are highly correlated; The correlation coefficient of the encrypted image is close to zero, which illustrates there is little correlation among adjacent pixels. All these show the pixels of the encrypted image are randomly distributed. The encrypted image can effectively resist the attacks of the relevant statistical techniques, and its security is good.

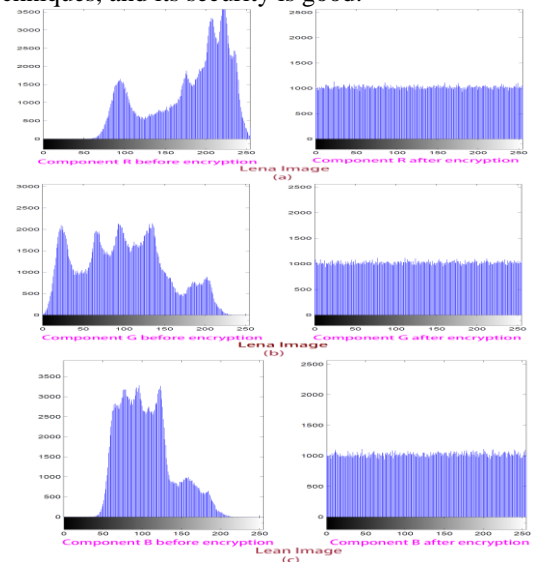


Fig.7 Histogram before and after encryption

Table 1 Correlation Coefficient

	Lena		Xuexiao	
	Original Image	Encrypted Image	Original Image	Encrypted Image
R	0.98663	0.00077537	0.91771	0.00020332
G	0.985	0.0012447	0.91698	0.0057597
B	0.9687	0.00068893	0.93997	0.0036447

6. Conclusion

This paper adopts an effective method to implement the image encryption operation. The method is based on the chaotic sequence generated by the fractional-order Chen system, and combines the double encrypted technique including the pixels position scrambling of image and the pixels value transform of image. The experimental results and performance analysis show that this method not only has good encryption effect, but also has high security.

Acknowledgements

This work was supported in part by the Young Scientists Fund of the National Natural Science Foundation of China (Grant No. 11202148), the Natural Science Foundation of China (Grant No. 61174094).

References

1. Dong W, Zhang L, Shi G, Li X, Non-Locally centralized sparse representation for image restoration, *IEEE Transactions on Image Processing*. 22(4) (2013) 1620-1630.
2. Liao X, Lai S, Zhou Q, A novel image encryption algorithm based on self-adaptive wave transmission, *Signal Processing*. 90(9) (2010) 2714-2722.
3. Jin Bing, Qi Lilei, JIA Yuzhen, Research of chaos cross-encryption algorithm based on Logistic mapping, *Computer & Digital Engineering*. 39(1) (2011) 93-94.
4. Wang Xiao, Zhao Dong. Double image encryption method with resistance against the specific attack based on asymmetric algorithm, *Optics Express*. 20(11) (2012) 11994-12003.
5. ZHANG Xiaoyan, WANG Chao, SUN Zhiren, et al. An image encryption scheme based on sequential CA, *Optics and Precision Engineering*. 16(9) (2008) 1781-1786.
6. Nooshin B, Yousset F, Karim A, A robust hybrid method for image encryption based on Hopfield neural network, *Computer & Electrical Engineering*. 38(2) (2012) 356-369.
7. Liu Lili, Zhang Qiang, Wei Xiaopeng, A RGB image encryption algorithm based on DNA encoding and chaos map, *Computer and Electrical Engineering*. 38(5) (2012) 1240-1248.
8. Zhang Yonghong, Zhang Bo, Algorithm of image encrypting based on logistic chaotic system, *application research of Computer*. 32(6) (2015) 1770-1773
9. Zhang Jian, Fang Dongxin, Image encryption technology applied chaotic maps index and DNA coding, *Computer Engineering and Design*. 36(3) (2015) 613-618.

Mobile Camera based Motion Segmentation by Image Resizing

Chunyu Yu

Department of Electrical Engineering and Computer Science
Syracuse University, Syracuse, NY 13244-1240
Email: cyu07@syr.edu

Abstract

The need of detecting moving object like human and vehicle by mobile camera is increasing in commerce and industry. In this paper, an image-resize methodology which can abstract motion segmentation and detect moving object from moving background is proposed. First, edges images are computed. Then movement vector between frame images are computed and the relative background motion is compensated. By adjusting the parameters of resize algorithm, human liked object or vehicle liked object can be segmented separately and the segmentation can be used for further detection. Experiments have been performed under three different environments for human detection and vehicle detection.

Keywords: mobile camera, motion segmentation, edge-based alignment, object detection.

1. Introduction

Real-time human detection is a key study field in computer vision. This technique is widely used in automotive engineering, traffic monitoring, robotics, human-computer interaction, security, military and many other applications. In literature, there are a lot of researchers focused on stationary camera based object detection. Main technique used is image difference to find the difference of two image pixel by pixel. However, when camera is moving during the recording, the whole background is changing. To resolve this problem, [1-4] developed different algorithms to against the light changes.

Another widely used method is statistical theory which classifies pixels into background and foreground. C. Rasmussen and G. D. Hager combine Maximum A posteriori Probability (MAP) with a Probabilistic Data Association Filter [5]. N. Vaswani, A. Tannenbaum, and A. Yezzi unified geometric active contours and level sets within Particle Filter [6] and R. Stolkin, A. Greig, M. Hodgetts, and J. Gilby, proposed an algorithm which

combines Expectation Maximization and extended-Markov Random Field [7]. Another method is wavelets based. The main idea is to analysis the difference part's frequency. For instance, [8] presented a motion segmentation based on Galilean wavelets. In 1980 Horn and Schunch first proposed a new method named optical flow [9]. After that, many researchers made improvement on it such as J. Zhang, F. Shi, J. Wang, and Y. Liu [10].

In this paper, an image resizing based motion segmentation method is proposed. Unlike other computational expensive method, this algorithm only relies on a new edge alignment method and fast image resizing according to object morphology. First, edges in two consecutive frame images are detected. Then the new edge-based alignment method is adopted to find the motion vector between two images. Motion compensation is performed before motion segmentation. Then the image is resized according to object morphology. After filtering pixels lower than threshold value, object is stand out of the background. The experiment was performed by MATLAB 2014a on i5-2450m and 6GB RAM in three different scenarios for

human liked object detection and vehicle liked object detection. The results illustrate that the accuracy rate can reach as high as 93.04%, and the execution time is

highly speeded up (approximately 0.82s per frame).

The paper is organized as follows. The proposed method for motion segmentation and object detection is described in section 2 and section 3 presents the experiment results and the conclusion part is in section 4.

2. Proposed Method

2.1 Finding global minima

Take human liked object detection as an example. Two consecutive frame images f_1 and f_2 are loaded first. By using Canny edge detector, two binary edge images are obtained. Ideally, the camera is stable and the background is not moved, so in the difference image ($f_2 - f_1$), only moving object is visible and background is offset. Virtually, the camera may slide a very small distance in a direction, so the background and people are moved simultaneously when two consecutive images are compared. Therefore, eliminate the movement of background is essential.

Assume people are most likely appear in the central area of an image, when detecting background movement, only edges at the margin of images are compared. Specifically, fill zero into the central area of two images and find out the relative movement between the background in 8 directions (vertical, horizontal and diagonal) (Fig.1). By the algorithm in table 1, relative motion direction and distance are achieved. Base on experiments, the movement between two frames is always 3 to 6 pixels, so 10 pixels are sufficient for searching in our algorithm.

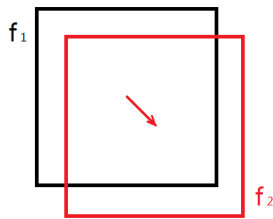


Fig. 1 One of eight directions of relative movement between two images

Table 1 Algorithm for finding relative motion direction and distance

```

for 1 to 8 directions
  for 1 to 10 pixels
    m[i][j]=abs(tailored(f1,-direction,pixel)-tailored(f2,direction,pixel))
  direction = minima(m).direction
  distance = minima(m).pixel

```

According to the direction and movement distance, tailor pixels from two images respectively. After that, beside the people, backgrounds are almost in the same position in two images (say, reach the global minima).

2.2 Resizing image algorithm

Even global minima is reached, virtually the edges in two images cannot be overlapped exactly. As a result, when difference image ($f_2 - f_1$) is calculated, background edges of two images can hardly offset each other. The background may become even more complicated than human outline. As a result, the human cannot stand out of background (Fig.2).

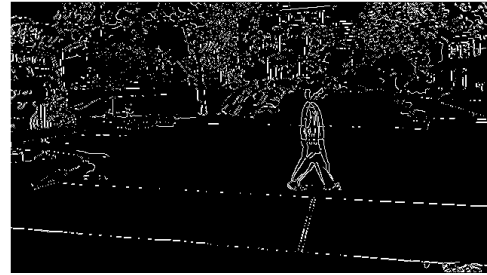


Fig. 2 Difference image acquired without resizing algorithm

To resolve the problem, an image resizing algorithm is adopted. Table 2 is the matrix of yellow rectangle in Fig. 2 which is achieved without dilating images. Table 3 is the result acquired after dilating images. By compare two tables, we can notice that the number of pixels which value is 1 is decreased and they are more scattered in Table 3. In terms of the whole image, dilating images results to more mottled background.

Table 2 Difference image acquired without dilating
(1-value pixels: 15)

	258	259	260	261	262	263	264	265	266	267
391	0	0	0	0	0	0	0	0	0	0
392	1	1	1	1	1	0	0	0	0	0
393	1	1	1	1	1	0	0	0	0	0
394	0	0	0	0	0	0	0	0	0	0
395	0	0	0	0	0	0	0	0	0	0
396	0	0	0	0	0	0	0	0	0	1
397	0	0	0	0	0	0	0	0	0	0
398	0	0	0	0	0	0	0	0	1	0
399	0	0	0	0	0	0	0	0	1	1
400	0	0	0	0	0	0	0	0	0	1

Table 3 Difference image acquired after dilating (1-value pixels: 13)

	258	259	260	261	262	263	264	265	266	267
391	1	1	1	1	1	1	0	0	0	0
392	0	0	0	0	0	0	0	0	0	0
393	0	0	0	0	0	0	0	0	0	0
394	1	1	1	1	1	0	0	0	0	0
395	0	0	0	0	0	0	0	0	1	0
396	0	0	0	0	0	0	0	0	0	0
397	0	0	0	0	0	0	0	1	0	0
398	0	0	0	0	0	0	0	1	0	0
399	0	0	0	0	0	0	0	0	0	0
400	0	0	0	0	0	0	0	0	0	0

As moving human most likely look like vertical rectangles, they are more robust than noise (remained background) in terms of vertical image resizing. Therefore, based on the result in Table 3, the image is resized in vertical direction and then restored. After that pixels' value are between -1 and 1.

Table 4 Matrix after image resizing

	258	259	260	261	262	263	264	265	266	267
391	0.31	0.31	0.31	0.31	0.23	0.23	0.00	-0.04	0.01	0.00
392	0.34	0.34	0.34	0.34	0.23	0.23	-0.00	-0.00	0.04	0.00
393	0.31	0.31	0.31	0.31	0.16	0.17	-0.02	0.07	0.11	0.00
394	0.25	0.25	0.25	0.25	0.08	0.08	-0.04	0.17	0.18	0.00
395	0.19	0.19	0.19	0.19	0.01	0.01	-0.04	0.25	0.23	0.00
396	0.14	0.14	0.14	0.14	-0.02	-0.02	-0.00	0.29	0.23	-0.00
397	0.09	0.09	0.09	0.09	-0.02	-0.05	0.07	0.31	0.16	-0.01
398	0.03	0.03	0.03	0.03	-0.01	-0.05	0.17	0.31	0.08	-0.02
399	-0.00	-0.00	-0.00	-0.00	-0.00	-0.04	0.25	0.29	0.00	-0.02
400	-0.02	-0.02	-0.02	-0.02	0.00	-0.00	0.26	0.25	-0.02	0.01

Due to the distortion, mottled background faded dramatically compared to human outline. It can be eliminated by deleting pixels which value is lower than specific threshold value. According to the environment and object, 0.5 is adopted in this experiment. Therefore, all the pixels in Table 4 will be 0. Compare to Fig. 2, the road line in Fig. 3 is eliminated (yellow rectangle) and human is out stand of background.



Fig. 3 Difference image acquired by resizing algorithm

The following step are dilating image, filling image hole and eroding image. The largest block in the image is the object.



Fig. 4 segmentation achieved by resizing algorithm (sinister) versus without resizing algorithm (dexter)

The following assumptions are made in proposed algorithm. Firstly, there must be sufficient edges in the margin of the images as they are used to find motion vector. Secondly, there must be sufficient movement of the object. If the object is stationary, it will be considered as background. Finally, the object should large enough in terms of the image scale as the largest block is selected as object in the final step.

3. Experiment Results

Without loss of generality, the experiment was performed to test vertical resizing and horizontal resizing in three different scenarios: (1) human walk indoor, (2) human walk outdoor and (3) human walk outdoor with moving vehicle in background. The dataset of Zheng et al.'s experiment was adopted [11].

3.1. Human walk indoor without moving object

231 frames of a video were tested in this experiment. Fig. 5 as part of results illustrates that the movement segmentation is highly accurate and almost overlaps with the human body. Thus the segmentation will decrease the running time largely for further HOG detection. Even though illumination sometimes disturbs the detection, the overall successful detection rate for whole frames is 77.56%.

3.2. Human walk outdoor without moving vehicle

In this experiment, 273 frames were tested and the accurate detection rate is 93.04%. Similar to the results of indoor experiment, the segmentation part is highly overlapped with the human body (Fig. 6). Human walk outdoor with moving vehicle in the background

3.3. Human walk outdoor with moving vehicle in the background

100 frames were tested for human and vehicle. The detection rate is 86% and 83.1% respectively. As shown in Fig.7 and Fig.8, the moving vehicle can be distinguished from stopped bus.

4. Conclusions

In this paper, a fast and simple motion segmentation method for moving background is proposed. Zheng et al.'s dataset was tested in the experiment. The results show that the proposed method is highly accurate especially in complex environment. In the future, prior knowledge will be considered. The position of yellow box can be limited in a range according to its position in prior frame. Thus the algorithm can be more robust to fast light changing. Due to pretty accurate segmentation region, further detection such as HOG in this region can be speed up largely.

References

1. A. Cavallaro, O. Steiger, and T. Ebrahimi, "Tracking Video Objects in Cluttered Background," IEEE Transactions on Circuits and Systems for Video Technology, vol. 15, no. 4, pp. 575–584, 2005.
2. F.-H. Cheng and Y.-L. Chen, "Real time multiple objects tracking and identification based on discrete wavelet transform," Pattern Recognition, vol. 39, no. 6, pp. 1126–1139, 2006.
3. R. Li, S. Yu, and X. Yang, "Efficient spatio-temporal segmentation for extracting moving objects in video sequences," IEEE Transactions on Consumer Electronics, vol. 53, no. 3, pp. 1161–1167, Aug. 2007.
4. A. Colombari, A. Fusiello, and V. Murino, "Segmentation and tracking of multiple video objects," Pattern Recognition, vol. 40, no. 4, pp. 1307–1317, 2007.
5. C. Rasmussen and G. D. Hager, "Probabilistic data association methods for tracking complex visual objects," IEEE Transactions on Pattern Analysis and Machine Intelligence, vol. 23, no. 6, pp. 560–576, 2001.
6. N. Vaswani, A. Tannenbaum, and A. Yezzi, "Tracking deforming objects using particle filtering for geometric active contours," IEEE Transactions on Pattern Analysis and Machine Intelligence, vol. 29, no. 8, pp. 1470–1475, 2007.
7. R. Stolkin, A. Greig, M. Hodgetts, and J. Gilby, "An em/e-mrf algorithm for adaptive model based tracking in extremely poor visibility," Image and Vision Computing, vol. 26, no. 4, pp. 480–495, 2008.
8. M. Kong, J.-P. Leduc, B. Ghosh, and V. Wickerhauser, "Spatio-temporal continuous wavelet transforms for motion-based segmentation in real image sequences," Proceedings of the International Conference on Image Processing, vol. 2, pp. 662–666 vol.2, 4-7 Oct 1998.
9. B. K. Horn and B. G. Schunck, "Determining optical flow," Cambridge, MA, USA, Tech. Rep., 1980.
10. J. Zhang, F. Shi, J. Wang, and Y. Liu, "3d motion segmentation from straight-line optical flow," in Multimedia Content Analysis and Mining, 2007, pp. 85–94.
11. Y. Zheng, "Detection of moving people with mobile cameras by fast motion segmentation", 2013 Seventh International Conference on Distributed Smart Cameras (ICDSC), pp.1-6, Oct. 29-Nov. 1 2013.

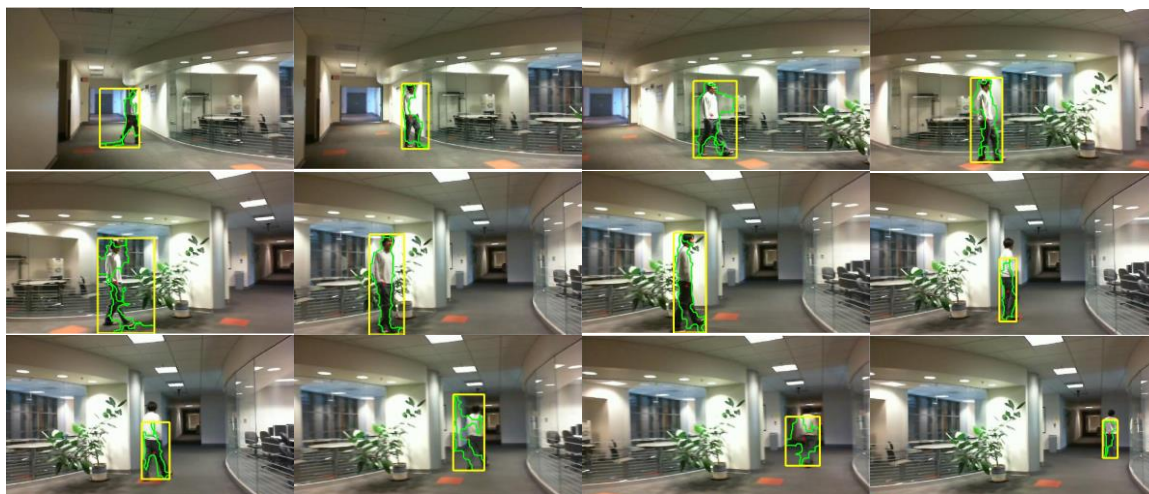


Fig. 5 Indoor sequence. The green line outlines the largest block and the yellow box indicates the possible human region

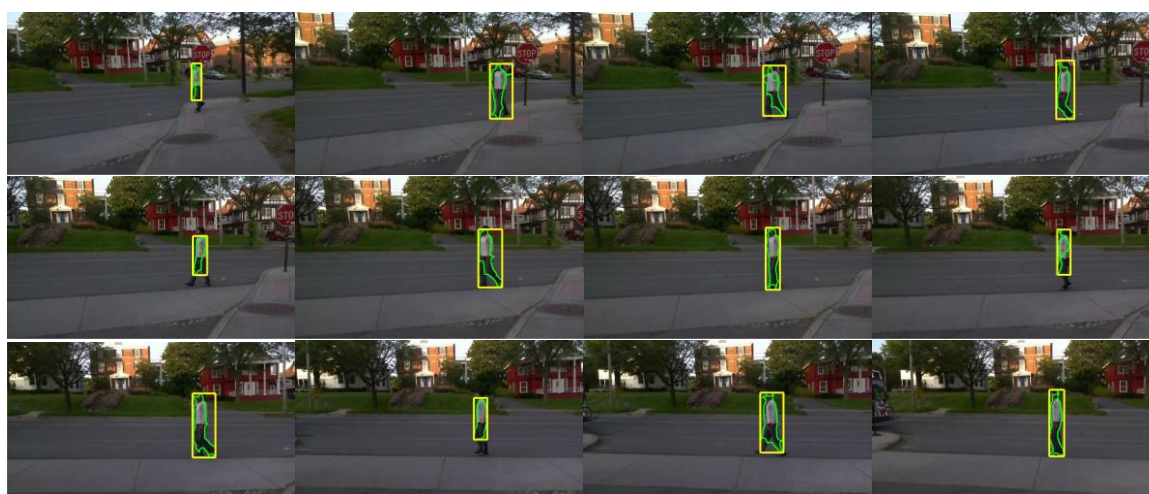


Fig. 6 Outdoor sequence. The green line outlines the largest block and yellow box indicates the possible human region

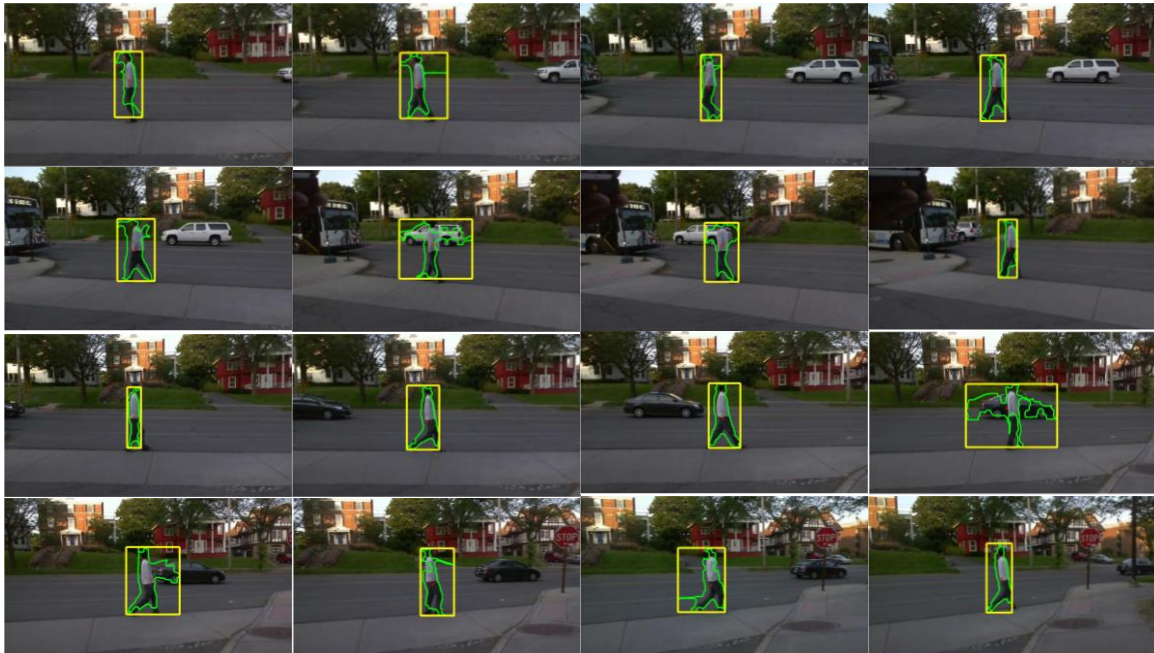


Fig. 7 Outdoor sequence with moving car in background. The green line outlines the largest block and yellow box indicates the possible human region

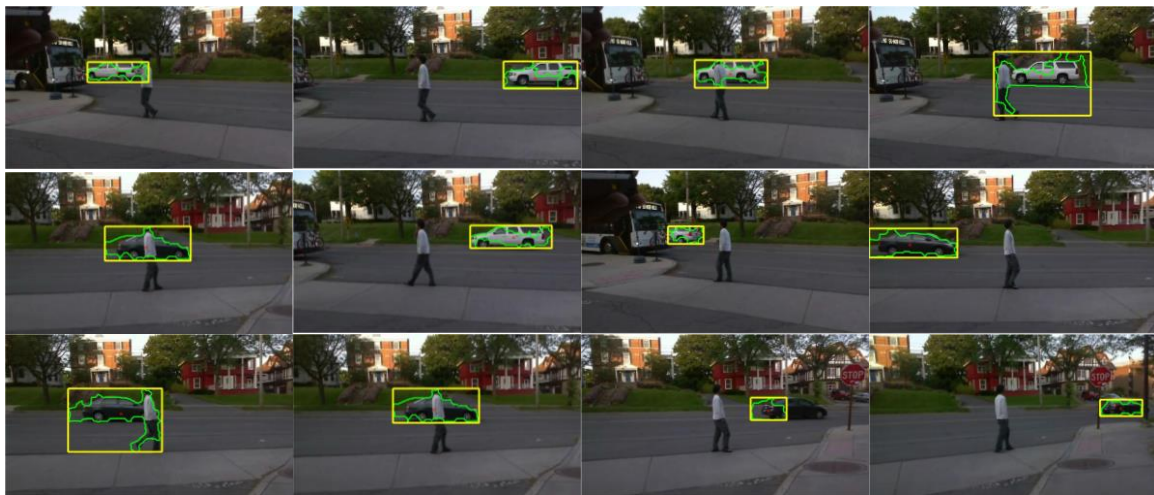


Fig. 8 Outdoor sequence with moving car in background. The green line outlines the largest block and yellow box indicates the possible vehicle region.

Synchronization of the Fractional-order Permanent Magnet Synchronous Motor

Wei Xue

*Department of Automation, Tianjin University of Science and Technology,
1038 Daguanlu Road, Hexi District, Tianjin 300222, PR China*

Xue Li

*Department of Automation, Tianjin University of Science and Technology,
1038 Daguanlu Road, Hexi District, Tianjin 300222, PR China
E-mail: xuwei@tust.edu.cn, lixueTJKJ@163.com
www.tust.edu.cn*

Abstract

In this paper, the chaotic synchronization of the fractional-order permanent magnet synchronous motor is investigated. The presented control scheme is simple and flexible, and it is suitable both for design and implement in practice. According to the stability theory of fractional-order linear system, the chaotic synchronization of the drive system and the response system is achieved. Adopting the nonlinear feedback method, a nonlinear feedback controller in theoretical analysis is designed. The obtained numerical simulation results agree with that of theoretical analysis, which can further demonstrate the feasibility and effectiveness of the proposed synchronization scheme.

Keywords: Chaos; Fractional-order; Permanent magnet synchronous motor; Nonlinear feedback synchronization; Numerical simulation.

1. Introduction

Since permanent magnet synchronous motor (PMSM) has excellent properties such as simple structure, high torque-to-weight ratio, low manufacturing cost and high torque-to-inertia ratio, it is used in the industrial applications more widely. Studies have shown that, when the motor works under certain parameters and operating conditions, the chaotic behavior will occur, such as intermittent ripples of torque, the low-performance property speed control, irregular current system noise and so on. The study of the integer-order chaotic model of the PMSM is comprehensive. For PMSM, the fractional-order chaotic model can reflect its chaotic characteristics more accurately. Some investigation of fractional-order PMSM are still in its infancy. Many scholars have researched on fractional-order chaotic systems, such as fractional-order Rössler system,¹ fractional-order Chen system,² fractional-

order Liu system,³ fractional-order Lü system,⁴ and fractional-order generalized augmented Lü system.⁵

The chaotic behavior of PMSM is harmful in most cases. However, the chaotic behavior of PMSM can also be useful in some applications, such as in industrial mixing process, the chaotic motion itself gives the extension and folding characteristics of good mixing. It is of practical significance to improve the efficiency of industrial mixing. Therefore, it is necessary to study the chaos synchronization of fractional-order PMSM. Recently, many synchronization approaches to the chaotic system have been proposed such as linear feedback synchronization,⁶ adaptive synchronization,⁷ impulse synchronization,⁸⁻⁹ projective synchronization,¹⁰ active synchronization,¹¹ generalized synchronization,¹² sliding mode control,¹³ and lag synchronization.¹⁴ Adopting the nonlinear feedback method, a nonlinear feedback controller in theoretical analysis is designed. And the synchronization of the fractional-order PMSM is achieved according to the stability theory of

fractional-order linear system. The obtained numerical simulation results agree with the theoretical analysis results, which can further demonstrate the feasibility and effectiveness of the proposed synchronization scheme.

2. Synchronization of fractional-order PMSM

2.1. General nonlinear feedback synchronization scheme

Here, the fractional-order chaotic system is considered as follow:

$$\frac{d^\alpha x}{dt^\alpha} = Ax + f(x) \quad (1)$$

where $\alpha \in (0,1]$, $A \in R^{n \times n}$ is the matrix of system parameters, $\mathbf{x} = (x_1, x_2, \dots, x_n)^T \in R^n$ is the state variable

$f(\mathbf{x}) = (f_1(x), f_2(x), \dots, f_n(x))^T \in R^{n \times 1}$ is continuous nonlinear vector function. The system(1) can be used as a driving system, and the corresponding response system is given by:

$$\frac{d^\alpha y}{dt^\alpha} = By + g(y) + u \quad (2)$$

where $\alpha \in (0,1]$, $B \in R^{n \times n}$ is the matrix of system parameters, $\mathbf{y} = (y_1, y_2, \dots, y_n)^T \in R^n$ is the state variable, $g(\mathbf{y}) = (g_1(y), g_2(y), \dots, g_n(y))^T \in R^{n \times 1}$

is the state variable and $\mathbf{u} = (u_1, u_2, \dots, u_n)^T$ is the controller to be determined in order to realize nonlinear feedback synchronization.

Let the error vector be $\mathbf{e} = \mathbf{y} - \mathbf{x} = (e_1, e_2, \dots, e_n)^T$, and the appropriate controller \mathbf{u} should be designed to make $\lim_{t \rightarrow \infty} \mathbf{e} = 0$.

The chaotic model of PMSM can be expressed as the following form¹⁵:

$$\begin{cases} \frac{d^\alpha x_1}{dt^\alpha} = -x_1 + x_2 x_3 \\ \frac{d^\alpha x_2}{dt^\alpha} = -x_2 - x_1 x_3 + \gamma x_3 \\ \frac{d^\alpha x_3}{dt^\alpha} = \sigma(x_2 - x_3) \end{cases} \quad (3)$$

where $\alpha \in (0,1]$ is the fractional order, $\sigma > 0$ and $\gamma > 0$ are constants.

In order to observe the nonlinear feedback synchronization of PMSM, the response systems can be defined as follow:

$$\begin{cases} \frac{d^\alpha y_1}{dt^\alpha} = -y_1 + y_2 y_3 + u_1 \\ \frac{d^\alpha y_2}{dt^\alpha} = -y_2 - y_1 y_3 + \gamma y_3 + u_2 \\ \frac{d^\alpha y_3}{dt^\alpha} = \sigma(y_2 - y_3) + u_3 \end{cases} \quad (4)$$

where $\mathbf{u}^T = (u_1, u_2, u_3)$ is the nonlinear controller to be designed for PMSM with the same parameters σ and γ in spite of the differences in initial conditions.

2.2. Design of synchronization controller

The drive system(3) can be described as system(1) in the form of:

$$\frac{d^\alpha x}{dt^\alpha} = \begin{pmatrix} -1 & 0 & 0 \\ 0 & -1 & \gamma \\ 0 & \sigma & -\sigma \end{pmatrix} x + \begin{pmatrix} +x_2 x_3 \\ -x_1 x_3 \\ 0 \end{pmatrix}$$

(5)

Similarly, the response system(4) is written in the form of system(2) as follow:

$$\frac{d^\alpha y}{dt^\alpha} = \begin{pmatrix} -1 & 0 & 0 \\ 0 & -1 & \gamma \\ 0 & \sigma & -\sigma \end{pmatrix} y + \begin{pmatrix} +y_2 y_3 \\ -y_1 y_3 \\ 0 \end{pmatrix} + u. \quad (6)$$

Here, the nonlinear feedback method to realize the synchronization of PMSM is adopted. And controller $\mathbf{u} = f(\mathbf{x}) - g(\mathbf{y}) - K\mathbf{e}$ can be selected as the following form:

$$u = f(x) - g(y) - Ke = \begin{pmatrix} x_2 x_3 \\ -x_1 x_3 \\ 0 \end{pmatrix} - \begin{pmatrix} y_2 y_3 \\ -y_1 y_3 \\ 0 \end{pmatrix} - Ke \quad (7)$$

Where $\mathbf{e} = \mathbf{y} - \mathbf{x} = (e_1, e_2, e_3)^T$.

From Eq.(5), Eq.(6), and Eq.(7), the error system is obtained, which can be expressed as:

$$\frac{d^\alpha e}{dt^\alpha} = \begin{pmatrix} -1 & 0 & 0 \\ 0 & -1 & \gamma \\ 0 & \sigma & -\sigma \end{pmatrix} e - Ke \quad (8)$$

$$K = \begin{pmatrix} 0 & 0 & 0 \\ 0 & 0 & \gamma \\ 0 & \sigma & 0 \end{pmatrix} \quad (9)$$

From Eq.(8) and Eq.(9), the error system is obtained as follow:

$$\frac{d^\alpha e}{dt^\alpha} = \begin{pmatrix} -1 & 0 & 0 \\ 0 & -1 & 0 \\ 0 & 0 & -\sigma \end{pmatrix} e \quad (10)$$

From Eq.(10), the eigenvalues are $\lambda_1 = -1$, $\lambda_2 = -1$, and $\lambda_3 = -\sigma$. Because $\sigma > 0$, all eigenvalues λ_i ($i=1,2,3$)

are negative, that is $|\arg(\lambda_i)| > \frac{\alpha\pi}{2}$. According to

Ref.[16], it will be asymptotical stability of the origin of the error system, which means that $\lim_{t \rightarrow \infty} e = 0$.

Therefore, the goal of synchronizing the fractional-order PMSM is achieved.

3. Numerical simulation

From system(3), the phenomenon of chaos can be observed when $\alpha=0.95$, therefore we will concentrate on the 2.85-order system in the following part. By adopting the time domain method based on predictor-corrector to conduct the numerical simulation, the chaotic attractors of system(3) is obtained. When $\alpha=0.95, \sigma=11$, and $\gamma=90$, and phase portraits are shown in Fig.1:

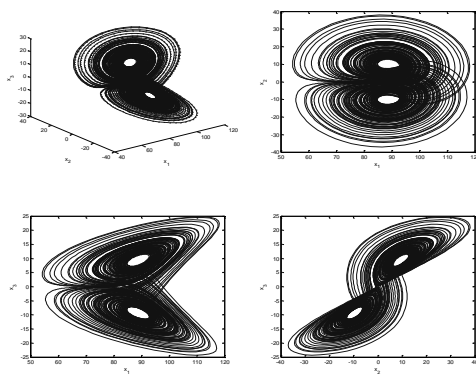


Fig.1. Phase portraits of system(3) with $\alpha=0.95, \sigma=11$, and

$\gamma=90$: (a) $x_1 - x_2 - x_3$; (b) $x_1 - x_2$; (c) $x_1 - x_3$; (d) $x_2 - x_3$.

In this section, we conduct the numerical simulation of the synchronization via Matlab, taking the 2.85-order PMSM as an example. The system parameters are chosen to be $\alpha = 0.95, \sigma = 11$, and $\gamma = 90$, and in time steps of 0.01. The initial states of the drive system and response system are assumed as $x_1(0) = 0.8, x_2(0) = 5, x_3(0) = 1.3, y_1(0) = 3, y_2(0) = 6$, and $y_3(0) = 1$, respectively. It can be observed that the drive system and the response system are in asymptotic synchronization in Fig.2. In addition, the curves of synchronization error is obtained as shown in Fig.3. It's clearly showed the synchronization error vector converge to zero as time goes to infinity. The obtained numerical simulation results agree with theoretical analysis results.

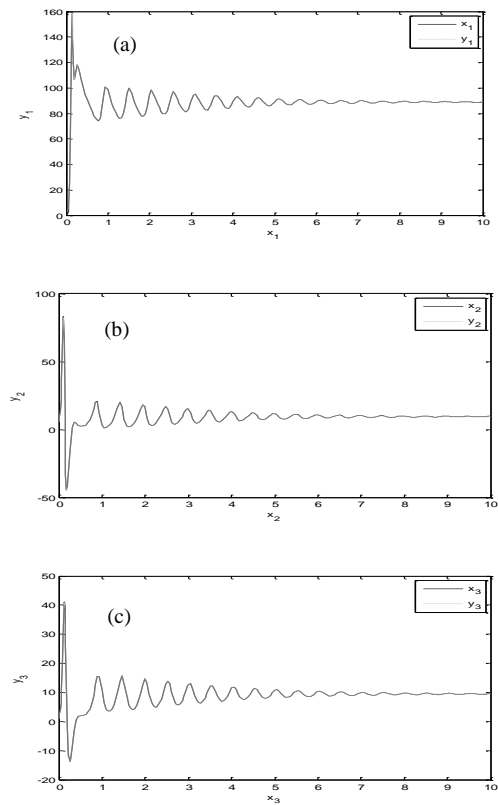


Fig.2. Variation of state variables with time: (a) (x_1, y_1) ; (b) (x_2, y_2) ; (c) (x_3, y_3) .

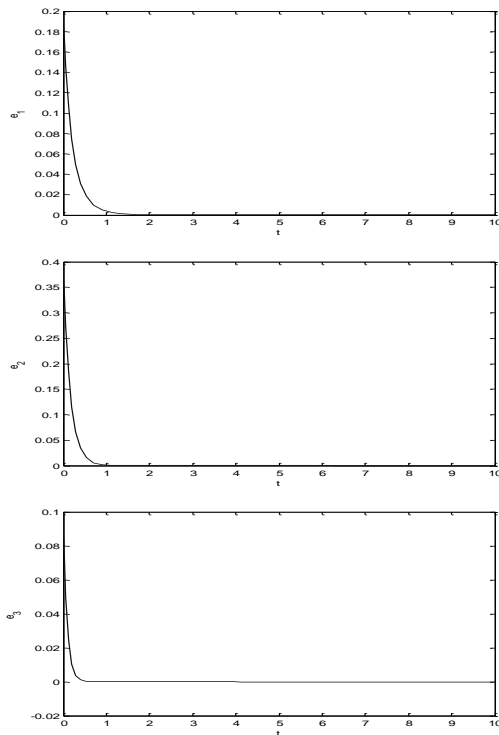


Fig.3 Synchronization errors versus time t (a) $e_1 - t$;
(b) $e_2 - t$;(c) $e_3 - t$.

4. Conclusion

In this paper, a general nonlinear feedback chaotic synchronization scheme for fractional-order PMSM is introduced. By analyzing phase portraits of fractional-order PMSM, we have found there are abundant dynamical behaviors in the fractional-order PMSM. Moreover, the synchronization problem of the fractional-order PMSM has been investigated. Based on the nonlinear feedback method, the synchronization controller to achieve synchronization between the drive system and the response system is designed. The obtained numerical simulation results agree with theoretical analysis, which can further demonstrate the feasibility and effectiveness of the proposed synchronization scheme.

5. Acknowledgement

This work is supported by the Young Scientists Fund of the National Natural Science Foundation of China (Grant No.11202148).

6. References

1. Li C G, Chen G R. Chaos and hyperchaos in the fractional order Rössler equations. *Physics Letters A*. 2004, 341: 55-61.
2. Li C P, Peng G J. Chaos in Chen's system with a fractional order. *Chaos, Solitons and Fractals*. 2004, 22: 443-450.
3. Daftardar-Gejji V, Bhalekar S. Chaos in fractional ordered Liu system. *Computers and Mathematics with Applications*. 2010, 59(3): 1117-1127.
4. Lu J G. Chaotic dynamics of the fractional order Lü system and its synchronization. *Physics Letters A*. 2006, 354(4): 305-311.
5. Xue W, Xu J K, Cang S J, et al. Synchronization of the fractional-order generalized augmented Lü system and its circuit implementation. *Chinese Physics B*. 2014, 23(6): 060501.
6. Liu F, Ren Y, Shan X M, et al. A linear feedback synchronization theorem for a class of chaotic system. *Chaos, Solitons and Fractals*. 2002, 13(4): 723-730.
7. Wang Y W, Guan Z H, Wen X J. Adaptive synchronization for Chen chaotic system with fully unknown parameters. *Chaos, Solutions and Fractals*. 2004, 19(4): 899-903.
8. Ren Q S, Zhao J Y. Impulsive synchronization of coupled chaotic systems via adaptive-feedback approach. *Physics Letters A*. 2006, 356(3): 226-230.
9. Mohammad H, Mahsa D. Impulsive synchronization of Chen's hyperchaotic systems. *Physics Letters A*. 2006, 355(4, 5): 342-347.
10. Meng J, Wang X Y. Generalized projective synchronization of a class of delayed neural networks. *Physics Letters A*. 2008, 22(3): 181-190.
11. Li G H. An active synchronization for two modified chua circuits. *Chinese Physics B*. 2005, 14(3): 472-475.
12. Shih Y L, Zheng M G. Generalized synchronization of chaotic systems with different order by fuzzy logic constant controller. *Expert Systems with Applications*. 2011, 38(3): 2302-2310.
13. Yau H T, Yan J J. Design of sliding mode controller for Lorenz chaotic system with nonlinear input. *Chaos, Solitons and Fractals*. 2004, 19(4): 891-898.
14. Shahverdiev E M, Sivaprakasam S, Shore K A. Lag synchronization in time-delayed systems. *Physics Letters A*. 2002, 292(6): 320-324.
15. Xue W, Li Y L, Cang S J, Jia H Y, Wang Z H. Chaotic behavior and circuit implementation of a fractional-order permanent magnet synchronous motor model. *Journal of the Franklin Institute*. 2015, 352: 2887-2898.
16. Matignon D. Stability results for fractional differential equations with application to control processing. In *Computational Engineering in Systems and Application multiconference, Lille*. 1996, 2: 963-968.

Analog Circuit Implementation and Full State Observation of Chua's Circuit

Hong Niu

*College of Electronic Information and Automation, Tianjin University of Science & Technology
80 Mailbox, Tianjin University of Science & Technology, No. 1038 Dagu Nanlu, Hexi District, Tianjin, China 300222*

Dongcheng Tan

*College of Electronic Information and Automation, Tianjin University of Science & Technology
Tianjin, 300222, China*

Yongjun Wu

*College of Electronic Information and Automation, Tianjin University of Science & Technology
Tianjin, 300222, China
E-mail: spots@163.com
www.tust.edu.cn*

Abstract

In this paper, an inductance simulator and a nonlinear resistor, which are constructed by operational amplifiers and resistors, are applied to complete the analog circuit implementation of Chua's circuit as well as improve the accuracy of circuit parameters. For the observation of all variables, the state variable z , which represents the product of the linear resistance and the inductor current in Chua's circuit, should be observed even if it is not an actual measurable physical quantity. It is found that z can be obtained via scaling of the voltage of the resistor in the inductance simulator. The real chaotic curves generated from the analog Chua's circuit are displayed on the oscilloscope clearly and correctly. It demonstrates that the realization of Chua's circuit is correct and available for other research such as chaos synchronization of Chua's circuits.

Keywords: Chua's circuit; inductance simulator; circuit implementation; scaling; full state observation

1. Introduction

Chua's circuit was introduced in 1983 by Leon Ong Chua.¹ It is a three-dimensional autonomous electronic circuit that exhibits classic chaos behavior. Because Chua's circuit has rich chaotic dynamics and a simple circuit structure, it has been one of the best chaotic circuits for experimental observation and study.²⁻⁶

In Ref. 7 and Ref. 8, hybrid realizations of Chua's circuit, combining the circuit topologies proposed for nonlinear resistor and inductor element, are presented. However, there is no study on how to observe the state variable $z= Ri_L$ which represents the product of the

resistance R and the inductor current i_L . In this paper, Chua's circuit will be implemented by an inductance simulator and a piecewise linear resistor consisting of six resistors and two operational amplifiers, as shown in Ref. 8. Moreover, the variable z will be obtained via scaling of the voltage of the resistor in the inductance simulator to show the chaotic attractors of Chua's circuit completely.

2. Chua's Circuit

Chua's circuit consists of two capacitors, one inductor, one linear resistor and one nonlinear resistor named Chua's diode, as shown in Fig. 1. The inductance,

resistance, and capacitances respectively are $L = 21.83$ mH, $R = 1.875$ k Ω , $C_1 = 10$ nF and $C_2 = 100$ nF.

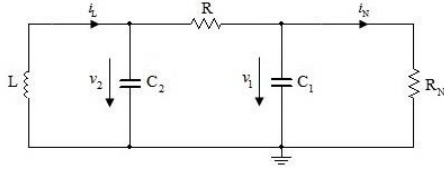


Fig. 1. Chua's circuit

The dynamic equation of Chua's circuit is represented as

$$\begin{aligned}\dot{x} &= \alpha [y - x - h(x)], \\ \dot{y} &= x - y + z, \\ \dot{z} &= -\beta y.\end{aligned}$$

Where $\alpha = C_2/C_1 = 10$, $\beta = (R^2 C_2)/L = 16.1$, and

$$h(x) = m_1 x + \frac{1}{2} (m_0 - m_1) [|x + E| - |x - E|].$$

Where $E=1.1$, $m_0 = -1.4205$, and $m_1 = -0.7671$.

Let the initial values of Chua's circuit be $(x_0, y_0, z_0) = (0.1, 0.2, 0.5)$, then the Lyapunov exponents are $\lambda_1 = 0.3193 > 0$, $\lambda_2 = -0.0001 \approx 0$ and $\lambda_3 = -3.1683 < 0$. It indicates that the system is chaotic. The simulation phase portraits of Chua's circuit are shown in Fig. 3(a1)-(a3).

3. Implementation of Chua's Circuit

3.1. Inductance simulator

Because the internal resistance of an ordinary inductor is too large and the inductance is difficult to alter, it is not suitable to put an ordinary inductor in a chaotic circuit which is very sensitive to the parameters. Hence, an inductance simulator should be used to construct Chua's circuit instead of an ordinary inductor.⁶⁻⁸ The equivalent circuit of the inductance simulator is shown in the left dashed box of Fig. 2, where $R_1 = R_2 = R_3 = 1$ k Ω , $R_4 = 2.183$ k Ω and $C_5 = 10$ nF. The operational amplifiers used in this paper are TL082CP and their supply voltages are ± 9 V, so that their output saturation voltage is 8.3V. The inductance simulator has no

equivalent internal resistance, and its inductance is easy to adjust.

Assume that the currents through the resistors R_1, R_2, R_3, R_4 and the capacitor C_5 respectively are i_1, i_2, i_3, i_4 and i_5 , whose reference directions are all from top to bottom. When the operational amplifiers U1A and U1B are being operated in linear mode, it is obtained that

$$i_2 = i_3, i_4 = i_5, i_1 R_1 = -i_2 R_2, i_3 R_3 = -i_5 (1/j\omega C_5).$$

By solving the equations above, the relationship between the currents i_1 and i_4 is expressed as

$$i_4 = (j\omega R_1 R_3 C_5 / R_2) i_1.$$

According to the definition of two-terminal network impedance, the equivalent impedance of the inductance simulator is

$$Z = i_4 R_4 / i_1 = j\omega R_1 R_3 R_4 C_5 / R_2 \rightarrow L = 21.83 \text{ mH}.$$

As a result, the desired inductance is obtainable by adjusting the resistance of the resistor R_4 .

3.2. Chua's diode

Chua's diode consists of two operational amplifiers U2A, U2B and six resistors, as shown in the right dotted box of Fig. 2. The resistances are $R_6 = R_7 = 22$ k Ω , $R_8 = 3.3$ k Ω , $R_9 = R_{10} = 220$ Ω and $R_{11} = 2.2$ k Ω . The design procedure of Chua's diode's equivalent circuit can be found in detail in Ref. 6.

3.3. Realization of Chua's circuit

Chua's circuit is implemented by replacing the ordinary inductor and Chua's diode shown in Fig. 1 with the inductance simulator and the equivalent circuit of Chua's diode. The whole analog Chua's circuit is presented in Fig. 2.

4. Phase Portraits of Chua's Circuit

4.1. Observation of state variable z

For the observation of all variables of Chua's circuit, the state variable $z = Ri_L$ should be observed even if it is not an actual measurable physical quantity. The observation circuit of z consists of four operational amplifiers U3A, U3B, U4A, U4B and some related resistors, as shown in

Fig. 2. The resistances are $R_{12} = R_{13} = R_{14} = R_{15} = R_{16} = R_{18} = 10 \text{ k}\Omega$, and the resistance of the resistor R_{17} is variable.

The relationship between the voltage u_{R1} and the state variable z can be described as

$$i_L = -i_1 \rightarrow z = Ri_L = -\frac{R}{R_1} u_{R1} = -\frac{R_{17}}{R_{16}} u_{R1}.$$

Thus, the design procedure of the observation circuit can be divided into three parts. Firstly, U3A and U3B are two input voltage followers used to get the potentials of both ends of R_1 . Secondly, U4A and the resistors R_{12} - R_{15} constitute the differential input proportion operational circuit used to work out the voltage u_{R1} . Finally, the state variable z can be obtained from the output of the inverse proportion operational circuit consisting of U4B and the resistors R_{16} and R_{17} . Furthermore, the operational amplifiers U3A and U3B can also insulate the main Chua's circuit from impact of the observation circuit.

It is found that some peak (valley) values of z are larger than the output saturation voltage of the operational amplifier by numerical simulation, such that the cut-off (saturation) distortion will occur when observing the experiment phase portraits of x - z and y - z on the oscilloscope. Hence, scaling of z should be performed. Adjust the resistance of the resistor R_{17} to $R_{17} = 14.77 \text{ k}\Omega$, then the distortions will no longer occur. Consequently, the experiment value of z is about 0.8 times its simulation value. For a convenient comparison, the simulation value of z is adjusted to 0.8 times its original value in Fig. 3(a2)-(a3).

4.2. Comparison of simulation and experiment phase portraits

The experiment phase portraits of Chua's circuit are shown in Fig. 3(b1)-(b3). The scales of x , y and z are 2 V/Div, 0.5 V/Div and 2 V/Div, respectively. By comparing figures (b1)-(b3) with (a1)-(a3), it can be confirmed that here is a good qualitative agreement between the numerical simulation and the experimental realization. It demonstrates that the realization of Chua's circuit is correct and available for other research such as chaos synchronization of Chua's circuits.

5. Conclusions

The hybrid analog circuit implementation of Chua's circuit, which exploits the circuit topologies for the inductor element and nonlinear resistor, is proposed in this paper. The observation circuit for the directly nonmeasurable variable z is also designed for comprehensive investigation of the chaotic attractors of Chua's circuit. It is necessary to observe all chaotic state variables, especially for full state chaos synchronization. For example, in synchronization physical test of two identical three-dimensional chaotic circuits, the assumption that all three states would synchronize as long as two of them synchronized may be incorrect, so that all of the states generated from the circuits should be investigated to verify the synchronization phenomena. Therefore, the study in this paper has some engineering significance.

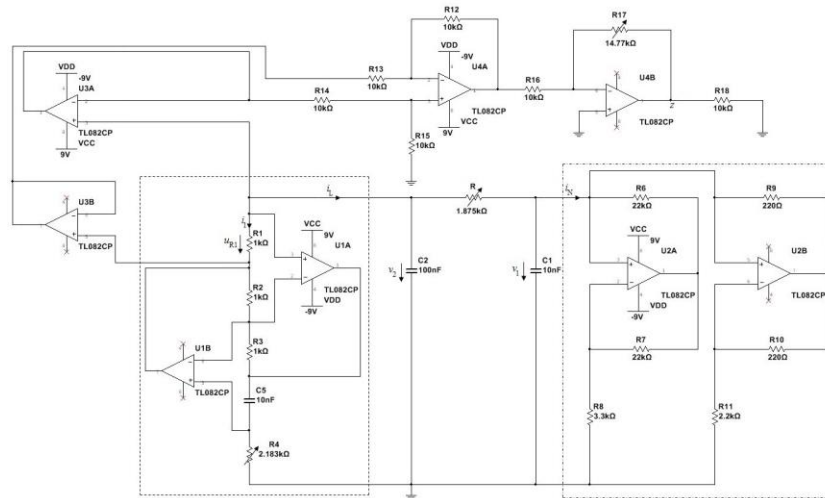


Fig. 2. Analog Chua's circuit

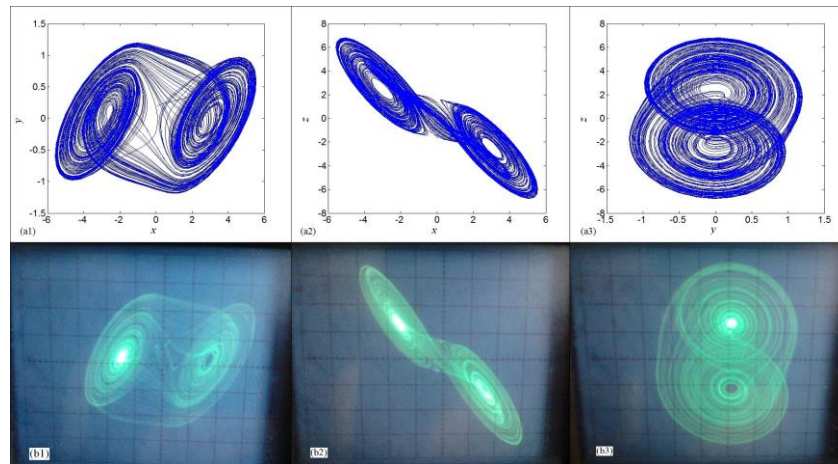


Fig. 3. Comparison of phase portraits: Simulation-Experiment: (a1)-(b1) x - y ; (a2)-(b2) x - z ; (a3)-(b3) y - z

References

1. T. Matsumoto, A chaotic attractor from Chua's circuit, *IEEE Trans. on Circuits and Systems* **31**(12) (1984) 1055–1058.
2. Z. Yang, J. Zhang, Y. Ma, Y. Bai and S. Ma, Design and realization of Chua's circuit based on current conveyers, *Acta Physica Sinica* **59**(5) (2010) 3007–3016.
3. B. Bao, W. Hu, J. Xu, Z. Liu and L. Zou, Analysis and implementation of memristor chaotic circuit, *Acta Physica Sinica* **60**(12) (2011) 63–70.
4. E. Lv and S. Huang, The equivalent circuit design of Chua's circuit and application thereof, *Chinese Journal of Electron Devices* **37**(5) (2014) 891–895.
5. X. Zhang, H. Sun, J. Zhao, J. Liu, Y. Ma and T. Han, Equivalent circuit in function and topology to Chua's circuit and the design methods of these circuits, *Acta Physica Sinica* **63**(20) (2014) 95–102.
6. S. Yu, *Chaotic Systems and Chaotic Circuits: Principle, Design and Its Application in Communications* (XiDian University Publishing House, Xi'an, 2011).
7. R. Kiliç, A comparative study on realization of Chua's circuit: Hybrid realizations of Chua's circuit combining the circuit topologies proposed for Chua's diode and inductor elements, *International Journal of Bifurcation and Chaos* **13**(6) (2003) 1475–1493.
8. H. Liu, F. Jiang, B. Xia and L. Yue, The experiment study of multiscroll chaotic circuit based on a stimulated inductor circuit, *Journal of Northeast Normal University (Natural Science Edition)* **39**(2) (2007) 55–59.

Research on Visualized Rescue Robot

Yuanli Yue, Fengzhi Dai *, Qijia Kang, Pengfei Xie

College of Electronic Information and Automation, Tianjin University of Science and Technology, China

E-mail *: daifz@tust.edu.cn

Abstract

Aimed at the shortcomings of the low efficiency and the limitation of the search and rescue robot, this paper presents a visualized search and rescue robot based on Arduino platform. The infrared detector for searching human body is used to detect lives, and the camera can transmit the information back to the mobile phone or computer terminal in real-time. The track wheel improves the capability of shuttle and over obstacle, and can easily cope with complex terrain. The mounded manipulator can complete many missions, such as clean up the road block and deliver essential supplies to small space. It can replace humans to carry out the task into the dangerous environment and search-and-rescue person into the confined space.

Keywords: visualized, Arduino, track, search-and-rescue

1. Introduction

With the rapid development of science and technology, the application of search and rescue robots become wider ¹. By virtue of superior mobility and well adapt ability in various environments, search and rescue robot have already been paid more and more attention. The search and rescue robot is experiencing rapid development, such as earthquake rescue robots, it is a robot used to search for survivors in the rubble of the underground shopping mall after the earthquake, which is equipped with a color camera, thermography and communication system ². The robot can replace the rescue workers into the dangerous environment, then implement the rescue work and transport the necessary supplies for the trapped persons. Therefore, it is important to develop a rescue robot that can replace or partially replace the relief workers into the unknown environment ³.

Search and rescue robot is different from the household robot or industrial robot. Its working

environment is uncertain or serious. So we have higher requirements for the robot. Search and rescue robots generally have the following advantages ⁴⁻⁵:

1. Walking through the ruins to detect signs of life freely with small size and flexible operation.
2. Having strong adaptability in various environment, which can arrive at the high temperature and high pressure place where the rescue workers cannot arrive in.
3. Being equipped with other functional sensors and detection equipment, such as infrared detector for human body and cameras.
4. Using lithium-ion batteries with low power consumption and strong battery life, so it can work for a long time.

2. Research at home and abroad

Since 1980s, the concept of search and rescue robot has been put forward, then, it gradually plays an irreplaceable role in the rescue activities. The study of search and rescue robots has several stages. One

landmark event is the explosion of the Federal Building in Alfred, Oklahoma in 1995. It is the first time that the search and rescue robots appeared in public ⁶. In 2001, 911 event, which is a case of search and rescue robot actual maneuver. The following agencies to participate in the rescue activities: The SOLEM system in Foster-Milker, the VGTV system in Tolon and the Microtac system in Inuktun. At the same time, many problems of search and rescue robots are exposed, including the choice of the control strategy and the problem of water proofness ⁷.

Since the 911 event, countries step up the pace of research on the rescue robots and set off a new wave of research. Then, research on search and rescue robots have a huge leap. Not only in theoretical and practical aspects, people have made big progress, but also published a lot of research results. And in appearance, functionality and performance, robots are becoming more and more perfect. Then, with the development of the technology and science, the crawler robots, snake-like robots and spider-shaped robots have been appeared.

Owing to the frequent earthquake and tsunami, Japan's search and rescue robot has been at the forefront of the world ⁸. The Japanese spider-shaped robot, by mimicking the spider's movement, the multiple feet are coordinate with each other to complete a variety of actions, or jump over the obstacles. Better than crawler robots or snake-like robots, spider-shaped robots has a greater ability to adapt to the complex environment and to through the narrow space. In a word, it can quickly and efficiently complete the search and rescue mission. The "Asterisk" was developed by Professor Nii Kenzo at the Osaka University in Japan ⁹. Not only the Asterisk's six feet can move on different ground, but also can it be used as a hand to move on the ceiling. Thus, it has a good prospect in the future.

Because of the complexity and the unknown environment, the robot must have better performance. And in order to better completing the search and rescue work, it should have an outside perception, by which it can work fine and transmit the current information in real-time with harsh environment. Therefore, this paper on the basis of studying both at home and abroad, then combined with the advantages and disadvantages of the practical application, we studied a new visualized rescue robot that has a greater ability to adapt to the complex environment and more powerful rescue capability ¹⁰.

3. The overall scheme design of search and rescue robots

Firstly, search and rescue robots enter the rescue scene. Second, gathering the information of the environment. Finally, using the camera to transmit images to mobile phone or computer terminal in real-time by wireless technology. Not only the search and rescue robots should have the ability of adapting to changeable environment, but also need the following functions:

- Collecting parameters in spot environment:

Search and rescue robots arrive at the accident scene to implement missions, which requires robots gathering information accurately and efficiently. The main functions are as follows: capturing motion video, infrared detector for human body and information transmission in real-time.

- Excellent overstepping capability:

Overstepping capability is an important index for search and rescue robot. When a rescue robot encounters obstacles, it can clear obstacles by mechanical arm. If the obstacle is big, it can also cross with a mechanical arm as main origin of force.

- Feedback capability in real-time

Visualization is a major feature of rescue robots, which can send the location information back to the outside world. Therefore, relief workers can get environment information and physical condition of the trapped personnel in real-time. In a word, it can provide more valuable information for the rescuer.

The overall scheme design of search and rescue robots as shown in the Fig.1:

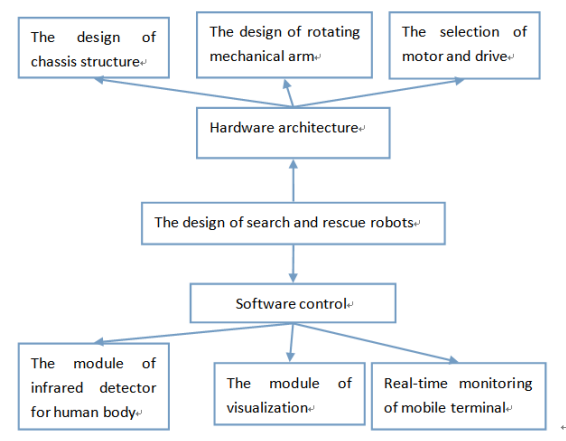


Fig.1 The overall scheme design of search and rescue robots

4. Design of mechanical structure

The mechanical structure design of search and rescue robots includes the design of the car chassis and the design of the manipulator. In the mechanical design process, the main part is car chassis, which determines maneuvering capability and it is important for overstepping obstacles.

Through analyzing the rescue robot chassis, we can conclude that the design is turned up, in the front of the car tracks, with an oblique angle (as shown in Fig 2.), this design can greatly enhance the ability to climb obstacles.

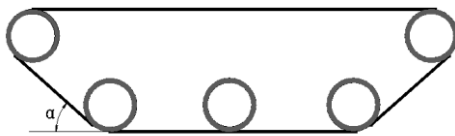


Fig 2. Crawler design of search and rescue robot

The design uses a rhombus frame structure. At the same time, the material selected guarantees the frame's strength as well as lower weight. Thus, in the main bearing part, installing reinforced steel plate to enhance strength. The height of overcoming obstacles is determined by the position of the robot's center of gravity and the length of the track, therefore, we lengthen the length of the track in the design of crawler structure and using symmetrical structure in the design of car body. The crawler mechanical structure has many advantages, such as gripping firmly, improving the ability of climbing and having good ability to overcome obstacles.

5. The circuit control unit

Circuit control unit includes the following sections: main control chip, driving motor, sensing scheme and remote signal transmission module. The sensing scheme includes a variety of sensing modules. For example, rotating machine arm function module, visual operation function module and the human infrared sensor module for detecting life characteristics. Finally, all these modules consist function platform of search and rescue robots.

5.1. Main control chip

The control circuit choose the ATmega128-AU as the main chip, which is used to control and deal with a variety of information from sensors. Its voltage is 3.3-5 V and it has 16M high speed crystal. At the same time, which can provide a high clock frequency. The main control chip have a high processing speed, so it can process the data from sensors more timely and more quickly.

ATmega128 in ATMEL is a CMOS 8 bit microcontroller based on the AVR with low power and high performance. The structure of the AVR is the Harvard, with independent data and program bus. ATmega128 contains EEPROM of 4K bytes, which can meet the needs of the program. The EEPROM as a separate department of data space, which reads and writes processes in bytes. At the same time, the EEPROM's life is at least 100000 times. The point of ATmega128 SCM and main control chips shown in the Fig 3.

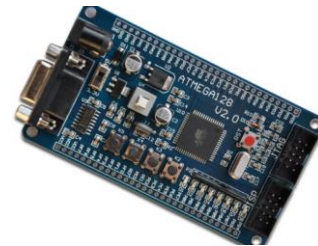


Fig 3. Main control chip

5.2. Motor selection

The motor provides power for the whole search and rescue robot. Through the motor mutual cooperation, it can complete a variety of different actions. As for motor selection, large torque motor can provide enough power in the progress of moving ahead. Therefore, the robot use 37GB-500 permanent-magnet direct current speed reduction motor, which rated voltage of 1.5-36 V, rated speed of 5-3000 (rpm) and rated torque of 0.02-30 (NM).



Fig 4. DC geared motor

6. Introduction of functional modules

The sensor parameter gathering and human detection are very important aspects in the field of search and rescue robot. With a variety of auxiliary function modules, search and rescue robot can detect the location information and life characteristics of the trapped personnel, by which the rescue work can complete in real time. The data-collection of a single sensor is limited, so that it only gets partial environment information and does not let rescue workers get enough information of the trapped people. Thus, integrating multiple sensors into one piece instead of a single sensor, which has several advantages: enhancing detecting precision, reducing the costs of getting information, improving the intelligence level of search and rescue robots and completing the task in the shortest time.

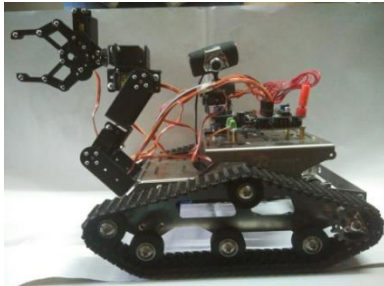


Fig 5. The overall structure figure

6.1. The module of infrared detector for human body

The visualized rescue robot can search and rescue trapped person in dangerous areas or in ruins, therefore, it need to carry the module of infrared detector for human body. In nature, all the objects will appear the phenomenon of infrared spectrum, so long as its absolute temperature exceeds -273°C . Such as: human body, stones, mountains, etc. But they have different wavelengths in the infrared spectrum. According to this natural phenomenon, it can be applied to the search and rescue work. From other sources: Normal body temperature is $36\sim 37^{\circ}\text{C}$ and human body products wavelength of infrared spectrum is $9\sim 10\ \mu\text{m}$. Thus, in the rescue, pyroelectric infrared detector can be used to shorten the search and rescue time and increase the efficiency of search and rescue.

Pyroelectric effect is a polarization phenomenon that pyroelectric crystal will changes with the change of

temperature. When the external alternating infrared radiation shines on pyroelectric crystal, the temperature of the crystal surface will have a significant change, so a strong external electric field is formed. Instead, when the external alternating infrared radiation does not shine on pyroelectric crystal, the temperature of the crystal surface will not have a significant change, so a strong external electric field is not formed. The characteristic of pyroelectric crystal can be applied to detect alternating infrared, but cannot detect the constant infrared. Pyroelectric crystal is generally produce electrical charge, so it needs to be converted into voltage and then put into use. Pyroelectric infrared sensors can detect whether the life exists, because the thickness of the filter is generally $14\sim 8\ \text{m}$, it can cover the body's infrared. Thus, the sensors of infrared detector for human body achieve the effect, detecting human infrared. The sensors of infrared detector for human body as shown in the Fig 6.



Fig 6. The sensors of infrared detector for human body

6.2. Rotating mechanical arm

Search and rescue robot has a six-degree of freedom Rotating mechanical arm, which is an important part for search and rescue robot. When a small obstacle is in front of the robot, it can easily pass it by the rotating mechanical arm. If the obstacle is too big, the mechanical arm helps the crawler to climb. Thus, it has a stronger adaptability in complex environment. The rotating mechanical arm is made up of upper arm, lower arm and rotary frame. Upper arm and lower arm are mounted on the rotating frame by two large torque servo to drive, which has enough strength to carry goods. And when the lower arm moves, there's no need for additional arm operation, handling or cleaning operation can be controlled by a mechanical linkage firmware. The advantage of it is vastly simplifying operational. And the rotating frame is a support part of the whole mechanical arm system, on one side of it is equipped

with a high torque servo for rotating run the entire system.

Some parameters of the rotating mechanical are as follows: The rotating angle can reach on 180 degrees, the gyration radius is 355mm, the maximum height is 460mm (the gripper closed), the maximum of the opening in front of the gripper is 55mm and the widest range of the clipped goods is 98mm. Rotating mechanical arm is shown in the Fig.7.



Fig 7. Rotating mechanical arm

6.3. The function of visualization

Search and rescue robot has a function of visualization. In the upper part of the robot was equipped with two small geared motors that control the camera to move up and down or left and right, which is a major video capture device. The function of visualization is the primary mean to providing the environment information for rescuer in real-time, which we can see the importance of it. The situation of collapsed may be in poor light, thus, using lights may cause secondary damage to the affected people. In order to avoid this situation, the infrared camera is been selected, which with the function of wireless transmission. The model of the camera is SP-H01W (as shown in Fig 8), which wide-angle is 3.6mm and effective distance is 10m. And it has video recording function, which provides valuable data for the disaster relief.

The camera has the following features:

(1) The module of wireless transmission optimizes the H.264 lossless compression arithmetic, this method can decrease the transmission data and time in effect, which ensures high picture quality.

(2) With infrared light, the camera automatically switches between modes of day and night by the IR-CUT. In this way, it can guarantee the accuracy and

clarity in the image transmission when the disaster scene is in poor light.

(3) The camera have the TF card slot in which video and image information can be saved in the rescue and relief operations. Therefore, it is convenient to optimize path in the progress of follow-up succor.

(4) The visual angle rotates 360 degrees and the camera rotates 80 degrees to ensure video capture in narrow space.



Fig 8. Video camera

7. The realization of the overall function

7.1. Selection of rescue route

Since we have finished the construction of Hardware and software platform of search and rescue robot, the last step is to process information from the robot and plan the path to reach to the scene. The information processing style is based on fuzzy reasoning, at the same time, the path planning based on the combination of artificial potential field method and grid method. Ultimately, through the test and analysis of the test results, it can be improved that the search and rescue robot is feasible.

Grid method has some disadvantages. First, the intensity of dividing the grip is difficult to control. Then, in order to accurately represent the location of the robots and obstacles, a large amount of storage space is occupied by much smaller grid granularity. But on the contrary, if the grid size is too large, it will make the robot path planning very inaccurate.

The artificial potential field method raised by Khatib is a virtual method, its basic idea is that we consider the motion of the robot in surrounding environment as a motion in a artificial gravitational field. The target point exerts a gravitational pull, on the contrary, the obstacle exerts repulsion to the mobile

robot. Finally, the movement of the mobile robot is controlled by the resultant force. In the process of search and rescue, to avoid crashing into obstacles and to approach the target gradually, the method is generally smooth and safe. But at the same time, the method has a defect of locally optimum.

The problem of path planning based on the combination of artificial potential field method and grid method. It is obvious that the two can learn from each other. Not only solving the problem of path planning inaccurately caused by grid granularity dividing, but also can we find the exact target coordinates by the artificial potential field method.

7.2. Testing

By the test of the search and rescue robot, the following data is obtained. The maximum height of the barrier crossing is 120 mm, the maximum angle of climbing is 38, the maximum range of detection is a circle of radius 1, and the maximum distance of transmission is 22m. Through the above analysis of the data, which can basically meet the needs of rescue.

8. Conclusion

On the basis of analyzing current robot, a kind of visualized rescue robot was designed. The robot has more perfect functions better than current rescue robot. On the one hand, the design of walking manner is based on the crawler structure with an oblique angle, and cooperate with rotating mechanical arm, which improve the ability of climbing. On the other hand, using camera and the technology of wireless transmission to transmit the image information to the control terminal in real-time. At the same time, with the sensors of infrared detector for human body, the rescue robot can detect the affected person on a wide range, through these functions, the search and rescue robot can achieve timely rescue. In the design, the final step is test, which include the ability of climbing, the accuracy of infrared detector for human body and the relationship between wireless transmission distance and obstacle. Finally, the test result shows that the visualized search and rescue robot have a good ability to overcome obstacles and can basically meet the needs of rescue.

Acknowledgements

The research is partly supported by the Research Fund for the Doctoral Program of Higher Education of China (20131208110005).

References

1. Guohua Xu, Min Tan. The development and tendency of mobile robots. *Robot Technique and Application*, 2001, (3): 7-14.
2. You He, Guohong Wang, Dajin Lu. Multi-sensor information fusion (Continued). *Infrared and Laser Engineering*, 1999, 28(2): 10-15.
3. Yinghui Huo, Lianming Zhang, A path planning algorithm for mobile robot. *Techniques of automation and applications*, 2003, 22(5): 8-10.
4. Lei Li, Tao Ye, etc. The research and future research of mobile robot technology. *Robot*, 2002, 24(5): 475-480.
5. Xiaodong Zhuang, Qingchun Meng. The robot path search method based on fuzzy concept in dynamic environment. *Robot*, 2001, 23(5): 397-399.
6. Jun Wang, Xinhua Huang. Obstacle avoidance control of two wheeled mobile robot based on neural network learning. *Robot*, 1996, 18(5): 292-297.
7. Shiyong Li. The theory of fuzzy control and intelligent control. Harbin Institute of Technology Press, 1999
8. Qingzhong Li, etc. A path planning method for mobile robot based on genetic algorithm. *Pattern Recognition and Artificial Intelligence*. 2002, 15(2): 161-165.
9. Zhiwen Wang, Ge Guo. The present situation and prospect of mobile robot navigation technology. *Robot*, 2003, 25(5): 470-474.
10. Leize Jin, Zhenjun Du, Kaijia. The research on simulation of path planning for mobile robot based on potential field method. *Computer Engineering and Applications*. 2007, 43(24): 226-228.

Development of Training Instrument for Upper Limb Muscle Rehabilitation

Qijia Kang, Fengzhi Dai *, Yuanli Yue, Bo Liu, Hongtao Zhang

College of Electronic Information and Automation, Tianjin University of Science and Technology, China

E-mail *: daifz@tust.edu.cn

Abstract

This equipment can work in multiple degrees. By the single joint and composite motion, it imitates human upper limb movement. Composite motion can be multiple degrees of freedom, so that the equipment can fit with the physiological structure of human body well. Upper limb strength can be recovered efficiently and the muscle contraction can also be well preserved as expected. Obtaining vibration module, it enhances the effect of recovering. Wireless transceiver module makes the wireless monitoring and data wireless transmission be a feasible way. It is connected with the computer, and the recover information of patients could be gathered, analyzed and recorded in computer as well. Data can also be transmitted by the internet, so as to offer the recover information to medical institution.

Keywords: multiple degrees, efficiently, recovering, muscle contraction, training instrument

1. Introduction

With the rapid development of economy, people's living standards have improved significantly since the 21st century. So modern people pay more attention to the improvement of life quality. High incidence of diseases such as apoplectic hemiplegia is seriously threatening the health of human body. How to deal with those ills has become a problem to be solved.

The symptoms of apoplectic hemiplegia mainly embodies in the patient's physical activity, which is that the limbs can't be controlled by the brain. Due to the severity of the disease, the symptoms will show in a variety of sides. The limbs of the most serious cases are completely unable to motion. Some patients only show that physical activity becomes awkward and action becomes inconvenient. The physical activity of others performances worse and worse and due to the untimely recovery treatment, the illness becomes more serious. The clinical manifestations of this kind of patients are

paralysis or half paralyzed. The symptoms are that upper limbs are not controlled by the brain, upper limb activity was blocked, and even lost independent living skills. It can cause muscle belly shortening in a short time, then will harden the soft tissues which are near the muscles and joints and make the joint contracture, over time can lead to loss of muscle contraction function and muscle atrophy. It was called disuse atrophy. It will produce adverse effect on the digestive system and cardiovascular system and worsen the condition. From what has been mentioned above, we can come to the conclusion that it is important to develop the equipment that it can help patients with muscle rehabilitation ¹.

Rehabilitation training not only can effectively alleviate the exacerbation of illness. Insisting for a long time to arm rehabilitation exercise, the patients also can obtain good effect, such as make muscle cross-sectional area increase, the enlargement of muscle fibers. Then can enhance the shoulder muscle strength and muscular endurance and prevent muscle contracture around

shoulder joint ². Muscles exercise can speed up the upper limb blood flow, and indirectly enhances the cardiovascular function, meanwhile, patients can get some relief in psychological and spiritual aspects. Rehabilitation exercise can be divided into the passive motion, the massage movement, the help active movement, the active movement, the resistance movement and so on. The research shows that the guidance of proper upper limb movements and auxiliary recovery can restore upper limb movement, strengthen the upper body strength, repair the damaged motor function and prevent malformation, paralysis and atrophy of upper limbs. Thus, it can play a positive recovery effect.

Upper limb rehabilitation equipment is a kind of modern device which can help paralyzed patients to avoid to lose function of upper limbs and help upper limbs muscle rehabilitation. But this kind of auxiliary recovery equipment research is still in its infancy. There aren't finished products on sale on the market. And most of instrument developed by the researchers at home and abroad has its limitations. There is a lot of difficulty which hasn't been overcome in technical and functional aspects ³⁻⁴. Problems are mainly manifested in the following aspects:

(1) Safety performance. Safety is the primary premise. Safety should be considered firstly in the rehabilitation process. It includes that the limitation of human upper limb movement should be considered. For example, in order to avoid the harmless to human body health, it should be taken into account when rehabilitation equipment is in action group.

(2) The man-machine comfort. For complete relax in the recovery process can help enhance recovery effect, it requires equipment should have good comfort and can't make the patient produces psychological resistance.

(3) Portability. Because the existing recovery area of some hospital is too large, mobility is not convenient, and restricted by regional recovery process, Patients need spend too much time and energy on treatment. Those require that the recovery equipment should be in small shape, easy to move, recover at home and save time and effort.

(4) Working time. Because the recovery equipment need motor to drive the human upper limb and cost more power, the arm recovery equipment need have

long life battery and ensure the recovery time meet the requirements.

2. Research of the field

Many experts from elite schools domestic and overseas have done a lot of researches about the upper limb rehabilitation equipment ⁵. Such as the six degree of freedom robot ROBOTHERAPIST designed by Takehito Kiuchi team from Osaka University. The whole robot use external traction structure, through measuring the hand position of patients, it couple back training information, patients can also have access to movement information through screen with the virtual reality technology. This robot can make patients recover preferably, and add more interest into recover training. But the cost of manufacture is too high to popularize to public, it's more suitable to deploy in professional places such as hospital.

Helparm rehabilitation equipment produced by Kinsman company ⁶, use pulley winded by wire rope to motive patient upper limb to achieve rehabilitation training. With simple structure, each side of patients can be trained partly, it has strong controllability, which make it easy to achieve rehabilitation training at home or in community. The defect is it's hard to control and can only provide several movements, which can't make a full recovery.

3. Design of mechanical structure

Upper limb auxiliary recovery equipment should have sufficient strength, and can withstand the pressure of human arm and pulling force. In the aspect of material selection, use the high strength aluminum plate, and use organic glass in upper limbs fixed place. Organic glass plate is bent into a radian. The radian which accords with human body upper limb physiological radian makes patients without the feeling of discomfort after tighten the arm. Recovery device based on a chair. It gives patients a more comfortable experience. In order to make patients in rehabilitation has the best effect, mechanical structure was designed into the shape of human upper limb exoskeleton to making it easier for upper limb when fixed.

The designed machinery structure considered the actual situation of different patients. In order to meet the different needs, can adjust the length of the forearm and

the big arm with more holes on the fittings. There also design the adjustable artifacts, which can slightly adjust in the design of the shoulder. A rough adjustment is controlled by a set of three cross slide guide rail. Stepper motor provides power supply, which by remote control can automatically adjust. The design meets the different patients demand, making it to have a wider range of use.

The hardware structure of the mechanical structure parts takes the design of the stationary. For small land occupation, the whole hardware of device fixed on the seat. On the design of some adjustable parts innovate boldly, by adjust the spacing and density of drilling hole to achieve the adjustment of dimension. 3 d figure of the overall and local figure as shown in figure 2-1, 2-2 and 2-3. Material selection is 6 mm thick aluminum plate. The density of aluminum plate $\rho = 2700 \text{ (kg/m}^3\text{)}$. Take the person of weight 75 kg, height 75 cm as an example by check data. The weight of Human upper limb a single arm materials is about 3.5 kg⁷. Through the data calculation and finite element analysis, 6 mm thick aluminum plate can support the weight of the human upper limb and meet the required strength requirements. Three-dimensional structure are shown in Fig 1.

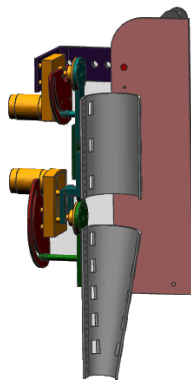


Fig 1. Three-dimensional structure

4. Research on human upper limb rehabilitation equipment

4.1. Review of circuit system

In the aspect of software: Synthetically analyzing the strength needed by the human upper limbs and calculating the steering engine power and torque need output pulse signal to control steering gear rotation.

© The 2016 International Conference on Artificial Life and Robotics (ICAROB 2016), Jan. 29-31, Okinawa Convention Center, Okinawa, Japan

Need low speed large torque in the rehabilitation process .Large torque servo provide tangential force to do twist motion, generate bigger torque in a smaller space and provide convenience for shoulder structure design .The large steering engine is used to complete the training of rehabilitation.

4.2. Construction of circuit system

In the aspect of electric system's control: Master control chip is Freescale 32-bit Kinetis (ARM Cortex - the M4) micro controller .It has the advantages of high performance, low cost and low power consumption .The steering gear control panel is used on the control and execution of the action. The steering gear control panel can provide more accurate rotation Angle. Realize the communication between the servo control board and the stm32 chip. In the servo control board keep several sets of action in advance. When the steering gear control panel and stm32 chip make communication each other, draw on the inner recovery process according to the demand of the patients. There have set a few buttons on the back of arm recovery equipment. Family members of patients or doctors can choose different rehabilitation movement patterns according to the needs. The function of control system as shown in Fig 2.

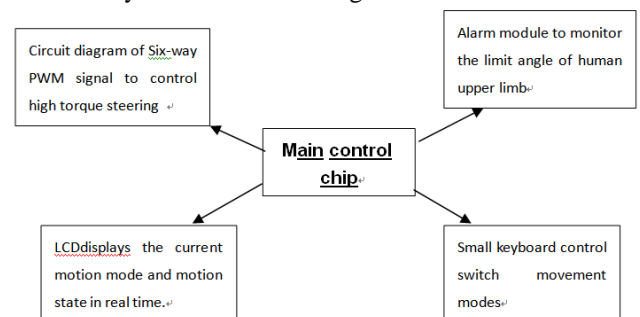


Fig 2. The function of control system

4.3. Limit size of upper limb

The upper limb rehabilitation equipment is designed to help patients recover in a safe and comfortable way, as a result, the extreme dimension is necessary while designing in case injury may happen during training. Through consulting data the author found: In the human body, the limit of the physiological structure of the upper limb of is 80°~90°.When the degree is based on the upright standing human body with arm dropping, the angle of lifting arm upward is 170°and extending arm

backward is 40° . The range of swing arms left and right is 70° to 60° . In order to prevent accident that do harm to the patient during the recovery process, we must set aside scope of safety margin during compile program of rehabilitation action. Setting the security range (should not exceed the limit angle) is as follows: the range of lifting arm upward is $0^\circ \sim 130^\circ$ and extending arm backward is $0^\circ \sim 10^\circ$ and the range of swing arms left and right is $0^\circ \sim 30^\circ$. It must fit with the physiological characteristics of human body at the same time, and refer to the dimension of human upper limb and range of motion of the body.

4.4. Realize alarm function

Upper limb rehabilitation auxiliary equipment also has the function of ultralimit alarming. When the duty cycle adjusts the output, it may be result steering rotational angle is too large from adjusting the duty cycle is too large. Thus, it will lead to accidents if it is beyond the scope of the human upper limb. According to the human upper limb medical data, we pre-configured angular range of human upper limb movement in the mechanical design and program. In the recovery process, if the equipment will exceed the limited data, the angle monitor will detect the change. As the same time, it will send the feedback to the main control chip, and then trigger the alarm to prevent the action. It makes the equipment keep in a safe range and prevent damage to patients. In a word, the mode of automatic alarm and reset has a protective effect on patients and enhances safety performance. The main function as shown in Fig 3.

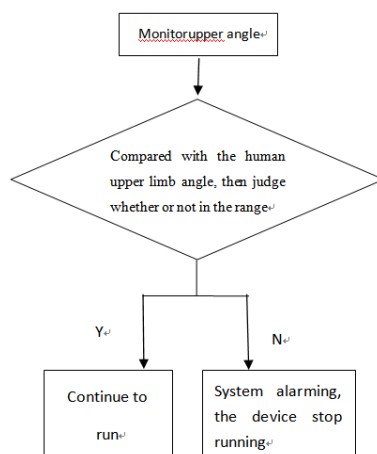


Fig 3. The main function

4.5. Current and voltage

At the same time, Aiming at different voltage requirements of chip and motor in the system, adopt the power supply method of different lines with different voltage. In the aspect of power supply, high-power, multi-voltage output switching power supply as the power supply equipment, chip with 5V voltage of power supply, motor power supply with 12V voltage. those not only meet the requirements of the voltage of the motor, make the motor has enough energy to drive the upper limb movement, but also can satisfy the requirement of the chip safe voltage^[8]. Equipment as shown in Fig 4.

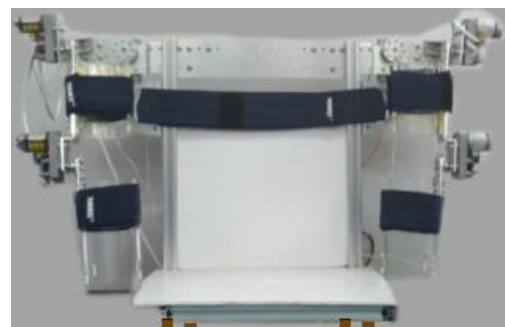


Fig 4. Equipment

4.6. LCD and data transmission

Upper limb rehabilitation system is equipped with liquid crystal display, which not only can display the current patterns, exercise and other information, but also show that the rehabilitation training time and rehabilitation action group. The design so as to patients and their family members can better understand the current state of motion and reasonably arrange rehabilitation exercise group, training time and intensity of training. LCD shown in Fig 5.



Fig 5. LCD shown

The equipment is different from the traditional device. It is equipped with vibration module, in the recovery process, the vibrating plate is attached to the patient's arm by the control unit to control it. It can stimulate the patient's muscles, blood circulation and peripheral nerve, at the same time, combined with the recovery design of professional doctors. Then you can achieve better and faster recovery of upper limb motor function.

The wireless transceiver module, which is introduced in the device, can realize wireless monitoring and wireless transmission of motion data. By the module, the doctor can monitor remotely the patient's motion state, and change the program in real time. The computer terminal equipment can summarize and analyze the recovery information of patients, and can record the recovery of patients, which helps medical workers to analyze and improve the action group. It provides the basis for the record of the rehabilitation data and provides the basis for the future data processing, by the Internet, it can provide rehabilitation data for medical institutions.

5. Medical foundation of upper limb rehabilitation

The movement of the human body shoulder joint is accomplished by movement of the arm movement. To design a reasonable shoulder joint rehabilitation training plan, need to analyze the mode of Human arm motion. According to the theory of the human anatomy, when the body vertically stands on the ground, call the axis which is perpendicular to the ground and through the body vertical axis, call the axis which through the body of the front and rear and is perpendicular to vertical axis sagittal axis, call the axis which through the body and is perpendicular to the above two axes coronal axis. The human body is divided into three planes by the human anatomy. They are defined as:

- Horizontal plane (cross section): It parallels to the ground and through the sagittal axial and coronal axis. The plane divides the human body into Upper and lower two parts.
- Coronal plane (frontal plane): It is perpendicular to the sagittal axis and through the coronary axis and vertical axis. The plane divides the human body into front and back two parts.
- Sagittal plane (longitudinal section): It is perpendicular to coronal axis and through the

sagittal axis and vertical axis. The plane divides the human body into left and right two parts.

The shoulder joint motion is defined into three kinds: flexion and extension movement, outreach and adduction movement and extorsion and intorsion movement by Human anatomy⁹.

(1) Flexion and extension movement: Arms move around the coronary axis in the sagittal plane. Forward is flexion. Backward is extension.

(2) Outreach and adduction movement: Arms move around sagittal axis in the coronal plane. Away from the trunk is outreach. Near the trunk is adduction.

(3) Extorsion and intorsion movement: Arms move around the vertical axis movement in the horizontal plane. Away from the trunk is extorsion. Near the trunk is intorsion.

Upper limb movement is divided into two categories in accordance with degree of freedom of the movement.

(1) Single joint movement

Single joint movement is only a single joint training, such as the elbow bend and stretch. It is a training methods which is adopted in the early stages of the rehabilitation training, or to improve the strength of a particular muscle group. The way of movement is simple. The purpose is clearer. It can strengthen the impression of the nervous system to specific actions and promote the rapid recovery of neural function.

(2) Compound movement

Compound movement is the most popular way in rehabilitation exercise. Patients' muscle groups must be achieved through multiple joints movement, and multi-joint muscle in the majority in the joints and muscles. So the compound training must be conducted: compound movement can exercise the coordination of muscle, and the control of multiple muscle groups. Compound movement mainly adopt the way of a specific task to achieve, such as take water glass to drink. This series of composite action, must pass through joint movement to achieve. At the same time, treat patients from the psychological and improve the rehabilitation confidence of patients. It must be very careful when composite motion do, avoid muscle damage.

For normal human upper limb movement, the brain controls the upper limb different muscle contraction in order to realize the upper limb movement, then complete a series of actions. Upper auxiliary

rehabilitation equipment according to the human upper limbs motion common action to drive the upper limb muscle contraction and expansion. Action group is divided into different movement patterns: the horizontal motion model, the vertical movement patterns and stretching model. Different patterns train different muscle tissue. This can get better effect.

6. Conclusion

Upper secondary recovery equipment is a kind of for upper limb movement disorder patients recovery equipment. The recovery equipment based on the analysis of the human body of medical knowledge, mechanical structure design, and the construction of the circuit system, combined with the test data and so on comes out the conclusion. Through mode selection for designed recovery actions in advance group then moves to restore, restored information real-time display on the LCD screen.

The innovation points of this paper is to design the adjustable mechanical structure and recovery of real-time display. This device can replace physical therapy for patients with rehabilitation massage in some degree, achieve the effect of upper limb rehabilitation. At the same time, consider the characteristics of less occupied area, easy to move and portable. Therefore the rehabilitation equipment made into the shape of a chair. In order to reduce the cost of production, adopt standard parts as far as possible in the meantime. with 24V safe voltage, make it safe and reliable to use.

Synthetically consider arm recovery equipment simplicity, aesthetics, and security of human body recovery and comfort of the design. Ultimately determines the design of upper limbs restoration equipment:

(1) From a security perspective come out the extreme dimension of human upper limb. With alarm device to monitor the data.

(2) From the point to achieve the best recovery effect, design different action group to implement the recovery of upper limb different muscles.

(3) From the humanistic perspective, the display screen shows the currently executing movement patterns and can be adjusted and chosen according to need.

In this paper, the design of upper limbs restoration equipment adopted a large number of aluminum and its standard fittings in structural design. Under the premise

of meeting the structure and strength requirement, greatly reduced the quality of ontology and control the manufacturing cost. Equipment test result and the effect of human movement experiment of upper limbs to restore movement basically corresponds. It shows that the design of the upper limbs restoration equipment structure design is reasonable. In the design of the upper limbs restoration movement groups, can achieve the effect of upper limbs to restore, feel safe and comfortable and provide certain help for upper limb disorders.

Acknowledgements

The research is partly supported by the Research Fund for the Doctoral Program of Higher Education of China (20131208110005).

References

1. Yonglian Zhu, Ruihua Wang, Dinghua Fang, Neurorehabilitation, BeiJing, People's Military Medical Publisher, 2001
2. Ming Yang, Research on rehabilitation training device of elbow join. Wu Han, Huazhong University of Science and Technology, 2008
3. Yuchuan Hu, Linhong Ji. Discussion on the design of rehabilitation training robot for upper limb rehabilitation from the medical point of view. Chinese Journal of Clinical Rehabilitation, 8(34): 7754-7756
4. Hesheng Wang, Yunhui Liu, Dongxiang Zhou. Adaptive Visual Servoing Using Point and Line Features With an Uncalibrated Eye-in-Hand Camera, IEEE TRANSACTIONS ON ROBOTICS VOL. 24, NO. 4, AUGUST 2008
5. Feng Cai. Design and research of shoulder joint rehabilitation training robot. Dalian, Dalian Jiaotong University, 2012
6. Dequan Guo, Hui Ju, Yuqin Yao. Research of Manipulator Motion Planning Algorithm Based on Vision. 2009 Sixth International Conference on Fuzzy Systems and Knowledge Discovery. 2009
7. GB1000-88. Human dimensions of Chinese adults. Beijing: China Standards Press, 1988
8. Zhiyan Jin. Rehabilitation nursing of stroke patients with hemiplegia. Journal of Clinical Nursing, 2006, 4: 5-2.
9. Qiaoyun Li. Rehabilitation nursing of patients with hemiplegia shoulder. Journal of Changzhi Medical College, 2000, 3:14.

Haptic system with fuzzy controller for extended control of Teleoperation mine detector wheeled robots

Yekkehfallah Majid

School of electronic and information engineering, Xi'an Jiaotong University, Xi'an 710049, China

Yuanli Cai ,Guao Yang, Naebi Ahmad, Zolghadr Javad

School of electronic and information engineering, Xi'an Jiaotong University, Xi'an 710049, China

Majid.fallah@stu.xjtu.edu.cn, ylicai@mail.xjtu.edu.cn, gayang@mail.xjtu.edu.cn, ahmad.naebi@stu.xjtu.edu.cn, javad.zolghadr@gmail.com

Abstract

In the tele-operation robots one of the big challenges is operator's error in urgent situations that can make big problem for robot and other systems which working beside the robot. This paper proposes an approach of haptic system and fuzzy logic system with implementation on tele-operation deminer robot, in order to reduce operator's error through fusion of haptic system and fuzzy logic controller, The haptic system convey vibration to user's hand and fuzzy controller, controlled rate of the vibration in different situation to user hand and controlled the speed of the robot.

Keywords: Haptic system, fuzzy logic, deminer robot, vibrotactile, magnetic field.

1. Introduction

Tasks of deminer robot is detecting mine in landmine and marks it with tools mounted on the robot (fig. 1) and rescue robots [1]. Currently robots controlled by human operators [2] with visual display (fig. 2) and operators are limited in their interact with the robot and because of difficult situation and the low threshold for dealing on demine tasks. Minimizing operator's error while care for high level of accuracy and speed is difficult also if operator can't clearly hear or see data from mine detector sensor (MDS) in operator GUI (fig.2) or for some other problem as communication delay between operator and robot so the robot will enter to hazardous region. For these reasons we used vibrotactile feedback according to the level of MDS's output to inform user when robot is near dangerous touch with environment.

Accordingly, we investigated the use of a force three-dimensional joystick for applying forces and vibrations on user hand. This joystick connected to operator computer in (fig. 5) the joystick haptic device also used to control the robot speed and robot navigation [3].

This approach presents a fuzzy logic system (FLS) based force feedback generation method for deminer robots in teleoperation manipulators deminer robot. The approach utilizes the MDS's output and position of arm to generate desire vibrotactile using FLS.

In this paper, we investigated problems of previous work on deminer robot such as safety controlling, communication time delays, communication fail, and operator's error. The structure of this paper is in the following: in section 2 we described completely previous work on demine robot, in section 3 we explained new approach in detail. In section4 where we implemented FLS and haptic system in MATLAB fuzzy tools, while in section 5 we concluded result of implementation in section 4.

2. Background

2.1. Deminer robot

Basically mobile deminer teleoperation robot uses for detection mine in landmine with MDS mounted on

the robot and user controls this robot by joystick, but user just send command to robot by joystick and monitoring robot is through visual display (fig. 2) and sound without any repulsive feedback from MDS in urgent situations.



Fig. 1: photographs of the deminer robot.

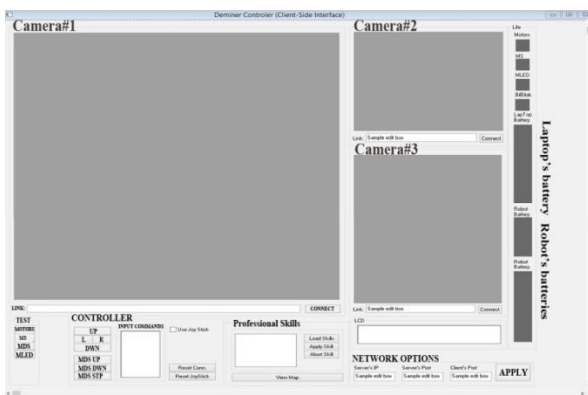


Fig. 2: operator GUI which contained: camera monitoring, robot controller, mine illustrates, network monitoring, robot's batteries status illustrates, laptop's battery status illustrates, motors statues indicators.

This console developed in windows and this is a graphical consol between operator and robot, this console installed in operator computer (fig. 5)

2.2. Mine Detector sensor (MDS)

MDS work on the principle of transmitting a magnetic field and analyzing a return signal from the target and environment. These systems may use a single coil as both transmitter and receiver, or they may have two or even three coils working together. In this project we used two coils first coil is transmitter and second one is receiver signal fig. 3.

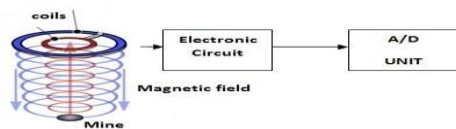


Fig 3: Overall hardware of mine detector sensor

2.3. Electromagnetic induction

As we mentioned before, in this section there are two parts first one is transmitter and second one is receiver we simulated this two coils with FEMM (fig. 4) [4][5]. FEMM is one of power full software that uses for designing and analyzing magnetic problems[6][7].

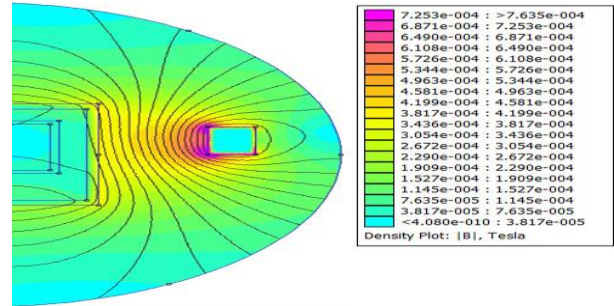


Fig.4: color flux density plot of two coils with mine. we added a mine in analyzed region, most of flux passed through mine because reluctance of mine is smaller than air therefore most flux passed through low reluctance and least flux passed through receiver coil and caused least EMF induced in receiver coil.

3. Haptic system and fuzzy logic controller

3.1 New approach

Our solutions for those problems we mentioned in previous section (2.1) are haptic system and fuzzy logic controller. Haptic system solved feedback problem we suggest two ways for using haptic system in this project the first one is vibrating electric motors in joystick and second suggestion is haptic force three-dimensional joystick (fig.5) actually this joystick is a haptic system contains the vibration electric motors and joystick (fig.5). Haptic increases human sensitivity from environment and user's hand can feel environment through vibrotactile feedback.

The level of vibrotactile with respect to different situations as MDS sense, robot speed and robot's arm status is variable, for controlling level of vibrations and velocity of robot we used fuzzy logic controller.

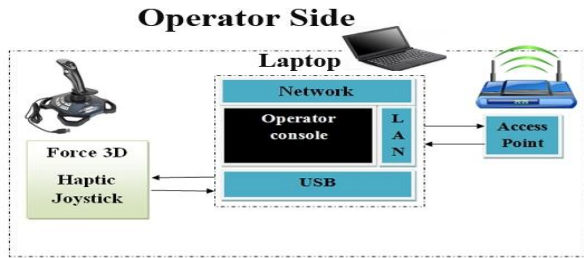


Fig. 5: overall framework of operator side controller. In new approach we added force three dimensional haptic joystick in this part.

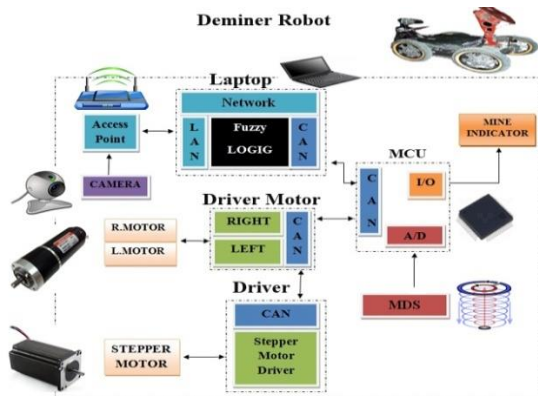


Fig. 6: overall framework of deminer robot.

4. Implementation

Trap membership function used for MDS inputs and outputs in two FLSs, (fig. 8) and (fig. 10). the rule based in this work is shown in Table 1 and Table 2. The commonly used Madman's min-max implication function was utilized. Finally for defuzzification we used centroid technique because it's very accurate. The control surface generated by the rule base and the given fuzzy sets is depicted in (fig. 9) and (fig. 11). Detail of fuzzy logic system could find in literature [8] [9].

4.1. Fuzzy logic system for dealing with haptic system

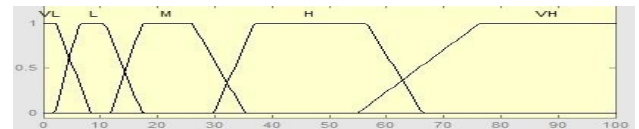
MDS OUTPUT	ARM STATUS	DP	OAP	RTP
VL	VH	M	M	VL
L	H	M	M	VL
M	M	M	M	VL
H	S	M	M	VL
VH	VS	L	L	VL

Table1: Rule table of the vibrotactile controller with respect to MDS output and arm status.

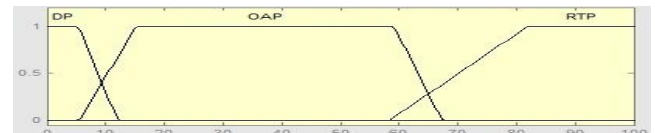
Respectively, they are decomposed into five fuzzy partitions for output, such as very low (VL), low (L), medium (M), high (H), very high (VH), and three partition

for arm status as : Down position (DP), obstacle avoidance position (OAP), rest time position (RTP) in last portions related to vibrotactile signal as: very slow (VS), slow (S), medium (M), fast (F), very fast (VF) and nothing (NOP).

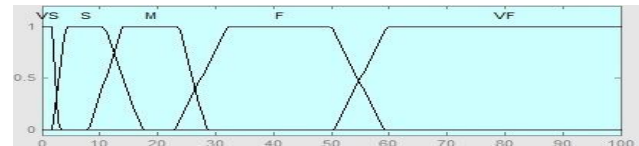
Since one input divided to five fuzzy sets and another one divided to three fuzzy sets, thus fifteen fuzzy rules for vibrotactile controller must be determined. Following the output signal of MDS directly related to distance between coil and mine in the ground therefore when the robot is far from the mine sensed a mine with very low level and fuzzy logic gets the level of the MDS and give very slow vibrotactile to haptic system and haptic system transfer vibration to user hand and user feels mine through vibration.



(a)



(b)



(c)

Fig. 7: (a) membership functions of MDS. (b) Membership functions of arm status. (c) Membership functions of vibrotactile.

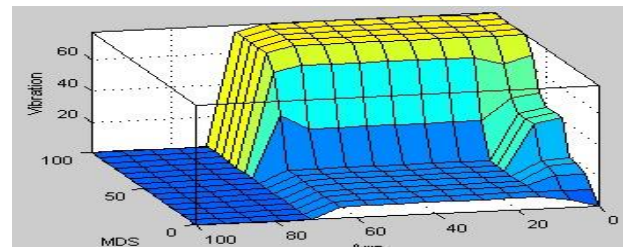


Fig. 8: The output surface of the implemented fuzzy vibrotactile generator.

Three-dimensional curve that represents mapping from MDS and arm to level of the vibration, because this curve represents a two-input and one output case. As this curve is obvious when the arm is in down position and MDS level is increased therefore vibrotactile corresponding with MDS's level increases.

4.2. Fuzzy logic system for velocity controller

This section is similar to section (4.1) inputs of FLS are same as last one just output is different.

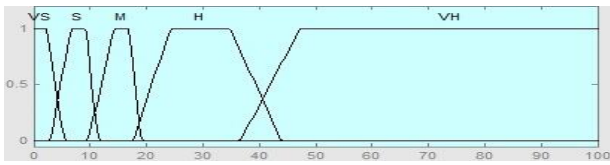


Fig9: Membership function of velocity.

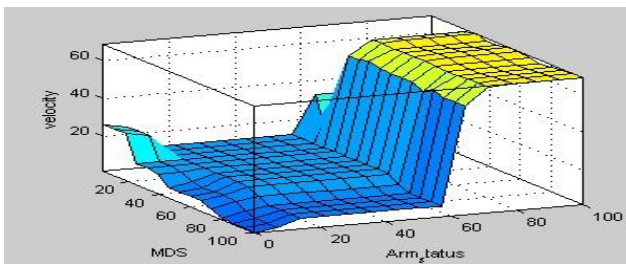


Fig 10: The output surface of the implemented fuzzy velocity controller.

Three-dimensional curve that represents mapping from MDS and arm to robot velocity, because this curve represents, a two-input and one output case. As this curve is obvious when the arm is in down position and MDS level is increasing in other side velocity with respect to MDS's level reduces.

5. CONCLUSION

This paper presented a dynamic, real-time fuzzy logic based force feedback control for deminer robot in remotely operated robot manipulators. The presented method utilizes distance from the mine to the robot, it needs consider two items first one is mine distance to robot and second one is arm's position with respect to these items new approach generates force feedback and control speed of the robot. The presented method was implemented on a deminer robot and for simulate and illustrates result of vibrotactile data and velocity controller we used MATLAB.

The results shows which fuzzy logic controller and haptic system, significantly reduced operator's fault and also fuzzy logic can prevent dangerous contact between the robot and mine when network connection drops, with this method operator drives robot with confidence because this system warned the operator in urgent situation.

6. ACKNOWLEDGMENT

This work supported in part by grant from the XI'AN JIOTONG UNIVERSITY and MRL laboratory of QIAU.

References

- [1] Sibert, John, et al. "Vibrotactile feedback for enhanced control of urban search and rescue robots." *Proceedings of the IEEE International Workshop on Safety, Security and Rescue Robotics*. 2006. Page1
- [2] Smith, F. M., D. K. Backman, and Stephen C. Jacobsen. "Telerobotic manipulator for hazardous environments." *Journal of Robotic Systems* 9.2 (1992): 251-260.
- [3] Pantelios, Michael, et al. "Haptics technology in Educational Applications, a Case Study." *JDIM* 2.4 (2004): 171-178.
- [4] Meeker, David. "FEMM 4.2 Electrostatics Tutorial1." (2006).
- [5] Jin, Jian-Ming. *The finite element method in electromagnetics*. John Wiley & Sons, 2014.
- [6] Turner, Robert. "Gradient coil design: a review of methods." *Magnetic Resonance Imaging* 11.7 (1993): 903-920.
- [7] Singh, Isha, and Rajul Mishra. "Analysis of Magnetic Field of Air Cored Solenoid using FEMM."
- [8] Mizumoto, Masaharu, and Hans-Jürgen Zimmermann. "Comparison of fuzzy reasoning methods." *Fuzzy sets and systems* 8.3 (1982): 253-283.
- [9] Iancu, Ion. *A Mamdani type fuzzy logic controller*. INTECH Open Access Publisher, 2012.

Effects of System Parameters and Controlled Torque on The Dynamics of Rigid-Flexible Robotic Manipulator

Sachindra Mahto

*Mechanical Engineering Department
NERIST, Itanagar, Arunachal Pradesh-791109, India
E-mail: smh@nerist.ac.in
www.nerist.ac.in*

Abstract

This work illustrates the effects of various system parameters on the dynamics of flexible link of revolute-jointed rigid-flexible manipulator. Flexible link is considered as a Euler-Bernoulli beam and finite element based on Lagrange approach is employed for dynamic analysis. A comparative study is carried out for comparative dynamic response for the variation of system parameters and controlled torque excitation.

Keywords: Rigid-flexible revolute manipulator, Euler-Bernoulli beam, Shape optimization, Finite element method, Parametric study

1. Introduction

In the last few decades, dynamics and control of the flexible manipulators have received a considerable research attention. Flexible robotics systems have several advantages over the convention systems. However, due to lightweight of flexible systems, stiffness is low and there is a serious problem of vibration. Sometimes, to retain the advantages of the flexible system, some of the links are made flexible and some are rigid. Still the dynamic behaviour improvement, optimal design and proper control strategy is the research interest for flexible manipulator.

Most of the researchers contributed their works in different ways of dynamic modeling and control aspects of flexible robotic manipulators. Sunada and Dubowsky [1] developed a lumped parameter FEM model for analyzing the complete behavior of industrial robotic manipulator with complex-shape flexible links. Fakuda and Arakawa [2] studied the modeling and dynamic characteristics of two-link flexible robotic arms and controlled the vibration by taking into account

the gravity, payload, and the coupled vibration between the first and second arm. Usoro et al. [3] developed finite element models to describe the deflection of a planar multi-link model. Ower and Vegte [4] used a Lagrangian approach to model the planar motion of a manipulator consisting of two flexible links and two rotary joints. Benati and Morro [5] developed a Lagrangian approach for the dynamics of chain with flexible links..

Bayo [6] used FEM to deal with multi-link flexible manipulator considering Timoshenko beam theory and including nonlinear Coriolis and centrifugal effects for the elastic behavior. Jonker [7] presented a nonlinear finite element based formulation for analyzing the dynamic behavior of flexible manipulators. De Luca and Siciliano [8] presented closed-form equations of motion for planar flexible multi-link robot arm. Morris and Madani [9] studied the accurate modeling based on Lagrange-Euler formulation of a two link flexible manipulators.

Dogan and Iftar [10] carried out the modeling and control of two-link robot manipulator whose first

link is rigid and second link is flexible. Everett et al. [11] showed that it is possible to design a two-link flexible manipulator that has nearly position invariant first natural frequency with wide separation between the first two natural frequencies, to have its behaviour like rigid manipulator. Chen [12] developed a linearized dynamic model for multi-link planar flexible manipulator. Yang et al. [13] studied the tip trajectory tracking control for flexible multi-link manipulator using Lagrangian assumed mode method. Zhang et al. [14] derived a partial differential equation model for a flexible two-link manipulator using Hamilton's principle.

Some researchers presented their works on shape optimization of static/rotating beams. Karihaloo and Niordson [15] determined the optimum tapering of a cantilever beam carrying an end mass to maximize fundamental frequency. Wang [6] addressed optimum design of a single link manipulator to maximize its fundamental frequency. Yoo et al. [17] used the assumed mode method for dynamic modelling of rotating flexible manipulator for modal analysis and shape optimization to increase the fundamental frequency of the beam. Dixit et al. [18] presented a finite element model of single link robotic manipulator for revolute as well as prismatic joint. They used SQP for optimizing beam shapes under different optimization conditions.

From the above survey, it is observed that there is no much research contribution for the effects of system parameters in the dynamics of rigid-flexible robotic manipulator. In this paper, the dynamic behavior of robotic manipulator is presented for the variation of system parameters and improvement through control strategy.

2. Modeling and Solution Technique

The finite element formulation has been adopted here as described by Usoro et al. [3]. Fig. 1(a) shows rigid-flexible manipulator comprised of two links, two joints and tip load. The links are clamped on the joints. Shoulder joint (joint 1) is located at the origin of XOY represents the stationary co-ordinate frame and elbow joint (joint 2) is located at the origin of $X_1O_1Y_1$ and $X_2O_1Y_2$ which represent the moving co-ordinate frames. manipulator is considered slender. Flexible link is

treated as a Euler-Bernoulli beam and gravity force is neglected.

Consider a point P in the i^{th} element on the manipulator at a distance ' x ' from the elbow hub. The point P attains the position P' with respect to inertial frame of reference (XOY) after having rigid body motion $\theta_1(t)$ and $\theta_2(t)$ of shoulder and elbow joint respectively and flexural deflection $w(x, t)$. Flexural deflection $w(x, t)$ of point P is approximated in finite element technique using Hermitian shape functions as

$$w(x, t) = N_1 w_{2i-1} + N_2 w_{2i} + N_3 w_{2i+1} + N_4 w_{2i+2} = [N] \{W\}, \quad (1)$$

where $[N] = [N_1 \ N_2 \ N_3 \ N_4]$

and $\{W\}^T = [w_{2i-1} \ w_{2i} \ w_{2i+1} \ w_{2i+2}]$.

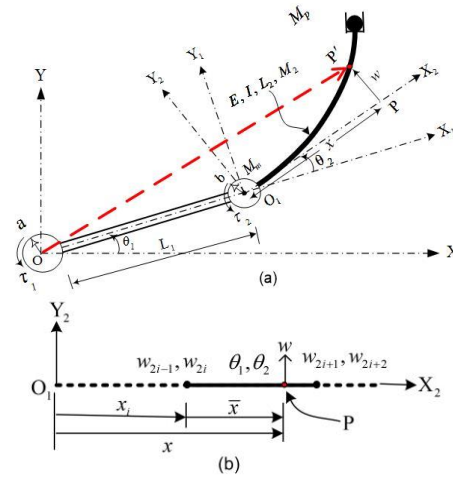


Fig. 1. (a) Configuration of rigid-flexible manipulator, (b) Typical i^{th} element with six dof

In FEM formulation, the manipulator is divided into finite number of elements with each element having six degrees of freedom. Detail of i^{th} element of the link is shown in Fig. 1(b), where θ_1 and θ_2 are the hub rotation of shoulder and elbow joints respectively, w_{2i-1} , w_{2i} and w_{2i+1} , w_{2i+2} are the transverse deflection and slope at the first and second node of the element respectively. The position vector of P' with respect to inertial system XOY is given by Eq. 2. For the prediction of approximate dynamic behaviour of the optimized beams, smaller excitation torque is considered for linearization of system modelling. Global position vector of the point P' under smaller angular and flexural displacement is given by

$$\mathbf{r} = \mathbf{op}' = \begin{bmatrix} X \\ Y \\ 1 \end{bmatrix} = \begin{bmatrix} a + L_1 + b + (i-1)h + \bar{x} \\ (a + L_1)\theta_1 + ((i-1)h + \bar{x} + b)(\theta_1 + \theta_2) + [N] \{W\} \\ 1 \end{bmatrix}, \quad (2)$$

In finite element method, variables are converted into nodal variables.

$$\mathbf{r} = \mathbf{op}' = f(\theta_1, \theta_2, w_{2i-1}, w_{2i}, w_{2i+1}, w_{2i+2}). \quad (3)$$

Let $Z = [\theta_1 \ \theta_2 \ w_{2i-1} \ w_{2i} \ w_{2i+1} \ w_{2i+2}]$, then absolute velocity of the point P of the flexible link is obtained as

$$\frac{\partial \mathbf{r}}{\partial t} = \left[\frac{\partial \mathbf{r}}{\partial Z} \right] \dot{Z}^T. \quad (4)$$

2.1 Kinetic Energy Computation of the Link Element

The Kinetic energy of the i^{th} element of the link is given by

$$K_i^e = \frac{1}{2} \int_0^h m_2 \left[\frac{\partial \mathbf{r}^T}{\partial t} \cdot \frac{\partial \mathbf{r}}{\partial t} \right] d\bar{x}. \quad (5)$$

We have

$$\frac{\partial \mathbf{r}^T}{\partial t} \cdot \frac{\partial \mathbf{r}}{\partial t} = \dot{Z}^T \left[\frac{\partial \mathbf{r}}{\partial Z} \right]^T \left[\frac{\partial \mathbf{r}}{\partial Z} \right] \dot{Z}. \quad (6)$$

Substituting Eq. 10 in Eq. 9, we have

$$K_i^e = \frac{1}{2} \dot{Z}^T \left[\int_0^h m_2 \left[\frac{\partial \mathbf{r}}{\partial Z} \right]^T \cdot \left[\frac{\partial \mathbf{r}}{\partial Z} \right] d\bar{x} \right] \dot{Z}, \quad (7)$$

and the elemental mass matrix is given by

$$M_i^e = \int_0^h m_2 \left[\frac{\partial \mathbf{r}}{\partial Z} \right]^T \cdot \left[\frac{\partial \mathbf{r}}{\partial Z} \right] d\bar{x} \\ M_i^e = \begin{bmatrix} M_{11} & M_{12} & M_{13} & M_{14} & M_{15} & M_{16} \\ M_{21} & M_{22} & M_{23} & M_{24} & M_{25} & M_{26} \\ M_{31} & M_{32} & & & & \\ M_{41} & M_{42} & & P_i(4 \times 4) & & \\ M_{51} & M_{52} & & & & \\ M_{61} & M_{62} & & & & \end{bmatrix}. \quad (8)$$

All the constants of the above matrix in Eq. 8 are obtained by proper integration.

2.2 Elastic Potential Energy of the Link Element

The potential energy of the i^{th} element of link due to elastic deformation is given by

$$V_i^e = \frac{1}{2} \int_0^h EI \left[\frac{\partial^2 w}{\partial x^2} \right]^2 d\bar{x} = \{W\}^T \frac{1}{2} \int_0^h EI \left[N'' \right]^T \left[N'' \right] d\bar{x} \{W\}. \quad (9)$$

Thus, elemental stiffness matrix is given by

$$K_i^e = EI \int_0^h \left[N'' \right]^T \left[N'' \right] d\bar{x} \\ K_i^e = \frac{EI}{h^3} \begin{bmatrix} 0 & 0 & 0 & 0 & 0 & 0 \\ 0 & 0 & 0 & 0 & 0 & 0 \\ 0 & 0 & 12 & 6h & -12 & 6h \\ 0 & 0 & 6h & 4h^2 & -6h & 2h^2 \\ 0 & 0 & -12 & -6h & 12 & -6h \\ 0 & 0 & 6h & 2h^2 & -6h & 4h^2 \end{bmatrix}. \quad (10)$$

2.3 Lagrange's Equation of Motion in Discretized Form

First link is rigid and posses kinetic energy only. However, being second link flexible it posses both kinetic and potential energy. The kinetic energy and the potential energy of the system are obtained by computing energy of rigid link and the energy of each element of the flexible link and then summing over all the elements. The global mass matrix and global stiffness matrix can be obtained as

$$T = \frac{1}{2} [\dot{q}]^T [M] [\dot{q}] \text{ and } V = \frac{1}{2} [q]^T [K] [q] \quad (11)$$

respectively.

Here $[q] = [\theta_1 \ \theta_2 \ w_1 \ w_2 \ \dots \ w_{2n+1} \ w_{2n+2}]$ is the global nodal vector. The Lagrangian of the system is given by $L = T - V$ and then Lagrange's equations of motion of this dynamic system may be written as

$$\frac{\partial}{\partial t} \left[\frac{\partial L}{\partial \dot{q}} \right] - \frac{\partial L}{\partial q} = F_q, \quad (12)$$

where F_q is the generalized force vector. Due to modelling linearization, global mass and stiffness matrices are constant and equation of motion of undamped system is expressed as

$$[M] \{\ddot{q}\} + [K] \{q\} = \{F\}. \quad (13)$$

Global load vector $\{F\}$ and global nodal displacement vector $\{q\}$ for ' n ' number of finite elements are given by $\{F\} = [\tau_1 \ \tau_2 \ 0 \ 0 \dots 0 \ 0]^T$.

3. Optimization Procedure

To retain and optimize the advantage, upper limit of the optimized mass (M^*) is constraint to the prescribed mass (M). In the rigid-flexible robotic system, flexible link is considered for the shape optimization. $X = [d_1 \ d_2 \ \dots \ d_n]^T$ is the design vector with d_i indicating diameter of the i^{th} finite element of link 2.

Table 1. Different Optimization Problems

Optimization Problem/Objective	Constraint
Maximization of fundamental beam frequency	$M^* - M \leq 0$
Permissible Bound : $X^{UB} < X < X^{LB}$	

Minimum and maximum diameter of the beam elements (X) are denoted by X^{LB} , X^{UB} respectively. The MATLAB function “*fmincon*” employing sequential quadratic programming (SQP) technique is used for constrained optimization of nonlinear function.

4. Results and Discussion

Modeling of this system is highly complex and nonlinear in nature. However, linearized model is preferred and considered in this work to predict its approximate dynamic behavior. Structural dimensions of this revolute-jointed rigid-flexible robotic manipulator for numerical experiments are taken as lengths 0.75m and 0.75m, diameters 0.03m and 0.01m, mass densities 2710 kg/m³ and 2710 kg/m³, hub radii 0.02m and 0.01m, hub inertias 0.03 kgm² and 0.03 kgm² for first and second link respectively. Young's modulus 7.11×10^{10} N/m² and mass of the motor 0.1 kg is considered.

Excitation torque $\tau = \tau_m \sin 2\pi t$ Nm is considered for both the joints for 2 seconds action. Torque amplitude 3.0 Nm and 1.0 Nm are considered for shoulder and elbow joints respectively. Static load of 1N is considered at the tip of the manipulator for comparative static beam deflections. The ratio of payload (M_p) to the mass of second link (M_2) is denoted by μ_2 ; ratio of motor mass (M_m) to mass of the first link (L_1) is denoted by μ_1 and ratio of the second link length (L_2) to first link length (L_1) is denoted by (L^*).

4.1 Effects of Different Link Length

As the second link is flexible, its length is varied with respect to the first link length. Effects of variation of

link lengths in its natural frequencies, static tip deflection, hub angles, and dynamic response are plotted in Fig. 2 to Fig. 5. Natural frequencies of the flexible links decrease with increase of its length and vice versa. Static link deflection increases with increase of its length. Hub angles increase with decrease of its length and vice-versa. Residual vibration increases with increase of length of the flexible link.

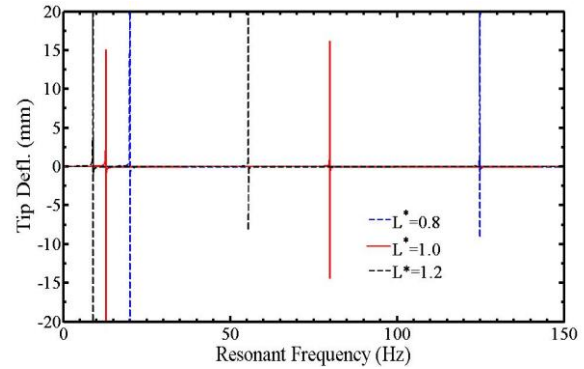


Fig. 2. Beam frequencies of flexible link for different link lengths

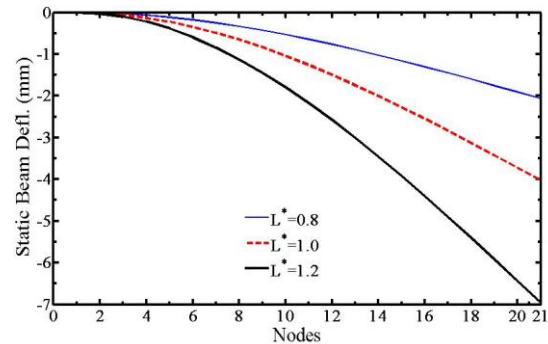


Fig. 3. Static deflection of flexible link due to 1N force at tip for different link lengths

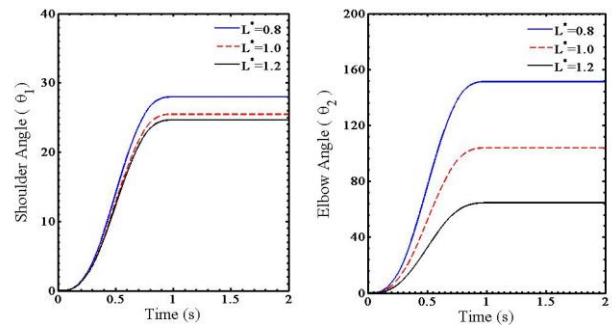


Fig. 4. Hub angles due to excitation torques for different link lengths

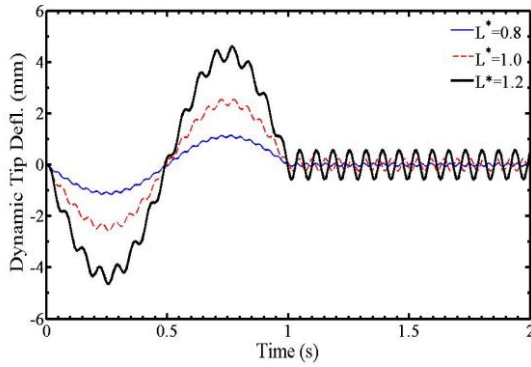


Fig. 5. Vibration residual of the tip of flexible link for different link lengths

4.2 Effects of Different Payload, Motor Mass and Hub Inertia

Robotic system means to take load and due to flexible links, there is always flexural vibration. Changes in the dynamics of the manipulator due to the change of payload, motor mass and hub inertia are plotted in Fig. 6 to Fig. 11. Hub angle decrease and residual vibration of flexible link tip increases with the increase of payload and vice-versa. By increasing the motor mass which is acting as a payload for link 1 has significant effect on shoulder joint angle for a given set of torques but less effect on elbow joint, however residual vibration increases. By increasing the hub-inertia of the shoulder joint, hub angles of shoulder joint decreases and elbow joint increase for a given set of applied torque and very less effect on the residual vibration of the flexible link tip.

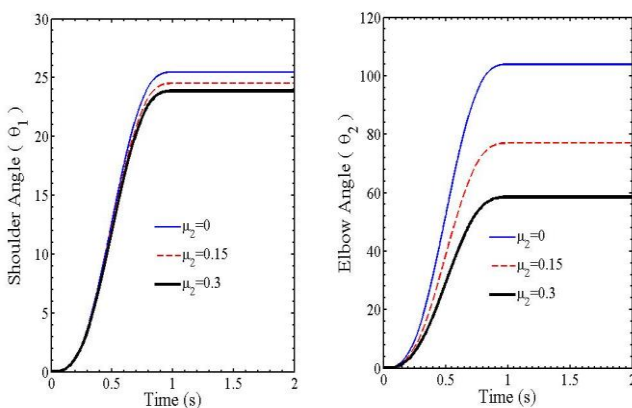


Fig. 6. Hub angles for different payloads for set of applied torques

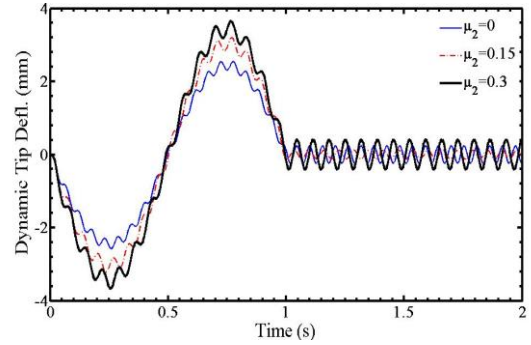


Fig. 7. Dynamic flexible tip deflection for different payloads

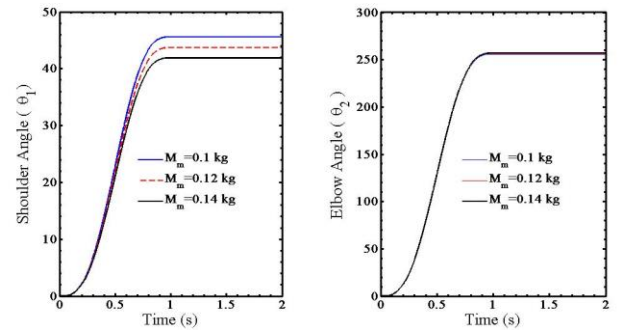


Fig. 8. Hub angles for different motor mass for set of applied torques

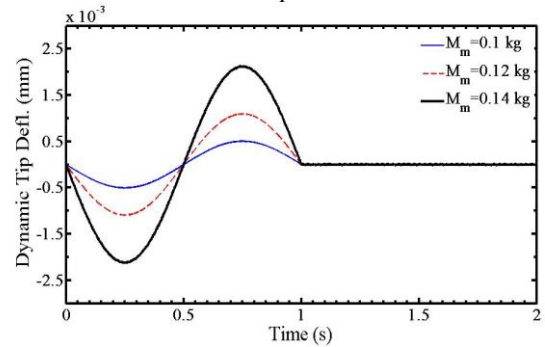


Fig. 9. Dynamic flexible tip deflection for different motor mass

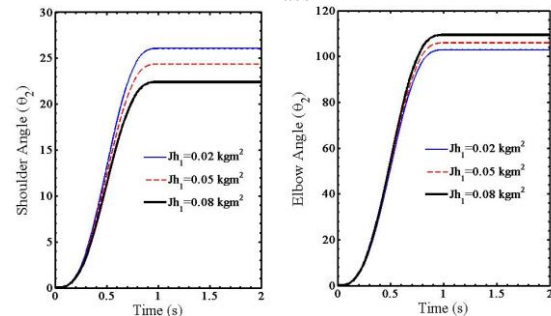


Fig. 10. Hub angles for different hub inertia for set of applied torques

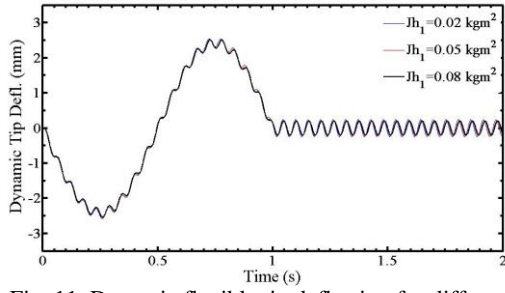


Fig. 11. Dynamic flexible tip deflection for different hub inertia

4.3 Effects of Mass Distribution of Link

Optimal design has a great importance in engineering applications. Shape optimization is done as per the optimization problem (Table 1) to increase the fundamental frequency and the optimized shape of the flexible link is shown in Fig. 12, where the mass of the link is re-distributed. It is observed that mass is concentrated more towards the root side in shape optimization. Static link deflection due to 1N force at tip, natural frequencies of the optimized flexible link are plotted in Fig. 13 and Fig. 14 and its dynamics (hub angles and residual vibration) are plotted in Fig. 15 and Fig. 16 respectively for set of excitation torque. It is observed that parameters *viz.*, static tip deflection, natural frequencies, hub angle and residual vibration are improved.

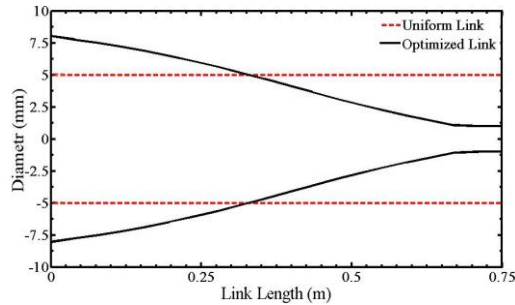


Fig. 12. Optimized shape of flexible link

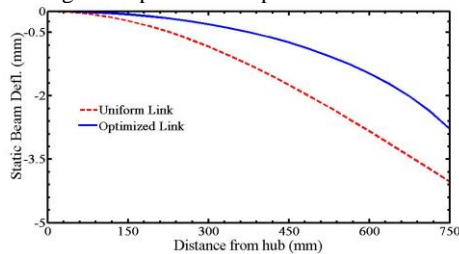


Fig. 13. Static beam deflection due to 1 N force at the tip of optimized link

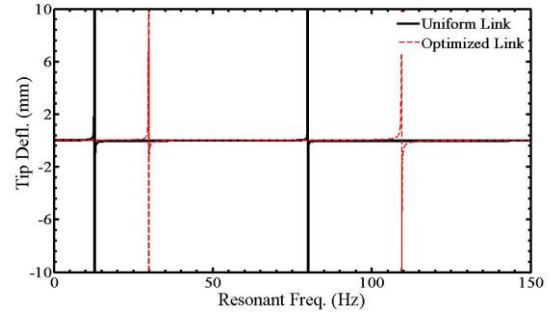


Fig. 14. Comparison of natural frequencies

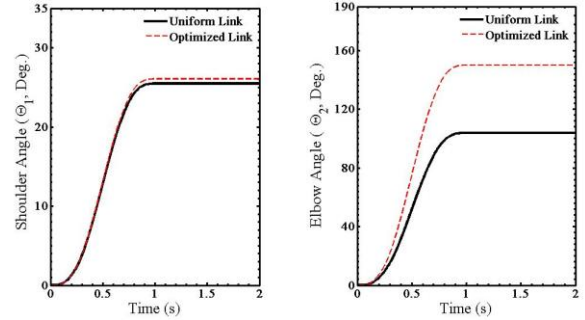


Fig. 15. Comparison of joint angles for set of applied torques

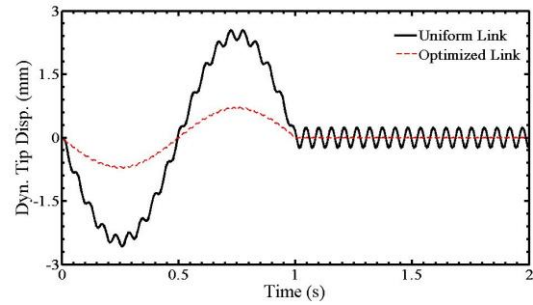


Fig. 16. Comparison of tip residuals for set of applied torques

4.4 Effects of Controlled Torque

Yigit [19] presented the position and derivative (PD) control torque for single link revolute-jointed flexible manipulator as given below

$$\tau_{PD} = -K_p(\theta - \theta_f) - K_v(\dot{\theta}). \quad (14)$$

The feedback gains K_p and K_v depend upon the equivalent rigid system parameters and are expressed as

$$K_p = (J_h + \frac{1}{3}mL^3 + M_pL^2)f_n^2, \quad (15)$$

and

$$K_v = 2(J_h + \frac{1}{3}mL^3 + M_pL^2)f_n. \quad (16)$$

where ' m ' is the mass per unit length, ' L ' is the link length, ' J_h ', ' θ_f ' is the final angular position, and ' f_n ' is the fundamental frequency. PD controller is able to stabilize the system but vibration of the flexible beam can not be controlled. Ge et al. [20] extended the work of Yagit [19] and introduced energy-based robust (EBR) control law and added the nonlinear deflection feedback to improve the performance of the PD controller by adding the nonlinear control term as given by

$$\tau_{EBR} = \tau_{PD} - K_f y(L, t) \int_0^t \dot{\theta}(\sigma) y(L, \sigma) d\sigma, \quad (17)$$

where K_f is the gain constant of robust control, σ is the dummy variable, $\dot{\theta}$ is the hub angular acceleration and y is the deflection at the tips. Above control law is also applicable for multi-link robotic revolute jointed systems.

Elbow angle due to the controlled torque is plotted in Fig. 17 and residual vibration is shown in Fig. 18. It is observed that hub angle is achieved faster by controlled torque and tip vibration is lesser than the sinusoidal excitation.

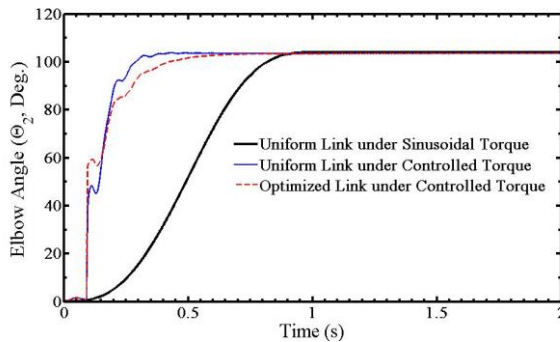


Fig. 17. Comparison of elbow angles for different excitation

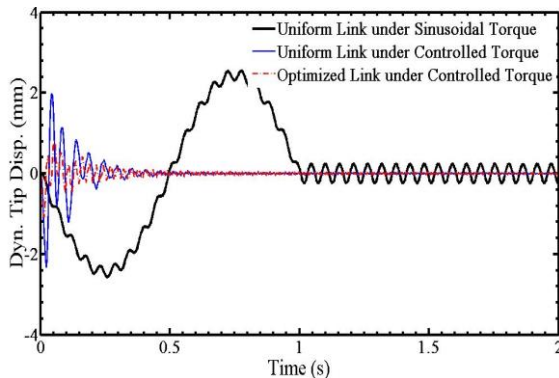


Fig. 18. Comparison of dynamic tip response for different excitation

5. Conclusion

In this work, finite element analysis of revolute-jointed rigid-flexible manipulator has been performed through linear modeling. Classical nonlinear optimization is used to solve the constrained shape optimization. From the numerical experiments, it is observed that there is a great role of system parameters (link lengths, payloads, hub-inertia, link shape) in its system dynamics and should be analyzed properly during the design. It is also observed that controlled torque improves the system dynamics further.

References

1. W. Sunada and S. Dubowsky, On the dynamic analysis and behaviour of industrial robotic manipulators with elastic members, *ASME Journal of Mechanism, Transmissions and Automation in Design*, **105**(1) (1983), pp. 42–51.
2. T. Fukuda and A. Arakawa, Modeling and control characteristics for a two-degrees-of-freedom coupling system of flexible robotic arms, *JSME, Series C*, **30**, pp (1987). 1458–1464.
3. P.B. Usoro, R. Nadira and S.S. Mahil, S.S., A finite element/Lagrangian approach to modeling light weight flexible manipulators, *ASME Journal of Dynamic System, Measurement and Control*, **108** (1986), pp. 198–205.
4. J.C. Ower and J.V. Vegte, Classical control design for a flexible manipulator: modeling and control system design, *IEEE Journal of Robotics and Automation*, **RA**, 3(5) (1987), pp. xx-xx.
5. M. Benati and A. Morro, Dynamics of chain of flexible links, *ASME J. of Dyn. Sys., Meas., and Control*, **110** (1988), pp. 410–415.
6. E. Bayo, Timoshenko versus Bernoulli-Euler beam theories for inverse dynamics of flexible robots, *International Journal of Robotics and Automation*, **4**(1) (1989), pp. 53–56.
7. B. Jonker, A finite element dynamic analysis of flexible manipulators, *The International Journal of Robotics Research*, **9**(4) (1990), pp. 59–74.
8. A. DeLuca and B. Siciliano, Closed form dynamic model of planar multilink lightweight robots, *IEEE*

- Transactions on Systems, Man and Cybernetics SMC-21*, **4** (1991), pp. 826–839.
9. A.S. Morris and A. Madani, Static and dynamic modeling of a two-flexible-link robot manipulator, *Robotica*, **14**(3) (1995), pp. 289–300.
 10. A. Dogan and A. Iftar, Modeling and control of a two-link flexible robot manipulator, In *Proceedings of the IEEE International Conference on Control Applications*, **2** (1998), pp. 761–765.
 11. L.J. Everett, T. Jennchen and M. Compere, Designing flexible manipulators with the lowest natural frequency nearly independent of position, *IEEE Trans. on Robotics and Automation*, **15**(4) (1999), pp. 605–611.
 12. W. Chen, Dynamic modeling of multi-link flexible robotic manipulators, *Computers and Structures*, **79**(2) (2001), pp. 183–195.
 13. T.W. Yang, W.L. Xu and S.K. Tso, Dynamic modeling based on real-time deflection measurement and compensation control for flexible multi-link manipulators, *Dynamics and Control*, **11**(1) (2001), pp.5–24.
 14. X. Zhang, W. Xu, S.S. Nair, and V.S. Chellabonia, PDE modeling and control of a flexible two-link manipulator, *IEEE Transactions on Control Systems Technology*, **13**(2) (2005), pp. 301–312.
 15. B.L. Karihaloo and F.I. Niordson, Optimum design of vibrating cantilever. *Journal of Optimization, Theory and Applications*. **11**(6) (1973), pp. 638–654.
 16. F.Y. Wang, On the External Fundamental Frequencies of one Link Flexible Manipulators. *The International Journal of Robotics Research*, **13** (1994), pp. 162–170.
 17. H.H. Yoo, J.E. Cho, and J. Chung, Modal analysis and shape optimization of rotating cantilever beams, *Journal of Sound and Vibration*, **290** (2006), pp. 223–241.
 18. U.S. Dixit, R. Kumar, and S.K. Dwivedy, Shape optimization of flexible robotic manipulators, *ASME Journal of Mechanical Design*, **128** (2006), pp. 559–565.
 19. A.S. Yigit, On the stability of PD control for a two-link rigid-flexible manipulator, *J. of Dyn. Sys., Meas., and Control*, **116** (1994), pp. 208–215.
 20. S.S. Ge, T.H. Lee, G. Zhu, Energy-based robust controller design for multi-link flexible robots, *Mechatronics*, **6**(7) (1996), pp. 779–798.

Modeling of Mobile Manipulator and Adaptive Super-Twisting Backstepping Control

Seong-Ik Han

*Dept. of Electronic Eng., Pusan National University, Jangjeon-dong, Geumjeong-gu
Busan, 609-735, Korea Republic*

Deok-Su Kim

*Dept. of Electronic Eng., Pusan National University, Jangjeon-dong, Geumjeong-gu
Busan, 609-735, Korea Republic*

Hyun-Uk Ha

*Dept. of Electronic Eng., Pusan National University, Jangjeon-dong, Geumjeong-gu
Busan, 609-735, Korea Republic*

Jang-Myung Lee

*Dept. of Electronic Eng., Pusan National University, Jangjeon-dong, Geumjeong-gu
Busan, 609-735, Korea Republic*

*E-mail: skhan@pusan.ac.kr, deoksu1696@pusan.ac.kr, hyunuk.ha@gmail.com, jmlee@pusan.ac.kr
www.pusan.ac.kr*

Abstract

A mobile manipulator with three wheels and three DOF links is modeled by using Euler-Lagrange method and vector orientated constraint conditions. In this modeling process, the conventional complex nonholonomic constraint transformation need not be considered in mobile robot system and then much simpler dynamic model can be obtained. Next, the super-twisting sliding mode control is combined with nonlinear backstepping control to obtain the systematic nonlinear controller design, fast response speed, and improved robustness to uncertainty due to dynamic coupling and disturbance. Simulation and experiment were carried out to prove the effectiveness of the proposed control methodology.

Keywords: Mobile-manipulator, Super-twisting sliding mode control, Backstepping control.

1. Introduction

In recent years, there has been a great interest for researches of multi-agent systems, whose applications include spacecraft, mobile robots, sensor networks, etc. Interesting research directions are containment control, consensus, formation, and flocking control [1]. These problems focus on two cases, namely, the case that there does not exist a leader and the case where there exists a leader. The coordinate tracking problems to track a single leader have been investigated for followers with single-integrator, double-integrator, high-order dynamics, nonlinear or Euler-Lagrange dynamics [2-5]. Linear control theory and variable structure control methods in most researches are used. On the other hand, there are few examples that use the backstepping control technique [6] for nonlinear or Euler-Lagrange multi-agent system. In this method, the problem of unmatched uncertainty and neglecting the efficient

nonlinearities is overcome via adopting step-by-step recursive process.

However, although a controller designed using this theorem guarantees the infinite-time stability of a closed-loop system, it has drawbacks such as a slow convergence rate and reduced robustness to uncertainty. On the other hand, systems with finite-time settling-time design possess attractive features such as improved robustness and disturbance rejection properties [7]. In this paper, terminal backstepping control based multi-agent consensus control for Euler-Lagrange system with one-leader and multi-followers is developed.

2. Background and Preliminaries

© The 2016 International Conference on Artificial Life and Robotics (ICAROB 2016), Jan. 29-31, Okinawa Convention Center, Okinawa, Japan

2.1. Description of the Mobile-Manipulator

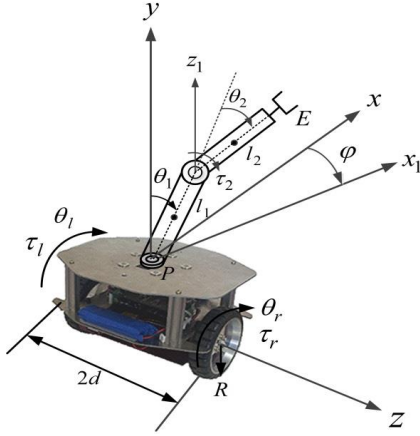


Fig. 1 Schematic diagram of the two-link and two-wheeled mobile manipulator.

The following variables are selected to describe the two-link and two-wheeled mobile manipulator shown in Fig. 1: τ_r, τ_l , and τ_2 are the torques of two wheels and the joint2; θ_r and θ_l are the rotation angles of the right and left wheels of the mobile platform, respectively; x and φ are the forward distance and the rotation angle of the mobile platform, respectively; θ_1 and θ_2 are the rotation angle of the links 1 and 2, respectively; $m_p = 5\text{kg}$, $m_w = 0.58\text{kg}$, $m_1 = 2\text{kg}$, and $m_2 = 0.5\text{kg}$ are the masses of the mobile platform, wheel, link 1, and link 2, respectively; I_p, I_1 , and I_2 are the moment of inertia of the mobile platform, link 1, and link 2 with respect to y axis, respectively; $I_{\theta_1}, I_{\theta_2}$, and I_w are the moment of inertia of link 1, link 2, and each wheel with respect to the z and z_1 axis, respectively; $d = 0.145\text{m}$ is the distance between point P and the wheels; $R = 0.08\text{m}$ is the radius of the wheels; $l_1 = 0.25\text{m}$ and $l_2 = 0.2\text{m}$ are the lengths of link 1 and link 2; and r_1 and r_2 are the distances between the joints and the center of mass of the links.

The generalized coordinated is selected as $q = [x, \varphi, \theta_1, \theta_2, \theta_l, \theta_r]^T$. The total kinematic energy is given as,

$$T = \frac{1}{2}(m_p + m_1 + m_2 + 2m_w)\dot{x}^2 + \frac{1}{2}(I_p + I_w + I_1 + I_2)\dot{\varphi}^2 + \frac{1}{2}(m_1 r_1^2 + I_{\theta_1})\dot{\theta}_1^2 + \frac{1}{2}m_2[r_1^2\dot{\theta}_1^2 + r_2^2(\dot{\theta}_1 + \dot{\theta}_2)^2 + 2r_1 r_2(\dot{\theta}_1^2 + \dot{\theta}_1 \dot{\theta}_2)c\theta_2] + \frac{1}{2}I_{\theta_2}\dot{\theta}_2^2 + \frac{1}{2}\left(m_w + \frac{I_{zw}}{R^2}\right)\dot{x}_r^2 + \frac{1}{2}\left(m_w + \frac{I_{zw}}{R^2}\right)\dot{x}_l^2, \quad (1)$$

where $I_1 = \frac{1}{3}m_1(l_1 s\theta_1)^2$ and $I_2 = \frac{1}{3}m_2(l_1 s\theta_1 + r_2 s\theta_{12})^2$.

The potential energy is obtained as follows:

$$V = m_1 g r_1 c\theta_1 + m_2 g(l_1 c\theta_1 + r_2 c\theta_{12}). \quad (2)$$

The dynamics are obtained using the Euler-Lagrangian method. From the tire dynamics, we obtain

$$I_{zw}\ddot{\theta}_l = \tau_l, \quad (3)$$

$$I_{zw}\ddot{\theta}_r = \tau_r, \quad (4)$$

with the kinematic relations $x = (x_r + x_l)/2$, $\ddot{x} = (\ddot{x}_r + \ddot{x}_l)/2$, $\theta_r = x_r/R$, $\theta_l = x_l/R$, $\ddot{\theta}_l = \ddot{x}_l/R$, and $\ddot{\theta}_r = \ddot{x}_r/R$, which is obtained from the assumption that a slip does not occur between tire and contact surface. Therefore, we obtain

$$F_l = \frac{\tau_l}{R} - \left(\frac{I_{zw}}{R^2} + M_l\right)\ddot{x}_l, \quad (5)$$

$$F_r = \frac{\tau_r}{R} - \left(\frac{I_{zw}}{R^2} + M_r\right)\ddot{x}_r. \quad (6)$$

Under the assumption of no sideslip, the relationships of $M_r = M_l = M_w$, $\ddot{x} = (\ddot{x}_l + \ddot{x}_r)/2$, $\dot{\varphi} = R(\dot{\theta}_l - \dot{\theta}_r)/2d = (\dot{x}_l - \dot{x}_r)/2d$, and $\ddot{\varphi} = R(\ddot{\theta}_l - \ddot{\theta}_r)/2d = (\ddot{x}_l - \ddot{x}_r)/2d$ give

$$F_l + F_r = \frac{\tau_l}{R} + \frac{\tau_r}{R} - \left(\frac{I_{zw}}{R^2} + M_w\right)(\ddot{x}_l + \ddot{x}_r) = \frac{\tau_l}{R} + \frac{\tau_r}{R} - 2\left(\frac{I_{zw}}{R^2} + M_w\right)\ddot{x}, \quad (7)$$

$$F_l - F_r = \frac{\tau_l}{R} - \frac{\tau_r}{R} - \left(\frac{I_{zw}}{R^2} + M_w\right)(\ddot{x}_l - \ddot{x}_r) = \frac{\tau_l}{R} - \frac{\tau_r}{R} - 2d\left(\frac{I_{zw}}{R^2} + M_w\right)\ddot{\varphi}. \quad (8)$$

Finally, the reduced generalized coordinate is given as $q_r = [x, \varphi, \theta_1, \theta_2]^T$. The derived dynamic equation is written as

$$M(q_r)\ddot{q}_r + C(q_r, \dot{q}_r)\dot{q}_r + G(q_r) = B(q_r)\tau, \quad (9)$$

Where,

$$M(q_r) = \begin{bmatrix} m_{11} & 0 & m_{13} & m_{14} \\ 0 & m_{22} & 0 & 0 \\ m_{31} & 0 & m_{33} & m_{34} \\ m_{41} & 0 & m_{43} & m_{44} \end{bmatrix},$$

$$C(q_r, \dot{q}_r) = \begin{bmatrix} 0 & 0 & 0 & 0 \\ 0 & 0 & l_{eq1} & l_{eq2} \\ 0 & 0 & -m_2 r_1 r_2 \dot{\theta}_2 s\theta_2 & -m_2 r_1 r_2 \dot{\theta}_2 s\theta_2 \\ 0 & 0 & -m_2 r_1 r_2 \dot{\theta}_1 s\theta_2 & 0 \end{bmatrix},$$

$$B(q_r) = \begin{bmatrix} 1/R & d/R & 0 & 0 \\ 1/R & -d/R & 0 & 0 \\ 0 & 0 & 0 & 1 \end{bmatrix}^T, \text{ and } \tau = [\tau_l, \tau_r, \tau_2]^T.$$

By denoting v and m as suffixes of the mobile platform and manipulator, respectively, the coordinates q_r can be decomposed as $q = [q_v^T, q_m^T]^T$, $q_v = [x, \varphi, \theta_1]^T$, and $q_m = \theta_2$. Thus, (51) can be written as follows:

$$\begin{bmatrix} M_v & M_{vm} \\ M_{mv} & M_m \end{bmatrix} \begin{bmatrix} \ddot{q}_v \\ \ddot{q}_m \end{bmatrix} + \begin{bmatrix} C_v & C_{vm} \\ C_{mv} & C_m \end{bmatrix} \begin{bmatrix} \dot{q}_v \\ \dot{q}_m \end{bmatrix} + \begin{bmatrix} G_v \\ G_m \end{bmatrix} + \begin{bmatrix} \tau_{dv} \\ \tau_{dm} \end{bmatrix} = \begin{bmatrix} B_v & 0 \\ 0 & B_m \end{bmatrix} \begin{bmatrix} \tau_v \\ \tau_m \end{bmatrix}. \quad (10)$$

The state space model of the mobile platform of (10) can be expressed as follows:

$$\begin{aligned} \dot{x}_1 &= x_2, \\ \dot{x}_2 &= -M_v^{-1}(C_v x_2 + G_v + F_{dv}) + M_v^{-1} B_v u_2 \\ y_v &= x_1, \end{aligned} \quad (11)$$

where $x_1 = q_v$, $x_2 = \dot{q}_v$, $F_{dv} = M_{vm} \ddot{q}_m + C_{vm} \dot{q}_m + \tau_{dv}$, and $u_2 = \tau_v$. The state space model of the manipulator from (10) can be expressed as follows:

$$\begin{aligned} \dot{x}_3 &= x_4, \\ \dot{x}_4 &= -M_m^{-1}(C_m \dot{q}_m + G_m + F_{dm}) + M_m^{-1} B_m u_4, \\ y_m &= x_3, \end{aligned} \quad (12)$$

where, $x_3 = \theta_2$, $x_4 = \dot{\theta}_2$, $F_{dm} = M_{mv} \ddot{q}_v + C_{mv} \dot{q}_v + \tau_{dm}$, and $u_4 = \tau_m$. The state variables of the mobile manipulator system are selected as $x_1 = [x_{1,1}, x_{2,1}, x_{3,1}]^T = [x, \varphi, \theta_1]^T$, $x_2 = [x_{1,2}, x_{2,2}, x_{3,2}]^T = [\dot{x}, \dot{\varphi}, \dot{\theta}_1]^T$, $x_3 = x_{4,1} = \theta_2$, and $x_4 = x_{4,2} = \dot{\theta}_2$. The control objective is that the outputs track the desired command in finite-time, and the tilting angle, θ_1 , should be maintained stably in the vertical position.

3. Design of Finite-Time Controller Design and Stability Analysis

3.1 Design of a STA backstepping controller for a mobile platform

The auxiliary tracking error and new states are defined as

$$z_{v1} = q_v - q_{vd}, \quad (13)$$

$$\zeta_{v1,1} = k_{v1} z_{v1} + |z_{v1}|^{1/2} \text{sign}(z_{v1}), \quad (14)$$

$$\begin{aligned} \zeta_{v1,2} &= -\beta_{v1,2} \int_0^t [k_{v1}^2 z_{v1} + (3/2)k_{v1} |z_{v1}|^{1/2} \text{sign}(z_{v1}) \\ &\quad + \gamma_{v1} \text{sign}(z_{v1})] d\tau. \end{aligned} \quad (15)$$

$$\dot{\zeta}_{v1,1} = \xi_{v1}(x_{v2} - \dot{q}_{vd}), \quad (16)$$

$$\dot{\zeta}_{v1,2} = -\xi_{v1} \beta_{v1,2} \zeta_{v1,1}, \quad (17)$$

where $\xi_{v1} = k_{v1} + \gamma_{v1} |z_{v1}|^{\gamma_v - 1}$. Define the virtual error surface and new states as

$$z_{v2} = x_{v2} - \alpha_{v1}, \quad (18)$$

$$\zeta_{v2,1} = k_{v2} z_{v2} + |z_{v2}|^{1/2} \text{sign}(z_{v2}), \quad (19)$$

$$\begin{aligned} \zeta_{v2,2} &= -\beta_{v2,2} \int_0^t [k_{v2}^2 z_{v2} + (3/2)k_{v2} |z_{v2}|^{1/2} \text{sign}(z_{v2}) \\ &\quad + \gamma_{v2} \text{sign}(z_{v2})] d\tau, \end{aligned} \quad (20)$$

If we select the virtual control as follows:

$$\alpha_{v1} = -\beta_{v1,1} \zeta_{v1,1} + \dot{q}_{vd} + \zeta_{v1,2}, \quad (21)$$

(21) can be expressed as

$$\dot{\zeta}_{v1,1} = -\beta_{v1,1} \xi_{v1} \zeta_{v1,1} + \xi_{v1} \zeta_{v1,2} + \xi_{v1} z_{v2}. \quad (22)$$

$$\begin{aligned} \dot{\zeta}_{v1} &= [\dot{\zeta}_{v1,1} \quad \dot{\zeta}_{v1,2}]^T \\ &= \xi_{v1} A_{v1} \zeta_{v1} + \xi_{v1} B_{z1}, \end{aligned} \quad (23)$$

where $A_{v1} = \begin{bmatrix} -\beta_{v1,1} & 1 \\ -\beta_{v1,2} & 0 \end{bmatrix}$ and $B_{z1} = \begin{bmatrix} z_{v2} \\ 0 \end{bmatrix}$. Defining the

Lyapunov function candidate $V_{v1} = (1/2) \zeta_{v1}^T P_{v1} \zeta_{v1}$,

$$\dot{V}_{v1} \leq -\xi_{v1} \zeta_{v1}^T Q_{v1} \zeta_{v1} + \xi_{v1} \psi_{v1} \zeta_{v1} z_{v2}, \quad (24)$$

where $\psi_{v1} = (c_{v1} + 4\varepsilon_{v1}^2) \zeta_{v1,1} - 2\varepsilon_{v1} \zeta_{v1,2}$; P_{v1} is a positive definite matrix defined with constants $c_{v1} > 0$, $\varepsilon_{v1} > 0$,

$P_{v1} = \begin{bmatrix} c_{v1} + 4\varepsilon_{v1}^2 & -2\varepsilon_{v1} \\ -2\varepsilon_{v1} & 1 \end{bmatrix}$ and is a solution of an

algebraic Lyapunov equation (ALE)

$A_{v1}^T P_{v1} + P_{v1} A_{v1} = -2Q_{v1}$, and a positive definite symmetric matrix Q_{v1} is defined as

$$Q_{v1} = \begin{bmatrix} \beta_{v1,1}(c_{v1} + 4\varepsilon_{v1}^2) - 4\beta_{v1,2}\varepsilon_{v1} & (c_{v1} + 4\varepsilon_{v1}^2) - 2\varepsilon_{v1}\beta_{v1,1} + \beta_{v1,2} \\ (c_{v1} + 4\varepsilon_{v1}^2) - 2\varepsilon_{v1}\beta_{v1,1} + \beta_{v1,2} & 4\varepsilon_{v1} \end{bmatrix}.$$

Defining the state vector as $\zeta_{v2} = [\zeta_{v2,1} \quad \zeta_{v2,2}]^T$ and one can then obtain that

$$\dot{\zeta}_{v2,1} = \xi_{v2} [-M_v^{-1} C_v \dot{q}_v - \rho_v + \bar{g}_v \tau_v] - \dot{\alpha}_{v1}, \quad (25)$$

$$\dot{\zeta}_{v2,2} = -\xi_{v2} \beta_{v2,2} \zeta_{v2,1}, \quad (26)$$

If we select the control law τ_v as

$$\tau_v = g_v^+ \left[-\beta_{v2,1} \zeta_{v2,1} + M_v^{-1} C_v \dot{q}_v + \hat{\rho}_v - \frac{\xi_{v1} \psi_{v1} \zeta_{v1}}{\xi_{v2} \psi_{v2} \zeta_{v2}} z_{v2} + \dot{\alpha}_{v1} \right], \quad (27)$$

Defining the following Lyapunov function candidate as

$$V_{v2} = V_{v1} + (1/2) \zeta_{v2}^T P_{v2} \zeta_{v2} + (1/2\eta_v) \tilde{\rho}_v^T \tilde{\rho}_v, \quad (28)$$

where $\eta_v > 0$ is constant. The time derivative of V_{v2} is written as

$$\begin{aligned} \dot{V}_{v2} &= \dot{V}_{v1} + \zeta_{v2}^T P_{v2} \dot{\zeta}_{v2} + \frac{1}{\eta_{\rho v}} \tilde{\rho}_v^T \dot{\tilde{\rho}}_v \\ &\leq -\sum_{i=1}^2 \xi_{vi} \zeta_{vi}^T Q_{vi} \zeta_{vi} + \xi_{v1} \psi_{v1} z_{v2} - \xi_{v1} \psi_{v1} z_{v2} \\ &\quad + \tilde{\rho}_v^T \left(\xi_{v2} \psi_{v2} \zeta_{v2} - \frac{1}{\eta_v} \dot{\tilde{\rho}}_v \right), \end{aligned} \quad (29)$$

where $\psi_{v2} = (c_{v2} + 4\varepsilon_{v2}^2) \zeta_{v2,1} - 2\varepsilon_{v2} \zeta_{v2,2}$. If we select an adaptive law as

$$\dot{\hat{\rho}}_v = \eta_v (\xi_{v2} \psi_{v2} \zeta_{v2} - \eta'_v \hat{\rho}_v), \quad (30)$$

where $\eta'_{pv} > 0$ are constants, (50) can be written as:

$$\begin{aligned} \dot{V}_{v2} &\leq -\sum_{i=1}^2 \xi_{vi} \zeta_{vi}^T Q_{vi} \zeta_{vi} + \eta'_v \tilde{\rho}_v^T \hat{\rho}_v \\ &\leq -\sum_{i=1}^2 \xi_{vi} \zeta_{vi}^T Q_{vi} \zeta_{vi} - \frac{\eta'_{pv} \tilde{\rho}_v^T \tilde{\rho}_v}{2} + \frac{\eta'_{pv} \rho_v^T \rho_v}{2}. \end{aligned} \quad (31)$$

3.2. Design of a STA backstepping controller for a mobile platform

The auxiliary tracking error and new states are defined as:

$$z_{m1} = q_m - q_{md}, \quad (32)$$

$$z_{m2} = x_{m2} - \alpha_{m1}, \quad (33)$$

$$\zeta_{m1,1} = k_{m1} z_{m1} + |z_{m1}|^{1/2} \text{sign}(z_{m1}), \quad (34)$$

$$\begin{aligned} \zeta_{m1,2} &= -\beta_{m1,2} \int_0^t [k_{m1}^2 z_{m1} + (3/2)k_{m1} |z_{m1}|^{1/2} \text{sign}(z_{m1}) \\ &\quad + \gamma_{m1} \text{sign}(z_{m1})] d\tau, \end{aligned} \quad (35)$$

$$\zeta_{m2,1} = k_{m2} z_{m2} + |z_{m2}|^{1/2} \text{sign}(z_{m2}), \quad (36)$$

$$\begin{aligned} \zeta_{m2,2} &= -\beta_{m2,2} \int_0^t [k_{m2}^2 z_{m2} + (3/2)k_{m2} |z_{m2}|^{1/2} \text{sign}(z_{m2}) \\ &\quad + \gamma_{m2} \text{sign}(z_{m2})] d\tau. \end{aligned} \quad (37)$$

We select the virtual control, the control law, and adaptive law as follows:

$$\alpha_{m1} = -\beta_{m1,1} \zeta_{m1,1} + \dot{q}_{md} + \zeta_{m1,2}, \quad (38)$$

$$\begin{aligned} \tau_m &= g_m^{-1} \left[M_m^{-1} (C_m \dot{q}_m + G_m) - \beta_{m2,1} \zeta_{m2,1} \right. \\ &\quad \left. - \frac{\xi_{m1} \psi_{m1} \zeta_{m1}}{\xi_{m2} \psi_{m2} \zeta_{m2}} z_{m2} + \hat{\rho}_m + \dot{\alpha}_{m1} \right], \end{aligned} \quad (39)$$

$$\dot{\hat{\rho}}_m = \eta_{pm} (\xi_{vm} \psi_{m2} \zeta_{m2} - \eta'_{pm} \hat{\rho}_m). \quad (69)$$

4. Simulation Example

To validate the proposed control scheme, the following group of one leader indexed by 0 and four followers indexed by 1, 2, 3, and 4, respectively as shown in Fig. 1. The strict feedback state equations of each agent are expressed as:

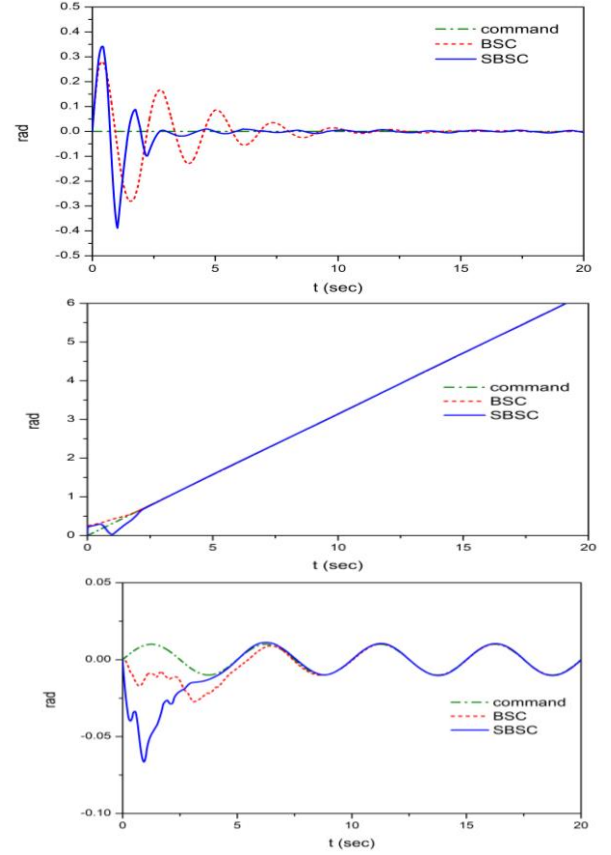
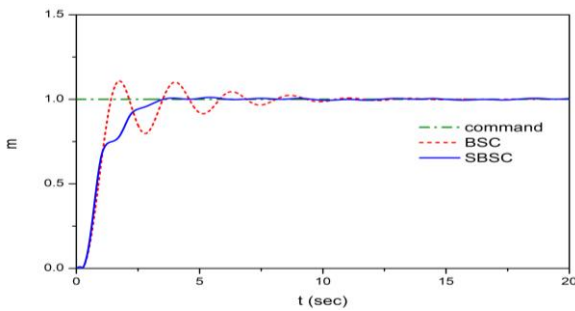


Fig. 2. Simulation result for proposed algorithm. (a) Mobile platforms tracking performance, (b) Pitch control of mobile platform, (c) Yaw control of mobile platform (d) Manipulator's position control(Sinusoidal input).

Above figure 2 illustrates simulation result for vehicle's tracking performance, pitch and yaw control, and manipulator's sinusoidal position control.

5. Conclusion

A terminal backstepping control scheme to guarantee the fast error convergence and small tracking error performance for a multi-agent Euler-Lagrange system is developed in this paper. A virtual finite-time error surface is defined to design a virtual control. The finite-time convergence is proved by the finite-time stability analysis of Lyapunov function. Simulation for one-link manipulator agents confirms the theoretical proposal.

Acknowledgements

This work was supported by the National Research Foundation of Korea(NRF) grant funded by the Korea government(MSIP) (NRF-2015R1A2A2A01004457).

Self-tuned Local Feedback Gain Based Decentralized Fault Tolerant Control of Reconfigurable Manipulators

Bo Zhao

*The State Key Laboratory of Management and Control for Complex Systems, Institute of Automation,
Chinese Academy of Sciences, Beijing 100190, China*

Bo Dong, Yan Li

*Department of Control Science and Engineering, Changchun University of Technology,
Changchun 130012, China*

Fumitoshi Matsuno

*Department of Mechanical Engineering and Science, Graduate School of Engineering, Kyoto University,
Kyoto Daigaku-Katsura, Nishikyo-ku, Kyoto 615-8540, Japan*

Yuanchun Li*

*Department of Control Science and Engineering, Changchun University of Technology,
Changchun 130012, China (Corresponding Author)*

E-mail: zhaobo@ia.ac.cn, dongbo@ccut.edu.cn, liyandianqi@ccut.edu.cn, matsuno@me.kyoto-u.ac.jp, liyc@ccut.edu.cn

Abstract

This paper investigates the decentralized fault tolerant control (DFTC) scheme based on self-tuned local feedback gain to against partial loss of actuator effectiveness of reconfigurable manipulators. Consider the entire system as a set of interconnected subsystems due to its modularity property, the decentralized control method is proposed by employing two neural networks for the system fault-free. For the subsystem suffers to partial loss of actuator effectiveness, the self-tuned local feedback gain is added to the proposed decentralized control method to guarantee the control performance. Finally, a simulation example is provided to demonstrate the effectiveness of the present DFTC scheme. The main contributions of this method are: i) The fault tolerant control structure is simple since it is no need to be redesigned in the presence of partial loss of actuator effectiveness; ii) The actuator fault can be handled in its local subsystem, it implies that the performance degradation of the faulty subsystem can not affect the fault-free subsystems.

Keywords: Fault tolerant control; Decentralized control; Neural networks; Partial loss of effectiveness; Reconfigurable manipulators.

1. Introduction

Reconfigurable manipulators consist of a set of joint and link modules in standard size and interface¹⁻². By adding or removing the modules, they can change their configurations and degree of freedoms (DOF) to adapt different tasks. Hence, the flexible structure serves plenty of potential applications. However, failures of actuators, sensors or other components will inevitably

occur after working for a long time. They bring performance degradation or system damaged if they can not be repaired timely.

As the modularity property of reconfigurable manipulators, the decentralized control architecture is more feasible than the centralized one. Zhu et al.³ proposed a decentralized adaptive fuzzy sliding mode control scheme so that the system was guaranteed to be stable joint by joint. K. Sato et al.⁴ investigated a

decentralized control scheme in which phasic and tonic control were well coordinated, this scheme obtained success on a snake-like robot. Liu et al.⁵ presented a DFTC based on an observer for fault detection of modular reconfigurable robot with joint torque sensing. Motivated by it, Yuan et al.⁶ developed an independent joint power efficiency estimation-based health monitoring and fault detection method. Zhao et al.⁷ investigated an active DFTC strategy for reconfigurable manipulators based on local joint information and an unknown input observer. They also⁸ proposed an active DFTC scheme based on signal reconstruction to against the sensor fault in reconfigurable manipulators.

This paper presents a self-tuned local feedback gain based FTC scheme for reconfigurable manipulators with partial loss of actuator effectiveness. For the fault-free system, a decentralized neural network control is developed to stabilize the closed-loop reconfigurable manipulator system. By adding a self-tuned local feedback gain, the trajectory tracking can be guaranteed to the acceptable level though the fault occurs. The simulation of 2-DOF reconfigurable manipulator shows the effectiveness of the proposed method.

2. Problem Statement

For the development of the decentralized control, each joint is considered as a subsystem of the entire manipulator system interconnected by coupling torques. And then the dynamical model of the i th subsystem suffers to partial loss of actuator effectiveness can be formulated in joint space as

$$M_i(q_i)\ddot{q}_i + C_i(q_i, \dot{q}_i)\dot{q}_i + G_i(q_i) + Z_i(q, \dot{q}, \ddot{q}) = \rho_i u_i \quad (1)$$

with

$$\begin{aligned} Z_i(q, \dot{q}, \ddot{q}) = & \left\{ \sum_{j=1, j \neq i}^n M_{ij}(q)\ddot{q}_j + [M_{ii}(q) - M_i(q_i)]\ddot{q}_i \right\} \\ & + \left\{ \sum_{j=1, j \neq i}^n C_{ij}(q, \dot{q})\dot{q}_j + [C_{ii}(q, \dot{q}) - C_i(q_i, \dot{q}_i)]\dot{q}_i \right\} \\ & + [\bar{G}_i(q) - G_i(q_i)] \end{aligned}$$

where $i=1,2,\dots,n$, $q_i, \dot{q}_i, \ddot{q}_i$ are the vectors of joint displacement, velocity and acceleration, $M_i(q_i)$ is the inertia matrix, $C_i(q_i, \dot{q}_i)$ is the Coriolis and centripetal force, $G_i(q_i)$ is the gravity term, $Z_i(q, \dot{q}, \ddot{q})$ is the interconnected term, and u_i is the applied joint torque of the i th subsystem, respectively. ρ_i is the

effectiveness factor of the i th subsystem with $0 < \rho_i \leq 1$ holds, which presents the degree of fault.

Let $x_i = [x_{i1}, x_{i2}]^T = [q_i, \dot{q}_i]^T$, (1) can be expressed as

$$S_i : \begin{cases} \dot{x}_{i1} = x_{i2} \\ \dot{x}_{i2} = f_i(q_i, \dot{q}_i) + g_i(q_i)\rho_i u_i + h_i(q, \dot{q}, \ddot{q}) \\ y_i = x_{i1} \end{cases} \quad (2)$$

where x_i and y_i are the state and the output of the subsystem S_i , respectively, and

$$f_i(q_i, \dot{q}_i) = M_i^{-1}(q_i)[-C_i(q_i, \dot{q}_i)\dot{q}_i - G_i(q_i)]$$

$$g_i(q_i) = M_i^{-1}(q_i)$$

$$h_i(q, \dot{q}, \ddot{q}) = -M_i^{-1}(q_i)Z_i(q, \dot{q}, \ddot{q})$$

The control objective is to design a DFTC scheme for the faulty subsystem of reconfigurable manipulators (1) to make the joint displacements to follow their desired trajectories.

3. Decentralized Fault Tolerant Controller Design

3.1. Decentralized control design for the fault-free system

Assumption 1. The desired trajectories are bounded as

$$\begin{bmatrix} q_{id} \\ \dot{q}_{id} \\ \ddot{q}_{id} \end{bmatrix} \leq q_A \quad (3)$$

where $q_A > 0$ is a known constant.

Define the tracking error as

$$e_{i1} = x_{i1} - x_{i1d} \quad (4)$$

where x_{i1d} is the desired displacement of the i th joint.

Introducing a first order filter as

$$s_i = \lambda_i e_{i1} + \dot{e}_{i1} \quad (5)$$

where $\lambda_i > 0$ is a known constant.

Assumption 2. The interconnected term $h_i(q, \dot{q}, \ddot{q})$ is norm-bounded as³

$$\|h_i(q, \dot{q}, \ddot{q})\| \leq \sum_{j=1}^n d_{ij} S_j \quad (6)$$

where $d_{ij} \geq 0$ and $S_j = 1 + |s_j| + |s_j|^2$.

For the system (1) in fault-free, i.e., $\rho_i = 1$, differentiating (5) and using (4), one has

$$\begin{aligned} \dot{s}_i &= \lambda_i \dot{e}_{i1} + \ddot{e}_{i1} \\ &= \lambda_i \dot{e}_{i1} + f_i(q_i, \dot{q}_i) + g_i(q_i)u_i + h_i(q, \dot{q}, \ddot{q}) - \ddot{q}_{id} \end{aligned} \quad (7)$$

where the nonlinear terms $f_i(q_i, \dot{q}_i)$ and $g_i(q_i)$ are approximated by employing two ideal radial basis function (RBF) neural networks as

$$f_i(q_i, \dot{q}_i, W_{if}^T) = W_{if}^T \sigma_{if}(q_i, \dot{q}_i) + \varepsilon_{if}, \|\varepsilon_{if}\| \leq \varepsilon_1 \quad (8)$$

$$g_i(q_i, W_{ig}^T) = W_{ig}^T \sigma_{ig}(q_i) + \varepsilon_{ig}, \|\varepsilon_{ig}\| \leq \varepsilon_2 \quad (9)$$

where W_{if} and W_{ig} are the ideal weight vectors from the hidden layer to the output layer, σ_{if} and σ_{ig} are the basis function vectors, ε_{if} and ε_{ig} are their approximation errors, ε_1 and ε_2 are known positive constants, respectively.

Let \hat{W}_{if} and \hat{W}_{ig} be the estimation of W_{if} and W_{ig} , $\hat{\sigma}_{if}$ and $\hat{\sigma}_{ig}$ are the estimation of σ_{if} and σ_{ig} , we have

$$\hat{f}_i(q_i, \dot{q}_i, \hat{W}_{if}^T) = \hat{W}_{if}^T \hat{\sigma}_{if}(q_i, \dot{q}_i) \quad (10)$$

$$\hat{g}_i(q_i, \hat{W}_{ig}^T) = \hat{W}_{ig}^T \hat{\sigma}_{ig}(q_i) \quad (11)$$

Let $\tilde{W}_{if} = W_{if} - \hat{W}_{if}$, $\tilde{W}_{ig} = W_{ig} - \hat{W}_{ig}$ be the weight estimation errors, we have

$$\begin{aligned} f_i(q_i, \dot{q}_i, W_{if}^T) - \hat{f}_i(q_i, \dot{q}_i, \hat{W}_{if}^T) \\ = \tilde{W}_{if}^T \hat{\sigma}_{if}(q_i, \dot{q}_i) + W_{if}^T \tilde{\sigma}_{if}(q_i, \dot{q}_i) + \varepsilon_{if} \end{aligned} \quad (12)$$

$$\begin{aligned} g_i(q_i, W_{ig}^T) - \hat{g}_i(q_i, \hat{W}_{ig}^T) \\ = \tilde{W}_{ig}^T \hat{\sigma}_{ig}(q_i) + W_{ig}^T \tilde{\sigma}_{ig}(q_i) + \varepsilon_{ig} \end{aligned} \quad (13)$$

where the output errors of the basis functions $\sigma_{if}(\cdot)$ and $\sigma_{ig}(\cdot)$ are defined as

$$\tilde{\sigma}_{if}(q_i, \dot{q}_i) = \sigma_{if}(q_i, \dot{q}_i) - \hat{\sigma}_{if}(q_i, \dot{q}_i) \quad (14)$$

$$\tilde{\sigma}_{ig}(q_i) = \sigma_{ig}(q_i) - \hat{\sigma}_{ig}(q_i) \quad (15)$$

Define the whole approximated error as

$$\omega_i = W_{if}^T \tilde{\sigma}_{if}(q_i, \dot{q}_i) + W_{ig}^T \tilde{\sigma}_{ig}(q_i) u_i + \varepsilon_{if} + \varepsilon_{ig} u_i \quad (16)$$

Assumption 3. The whole approximated error ω_i is norm-bounded as

$$\|\omega_i\| \leq \xi_i \quad (17)$$

where $\xi_i > 0$ is a known constant.

The decentralized controller can be designed as

$$\begin{aligned} u_i = - \left(k_i s_i + \hat{f}_i(q_i, \dot{q}_i, \hat{W}_{if}^T) + \hat{\sigma}_i \operatorname{sgn}(s_i) S_i - \ddot{q}_{id} \right. \\ \left. + \lambda_i \dot{e}_{i1} + \hat{\xi}_i \operatorname{sgn}(s_i) \right) / \hat{g}_i(q_i, \hat{W}_{ig}^T) \end{aligned} \quad (18)$$

where $k_i > 0$ is a known constant, \hat{W}_{if} , \hat{W}_{ig} , $\hat{\sigma}_i$ and $\hat{\xi}_i$ are updated by

$$\dot{\hat{W}}_{if} = \Gamma_{if} s_i \hat{\sigma}_{if}(q_i, \dot{q}_i) \quad (19)$$

$$\dot{\hat{W}}_{ig} = \Gamma_{ig} s_i \hat{\sigma}_{ig}(q_i, \dot{q}_i) u_i \quad (20)$$

$$\dot{\hat{\sigma}}_i = \Gamma_{i\delta} |s_i| S_i \quad (21)$$

$$\dot{\hat{\xi}}_i = \Gamma_{i\xi} |s_i| \quad (22)$$

where Γ_{if} , Γ_{ig} , $\Gamma_{i\delta}$ and $\Gamma_{i\xi}$ are positive constants.

Theorem 1. For the system (1) in fault-free, consider the assumptions 1-3, the decentralized control law (16) with the adaptive updated laws (17)-(20) can guarantee the tracking errors of the closed-loop system converge to zero asymptotically.

Proof. Define $\tilde{\delta}_i = \delta_i - \hat{\delta}_i$ and $\tilde{\xi}_i = \xi_i - \hat{\xi}_i$, and select the Lyapunov candidate function as

$$\begin{aligned} V_i = \frac{1}{2} s_i^T s_i + \frac{1}{2} \tilde{W}_{if}^T \Gamma_{if}^{-1} \tilde{W}_{if} + \frac{1}{2} \tilde{W}_{ig}^T \Gamma_{ig}^{-1} \tilde{W}_{ig} \\ + \frac{1}{2} \tilde{\delta}_i^T \Gamma_{i\delta}^{-1} \tilde{\delta}_i + \frac{1}{2} \tilde{\xi}_i^T \Gamma_{i\xi}^{-1} \tilde{\xi}_i \end{aligned} \quad (23)$$

Taking its time derivative and noticing (7), we have

$$\begin{aligned} \dot{V}_i = s_i^T \dot{s}_i - \tilde{W}_{if}^T \Gamma_{if}^{-1} \dot{\tilde{W}}_{if} - \tilde{W}_{ig}^T \Gamma_{ig}^{-1} \dot{\tilde{W}}_{ig} \\ - \tilde{\delta}_i^T \Gamma_{i\delta}^{-1} \dot{\tilde{\delta}}_i - \tilde{\xi}_i^T \Gamma_{i\xi}^{-1} \dot{\tilde{\xi}}_i \\ = s_i^T (\lambda_i \dot{e}_{i1} + f_i + g_i u_i + h_i - \ddot{q}_{id}) - \tilde{W}_{if}^T \Gamma_{if}^{-1} \dot{\tilde{W}}_{if} \\ - \tilde{W}_{ig}^T \Gamma_{ig}^{-1} \dot{\tilde{W}}_{ig} - \tilde{\delta}_i^T \Gamma_{i\delta}^{-1} \dot{\tilde{\delta}}_i - \tilde{\xi}_i^T \Gamma_{i\xi}^{-1} \dot{\tilde{\xi}}_i \end{aligned} \quad (24)$$

Substituting (16) into (22), one can obtain

$$\begin{aligned} \dot{V}_i = s_i^T (-k_i s_i + f_i - \hat{f}_i + (g_i - \hat{g}_i) u_i + h_i \\ - \hat{\delta}_i \operatorname{sgn}(s_i) S_i - \hat{\xi}_i \operatorname{sgn}(s_i)) - \tilde{W}_{if}^T \Gamma_{if}^{-1} \dot{\tilde{W}}_{if} \\ - \tilde{W}_{ig}^T \Gamma_{ig}^{-1} \dot{\tilde{W}}_{ig} - \tilde{\delta}_i^T \Gamma_{i\delta}^{-1} \dot{\tilde{\delta}}_i - \tilde{\xi}_i^T \Gamma_{i\xi}^{-1} \dot{\tilde{\xi}}_i \\ = s_i^T (-k_i s_i + \tilde{W}_{if}^T \hat{\sigma}_{if} + \tilde{W}_{ig}^T \hat{\sigma}_{ig} u_i + \omega_i + h_i \\ - \hat{\delta}_i \operatorname{sgn}(s_i) S_i - \hat{\xi}_i \operatorname{sgn}(s_i)) - \tilde{W}_{if}^T \Gamma_{if}^{-1} \dot{\tilde{W}}_{if} \\ - \tilde{W}_{ig}^T \Gamma_{ig}^{-1} \dot{\tilde{W}}_{ig} - \tilde{\delta}_i^T \Gamma_{i\delta}^{-1} \dot{\tilde{\delta}}_i - \tilde{\xi}_i^T \Gamma_{i\xi}^{-1} \dot{\tilde{\xi}}_i \end{aligned} \quad (25)$$

According to assumptions 2-3, and using (17)-(19), we have

$$\dot{V}_i \leq -k_i s_i^2 + s_i^T \sum_{j=1}^n d_{ij} S_j - \hat{\delta}_i |s_i| S_i - \tilde{\delta}_i^T \Gamma_{i\delta}^{-1} \dot{\tilde{\delta}}_i \quad (26)$$

Then,

$$\begin{aligned}
\dot{V} &= \sum_{i=1}^n \dot{V}_i \\
&= \sum_{i=1}^n (-k_i s_i^2 + s_i^T \sum_{j=1}^n d_{ij} S_j - \hat{\delta}_i |s_i| S_i - \tilde{\delta}_i^T \Gamma_{i\delta}^{-1} \dot{\hat{\delta}}_i) \\
&\leq \sum_{i=1}^n \left(-k_i s_i^2 - \tilde{\delta}_i^T \Gamma_{i\delta}^{-1} \dot{\hat{\delta}}_i + \max_{ij} \{d_{ij}\} \sum_{i=1}^n |s_i| \sum_{j=1}^n S_j - \hat{\delta}_i |s_i| S_i \right)
\end{aligned} \quad (25)$$

Noticing $|s_i| \leq |s_j| \Leftrightarrow S_i \leq S_j$, and using Chebyshev inequality, we have

$$\sum_{i=1}^n |s_i| \sum_{j=1}^n S_j \leq n \sum_{i=1}^n |s_i| S_i \quad (26)$$

Thus we have

$$\begin{aligned}
\dot{V} &\leq \sum_{i=1}^n (-k_i s_i^2 - \hat{\delta}_i |s_i| S_i - \tilde{\delta}_i^T \Gamma_{i\delta}^{-1} \dot{\hat{\delta}}_i) \\
&\quad + n \max_{ij} \{d_{ij}\} \sum_{i=1}^n |s_i| S_i
\end{aligned} \quad (27)$$

Let $\delta = n \max_{ij} \{d_{ij}\}$, so we have

$$\dot{V} \leq \sum_{i=1}^n (-k_i s_i^2 + \tilde{\delta}_i^T |s_i| S_i - \tilde{\delta}_i^T \Gamma_{i\delta}^{-1} \dot{\hat{\delta}}_i) \quad (28)$$

Substituting (20) into (28), we have

$$\dot{V} \leq \sum_{i=1}^n (-k_i s_i^2) \leq 0 \quad (29)$$

So we can know $V(t) \leq V(0)$, which implies s_i is

bounded. Integrating $\sum_{i=1}^n k_i s_i^2$ with respect to time

$$\int_0^t \sum_{i=1}^n k_i s_i^2 dt \leq -\int_0^t \dot{V} dt = V(0) - V(t) \quad (30)$$

Because $V(0)$ is bounded, and $V(t)$ is bounded from below and is non-increasing with time, so the following result is obtained:

$$\lim_{t \rightarrow \infty} \int_0^t \sum_{i=1}^n k_i s_i^2 dt < \infty \quad (31)$$

It implies that $s_i \in L_2$. From (7), \dot{s}_i is bounded for all time, so according to Barbalat's Lemma, it concludes that $\lim_{t \rightarrow \infty} s_i(t) = 0$, so the joint tracking error e_i will also converge to zero asymptotically. \square

3.2. Self-tuning local feedback gain based DFTC

Through observing the system (1) with actuator failure, if we can estimate the effectiveness factor ρ_i in real-time, and then adding it to the decentralized control

scheme proposed in section 3.1, the DFTC can be achieved.

The decentralized fault tolerant controller is designed as

$$\bar{u}_i = \hat{\rho}_i^{-1} u_i \quad (32)$$

where $\hat{\rho}_i$ can be updated by the following adaptive law:

$$\dot{\hat{\rho}}_i = \Gamma_{i\rho} \hat{\rho}_i^{-1} s_i^T \hat{g}_i u_i \quad (33)$$

where $\Gamma_{i\rho} > 0$ is a known constant.

Theorem 2. Consider the system (1) with partial loss of actuator effectiveness, the proposed self-tuned local feedback gain based DFTC scheme can guarantee all the variables of the closed-loop system to be uniformly ultimately bounded (UUB).

Proof. Define $\tilde{\rho}_i = \rho_i - \hat{\rho}_i$, and select the Lyapunov candidate function as

$$V_{if} = V_i + \frac{1}{2} \tilde{\rho}_i^T \Gamma_{i\rho}^{-1} \tilde{\rho}_i \quad (34)$$

So its time derivative is

$$\begin{aligned}
\dot{V}_{if} &= \dot{V}_i + s_i^T (\tilde{\rho}_i^T \hat{g}_i \hat{\rho}_i^{-1} u_i + \tilde{\rho}_i^T \tilde{g}_i \hat{\rho}_i^{-1} u_i) - \tilde{\rho}_i^T \Gamma_{i\rho}^{-1} \dot{\tilde{\rho}}_i \\
&= -k_i s_i^2 + \tilde{\rho}_i^T (s_i^T \hat{g}_i \hat{\rho}_i^{-1} u_i - \Gamma_{i\rho}^T \dot{\hat{\rho}}_i) + s_i^T \tilde{\rho}_i^T \tilde{g}_i \hat{\rho}_i^{-1} u_i
\end{aligned} \quad (35)$$

Assuming that $\|s_i^T \tilde{\rho}_i^T \tilde{g}_i \hat{\rho}_i^{-1} u_i\| \leq \xi_{if}$, where $\xi_{if} > 0$ is a known constant. Substituting (33) into (35), we have

$$\dot{V}_{if} = -k_i s_i^2 + \xi_{if} \quad (36)$$

Thus $\dot{V}_{if} < 0$ as long as $|s_i| > \sqrt{\xi_{if}/k_i}$. According to Lyapunov direct method, the tracking error is UUB. \square

4. Simulation Study

In this section, a 2-DOF reconfigurable manipulator (Configuration *a* in reference 3, as well as the dynamic model, the desired trajectories) is employed to verify the effectiveness of the proposed DFTC scheme.

The actuator failure is injected into joint 1, and the effectiveness factor is chosen as

$$\rho_1 = \begin{cases} 1, & t < 4s \\ 0.8, & 4s \leq t \leq 10s \end{cases} \quad (37)$$

The control parameters are set as $\lambda_i = 5$, $k_i = 10$, $\Gamma_{if} = 0.002$, $\Gamma_{ig} = 0.002$, $\Gamma_{i\delta} = 500$, $\Gamma_{i\xi} = 400$ and $\Gamma_{i\rho} = 2000$.

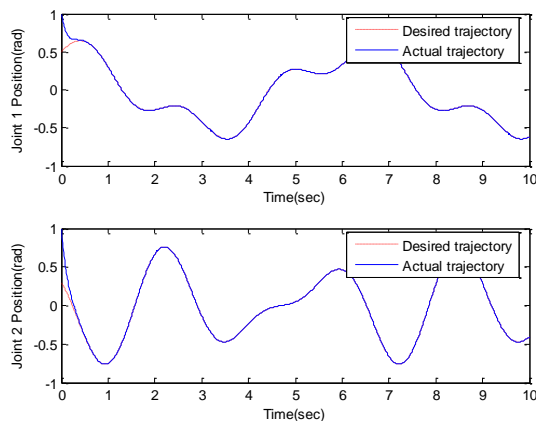


Fig.1. Tracking curves

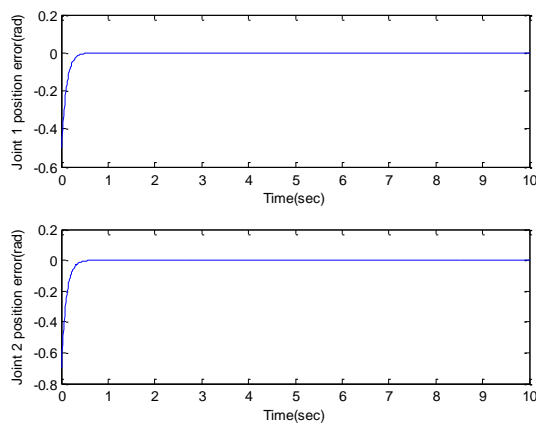


Fig.2. Tracking error curves

Fig.1 illustrates the trajectory tracking curves by using the proposed DFTC scheme, from where we can observe that the trajectory tracking is successfully guaranteed though the fault occurs after $t = 4s$. Meanwhile, the fault-free subsystem's control performance is not affected by the faulty one. The tracking errors in Fig.2 demonstrate this conclusion. Hence, the proposed self-tuned local feedback gain based DFTC is effective to deal with partial loss of actuator effectiveness.

5. Conclusions

A self-tuned local feedback gain based DFTC scheme is developed to deal with the partial loss of actuator effectiveness of reconfigurable manipulators. The decentralized neural network controller is designed for the fault-free system. Once the system suffers to partial

loss of actuator effectiveness, only a self-tuned local feedback gain is added to guarantee the system stable. This control architecture is simple since it is no need to redesign the fault tolerant controller once the system suffers to the partial loss of actuator effectiveness. Meanwhile, the fault is handled only in its local subsystem, rather than the entire system.

Acknowledgements

This work is supported in part by the National Natural Science Foundation of China under grant 61374051, and in part by the Scientific and Technological Development Plan Project in Jilin Province of China under grant 20150520112JH.

References

1. M. Yim, K. Roufas, D. Duff, et al. *Modular reconfigurable robots in space applications*, Autonomous Robots, **14**(2-3) (2003) 225-237.
2. C. Paradis, H. Brown and P. Khosla. *A rapidly deployable manipulator system*. Rob Auton Syst. **21**(1997) 289-304.
3. M. Zhu, Y. Li, *Decentralized adaptive fuzzy sliding mode control for reconfigurable modular manipulators*, International Journal of Robust and Nonlinear Control, **20**(4) (2010) 472-488.
4. T. Sato, T. Kano and A. Ishiguro, *A decentralized control scheme for an effective coordination of phasic and tonic control in a snake-like robot*, Bioinspiration & Biomimetics. **7**(1) (2012) 016005.
5. S. Abdul, G. Liu, *Decentralised fault tolerance and fault detection of modular and reconfigurable robots with joint torque sensing*, in Proc. 2008 IEEE Int. Conf. Robotics and Automation, pp. 3520-3526.
6. J. Yuan, G. Liu and B. Wu, *Power efficiency estimation-based health monitoring and fault detection of modular and reconfigurable robot*, IEEE Transactions on Industrial Electronics, **58**(10)(2011) 4880-4887.
7. B. Zhao, Y. Li, *Local joint information based active fault tolerant control for reconfigurable manipulator*, Nonlinear Dyn. **77**(2014) 859-876.
8. B. Zhao, Y. Li, *Signal reconstruction based active decentralized fault tolerant control for reconfigurable manipulators*, Acta Sinica Automatica. **40**(9)(2014) 1942-1950.

Study on Decentralized Integral Nested Sliding Mode Control for Constrained Reconfigurable Manipulator with Harmonic Drive Transmission

Bo Dong¹, Zeyu Dong¹, Bo Zhao², Yan li¹, Fumitoshi Matsuno³ and Yuanchun Li^{1,*}

¹*Department of Control Engineering, Changchun University of Technology
Changchun 130012, China*

²*The State Key Laboratory of Management and Control for Complex Systems, Institute of Automation,
Chinese Academy of Sciences, Beijing 100190, China*

³*Department of Mechanical Engineering and Science*

Graduate School of Engineering, Kyoto University, Japan

E-mail: ¹liyc@ccut.edu.cn (*Corresponding Author) ²zhaobo@ia.ac.cn ³matsuno@me.kyoto-u.ac.jp

Abstract

This paper addresses the problems of trajectory tracking control of a constrained reconfigurable manipulator with harmonic drive transmission under a decentralized integral nested sliding mode control (INSMC) method, and a high-performance control is achieved without using force/torque sensor. The dynamic model of the constrained reconfigurable manipulator is formulated with a nonlinear harmonic drive model. Based on only local dynamic information of each module, a decentralized integral nested sliding mode control method is proposed to reduce the chattering effect of the controller and compensating the model uncertainties. Finally, simulations are performed for a constrained 2-DOF reconfigurable manipulator to study the effectiveness of the proposed method.

Keywords: Reconfigurable manipulator, harmonic drive, decentralized control, sliding mode control

1. Introduction

Reconfigurable manipulator consists of the manipulator modules that incorporate power electronics, computing systems, sensors and actuators. These modules can be serially connected with standard electromechanical interfaces and assembled to desirable configuration for satisfying the requirements of various tasks. Besides, reconfigurable manipulator needs an appropriate control system to provide accuracy and stability.

Harmonic drives have been widely used in manipulator design due to the excellent properties such as high reduction ratio, compact size, light weight, and coaxial assembly. A typical harmonic drive includes a wave generator, a circular spline, and a flexspline placed in between. Numerous studies have been carried out on analytical description of harmonic drives based systems¹⁻⁵. However, in conventional methods, the kinematic error⁶ between the measured and expected flexspline output is always neglected and this may lead to a local torque ripple, which is introduced in harmonic harmonic drive should be considered when formulating the dynamic model of reconfigurable manipulator. Decentralized control is a particularly promising concept in implementing reconfigurable manipulator

system. Some researchers have studied the decentralized control method for reconfigurable manipulator⁷⁻⁹, and combining it with the sliding mode control method^{10,11}. However, the main drawback for these control strategies is the so-called “chattering effect”, which will be aggravated due to harmonic drive based reconfigurable manipulator is with the joint flexibility. Therefore, an excellent control approach for reconfigurable manipulator should be able to compensate the model uncertainty accurately and reduce the chattering effect of the controller.

In this paper, a decentralized integral nested sliding mode control method is proposed for constrained reconfigurable manipulator with harmonic drive transmission. The dynamic model of the constrained reconfigurable manipulator is formulated with a nonlinear harmonic drive model. An integral nested sliding surface¹², which is designed by employing a pseudo-sliding surface block, is implemented to reduce the chattering effect of the controller. Model uncertainties, including unmodeled subsystem dynamics, friction modeling error and the interconnected dynamic coupling, are compensated by using a variable gain super twisting algorithm (VGSTA) based decentralized

controller. Finally, simulations are performed for a constrained 2-DOF reconfigurable manipulator to illustrate the effectiveness of the proposed method.

2. Problem Formulation

According to the dynamic model of a n -DOF reconfigurable manipulator which is formulated as a synthesis of interconnected subsystems⁷, the dynamic model of i th subsystem of reconfigurable manipulator is given as follows

$$I_{mi}\ddot{\theta}_i + f_i(\theta_i, \dot{\theta}_i) + I_{mi} \sum_{j=1}^{i-1} z_{mi}^T z_{\theta j} \ddot{\theta}_j + I_{mi} \sum_{j=2}^{i-1} \sum_{k=1}^{j-1} z_{mi}^T (z_{\theta k} \times z_{\theta j}) \dot{\theta}_k \dot{\theta}_j + \frac{\tau_{fci}}{\gamma_i} = \tau_i \quad (1)$$

where $I_{mi} \sum_{j=1}^{i-1} z_{mi}^T z_{\theta j} \ddot{\theta}_j + I_{mi} \sum_{j=2}^{i-1} \sum_{k=1}^{j-1} z_{mi}^T (z_{\theta k} \times z_{\theta j}) \dot{\theta}_k \dot{\theta}_j$ is the dynamic coupling term, I_{mi} is the moment of inertia of the rotor about the axis of rotation, τ_i is the motor output torque, z_{mi} and $z_{\theta i}$ are the unity vectors along the axis of rotation of the i th rotor and joint respectively, τ_{fci} is the certain part of the estimated joint torque using only position measurements⁵, and can be represented as following

$$\tau_{fci} = \frac{1}{c_f} \tan \left(c_f k_{f0} \left(\Delta \theta_i - \frac{\text{sgn}(\tau_{wi})}{\gamma_i c_w k_{w0}} (1 - e^{-c_w |\tau_{wi}|}) \right) \right) \quad (2)$$

where k_{f0} , k_{w0} , c_f and c_w are the constants to be determined, $\text{sgn}(\cdot)$ is the normal sign function, $\Delta \theta_i$ is the torsional angle of the harmonic drive, which is obtained by combining the measured link side with the motor side position measurements, and the wave generator torque τ_{wi} can be approximated by the motor torque command. Note that the term $f_i(\theta_i, \dot{\theta}_i)$ in (1) is the frictional torque term which is considered as a function of the joint position and velocity¹³, and given as follows

$$f_i(\theta_i, \dot{\theta}_i) = b_{fi} \dot{\theta}_i + \left(f_{ci} + f_{si} e^{(-f_{ti} \dot{\theta}_i^2)} \right) \text{sgn}(\dot{\theta}_i) + f_{\theta i}(\theta_i, \dot{\theta}_i) \quad (3)$$

where f_{ci} denotes the Coulomb friction-related parameter; f_{si} denotes the static friction-related parameter; f_{ti} is a position parameter about the Stribeck effect, b_{fi} is the viscous friction coefficient, $f_{\theta i}(\theta_i, \dot{\theta}_i)$ is the position dependency of friction and friction modeling errors. Let $x_i = [x_{i1}, x_{i2}]^T = [\theta_i, \dot{\theta}_i]^T$ for $i = 1, 2, \dots, n$. According to (1), the following state equation is obtained:

$$S_i : \begin{cases} \dot{x}_{i1} = x_{i2} \\ \dot{x}_{i2} = Fr_i(\theta_i, \dot{\theta}_i) + \Psi_i(\theta_i, \dot{\theta}_i) + h_i(\theta_i, \dot{\theta}_i, \ddot{\theta}_i) - b_i u_i \\ y_i = x_{i1} \end{cases} \quad (4)$$

where x_i is the state vector and y_i is the output of S_i . $b_i = (I_{mi} \gamma_i)^{-1} \in \mathbb{R}^+$, $\Psi_i(\theta_i, \dot{\theta}_i)$, $Fr_i(\theta_i, \dot{\theta}_i)$ and $h_i(\theta_i, \dot{\theta}_i, \ddot{\theta}_i)$ is defined as

$$\begin{aligned} \Psi_i(\theta_i, \dot{\theta}_i) &= -(I_{mi} \gamma_i)^{-1} (\tau_{fci} / \gamma_i) \\ Fr_i(\theta_i, \dot{\theta}_i) &= -(I_{mi} \gamma_i)^{-1} f_i(\theta_i, \dot{\theta}_i) \\ h_i(\theta_i, \dot{\theta}_i, \ddot{\theta}_i) &= -(I_{mi} \gamma_i)^{-1} \left(I_{mi} \sum_{j=2}^{i-1} \sum_{k=1}^{j-1} z_{mi}^T (z_{\theta k} \times z_{\theta j}) \dot{\theta}_k \dot{\theta}_j + I_{mi} \sum_{j=1}^{i-1} z_{mi}^T z_{\theta j} \ddot{\theta}_j + \tau_{ui} \right) \end{aligned} \quad (5)$$

where τ_{ui} is the output torque ripple that is considered as a model uncertain term and will be compensated in the next section.

3. Control Design

In this section, a decentralized integral nested sliding mode control approach is proposed based on VGSTA.

Assumption 1. Desired trajectory $y_{ir1}(t)$ is bounded and second order derivable.

Assumption 2. The interconnected dynamic coupling term $h_i(\theta_i, \dot{\theta}_i, \ddot{\theta}_i)$ is bounded, and satisfy

$$\|h_i(\theta_i, \dot{\theta}_i, \ddot{\theta}_i)\| \leq g_{i0} + \sum_{j=1}^n g_{ij} \quad (6)$$

where g_{i0} is a positive constant, g_{ij} is a smooth Lipschitz function. Define the tracking position error and its time derivative as

$$e_{i1} = x_{i1} - y_{ir1}(t), \quad \dot{e}_{i1} = x_{i2} - \dot{y}_{ir1}(t) \quad (7)$$

Define the pseudo-sliding surface s_{i1} for the first block as

$$s_{i1} = e_{i1} + z_{i1}, \quad z_{i1}(0) = -e_{i1}(0) \quad (8)$$

and the derivative of s_{i1} can be given as follows

$$\dot{s}_{i1} = \dot{e}_{i1} + \dot{z}_{i1} = x_{i2} - \dot{y}_{ir1}(t) + \dot{z}_{i1} \quad (9)$$

In (8) and (9), z_{i1} is an integral variable which will be defined later. It is of importance to introduce the second block of sliding surface, defined as follows

$$s_{i2} = e_{i2} + z_{i2}, \quad z_{i2}(0) = -e_{i2}(0) \quad (10)$$

where z_{i2} is an integral variable to be determined, and e_{i2} , which is used to design the second block of sliding surface, can be defined as

$$e_{i2} = x_{i2} - y_{ir2}(t) \quad (11)$$

where $y_{ir2}(t)$ is defined as

$$y_{ir2}(t) = y_{ir2,0}(t) + y_{ir2,1}(t) \quad (12)$$

In (12), $y_{ir2,0}(t)$ is the nominal part of the control design, and $y_{ir2,1}(t)$ is used to design the control law for the purpose of compensating the unmodeled subsystem dynamics.

Substituting (11) into (10), one can obtain that

$$\dot{x}_{i2} = \dot{s}_{i2} + \dot{y}_{ir2}(t) - \dot{z}_{i2} \quad (13)$$

Combining (9) with (13), the derivative of the pseudo-sliding surface s_{i1} can be rewritten as

$$\dot{s}_{i1} = \dot{s}_{i2} - \dot{z}_{i2} + \dot{y}_{ir2,0}(t) + \dot{y}_{ir2,1}(t) - \dot{y}_{ir1}(t) + \dot{z}_{i1} \quad (14)$$

Choose \dot{z}_{i1} as the form of

$$\dot{z}_{i1} = -(s_{i2} - z_{i2} + y_{ir2,0}(t)) \quad (15)$$

Then, combining (10), (14), with (15), the derivative of s_{i1} and z_{i1} can be represented as

$$\dot{s}_{i1} = y_{ir2,1}(t) - \dot{y}_{ir1}(t), \quad \dot{z}_{i1} = -e_{i2} - y_{ir2,0}(t) \quad (16)$$

With the initial condition $z_{i1}(0) = -e_{i1}(0)$, define $y_{ir2,0}(t)$ and $y_{ir2,1}(t)$ as

$$y_{ir2,0}(t) = -k_1 e_{i1}, \quad y_{ir2,1}(t) = -\sigma_1 \text{sigm}(\varepsilon_1, s_{i1}) \quad (17)$$

where k_1 , σ_1 and ε_1 are positive constants to be determined. $\text{sigm}(\cdot)$ is a sigmoid function which can be defined as follows

$$\text{sigm}(\varepsilon_1, s_{i1}) = \tanh(\varepsilon_1 s_{i1}) \quad (18)$$

Then, we can obtain the time derivative of s_{i2} as

$$\dot{s}_{i2} = \dot{e}_{i2} + \dot{z}_{i2} = \dot{x}_{i2} - \dot{y}_{ir2}(t) + \dot{z}_{i2} \quad (19)$$

According to (17), one can obtain that $\dot{y}_{ir2}(t)$ is represented as

$$\dot{y}_{ir2}(t) = -k_1 \dot{e}_{i1} + \sigma_1 \varepsilon_1 (1 - \tanh^2(\varepsilon_1 s_{i1})) (\sigma_1 \text{sigm}(\varepsilon_1, s_{i1}) + \dot{y}_{ir1}(t)) \quad (20)$$

Substituting (4) into (19), we can rewrite \dot{s}_{i2} as

$$\dot{s}_{i2} = \Psi_i(\theta_i, \dot{\theta}_i) + Fr_i(\theta_i, \dot{\theta}_i) + h_i(\theta, \dot{\theta}, \ddot{\theta}) - b_i u_i - \dot{y}_{ir2}(t) + \dot{z}_{i2} \quad (21)$$

where \dot{z}_{i2} is chosen as

$$\dot{z}_{i2} = -k_2 \dot{e}_{i1} + \sigma_2 \varepsilon_1 (1 - \tanh^2(\varepsilon_1 s_{i1})) (\sigma_1 \text{sigm}(\varepsilon_1, s_{i1}) + \dot{y}_{ir1}(t)) \quad (22)$$

where k_2 and σ_2 are positive constants to be determined. For the purpose of compensating the different terms of the derivative of the sliding surface, we can design the control law as the form of $u_i = u_{i0} + u_{i1} + u_{i2}$. So that (21) can be rewritten as

$$\begin{aligned} \dot{s}_{i2} = & Fr_i(\theta_i, \dot{\theta}_i) - b_i u_{i0} + \Psi_i(\theta_i, \dot{\theta}_i) - b_i u_{i1} \\ & + h_i(\theta, \dot{\theta}, \ddot{\theta}) - b_i u_{i2} - \dot{y}_{ir2}(t) + \dot{z}_{i2} \end{aligned} \quad (23)$$

First, design the control law u_{i0} to compensate the effect of joint friction $Fr_i(\theta_i, \dot{\theta}_i)$.

$$u_{i0} = \hat{b}_{fi} \dot{\theta}_i + (\hat{f}_{ci} + \hat{f}_{si} e^{(-\hat{f}_{si} \dot{\theta}_i^2)}) \text{sgn}(\dot{\theta}_i) + u_{i0}^1 + Y(\dot{\theta}_i) (u_{i0}^2 + u_{i0}^3) \quad (24)$$

where $Y(\dot{\theta}_i)$ can be defined as follows

$$Y(\dot{\theta}_i) = [\dot{\theta}_i, \text{sgn}(\dot{\theta}_i), e^{(-\hat{f}_{si} \dot{\theta}_i^2)} \text{sgn}(\dot{\theta}_i), -\hat{f}_{si} \dot{\theta}_i^2 e^{(-\hat{f}_{si} \dot{\theta}_i^2)} \text{sgn}(\dot{\theta}_i)] \quad (25)$$

In order to incorporate variable parametric model uncertainty compensation, we can design

$$\tilde{F}^i = [\hat{b}_{fi} - b_{fi}, \hat{f}_{ci} - f_{ci}, \hat{f}_{si} - f_{si}, \hat{f}_{\tau i} - f_{\tau i}]^T = \tilde{F}_c^i + \tilde{F}_v^i \quad (26)$$

where \tilde{F}_c^i and \tilde{F}_v^i are constant and variable unknown vector respectively. And \tilde{F}_v^i is bounded as

$$|\tilde{F}_{vn}^i| < \rho_n^i, n = 1, 2, 3, 4 \quad (27)$$

In (25), \hat{b}_{fi} , \hat{f}_{ci} , \hat{f}_{si} , $\hat{f}_{\tau i}$ are the normal friction parameters, u_{i0}^1 is the term designed to compensate the nonparametric uncertainty $f_{\theta i}(\theta, \dot{\theta})$ in (3). The terms u_{i0}^2 and u_{i0}^3 are designed to compensate for the parameter uncertainty \tilde{F}_c^i and \tilde{F}_v^i , respectively. The friction compensation is of the same form for all the joints, and hence, for the i th joint, the compensators, u_{i0}^1 , u_{i0}^2 , u_{i0}^3 are defined by

$$\begin{aligned} u_{i0}^1 &= -\rho_{fi} \frac{s_{i2}}{|s_{i2}|} \quad |s_{i2}| > \varepsilon^i, \quad -\rho_{fi} \frac{s_{i2}}{\varepsilon^i} \quad |s_{i2}| \leq \varepsilon^i \\ u_{i0}^2 &= -k_3 \int_0^t Y(\dot{\theta}_i)^T s_{i2} dt \\ u_{i0}^3 &= -\rho_n^i \frac{\delta_n^i}{|\delta_n^i|} \quad |\delta_n^i| > \varepsilon_{pn}^i, \quad -\rho_n^i \frac{\delta_n^i}{\varepsilon_{pn}^i} \quad |\delta_n^i| \leq \varepsilon_{pn}^i \end{aligned} \quad (28)$$

where $\delta^i = Y(\dot{\theta}_i)^T s_{i2}$, and ρ_{fi} , ρ_n^i are the parametric uncertainty bounds. ε^i , ε_{pn}^i are parameters to be determined.

Second, design the control law u_{i1} to compensate the terms of $\Psi_i(\theta_i, \dot{\theta}_i)$, $\dot{y}_{ir2}(t)$, and \dot{z}_{i2}

$$u_{i1} = b_i^{-1} \left((k_1 - k_2) \dot{e}_{i1} + k_3 \text{sat}(\varepsilon_s, s_{i2}) + (\sigma_1 - \sigma_2) (1 - \tanh^2(\varepsilon_1 s_{i1})) \right) \quad (29)$$

where ε_s and k_3 are positive constants to be determined. $\text{sat}(\cdot)$ is a saturation function, which is defined as follows

$$\text{sat}(\varepsilon_s, s_{i2}) = \begin{cases} \text{sgn}(s_{i2}) & |s_{i2}| > \varepsilon_s \\ s_{i2} / \varepsilon_s & |s_{i2}| \leq \varepsilon_s \end{cases} \quad (30)$$

Third, based on the VGSTA theory^{8, 14}, design the control law u_{i2} to compensate the interconnected dynamic coupling term $h_i(\theta, \dot{\theta}, \ddot{\theta})$ which is represented as the following form

$$h_i(\theta, \dot{\theta}, \ddot{\theta}) = g_{i1}(\theta, t) + g_{i2}(\theta, t) \quad (31)$$

where $g_{i1}(\theta, t)$ and $g_{i2}(\theta, t)$ are bounded by

$$\begin{cases} |g_{i1}(\theta_i, t)| \leq \varsigma_{i1}(\theta_i, t) |\phi_{i1}(s_{i2})| \\ \left| \frac{dg_{i2}(\theta_i, t)}{dt} \right| \leq \varsigma_{i2}(\theta_i, t) |\phi_{i2}(s_{i2})| \end{cases} \quad (32)$$

where $\varsigma_{i1}(\theta_i, t) > 0$ and $\varsigma_{i2}(\theta_i, t) > 0$ are known continuous functions. $\phi_{i1}(s_{i2})$ and $\phi_{i2}(s_{i2})$ are defined as

$$\begin{cases} \phi_{i1}(s_{i2}) = |s_{i2}|^{1/2} \text{sgn}(s_{i2}) + \kappa_{i3}(t) s_{i2} \\ \phi_{i2}(s_{i2}) = \frac{1}{2} \text{sgn}(s_{i2}) + \frac{3}{2} \kappa_{i3}(t) |s_{i2}|^{1/2} \text{sgn}(s_{i2}) + \kappa_{i3}^2(t) s_{i2} \end{cases} \quad (33)$$

where $\kappa_{i3}(t)$ is a positive gain to be determined. Substituting (31) into (23), one can obtain that

$$\begin{aligned} \dot{s}_{i2} = & F c_i(\theta_i, \dot{\theta}_i) - b_i u_{i0} + \Psi_i(\theta_i, \dot{\theta}_i) - b_i u_{i1} \\ & + g_{i1}(\theta_i, t) + g_{i2}(\theta_i, t) - b_i u_{i2} - \dot{y}_{ir2}(t) + \dot{z}_{i2} \end{aligned} \quad (34)$$

Design the control law u_{i2} to compensate the inter-connected dynamic coupling term, shown as follows

$$u_{i2} = b_i^{-1} \left(\kappa_{i1}(t) \phi_{i1}(s_{i2}) + \int_0^t \kappa_{i2}(t) \phi_{i2}(s_{i2}) dt \right) \quad (35)$$

where the variable gains $\kappa_{i1}(t)$ and $\kappa_{i2}(t)$ are chosen as

$$\begin{cases} \kappa_{i1}(t) = \frac{1}{\rho_v} \left\{ \frac{1}{4\varepsilon_2} (2\varepsilon_2 \varsigma_{i1} + \varsigma_{i2})^2 + 2\varepsilon_2 \varsigma_{i2} \right\} + \varphi \\ \kappa_{i2}(t) = \rho_v + 4\varepsilon_2^2 + 2\varepsilon_2 \kappa_{i1}(t) \end{cases} \quad (36)$$

where φ , ρ_v , ε_2 are positive constants to be determined. Therefore, combine (24), (29) with (35), the decentralized integral nested sliding mode control law u_i for the i th joint can be defined as follows

$$\begin{aligned} u_i = & b_i^{-1} \left(b_i \left(\hat{b}_{ji} \dot{\theta}_i + Y(\dot{\theta}_i) (u_{i0}^3 + u_{i0}^1) \right) + (k_1 - k_2) \dot{e}_{i1} \right. \\ & + \left(\hat{f}_{ci} + \hat{f}_{si} e^{-\hat{f}_{si} \theta_i^2} \right) \text{sgn}(\dot{\theta}_i) \\ & + (\sigma_1 - \sigma_2) (1 - \tanh^2(\varepsilon_1 s_{i1})) + k_3 \text{sat}(\varepsilon_s, s_{i2}) \\ & \left. + \kappa_{i1}(t) \phi_{i1}(s_{i2}) + \int_0^t \kappa_{i2}(t) \phi_{i2}(s_{i2}) dt \right) \end{aligned} \quad (37)$$

Theorem. Given a constrained n -DOF reconfigurable manipulator, with the dynamic model as formulated in (1), and the model uncertainties that existed in (5). The closed-loop system is stable under the decentralized integral nested sliding mode control law defined by (37). **Proof.** Refer to Ref. 12.

4. Simulations

To study the effectiveness of the proposed decentralized control approach, in this paper, two different configurations of the constrained reconfigurable manipulator with harmonic drive transmission are used to conduct the simulations. The dynamic model and the parameters of controller are chosen as Ref. 12.

To verify the effectiveness and precision of the proposed control method, in this paper, the simulations are conducted with two different controllers respectively,

that including the conventional one-order sliding mode controller (SMC) and the proposed integral nested sliding mode controller (INSMC). The simulation results are shown in the following figures. Fig. 1 shown the joint position error curves and the control torque curves of two different configurations under the SMC. Fig. 2 shown the joint position error curves and the control torque curves of configurations A and B under the INSMC. Fig. 3 shown the constrained force and trajectory tracking curves of the end-effector.

From these figure we can conclude that the chattering effects in both the error curves and the control torque curves are relatively obvious under the conventional SMC method. However, the tracking performance of the joint positions is improved under the INSMC method because the model uncertainty has been compensated accurately. The chattering effect can be reduced in a short time interval by using the proposed integral nested sliding surface design, and the desired trajectory of end-effector can be tracked accurately under the proposed INSMC method.

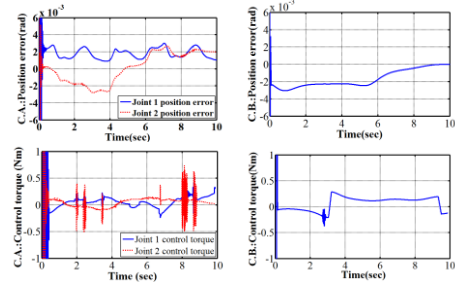


Fig. 1. Position error and control torque curves of configurable A and B under SMC

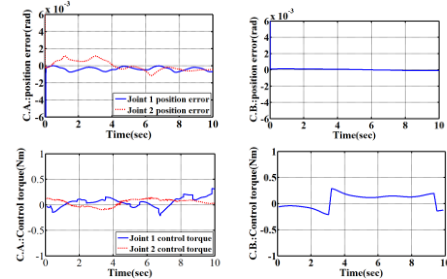


Fig. 2. Position error and control torque curves of configurable A and B under INSMC

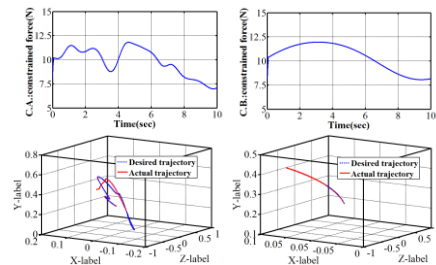


Fig. 3. Constrained force and trajectory tracking curves of end-effector

5. Conclusion

This paper studies on constrained reconfigurable manipulator with harmonic drive transmission, and addresses the problems of trajectory tracking control without using force/torque sensor. The dynamic model is formulated based on a nonlinear harmonic drive model. A decentralized INSMC method based on VGSTA is proposed to reduce the chattering effect and compensating the model uncertainties. Finally, simulations are performed to study the effectiveness of the proposed method.

Acknowledgment

This work is financially supported by: National Natural Science Foundation of China (Grant No. 61374051).

References

1. M. Hashimoto, T. Kiyosawa, and R. P. Paul, "A torque sensing technique for robots with harmonic drives," *IEEE Trans. on Robot. Automat.*, vol. 9, no. 1, pp. 108-116, Feb. 1993.
2. H. Zhang, S. Ahmad and G. Liu, "Modeling of torsional compliance and hysteresis behaviors in harmonic drives," *IEEE/ASME Trans. on Mech.*, vol. 20, no. 1, pp. 178-184, Feb. 2015.
3. W. Zhu, T. Lamarche, E. Dupuis, D. Jameux, P. Barnard, and G. Liu, "Precision control of modular robot manipulators: the VDC approach with embedded FPGA," *IEEE Trans. on Robot.*, vol. 29, no. 5, pp. 1162-1179, Oct. 2013.
4. C. Kennedy and J. Desai, "Modeling and control of the mitsubishi pa-10 robot arm harmonic drive system," *IEEE/ASME Trans. on Mech.*, vol. 10, no. 3, pp. 263-274, Jun. 2005.
5. H. Zhang, S. Ahmad and G. Liu, "Torque Estimation for Robotic Joint With Harmonic Drive Transmission Based on Position Measurements", *IEEE Trans. Robot.*, vol. 31, no. 2, pp. 322-330, 2015.
6. Y. Shigeo, S. Ishizuka, T. Yamaguchi, and I. Masaki, "Torsional stiffness of harmonic drive reducers," *Trans. Japan Soc. Mechanic. Eng.*, part C, (in Japanese), vol. 55, no. 509, pp. 216-221, 1989.
7. B. Dong and Y. C. Li, "Decentralized reinforcement learning robust optimal tracking control for time varying constrained reconfigurable modular robot based on ACI and Q-function," *Mathematical Problems in Engineering*, vol. 2013, Article ID 387817, 16 pages, 2013. doi:10.1155/2013/387817.
8. Y. C. Li and B. Dong, "Decentralized ADRC control for reconfigurable manipulators based on VGSTA-ESO of sliding mode," *Information-An International Interdisciplinary Journal*, vol. 15, no. 6, pp. 2453-2466, 2012.
9. G. Liu, S. Abdul, and A. A. Goldenberg, "Distributed control of modular and reconfigurable robot with torque sensing," *Robotica*, vol. 26, no. 1, pp. 75-84, 2008.
10. M. C. Zhu and Y. C. Li, "Decentralized adaptive fuzzy sliding mode control for reconfigurable modular manipulators," *International Journal of Robust and Nonlinear Control*, vol. 20, no. 4, pp. 472-488, 2010.
11. M. C. Zhu and Y. C. Li, "Decentralized adaptive sliding mode control for reconfigurable manipulators using fuzzy logic," *Journal of Jilin University Engineering and Technology Edition*, vol. 39, no. 1, pp. 170-176, 2009.
12. B. Dong and Y. C. Li, "Decentralized integral nested sliding mode control for time varying constrained modular and reconfigurable robot" *Advances in Mechanical Engineering* 2015. doi:10.1155/2014/317127.
13. G. Liu, A. A. Goldenberg and Y. Zhang, "Precise slow motion control of a direct-drive robot arm with velocity estimation and friction compensation," *Mechatronics* vol. 14, no. 7, pp. 821-834, Sep. 2004.
14. T. Gonzalez, J. A. Moreno and L. Fridman, "Variable gain super-twisting sliding mode control," *IEEE Transactions on Automatic Control*, vol. 57, no. 8, pp. 2100-2105, 2012.

A Number of Mobile Manipulator Control for Moving an Object by using Cooperative Control

Deok-Su Kim

*Dep. of Electronic Eng., Pusan National University, Jangjeon-dong, Geumjeong-gu
Busan, 609-735, Korea Republic*

Dong-Eon Kim

*Dep. of Electronic Eng., Pusan National University, Jangjeon-dong, Geumjeong-gu
Busan, 609-735, Korea Republic*

Seong-Ik Han

*Dep. of Electronic Eng., Pusan National University, Jangjeon-dong, Geumjeong-gu
Busan, 609-735, Korea Republic*

Jang-Myung Lee

*Dep. of Electronic Eng., Pusan National University, Jangjeon-dong, Geumjeong-gu
Busan, 609-735, Korea Republic*

*E-mail: deoksu1696@pusan.ac.kr, hyunuk.ha@gmail.com, dongeon1696@pusan.ac.kr, jmlee@pusan.ac.kr
www.pusan.ac.kr*

Abstract

In this paper, we propose a method of cooperative control of a three mobile manipulator for moving an object. These robots go to desired position independently by using encoder data and inverse kinematics and after arriving in the position, they grasp and lift the object. For the carrying operation, the lifting operation is implemented by using the manipulator mounted on the top of the mobile robots cooperatively. In this system, master-slave mode is used for finding each position of robots and for coordinative control among the robots. During the moving operation, a trajectory planning has been kept constantly. The real cooperative carrying motions was implemented to check the possibility of the master-slave mode control based on the mobile manipulator's kinematics.

Keywords: Cooperative Control, Kinematics, Mobile Manipulator, Master-Slave.

1. Introduction

Due to rapid growth of the intelligent robot industry in the modern society, role of robot has been increased. so it is used in ordinary life as well as industries[1]. recent studies of mobile robot is extended from single action

plan of a robot to cooperation of a number of robots.[2] the cooperation system with robots can solve impossible problems that can't do with performance of each robots.[3] to achieve goal in cooperative robotic systems, a strategy for the cooperation between robots is essential.

© The 2016 International Conference on Artificial Life and Robotics (ICAROB 2016), Jan. 29-31, Okinawa Convention Center, Okinawa, Japan

recently a theory of intelligent communities make it possible that solving complex missions by serving flexible way.[4] cooperative robot system is classified behavior control technology, situation recognizing technology, networking technology, clustering technology, and in this paper, we want to propose the overall system about cooperative robot. situation, and action is given, so we just investigated for moving and communicating method.

In this paper, we studied cooperative control for carrying an object by using three mobile manipulator. We suggest method of cooperative control for moving an object by using three mobile manipulator. and we explain the position control by using encoder value and trajectory plan after that we conclude this paper.



Fig. 1. Mobile robot.

2. Cooperative Control System

The robot in Fig. 1 was made for experiment. for position control it use two motors and it was controlled by Embedded Computer. The manipulator is composed of three-wheeled and three-linked mobile manipulator system.

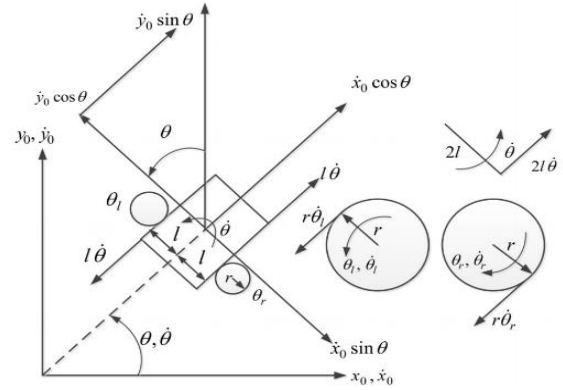


Fig. 3. Schematic description of a mobile part.

$$\begin{aligned}
 & + \frac{1}{2} m_2 [\dot{x} - r_2 \dot{\theta}_2 s_{\theta_2} c_{\varphi\theta_1} - r_2 (\dot{\varphi} + \dot{\theta}_1) c_{\theta_2} s_{\varphi\theta_1}]^2 \\
 & + \frac{1}{2} m_2 [\dot{y} - r_2 \dot{\theta}_2 s_{\theta_2} s_{\varphi\theta_1} + r_2 (\dot{\varphi} + \dot{\theta}_1) c_{\theta_2} c_{\varphi\theta_1}]^2 \\
 & + \frac{1}{2} I_{z2} [(\dot{\varphi} + \dot{\theta}_1)^2 + \dot{\theta}_2^2] \\
 & + \frac{1}{2} m_3 [\dot{x} - l_2 \dot{\theta}_2 s_{\theta_2} c_{\varphi\theta_1} - l_2 (\dot{\varphi} + \dot{\theta}_1) c_{\theta_2} s_{\varphi\theta_1} - r_3 (\dot{\theta}_2 + \dot{\theta}_3) s_{\theta_23} c_{\varphi\theta_1} \\
 & \quad - r_3 (\dot{\varphi} + \dot{\theta}_1) c_{\theta_23} s_{\varphi\theta_1}]^2 + \frac{1}{2} m_3 [\dot{y} - l_2 \dot{\theta}_2 s_{\theta_2} s_{\varphi\theta_1} \\
 & \quad + l_2 (\dot{\varphi} + \dot{\theta}_1) c_{\theta_2} c_{\varphi\theta_1} - r_3 (\dot{\theta}_2 + \dot{\theta}_3) s_{\theta_23} s_{\varphi\theta_1} + r_3 (\dot{\varphi} + \dot{\theta}_1) c_{\theta_23} c_{\varphi\theta_1}]^2 \\
 & + r_3 (\dot{\varphi} + \dot{\theta}_1) c_{\theta_23} c_{\varphi\theta_1}]^2 + \frac{1}{2} I_{z3} [(\dot{\varphi} + \dot{\theta}_1)^2 + (\dot{\theta}_2 + \dot{\theta}_3)^2].
 \end{aligned}$$

The potential energy is obtained as follows:

$$V = m_2 g r_2 s_{\theta_2} + m_3 g (l_2 s_{\theta_2} + r_3 s_{\theta_23})$$

And we use Bumblebee stereo camera to detecting object and get depth information of it. We use triangulation algorithm which refers to the process of determining a point in 3D space given its projections over two or more images. Now, we recognize our mobile robot's velocity, torque, object's position and depth information. We propose an approach to control the communication among 3 mobile robots. In our system, 3 mobile robots which take role of clients are worked under the control of a computer server. Status data coming from mobile robot, which contains the information about robot's position, orientation and end-effector's posture, is transferred to computer. In server term, after collecting data from 3 robots, the programed calculation process is operated. The result of this process is the next status data for 3 mobile robots, is then sent to all slaves by using wireless communication. Our mobile robot system is set

up with the architecture of sever & multi-client, which is include one computer and three autonomous mobile robots. Computer takes a role of server device, which is in charge of receiving the status of each mobile robot, and then, after calculation process, it send back the command to each client (mobile robot). In term of mobile robot, after sending the status containing the information about position of the platform and the angler of each link in end-effector, it will wait until receive the command from server. Depend on the data coming from computer, mobile robot will move to next position. In mobile robot, we use embedded system to control whole process. The device using in our experiment is IEC1000 series industrial embedded computer & HMI, which is supported to use external HNS wireless card. Schematic description of a mobile part(Fig.3), the dynamic equations of mobile robot is describe as the following equation:

$$\begin{bmatrix} \dot{x}_o \\ \dot{y}_o \\ \dot{\theta} \\ \dot{\theta}_r \\ \dot{\theta}_l \end{bmatrix} = \begin{bmatrix} \frac{r}{2l(l\cos\theta - d\sin\theta)} & \frac{r}{2l(l\cos\theta + d\sin\theta)} \\ \frac{r}{2l(l\sin\theta + d\sin\theta)} & \frac{r}{2l(l\sin\theta - d\cos\theta)} \\ \frac{r}{2l} & -\frac{r}{2l} \\ 1 & 0 \\ 1 & 0 \end{bmatrix} \cdot \begin{bmatrix} \dot{\theta}_r \\ \dot{\theta}_l \end{bmatrix} \quad (1)$$

■ $q_v = [x_o \ y_o \ \theta \ \theta_r \ \theta_l]^T$: The generalized coordinates of the mobile platform.

Where

- $x_o \ y_o$: The position of mobile robot.
- θ : The rotation angler of mobile robot's platform.
- $\theta_r \ \theta_l$: The rotation angler of left wheel and right wheel, respectively.

■ r : The radius of the wheels.

■ $2l$: The distance between 2 wheels.

From eq.(1), if the desired velocity vector of the left and right wheel is given, the translational velocity, with respect to x-axis and y-axis respectively, and angular velocity of the platform is also specified. Consequently, after sending the status data (platform's position and direction, end-effector's posture) to computer, mobile robot is waiting for the command coming from computer, which contains the information about desired velocity of the left and right wheel. Client's processor controls all other parts based on the data coming from server. Client-Server (CS) mode is an information sharing mode which is widely used in information system. The core of CS system structure is the distribution of task-level application between client and server. In the C/S system Clients and servers can be linked through LAN,

WAN or internet. In client-Server module, it allows to share information and resource among the systems like files, disk space, processors and peripherals which can collaborate and deliver message inevitably between many processors. Therefore, The mechanism which get the other machine's network address while communicating between network. A server (computer) maintains the communication with the three clients. Therefore, it is needed to apply several way to separate the mobile robot's connection time between server. Therefore, in this case, multi-thread is applied for server programming. The key of the multi-thread create the main server socket object in the main program. As each client connects to the server, the main program creates a separate thread to handle the communication.

Many methods have been suggested for the control of autonomous mobile robot like behavior-based approach, virtual structural approach. To control the three multi mobile robots we used leading-follow approach and virtual architecture. Behavioral approach use the distance between the robot to control the other action like evasion, maintaining the position and the movement. It is mainly used when lots of robots search the space, it is easy to derive a control strategy when a plurality of tasks are given. Virtual structure approach is the method that as robots moving keep the charge point to maintain the specific structure. This method defines a desired virtual structure and convert the virtual structural movement to the path that robots move. Finally, leading-follow approach is a way to maintain the overall position by keeping the robot along a desired distance and angle tracking robots. In this paper, we decide the sequence of operations and make different behavior depending in the order of the conditions. The driving method will be different according to the robot is holding a object or not. Also, when lifting the object the movement of the robot is changing. It divided into three conditions to have a driving and the operation patterns for each situation. 1. The case that the robot does not holding an object. First, the mobile robot need the finding action to find the object. It use the bumblebee camera to identify the location through the object recognition. In addition, the starting position of the mobile robot is fixed point. So the first step is to access a place that exist the object to lift. The mobile robot that knows the target location and the start location is easily accessible to the target position. 2. When lifting the object. The robot knows the coordinates of the current location. To lift an object we set the manipulator movement by inverse kinematics analysis. We consider the approach

© The 2016 International Conference on Artificial Life and Robotics (ICAROB 2016), Jan. 29-31, Okinawa Convention Center, Okinawa, Japan

distance of the mobile robot to the inverse kinematics analysis. 3. When mobbing with the holding object. After lift the object, three mobile robots should move in the same direction at the same time. Additionally, the distance and angle between the robot to be held constant. Three robot is composed of a single Master and two Slave robot. Master robot determine the each situation and receive communication information with the slave robot. A control algorithm of a robot can be seen from Figure 3.

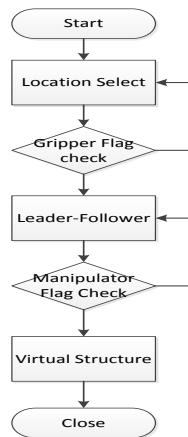


Fig. 3. Algorithm for swarm robots.

The first three robots must go to find their target position. If all three robot reaches the correct position, the robot takes an object with stretched arms. At that time the Slave robot sends the signal to determine the objects caught to the Master robot. When Master robot notice that three robots grab the object it will lift the object on. This algorithm inform to master robot that slave robot holding all of the objects and when master robot is holding the object is lifted on it will drive with maintaining the present distance and angle based on position of leader robot. Each of the conditions will be noticed using camera. Each robot is controlled by Embedded Computer. We can confirm that driving works well by using PD controller in the Encoder value.

Conclusion

In this paper, we proposed the method of navigation of Mobile Robot using recognition and distance information with Bumblebee stereo camera. And controlling the communication which use Wifi-comm based on the socket programing applying wireless communication in



Fig. 4. Mobile Robots in formation based on the Vision.

three mobile robot system,. By applying structure of multi-thread server, computer can handle the communication with three mobile robots without collision. We deal with the multiple robot coordination control system using inverse kinematics analysis.

Acknowledgements

This work was supported by the National Research Foundation of Korea(NRF) grant funded by the Korea government(MSIP) (NRF-2015R1A2A2A01004457). This research was supported by the MOTIE (Ministry of Trade, Industry & Energy), Korea, under the Industry Convergence Liaison Robotics Creative Graduates Education Program supervised by the KIAT (N0001126).

References

- [1] M.-H. Tak, Y.-J. Cho, and Y.H. Joo, "Behavior Control for Cooperative Exploration for Swarm Robots", Proceedings of KIIS Fall Conference, vol. 21, no.2, Korea, pp.169-170, Dec, 2011.
- [2] D.-W. Lee, and K.B. Sim, "Study on Cooperative Behaviors and Cooperative Control in Collective Autonomous Mobile Robots", Proceedings of Institute of Electronics and Information Engineers Conference, Korea, pp.68-71, Jan, 1997.
- [3] H.-C. Kim, J.-S. Kim, Y.-K. Ji, and J.-H. Park, "Path Planning of Swarm Mobile Robots Using Firefly Algorithm", Journal of Institute of Control, Robotics and Systems, vol. 19, no.5, pp.435-441, May, 2013.
- [4] J.-S. Kim, D.-H. Yeom, Y.-H. Joo, and J.B. Park, "Hierarchical Control of Multiple Mobile Robots", Proceedings of KIEE Summer Conference, Pyeongchang-gun, Korea, pp.1890-1891, Jul, 2011.

Adaptive Control of Discrete-Time Systems Using Multiple Fixed and One Adaptive Identification Models

Yuzhen Zhang

School of Automation and Electrical Engineering, University of Science and Technology Beijing, 30#Xueyuan Road, Haidian District, Beijing, China

Qing Li

School of Automation and Electrical Engineering, University of Science and Technology Beijing, 30#Xueyuan Road, Haidian District, Beijing, China

Weicun Zhang

School of Automation and Electrical Engineering, University of Science and Technology Beijing, 30#Xueyuan Road, Haidian District, Beijing, China

*E-mail: luxuhuiluxuhui@163.com, ymjia@buaa.edu.cn
www.buaa.edu.cn*

Abstract

The adaptive control of a linear time-invariant discrete-time system using multiple models is considered in this paper. Based on the prediction errors of a finite number of fixed and one adaptive identification models, a new weighting algorithm is proposed for improving system performance. The principal contributions of the paper are the proofs of global stability and the convergence of the overall system. Computer simulation results are included to complement the theoretical results.

Keywords: discrete-time; multiple model adaptive control; weighting algorithm; stability; convergence.

1. Introduction

The control of dynamical systems with large uncertainties is of great interest. Such problem arises when there are large parameter variations. So, an approach gains development: the use of multiple models to identify the unknown plant. In any time, the closest model will be identified according to the performance index.¹ Then, the corresponding controller is used to control the system.

The earliest research on weighted multiple model adaptive control (WMMAC) appeared in 1970's.^{2, 3} In that system, posterior possibility evaluator (PPE) algorithm played the key role. Later, K. S. Narendra put forward the concept of indirect multi-model adaptive control.⁴ The basic idea is that multiple fixed models are established off-line to cover uncertainty plant. At the same time, one or two adaptive identification models are present for global stability and the convergence of the overall system.⁴ The scheme is designed easily.

Therefore it has been widely used in recent years. This is also one basis of the algorithm in this paper.

In this paper, we made efforts from two aspects to improve the stability of WMMAC. On one side, a new algorithm for calculating controller weights is proposed. On the other side, a finite number of fixed and one adaptive identification models are designed.

It is worth noting that this paper is focused on the linear time-invariant discrete-time system because most practical systems are controlled by computers that are discrete in nature.³

2. Description of Weighted Multiple Model Adaptive Control

In order to analyze system clearly, a concise block diagram is shown in Fig.1. The simplified block diagram shows a general discrete-time WMMAC system. The details of every local control strategy and weighting algorithm are omitted.

The meanings of symbols are shown: P is the uncertainty plant; C_i is a local controller, which is corresponded to the fixed model; C_θ is the local controller corresponded to the adaptive identification model; $p_i(k)$ is a weight for its local controller; $p_\theta(k)$ is the weight for the adaptive identification controller. Through the algorithm, local controller weights are known. Then, the weighed sum $u(k)$ is obtained by the local controller weights.

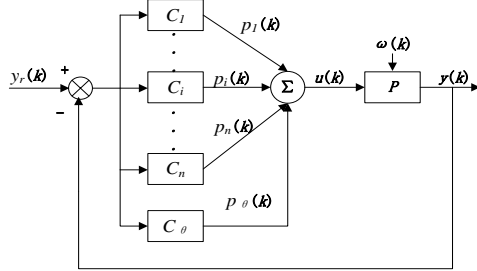


Fig. 1. Concise block diagram of a general WMMAC system

Consider the following discrete-time dynamical plant P , the mathematical model is

$$A(z^{-1})y(k) = z^{-d}B(z^{-1})u(k) + \omega(k) \quad (1)$$

where

$$A(z^{-1}) = 1 + a_1 z^{-1} + a_2 z^{-2} + \cdots + a_{n_a} z^{-n_a} \quad (2)$$

$$B(z^{-1}) = b_0 + b_1 z^{-1} + b_2 z^{-2} + \cdots + b_{n_b} z^{-n_b} \quad (3)$$

$y(k)$ and $u(k)$ are the output and the input. The $\omega(k)$ is a zero-mean white noise with constant variance.

The plant P also can be written as

$$y(k) = \varphi^T(k)\theta + \omega(k) \quad (4)$$

where

$$\varphi(k) = [-y(k-1), \dots, -y(k-n_a), u(k-d), \dots, u(k-d-n_b)] \quad (5)$$

$$\theta = [a_1, \dots, a_{n_a}, b_0, \dots, b_{n_b}] \quad (6)$$

$M = \{M_i, M_\theta, i=1, 2, \dots, N\}$ is the model set that includes a finite number of fixed and one adaptive identification models in this system. For every fixed model, the corresponded controller is designed by pole placement control. At the same time, the one adaptive identification model is designed by indirect pole assignment self-tuning control. The forgetting factor recursive extended least square is used to estimated parameter⁵. That is

$$\begin{cases} \hat{\theta}(k) = \hat{\theta}(k-1) + K(k)[y(k) - \hat{\varphi}^T(k)\hat{\theta}(k-1)] \\ K(k) = \frac{P(k-1)\hat{\varphi}(k)}{\lambda + \hat{\varphi}^T(k)P(k-1)\hat{\varphi}(k)} \\ P(k) = \frac{1}{\lambda}[I - K(k)\hat{\varphi}^T(k)]P(k-1) \end{cases} \quad (7)$$

where

$$\begin{cases} \hat{\varphi}(k) = [-y(k-1), \dots, -y(k-n_a), u(k-d), \dots, u(k-d-n_b)] \\ \hat{\theta}(k) = [\hat{a}_1, \dots, \hat{a}_{n_a}, \hat{b}_0, \dots, \hat{b}_{n_b}]^T \end{cases} \quad (8)$$

For each model, including the adaptive identification model certainly, its output $y_{mi}(k)$ is used to define the output error. That is

$$e_i(k) = y(k) - y_{mi}(k) \quad (9)$$

which is used to calculate the weight for the local controller. As shown in Fig.1, the global control $u(k)$ is obtained by

$$u(k) = \sum_{i=1}^{N+1} p_i(k) u_i(k) \quad (10)$$

In this paper, the algorithm to calculate weight is proposed, that is

$$p_i(0) = l_i(0) = \frac{1}{N+1} \quad (11)$$

$$l'_i(k) = \alpha + \frac{1}{k} \sum_{j=1}^k e_i^2(j) \quad (12)$$

where $\alpha > 0$, which is a small constant to avoid $l'_i(k) = 0$

$$l'_{\min}(k) = \min_i \{l'_i(k)\} \quad (13)$$

$$l_i(k) = \frac{l'_{\min}(k)}{l'_i(k)} l_i(k-1) \quad (14)$$

$$p_i(k) = \frac{l_i(k)}{\sum_{j=1}^{N+1} l_j(k)} \quad (15)$$

This algorithm is very simple in calculation. The results and their proofs regarding its convergence character are presented in Ref. 3 and 6-8.

3. Simulation Studies

In the previous section, the algorithm for calculating controller weights is presented. And a finite number of fixed and one adaptive identification models are discussed. In this section, the results of computer simulations will be presented. Using a single example, the effectiveness of the adaptive control of discrete-time systems with multiple fixed and one adaptive identification models, is discussed in detail.

Consider an uncertain discrete-time plant

$$(1 + a_1 z^{-1} + a_2 z^{-2})y(k) = z^{-1}(b_0 + b_1 z^{-1})u(k) + \omega(k) \quad (16)$$

where $\omega(k)$ is a zero-mean white noise with constant variance. This discrete-time model can be obtained by the simple continuous-time in (17) with sample time $t_s = 0.5s$ and the zero order hold.

$$G(s) = \frac{k}{s^2 - 3s + 2} \quad (17)$$

For simplicity, four fixed local models are used as the uncertainty of k , that is, $k_1 = 0.7$, $k_2 = 0.8$, $k_3 = 1.2$, $k_4 = 1.3$. The four corresponded controllers are designed by pole placement control. At the same time, the one adaptive identification model is designed by indirect pole assignment self-tuning control. The forgetting factor recursive extended least square is used to estimated parameter.

The controller 1 is

$$\begin{aligned} & (1 - 4.3670z^{-1} + 4.4817z^{-2})y(k) \\ & = q^{-1}(0.1473z^{-1} + 0.2428z^{-2})u(k) + \omega(k) \end{aligned} \quad (18)$$

The controller 2 is

$$\begin{aligned} & (1 - 4.3670z^{-1} + 4.4817z^{-2})y(k) \\ & = q^{-1}(0.1683z^{-1} + 0.2775z^{-2})u(k) + \omega(k) \end{aligned} \quad (19)$$

The controller 3 is

$$\begin{aligned} & (1 - 4.3670z^{-1} + 4.4817z^{-2})y(k) \\ & = q^{-1}(0.2525z^{-1} + 0.4163z^{-2})u(k) + \omega(k) \end{aligned} \quad (20)$$

The controller 4 is

$$\begin{aligned} & (1 - 4.3670z^{-1} + 4.4817z^{-2})y(k) \\ & = q^{-1}(0.2735z^{-1} + 0.4510z^{-2})u(k) + \omega(k) \end{aligned} \quad (21)$$

The controller 5 is designed according to the adaptive identification model by indirect pole assignment self-tuning control. The forgetting factor recursive extended least square is used to estimated parameter. The initial value of θ is $0.001 * \text{ones}(na + nb + 1, 1)$; the initial value of P is $10^6 * \text{eye}(na + nb + 1)$. The forgetting factor λ is 1. The calculation in detail is shown in formula (7) and (8).

The expected closed-loop characteristic polynomial is corresponds to the characteristic polynomial of the following continuous-time second-order system

$$\frac{\omega_n^2}{s^2 + 2\xi\omega_n s + \omega_n^2} \quad (22)$$

where ξ is 0.7, ω_n is 1.

The true model of plant is not included in the four fixed model, which k is 1. The simulation results are shown in Fig.2 to Fig.4.

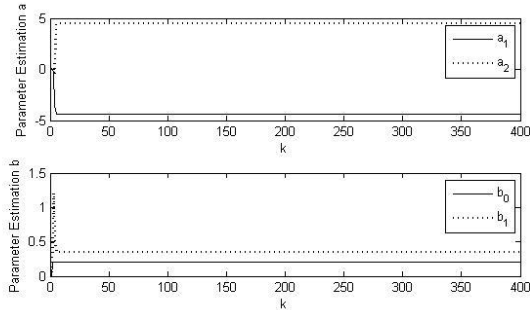


Fig. 2. Parameter estimation of the adaptive identification model

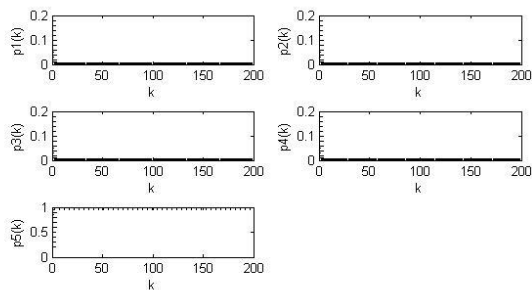


Fig. 3. Controller weight signals

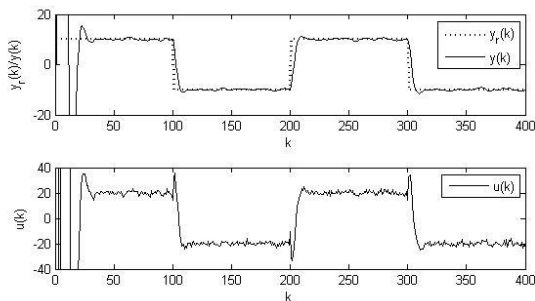


Fig. 4. Output, reference and control signals

As shown in Fig. 3, if the true model of plant is not included in the four fixed models, controller 5 designed according to the adaptive identification model is chosen rapidly in a good performance.

4. Conclusions

In this paper, a finite number of fixed and one adaptive identification models are designed. At the same time, the new algorithm for calculating controller weights is proposed. The weighted value can converge quickly. The controller designed according to the adaptive identification model performs well when the true one is not included in the fixed models, which improves the stability of WMMAC.

Acknowledgements

This work is supported by the National Basic Re-search Program of China (973 Program: 2012CB821200, 2012CB821201) and the NSFC (61134005, 60921001, 61327807).

References

1. K. S. Narendra and X. Cheng, Adaptive control of discrete-time systems using multiple models, *IEEE Transactions on Automatic Control* **45**(9) (2000) 1669-1686.
2. D. G. Lainiotis, Partitioning: a unifying framework for adaptive systems - I: Estimation - II: Control, *Proceedings of the IEEE* **64**(8) (1976) 1126-1143 and 1182-1197.
3. W. Zhang, Stable weighted multiple model adaptive control: discrete-time stochastic plant, *International Journal of Adaptive Control and Signal Processing* **27**(7) (2013) 562-581.
4. F. Li, Robust multiple model adaptive control base on dynamic optimization model bank, *Master Thesis, South China University of Technology*, 2004.
5. Z. Pang and H. Cui, System identification and adaptive control MATLAB simulation (*Beihang University Press, Beijing*, 2009), pp. 175-189.
6. W. Zhang, T. Chu, L. Wang, A new theoretical framework for self-tuning control, *International Journal of Information Technology* **11**(11) (2005) 123-139.
7. W. Zhang, On the stability and convergence of self-tuning control - virtual equivalent system approach, *International Journal of Control* **83**(5) (2010) 879-896.
8. W. Zhang, Stability of weighted multiple model adaptive control, *Journal of Control Theory and Applications* **29**(12) (2012) 1658-1660.

Adaptive Polynomial Regression and Its Application to Gene Selection of Rat Liver Regeneration

Juntao Li

Henan Engineering Laboratory for Big Data Statistical Analysis and Optimal Control, School of Mathematics and Information Science, Henan Normal University, 46 Jianshe Road, Xinxiang, 453007, P.R. China

Yimin Cao

Henan Engineering Laboratory for Big Data Statistical Analysis and Optimal Control, School of Mathematics and Information Science, Henan Normal University, 46 Jianshe Road, Xinxiang, 453007, P.R. China

Xiaoyu Wang

Henan Engineering Laboratory for Big Data Statistical Analysis and Optimal Control, School of Mathematics and Information Science, Henan Normal University, 46 Jianshe Road, Xinxiang, 453007, P.R. China

Cunshuan Xu

State Key Laboratory Cultivation Base for Cell Differentiation Regulation, Henan Normal University, 46 Jianshe Road, Xinxiang, 453007, P.R. China

*E-mail: juntaolimail@126.com, cao_yimin@126.com, 49207543@qq.com, cellkeylab@126.com
www.henannu.edu.cn*

Abstract

To deal with multi-class classification problem for gene expression data, this paper proposed an adaptive polynomial regression by incorporating multi-class adaptive elastic net penalty into polynomial likelihood loss. The adaptive polynomial regression was proved to adaptively select relevant genes in groups in performing multi-class classification. The proposed method was successfully applied to gene expression data for rat liver regeneration and the relevant genes were selected. The pathway relationships among the selected genes were also provided to verify their biological rationality.

Keywords: multi-class classification, polynomial regression, gene selection, rat liver regeneration

1 Introduction

Statistical machine learning methods, e.g., support vector machine, lasso and their extensions,¹⁻³ have been successfully applied to the microarray classification and gene selection. Note that multiple decision functions are

required and each is decided by the coefficients corresponding to the different gene groups. Hence, it is a challenge to select the proper genes for the microarray multi-class classification problem.

To deal with the aforementioned problem, some new statistical learning methods have been proposed. For

© The 2016 International Conference on Artificial Life and Robotics (ICAROB 2016), Jan. 29-31, Okinawa, Japan

example, Ref. 4 proposed L_1 -norm multi-class support vector machine (MSVM), Ref. 5 proposed the adaptive sup-norm MSVM. In particular, by using the initial estimator, Ref. 6 proposed an adaptive MSVM which can adaptively select the related genes.

Recently, the polynomial regression have attracted much attention.⁷⁻⁹ Ref. 7 proposed variational bayesian polynomial probit regression model and provide the R package. Ref. 8 proposed the regularized polynomial regression and applied it to multiple alignments of protein sequences. Ref. 9 proposed the multinomial regression and proved its performance of the grouped gene selection. However, these polynomial regression methods can not adaptively select the related genes.

Motivated by Ref. 6, this paper present a new polynomial regression method by introducing the multi-class adaptive elastic net penalty. The adaptive gene selection performance is analyzed and experiment results on the gene expression data for rat liver regeneration are provided which demonstrate the effectiveness of the proposed method.

2 Problem description

Given the microarray set $\{(x_1, y_1), (x_2, y_2), \dots, (x_n, y_n)\}$, where $K \geq 3$ represents the number of classes, $x_i = (x_{i1}, x_{i2}, \dots, x_{ip})$ is the input vector and $y_i \in \{1, 2, \dots, K\}$ is sample label. Similar to Ref 6, Let $Y = (y_1, \dots, y_n)^T$, $X = (x_1; x_2; \dots; x_n) = (x_{(1)}, x_{(2)}, \dots, x_{(p)})$, $x_{(j)} = (x_{1j}, \dots, x_{nj})^T$. Suppose that the predictors $x_{(j)}$, $j = 1, \dots, p$ are standardized, the response has zero mean value. The objective of this paper is to perform classification and select genes by building the following classifier

$$\phi(x) = \arg \max_{k=1,2,\dots,K} f_k(x).$$

For the sake of convenience, we adopt the notations in Ref. 9. $f_k(x) = b_k + w_k^T x$, $(k=1, 2, \dots, K)$ be the k th decision function, $w_k = (w_{k1}, \dots, w_{kp})^T$ be the k th row vector of matrix W , $w_{(j)} = (w_{1j}, \dots, w_{Kj})^T$ be the j th column vector of matrix W . By using the multi elastic net penalty and the polynomial likelihoods loss, Ref. 9 proposed the regularized polynomial regression

$$\min_{(b,w)} \left\{ -\frac{1}{n} \sum_{i=1}^n \sum_{k=1}^K y_{ik} (b_k + w_k^T x_i) - \log \sum_{k=1}^K e^{(b_k + w_k^T x_i)} \right\} + \lambda_2 \sum_{k=1}^K \sum_{j=1}^p w_{kj}^2 + \lambda_1 \sum_{k=1}^K \sum_{j=1}^p |w_{kj}|$$

$$s.t. \quad 1^T b = 0, 1^T w_j = 0, (j=1, 2, \dots, p)$$

© The 2016 International Conference on Artificial Life and Robotics (ICAROB 2016), Jan. 29-31, Okinawa, Japan

(1)

Although this method can select genes in groups during performing classification, it can not adaptively identify the important gene in the selected groups. This paper is devoted to solving the problem.

3 Main Result

3.1 Adaptive Polynomial Regression Model

Similar to Ref. 6, let $V = (v_{ik})_{n \times K} = [v_1^T; v_2^T; \dots; v_n^T]$ denote the index matrix, where v_i^T represents vector code corresponding to label y_i . By introducing multi-class adaptive elastic net penalty, the adaptive polynomial regression can be represented by

$$\min_{(b,w)} \left\{ -\frac{1}{n} \sum_{i=1}^n \sum_{k=1}^K y_{ik} (b_k + w_k^T x_i) - \log \sum_{k=1}^K e^{(b_k + w_k^T x_i)} \right\} + \sum_{k=1}^K \sum_{j=1}^p t_j (\lambda_2 w_{kj}^2 + \lambda_1 |w_{kj}|)$$

$$s.t. \quad 1^T b = 0, 1^T w_j = 0, (j=1, 2, \dots, p)$$

(2)

where

$$t_j = \|\tilde{w}_{(j)}\|^{-1}, \quad \tilde{w}_{kj} = \frac{\sum_{i=1}^n x_{ij} v_{ik}}{\sum_{i=1}^n x_{ij}^2}.$$

(3)

\tilde{w}_{kj} and t_j are the estimated contributions of the j th gene to the k th classifier and the whole classifier. Compared with the regularized polynomial regression (1), the weight t_j ($j=1, 2, \dots, p$) can be viewed as leverage vector which controls shrinkage of parameters adaptively. Substituting the constraint condition into objective function, the constrained optimization problem (2) can be transformed into unconstrained optimization problem. The altered objective function is shown as follows:

$$\bar{L}(\lambda_1, \lambda_2, b, w) = -\frac{1}{n} \sum_{i=1}^n \left\{ y_{ik} \left[-\sum_{k=1}^{K-1} b_k + \left(-\sum_{k=1}^{K-1} w_k \right) x_i \right] + \sum_{k=1}^K y_{ik} (b_k + w_k^T x_i) \right. \\ \left. - \log \left(\sum_{k=1}^{K-1} e^{b_k + w_k^T x_i} + e^{[-\sum_{k=1}^{K-1} b_k + (-\sum_{k=1}^{K-1} w_k) x_i]} \right) \right\} \\ + \lambda_2 \sum_{k=1}^{K-1} \sum_{j=1}^p t_j w_{kj}^2 + \lambda_2 \sum_{j=1}^p t_j \left(-\sum_{k=1}^{K-1} w_{kj} \right)^2 \\ + \lambda_1 \sum_{k=1}^{K-1} \sum_{j=1}^p t_j |w_{kj}| + \lambda_1 \sum_{j=1}^p t_j \left| -\sum_{k=1}^{K-1} w_{kj} \right|$$

(4)

3.2 Gene Selection performance

Note that the parameters corresponding to the j th gene for each classifiers is assigned the same weight t_j in

adaptive polynomial regression. Hence, the weighted L_1 norm penalty can shrink the parameters corresponding to the non-significant genes converge to 0 adaptively. Meanwhile, it can also reduce shrinkage error of the parameters corresponding to important genes and emerge sparsity. In another words, the adaptive polynomial regression can select the relevant genes in groups adaptively by estimating their contribution to K classifiers. This performance of gene selection can be described by the following Theorem.

Theorem 1. *Given the sample set (X, Y) and regularized parameters (λ_1, λ_2) . Let \hat{b}, \hat{w} be the solution of adaptive polynomial regression (2), $x_{(m)} \in R^n, x_{(l)} \in R^n$ be the columns of X corresponding to $\hat{w}_{(m)}, \hat{w}_{(l)}$. If predictors $\hat{w}_{(m)}$ and $\hat{w}_{(l)}$ are standardized, then*

$$\|\hat{w}_{(m)} - \hat{w}_{(l)}\|_2 \leq \frac{2\sqrt{K}}{\sqrt{n}\lambda_2} \sum_{i=1}^n |t_m^{-1}x_{im} - t_l^{-1}x_{il}| \quad (5)$$

holds.

Proof. Construct the following coefficient matrices

$$b^* = \hat{b} \quad w_{kj}^* = \begin{cases} \frac{t_m}{t_m + t_l} \hat{w}_{km} + \frac{t_l}{t_m + t_l} \hat{w}_{kl}, & j = m, l \\ \hat{w}_{kj}, & j \neq m, l \end{cases}$$

Note that (\hat{b}, \hat{w}) be the solution of adaptive polynomial regression. Hence, we have

$$0 \leq \bar{L}(\lambda_1, \lambda_2, b^*, w^*) - \bar{L}(\lambda_1, \lambda_2, \hat{b}, \hat{w}) \quad (6)$$

Following the similar procedure in Ref. 6, we have

$$\|\hat{w}_{(m)} - \hat{w}_{(l)}\|_2 \leq \frac{2\sqrt{K}}{\sqrt{n}\lambda_2} \sum_{i=1}^n |t_m^{-1}x_{im} - t_l^{-1}x_{il}| \quad (7)$$

□

Let $\rho = x_{(m)}^T x_{(l)} = \sum_{i=1}^n x_{im} x_{il}$, $\gamma = 2t_m t_l / (t_m^2 + t_l^2)$. By some simple calculations, we have

$$\begin{aligned} \frac{2\sqrt{K}}{n\lambda_2} \|t_m^{-1}x_{(m)} - t_l^{-1}x_{(l)}\|_1 &= \frac{2\sqrt{K}}{n\lambda_2} \sqrt{n} \|t_m^{-1}x_{(m)} - t_l^{-1}x_{(l)}\|_2 \\ &= \frac{2\sqrt{K}}{n\lambda_2} \sqrt{t_m^{-2} + t_l^{-2}} \cdot \sqrt{1 - \gamma\rho} \end{aligned} \quad (8)$$

When $K = 2$, it can yield that

$$|\hat{w}_{(lm)} - \hat{w}_{(ll)}| \leq \frac{2}{\sqrt{n}\lambda_2} \sqrt{2(1 - \rho)}$$

Note that $\gamma = 1$ if and only if $t_m = t_l$. Hence, the adaptive polynomial regression will assign the same coefficients to the corresponding genes only if $x_{(m)}$ and $x_{(l)}$ are highly correlated and these genes show the

same overall importance to the all K classifiers, i.e. $\|\tilde{w}_{(m)}\|_1 = \|\tilde{w}_{(l)}\|_1$. In other words, adaptive polynomial regression can adaptively identify the important gene in the selected gene groups. According the terms in Ref.6, we call it the adaptive grouping gene selection p. Different from Ref.6, the pathwise coordinate descent algorithm (PCD) presented in Ref. 10 can be improved to solve the adaptive polynomial regression model.

4 Experiment

To demonstrate the performance of the proposed model, we apply the adaptive polynomial regression to the gene chip data of rat liver regeneration. This data set is produced by the State Key Laboratory Cultivation Base for Cell Differentiation Regulation, Henan Normal University, which is available in the NCBI database with accession number: GSE55434.

Note that rat liver regeneration process has different physiological activity at every moment. Hence, we treat it as 9-classes classification problem which has 81 sample points, where each class has 9 sample points and each point contains 24618 genes. In our experiments, 54 sample points are used to train the regression model and the rest 27 for testing. In order to guarantee the balance of different classes, we take 6 samples out of each class for training and the rest 3 for testing. Fig.1 (a) shows the tenfold cross-validation error of the adaptive polynomial regression on operation group training set. From Fig.1(a) we can see that when $\ln \lambda \leq -1$, i.e. $\lambda \leq 0.3678794$ the cross-validation error is the least. Thus, we choose the optimal $\lambda = 0.220036243$ and determine the solution of adaptive polynomial regression model. Then we use the obtained coefficients to predict on test set and get 100% classification accuracy. Further, we determine 196 relevant genes using nonzero coefficients.

In order to eliminate the operation error and the influence of other noisy points, we also perform experiments on sham operation group data. Fig.1 (b) shows the tenfold cross-validation error of the adaptive polynomial regression model on sham operation group training set. Similar to the case of operation group data, we choose $\lambda = 0.1826835$ and obtain 83 genes. By eliminating the genes existing in sham operation group from 196 genes in operation group, the rest 113 genes are considered to be the relevant genes of rat liver

regeneration. To verify the biological rationality, we conduct pathway relationships among the selected genes by using the pathway studio 8. Fig.2 shows there exists two gene pathways.

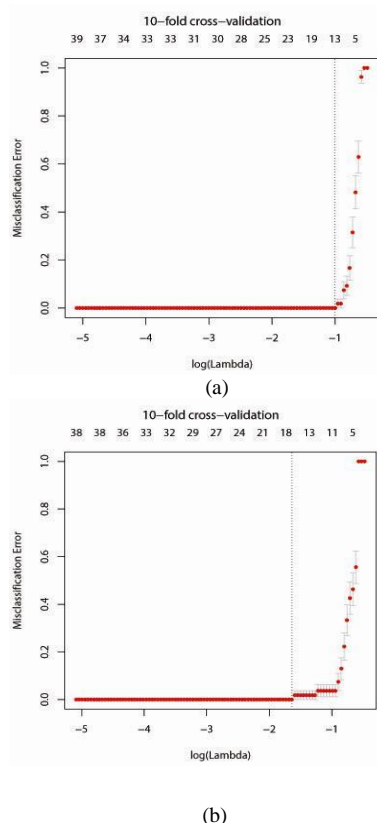


Fig.1, (a) $\alpha=0.5$ tenfold cross-validation error of the adaptive polynomial regression on operation group training set. (b) $\alpha=0.5$ tenfold cross-validation error of the adaptive polynomial regression on shame operation group training set.

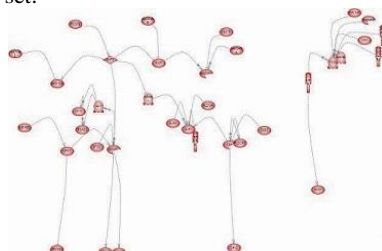


Fig.2, Regulative relation of relevant genes of rat liver Regeneration.

5 Conclusion

By combining polynomial likelihood loss and the multi-class adaptive elastic net penalty, an adaptive

polynomial regression was proposed in this paper. The proposed model can adaptively select genes in groups. PCD algorithm can be improved to solve the proposed model. The proposed method was successfully applied to the gene expression data for rat liver regeneration and the relevant genes were selected. Furthermore, the pathway relationships among the selected genes were analyzed by using the pathway studio 8, which verifies their biological rationality.

Acknowledgements

This work is supported by Natural Science Foundation of China (61203293), Program for Science and Technology Innovation Talents in Universities of Henan Province (13HASTIT040).

References

1. I. Guyon, et al., Gene selection for cancer classification using support vector machine, *Machine Learning* **46**(1) (2002) 389-422.
2. L. Wang, et al., Hybrid huberized support vector machine for microarray classification and gene selection, *Bioinformatics* **24**(3) (2008) 412-419.
3. R. Tibshirani, Regression shrinkage and selection via the lasso, *Journal of the Royal Statistical Society, Series B (Statistical Methodology)* **58**(1) (1996) 267-288.
4. L. Wang and X. Shen, On L1-norm multi-class support vector machine: method and theory, *Journal of American Statistical Association* **102**(478) (2007) 583-594.
5. H. H. Zhang, et al., Variable selection for the multicategory SVM via adaptive sup-norm regularization, *Electronic Journal of Statistics* **2**(2008) 149-167.
6. J. Li, et al., Adaptive Multi-class Support Vector Machine for Microarray Classification and Gene Selection, *ICROS-SICE International Joint Conference, (Japan, Fukuoka, 2009)*, pp. 2658-2663.
7. L. Nicola and M. Girolami, vbmp: Variational bayesian multinomial probit regression for multi-class classification in R, *Bioinformatics* **24**(1) (2008) 135-136.
8. J. Sreekumar et al., Correlated mutations via regularized multinomial regression, *BMC Bioinformatics* **12**(22) (2011) 444-456.
9. L. Chen, et al., Multinomial regression with elastic net penalty and its grouping effect in gene selection, *Abstract and Applied Analysis* **7**(1) (2014) 558-577.
10. J. Friedman, et al., Regularization path for generalized linear models via coordinate descent, *Journal of Statistical Software* **33**(1) (2010) 1-22.

Adaptive Consensus via Dynamic Feedback Control for Lipschitz Nonlinear Multi-Agent Systems

Lin Li

Department of Control Science and Engineering, University of Shanghai for Science and Technology, 516 JunGong Road, Shanghai, 200093, P.R.China

Heyang Wang

Department of Control Science and Engineering, University of Shanghai for Science and Technology, 516 JunGong Road, Shanghai, 200093, P.R.China

*E-mail: lilin0211 @163.com, wangheyang2015@163.com
www.usst.edu.cn*

Abstract

This paper deals with the consensus problem for multi-agent systems with fixed topologies. The agents are described by Lipschitz nonlinear systems. Only output information of each agent can be obtained from its neighbor agents. A distributed adaptive consensus algorithm via dynamic output feedback is proposed, in which the coupling weights between adjacent agents are time-varying and satisfy some designed adaptive laws. Provided examples are included to demonstrate the effectiveness of the proposed consensus algorithm.

Keywords: consensus, multi-agent systems, adaptive protocol, dynamic output feedback, Lipschitz nonlinear

1. Introduction

With the rapid development of science and technology, the distributed coordinated control problem for multi-agent systems (MASs) has received increasing attention. Consensus is an important and fundamental issue for coordinated control of the MASs, and has received more and more attention due to its broader range applications, such as flocking control, tracking control, unmanned aerial vehicle formation, underwater robot coordinated search and rescue, etc. Over the past decade, research on consensus problem has achieved numerous meaningful results.¹⁻⁶ Above the existing works that about consensus control for MASs are based on static

state-feedback under a restrictive assumption that all the agents' states can be measured, while the global information, for example the eigenvalue of the Laplace matrix, is used. But we know that in many real applications, the full states of the agents cannot be got, and the global information of the MASs may be unknown. Recently, an adaptive protocol was proposed to solve consensus for general linear MASs,⁷ where the states of agents were supposed to be known. The observer-based protocol was investigated.⁸

In this paper, the consensus problem of MASs with Lipschitz nonlinear dynamics under a fixed undirected connected topology is in focus. A distributed output feedback protocol is proposed, in which the output errors of the agents and the controller states' errors are

used to be the controller input. And in this designed protocol, the coupling weights between agents satisfy some designed adaptive law, in this way, the global information are avoided. Sufficient condition for the existence of this protocol is derived. Finally, numerical simulation shows the effectiveness of our obtained method.

2. Problem Formulation

The communication topology among agents is represented by a weighted connected undirected graph $G=(V,E,A)$. Hereinto, V represents the set of nodes with $V=\{v_1, v_2, \dots, v_N\}$, E is the set of undirected edges, and $A=[a_{ij}]$ is the weighted adjacency matrix with $a_{ii}=0, a_{ij}>0$. An undirected edge a_{ij} is denoted by the pair of nodes $(v_i, v_j) \in E$. The in-degree of nodes v_i is defined by $D_{in}(i) = \sum_j a_{ij}$. Laplace matrix is defined as $L=[l_{ij}] = \Delta - A$, $\Delta = \text{diag}\{D_{in}(1), \dots, D_{in}(N)\}$.

Consider a multi-agent system consisting of N agents, and the dynamic of the i th agent is

$$\begin{aligned} \dot{x}_i(t) &= Ax_i(t) + f(x_i) + Bu_i(t) \\ y_i(t) &= Cx_i(t) \quad i=1, 2, \dots, N \end{aligned} \quad (1)$$

where $x_i(t)$ is the state, $y_i(t)$ is the measured output, and $u_i(t)$ is the control input of the i th agent. A, B and C are known real matrices. The nonlinear function $f(x_i)$ satisfies the following Lipschitz condition:

$$\|f(x) - f(y)\| \leq \mu \|x - y\| \quad (2)$$

where $\mu > 0$ is the known Lipschitz constant.

For system (1), since some states cannot be measured in many cases, consider the following distributed consensus protocol

$$\begin{aligned} \dot{x}_{oi}(t) &= A_o x_{oi}(t) + f(x_{oi}) + B_o \sum_j c_{ij}(t) a_{ij} \\ &\quad [y_i(t) - y_j(t) + C(x_{oi}(t) - x_{oj}(t))] \end{aligned} \quad (3)$$

$$u_i(t) = C_o x_{oi}(t) \quad i=1, 2, \dots, N$$

where $x_{oi}(t)$ is the state, A_o, B_o and C_o are the gain matrices to be determined, $c_{ij}(t)$ is the time-varying coupling weight of agent i and agent j satisfying $c_{ij}(0) = c_{ji}(0)$.

The objective of this paper is to design a distributed consensus protocol (3) with an adaptive law about the $c_{ij}(t)$ for the group of agents such that the states of system (1) achieve consensus asymptotically. That is, for any initial states $x_i(0)$, the following is satisfied

$$\lim_{t \rightarrow \infty} \|x_i(t) - x_j(t)\| = 0, i, j = 1, 2, \dots, N$$

Denote

$$e_i(t) = x_i(t) - \frac{1}{N} \sum_{j=1}^N x_j(t)$$

and

$$e_i(t) = x_i(t) - \frac{1}{N} \sum_{j=1}^N x_j(t).$$

Then, it follows from (1) and (3) that

$$\dot{e}_i(t) = Ae_i(t) + f(x_i) - \frac{1}{N} \sum_{j=1}^N f(x_j) + BC_o e_{oi}$$

$$\begin{aligned} \dot{e}_{oi}(t) &= A_o e_{oi}(t) + f(x_{oi}) - \frac{1}{N} \sum_{j=1}^N f(x_{oj}) + B_o C \sum_j c_{ij}(t) a_{ij} (e_i(t) - e_j(t)) \\ &\quad + B_o C \sum_j c_{ij}(t) a_{ij} (e_{oi}(t) - e_{oj}(t)) \end{aligned} \quad (4)$$

Choose the adaptive law described as follows

$$\dot{c}_{ij}(t) = -a_{ij} [(e_{oi}(t) - e_{oj}(t))^T QB_o C (e_i(t) - e_j(t))]$$

(5)

$$+ (e_{oi}(t) - e_{oj}(t))^T QB_o C (e_{oi}(t) - e_{oj}(t)), i, j = 1, 2, \dots, N$$

$$\lim_{t \rightarrow \infty} \|e_i(t) - e_j(t)\| = 0 \text{ and } \lim_{t \rightarrow \infty} \|e_{oi}(t) - e_{oj}(t)\| = 0.$$

We can get that $\lim_{t \rightarrow \infty} \|x_i(t) - x_j(t)\| = 0$. Then, the

consensus problem of system (1) is equal to the asymptotical stability of the error system (4). In the following, we will focus on the asymptotical stability of system (4).

3. Main Result

Theorem 1. Given positive scalar μ , if there exist a constant $\beta > 0$, positive definite matrices P, R , and three matrices $V_i (i=1, 2, 3)$ such that the following LMI holds

$$\begin{bmatrix} (1,1) & BV_3 & V_2 & P & 0 & 0 & 0 \\ * & (2,2) & V_2 & 0 & P & \mu R & C^T \\ * & * & -I & 0 & 0 & 0 & 0 \\ * & * & * & -I & 0 & 0 & 0 \\ * & * & * & * & -I & 0 & 0 \\ * & * & * & * & * & -I & 0 \\ * & * & * & * & * & * & -\beta I \end{bmatrix} < 0$$

(6)

where $(1,1) = AP + PA^T + \mu^2 I, (2,2) = V_1 + V_1^T$. The signal

$*$ denotes the symmetry part of a symmetry matrix. Then, under the protocol (3) with the adaptive law (5), the consensus of multi-agent system (1) can be solved. And the gain matrices of this protocol can be taken as:

$$A_o = R^{-1}V_1P^{-1}, B_o = R^{-1}V_2, C_o = V_3P^{-1}$$

Proof: For system (4), consider the following Lyapunov-Krasovskii functional candidate

$$V(t) = \sum_{i=1}^N e_i^T(t)P^{-1}e_i(t) + \sum_{i=1}^N e_{oi}^T(t)Qe_{oi}(t) + \sum_{i=1}^N \sum_{j=1}^N \frac{(c_{ij}(t) + \alpha)^2}{2} \quad (7)$$

where α is some appropriate constant. Taking the time derivative of Lyapunov functional $V(t)$ along the trajectory of system (4), we get

$$\begin{aligned} \dot{V}(t) &= 2 \sum_{i=1}^N e_i^T(t)P^{-1}\dot{e}_i(t) + 2 \sum_{i=1}^N e_{oi}^T(t)Q\dot{e}_{oi}(t) \\ &\quad + \sum_{i=1}^N \sum_{j=1}^N (c_{ij}(t) + \alpha)\dot{c}_{ij}(t). \end{aligned}$$

From (4) and (5), we have

$$\begin{aligned} \dot{V}(t) &= 2 \sum_{i=1}^N e_i^T(t)P^{-1}[Ae_i(t) + f(x_i) - \frac{1}{N} \sum_{j=1}^N f(x_j) \\ &\quad + BC_o e_{oi}] + 2 \sum_{i=1}^N e_{oi}^T(t)Q[A_o e_{oi}(t) + f(x_{oi}) - \frac{1}{N} \sum_{j=1}^N f(x_{oj})] \\ &\quad + \alpha B_o C \sum_{j=1}^N c_{ij}(t)a_{ij}(e_i(t) - e_j(t) + e_{oi}(t) - e_{oj}(t)) \end{aligned} \quad (8)$$

Since $c_{ij}(t) = c_{ji}(t)$, we get

$$\begin{aligned} &2 \sum_{i=1}^N e_{oi}^T(t)QB_o C \sum_{j=1}^N c_{ij}(t)a_{ij}(e_{oi}(t) - e_{oj}(t)) \\ &= \sum_{i=1}^N \sum_{j=1}^N c_{ij}(t)a_{ij}(e_{oi}(t) - e_{oj}(t))^T QB_o C(e_{oi}(t) - e_{oj}(t)) \end{aligned} \quad (9)$$

Denote $\bar{x} = \frac{1}{N} \sum_{j=1}^N x_j(t)$, $\bar{x}_o = \frac{1}{N} \sum_{j=1}^N x_{oj}(t)$, we have

$$\begin{aligned} f(x_i) - \frac{1}{N} \sum_{j=1}^N f(x_j) &= f(x_i) - f(\bar{x}) + f(\bar{x}) - \frac{1}{N} \sum_{j=1}^N f(x_j) \\ f(x_{oi}) - \frac{1}{N} \sum_{j=1}^N f(x_{oj}) &= f(x_{oi}) - f(\bar{x}_o) + f(\bar{x}_o) - \frac{1}{N} \sum_{j=1}^N f(x_{oj}) \end{aligned}$$

In addition, because $\sum_{i=1}^N e_i(t) = 0$, $\sum_{i=1}^N e_{oi}(t) = 0$, we get

$$\begin{aligned} 2 \sum_{i=1}^N e_i^T(t)P^{-1}[f(\bar{x}) - \frac{1}{N} \sum_{j=1}^N f(x_j)] &= 0 \\ 2 \sum_{i=1}^N e_{oi}^T(t)Q[f(\bar{x}_o) - \frac{1}{N} \sum_{j=1}^N f(x_{oj})] &= 0 \end{aligned}$$

Then, it follows from the Lipschitz condition (2) that

$$\begin{aligned} 2e_i^T(t)P^{-1}[f(x_i) - \frac{1}{N} \sum_{j=1}^N f(x_j)] &\leq e_i^T(t)(\mu^2(P^{-1})^2 + I)e_i(t) \\ 2e_{oi}^T(t)Q[f(x_{oi}) - \frac{1}{N} \sum_{j=1}^N f(x_{oj})] &\leq e_{oi}^T(t)(\mu^2Q^2 + I)e_{oi}(t) \end{aligned} \quad (10)$$

Let

$$\tilde{e} = [e_1^T(t), e_2^T(t), \dots, e_N^T(t)]^T$$

$$\tilde{e}_o = [e_{o1}^T(t), e_{o2}^T(t), \dots, e_{oN}^T(t)]^T$$

$$\xi = [\tilde{e}^T, \tilde{e}_o^T]^T$$

Combing (5), (9) and (10) in to (8) yields

$$\dot{V}(t) \leq \xi^T \Phi \xi \quad (11)$$

where

$$\Phi = \begin{bmatrix} \Phi_{11} & \Phi_{12} \\ * & \Phi_{22} \end{bmatrix},$$

$$\Phi_{11} = I_N \otimes (P^{-1}A + A^T P^{-1} + \mu^2(P^{-1})^2 + I)$$

$$\Phi_{12} = I_N \otimes (P^{-1}BC_o) + \alpha L \otimes QB_o C$$

$$\Phi_{22} = I_N \otimes (QA_o + A_o^T Q + \mu^2Q^2 + I) + 2\alpha L \otimes QB_o C$$

The graph \mathcal{G} is connected, zero is a simple eigenvalue of Laplace matrix L , and all the other eigenvalues are positive. Then, there exists a unitary matrix $U \in \mathbb{R}^{N \times N}$ such that $U^T L U = \bar{L} = \text{diag}\{0, \lambda_1, \lambda_2, \dots, \lambda_N\}$, where $\lambda_i (i = 2, 3, \dots, N)$ are positive eigenvalues of L .

Let $\bar{\xi} = \text{diag}\{U^T \otimes I_N, U^T \otimes I_N\} \xi$, we have

$$\dot{V}(t) \leq \bar{\xi}^T \bar{\Phi} \bar{\xi} \quad (12)$$

If the inequality (6) is satisfied, choose α such

that $\alpha^2 \leq \frac{\beta}{\lambda_N^2}$, and let $R = PQ$, it is easy to get

that $\dot{V}(t) < 0$. Hence, $V(t)$ is bounded. By using the LaSalle's Invariance Principle, the error system (4) is asymptotically stable. Then, the consensus problem of system (1) is solved. This completes the proof.

4. Simulation Example

A simulation example is illustrated to show the effectiveness of our results. Consider an undirected graph \mathcal{G} , the communication topology is the same as Fig. 1⁸, in which there are eight agents. The elements of adjacency matrix A satisfy $a_{ij} = a_{ji} = 1$ with $(v_i, v_j) \in E$. Consider system (1) with

$$A = \begin{bmatrix} -0.9 & 0 \\ 0 & -2 \end{bmatrix}, B = \begin{bmatrix} 0.1 \\ 0.2 \end{bmatrix}, C = \begin{bmatrix} 0.5 & 0.2 \\ 0 & 0.3 \end{bmatrix},$$

$$f(x_i) = [0 \quad -0.1 \sin(x_{i2})]^T$$

It is easy to see that the nonlinear dynamic $f(x_i)$ satisfies the condition (2) with $\mu = 0.1$. Suppose the initial states of system (1) are $x_1(0) = [5 \quad 1]^T$, $x_2(0) = [0 \quad -1]^T$, $x_3(0) = [9 \quad 1]^T$, $x_4(0) = [-5 \quad 1]^T$, $x_5(0) = [2 \quad 0]^T$, $x_6(0) = [-1.8 \quad -1]^T$, $x_7(0) = [-6 \quad 2]^T$.

By solving the inequality (6), we can obtain the dynamic output feedback gain matrices are

$$A_o = \text{diag}(-0.2, -0.2), B_o = \begin{bmatrix} -0.2040 & 0 \\ 0 & -0.2040 \end{bmatrix}$$

$$C_o = [1.3945 \quad 1.9870]$$

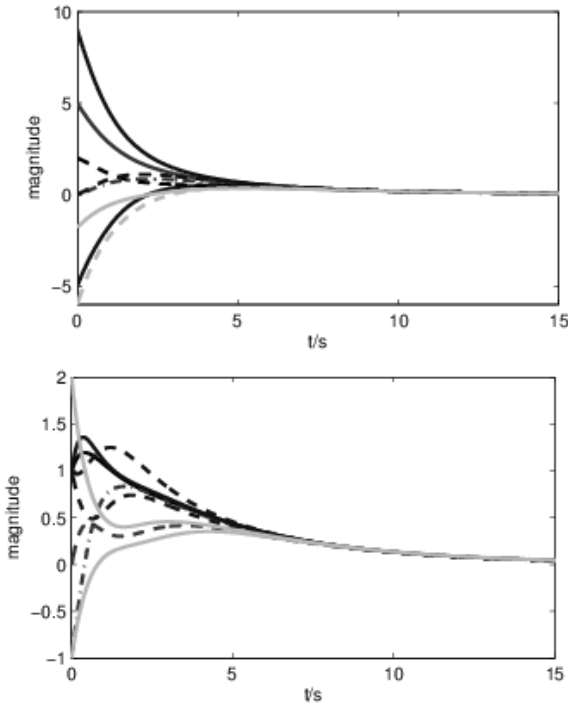


Fig. 1. The states of multi-agent system (1)

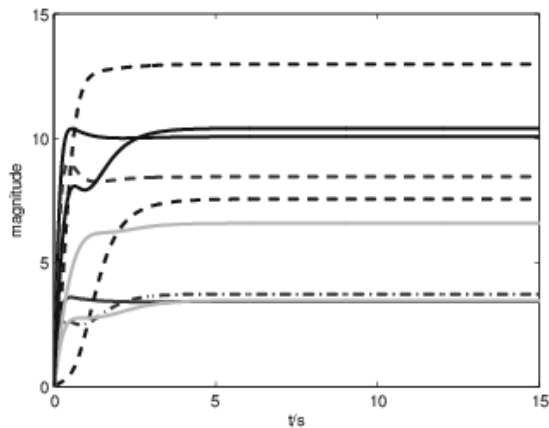


Fig. 2. The coupling weights $c_{ij}(t)$

The state trajectories of nonlinear multi-agent system (1) are shown in Fig. 1. From Fig.1, we can see that the

consensus control problem of system (1) under the distributed adaptive protocol (3) can be asymptotically solved. Curves of coupling weights are given in Fig.2.

5. Conclusion

The state consensus problem for multi agent systems with Lipschitz nonlinear dynamics has been investigated. Under that consideration of the unmeasured agent state, a distributed dynamic output feedback protocol with time varying coupling weights was designed. The coupling weights satisfy the designed adaptive law. A simulation example shows that the consensus problem under the designed distributed adaptive protocol can be asymptotically solved.

Acknowledgements

This paper is supported by the National Natural Science Foundation (61203143), and the Hujiang Foundation of China (C14002).

References

1. T. Li, M.Y. Fu, L.H. Xie, J.F. Zhang, Distributed consensus with limited communication data rate, *IEEE Transaction on Automatic Control* **56**(2) (2011) 279-291.
2. Z.W. Liu, et al, Consensus of multi-agent networks with a periodic sampled communication via impulsive algorithms using position-only measurement, *IEEE Transaction on Automatic Control* **57**(10) (2012) 2639-2643.
3. M. Ji and M. Egerstedt, Distributed coordination control of multi-agent systems while preserving connectedness, *IEEE Transactions on Robotics* **23**(4) (2007) 693-703.
4. R. Olfati-Saber and R.M. Murry, Consensus problems in networks of agents with switching topology and time-delays, *IEEE Transaction on Automatic Control* **49**(9) (2004) 1520-1533.
5. W. Ren and E.M. Atkins, Distributed multi-vehicle coordinated control via local information exchange, *International Journal of Robust and Nonlinear Control* **17**(1011) (2007) 1002-1033.
6. P. Lin, Y. Jia, Distributed robust H_∞ consensus control in directed networks of agents with time-delay, *Systems & Control Letters* **57**(8) (2008) 643-653.
7. J. Hu, et al., Consensus of nonlinear multi-agent systems with observer-based protocols, *Systems & Control Letters* **72**(10) (2014) 71-79.
8. Z. Li, et al., Consensus of multi-agent systems with general linear and Lipschitz nonlinear dynamics using distributed adaptive protocols, *IEEE Transactions on Automatic Control* **58**(7) (2013) 1786-1791.

Iterative Learning Based Thrust Ripple Suppression for PMLSM

Caixia Gao

School of Electrical Engineering and Automation, Henan Polytechnic University, Jiaozuo 454000 P.R.China

Fuzhong Wang

School of Electrical Engineering and Automation, Henan Polytechnic University, Jiaozuo 454000 P.R.China

Ziyi Fu

School of Electrical Engineering and Automation, Henan Polytechnic University, Jiaozuo 454000 P.R.China

gcx@hpu.edu.cn; wangfzh@hpu.edu.cn; fzy@hpu.edu.cn

Abstract

A fuzzy-PID-based control strategy was provided to deal with thrust ripple of multi-segment primary Permanent Magnet Linear Synchronous Motor. First these thrust ripple suppression model is proposed. The iterative learning algorithm is then synthesized with the velocity regulation for current compensation. Simulation results verify the strong suppression of thrust ripple even with periodic disturbances.

Keywords: multi-segment primary Permanent Magnet Linear Synchronous Motor, thrust ripple, iterative learning control, feedforward compensation.

1. Introduction

PMLSM vertical hoisting system consists of multi-segment primary armature windings, rotor and lifting container. Primary armature windings are evenly placed in the fixed frame (hoist Guide); the no-salient pole type rotor consists of permanent magnet and the rest. The car platform moves vertically with the rotor. Without the trouble of mechanical transmission device it employs the segmented power supply mode and does not need any electricity in the whole process, it is energy -saving, and efficient. Due to its significant economic and social benefits, more and more attention is being paid to PMLSM. However, in the actual operation process, the permanent magnet will be disturbed inevitably, if the disturbance can not be solved in time, it will make the

system run out of synchronization, the rotor and cage motor will decline dramatically due to the gravity, causing serious accidents. Therefore, the application of new control strategy is necessary to limit the force ripple and avoid the accident.

Many experts and scholars have done a lot of work in the thrust fluctuation suppression of linear motor. Their methods can be grouped into two kinds: One is to reduce the force ripple by optimizing the motor structure. The other is to compensate and restrain the force ripple by algorithmic control.

Based on its characteristics, this paper builds the mold of force ripple for PMLSM. It realizes the advanced control of the force ripple through the feedforward compensation of PMLSM.

2. The basic structure and working principle of segmented PMLSM hoisting system

As shown in figure 1, the segmented PMLSM hoisting system uses the double hidden pole. By rolling pulley, it moves up and down on the track. The length of the track of the rotor is equal to the total length of the table and the longitudinal length of the interval so as to make the coupling field area of the primary and the permanent magnet unchanged in the process of longitudinal motion of the rotor.

The air gap magnetic field will be generated when the three-phase windings of PMLSM are connected to the three sine alternating current. If the longitudinal end effect caused by the opening of the two ends is not considered, the air gap magnetic field can be regarded as the sine wave distributed along the straight line. When the three-phase current changes with time, the air gap magnetic field will move along a straight line in the sequence of A、B、C (or A、C、B), which is called the travelling magnetic field. The interaction of permanent magnet magnetic field and the travelling magnetic field generated by the armature winding will produce electromagnetic force. With the force, the rotor will do linear movement along the direction of the travelling magnetic field because of the fixed stator armature winding Group.

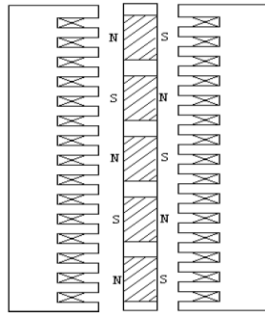


Fig.1 Double-side non-salient pole PMLSM

3. The analysis of segmented permanent magnet linear motor

The thrust wave is generated in the process of the segmented permanent magnet linear synchronous motor. The main reasons of the production of thrust fluctuation are: the breaking of the end core, which produces the unique end effect of the linear motor, that is, the force

of the end, the differences of magnetic permeance between the core and the groove produce the cogging effect, which is the same as that in rotary motor. That is cogging force; the frequent transformation of the motor stator armature winding during the operation will change the parameters of the motor caused by the change of the air gap.

The equation for the thrust is:

$$F(t) = ki_q(t) \quad (1)$$

$$F(t) = M \ddot{x} + f_s(t) + f_m(x) + f_g(x) + f_q(t) \quad (2)$$

In the above equations: $F(t)$ is the thrust, $f_s(t)$ is the carrying capacity, $f_m(x)$ is force of friction, $f_g(x)$ is ripple thrust, and $f_q(t)$ is other disturbance. Since the Double-side non-salient pole mode is adopted, the force of friction is ignored in this study; x is the position of the motor.

The ripple thrust caused by frequent switching of the motor stator armature winding and the uneven density of the air-gap field caused by slot effect and end effect bear direct relationship with the motion position of the permanent linear motor. And the mathematical model for the ripple thrust is:

$$\begin{aligned} f_g(x) &= A_g \sin(wx + \varphi) \\ &= A_{g1} \cos wx + A_{g2} \sin wx \end{aligned} \quad (3)$$

In formula (3), A_g is the amplitude of the ripple thrust; A_{g1} and A_{g2} are the constants; w is the angular velocity of the constant displacement; φ is the initial phase angle. $A_g, A_{g1}, A_{g2}, w, \varphi$ are all related to the structure of the linear motor.

4. Suppression strategy of force ripple of segmented permanent magnet synchronous motor

Force ripple Suppression strategy principle control is shown in figure2. The systematical control includes a master controller and a feedforward controller based on iterative learning control. Influenced by the force ripple caused by the side effect of the linear motor, the controlling effect would not be good if the master controller is applied. Therefore, iterative learning controller is used to predict the force ripple and compensate the main control system so as to reduce the

influence of the force ripple on the performance of the linear motor control.

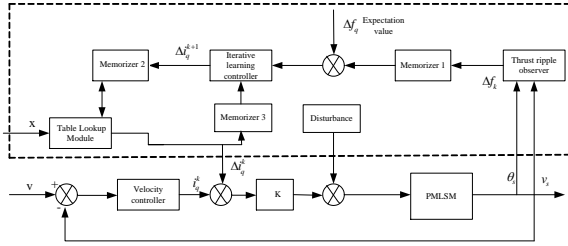


Fig.2 Iterative learning based thrust ripple suppression diagram for PMLSM

4.1. Force ripple observer

The working principle of the force ripple observer is as following: according to the actual position and the speed of the linear motor, it can calculate the thrust of the push and then put it into the memory, and then to the Iterative learning controller.

According to the analysis of force angle characteristics of permanent magnet linear motor, the relationship of the speed between thrust power and Angular (position) can be obtained.

$$F(t) = \frac{3E_0 U_s}{vZ} \sin(\theta + \alpha) - \frac{3E_0^2 R_s}{vZ^2} \quad (4)$$

$$\theta = \frac{\pi}{\tau} x - \omega t = \frac{\pi}{\tau} x - \frac{\pi}{\tau} v t \quad (5)$$

$$\Delta f_k = k i_q^*(t) - \frac{3E_0 U_s}{v_k Z} \sin\left(\frac{\pi}{\tau} x_k - \frac{\pi}{\tau} v_k t\right) + \frac{3E_0^2 R_s}{v_k Z^2} \quad (6)$$

In formula (4),(5) and (6), $\alpha = \arctan R_s / X_T$, Δf_k is the dynamic thrust after K times iteration; $i_q^*(t)$ is the given electric current; x_k and v_k are position and speed after k times iteration; Z is the synchronous impedance, E_0 is the no-load electric potential of the motor, U_s is the imposed voltage on the linear motor stator armature winding.

4.2. Iterative learning controller

Through the formula 3, it can be seen that there is a direct relationship between the ripple thrust and the position (time) of the permanent magnet linear motor.

When the vertical motion of the linear motor is repeated, the relationship between the ripple thrust and the position (time) of the permanent magnet linear motor remains the same. Therefore, this paper uses an iterative learning controller to compensate for the ripple thrust and eliminate the thrust fluctuation.

The operation principle of the iterative learning controller is as following: after k times iteration and before the next target position, the controller finds out the offset current in Memory 2 via lookup table. And linear motor, compensates the thrust ripple and stores then it will send the current to the major loop of the Δi_q^k in Memory 3; Afterwards it will store Δf_k sent by

thrust observer in Memory 1 and learn $\Delta i_q^k(t)$ in Memory 3 and the difference value between the controller-predicted thrust ripple Δf_k and expected thrust ripple Δf_q , namely, $e_k(t) = \Delta f_k - \Delta f_q$. As the offset current after k+1 times iteration, the newly obtained offset current $\Delta i_q^{k+1}(t)$ will do the above operations again and realize feedforward compensation effect.

The learning scheme is the iterative learning control scheme. This paper uses PID as the learning scheme, namely, the last control information and current errors are used as correction terms.

Applied in study, the designed learning scheme of the iterative learning is:

$$\begin{aligned} \Delta i_q^{k+1}(t) = & \Delta i_q^k(t) + \Gamma_p e_k(t) \\ & + \Gamma_i \int_0^t e_k(\tau) d\tau + \Gamma_D \frac{de_k(t)}{dt} \end{aligned} \quad (7)$$

Repeated interactive learning results in thrust ripple approaching zero as close as possible.

5. Simulink Simulation

In order to analyze the control effect of the controller designed in this paper, the iterative learning based thrust ripple suppression system for PMLSM is simulated through the platform of Matlab or Simulink, and a disturbing force with its amplitude and mean at 6N is added according to the actual interference condition of the linear motion actuator.

The parameters of the permanent magnet linear motor are set as follows : the weight of the active cell is 20kg; the number of the active cell pole- pairs is 2;

the polar distance of permanent magnet is 30mm, the thrust coefficient is 11.45N/A; the armature resistance of the active cell is 1.30Ω; and its inductance is 5.30mH with coefficient potential as 1.05×10^{-3} (Wb.s)/m.

The following result is concluded from the stimulation:

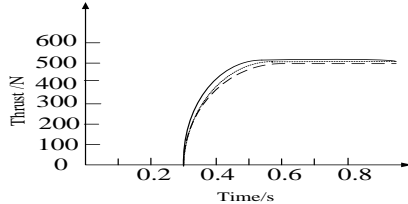


Fig.3 The thrust curve under different iteration times

From figure.3 it is loaded at 0.3s. The solid line is the given thrust curve, the dense dotted line is the thrust curve after 20 times iteration and the sparse dotted line is it after 10 times iteration.

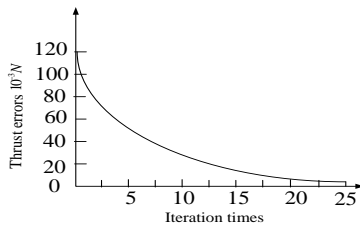


Fig.4 Maximum thrust error under different iteration times

From figure.5, the maximum thrust error after 10 times iteration is 40×10^{-3} N, which is reduced to 10×10^{-3} N after 20 times iteration. So more iterations can reduce the thrust error.

6. Conclusions

(1) This paper employs the control strategy of a combination of the iterative learning controller and the thrust fluctuation observer to control the thrust fluctuation in advance.

(2) The thrust fluctuation compensation strategy takes the impact of the thrust fluctuations into consideration.

The results of the simulation show that the control strategy has strong power to suppress the thrust fluctuation so as to improve the stability of the linear motor.

References

1. M. Sun, Z. Li. Characteristic Models and Iterative Learning Control Methods of PMLSM Servo-system, *Science Technology and Engineering*, **12**(13) (2012) 3126-3133,.
2. J. Yang, et al., Disturbance rejection for PMLSM based on iterative learning control, *Journal of Shenyang University of Technology*, **32**(1) (2010) 6-10.
3. Z. MA and Y. Nan, Position control for Permanent Magnet Linear motor using Iterative Learning Control, *Small & Special Electrical Machines*, **4**(3) (2008), 49-51.
4. K. Tan, S. Zhao, Adaptive force ripple suppression in iron-core permanent magnet linear motors, *Proceedings of the 2002 IEEE International Symposium on Intelligent Control*, (Canada, Vancouver, 2002), pp. 27-30.

Adaptive Sliding Mode Control for A 2 DOF Magnetic Levitation System with Uncertain Parameters

Meng Duan

*The Seventh Research Division, Beihang University (BUAA)
Beijing 100191, China*

Yingmin Jia

*The Seventh Research Division, Beihang University (BUAA)
Beijing 100191, China*

*E-mail: duanmeng90@126.com; ymjia@buaa.edu.cn
www.buaa.edu.cn*

Abstract

This paper investigates the stability control for a 2 DOF magnetic levitation system with uncertain parameters and external disturbance. The electromagnetic forces between the magnets and coils are obtained by numerical calculation. Then, an adaptive sliding mode controller is proposed to deal with the parameter uncertainties in the system matrices. The robust stability of the closed-loop system is proved by Lyapunov stability theory. Simulation results are presented to verify the effectiveness of the proposed control strategy.

Keywords: adaptive sliding mode control, magnetic levitation, numerical calculation, uncertain input

1. Introduction

In recent years, magnetic levitation technology becomes more and more important in the modern industry, like high precision transportation, because magnetic levitation technology can eliminate the friction, vibrations and wear caused by contact. And these machines have to move in multiple degrees of freedom(DOF). In Ref. 1-2, two kinds of planar motors using Halbach permanent magnet arrays which can move in a large horizontal plane have been proposed. Ref. 3 designed a long stroke 6 DOFs direct drive machine, the mover was constructed by symmetric linear magnet arrays and control currents generated by manufactured PCBs.

However, large rotation ranges are limited by the distribution of magnetic field in the above mentioned technologies, forces and torques in six DOFs can not be calculated sufficiently accurately in real time.⁴ To this

end, Ref. 5 proposed a novel single-deck planar maglev stage, its electromagnetic forces and torques are analyzed by the ANSOFT software. Refs. 6 also used numerical calculation method to obtain accurate electromagnetic forces and torques, and large rotation ranges have been realized.

Inspired by those works, this paper mainly focus on the problem of stability control for a 2-DOF magnetic levitation system subjects to parameter uncertainties. The contributions include that

- (i) In the modeling process of electromagnetic forces, the errors between the real position and preset one are described as the uncertainties of control matrix.
- (ii) Based on the sliding mode method, an adaptive controller is designed to guarantee the robust stability of the closed-loop system which has uncertain parameters and external disturbances.

This paper is organized in six sections. Section 2 describes electromagnetic forces numerical calculation model; Section 3 analyses the uncertain parameters of system dynamic model; Section 4 presents the controller design. Simulation results are presented in section 5. And the conclusions are given in section 6.

2. Electromagnetic Force Model

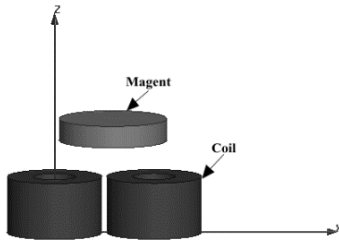


Fig. 1. Magnetic levitation system

In this paper, we investigate a 2 DOFs magnetic levitation system that consists of one disk magnet and two cylindrical coils shown in Fig.1, Assumed that the levitated magnet can only move through x-axis and z-axis but can not rotate.

Generally, electromagnetic forces are calculated by Lorentz's formula at a fixed relative position between the magnet and coils. The total forces are calculated as the volume integrals:

$$F = \iiint_V J \times B_m dV = \frac{I}{A} \iiint_V a \times B_m dV \quad (1)$$

where J is the vector of the current density of coils, I is the coil current, A is the cross-sectional area of the coil, a is the direction of the current, B_m is the vector of magnetic field density generated by the magnet and it is the function of the relative position of the magnet and the coils, V is the volume of coils. From Eq. (1) we can get that the electromagnetic forces are proportional to the magnitude of coil currents at a fixed relative position. So we can write Eq. (1) as follow:

$$F = \hat{b}I \quad (2)$$

where $\hat{b} = \frac{1}{A} \iiint_V a \times B_m dV$.

In practice, the impact between coils can be ignored, so the forces generated by each coil are independent, the

total forces can be calculated simply by adding the forces generated by each coil. The forces can be written as :

$$F = \sum \hat{b}_i I_i = \hat{B}I \quad i=1,2 \quad (3)$$

where $I = [I_1, I_2]^T$, $\hat{B} = [\hat{b}_1, \hat{b}_2]^T$.

Because the forces generated by each coil current are proportional and independent, a numerical model can be established that only includes one magnet and one coil, the electromagnetic forces are calculated in this model on each preset position along x-axis and z-axis with a unit ampere of current to get \hat{b}_i , then use Eq. (3) to get F .

But the preset positions in numerical calculation model are discrete, when the magnet moves on the positions that have not been numerical calculated, we can not find the matrix \hat{B} . In Ref. 6, B. Peter uses nearest-neighbor positions to replace real positions, so the \hat{B} is not certain at some positions, in this paper, the uncertainties of \hat{B} are introduced as $D\hat{B}$, obviously, it is bounded, so the electromagnetic forces can be written as:

$$F = (\hat{B}_0 + D\hat{B})I \quad (4)$$

where \hat{B}_0 is the nominal part of \hat{B} .

3. Model Analysis

The dynamic model of the magnetic levitation system can be derived by using Newton's Law as follow:

$$\begin{aligned} F_x &= \sum f_{xi} = m\ddot{x} \\ F_z &= \sum f_{zi} = m\ddot{z} - mg \end{aligned} \quad i=1,2 \quad (5)$$

where m is the mass of magnet, g is acceleration of gravity. Choose $X = [x_1, x_2, x_3, x_4] = [x, \dot{x}, z, \dot{z}]$, apply Eq. (4) to Eq. (5), the dynamic model can be expressed as follow:

$$\dot{X} = f(X) + (B + \Delta B)I \quad (6)$$

where $f(X) = [x_2, 0, x_4, -g]^T$, $I = [I_1, I_2]^T$, $\Delta B = \Delta\hat{B}/m$,

$$B = \begin{bmatrix} 0 & \hat{b}_{11} & 0 & \hat{b}_{21} \\ 0 & \hat{b}_{12} & 0 & \hat{b}_{22} \end{bmatrix}^T / m = \begin{bmatrix} 0 & b_{11} & 0 & b_{21} \\ 0 & b_{12} & 0 & b_{22} \end{bmatrix}^T.$$

Simultaneously consider the uncertain parameters of system dynamic model and external disturbances, write dynamical model as follow:

$$\dot{\tilde{X}} = f_o(X) + Df(X) + (B_o + DB)I + w \quad (7)$$

where $f_o(X)$ is the nominal part of $f(X)$, $Df(X)$ is the uncertain part of $f(X)$, w is external disturbance, assumed that both of them are bounded.

4. Adaptive Sliding Mode Controller Design

Define the desired state as $X_d = [x_{d1}, x_{d2}, x_{d3}, x_{d4}]^T$, the tracking error can be written as:

$$E = \begin{bmatrix} e_1 \\ e_2 \end{bmatrix} = X_d - X \quad (8)$$

where $e_1 = [E(1), E(2)]^T$, $e_2 = [E(3), E(4)]^T$.

Because the levitated magnet moves along two axes, the sliding-surface function can be introduced as:

$$s = [s_1, s_2]^T = \begin{bmatrix} c_1 \\ c_2 \end{bmatrix} e_1, c_2^T e_2^T \quad (9)$$

where $c_1 = [c_{11}, c_{12}]^T$, $c_2 = [c_{21}, c_{22}]^T$. The constant $c_{11}, c_{12}, c_{21}, c_{22}$ are chosen to be positive to make sure that the polynomial $c_{11}\lambda + c_{12}$ and $c_{11}\lambda + c_{12}$ is Hurwitz.

Differentiating s yields:

$$\dot{s} = c^T f(X) - c^T \dot{X}_d + c^T B_o I + W(X, I) \quad (10)$$

where $c = \begin{bmatrix} c_1 \\ c_2 \end{bmatrix}$, $W(X, I)$ is the lumped uncertain parameters and external disturbance:

$$W(X, I) = [W_1, W_2]^T = c^T \Delta f(X) + c^T \Delta B I + c^T w \quad (11)$$

in practice, the input coil currents are bounded, we can guarantee that $W(X, I)$ is bounded.

we design the control input I to be:

$$I = I_o + I_s \quad (12)$$

where

$$I_o = -(c^T B_o)^{-1} (c^T f(X) - c^T \dot{X}_d) \quad (13)$$

$$I_s = -(c^T B_o)^{-1} \hat{P} \text{sgn}(s) = -(c^T B_o)^{-1} \begin{bmatrix} \hat{P}_1 \text{sgn}(s_1) \\ \hat{P}_2 \text{sgn}(s_2) \end{bmatrix} \quad (14)$$

and \hat{P}_1 and \hat{P}_2 are adjustable parameters, and the adaptive law is:

$$\dot{\hat{P}} = \begin{bmatrix} \frac{1}{\rho_1} \|s_1\|, \frac{1}{\rho_2} \|s_2\| \end{bmatrix}^T \quad (15)$$

where r_1 and r_2 are the adaptation gain and both are positive. Assume that P_{d1} and P_{d2} are the terminal solution

of \hat{P}_1 and \hat{P}_2 which satisfy $|W_1| \leq P_{d1}$, $|W_2| \leq P_{d2}$ respectively.

Choose the adaption error as:

$$\tilde{P} = \begin{bmatrix} \hat{P}_1 - P_{d1} \\ \hat{P}_2 - P_{d2} \end{bmatrix} = \begin{bmatrix} \tilde{P}_1 \\ \tilde{P}_2 \end{bmatrix}. \quad (16)$$

Define a Lyapunov candidate function as:

$$V = \frac{1}{2} s^T s + \frac{1}{2} \tilde{P}^T \begin{bmatrix} \rho_1 & 0 \\ 0 & \rho_2 \end{bmatrix} \tilde{P}. \quad (17)$$

The time derivative of the Lyapunov candidate function can be found to be:

$$\begin{aligned} \dot{V} &= s^T \dot{s} + \tilde{P}^T \begin{bmatrix} \rho_1 & 0 \\ 0 & \rho_2 \end{bmatrix} \dot{\tilde{P}} \\ &= s^T (c^T f(X) - c^T \dot{X}_d + c^T B_o I + W(X, I)) + \begin{bmatrix} \rho_1 (\hat{P}_1 - P_{d1}) \\ \rho_2 (\hat{P}_2 - P_{d2}) \end{bmatrix}^T \dot{\tilde{P}} \\ &= s^T (W(X, I) - \begin{bmatrix} \hat{P}_1 \text{sgn}(s_1) \\ \hat{P}_2 \text{sgn}(s_2) \end{bmatrix}) + \begin{bmatrix} \hat{P}_1 - P_{d1} \\ \hat{P}_2 - P_{d2} \end{bmatrix}^T \begin{bmatrix} s_1 \text{sgn}(s_1) \\ s_2 \text{sgn}(s_2) \end{bmatrix} \\ &= s_1 W_1 + s_2 W_2 - |s_1| P_{d1} - |s_2| P_{d2} \leq 0. \end{aligned}$$

Because $V \in L_2$, \dot{V} is bounded, according to Barbalat Lemma, V would converge to zero, so the tracking error E would converge to zero. In order to alleviate the input chattering caused by the discontinuous term $\text{sgn}(s_i)$ in Eq. (14), the saturation function $\text{sat}(s_i/f)$ is used to replace $\text{sgn}(s_i)$,⁷ where f is constant.

5. Simulation Results

In this paper, the electromagnetic force model is calculated by Radia which is a free 3D magnetostatics computation software package developed by ESRF and running in Mathematica. The numerical calculation model established in Radia is shown in Fig. 2. The coil in

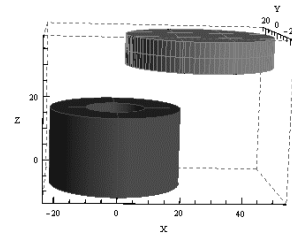


Fig. 2. Numerical calculation model.

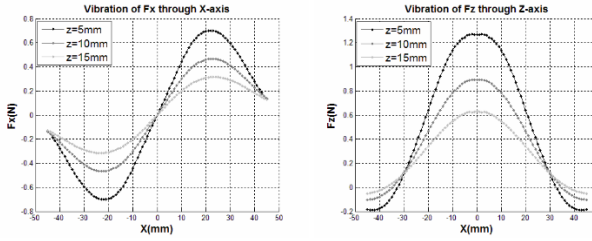


Fig. 3. Vibration of electromagnetic forces along x-axis with different air gaps

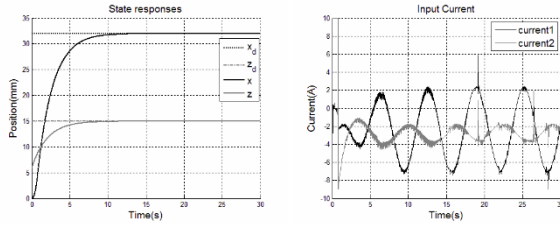


Fig. 4. Position tracking response performance.

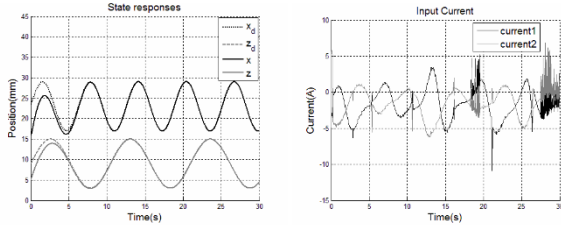


Fig. 5. Trajectory tracking response performance

the numerical calculation model is 26mm in height, 20mm in the inside diameter and 44mm in the outside diameter. The current density in the coil is 0.97A/mm². The magnet is cylindrical with 50mm in diameter and 10mm in height, its material is NdFeB and the remnant magnetization is 1.22T. The calculation sampling interval is 1mm along z-axis and x-axis. Figure. 3 shows that vibration of electromagnetic forces when the magnet moves along x-axis with different air gaps.

In this section, two typical simulation results which including the trajectory and position tracking are presented. In both two simulations, $Df(X)$ is supposed to be $[0.3\sin t(|x_1| + |x_2|), 0, 0.2\cos t(|x_1| + |x_2|), 0]^T$, w is designed as $[0, \sin t, 0, \sin t]^T$, and the parameters of the controller are designed as: $c_1 = c_2 = [0.5, 1]$, $r_1 = r_2 = 0.5$, $\hat{P}_1(0) = 30$, $\hat{P}_2(0) = 70$, $f = 0.1$.

The position tracking response performance of the 2-DOF magnetic levitation system is shown in Fig. 4, where the levitated magnet can track the desire position $x = 32 \text{ mm}$ and $z = 15 \text{ mm}$. From the tracking curve shown in Fig. 4, we can see that the magnet can reach and keep balance at the desired position with small currents.

The trajectory tracking response performance is shown in Fig. 5, from the simulation results, we can see that the levitated magnet can track the desired trajectories $x = 6\sin t + 22 \text{ mm}$ and $z = 6\sin(0.6t) + 9 \text{ mm}$.

6. Conclusions

In this paper, electromagnetic forces obtained by the method of numerical calculation, which brings the uncertainties to the control matrix, to deal with this, an adaptive sliding model controller has been developed and applied to the 2-D maglev system, the simulations confirmed the efficacy of the proposed controllers.

Acknowledgements

This work was supported by the National Basic Research Program of China (973 Program: 2012CB821200, 2012CB821201) and the NSFC (61134005, 60921001, 61327807).

References

1. H.-S. Cho and H.-K. Jung, Analysis and design of synchronous permanent-magnet planar motors, *IEEE T ENERGY CONVER.* 17(4)(2002)492 -499.
2. J. W. Jansen, Magnetically levitated planar actuator with moving magnets, *IEEE T IND APPL.* 46(5)(2008)1108-1115.
3. X. Lu and I.-U.-R. Usman, 6D direct-drive technology for planar motion stages, *CIRP ANN-MANUF TECHN.* 61(1)(2012)359 -362.
4. M. B. Khamesee and E. Shamel, Regulation technique for a large gap magnetic field for 3D non-contact manipulation, *Mechatronics.* 15(2005)1073 -1087.
5. Y.-C. Lai, Y.-L. Lee and J.-Y. Yen, Design and servo control of a single-deck planar maglev stage, *IEEE T MAGN.* 43(6)(2007)2600 -2602.
6. B. Peter and D. Michael, Magnetic levitation over large translation and rotation ranges in all directions, *IEEE-ASME T MECH.* 18(1)(2013) 44 -52.
7. Y.-J. Huang, T. C. Kuo and S.-H. Chang, Adaptive sliding-mode control for nonlinear systems with uncertain parameters, *IEEE T SYST MAN CY B.* 38(2)(2008)534 -539.

Undershoot Reduction in Discrete-Time ADRC of NMP Plant by Parameters Optimization

Tong Wu

*School of Automation and Electrical Engineering,
University of Science and Technology Beijing, #30 Xueyuan Rd, Haidian District,
Beijing, 100083, P. R. China*

Weicun Zhang

*School of Automation and Electrical Engineering,
University of Science and Technology Beijing, #30 Xueyuan Rd, Haidian District,
Beijing, 100083, P. R. China
E-mail: luxuhuiluxuhui@163.com, ymjia@buaa.edu.cn
www.buaa.edu.cn*

Abstract

Undershoot phenomena caused by unstable zeros of non-minimum-phase (NMP) plant is difficult to deal with in active disturbance rejection control (ADRC). This paper proposes a new method to reduce undershoot by optimizing the controller parameters of discrete-time ADRC system. Simulation results are given to verify the effectiveness of the proposed scheme.

Keywords: ADRC, NMP System, Discrete Control, Parameters Optimization

1. Introduction

Active disturbance rejection control (ADRC), first proposed by Han Jingqing, as a novel control design method has been applied to solve various control problems since 2000s¹. The ADRC technique, including Extended State Observer (ESO), mentioned in Han's book² is a kind of non-linear technique which shows great advantages in dynamic performance, robust performance, and disturbance rejection performance. But it confronts with much trouble in finding appropriate tuning method to deal with ADRC parameters for different plants. Gao Zhiqiang focuses on

the linearized ADRC and gives a bandwidth-parameterization method to solve the linear ADRC tuning problem.³ The number of ADRC parameters to be tuned can be decreased to two in this method which largely simplifies the task of ADRC design.

The discrete control technology as an emerging technology has been widely applied in control system. Various discrete techniques have been proposed to solve control problems.^{4, 5} In This paper, a discrete ADRC is designed to achieve the control task for NMP system which having the undershoot problem due to the unstable zeros.^{6, 7} A modified method of using appropriate non-linear function for parameters

optimization to reduce undershoot will be discussed in the following sections. For simplicity, the subject to be discussed in this paper is the second order system.

2. Discrete Active Disturbance Rejection Control

2.1. Discrete Extended State Observer

The linear extended state observer (LESO)³ can be constructed as

$$\begin{aligned}\dot{z} &= Az + Bu + L(y - \hat{y}) \\ \hat{y} &= Cz\end{aligned}\quad (1)$$

where

$$\begin{aligned}A &= \begin{bmatrix} 0 & 1 & 0 \\ 0 & 0 & 1 \\ 0 & 0 & 0 \end{bmatrix}, B = \begin{bmatrix} 0 \\ b_0 \\ 0 \end{bmatrix}, \\ C &= [1 \ 0 \ 0], L = \begin{bmatrix} \beta_1 \\ \beta_2 \\ \beta_3 \end{bmatrix}\end{aligned}\quad (2)$$

Using ω_0 -Parameterization method mentioned in Ref. 3, the observer gain vector L can be get as

$$\beta_1 = 3\omega_0, \beta_2 = 3\omega_0^2, \beta_3 = \omega_0^3 \quad (3)$$

where ω_0 is the bandwidth of the observer. And the value of b_0 falls in the range from 20 to 100. The extended state observer can be discretized as^{8,9}

$$\begin{aligned}z(k+1) &= \Phi z(k) + \Gamma u(k) + L_p(y(k) - \hat{y}(k)) \\ \hat{y}(k) &= Hz(k)\end{aligned}\quad (4)$$

where

$$\Phi = e^{Ah}, \Gamma = \left(\int_0^h e^{At} dt\right)B, H = C, L_p = \begin{bmatrix} \beta_1 \\ \beta_2 \\ \beta_3 \end{bmatrix} \quad (5)$$

h is the sample period. And the estimator gain vector L_p is determined by the equation

$$\lambda(z) = |zI - (\Phi - L_p H)| = (z - \beta)^3 \quad (6)$$

Combine equation (2) and (5), and solving (6) for L_p yields⁸

$$\begin{aligned}\Phi &= \begin{bmatrix} 1 & h & \frac{h^2}{2} \\ 0 & 1 & h \\ 0 & 0 & 1 \end{bmatrix}, \Gamma = b \times \begin{bmatrix} \frac{h^2}{2} \\ h \\ 0 \end{bmatrix}, \\ H &= [1 \ 0 \ 0], L_p = \begin{bmatrix} 3-3\beta \\ \frac{(\beta-1)^2(\beta+5)}{2h} \\ -\frac{(\beta-1)^3}{h^2} \end{bmatrix} \quad (7) \\ \beta &= e^{-\omega_0 h} \quad (8)\end{aligned}$$

where b is a constant.

2.2. Discrete ADRC control law

The parameterized control law can be constructed as^{3,8}

$$u_0(k) = k_p(r(k) - z_1(k)) - k_d z_2(k) \quad (9)$$

$$u(k) = \frac{u_0(k) - z_3(k)}{b} \quad (10)$$

where

$$\omega_0 = 2 \sim 5\omega_c, k_p = \omega_c^2, k_d = 2\omega_c \quad (11)$$

3. Optimization of ADRC Parameters

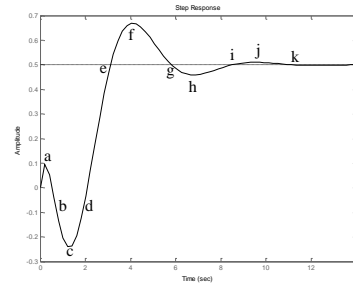


Figure 1 step response of NMP system

For the controller design, we need a bigger proportional gain at a, c, f, h and j, and a smaller one at b, e, g, i and k in Fig. 1. A bigger differential gain between a and b, c and d, f and g, h and i and j and k, and a smaller one between b and c, e and f, g and h and i and j in Fig. 1¹⁰.

Generally this is not realizable where controller

parameters are found being fixed. But we can choose appropriate non-linear functions to optimize the proportional gain and differential gain of the controller as a solution to this problem¹⁰.

We assume y_d as the derivative of the output, y_{d2} as the second derivative of the output, and $e(k)$ as the error between the reference and the output of the system. Using non-linear function, controller parameters can be constructed as

$$e(k) = r - z_1(k) \quad (12)$$

$$y_d(k) = \frac{z_1(k) - z_1(k-1)}{h} \quad (13)$$

$$y_{d2}(k) = \frac{y_d(k) - y_d(k-1)}{h} \quad (14)$$

$$K_p = K_{pr} \times \left(1 + \frac{2}{e^{y_d} + e^{-y_d}}\right) \quad (15)$$

$$K_d = \frac{K_{dr}}{(1 + e^{-2\text{sign}(y_d)\text{sign}(y_{d2})|e(k)|})} \quad (16)$$

where K_{pr} , K_{dr} is the original proportional gain and original differential gain of the controller which can be settled using the method mentioned in (9) and (11). And $z_1(k)$ is the state of the extended observer which is used to estimate the output of the plant.

4. Design Example

A simulation of NMP system is used to demonstrate the control design procedure and its resulting performance. The plant is modeled as

$$G(s) = \frac{-s+2}{s^2+40s+400} \quad (17)$$

Its corresponding z transfer function and difference equation is shown as (18) and (19)

$$G(z) = \frac{-0.004501z + 0.004546}{z^2 - 1.81z + 0.8187} \quad (18)$$

$$\begin{aligned} y(k) &= 1.81y(k-1) - 0.8187y(k-2) \\ &- 0.004501u(k-1) + 0.004546u(k-2) \end{aligned} \quad (19)$$

The sample period h is taken as 0.005s. The discrete extended state observer can be constructed as

$$\begin{aligned} z(k+1) &= \Phi z(k) + \Gamma u(k) + L_p(y(k) - \hat{y}(k)) \\ \hat{y}(k) &= H z(k) \end{aligned} \quad (20)$$

As is mentioned in Ref. 2, the extended state is fed back to cancel the model uncertainty. ω_0 is selected as 100 rad/sec and using bandwidth-parameterization,

parameters of discrete ESO are chosen as

$$\begin{aligned} u(k) &= \frac{u_0(k) - z_3(k)}{b} \\ (21) \Phi &= \begin{bmatrix} 1 & 0.005 & 1.25 \times 10^{-5} \\ 0 & 1 & 0.005 \\ 0 & 0 & 1 \end{bmatrix}, \Gamma = b \times \begin{bmatrix} 1.25 \times 10^{-5} \\ 0.005 \\ 0 \end{bmatrix}, \\ H &= [1 \ 0 \ 0], L_p = \begin{bmatrix} 1.2 \\ 86.8 \\ 2436.6 \end{bmatrix} \end{aligned} \quad (22)$$

where $b = 120$.

Finally the controller can be designed as (23) to control augmented system where r is the setpoint. The value of ω_c is 25 rad/sec.

$$\begin{aligned} u_0(k) &= K_p(r - z_1(k)) - K_d z_2(k) \\ K_p &= \omega_c^2 \times \left(1 + \frac{2}{e^{y_d} + e^{-y_d}}\right) \\ K_d &= \frac{2\omega_c}{(1 + e^{-2\text{sign}(y_d)\text{sign}(y_{d2})|e(k)|})} \end{aligned} \quad (23)$$

The result for the simulation mentioned above is shown in figure 2. The dash line represents the step response of regular discrete ADRC and the solid line represents the step response of modified discrete ADRC. Intuitively, the undershoot of modified discrete ADRC is lower than that of regular discrete ADRC.

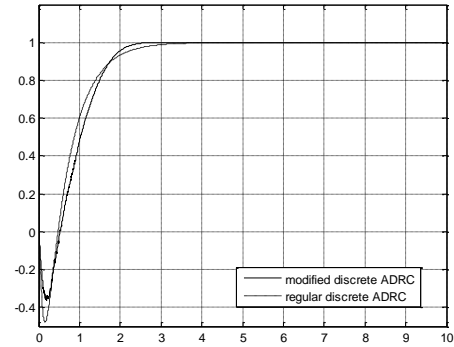


Figure 2 Step response of regular discrete ADRC and modified discrete ADRC

5. Conclusion Remarks

In this paper, a method of ADRC parameters optimization using nonlinear function has been discussed. It is shown that the modified discrete ADRC

has smaller undershoot than the regular one. Simulation result has been shown to verify the effectiveness of the proposed scheme.

Acknowledgements

The author would like to thank the anonymous reviewers for their constructive and insightful comments for further improving the quality of this work. This work was supported by the Major State Basic Research Development Program (973 Program) (No. 2012CB821200).

References

1. Z. Gao, On the Foundation of Active Disturbance Rejection Control, *Control Theory & Applications*, **30**(12) (2013) 1498-1510.
2. J. Han, *Active Disturbance Rejection Control Technique-the technique for estimating and compensating the uncertainties* (National Defense Industry Press, Beijing, 2008).
3. Z. Gao, Scaling and Bandwidth- Parameterization Based Controller Tuning, *American Control Conference*, (USA, Denver, 2003), pp. 4989-4996.
4. D. V. Stallard, Discrete Optimal Terminal Control, with Application to Missile Guidance, *IEEE Transactions on Automatic Control*, **18**(4) (1973) 373-377.
5. D. Zhou and C. Gao, Variable Structure Control of Discrete System with Time-delay, *Systems and Control in Aerospace and Astronautics*, (China, Shenzhen, 2008), pp. 1-5.
6. S. Zhao and Z. Gao, Active Disturbance Rejection Control for Non-minimum Phase Systems, *Chinese Control Conference*, (China, Beijing, 2010), pp. 6066-6070.
7. M. Tang and P. Wu. Control of Non-minimum Phase Servo System Based on Auto Disturbance Rejection, *Radar Science and Technology*, **11**(3) (2013) 335-340.
8. R. Miklosovic, A. Radke, Z. Gao, Discrete Implementation Generalization of the Extended State Observer, *American Control Conference*, (USA, Minneapolis, 2006), pp. 2209-2214.
9. C. Zhang, J. Zhu, Y. Gao, Active Disturbance Rejection Controller Based on Deadbeat Observer Design and Performance Analysis, *Control Theory & Applications*, **32**(1) (2015) 29-34.
10. D. Zhang, K. Liu, B. Fang, Non-minimum Phase System Control Based on Nonlinear PID, *Microcomputer Development*, **14**(12) (2004) 4-6.

Development of a Tool to Keep Consistency between a Model and a Source Code in Software Development Using MDA.

Yuuki Kikkawa*, Tetsuro Katayama*, Yoshihiro Kita†,
Hisaaki Yamaba*, Kentaro Aburada‡ and Naonobu Okazaki*

*University of Miyazaki, Japan, †Tokyo University of Technology, Japan

‡Oita National College of Technology, Japan

kikkawa@earth.cs.miyazaki-u.ac.jp, kat@cs.miyazaki-u.ac.jp, kitayshr@stf.teu.ac.jp,
yamaba@cs.miyazaki-u.ac.jp, aburada@oita-ct.ac.jp, oka@cs.miyazaki-u.ac.jp

Abstract

This study improves efficiency of software development using MDA. This paper develops the tool that keeps consistency between a model and a source code in software development using MDA. The tool has two functions: (i) Generating a source code and (ii) Keeping consistency between a model and a source code. A simple ATM example is used in order to confirm effectiveness of the tool. The tool can reduce time and effort to keep consistency between models and a source code.

Keywords: MDA (Model Driven Architecture), Extended Activity Diagram, Activity diagram, Detail specification.

1. Introduction

MDA (Model Driven Architecture) is a concept of software development.¹ MDA defines five models: business model, requirement model, platform independent model (PIM), platform specific model (PSM), and physics model. Each model has different abstraction level. A developer defines models and generates a less abstract model by software development in MDA. Here, MDA tools are used to generate a less abstract model. A developer uses UML (Unified Modeling Language)² for modeling PIM and PSM.

Before generation of a less abstract model, a developer must define generation rules of high abstract model. A method to support the definition of a generation rule is researched.³

One of the MDA's problems is how to keep consistency between the original model and an edited model which is generated from the original. A

modification tool of PIM to keep consistency with PSM is researched.⁴

Also, there is no consistency if a developer edits the original model. A developer can keep consistency if a MDA tool generates models from the edited models again. Here, some MDA tools can generate a complete model from models including detail specification. A framework that generates the executable source code from a class diagram and a state machines diagram is researched.⁵ However, MDA tools cannot generate complete models from abstract models because these models do not have detail specification of a system. The developer must modify generated models to fit the modified original models or generate a new model from the modified models with a MDA tool and then add the detail specification to the new model by hand again.

This study improves efficiency of software development using MDA. We proposed a modification method of a source code to correspond with a modified model in MDA.⁶ However, we did not implement the method. In this paper, we develop the tool that keeps

consistency between a model and a source code in software development using MDA. This paper introduces the tool and describes how we implement the tool.

2. The Developed Tool

This chapter describes functions and an overview of the tool. Here, the tool treats with activity diagram of UML and programming language C++.

2.1. Functions

The tool has two functions: (i) generating a source code, (ii) keeping consistency between a model and a source code. (ii) consists of 3 steps. Fig. 1. shows each function.

An input of (i) is an activity diagram, and an output of (i) is the source code based on the activity diagram. Inputs of (ii) are an unmodified activity diagram, the modified activity diagram, and the source code including the detail specification. An output of (ii) is a source code which is consistent with the modified activity diagram and includes the detail specification.

In executing (ii), the tool generates an EAD (Extended Activity Diagram) as intermediate data. An EAD is a format of the data added a part of the source code which has the detail specification to the activity diagram.

2.2. Overview

Fig. 2 shows an overview of the tool. The tool consists of 4 parts shown below.

- (i) Menu bar.
- (ii) Mode select panel.
- (iii) Multipurpose panel.
- (iv) Paint panel.

A developer can execute a function of the tool by (i). By using (ii), a developer can select an operation he wants to do on (iv). (iii) assists the selected operation on (iv). (iv) shows activity diagram.

3. Implementation

This chapter describes how to implement each function. Here, the tool sets node ID and edge ID in the node and the edge that the developer describes. Node ID and edge ID are unique number in a diagram.

© The 2016 International Conference on Artificial Life and Robotics (ICAROB 2016), Jan. 29-31, Okinawa Convention Center, Okinawa, Japan

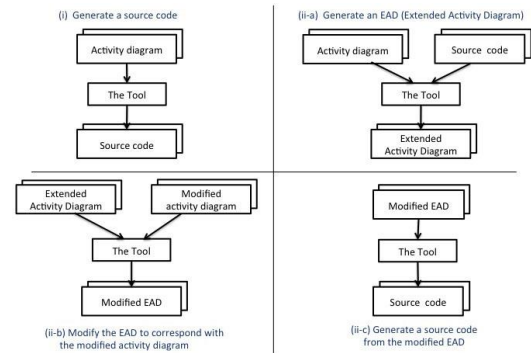


Fig. 1. Functions of the tool.

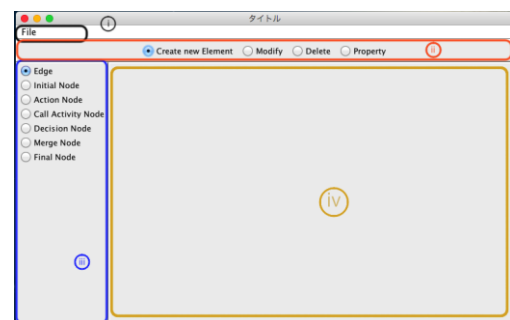


Fig. 2. Overview of the tool.

3.1. Generating a source code

The tool generates a source code from the activity diagram. The steps to generate a source code are shown as below.

- (i) Acquire the function name
The tool generates a skeleton of source code. The function name is the activity name that is described in the activity diagram. Here, the type and the parameter of the function are void.
- (ii) Select the initial node
The tool selects the initial node.
- (iii) Implement the function
The tool executes the process as below depending on the type of the selected node.
 - Call activity node
Write the name of the call activity node to the source code.
 - Decision node
Write an if-statement to the source code. Conditions of if-statement are guard conditions of this node.

- Activity final node
Finish the generation of the source code.
 - Other than the above
Do nothing.
- (iv) Select another node
The tool reselects the node connected by the outgoing edge of the selected node and go to (iii).

3.2. Generating an EAD

The tool keeps consistency between a model and a source code. At the first step of the function, the tool generates an EAD. The steps to generate an EAD are shown as below.

- (i) Select the first line of the source code added the detail specification.
 - We call the selected source code “LOS (line of selected)”
- (ii) Generate and extract a line of source code from the activity diagram.
 - Generation rule of a source code is same as the function (i) of the tool.
- (iii) If (ii) and the LOS are not same character string, execute the process shown as below.
 - (a) Write the LOS to the activity diagram.
 - (b) Encircle lines written in (a) as a node.
 - (c) Select the original node of the generated source code in (ii).
 - (d) Connect the incoming edge for the selected node to the node generated in (b).
 - (e) Make an edge connected with the selected node and the node generated in (b).
 - (f) Change the LOS to the next line of the current LOS.
 - (g) Go to (iii).
- (iv) Change the LOS to the next line of the current LOS.
- (v) Go to (ii).

Later, we call an encircle node a platform specific node. We define a node other than a platform specific node as a platform independent node. We define an edge connected with a platform specific node as a platform specific edge. We define an edge other than a platform specific edge as a platform independent edge.

3.3. Modifying the EAD

At the second step of the function which keeps consistency between a model and a source code, the tool modifies the EAD to correspond with the modified activity diagram. The steps to modify the EAD are shown as below.

- (i) Add an edge adjacent to a platform specific node.
 - (a) Select a platform independent edge from an EAD.
 - (b) If selected edge connects a platform specific node to a platform independent node and the platform independent node does not exist in the modified activity diagram, execute the process shown as below.
 1. Select a node in the modified activity diagram which has the same node ID as the selected node.
 2. Select a next node of the current selected node in the modified activity diagram.
 3. Select a node in the EAD which has the same node ID as the selected node in the modified activity diagram.
 4. Make an edge connected with the first selected node and the second selected node in the EAD.
 - (c) If the selected edge connects a platform independent node to a platform specific node and the platform independent node does not exist in the modified activity diagram, execute the process shown as below.
 1. Select a node in the modified activity diagram which has the same node ID as the selected node.
 2. Select a previous node of the current selected node in the modified activity diagram.
 3. Select a node in the EAD which has the same node ID as the selected node in the modified activity diagram.
 4. Make an edge connected with the first selected node and the second selected node in the EAD.
 - (d) If there is an unselected node, select an unselected node and go to (b).
- (ii) Delete edges and nodes.
 - (a) Select a node or edge from the EAD.

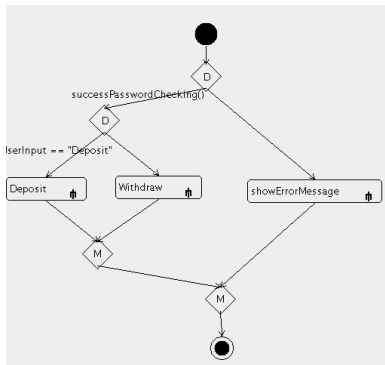


Fig. 3. The activity diagram of the ATM system.

- (b) If the modified activity diagram does not consist of a node or edge which has the same ID as a selected node or an edge, delete the selected node or edge.
- (c) If there is an unselected node or edge in the EAD, select an unselected node or edge and go to (b).
- (iii) Add edges or nodes.
 - (a) Select a node or edge from the modified activity diagram.
 - (b) If the EAD does not consist of a node or edge which has the same ID as a selected node or edge, add the selected node or edge to EAD.
 - (c) If there is an unselected node or edge in the modified activity diagram, select an unselected node or edge and go to (b).

3.4. Generating the source code from the EAD

The tool generates a source code from the EAD. The steps to generate a source code are same as section 3.1. If the tool selects a platform specific node, the tool writes its name to the source code.

4. Application Example

We use a simple ATM as an example to confirm effectiveness of the tool. This ATM system executes password checking process. If a user successes

```

void Transaction(){
    if(successPasswordChecking()){
        if(UserInput == "Deposit"){
            Deposit();
        }else{
            Withdraw();
        }
    }else{
        showErrorMessage();
    }
}
    
```

Fig. 4. The generated source code.

password checking, this system executes a withdrawal process or a depositing process by a user's input. Fig. 3 shows the activity diagram of the ATM system.

The tool generates a source code from the activity diagram. Fig. 4 shows a generated source code.

The developer adds the detail specification to the generated source code in order to execute it. Fig. 5. shows the source code added the detail specification.

Suppose a case that the requirement of specification is changed, after adding the detail specification. The developer needs to modify the activity diagram by deleting and adding some elements of the activity diagram. Fig. 6 shows a modified activity diagram. The developer deletes the password checking process to sequence of deposit.

The tool generates a new source code from the source code including the detail specification, the modified activity diagram, and original activity diagram. Fig. 7 shows a generated source code. The source code includes the detail specification.

5. Discussion

MDA Tools such as EA⁷ (Enterprise Architecture) can generate a skeleton of a source code from a class diagram. In addition, EA can generate a source code from an activity diagram or a state machine diagram. However, the source code generated by EA does not have the detail specification. It takes time and effort that the developer adds the detail specification to the source code generated from the modified activity diagram.

```

void Transaction(){
    string UserInput;
    cin >> UserInput;
    if(successPasswordChecking()){
        if(UserInput == "Deposit"){
            Deposit();
        }else{
            Withdraw();
        }
    }else{
        showErrorMessage();
    }
}

```

Fig. 5. The source code added the detail specification.

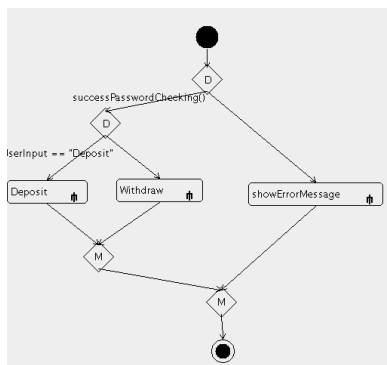


Fig. 6. The modified activity diagram.

The developed tool can generate a source code including the detail specification. The tool can reduce time and effort to add the detail specification to the source code generated from the modified activity diagram. Moreover, it can reduce time and effort to keep consistency between models and a source code after the requirement specification is modified. Therefore, the tool is useful for efficiency of software development using MDA.

6. Conclusion

This paper develops the tool that keeps consistency between a model and a source code in software development using MDA. The tool can generate the source code that corresponds with the modified activity diagram and has information about the detail specification.

We have confirmed that the tool can generate a source code including the detail specification from the original activity diagram, the modified activity diagram, and the original source code. Therefore, the tool is useful for efficiency of software development.

© The 2016 International Conference on Artificial Life and Robotics (ICAROB 2016), Jan. 29-31, Okinawa Convention Center, Okinawa, Japan

```

void Transaction(){
    string UserInput;
    cin >> UserInput;
    if(UserInput == "Deposit"){
        Deposit();
    }else{
        if(successPasswordChecking()){
            Withdraw();
        }else{
            showErrorMessage();
        }
    }
}

```

Fig. 7. The source code corresponded with the modified activity diagram.

Future issues are as follows.

- Improvement of the tool to treat with other statements except if-statement.
- Improvement of the tool to treat with programming language Java.

References

1. MDA (Model Driven Architecture), <http://www.omg.org/mda> (accessed November 30, 2016).
2. UML (Unified Modeling Language), <http://www.omg.org/spec/UML/2.4.1> (accessed November 30, 2016).
3. D. Lopes, S. Hammoudi, J. Bézivin, F. Jouault: Mapping Specification in MDA: From Theory to Practice, *Interoperability of Enterprise Software and Applications*, (Springer-Verlag London Ltd 2006), pp.253-264,
4. Lionel C. Briand, Yvan Labiche, Tao Yue: Automated traceability analysis for UML model refinements, *Information and Software Technology*, Vol. 51 (2009), Issue2, pp. 512-527.
5. A. Derezinska, Code Generation and Execution Framework for UML 2.0 Classes and State Machines, *IMCSIT*, (2008), pp. 517-524.
6. Yuuki Kikkawa, Tetsuro Katayama, Yoshihiro Kita, Hisaaki Yamaba, Kentaro Aburada and Naonobu Okazaki, Proposal of a Modification Method of a Source Code to Correspond with a Modified Model in MDA, *International Conference on Artificial Life and Robotics*, (2015), pp. 384-387.
7. Enterprise Architect, <http://www.sparxsystems.jp> (accessed November 30, 2016).

Necessary spaces for seven-way four-dimensional Turing machines to simulate four-dimensional one-marker automata

Makoto Nagatomo, Shinnosuke Yano, Makoto Sakamoto, Satoshi Ikeda, and Hiroshi Furutani

Faculty of Engineering, University of Miyazaki,

1-1 Gakuen Kibanadai Nishi, Miyazaki, Miyazaki 889-2192, Japan

E-mail: je.suis.makoto@gmail.com, shinchandx@ezweb.ne.jp, sakamoto@cs.miyazaki-u.ac.jp, bisu@cs.miyazaki-u.ac.jp, furutani@cs.miyazaki-u.ac.jp

Takao Ito and Tsutomu Ito

Institute of Engineering, Hiroshima University, 4-1, Kagamiyama 1-chome

Higashi-Hiroshima, Hiroshima 739-8527, Japan

E-mail: itotakao@horoshima-u.ac.jp, Ova71-2538f211n@ezweb.ne.jp

Yasuo Uchida

Department of Business Administration, Ube National College of Technology, Tokiwadai

Ube, Yamaguchi 755-8555, Japan

E-mail: uchida@ube-k.ac.jp

Tsunehiro Yoshinaga

Department of Computer Science & Electronic Engineering,

National Institute of Technology, Tokuyama College, Gakuendai

Shunan, Yamaguchi 745-8585, Japan

E-mail: yosinaga@tokuyama.ac.jp

Abstract

We think that recently, due to the advances in many application areas such as motion image processing, computer animation, and so on, it is very useful for analyzing computational complexity of multi-dimensional information processing to explicate the properties of four-dimensional automata, i.e., three-dimensional automata with the time axis. As far as we know, there is no investigation about four-dimensional automata. Then, in 2002, we first introduced four-dimensional finite automata in the world. In 2003, we investigated four-dimensional alternating Turing machines. In 2015, we show the sufficient spaces for four-dimensional Turing machines to simulate four-dimensional one-marker automata. In this paper, we continue the investigations, and deal with the necessary spaces for four-dimensional Turing machines to simulate four-dimensional one-marker automata.

Keywords: computational complexity, finite automaton, lower bounds, marker, simulation, Turing machine.

1. Introduction

An improvement of picture recognizability of the finite automaton is the reason why the marker automaton was introduced. That is, a two-dimensional one-marker automaton can recognize connected pictures. This automaton has been widely investigated in the two- or three-dimensional case [2]. A multi-marker automaton is a finite automaton which keeps marks as ‘pebbles’ in the finite control, and cannot rewrite any input symbols but

can make marks on its input with the restriction that only a bounded number of these marks can exist at any given time[1].

As is well known among the researchers of automata theory, one-dimensional one-marker automata are equivalent to ordinary finite state automata. In other words, there is no need of working space usage for one-way Turing machines to simulate one-marker automata, as well as finite state automata.

In the two-dimensional case, the following facts are known : the necessary and sufficient space for three-way two-dimensional deterministic Turing machines $TR2\text{-}DTM$'s to simulate two-dimensional deterministic (nondeterministic) finite automata $2\text{-}DFA$'s ($2\text{-}NFA$'s) is $m \log m$ (m^2) and the corresponding space for three-way two-dimensional nondeterministic Turing machines $TR2\text{-}NTM$'s is m (m), whereas the necessary and sufficient space for three-way two-dimensional deterministic Turing machines $TR2\text{-}DTM$'s to simulate two-dimensional deterministic (nondeterministic) one-marker automata $2\text{-}DMA_1$'s ($2\text{-}NMA_1$'s) is $2^{m \log m}$ (2^{m^2}) and the corresponding space for $TR2\text{-}NTM$'s is $m \log m$ (m^2), where m is the number of columns of two-dimensional rectangular input tapes.

In the three-dimensional case, the following facts are known : the necessary and sufficient space for five-way three-dimensional deterministic Turing machines $FV3\text{-}DTM$'s to simulate three-dimensional deterministic (nondeterministic) finite automata $3\text{-}DFA$'s ($3\text{-}NFA$'s) is $m^2 \log m$ (m^3) and the corresponding space for five-way three-dimensional nondeterministic Turing machines $FV3\text{-}NTM$'s is m^2 (m^2), whereas the necessary and sufficient space for five-way three-dimensional deterministic Turing machines $FV3\text{-}DTM$'s to simulate three-dimensional deterministic (nondeterministic) one-marker automata $3\text{-}DMA_1$'s ($3\text{-}NMA_1$'s) is $2^{lm \log lm}$ ($2^{l^2 m^2}$) and the corresponding space for $FV3\text{-}NTM$'s is $lm \log lm$ ($l^2 m^2$), where $l(m)$ is the number of rows (columns) on each plane of three-dimensional rectangular input tapes.

In the four-dimensional case, we showed the sufficient spaces for four-dimensional Turing machines to simulate four-dimensional one-marker automata [3]. In this paper, we continue the investigations, and deal with the necessary spaces for four-dimensional Turing machines to simulate four-dimensional one-marker automata.

2. Preliminaries

An ordinary finite automaton cannot rewrite any symbols on input tape, but a marker automaton can make a mark on the input tape. We can think of the mark as a 'pebble' that M puts down in a specified position. If M has already put down the mark, and wants to put it down elsewhere, M must first go to the position of the mark and pick it up. Formally, we define it as follows.

Definition 2.1. A four-dimensional nondeterministic one-marker automaton ($4\text{-}NMA_1$) is defined by the 6-tuple $M = (Q, q_0, F, \Sigma, \{+, -\}, \delta)$, where

- (1) Q is a finite set of states ;
- (2) $q_0 \in Q$ is the initial state ;
- (3) $F \subseteq Q$ is the set of accepting states ;
- (4) Σ is a finite input alphabet ($\# \notin \Sigma$ is the boundary symbol);
- (5) $\{+, -\}$ is the pair of signs of presence and absence of the marker ; and
- (6) $\delta : (Q \times \{+, -\}) \times ((\Sigma \cup \{\#\}) \times \{+, -\}) \rightarrow \times 2^{Q \times \{+, -\} \times ((\Sigma \cup \{\#\}) \times \{+, -\}) \times \{\text{east, west, south, north, up, down, future, past, no move}\}}$ is the next-move function, satisfying the following : For any $q, q' \in Q$, any $a, a' \in \Sigma$, any $u, u', v, v' \in \{+, -\}$, and any $d \in \{\text{east, west, south, north, up, down, future, past, no move}\}$, if $((q', u'), (a', v'), d) \in \delta((q, v), (a, v))$ then $a = a'$ and $(u, v, u', v') \in \{(+, -, +, -), (+, -, -, +), (-, +, -, +), (-, +, +, -), (-, -, -, -)\}$.

We call a pair (q, u) in $Q \times \{+, -\}$ an *extended state*, representing the situation that M holds or does not hold the marker in the finite control according to the sign $u = +$ or $u = -$, respectively. A pair (a, v) in $\Sigma \times \{+, -\}$ represents an input tape cell on which the marker exists or does not exist according to the sign $u = +$ or $u = -$, respectively.

Therefore, the restrictions on δ imply the following conditions. (i) When holding the marker, M can put it down or keep on holding. (ii) When not holding the marker, and ① if the marker exists on the current cell, M can pick it up or leave it there, or ② if the marker does not exist on the current cell, M cannot create a new marker any more.

Definition 2.2. Let Σ be the input alphabet of $4\text{-}NMA_1$ M . An *extended input tape* \tilde{x} of M is any four-dimensional tape over $\Sigma \times \{+, -\}$ such that for some $x \in \Sigma^{(4)}$,

- (i) for each j ($1 \leq j \leq 4$), $l_j(\tilde{x}) = l_j(x)$,
- (ii) for each i_1 ($1 \leq i_1 \leq l_1(\tilde{x})$), i_2 ($1 \leq i_2 \leq l_2(\tilde{x})$), i_3 ($1 \leq i_3 \leq l_3(\tilde{x})$), and i_4 ($1 \leq i_4 \leq l_4(\tilde{x})$), $\tilde{x}(i_1, i_2, i_3, i_4) = x((i_1, i_2, i_3, i_4), u)$ for some $u \in \{+, -\}$.

Definition 2.3. A *configuration* of $4\text{-}NMA_1$ $M = (Q, q_0, F, \Sigma, \{+, -\}, \delta)$ is a pair of an element of $((\Sigma \cup \{\#\}) \times \{+, -\})^{(4)}$ and an element of $C_M = (\mathbb{N} \cup \{0\})^{(4)} \times (Q \times \{+, -\})$. The first component of a configuration $c = (\tilde{x}, ((i_1, i_2, i_3, i_4), (q, u)))$ represents the extended input tape of M . The second component (i_1, i_2, i_3, i_4) of

c represents the input head position. The third component (q, u) of c represents the extended state. An element of C_M is called a *semi-configuration* of M . If q is the state associated with configuration c , then c is said to be an *accepting configuration* if q is an accepting state. The *initial configuration* of M on input x is $I_M(x) = (x^-, ((1,1,1,1), (q_0, +)))$, where x^- is the special extended input tape of M such that $x^-(i_1, i_2, i_3, i_4) = (x(i_1, i_2, i_3, i_4), -)$ for each i_1, i_2, i_3, i_4 ($1 \leq i_1 \leq l_1(x^-), 1 \leq i_2 \leq l_2(x^-), 1 \leq i_3 \leq l_3(x^-), 1 \leq i_4 \leq l_4(x^-)$). If M moves deterministically, we call M a four-dimensional deterministic one-marker automaton (4-DMA₁).

Definition 2.4. Given a 4-NMA₁ $M = (Q, q_0, F, \Sigma, \{+, -\}, \delta)$, we write $c \vdash_M c'$ and say c' is a *successor* of c if configuration c' follows from configuration c in one step of M , according to the transition rules δ . \vdash_M^* denotes the reflexive transitive closure of \vdash_M . The relation \vdash_M is not necessarily single-valued, because δ is not. A *computation path* of M on x is a sequence $c_0 \vdash_M c_1 \vdash_M \dots \vdash_M c_n$ ($n \geq 0$), where $c_0 = I_M(x)$. An *accepting computation path* of M on x is a computation path of M on x which ends in an accepting configuration. We say that M *accepts* x if there is an accepting computation path of M on input x .

Let $L(l, m, n) : \mathbf{N}^3 \mapsto \mathbf{R}$ be a function. A seven-way four-dimensional Turing machine M is said to be $L(l, m, n)$ *space-bounded* if for each $l, m, n \geq 1$ and for each x with $l_1(x) = l, l_2(x) = m$, and $l_3(x) = n$, if x is accepted by M , then there is an accepting computation path of M on x in which M uses no more than $L(l, m, n)$ cells of the storage tape. We denote an $L(l, m, n)$ space-bounded SV4-DTM (SV4-NTM) by $SV4-DTM(L(l, m, n))$ ($SV4-NTM(L(l, m, n))$).

Definition 2.5. For any four-dimensional automaton M with input alphabet Σ , define $T(M) = \{x \in \Sigma^{(4)} \mid M \text{ accepts } x\}$. Furthermore, for each $X \in \{D, N\}$, define

$$\mathbb{S}[4-XMA_1] = \{T \mid T = T(M) \text{ for some } 4-XMA_1\},$$

$$\mathbb{S}[SV4-XTM(S(l, m, n))] = \{T \mid T = T(M) \text{ for some } SV4-XTM(S(l, m, n))\}, \text{ and}$$

$$\mathbb{S}[SV4-XTM(L(l, m))] = \{T \mid T = T(M) \text{ for some } SV4-XTM((l, m))\}.$$

3. Necessary spaces

In this section, we investigate the necessary spaces (i.e., lower bounds) for seven-way Turing machines to simulate one-marker automata.

© The 2016 International Conference on Artificial Life and Robotics (ICAROB 2016), Jan. 29-31, Okinawa Convention Center, Okinawa, Japan

Definition 3.1. Let x be in $\Sigma^{(4)}$ (Σ is a finite set of symbols) and $l_1(x)=l, l_2(x)=m, l_3(x)=n$. For each j ($1 \leq j \leq Q[l_4(x)/lmn]$) (where $Q[l_4(x)/lmn]$ denotes the quotient when $l_4(x)$ is divided by lmn),

$$x[(1, 1, 1, (j-1)lmn+1), (l, m, n, jlmn)]$$

is called the j th (l, m, n) -block of x . We say that the tape x has exactly k (l, m, n) -blocks if $l_4(x)=klmn$, where k is a positive integer.

Definition 3.2. Let $(l_1, m_1, n_1), (l_2, m_2, n_2), \dots$, be a sequence of points (i.e., pairs of three natural numbers), and let $\{(l_i, m_i, n_i)\}$ denote this sequence. We call a sequence $\{(l_i, m_i, n_i)\}$ the *regular sequence of points* if $(l_i, m_i, n_i) \neq (l_j, m_j, n_j)$ for $i \neq j$.

Lemma 3.1. Let $T_1 = \{x \in \{0, 1\}^{(4)} \mid \exists l \geq 1, \exists m \geq 1, \exists n \geq 1 [l_1(x)=l \text{ and } l_2(x)=m \text{ and } l_3(x)=n \text{ and (each plane of } x \text{ contains exactly one '1') and } \exists d \geq 2 [(x \text{ has exactly } d \text{ (} l, m, n \text{)-blocks, i.e., } l_4(x)=dlmn) \text{ and (the last (} l, m, n \text{)-block is equal to some other (} l, m, n \text{)-block)}]]]\}$. Then,

(1) $T_1 \in \mathbb{S}[4-DMA_1]$, but

(2) $T_1 \notin \mathbb{S}[SV4-DTM(2^{L(l, m, n)})]$ (so, $T_1 \notin \mathbb{S}[SV4-NTM(L(l, m, n))]$) for any function $L(l, m, n)$ such that $\lim_{i \rightarrow \infty} [L(l_i, m_i, n_i)/(l_i m_i n_i \log l_i m_i n_i)] = 0$, for some regular sequence of points $\{(l_i, m_i, n_i)\}$.

Proof: (1): We construct a 4-DMA₁ M accepting T_1 as follows. Given an input x with $l_1(x) = l, l_2(x) = m$, and $l_3(x) = n$, M first checks, by sweeping plane by plane, that each plane of x contains exactly one '1', and M then checks, by making a zigzag of 45° -direction from top plane to bottom plane, that x has exactly d (l, m, n) -blocks for some integer $d \geq 2$. After that, M tests by utilizing its own marker whether the last (l, m, n) -block is identical to some other (l, m, n) -block. M then finds the '1' position on the plane and move up vertically from this position. In this course, each time M meets a '1' position, it checks whether or not there is a marker on the plane (containing the '1' position).

(i): If there is a marker on the plane, M knows that the k th planes of the h th and the last (l, m, n) -blocks are identical, and so M then tries to check whether the next $(k+1)$ th planes of the h th and the last (l, m, n) -blocks are identical.

(ii): If there is no marker on the plane, M goes back to the '1' position on the plane, and vertically moves up again to find the next '1' position.

In this case, if M eventually encounters the top boundary, M knows that the k th planes of the h th and the last (l, m, n) -blocks are different (thus, the h th (l, m, n) -block is not

identical to the last (l, m, n) -block), and so M then tries to check whether the next $(h+1)$ th (l, m, n) -block is identical to the last (l, m, n) -block.

In this way, M enters an accepting state just when it finds out some (l, m, n) -block, each of whose planes is identical to the corresponding plane of the last (l, m, n) -block. It will be obvious that $T(M) = T_1$.

(2): Suppose to the contrary that there exists an SV4-DTM $(2^{L(l, m, n)})$ M accepting T_1 , where $L(l, m, n)$ is a function such that

$$\lim_{i \rightarrow \infty} [L(l_i, m_i, n_i) / (l_i m_i n_i \log l_i m_i n_i)] = 0.$$

For some regular sequence of points $\{(l_i, m_i, n_i)\}$. Let s and t be the numbers of states in the finite control and storage tape symbols of M , respectively. We assume without loss of generality that if M accepts an input, then M enters an accepting state on the bottom boundary. For each $l \geq 1, m \geq 1, n \geq 1$, let

$V(l, m, n) = \{x \in T_1 \mid l_1(x) = l \text{ and } l_2(x) = m \text{ and } l_3(x) = n \text{ and } x \text{ has exactly } ((lmn)^{lmn} + 1) \text{ } (l, m, n)\text{-blocks}\}$. For each $x \in V(l, m, n)$, let $B(x) = \{b \in \{0, 1\}^{(4)} \mid \exists h (1 \leq h \leq (lmn)^{lmn}) [b \text{ is the } h\text{th } (l, m, n)\text{-block of } x]\}$, and let $S(l, m, n) = \{B(x) \mid x \in V(l, m, n)\}$. Note that for each $x \in V(l, m, n)$, there is a sequence of configurations of M which leads M to an accepting state. Let $\text{conf}(x)$ be the semi-configuration just after M leaves the second-to-last (l, m, n) -block of x . Then, we get following proposition.

Proposition 3.1. *For any two tapes $x, y \in V(l, m, n)$, if $B(x) \neq B(y)$, then $\text{conf}(x) \neq \text{conf}(y)$.*

Proof of Lemma 3.1 (continued): There are at most

$$E(l, m, n) = (l+2)(m+2)(n+2)s^{2^{L(l, m, n)}}t^{2^{L(l, m, n)}}$$

different semi-configurations of M just when M enters the last (l, m, n) -block of tapes in $V(l, m, n)$. On the other hand,

$$|S(l, m, n)| = 2^r - 1 \quad (r = (lmn)^{lmn}).$$

Thus, from the assumption concerning the function $L(l, m, n)$, it follows that there exists a point (l_i, m_i, n_i) such that $|S(l_i, m_i, n_i)| > E(l_i, m_i, n_i)$. For such (l_i, m_i, n_i) , there exist two tapes x, y in $V(l_i, m_i, n_i)$ such that $B(x) \neq B(y)$ and $\text{conf}(x) \neq \text{conf}(y)$. This contradicts Proposition 3.1. This completes the proof of (2). \square

From Lemma 3.1, we can conclude as follows.

Theorem 3.1. *To simulate 4-DMA₁'s,*

- (1) *SV4-NTM's require $\Omega(lmn \log lmn)$ space, and*
- (2) *SV4-DTM's require $2^{\Omega(lmn \log lmn)}$ space.*

By using the same technique as in the proof of Theorem 3.1, we can get as follows.

Theorem 3.2. *To simulate 4-NMA₁'s,*

- (1) *SV4-NTM's require $\Omega(l^2 m^2 n^2)$ space, and*
- (2) *SV4-DTM's require $2^{\Omega(l^2 m^2 n^2)}$ space.*

4. Conclusion

In this paper, we showed the necessary spaces for four-dimensional Turing machines to simulate four-dimensional one-marker automata. It will be interesting to investigate how much space is necessary and sufficient for seven-way four-dimensional deterministic or nondeterministic Turing machines to simulate four-dimensional 'alternating' one-marker automata.

References

1. M. Blum and C. Hewitt, "Automata on a two-dimensional tape", IEEE Symposium on Switching and Automata Theory, pp.155-160 (1967).
2. M. Sakamoto, "Three-dimensional alternating Turing machines", Ph.D. Thesis, Yamaguchi University (1999).
3. M. Nagatomo, M. Sakamoto, H. Susaki, T. Zhang, S. Ikeda, H. Furutani, T. Ito, Y. Uchida, and T. Yoshinaga, "Sufficient spaces for seven-way four-dimensional Turing machines to simulate four-dimensional one-marker automata", Proceedings of the International Conference on Artificial Life and Robotics (ICAROB2015), Horuto Hall, Oita, Japan, OS6-1, pp.340-343(CD-ROM) (2015).

Analysis for 4×12 board of Othello

Yuki Takeshita

*Graduate School of Engineering, Miyazaki University
Japan, hf11031@student.miyazaki-u.ac.jp*

Makoto Sakamoto

*Department of Computer Science and System Engineering, Miyazaki University
Japan, sakamoto@cs.miyazaki-u.ac.jp*

Takao Ito

*Graduate School of Engineering, Hiroshima University
Japan, itotakao@hiroshima-u.ac.jp*

Satoshi Ikeda

*Department of Computer Science and System Engineering, Miyazaki University,
Japan, bisu@cs.miyazaki-u.ac.jp*

Abstract

More than 20 years has passed since J. Feinstein (1993) found by using computer that perfect play on 6×6 board of Othello gives 16-20 loss for the first player. During this time, computers have improved drastically, however, standard 8×8 board remain unsolved. In our previous paper, we were able to obtain the perfect plays on 6×6 board and 4×10 board. In this paper, we challenge the unsolved problem of 4×12 board by dividing it into about 100 small distinct sub-problems.

Keywords: combinatorial theory, combinatorial optimization, perfect play, rectangular Othello

1. Introduction

Othello is a board game derived from Reversi by Goro Hasegawa (JPN) in 1973. Othello rules¹ are completely unified, whereas Reversi has many local rules. According to the Japan Othello Association established by Hasegawa, World Championship has been held every year since 1977, tournament is held in Japan, the United States and European countries.

Othello is categorized into two-player zero-sum finite deterministic games of perfect information². Games in this class are possible to look ahead in theory, thus if both players choose constantly the best move, these are classified into win, loss or draw game for the first player³

(the sequence obtained in this case is called perfect play). In 1993, Joel Feinstein reported that perfect play on 6×6 board of Othello gives 16-20 loss for the first player⁴(Fig. 1); we confirmed that the sequence reported by him is one of the perfect plays⁵. Othello on standard 8×8 board has not been solved, since the number of positions is too large; according to some strong programs, it seems theory of becoming draw is strong⁶. In our previous paper⁷, we were able to obtain some perfect plays on 6×6 board and 4×10 board. In this paper, we challenge the unsolved problem of 4×12 board by dividing it into about 100 small distinct sub-problems.

28	9	8	7	31	32
22	14	1	4	17	16
27	13	○	●	6	15
19	2	●	○	5	12
24	23	3	10	26	29
21	18	20	11	25	30

Fig. 1. Feinstein's perfect play.

2. Othello

First of all, we will introduce the rules of Othello. The game always begins with the setup as shown in Fig. 2, however, since we deal with 4×12 board of Othello in this paper, the disposition such as shown in Fig. 3 is the starting position. One player uses the black side of the pieces (circular chips), the other the white side. Black always moves first.

Each player puts a piece of own color to an empty square in own turn. A player's move consists of outflanking his opponent's the pieces, he flips outflanked pieces to his color. To outflank means to place the piece on the board so that his opponent's rows of the piece are bordered at each end by the piece of his color. If a player cannot make any move, then he has to pass. If he is able to make a valid move, then passing is not allowed. The game ends when neither player can make any valid move. The winner is the player who has more pieces than his opponent.

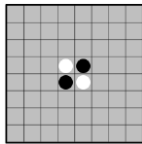
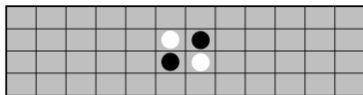


Fig. 2. Othello's setup.

Fig. 3. The starting position on 4×12 board of Othello.

3. Computer Othello

For perfect analysis of strategy board game such as Othello, it is useful to refer thinking routines of game

program. This is because end-game routine of game program is the perfect analysis exactly, and evaluation function in the middle-game routine is available for the ordering of the search in perfect analysis.

In addition, end-game routine is classified into solving for WLD (win/loss/draw) score and solving for exact score. Both are the perfect analysis, but there is a difference in the evaluation of the end. For an exact score solve, the end is evaluated with the piece difference. This routine can find best one move. For WLD score solve, the end is evaluated in three ways win, loss, and draw. It generates relatively many pruning (Alpha-Beta Pruning⁸) if the range of the evaluation value is small. Therefore, an execution time for the exact score is estimated to be several times of the execution time for the WLD score.

4. Perfect analysis for $4 \times 2n$ board of Othello

Table 1 is the results that we analyzed from the starting position for $4 \times 2n$ board of Othello. See Table 1, we see that rectangular Othello has the feature that gives the first player an advantage according to extended board size. Therefore, we suppose that there is a strong possibility that first move wins in 4×12 board of Othello.

Table 1. The analysis results for $4 \times 2n$ board of Othello.

	Winner	Perfect Play
4×4	White	B: 03, W: 11
4×6	Black	B: 20, W: 04
4×8	Black	B: 28, W: 00
4×10	Black	B: 39, W: 00

5. Estimate the number of the final positions

See Fig. 4, it is changes in the number of the final positions for $4 \times 2n$ board of Othello. By Fig. 4, the number of the final positions in 4×12 board seems to be about 10^{16} . However, in 4×12 board, since the white is often wiped out in the middle, it is assumed to be 10^{15} . Therefore, since execution time in 4×10 board is six days, we suppose that execution time in 4×12 board is about six thousand days. In this paper, by dividing it into about 100 distinct sub-problems, we solve each sub-problem in 4×12 board of Othello within sixty days.

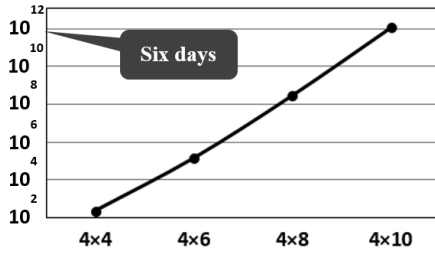


Fig. 4. Changes in the number of the final positions for 4×2n board of Othello.

6. Perfect Analysis with the fixed moves

We found an initial position of 4×12 board as shown Fig. 5, which fixed from move 1 to move 6 in 4×12 board. This position gives win for the first player. This position is also the sequence of perfect play which is consistent with 4×8 board and 4×10 board. This is the reason why we choose this sequence. See Fig. 6, it is perfect play under starting position Fig. 6. If this sequence is the best move for both players, it shows that 4×12 board of Othello gives win for the first player. Therefore, it is necessary to check some positions which branched from white turn. Concretely, they are move 2, move 4 and move 6.

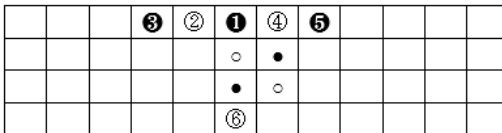


Fig. 5. A fixed position from move 1 to move 6.

29	19	18	●	●	●	●	●	13	32	41	
30	24	17	16	14	○	●	10	20	31		
35	36	21	23	15	○	○	22	33	34	39	
37	25	26	8	7	○	11	9	12	27		

Fig. 6. Perfect play fixed from move 1 to move 6 in 4×12 board. The black wins 48-0. PASS is 28, 30, and 40.

7. Experiments

We use six computers with quad-core to solve the sub-problems for 4×12 board. Our solver has the exact score as evaluation value for perfect analysis.

Fig. 7, Fig. 8 and Fig. 9 are three positions that must be checked in order to prove that gives win for the first player on 4×12 board. The Greek alphabets in these

figures mean all of places that the second player can put in his turn. 'F' in each figure means 'Finish', this is a place which already finished the search when we check in descending order (Depth 6, Depth 4, and Depth 2).

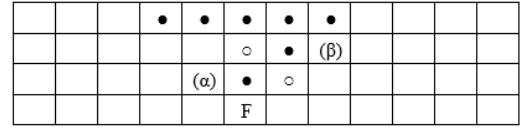


Fig. 7. Depth 6.

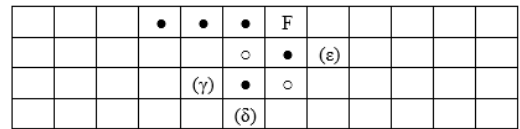


Fig. 8. Depth 4.

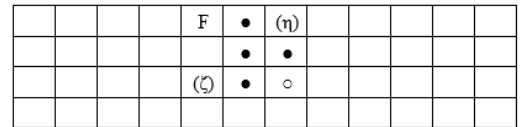


Fig. 9. Depth 2.

Table 2 shows a part of the position that is fixed from move 1 to move 6 in 4×12 board of Othello. These are currently analyzing sub-problems for this board. For every element in Table 2, the first Greek alphabets show the places as mentioned above. The following character strings are a sequence to move 6 corresponding to the coordinates in Fig. 10. For further details on the sub-problems, refer to Appendix Table 3.

Table 2. Currently checking problems for each position.

Depth 6	Depth 4	Depth 2
(a)	(γ)e4g1	(ζ)f4e1d1g1
(β)	(γ)e4h2	(ζ)f4e1d1h2
	(γ)e4f4	(ζ)f4g1h1h2
	(γ)f4g1	(η)h1e1d1e3
	(δ)h4h1	(η)h1e1d1f4
	(δ)h4h2	(η)h1e1d1h2
	(δ)h4h3	(η)h1e3g4h3
	(ε)h3f4	(η)h1e3h4h3
	(ε)h3h4	
	(ε)h4e2	
	(ε)h4e4	
	(ε)h4g4	
	(ε)h1g1	

a1	b1	c1	d1	e1	f1	g1	h1	i1	j1	k1	l1
a2	b2	c2	d2	e2	○	●	h2	i2	j2	k2	l2
a3	b3	c3	d3	e3	●	○	h3	i3	j3	k3	l3
a4	b4	c4	d4	e4	f4	g4	h4	i4	j4	k4	l4

Fig. 10. Coordinates on 4×12 board.

8. Consideration

(ζ)f4e1d1g1, (γ)e4g1 and (η)h1e1d1f4 in Table 2 have already finished. Both results are the black win 48-0. When all of the execution given in Table 2 are over, if their results are the black win, it is proven that the first player wins in 4×12 board of Othello. Moreover, if all of them are complete victories of the first player, it is proven that a sequence given in Fig. 6 is one of the perfect plays on 4×12 board of Othello.

9. Future work

The next challenge is the analysis for 6×8 board of Othello. It is necessary to estimate the size of game tree in the 6×8 board accurately. After that, we will implement the distributed processing for transferring to the cloud servers.

References.

1. Japan Othello Association: Nihon osero renmei kyougi ru-ru, [online]www.othello.gr.jp/r_info/rule.html (Retrieved 10 December. 2015)
2. J. V. Neumann and O. Morgenstern: Theory of Games and Economic Behavior, Princeton University Press (1944).
3. J. Schaeffer, N. Burch, Y. Björnsson, A. Kishimoto, M. Müller, R. Lake, P. Lu and S. Sutphen: "Checkers Is Solved," Science, Vol. 317, pp. 1518-1522 (2007).
4. British Othello Federation: Forty Billion Nodes Under The Tree - The Newsletter of the British Othello Federation, [online]www.britishothello.org.uk/fbnall.pdf (Retrieved 1 December. 2015), pp. 6–8 (1993).
5. Y. Takeshita, S. Ikeda, M. Sakamoto and T. Ito: "Perfect Analysis in miniature Othello," Proceedings of the 2015 International Conference on Artificial life and Robotics, pp.39 (2015).
6. B. Rose: Othello - A Minute to Learn... A Lifetime to Master, [online]www.ffothello.org/livres/othello-book-Brian-Rose.pdf (Retrieved 1 December. 2015) (2005).
7. Y. Takeshita, S. Ikeda, M. Sakamoto and T. Ito: "Perfect Play in Miniature Othello," Proceedings of the Ninth International Conference on Genetic and Evolutionary Computing, pp.281-290 (2015).

8. D. E. Knuth and R. W. Moore: "An Analysis of Alpha-Beta Pruning," Artificial Intelligence, Vol. 6, pp. 293–326 (1975).

Appendix

Table 3. The other problems fixed to move 6 on 4×12 board.

Depth 4	Depth 2		
(γ)e2g1	(ζ)f4e1e2g1	(ζ)f4g1d3e4	(η)h1e1h3h2
(γ)e2h1	(ζ)f4e1d3d4	(ζ)f4g1h2e1	(η)h1e1h3h4
(γ)g4h1	(ζ)f4e1d3g1	(ζ)f4g1h2e4	(η)h1e1h3i1
(γ)g4h2	(ζ)f4e1d3h2	(ζ)f4g1h2g4	(η)h1e3d4d3
(γ)g4h2	(ζ)f4e1g4g1	(ζ)f4g1h2h3	(η)h1e3d4e1
(γ)g4h3	(ζ)f4e1g4h2	(ζ)f4g1h2h4	(η)h1e3e4e1
(γ)g4h4	(ζ)f4e1g4h3	(ζ)f4g1h2i2	(η)h1e3f4e1
(γ)h4g1	(ζ)f4e1g4h4	(ζ)f4g1h2i3	
(γ)h4h1	(ζ)f4e1h2g1	(ζ)f4g1h3e1	
(γ)h4h3	(ζ)f4e1h2h3	(ζ)f4g1h3g4	
(δ)e2g1	(ζ)f4e1h2h4	(ζ)f4g1h3h2	
(δ)e2h1	(ζ)f4e1h2i2	(ζ)f4g1h3h4	
(δ)e4g1	(ζ)f4e1h3g1	(ζ)f4g1h3i3	
(δ)e4h2	(ζ)f4e1h3h2	(η)h1e1e2e3	
(δ)e4e3	(ζ)f4e1h3h4	(η)h1e1e2i1	
(δ)e4d4	(ζ)f4e1h3i3	(η)h1e1e3d3	
(δ)g4h1	(ζ)f4g1d2d3	(η)h1e1e3i1	
(δ)g4h2	(ζ)f4g1d2d4	(η)h1e1g4f4	
(δ)g4h3	(ζ)f4g1d2e1	(η)h1e1g4h2	
(δ)g4h4	(ζ)f4g1d3c3	(η)h1e1g4h4	
(e)h1e3	(ζ)f4g1d3d4	(η)h1e1g4i1	
(e)h1f4	(ζ)f4g1d3e1	(η)h1e1h3f4	

A space lower-bound technique for four-dimensional alternating Turing machines

Makoto Nagatomo, Shinnosuke Yano, Makoto Sakamoto, Satoshi Ikeda and Hiroshi Furutani

Faculty of Engineering, University of Miyazaki,

1-1 Gakuen Kibanadai Nishi, Miyazaki, Miyazaki 889-2192, Japan

E-mail: je.suis.makoto@gmail.com, shinchandx@ezweb.ne.jp, sakamoto@cs.miyazaki-u.ac.jp, bisu@cs.miyazaki-u.ac.jp, furutani@cs.miyazaki-u.ac.jp

Takao Ito, Tsutomu Ito

Institute of Engineering, Hiroshima University, 4-1, Kagamiyama 1-chome

Higashi-Hiroshima, Hiroshima 739-8527, Japan

E-mail: itotakao@horoshima-u.ac.jp, 0va71-2538f211n@ezweb.ne.jp

Yasuo Uchida

Department of Business Administration, Ube National College of Technology, Tokiwadai

Ube, Yamaguchi 755-8555, Japan

E-mail: uchida@ube-k.ac.jp

Tsunehiro Yoshinaga

Department of Computer Science & Electronic Engineering,

National Institute of Technology, Tokuyama College, Gakuendai

Shunan, Yamaguchi 745-8585, Japan

E-mail: yosinaga@tokuyama.ac.jp

Abstract

Alternating Turing machines were introduced in 1981 as a generalization of nondeterministic Turing machines and as a mechanism to model parallel computation. On the other hand, we have no enough techniques which we can show that some concrete four-dimensional language is not accepted by any space-bounded four-dimensional alternating Turing machines. The main purpose of this paper is to present a technique which we can show that some four-dimensional language is not accepted by any space-bounded four-dimensional alternating Turing machines. Concretely speaking, we show that the set of all four-dimensional input tapes over $\{0,1\}$, which each top half part is equal to each bottom half part, is not accepted by any $L(m)$ space-bounded four-dimensional alternating Turing machines for any function $L(m)$ smaller than $\log m$.

Keywords: Alternation, Complexity, Computation Tree, Configuration, Four-Dimension, Turing machine

1. Introduction and Preliminaries

We have no enough techniques which we can show that some concrete four-dimensional language is not

accepted by any space-bounded four-dimensional alternating Turing machines [1, 2]. The main purpose of this paper is to present a technique which we can show

© The 2016 International Conference on Artificial Life and Robotics (ICAROB 2016), Jan. 29-31, Okinawa Convention Center, Okinawa, Japan

that some four-dimensional language is not accepted by any space-bounded four-dimensional alternating Turing machines. Concretely speaking, we show that the set of all four-dimensional input tapes over $\{0,1\}$, which each top half part is equal to each bottom half part, is not accepted by any $L(m)$ space-bounded four-dimensional alternating Turing machines for any function $L(m)$ such that $\lim_{m \rightarrow \infty} [L(m)/\log m] = 0$. We let each side-length of each four-dimensional input tape of these automata be equivalent in order to increase the theoretical interest.

Let Σ be a finite set of symbols. A three-dimensional tape over Σ is a four-dimensional rectangular array of elements of Σ . The set of all four-dimensional tapes over Σ is denoted by $\Sigma^{(4)}$. Given a tape $x \in \Sigma^{(4)}$, for each integer $j (1 \leq j \leq 4)$, we let $m_j(x)$ be the length of x along the j th axis. The set of all $x \in \Sigma^{(4)}$ with $l_1(x)=m_1, l_2(x)=m_2, l_3(x)=m_3$, and $l_4(x)=m_4$ denoted by $\Sigma^{(m_1, m_2, m_3, m_4)}$. If $1 \leq i_j \leq l_j(x)$ for each $j (1 \leq j \leq 4)$, let $x(i_1, i_2, i_3, i_4)$ denote the symbol in x with coordinates (i_1, i_2, i_3, i_4) . Furthermore, we define $x[(i_1, i_2, i_3, i_4), (i'_1, i'_2, i'_3, i'_4)]$, when $1 \leq i_j \leq i'_j \leq l_j(x)$ for each integer $j (1 \leq j \leq 4)$, as the four-dimensional tape y satisfying the following (i) and (ii):

- (i) for each $j (1 \leq j \leq 4)$, $l_j(y) = i'_j - i_j + 1$;
- (ii) for each $r_1, r_2, r_3, r_4 (1 \leq r_1 \leq l_1(y), 1 \leq r_2 \leq l_2(y), 1 \leq r_3 \leq l_3(y), 1 \leq r_4 \leq l_4(y))$, $y(r_1, r_2, r_3, r_4) = x(r_1 + i_1 - 1, r_2 + i_2 - 1, r_3 + i_3 - 1, r_4 + i_4 - 1)$. (We call $x[(i_1, i_2, i_3, i_4), (i'_1, i'_2, i'_3, i'_4)]$ $x[(i_1, i_2, i_3, i_4), (i'_1, i'_2, i'_3, i'_4)]$ -segment of x);

A four-dimensional alternating Turing machine (4-ATM) M is defined by the 7-tuple $M = (Q, q_0, U, F, \Sigma, \Gamma, \delta)$, where (1) Q is a finite set of states; (2) $q_0 \in Q$ is the initial state; (3) $U \subseteq Q$ is the set of universal states; (4) $F \subseteq Q$ is the set of accepting states; (5) Σ is a finite input alphabet ($\# \notin \Sigma$ is the boundary symbol); (6) Γ is a finite storage-tape alphabet ($B \in \Gamma$ is the boundary symbol), and (7) $\delta \subseteq (Q \times (\Sigma \cup \{\#\}) \times \Gamma) \times (Q \times (\Gamma - \{B\}) \times \{\text{east, west, south, north, up, down, past, future, no move}\} \times \{\text{right, left, no move}\})$ is the next-move relation.

A state q in $Q - U$ is said to be *existential*. The machine M has a read-only four-dimensional input tape with boundary symbols $\#$'s and one semi-infinite storage tape, initially blank. Of course, M has a finite control, an input head, and a storage-tape head. A position is assigned to each cell of the read-only input tape and to each cell of the storage tape. A step of M consists of reading one symbol from each tape, writing a symbol on the storage tape, moving the input and storage heads in specified directions, and entering a new state, in accordance with

the next-move relation δ . Note that the machine cannot write the blank symbol. If the input head falls off the input tape, or if the storage head falls off the storage tape (by moving left), then the machine M can make no further move.

A configuration of a 4-ATM $M = (Q, q_0, U, F, \Sigma, \Gamma, \delta)$ is a pair of an element of $\Sigma^{(4)}$ and an element of $C_M = (NU\{0\})^3 \times S_M$, where $S_M = Q \times (\Gamma - \{B\})^* \times N$ and N denotes the set of all the positive integers. The first component x of a configuration $c = (x, ((i_1, i_2, i_3, i_4), (q, \alpha, j)))$ represents the input to M . The second component $((i_1, i_2, i_3, i_4), (q, \alpha, j))$ of c represents the input-head position. The third component (q, α, j) of c represents the state of the finite control, nonblank contents of the storage tape, and the storage-head position. An element of C_M is called a *semi-configuration* of M and an element of S_M is called a storage state of M . If q is the state associated with configuration c , then c is said to be a *universal (existential, accepting)* configuration if q is a universal (existential, accepting) state. The initial configuration of M on input x is $I_M(x) = (x, (1, 1, 1, 1), (q_0, \lambda, 1))$, where λ is the null string.

Given $M = (Q, q_0, U, F, \Sigma, \Gamma, \delta)$, we write $c \vdash_M c'$ and say c' is a *successor* of c if configuration c' follows from configuration c in one step of M , according to the transition rules δ . The relation \vdash_M is not necessarily single-valued, because δ is not. A *computation path* of M on x is a sequence. $C_0 \vdash_M C_1 \vdash_M \cdots \vdash_M C_n$ ($n \geq 0$), where $C_0 = I_M(x)$. A *computation tree* of M is a finite, nonempty labeled tree with the following properties: (1) Each node v of the tree is labeled with a configuration $l(v)$, (2) If v is an internal node (a nonleaf) of the tree, $l(v)$ is universal and $\{c \mid l(v) \vdash_M c\} = \{c_1, \dots, c_k\}$, then v has exactly k children v_1, \dots, v_k such that $l(v_i) = c_i$ ($1 \leq i \leq k$), and (3) If v is an internal node of the tree and $l(v)$ is existential, then v has exactly one child u such that $l(v) \vdash_M l(u)$. A *computation tree* of M on input x is a computation tree of M whose root is labeled with $I_M(x)$. An *accepting computation tree* of M on x is a computation tree of M on x whose leaves are all labeled with accepting configurations. We say that M accepts x if there is an accepting computation tree of M on input x . Define $T(M) = \{x \in \Sigma^{(4)} \mid M \text{ accepts } x\}$.

In this paper, we shall concentrate on investigating the properties of 4-ATM's whose each side-length of each four-dimensional input tape is equivalent and whose storage tapes are bounded (in length) to use.

Let $L(m) : N \rightarrow N$ be a function with one variable m . With each 4-ATM M we associate a *space complexity function* SPACE that takes configurations to natural numbers. That is, for each configuration $c = (x, ((i_1, i_2, i_3, i_4), (q, \alpha, j)))$, let $\text{SPACE}(c) = |\alpha|$. We say that M is $L(m)$ *space-bounded* if for all $m \geq 1$ and for each x with $l_1(x) = l_2(x) = l_3(x) = l_4(x) = m$, if x is accepted by M , then there is an accepting computation tree of M on input x such that for each node v of the tree, $\text{SPACE}(l(v)) \leq L(m)$. We denote an $L(m)$ space-bounded 4-ATM by 4-ATM $(L(m))$. $\mathcal{L}[4\text{-ATM}(L(m))]$ = $\{T \mid T = T(M) \text{ for some } 4\text{-ATM}(L(m)) M\}$.

2. Main Result

[Theorem 1] Let $T = \{x \in \{0, 1\}^{(4)} \mid \exists m \leq 1 [l_1(x) = l_2(x) = l_3(x) = l_4(x) = 2m \ \& \ x[(1, 1, 1, 1), (2m, 2m, 2m, m)] = x[(1, 1, 1, m+1), (2m, 2m, 2m, 2m)]]\}$. Then, $T \notin \mathcal{L}[4\text{-ATM}(L(m))]$ for any $L(m) = o(\log m)$.

(Proof) Suppose that there exists a 4-ATM $(L(m))$ M accepting T , where $L(m) = o(\log m)$. We assume, without loss of generality, that M moves a storage-tape head after changing its state and writing a new symbol on the storage tape, and moves an input head finally. For each $m \leq 1$, let $V(m) = \{x \in T \mid l_1(x) = l_2(x) = l_3(x) = l_4(x) = 2m\}$. For each x in $V(m)$, let $t(x)$ be one fixed accepting computation tree of M on x such that each node v of the tree satisfies $\text{SPACE}(l(v)) \leq L(2m)$, where for each node v of $t(x)$, $l(v)$ represents the label of v . Without loss of generality, we assume that for any $t(x)$;

- (i) any two different nodes on any path of $t(x)$ are labeled by different configurations, and,
- (ii) if any different nodes of $t(x)$ have the same label, then the subtrees [of $t(x)$] with these nodes as the roots are identical.

For each x in $V(m)$, let $t(m)$, which we call the *reduced accepting computation tree* of M on x , be a tree obtained from $t(x)$ by the following procedure [for each node v of $t(x)$, we denote by $d(v)$ the length of the path from the root of $t(x)$ to v (i.e., the number of edges from the root of $t(x)$ to v)]:

Begin

1. $T_r = t(x)$
2. $i = 1$
3. Let $N(i) \triangleq \{v \mid v \text{ is node of } T_r \text{ and } d(v) \leq i\}$. Divide $N(i)$ as follows: $N(i) = P(1) \cup P(2) \cup \dots \cup P(j_i)$, where: (1) if $i_a = i_b$ ($1 \leq i_a, i_b \leq j_i$), then $P(i_a) \cap P(i_b) = \emptyset$, and (2) for each i_a ($1 \leq i_a \leq j_i$) and for each $v_a, v_b \in P(i_a)$, $l(v_a)$

$= l(v_b)$ (i.e., the labels of v_a and v_b are identical). For each i_a ($1 \leq i_a \leq j_i$), let $\text{dis}(i_a) = \min\{d(v) \mid v \in P(i_a)\}$ and let $n(i_a)$ be the leftmost node among those nodes v in $P(i_a)$ such that $d(v) = \text{dis}(i_a)$. Further, let $N'(i) = N(i) - \{n(1), n(2), \dots, n(j_i)\}$. By removing from T_r all the subtrees whose roots are included in $N'(i)$, we make the new T_r .

4. If the height of T_r (i.e., the length of the longest path of T_r) is less than or equal to i , then we let $t'(x) = T_r$. Otherwise, we let $i = i + 1$ and go to step 3.

end

[Example 1] Let $x \in V(m)$ and $t(x)$ be a tree. Here, suppose that nodes A and D have the same label, nodes B and C have the same label, and other nodes each have different labels. [From the preceding assumption (ii) concerning $t(x)$, identical.] Then, $t'(x)$ is a tree. That is, $t'(x)$ is obtained from $t(x)$ by moving the subtree with nodes C and D as the roots from $t(x)$.

It is easily seen that for each x in $V(m)$, all the nodes of $t'(x)$ have labels different from one another, and the set of all the paths from root of $t'(x)$ to the leaves of $t'(x)$ represents necessary and sufficient accepting computations of M on x . From $t'(x)$, we now define an *extended crossing sequence (ECS)* at the boundary between the top and bottom halves of x . The concept of ECS was first introduced in [3]. We relabel each node v of $t'(x)$, as follows. (We denote this new labeling by l' .) For each node v of $t'(x)$, let $f(v)$ denote the father node of v . Then, for each node v of $t'(x)$, where $x \in V(m)$, let if, for some storage states (q, α, j) and (q', α', j') ,

- (i) $l(f(v)) = (x, (i_1, i_2, i_3, m), (q', \alpha', j'))$ and $l(v) = (x, (i_1, i_2, i_3, m+1), (q, \alpha, j))$, or
- (ii) $l(f(v)) = (x, (i_1, i_2, i_3, m+1), (q', \alpha', j'))$ and $l(v) = (x, (i_1, i_2, i_3, m), (q, \alpha, j))$, then $l'(v) = ((i_1, i_2, i_3), (q, \alpha, j))$

else

$l'(v) = *$.

That is, if the movement of M from $f(v)$ to v represents the action of crossing the boundary between the top and bottom halves of x , then v is newly labeled by $(i_1, i_2, i_3), (q, \alpha, j)$, where (q, α, j) is the storage state component of $l(v)$. Otherwise, v is newly labeled by $*$. From the newly labeled $t'(x)$, we extract those nodes v such that $l'(v) = *$, and by using these nodes, we construct a tree $t''(x)$ satisfying the following condition:

- (A) For any node v of $t''(x)$, nodes v_1, v_2, \dots, v_s are children of v if and only if v_1, v_2, \dots, v_s are descendants of v in $t'(x)$ and $l'(u) = *$ for each node u on the path

from v to each v_i . In general, there can be two or more such trees $t''(x)$. Let these trees be $t_1''(x), \dots, t_n''(x)$. For each node v of each $t_i''(x)$ ($1 \leq i \leq n$), we now define an element of ECS (EECS) inductively as follows: Let

$$l'(v) = ((i_1, i_2, i_3), (q, \alpha, j)).$$

(1) If v is a leaf, then $(((i_1, i_2, i_3), (q, \alpha, j)))$ is an EECS of v .

(2) If v has only one child v_1 and $Q_1 = [((i_{11}, i_{21}, i_{31}), (q_1, \alpha_1, j_1))P]$ is an EECS of v_1 , then $(((i_1, i_2, i_3), (q, \alpha, j)))$ is an EECS of v .

(3) If v has $d(\geq 2)$ children v_1, \dots, v_d and Q_1, \dots, Q_d are EECS's of v_1, \dots, v_d , respectively, then $(((i_1, i_2, i_3), (q, \alpha, j))) Q_{\sigma(1)} \dots Q_{\sigma(d)}$ is an EECS of v for any permutation $\sigma : \{1, \dots, d\} \rightarrow \{1, \dots, d\}$.

(4) An EECS of v is defined only by the preceding statements (1), (2), and (3).

Now, let Q_1, \dots, Q_n be EECS's of the root nodes of $t_1''(x), \dots, t_n''(x)$, respectively. Then, for any permutation $\sigma : \{1, \dots, n\} \rightarrow \{1, \dots, n\}$, we call $Q_{\sigma(1)}, \dots, Q_{\sigma(n)}$ an ECS of x . As is easily seen from the definitions, there can be two or more EECS's of each node v of each $t''(x)$, and there can be two or more ECS's of x . Let Q_1 and Q_2 be any two EECS's. If the following condition (B) is satisfied, we say Q_1 and Q_2 are equivalent and write $Q_1 \equiv Q_2$:

(B) Let $Q_1 = [((i_{11}, i_{21}, i_{31}), (q_1, \alpha_1, j_1)) \dots ((i_{1n}, i_{2n}, i_{3n}), (q_n, \alpha_n, j_n)) P_1 \dots P_s]$, $Q_2 = [((i'_{11}, i'_{21}, i'_{31}), (q'_1, \alpha'_1, j'_1)) \dots ((i'_{1n}, i'_{2n}, i'_{3n}), (q'_n, \alpha'_n, j'_n)) P'_1 \dots P'_s]$. Then $n = n'$, $s = s'$, and $((i_{1k}, i_{2k}, i_{3k}), (q_k, \alpha_k, j_k)) = ((i'_{1k}, i'_{2k}, i'_{3k}), (q'_k, \alpha'_k, j'_k))$ for each k ($1 \leq k \leq n$), and there exists a permutation $\sigma : \{1, \dots, s\} \rightarrow \{1, \dots, s\}$ such that $P_i \equiv P'_{\sigma(i)}$ for each i ($1 \leq i \leq s$), where $n, s \geq 0$, and $((i_1, i_2, i_3), (q, \alpha, j))$'s and $((i'_1, i'_2, i'_3), (q', \alpha', j'))$'s are pairs (coordinates along the fourth axis, storage state), and further P, P' are EECS's.

Let $Q = Q_1 \dots Q_n$, $Q' = Q'_1 \dots Q'_n$ be any two ECS's. We say that Q and Q' are equivalent if $n = n'$ and there exists a permutation $\sigma : \{1, \dots, n\} \rightarrow \{1, \dots, n\}$ such that $Q_i \equiv Q'_{\sigma(i)}$ for each i ($1 \leq i \leq n$). [As is easily seen from the definition, any two ECS's of x are equivalent for any x in $V(m)$.] For any ECS Q , the length of Q is the number of pairs (coordinates along the fourth axis, storage state) in Q , and is denoted by $|Q|$. For each $m \geq 1$, let $E(m) = \{Q \mid Q \text{ is an ECS of } x \text{ for some } x \text{ in } V(m)\}$. Then, the following two propositions must hold :

[Proposition 1] $|E(m)| = Z(m)^{dZ(m)}$, where $Z(m) = (2m + 2)^3 rL(2m)s^{L(2m)}$, r and s are the numbers of states (of

the finite control) and storage-tape symbols of M , and d is a positive constant.

[Proposition 2] Let x and y be any two different tapes in $V(m)$, and let Q_x and Q_y be any ECS's of x and y , respectively. Then, Q_x and Q_y are not equivalent.

Clearly, $|V(m)| = 2^{8t} (t = m^4)$. Because $L(m) = o(\log m)$, it follows from Proposition 1 that $|V(m)| > |E(m)|$ for large m . For such a large m , there must exist two different tapes $x, y \in V(m)$ such that some ECS of x and some ECS of y are equivalent, which contradicts Proposition 2. This completes the proof. \square

3. Conclusion

In this paper, we presented a technique which we can show that a four-dimensional language is not accepted by any space-bounded alternating Turing machines. It will be interesting to investigate infinite space hierarchy properties of the classes of sets accepted by 4-ATM's with spaces of size smaller than $\log m$.

References

- [1] A.K.Chandra, D.C.kozen, and L.J.Stockmeyer: Alternation, *J.ACM*, Vol. 28, No. 1 pp.114-133 (1981).
- [2] M.Sakamoto, K.Inoue, and I.Takanami: A note on three-dimensional alternating Turing machines with space smaller than $\log m$, *Inform. Sci., ELSEVIER*, Vol. 72, pp. 225-249 (1993).
- [3] H.Yamamoto and S.Noguchi: Time-and-leaf bounded 1-tape alternating Turing machines, *The Trans. of IECE*, J68-D, pp.1719-1726 (1985).

Socialized Multi-Agent System Rendezvous via Networks of Networks

Yunzhong Song

College of Electrical Engineering and Automation, Henan Polytechnic University, 2001 Century Avenue, Jiaozuo 454003, P.R.China

Ziyi Fu

College of Electrical Engineering and Automation, Henan Polytechnic University, 2001 Century Avenue, Jiaozuo 454003, P.R.China

Fuzhong Wang

College of Electrical Engineering and Automation, Henan Polytechnic University, 2001 Century Avenue, Jiaozuo 454003, P.R.China

*E-mail: songhpu@126.com, fzy@hpu.edu.cn, wangfzh@hpu.edu.cn
www.hpu.edu.cn*

Abstract

Networks of networks based rendezvous of leader-follower multi-agent system, where the rendezvous actors including the target object, the leader agents, the informed follower agents and the isolated follower agents, was toughed upon here. To be specific, humanized system inspired strategies were investigated, and results demonstrated that the mixed strategy, could be the most prior policy in balancing of the convergent speed and the utmost task of success of rendezvous.

Keywords: networks of networks, leader-follower multi-agent network, rendezvous problems, the democracy strategy, the autarchy strategy, the mixed strategy

1. Introduction

In recent years, the distributed control of multi-agent network has been paid more attentions from different disciplines. For instance, Ref. 1 analyzed the issue of how the ratio of leaders to followers affects connectivity. Ref. 2 discussed the consensus problems in undirected networks of agents with fixed topology and switching topology. In Ref. 3, the direct control laws were used in

a heterogeneous network. Ref. 4 provided sufficient conditions for rendezvous in first order leader-follower network; Ref. 5 studied the distributed tracking control of the leader-follower directed network with noisy measurement. Ref. 6 investigated the consensus problems in leader-follower network with fixed topology and switching topology.

Although the consensus research of multi-agent networks and leader-follower multi-agent networks provided valuable results, there still have been some

© The 2016 International Conference on Artificial Life and Robotics (ICAROB 2016), Jan. 29-31, Okinawa, Japan

obvious limitations. For instance, the realization mechanism of the swarm has been considered rarely. But in actual society, the swarm members can interact with each other in various styles, for example, the followers may be kept in the group or be left alone according to the different utmost objectives; and as the same way, the leaders may also play with the followers in the unselfish ways or in the selfish ways, that can be boiled down to the costs and the capabilities of the leaders. Lately, the networks of networks, like Ref.7 which paid much more attention to the coupling among the networks, was much more powerful in modeling the real world systems, where interdependence of networks and the effect of this interdependence on the structural and functional behavior of the coupled system were considered into detail. So, it is necessary to be clarified that whether the networks of networks form mechanism can be verified feasible or not in leader-follower multi-agent systems. The already existing results including the different layers built according to the different relationship among agents, for example, one layer can be used to express the relationship from the spatial location of the agents, that is, if they are near each other enough in spatial physical distance, they can have connections with each other; and the another layer can be assigned to express their social relationships, such as friendships, and classmates, that is if they are friends or have been classmates before, they can be categorized into one layer, and the connection strength can be determined with their intimateness. The style we deal with networks of networks here can enrich the results of networks of networks and it can be referred further. In this paper, the three strategies namely the democracy strategy, the autarchy strategy and the mixed strategy would be used in rendezvous problem of leader-follower network. Specific to leader-follower multi-agent network, the democracy strategy means that the motion of agent is affected by the other ones located within the sensing zone of the agent. And the autarchy strategy is such a strategy, in which the motion of leader is not affected by any agents, while follower only gets the influence of the initial nearest leader within its sensing zone. The mixed strategy is composed of the autarchy one and the democracy one. In the mixed strategy, all the leaders and some followers which are affected by leader initially take the autarchy strategy, while the

other followers which are called isolated followers take the democracy strategy.

Here, we must note that in case of brevity and the limited space of the paper, only the democracy strategy is covered.

2. Preliminaries

Consider N agents evolving in R^2 . We use single integrator agents whose motions obey the model:

$$\dot{x}_i^j = u_i^j, i \in N = \{1, \dots, N\}, j \in N = \{1, \dots, M\}, \quad (1)$$

Where the subscript denotes the order number of the agents in the corresponding layer, whereas the superscript denotes the order number of the layer that agents belong to. So, here in (1), N and M denote the biggest order number of intra-layer and inter-layer. And the rest can be done in the same manner. In case of convenience, the node order number and its corresponding expression in networks of networks style is listed in Table 1.

TABLE 1 THE NODE ORDER NUMBER AND ITS CORRESPONDING EXPRESSION IN NETWORKS OF NETWORKS STYLE

Followers				Leaders			Target		
V1	V2	V3	V4	V5	V6	V7	V8	V9	V10
x_1^3	x_2^3	x_3^3	x_4^3	x_1^4	x_5^3	x_1^2	x_2^2	x_3^2	x_1^1

Let $g=\{V, E\}$ describe the group topology, that consists of a set of vertices, $V=\{1, \dots, N\}$, representing the team members, and a set of edges, $E=\{(i, j) \in V \times V \mid i \in N\}$ representing the active inter-agent communication links. If g is an undirected graph, there is a line between node i and j , representing the impact between them is mutual. If g is a directed graph, the line (i, j) is directed, which consists of starting point i and finishing point j , representing node i makes an impact on node j .

According to the different functions of the agents in leader-follower network, the agents can be divided into two categories, i.e. leaders and followers. The leaders were capable of knowing the details of the global task that is to come to a given target, while the followers just need to keep in touch with leaders to reach the target. The agents belong either to the subset of leaders, N_l , or to the subset of followers, N_f , where $N_l \cup N_f = N$, $N_l \cap N_f = \emptyset$ and the number of agents in each set is given by $|N_l|=N_l$ and $|N_f|=N_f$ respectively. Due to

limited sensing capability of the sensors, each agent has a limited sensing zone of radius $\Delta > 0$. At any given time, the set of agents located within the sensing zone of agent $i \in N$ are referred to as the neighbours of agent i ,

	Followers					Leaders				Target
	1	2	3	4	5	6	7	8	9	10
x	27.5	28	28	28	32	17	21.5	22	21	0
y	0	-2	-4	4	-1	-2	-1	.5	1	0

$N_i = \{j \in N: |x_i - x_j| \leq \Delta\}$. Each agent has knowledge of the relative coordinates to its neighbouring agents, but cannot detect or communicate with agents outside its sensing zone. Note that both g and N_i are time-varying. The difference between leaders and followers is that leaders are aware of the location of the target and can control group but the followers cannot.

We start by introducing a notation for the distance between two arbitrary agents i and j . Let

$$\delta_{i,j}^{k,l} = \delta_{j,i}^{l,k} = |x_i^k - x_j^l| = \sqrt{(x_i^k - x_j^l)^T (x_i^k - x_j^l)} \geq 0$$

Since we are considering a physical system we can assume that $x_k(t)$ is a continuous function for any agent $k \in N$. The time derivative $\dot{\delta}_{ij}^k$ is not directly defined when

$$\delta_{i,j}^{k,l} = 0 \text{ so here we shall instead consider the time}$$

derivative of $(\delta_{i,j}^{k,l})^2$

$$\frac{d(\delta_{i,j}^{k,l})^2}{dt} = 2\delta_{i,j}^{k,l} \dot{\delta}_{i,j}^{k,l} = 2(x_i^k - x_j^l)^T (\dot{x}_i^k - \dot{x}_j^l) \quad (2)$$

To describe the relationship between leaders and target, the target attraction function is defined as

$$F(x_j^l, d) = \begin{cases} f(\delta_j^l) \frac{d - x_j^l}{\delta_j^l}, & \delta_j^l > 0 \\ 0, & \delta_j^l = 0. \end{cases} \quad (3)$$

where d is the location of the target and define $\delta_j^l = |x_j^l - d|$ representing the agent x_j^l 's distance to the target. At any given position $x_j^l \neq d$, the direction of $F(x_j^l, d)$ is towards the target and the magnitude is decided by the continuous scalar function $f(\delta_j^l) \geq 0$.

In the following analysis, the leader-follower multi-agent network that consists of four leaders and five followers is illustrated. The agents are tagged with numbers, starting at 1 at first, followed with 2, 3 and the

other numbers, where agents from 1 to 5 belong to follower agents, whereas 6 to 9 belong to leader agents and node 10 is the target. Without loss of generality, we assume that the target is the origin of coordinates and $f(\delta_j) = \beta \delta_j$, $\beta = 0.5$. The initial configuration of each agent can be seen in Tab. 2.

TABLE 2 INITIAL VALUES OF THE SIMULATION WORK

3. Results and Analysis

In the democracy strategy, the motion of agent is affected by the other ones located within the sensing zone of the agent. If agent i has an impact on j , agent i is also affected by j . In other words, interactions among each agent are undirected. The topology of group is thus described by undirected graph $g1 = \{V1, E1\}$.

The dynamics for an arbitrary follower agent $i \in N_f$ are

$$\dot{x}_i^j = -\sum_{k \in N_i^j} (x_i^j - x_k^l) = -N_i^j x_i^j + \sum_{k \in N_i^j} x_k^l \quad (4)$$

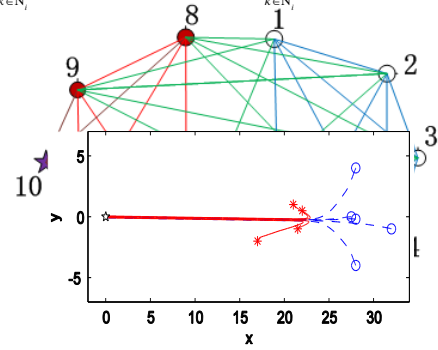


Fig. 1, simulation results in the democracy strategy.

(a) Topological structure (b) Position rendezvous

Where x_i^j denotes the i^{th} agent is in the j^{th} layer, and x_k^l denotes the k^{th} neighbor of x_i^j , which is in the l^{th} layer of the networks. We can conclude that the motions of followers are decided by their neighbours. Considering the situation of two dimensions, the dynamics can be looked as the resultant vectors of themselves and their neighbors, where the directions of all the agents are the same corresponding to the resultant vectors, and the speeds of the swarm motion members can also be decided by the norm of the resultant vectors. For an arbitrary leader agent $j \in N_l$, the dynamics are described by

$$\dot{x}_j^l = -N_j^l x_j^l + \sum_{k \in N_j^l} x_k^m + F(x_j^l, d) \quad (5)$$

and x_j^l and x_k^m can be defined accordingly. By contrast, the dynamics for leaders are the same as the followers in some way, except for the impact from the target, which is the leaders' feature. The simulation results in the democracy strategy can be seen in Fig.1. In the process of simulation, the distances between the agents from the leader group and the follower group and the target agent are used to measure the rendezvous time indirectly, where all the distances are turned into be zero is regarded as the network rendezvous. It is not difficult to recognize that during the democracy strategy, the information flow among the different layers is fully utilized, and the enjoyment of the overall information via the shared cooperation realized win-win policy of the agents. That kinds of profit can only be available depend on the interdependency among the networks of networks. In order to elucidate the democracy in the ways of networks of networks further, the paradigm for democracy of networks of networks is illustrated as Figure 2.

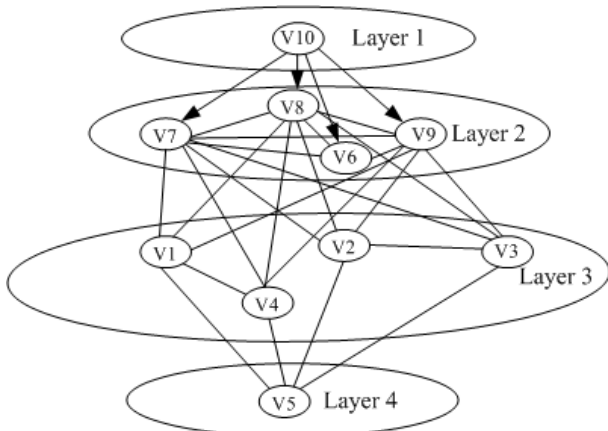


Fig. 2, the paradigm for democracy of networks of networks

4. Conclusion

In this paper, according to the paradigm of networks of networks we turned the leader-follower agent systems into four different layers, and each of these layers can be equivalent to one sub-network, the

connections among them can be viewed as the interdependency of the networks of networks, and we have examined and discussed the convergent characteristics of the democracy strategy. The simulation of leader-follower multi-agent network which consisted of four leaders and five followers demonstrated the potential usage of our suggested scheme.

Acknowledgements

This work is partially supported by NSFC Grant (61340041 and 61374079) and the Project-sponsored by SRF for ROCS, SEM to Yunzhong Song.

References

1. A. Ji, Rahmani, M. Mesbahi, et al., Controllability of multi-agent systems from a graph-theoretic perspective, *SIAM Journal on Control and Optimization*, **48**(1) (2009) 162-186.
2. R. Olfati-Saber, R. M. Murray, Consensus problems in networks of agents with switching topology and time-delays, *IEEE Transactions on Automatic Control*, **49**(9) (2004) 1520-1533.
3. M. Zavlanos, G. Pappas, Distributed connectivity control of mobile networks, *IEEE Transaction on Robotics*, **24**(6) (2008) 1416-1428.
4. T. Gustavi, D. V. Dimarogonas, M. Egerstedt, et al., Sufficient conditions for connectivity maintenance and rendezvous in leader-follower networks, *Automatica*, **46**(1) (2010) 133-139.
5. J. Hu, G. Feng, Distributed tracking control of leader-follower multi-agent systems under noisy measurement, *Automatica*, **46**(8) (2010) 1382-1387.
6. W. Ni, D. Cheng, Leader-following consensus of multi-agent systems under fixed and switching topologies, *Systems & Control Letters*, **59**(3-4) (2010) 209-217.
7. R. Lu, W. Yu, J. Lü and A. Xue, Synchronization on complex networks of networks, *IEEE Transactions on Neural Networks and Learning Systems*, **25**(11) (2014) 2110-2118.

Global sensor selection for maneuvering target tracking in clutter

Wenling Li

*The Seventh Research Division, Beihang University
37 Xueyuan Road, Haidian District, Beijing, 100191, China*

Yingmin Jia

*The Seventh Research Division, Beihang University
37 Xueyuan Road, Haidian District, Beijing, 100191, China
E-mail: lwlmath@buaa.edu.cn, ymjia@buaa.edu.cn*

Abstract

This paper studies the problem of sensor selection for maneuvering target tracking in the cluttered environment. By modeling the target dynamics as jump Markov linear systems, a decentralized tracking algorithm is developed by applying the extended Kalman filter and the probabilistic data association technique. A cost function that minimizes the expected filtered mean square position error is utilized and a sensor selection scheme is proposed. A numerical example is provided to illustrate the effectiveness of the proposed approach.

Keywords: Sensor selection, Jump Markov system, Extended Kalman filter, Maneuvering target tracking, Clutter

1. Introduction

Sensor or node selection *has* been found a wide range of applications in diverse civilian and military areas such as sensor placement for structures,¹ chemical plant control² and wireless networks.^{3,4} In recent years the problem of sensor selection for target tracking has been investigated. As pointed out in Ref. 5, the main idea beyond sensor selection is to optimize a cost function that represents the localization accuracy constrained by the number of active sensors. A cost function that minimizes the geometrical dilution of precision (GDOP) is used to derive the sensor selection scheme where the best three sensors are selected. Based on the GDOP measure, an adaptive sensor selection strategy has been proposed in which the signal power measurements are used. By combining with the prior information, which is not accounted for the GDOP measure, global sensor

selection method that minimizes the expected filtered mean square position error have been studied for bearing-only tracking. Especially, two strategies including the 'add one sensor node at a time' and the 'simplex' have been developed for selecting the best subset of active sensors.⁶ These results are extended to propose local sensor selection schemes which do not require the knowledge of all the sensors locations in the networks.

In the target tracking community, the single model approach is used mainly for targets with fixed kinematic behaviors while for targets with multiple kinematics behaviors (i.e., maneuvering targets), the multiple model tracking algorithm is preferred.⁷ The problem of sensor selection for maneuvering target tracking has been investigated in Ref. 8 and 9. To our knowledge, little research has been done to deal with the problem of

sensor selection for target tracking in the cluttered environment.

In this paper, we consider the problem of sensor selection for maneuvering target tracking in the cluttered environment. By using the global knowledge of all sensors locations, a cost function that minimizes the expected filtered mean square localization error is developed to select a given number of active sensors. As the cost function is derived based on the decentralized structure, we investigate how to derive the decentralized fusion formula by applying the basic extended Kalman filter (EKF) and the PDA technique so that the clutter information can be combined into the cost function. Meanwhile, we have to circumvent the difficulty encountered in multiple model decentralized fusion.¹⁰ By minimizing the cost function, a sensor selection scheme is proposed based on the 'add one sensor node at a time' strategy. Simulations are provided to illustrate the effectiveness of the proposed algorithm.

2. Problem formulation

In this paper, we consider a two-dimensional (2-D) target-observer scenario. The target dynamics is modeled as the following coordinated turn model

$$x_{k+1} = \begin{bmatrix} 1 & 0 & \frac{\sin(\omega T)}{\omega} & -\frac{1-\cos(\omega T)}{\omega} \\ 0 & 1 & \frac{1-\cos(\omega T)}{\omega} & \frac{\sin(\omega T)}{\omega} \\ 0 & 0 & \cos(\omega T) & \sin(\omega T) \\ 0 & 0 & \sin(\omega T) & \cos(\omega T) \end{bmatrix} x_k + w_k$$

where $x_k = (x_k, y_k, \dot{x}_k, \dot{y}_k)^T$ denotes the target state. (x_k, y_k) and (\dot{x}_k, \dot{y}_k) represent the target position and velocity components, respectively. ω denotes the turn rate and T is the sampling time period. w_k is zero-mean white Gaussian noise with covariance Q_k .

To formulate the target dynamics into the framework of jump Markov systems, we assume that at any time the target motion obeys one of M dynamic behavior models, which can be described by the above coordinated turn model with different turn rate. The switching between models is governed by a time-homogeneous first-order Markov chain r_k with known transition probability $\pi_{ij} = P\{r_k = j | r_{k-1} = i\}$.

A radio receiver that provides the signal power measurement is used throughout this paper. The target-

originated power measurement from sensor s can be modeled in a logarithmic form

$$z_{k,s} = K - 10\eta \log_{10}(r_{k,s}) + v_{k,s}$$

$$r_{k,s} = \sqrt{(x_k - x_s)^2 + (y_k - y_s)^2}, \quad s = 1, 2, \dots, N$$

where K and $\eta \in [2, 5]$ denote the transmission power and the path loss exponent, respectively. They are dependent on the radio environment, the antenna characteristics and so on. (x_s, y_s) represents the position of sensor s and $r_{k,s}$ is the relative distance between sensor s and the target. N is the number of sensors. $v_{k,s}$ is zero-mean white Gaussian with variance $R_{k,s}$.

Our aim is to find the set of active sensors that optimizes the cost function. As the clutter is considered, we should investigate how to combine the clutter information into the cost function.

3. SENSOR SELECTION FOR MANEUVERING TARGET TRACKING IN CLUTTER

Decentralized fusion of EKF-PDA

Assume that the target dynamics and the measurement model can be represented by

$$\begin{aligned} x_{k+1} &= \Phi_k x_k + w_k \\ z_{k,s} &= h_s(x_k) + v_{k,s}, \quad s = 1, 2, \dots, N \end{aligned}$$

where Φ_k and the covariance Σ_k of w_k are derived by the best-fitting Gaussian approximation. h_s is the nonlinear measurement function of sensor s . By combining the EKF and the PDA technique, a single forward run of the tracking algorithm proceeds as follows for each sensor s .

First of all, the predicted mean and covariance are obtained by using a standard Kalman filter

$$\begin{aligned} \hat{x}_{k|k-1}^s &= \Phi_{k-1} \hat{x}_{k-1|k-1}^s \\ P_{k|k-1}^s &= \Phi_{k-1} P_{k-1|k-1}^s \Phi_{k-1}^T + \Sigma_{k-1} \end{aligned}$$

Then, the predicted measurement and the innovation covariance can be derived as

$$\begin{aligned} \hat{z}_{k|k-1}^s &= h_s(\hat{x}_{k|k-1}^s) \\ v_{k,s}^i &= z_{k,s}^i - \hat{z}_{k|k-1}^i \\ S_{k,s} &= H_{k,s} P_{k|k-1}^s H_{k,s}^T + R_{k,s} \end{aligned}$$

where $H_{k,s}$ is the Jacobian matrix of the nonlinear function h_s evaluated at $\hat{x}_{k-1|k-1}^s$.

After receiving the measurements $Z_{k,s}$ by sensor s , $z_{k,s}^i$ is validated if

$$[z_{k,s}^i - \hat{z}_{k|k-1}^s]^T S_{k,s}^{-1} [z_{k,s}^i - \hat{z}_{k|k-1}^s] < \gamma$$

where γ is the gate threshold.

By assuming that the number of clutter in the validated region is assumed to be Poisson distributed, a parametric PDA technique is used to generate the association event probability

$$\beta_{k,s}^0 = \frac{b_{k,s}}{b_{k,s} + \sum_{j=1}^{m_{k,2}} d_{k,s}^j}$$

$$\beta_{k,s}^i = \frac{b_{k,s}}{b_{k,s} + \sum_{j=1}^{m_{k,2}} d_{k,s}^j}, i=1, \dots, m_{k,s}$$

Where

$$d_{k,s}^i = \exp(-0.5[v_{k,s}^i]^T S_{k,s}^{-1} v_{k,s}^i)$$

$$b_{k,s} = \lambda |2\pi S_{k,s}|^{1/2} \frac{1-P_D P_G}{P_D}$$

p_D is the detection probability, p_G is the probability that the measurement originated from the target falls into the validated region, and λ is the spatial density of clutter. Finally, the updated estimates can be computed by

$$\hat{x}_{k|k}^s = \hat{x}_{k|k-1}^s + K_{k,s} v_{k,s}$$

$$\hat{P}_{k|k}^s = \hat{P}_{k|k-1}^s - K_{k,s} (S_{k,s} - B_{k,s}) K_{k,s}^T$$

where

$$v_{k,s} = \sum_{i=1}^{m_{k,2}} \beta_{k,s}^i v_{k,s}^i$$

$$K_{k,s} = P_{k|k-1}^s H_{k,s}^T S_{k,s}^{-1}$$

$$B_{k,s} = \beta_{k,s}^0 S_{k,s} + \sum_{i=1}^{m_{k,2}} \beta_{k,s}^i v_{k,s}^i [v_{k,s}^i]^T - v_{k,s} v_{k,s}^T$$

In order to develop the decentralized fusion formula, we would like to rewrite the updated mean and covariance as the same form of the usual Kalman filter, i.e.,

$$\hat{x}_{k|k}^s = \hat{x}_{k|k-1}^s + \tilde{K}_{k,s} (\tilde{z}_{k,s} - \hat{z}_{k|k-1}^s)$$

$$P_{k|k}^s = P_{k|k-1}^s - \tilde{K}_{k,s} \tilde{S}_{k,s} \tilde{K}_{k,s}^T$$

$$\tilde{K}_{k,s} = P_{k|k-1}^s H_{k,s}^T \tilde{S}_{k,s}^{-1}$$

$$\tilde{S}_{k,s} = H_{k,s} P_{k|k-1}^s H_{k,s}^T - \tilde{R}_{k,s}$$

It can be observed that our aim is to define $\tilde{z}_{k,s}$ and

$\tilde{R}_{k,s}$. To this end, we have

$$\tilde{K}_{k,s} \tilde{S}_{k,s} \tilde{K}_{k,s}^T = P_{k|k-1}^s H_{k,s}^T \tilde{S}_{k,s}^{-1} H_{k,s} P_{k|k-1}^s$$

$$= K_{k,s} S_{k,s} \tilde{S}_{k,s}^{-1} S_{k,s} K_{k,s}^T$$

$$\tilde{S}_{k,s} = (S_{k,s}^{-1} - S_{k,s}^{-1} B_{k,s} S_{k,s}^{-1})^{-1}$$

$$= S_{k,s} - S_{k,s} S_{k,s}^{-1} (S_{k,s}^{-1} S_{k,s} S_{k,s}^{-1} - B_{k,s}^{-1})^{-1} S_{k,s} S_{k,s}^{-1}$$

$$= S_{k,s} + (B_{k,s}^{-1} - S_{k,s}^{-1})^{-1}$$

Therefore,

$$\tilde{R}_{k,s} = R_{k,s} + (B_{k,s}^{-1} - S_{k,s}^{-1})^{-1}$$

On the other hand, we have

$$K_{k,s} v_{k,s} - \tilde{K}_{k,s} (\tilde{z}_{k,s} - \hat{z}_{k|k-1}^s) = 0$$

which leads to

$$\tilde{z}_{k,s} = [I + (B_{k,s}^{-1} - S_{k,s}^{-1})^{-1} S_{k,s}^{-1}] v_{k,s} + \hat{z}_{k|k-1}^s$$

Based on the above EKF-PDA tracking algorithm, we can obtain the decentralized fusion formula. We assume that each sensor knows its position and they share the common prior information. Suppose each active sensor have obtained estimates $\hat{x}_{k-1|k-1}$ and $P_{k-1|k-1}$ at time step $k-1$, the filtered estimates can be derived by each sensor via communicating with other active sensors

$$\hat{x}_{k|k-1} = \Phi_{k-1} \hat{x}_{k-1|k-1}$$

$$P_{k|k-1} = \Phi_{k-1} P_{k-1|k-1} \Phi_{k-1}^T + \Sigma_{k-1}$$

$$\hat{x}_{k|k} = P_{k|k} [P_{k|k-1}^{-1} \hat{x}_{k|k-1} + \sum_{s \in N_a} H_{k,s}^T \tilde{R}_{k,s}^{-1} [\tilde{z}_{k,s} - h_s(\hat{x}_{k|k-1})] + H_{k,s} \hat{x}_{k|k-1}]$$

$$P_{k|k}^{-1} = P_{k|k-1}^{-1} + \sum_{s \in N_a} H_{k,s}^{-1} \tilde{R}_{k,s}^{-1} H_{k,s}$$

Sensor selection

When the signal power measurement is applied, the updated covariance for the decentralized fusion of EKF-PDA can be rewritten as

$$J_f = J_p + \begin{bmatrix} J, 0 \\ 0, 0 \end{bmatrix}$$

Where $J_f = P_{k|k}^{-1}$, $J_p = P_{k|k-1}^{-1}$ and

$$J = (10\eta \log_{10} e)^2 \sum_{s \in N_a} \tilde{R}_{k,s}^{-1} r_{k,s}^{-2} \begin{bmatrix} \cos^2 \phi_{k,s}, \sin \phi_{k,s} \cos \phi_{k,s} \\ \sin \phi_{k,s} \cos \phi_{k,s}, \sin^2 \phi_{k,s} \end{bmatrix}$$

Note that

$$H_{k,s} = -10\eta \log_{10} e [r_{k,s}^{-1} \cos \phi_{k,s}, r_{k,s}^{-1} \sin \phi_{k,s}, 0, 0]$$

where $(r_{k,s}, \phi_{k,s})$ is the position of sensor s relative to the predicted target position in polar coordinates.

The aim of sensor selection is to search for the minimum expected mean square posterior error which can be expressed in terms of the posterior Fisher information matrix. Specifically, the cost function to be minimized for sensor selection is

$$\rho(N_a) = [J_f^{-1}]_{1,1} + [J_f^{-1}]_{2,2}$$

Where $[A]_{i,j}$ denotes the (i,j) th element of the matrix A

$$\rho(N_a) = \frac{\text{tr}\{\tilde{J}_p\} + \text{tr}\{J\}}{|\tilde{J}_p + J|} = \frac{\text{tr}\{\tilde{J}_p\} + \text{tr}\{J\}}{|\tilde{J}_p| + |J| + J_k^d}$$

where ‘tr’ represents the trace of the matrix, and

$$\begin{aligned} \tilde{J}_p &= [J_p]_{1:2,1:2} - [J_p]_{1:2,3:4} ([J_p]_{3:4,3:4})^{-1} [J_p]_{3:4,1:2} \\ J_k^d &= (10\eta \log_{10} e)^2 \sum_{s \in N_a} [\tilde{J}_p]_{1,1} \tilde{R}_{k,s}^{-1} r_{k,s}^{-2} \sin^2 \phi_{k,s} \\ &\quad + [\tilde{J}_p]_{2,2} \tilde{R}_{k,s}^{-1} r_{k,s}^{-2} \cos^2 \phi_{k,s} - 2[\tilde{J}_p]_{1,2} \tilde{R}_{k,s}^{-1} r_{k,s}^{-2} \sin \phi_{k,s} \cos \phi_{k,s} \end{aligned}$$

A practical strategy called as ‘add one sensor node at a time’. For this strategy, an initial active set is established by using the exhaustive search, which includes two active sensor nodes and requires evaluating $\rho(N_a)$ over $N(N-1)/2$ configurations. Then the rest of sensor nodes are added to the initial active set one at a time by minimizing $\rho(N_a)$.

4.SIMULATIONS

Three models corresponding to different turn rates are used. The sampling period is taken to be 1 s for target motion model. The network consists of 30 sensors randomly scattered over a field. The sensing range for each sensor is 25 m. For the signal power measurements, the transmission power is taken to be 9 dBm and the path loss exponent is 3. The variance of the measurement noise is 0.2 for all sensors. The detection probability and the gate probability are set to 0.997 and 0.999, respectively. The gate threshold is 16 and the spatial density of clutter is 0.1.

In the simulations, the root mean square error (RMSE) in position is used for performance comparison. The RMSE in position of the proposed algorithm with different numbers of active sensors is shown in Fig.1. It can be observed that the tracking performance is improved as the number of active sensors is used and the best performance is achieved when all the active sensors in the sensing range are utilized.

5.CONCLUSION

In this paper, we propose a global sensor selection scheme for tracking maneuvering target in the cluttered environment. A formulation of PDA for decentralized fusion is derived which helps the definition of the cost function for sensor selection. This is implemented by developing novel measurement vector and noise covariance matrix combining the clutter information. Simulation results are provided to verify that the proposed algorithm.

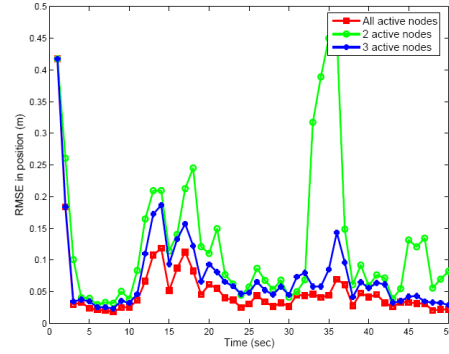


Fig.1 RMSE in position of the proposed filter.

REFERENCES

1. D. Kammer, Sensor placement for on-orbit modal identification and correlation of large space structures, *Journal of Guidance, Control, and Dynamics*, **14**(2) (1991) 251-259.
2. K. Kookos and J. Perkins, A systematic method for optimum sensor selection in inferential control systems, *Industrial Engineering Chemistry Research*, **38**(11) (1999) 4299-4308.
3. F. Zhao and L. Guibas, *Wireless Sensor Networks: An Information Processing Approach*. (Morgan Kaufmann, San Mateo, 2004).
4. H. Rowaihy, et al., A survey of sensor selection schemes in wireless sensor networks, *Proceedings of the SPIE*, (2007), 6562-65621.
5. L. M. Kaplan, Global node selection for localization in a distributed sensor network, *IEEE Transactions on Aerospace and Electronic Systems*, **42**(1) (2006) 113-135.
6. L. M. Kaplan, Local node selection for localization in a distributed sensor network, *IEEE Transactions on Aerospace and Electronic Systems*, **42**(1) (2006) 136-146.
7. X. R. Li and V. P. Jilkov, Survey of maneuvering target tracking. Part V: multiple-model methods, *IEEE Transactions on Aerospace and Electronic Systems*, **41**(4) (2005) 1255-1321.
8. Q. Le, et al., Multiple-mode Kalman filtering with node selection using bearings-only measurements, *Proceedings of the 36th IEEE Southeastern Symposium on System Theory*, (USA, Atlanta, 2004), pp.185-189.
9. S. Zhang et al., IMM filter based sensor scheduling for maneuvering target tracking in wireless sensor networks, *Proceedings of the 3rd International Conference on Intelligent Sensors, Sensor Networks and Information*, (Melbourne, Qld, 2007), pp. 287-292.
10. W. L. Li and Y. M. Jia, Distributed interacting multiple model H^∞ filtering fusion for multiplatform maneuvering target tracking in clutter, *Signal Processing*, **90**(5) (2010) 1655-1668.

Attitude/Position Estimation of Rigid-Body using Inertial and Vision Sensors

Shihao Sun

*The Seventh Research Division, Beihang University (BUAA),
37 XueYuan Road, Beijing, 100191, P.R. China*

Yingmin Jia

*The Seventh Research Division, Beihang University (BUAA),
37 XueYuan Road, Beijing, 100191, P.R. China
E-mail: jxcrssh@126.com, ymjia@buaa.edu.cn
www.buaa.edu.cn*

Abstract

This paper is concerned with the attitude/position estimation of a rigid-body using inertial and vision sensors. By employing the Newton-Euler method, a kinematic model is developed for the rigid-body by treating the inertial measurements as inputs. Based on the coordinate transformation, a nonlinear visual observation model is proposed by using the image coordinates of feature points as observations. Then the Extended Kalman filter (EKF) is utilized to estimate the attitude/position recursively. The effectiveness of the proposed algorithm is evaluated by simulation.

Keywords: attitude and position estimation, EKF, inertial sensor, vision sensor.

1. Introduction

Accurate attitude/position estimation of rigid-body has received considerable attention in the past decades. This is partly due to the fact that it is generally required in many typical applications such as estimating the motion of a robot end-effector¹, navigation for small unmanned aerial vehicle², spacecraft relative navigation in rendezvous³ etc. The widely used way of obtaining position and orientation is using an inertial measurement unit (IMU) as the navigation sensor, which consists of a tri-axis gyroscope and a tri-axis accelerometer. However, integration over a long time period may lead to unbounded estimation errors if noises, offsets, scale errors and uncertainty in navigation model are present. Using vision as a standalone sensor for attitude/position estimation is also quite a standard way⁴, because of the ability to sense the actual attitude/position without accumulative errors. However, vision sensors can only sense the actual position but not the velocity and

accelerate. Therefore, an underlying dynamic model for the motion of rigid-body is needed for accurate estimation when we use vision sensor alone.

Motivated by the discussions above, the combination of the vision and inertial sensors has been recognized as a promising choice for accurate attitude and position estimation. For example, rigid body pose estimation using inertial sensors and a monocular camera is considered in Ref. 5, and it is shown how rotation estimation can be decoupled from position estimation. In Ref. 6, Chen studied the problem of the pose estimation of robotic end-effector with inertial and $SE(3)$ measurements. Among these literature, the measurements of vision sensor are the actual attitude and position that can be obtained by using machine vision algorithms like PNP, stereo-vision. Although the observation model is linear in such way, the expression of observation noises is complicated according to the complicated machine vision algorithms and costs huge computations. An alternative

way is applying the image coordinates of feature points as observations directly.

In this paper, we attempt to estimate the orientation of a rigid-body using inertial and vision sensors. The inertial measurements are treated as inputs for developing the kinematic model, and a novel non-linear observation model is proposed by using the image coordinates of feature points. The EKF is utilized to address the nonlinear filtering problem. Simulation results are provided to evaluate the performance of the proposed algorithm.

2. Problem Statement

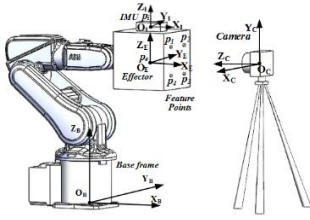


Fig. 1. System configuration and coordinate frames

In this paper, we consider the case in which the motion of a rigid-body (noted as effector) is controlled by the ABB-120 robot as shown in Fig.1. The effector is equipped with a strap-down IMU and four infrared LED feature points. The vision sensor is a camera equipped with an infrared filter, which is fixed at a certain location in the base frame.

2.1. Effector Kinematics

As shown in Fig. 1. Denote ${}^B p_e \in R^3$ as the effector position in the base frame, evolving as:

$${}^B \dot{p}_e = {}^B v_e \quad {}^B \ddot{p}_e = {}^B a_e \quad (1)$$

where ${}^B v_e \in R^3$ and ${}^B a_e \in R^3$ are referred as the translational velocity and acceleration of SCP in the base frame, respectively.

Denote Euler (3-2-1) rotation angles $\Phi = [\alpha \ \beta \ \gamma]^T$ as the effector attitude observed in the base frame, according to attitude kinematics:

$$\dot{\Phi} = T(\Phi) {}^E \omega_e \quad (2)$$

where ${}^E \omega_e \in R^3$ is the angular velocity of the effector as viewed in the effector frame and

$$T(\Phi) = \begin{bmatrix} 0 & \sin \gamma / \cos \beta & \cos \gamma / \cos \beta \\ 0 & \cos \gamma & -\sin \gamma \\ 1 & \sin \gamma \tan \beta & \cos \gamma \tan \beta \end{bmatrix} \quad (3)$$

Discretization of equations (1) and (2) is needed to design a Kalman Filter. Assume that ${}^B a_e$ and ${}^E \omega_e$ are

constants in each sampling interval $[kT_s, (k+1)T_s]$ with sampling period T_s .

The state transition can be approximated by:

$$\begin{aligned} {}^B p_e(k+1) &= {}^B p_e(k) + T_s {}^B v_e(k) + \frac{T_s^2}{2} {}^B a_e(k) \\ {}^B v_e(k+1) &= {}^B v_e(k) + T_s {}^B a_e(k) \\ \Phi(k+1) &= \Phi(k) + T_s T(\Phi(k)) {}^E \omega_e(k) \end{aligned} \quad (4)$$

2.2. Transition models using IMU measurements

The IMU in Fig. 1 consists of a tri-axis gyroscope and a tri-axis accelerometer that output:

$$\begin{aligned} \bar{\omega}_{imu} &= {}^I \omega_i + {}^I m_{\omega} \\ \bar{a}_{imu} &= {}^I a_i + {}^I g + {}^I m_a \end{aligned} \quad (5)$$

where $\bar{\omega}_{imu}$ and \bar{a}_{imu} are IMU measurements, m_{ω} and m_a are measurement noises, and g is the gravity vector.

According to the rigid kinematic theorem, the angular velocity and acceleration relations between point p_i and p_e are as follows:

$$\begin{aligned} {}^E \omega_e &= {}^E R_i {}^I \omega_i \\ {}^B a_e &= {}^B R_E {}^E R_i ({}^I a_i + S({}^I a_i) {}^I r_{ei} + S({}^I \omega_i) S({}^I \omega_i) {}^I r_{ei}) \end{aligned} \quad (6)$$

where ${}^E R_i$ is a constant orientation matrix referred as the IMU frame attitude observed in the effector frame; ${}^I r_{ei}$ is the position vector of p_e relative to p_i in IMU frame; ${}^I a_i$ is the angular acceleration of the IMU, according to the assumption that ${}^E \omega_e$ is constant in each sampling interval, then ${}^I a_i(k) = 0$; ${}^B R_E$ is the orientation matrix referred as the end-effector attitude observed in the base frame, which is given by

$${}^B R_E = \begin{bmatrix} \cos \alpha \cos \beta & -\sin \alpha \cos \beta & \cos \alpha \sin \beta \sin \gamma & \sin \alpha \sin \beta \sin \gamma \\ \sin \alpha \cos \beta & \cos \alpha \cos \beta & \sin \alpha \sin \beta \sin \gamma & -\cos \alpha \sin \beta \sin \gamma \\ -\sin \beta & \cos \beta \sin \gamma & \cos \beta \cos \gamma & \end{bmatrix};$$

and $S(\bullet)$ is the cross product operator transforms a vector $c = [c_1 \ c_2 \ c_3]^T$ to a skew-symmetric matrix

$$S(c) = \begin{bmatrix} 0 & -c_3 & c_2 \\ c_3 & 0 & -c_1 \\ -c_2 & c_1 & 0 \end{bmatrix}.$$

Given (5) and (6) at the sampling interval, we have

$$\begin{aligned} {}^E \omega_e(k) &= {}^E R_i \bar{\omega}_{imu}(k) - {}^E R_i {}^I m_{\omega}(k) \\ {}^B a_e(k) &= {}^B R_E ({}^E R_i ({}^I \bar{a}_{imu}(k) + {}^I m_a(k)) + S({}^I \bar{\omega}_{imu}(k)) S({}^I \bar{\omega}_{imu}(k)) {}^I r_{ei} - {}^B g \\ &\quad - {}^B R_E ({}^E R_i (S({}^I \bar{\omega}_{imu}(k)) {}^I r_{ei} + S({}^I \bar{\omega}_{imu}(k)) S({}^I r_{ei})) {}^I m_{\omega}(k) \\ &\quad + {}^B R_E ({}^E R_i S({}^I m_a(k)) S({}^I m_a(k)) {}^I r_{ei} - {}^B m_a) \end{aligned} \quad (7)$$

Then the state transition equation (4) can be rewritten as

$$X(k+1) = \Phi[X(k), U(k)] + \Gamma[X(k), U(k)]W(k) \quad (8)$$

where $X(k) = \begin{bmatrix} {}^a p_e(k) & {}^a v_e(k) & \Phi(k) \end{bmatrix}^T$, $U(k) = \begin{bmatrix} \bar{\omega}_{imu}(k) & \bar{a}_{imu}(k) \end{bmatrix}^T$

$$W(k) = \begin{bmatrix} {}^i m_w(k) & {}^i m_a(k) & S({}^i m_w(k))S({}^i m_a(k))'r_a \end{bmatrix}^T, Cov\{W(k), W(j)\} = Q_k \delta_{kj}$$

$$\varphi[X(k)] = \begin{bmatrix} {}^a p_e(k) + T_s {}^a v_e(k) + \frac{T_s^2}{2} ({}^a \hat{R}_e(k) {}^a R_i(\bar{a}_{imu}(k) + S(\bar{\omega}_{imu}(k))S(\bar{\omega}_{imu}(k))'r_a) - {}^a g) \\ {}^a v_e(k) + T_s ({}^a \hat{R}_e(k) {}^a R_i(\bar{a}_{imu}(k) + S(\bar{\omega}_{imu}(k))S(\bar{\omega}_{imu}(k))'r_a) - {}^a g) \\ \Phi(k) + TT(\Phi(k)) {}^e R_{imu}(k) \end{bmatrix}$$

$$r[X(k)] = \begin{bmatrix} -\frac{T_s^2}{2} T_s {}^a R_i(k) {}^e R_i(S({}^i m_w(k))'r_a) + S(\bar{\omega}_{imu}(k))S({}^i r_a) & -\frac{T_s^2}{2} & \frac{T_s^2}{2} {}^e R_i(k) {}^e R_i \\ -T_s {}^a R_i(k) {}^e R_i(S({}^i m_w(k))'r_a) + S(\bar{\omega}_{imu}(k))S({}^i r_a) & -T_s & T_s {}^e R_i(k) {}^e R_i \\ TT(\Phi(k)) {}^e R_i & 0 & 0 \end{bmatrix}$$

2.3. Observation models of Camera

The rigid body in Fig. 1 contains four feature points noted as ${}^E p_i = \begin{bmatrix} {}^E p_{ix} & {}^E p_{iy} & {}^E p_{iz} \end{bmatrix}^T$, $i=1 \dots 4$, and the relation between the fixed camera and the base frame are noted as the orientation matrix ${}^C R_B$ and the translation vector ${}^C r_{bc}$. By using the homogeneous transform matrices between the frames of Base, Effector and Camera, we obtain

$$\begin{bmatrix} {}^C p_i \\ 1 \end{bmatrix} = \begin{bmatrix} {}^C R_B & {}^C r_{bc} \\ 0 & 1 \end{bmatrix} \begin{bmatrix} {}^B R_E & {}^B p_e \\ 0 & 1 \end{bmatrix} \begin{bmatrix} {}^E p_i \\ 1 \end{bmatrix} \quad i=1 \dots 4 \quad (9)$$

According to the camera pinhole model with the projective geometry, we obtain

$$u_i = f_x \frac{{}^c p_{ix}}{{}^c p_{iz}} + u_0$$

$$v_i = f_y \frac{{}^c p_{iy}}{{}^c p_{iz}} + v_0 \quad i=1 \dots 4 \quad (10)$$

where f_x and f_y are pixel magnification factors, (u_0, v_0) denotes the image coordinate of the camera's principal point, and (u_i, v_i) is the coordinate of the feature point p_i in the image plane. In view of (9) and (10), denote $Z_i(k)$ as the image coordinate $(u_i(k), v_i(k))$ at time k , then the observation model of camera can be written as

$$Z_i(k) = h_i[X(k), {}^E p_i] + V_i(k) \quad i=1 \dots 4 \quad (11)$$

where h_i is a 2-dim function derived by replacing ${}^c p_i$ in equation (10) using equation (9), $V(k)$ is the measurement noise and its covariance is $Cov\{V_i(k), V_j(j)\} = R_{ij} \delta_{ij}$.

3. Estimation based on EKF

Since the state transition model (8) and the observation model (11) are both nonlinear, the EKF is used to update the effector motion state estimate $\hat{X}(k|k)$ and its estimation error covariance matrix $P(k|k)$.

The EKF is implemented as follows:

1) *Prediction*. Denote $\hat{X}(k+1|k)$, $P(k+1|k)$, $\hat{Z}_i(k+1|k)$ as the one step predictions of estimation, covariance matrix and observation at the time $k+1$.

Then as to (8), they can be obtained

$$\hat{X}(k+1|k) = \varphi[\hat{X}(k|k), U(k)] \quad (12)$$

$$P(k+1|k) = \Psi[k+1|k]P(k|k)\Psi^T[k+1|k] + \Gamma[\hat{X}(k|k), U(k)]Q_k\Gamma^T[\hat{X}(k|k), U(k)] \quad (13)$$

where $\Psi[k+1|k] = \frac{\partial \varphi[X(k), U(k)]}{\partial X(k)} \Big|_{X(k) = \hat{X}(k|k)}$

$$\hat{Z}(k+1|k) = h[\hat{X}(k+1|k), {}^E p_i] \quad (14)$$

where $\hat{Z} = [\hat{Z}_1, \hat{Z}_2, \hat{Z}_3, \hat{Z}_4]^T$ and $h = [h_1, h_2, h_3, h_4]^T$ represent four feature points.

2) *Observation*. As the feature points are infrared LED and the camera is equipped with an infrared filter, we can easy obtain the coordinates $Z_i(k+1)$ of the feature point p_i in the image plane at the time $k+1$.

3) *Update*. When the new image is obtained at time $k+1$, the filter can be computed as

$$K(k+1) = P(k+1|k)H^T(k+1)O(k+1) \quad (15)$$

where $O(k+1) = [H(k+1)P(k+1|k)H^T(k+1) + \text{diag}[R_{ij}]_{i,j=1 \dots 4}]^{-1}$

$$H(k+1) = \frac{\partial h[X(k+1), {}^E p_i]}{\partial X(k+1)} \Big|_{X(k+1) = \hat{X}(k+1|k)}$$

Then the state estimate $\hat{X}(k+1|k+1)$ and its estimation error covariance matrix $P(k+1|k+1)$ at time $k+1$ can be computed by

$$\hat{X}(k+1|k+1) = \hat{X}(k+1|k) + K(k+1)[Z(k+1) - \hat{Z}(k+1|k)] \quad (16)$$

$$P(k+1|k+1) = [I - K(k+1)H(k+1)]P(k+1|k) \quad (17)$$

4. Simulation results

As stated in section 2, the effector is controlled by the robot, in which the revolute joints are programmed as

$$q = \frac{\pi}{180} [40 \ 10 \ -5 \ 60 \ 8 \ 10] \cos\left(\frac{t}{100}\right) (\text{rad}) \quad t \in [0, 100\pi]$$

And the robot forward kinematics with nominal D-H parameters is used to provide the attitude /position of the effector relative to base frame, which serve as the real. The sampling period of IMU and camera are both set as 0.1s, ignored the different sampling rate of the sensors. The noises of the IMU and camera sensors are assumed as $m_w \sim N(0, 0.1^2)$, $m_a \sim N(0, 2.5^2)$, $V \sim N(0, 5^2)$. The plots in Fig.2 and Fig.3 show the estimate results based on EKF and transition models only use IMU, respectively.

The simulation results suggest the effectiveness of the pro-posed method.

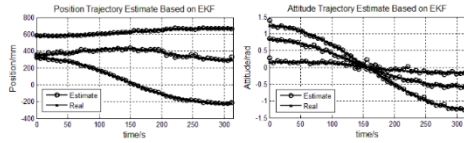


Fig. 2. Estimate of Effector Motion Based on EKF

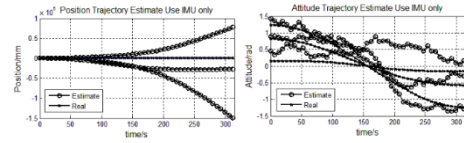


Fig. 3. Estimate of Effector Motion Use IMU Only

The measure model $Z(k) = X(k) + V(k)$, which can be obtained by using the PNP algorithm (refer to solvepnp function in OpenCV), is also applied in EKF to compare against the proposed observation models noted as Pixels Measure. To illustrate the performance of the observation models, the root mean square error (RMSE) in position and attitude are shown and the simulation results are derived from 100 Monte Carlo runs. The RMSE in position and attitude are shown in Fig. 4. The simulation results suggest that the performance of the EKF can be improved by using the image coordinates (Pixels) of feature points as observations.

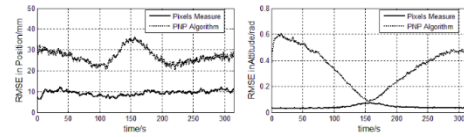


Fig. 4. The RMSE in position and attitude

Notice from (7) that the IMU's acceleration measurement is affected by the effector acceleration and the gravity, and the effector acceleration is much smaller than gravity in this simulation. Thus, it is very sensitive to noise, and lead to the estimate errors of position use IMU only are very large as shown in Fig.3.

Because of the complex computation, the measurement noises covariance matrices in measurement model obtained by PNP algorithm are not calculated based on the pixels noises of the camera, it is set based on our experience in this simulation. Besides, the errors of the attitude measure are shown in Fig.5. It's clear from the figure that the error is non-Gaussian.

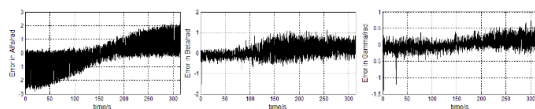


Fig. 5. The errors of the attitude measure

© The 2016 International Conference on Artificial Life and Robotics (ICAROB 2016), Jan. 29-31, Okinawa Convention Center, Okinawa, Japan

5. Conclusion

This paper investigated the attitude/position estimation of a rigid-body by using a measurement system consist of an inertial sensor and a vision sensor, and an EKF is applied to fuse these measurements. The motion states are propagated in time using the inertial measurements processed through the Newton-Euler equations, and the pixels coordinates of feature points are used as observation directly, which is different from using position and attitude coordinates in the camera frame. Simulation results suggest that the performance of the EKF can be improved by using the pixels coordinates of feature points as observations than calculating position and attitude coordinates through PNP algorithm. Future work would focus on the on-line tracking estimation experiments.

Acknowledgements

This work is supported by the National Basic Research Program of China (973 Program: 2012CB821200, 2012CB821201) and the NSFC (61134005, 61221061, 61327807, 61520106010).

References

1. Wang C, Chen W, Tomizuka M., Robot end-effector sensing with position sensitive detector and inertial sensors, in *Proc. IEEE Int. Conf. Robotics and Automation*. (Minnesota, USA, 2012), 5252-5257.
2. Williamson, Walton R., et al, Sensor Fusion Applied to Autonomous Aerial Refueling, *J. Guid Control Dynam.* **32**(1) (2009) 262-275.
3. Zhang G, M. Kontitsis, et al, Cooperative Relative Navigation for Space Rendezvous and Proximity Operations using Controlled Active Vision, *J. Field Robot.* **00**(0) (2015) 1-24.
4. D. B. Gennery. Visual Tracking of Known Three Dimensional Objects, *Int J Comput Vision*, **7**(3) (1992), 243-270.
5. H Rehbindler, B.K. Ghosh, Pose estimation using line based dynamic vision and inertial sensors. *IEEE T Automat Contr*, **48**(2) (2003) 186 - 199.
6. Chen X, et al. Pose estimation of robotic end-effectors under low speed motion using EKF with inertial and SE(3) measurements, in *Proc. IEEE Int. Conf. Advanced Intelligent Mechatronics*, (Busan, Korea 2015) 1585-1590.

Modeling and Control of a Suspended Gravity Compensation System with Rigid-Flexible Coupling

Jiao Jia

*The Seventh Research Division, Beihang University (BUAA)
Beijing, 100191, China*

Yingmin Jia

*The Seventh Research Division, Beihang University (BUAA)
Beijing, 100191, China*

Shihao Sun

*The Seventh Research Division, Beihang University (BUAA)
Beijing, 100191, China
E-mail: annebuaa@hotmail.com; ymjia@buaa.edu.cn; jxcrssh@126.com
www.buaa.edu.cn*

Abstract

In this paper, the suspension gravity compensation system (SGCS) is modeled and the corresponding controller is designed. The system is a servo platform consisting of three sub-systems by which a micro-gravity environment can be established. Especially, a novel zero stiffness suspension sub-system and a creative unconstrained structure are proposed. The system model is deduced based on Lagrange equation. A PID controller is designed by using the feedback linearization approach. Simulation results show the effectiveness of the proposed method.

Keywords: gravity compensation, rigid-flexible coupling, Lagrange method, feedback linearization, PID

1. Introduction

One of the vital differences between the space environment and the ground laboratory environment is that the space is micro-gravity. In order to represent the spacecraft motion in space on the ground and improve the fidelity of ground verification of guidance and control system, the micro-gravity environment should be built. Up to now, the gravity compensation methods have been developed such as weight loss, neutral buoyancy, air-bearing and suspension system¹⁻⁵. There are both advantages and disadvantages of these approaches. Among them the suspension method⁵⁻⁷ becomes an economical, practical and reliability method.

There are two kinds of suspension compensation methods passive suspension compensation⁵ and active suspension compensation.⁶⁻⁷ The active suspension method performs much better than the passive one. The compensation accuracy of the suspend system depends on the structure and controller of the vertical direction sub-system greatly. Usually, the wire rope is one of the necessary parts of the vertical direction sub-system. However, when a force which is opposite to or greater than the object gravity functions on the object, the rope will be invalid. To solve this problem, a spring is combined with rope, but the compensation accuracy is affected by the rope reversing. In this paper, we develop a new means that combines a spring buffer unit with the

transmission unit to avoid the shortage of the wire rope. Besides, there are rarely papers or researches that concern how to guarantee the object rotation freedoms when it is suspended to the compensation platform. In this paper, a creative mechanical structure is presented.

2. System Design

The platform is a servo system consisting of a level-servo sub-system (LSS), a zero stiffness suspension sub-system (ZSSS), an unconstrained suspension sub-system (USS) and a circuit control section (CCS). The LSS can follow the object's horizontal movement and maintain the ZSSS vertically. The ZSSS could compensate the gravity of the object suspended to the USS and assure its gravity wouldn't affect its movement. The USS holds the object and such that the object would rotate freely. Note that they work cooperatively to create a micro-gravity environment.

As described in Fig.1, the object connects to the platform through the USS. The USS is composed of twelve rolling bearings and their fixations, which guarantees the equivalent suspension point coincides with the object centroid. Hence, the object can keep balance at any random attitude. The USS links to the spring buffer. The spring buffer attaches to the ZSSS. Besides, the ZSSS includes universal joint, Z direction mechanism and motor 3. The dual-axis tilt sensor is fixed to a spring buffer through an aluminum panel. The spring buffer and the tension sensor are connected by the universal joint. Therefore, when the object moves, the spring buffer swings around the universal joint. The dual-axis tilt sensor can measure the swing angle. The tension sensor connects to the Z direction mechanism. Z direction mechanism transmits by a rack and a pinion driven by motor 3. The ZSSS installs on the LSS specifically on the Y direction mechanism. In addition, The LSS comprises motor 2, the X direction mechanism and motor 1. The Y direction mechanism mounts on the X direction mechanism and they are driven by motor 2 and motor 1 respectively. The X direction mechanism fixes on the supporting frame.

The USS consists of twelve bearings and their fixations as presented in Fig.2. The bearings are classified into yaw bearings, roll bearings and pitch bearings according to their corresponding support rotation of the object.

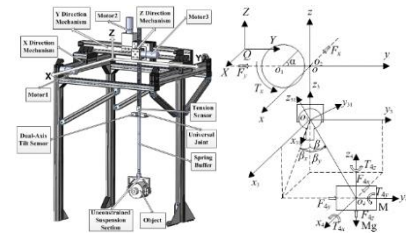


Fig.1. Structure and coordinate system of SGCS

The CCS contains the dual-axis tilt sensor, the tension sensor, drive control cards, an acquisition card and a PC. The working principle of the platform is as follows. When the object moves along the horizontal plane the dual-axis tilt sensor can measure the swing angles. Then the motor 1 and motor 2 can drive the X and Y direction mechanism to eliminate the swing angle to maintain the spring buffer vertically. When the object moves vertically the length of the spring will vary. The tension sensor will detect the variation and then the motor 3 actuates the Z direction mechanism to eliminate the variation. So the vertical movement of the object wouldn't be affected by its own gravity. The object is in a micro-gravity environment.

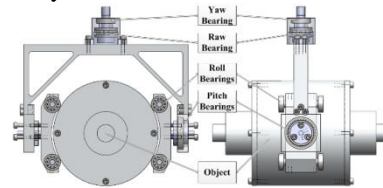


Fig.2. Structure of USS

3. Model Building

The SGCS coordinate system is shown in Fig.1, right. Among it, the spring buffer and the application of USS are equivalent to a spring and a rope linked to the centroid of the object respectively. The meaning of each part is as below.

- m_0 , the load of LSS,
- m_1, m_2 , the mass of the pinion and rack resp.,
- M , the mass of object,
- α , the rotation angle of the pinion
- $Q-XYZ$, static coordinate system
- O , centroid of m_0
- O_1, O_2, O_4 , centroids of m_1, m_2, M resp.,
- O_3 , centroid of the universal joint,
- F_x, F_y , motor 1&2 driving forces on X&Y
- T_x , motor 3 output torque on the pinion

- F_{4x}, F_{4y}, F_{4z} , the object driving force
- T_{4x}, T_{4y}, T_{4z} , the object driving torque
- β , wing angle between spring buffer & vertical
- β_x, β_y , orthogonal decomposition of β
- $O-xyz$, coordinate moves with O ,
- $O_i-x_iy_iz_i, i=3,4$, coordinates move with O_3 & O_4 ,
- $O_3-x_{31}y_{31}z_{31}$, coordinate rotate along the buffer.

From the definition above, the coordinates of O, O_1, O_2 are $(x, y, 0), (x, y-R, 0)$ and $(x, y, \alpha R)$.

And the velocity of each point is $(\dot{x}, \dot{y}, 0), (\dot{x}, \dot{y}, 0)$ and $(\dot{x}, \dot{y}, \dot{\alpha}R)$.

Define $l_1 = \frac{Mg}{k}, d = l_0 + l_1 + l$ Then O_4 is

$$(x + d \sin \beta_x \cos \beta_y, y + d \sin \beta_y, \alpha R - 0.5h_0 - d \cos \beta_x \cos \beta_y)$$

h_0 is the length of the rack. O & O_2 coincide at the initial position. l is the variation length of the spring. Set $l = 0$, when the force of the spring is equal to Mg .

For $\beta \leq 5^\circ$, $\sin \beta \approx \beta, \cos \beta \approx 1$, then

$$(x + d\beta_x, y + d\beta_y, \alpha R - 0.5h_0 - d)$$

The velocity of O_4 is

$$(\dot{x} + \dot{l}\beta_x + d\dot{\beta}_x, \dot{y} + \dot{l}\beta_y + d\dot{\beta}_y, \dot{\alpha}R - \dot{l})$$

The attitudes of the object will be changed when T_{4x}, T_{4y}, T_{4z} is valid, and therefore the angular velocity is time-varying. But when we choose x, y, α, l, β_x & β_y as system generalized coordinates, they are independent of the object rotational kinetic energy. Hence, we could ignore it when we calculate the system kinetic energy.

We define m_0 as the load of LSS. The pinion and rack move along the X&Y direction mechanism at the horizontal direction, so this part of kinetic energy is included in $0.5m_{0x}v_{m0x}^2 + 0.5m_{0y}v_{m0y}^2$ (m_{0x}, m_{0y} the load of X, Y direction resp.).

The system kinetic energy is

$$T = \frac{1}{2} \left(\frac{1}{2} m_1 R^2 \right) \dot{\alpha}^2 + \frac{1}{2} m_2 (\dot{\alpha} R)^2 + \frac{1}{2} m_{0x} v_{m0x}^2 + \frac{1}{2} m_{0y} v_{m0y}^2 + \frac{1}{2} M (v_{Mx}^2 + v_{My}^2 + v_{Mz}^2)$$

Choose xOy plane as zero potential energy surface and the system potential energy is

$$V = m_2 g \alpha R + 0.5k(l + l_1)^2 + Mg(\alpha R - 0.5h_0 - d) \quad (1)$$

Lagrange equation

$$\frac{d}{dt} \left(\frac{\partial L}{\partial \dot{q}} \right) - \frac{\partial L}{\partial q} = Q_j (j=1, 2, \dots) \quad (2)$$

Substitute Eq. (1) into Eq. (2) and define

$$m = \frac{1}{2} m_1 + m_2 + M, \eta_x = \frac{M + m_{0x}}{M}, \eta_y = \frac{M + m_{0y}}{M}$$

$$\eta = \frac{m}{M}, \eta_2 = \frac{m_2 + M}{M}, \varsigma = \frac{k}{M}, \rho = \frac{1}{M}$$

$$\beta^2 = \beta_x^2 + \beta_y^2, \beta_x^y = \beta_x \dot{\beta}_x + \beta_y \dot{\beta}_y$$

The equations deduced from Eq. (2) can be formatted in a compact form

$$\begin{bmatrix} \eta_x & 0 & 0 & \beta_x & d & 0 \\ 0 & \eta_y & 0 & \beta_y & 0 & d \\ 0 & 0 & \eta R^2 & -R & 0 & 0 \\ \beta_x & \beta_y & -R & \beta^2 + 1 & d\beta_x & d\beta_y \\ d & 0 & 0 & d\beta_x & d^2 & 0 \\ 0 & d & 0 & d\beta_y & 0 & d^2 \end{bmatrix} \begin{bmatrix} \ddot{x} \\ \ddot{y} \\ \ddot{\alpha} \\ \ddot{l} \\ \ddot{\beta}_x \\ \ddot{\beta}_y \end{bmatrix} + \begin{bmatrix} 0 & 0 & 0 & 2\dot{\beta}_x & 0 & 0 \\ 0 & 0 & 0 & 2\dot{\beta}_y & 0 & 0 \\ 0 & 0 & 0 & 0 & 0 & 0 \\ 0 & 0 & 0 & 2\dot{\beta}_x^y & 0 & 0 \\ 0 & 0 & 0 & 2d\dot{\beta}_x & 0 & 0 \\ 0 & 0 & 0 & 2d\dot{\beta}_y & 0 & 0 \end{bmatrix} \begin{bmatrix} \dot{x} \\ \dot{y} \\ \dot{\alpha} \\ \dot{l} \\ \dot{\beta}_x \\ \dot{\beta}_y \end{bmatrix} + \begin{bmatrix} 0 \\ 0 \\ \eta_2 g R \\ \varsigma l \\ 0 \\ 0 \end{bmatrix} = \rho \begin{bmatrix} F_x \\ F_y \\ T_x \\ F_{4z} \\ F_{4x} \\ F_{4y} \end{bmatrix} \quad (3)$$

We classify the system generalized coordinates into two parts based on their controllability that x, y, α only controlled by the motors and the other ones are affected by the driving forces of the object simultaneously.

Define $q_1 = [x \ y \ \alpha]^T, q_2 = [l \ \beta_x \ \beta_y]^T$, and

$$M_1 \ddot{q}_1 + M_2 \ddot{q}_2 + C_1 \dot{q}_1 + C_2 \dot{q}_2 + G_1 = F_1 \quad (4)$$

$$M_2^T \ddot{q}_1 + M_3 \ddot{q}_2 + C_3 \dot{q}_1 + C_4 \dot{q}_2 + G_2 = F_2 \quad (5)$$

Obviously, M_2 is invertible

Let Eq.(4) - $M_1 M_2^{-T}$ Eq.(5). And $C_1 = C_3 = 0$ we gain

$$M_m \ddot{q}_2 + C \dot{q}_2 + G = F_1 - M_1 M_2^{-T} F_2 \quad (6)$$

$$M_m = M_2 - M_1 M_2^{-T} M_3, C = C_2 - M_1 M_2^{-T} C_4,$$

$$G = G_1 - M_1 M_2^{-T} G_2$$

4. Controller Design

Since $F_2 = [F_{4z} \ F_{4z} \ F_{4z}]^T$ depends on the object movement requirements and is uncontrollable for SGCS, it's regarded as interferences. So the model is a time-varying coupling model with disturbances. A PID controller is designed by using the feedback linearization approach.

$$F_1 = F_{11} + M_m F_{12} \quad (7)$$

$$F_{11} = C\dot{q}_2 + G \quad (8)$$

$$F_{12} = -(K_P q_2 + K_I \int q_2 + K_D \dot{q}_2) \quad (9)$$

$$K_P = \begin{bmatrix} K_{Pz} & K_{Px} & K_{Py} \end{bmatrix}, K_I = \begin{bmatrix} K_{Iz} & K_{Ix} & K_{Iy} \end{bmatrix}$$

$$K_D = \begin{bmatrix} K_{Dz} & K_{Dx} & K_{Dy} \end{bmatrix}$$

F_{11} is used to counterweigh $C\dot{q}_2 + G$ of Eq. (6). Substitute Eq. (7) in Eq. (6), and we gain

$$M_m \ddot{q}_2 = M_m F_{12} - M_1 M_2^{-T} F_2 \quad (10)$$

It's easy to verify the existence of the inverse of M_m . Eq. (10) simplifies to

$$\ddot{q}_2 = F_{12} + d(t), d(t) = -M_1 M_2^{-T} F_2 \quad (11)$$

Where F_{12} is a PID controller. PID parameters adjustment rules are employed to find suitable control parameters for the system.

5. Simulation Results

Firstly, the control target is $q_2 = 0$. It means the gravity of the object is compensated completely.

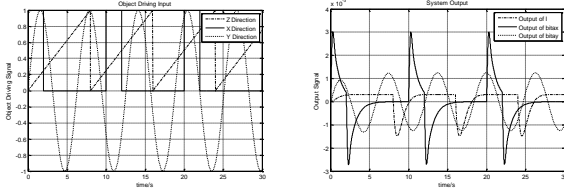


Fig.3. The object driving input and output of the system

The object driving input is shown in Fig.3.left which is regarded as the system disturbance. From Fig.3.right, the system spring variation error is less than 0.0015 m which means the compensation accuracy is up to 99%.

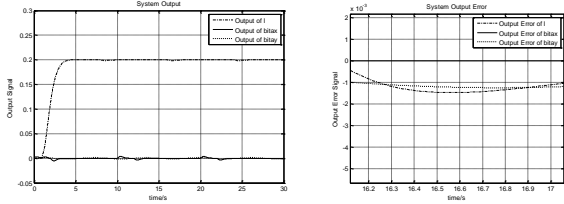


Fig.4. The system response & output error of the 0.2step input

Then set $q_2 = [u(t) \ 0 \ 0]^T$. $u(t)$ is the reference input of the system which means when the spacecraft is not complete weightlessness and it varies according to the law role of the gravity effect.

Fig.4. shows the system response and output error at 0.2step reference input with the same disturbance as shown in Fig.3.left. The compensation accuracy is up to 99%. The simulation results show that smaller of spring stiffness coefficient the higher compensation accuracy.

6. Conclusions

In this paper, a novel compensation platform reflecting in the ZSSS and USS is proposed and then the mathematic model based on Lagrange equation is developed. Lastly, a stable and high compensation accuracy controller is given. However, the existence of the sensor errors and modeling errors, we can't compensate the nonlinear parts. Depth study should be conducted to find more practical controllers.

Acknowledgements

This work was supported by the National Basic Research Program of China (973 Program: 2012CB821200, 2012CB821201) and the NSFC (61134005, 60921001, 61327807).

References

1. Y. Watanabe, et al., Microgravity experiments for a visual feedback control of a space robot capturing a target, *Proceedings of the IEEE/RSJ International Conference on Intelligent Robots and Systems*, (USA, Piscataway, 1998), pp. 1993-1998.
2. H. Sawada, et al., Micro-gravity experiment of a space robotic arm using parabolic flight, *Advanced Robotics* **18**(3) (2004) 247-267.
3. C. Menon, et al., Issues and solutions for testing free-flying robots, *Acta Astronautica* **60**(12) (2007) 957-965.
4. A. Robertson, et al., Spacecraft formation flying control design for the Orion mission, *AIAA Guidance, Navigation, and Control Conference*, (USA, Reston, 1999), pp. 1562-1575.
5. D. A. Kienholz, et al., Very low frequency suspension systems for dynamic testing, *Proceedings of the 30th Structures, Structural Dynamics and Materials*, (USA, Mobile, 1989), pp. 327-336.
6. G. C. White and Y. S. Xu, Active vertical-direction gravity compensation system, *IEEE Transactions on Instrumentation and Measurement* **43**(6) (1994) 786-792.
7. O. Han, et al., Gravity-offloading system for large-displacement ground testing of spacecraft mechanisms, *Proceedings of 40th aerospace mechanisms symposium*, (USA, FL, 2010), pp. 119-132.

Trajectory Tracking Control for Omnidirectional Mobile Robots with Input Constraints

Wenhao Zheng

*The Seventh Research Division and the Department of Systems and Control, Beihang University (BUAA)
Beijing, 100191, China*

Yingmin Jia

*The Seventh Research Division and the Department of Systems and Control, Beihang University (BUAA)
Beijing, 100191, China*

*E-mail: zhengwenhao@163.com, ymjia@buaa.edu.cn
www.buaa.edu.cn*

Abstract

In this paper, a trajectory tracking controller based on kinematics for omnidirectional mobile robots with input constraints is presented. The tracking error model with the control law is proved to be global asymptotic stability by Lyapunov stability theory. The input limits can be described as an octahedron in three-dimensional space, so that a spatial vector analysis method is proposed to design time-varying feedback parameters to limit robot inputs. Simulation results show the feasibility and effectiveness of the control strategy.

Keywords: omnidirectional mobile robot, tracking control, input constraints, time-varying feedback control.

1. Introduction

Omnidirectional mobile robots, with the ability of three degree-of-freedom motion in the plane, have been widely applied in different fields of the society, which has brought to the forefront in recent years. Many methods about tracking control have been proposed, such as sliding mode control¹, model predictive control², fuzzy control³ and their combinations. In the practical systems, the velocities of driving motors is limited, which means that the inputs of the mobile robot are subject to constraints. The control law will be affected by input constraints. Some results about tracking control with input constraints can be found. In Ref.4, the control signal to a given reference system was modified to make the error dynamics robust to the saturation constraints. In Ref.5, the diamond-shaped input constraints was considered which made the controller more effective.

This paper mainly focuses on the tracking control of omnidirectional mobile robots with input constraints. The control law is proposed with time-varying feedback parameters to satisfy the input constraints. Then, a spatial vector analysis method is used to design parameters which is devoted to find a suitable robot inputs in the restricted area. And the tracking error system can be global asymptotic stability with the controller. Comparing with existing results, this paper primarily contributes to the novel solution of input constraints of omnidirectional mobile robots.

The structure of the rest paper is organized as follows. The section 2 introduces the tracking error system. In the section 3, the tracking controller is designed with input constraints using the spatial vector analysis method. Simulation results are presented to show the validity of the control law in the section 4. In the end, the section 5 summarizes the whole paper and draws the conclusion.

2. Problem Statement

2.1. Kinematic model of omnidirectional mobile robot

As shown in Fig.1.(a), the four wheeled omnidirectional mobile robot is considered in this paper. The kinematic of omnidirectional mobile robots is

$$\begin{pmatrix} \dot{x} \\ \dot{y} \\ \dot{\theta} \end{pmatrix} = \begin{pmatrix} \cos \theta & -\sin \theta & 0 \\ \sin \theta & \cos \theta & 0 \\ 0 & 0 & 1 \end{pmatrix} \begin{pmatrix} v_x \\ v_y \\ \omega \end{pmatrix} \quad (1)$$

Where (x, y) are the robot position in Cartesian coordinates and θ is the robot orientation. The control inputs of the robot are (v_x, v_y, ω) : (v_x, v_y) here denote robot's longitudinal velocity and transverse velocity, and ω represents the rotate speed of the robot. As a matter of fact, the kinematic of all kinds of omnidirectional robots including three wheeled robots or others with different omnidirectional wheels can be expressed as equation (1).

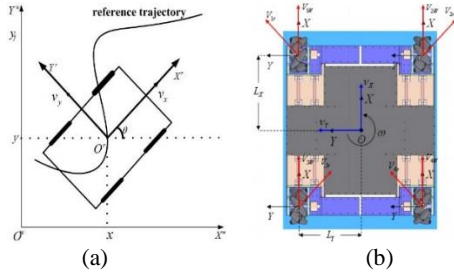


Fig. 1. The schematic of trajectory tracking (a) and Four-wheel structure of the robot (b).

In the Fig.1.(b), the framework of omnidirectional mobile robot has been proposed. The transformation relation between the speeds $(v_{1w}, v_{2w}, v_{3w}, v_{4w})$ of the four driving wheels and the omnidirectional robot's speed (v_x, v_y, ω) is described as the equation (2), where $d = L_x + L_y$ and L_x is the X-axis distance from each wheel to the center of gravity (the similar definition for L_y).

$$\begin{pmatrix} v_{1w} \\ v_{2w} \\ v_{3w} \\ v_{4w} \end{pmatrix} = \begin{pmatrix} 1 & -1 & -d \\ 1 & 1 & d \\ 1 & 1 & -d \\ 1 & -1 & d \end{pmatrix} \begin{pmatrix} v_x \\ v_y \\ \omega \end{pmatrix} \quad (2)$$

2.2. Input constraints

In the practical systems, the velocities of motors are limited. Assume that four driving wheels have the same mechanical characteristics, therefore, it is obvious that the same input constraint $|v_{iw}| \leq V$ ($i = 1, 2, 3, 4$) should be satisfied, and V is the maximum wheel velocity. Using the constraint and the equation (2), we can deduce the equation (3) as follows:

$$\left| \frac{v_x}{V} \right| + \left| \frac{v_y}{V} \right| + \left| \frac{\omega}{V/d} \right| \leq 1 \quad (3)$$

which can be described in three-dimensional space as shown in Fig.2: the restricted zone of robot inputs is an octahedron with the geometric representation.

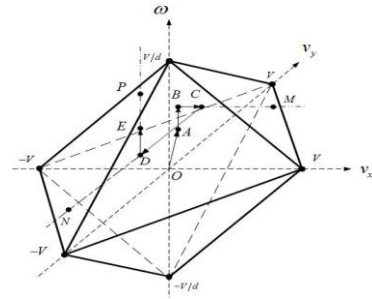


Fig. 2. Input constraints area in three-dimensional space

2.3. Error model of trajectory tracking

Assume that the reference trajectory for the omnidirectional mobile robot satisfies the kinematic

$$\begin{pmatrix} \dot{x}_r \\ \dot{y}_r \\ \dot{\theta}_r \end{pmatrix} = \begin{pmatrix} \cos \theta_r & -\sin \theta_r & 0 \\ \sin \theta_r & \cos \theta_r & 0 \\ 0 & 0 & 1 \end{pmatrix} \begin{pmatrix} v_{xr} \\ v_{yr} \\ \omega_r \end{pmatrix} \quad (4)$$

and the input constraints

$$\left| \frac{v_x}{V} \right| + \left| \frac{v_y}{V} \right| + \left| \frac{\omega}{V/d} \right| \leq 1 - \varepsilon \quad (5)$$

In the equation (4) and (5), $(x_r, y_r, \theta_r, v_{xr}, v_{yr}, \omega_r)$ are the desired values for $(x, y, \theta, v_x, v_y, \omega)$. Besides, ε is a constant with the condition $0 < \varepsilon < 1$ which guarantees the robot has the ability to track the reference trajectory successfully.

We can define the tracking errors as follows:

$$\begin{pmatrix} x_e \\ y_e \\ \theta_e \end{pmatrix} = \begin{pmatrix} \cos \theta & \sin \theta & 0 \\ -\sin \theta & \cos \theta & 0 \\ 0 & 0 & 1 \end{pmatrix} \begin{pmatrix} x_r - x \\ y_r - y \\ \theta_r - \theta \end{pmatrix} \quad (6)$$

Combining the equation (1) and (4) with differentiating both side of (6), error model can be expressed as

$$\begin{aligned} \dot{x}_e &= v_{xr} \cos \theta_e - v_{yr} \sin \theta_e + \omega y_e - v_x \\ \dot{y}_e &= v_{xr} \sin \theta_e + v_{yr} \cos \theta_e - \omega x_e - v_y \\ \dot{\theta}_e &= \omega_r - \omega \end{aligned} \quad (7)$$

The destination of control law design is to find the appropriate inputs (v_x, v_y, ω) which are subject to the input constraints (3) to meet the desired outcome:

$$\lim_{t \rightarrow 0} x_e \rightarrow 0, \lim_{t \rightarrow 0} y_e \rightarrow 0, \lim_{t \rightarrow 0} \theta_e \rightarrow 0 \quad (8)$$

3. Controller Design

3.1. Control law design without input constraints

Inspired by the tracking error model and tracking control methods for differential-drive mobile robots, we come up with the control law

$$\begin{aligned} v_x &= v_{xr} \cos \theta_e + k_x x_e \\ v_y &= v_{yr} \cos \theta_e + k_y y_e \\ \omega &= \omega_r + k_t (v_{xr} y_e - v_{yr} x_e) \sin \theta_e / \theta_e + k_\theta \theta_e \end{aligned} \quad (9)$$

Where k_x, k_y, k_θ are positive time-varying parameters and k_t is positive constants. In order to ensure the continuity of the robot inputs, we define $\sin \theta_e / \theta_e = 1$ when $\theta_e = 0$. And it's noticeable that $\sin \theta_e / \theta_e$ is bounded. The tracking errors x_e, y_e and θ_e will converge to zero under the control law (9), which can be proven as follows:

Let Lyapunov function be

$$V = \frac{1}{2} \left(x_e^2 + y_e^2 + \frac{\theta_e^2}{k_t} \right) \quad (10)$$

Considering the tracking error system (7) and the controller (9), the derivative of this Lyapunov function can be expressed as $\dot{V} = -k_x x_e^2 - k_y y_e^2 - (k_\theta / k_t) \theta_e^2$. When the conditions $k_x, k_y, k_\theta, k_t > 0$ are satisfied, we can infer $\dot{V} \leq 0$ and $V(t) \leq V(0)$. Furthermore, it's

convenient to get the conclusion that $x_e, y_e, \theta_e \rightarrow 0$ as $t \rightarrow \infty$ with Barbalat's lemma.

3.2. Feedback parameters design with input constraints

Define the space vectors

$$\begin{aligned} \overline{OE} &= (v_x \quad v_y \quad \omega_r)^T \\ \overline{OA} &= (v_{xr} \cos \theta_e \quad v_{yr} \cos \theta_e \quad \omega_r)^T \\ \overline{AB} &= (0 \quad 0 \quad k_t (v_{xr} y_e - v_{yr} x_e) \sin \theta_e / \theta_e)^T \\ \overline{BC} &= (k_x x_e \quad 0 \quad 0)^T, \overline{CD} = (0 \quad k_y y_e \quad 0)^T \\ \overline{DE} &= (0 \quad 0 \quad k_\theta \theta_e)^T \end{aligned} \quad (11)$$

The controller (7) can be expressed as a space vector $\overline{OE} = \overline{OA} + \overline{AB} + \overline{BC} + \overline{CD} + \overline{DE}$. Fig.2 shows the relationships of the vectors. According to the equation (5),

$$\left| \frac{v_{xr} \cos \theta_e}{V} \right| + \left| \frac{v_{yr} \cos \theta_e}{V} \right| + \left| \frac{\omega_r}{V/d} \right| \leq 1 - \varepsilon \quad (12)$$

\overline{OA} is in the input area.

If the condition

$$k_t = \frac{\mu \varepsilon}{2d \sqrt{V(0) + \alpha}} \quad (\alpha > 0, 0 < \mu < 1) \quad (13)$$

holds, \overline{OB} is in the octahedron. We can prove this result as follows:

$$\begin{aligned} & \left| \frac{v_{xr} \cos \theta_e}{V} \right| + \left| \frac{v_{yr} \cos \theta_e}{V} \right| + \left| \frac{\omega_r + k_t (v_{xr} y_e - v_{yr} x_e) \sin \theta_e / \theta_e}{V/d} \right| \\ & \leq \left| \frac{v_{xr} \cos \theta_e}{V} \right| + \left| \frac{v_{yr} \cos \theta_e}{V} \right| + \left| \frac{\omega_r}{V/d} \right| + \\ & k_t \left| \frac{(v_{xr} y_e - v_{yr} x_e) \sin \theta_e / \theta_e}{V/d} \right| \\ & \leq 1 - \varepsilon + dk_t (|x_e| + |y_e|) \leq 1 - \varepsilon + dk_t \sqrt{4V(t)} \\ & \leq 1 - \varepsilon + 2dk_t \sqrt{V(0)} < 1 - \varepsilon + \mu \varepsilon < 1 \end{aligned}$$

We can obtain the value of k_t from equation (13)

$$k_t = \frac{-\theta_e^2(0)d + \sqrt{\theta_e^4(0)d^2 + 2[x_e^2(0) + y_e^2(0) + 2\alpha]\mu^2\varepsilon^2}}{2[x_e^2(0) + y_e^2(0) + 2\alpha]d}$$

Define a function $\eta(x)$ which has three features: $\eta(x) \in [0, 1]$ for $x \in [0, \infty)$, $\eta(x)$ is non-decreasing and $\eta(0) = 0, \eta(\infty) = 1$. In order to design the time-varying

feedback parameters k_x, k_y, k_θ , we come up with a geometric method. Sign function is defined as $\text{sign}(x)$.

As shown in Fig.2, we can make a line through B and in parallel with v_x , which goes through the constrained boundary with a point of intersection M . Take $\overline{BC} = \eta(|x_e|)\overline{BM}$, then, we can get the expression of k_x . And construct another line going through C and in parallel with v_y , there will be another intersection N in the constrained boundary, then make $\overline{CD} = \eta_2(|y_e|)\overline{CN}$. It is easy to get the expression of k_y . We can use the same thought to define P and $\overline{DE} = \eta_3(|\theta_e|)\overline{DP}$.

In the end, we can get the controller

$$\begin{aligned} v_x &= v_{xr} \cos \theta_e + \eta_1(|x_e|)[\text{sign}(x_e)(V - |v_{yr} \cos \theta_e| - \\ &\quad d[\omega_r + k_t(v_{xr}y_e - v_{yr}x_e) \sin \theta_e / \theta_e] - v_{xr} \cos \theta_e] \\ v_y &= v_{yr} \cos \theta_e + \eta_2(|y_e|)[\text{sign}(y_e)(V - |v_{xr} \cos \theta_e| - \\ &\quad d[\omega_r + k_t(v_{xr}y_e - v_{yr}x_e) \sin \theta_e / \theta_e] - v_{yr} \cos \theta_e] \\ \omega &= \omega_r + k_t(v_{xr}y_e - v_{yr}x_e) \sin \theta_e / \theta_e + \\ &\quad \eta_2(|\theta_e|)[\text{sign}(\theta_e)(V - |v_x| - |v_y|) / d \\ &\quad - \omega_r - k_t(v_{xr}y_e - v_{yr}x_e) \sin \theta_e / \theta_e] \end{aligned} \quad (15)$$

And the time-varying feedback parameters can be expressed as $k_x = \eta_1(|x_e|)[\text{sign}(x_e)(V - |v_{yr} \cos \theta_e| - d[\omega_r + k_t(v_{xr}y_e - v_{yr}x_e) \sin \theta_e / \theta_e] - v_{xr} \cos \theta_e] / x_e$, $k_y = \eta_2(|y_e|)[\text{sign}(y_e)(V - |v_{xr} \cos \theta_e| - d[\omega_r + k_t(v_{xr}y_e - v_{yr}x_e) \sin \theta_e / \theta_e] - v_{yr} \cos \theta_e] / y_e$ and $k_\theta = \eta_3(|\theta_e|)[\text{sign}(\theta_e)(V - |v_x| - |v_y|) / d - \omega_r - k_t(v_{xr}y_e - v_{yr}x_e) \sin \theta_e / \theta_e]$.

4. Simulation Results

Set the reference trajectory as $x_r = 0.75 \sin(2\pi t / 45)$, $y_r = \sin(4\pi t / 45)$ and $\theta_r = \pi \cos(\pi t / 16) / 4$, and the initial robot pose is $(x(0), y(0), \theta(0)) = (-0.5m, 0.2m, 0)$. Let $V = 2m/s, d = 0.7m, \varepsilon = 0.01, \alpha = 1, \mu = 0.99$. Thus $k_t = 1.6203e-04$. The simulation results are presented in Fig.3 and Fig.4.

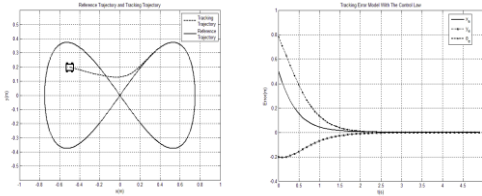


Fig. 4. Tracking trajectory and tracking errors.

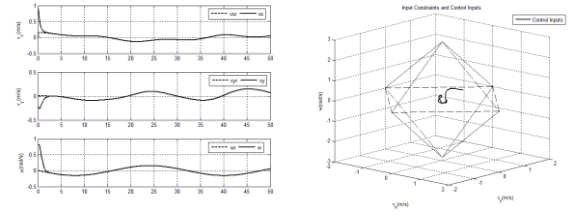


Fig. 4. Tracking velocity and control inputs.

Fig.3 and Fig.4 show that the tracking errors will converge to zero with the control law (15), and the control inputs are always in the area of input constraints.

5. Conclusion

In this paper, the tracking control problem of omnidirectional mobile robot with input constraints has been solved. A controller with time-varying feedback parameters is proposed using the spatial vector analysis method. The simulation results show that the control law can guarantee great tracking performance and the inputs will be located in the restricted area.

Acknowledgements

This work was supported by the National Basic Research Program of China (973 Program: 2012CB821200, 2012CB821201) and the NSFC (61134005, 60921001, 61327807).

References

1. Li, Yunqi, et al. "Sliding mode trajectory tracking control based on dynamic model for four-wheel drive omnidirectional mobile robots." *Science Mosaic* (2014).
2. Zeng, Zhi Wen, et al. "Trajectory tracking based on model predictive control for omni-directional mobile robot." *Control Engineering of China* (2011).
3. Hashemi, Ehsan, M. G. Jadidi, and N. G. Jadidi. "Model-based PI-fuzzy control of four-wheeled omni-directional mobile robots." *Robot. Auton. Syst.* 59.11(2011):930-942.
4. A. Leonessa, W. M. Haddad, T. Hayakawa, and Y. Morel, "Adaptive control for nonlinear uncertain systems with actuator amplitude and rate saturation constraints." *Int. J. Adapt. Control Signal Process.* 23.1(2009):73-96.
5. Chen, Xiaohan, Y. Jia, and F. Matsuno. "Tracking control for differential-drive mobile robots with diamond-shaped input constraints." *IEEE Trans. Control Syst. Technol.* 22.5(2014):1999-2006.

Parameters tuning approach for prescribed performance function based active disturbance rejection control

Wei Wei

School of Computer and Information Engineering, Beijing Technology and Business University, 11 FuCheng Road, 100048, P.R. China

Bo Liang

School of Computer and Information Engineering, Beijing Technology and Business University, 11 FuCheng Road, 100048, P.R. China

Weijun Su

School of Computer and Information Engineering, Beijing Technology and Business University, 11 FuCheng Road, 100048, P.R. China

*E-mail: weiweizdh@163.com, liangbo@st.btbu.edu.cn, swj6843@163.com
www.btbu.edu.cn*

Abstract

Active disturbance rejection control (ADRC) is a control approach which needs less information of the controlled plants/processes. However, there are many parameters in the nonlinear functions utilized in ADRC, so many parameters make the tuning of ADRC be a challenge. Prescribed performance function based ADRC is proposed and the tuning approach is studied in this paper. Some typical controlled plants are considered in the simulations. Numerical results are presented to support the proposed control approach and its tuning method.

Keywords: ADRC, prescribed performance function, parameter tuning

1. Introduction

Active disturbance rejection control (ADRC) is a control approach first proposed by Prof. Han in early 1990s.¹ ADRC was proposed by reconsidering the essence of control problem. Its basic idea is to make the control system be more robust to disturbance and uncertainties by estimating and compensating those factors actively in real time.

For the idea of ADRC, standard form of any system is the chain of integrators. The difference between the model and standard form will be viewed as disturbance

or uncertainties. Extended state observer (ESO), the key part of ADRC, composed of the state observer and an extended state, is designed to estimate the disturbance and uncertainties in real time. And any control law can be designed in order to achieve the desired performance.

Nowadays, ADRC is relatively common in numerous applications, such as superconducting RF cavities,² piezoelectric beam,³ nanopositioning.⁴ The theoretical analysis is also given in Ref. 5, 6 and 7. Although there are many successful applications and valid theoretical analysis, the number of controller parameters one has to determine is a headache for engineers. In other words, engineers are difficult to set a

© The 2016 International Conference on Artificial Life and Robotics (ICAROB 2016), Jan. 29-31, Okinawa, Japan

group of applicable values for those tunable parameters. The value of parameters depends greatly on experience of engineers. Such problem limits ADRC's application more or less, even if ADRC is effective in control engineering.

As a matter of fact, for our part, the reason for the difficulties in tuning is that the parameters are of no physical explanations in ADRC.

With an attempt to get an easier and a more effective approach to fix the parameters of ADRC, Prof. Gao propose a bandwidth-parameterization based controller tuning approach.⁸ By such proposal, engineers are able to get a clearer physical explanation for tunable parameters, and the tuning work becomes easier. However, such approach is based on the linear version of ADRC, i.e. LADRC. Tunable parameters can be got by an easier way, but the performance will be reduced as a result of taking linear extended state observer (LESO) or LADRC.

How to get an easier tuning approach and also retain the control performance by utilizing nonlinear function? This is a desired goal from both practical and theoretical view of point. In this paper, we have proposed prescribed performance function based active disturbance rejection control (PPF-ADRC), and given out the tuning approach. The parameters one has to determine have clear physical explanations and the simulation results confirm the proposed approach.

The remainder of the paper is organized as follows. Section 2 gives out the basic structure of LADRC. PPF-ADRC is designed in Section 3. Simulation results and conclusions are offered in Section 4 and 5 respectively.

2. Linear Active Disturbance Rejection Control

Generally, LADRC is designed by linearize the estimation error, the control block diagram for 3rd-order LADRC can be shown in Fig. 1.

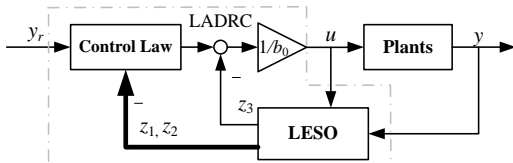


Fig. 1 Control block diagram for 3rd-order LADRC

The dynamics of LADRC can be described as⁸

$$\begin{cases} \dot{\xi}_1 = z_2 + \beta_1 e(t) \\ \dot{\xi}_2 = z_3 + \beta_2 e(t) + b_0 u \\ \dot{\xi}_3 = \beta_3 e(t) \end{cases} \quad (1)$$

$$u = [k_p(y_r - z_1) - k_d z_2 - z_3]/b_0 \quad (2)$$

where y_r is the desired system output, u is the control input, k_p, k_d are control gains, b_0 is the coefficient of control input, $e(t)$ is the estimation error, and $e(t) = y - z_1$. z_1, z_2 and z_3 are outputs of LESO respectively. z_1 estimates system output y , z_2 estimates \dot{y} , z_3 is the estimation of total disturbance and uncertainties. β_1, β_2 and β_3 are gains of LESO.

3. Prescribed Performance Function based Active Disturbance Rejection Control Design

In order to improve the efficiency of LESO, in this paper, we still take advantage of nonlinear function in ESO, but the parameters for the nonlinear function have clear physical explanations.

Firstly, a prescribed performance function, a positive decreasing smooth function, is introduced.

$\rho(t): R^+ \mapsto R^+$, and $\lim_{t \rightarrow \infty} \rho(t) = \rho_\infty > 0$, it can be defined as

$$\rho(t) = (\rho_0 - \rho_\infty) \exp(-lt) + \rho_\infty \quad (3)$$

where $\rho_0 > \rho_\infty, l > 0$. ρ_0 is the maximum value of allowable estimation error, ρ_∞ is the maximum value of allowable steady estimation error, l determines the decreasing rate of $\rho(t)$.

Then, we may define $\gamma(t)$ satisfying,⁹

$$-\underline{\delta}\rho(t) < \gamma(t) < \bar{\delta}\rho(t) \quad (4)$$

where $0 < \underline{\delta}, \bar{\delta} \leq 1$ are prescribed scalars. By (4), we can see that function $\gamma(t)$ is defined in a prescribed range.

For the sake of satisfying the constrained condition (4), a smooth and strictly increasing function $S(x)$ can be defined,

$$-\underline{\delta} < S(x) < \bar{\delta} \quad (5)$$

$$\lim_{x \rightarrow \infty} S(x) = \bar{\delta}, \lim_{x \rightarrow -\infty} S(x) = -\underline{\delta} \quad (6)$$

We can introduce a transformation

$$\gamma(t) = \rho(t)S(x) \quad (7)$$

then property (4) can be described as,

$$-\underline{\delta}\rho(t) < \gamma(t) = \rho(t)S(x) < \bar{\delta}\rho(t) \quad (8)$$

If we let $\gamma(t)$ be estimation error, from inequality (8), we can see clearly that estimation error will be always within the prescribed range.

Actually, the estimation error reflects the system's ability of disturbance estimation and compensation in a

great extent. If estimation error is within a prescribed range from the beginning, it means that ESO has stronger power in estimation and compensation disturbance and uncertainties. Therefore, we introduce a transformation. Let $x = e(t)$, then transformation (7) can be rewritten as

$$e_o(t) = \rho(t)S(e(t)) \quad (9)$$

where $e_o(t)$ is the transformed estimation error, which satisfies property (8).

Then we use the transformed estimation error $e_o(t)$ in error transformation based ESO (ETESO),

$$\begin{cases} \dot{\hat{x}}_1 = z_2 + \beta_1 e(t) \\ \dot{\hat{x}}_2 = z_3 + \beta_2 e_o(t) + b_0 u \\ \dot{\hat{x}}_3 = \beta_3 e_o(t) \end{cases} \quad (10)$$

In the design, we choose function $S(x)$ as

$$S(x) = \frac{\bar{\delta} \exp(x) - \underline{\delta} \exp(-x)}{\exp(x) + \exp(-x)}$$

Accordingly, PPF-ADRC can be obtained((2) and (10)).

4. Simulation Results

With an attempt to verify the performance of PPF-ADRC, we have performed two simulations. Refer to Ref. 10, two plants are considered.

Table 1. Plants and its models

Plant	Model
P ₁	$G_1(s) = \frac{e^{-5s}}{(s+1)^3}$
P ₂	$G_2(s) = \frac{1-2s}{(s+1)^3}$

For the plants shown in Table 1, we design both PPF-ADRC and LADRC. Controller parameters chosen approach refers to Ref. 8.

For the controller part, we take the bandwidth-parameterization approach. For the ETESO part, $\beta_1, \beta_2, \beta_3$ are also taken bandwidth-parameterization approach into consideration. Parameters for error transformation part refer to their physical explanations. Parameter values chosen in simulations are shown in Table 2.

Table 2 PPF-ADRC parameters

	b_0	ω_o	ω_c	ρ_0	ρ_∞	l	$\underline{\delta}$	$\bar{\delta}$
P ₁	3	1.6	0.3	0.291	0	0.3	1	0.8
P ₂	15	4	1	.18	0	1	1	0.1

In simulations, controller parameters and the gain of ESO in LADRC and PPF-ADRC are chosen the same value. Simulation results are shown in Fig. 2 and 3, respectively. Both subfigures (e) and (f) in Fig. 2 and 3 depict the tracking error $e_c(t)$, i.e. the error curves between y and y_r .

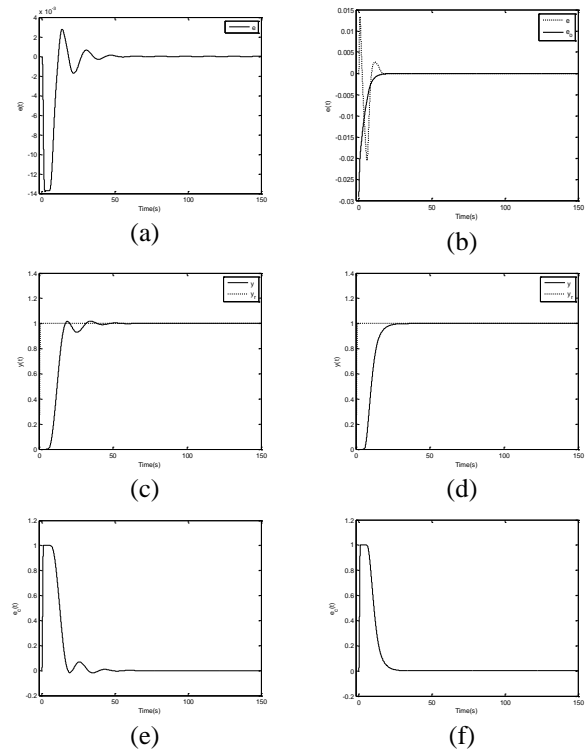


Fig. 2 Comparisons of system response(for P₁)

Table 3. Comparisons of IAE Values(For P₁)

Controller	IAE Value
LADRC	12.4144
PPF-ADRC	10.8236

From Fig. 2, we can see clearly that the response of LADRC ((a),(c), and (e)) is inferior to the response of PPF-ADRC((b),(d),and (f)), when control parameters and the gains of ESO are chosen the same. Comparisons of integral of absolute error (IAE) values are given in Table 3.

Fig. 3 demonstrates that PPF-ADRC is also superior to LADRC when control parameters and the gains of ESO are chosen the same. Comparisons of IAE values are shown in Table 4.

In this section, typical systems including delay and unstable unit are considered. Both system response and IAE values confirm that PPF-ADRC has better performance than LADRC. Actually, advanced design idea guarantees better performance of PPF-ADRC.

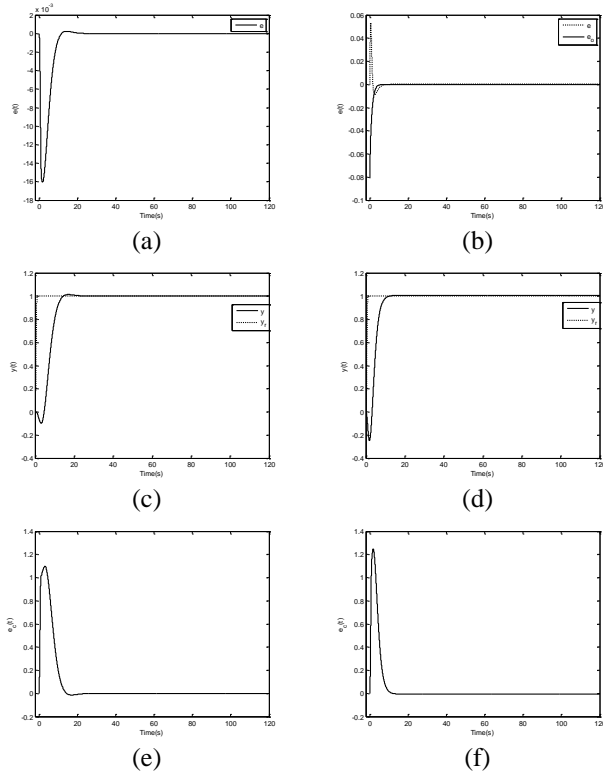


Fig. 3 Comparisons of system response(for P₂)

Table 4. Comparisons of IAE Values(For P₂)

Controller	IAE Value
LADRC	7.8713
PPF-ADRC	5.9112

5. Conclusion

In this paper, based on the prescribed performance function and the idea of error transformation, we have proposed PPF-ADRC. Parameters of PPF-ADRC are chosen according to the bandwidth-parameterization approach and the physical explanation of prescribed performance function. Two typical examples are taken to confirm PPF-ADRC and its parameters tuning method. Numerical results confirm that, by introducing

nonlinear prescribed performance function and error transformation, PPF-ADRC not only has a relatively easier tuning approach, but also can improve the control performance effectively.

Acknowledgements

This work is supported by National Natural Science Foundation of China (61403006), Beijing Natural Science Foundation (4132005), The Importation and Development of High-Caliber Talents Project of Beijing Municipal Institutions (YETP1449), Project of Scientific and Technological Innovation Platform (PXM2015_014213_000063).

References

1. J.Q. Han, Auto-disturbance-rejection controller and it's applications, *Control and Decision* **13**(1) (1998) 19-23 (in Chinese).
2. J. Vincent, et al., On active disturbance rejection based control design for superconducting RF cavities, *Nuclear Instruments and Methods in Physics Research A*, **643**(1) (2011) 11-16.
3. Q.L. Zheng, et al., Active disturbance rejection control for piezoelectric beam, *Asian Journal of Control* **17**(1) (2015) 1-11.
4. W. Wei, et al., Compound active disturbance rejection control for resonance damping and tracking of nanopositioning, in *Proceeding of Chinese Control Conference*, (China, Nanjing, 2014), pp. 5906-5909.
5. Q. Zheng, et al., On stability analysis of active disturbance rejection control for nonlinear time-varying plants with unknown dynamics, in *Proceeding of the 46th IEEE conference on decision and control*, (USA, New Orleans, 2007), pp. 12-14.
6. Y. Huang and W. Xue, Active disturbance rejection control: methodology and theoretical analysis, *ISA Transactions* **53**(4) (2014) 963-976.
7. Z. Chen et al., On the stability of linear active disturbance rejection control, *Acta Automatica Sinica* **39**(5) (2013) 574-580 (in Chinese).
8. Z. Gao, Scaling and Bandwidth-Parameterization Based Controller Tuning, in *Proceedings of American Control Conference*, (USA, Denver, 2003), pp. 4989-4996.
9. W. Wang and C. Wen, Adaptive actuator failure compensation control of uncertain nonlinear systems with guaranteed transient performance, *Automatica* **46**(12) (2010) 2082-2091.
10. X. Chen, Active disturbance rejection controller tuning and its applications to thermal processed, Master Degree Thesis, (Tsinghua University, 2008).

Moving Robots Lies and Their Minds with Degree of Confidence in a Decentralized Autonomous FMS

Shizuka Tanaka

*Human and Information System Division, Gifu University, 1-1, Yanagido
Gifu-shi, Gifu, 501-1193, Japan*

Hidehiko Yamamoto

*Department of Mechanical Engineering, Gifu Univ., 1-1, Yanagido
Gifu-shi, Gifu, 501-1193, Japan*

Takayoshi Yamada

*Department of Mechanical Engineering, Gifu Univ., 1-1, Yanagido
Gifu-shi, Gifu, 501-1193, Japan
E-mail: t3128020@edu.gifu-u.ac.jp, yam-h@gifu-u.ac.jp, yamat@gifu-u.ac.jp
www1.gifu-u.ac.jp/~yamlab/*

Abstract

According to the previous study of a decentralized autonomous FMS using a mind, it is found that the production outputs decreased because an agent sometimes lies. To solve this problem, we study an AGV's lie. The study is that AGVs recognize the lie that each AGV sends. To do this, we propose to give a degree of confidence to the mind that each AGV has. By performing the production simulations with the degree of confidence, we improve the increase of the production outputs.

Keywords: Decentralized Autonomous FMS, AGVs Lie, Minimum Unit of Mind, Degree of Confidence.

1. Introduction

We've developed the computer control systems to realize a decentralized autonomous flexible manufacturing system (FMS). To do this, it is necessary to avoid the path interference of automated guided vehicles (AGVs) in a decentralized autonomous FMS. To solve this problem, we inserted an arrogant mind and a modest mind into AGVs to control AGVs' moving.

In a decentralized autonomous FMS with minds, it is assumed that the information provided by the agents is always correct. However, this is not the case in a real factory, where incorrect information can sometimes be sent as a result of machine failures. In this study, we define and find this incorrect information as a "lie" of AGV. Then, in the decentralized autonomous FMS including AGVs lies, we perform the moving control of the AGVs in order not to have a low productivity.

Specifically, we propose the method of finding lies using the AGV's position information. We also propose the method of controlling the AGV's moving using a degree of confidence.

2. Mechanism of Decentralized Autonomous FMS

2.1. Description of Decentralized Autonomous FMS

Fig.1 shows the example of a decentralized autonomous FMS factory. The factory floor has been divided into a grid pattern where AGV moves on the line. Then, a system of automated factory performs the production by carrying the product to parts of the warehouse and machining centers (MCs). A decentralized autonomous FMS does not have a management mechanism that controls the whole system between agents that constitute the system to the knowledge exchange, to determine the behavior by coordination.

© The 2016 International Conference on Artificial Life and Robotics (ICAROB 2016), Jan. 29-31, Okinawa Convention Center, Okinawa, Japan

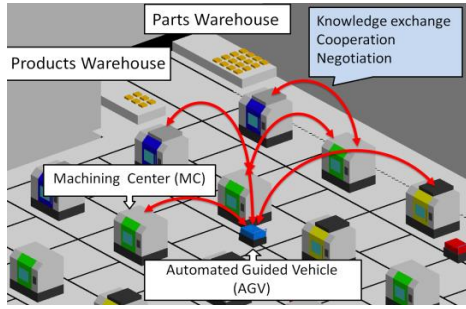


Fig.1. Example of decentralized autonomous FMS

2.2. Model of the Mind and Behavior of AGV

In the decentralized autonomous FMS, all AGVs use the position information received from the other AGVs and determine each behavior autonomously. In order to realize the autonomous behavior, we give a mind to AGVs. In the present study, in order to perform the behavior efficiently; we give the arrogant mind and the modest mind to AGVs. AGV with arrogant mind takes action approaching the destination forcibly. AGV with modest mind takes the action to give way to other AGV.

This mind is expressed in mind model in Fig.2, Minimum Unit of Mind (MUM)^[1]. Then, A1 and A2 called as unit, X is load, and arrow is a stimulation vector. The threshold is determined by the unit. If the internal value reaches the threshold, we call it "excited". And if it does not reach the threshold, we call it "normal".

When a signal is sent to the unit, it sends a signal to the direction of the arrow if it is excited, and it is not sent if it is normal. Load has the function to change the internal value of the unit. When the signal is sent to the load, the value of the unit is increased by the value of X. Stimulation vector is a line connecting the load and the unit, and it gives a signal to the load or unit if the signal comes. When A1 is kept excited, we call it "modest mind", and when normal, we call it "arrogant mind".

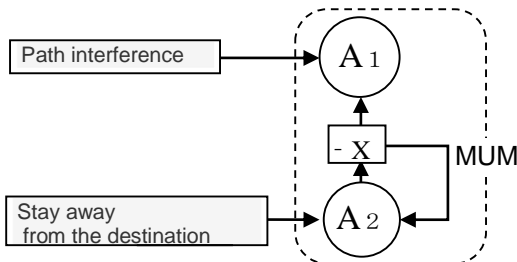


Fig.2. MUM

By the amount of the signal input to the unit, MUM changes the mind to arrogant or modest frequently.

Next, we describe the internal functions of MUM. When the arrogant AGV has path interference, A1 is increased by 1. Keeping the situation of the interference and being

increased by 1, the A1 value becomes the threshold, and the AGV is changed to a modest one.

When AGVs with a modest mind keep giving a way, the value of A2 is increased by 1. When the situation is repeated at optional times, A2 becomes excited and a signal is sent to a load. The received load decreases the values of units A1 and A2 by optional values. Owing to this, A1 and A2 are returned to normal and a modest mind is changed to an arrogant mind. In this way, AGV avoids the path interference by the change of heart.

3. Finding AGV's Lies

In the decentralized autonomous FMS using a mind from previous studies, each agent transmitted the information, treats the received information as all correct, works in cooperation each other. However, trouble including short-period stop occurs in the real FMS factory. To realize this real factory in this study, we adopt the decentralized autonomous FMS where failure occurs. We define the AGV as "liar" when the AGV sends a incorrect information and "honest" when the AGV sends a correct information. In this study, we focus on the lie that especially takes the AGV among the lie of the agent.

AGV's lies are defined as the following three types.

1. Although the current position is correctly taken, an AGV sends incorrect information to other AGVs. We call this as "USO1".
2. An AGV sometimes takes the current position for a different one and sends it. We call this as "USO2".
3. An AGV sometimes fails to read the current position and does not update the information. We call this as "USO3".

The state of the USO1 is shown in Fig 3. When USO1 occurs, correct position information is saved in the AGV that lied. However, incorrect information is saved in the other AGVs.

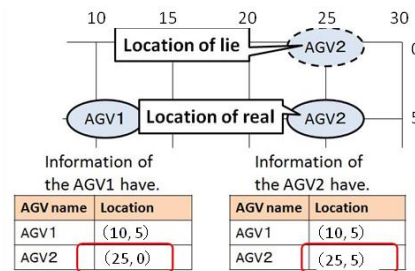


Fig.3. USO1

The state of the USO2 is shown in Fig 4. When USO2 occurs, both AGV that lied and other AGVs save incorrect information.

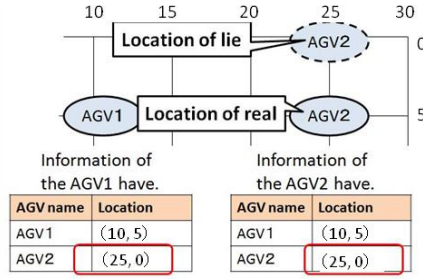


Fig.4. USO2

The state of the USO3 is shown in Fig 5. When USO3 occurs, the AGV that lied fails to read the current position. The AGV does not update the location information and does not send the information to other AGVs.

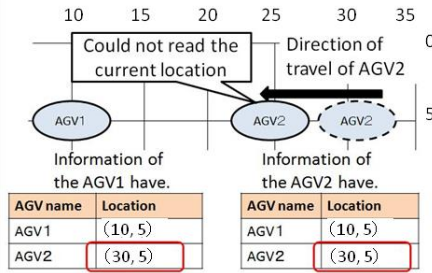


Fig.5. USO3

We propose the three methods to find the lies.

[1] The AGVs except for the liar AGV receive the information from the liar AGV, compare the liar AGV's current position with its previous positions and find the incorrect information. This is the method to find USO1.

When the information transmitted from the other AGV satisfies Equation (1), the AGV that has transmitted the information is defined as USO1.

$$|(\text{Past X-coordinate}) - (\text{Current X-coordinate})|$$

$$+ |(\text{Past Y-coordinate}) - (\text{Current Y-coordinate})| > 5 \quad (1)$$

[2] When the difference between the own current position and the previous position becomes big, the situation is called as USO2. When the AGV's information satisfies Equation (2), the AGV realizes as USO2.

$$|(\text{Past X-coordinate}) - (\text{Current X-coordinate})|$$

$$+ |(\text{Past Y-coordinate}) - (\text{Current Y-coordinate})| > 10 \quad (2)$$

[3] This is the method to find the USO3. When the AGV's information satisfies Equation (3), the AGV realizes as USO3

$$|(\text{Past X-coordinate}) - (\text{Current X-coordinate})|$$

$$+ |(\text{Past Y-coordinate}) - (\text{Current Y-coordinate})| = 10 \quad (3)$$

4. Mind with Degree of Confidence

If there are AGVs that lie, AGV that uses the incorrect information takes the wrong action. As a result, the number of production is reduced. In this study, we get the

© The 2016 International Conference on Artificial Life and Robotics (ICAROB 2016), Jan. 29-31, Okinawa Convention Center, Okinawa, Japan

honest AGV to work preferentially to solve this problem. To do this, we find the AGV to lie, to distinguish honest AGVs and liar AGVs. In order to achieve the distinguishing, we propose the new degree of confidence in the mind of AGV. And we adopt the method that higher confidence AGV acts preferentially.

In this study, we define the degree of confidence as "the degree which an AGV can correctly work without lie". When an AGV passes through the intersection without lie, the confidence of the mind of the AGV is increased. The higher the confidence, the more arrogant the AGV becomes. Because of this, the AGV does the work preferentially.

The way to give confidence is shown as the following.

1. When the AGV is passed through the intersection without lie, the mind of confidence is increased by 1.
2. If confidence has reached a threshold, the threshold value of the unit A1 is increased by 1, and the mind sets the confidence as 0.

The new mind model of Fig.6. is generated by adding MUM of Fig2 to a unit C, load Y, Z, and the stimulus vector. We define it as MUMS (MUM with Self-confidence degree). Unit C of MUMS is called degree of confidence; unit C has a threshold C[T] and excitement value C[E]. Load Y indicating by the triangle of Fig.6 sends a signal to the threshold A1[T]. Load -Z sends a signal to the excitement value C[E] of the unit C.

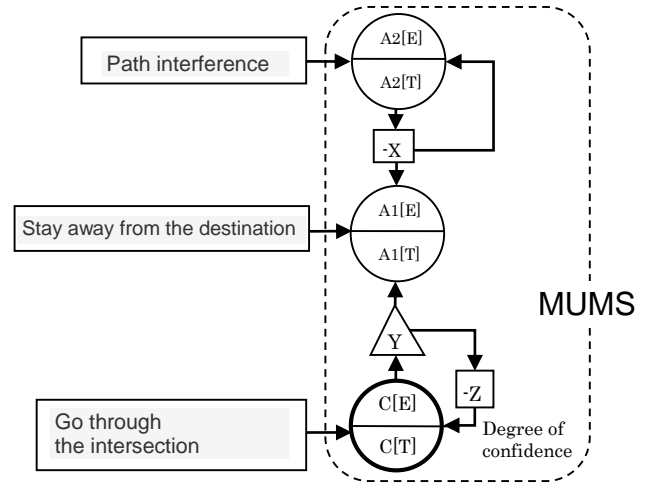


Fig.6 MUMS

Further, an function of the MUMS is shown below. When an AGV passes through the intersection without lie, a signal is sent to C[E]. In other words, the degree of confidence is increased. When C[E] continues to receive the signal, unit C becomes excited and sends a signal to the load Y and load -Z. Load Y increases A1[T], load -Z

reduces $C[E]$. In this way, when an AGV passes through the intersection without lie, $A1[T]$ is increased. When $A1[T]$ increases, unit $A1$ is hard to become the excited condition, that is, it is easy to have an arrogant mind. On the other hand, when an AGV passes through the intersection with lie, the signal is not sent to the unit C . Because of it, $A1[T]$ is not changed.

5. Simulation Results and Consideration

We simulated the production results. We set AGVs lie with a certain probability and carried out the production simulations by using the following four conditions.

- FMS just using honest AGVs
- FMS including AGVs that lie
- FMS including AGVs that lie, and the AGVs with MUMS (Set the threshold value $C[T]$ shown in Fig.6 as 500)
- FMS including AGVs that lie, and the AGVs with MUMS (Set the threshold value $C[T]$ shown in Fig.6 as 900)

The production simulations were carried out seven times under these conditions. Table.1 shows the average of the output of simulation production, the total number of collisions and the efficiency of each AGV.

Table.1. Simulation Results

	Honesty	Liar	Degree of Confidence(500)	Degree of Confidence(900)
Production Outputs	158.7	133.7	138.4	140.4
Collision Number	0	2159.9	2385.1	2236.7
Efficiency	AGV1	0.591	0.414	0.408
	AGV2	0.901	0.716	0.707
	AGV3	0.847	0.646	0.622
	AGV4	0.686	0.506	0.495
	AGV5	0.774	0.559	0.551

Table.2 also shows the adopted stimulus values of the degrees of confidence of AGVs.

Table.2. Stimulus number in the degree of confidence

	AGV1	AGV2	AGV3	AGV4	AGV5
$C[T]=500$	2	11	9	8	9
$C[T]=900$	0	6	4	6	4

From Table.1, comparing honest FMS with FMS including liar AGVs, the latter FMS reached to a bad production results 25 products, lower than the former FMS. Comparing the latter FMS with the FMS including AGVs with confidence, the number of production for the FMS with confidence was increased. The number of production for each condition, 500 and 900, was increased. The number of production with confidence

was close to the number of production with honest FMS. Because AGVs that have the characteristics easy to become arrogant and modest exist by confidence, the time required path interference avoidance is reduced.

In addition, comparing 500 with 900, the number of production for 900 is two more than 500. Table.2 shows that the case of $C[T]=500$ gave a lot of stimulations to the mind of AGVs. If $C[T]$ is too small, many signals are sent to $A1[T]$ and $A1[T]$ becomes too large. The larger $A1[T]$ is, the longer the time until the change of the mind is. As a result, the time to perform the judgment of the path interference avoidance becomes longer. Because of this, the magnitude of $C[T]$ affects the ease of the change of the mind and the number of production.

However, even using the degree of confidence, it was not possible to reduce the total interference number. This is because the interference occurs together with the lie. Even if using the degree of confidence, it is not possible to reduce the number of the lie itself.

6. Conclusions

This study found that finding the lie and a degree of confidence are useful for improving the production number in a decentralized autonomous FMS including AGVs that lie. This study also found that the magnitude of $C[T]$ affects the ease of the change of the mind and the number of production. We can establish the foundation of the way how to handle the lie.

In this study, the threshold value of the degree of confidence was determined in accordance with a certain probability of the lie happening. In the actual FMS factory, however, the agent does not lie with a certain probability. Therefore, it is necessary to determine the threshold of the confidence flexibly in a future work.

References

1. Hidehiko YAMAMOTO, Takayoshi YAMADA and Shinsuke KATO, AGV Mind Model and its Usage for Decentralized Autonomous FMS by Change of Mind, Proceeding of Third KES International Symposium, KES-AMSTA 2009, Agent and Multi- Agent Systems : Technologies and Applications, Lecture Notes in Artificial Intelligence, Edited by Anne Hakansson, Ngoc Thanh Nguyen etc. , ISSN 0302-9743, Uppsala, Sweden, pp.744-753, June(2009), Springer.

Conquest Oriented Robot Knowing Its Own Availability

Sho Yamauchi

*Future University Hakodate, 116-2, Kameda Nakanochi,
Hakodate-shi, Hokkaido, 041-0803, Japan,*

Keiji Suzuki

*Future University Hakodate, 116-2, Kameda Nakanochi,
Hakodate-shi, Hokkaido, 041-0803, Japan,
E-mail: yamauchi@fun.ac.jp, kjsuzuki@fun.ac.jp
www.fun.ac.jp*

Abstract

Robot is designed for achieving specific task. However, robot is able to do much more things than it is expected by its own hardware. In this paper, concept of conquest oriented robot is proposed to know its availability systematically and autonomously. Algorithm of conquest oriented robot and its experimental result in simulation field for the first step is shown in this paper.

Keywords: autonomous, conquest, robot, availability

1. Introduction

Robot is designed for achieving specific task. Cleaner robot is designed to collect dusts in room and industrial robot is designed to assemble some kind of merchandise in factory. These tasks are designed by human and the only thing robots do is complete the tasks. Previously, robot is just a tool to achieve some tasks that are hard for human or tool for automation. However, robot can do much more things by their body even though the thing is not expected to do by human. For example, Cleaner robot with two wheels can push something as well as cleaning. This means that the cleaner robot might bring something heavy and might communicate with human by pushing their hands, for example. Robot has lots of possibility by their given body and this possibility is not limited to the purpose expected by human. From these points of view, concept of conquest oriented

robot is proposed in this paper. Base algorithm to find what they can do by its body is proposed for the first step and experimental result using the algorithm is shown.

2. Concept of conquest oriented robot

The purpose of conquest oriented robot is finding, increasing and maintaining available things of the robot. Robot has its own available event in its existing environment (Fig. 1). In other words, conquest oriented robot tries to increase event that robot can execute with high probability, increase the probability and maintain its events and probability.

Comparison between previous robot design and conquest oriented robot is shown in Fig. 2. Robot is designed to reach only one event, it means “task”, previously. However, if the task is changed, robot must be re-

designed to achieve new task. On the other hand, conquest oriented robot researches its own availability previously and it can change its task easily if the new task is within its availability.

What is an advantage of conquest oriented robot? If robot knows its own availability, robot is able to do maximum work even though it does not know the task preliminarily. If the task is unavailable, robot is able to know it is unavailable by its given hardware. In this case, human should prepare another robot that has suitable hardware.

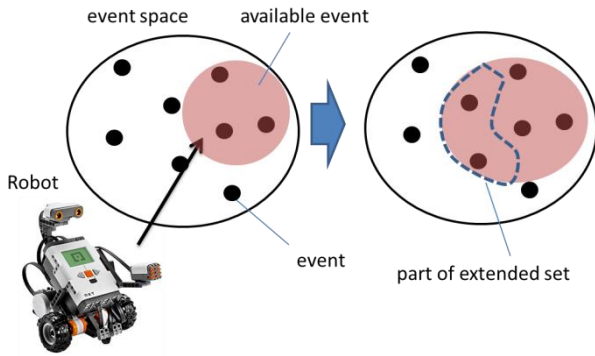


Fig. 1. Conquest oriented robot concept. Event space means a set of all the events that might happen in current environment. Conquest oriented robot tries to extend a set of event that is able to happen at any time.

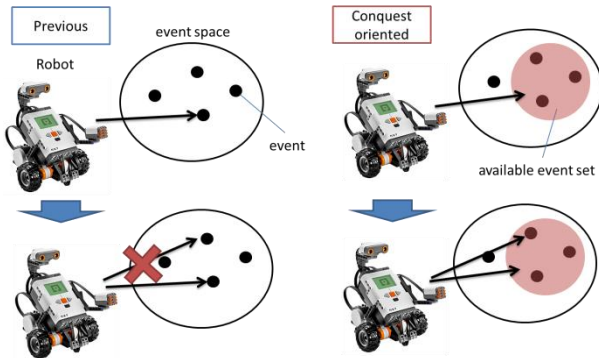


Fig. 2. Previous robot design and conquest oriented design. In previous robot design, the specific event is focused and robot tries to achieve the specific task. However, conquest oriented robot tries to find “what it can do” and maintain those things.

3. Action Fragment and Variable Action Generation

As a unit of robot’s available event, action fragment is introduced. Action fragment is a part of time-series data

of robot’s action as shown in Fig. 3. Action fragment \mathbf{F} is defined as

$$\mathbf{F} = [\vec{x}_1, \vec{x}_2, \vec{x}_3, \dots, \vec{x}_n] \quad (1)$$

$$\vec{x}_i = \begin{bmatrix} x_i^{(1)} \\ x_i^{(2)} \\ \vdots \\ x_i^{(m)} \end{bmatrix} = \begin{bmatrix} a_i^{(1)} \\ a_i^{(2)} \\ \vdots \\ a_i^{(n_a)} \\ b_i^{(1)} \\ b_i^{(2)} \\ \vdots \\ b_i^{(n_b)} \end{bmatrix} \quad (2)$$

where $a_i^{(k)}, b_i^{(k)}$ are k-th actuator output and sensor input at time i respectively .

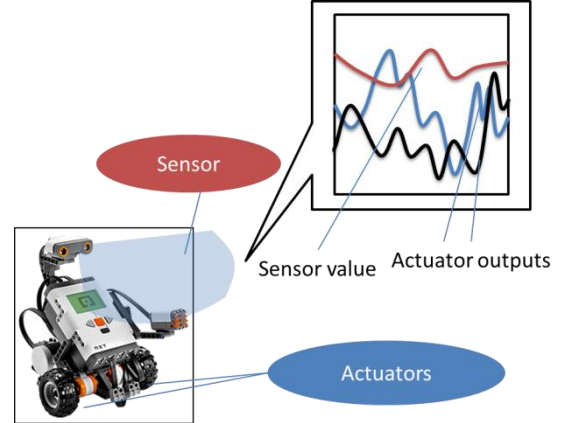


Fig. 3. Action fragment of conquest oriented robot. Action fragment is made of time series data of sensors and actuators.

Use Fourier series expansion to generate various types of time-series action for robot. Equation is as follows.

$$f(\omega t) = \frac{a_0}{2} + \sum_{n=1}^{n_{\max}} (a_n \cos n\omega t + b_n \sin n\omega t) \quad (3)$$

If coefficients a_n, b_n are changed periodically, various types of wave would be generated and this wave is used as actuator output of robot for generating various actions. To find new action fragment, robot has to detect whether the action fragment is different from all other experienced action fragments. It means that criterion to measure the difference between two action fragments is needed. For this purpose, criterion \mathbf{G} is introduced as follows.

$$G(\mathbf{F}_A, \mathbf{F}_B) = \frac{AMSS(\mathbf{F}_A, \mathbf{F}_B)}{S_{\max}} \quad (4)$$

$$S_{\max} = AMSS(\mathbf{F}_{\text{long}}, \mathbf{F}_{\text{long}}) \quad (5)$$

$$\mathbf{F}_{\text{long}} = \arg \max_{\mathbf{F} \in \{\mathbf{F}_A, \mathbf{F}_B\}} \{len(\mathbf{F})\} \quad (6)$$

where $\mathbf{F}_A, \mathbf{F}_B$ are compared action fragments. Function $len()$ returns length of action fragment's time series data. Function $AMSS()$ is also returns the value of AMSS between two action fragments. AMSS(Angular Metrics for Shape Similarity)[Ref. 1] is method to compare two time series data and calculate similarity. AMSS assume time series data as vector and calculate similarity by cos similarity and dynamic programming. It can be applied to time series data that are different length. In criterion \mathbf{G} , similarity is normalized and all the results can be compared with each other. The value of criterion \mathbf{G} is called similarity rate in this paper.

Robot stores new action fragment if new action fragment is different enough comparing with all the action fragments stored already as follows.

For all i , if similarity rate r_i satisfies condition

$$r_i = G(\mathbf{F}, \mathbf{F}_i) < c_{\text{acc_l}} \quad (7)$$

then store action fragment \mathbf{F}

where $c_{\text{acc_l}} (0 < c_{\text{acc_l}} \leq 1)$.

The process to store new action fragment is called “accumulate” in this paper. “Accumulate” is considered as the first step of conquest oriented robot.

4. Experiment

Confirm the process of “accumulate” in simple experiment. Consider a robot in 2D physics simulation field shown in Fig. 4. In this simulation field, a differential wheeled robot and two objects are placed. The robot can detect object in front of it and obtain the distance from detected object. It means that this robot has 1 sensor and 2 actuators.

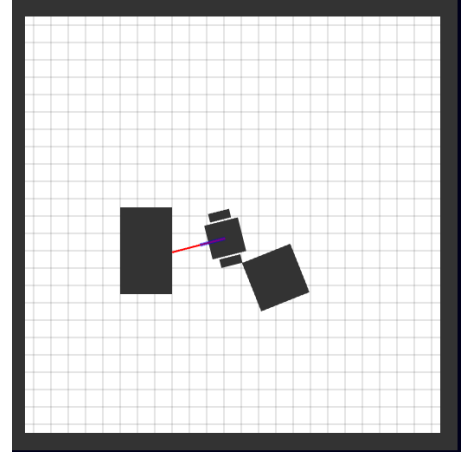


Fig. 4. 2D physics experimental field. Red line indicates the sensor of differential wheeled robot. Two objects are also placed.

Friction between wheels of robot and floor, objects and floor exists. Robot starts “accumulation” in this field and store action fragments. All the fragments have the same fixed length in this time. In this experiment, two types of action generating methods are applied. One changes coefficients in equation (3) periodically. Another does not change coefficients. If coefficients are changed periodically, various types of action of robot would be generated and number of action fragments is supposed to increase. However, action of robot is limited, so the number of action fragment is expected to be saturated eventually. On the other hand, if coefficients in equation (3) are fixed, generated action of robot is far more limited and number of stored action fragment is expected to be smaller.

Experimental result is shown in Fig. 5.

Horizontal axis denote time step and vertical axis mean s number of action fragments. “Update” is a case that coefficients in equation (3) are periodically updated.

“Fixed” means coefficients in equation (3) are fixed. As expected, number of action fragment saturated in both case. Also, as we expected, the number of action fragment in “Fixed” case is smaller than “Update”. This result means that criterion **G** for similarity rate works properly and “accumulation” phase algorithm works properly.

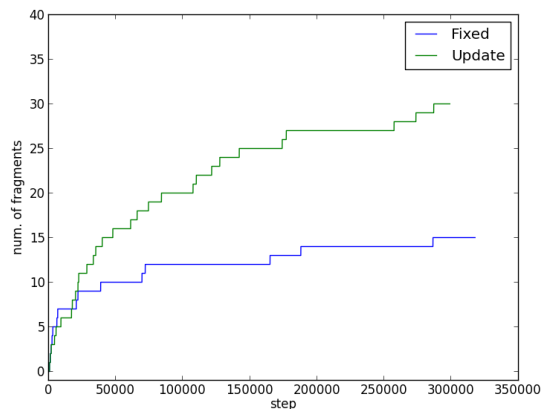


Fig. 5. Experimental result. Horizontal axis denote time steps and Vertical axis denote number of action fragments..

5. Conclusion

The concept of conquest oriented robot that tries to know its own availability is proposed in this paper. For the first step, algorithm of “accumulate”, the first phase of conquest oriented robot algorithm, is proposed. AMSS based similarity criterion is also introduced. “Accumulate” phase process is confirmed by experiment using differential wheeled robot in 2D physics simulation experiment field. We develop second and third phase of conquest oriented robot algorithm for the future work.

References

1. Tetsuya NAKAMURA, Keishi TAKI, Hiroki NOMIYA and Kuniaki UEHARA, *AMSS: A Similarity Measure for time Series Data*, *IEICE TRANSACTIONS on Information and Systems*, Vol.J91-D, No.11, pp.2579-2588, 2008.

A Consideration on Feature Extraction for Operation Skill Based on Control Engineering Approach

Kazushige Koiwai

*Institute of Engineering, Hiroshima University,
1-4-1, Kagamiyama, Higashihiroshima City, Hiroshima, 739-8527, Japan*

Yuntao Liao

*Graduate School of Engineering, Hiroshima University,
1-4-1, Kagamiyama, Higashihiroshima City, Hiroshima, 739-8527, Japan*

Toru Yamamoto

*Faculty of Engineering, Hiroshima University,
1-4-1, Kagamiyama, Higashihiroshima City, Hiroshima, 739-8527, Japan*

Takao Nanjo, Yoichiro Yamazaki, Yoshiaki Fujimoto

*Global Engineering Center, KOBELCO Construction Machinery CO., LTD.,
2-2-1, Itsukaichikou, Saeki-ku, Hiroshima City, Hiroshima, Japan*

*E-mail: koiwaik@hiroshima-u.ac.jp, liao-yuntao@hiroshima-u.ac.jp, yama@hiroshima-u.ac.jp
<http://www.hiroshima-u.ac.jp>*

Abstract

Social issue of reducing and aging population create difficulty in the transfer of professional skills on the field where the human-skill is needed for operation of some equipments. In this study, the operator is considered as a kind of controller that consists of CMAC-PID. CMACs calculate PID parameters to evaluate human-skill by their trajectories. As an example, the comparison of operator skills for an excavator will be performed.

Keywords: PID Controller, Human Skill Analysis, Neural Network

1. Introduction

Technologies of automation or manpower-saving are innovated in production fields. However, there are many industrial equipments to need human operation, i.e. the construction site, the crane operation and the building demolition work. The human-skill optimized by professionals exists in those fields. However, the transfer of skills is not processing in leading countries because of decreasing employed population, aging of professionals, increasing multinational workers and others. Therefore the quantification of the human-skill is required to

transfer and educate the optimized skills. Moreover, the quantification of human skill can be applied to automation and efficiency for the work.

As precedent studies, adaptive control of deburring robots based on human skill models is proposed by Liu and Asada¹. And the human-skill is considered as a kind of nonlinear controller. It consists of PID controller that interpret trajectories of parameters as a way to evaluate human skill². Then neural network is utilized for the architecture of nonlinear controller³. As one of artificial NNs, a cerebellar model articulation controller (CMAC) has been proposed that advantages are a simple structure

and short learning time⁴. Moreover CMAC-PID is proposed⁵ and the controller is applied to human skill evaluation⁶.

In this paper, human skills are evaluated by using CMAC-PID. As an application example, the comparison of operator skills for an excavator will be performed. The feature of professional skills will be extracted by trajectories of PID parameters.

2. Scheme for Evaluation of Human Skill

2.1. CMAC

The CMAC is a mathematical model based on a cerebellar information processing mechanism by using mapping function. The simple example of CMAC with 3weights, 4 labels and 2-dimensional input is shown in Fig.1. The input signals of S (3, 6) are mapped to the set of labels M {B, F, J} and {c, g, k}. Those labels indicate the location of weight tables and select the numbers 8, 9 and 3 form each weight. The sum of them 20 is the output of CMAC. If the teacher signal is 14, each weight are adjusted by the differential of the output and teachers signal 6 into the total weight number 3.

2.2. Architecture of Human Skill Evaluation

The architecture of human skill evaluation is shown in Fig.2. $y^*(t)$ and $u^*(t)$ are denoted as the system output and the system input by human operation. To evaluate the human skill, the human is considered as PID controller using CMACs that tune parameters. The following control law with the PID controller is considered:

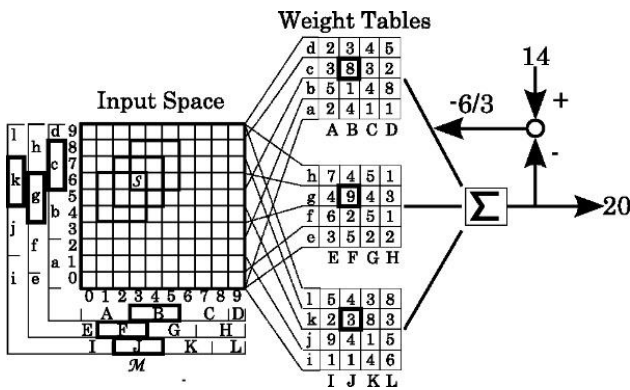


Fig. 1 The Sample of the CMAC Model

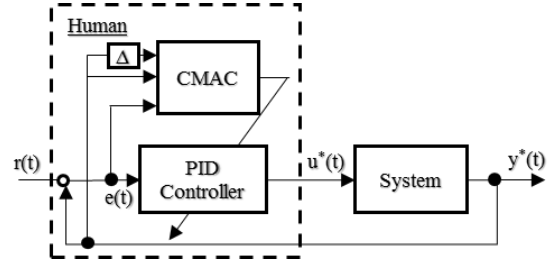


Fig. 2 The Architecture of Human skill Evaluation

$$\Delta u(t) = K_I e(t) - K_P \Delta y(t) - K_D \Delta^2 y(t) \quad (1)$$

where the control error signal of $e(t)$ is defined as $e(t) := r(t) - y(t)$ and the difference operator of Δ is defined as $\Delta := 1 - z^{-1}$. Each CMAC has some weights to calculate PID parameters in Eq.(2).

$$\begin{aligned} K_P(t) &= \sum_{h=1}^K W_{P,h}(t) \\ K_I(t) &= \sum_{h=1}^K W_{I,h}(t) \\ K_D(t) &= \sum_{h=1}^K W_{D,h}(t) \end{aligned} \quad (2)$$

$h = 1, 2, \dots, K$ is defined as the number of weight tables in each CMAC. CMACs which calculate PID parameters has 3-dimensional inputs of $e(t)$, $y(t)$ and $\Delta y(t)$. In Fig.3, the diagram of off-line learning manner is shown. CMACs learn those weights by using human skill data of $y^*(t)$ and $u^*(t)$. Those weights are updated by using the steepest descent method of the following Eq.(3). In the learning process, the differential of teachers signal $u^*(t)$ and the controller input signal $u(t)$ is reduced to express the human skill by PID controller.

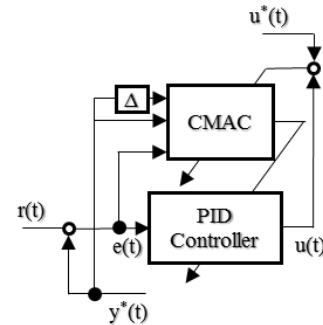


Fig. 3 The Learning Structure of Human Skill Evaluation

$$W_{P,h}^{new}(t) = W_{P,h}^{old}(t) - g(t) \frac{\partial J}{\partial K_p} \frac{1}{K}$$

$$W_{I,h}^{new}(t) = W_{I,h}^{old}(t) - g(t) \frac{\partial J}{\partial K_i} \frac{1}{K} \quad (3)$$

$$W_{D,h}^{new}(t) = W_{D,h}^{old}(t) - g(t) \frac{\partial J}{\partial K_d} \frac{1}{K}$$

where $g(t)$ is defined as the gradient to update weight and J is defined as the error criterion. Following equation are shown them.

$$g(t) = \frac{1}{c + a \cdot \exp(-b|u^*(t) - u(t)|)} \quad (4)$$

$$J(t) = \frac{1}{2} \epsilon(t)^2 \quad (5)$$

$$\epsilon(t) = u^*(t) - u(t) \quad (6)$$

Appropriate positive constant is set in a , b and c . And each partial differential of Eq.(3) is calculated as follows:

$$\frac{\partial J}{\partial K_p} = \epsilon(t) \Delta y(t)$$

$$\frac{\partial J}{\partial K_i} = -\epsilon(t) e(t) \quad (7)$$

$$\frac{\partial J}{\partial K_d} = \epsilon(t) \Delta^2 y(t)$$

3. Application Example

3.1. Equipment

The proposed scheme is applied to the excavator swing operation. The excavator which is used for experiment is SK200-9 by Kobelco Construction Machinery in Fig.4. Operators are accelerated by the maximum input from the starting point where is defined as 0 degree. After acceleration, they stop accurately at the target point that are 90 degrees. The skill for the stop operation is evaluated.

3.2. Application result

In this experiment, the system output value of $y^*(t)$ is the angle of swing and the system input value of $u^*(t)$ is the pilot pressure. The following procedure is performed to compare the professional skill and the beginner skill.

© The 2016 International Conference on Artificial Life and Robotics (ICAROB 2016), Jan. 29-31, Okinawa Convention Center, Okinawa, Japan



Fig. 4 Excavator for the Experiment

- (1) Obtain the data by operators. Here, those obtained data are normalized. And the sampling time of T_s should be 200ms with consideration for the human quickness of a response.
- (2) Calculate the initial values of PID parameters by the least squared method.
- (3) Learn CMACs according to Eq.(3)-(7). Here, each CMACs are designed as the number of weight tables and labels are 10 both of them.

The results by a professional operator and a beginner operator are shown in Fig.5 and Fig.6. The period of stop motions are 3 seconds to 5seconds on the both of them. Typically, the PID parameters have the following properties. The proportional action shows the responsiveness for the current information. The integral action shows the following performance based on the past information. In addition, the derivative action shows the forecast in the future. The following features are extract by the comparison of those result.

- (1) The beginner has higher proportional gain K_p and higher derivative gain K_d then the professional.
- (2) The professional decreases the proportional gain and increases the integrated gain and the derivative gain when the stop motion is started.
- (3) The beginner increases the proportional gain and decreases the derivative gain and the integrated gain at the stop.
- (4) The professional parameters are changed slightly. On the other hand, the changes of beginner is bigger than the professional relatively.

The professional changes parameters properly at the appropriate position. Increasing the derivative gain is to prevent the overshoot, and increasing the integrated gain is to follow the target value. And the decreasing of proportional gain keep the stability of system. That is, he keep the stability and following performance, and predict

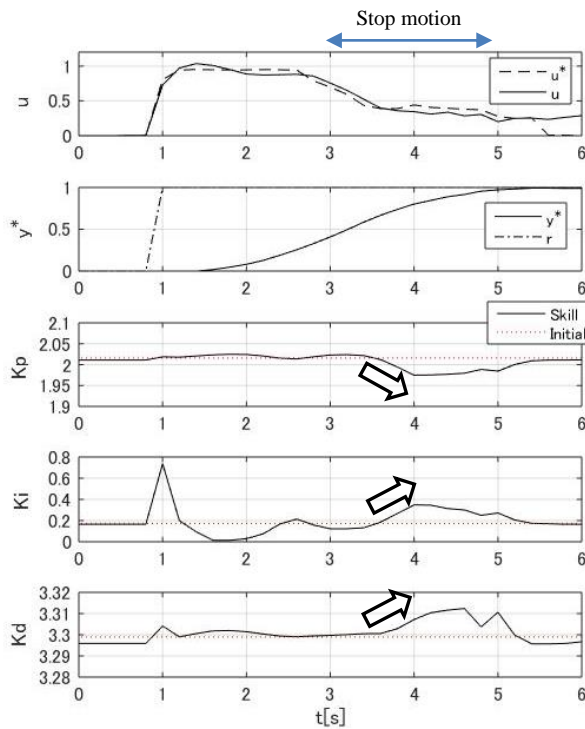


Fig. 5 Result of professional Skill Evaluation

the future. On the other hand, the beginner has the opposite reaction of all gains. He focuses to only the current information to give the higher proportional gain. And the initial values shows the stability margin. The beginner has bigger proportional and derivative gains than the professional. Therefore, the beginner is difficult to control the system properly by having bigger gains.

4. Conclusion

In this study, the evaluation scheme of human skill is proposed by using CMAC-PID. In order to verify the proposed scheme, it is applied to the excavator operation and the comparison of the beginner and professional is carried out. The feature of operation is extracted through trajectories of PID parameters are considered. It is possible to interpret operation skills from the control engineering approach. For the future work, it will be extended to another operation and other type of operator. And the stochastic method will be introduced.

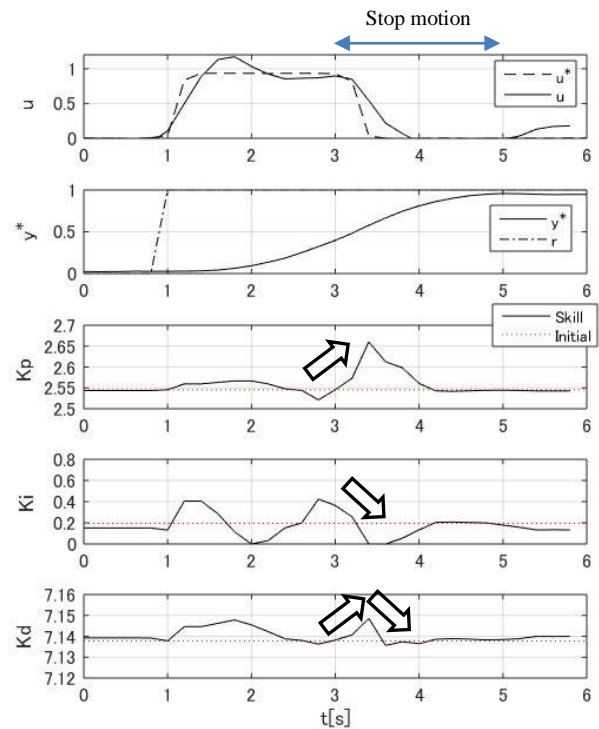


Fig. 6 Result of Beginner Skill Evaluation

5. References

1. S.Liu and H.Asada, Adaptive Control of Deburring Robots Based on Human Skill Models, *Proc. of IEEE Conf. on Decision and Control*, Brighton(1991), pp.348-353.
2. M.Kato, T.Yamamoto and S.Fujisawa A Skill-Based PID Controller Using Artificial Neural Networks, *Proc. of Int. Conf. on Computational Intelligence for Modeling, Control and Automation*, Vienna(2005), pp.702-705.
3. M.Tokuda, T.Yamamoto and Y.Monden, A Design of Multiloop PID Controllers with a Neural-Net Based Decoupler, *Asian Journal of Control*, Vol.7(3), (2005) pp.275-285
4. J.S.Albus A New Approach to Manipulator Control Cerebellar Articulation Control (CMAC), *Trans. on ASME, J. of Dynamics Systems, Measurement, and Control*, Vol.97, No.9,(1975), pp.220-227.
5. T.Yamamoto, R.Kurozumi and S.Fujisawa A Design of CMAC Based Intelligent PID Controllers, *Artificial Neural Networks and Neural Information Processing, Lecture Notes in Computer Science*, Vol.2714,(2003) pp.471-478.
6. K.Koiwai, K.Kawada and T.Yamamoto, Design and Experimental Evaluation of an Intelligent PID Controller using CMAC, *Proc. of IEEE Int. Conf. on Networking, Sensing and Control*, Okayama,(2009), pp740-745.

Design of a Data-Driven Control System for a Hydraulic Excavator

Takuya Kinoshita

*Graduate School of Engineering, Hiroshima University,
1-4-1, Kagamiyama, Higashihiroshima city, Hiroshima, Japan*

Kazushige Koiwai

*Collaborative Research Division, Institute of Engineering, Hiroshima University,
1-4-1, Kagamiyama, Higashihiroshima city, Hiroshima, Japan*

Toru Yamamoto

*Faculty of Engineering Division of Electrical, Systems and Mathematical Engineering, Hiroshima University,
1-4-1, Kagamiyama, Higashihiroshima city, Hiroshima, Japan*

Takao Nanjo, Yoichiro Yamazaki, Yoshiaki Fujimoto

*Global Engineering Center, KOBELCO Construction Machinery CO., LTD.,
2-2-1, Itsukaichikou, Saeki-ku, Hiroshima City, Hiroshima, Japan*

*E-mail: takuya--kinoshita@hiroshima-u.ac.jp, koiwaik@hiroshima-u.ac.jp, yama@hiroshima-u.ac.jp
<http://www.hiroshima-u.ac.jp>*

Abstract

PID control schemes have been widely used in most industrial systems. However, it is difficult to achieve the desired control performance for nonlinear systems such as hydraulic excavators by using fixed PID parameters. In order to overcome such a problem, data-driven PID control scheme based on database has been proposed. Moreover, data-driven scheme has a learning method in off-line by using closed-loop data. In this paper, data-driven control scheme is applied to a hydraulic excavator to get desired control performance.

Keywords: PID controller, Data-driven controller, Hydraulic excavators, off-line learning.

1. Introduction

In most industries, it is very important to get desired control performance by using some control schemes. PID control schemes^{1, 2} have been widely used because control parameters have a clear physical meaning and control structure is simple. However, it is very difficult to get desired control performance for nonlinear systems such as hydraulic excavators by using fixed PID parameters. In order to overcome such problem, data-driven PID control scheme³ based on database has been proposed. It

is a controller for nonlinear system and it has an off-line learning method by using closed-loop data.

In this paper, data-driven control scheme is applied to a hydraulic excavator to improve control performance. The effectiveness of the proposed scheme is numerically verified by using a simulation example.

2. Schematic Figure of a Hydraulic System

Fig.1 shows schematic of a hydraulic system⁴. As the system, the motion of system is swing operation. The input should be the direction of flow rate for a hydraulic pump, and the output should be this torque. In the

system, the relief valve works in order to prevent increasing hydraulic pressure. Therefore, the hydraulic system is a kind of time-variant system include a derivative element after the relief valve work. That why, it is difficult to get desired control performance by using fixed controller.

3. Schematic of Data-Driven Control System

Schematic of data-driven control system is shown in fig.2. The current information of controlled object is stored in a database and suitable control parameters are calculated by historical data in the database. Moreover, off-line learning method is utilized to avoid on-line learning time cost. The specific design procedure of data-driven scheme is described in section 7.

4. Controlled Object

A controlled object can be described by following nonlinear system:

$$y(t) = f(\phi(t-1)), \quad (1)$$

where $y(t)$ is system output, $f(\cdot)$ is function of nonlinear and $\phi(t-1)$ is information vector. $\phi(t-1)$ is defined as follows:

$$\phi(t-1) := [y(t-1), \dots, y(t-n_y), u(t-1), \dots, u(t-n_u)], \quad (2)$$

where $u(t)$ is system input, and n_y, n_u are the order of system output and input respectively. In data-driven control scheme, I/O data (equation (2)) are stored in the database.

5. Control law

Hydraulic system in Fig. 1 has derivative element. Therefore, controller with double integral element is needed and PII²D controller is defined as follows:

$$\Delta^2 u(t) = K_{II} e(t) + K_I \Delta e(t) - K_P \Delta^2 y(t) - K_D \Delta^3 y(t) \quad (3)$$

$$e(t) := r(t) - y(t), \quad (4)$$

where $e(t)$ denotes control error, and K_P, K_I, K_D and K_{II} respectively are proportional gain, integral gain, derivative gain and double integral gain. Furthermore, Δ denotes a difference operator.

6. Fictitious Reference Iterative Tuning: FRIT

FRIT⁵ is a scheme to calculate control parameters directly from closed-loop data which are input $u_0(t)$, output $y_0(t)$ and $e_0(t) = \tilde{r}(t) - y_0(t)$.

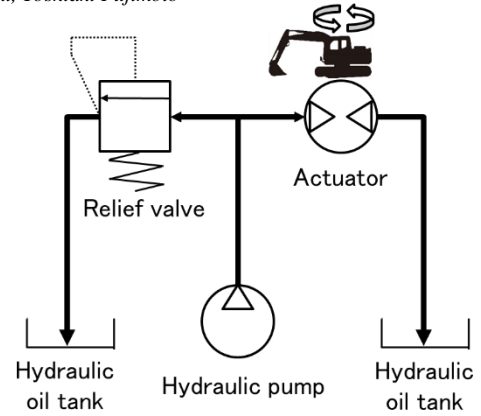


Fig. 1. Schematic of a hydraulic system.

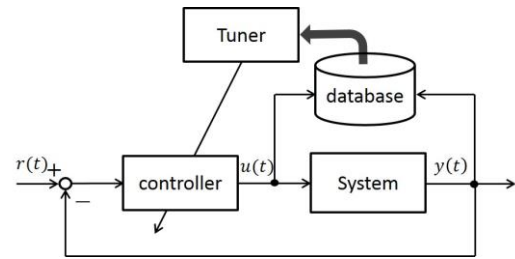


Fig. 2. Schematic of the data-driven control system.

$$\Delta^2 u_0(t) = K_{II} e_0(t) + K_I \Delta e_0(t) - K_P \Delta^2 y_0(t) - K_D \Delta^3 y_0(t) \quad (5)$$

Therefore, $\tilde{r}(t)$ is derived as follows:

$$\tilde{r}(t) = [\Delta^2 u_0(t) + K_I \tilde{r}(t-1) + \Delta^2 K_P y_0(t) + \Delta K_I y_0(t) + \Delta^3 y_0(t) + K_{II} y_0(t)] / (K_{II} + K_I). \quad (6)$$

In addition, user set a desired reference model expressed by following equation:

$$\tilde{y}_m(t) = \frac{z^{-1} P(1)}{P(z^{-1})} \tilde{r}(t), \quad (7)$$

where $\tilde{y}_m(t)$ is reference model output and $P(z^{-1})$ is user-specified polynomial. In FRIT, Control parameters are calculated to minimize difference between $\tilde{y}_m(t)$ and $y(t)$.

Here, $P(z^{-1})$ is designed based on the reference design as follows:

$$P(z^{-1}) := 1 + p_1 z^{-1} + p_2 z^{-2} \quad (8)$$

$$\left. \begin{aligned} p_1 &= -2 \exp\left(-\frac{\rho}{2\mu}\right) \cos\left(\frac{\sqrt{4\mu-1}}{2\mu} \rho\right) \\ p_2 &= \exp\left(-\frac{\rho}{\mu}\right) \\ \rho &:= \frac{T_s}{\sigma} \\ \mu &:= 0.25(1-\delta) + 0.51\delta \end{aligned} \right\} \quad (9)$$

where σ is a parameter related to the rise-time and δ is a parameter related to the damping oscillation. User set

them arbitrarily. σ denotes the time when output reaches about 60% of the step reference value. Moreover, δ is set between $0 \leq \delta \leq 2.0$ desirably. In particular, $\delta = 0$ indicates the response of Butterworth model and $\delta = 1.0$ indicates the response of Binominal model.

7. Design of a Data-Driven Controller

7.1. Design procedure

[STEP 1] Create an initial database.

The historical data is needed to use data-driven control scheme. Therefore, initial database is created by using Ziegler & Nichols: ZN method¹ and Chien, Hrones & Reswick: CHR method². The database are constructed by following information vector:

$$\phi(j) := [\bar{\phi}(j), K(j)] \quad (j = 1, 2, \dots, N) \quad (10)$$

$$\bar{\phi}(j) := [r(t+1), r(t), y(t), \dots, y(t-n_y+1), u(t-1), \dots, u(t-n_u)] \quad (11)$$

$$K(j) := [K_p(t), K_I(t), K_D(t), K_{II}(t)], \quad (12)$$

where N denotes the number of data. Since initial control parameters are fixed, which indicates $K(1) = K(2) = \dots = K(N)$.

[STEP 2] Calculate distance and select neighbors' data.

Distance between Query $\bar{\phi}(t)$ and $\bar{\phi}(j)$ is calculated by using the following L1-norm with some weights:

$$d(\bar{\phi}(t), \bar{\phi}(j)) = \sum_{l=1}^{m_y+n_u+1} \left| \frac{\bar{\phi}_l(t) - \bar{\phi}_l(j)}{\max \bar{\phi}_l(m) - \min \bar{\phi}_l(m)} \right| \quad (13)$$

$(j = 1, 2, \dots, N)$

$\bar{\phi}_l(j)$ denotes the l th element of query $\bar{\phi}(j)$.

$\max \bar{\phi}_l(m)$ is a maximum l th element in database. In contrast, $\min \bar{\phi}_l(m)$ is a minimum l th element. In addition, the number of neighbors' data k are selected, which data are based on smallest distance d .

[STEP 3] Calculate control parameters.

Control parameters are calculated by using the following linearly weighted average (LWA):

$$K(t) = \sum_{i=1}^k w_i K(i), \quad \sum_{i=1}^k w_i = 1, \quad (14)$$

where w_i is the weight corresponding to the i th information vector $\bar{\phi}(i)$ in the selected neighbors. It is calculated by following equation:

$$w_i = \frac{1/d_i}{\sum_{i=1}^k 1/d_i}. \quad (15)$$

In order to calculate effective control parameters, a learning method is needed. Therefore, an off-line learning method is described in next section.

7.2. Off-line learning method in Data-Driven Control scheme by using FRIT

In this section, an off-line learning method is described by using FRIT. At first, the number of neighbors' data k is selected and $K^{old}(t)$ is calculated by equation (14) using closed-loop data $u_0(t)$ and $y_0(t)$. Next, the following steepest descent method is utilized to modify the control parameters:

$$K^{new}(t) = K^{old}(t) - \eta \frac{\partial J(t+1)}{\partial K(t)} \quad (16)$$

$$\eta = [\eta_p, \eta_I, \eta_D, \eta_{II}],$$

where η denotes the learning rate and $J(t+1)$ is defined as following error criterion:

$$J(t) := \frac{1}{2} \epsilon(t)^2 \quad (17)$$

$$\epsilon(t) := y_0(t) - \tilde{y}_m(t), \quad (18)$$

The each partial differential of equation (16) are developed as follows:

$$\left. \begin{aligned} \frac{\partial J(t+1)}{\partial K_p(t)} &= \frac{\partial J(t+1)}{\partial \tilde{y}_m(t+1)} \frac{\partial \tilde{y}_m(t+1)}{\partial \tilde{r}(t)} \frac{\partial \tilde{r}(t)}{\partial K_p(t)} \\ &= \frac{\epsilon(t+1)P(1)\Delta^2 y_0(t)}{K_I + K_{II}} \\ \frac{\partial J(t+1)}{\partial K_I(t)} &= \frac{\partial J(t+1)}{\partial \tilde{y}_m(t+1)} \frac{\partial \tilde{y}_m(t+1)}{\partial \tilde{r}(t)} \frac{\partial \tilde{r}(t)}{\partial K_I(t)} \\ &= \frac{\epsilon(t+1)P(1)\Delta y_0(t)}{K_I + K_{II}} \\ \frac{\partial J(t+1)}{\partial K_D(t)} &= \frac{\partial J(t+1)}{\partial \tilde{y}_m(t+1)} \frac{\partial \tilde{y}_m(t+1)}{\partial \tilde{r}(t)} \frac{\partial \tilde{r}(t)}{\partial K_D(t)} \\ &= \frac{\epsilon(t+1)P(1)\Delta^3 y_0(t)}{K_I + K_{II}} \\ \frac{\partial J(t+1)}{\partial K_{II}(t)} &= \frac{\partial J(t+1)}{\partial \tilde{y}_m(t+1)} \frac{\partial \tilde{y}_m(t+1)}{\partial \tilde{r}(t)} \frac{\partial \tilde{r}(t)}{\partial K_{II}(t)} \\ &= \frac{\epsilon(t+1)P(1)\{y_0(t) - \tilde{r}(t-1)\}}{K_I + K_{II}} \end{aligned} \right\} \quad (19)$$

Therefore, control parameters can be learned off-line by using closed-loop data in equation (16) and (19).

8. Numerical Example

In this section, the effectiveness of the proposed scheme is verified. Table 1 shows the user-specified parameters included in proposed scheme.

Fig. 3 shows control results by using fixed PII²D control and proposed scheme. Initial control parameters in fixed PII²D controller are set as follows:

Table 1. User-specified parameters included in proposed scheme.

Rise-time	$\sigma = 0.2$
Damping property	$\delta = 0$
Order of information vector	$n_u = 4, n_y = 3$
Learning rate : $t \leq 4.0[s]$	$\eta = [2 \times 10^{-13}, 10^{-15}, 10^{-13}, 0]$
: $t > 4.0[s]$	$\eta = 3 \times [10^{-24}, 10^{-24}, 10^{-24}, 10^{-24}]$
Number of neighbors' data	$k = 3$
Reference signal	$r = 100$

$$K_p = 1.8 \times 10^{-6}, K_I = 9.0 \times 10^{-8}, K_D = 1.8 \times 10^{-5}, K_{II} = 0. \quad (20)$$

In equation (20), K_{II} equals to zero because this parameter is for a system without derivative element between $t = 2[s] - 4.0[s]$

In this case, system output can be reached to reference signal between $t = 2[s] - 4.0[s]$. However, after $4.0[s]$, it cannot be reached to reference signal because the system includes derivative element.

In proposed scheme, control performance is better than above control result since control parameters are adjusted. Trajectories of control parameters are show in Fig. 4. K_{II} is adjusted largely after $t = 4[s]$ because system has derivative elements.

9. Conclusion

This paper has proposed a data-driven control system for a hydraulic excavator. Control parameters should be adjusted because a hydraulic excavator is nonlinear system. In this paper, controller has been designed as PII^2D controller for derivative system. The effectiveness of proposed scheme has been numerically verified by using simulation example.

References

1. J.G.Ziegler and N.B.Nichols, "Optimum Settings for Automatic Controllers", *Trans. on ASME*, **64**(8) (1942) 759–768.
2. K.L.Chien, J.A.Hrones and J.B.Reswick, "On the automatic Control of Generalized Passice Systems", *Trans. ASME*, **74** (1952).
3. T. Yamamoto and K. Takao and T. Yamada, "Design of a Data-Driven PID Controller", *IEEE Trans on control systems Technology*, **17**(1) (2009) 29–39.
4. S. Okabe, "A Complete Work on Hydraulic Excavator (in Japanese)", Japan Industrial Publishing Co., LTD (2007).
5. S. Soma, O. Kaneko and T.Fujii, "A New Approach to Parameter Tuning of Controllers by Using One-Shot Experimental Data: A Proposal of Fictitious Reference Iterative Tuning (in Japanese)", *Trans. of the Institute of*

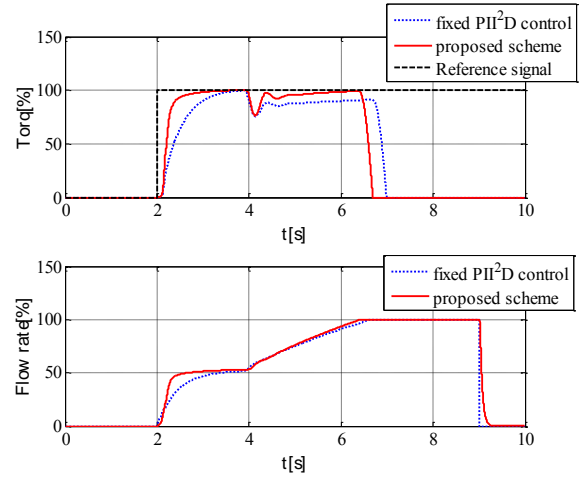
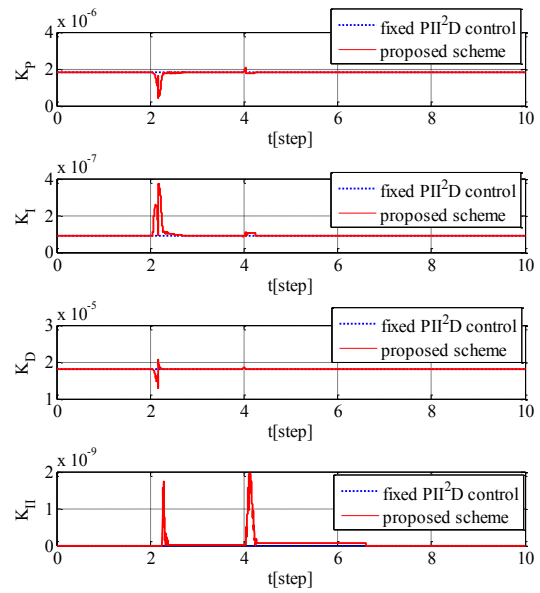
Fig. 3. Control results by fixed PII^2D control and proposed scheme.

Fig. 4. Trajectories of control parameters corresponding to Fig. 3.

systems, Control and Information Engineers, **17**(2) (2004) 528–536.

An Optimization of Spatio-Spectral Filter Bank Design for EEG Classification

Masanao Obayashi¹, Takuya Geshi², Takashi Kuremoto³ and Shingo Mabu⁴
Information Science and Design Engineering, Yamaguchi University, Tokiwadai 2-16-1
E-mail: {¹m.obayas,²t015vk,³wu,⁴mabu}@yamaguchi-u.ac.jp

Abstract

How to select the appropriate frequency band to classify EEG signal by motor imagery is discussed in this paper. Our proposal is an improvement of the conventional Bayesian Spatio-Spectral Filter Optimization (BSSFO). Defect of BSSFO is on the way to generate the renewal particle of the filter bank, such a random number generation. To avoid a local optimum, an evolutionary update method of particles is introduced. It is shown that performance of the EEG classification ability is improved.

Keywords: spatio-spectral filter, EEG, classification, .optimization, mutual information, common spatial filter

1. Introduction

Recently, researches using brain computer interface (BCI) have been actively studied. To precisely identify EEG signal, it is necessary to remove the artifact and noise by using appropriate spatial and spectral filter, Refs. 1-2. Furthermore, the best frequency bands identifying EEG signals depend on individuals and measurement environment, Ref. 3. Bayesian Spatio-Spectral Filter Optimization (BSSFO) is known as a powerful method to solve these problems, Ref. 4. However, BSSFO has also drawbacks that the obtained solution by it falls into sub-optimum. To overcome this drawback, we propose improvements of the preprocessing and update method of the filter bank in Ref. 4, to result in confirming effectiveness of our proposal.

2. Classification System

The classification system of EEG signals proposed by K. Suk, et al. Ref. 1 that is improved in this paper by us is shown in Fig.2. According to the flow of Fig.1, the contents are described in the following subsections.

2.1 Preprocessing

© The 2016 International Conference on Artificial Life and Robotics (ICAROB 2016), Jan. 29-31, Okinawa Convention Center, Okinawa, Japan

Laplacian smoothing is applied to all the EEG signals to reduce artifacts and noise as follows. The weight of the data in attention electrode surrounded by a green circle is 4 and that of each of four surrounding electrodes surrounded by red circles is -1. (See Fig.1) These weights are changed to optimal values in Section 3 by us (Improvement 1).

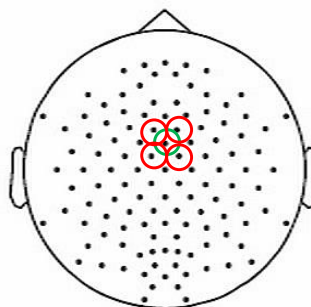


Fig. 1 Explanation of the weights of the EEG electrodes in smoothing of the EEG signal in the extended international 10/20 system used in this study

2.2 Spectral Filtering

The filter used in this paper is a fifth-order Butterworth bandpass-filter. The EEG signals of all the data sets are

bandpass-filtered between 4 Hz and 40 Hz covering both the μ -rhythm(8–14Hz) and β -rhythm(14–30Hz).

2.3 Common Spatial Pattern

Common Spatial Pattern (CSP) proposed by H. Ramoser, et al. in Ref. 2 is used in this paper. CSP is applied to the signals after bandpass filtering. CSP algorithm is for searching for the spatial weight to multiply to the EEG signals. The spatial weight W is gotten by solving the optimization problem of following a generalized eigenvalue problem:

$$\arg \max_W \frac{W^T \Sigma_1 W}{W^T \Sigma_2 W}, \quad (1)$$

where Σ_1 and Σ_2 are covariance matrices of each class. Σ_1 and Σ_2 are calculated as follows:

$$\Sigma_{1,2} = \mathbf{X}\mathbf{X}^T / \text{trace}(\mathbf{X}\mathbf{X}^T), \quad (2)$$

where \mathbf{X} means EEG signal matrix, and following:

$$\mathbf{X} = \begin{pmatrix} x_{1,1} & \cdots & x_{1,N} \\ \vdots & \ddots & \vdots \\ x_{C,1} & \cdots & x_{C,N} \end{pmatrix}, \quad (3)$$

where N is the number of signal samples, C means the number of electrodes. The first and last row vectors are taken as spatial patterns for class 1 and class 2, respectively.

2.4 Bayesian Spatio Spectral Filter Optimization (BSSFO)

Algorithm : BSSFO filter optimization algorithm

Input Data: $\{\mathbf{X}, \Omega\}$, K , m ,

$\mathbf{X} = \{\mathbf{x}_i\}_{i=1}^D$: Set of EEG signal, D : amount of trial,

$\Omega = \{\omega_i\}_{i=1}^D$: Set of class labels, where $\omega_i \in \{+1, -1\}$,

K : The number of particles,

m : The half number of spatial patterns to be determined in a spatial pattern learning algorithm

Output Data :

$\hat{B} = \{\hat{\mathbf{b}}_j, \hat{\pi}_j\}_{j=1}^\eta$: Set of optimal particles,

$\hat{W} = \{\hat{W}_j\}_{j=1}^\eta$: Set of optimal spatio filters,

η : the number of particles

Optimization:

Initialization :

• $\hat{\mathbf{B}}^{old} = \{\mathbf{b}_k^{old}, \pi_k^{old}\}_{k=1}^K$

- $\mathbf{b}_k^{old} = \{b_k^s, b_k^e\}$

- $\pi_k^{old} = \frac{1}{K}$: Weight of k th particle

while stopping criterion not satisfied **do**

if the first iteration **then**

$B^{new} = B^{old}$

else

$B^{old} = B^{new}$

$\psi(k) = 0, \forall k \in \{1, \dots, K\}$

for $k = 1$ to K **do**

Generate a random number $r \in \{0, 1\}$, uniformly distributed.

Find the largest j for which $r \geq \sum_{n=1}^j \pi_n$,

$\psi(j) = \psi(j) + 1$,

Improve $\mathbf{b}_k^{new} = \begin{cases} \mathbf{b}_j^{old} + N(0, \mathbf{R}) & \text{if } \psi(j) > 1 \\ \mathbf{b}_j^{old} & \text{otherwise} \end{cases}$

end

end

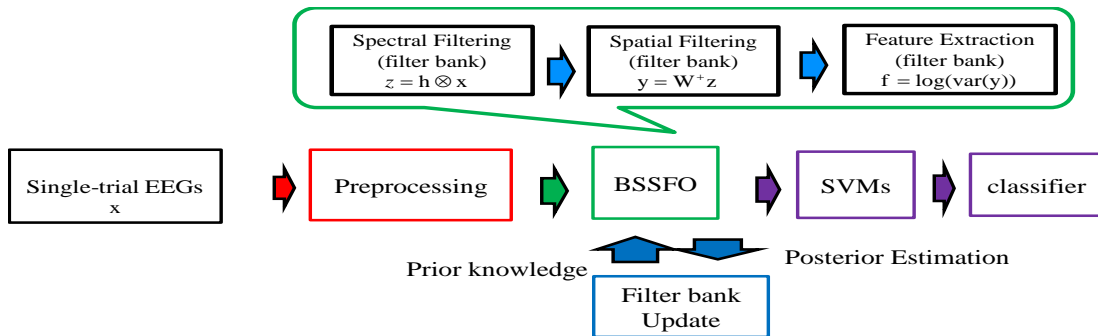


Fig. 2 Whole structure of the EEG classification system proposed by K. Suk, et al. Ref. 1

```

for k=1 to K do
   $\mathbf{Z}_k = \mathbf{h}_k^{new} \otimes \mathbf{X}$  /* Perform a bandpass filter */
  Solve  $\mathbf{W}_k (\sum^{(+)} + \sum^{(-)}) \mathbf{W}_k = \mathbf{I}$ 
  /* Perform a CSP algorithm */
   $\hat{\mathbf{W}}_k$  = the first m and the last m column vectors in  $\mathbf{W}_k$ 
  for i = 1 to D do
     $\mathbf{f}_k^i = \log [\text{var} (\hat{\mathbf{W}}_k^+ \mathbf{z}_k^i)]$  /*  $\mathbf{F}_k = \{\mathbf{f}_k^i\}_{i=1}^D$  */
  end
   $\mathbf{I}(\mathbf{F}_k; \Omega) = \mathbf{H}(\mathbf{F}_k) - \{\mathbf{H}(\mathbf{F}_k | \omega = +1)\} + \mathbf{H}(\mathbf{F}_k | \omega = -1)\}$ 
   $p(\mathbf{F}_k, \Omega | \mathbf{B}_k) \equiv \exp\{\mathbf{I}(\mathbf{F}_k; \Omega)\}$ 
  /* Update the weight of particles */
  end
   $\mathbf{B}^{new} = \{\mathbf{b}_k^{new}, \hat{\pi}_k^{new}\}_{k=1}^K$ 
end
 $S = \bigcup_k (\pi_k > \tau), k \in \{1, 2, \dots, K\}$ 
 $\hat{\mathbf{B}} = \{\mathbf{b}_j^{new}, \hat{\pi}_j^{new}\}_{j \in S}, \hat{\mathbf{W}} = \{\hat{\mathbf{W}}_j\}_{j \in S}$ 

```

2.5 Feature Extraction

After spectral and spatial filtering, we get the feature vector \mathbf{F}_k of k th particle as follows:

$$\mathbf{F}_k = \{\mathbf{f}_k^i\}_{i=1}^D, \quad \mathbf{f}_k^i = \log [\text{var} (\hat{\mathbf{W}}_k^+ \mathbf{z}_k^i)]. \quad (4)$$

Using \mathbf{F}_k , mutual information $\mathbf{I}(\mathbf{F}_k; \Omega)$ between \mathbf{F}_k and class label Ω is calculated as follows:

$$\mathbf{I}(\mathbf{F}_k; \Omega) = \mathbf{H}(\mathbf{F}_k) - \{\mathbf{H}(\mathbf{F}_k | \omega = +1)\} + \mathbf{H}(\mathbf{F}_k | \omega = -1)\}, \quad (5)$$

where $\mathbf{H}(\mathbf{F}_k)$ and $\mathbf{H}(\mathbf{F}_k | \omega = c)$ are defined as following equations.

$$\mathbf{H}(\mathbf{F}_k) \cong -\frac{1}{D} \sum_{i=1}^D \log \left[\frac{1}{D} \sum_{j=1}^D \hat{p}(\mathbf{f}_k^i) \right], \quad (6)$$

$$\mathbf{H}(\mathbf{F}_k | \omega = c) \cong -\frac{1}{D_c} \sum_{i \text{ s.t. } \omega_i = c} \log \left[\frac{1}{D_c} \sum_{j \text{ s.t. } \omega_j = c} \hat{p}(\mathbf{f}_k^i - \mathbf{f}_k^j, \nu) \right], \quad (7)$$

$$\hat{p}(\mathbf{f}_k) = \frac{1}{D} \sum_{i=1}^D \varphi(\mathbf{f}_k - \mathbf{f}_k^i, \nu), \quad (8)$$

$$\varphi(\mathbf{a}, \nu) = \frac{1}{(2\pi)^{d/2} \nu^d |\Sigma|^{1/2}} \exp \left[-\frac{\mathbf{a}^+ \Sigma^{-1} \mathbf{a}}{2 \nu^2} \right], \quad (9)$$

where D and D_c are the total number and class c of trials and Σ is the covariance matrix. The weight π_k of the classification result weight of particle k is calculated as follows:

$$\pi_k = \frac{\exp[\mathbf{I}(\mathbf{F}_k; \Omega)]}{\sum_j \exp[\mathbf{I}(\mathbf{F}_j; \Omega)]}. \quad (10)$$

© The 2016 International Conference on Artificial Life and Robotics (ICAROB 2016), Jan. 29-31, Okinawa Convention Center, Okinawa, Japan

2.6 Classifier

A Gaussian kernel-based SVM is used in this paper. An optimal filter bank S with the set of class-discrimination frequency bands selected by the following rule:

$$S = \bigcup_k (\pi_k > \tau), \quad (11)$$

where $k \in \{1, 2, \dots, K\}$ and τ denotes a threshold parameter that is determined empirically. The class label is determined by the following rule:

$$\hat{c} = \arg \max_{c \in \{+, -\}} \left\{ \sum_{k=1}^{|S|} \pi_k \cdot \Phi_k^c(\mathbf{f}_k^*) \right\}, \quad (12)$$

where $|S|$ denotes the size of the optimal filter bank S , \mathbf{f}_k^* denotes the feature vector from the input signal-trial EEG \mathbf{x}_i^* , and $\Phi_k^c(\mathbf{f}_k^*)$ is the result of a SVM which classifies the EEG into the class c , in the k th frequency band.

3. Improvement of the method

We propose two improvements of the method mentioned above.

3.1 Improvement 1

The first is that in the Laplacian smoothing, the weight value 4 of the data in attention electrode surrounded by a green circle in Fig. 1 is changed to 5 to enhance the signal of the attention electrode. .

3.2 Improvement 2

The second is that the improvement as to the update method of the particles which are for band start and end positions of bandpass filter. Use of the update method of the conventional method results in that particles with semi higher amount of information are remained, as a result, particles would be biased. For improvement, remove the half of all particles from the lower amount of information. Then, two particles with higher amount of information are selected stochastically, crossing them, new particles are generated. After that, particles between 1/4 and half from highest amount of information are re-initialized shown in Fig. 3.

Re-initializing of particles is to generate particles by use of following probability density function:

$$p(\mathbf{B}) = \frac{1}{2} N(\boldsymbol{\mu}, \Sigma_{\boldsymbol{\mu}}) + \frac{1}{2} N(\boldsymbol{\beta}, \Sigma_{\boldsymbol{\beta}}) \quad (13)$$

The crossing method of two particles is as follows:

$$(b_k^s, b_k^e)^{new} = \alpha_1 (b_k^s, b_k^e)^{old1} + \alpha_2 (b_k^s, b_k^e)^{old2}, \quad (14)$$

where the weights α_1, α_2 are set to 0.9 and 0.1, respectively, in next simulation to avoid generation of particles that both particles become far away.

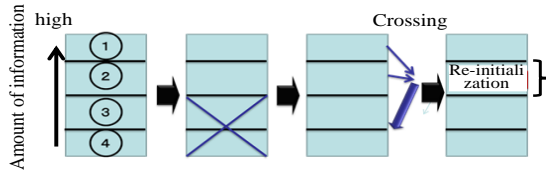


Fig. 3 Our proposed update method of particles

4. Computer simulation

4.1 Data set, simulation condition and results

EEG data set used in this simulation is Data set Iva in the BCI Competition III, in Ref. 5. The conditions to take these data is shown in Table 1. Table 2, 3, and 4 show the simulation results that update method of particles of both conventional and improvement 2 are common, but without preprocessing, with conventional preprocessing, and with preprocessing improvement 1, respectively. In all cases, our proposed method is superior to conventional one.

Table 1 Simulation condition

EEG data	
the number of sampling	200
sampling rate	100 [Hz]
used time of EEG data	0.5[s]~2.5[s]
the number of electrodes	118
BSSFO	
the number of particles	15
width of frequency band	4 ~ 40 [Hz]
The number of loop algorithm	10

Table 2 Simulation results of both update methods of particles without preprocessing

update method		subjects					average
		aa	al	av	aw	ay	
conventional	average	70.54	99.82	60.56	76.25	56.67	72.77
Improvement 2	average	72.86	99.64	63.21	70.58	69.13	75.08

Table 3 Simulation results of both update methods of particles with conventional preprocessing

update method		subjects					average
		aa	al	av	aw	ay	
conventional	average	40.29	87.5	56.68	64.06	49.6	61.43
Improvement 2	average	53.57	91.61	53.67	65.54	50.36	63.95

Table 4 Simulation results of both update methods of particles with preprocessing with improvement 1

update method		subjects					average
		aa	al	av	aw	ay	
conventional	average	72.23	98.75	60.51	677.1	55.36	72.79
Improvement 2	average	73.3	99.64	61.99	74.91	69.88	75.9

5. Conclusion

In this paper, we intended to improve the update method of particles of the conventional method “BSFFO” that mean improvement of frequency bandpass filters and also to improve the preprocessing method. As a result, it is verified that our method is useful.

References

1. H. Ramoser, J. Muller-Gerking, and G. Pfurtscheller, “Optimal Spatial Filtering of Single Trial EEG during Imagined Hand Movement”, IEEE Trans. Rehabilitation Eng., vol. 8, no. 4, pp.441-446, Dec. 2000.
2. Fikri Goksu, Nuri F. Ince, Ahmed H. Tewfik, “Greedy solutions for the construction of sparse spatial and spatio-spectral filters in brain computer interface applications”, Neurocomputing, vol. 108, no. 2, pp.69-78, May. 2013.
3. H. Ramoser, J. Muller-Gerking, and G. Pfurtscheller, “Optimal Spatial Filtering of Single Trial EEG during Imagined Hand Movement”, IEEE Trans. Rehabilitation Eng., vol. 8, no. 4, pp.441-446, Dec. 2000.
4. Heung-Il Suk, Seong-Whan Lee, “A Novel Bayesian Framework for Discriminative Feature Extraction in Brain-Computer Interfaces”, IEEE Transactions. Pattern Analysis and Machine Intelligence, vol. 35, no. 2, pp.286-299, Feb. 2013.
5. http://bbci.de/competition/iii/desc_IVa.html

Design and Analog Circuit Implementation of a Dynamic Feedback Control System Based on RLC Series Circuit

Hong Niu

*College of Electronic Information and Automation, Tianjin University of Science & Technology
80 Mailbox, Tianjin University of Science & Technology, No. 1038 Dagu Nanlu, Hexi District, Tianjin, China 300222*

Yongjun Wu

*College of Electronic Information and Automation, Tianjin University of Science & Technology
Tianjin, 300222, China*

Dongcheng Tan

*College of Electronic Information and Automation, Tianjin University of Science & Technology
Tianjin, 300222, China
E-mail: spots@163.com
www.tust.edu.cn*

Abstract

The purpose as expected performance. The simulation results of the theoretical model and the corresponding results of the real analog circuit implementation are given in the paper to illustrate that the circuit can accomplish the track of this paper is to verify that a dynamic feedback control system can be realized by a simple small analog circuit. A normal RLC series circuit, which is an electrical two-order circuit only consisting of one resistor, one inductor and one capacitor, is taken as the controlled object, and the voltage of the capacitor is taken as the output of the system. The engineering design method of regulator in DC drive control system is applied to design the dynamic feedback compensator, so that the output of the system can track the given input, and the system is stabilized and having function of dynamic feedback control system.

Keywords: dynamic output feedback; engineering design method; dynamic compensator; analog circuit implementation

1. Introduction

The servo system is a normal type in electric driving automatic control system. To facilitate engineering applications, scholars have put forward a variety of engineering design methods to simplify the regulator design procedure.¹⁻⁵ The purpose of this paper is to design a dynamic feedback compensator with the engineering design method and make the design procedure separate from the complex application background of electric drive system. In this paper, a

simple analog circuit will be implemented to achieve the input tracking performance of the servo system.

2. Design of Dynamic Feedback Compensator Based on Engineering Design Method

The structure of RLC series circuit is shown in Fig. 1. From Fig. 1, the state equation of the circuit can be formulated as

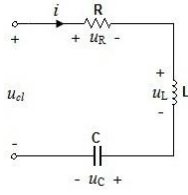


Fig. 1. RLC series circuit

$$u_{cl} = u_L + u_R + u_C = LC \frac{d^2 u_C(t)}{dt^2} + RC \frac{du_C(t)}{dt} + u_C(t). \quad (1)$$

Take the RLC series circuit as the controlled object, and let the voltage of the capacitor u_C be the output of the system. The transfer function of the RLC series circuit can be presented as

$$G(s) = \frac{U_C(s)}{U_{cl}(s)} = \frac{1}{LCs^2 + RCs + 1}. \quad (2)$$

Where $u_C(0) = 0$, and $i(0) = 0$.

Let $L = 10$ mH and $C = 1$ μ F. To make the circuit non-oscillatory, the resistance of the resistor R should be $R > (L/C)^{1/2} = 200 \Omega$.

Eq. (2) is transformed as

$$G(s) = \frac{1}{\left(\frac{1}{R}s + 1\right)(RLCs + 1)} = \frac{1}{(T_1s + 1)(T_2s + 1)}. \quad (3)$$

So that the engineering design method can be applied to design the dynamic feedback compensator.

To make Eq. (3) and Eq. (2) equal, the resistance should be $R = [1/C/(1-L)]^{1/2} \approx 1$ k $\Omega > 200 \Omega$, which satisfies the non-oscillatory condition. Then, $T_1 = 1/R = 10^{-3}$, and $T_2 = RLC = 10^{-5}$.

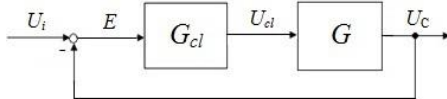


Fig. 2. Block diagram of dynamic feedback control system

The block diagram of the dynamic feedback control system is shown in Fig. 2. The engineering design method, which is simple and can simplify the design procedure, is often used to design the regulator for the DC drive control system. In this paper, the engineering design method is applied to design the dynamic feedback compensator $G_{cl}(s)$, such that the output signal $u_C(t)$ can track the given input signal $u_i(t)$.

To ensure the safety requirements of the elements and the performance of the closed-loop system, such as stability, accuracy and rapidity, the closed-loop system should be designed as a typical I system according to Ref. 1, because the overshoot of the typical I system is smaller than that of the typical II system. Moreover, the typical I system has an acceptable dynamic performance that satisfies the control require of this paper. The open-loop transfer function of the typical I system is

$$G_1(s) = G_{cl}(s)G(s) = \frac{K}{s(Ts + 1)}. \quad (4)$$

From Eq. (4) and Eq. (3), the dynamic feedback compensator $G_{cl}(s)$ can be formulated as

$$G_{cl}(s) = \frac{K_{pi}(\tau_1s + 1)}{\tau_1s}. \quad (5)$$

Where $\tau_1 = T_1 = 10^{-3}$. Thus, the control signal $u_{cl}(t)$ is represented as

$$u_{cl}(t) = K_{pi}e(t) + \frac{K_{pi}}{\tau_1} \int e(t)dt. \quad (6)$$

Substitute Eq. (3) and Eq. (5) into Eq. (4). Then,

$$G_1(s) = G_{cl}(s)G(s) = \frac{K_{pi}/\tau_1}{s(T_2s + 1)} = \frac{K}{s(Ts + 1)}. \quad (7)$$

Where $K = K_{pi}/\tau_1$, and $T = T_2 = 10^{-5}$.

To guarantee the good tracking performance of the system, let $KT = 0.5$ so that the damping ratio of the system is $\xi = 0.707$. Therefore, $K_{pi} = K\tau_1 = 0.5\tau_1/T = 50$.

From Fig. 2 and Eq. (7), the closed-loop transfer function is formulated as

$$\varphi(s) = \frac{G_1(s)}{1 + G_1(s)} = \frac{K}{Ts^2 + s + K}. \quad (8)$$

It is easy to prove that all of the eigenvalues of Eq. (8) have the negative real parts, so the closed-loop system is stabilized.

When the given input signal is a step signal whose amplitude is a , i.e., $u_i(t) = a \cdot 1(t)$ and $U_i(s) = a/s$, the steady-state error of the system (8) is

$$e_{ss} = \lim_{s \rightarrow 0} sE(s) = 0. \quad (9)$$

When the given input signal is a ramp signal whose slope is b , i.e., $u_i(t) = b \cdot t \cdot 1(t)$ and $U_i(s) = b/s^2$, the steady-state error of the system (8) is

$$e_{ss} = \lim_{s \rightarrow 0} sE(s) = b/K. \quad (10)$$

According to the output saturation voltage of the operational amplifier, the parameters a and b should not be too large to avoid distortion of the output signal. Because the parameter $K = K_{pi}/\tau_1 = 5 \times 10^4$, which is large enough, the steady-state error of the system (8) under the ramp signal input is also equal to 0, i.e., $e_{ss} = 0$.

When the given input signal is a sine signal whose amplitude is A , i.e., $u_i(t) = A \cdot \sin(\omega t)$ and $U_i(s) = A\omega/(s^2 + \omega^2)$, the steady-state error of the system (8) is

$$e_{ss} = \lim_{s \rightarrow 0} sE(s) = 0. \quad (11)$$

Similarly, the amplitude of the input sine signal should also be kept in a proper range.

3. Numerical Simulation

In this paper, there are three different given input signals. The first one is a square wave, the second one is a triangular wave, and the third one is a sine wave, as shown in Fig. 3(a). The corresponding output response waves are shown in Fig. 3(b).

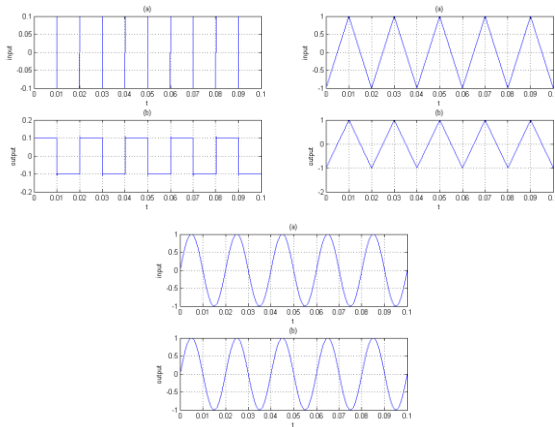


Fig. 3. Waves of the input signal and the output signal: (a) input; (b) output

The numerical simulation waves illustrate that the output signals can track the different given input signals

well. It demonstrates that the dynamic feedback compensator designed by the engineering design method is feasible and effective.

4. Circuit Implementation

The analog circuit implementation of the servo system (8) is shown in Fig. 4. The type and parameters of the elements have been labelled in the figure. The real output response waves under the same input signals of the numerical simulation are shown in Fig. 5.

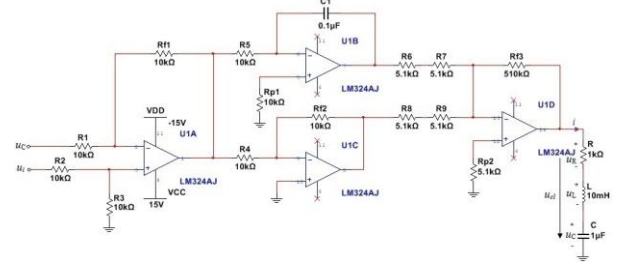


Fig. 4. Analog circuit implementation of the servo system (8)

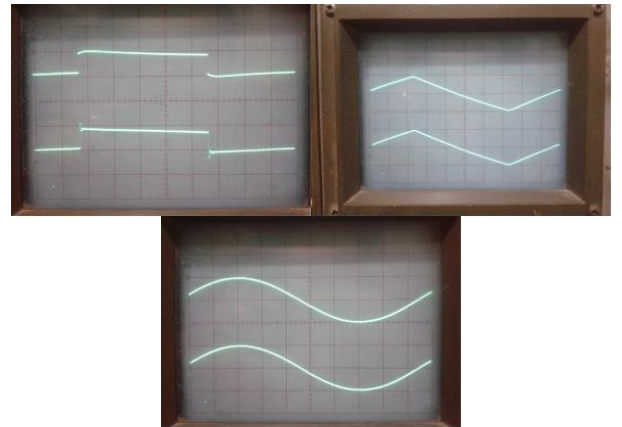


Fig. 5. Real waves of the input signal and the output signal: (up) input; (down) output

By comparing Fig. 5 with Fig. 3, it can be verified that there is a good qualitative agreement between the numerical simulation and the experimental realization. It shows that the real analog circuit accomplishes the purpose of tracking the given input signals.

Furthermore, the amplitude of the given input signal is limited to the output saturation voltage of the operational amplifier. Hence, it should not be too large, otherwise, the distortion of the output signal would occur, and the elements would even be destroyed.

5. Conclusions

In this paper, a servo system is implemented by a simple analog circuit only consisting of nineteen elements. The numerical simulation results, as well as the experiment realization results, prove that the output voltage of the capacitor in the RLC series circuit tracks the different given input signals well. The proposed circuit can be used as an example for the courses of control theory and application, such as the course of automatic control theory, the course of motion control system and so on.

References

1. B. S. Chen, *Electric Drive Automatic Control System (Motion Control System)*, 3rd edn. (China Machine Press, Beijing, 2003).
2. G. Z. Yu, The design of regulator in engineering, *Journal of Changchun Institute of Optics and Fine Mechanics* **23**(2) (2000) 48–51.
3. Y. F. Wen, The digital simulation of engineering designs for a double closed loop speed-regulation system, *Modern Electric Power* **17**(1) (2000) 76–81.
4. X. L. Ma, Decoupling and regulator design of vector control systems, *Electric Drive* **39**(1) (2009) 3–6.
5. H. Dong, H. Wang and K. Y. Huang, Design of PMSM drive system digital PI adjuster parameters, *Electric Drive* **39**(1) (2009) 7–10.

Simulation Study on the Tracking Technology of the Maximal Power Point of the Solar Photovoltaic Based on the Model Predictive Control

Xia Zhao

School of Electrical and Electronic Engineering, Shanghai Institute of Technology, Shanghai, China

Huailin Zhao

School of Electrical and Electronic Engineering, Shanghai Institute of Technology, Shanghai, China

Masanori Sugisaka

Alife Robotics Cooperation LTD, Oita, Japan

E-mail: zhl@sit.edu.cn, 156101128mail@sit.edu.cn

www.sit.edu.cn

Abstract

The solar photovoltaic battery is a new type of renewable distributed energy's important part of the key research development at home and abroad, but its output power is directly affected by light intensity and temperature, voltage-current characteristics have obvious nonlinear features. Therefore, a new MPPT technology based on model predictive control (MPC) is proposed in this paper, the simulation results show that the method can quickly track the maximum power point under the current environmental conditions, and improve the energy conversion efficiency of the system.

Keywords: Photovoltaic cell; Maximum power point tracking; Solar energy; Matlab/Simulink;

1. Introduction

Currently the survival of humanity is inseparable from the use of energy. Along with the increasing depletion of non-renewable energy, development of renewable energy has become the theme of today's world. Solar energy as a clean and renewable energy attracts the people's attention. That photovoltaic cells convert solar energy into electricity by some way is called as photovoltaic.

Because of its affection of environment and the load, and consideration of the input and output characteristics of nonlinear, this paper presents the maximum power point tracking (MPPT) principles and methods, mentions several MPPT method, and compare the advantages and disadvantages of the algorithm .

2. MODELING THE SOLAR CELL

Photovoltaic cell is the device that can convert the sun

light into electricity using the photovoltaic effect. The critical element of a photovoltaic cell is a semiconductor diode that P-N junction is exposed to light. The incidence of light on the cell is generates charge carrier that originate an electric current if the cell is short-circuited [1]. Charge are generated when the energy of the incident photon is sufficient to detach the covalent electrons of the semiconductor, and this phenomenon depends on the semiconductor material and the wavelength of the incident light. Basically, the PV phenomenon may be described as the absorption of solar radiation, the generation and transport of free carriers at the p-n junction, and the collection of these electric charges at the terminals of the photovoltaic device [2]. If the terminal of cell is connected with external load, electrons flow through it which is cause of current in the circuit. The commonly accepted solar cell model is a one diode model [3], which is shown in Fig. 1. This Photovoltaic cell model is a nonlinear device and can be represent as a current source model. The output of the current source is directly dependent on the solar irradiance and the ambient temperature. The I-V characteristics of a photovoltaic cell is similar to diodes characteristic, and which is represent by the following equation [2] [3] [4]:

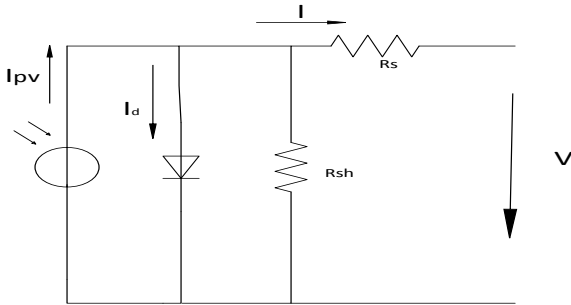


Fig. 1. The circuit diagram of the photovoltaic cell.

$$I = I_{pv,cell} - I_{o,cell} \left(\exp \left(\frac{qV}{aKT} \right) - 1 \right) \quad (1)$$

Actually, we care more about photovoltaic arrays, instead of a single cell. In each array, cells connected in parallel increase current and cells connected in series provide greater output voltages. And if there have parallel connection of cells in array, the photovoltaic and saturation current can be expressed as $I_{pv} = N_p I_{pv,cell}$, $I_o = N_p I_{o,cell}$. Also the characteristic of photovoltaic arrays can be mathematically described as:

$$I = I_{pv} - I_o \left\{ \exp \left(\frac{q(V_o + IR_s)}{aN_s KT} \right) - 1 \right\} - \frac{V_o + IR}{R_{sh}} \quad (2)$$

$$I_{pv} = (I_{pv,nom} + K_i \Delta T) \frac{G}{G_{nom}} \quad (3)$$

$$I_o = I_{o,nom} \left(\frac{T_{nom}}{T} \right)^3 \exp \left[\frac{qE_g}{aK} \left(\frac{1}{T_{nom}} - \frac{1}{T} \right) \right] \quad (4)$$

$$I_{pv,nom} = I_{SC} \frac{R_{sh} + R_s}{R_{sh}} \quad (5)$$

$$I_{o,nom} = \frac{I_{SC}}{\exp \left(\frac{V_{OC}}{aV_{t,nom}} \right) - 1} \quad (6)$$

whereand are the output current and voltage of the photovoltaic cell, respectively, is the generated current under a given in solution, is the reverse saturation current, is the charge of an electron (value is), is the Boltzmann's constant (value is), is the ideality factor(usually, and the choice depends on other parameters of the I-V model. And here is taken as 1), T is the temperature (in Kelin) of the p-n junction of photovoltaic cell, is the number of photovoltaic cell for each array, is the internal series resistance, is the internal shunt resistance of the photovoltaic cell, is the light-generated current at the nominal situation , is the difference between actual and nominal temperature, is the short circuit current/temperature coefficient, G is the irradiation on the device surface, is the nominal irradiation, is the band gap energy of the semiconductor, and is the thermal voltage of photovoltaic array at the nominal temperature .

The equation (2-2) have a wide application in theoretical analysis of photovoltaic cell. But it is not suitable for engineering application, due to the parameters,, K, and are relative to the solar irradiance and the ambient temperature, and the value of them is hard to determined. Consider that the value of is very small, but is very large. So we can approximately see $(V_o + I_o R_s)/R_{sh}$ equal to zero [4]. Also there have other parameters are very important to photovoltaic arrays, such as Open Circuit Voltage, Open Circuit Current , Maximum Power Voltage, Maximum Power Current, and Maximum Power. And the normalized value (work at

standard test condition, namely, 25 and 1000 w/m^2) of them are provided by manufactures. For example, the Solarex MSX60, a typical 60W photovoltaic module, its parameter as the table 1 described [3].

Table.1. The parameters of the Solarex MSX60 photovoltaic panel

At temperature	T	25	
Open Circuit Voltage		21.0	V
Short Circuit Current		3.74	A
Maximum Power Voltage		17.1	V
Maximum Power Current		3.5	A
Maximum Power		59.9	W

For the purpose of efficiency and stability, a maximum power point tracker (MPPT) is a power electronic DC-DC converter inserted between the photovoltaic array and its load. By using an intelligent algorithm, it has ability to predict and control the photovoltaic module use the history data of solar irradiance, so it ensure the photovoltaic array always works at its maximum power point as the temperature, insolation and load vary.

3. Maximum Power Point Tracking Algorithms

The operation of photovoltaic array are influenced by solar radiation, temperature and load values. The output power of photovoltaic cell decreasing with the temperature increasing, and increasing with the solar radiation increasing. At a given condition of irradiation and temperature, a photovoltaic cell can work at difference operation point, but there is a unique operation point of the photovoltaic array with maximum output power, that is Maximum power point (MPP). Obviously, it is necessary to take some measure to maintain the photovoltaic array work at MPP, and it also can improve the efficiency of photovoltaic power system. These measures called Maximum Power Point Tracking (MPPT), which draws maximum power from the photovoltaic array regardless of weather or load condition [5]. The principle of maximum power point tracking is through adjusting the load impedance to make the photovoltaic power generation system always work at the near maximum power point, under different environmental condition [6].

Many research papers have produced with various schemes for the MPPT in photovoltaic power generation system. There are many methods of MPPT techniques applied to photovoltaic power system. Such as one cycle control method, feedback voltage and current method, and feedback of power variation with voltage and current [5]. At now the commonly used method about the maximum power point tracking of photovoltaic generation are the constant voltage method (CVT), the perturbation and observation method (P&O) [7], and the incremental conductance method (INC) [8]. Moreover, the fuzzy logic based method could found in [9] [10] [11]. Among all these methods, due to the poor accuracy, the constant voltage method are not widely applied in industry. And the incremental conductance method (INC) and the perturbation and observation method (P&O) are applied widely. In the next section, we will discuss the two basic MPPT algorithms in detail.

A. Perturbation and Observation method (P&O)

The P&O method maintain the operating point near the maximum power point by a small voltage change ΔV called voltage disturbance signal. At the beginning, it has to measure photovoltaic voltage and current at the moment atmosphere condition, and to calculate the output power P_1 . And then periodically increasing (or decreasing) the photovoltaic array voltage, that is $V_2 = V_1 + \Delta V$, and also to calculate the output power P_2 . The photovoltaic power P_1 and P_2 are compared, if P_2 is more than P_1 , then the perturbation is correct otherwise it should be reversed. This method has major drawback are occasional deviation from the maximum due to its inability to relate the change in the photovoltaic array power to the change in the atmospheric condition. [9]. Moreover, when the MPP is reached, the P&O method will oscillate around it in case of constant or slowly varying atmospheric condition. In order to avoid these, the value of ΔV is very small. The simulation result of this method will be analysis in the next section.

B. Incremental Conductance method (INC)

According to the P – V characteristic curve, when a photovoltaic array work at maximum power point the slope of P – V curve is zero, namely $\frac{dP}{dV} = 0$. These relation can further be written as following:

$$\frac{dP}{dV} = \frac{d(VI)}{dV} = I + V \frac{dI}{dV} \quad (7)$$

Namely

$$\frac{dI}{dV} = -\frac{I}{V} \quad (8)$$

The control strategy of the incremental conductance algorithms can be written in the following simple equations:

$$\frac{dI}{dV} > -\frac{I}{V}, \text{ that is } \frac{dI}{dV} > 0, \text{ means } V < V_{\max}, \text{ then}$$

$$V = V + \Delta V;$$

$$\frac{dI}{dV} < -\frac{I}{V}, \text{ that is } \frac{dI}{dV} < 0, \text{ means } V > V_{\max}, \text{ then}$$

$$V = V - \Delta V;$$

$$\frac{dI}{dV} = -\frac{I}{V}, \text{ that is } \frac{dP}{dV} = 0, \text{ means the}$$

photovoltaic array work at maximum power point, and then $V = V_{\max}$.

Hence, the photovoltaic cell terminal voltage can be adjusted relative to the maximum power point voltage by measuring the incremental (dI/dV) and instantaneous array conductance (I/V) and make use of the mentioned control strategy. In practical application, the incremental are approximated as: $dI = I - I_{bef}$ and $dV = V - V_{bef}$. Where I_{bef}, V_{bef} are the last time measured value of current and voltage. This method can compare directly the photovoltaic array conductance. It has better track of any changes either in load or photocurrent rather than the perturbation and observation method, but this way of tracking still has some oscillation which cannot be avoided. Also the simulation result of the incremental conductance algorithms will be discussed in next section.

4. Model Predictive Control based Maximum Power Point Tracking

As mentioned above, conventional methods to track the maximum power point the result are not as good as expected, most of them have oscillation and cannot be avoided. We want the output power of photovoltaic array is stable and smooth without oscillation, or the oscillation is small that can be ignored. It is needful to find a new way of tracking to improve the stability of the output power and the conversion efficiency of photovoltaic array. And this paper we consider a model predictive control based MPPT technique applied to photovoltaic module.

© The 2016 International Conference on Artificial Life and Robotics (ICAROB 2016), Jan. 29-31, Okinawa Convention Center, Okinawa, Japan

Model predictive control (MPC) is widely applied in industrial control with several advantages over the conventional control technique. The main characteristic of model predictive control is predicting the future behavior of the desired control variables until a predefined horizon in time based on the present data of input or output. Also this control variables will be optimized by minimizing a cost function to obtain a satisfying control performance of overall system.

This paper we consider a islanded operation photovoltaic generation system as controlled member, which main consist of a photovoltaic array, a DC-DC boost converter, and a MPC controller as shown in Fig.2.

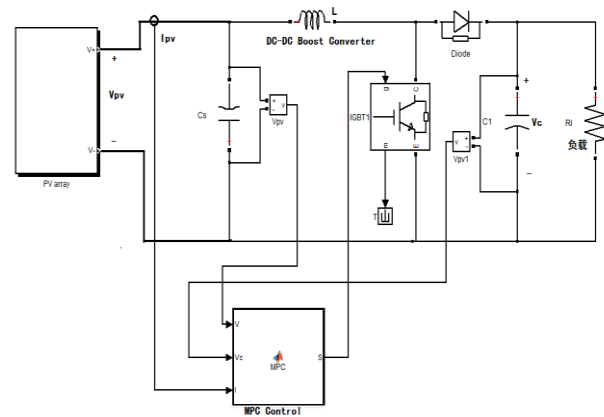


Fig. 2. Control block diagram of overall islanded photovoltaic system configuration implementing MPC based MPPT technique

The photovoltaic array generates electric power directly from solar radiation. And then the power is delivered to DC load through a DC-DC boost converter, whose switch (IGBT) is operated by the MPC controller. The MPC controller applied a model predictive control based maximum power point tracking algorithm. And the states of switch are controlled by the output (S) of MPC controller. Due to the switch have two basic states (open and close) there have two equivalent circuits to represent the DC-DC boost converter to analyze.

When the switch is considered as open, the equivalent circuits of the boost converter shown as Fig.3. And we use the following equations to describe the operation of boost converter.

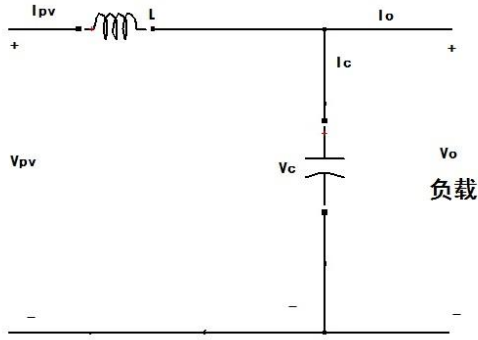


Fig. 3. Equivalent circuits for boost converter when the switch is open (S=0)

$$L \frac{dI_{pv}}{dt} = V_{pv} - V_C \quad (9)$$

$$C \frac{dV_C}{dt} = I_{pv} - \frac{V_C}{R} \quad (10)$$

The Euler approximation is then used to obtain the discrete model of the system:

$$I_{pv}(k+1) = \frac{T_s}{L} V_{pv}(k) - \frac{T_s}{L} V_C(k) + I_{pv}(k) \quad (11)$$

$$V_C(k+1) = \frac{1}{C} I_{pv}(k) - \frac{1}{RC} V_C(k) + V_C(k) \quad (12)$$

$$V_{pv}(k+1) = \frac{L}{T_s} (I_{pv}(k+1) - I_{pv}(k)) + V_C(k) \quad (13)$$

When the switch is closed, the equivalent circuits of the boost converter shown as Fig.4. and the equations as following:

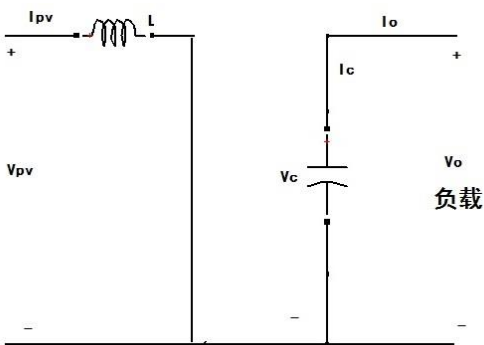


Fig. 4. Equivalent circuits for boost converter when the switch is open (S=1)

$$V_{pv} = L \frac{dI_{pv}}{dt} \quad (14)$$

$$\frac{dV_C}{dt} = -\frac{1}{RC} V_C \quad (15)$$

The discrete model of the system as following:

$$I_{pv}(k+1) = \frac{T_s}{L} V_{pv}(k) + I_{pv}(k) \quad (16)$$

$$V_C(k+1) = \left(1 - \frac{T_s}{RC}\right) V_C(k) \quad (17)$$

$$V_{pv}(k+1) = \frac{L}{T_s} (I_{pv}(k+1) - I_{pv}(k)) \quad (18)$$

Where T_s is sampling frequency, make use of the equation (11), (12), (13) or (16), (17), (18), the behavior of the controlled variable I_{pv} , V_{pv} and V_C can be predicted for the next sampling instant. And we can utilize the predicted value of this control variables to distinguish whether the photovoltaic array work at the maximum power point. All of this variable estimated and optimized based on the evaluation of a cost function. In this paper, the cost function can be expressed as:

$$J = \left| I_{pv}(k+1) + V_{pv}(k+1) \frac{I_{pv}(k+1) - I_{pv}(k)}{V_{pv}(k+1) - V_{pv}(k)} \right|_{S=0,1} \quad (19)$$

For each sampling sequence the cost function is calculated twice for each switching states. And the cost function for each switch states are compared to determine the control actions for the following time instant. Fig.5. depicts the process of the model predictive control based MPPT control scheme.

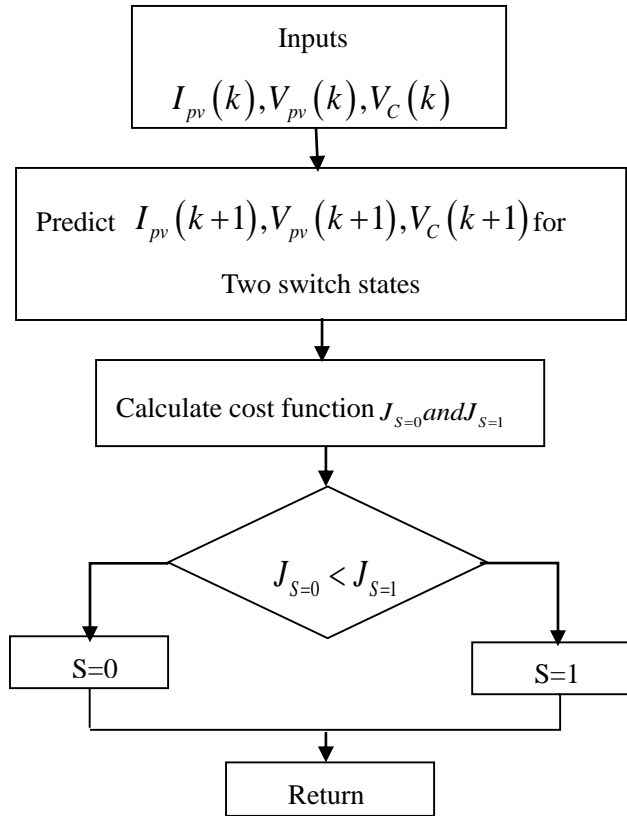


Fig. 5. Flow chart of MPC based MPPT controller

5. Simulation and Result

According to the mathematical model of the solar photovoltaic module described above, build a mathematical model of solar photovoltaic cells in the Matalab/Simulink environment. Simulation were designed based on IMC and MPC described above. In the simulation process of Solar photovoltaic cells, assuming the ambient temperature is maintained at 25 degrees, just considering the changes of the solar illumination and that three time points were given light $700\text{w}/\text{m}^2$, $900\text{w}/\text{m}^2$ and $1000\text{w}/\text{m}^2$. In the simulation, simulate the mutations of the light intensity at different moments with three step signal observe and compare the maximum power output tracking situation in the current environment conditions with the use of solar photovoltaic cells under the control of MPC and INC. The simulation results are shown in the following figure.

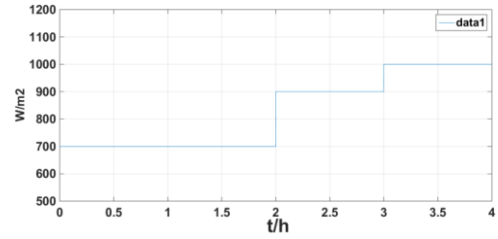


Fig. 6. light changing after time

The initial value of light was 700, at the second the light increases by 200, at the third second the light changed into 1000, and the changes of the moments are mutations. Change of the light is shown in Figure 6.

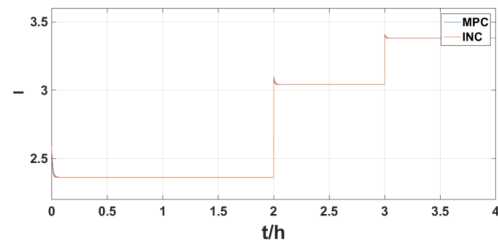


Fig. 7. current changing after time

Output current is shown in Figure 7, since the output of photovoltaic solar cells is directly proportional to the light intensity of the sun, when the sunlight changes, the current of the photovoltaic cell can quickly track changes of the light; since the influence of an external circuit device received by the output current, there is no difference in the use of MPC and lower INC to control the current, and all changes after the light steeply.

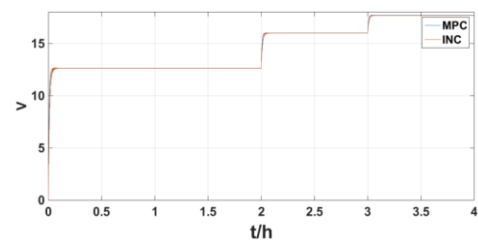


Fig. 8. voltage changing after time

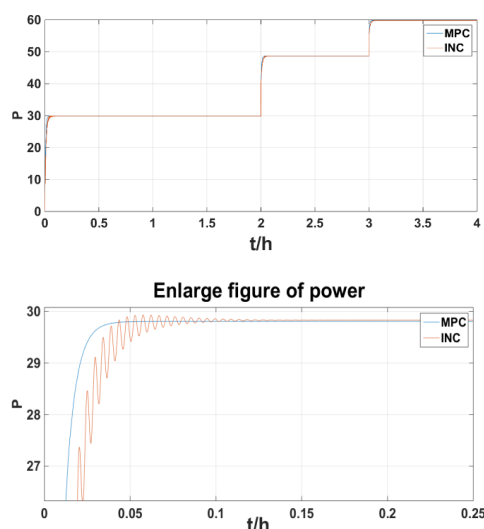


Fig. 9. output power

Output voltage and power as respectively shown in figure 9 and figure 9. shown as the right figure, when the light intensity changes, whether it is the use of MPC or INC to output voltage and power, they are able to follow the changes in light intensity. But the MPC control system is no shock, and the tracking speed is significantly faster than the INC. it is more obviously in the output power. In order to clearly demonstrate the dynamic process of system output under two different control methods, amplified the dynamics process of the change of the power amplification. From the enlarged graph, MPC track the maximum power relatively stable and the method of INC has severe shock that the effect is less good than predicted.

This paper analyzes principle when solar photovoltaic cells work, and relationship between output of current, voltage and power. Under certain light intensity and ambient temperature, the output of power and operating voltage is obviously nonlinear. It is difficult to operate at the maximum outputting point of power. Therefore, in order to improve the conversion rate of solar energy, solar photovoltaic cells designed the predictive control based on the maximum power point tracking technology. According to the solar photovoltaic cell model, predict the output power of the PV array in the current environment, control full-controlled device in the converter circuit, Regulate the operating voltage of the solar cell to operate at maximum power point. The simulation shows that this method can quickly adjust the solar cell operating voltage and track the maximum

power point fast, at the same time overcome the shock and other issues brought by the classic disturbance observer and incremental admittance MPPT technology. The accuracy and speed of tracking maximum power point have improved significantly.

References

1. A.Lasnier and T.G.Ang, Photovoltaic Engineering Handbook. NewYork: Adam Hilger, 1990.
2. M.G. Villava, J.R. Gazoli, and E.R. Filho, Comprehensive Approach to Modeling and Simulation of Photovoltaic Arrays [J]. Power Electronics, IEEE Transactions, 2009, Vol.24, No.5, pp.1198-1208.
3. Geoff Walker. Evaluating MPPT Converter Topologies Using a Matlab PV Model [J]. Innovation for Secure Power, Queensland University of Technology, Brisbane, Australia, 2000, PP. 138-143
4. ZENG Zhuoying and LIU Dong. Study on Cyber-Physical System Modeling on Coordinated Control of Photovoltaic Generation and Battery Energy Storage System [J]. Power System Technology, Jun/2013, Vol.37, No.6, pp.1506-1513.
5. Li Wei, Zhu Xinjian, "The Maximum Power Point Tracking Control of a Photovoltaic Power System" Computer Simulation, Vol. 23, No. 6, pp.239 243, June 2006.
6. Yang Xue; Sha Wang; Photovoltaic Cell Modeling and the Maximum Power Point Tracking Simulation; Materials for Renewable Energy and Environment (ICMREE), 2013 International Conference on; 2013, pp.119-123
7. Radwan, H. ; Abdelkarem, E. ; Ahmed, M. ; Orabi, M.;The non ideality effect of optimizing the P&O MPPT algorithm for PV battery charger applications telecommunications Energy Conference (INTELEC), 2011 IEEE 33rd International; 2011.
8. K. H. Hussein; Maximum photovoltaic power tracking: An algorithm for rapidly changing atmospheric conditions; Proc.Inst.Electr.Eng.—Generation,Transmission, Distribution, vol. 142, no. 1, pp. 59–64, Jan. 1995.
9. Anaadhakumar,G.; Venkateshkumar,M.; Shankar, P.; Intelligent controller based MPPT method for the Photovoltaic Power system; Human Computer Interactions (ICHCI), 2013 International Conference; 2013, pp.1-6.
10. Al-Mohaya; M.A.M. Mahamad, A.K.; Saon, S.; Implementation of Field Programmable Gate Array based Maximum Power Point Tracking Controller of Photovoltaic System;Power Engineering and Optimization Conference (PEOCO), 2013 IEEE 7th International; 2013, pp. 718-721.
11. Shijie Yan; Jia Yuan Lei Xu; Fuzzy Logic Control of MPPT for Photovoltaic Power System; Fuzzy Systems and Knowledge Discovery (FSKD), 2012 9th International Conference; 2012, pp.448-451.

Analysis and unidirectionally coupled synchronization of a novel chaotic system

Xue Li

*Department of Automation, Tianjin University of Science and Technology,
1038 Daguanlu Road, Hexi District, Tianjin 300222, PR China*

Wei Xue

*Department of Automation, Tianjin University of Science and Technology,
1038 Daguanlu Road, Hexi District, Tianjin 300222, PR China
E-mail:lixueTJKJ@163.com,xuewei@tust.edu.cn
www.tust.edu.cn*

Abstract

In this paper, a new three-dimensional autonomous chaotic system is proposed. By means of theoretical analysis and numerical simulation, some basic dynamical properties, such as dissipation, fractal dimension, Lyapunov exponent spectrum and chaotic dynamical behaviors of the new chaotic system are illustrated. The obtained results show clearly that this system is a new chaotic system. Furthermore, based on Lyapunov stability theory of the system, unidirectionally coupled synchronization of the new three-dimensional chaotic system through designing the appropriate coupling coefficient is investigated. Results of numerical simulation validate the accuracy and effectiveness of synchronization scheme of the presented system.

Keywords: Chaos; New chaotic system; Lyapunov exponent; Unidirectionally coupled synchronization.

1. Introduction

In 1963, American mathematical meteorologist Lorenz discovered chaos in a simple system of three autonomous ordinary differential equations, called the Lorenz system,¹ a lot of work have been reported on finding the new chaotic attractors. As the first chaotic model, the Lorenz system has become a paradigm of chaos research. In 1976, Rössler presented a three-dimensional quadratic autonomous chaotic system.² Recently, there have been increasing attentions in generating chaotic system since Chen found a new Lorenz-like chaotic system in 1999, namely, the Chen system.³ In 2002, Lü and Chen found a new chaotic system, called the Lü chaotic system,⁴ which represents the transition between the Lorenz system and Chen system. In 2003, Liu created a new chaotic system and

researched its basic dynamical characteristics, as the name of Liu chaotic system.⁵ In 2005, Qi reported a three-dimensional continuous quadratic autonomous chaotic system modified from the Lorenz system,⁶ in which each equation contains a single quadratic cross-product term. In this paper, a novel three-dimensional autonomous chaotic system is introduced. Numerical analysis shows that the proposed chaotic attractor is a new attractor, which is not topologically equivalent to the original chaotic system, or the Lorenz system, or the Chen system, or the Lü system, or even the Lorenz system family.

In the past few decades, synchronization of the chaotic systems have attracted considerable interests because of their practical applications in the fields of image encryption, secure communication, electrical

engineering, neural network, control processing and so on. Many synchronization approaches have been proposed in order to synchronizing the chaotic systems. For example, linear feedback synchronization,⁷ active synchronization,⁸ adaptive synchronization,⁹ projective synchronization,¹⁰⁻¹¹ sliding mode synchronization,¹² unidirectionally coupled synchronization,¹³ and lag synchronization.¹⁴⁻¹⁵ By means of Lyapunov stability theory of the system, unidirectionally coupled synchronization of the new three-dimensional chaotic system is investigated. Numerical simulation results verify the accuracy and effectiveness of the synchronization scheme presented in this paper.

2. The new chaotic system and its basic dynamical properties

2.1. The new three-dimensional chaotic system

In this paper, a new three-dimensional autonomous system is proposed, which can be expressed as the following form:

$$\begin{cases} \dot{x} = ay - ax - yz \\ \dot{y} = bx + y + xz \\ \dot{z} = -dz + cy^2 \end{cases} \quad (1)$$

When the parameters are fixed as $a=33$, $b=50$, $c=3$, and $d=15$, the chaotic behavior of system(1) is obvious. By adopting the time domain method based on predictor-corrector, the phase portrait of system(1) is shown in Fig.1 and the three Lyapunov exponents are 5.767 3, 0.003 4, -7.823 6, respectively.

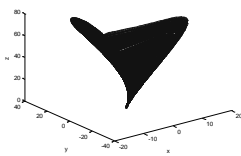


Fig.1 Phase portrait of system(1) with $a=33$, $b=50$, $c=3$, and $d=15$.

2.2. Basic dynamical properties of the new chaotic system

(I)Dissipation:

The dissipativity of system(1) is described as:

$$\Delta V = \frac{\partial \dot{x}}{\partial x} + \frac{\partial \dot{y}}{\partial y} + \frac{\partial \dot{z}}{\partial z} = -(a-1+d)$$

Therefore, when a, d satisfy $a+d > 1$, system(1) is dissipative, and with an exponential rate:

$$\frac{dV}{dt} = e^{-(a-1+d)t}$$

It means that a volume element V_0 is apparently contracted by the flow into a volume element $V_0 e^{-(a-1+d)t}$ versus time t . That is, each volume element containing the trajectories of this dynamical system shrinks to zero as $t \rightarrow \infty$ at an exponential rate. Therefore, all the orbits of the new system(1) are ultimately confined to a specific subset that has zero volume, and the asymptotic motion of system(1) will settle onto an attractor of the system.

(II)The Lyapunov exponents

As is known, the Lyapunov exponents measure the exponent rates of the divergence and convergence of nearby trajectories in phase space of system. Three Lyapunov exponents of system(1) are calculated as $L_1 = 5.7673$, $L_2 = 0.0034$, and $L_3 = -7.8236$. The Lyapunov exponent spectrum of the new system(1) is showed in Fig.2, when the parameters is taken as $a=33$, $b=50$, $c=3$, and $d \in (0,30)$. Thus, the Lyapunov dimension of the new chaotic system(1) is

$$D_L = 2 + \frac{1}{|L_3|} \sum_{i=1}^2 L_i = 2 + \frac{L_1 + L_2}{|L_3|} = 2 + \frac{5.7673 + 0.0034}{|-7.8236|} = 2.7376$$

Which means the system(1) is a chaotic system since the Lyapunov dimension of the system(1) is fractional.

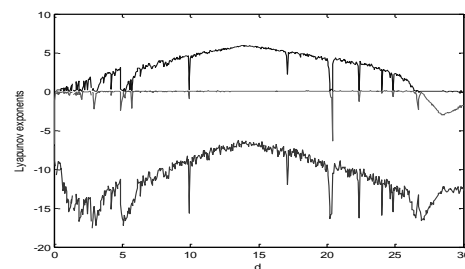


Fig.2 Lyapunov exponent diagrams of system(1) on x -axis versus parameter $d \in (0,30)$

3. Unidirectionally coupled synchronization of the new chaotic system

In order to realize the unidirectionally coupled synchronization of the new chaotic system, the drive system is defined as follow:

$$\begin{cases} \dot{x}_1 = ax_2 - ax_1 - x_2x_3 \\ \dot{x}_2 = bx_1 + x_2 + x_1x_3 \\ \dot{x}_3 = -dx_3 + cx_2x_2 \end{cases} \quad (2)$$

and the response system can be described in the form of:

$$\begin{cases} \dot{y}_1 = ay_2 - ay_1 - y_2y_3 - k(y_1 - x_1) \\ \dot{y}_2 = by_1 + y_2 + y_1y_3 - k(y_2 - x_2) \\ \dot{y}_3 = -dy_3 + cy_2y_2 - k(y_3 - x_3) \end{cases} \quad (3)$$

Where $e_1 = y_1 - x_1$, $e_2 = y_2 - x_2$, and $e_3 = y_3 - x_3$. And k is the coupling coefficient, it can make system(2) and system(3) compose a coupling system.

From Eq.(2) and Eq.(3), the error system is obtained which can be expressed as:

$$\dot{e}_1 = de_1 - ae_1 - y_2e_3 - y_3e_2 + e_2e_3 - ke_1 \quad (4)$$

Eq.(4) utilizes Laplace transform, the error system is provided which is described by:

$$\begin{cases} sE_1(s) - e_1(0) = aE_2(s) - aE_1(s) - L\{y_2e_3\} \\ \quad - L\{y_3e_2\} + L\{e_2e_3\} - kE_1(s) \\ sE_2(s) - e_2(0) = bE_1(s) + E_2(s) + L\{y_1e_3\} \\ \quad + L\{y_3e_1\} - L\{e_1e_3\} - kE_2(s) \\ sE_3(s) - e_3(0) = -dE_3(s) + cL\{y_2e_2\} + cL\{y_2e_2\} \\ \quad - cL\{e_2e_2\} - kE_3(s) \end{cases} \quad (5)$$

From Eq.(5), the error system is obtained as follow:

$$\begin{cases} E_1(s) = \frac{aE_2(s)}{s+k+a} - \frac{e_1(0)}{s+k+a} - \frac{L\{y_2e_3\}}{s+k+a} \\ \quad - \frac{L\{y_3e_2\}}{s+k+a} + \frac{L\{e_2e_3\}}{s+k+a} \\ E_2(s) = \frac{bE_1(s)}{s+k-1} + \frac{e_2(0)}{s+k-1} + \frac{L\{y_1e_3\}}{s+k-1} \\ \quad + \frac{L\{y_3e_1\}}{s+k-1} - \frac{L\{e_1e_3\}}{s+k-1} \\ E_3(s) = -\frac{e_3(0)}{s+k+d} + \frac{cL\{y_2e_2\}}{s+k+d} + \frac{cL\{y_2e_2\}}{s+k+d} \\ \quad - \frac{cL\{e_2e_2\}}{s+k+d} \end{cases} \quad (6)$$

Based on the final value theorem of Laplace transform, the error system is described in the form of:

$$\begin{aligned} \lim_{t \rightarrow \infty} e_1(t) &= \lim_{s \rightarrow 0} E_1(s) = \frac{a}{s+k+a} \lim_{t \rightarrow \infty} e_2(t) - \lim_{s \rightarrow 0} \frac{sL\{y_2e_3\}}{s+k+a} \\ &\quad - \lim_{s \rightarrow 0} \frac{sL\{y_3e_2\}}{s+k+a} + \lim_{s \rightarrow 0} \frac{sL\{e_2e_3\}}{s+k+a} \\ &= 0 \end{aligned} \quad (7)$$

$$\begin{aligned} \lim_{t \rightarrow \infty} e_2(t) &= \lim_{s \rightarrow 0} E_2(s) = \frac{b}{s+k-1} \lim_{t \rightarrow \infty} e_1(t) + \lim_{s \rightarrow 0} \frac{sL\{y_1e_3\}}{s+k-1} \\ &\quad + \lim_{s \rightarrow 0} \frac{sL\{y_3e_1\}}{s+k-1} - \lim_{s \rightarrow 0} \frac{sL\{e_1e_3\}}{s+k-1} \\ &= 0 \end{aligned} \quad (8)$$

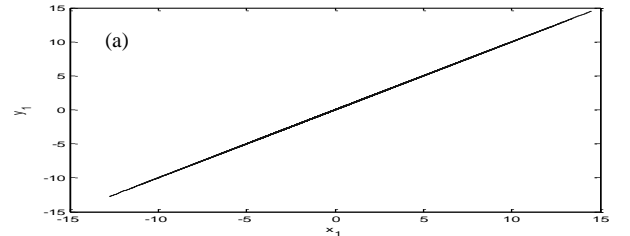
$$\begin{aligned} \lim_{t \rightarrow \infty} e_3(t) &= \lim_{s \rightarrow 0} E_3(s) = c \lim_{s \rightarrow 0} \frac{sL\{y_2e_2\}}{s+k+d} + c \lim_{s \rightarrow 0} \frac{sL\{y_2e_2\}}{s+k+d} \\ &\quad - c \lim_{s \rightarrow 0} \frac{sL\{e_2e_2\}}{s+k+d} \\ &= 0 \end{aligned} \quad (9)$$

From Eq.(7), Eq.(8), and Eq.(9), $\lim_{t \rightarrow \infty} e_i(t) = 0$ ($i=1,2,3$)

can be obtained. Theoretical analysis demonstrate system(2) can synchronize system(3) completely.

4. Numerical simulation

In following, unidirectionally coupled synchronization of the new three-dimensional chaotic system through designing the appropriate coupling coefficient is illustrated. The system parameters are chosen as $a=33$, $b=50$, $c=3$, and $d=15$. The initial values of the drive system(2) and the response system(3) are taken as $x_1(0)=-3$, $x_2(0)=0$, $x_3(0)=2$, $y_1(0)=-3$, $y_2(0)=-0.6$, and $y_3(0)=-1.6$, respectively. When the coupling coefficient is taken as $k=200$, the simulation results of state parameters are displayed in Fig.3. Furthermore, the curves of synchronization error is described in Fig.4. It's clearly showed that corresponding numerical simulations agree with the analytical results.



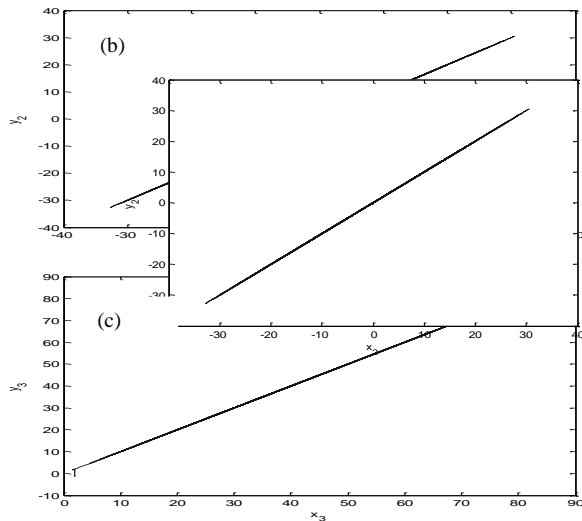


Fig.3 Curves of state variable (a) (x_1, y_1) ; (b) (x_2, y_2) ; (c) (x_3, y_3) .

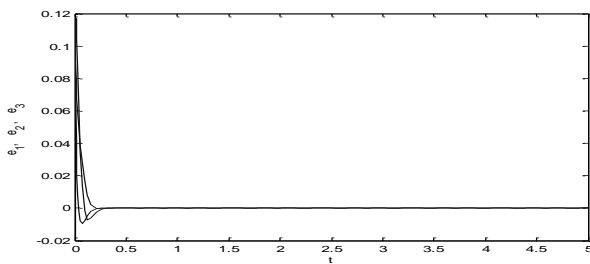


Fig.4 Synchronization errors versus time t

5. Conclusion

In this paper, a new three-dimensional autonomous chaotic system is proposed and investigated. By utilizing theoretical analysis and numerical simulation, some basic dynamical properties, such as dissipation, fractal dimension, Lyapunov exponent spectrum and chaotic dynamical behaviors of the new chaotic system are introduced. In addition, based on Lyapunov stability theory, unidirectionally coupled synchronization of the new chaotic system is illustrated. Numerical simulation are performed to validate the effectiveness of the presented synchronization scheme. The synchronization scheme proposed in our work can provide technical basis and support for the further study of the secure communication and automatic control.

6. Acknowledgement

This work is supported by the Young Scientists Fund of the National Natural Science Foundation of China (Grant No.11202148).

7. References

1. Lorenz E N. Deterministic nonperiodic Flow. *Journal of the Atmosphere Science*. 1963, 20(2): 130-141.
2. Rössler O E. An equation for continuous chaos. *Physics Letters A*. 1976, 57(3): 397-398.
3. Chen G R, Ueta T. Yet another chaotic attractor. *International Journal of Bifurcation and Chaos*. 1999, 9(7): 1465-1466.
4. Lü J H, Chen G R. A new chaotic attractor coined. *International Journal of Bifurcation and Chaos*. 2002, 12(3): 659-661.
5. Liu W B, Chen G R. A new chaotic system and its generation. *International Journal of Bifurcation and Chaos*. 2003, 13(1): 261-267.
6. Qi G Y, Du S Z, Chen G R, et al. On a 4-dimensional chaotic system. *Chaos, Solitons and Fractals*. 2005, 23: 1671-82.
7. Yassen M T. Controlling chaos and synchronization for new chaotic system using linear feedback control. *Chaos, Solitons and Fractals*. 2005, 26: 913-920.
8. Li G H. An active control synchronization for two modified chua circuits. *Chinese Physics B*. 2005, 14(3): 472-475.
9. Kim J H, Park C W, Kim E, et al. Adaptive synchronization of T-S fuzzy chaotic systems with unknown parameters. *Chaos, Solitons and Fractals*. 2005, 24: 1335-1361.
10. Meng J, Wang X Y. Generalized projective synchronization of a class of delayed neural networks. *Physics Letters A*. 2008, 22(3): 181-190.
11. Xu D L, Li Z. Controlled projective synchronization in nonpartially-linear chaotic systems. *Physics Letters A*. 2002, 292(6): 1395-1402.
12. Yau H T, Yan J J. Design of sliding mode controller for Lorenz chaotic system with nonlinear input. *Chaos, Solitons and Fractals*. 2004, 19(4): 891-898.
13. Yang X S. On the existence of generalized synchronization in unidirectionally coupled systems. *Computers and Mathematics with Applications*. 2001, 122(1): 71-79.
14. Shahverdiev E M, Sivaprakasam S, Shore K A. Lag synchronization in time-delayed systems. *Physics Letters A*. 2002, 292(96): 320-324.
15. Rosenblum M G, Pikovsky A S, Kurths J. From phase to lag synchronization in coupled chaotic oscillators. *Physics Letters A*. 1997, 78(22): 4193-4196.

Fast collective photographic subject detection without pixels by an assumption about a shoot and its elevation angle

Sora Tanioka

*Department of Computer Science, National Defense Academy of Japan, hasirimizu 1-10-20
yokosuka, kanagawa 239-8686, Japan*

Masao Kubo

*Department of Computer Science, National Defense Academy of Japan, hasirimizu 1-10-20
yokosuka, kanagawa 239-8686, Japan*

Hiroshi Sato

*Department of Computer Science, National Defense Academy of Japan, hasirimizu 1-10-20
yokosuka, kanagawa 239-8686, Japan
E-mail: {masaok,hsato}@nda. ac. jp
www. nda. ac. jp/cs/*

Abstract

In this paper a method that discovers socially attracted photographic subjects in real time is proposed. This needs only, not pixel information of a digital photograph for this discovery, but at time of shoot, a GPS location, a bearing of the shoot and so on. This information is sufficiently lightweight so that we expect that a congestion-free photo sharing wireless network service can be achieved. In this paper, a photography behavior model which considers an elevation angle of a shoot makes the accuracy better.

Keywords: Reality mining; Photograph, Event detection, Geo tagged images

1. Introduction

Interests at the present moment of others can be observed by current Information Communication Technology. Photograph based communication is more vivid and secure than a text based information sharing like Twitter. However, this communication system usually becomes much slow because the heavy congestion caused by transmission of hug pixel data. Therefore this framework has not been used for a real-time information sharing system. So far researches which attempt to improve this lower real time capability have been proposed. It has been proposed a method of transmitting only the best photos that match the viewing

request to the server while they are categorized only by not-pixel information of digital photograph. The information includes time to shoot, GPS and bearing of shoot so on. According to this method, photo pixel data congestion is unlikely because they are transmitted sequentially. However, in the conventional method, there is a practical problem that estimation accuracy of the object taken from the biased direction is worse. In order to solve this issue in this paper, we propose a method for estimating sterically an object by using the elevation angle (Fig.1). It is intended to improve the estimation accuracy by noting the characteristic of

tilting the camera in order to capture the entire subject into photographic frame.

This paper is organized as follows. First, related studies are introduced. Next the algorithm by using the elevation angle information is proposed. Finally, computer simulations perform, we verify the validity of the algorithm.

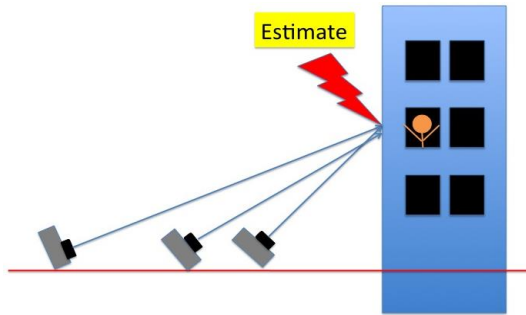


Fig.1 The concept of the proposed method: estimation of subject by a collection of elevation angle data in non pixel information in digital photographs.

2. Related works

Kubo et al. [1] introduces the photographer behavior model using the angle of view by composition. Thereby it realizes a method of automatically detecting its main subject in each image. As shown in Fig.2(a) the method that adopts a planar estimation in estimating the subject can be very accurately estimated when it is taken with a wide angle to the object. However, such a examples are rare in the real environment. Also when it is taken from a narrow angle, it can be pointed out that the accuracy is hardly improved even if information is increased as shown in Fig.2 (b).

3. The proposed system

3.1. Input data

Here, small mobile devices such as a smart phone is our main subject. The photographic information includes latitude, longitude, altitude, azimuth of GPS, elevation angle by accelerometer, and time to shoot in TIFF and Exif data .

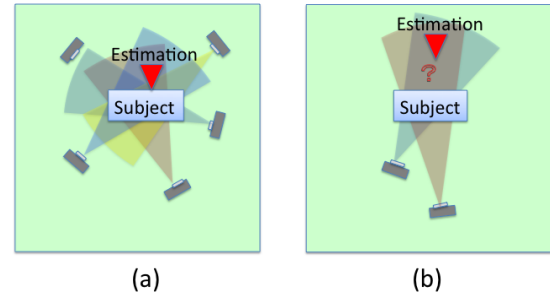


Fig.2 (a)A case conventional methods solve. (b) A difficult case for the conventional methods.

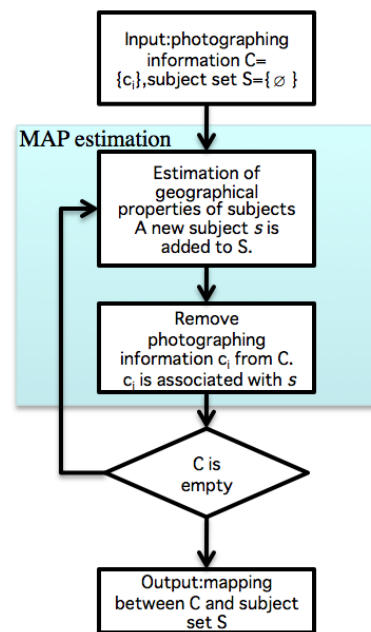


Fig.3 Subject location discovery algorithm by MAP estimation

3.2. Flow of the proposed system

Fig.3 describes the proposed algorithm. In this figure a set of photographic information is described by $C = \{c_1, \dots, c_N\}$. The each subject is estimated by MAP (Maximum a posteriori) estimation iteratively. Once a subject is found, c_i which seems to be a consequence of shooting the subject is removed from C . By this procedure, the proposed method can discover multiple subjects.



Fig.4 Search result of ‘building+photograph’

3.3. Photographer behavior model

The photographer behavior model is a probability distribution $P_{shoot}(c_{Ti}|s_j)$ that a photographer at c_{Ti} takes a photo for a given subject s_j .

$$P_{shoot}(c_{Ti}|s_j) = K_{motivation} \cdot V_{composition}(s_j) \quad (1)$$

where $K_{motivation}$ represents the motivation to take a photo and $V_{composition}(s_j)$ means the fitness of the composition. This consists of the elevation angle E and the bearing B .

$$V_{composition}(s_j) = f(E)f(B) \quad (2)$$

However, in this paper, we assume that the photographs that place a subject in the center of the frame are useful to viewers and $f(B)=1$.

3.4. Algorithm for estimation of subjects

First, the overview of the MAP estimation is described.

$$I_{o_{j,k}} = \sum_{x=1}^{|c_j|} \max \{ I_{R_{j,k}}(c_{Ti}|p_{j,k}, \Delta_x) I_0 \} + I_0 \quad (3)$$

For each grid s_j in a given area, a weight as $P_{shoot}(c_{Ti}|s_j)$ is added about C . After this weighting step, a grid of maximum weight is selected as a subject s in this iteration. c_i which seems to take a photo of this subject is removed and s with c_i is added the subject set S . The next iteration starts with the new C . If C is empty the algorithm stops..

3.5. Photographer behavior and elevation angle

Fig.4 illustrates the top 20 of the search result of “building” by Google image search. As these images tell, the elevation angle is nearly horizontally when a photo is taken from far. On the other hand, when it is taken from the vicinity of a building the elevation angle becomes large in order to include the top of the building in the photo. Thus it was found to be estimated by the elevation angle at the time of photographing the distance from the size and shooting point of the object.

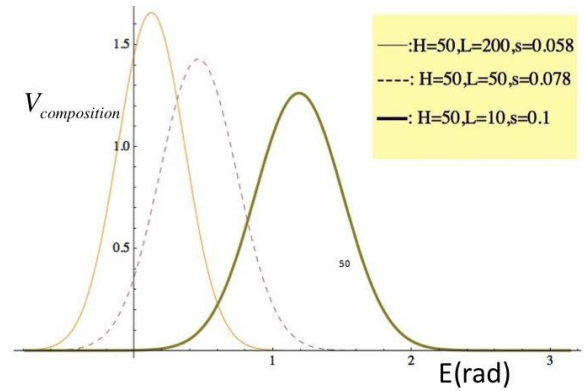


Fig.5 Examples of the proposed photographer behavior model of elevation angle

3.6. The proposed photographer behavior model of elevation

The photographer behavior model of elevation $f(E)$ is proposed in this section. This $f(E)$ is used for the Map estimation procedure in the algorithm in 3.4.

$$V_{composition}(s_j) = f(E) = \frac{1}{\sqrt{2\pi}\sigma} \exp\left(-\frac{(E-D)^2}{2\sigma^2}\right) \quad (4)$$

$$D = \arctan\left(\frac{H}{2L}\right) \quad (5)$$

The composition of a photograph is evaluated by an elevation angle E . We suppose that distribution of E obeys a normal distribution. D is the best elevation angle and H is the height of the subject and L is the distance to the subject. σ is a parameter.

Fig.5 shows examples of this $f(E)$. The motivation $k_{motivation}$ is constant among all photographer. The y axis indicates $E(\text{rad})$. The x axis shows the evaluation

$V_{compositional}$ There are 3 lines, namely the thin line, the dotted line, bold line. The thin line shows a case from far and the bold line indicates a case from a close point. Features of this model thing can sterically estimated. Photographing direction of the imaging information that could be collected by this can be accurately estimated even when biased. Although it is not easy to shoot at different locations, it is easy to take by changing the angle of the camera. The more shot people at least the number of each person is taken we can be expected to be able to estimate the location of the subject.

4. Experiment

By performing an experiment by computer simulations to evaluate the performance of the proposed method. The experiment is conducted in the configuration of estimating the subject that can be taken only from the direction of the difficult had been part in the conventional technique. Only one subject with the height of 40 meters sets at $(x,y) = (0,0)$. The dataset of photographic information is generated by Metropolis-Hastings algorithm. For reduction of memory resources, each elevation angle is discretized into 18 pattern from 0 degree to 85 degree.

Fig.6 shows the result of estimation of location of the subject. The bullet at $(x,y)=(0,0)$ indicates the subject. The result by the traditional method is $(x,y)=(4,-46)$ represented by '+' mark. On the other hand, the result of the proposed method is $(x,y)=(-6,8)$ shown by a 'x' mark. The proposed method can improve the accuracy.

5. Conclusion

Collect only the shooting information of digital photos, we have proposed a method for estimating a subject that has attracted the social attention. The proposed a photographer model using elevation and improved conventional been difficult case. Consequently, it was possible to improve the practicability.

This work is partially supported by JSPS 15K00433.

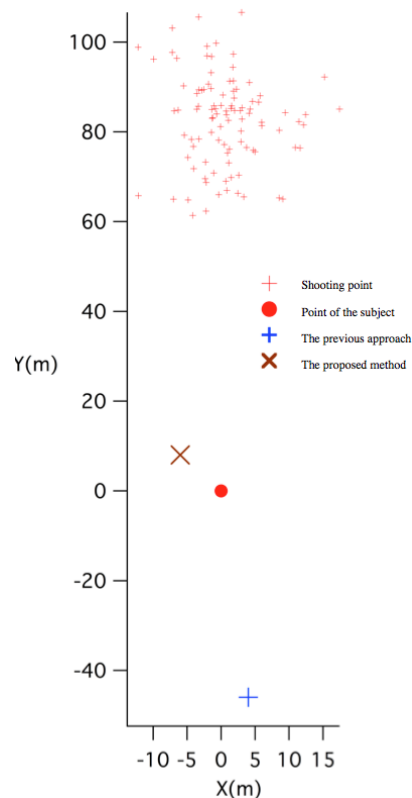


Fig.6 the result of the experiment

References

1. Y. Kubo, M. Kubo, H. Sato, M. Hirano, and A. Namatame, Understanding Geographic Attentions of Crowd from Photographing Information in *Journal of Advanced Computational Intelligence and Intelligent Informatics*, Vol. 17, No. 6(2013) 890-903.

Evaluation of a safety map generated from a collection of difference of Individuals

Viet Chau Dang

*Department of Computer Science, National Defense Academy of Japan, hasirimizu 1-10-20
yokosuka, kanagawa 239-8686, Japan*

Masao Kubo

*Department of Computer Science, National Defense Academy of Japan, hasirimizu 1-10-20
yokosuka, kanagawa 239-8686, Japan*

Hiroshi Sato

*Department of Computer Science, National Defense Academy of Japan, hasirimizu 1-10-20
yokosuka, kanagawa 239-8686, Japan*

Akira Namatame

*Department of Computer Science, National Defense Academy of Japan, hasirimizu 1-10-20
yokosuka, kanagawa 239-8686, Japan*

*E-mail: dangvietchau@gmail.com, {masaok,hsato,nama}@nda.ac.jp
www.nda.ac.jp/cs/*

Abstract

In this paper, a method to generate traffic safety maps automatically from a collection of GPS logs of a drivers' smartphone. So far methods that residents can update their traffic environment better by their opinion are required for. The proposed method which uses a collection of individual summary not raw data achieves a consistent safety map while their privacy is protected moderately. In this paper, the summarization method is explained.

Keywords: Traffic Safety Map; Risk Estimation; Smartphone Sensing; Collective Intelligence; Reality mining;

1. Introduction

In this paper, we propose a method for generating traffic safety maps based on differences in individual recognition of the road environment by using smartphone data from various users.

Safety map is a kind of risk analysis result of traffic environment. There are some works related to risk analysis. For example, Google Live Traffic is a service that utilizes GPS data from Android smartphones to estimate traffic jams based on average GPS speed. Honda initiated a project for traffic safety map in 2013

using data recorded by their Internavi in-vehicle unit, along with police reports and user contributions to their safety map website[8]. The locations where sudden brake occurs as risky spots are plotted automatically in the map.

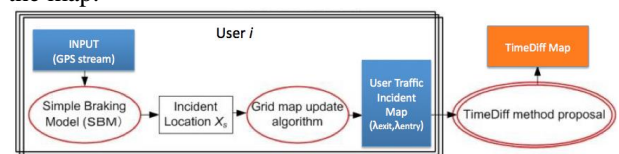


Fig.1. Process for generating traffic safety map

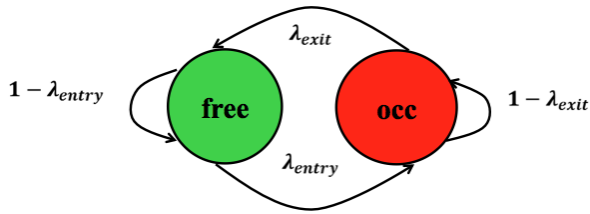


Fig.2. IMAC: it supposes that each grid forms a two-states Markov chain, which has with two states of being: free or occupied (free and occupied).

In this paper, we propose a method for integrating a collection of hazard locations based on differences in drivers' recognition of the road environment. The method is inspired by STEP technique of risk analysis in traffic safety field. We suppose that if every drivers have the same recognition of a crossroad, the level of danger will depend on one's driving skill. By contrast, where one driver recognizes a crossroad as passable and where other drivers recognize it as impassable, accidents are more likely to occur.

2. The Proposed Method

The process for generating the proposed traffic safety maps is depicted in Fig.1. We refer to the proposed traffic safety map as a TimeDiff map. The map integrates a collection of traffic-incident maps that are generated from users' smartphone log data (proposed in [1]). In this section, we explain the method for constructing a user's traffic-incident map which is the left side of Fig. 1. Finally, we describe the proposed summarization method for integrating these incident maps into a global hazard map which is shown by the right of Fig. 1.

2.1. Simple Braking Model(SBM)

We explain a method for generating a traffic incident map that can be used to interpret how a driver recognizes the road environment. The Simple Braking Model (SBM) is used for estimation of location of a hazard spot from a log stream of a smartphone.

We assume that whenever a vehicle encounters an incident, it always decreases its speed to avoid an

accident. The relation between the current speed and the moving distance is described in the following braking equation:

$$\frac{dx}{dt} = v_0 \left(1 - \frac{x}{X_s}\right)^n \quad (1)$$

where X_s is the initial distance to the incident, x is the current distance to the incident ($x=0$ when the vehicle begins to slow down), $n>0$, and v_0 is the initial speed. By fitting by eq(1), it can tell the distance X_s to an incident.

2.2. Generating a traffic-incident map with IMAC

We explain the method to estimate incident for generating a user's traffic-incident map [16], [17]. Saarinen's [16], Saarinen et al. proposed IMAC [2], a model, a method to describe for describing dynamic environment by environments with an occupancy grid map, and this model is utilized to represent a traffic incident map [1]. In incidents. With the IMAC model, an environment for mapping is evenly divided into grids. Each grid is modeled as a two-states Markov chain, which has with two states of being: free or occupied (free and occupied (see Fig.2)). The IMAC model is suitable for representing dynamic objects, such as traffic signals or incident in road environment by traffic incidents, with a grid map. Furthermore, IMAC is advanced used to estimate the transition probability parameters (λ_{exit} , λ_{entry}) by observe by observing the occurrence of the state occupied or free and the transitions between them.

To estimate the grid states from the observed events, Saarinen proposed a method to observe for observing two processes for in each grid in a dynamic environment as in Eq with Eqs. (4), (5), (2):

$$\lambda_{exit} = \frac{\# \text{occupied to free} + 1}{\# \text{occupied}}, \lambda_{entry} = \frac{\# \text{free to occupied} + 1}{\# \text{free}} \quad (2)$$



Fig. 3. Input: a log stream of smartphone


 Fig. 4. Output; the user's traffic-incident map

Fig.3 shows an example of a GPS log of a vehicle which is the input to generate a traffic incident map. Fig.4 and 5 illustrate the traffic incident map, Fig.4 shows the IMAC map of λ_{exit} and Fig.5 depicts the map of λ_{entry} . Small circles indicate incidents of this driver. As these figures show the proposed method can detect incidents at each corner adequately. In the next section we explain a method to merge multiple users' traffic incident maps.

2.3. TimeDiff method[1]

This section proposes an integration method for generating a global map from a collection of IMAC users' grid maps for $(\lambda_{exit}, \lambda_{entry})$. This method is based on the average time that users hold a different recognition of the same road environment. We call this the TimeDiff method. The global map (i.e., the TimeDiff map) shows the total time for road-recognition differences between users in a given area.

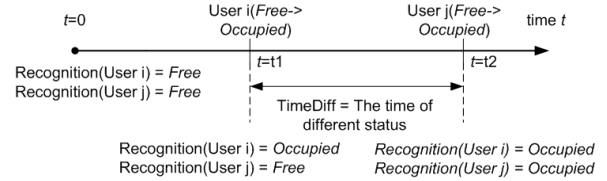


Fig. 5. Time differences in the judgment of a road environment

Consider a scenario where two vehicles are driving along a road. At this time, the road upon which the vehicles are traveling is recognized as *Free* (see Fig. 5). As the two vehicles approach a red traffic signal, they encounter an incident, and the road at this location is recognized as *Occupied*. Consequently, both vehicles come to a stop. At this time, both vehicles must change their recognition of the road environment from *Free* to *Occupied*. The TimeDiff method focuses on the time that each vehicle changes its status. It is clear that the occurrence of an accident depends on the recognition of both drivers. If two vehicles change their status at the same time, they both have the same recognition of road environment. Thus, an accident will not occur unless a driver makes a mistake in controlling the vehicle. By contrast, the more difference in time between when the recognition changes - that is, between when one vehicle recognizes the road as *Free* and other recognizes it as *Occupied* - the higher the likelihood of a collision. Thus, the global TimeDiff map is based on the road-recognition level of the users.

Let D be the set of users. We assume that all users generate their own traffic incident map $(\lambda_{exit}, \lambda_{entry})$ by using the update method in Eq. (2). We define the hazard level of each grid g in the global map with Eq. (3). Suppose two users, i and j in D , initially report an *Occupied* status. Suppose further that user i changes this status to *Free* before user j does. Alternatively, suppose that i and j initially report a *Free* status, and that the status from user i switches to *Occupied* before that of user j . The total difference in time between such status changes (whether *Occupied* or *Free*) from all pairs of users i and j in D is calculated as follows:

$$TimeDiff_g = \sum_{i \in D} \sum_{j \neq i \in D} c_{ij} (E(P_{dif}^f(i, j)) + E(P_{dif}^o(i, j))) \quad (3)$$

where $E(P_{dif}^f(i, j))$ is the difference in time between switches when each pair of users initially reports a *Free* status, and $E(P_{dif}^o(i, j))$ is the difference in time between switches when each pair of users initially

reports an *Occupied* status. c_{ij} is a probability that user i and j meet.

$$E(P_{dif}^f(i, j)) = \int_0^{B_f} t \cdot \text{Prob}[X_i = occ \leq t](1 - \text{Prob}[X_j = occ > t])dt \quad (4)$$

$$E(P_{dif}^o(i, j)) = \int_0^{B_o} t \cdot \text{Prob}[X_i = free \leq t](1 - \text{Prob}[X_j = free > t])dt \quad (5)$$

We suppose that this follows a Poisson process so that these 2 terms can be calculated briefly. For example, when $\lambda_{i,exit} = 0.01$, $\lambda_{j,exit} = 0.1$, $B_o = 10$, $c_{ij} = 1$, then $E(P_{dif}^o(i, j)) = 1.5505$.

3. Experiment

The global hazard map (i.e., the proposed TimeDiff map) is shown in Fig.6. In the Fig.6 the spots where accidents occurred in the last 5 years are also illustrated. This proposed map agrees with the accident data.

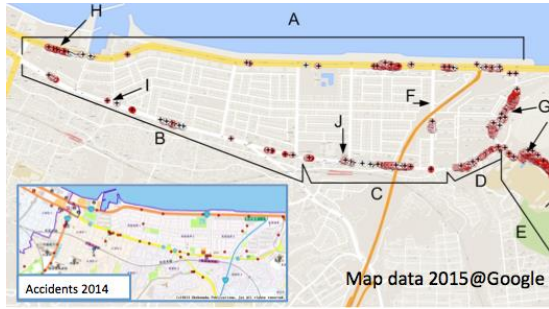


Fig. 6. Process for generating traffic safety map

Also spots where a field survey is conducted are shown in Fig.6. For example spot J has many pedestrians because it is in front of a gate of a train station. Spot H is an exit of a parking area of restaurants. Fig.7 shows spot F. Spot F is on a straight road, but some accidents have been occurring. As shown by Fig.7 spot F is along a park and has a zebra crossing. The proposed safety map can detect a zebra crossing without a signal.



Fig. 7. Spot F

4. Conclusion

In this paper, a method for generating traffic safety maps based on differences in individual recognition of the road environment by using smartphone data from various users is proposed.

References

1. V. C. Dang, H. Sato, M. Kubo and A. Namatame, Building Safety Road Maps Based on Difference of Judgment of Road Users by their Smartphone, International Journal of Advanced Computer Science and Applications(IJACSA), 6(9)(2015) 15-23.
2. J. Saarinen, A. Henrik, and J. L. Achim, Independent Markov chain occupancy grid maps for representation of dynamic environment., in Proceedings of IEEE/RSJ International Conference on Intelligent Robots and Systems (IROS)(2012)3489-3495.

Endeavor to adopt GIS data on evacuation decision making model

Saori Iwanaga

*Department of Maritime Safety Technology, Japan Coast Guard Academy, 5-1 Wakaba
Kure, Hiroshima 7378512, Japan*

Akira Namatame

*Computer Science Department., National Defense Academy, 1-10-20 Hashirimizu
Yokosuka, Kanagawa 2398686, Japan
E-mail: s-iwanaga@jcga.ac.jp, nama@nda.ac.jp*

Abstract

By Multi Agent Simulation MAS, we focused on contagion of evacuation decision making on real map assuming that not all people evacuate at the time of disaster. Then, we found that for contagion of evacuation decision making, local neighborhood is needed and connection of sub network is needed. But, there we faced on difficulty of obtaining realistic population data on map, because Census Bureau data consists of not position data but numbers and properties. In this paper, we attempt to use geographic information system GIS data and population data, then we will simulate population with heterogeneous agents and their decision making.

Keywords: Multi agent simulation, Evacuation, GIS data, Population data.

1. Introduction

The Great East Japan Earthquake was a 9.0 magnitude undersea mega thrust earthquake that occurred on Friday, March 11, 2011. After the earthquake, since there were many people who were unable to effectively evacuate, damage was considered to have spread. In fact, the ratio of victims to the residents in the Great East Japan Earthquake was lower than that in the Meiji Sanriku Earthquake, which was an 8.2 magnitude undersea mega thrust earthquake that occurred off the Pacific coast of Japan on June 15, 1896. It is believed that various disaster prevention methods take effect¹. Although according to a questionnaire and interview, about 30% of the people evacuate in Japan².

In our former study³, we adopted a multi-agent simulation that focused on psychological conditions at

time of disaster. We supposed that all agents evacuate. We confirm that it takes more time to complete evacuations if psychological conditions exist at the time of disaster. There, similar to other evacuation simulations, we set that all people decide to evacuate. In another study⁴, to deal with the condition that not all people decide to evacuate and we deal with contagion of evacuation decision making by cascade model. We found that for contagion of evacuation decision making, local neighborhood is needed and connection of sub network is needed. In these studies, we faced on difficulty of obtaining realistic population data on map, because Census Bureau data consists of not position data but numbers and properties. By Wise⁵, acquiring good data is frequently a challenge in research efforts, and many techniques have been devised in order to address this need. MAS incorporate theoretically boundless

© The 2016 International Conference on Artificial Life and Robotics (ICAROB 2016), Jan. 29-31, Okinawa Convention Center, Okinawa, Japan

heterogeneity, and consequently can be designed to take extremely rich data. For extension to many cities, it is important to obtain realistic population data on map. In this paper, we attempt to use geographic information system GIS data and population data, then we will simulate of population with heterogeneous agents and their decision making.

2. Population Synthesis and arrangement

People are arranged in houses and workers or students are arranged in their workplaces or schools. In this paper, we focus on population arranged in houses. Almost Census data include population and the number of homes in Census tract, but it is difficult to find the data including geographic locations of houses in the town.

2.1. Our method

In our former this study, we adopted 10 towns in Kure city where my academy located and 30 shelters, as shown in Fig. 1. We follow the Ohata's model⁶, which simulate of evacuation from Tsunami in Hokkaido area, and reproduced on Multi agent simulator Artisoc⁷. The area is 2.28km by 1.88km. According to the Census data of March 31, 2013, the residents per household averaged 1.937. We set an agent as two people, which is the average population of a household. It is reported that many people evacuated by family unit⁸. And we set many roads and intersections on Bing map by manual as shown in Fig. 1. And we set agents on an intersection node for each town at the first time step. Number of agents are 10,088 and number of intersection nodes and links are 213 and 384.



Fig. 1. Town, shelters and network of roads in Kure city.

2.2. Wise⁵ Method

Wise used method discussed the statistical quality of the generated population by Barthelemy and Toint⁹. It proceeds in three main successive steps: generation of individuals, generation of household type's joint distributions, and generation of households by gathering individuals. The main idea in these generation steps is to use data at the most disaggregated level possible to define joint distributions, from which individuals and households are randomly drawn. The method also makes explicit use of both continuous and discrete optimization and uses the χ^2 metric to estimate distances between estimated and generated distributions. The new generator is applied for constructing a synthetic population of 10,300,000 individuals and 4,350,000 households localized in the 589 municipalities of Belgium.

To automatically generate reasonable housing distributions, the set of all roads labeled "residential" by OpenStreetMap are extracted, and roads are assigned to Census tracts if both of their end points are located within the tract. Going tract by tract, the number of homes in the tract from the Census data is determined and the implied density of housing is calculated through the relative cumulative length of residential roads and number of housing units associated with the specific tract. The process then generates houses at the given density along all of the residential roads. After they have been assembled, households are assigned to these generated houses.

2.3. Crooks¹⁰ Method

The model combines and utilizes both raster and vector data structures into a single simulation, utilizing both ESRI grid and shapefiles with a range of different resolutions. These data capture information about the target location, an 8 by 6 km area around Haiti's capital and most densely populated city, Port-au-Prince. To initialize the population of agents in a way that realistically parallels the distribution of individuals throughout the city, to estimate of population distribution over the study area, they use population counts from the 2009 LandScan¹¹ (2011). LandScan data divides the

Table 1. The planning and control components.

		Our method	Wise method	Crooks method
Population synthesis	Data	Population	Census data	Census data
		Households	Population/2	Barthelemy methodology
Arrangement of population	Data	Homes	Bing Map	OpenStreetMap
		Roads	Bing Map	OpenStreetMap
	Position	Roads	Manual	Automatic
		Nodes	Manual	Automatic
		Homes	Manual	Along residential roads
			Evenly distribute	on grid

world into roughly 1 km by 1 km squares and assigns a population count to each cell. Such a data source is useful for estimating baseline populations where census data is missing. When using this data to initialize our agents, they assume that the agents are evenly distributed throughout the 1 km by 1 km area, excluding the parts of the environment that are determined from other GIS data to contain water or similar obstacles. Based on this information and methodology, the simulation is initialized with approximately 1.3 million agents.

3. Discussion

Almost towns have distorted boundary, but, computer simulation well-acquainted grid or cell data. So, to consider arrange of population, it is easy to use LandScan data for population synthesis. But, definition of agent depends on the case of simulation. For evacuation of disaster, it is reasonable to set agent as households.

As for arrangement of population, for extension to many cities, it is easy to use GIS data, such as OpenStreetMap. For behavior of agents, it is good to set agents on node not on over cell at first step, to easily walk on the road.

4. Example

For population synthesis, we will adapt LandScan data, which divides the 1 km by 1 km squares and assigns a population count to each cell. Fig. 2 is example of model of 8 km by 6 in Port-au-Prince, Haiti¹². A cell means 1 km by 1 km square and large population area is deep in color. We export layer file (lyr) of population to text file by ArcGIS¹³ and convert to comma separated values file (csv), then we import to Multi agent simulator Artisoc⁷.

For arrangement of population, we will adapt shapefile of road (shp), which is GIS data. Because, there are so many nodes, we thin down the data by GIS Data Converter¹⁴. Nodes are shown in Fig.2, too. In fact, the nodes have links. We arrange agents on the nodes at first based on population of the 1 km by 1 km cell.

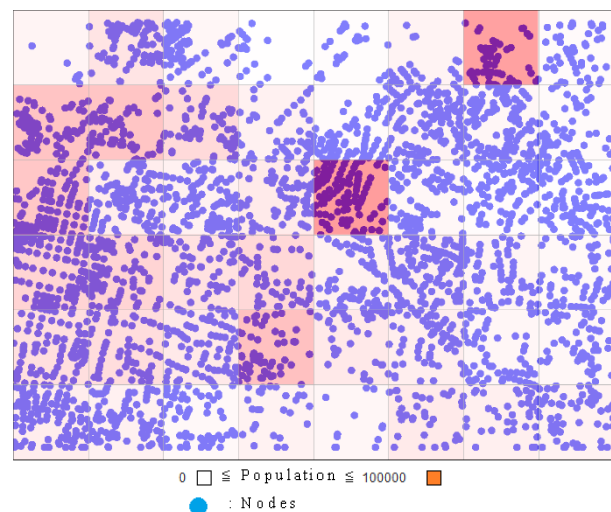


Fig. 2. Population and nodes in Port-au-Prince, Haiti.

References

1. M. Ushiyama and S. Yokomaku, Great East Japan Earthquake and Disaster Information <Special Edition> Feature of human damage (in Japanese), *Journal of Disaster Information Studies* **10** (2012) 7-13
2. H. Hirose, *Why Do People Fail to Escape* (in Japanese) (Shueisha, Tokyo, 2004)
3. S. Iwanaga and Y. Matsuura, Considering Psychological Conditions in a Tsunami Evacuation Simulation, *Information Processing and Management of Uncertainty*

- in Knowledge-Based Systems: series Communications in Computer and Information Science* **442** (2014) 437-446
4. S. Iwanaga and A. Namatame, Contagion of evacuation decision making on real map, in *Proc. of 8th International Conference on Bio-inspired Information and Communications Technologies* (ACM Digital Library, 2014)
 5. S. Wise, Using social media content to inform agent-based models for humanitarian crisis response (George Mason University, 2014)
 6. D. Ohata, N. Takai and H. Kagami, Spatial evaluation of tsunami refuge facilities in the central Kushiro city: Simulation of evacuation behavior from tsunami utilizing multi-agent system Part 2 (in Japanese), *Architectural Institute of Japan* **612** (2007) 87-91
 7. S. Yamakage, Modeling and expanding artificial societies -The possibilities of an artificial society (Shosekikobo Hayama Publishing, Tokyo, 2009)
 8. T.E. Drabek, and K. Boggs, Families in disaster: reactions and a relatives, *Journal of Marriage and the Family* (1968) 443-451
 9. J. Barthelemy and Ph.L. Toint, Synthetic Population Generation Without a Sample, *Transportation Science* **47** (2012) 266 – 279
 10. A.T. Crooks and S. Wise, GIS and agent-based models for humanitarian assistance, *Computers, Environment and Urban Systems* **4** (2013) 100–111
 11. LandScan, <http://www.ornl.gov/sci/landscan/>, Accessed 06. Aug. 2015
 12. Haiti model, <http://finder.geocommons.com/overlays/20302>, Accessed 06. Aug. 2015
 13. ArcGIS, <http://www.esri.com/>, Accessed 06. Aug. 2015
 14. GIS Data Converter for Artisoc, <http://mas.kke.co.jp/modules/tinyd0/index.php?id=12>, Accessed 06. Aug. 2015

Automatic Generation, Creativity, and Production of Narrative Contents

Takashi Ogata

*Faculty of Software and Information Science, Iwate Prefectural University
152-52, Sugo Takizawa, Iwate 020-0693, Japan*

E-mail: t-ogata@iwate-pu.ac.jp

Abstract

According to the concept of this organized session, in this presentation, we will consider the study of automatic narrative or story generation as a research field of artificial intelligence in the following levels: generation, creation, and production. Firstly, we study the technologies of narrative or story generation systems based on mainly artificial intelligence and cognitive science. Next, the artistic and aesthetic problems of narrative creation are considered in the relationships with the technologies and systems of narrative generation. Further, issues toward organizational or social narrative production are presented. The survey and discussion will conduct based on topics in this session relating to a game and advertising systems and our integrated narrative generation system.

Keywords: Multiple narrative structures model, Integrated narrative generation system (INGS), Geino information system (GIS), Narrative generation, Narrative production, Narrative creation.

1. Introduction

This organized session, *Automatic Generation, Creativity, and Production of Narrative Contents*, considers the study of automatic narrative or story generation as a highly interdisciplinary research field of information technologies, such as artificial intelligence (AI) and cognitive science, and literary theories, such as narratology.

For the author, this issue can be focused on the following levels: generation, production, and creation. The first automatic narrative “generation” means the technological aspect of systems that automatically generate narrative texts. In particular, it indicates narrative generation mechanism as a single subject. By contrast, we call narrative generation phenomenon as a collective and organizational level narrative “production”. This differentiation is dependent upon a narrative model by multiple narrative structures that the author has proposed as in the following section. The

word of production is closely associated with the organizational or social narrative making. On the other hand, the narrative “creation” is a word in a different level that has an artistic and aesthetic nuance.

This paper, at first, present the author’s multiple narrative structures model as a background of this consideration. Next, we respectively explain “Integrated Narrative Generation System: INGS”¹ and “Geino Information System: GIS”² as frameworks for single level narrative generation and multiple level narrative production. Lastly, according the above frameworks, we discuss the possibilities of narrative-based systems and contents technologies based on the relationships among narrative generation and production, future narrative creation as the level of the artistic and aesthetic problems of narrative.

2. A Model of Multiple Narrative Structures

©The 2016 International Conference on Artificial Life and Robotics (ICAROB 2016), Jan. 29-31, Okinawa Convention Center, Okinawa, Japan

For the author, one of the basic concepts for narrative generation is “multiplicity”. Narrative generation systems are necessary to design as the model of multiple narrative structures. Although this model has various sides from the formal aspect of narrative to the aspect of narrative semantics, an important characteristic is that narrative generation is divided into the next two aspects: narrative generation and reception process based on a single subject and narrative production and consumption process based on many subjects or collective authors. In other words, narrative production (and consumption) process contain many narrative generation (and reception) process. Narrative production and consumption process is the field that is socially opened and is also strongly related to documents and narratives produced by people on WWW.

Further, there exists the narrative multiplicity among various elements, such as story and character, in a narrative. For instance, in character of the *kabuki*, an actor in a work appears with the multiplicity, such as one or several characters in the drama, a person having actual and contemporary body, a person as an existence having the life story with the historical inheritance, etc.

From the viewpoint of the “Expanded Literary Theory: ELT”³ of the author, this model is partially related to the theory of polyphony by Bakhtin⁴ and the theory of inter-textuality by Kristeva⁵. The theory by

Bakhtin calls polyphony novels such types of novels that are not integrated by single voice of an author and the theory by Kristeva proposed an idea that all types of documents can respectively be exists in the network with many documents and the fragments including novels and the other genres, whether or not the author is conscious the fact. Both theories amplified narrative multiplicity in respective ways. The multiple narrative structures model comprises these theoretical frameworks.

3. Integrated Narrative Generation System

INGS is a developing narrative generation architecture that corresponds to a single level narrative generation subject. Fig. 1 shows the overview of INGS that various narrative techniques and knowledge are organized in a synthesizing system associating some literary theories for realizing ELT.

INGS is consisted of several components related to narrative generation process and control, narrative techniques for narrative structures’ generation, and narrative knowledge including relatively large-scale dictionaries.

At first, the generation process is divided into the three phases: story, discourse, and expression. A “story” generated by the story generation mechanism means the content of a narrative or a temporal sequence of events.

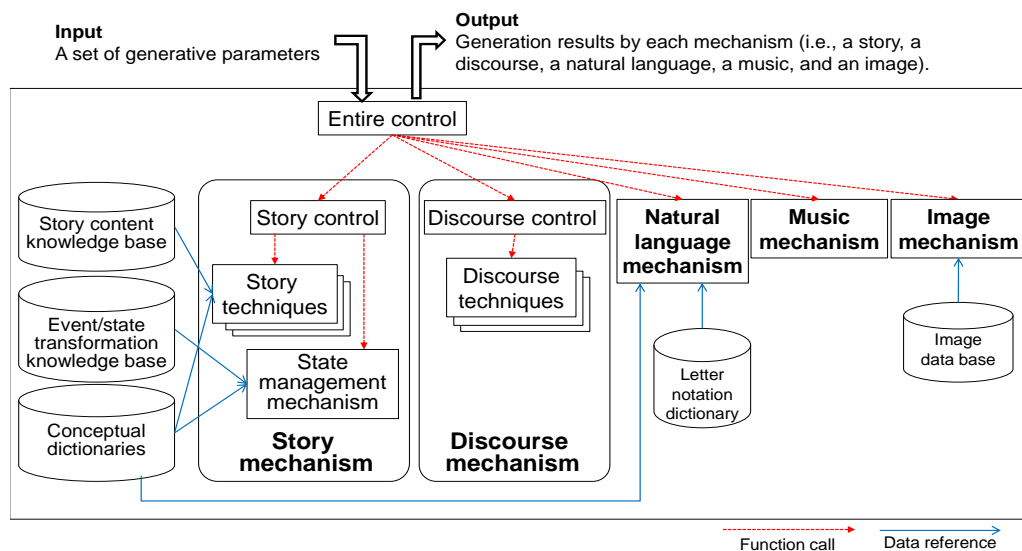


Fig. 1. An overall architecture of INGS¹

A story is represented by a tree structure consisting of the three basic units: event, relation, and state. A story structure is generated using one or more story techniques and states associating with the events are made according to another mechanism. Through this processing, an event that is a basic element of a story and a discourse are also generated. Each event is basically consisted of a verb concept and some noun and other concepts. A “discourse” transformed by the discourse mechanism means the structural aspect of how to narrate a story. A discourse structure and the surface media to narrate it are distinguished and accordingly it is described with a conceptual representation form. “Expression” means the aspect of narrative representation by various surface media including natural language, visual media, and music.

The control mechanism relating to the process, in many parts, currently utilizes a tentative approach based on parameters and rules for the above three phases. And a circulative process control, which does not limit the generation order among the phase to fixed order, is also adopted in the meta-level mechanism.

The generation of each tree structure of a story and a discourse is performed by using story techniques and discourse techniques that generate or transform from an old tree structure to a new tree structure using knowledge elements including conceptual dictionaries for verb and noun concepts. The surface narrative representation is conducted on the process.

An important design concept is “versatile” which means the potential to be used and applied to any purposes relevant to narrative generation without the limitations of themes and genres. In the future perspective of INGS, we aim at developing a versatile narrative generation architecture through which diverse narratives’ generation with various themes, genres, structures, etc is done. It means that INGS can be applied to various narrative production mechanisms as a single level narrative generation subject.

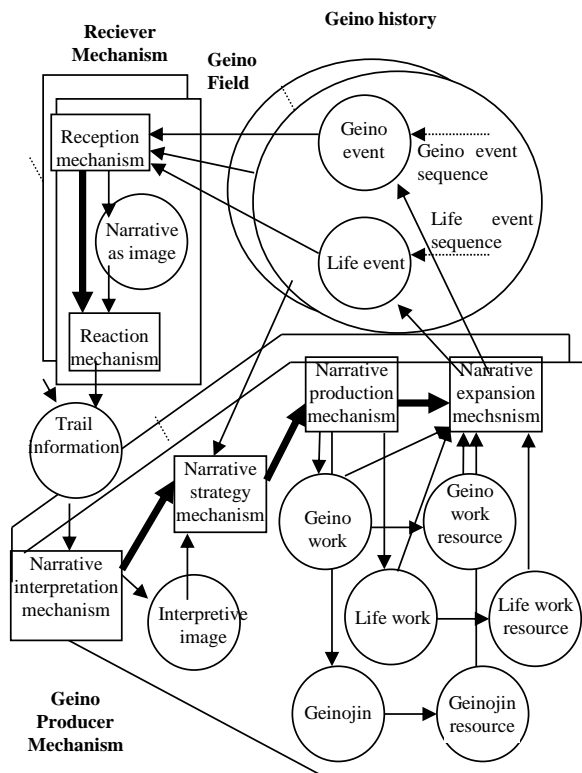
4. Geino Information System

The Japanese word *geino* has a complex meaning that includes elements of shrine rituals, entertainment, and amusement. From the viewpoint of narrative generation research, a *geino* system a whole that multiply contains

diverse narrative generation processes and is a multiple narrative phenomenon. For the author’s research plan, INGS is contained in GIS.

GIS is a model in which multiple narrative generation and production mechanisms are conducted to do the social level tasks of narrative. INGS and GIS respectively correspond to narrative generation-reception and narrative production-consumption. In GIS, various levels of narrative generation processes are driven by authors, receivers, characters, actors, and actresses. For example, a *kabuki* play is a collection of multiple narratives built around original scenarios, authentic related histories, and the actors’ private scenes. The construction will be connected with the plan for a future narrative generation system comprised of several other narrative generation systems.

Fig. 2 shows an original conceptual version of GIS². This idea of a conceptual model labelled GIS was originally based on the survey and analysis of Japanese folklore, performing arts including the *kabuki*, and angles of the modern entertainment business. A *geino* organization such as an entertainment agency or promoter is a synthetic narrative production-consumption system that aggregates a variety of narrative generation-reception processes of scenarios, lives of actors and actresses, etc. GIS is a comprehensive and multiple framework in which various narrative generation processes are driven by authors, receivers, characters, actors and actresses, directors, producers, etc. It is therefore one of the systems of multiple narrative structures.

Fig. 2. The original GIS model²

5. Generation, Production, and Creation of Narrative

Although INGS is a tentative, but progressing system that has been developing, GIS remains conceptual design level. The design and development of GIS for bridging narrative generation-reception by INGS and the narrative production-consumption is planned dependent upon the following process through application systems' development and experiment.

For example, we have developed a multimedia narrative generation system called KOSERUBE⁶. It was designed as an application using INGS inside the system, but we do not intend to have a function through which narrative generation and reception process is repeated to store a kind of history of narrative generation, namely narrative production. By designing as such circulative production-consumption system, we will implement a prototype of GIS based on the KOSERUBE.

On the other hand, Kawamura⁷ and Ogata⁸ have developed advertising generation systems based on each original ideas. Advertisement as a social system is

necessary to have a history or a story through the circulative generation, namely the level of narrative production-consumption. In the advertisement study as narrative in Ogata, in particular, INGS or the part as a single advertising generation mechanism will be able to be integrated into GIS.

Such an approach to GIS through narrative generation application systems design and development will be possible in a variety of systems, such as an entertainment game system⁹, a new narrative approach by the model of the kabuki, and so on. Further, narrative production and consumption model in which GIS is included will link to the world of contents business including the results of narrative generation and narrative generation function itself.

On the other hand, there is an important issue in another direction. By the word of narrative "creation", we mean various values beyond only generation and production of narrative. In particular, the problem of creativity of narrative is associated to diverse values, such as entertaining value, artistic value, literary value, aesthetic value, managerial value, etc. For instance, a contents business company relating to narrative production needs to sell any values through providing any narrative contents. For the author, this problem is related to the problem of narrative multiplicity or multiple narrative structures model. We have an idea that narrative multiplicity results in narrative values. The verification of this idea or hypothesis will be attempted dependent upon the development and social practice of GIS through various application systems.

6. Conclusion

This paper presented the author's multiple narrative structures model as a background of this consideration and respectively introduced INGS and GIS as frameworks for single level narrative generation and multiple level narrative production. Next, based on the above frameworks, we discussed the possibilities of narrative-based systems and contents technologies based on the relationships among narrative generation and production, further narrative creation as the level of artistic and aesthetic problems of narrative.

In the future, INGS and GIS are necessary to organically linked as an integrated system, therefore, levels of narrative generation-reception and production-

consumption also need to be associated each other. Further, the level of narrative creation should to be considered in the relationships the above multiple system framework. Designing, developing, and experimenting (including social level) INGS, GIS, and the application system are main future works.

References

1. T. Akimoto and T. Ogata, An Information Design of Narratology: The Use of Three Literary Theories in a Narrative Generation System, *Int. J. Visual Design* 7(3) (2014), pp.31-61.
2. T. Amino, Y. Kawamura and T. Ogata, Hierarchical Generation of Geino-Idol Stories: Toward Geino Information System and Narrative Marketing, *Proc. 17th Congress of the International Association of Empirical Aesthetics* (2002), pp.549-552.
3. T. Ogata, Expanded Literary Theory for Automatic Narrative Generation, *Proc. Joint 7th International Conference on Soft Computing and Intelligent Systems and 15th International Symposium on Advanced Intelligent Systems* (2014), pp.1558-1563.
4. M. Bakhtin (М. М. Бахтин), *Проблемы поэтики Достоевского*, Изд, 2е. (Москва, 1963). Transl. C. Emerson, *Problems of Dostoevsky's Poetics*. (University of Minnesota Press, 1984).
5. J. Kristeva, *Desire in Language: A Semiotic Approach to Literature and Art*. (Columbia University Press, 1980).
6. S. Imabuchi, T. Akimoto, J. Ono, and T. Ogata, T., KOSERUBE: An Application System with a Propp-based Story Grammar and Other Narrative Generation Techniques, *Proc. the 6th International Conference on Soft Computing and Intelligent Systems & the 13th International Symposium on Advanced Intelligent Systems* (2012), pp.248-253.
7. Y. Kawamura, An Analysis of the Rhetoric of Commercial Film: Toward the Building of a Commercial Film Production Support System based on Image Rhetoric, *Proc. the 2003 IEEE International Conference on Systems, Man and Cybernetics* (Washington, DC, 2003), pp.993-1000.
8. Y. Zhang, J. Ono and T. Ogata, An Advertising Rhetorical Mechanism for Single Event Combined with Conceptual Dictionary in Narrative Generation System, *7th Intl Conf. on Natural Language Processing and Knowledge Engineering* (2011), pp.340-343.
9. J. Ono and T. Ogata, Architecture of a Narrative Generation System based on a TRPG Model: The Use of an Integrated Narrative Generation System for Knowledge Acquisition (Preliminary Version), *Proc. the 3rd Int. Symposium on Computer and Networking*, (Sapporo, 2015).

A Design Plan of a Game System including an Automatic Narrative Generation Mechanism: The Entire Structure and the World Settings

Jumpei Ono

*Graduate School of Software and Information Science, Iwate Prefectural University
152-52, Sugo, Takizawa, Iwate 020-0693, Japan*

Takashi Ogata

*Faculty of Software and Information Science, Iwate Prefectural University
152-52, Sugo, Takizawa, Iwate 020-0693, Japan
E-mail: g236m001@s.iwate-pu.ac.jp, t-ogata@iwate-pu.ac.jp*

Abstract

In this paper, we propose a narrative generation system based on the scenario generation method in tabletop role-playing games (TRPGs). This system uses an integrated narrative generation system (INGS) that synthesizes various narrative generation mechanisms. The TRPG is an analog game in which one or more players (PLs) play the role of characters within the framework of the narrative prepared by the game master (GM). A PL promotes the development of scenes, which leads to the completion of the narrative. In particular, we concentrate on the “world setting” that consists of the rules or constricts for a narrative and also the components defined by the rules and the stage setting of the narrative. In an ordinary scenario, a GM sets a basic world setting for the narrative generation through the interaction between the PLs. We consider preliminarily prepared scripts corresponding to various world settings in addition to the detailed mechanism to use it.

Keywords: integrated narrative generation system, narrative generation, table-top role playing game, world setting

1. Introduction

We design a narrative generation system based on a game format that refers to a scenario generation method in tabletop role-playing games (TRPGs)¹. This system is an application of the integrated narrative generation system (INGS)²⁻⁴ that was developed using the game method; the proposed system generates a narrative based on the interactions between a user and the system.

The INGS consists of a concept generation mechanism to generate a structure of narrative, and a surface representation mechanism to represent the narrative through sounds, words and pictures. The INGS has noun conceptual dictionary and verb conceptual dictionary for constructing an event concept in the

narrative⁵, story content knowledge for constituting the structure of the narrative⁶, each event concept in the conceptual structure of narrative is connected in front state and behind it by a state-event translation knowledge base⁴.

2. Overview of the TRPG

The TRPG is an analog game where a player (PL) becomes a character and plays each role within the framework of a narrative prepared by the game master (GM). This role-playing by the character reaches a conclusion as the scene develops, and as a result, a big narrative is completed.

Further, Fig. 1 shows the relationship between the concepts of a “scenario.” The “scenario” consists of the

“world setting” and the “scene sequence. The “scenario” is formed during the progression of a game through the interaction between the GM and a PL.

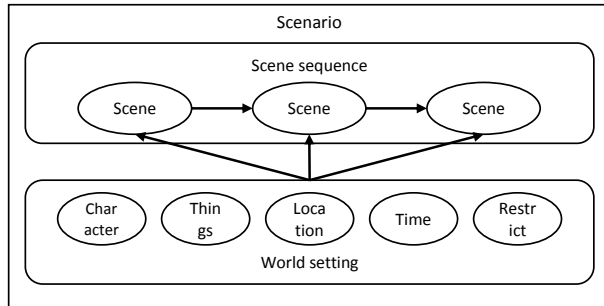


Fig. 1 Scenario and its components

We will now discuss the TRPG in detail. First, a “scene sequence” in the “scenario” is created based on the actual incident or fictitious it. Next, the “scene sequence” by the GM is modified and expanded as the game progresses. The “world setting” includes the setting of the game such as the place and time and consists of the limitations or rules applicable to the “scenario.”

3. Generation Process

The generation process is divided into three steps—“preparation of necessary information,” “generation of narrative,” and “output for a conclusive result.

In the “Preparation of necessary information” step implies the preparations required to obtain the information for an initial scenario prepared by the GM. The user inputs the information that is necessary for the GM to generate the initial state of the world setting and the scene sequence. Based on the “world setting”, the user inputs the editing contents of the conceptual dictionary, as described. The user can operate the limitations of a verb. For example, if the user adds “a cat” to the limitations of a verb concept “buy,” a cat becomes to be able to “buy” a thing like a human.

By using the initial scene sequence, a user inputs an event that will play a key role in the scenario; for example, “a man obtains a treasure.” An initial scene sequence will consist of elements. This scene will be a partial structure of a story expressed in a conceptual form. It consists of states indicating the static information of characters, things, locations, events

indicating the dynamic change in a state, and the relationships among them that can be used to connect these events structurally. The narrative is a structure consisting of events and relationships in the INGS. This is called an attribute frame. It records the properties and characteristics of individual elements and is connected to an event through an ID.

In the “generation of narrative” step, the scenario was fleshed out of the scene sequence based on the exchanges between the GM and the PL. Therefore, this part is the core of the system.

On the basis of a scene shown by the GM, the PL suggests a scene. The scene chain expansion utilizes the story (story contents) generation function of the INGS. The extended scene sequence is shown as a scenes sequence to the PL by the above mentioned process. When a progress condition is met in the present person, attribute frame of a thing, the place after this processing, GM stop that GM receives the suggestion of the scene from PL temporarily and show a “scene (climax)” and a “scene (ending)”.

In the “Output of a conclusive result” refers to the stage that outputs the scenario information in the final stage, expanding the scene sequence one way or another. For example, a novel-like sentence is thought to be created and produced as output. In this case, the game process is equivalent to a novel generation process. The system outputs a sentence as shown in the generation process. A structured text is obtained by compiling the sentences outputted for every scene. The user includes more names in the scenes and completes a story by modifying the outputted end results.

4. World Setting

This section shows a conceptual dictionary in the INGS, and describes the “world setting”.

4.1 Conceptual dictionary in the INGS

The conceptual dictionary is related to the “world setting”. The conceptual dictionary is used for controlling the world setting in a designed system. The conceptual dictionary includes a noun conceptual dictionary, verb conceptual dictionary, and modifier conceptual dictionary (conceptual dictionary for adjective, adjective verb, and adverb); it stores knowledge at the conceptual level as components. A

characteristic function in verb conceptual dictionary is to describe the “restriction” while using the elements in events such as “~ do ~.” To adjust this “restriction,” the system should be able to modify a realistic event such as “Taro eats an ice cream” into an unrealistic event such as “The car eats an ice cream.”

5.2 Elements in the World Setting

The “world setting” is like a stage for the progression of a narrative. The “world setting”, define the type of characters, things, locations, time, event and action that characters can perform. As a similar example, Nomura suggested the “background world”⁷. The “background world” consists of “space”, “existence”, “time”, and the component generates “phenomenon” and “event”.

Here, we mention each element in the “world setting”.

A) Restrictions

The “world setting” including the stage setting of the games such as places or times, has a kind of limitation in a “scenario.” The narrative could include “a human cannot fly in the sky without a vehicle” in the realistic “world setting.” On the other hand, “a person can fly in the sky” in the fantastic “world setting.” In this way, the restriction is a kind of a rule for the action possibility.

B) Locations

“Locations” is the space where characters or things exist and, for the objective achievement of a character, it can be either a beneficial or an unfavorable element. They show the environment of the stage for the narrative. For example, a character is police, climate etc. in the realistic “locations”.

C) Time

“Time” is the time when characters or things exist and affects the styles of characters or things. For example, for the case “to light,” the character of the reality world uses a lighter, whereas a more primitive world character uses a firestone.

D) Characters

“Characters” are all the people appearing in the narrative, which include the characters controlled by the user. Each character has the purpose, in the case of a character being controlled by a PL, and the PL defines the purpose of the character as the game progresses; other characters are defined by the GM at the start of the

game. Those purpose is stored an attribute frames in the states.

E) Things

“Things” represent the tools that a character uses; particularly these are the elements that are necessary for achieving the purpose of the character.

The above five elements are the “world setting” component. When the designed system generates a narrative and progresses game, the elements is required relationship between characters, things, locations, that are included in the “world setting”. Concretely, there is (1) a relationship among characters, things, and locations, (2) an ability to achieve a certain purpose, (3) a motive of each character. In addition, for (2), the restrictions in the “word setting” limit the ability of each element.

5.3 Generation of a Narrative through the World Setting

Fig.2, Fig.3 and Fig.4 show (1) a relationship among characters, things, and locations (Fig.2), (2) an ability to achieve a certain purpose (Fig.3), (3) a motive of each character (Fig.3).

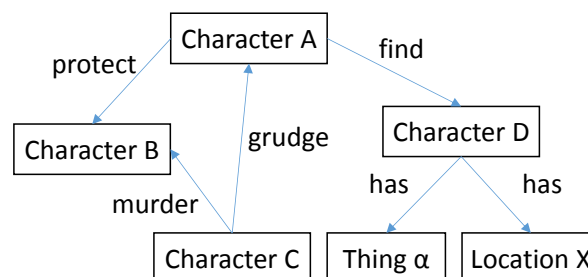


Fig. 2 (1) Relationship among characters, things, and locations

“Character A” can search [any person]
 “Character A” can fight against [any person]
 “Character B” dies of a [disease]
 “Character C” can interfere with “Character A”
 “Character C” can fight against [any person]
 “Character D” can cure [disease] using “thing α” at “location X”

Fig. 3 (2) Ability to achieve a certain purpose

<p>“Character A” wants to help “Character B” “Character C” wants to disturb “Character A” “Character C” wants to kill “Character B” “Character D” wants money</p>
--

Fig. 4 (3) Motive of each character

The system generates a “scene sequence” shown in Fig. 5 by using the relationship (Fig. 3) and motive (Fig. 4). The “Character C” inserts “C interferes with A” into behind either scene for to achieve its own purpose.

<p>Scene 1. “B” gets a [disease]→ Scene 2. “A” searches for a doctor→ Scene 3. “A” hears the wish of “D”→ Scene 4. “A” grants the wish of “D”→ Scene 5. “D” starts the treatment of “B”→ Scene 6-a. “B” is saved, or Scene 6-b. “B” is not saved</p>

Fig. 5 Generated scene sequence

The system gives an appearance based on the world setting in Fig. 2, as shown in Fig. 5. The appearances of each element are change based on “world setting”. For example, in the realistic “world setting,” the “character A” is a detective and the “character C” is a climate. In contrast, in the fantastic “world setting,” the “character A” is hero, “[disease]” is a curse, and the “character C” is a devil.

5. Conclusion

In this paper, we proposed a narrative generation system based on a game format that refers to the scenario generation method in a TRPG. This system can support story generation through the interactions with the user.

In the present conditions, the system design assumes that a human being controls the PL side and generates a story accordingly. When a system computer controls the PL side, there is a possibility of generation of a story that is unexpected for a human user. However, in the present conditions, the scene for the PL side is decided by the user and the procedure for this generation is not clear. Therefore, the scene is difficult to be designed by an automated PL. In future, we would like to automate the process of scene generation on the PL side.

References

1. “Tabletop role-playing game - Wikipedia, the free encyclopedia”, https://en.wikipedia.org/wiki/Tabletop_role-playing_game (Last access, 2015, July).
2. T. Ogata and A. Kanai, *An Introduction of Informatics of Narratology: on Thought and Technology of Narrative Generation* (Gakubunsha, Tokyo, 2010). (In Japanese)
3. T. Akimoto and T. Ogata, An Information Design of Narratology: The Use of Three Literary Theories in a Narrative Generation System, *The International Journal of Visual Design*, 7(3) (2014) 31-61.
4. T. Ogata, Development of the Integrated Narrative Generation System, *Proc. of the 13th Forum on Information Technology* (2), (2014) 323-330. (In Japanese)
5. T. Ogata, Building Conceptual Dictionaries for an Integrated Narrative Generation System, *Journal of Robotics, Networking and Artificial Life*, 1(4) (2015) 270-284.
6. T. Ogata and J. Ono, Language Notation Dictionaries and the Use in an Integrated Narrative Generation System, *IEICE Technical Report*, 115(69) (2015) 25-30. (In Japanese)
7. K. Nomura, *Sory Sekai no Tsukurikata (How to Making a Story World)* (Shinkigensya, Tokyo, 2014). (In Japanese)

A Way for using the Verb Conceptual Dictionary in an Integrated Narrative Generation System: the Use of Co-occurrence Information on Verb Concepts

Takashi Ogata

*Faculty of Software and Information Science, Iwate Prefectural University
152-52, Sugo Takizawa, Iwate 020-0693, Japan*

Jumpei Ono

*Graduate School of Software and Information Science, Iwate Prefectural University
152-52, Sugo Takizawa, Iwate 020-0693, Japan
E-mail: t-ogata@iwate-pu.ac.jp, g236m001@s.iwate-pu.ac.jp*

Abstract

This study presents a method of selecting verb concepts based on analysis of co-occurrence information of verbs in modern Japanese novels collected from the Japanese digital library, “Aozora Bunko”. We plan to incorporate the proposed method into an integrated narrative generation system (INGS) that synthesizes various mechanisms (story generation, sentence generation, and so on) for narrative generation. We are currently developing such a system. In this study, we provide an overview of INGS and examine mechanisms related to the proposed method. In a verb conceptual dictionary that we have developed, as verb concepts of a variety of difficulty (comprehensibility) are mixed, the objective in this study is to adjust difficulty of verb concepts by using co-occurrence information on verb concepts. Our hypothesis is that the original concepts of co-occurrence and the resulting concepts have a proportional relationship. We investigate this hypothesis by incorporating proposed mechanism into an INGS.

Keywords: Co-occurrence information, Integrated narrative generation system, Verb conceptual dictionary, Verb concept

1. Introduction

This paper mainly focuses on an event generation in the story generation mechanism and verb conceptual dictionary in an integrated narrative generation system (INGS)¹⁻³ (these details are mentioned in the section 2). An event composed of a verb concept and noun concepts. However, their concepts are selected randomly in an event generation in the INGS. Therefore, we previously proposed a method of the verb concept selection based on frequency information⁴. Here, we propose a method of the verb concept selection based on co-occurrence information.

2. The Architecture of an Integrated Narrative Generation System

The architecture of our INGS is shown in Fig. 1. The system is composed of a concept generation mechanism used to generate a story structure and edit it (discourse), and a surface representation mechanism to represent a narrative. These mechanisms use dictionaries (stored concepts⁵, language notations⁶), story contents knowledge base (stored knowledge for generating structure of narrative)⁷, the state-event translation knowledge base (stored knowledge for connecting between each event and states in the conceptual structure)³.

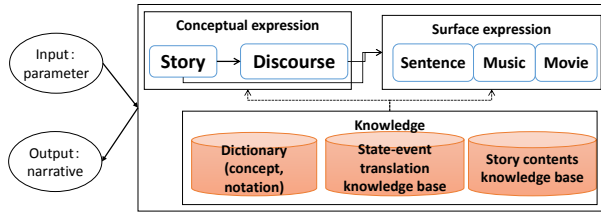


Fig. 1. Architecture of INGS

3. Overview of Conceptual Dictionaries

Conceptual dictionaries have a hierarchical structure from higher to lower concepts.

A) Hierarchy of Noun Concepts

The noun conceptual dictionary currently contains 115,765 terminal concepts and 5,809 intermediate concepts. Each intermediate concept has a list of hyponymy terminal concepts, the number of depths in the hierarchy, the super-ordinate concepts, and a list of the hyponymy intermediate concepts.

B) Hierarchy of Verb Concepts

The verb conceptual dictionary has 11,951 terminal concepts and 36 intermediate categories. Fig. 2. shows the description of the verb concept “bite.” Each terminal verb concept has the following three elements: 1) a sentence that includes the verb (“sentence-pattern” in Fig.2.), 2) the types of required noun cases (“case-frame”), and 3) defining the range which each noun concept in the case-frame(s) requires (“constraint”).

```
((name 齧る 2 [bite])
(sentence-pattern
  "N1 が N2 を齧る" [N1 bite N2])
(case-cons-set
((case-frame
  ((agent N1) (object N2) ...))
(constraint
  ((人[human] -死人[corpse] -人間<人称>
    [human<person>]-準人間[semi-human])
  (食料[food] -調味料[flavoring] -飲物・た
    ばこ[drink・cigarette] -汁[soup]))))
...))
```

Fig. 2. Description of the verb concept “bite”

C) Generating an Event Concept in the Story Generation Mechanism

A story generation process expands a story structure by using story techniques. This process includes an event generation. An event is generated based on the description of the case-frame. A verb concept that is used in an event concept generation is decided based on

© The 2016 International Conference on Artificial Life and Robotics (ICAROB 2016), Jan. 29-31, Okinawa Convention Center, Okinawa, Japan

story techniques and story contents knowledge. The objective of this paper is to revise this selecting method.

4. Acquiring Co-occurrence Information

A) Used Texts and Method

We used “Aozora Bunk”, which includes 4980 texts of primarily Japanese novels published from 1872 to 1963, to acquire co-occurrence data of verbs. At first, co-occurrence information of all verbs in the texts was acquired.

The following (1) is a formula in KH Coder⁷ to calculate the co-occurrence data. In the formula, S_a is equal to the total number of sentences that include verb a in the text; S_b is the total number of sentences that include verb b in the text; $S_a \cap S_b$ is the total number of sentences including both a and b in the text; and S_{all} is the total number of sentences included in the text.

$$f = \frac{|S_a \cap S_b|}{|S_a|} / \frac{|S_b|}{S_{all}} \quad (1)$$

B) Result

The co-occurrence information was corresponded to 4866 terminal verb concepts in the verb conceptual dictionary in INGS. As an example, Table. 1 shows co-occurrence data of “bite”. Each verb concept connects to 143.44 verb concepts in average.

Table. 1. Co-occurrence data of “bite”

Co-occurrence information	Relating verb concepts
141.1954	打ち上げる 1[shoot up], 慕う 1[pout], etc.
70.5977	飽きる 1[loss intent], 謀る 1[deceive], etc.
	...<Omitted>...
1.035663	出来る 7[be able to]
1.001386	戻る 1[return]

5. Preliminary Questionable Research

We evaluated the effectiveness in the verb concepts selection based on the acquired co-occurrence information.

5.1 Preparation

Four lists of verb concepts, which were extracted from the stories generated by using a partial mechanism in

INGS, were used in the questionable research.

A) A Used Story Generation Method in INGS

The story structures were generated by using “story contents grammar”⁸ and the mechanism that we have been developing for a part in INGS. A hierarchy of the story contents grammar has a layer of “functions”. The level is the most fundamental and a sequence of functions form a basic structure of a story. And, each function is extended to the lower level where one or more verb concepts are instantiated by selected from the candidates.

Fig. 3. shows used functions and the fixed sequence. Each of the functions is rewritten by the lower levels to reach to the level of one or more concrete verb concepts.

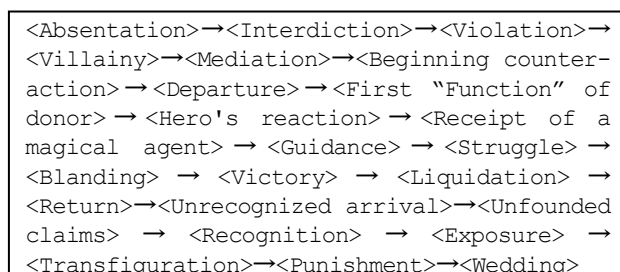


Fig.3. A used sequence of functions

B) Making Verb Concept Lists

We acquired co-occurrence data using the above story generation mechanism by the following method. When the mechanism selects a concrete verb concept from generally many verb concepts, it utilizes co-occurrence data as shown in the next types.

[Max] The story generation mechanism generated 5 stories by repeatedly using a verb concept that has the strongest co-occurrence with the prior verb concept and finally decided 39 verb concepts in one story selected randomly from the above stories.

[Middle] The mechanism generated 5 stories by repeatedly using a verb concept that has the medium co-occurrence with the prior verb concept and finally decided 41 verb concepts in one story selected randomly from the above stories.

[Min] The mechanism generated 5 stories by repeatedly using a verb concept that has the weakest co-occurrence with the prior verb concept and finally decided 47 verb

concepts in one story selected randomly from the above stories.

[Random] The mechanism generated 5 stories by repeatedly using a verb concept randomly for the prior verb concepts and finally decided 41 verb concepts in one story selected randomly from the above stories.

In addition, in the following cases, a verb concept is selected randomly: 1) the first verb concept in story generation, 2) when two or more candidates exist in the selection timing, 3) when no candidates with co-occurrence data in the selection timing.

5.2 First Evaluation

A) Goal and Process

The goal is to check the relationship between the degree of co-occurrence information and the degree of comprehensibility by the users. The subjects were five students. They read four kinds of verb concepts lists (max, middle, min, and random) to select a value from 1 (*easy*) to 5 (*difficult*). We set a time limit of five minutes for each verb list.

B) Result

As shown in Table. 2 shows the result, we could not see clear differences among the subjects. In short, co-occurrence information of verb concepts does not influence the comprehensibility.

Table. 2. Evaluation result

	A	B	C	D	E	Average
[Max]	1.23	2.54	2.87	3.08	2.82	2.51
[Middle]	1.29	2.73	3.00	2.80	3.10	2.59
[Min]	1.26	2.50	3.02	2.85	2.65	2.46
[Random]	1.15	2.60	2.93	2.80	2.63	2.42

This result was similar to the case of noun concept selection based on co-occurrence information that we previously implemented⁹. Also, frequency and co-occurrence are clearly different methods to adjust verb concepts selection in INGS.

5.3 Second Evaluation

A) Goal

On the other hand, in the noun concepts selection using co-occurrence information, we confirmed another

method. In the method, a noun concept is associated with other noun concepts that have the similar degree of co-occurrence information⁹. We adapt this method to verb concepts selection.

B) Process

For the above stories of max, middle, and min, we calculated the absolute values of difference (D) between the value of a verb concept X and the value of the next verb concept Y . Fig. 4 shows the procedure. As the case of noun concepts selection, we consider if D is lower, it indicates the similar comprehensibility. However, it is necessary to be actually investigated the consideration. In this paper, we check whether lower D is resulted by higher degree of co-occurrence. It enables to adjust selecting verb concepts using co-occurrence of verb concepts.

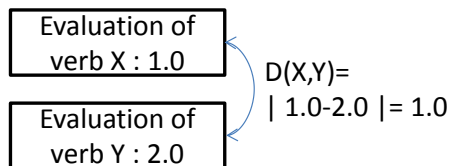


Fig. 4 Calculating D

C) Result

Table 3 shows the result of calculating D . In this Table 3, we did not use verb concepts that were selected randomly. The average of D in [Max] was smaller than others. If lower D is related to the similar degree of comprehensibility of the verb concepts, we may be able to use this result to adjust the degree of comprehensibility of verb concepts.

Table 3. The result of calculating D

Method	The number of the evaluated verb concepts	Average of D
[Max]	12	0.43
[Middle]	15	0.76
[Min]	14	0.96

6. Conclusion

This paper preliminarily proposed a method of a verb concept selection by using co-occurrence information for the conceptual event generation mechanism in INGS. The results indicate a next design direction of the verb concepts generation in INGS: to use verb concepts that

have co-occurrence relationship for prior verb concept enables to select them by similar degree of comprehensibility. The proposed method may useful to adjust the verb concepts selection in INGS.

In the future, we plan to precisely improve the method to finally integrate methods of concepts selection in event generation in INGS using frequency and co-occurrence of words.

References

1. Ogata, T. and Kanai, A.: An Introduction of Informatics of Narratology: On Thought and Technology of Narrative Generation, Gakubunsha, 2010. (In Japanese)
2. Akimoto, T. and Ogata, T.: "An Information Design of Narratology: The Use of Three Literary Theories in a Narrative Generation System", The International Journal of Visual Design, 7(3), 31-61, 2014.
3. Ogata, T.: "Development of the Integrated Narrative Generation System", Proc. of the 13th Forum on Information Technology II, 323-330, 2014. (In Japanese)
4. Ogata, T. and Ono, J.: "Controlling the use of Semantic Concepts in an Integrated Narrative Generation System: The use of the Verb Frequency Information", Proc. of 21st International Symposium on Artificial Life and Robotics, 2016. (to appear)
5. Ogata, T.: "Building Conceptual Dictionaries for an Integrated Narrative Generation System", Journal of Robotics, Networking and Artificial Life, 1(4), 270-284, 2015.
6. Ogata, T. and Ono, J.: "Language Notation Dictionaries and the Use in an Integrated Narrative Generation System", IEICE Technical Report, 115(69), 25-30, 2015. (In Japanese)
7. Higuchi, K.: "Quantitative Analysis of Textual Data: Differentiation and Coordination of Two Approaches", Sociological Theory and Methods, 19(1), 101-115, 2004.
8. Imabuchi, S. and Ogata, T.: "A Story Generation System Based on Propp Theory: As a Mechanism in an Integrated Narrative Generation System", Advances in Natural Language Processing, Springer, 7614, 312-321, 2012.
9. Ono, J. and Ogata, T.: "Noun Concepts Selection in Events Based on the Co-occurrence Relation in Verb Concepts and Noun Concepts: Mechanisms for the Story Generation in an Integrated Narrative Generation System", Proc. of the 14th Forum on Information Technology II, 239-242, 2015. (In Japanese)
10. Ono, J. and Ogata, T.: "Selecting Noun Concepts Based on Accounting Data: As a Mechanism in the Integrated Narrative Generation System", IEICE Technical Report, 114(366), 49-54, 2014. (In Japanese)

A Viewing Experiment on the Effects of Advertising Story

Yoji Kawamura

Faculty of Business Administration, Kinki University, 3-4-1 Kowakae

Higashi-osaka, Osaka 577-8502, Japan

E-mail: kawamura@bus.kindai.ac.jp

www.kindai.ac.jp

Abstract

This research lays out the conception and functions of developed Commercial Film Production Support System (CFPSS). The research then explains the results of a viewing experiment that utilized CFPSS. In this experiment where commercial films of beer were utilized, the following findings were obtained: in inducing interest, the evaluation of image type of advertising story is high; in stimulating willingness to buy, the evaluation of provider type is high; and mise-en-scène or editing attracts interest and the advertising story associated with product function and the supporting production and distribution stimulates willingness to buy. These findings gradually clarify the following creative know-how of the creator; to attract consumer interests by focusing on the stories of consumer situations in case consumers do not aware or understand their products or services; to arouse their willingness to buy by focusing on the products and stories of their acceptance and effects in case consumers have a certain level of understanding and interests in products or services.

Keywords: Commercial Film, Advertising Story, Editing, Viewing Experiment, Interest, Willingness to Buy

1. Introduction

There are case studies into effective commercial films with a focus on marketing and advertisement.¹ Some of these studies include elements of advertising expression that have been classified and extracted to enhance advertising effects. Alternatively, other studies classifying advertising expressions according to the nature of the information (comparative, unique selling proposition, preemptive, hyperbole, generic-informatic), and the nature of transformation (user image, brand image, use occasion, generic-transformatic) examine the ideas of advertising expressions.² However, these studies provide insight into advertising expressions from a particular vantage point, and are not conducive to developing specific rules for creating images at the microcosm level.

Related to print advertisements (text, photo, poster etc.), studies examine an interpretation and analysis of the

effect of advertising rhetoric on viewers.^{3,4,5} However, these studies do not include analyses related to commercial films.

This paper aims to extract rules to create more specific expressions of commercial films based on a viewing experiment using CFPSS.

This experiment aims to show how an advertising story influences viewers using commercial films derived from the four types of advertising stories generated from the image shots that were likely related to the viewer's associations and experiences.

2. CFPSS

Fig. 1 shows the plan of CFPSS.⁶ The concept of CFPSS is to generate the various commercial films adapted to the user's keywords and sentences (life scenario) input. CFPSS includes a database of 3643 image shots converted to a commercial film, that

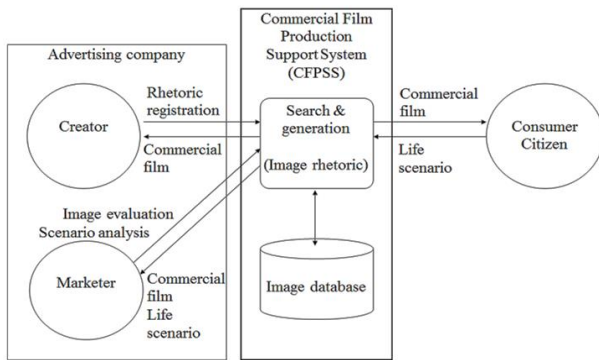


Fig. 1. CFPSS Plan.

searches and classifies image shots based on keywords and sentences. The system includes a function to generate the storyboard based on the selection of advertising story, and playback in the order arranged in the storyboard. The menu of advertising story is as follows;⁷

- Provider story type (PT): The primary structure expresses the provider's story (production and distribution, product function, effect on company). This is the "story of the product" and "story of the company."
- Consumer story type (CT): This primary structure expresses consumers' stories (consumption situation, product acceptance, consumption effect). This is the "story of consumption."
- Overall type (OT): This structure generally expresses both the provider's and consumer's stories. This is represented as PT + CT.
- Image type (IT): This structure expresses images related to the consumer situation, though does not express product acceptance and consumption effects in the film. Rather this structure represents a product function. This category also includes structures expressing an image that does not belong to the consumer, provider, or product function.

3. Viewing Experiment

3.1. Data and Method

In this experiment, commercial films of beer were utilized. For the study, 55 viewers provided four to five associated keywords about beer and simple sentences (approximately one to two lines) about the relationship

between beer and the viewer. The sample included 28 male and 27 female participants between from 20 to 23 years of age. The input from the viewers included such keywords and statements as:

- Asahi, foam, throat, bitter, mug
- A glass to drink when tired, such as after working a part-time job, is the best.
- Foam, twenty, summer, baseball, green soybeans
- The body gets itchy after drinking a beer.
- Alcohol, throat, bitter, taste, foam
- For me, beer is not something necessary, but I think it is necessary on social occasions.

The database was then searched for images using a summary of the viewers' sentences as input. An advertising story was selected from the OT, PT, CT, and IT types, and the generated image shot shown to viewers who provided their evaluations and feedback for each.

3.2. Results

Table 1 summarizes the image shot composition and order of the generated commercial film. The numbers in the advertising story columns indicate the order of the shots. Fig. 2 reports the viewer evaluations of interest and willingness to buy related to the four types of commercial films. IT has a greatest evaluation for interest, while PT has a greatest evaluation for willingness to buy.

The summary below shows the consolidated contents for films that stimulate interest and willingness to buy for items with responses in more than two cases. The frequency of comments is indicated in parentheses.

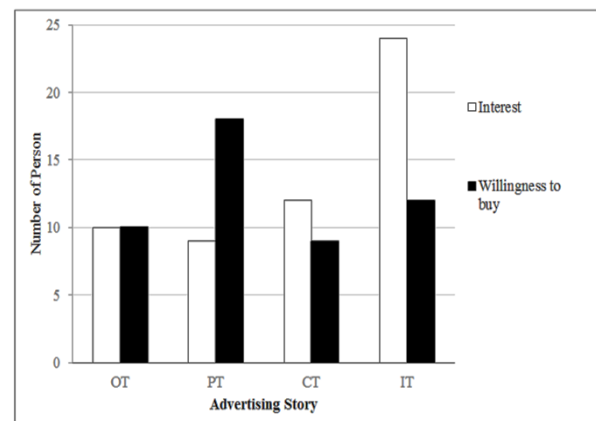


Fig. 2. Interest and willingness to buy by advertising story.

Table 1. Image shot composition and order of the generated commercial film.

Advertising Story Phase	Advertising Story				Abstract of Shots
	OT	PT	CT	IT	
Production and Distribution	1	1			Introduction of the production area of the beer
		2			Production process of the beer (low-temperature aging)
		3			Transporting the beer tank
	2	4			The cook sings a song while cooking
		5			The products are being transported on the belt conveyor
Consumption Situation	3		1	1	A lifesaver monitoring the sea
			2	2	A man walking toward home
				3	Appear to drink a beer, even without a glass
				4	People talking to the camera man
	4		3	5	The consumers asked to tour the factory
				6	People talking at the stock exchange
				7	People preparing meal at the poolside
Product Function			4	8	Attempting to borrow a bottle opener for beer at a seaside house
		6			Catch the copy of a product “All for Delight”
		7			Promotion of urban scenery and the product
	5	8	5	9	Foam spilling from the beer mug
Product Acceptance	6	9		10	Canned beer breaking the ice
	7		6		Consumer drinking beer in the cup
	8		7		Drinking beer while socializing
			8		Making a toast with a large number of people
Consumption Effect			9		Making a mysterious face
	9		10		Drinking beer and recounting funny stories
Effect on Company	10	10			Urban (overseas, China) scenery

3.2.1. Areas of Interest

Primarily related to the advertising story (including advertising concept):

- Copy added: “All for the customer’s ‘delight’!!” (4)
- Acceptance added: Demonstrations of an energetic way of drinking (2)
- Production added: When the provider’s efforts to provide delicious beer is apparent (3)

Primarily related to mise-en-scène:

- Product: When the beer is widely zoomed in (2)
- Buddy added: Where there are many people are having fun (6)
- Scene added: Scene showing that the beer is actually consumed with a gesture, even in the absence of a glass (14)

Primarily related to editing:

- Connection: The plot unravels gradually (2) / There is a perceived association from the creation of a professional story extending to the consumer’s consumption (2)
- Irregularity: The type of commercial message was initially unknown (2)

3.2.2. Willingness to Buy

Primarily related to the advertising story (including advertising concept):

- Copy added: Deceived by the phrase “All for the customer’s ‘delight’!!” (7)
- Situation added: A scene depicting drinking in a bar, imagining that the cuisine was easy (3) / A scene of a man going home (2)
- Acceptance added: Many scenes indicating product consumption (7)
- Effects added: The beer was consumed with zest (4)
- Production added: The story clearly shows the producer’s efforts to provide delicious beer (2)

Primarily related to mise-en-scène:

- Product: The beer overflows from the cup (2) / The beer package in ice representing the chill and delight (3)
- Scene added: Drinking beer with a gesture is impressive (2)

3.3. Discussion

3.3.1. Interest and Willingness to Buy

The IT type generated a high level of interest through a variety of image shots. However, the willingness to buy was highest for the PT type using image shots focusing on the product's function and production and distribution.

Fig. 3 summarizes the results in terms of interest and willingness to buy, or to the films' representation techniques (advertising story, mise-en-scène, editing). The results indicate that mise-en-scène and editing attracts interest, and the advertising story associated with the product function and illustrating production and distribution stimulates willingness to buy.

3.3.2. Strategic Rules of Advertising

From these results, it is conceivable to set the following strategic or tactical rules of advertising communications. These rules are applicable to the intelligent robot that has know-how of advertising communication between robot and human being.

- For the unfamiliar people for products, the robot stimulates the people's interest by presenting the wonder or extraordinary scene and information (for example, the environment or scene that the products are hidden consciously, the scene where there has been a lot of people etc.).
- The robot tries to grasp whether the people's interest has been evoked. If the people's interest has been aroused, the robot stimulates the willingness to buy by presenting a scene of functions, acceptance and effects of the product.

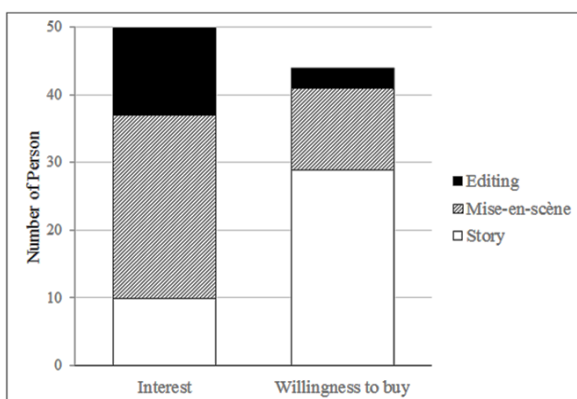


Fig. 3. Areas of interest and the willingness to buy.

4. Conclusion

An experiment using commercial films for beer generated the following findings:

- The IT type created the most interest through a variety of image shots.
- The PT type stimulated the highest willingness to buy using a variety of image shots showing the product function and the associated production and distribution.
- Mise-en-scène or editing attracts interest, and the advertising story associated with product function and the supporting production and distribution stimulates willingness to buy.

These findings gradually clarify the relationship between the commercial film techniques and their effects and significantly contribute to the symbolization and systematization of creator's inherent creative know-how.

Acknowledgements

This work was supported by JSPS KAKENHI Grant Number 22500102.

References

1. D. W. Stewart and D. H. Furse, *Effective television advertising: A study of 1000 commercials* (Lexington Books, Lexington, MA, 1986).
2. H. A. Laskey, E. Day and M. R. Crask, Typology of main message strategies for television commercial, *J. Advertising* **18**(1) (1989) 36-41.
3. E. F. McQuarrie and D. G. Mick, Figures of rhetoric in advertising language, *J. Consumer Research* **22**(4) (1996) 424-438.
4. B. A. Huhmann and P. A. Albinsson, Does rhetoric impact advertising effectiveness with liking controlled?, *European J. Marketing* **46**(11/12) (2012) 1476-1500.
5. I. G. Theodorakis, C. Koritos and V. Stathakopoulos, Rhetorical maneuvers in a controversial tide: assessing the boundaries of advertising rhetoric, *J. Advertising* **44**(1) (2015) 14-24.
6. Y. Kawamura, An analysis of the rhetoric of commercial film -toward the building of a commercial film production support system based on image rhetoric, in *Proc. 2003 IEEE Int. Conf. Systems, Man and Cybernetics*, (Washington, DC., 2003), pp.993-1000.
7. Y. Kawamura, An analysis on the story and editing techniques of commercial film -toward the building of a commercial film production support information system, *J. Advertising Science* **50** (2009) 16-32. (In Japanese).

Examination of Robotic Aerospace Engines Maintenance Supported by Augmented Reality through Cloud Manufacturing

Mosab Alrashed

*Manufacturing Department, School of Aerospace, Transport and Manufacturing, Cranfield University, Cranfield
Bedfordshire, MK43 0AL, UK*

Yaser Yadekar

*Manufacturing Department, School of Aerospace, Transport and Manufacturing, Cranfield University, Cranfield
Bedfordshire, MK43 0AL, UK*

John Ahmet Erkoyuncu

*Manufacturing Department, School of Aerospace, Transport and Manufacturing, Cranfield University, Cranfield
Bedfordshire, MK43 0AL, UK*

Yifan Zhao

*EPSRC Centre for Innovative Manufacturing in Through-life Engineering Services, Cranfield
Bedfordshire, MK43 0AL, UK*

E-mail: m.alrashed@cranfield.ac.uk, y.m.yadekar@cranfield.ac.uk, j.a.erkoyuncu@cranfield.ac.uk ,

*yifan.zhao@cranfield.ac.uk
www.cranfield.ac.uk*

Abstract

This Paper aims to develop a demonstration using a mobile device to apply augmented reality to allow remote maintenance activities. This research was focused primarily on the aerospace industry studies as there was a research gap as there are few relevant researches in the manufacturing field and accepted industry needs. The targets were achieved by developing and designing controls in the engineering steps to create the optimum conditions for augmented reality. The design process pursued in four stages: first, research the current practice of using augmented reality remotely in manufacturing maintenance; second, classify maintenance remote assisting problems and weakness in augmented reality; third, design and develop software and hardware, depending on the case study for a prototype solution to remote maintenance enhanced by the augmented reality that can be demonstrated and tested; finally, validate the developed software and demonstration using industrial experts and authentic reports. The results of this project were an open source software updated IDEA 2.0 and a hardware robot, dubbed McRobot, which was automated to conduct the inspection process and support the augmented reality requirement. Three type of evaluations were done at the end, and all of them recorded positive feedback, validating this project for future development.

Keywords: Augmented Reality, Virtual Reality, Mixed Reality, Cloud, NDT, Remote Maintenance, Robot Maintenance, Wearable Maintenance Gadgets.

1. Introduction

Maintenance is a costly process that requires time, money and effort. Maintenance duration is one of the main factors that must constantly be reduced as much as possible, as it has dire implications in terms of effort and money. This is particularly true in the aerospace field, where even one minute can have a significant cost implication. Major manufacturing and management teams in academic and industrial institutions have provided solutions to the maintenance quandary. In one such example, Toyota TM developed concepts and strategies to reduce maintenance as much as possible in terms of cost and time (Biehl et al. 2004). These days, technological gadgets have entered the arena and use cutting-edge technology to provide solutions to maintenance issues. While there are many technologies being developed for manufacturing activities, several come particularly recommended for future work and development (Akan et al. 2011; Fuhrmann & Encarnac n.d.; Neumann & Majoros 1998). One of the current developing technologies that is of increasing interest is augmented reality (AR). The focus on AR from some of the biggest industries and firms is growing, as these players are coming to realise the valuable benefits of the technology. Also, the use of new technologies in information systems and advanced networks such as Cloud Manufacturing has allowed the manufacturing industry to apply new and complex manufacturing systems. Cloud Manufacturing is one of the emerging technologies that helps to exceed the limitation that been faced in AR process. AR can be described as the coexistence of virtual content with the real world through the, compositing and supplementing of a particular area in the real world using powerful technology tools (Azuma et al. 2001). To understand AR, one must also be familiar with VR (virtual reality) and mixed-reality. Numerous definitions are available for VR, but they are all similar in meaning. A simple definition might be the simulation of virtual objects in a virtual environment through the use of a wearable gadget like glasses or gloves. (Steuer 1992). Mixed reality (or hybrid reality, as it was formerly known) can be defined as virtual objects that can be enhanced in a real environment or vice versa (Pan et al. 2006; Zauner et al. 2003). Virtual reality (VR)

is a part of augmented reality, and combining the two produces mixed reality. In Figure 1, the cross-section of the reality egg demonstrates the relationship between AR and VR: the egg shell represents mixed reality; the egg white signifies augmented reality; and the yolk is virtual reality.

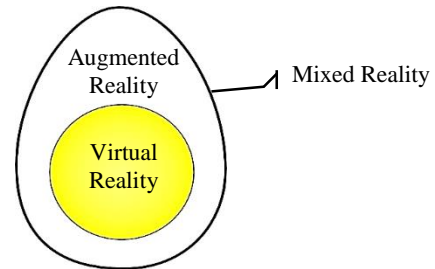


Fig. 1. Reality Egg representing the relation between augmented, virtual and mixed reality.

2. Methodology

The method for this project can be broken down into three stages. The first was a build-up stage, wherein collected data, gathered information and explored the technology as a research term. This phase also comprised a literature review and industrial requirements. By finishing the first phase and moving to the second stage, reserved for design and development, the whole project plan became clearer and was able to identify the gaps that needed to be filled. Finally, the last loop methodology stage included the process required to build up the design that was developed in stage two. It was beneficial to discover that moving backward from stage three (process) to stage two (design and development) could happen easily if updates are needed in the design or development algorithms. Moreover, the same goes for stage two (design and development) and stage one (research), if one needs to add new knowledge or correct some misunderstanding.

2.1. First Stage: Research

A literature review had been undertaken that included the basics of augmented reality, the reinforcement of AR, remote maintenance in manufacturing fields (with comparisons), the applications of AR, the benefits of using AR with remote support, and the scientific gaps that AR needs to fill. Also, one of the objectives of this project was to understand the real technology used in

industries and to evaluate its. Nuclear AMRC (Advanced Manufacturing Research Centre) in Sheffield was visited to review the latest projects that industrial companies are developing as this science centre is one of the biggest in the UK for developing technologies (Stuart Harrison 2015).

2.2. Second Stage: Design and Development

The project's core goal was a successful design and development phase. This stage summaries the ideas need to build in term of the core of the requirements and objectives by studying the process, data flow and tools available. One can break down the design process into two separate areas: software and hardware. The software was designed by using the software engineering tools like storyboard, sequence diagram and IDF0 for data flowing, while computer engineering tools like mock-up and prototype designs were used for the hardware. Not neglecting the application programs that need to edited with specific details as an example of the programming language or the framework simulating the scripts.

2.3. Third Stage: Process

This phase consists of five parts related to each other consecutively. They are hardware development, software development, experiments, analysis and validation.

3. Results

3.1. IDEA 2.0

An open source software run on Matlab was updated with new functionality to enhance the outcomes from the data presentation algorithms with AR technology. This software was developed originally by Multipolar Infrared Vision –Vision Infrarouge Multipolaire: MiViM, Laval University, Canada then it was updated at Cranfield University under the title of IDEA (Infrared Degradation Enhancement and Analysis).

3.2. Recognition Effectiveness

At first, to augment any multimedia type with regard to the samples that are in the project, there was the need to for recognise the location and calculate the size of the enhancement objects. The locations were learned using OpenCV libraries, as it is open source and customisable

to detect the damages to the composites materials. Then calculated the size to enhance in the top of the material needed to coincide the real world and acted as a real object. Finally, tracked the points detected and sizes calculated to provide the dynamic affecting the composite surface.

3.3. Image Enhancement

After developing the ability to recognise the size and location of the damage, the capability to enhance infrared images became easier and more practical. The only method that was new was calculating the size of the enhanced image related to the distance from the sample surface. The infrared images were generated from the same software (IDEA) after analysing the raw files that were taken from a previous project done at Cranfield University.

3.4. 3D Enhancement

The same technique of using image enhancement was used in 3D enhancement. These images were generated from IDEA software by analysing the infrared images analysed the RAW files together. The same method was used to calculate the size based on the distance moving on the sample surface.

4. Validation

The three types of evaluations were used for validation. The results support the idea of remote maintenance using augmented reality in manufacturing as the experts and specialists have industrials backgrounds.

4.1. Ultrasound, Infrared and Augmented Realty Comparison Results

One of the methods to evaluate the results of this this project was to compare the result of the previous project done on the same samples to calculate the damage size on the 30J damage shiny sample. The results were calculated with different tools; ultrasound (c-scan), an infrared (25 HZ) camera and an RGB camera (represent the AR). The results would not be the same, as each tool has a different accuracy, but the range result could provide positive conclusion about the validation level for the result and offer more ideas to build upon for future development and recommendations.

4.2. Experts and Specialists Feedback

Some experts and specialists were interviewed to corroborate the project's outcomes. Their feedback was separated into three parts according to IDEA output results and their recommendations for the termination.

The experts' positions are as follows:

- Lecturer in Digital Signal and Image Processing at Cranfield University.
- Research Fellow at EPSRC Centre in Through-Life Engineering Services at Cranfield University.
- Research Fellow in School of Aerospace, Transport and Manufacturing at Cranfield University.
- Lecturer in Service Simulation and Visualisation at Cranfield University.
- Software Development Engineer in School of Aerospace, Transport and Manufacturing at Cranfield University.

4.3. Authentic Similar Projects Contrast

As is known to the authors, there have been few papers published about robotics in manufacturing. Most of these papers, published and developed at the end of twentieth century, concern the early birth of ideas in this field. The most famous papers focus, on specific tasks or deliver an idea that the authors hope will be developed in a future work. They all tacitly agree on the benefits of robotic systems in many facets such as income, costs, time, quality and management (Karasic & Asada 2011; Chirn & McFarlane 2000; Luk et al. 2005; Mesa-barrameda et al. 2014).

5. Conclusions

All the requirements and qualifications needed to make a remote assistant for manufacturing using augmented reality were realised. An Open-source hardware and software were developed and available for any engineer to customise those in such way to fit the industry area. Remote assistance improved the quality of augmented reality supporting. Although there are some limitations with regard to big data and graphic process rendering these shortcomings could be addressed using a private cloud. The key advantage of this Cloud is the ability to control the Cloud infrastructure without third party intervention. The case study using augmented reality in

maintenance demonstrated a more rapid process in manufacturing workflow. The designed case study in the aerospace maintenance field pointed many further benefits than initially estimated.

References

1. Akan, B. et al., 2011. Intuitive industrial robot programming through incremental multimodal language and augmented reality. *Proceedings - IEEE International Conference on Robotics and Automation*, pp.3934–3939.
2. Azuma, R. et al., 2001. Recent Advances in Augmented Reality. *IEEE Computer Graphics and Applications*, 21(November), pp.1–15.
3. Biehl, M., Prater, E. & McIntyre, J.R., 2004. Remote repair, diagnostics, and maintenance. *Communications of the ACM*, 47(11), pp.100–106.
4. Fuhrmann, A. & Encarnac, L.M., *The Studierstube Augmented.*, pp.33–54.
5. Neumann, U. & Majoros, a., 1998. Cognitive, performance, and systems issues for augmented reality applications in manufacturing and maintenance. *Proceedings. IEEE 1998 Virtual Reality Annual International Symposium* (Cat. No.98CB36180).
6. Pan, Z. et al., 2006. Virtual reality and mixed reality for virtual learning environments. *Computers and Graphics* (Pergamon), 30(1), pp.20–28.
7. Steuer, J., 1992. Defining Virtual Reality: Dimensions Determining Telepresence. *Journal of Communication*, 42(4), pp.73–93.
8. Stuart Harrison, 2015. Advancing UK manufacturing. Available at: <http://namrc.co.uk/wp-content/uploads/2014/11/Nuclear-AMRC-brochure.pdf> [Accessed September 2, 2015].
9. Zauner, J. et al., 2003. Authoring of a mixed reality assembly instructor for hierarchical structures. *The Second IEEE and ACM International Symposium on Mixed and Augmented Reality*, 2003. *Proceedings*.
10. Karasic, G. & Asada, H., 2011. *For Aircraft Manufacturing and Maintenance*.
11. Chirn, J.-L.C.J.-L. & McFarlane, D.C., 2000. A holonic component-based approach to reconfigurable manufacturing control architecture. *Proceedings 11th International Workshop on Database and Expert Systems Applications*.
12. Luk, B.L. et al., 2005. Intelligent legged climbing service robot for remote maintenance applications in hazardous environments. *Robotics and Autonomous Systems*, 53(2), pp.142–152.
13. Mesa-Barrameda, E. et al., 2014. Sensor Deployment by a Robot in an Unknown Orthogonal Region : Achieving Full Coverage.

Unit Layout Design Supporting System of Cell Assembly Machine Using Two Robots by Reinforcement Learning

Yusaku Ikai

*Department of Human Information Systems, Gifu University, Yanagido 1-1,
Gifu-shi, Gifu 501-1194, JAPAN*

Hidehiko Yamamoto

*Department of Mechanical Engineering, Gifu University, Yanagido 1-1
Gifu-shi, Gifu 501-1194, JAPAN*

Takayoshi Yamada

*Department of Mechanical Engineering, Gifu University, Yanagido 1-1
Gifu-shi, Gifu 501-1194, JAPAN
E-mail: t3128002@gifu-u.ac.jp, yam-h@gifu-u.ac.jp, yamat@gifu-u.ac.jp
<http://www1.gifu-u.ac.jp/~yamlab/>*

Abstract

In this study, we explain the development of Design Supporting System for Cell Assembly Machine System (CAMS) which systemizes the decision of the unit layout that composes the assembly machine using two robots. CAMS uses Profit Sharing which is one of the Reinforcement Learning methods, determining each units layout. We apply CAMS to the assembly of the differential gear box in automotive parts to verify its validity.

Keywords: Reinforcement Learning, Profit Sharing, Differential Gear Box, Assembly Robot

1. Introduction

In recent years, the design of the assembly machine with a robot has been promoted. In designing such assembly machine, the good and bad product efficiencies are changed by the arrangement of each unit. However, because the placement of units is determined by the experience of engineers in many factories, it is questionable whether the determined placement is good or not. In order to solve this problem, we propose Design Supporting System for Cell Assembly Machine System(CAMS) that determines the efficient units placement of assembly machine and the job roles of the robot using Profit Sharing which is one of the

Reinforcement Learning methods. In addition, CAMS is applied to the design of the differential gear box assembling machine using two robots to verify its validity.

2. Differential Gear Box Assembly Machine

We develop a system to support units arrangement design of the assembly machine of the differential gear box. The gear box is an automobile part which has 5 units: differential case, side gear, pinion mate, jig and the storage station. Also, this assembly machine repeats the following five works using two robots as shown in Fig.1.

Work [1]: Take the differential case and assemble it on the jig.
 Work [2]: Take the side gears and assemble it into the differential case.
 Work [3]: Take the side gears and assemble it into the differential case.
 Work [4]: Take the pinion mate and assemble it into the differential case.
 Work [5]: Take the pinion mate and assemble it into the differential case.
 Work [6]: Put the finished product on the storage station.

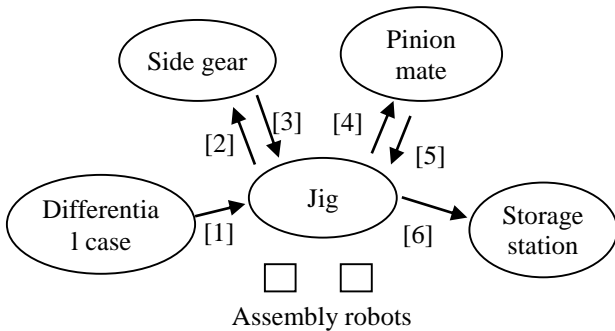


Fig.1 Assembly machine proceed

3. CAMS

3-1 Module configuration of the CAMS

CAMS consists of two modules, (i)the conditions making module, and (ii)the learning module as shown in Fig2.

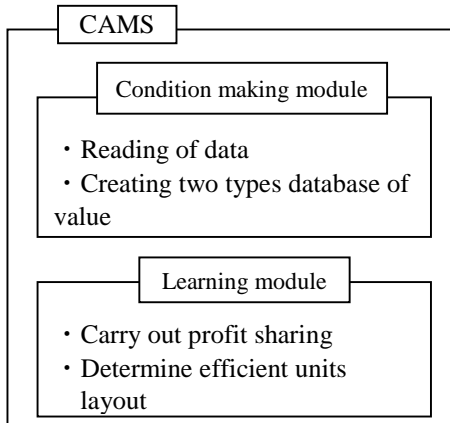


Fig.2 Outline of CAMS

The condition making module reads the learning data and creates two type databases whose values are necessary for the learning module. The two type databases determine the units layout and the robots job roles. In the

learning module, the units layout and the division of work are determined by Profit sharing.

3-2 Condition making module

The condition making module carries out the following processes.

Step1-1: Reading the learning data

The condition making module reads the information necessary for determining the unit arrangements and the robots job roles. The information to be read is the number of learning, initial values of a value, a basic reward value, one side size of an arrangement candidate place, and arrangement possible areas of each unit.

Step1-2: Create units value database.

As shown in Fig.3, the arrangement of possible area of each unit are divided square-shaped and each lattice are regarded as arrangement candidate place. And Units value database corresponding to each arrangement candidate place is created. It is used the decision of the units layout.

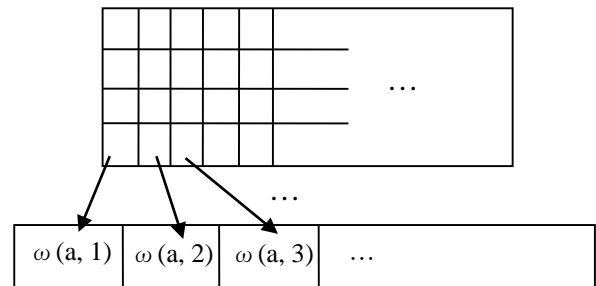


Fig.3 Each arrangement candidate place and its units value database

Step1-3: Create the robots job roles value database

As shown in Table.1, the robots job role value database of m-th steps is created for each robot.

Table.1 Database of value for the robots job roles

	1	2	...	m
Right robot	$\omega(R, 1)$	$\omega(R, 2)$...	$\omega(R, m)$
Left robot	$\omega(L, 1)$	$\omega(L, 2)$...	$\omega(L, m)$

Step1-4: Give an initial value to databases

The two type databases created in Step1-2 and 1-3 are given an initial value.

3-3 Learning module

Learning module using profit sharing performs the following processes.

Step2-1: Create the initial value of the reference time.

Parts are randomly placed regulation times, and its average evaluation time is defined as the initial value of the reference time.

Step2-2: Select units layout and robots job roles.

The units layout and the robots job roles are determined by roulette selection. Roulette selection randomly selects action by the ratio of the value. This probability is calculated by Eq. (1).

$$p(a | s) = \frac{\omega(s,a)}{\sum \omega(s,n)} \quad (1)$$

s: Unit a: Arrangement candidate place
n: The number of arrangement candidate place
 ω : Value of the arrangement candidate place

The left side of this equation indicates the probability of selecting the a-th arrangement candidate place of the unit s. The denominator of the right side means the sum of the value of the unit s. The molecule means a value of the a-th arrangement candidate place of the unit s. By the probability based on Eq. (1), the arrangement candidate places with higher values are likely to be located, the lower value are less likely to be located.

Step2-3: Calculate the unit work time of the robot

Using the determined units layout and the robots job roles, each working time of robots are calculated. In this study, we define that robot repeats the three operations to perform the work. In other words, the work is divided in the following three operations as shown in Fig.4, and a unit work time is the sum of the operation time.

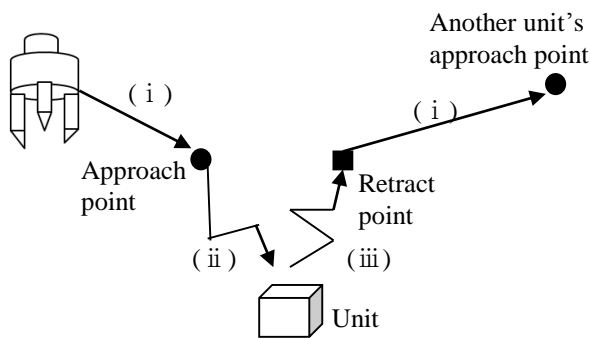


Fig.4 Operation of robot

(i) Fast-forward operation

Fast forward movement from the retract point of the unit to the approach point.

(ii) Acquiring or assembling operation

It is the operation that robot moves from the approach point to complete acquisition or assembly of the unit.

(iii) Retracting operation

The operation that moves to the retract point. The operation is carried out after (ii).

Fast forward operating time is calculated by calculating the moving distance of robot by Pythagorean theorem and dividing it by fast forward velocity. The acquiring or assembling operation time and the retracting operation time are any one of the values.

Step2-4: Calculate the evaluation time

The evaluation time is calculated using each working time that was calculated. The evaluation time is the time that is criteria of whether giving reward or not. Comparing T_R and T_L as shown in Fig.5, the longer one is defined as the evaluation time.

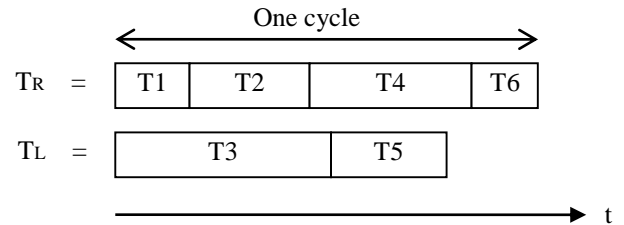


Fig.5 Calculate of the evaluation time

T_R : Total of 1 cycle work time of right robot

T_L : Total of 1 cycle work time of left robot

Step2-5: Compare the evaluation time and the reference time

The evaluation time which is obtained at Step2-4 is compared with the reference time which is obtained at Step2-1. If the evaluation time is larger than the reference time, proceed to Step2-6. If it is smaller than the reference time, proceed to Step2-2.

Step2-6: Compare the evaluation time and the minimum evaluation time

If the evaluation time is smaller than the minimum evaluation time, it is defined as minimum evaluation time. In this case, the current unit layout and the robots job roles are recorded as the best result. If the minimum evaluation time hasn't been determined, the evaluation time which is determined in Step2-4 is defined as the initial minimum evaluation time.

Step2-7: Distribution of reward

The units value database and the robots job roles value database which are currently selected are given reward to update the value. The reward used the value that is read in Step1-1.

Step2-8: Update of the reference time

The new reference time J_{n+1} is calculated by Eq.2.

$$J_{n+1} = \frac{T_1 + T_2 + \dots + T_n + T_{n+1}}{n+1} \quad (2)$$

T_n : The evaluation time that is less than the reference time in n -th times.

Step2-9 : End of learning

Learning module repeats Step2-2~2-8 regulation times. After that, unit layout and the robots job roles of the minimum evaluation time are adopted as the most efficient result in this simulation.

4. Simulation Application

We applied CAMS to the following differential gear box assembly machine to verify the goodness of CAMS. Learning conditions of the initial value is 10, the reward value is 10, the number of learning is 300,000 times. Unit arranged areas are set to five as shown in Fig.6, and one side of the arrangement candidate place is 100mm.

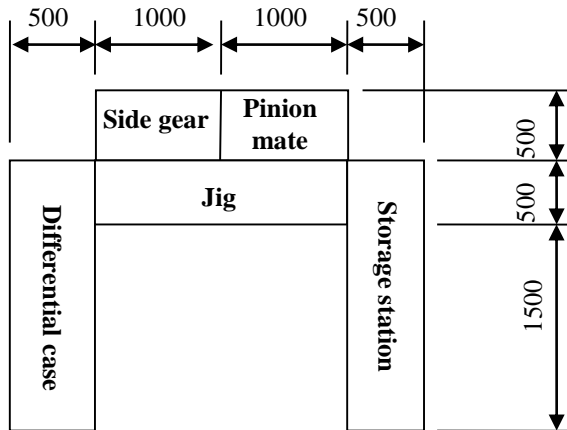


Fig.6 Units arranged area

We ran the simulations for the assembly machine which determined the random unit layout to compare the learning results. Two types of the average evaluation time and the minimum evaluation time of 10 times simulations are shown in Table.2. CAMS obtains good results from both of them as shown in Table.2. In particular, the average evaluation time, 24.84720[s], by

CAMS is about half of the average evaluation time, 42.86408[s], in random. Thus, we find that CAMS can stabilize determined efficient unit layout and robots job roles. Thereby, the validity of CAMS is verified. In addition, the unit layout of the shortest evaluation time in 10 times simulation by CAMS is shown in Fig.7. And, robots job roles is shown in Table.3.

Table.2 Average time of 10 times simulations

	Average evaluation time[s]	Minimum evaluation time[s]
Layout by random	42.86408	19.39125
Layout by CAMS	24.84720	18.897421

Table.3 Robots job roles by CAMS

	Work1	Work2	Work3	Work4	Work5	Work6
Robot	Right	Left	Left	Right	Left	Right

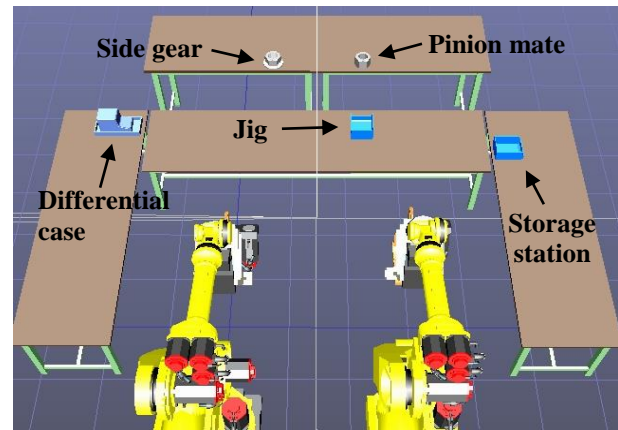


Fig.7 Units layout by CAMS

5. Conclusion

In this paper, we have described the development of CAMS in determining an efficient unit layout and robots job roles of the assembly machine using two robots. From the simulation results, it is found that the units layout and the robots job roles obtained by CAMS have shorter evaluation time than the random layout one. This makes it possible to verify the validity of CAMS. Furthermore, we are able to apply the reinforcement learning to decision of unit arrangement and the robots job roles.

Virtual Input Parts Decision System of Job-Shop Production Line by using GA with ON / OFF Gene

Junji Ito

*Department of Human Information Systems, Gifu University, Yanagido 1-1,
Gifu-shi, Gifu, 501-1194, JAPAN*

Hidehiko Yamamoto

*Department of Human Information Systems, Gifu University, Yanagido 1-1,
Gifu-shi, Gifu, 501-1194, JAPAN*

Takayoshi Yamada

*Department of Human Information Systems, Gifu University, Yanagido 1-1,
Gifu-shi, Gifu, 501-1194, JAPAN*

*E-mail: t3128003@gifu-u.ac.jp, yam-h@gifu-u.ac.jp, yamat@gifu-u.ac.jp
<http://www1.gifu-u.ac.jp/~yamlab/>*

Abstract

In this laboratory, priority allocation method to the machine tool that has the minimum machining time was developed. Moreover, to solve the problem of this system, to make better solutions .we have developed the determination system of parts using GA. If we apply GA to job shop production line, lethal gene and loss time of the problem occur. The problem of the lethal gene is a thing to use the concept of the ON/OFF gene, and the problem at loss time is solved by devising the order of turning on parts to begin the next cycle even if one cycle does not end to the last.

Keywords: Virtual Input Parts Decision System, GA, Job Shop Production, Loss time,

1. Introduction

In this study, the research aims to improve a production efficiency of a job-shop production line where one person carries parts, and to make the visualization of the production results. We already developed the existing priority allocation method to allocate parts to the machine tools. The method has the special characteristic that a part is allocated to the machine tool whose machining time is the shortest. To make better solutions, we develop the new system to find the input parts order using Genetic Algorithm (GA)

2. Virtual Input Parts Decision System

If we apply the conventional GA to find the order to put the parts into the machine tools in a job shop production line, a lethal gene problem occurs because of different

production conditions such that different types of parts need different manufacturing processes. Real genes have a directive information that sends the order to work when it is necessary and to stop when it isn't necessary. We express this directive information as the concept of ON / OFF (activation / deactivation) of the gene. This expression solves the lethal gene problem when it happens by inserting the concept of ON / OFF genes for switching the directive information into a chromosome. In this study, by using the concept of ON / OFF genes, we propose the simulator to decide the best parts input order. We call this simulator as Virtual Input Parts Decision by ON/OFF Genes (VIPDOG).

VIPDOG has 2 configuration systems as follows:

- 1) The parts order decision system to indicate the parts input and processing orders of a job shop production line.
- 2) The virtual production system that performs the visualization of the working environments acquired by

VIPDOG. The virtual production system can check what will happen in the future and some experienced engineers can discuss the problems to solve them.

2. 1 VIPDOG

Locus gene used in the GA of the VIPDOG is represented by three elements.

- i) Part name
- ii) Process name
- iii) Machine tool

The respective numerical value of the element in the locus gene shows the part and the necessary process and each machine tool specifically. In addition, Element numerical value of the process name shows the worker's work information ① and ② at the same time.

① The operator turns on the parts to machine tools

② The operator takes out the parts from the machine tool

Fig.1 shows an example of one of the locus gene.

[A,K(1),M(1)]

Fig.1 one of the locus gene

A of this locus indicates the part name. K (1) shows the process name. M (1) shows the machine tool. Numerical value of K () and M () to enter a positive integer. K (1) shows the process 1. M (1) shows the machine tool 1. If the number of K () is a positive integer, the gene show the work information ① at the same time.

As an example of the work information ②, it show the Fig.2.

[B,K(0),M(2)]

Fig.2 one of the locus gene

Only for K shown a process name, Numeric value of () exists that become zero. At this time, it show the work information ②.

2. 2 ON/OFF gene

Genes representing the work information ② in a gene used for GA in this study is expressed by ON / OFF gene wake up when needed.

The advantage of the ON / OFF gene prevents the occurrence of a lethal gene. ON / OFF gene is located between the normal genes that represent the working information ① as shown in Fig.3. As shown in fig.4 the switching ON / OFF is operated before and after the evaluation of fitness.

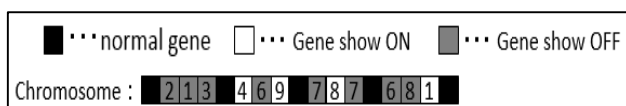


Fig3 ON / OFF genes sandwiched between normal genes

© The 2016 International Conference on Artificial Life and Robotics (ICAROB 2016), Jan. 29-31, Okinawa Convention Center, Okinawa, Japan

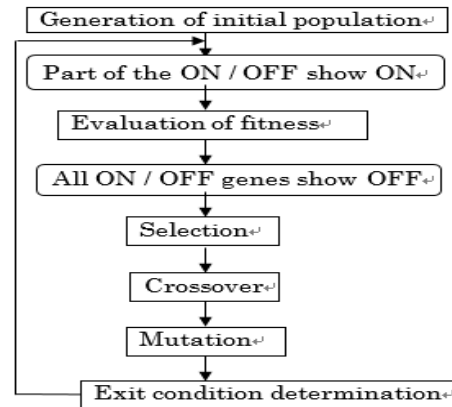


Fig4 Algorithm of ON / OFF switch

2. 3 ON/OFF gene not to occur lethal gene

The chromosomes of the parents that produce a lethal gene by crossover are shown in Fig5

Parent 1

[A,K(1),M(1)] [A,K(0),M(1)] [B,K(2),M(1)] [C,K(1),M(2)]

Parent 2

[B,K(2),M(1)] [B,K(0),M(1)] [A,K(1),M(1)] [D,K(1),M(3)]

Fig.5 Chromosome to be parents

The chromosomes of the children after circulation crossover are shown in Fig6.

Child 1

[A,K(1),M(1)] [B,K(0),M(1)] [B,K(2),M(1)] [D,K(1),M(3)]

Child 2

[B,K(2),M(1)] [A,K(0),M(1)] [A,K(1),M(1)] [C,K(1),M(2)]

Fig.6 Chromosome of children

To summarize the information of child 1 chromosome is as follows.

1. Put the part A to machine tool 1
2. Take out the part B from the machine tool 1
3. Put the part B to the machine tool 1
4. Put the part D to the machine tool 3

In the case of 2, there is a conflict when the operator wants to take the part B which has not being introduced into the machine tool 1. This is the occurrence of a lethal gene. The lethal gene problems can be solved by using the ON / OFF genes. ON / OFF gene is the gene that has a work information ②. That is, it was the gene with K a (0) in the locus. Inside the chromosomes, we use the ON/OFF gene and if we turn it OFF, the gene of the chromosome is not used. It is shown in Fig.7

Parent 1

[A,K(1),M(1)] [B,K(2),M(1)] [C,K(1),M(2)]

Parent 2

[B,K(2),M(1)] [A,K(1),M(1)] [D,K(1),M(3)]

Fig.7 OFF chromosome to be parents

Fig.8 shows the chromosomes of the children after circulation crossover.

Child 1

[A,K(1),M(1)] [B,K(2),M(1)] [D,K(1),M(3)]

Child 2

[B,K(2),M(1)] [A,K(1),M(1)] [C,K(1),M(2)]

Fig.8 OFF chromosome of children

The next three cases indicate to summarize the information of child 1 chromosome

1. Put the part A to machine tool 1
2. Put the part B to the machine tool 1
3. Put the part D to the machine tool 3

In the second case, the operator trying to put the part B into the machine tool. The machine tool already has the part A. The contradiction of work that putting part B is impossible occurs. This is the occurrence of a lethal gene. In order to avoid the lethal gene, we adopt to watch the lethal gene and all genes before the lethal gene, and change necessary and sleeping off gene to ON. The above example shows in fig.8 and fig.9. We watch [B,K(2),M(1)] corresponding to a child1 lethal gene and [A,K(1),M(1)] of fig.8. If the gene that has the information of taking out the part A from the machine tool 1 is between [A,K(1),M(1)] and [B,K(2),M(1)], the contradiction of work does not occur. [A,K(0),M(1)] of fig.9 change ON from an off gene.

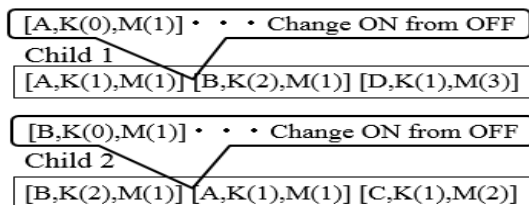


Fig. 9 ON chromosome of child

The next four works indicate the meaning of child1 of Fig.9.

1. Put the part A to machine tool 1
2. Take out the part A from the machine tool 1
3. Put the part B to the machine tool 1
4. Put the part D to the machine tool 2

The four works has no contradiction and lethal genes do not occur. By utilizing the ON / OFF gene, even after the crossover, it is possible to prevent the occurrence of lethal genes and to determine the best input order.

2. 4 Elimination of loss time between cycles

When determining the parts input order under the conditions that the target production ratio of parts is adopted as one cycle, the loss time corresponding that an

operator can't work occurs. This is because an operator stays for a long time till the next input cycle starts. To solve this problem, we adopt the different two machine tools, the last machine tool of a cycle and the first machine tool of the next cycle. Even if one cycle is not finished until the cycle last, the next cycle can start. Fig.10 shows the example of reducing the loss time.

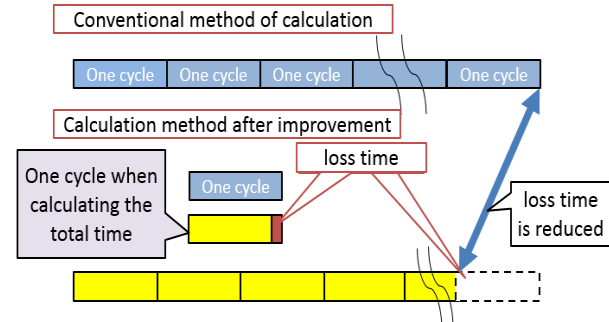


Fig.10 Example of reducing loss time

3. Simulation Applications

We applied VIPDOG to the job-shop production line as show in Fig.11 and simulated production results. The production conditions are shown below.

- 1 Operator's number : One person
- 2 Process : 15 types
- 3 Parts : 5 types
- 4 Ratio of the target production volume : 5 types
- 5 The number of machine tools : four

In addition, the ratio of the target production is shown in Table 1.

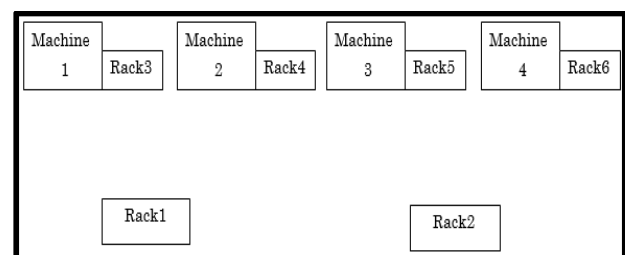


Fig.11 Layout of job shop production line

Table 1 The ratio of target production

		Type A	Type B	Type C	Type D	Type E
Target production ratio	P1	1	1	1	1	1
	P2	2	3	2	1	1
	P3	1	2	2	2	1
	P4	2	1	4	1	1
	P5	1	1	3	2	1

The conditions of GA are as follows

- 1 Population size: 100 individuals.
- 2 The number of generations: 500 generations.
- 3 Use a roulette selection and elite preservation strategy.
- 4 Use a circular crossover.
- 5 The probability of a mutation: 1%.

Using the above described various production conditions and the GA conditions, production simulation of 8 hours, 40 hours and 160 hours were carried out. We adopted two types of VIPDOG, one includes the loss time and the other doesn't. The former calls VIPDOG1 and the latter calls VIPDOG2. The production simulation results of VIPDOG2 are shown in Table2. The production simulation results of VIPDOG1 are shown in Table3. The results of the production simulator that do not use the GA compared to VIPDOG are shown in Table4. The number of occurrence of the lethal gene shows in Table5.

Table 2 Production simulation results of VIPDOG2

Production volume (the number)	8 hours	40 hours	160 hours
P1	21.81818	109.0909	436.3636
P2	12.11104	60.55519	242.2208
P3	13.89243	69.46217	277.8487
P4	13.02225	65.11124	260.445
P5	14.66395	73.31976	293.2791

Table 3 Production simulation results of VIPDOG1
(No loss time reduction)

Production volume (the number)	8 hours	40 hours	160 hours
P1	21.62487	108.1243	432.4974
P2	12.06257	60.31287	241.2515
P3	13.71723	68.58613	274.3445
P4	12.32191	61.60955	246.4382
P5	13.8367	69.1835	276.734

Table 4 Results of previous simulator without GA

Production volume (the number)	8 hours	40 hours	160 hours
P1	19.72603	98.63014	394.5205
P2	10.95057	54.75285	219.0114
P3	11.65992	58.2996	233.1984
P4	10.82707	54.13534	216.5414
P5	12	60	240

Table 5 The number of lethal gene

	Lethal gene
P1	0
P2	0
P3	0
P4	0
P5	0

Table 5 shows no occurrence of the lethal gene. VIPDOG can prevent the occurrence of lethal genes. As a result, we can have better result to use VIPDOG2. This is because we got the optimal solution by the GA and we reduced loss time. One shot example of visualized production results are shown in Fig.12.

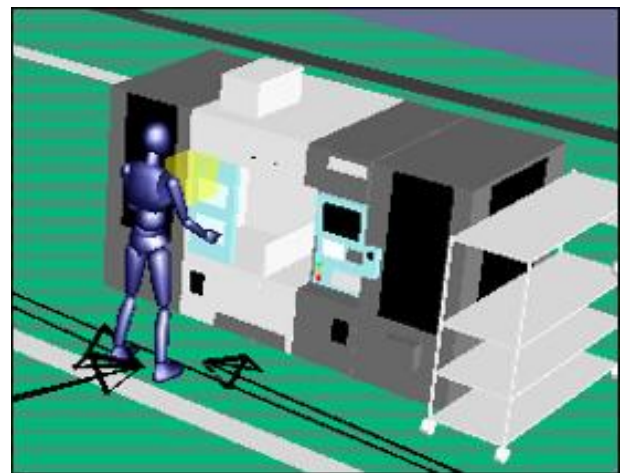


Fig.12 Visualization of VIPDOG

4. Conclusions

It is ascertained that VIPDOG including ON/OFF gene and not including the loss time can have good production results. In addition, we developed the visualized production results. The visualized system can check what will happen in the future and experienced engineers can discuss the problems to solve them.

References

- [1] Hidehiko Yamamoto, Takayoshi Yamada and Masanori Nakamura, Parts Layout Decision for Assembly Cell-Production by GA and Virtual Factory System, Transactions of Japan Society of Mechanical Engineers, Vol. 76, No.764, pp.210 -215, 2010

An Evolutionary Algorithm for Making Decision Graphs for Classification Problems

Shingo Mabu

*Graduate School of Science and Engineering, Yamaguchi University, Tokiwadai2-16-1
Ube, Yamaguchi 755-8611, Japan*

Masanao Obayashi

*Graduate School of Science and Engineering, Yamaguchi University, Tokiwadai2-16-1
Ube, Yamaguchi 755-8611, Japan*

Takashi Kuremoto

*Graduate School of Science and Engineering, Yamaguchi University, Tokiwadai2-16-1
Ube, Yamaguchi 755-8611, Japan*

E-mail: mabu@yamaguchi-u.ac.jp, m.obayas@yamaguchi-u.ac.jp, wu@yamaguchi-u.ac.jp

Abstract

As the exponential increase of data in the world, machine learning, pattern recognition, data mining etc. are attracting more attentions recently. Classification is one of the major research in pattern recognition and a large number of methods have been proposed such as decision trees, neural networks (NNs), support vector machines (SVMs). In order to easily understand and analyze the reason of the classification results, decision trees are useful comparing to NNs and SVMs. In this paper, to enhance the classification ability of decision trees, a new evolutionary algorithm for creating decision graphs is proposed as a superset of decision trees, where multi-root nodes and majority voting mechanism based on Maximum a posteriori are introduced. In the performance evaluation, it is clarified that the proposed method shows better classification ability than decision trees.

Keywords: evolutionary computation, decision graph, classification, majority vote, multi root nodes

1. Introduction

In the research fields of pattern recognition and machine learning, a large number of classification algorithms have been proposed¹, such as neural networks (NNs), support vector machines (SVMs)¹ and decision trees². NNs and SVMs mathematically create decision boundaries to separate classes with high accuracy and have applied to many applications such as intrusion detection³, prediction of stock market indexes⁴. As for the decision trees, typical learning algorithms are

classification and regression tree (CART)⁵, ID3 and C4.5². NNs, SVMs and their extended algorithms can create distinguished decision boundaries for accurate classification, however, they are black box models, thus the reason of the classification results is difficult to be shown to the end-users. On the other hand, decision trees can visually show the rules of classification explicitly by the tree structures, therefore, it is useful when users want to know the created rules and analyze the relationships between attributes in databases. However, when dealing with databases with a large

number of attributes, many rules have to be created by one tree, then the size of the tree would become too large. A large tree structure would cause over-fitting to the training data and decrease the generalization ability, therefore, a pruning of tree is to be executed. To enhance the generalization abilities of decision trees, some extended algorithms have been also proposed⁶.

In this paper, to enhance the representation ability of decision tree and obtain better classification accuracy, directed-graph based classifier with recurrent connections and its evolutionary algorithm are proposed. In the case of tree structure, the classification procedure starts from the root node, selects appropriate branches at non-terminal nodes, and finally classifies the data at the reached terminal node. Therefore, the node transition flows from the top layer to the bottom layers. In the case of graph structure, 1) any non-terminal nodes can become root nodes, and 2) the same nodes can be shared by several rules, therefore, many rules can be created by the smaller number of nodes and the program structure becomes quite compact.

In addition, this paper proposes some specific mechanisms to enhance the classification abilities of decision graph. First, multi root nodes are introduced to create various kinds of rules, while the standard decision tree uses one root node. Second, majority voting mechanism is introduced to enhance the generalization ability. In the proposed method, the classification process starts from one of the root nodes, selects branches at non-terminal nodes, and classifies a data into a certain class (vote for a certain class) at the transient terminal node. However, the transient terminal node has a connection to the next non-terminal node, therefore, the classification process continues and the same process is repeated until the fixed number of votes are executed. This multi-voting mechanism is expected to show better generalization ability.

The rest of this paper is organized as follows. In section 2, the basic structure of evolutionary decision graph and its gene expression is explained. In section 3, an evolutionary algorithm of decision graphs and how to classify data are explained. In section 4, after benchmark problems of classification and simulation conditions are explained, the results and analysis are described. Section 5 is devoted to conclusions.

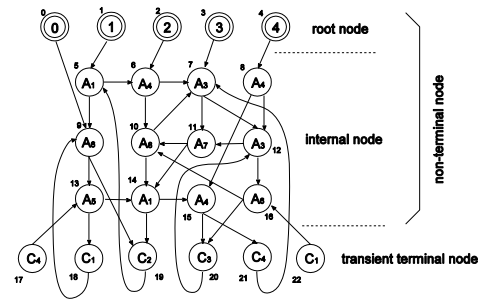


Fig. 1. Basic structure of evolutionary decision graph

2. Structure of Evolutionary Decision Graph

2.1. Basic structure

The basic structure of the decision graph is shown in Fig. 1, where there are three components: root nodes, internal nodes and transient terminal nodes. Here, root nodes and internal nodes are called non-terminal nodes. Root nodes have a function to start node transition and decide the next non-terminal node to which the current node transfers. The proposed decision graph has multi root nodes, and the node transition starts from each root node one by one, which results in considering various kinds of rules to make classification. The function of non-terminal nodes is the same as standard decision tree with multiple branches. In Fig 1, each non-terminal node has its own attribute A_i , $i \in \{1, 2, \dots, n\}$ to be judged, and when a data is inputted to the decision graph, an appropriate branch is selected according to the value of the data. The function of transient terminal node is to determine the class of the inputted data, and cast one vote to the class. For example, if the transient terminal node determines the class as "class 1", class 1 gets one vote. After the voting, the node transition continues depending on the connection from the transient terminal node. The detailed mechanism of making classification at each transient terminal node is explained in section 3.2.

2.2. Gene Structure

Fig. 2 shows the gene structure of node number k in a decision graph. NF_k shows a node function number: $NF_k=0$ is a root node, 1 is an internal node, and 2 is a transient terminal node. ATT_k shows an attribute number

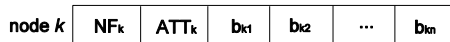


Fig. 2. Gene Structure of evolutionary decision graph

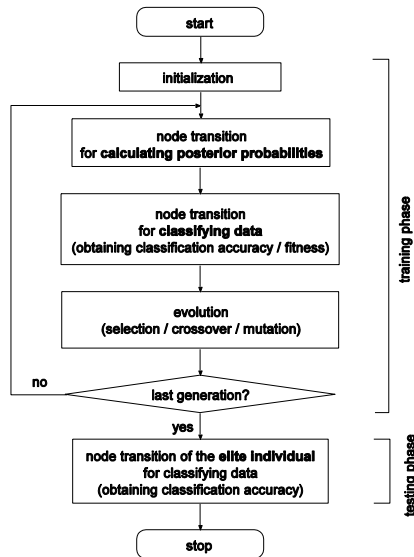


Fig. 3. Flowchart of training and testing phases in evolutionary decision graph

to be judged at non-terminal node k , or a class attribute to be assigned at transient terminal node k . b_{k1} , b_{k2} , ..., b_{kn} shows the next node number connected from node k . Transient terminal nodes have one branch to the next node, thus only b_{k1} is used at each node. Non-terminal nodes use b_{k1} , b_{k2} , ..., b_{kn} depending on the possible number of branches for ATT_k .

3. Evolutionary algorithm of decision graphs

Fig. 3 shows the flow of the whole implementation of evolutionary decision graph. In the training phase, after initializing the individuals, voting classes at transient terminal nodes are determined by posterior probabilities, and the classification accuracy for training data is obtained as the fitness for evolution. Then, evolutionary operations such as selection, crossover and mutation are carried out. The elite individual obtained in the final generation is picked up for the testing phase.

3.1. Initialization of an individual

First, the numbers of root nodes, internal nodes and transient terminal nodes are determined (NF_k is

determined) depending on the complexity of the target problem. Second, the values of ATT_k are randomly determined. ATT_k of non-terminal nodes are determined by randomly selecting one of the attributes in a database. ATT_k of transient terminal nodes are determined by maximum posterior probabilities explained in section 3.2. Finally, the branch connections are determined as follows. b_{k1} of transient terminal nodes are determined by randomly selecting one node number from non-terminal nodes. b_{k1} , b_{k2} , ..., b_{kn} of non-terminal nodes are determined by randomly selecting one node number from all the nodes.

3.2. Node transition for determining voting class at transient terminal nodes

To classify a data into an appropriate class, which class is assigned to each transient terminal node is very important. In this subsection, the procedure of assigning voting classes to each transient terminal node based on maximum posterior probabilities is explained in detail.

First, how to execute node transition is explained before introducing the class assignment mechanism. When a training data (tuple) d in a database is inputted, the node transition starts from root node 0 (node number $k=0$). The attribute ATT_0 of data d is examined and one of the branches among b_{01} , b_{02} , ..., b_{0n} is selected (here, suppose b_{01} is selected). If the selected node b_{01} is a non-terminal node, the same procedure as the root node is executed to determine the next node. Fig. 4 shows an example of the branch selection, where, in Fig. 4 (a), the value of attribute ATT_k of data d is in the range of $[0, 0.3]$, and its corresponding branch is b_{k1} , thus the

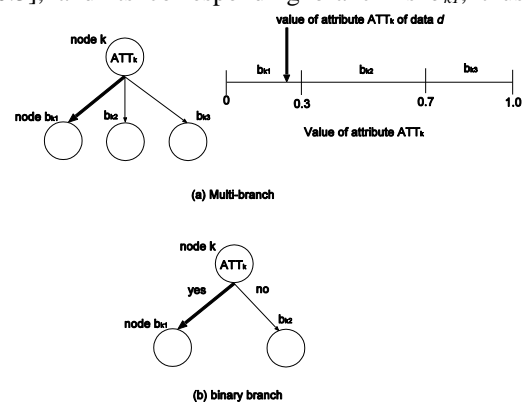


Fig. 4. An example of attribute division and branch decision

current node transfers to node b_{kl} . Fig. 4 (b) shows the case of binary branch where each non-terminal node executes yes-no branch selection. After repeating the branch selections at non-terminal nodes, if the current node reaches a transient terminal node t (Here, t shows the node number of transient terminal nodes), counter $N_i(t)$ increases by one, where i shows the class number of training data d . The current node transfers to the next node b_{kl} and continues the node transition until transient terminal nodes are visited predefined number of times, e.g., 10. However, if the node transition visits the same transient terminal nodes that have been already visited, the node transition restarts from the next root node, i.e., root node 1, to avoid the transition loop. In summary, the node transition starts from root node 0, and every time when a transition loop occurs, the node transition restarts from root node 1, 2, 3,... in the numerical order. By repeating the above node transition from the first data to the last one, the values of counters $N_i(t)$ of all the transient terminal nodes can be obtained. Then, the posterior probabilities of class i at transient terminal nodes t are calculated by

$$p(C_i|t) = \frac{N_i(t)}{N(t)} \quad (1)$$

where, $N(t)$ is the number of data visiting node t .

Finally, voting class (ATT_t in Fig. 2) at transient terminal node t is determined by

$$ATT_t = \arg \max_j P(C_j|t) \quad (2)$$

3.3. Node transition for classifying data

After the procedure described in sections 3.1 and 3.2, the classification of data d is carried out and fitness for evolution is obtained as follows.

The procedure of node transition is the same as section 3.2 except that, at transient terminal nodes, voting to one of the classes is carried out instead of counting the number of visits $N_i(t)$. When node transition reaches a transient terminal node t , it casts a vote to class ATT_t , then the current node transfers to the next node b_{kl} . The node transition continues until the predefined number of voting finishes. Finally, the class that wins the highest votes becomes the classification result. The above process is repeated for all the data d ,

then the classification accuracy is calculated as the fitness of the individual.

3.4. Genetic Operations in Evolutionary Decision Graphs

The individuals are evolved by selection, crossover and mutation. The genetic operations of evolutionary decision graphs are based on Ref. 7. In crossover, two parent individuals are selected by tournament selection and randomly selected nodes with the probability of P_C are exchanged between the parents. In mutation, one individual is selected by tournament selection, and the connections, attributes in non-terminal nodes, and root nodes are randomly changed with the probability of P_m .

Table 1. Dataset information

dataset	# of data	# of attributes	# of classes
Heart disease	303	13	2
Sonar	208	60	2
Hepatitis	155	19	2
Wine	178	13	3
Breast cancer	569	30	2

Table 2. Simulation condition

# of generations	2000
# of individuals	503
crossover rate	0.1
mutation rate	0.02
# of nodes	200
root nodes	50
internal nodes	50
transient terminal nodes	100

4. Simulations

The classification accuracy is evaluated using benchmark datasets downloaded from UCI machine learning repository⁸. The information of the datasets is shown in Table 1. The objective of this paper is to show the advantage over the conventional decision tree, but for more reference, the comparison with support vector machine (SVM) is also implemented. The parameters of the proposed method are set as shown in Table 2. The

simulations are implemented by 10-fold cross validation, and the mean classification accuracy is calculated. In the training, some variations are given to the training dataset to avoid over fitting. In detail, 10% of the training data consists of the data misclassified by the elite individual in the previous generation, and the rest of 90% of the training data are generated by bootstrap sampling⁹. The continuous attributes in the original datasets are binarized by the Fayyad and Irani's entropy based method¹⁰ executed by WEKA software¹¹.

4.1. Simulation results

The performance evaluation is executed using the elite individual obtained in the last generation in the training phase. Table 3 shows the classification accuracy obtained by the proposed decision graph, decision tree and SVM. From Table 3, we can see that the mean accuracy obtained by decision graph is better than decision tree. In addition, decision graph obtains higher accuracy than decision tree in four datasets out of five. Comparing the accuracy obtained by decision graph with that by SVM, decision graph shows comparable result, and decision graph obtains higher accuracy than SVM in three datasets out of five. Although the mean accuracy for the five datasets is almost the same as SVM, decision graph can show the classification rules to users like decision tree, therefore, when we want to know and analyze the obtained rules, decision graph can be an useful method. In the future, we will execute simulations using more datasets and analyze the generated classification rules and characteristics of the decision graph.

5. Conclusions

This paper proposed an evolutionary algorithm for creating decision graphs for classification problems. To enhance the classification abilities of the decision graph, some specific mechanisms such as multi-root nodes, unique genetic operators and majority voting were devised. From the simulation results, it was clarified that the proposed evolutionary algorithm improve the fitness (accuracy) of the individuals, and showed better classification accuracy comparing with decision tree and comparable accuracy to SVM. In the future, we will consider to apply impurity measures to the evaluation

Table 3. Testing results for benchmark datasets

dataset	Classification accuracy [%]		
	Decision graph	Decision tree	SVM
Heart disease	84.8	78.5	83.8
Sonar	82.2	71.2	76.0
Hepatitis	66.9	67.1	66.5
Wine	94.4	93.8	98.3
Breast cancer	94.9	93.1	97.7
mean	84.6	80.7	84.4

function of the evolutionary algorithm to clearly determine the decision boundaries of classes and improve the classification accuracy.

References

1. C. M. Bishop, et al., *Pattern recognition and machine learning* (Springer New York, 2006).
2. J. R. Quinlan, *C4.5: programs for machine learning*, (Morgan kaufmann, 1993).
3. S. J. Horng, M. Y. Su, Y. H. Chen, T. W. Kao, R. J. Chen, J. L. Lai, and C. D. Perkasa, A novel intrusion detection system based on hierarchical clustering and support vector machines, *Expert systems with Applications* **38**(1) (2011) 306–313.
4. E. Guresen, G. Kayakutlu, and T. U. Daim, Using artificial neural network models in stock market index prediction, *Expert Systems with Applications*, **38**(8) (2011) 10389–10397.
5. L. Breiman, J. Friedman, C. J. Stone, and R. A. Olshen, *Classification and regression trees*, (CRC press, 1984).
6. L. Breiman, Random forests, *Machine learning*, **45**(1) (2001) 5–32.
7. S. Mabu, K. Hirasawa, and J. Hu, A graph-based evolutionary algorithm: Genetic network programming (GNP) and its extension using reinforcement learning, *Evolutionary Computation*, **15**(3) (2007) 369–398.
8. UCI machine learning repository. Online available: archive.ics.uci.edu/ml/
9. Bradley Efron and Robert. J. Tibshirani, *An Introduction to the Bootstrap*, (Springer, 1993).
10. U. M. Fayyad and K. B. Irani, Multi-interval discretization of continuous valued attributes for classification learning, in *Proc. of the 13th International Joint Conference on Artificial Intelligence*, (Morgan Kaufmann, 1993), pp. 1022–1027.
11. Waikato environment for knowledge analysis, open source project for machine learning, Online available: www.cs.waikato.ac.nz/ml/weka/

Improvement of Computational Efficiency of UPF by Automatic Adjustment of the Number of Particles

Kenta Hidaka, Takuo Suzuki, and Kunikazu Kobayashi

School of Information Science and Technology, Aichi Prefectural University

1522-3 Ibaragabasama, Nagakute, Aichi 480-1198, Japan.

Tel: +81-561-76-8782, Fax: +81-561-64-1108

kobayashi@ist.aichi-pu.ac.jp

Abstract

In RoboCup Standard Platform League (SPL), the method using unscented particle filter (UPF) has been proposed for self-localization. The UPF resolves a problem of particle filter which cannot be sampled appropriately when the likelihood is too high or low. This filter can estimate accurate position when the more number of particles is. However, the more, the more computation time is needed. In the present paper, we propose an automatic adjustment method for the number of particles in UPF. The proposed method uses three kinds of feature values with respect to particles, i.e. centroid, standard deviation, and weight. Through computer simulations, we confirmed the improvement of computational efficiency of UPF.

Keywords: RoboCup, Self-localization, Unscented particle filter, Kalman filter, Particle

1. Introduction

The RoboCup (Robot Soccer World Cup) project sets a goal that a fully autonomous robot team shall win against the most recent winning team of FIFA World Cup in soccer by 2050. In the present paper, we treat one of major research issues in RoboCup, i.e. self-localization. In RoboCup, self-localization is required in a variety of situations, such as passing a ball to a teammate and intercepting a pass.

The RoboCup Standard Platform League (SPL) is a league that all teams compete with the same standard humanoid robot called NAO developed by Aldebaran Robotics. The robot operates fully autonomously, that is with no external control, neither by humans nor by computers. In RoboCup SPL, the robot must process all the calculations on vision processing and decision making using low-end CPU (Intel Atom 1.6GHz). In addition, the robot must devote a lot of computation time to percept a white goal and a mostly white ball in vision processing.

In the present paper, we focus on self-localization for reducing the computational cost. In conventional method using UPF^[1], since the number of particles is fixed during self-localization, it is possible to reduce the

computational cost by changing the number of particles and rejecting redundant particles depending on the situation. In RoboCup SPL, there is no method which can change the number of particles in UPF.

Yu et al. proposed an adaptive unscented particle filter, in which relative entropy is used for changing the number of particles^[2]. Yang et al. proposed another adaptive unscented particle filter, in which Kullback-Leibler divergence (KLD) sampling is employed^[3]. In contrast, the conventional self-localization method using UPF in RoboCup SPL uses 16 fixed particles^[4]. In RoboCup Middle Size League (MSL), the number of particles in the conventional self-localization method using KLD sampling is fixed as 75^[4]. In the present paper, in order to improve the computational efficiency of UPF, we propose an automatic adjustment method for changing the number of particles.

In Section 2, we explain fundamentals on UPF. Section 3 describes the proposed algorithm which can adaptively change the number of particles in UPF. In Section 4, we conduct some computer simulations and discuss the results. Section 5 summarizes our research and gives challenges for the future.

2. Unscented Particle Filter (UPF)

UPF has a combination of unscented Kalman filter (UKF)^[5] and particle filter^[6]. This filter can solve the problem in particle filter which resampling will fail if the new measurements appear in the tail of prior or if the likelihood is too peaked in comparison to the prior^[1]. In this section, we outline particle filter and UKF briefly.

2.1. Particle Filter

The particle filter is a type of non-parametric Bayesian filter. This filter can apply to nonlinear state equations with non-Gaussian probability distribution. The filter estimates the number of particles (state) by repeating the following three steps A, B, and C. This filter can precisely estimate state as more number of particles. Let the number of particles be N .

A. Motion update

The odometry information u_t obtained from robot estimates the current position $x_t = \{x_t^{[1]}, \dots, x_t^{[i]}, \dots, x_t^{[N]}\}$ from the previous position x_{t-1} .

$$p(x_t | u_t, x_{t-1}).$$

B. Measurement update

The weight w_t is calculated from x_t using measurement z_t .

$$w_t = \eta p(z_t | x_t),$$

where η is a constant.

C. Resampling

Some particles will be replaced with newly sampled ones.

draw i with probability $\propto w_t^{[i]}$,
add $x_t^{[i]}$ to state set X_t

2.2. Unscented Kalman Filter (UKF)

The UKF is a filter that handles nonlinear state equation as the following equation. Probability distributions can be used when the distribution follows from normality. This filter continues to update one state. UPF updates the the motion update in particle filter using UKF.

$$x(t+1) = f(x(t)) + bv(t),$$

$$y(t) = h(x(t)) + z(t),$$

where $x(t)$ is an n -dimensional vector, b is a constant. Assume that both variances of system noise $v(t)$ and

observation noise $z(t)$ follow from normal distributions. UKF approximates the non-linear function f and g using unscented transform^[1].

3. Proposed System

We propose an automatic adjustment method of the number of particles in UKF to reduce the computational cost. The proposed method realizes adjusting the number of particles by two steps, i.e. reset step and increase or decrease step as shown in Fig. 1.

3.1. Reset Step

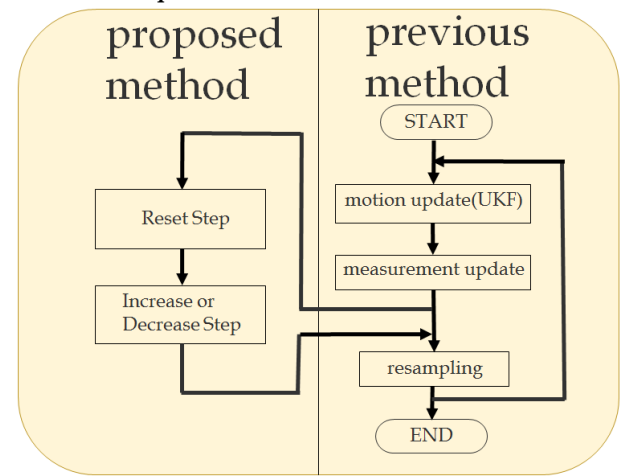


Fig. 1: Outline of the proposed method.

The reset step will be applied to increase the number of particles when robot is fallen or kidnapped. In RoboCup SPL, since there are so many such cases, a fallen or kidnapped robot must recover from disordered states. We therefore have to increase the number of particles to improve self-localization.

3.2. Increase or Decrease Step

In the increase or decrease step, the number of particles can be changed according to the estimation accuracy of self-localization. The detailed algorithm is illustrated in Fig. 2. Let $X = \{x_1, x_2, \dots, x_N\}$, $Y = \{y_1, y_2, \dots, y_n\}$ and X_{new} be sets. σ_n is the standard deviation of the particles with a weight more than α . e_1 and e_2 are any positive real values and used in order to adjust the size of σ_n at time n .

Algorithm 1 Increase or Decrease Step

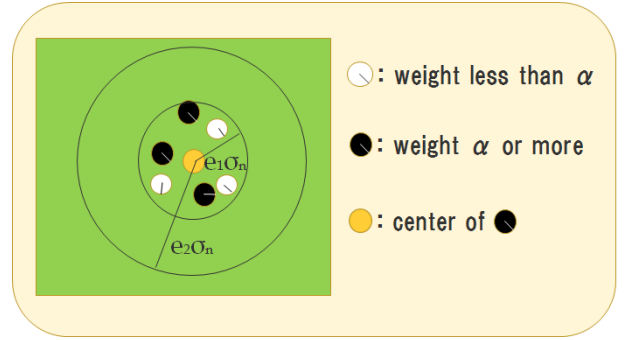
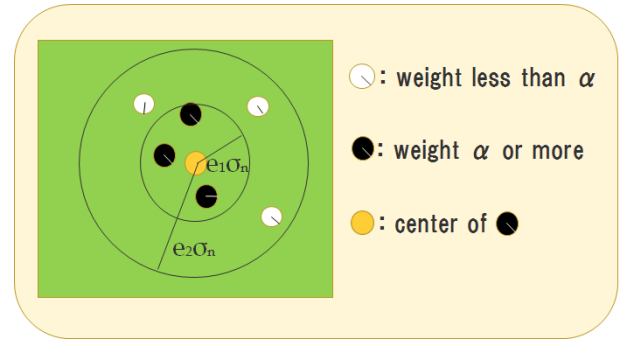
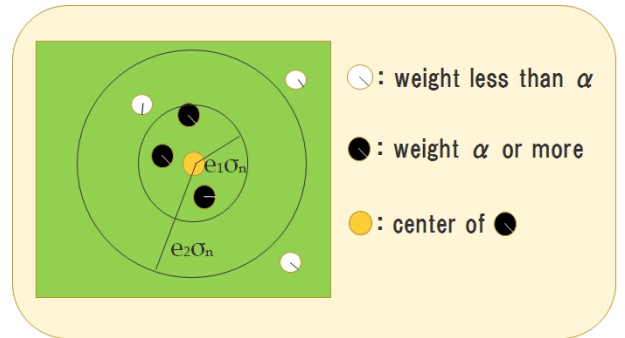
```

for  $i = 1$  to  $N$  do
  if  $\alpha \leq \text{weight}(x_i)$  then
     $X_{\text{new}} = X_{\text{new}} + x_i$ 
  end if
end for
if  $|X_{\text{new}}| \neq 0$  then
  if  $N = |X_{\text{new}}|$  then
     $Y = X_{\text{new}}$ 
     $e_1 = \text{parameter1}$ 
     $e_2 = \text{parameter2}$ 
  else
     $Y = X - X_{\text{new}}$ 
     $e_1 = \text{parameter3}$ 
     $e_2 = \text{parameter4}$ 
  end if
   $\mu = E[X_{\text{new}}]$ 
   $\sigma^2 = V[X_{\text{new}}]$ 
  for  $c = 1$  to  $|Y|$  do
    if  $\mu - e_1\sigma < y_c < \mu + e_1\sigma$  then
      if  $c = |Y|$  and  $N \neq N_{\min}$  then
         $X = X - \min(\text{weight}(Y))$ 
         $N = N - 1$ 
      end if
    else if  $\mu - e_2\sigma < y_c < \mu + e_2\sigma$  then
      if  $c = |Y|$  then
        break
      end if
    else
      if  $N = N_{\max}$  then
        break
      else
         $N = N + 1$ 
        break
      end if
    end if
  end for
end if

```

Fig. 2: Increase or decrease step in the proposed algorithm

The proposed algorithm will reduce the number of particles if the situation as shown in Fig. 3. In this figure, the white and black circles correspond to the particles with weights less than α and more than or equal to α , respectively and the yellow circle refers to the centroid of the black ones. If all the white circles are within the circle with radius $e_1\sigma_n$ and centered at the centroid of the black ones, i.e. the yellow circle, we can

**Fig. 3: An example of deleting a particle.****Fig. 4: An example of adding a particle.****Fig. 5: An example of fixing the number of particles.**

reduce the number of particles. On the other hand, if any of the white circles is beyond the circle with radius $e_2\sigma_n$, we cannot reduce any particles as shown in Fig. 4. If all the white circles are within the circle with radius $e_2\sigma_n$ and centered at the centroid of the black ones, we fix the number of particles.

4. Simulation

In this section, we show the validity of the proposed method through some computer simulations using

SimRobot simulator^[4]. Assume that the maximum number of particles is 16, i.e. $N_{\max}=16$ as the same with the conventional method^[4]. The values of parameters are set as follows: $N_{\min}=4$, parameter1=1, parameter2=2, parameter3=2, parameter4=3, and $\alpha=0.7$.

Figure 6 illustrates the difference between the centroid of particles and true position as the number of cycles. The

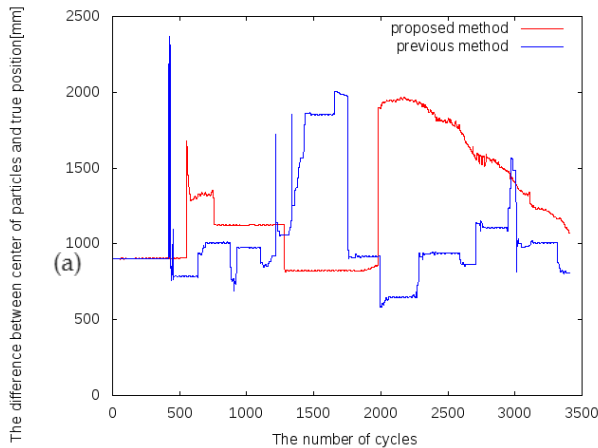


Fig. 6: Transition of the difference between the centroid of particles and true position.

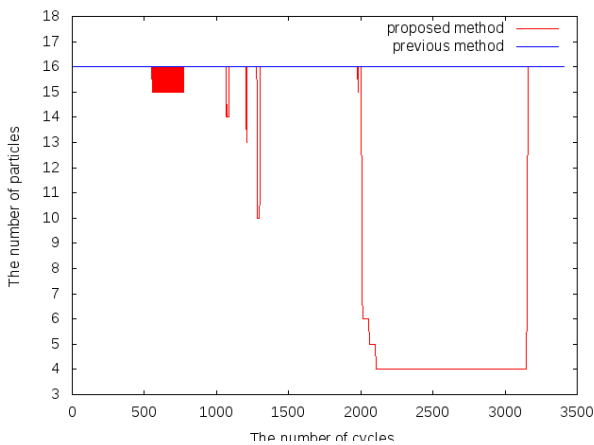


Fig. 7: Transition of the number of particles.

estimation accuracy of the self-localization using the proposed method is able to maintain the same level as the conventional method. However, the computational results confirm that the self-localization error and the number of particles is not proportional. The number of cycles for processing the self-localization was measured for 10 seconds. That for the conventional method and the

proposed method are 48,340 and 43,880 times, respectively. As a result, the computational efficiency was improved by about 10 percent.

5. Conclusion

In this paper, we focused on the self-localization in RoboCup SPL and proposed the automatic adjustment method of the number of particles in UPF. We suggested that the number of particles could be variable by using three values, i.e. the centroid, the standard deviation, and the weight of particles. Through computer simulations, we confirmed that the proposed method improved the computational efficiency as compared with the conventional method. As future issues, the number of particles and the self-localization error in the proposed method are required to be varied in proportion, because there is no need to increase the number of particles when the error is small.

Acknowledgements

This work was partly supported by President's Special Research Fund from Aichi Prefectural University, Japan.

References

1. R. van der Merwe, A. Doucet, N. de Freitas, and E. Wan, *The Unscented Particle Filter*, Proc. of NIPS, pp.584-590 (2000).
2. W. Yu, J. Peng, X. Zhang, S. Li, and W. Liu, *An Adaptive Unscented Particle Filter Algorithm through Relative Entropy for Mobile Robot Self-Localization*, Mathematical Problems in Engineering, Vol.2013, Article ID 567373 (2013).
3. J. Yang, X. Yuan, and Y. Zhang, *A Fast Initial Alignment Method for SINS Used Adaptive Sample Size Unscented Particle Filter*, Proc. of International Conference on Chemical, Material and Food Engineering, doi: 10.2991/cmfe-15.2015.157 (2015).
4. T. Röfer, T. Laue, J. Müller, D. Schütte, A. Böckmann, D. Jenett, S. Koralewski, F. Maaß, E. Maier, C. Siemer, A. Tsogias, and J. Vosteen, *B-Human Team Report and Code Release 2014* (2014).
5. S. J. Julier and J. K. Uhlmann, *A New Extension of the Kalman Filter to Nonlinear Systems*, Proc. of AeroSense: The 11th Int. Symp. On Aerospace/Defence Sensing, Simulation and Controls, pp.182-193 (1997).
6. N. J. Gordon, D. J. Salmond, and A. F. M. Smith, *Novel Approach to Nonlinear/non-Gaussian Bayesian State Estimation*, IEE Proceedings F (Radar and Signal Processing), Vol.140, No.2, pp.107-113 (1993).

Multi Objective Evolutionary Algorithms for Association Rule Mining: Advances and Challenges

Aswini Kumar Patra

Assistant Professor, Department of Computer Science & Engineering, NERIST, Itanagar, India

E-mail: akp@nerist.ac.in, aswinipatra@gmail.com

Abstract

Association rule mining is an important research area in data mining field. The challenge, posed by many methods, is the amount of time consumed for generating frequent items sets. To overcome this, evolutionary algorithms have been used widely. Moreover, apart from support and confidence, there are many other metrics available to measure the quality of association rules. That is the reason why multi-objective approach plays a crucial role. Therefore, two methodologies namely, multi-objective and evolutionary algorithms as a combination proved to be a preferred choice. Though numerous works have been proposed for mining association rules, use of multi-objective evolutionary algorithms are still in its infancy stage. This paper explores the challenges and advances that have been made in this regard in terms of nature of algorithm, encoding mechanism, objective functions and operators.

Keywords: Association Rule Mining, Categorical, Quantitative and Fuzzy Association Rules, MOEAs,

1. Introduction

The problem of association rule mining (ARM) was presented in 1993 and 1994 [2, 1]. The origin of Association Rules linked to well-known *market basket analysis*, where the purchase behavior of customers is analyzed. The goal is to discover regularities among products purchased in a supermarket. The rules were formed from transactional data (e.g., point-of-sale data), and the information codified by the rules (e.g., if buy(pen) and buy(paper) then buy(book) (in short, $\text{pen} \wedge \text{paper} \Rightarrow \text{book}$)), can later be utilized in order to take decisions involving promotions, product placement, etc. The idea is to discover *if-then* rules to infer interesting relations between variables in large databases. Nowadays, their use has found the way into many different fields, including electronic commerce, web usage mining, bioinformatics, intrusion detection, health care environment etc.

Many classical algorithms, so far, have been developed such as APRIORI, ECLAT or FP-GROWTH.[6] which are computationally expensive. These algorithms

work in two phases. First, frequent item-sets are detected by using a measure called *support count* and a user-defined parameter called *minimum support*. Second phase generates the rules using another user-defined parameter called *minimum confidence*. Evolutionary algorithms proved beneficial as they directly generate association rules skipping the frequent item set generation. Traditionally, support and confidence are maximized to have quality rules. But there are many other metrics available to measure the goodness of association rules [7]. Therefore, the problem of ARM can be posed as a multi objective optimization problem where the goal is to find association rules while optimizing several such goodness criteria simultaneously [5].

The rest of the paper is organized as follows: Section 2 briefs about the background and preliminaries. Section 3 surveys the research progresses that have been made for ARM involving evolutionary algorithms. Section 4 list out the challenges and difficulties and Section 5 concludes the paper.

© The 2016 International Conference on Artificial Life and Robotics (ICAROB 2016), Jan. 29-31, Okinawa, Japan

2. Background and Preliminaries

2.1 Types of Association Rules: Broadly, there are two types of association rules.

- Categorical Association Rule
- Quantitative Association Rule.

Fuzzy association rule is a variation of Quantitative Association Rule.

2.2 Multi objective Evolutionary Algorithms

Last two decades witnessed an increased interest in the use of GAs for multi objective optimization. Some of the most traditional multi-objective evolutionary methods are VEGA (Vector Evaluated Genetic Algorithm; Shaffer, 1985), MOGA (Multiple Objective Genetic Algorithm; Fonseca & Fleming, 1993), NPGA (Niche Pareto Genetic Algorithm; Horn & Nafpliotis, 1993), and NSGA (Non-dominated Sorting Genetic Algorithms; Srinivas & Deb, 1994). The newly developed evolutionary methods, that incorporate elitist strategy, are SPEA (Strength Pareto Evolutionary Algorithm; Zitzler & Thiele, 1999), PAES (Pareto Archived Evolution Strategy; Knowles & Corne, 1999), PESA (Pareto Enveloped-based Selection Algorithm; Knowles et al., 2000), SPEA2 (Strength Pareto Evolutionary Algorithm; Zitzler et al.,

- average of different objectives. Second, the lexicographical approach, in which the objectives are ranked in order of priority. Third, the Pareto approach, which consists of as many

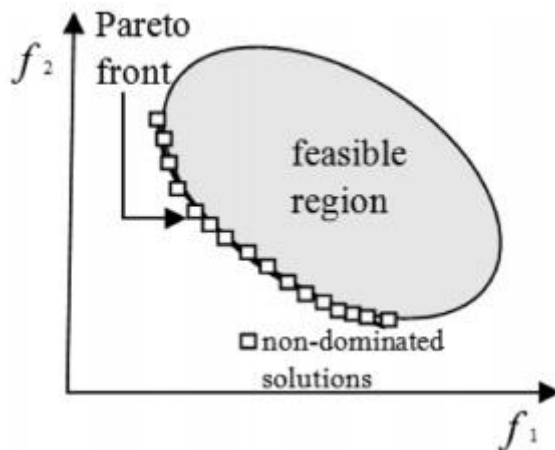


Fig 1. Pareto Front

2001) and NSGAI (Non-dominated Sorting Genetic Algorithm II; Deb et al., 2002). The researches for ARM use some of the standard algorithms, some variants and some non-standard (i.e. not same as above mentioned algorithms) MOEAs as well.

2.3 Terminologies for Evolutionary Algorithms

The Evolutionary algorithms are characterized by Encoding mechanism, objective functions, evolutionary operators.

- There are mainly two chromosome representation techniques. In the first approach (Pittsburgh approach), a set of possible association rules are encoded in each chromosome. The second method is Michigan approach, in which each chromosome represents exactly one rule. This approach is suitable for Association Rule Mining.
- There are three different approaches that can be found to tackle the objectives in fitness function in multi-objective problems [6]. First, the original multi-objective problem can be transformed into a single-objective problem by using a weighted function. It involves the use of a GA whose fitness function is the weighted non-dominated solutions as possible and returning the set of Pareto front to the user. Most of the studies using multi-objective GAs for ARM have been performed using the Pareto approach. Such a front is given in Fig 1 for two objectives f_1 and f_2 .
- Generally, both standard and varied *selection*, *crossover* and *mutation* operators used for Association Rule Mining.

3. MoEAs for Association Rule Mining

A comparison, of the proposed methods in the literature, is mentioned in Table 1, in terms of underlying MOO tool, encoding mechanism, objective functions, and evolutionary operators. The innovations, implementation details for each category of association rules are discussed in subsections below.

3.1. Categorical Association Rule Mining

The proposed works, related to categorical association rule mining, are discussed below.

- Ghosh et al. [8] proposed association rule mining as a multi objective problem rather than single objective one. The authors adopted

Michigan approach to represent the chromosomes (i.e. rules). Each chromosome has length $2n$, where 'n' is the number of items. Each gene, in the chromosome, represents an attribute. If the gene is 00, the attribute is in the antecedent part. If the gene is 11, the attribute is in the consequent part. The attribute does not exist in the rule, if the gene is 01 or 10. This method uses a Pareto based genetic algorithm to solve the multi-objective rule mining problem using three measures—comprehensibility, interestingness and the predictive accuracy (i.e. Confidence). This algorithm works on a sample of the original database, and used the random sampling method.

- In a similar approach as in [8], the work [9] uses binary encoding for the chromosomes with a little change. The presence of an attribute in the antecedent and consequent part are represented by bits 10 and 01, whereas other bit combinations represent the absence of the attribute from the rule. It uses Pareto based co-evolutionary algorithm in order to overcome the weakness of lexicographic order method. Two new measures, statistical correlation and comprehensibility, along with confidence as objection functions are proposed. The co-evolutionary operators, used, are Pareto neighborhood crossover operator, combination crossover and annexing operator. The outcome in terms of running time is compared with that of a classical method *F-growth* and found to be lesser.
- In [10], a non-standard MOEA is used for the ARM problem. Best solutions, encountered over generations, are filled into a secondary population called the "Pareto Archive". In the production process, elitism is applied in order to allow solutions from the "Pareto archive" to participate to the reproduction. The classical roulette selection based on the Pareto ranking is used. The proposed crossover operator has two versions depending upon the fact that the parents may share (or not) a common attribute: Crossover by value exchange and Crossover by insertion. Four mutation operators were used as mentioned in Table 1. This algorithm proposes to consider the ARM problem as a multi-objective combinatorial optimization problem

in order to be able to find non frequent but interesting rules.

- The work [11] uses NSGA II. Six different measures (support, confidence, interest, comprehensibility, cosine and attribute frequency) have been considered as objectives. Three of these measures have been taken at a time and optimized simultaneously. Because NSGA II known to perform well when the number of objective functions is at most three. Eventually, it demonstrates that this method obtains some rules which cannot be obtained by the traditional mining methods.
- Ali Hadian et al. [12] proposed the binary chromosome encoding as in [8]. The four measures Support, Confidence, Comprehensibility, and Interestingness are used as objectives. Cluster-Based Multi-Objective Genetic Algorithm (CBMOGA) is used which optimizes the support counting phase by clustering the database. Clusters are based on the number of items in each transaction. The benefit of CBMOGA is that it prevents some unnecessary comparisons as compared to MOGA. Though CBMOGA outperforms the MOGA, the speedup highly depends on the distribution of transactions in the cluster tables.
- The disadvantage of binary encoding scheme is that it leads to large chromosome length. To overcome this, an integer encoding scheme is being used in ARMMGA [13]. For example, if A_i represents the i th item, then the chromosome $\{3 \mid 2 \ 5 \ 4 \ 1 \ 3\}$ represents the rule $A_2A_5A_4 \Rightarrow A_1A_3$. However, this representation gives rise to a variable length chromosome length, thereby in need of a specialized crossover operator. The classical measures support and confidence are optimized simultaneously. It proposes a method without taking the minimum support and confidence into account. The promising point in this algorithm is that the value of the fitness function only specifies the order of chromosomes in population and has not any other effect on genetic algorithm operator; therefore, the algorithm is convergence with any usually arbitrarily fitness function.

Table1. Comparison of Association Rule Mining Methods using MOEAs (in Chronological Order)

Algorithm	Underlying Tool	Type	Encoding	Objective Functions	Evolutionary Operators
Ghosh and Nath[8], 2004	MOGA	Categorical	Binary(Michigan)	Confidence, Comprehensibility, Interestingness	Multi point cross over, Bit-flip mutation
Kaya and Alhajj[22], 2003 Kaya and Alhajj[23], 2004	SPEA Variant	Fuzzy	Real-valued (membership functions)	Number of large item sets, Time taken to find all large item sets	Multi-point cross over, Standard real-value mutation
Mehmet Kaya[24], 2005	Non-standard (Pareto based GA)	Fuzzy	. Real-valued (membership functions)	Strongness, Interestingness, Comprehensibility	Four point Crossover, Mutation not mentioned
Hu and Yang-Li[9], 2007	Pareto-based co evolutionary	Categorical	Binary(Michigan)	Statistical correlation, Comprehensibility	Pareto-neighbourhood cross over, Combination, annexing
Khabzaui et el.[10], 2008	Non-standard	Categorical	Not mentioned	Support, Confidence, J-measure, Interest, Surprise	Value exchange crossover, Insertion crossover, value/attribute mutation, insertion/deletion mutation
Altas et el.[14], 2008(MODE NAR)	MODE	Numeric	Mixed(integer+real)(Michigan)	Support, Confidence, Comprehensibility, Amplitude of interval	DE/rand/1
Alhajj and Kaya [25], 2008	SPEA Variant	Fuzzy	Real-valued (membership functions)	Number of large item sets, Time taken to find all large item sets	Multi-point cross over, standard real-value mutation
Chen et el.[26], 2008	MOGA	Fuzzy	Real-valued (membership functions)	Number of large 1-item sets, suitability of membership functions	Max-min arithmetic crossover, one point mutation
Anand et el.[11], 2009	NSGA-II	Categorical	Binary(Michigan)	Combination(3 at a time) of support, Confidence, Interest, Comprehensibility, Cosine, Attribute frequency	Crossover not mentioned, bit flip mutation.

Table 1(Continued)

Algorithm	Underlying Tool	Type	Encoding	Objective Functions	Evolutionary Operators
Ali Hadian et al.[12], 2010 (CBMOGA)	MOGA variant	Categorical	Binary(Michigan)	Support, Confidence, Comprehensibility, Interestingness	No specific mention of Crossover and Mutation
Qodmanan et al[13], 2011	Non-standard	Categorical	Integer(Michigan)	Support, Confidence	Order I crossover, random replacement mutation
Martin et al.[16], 2011(NSGA-II-QAR)	NSGA-II	Numeric	Real-valued(Michigan)	Lift, comprehensibility, performance(Support x Confidence)	Multipoint crossover, standard real-value mutation
Mathews et al.[27], 2011	NSGA-II	Fuzzy	Mixed(integer+real) (Michigan)	Temporal support, temporal confidence, fuzzy support, membership function width	Modified uniform crossover, random change mutation
K.Y.Fung et al.[17], 2012	NSGA-II	Categorical and numeric	Both Michigan and Pittsburgh	Accuracy, Comprehensibility, Definability.	Two point Crossover and bitwise Mutation, Arithmetic Crossover and polynomial Mutation
B. Minaei-Bidgoli et al[18], 2013(MOGAR)	Non-standard	Numeric	Michigan	Confidence, Interestingness, Comprehensibility,	K-point Crossover, Bit flip Mutation
D.Martin et al[19], 2014(QAR-CIP-NSGA-II)	NSGA-II variant	Numeric	Michigan	Interestingness, Comprehensibility, Performance	Standard Crossover and Mutation.
M.M.Ballesteros et al[20], 2014(GarNet)	NSGA-II	Numeric	Michigan	Support, accuracy and Confidence	Interval based crossover, probabilistic mutation.
Mehrdad Almasi et al[21], 2015(Rare-PEARs)	Non-Standard	Numeric	Michigan(integer+real)	Support, Confidence, Lift, Centrality Factor, Length of Rule and Coverage	One-point crossover, standard real-value mutation.

3.2. Quantitative Association Rule (QAR) Mining

The works related to QAR are briefed below.

- The chromosomes encode the lower and upper bounds of the intervals of the attributes participating in a rule. In [14], where the MODENAR algorithm uses such a

chromosome encoding where each attribute has three components. The first component indicates whether the attribute is present or absent in the rule, and if present, in which part (antecedent or consequent) in the rule it is. The second and third components indicate the lower and upper bounds of the ranges of the attribute. The first component can have integer

values 0, 1, or 2, which indicate the presence of the attribute in the antecedent of the rule, the presence of the attribute in the consequent of the rule, and the absence of the attribute from the rule, respectively. The second and third components can take real values from the corresponding attribute ranges. It is to be noted that as MODENAR uses differential evolution as an optimizer and works on real-valued chromosomes, the authors used a round-off operator to handle the integer part of the chromosome. Support, confidence value and the comprehensibility of the rule are maximization objectives while the amplitude of the intervals, which conforms the itemset and rule, is minimization objective. MODENAR used the standard version of the crossover and mutation operators adopted by the version of differential evolution called DE/rand/1. Additionally, a rounding operator is used to round off the first part of the attribute that requires an integer (0, 1, 2) for computing the objective function values. ARs are directly mined without generating frequent item sets.

- The work NSGA-II-QAR [16] uses the same encoding scheme as in [14]. The only difference is that in this case, the first part of the chromosome, instead of using the values 0, 1, 2, adopts the values 0, 1, and -1 , respectively, to denote the same meaning. In both cases, the algorithms used a Michigan encoding strategy. The three objectives interestingness, comprehensibility and performance are maximized. As evolutionary operator multipoint crossover is utilized and the two parts of the chromosome undergo two different mutations. It uses an extension of the well-known MOEA NSGA-II. This method follows a database-independent approach which does not rely upon the minimum support and the minimum confidence thresholds. An experimental comparison between NSGAII-QAR and MODENAR is provided in [16].
- In [17], a two-stage rule-mining approach is proposed to generate rules with a simple chromosome design in the first stage of rule mining. In the second stage of rule mining, entire rule sets are refined to determine solutions considering rule interaction. For a rule-mining problem, the proposed multi-

objective GA approach could simultaneously consider the accuracy, comprehensibility, and definability of approximate rules. The promising feature is that it uses both categorical and quantitative attributes and targets to define the design profile of a product. The proposed multi-objective GA approach could simultaneously consider the accuracy, comprehensibility, and definability of approximate rules as objectives.

- The work [18] uses the three measures; confidence, interestingness, and comprehensibility have been used as different objectives for our multi objective optimization which is amplified with genetic algorithms approach. The method uses *rough* values which are defined with upper and lower intervals to represent a range or set of values. Michigan approach is used for representing rules in chromosomes. Eventually, the best rules are obtained through Pareto optimality. It uses K-point crossover and bit flip mutation.
- QAR-CIP-NSGA-II [19] maximizes the comprehensibility, interestingness and performance of the objectives in order to mine a set of quantitative association rules with a good trade-off between interpretability and accuracy. This model extends NSGA II to perform an evolutionary learning of the intervals of the attributes and a condition selection for each rule. It uses Michigan type encoding for chromosomes and as similar as [16]. It uses standard crossover and mutation. Moreover, this proposal introduces an external population (EP) and a restarting process to the evolutionary model in order to store all the non-dominated rules found and improve the diversity of the rule set obtained. The results attained over nine real world datasets have shown how the EP and restarting process improves the percentage of patterns covered by the rules of the total patterns in the dataset and allows obtaining a greater number of rules than the classical approach.
- The work GarNet[20] is a multi-objective evolutionary algorithm for mining quantitative association rules that has been developed to discover gene association networks. It is based on NSGA II. The representation of an

individual consists of two data structures. The upper structure includes the intervals bounds of all the attributes of the dataset. The bottom structure indicates the membership of an attribute to the rule represented by an individual. The type of each attribute can have three values: 0 when the attribute does not belong to the rule and 1 or 2 if it belongs to the antecedent or the consequent of the rule, respectively. If an attribute is wanted to be retrieved for a specific rule, it can be done by modifying the value equal to 0 of the type by a value equal to 1 or 2 depending on the antecedent or consequent. Support, accuracy and Confidence are used as three objectives to be optimized simultaneously.

- In this paper [21], the proposed algorithm (Rare-PEARs) gives a chance to each rule with different length and appearance (antecedent and consequent parts of rules) to be created. Therefore, various interesting, rare or interesting and rare rules can be found. Some of these rules might be uninteresting (those that contain frequent item sets). However, it has been tried to avoid them by Rare-PEARs. To accomplish this goal, the method decomposes the process of association rule mining into N-1 sub-problems (N is the number of attributes, and each sub-problem is handled by an independent sub-process during Rare-PEARs execution). Each sub-process starts individually with a different initial population. It then explores the search space of its corresponding sub-problem to find rules with semi-optimal intervals for each of the attributes. This process is done by a new definition of Non-Dominated concept. Support, Confidence, Lift, Centrality Factor, Length of Rule and Coverage are used as objectives to be optimized.

3.3. Fuzzy Association Rules

One of the major problems of mining numeric association rules is that these algorithms deal with sharp boundaries between consecutive intervals. Thus, they cannot represent smooth changes from one interval to another, which can be easily handled by fuzzy association rules [5]. The OEA-based fuzzy ARM techniques have been developed in the past decade.

- Various MOEAs have been applied in different works on fuzzy ARM. Kaya *et al.* [22], [23], [25] used a variant of SPEA for fuzzy rule mining. In [26], a multi objective GA (MOGA) is used for this purpose. NSGA-II has been utilized in [27]. But, there is no mention of any comparison among different MOEAs for fuzzy rule mining in any of the work..
- There are two categories of chromosome representations for fuzzy ARM [5].
 1. In the first approach, a chromosome encodes a set of fuzzy clusters that correspond to each attribute. The goal is to find a suitable set of fuzzy clusters that partition the range of values in each attribute domain. This representation is employed in a series of works done by Kaya *et al.* in [22], [23], [25]. In these works, each chromosome represents the base values of a variable number of membership functions representing the fuzzy sets for each quantitative attribute. Fuzzy sets are represented by standard triangular membership functions. Chromosomes use real values. Here, a chromosome does not represent association rules. It represents a suitable fuzzy clustering of the attribute domains. The evolved fuzzy membership functions are then used as the linguistic values of the corresponding attributes [5]. Fuzzy association rules are mined using standard algorithms based on minimum support and minimum confidence criteria. The work [26] uses a similar encoding approach.
 2. In second approach, each chromosome directly represents association rule. This is a kind of Michigan approach. In [27], such an encoding mechanism is applied to mine temporal fuzzy association rules. A mixed representation, of chromosomes combining integer and real values, is used. The chromosome encodes the lower and upper bounds of the temporal interval in the rules as integers. The indices of the items participating in the rule are also

encoded as integers. Eventually, the real valued parameters of the triangular membership functions corresponding to each item are encoded in the chromosome. Thus, this representation induces variable-length chromosomes needing special evolutionary operators.

- In the works [22], [23], [25], two criterias are optimized, that is, number of large itemsets and time spent to obtain the large itemsets. So, there are two objectives to evolve a possible fuzzy clustering of the numeric attributes. First is maximizing the number of large itemsets while the other is minimizing the time required to obtain all large itemsets given the clustering. After optimizing the clustering, membership functions are used as linguistic values for the fuzzy association rules extracted based on minimum support and minimum confidence criteria. In [26], where a similar encoding strategy is adopted as in [22], two objective functions are optimized simultaneously. The first objective function is stability of the encoded membership functions, which has two components, that is, overlap factor and coverage factor [5]. The stability is optimized to avoid generation of too redundant and too separated fuzzy sets for an item. The second objective is to maximize the total number of large 1-itemsets for given minimum support values. Although this paper is a consequence of the works of Kaya et al. with modifications in the objective functions and evolutionary operators, no comparison has been made between the works to check which is better over the other approach. In [27], Michigan form of chromosomes the authors used for temporal fuzzy association rule mining. So, the objective functions are related to the optimization of the encoded rules. It used four objective functions, namely temporal support, temporal confidence, fuzzy support, and membership function widths. The first three objective functions are obvious; the last objective function is used to prevent a membership function from covering the whole range of attribute values. Without this objective function, the solutions could evolve to cover the complete range of attribute values,

since this gives higher support values as it includes more number of items [5].

- References [22], [23], have used standard multipoint crossover operations. In [25], arithmetic crossover is used. Also, they employed standard real-value mutation. In [26], the authors used max-min arithmetical crossover and one-point mutation. This crossover operator generates four offspring at a time out of which the two best offspring are chosen. The mutation operator is used to slightly change the center of the fuzzy set being mutated. Whenever mutation takes place at the center of a fuzzy membership function, it may disrupt the order of the resulting fuzzy membership functions. Hence, after the mutation, these fuzzy membership functions need rearrangement according to their center values. In [27], for a Michigan type of encoding, a modified uniform crossover operator is adopted. For mutating the genes representing the lower and upper bounds of the time interval, the values are generated within the endpoint range (*ep_r*) where the midpoint is the value of the current gene (*g*), such that the mutated value is a member of the set $\{-ep_r/2, \dots, g, \dots, ep_r/2\}$. This is done to reduce the effect of random sampling of the dataset [5].
- This paper [24] first introduces optimized fuzzy association rule mining in terms of three important criteria; strongness, interestingness and comprehensibility. Then, it proposes multi-objective Genetic Algorithm (GA) based approaches for discovering these optimized rules. Optimization technique according to given criterion may be one of two different forms; The first tries to determine the appropriate fuzzy sets of quantitative attributes in a pre-specified rule, which is also called as certain rule. The second deals with finding both uncertain rules and their appropriate fuzzy sets.

4. Points to Ponder

There are many challenges that have impacts on the overall performance of the proposed algorithms or methods. Those points that are found in literature listed out in this section.

- The use of minimum support and confidence thresholds has to be avoided as there is highly chance of missing out quality rules.
- Two major problems were encountered while obtaining rules using MOEAs. One is invalid rules and another is non-existent rules [11]. These two problems are reason for reduced performance of elitist MOEAs like NSGA-II to obtain more number of good rules. The search space tends to get stuck at local Pareto optimal solutions found so far or converge to very few Global Pareto optimal solutions if found[11].
- To improve the efficiency of an algorithm [8], which uses *sampling* of the database, some refinement is required because the sample may not truly reflect the actual database. Random sampling, regression based sampling or cluster based sampling could be a choice. A perfect sample will improve the correctness of the rules generated by the algorithm.
- Whenever a typical integer encoding scheme gives rise to variable length chromosomes [13], a specialized crossover operator is required.
- Finding the optimal interval of each rule's attribute is a challenge in QARs.
- Rapid convergence damages the efficiency of MOEAs. Some researches [19] solve this problem by restarting. They restart whenever it is found that the difference between two consecutive populations is less than " α " percent. To chose " α ", sufficient exploration is needed. If this value is high, current generations may not have the chance to produce elite chromosomes.
- Most of popular methods for association rule mining cannot be applied to the numerical data without data discretization. There have been efforts to resolve the problem of dealing with numeric data in [18].
- In fuzzy association rules mining, it is not an easy task to know apriori the most appropriate number of fuzzy sets and their membership functions in order to cover the domains of quantitative attributes. Moreover, it is not realistic that experts can always provide the most appropriate fuzzy sets [25].

5. Conclusion

This paper surveys the evolutionary algorithms used for association rule mining and briefed about the technicalities, innovations and goals of the works. Although ARM algorithms, based on MOEAs, have gained popularity in recent years, their use in real-life applications is still limited. It would be useful if future works will be directed to the use of rule mining for gene expressions, financial databases, text mining, and bioinformatics.

References

1. R. Agrawal, R. Srikant, Fast algorithms for mining association rules, *Proc. 20th Int. Conf. Very Large Data Bases VLDB*, vol. 1215, CiteSeer, pp. 487–499, 1994.
2. R. Agrawal, T. Imielin' ski, A. Swami, Mining association rules between sets of items in large databases, *News Lett. ACM SIGMOD 22 (2)*, pp.207–216, 1993.
3. J. Han and M. Kamber, *Data Mining: Concepts and Techniques*. San Francisco, CA, USA: Morgan Kaufmann, 2000.
4. A. Mukhopadhyay, U. Maulik, S. Bandyopadhyay, and C. A. Coello Coello, "A survey of multiobjective evolutionary algorithms for data mining: Part I," *IEEE Trans. Evol. Comput.*, Vol. 18, No. 1, pp. 4-19, February, 2014.
5. A. Mukhopadhyay, U. Maulik, S. Bandyopadhyay, and C. A. CoelloCoello, "A survey of multiobjective evolutionary algorithms for data mining: Part II," *IEEE Trans. Evolut. Comput.* Vol. 18, No. 1, pp. 20-35, February, 2014.
6. M. Jes'us, J. A. G'amez, P. Gonz'alez, and J. M. Puerta, "On the discovery of association rules by means of evolutionary algorithms," *Wiley Interdisc. Rev.: Data Min. Knowl. Discovery*, vol. 1, no. 5, pp. 397–415, 2011.
7. P.-N. Tan, V. Kumar, and J. Srivastava, "Selecting the right interestingness measure for association patterns," in *Proc. 8th ACM SIGKDD Int. Conf. KDD*, 2002, pp. 32–41.
8. A. Ghosh and B. Nath, "Multi-objective rule mining using genetic algorithms," *Inf. Sci.*, vol. 163, nos. 1–3, pp. 123–133, Jun. 2004.
9. J. Hu and X. Yang-Li, "Association rules mining using multi-objective co-evolutionary algorithm," in *Proc. Int. Conf. CISW*, 2007, pp. 405–408.
10. M. Khabzaoui, C. Dhaenens, and E.-G. Talbi, "Combining evolutionary algorithms and exact approaches for multiobjective knowledge discovery," *RAIRO—Oper. Res.*, vol. 42, no. 1, pp. 69–83, 2008.
11. R. Anand, A. Vaid, and P. K. Singh, "Association rule mining using multiobjective evolutionary algorithms:

- Strengths and challenges,” in *Proc. NaBIC*, 2009, pp. 385–390.
12. Ali Hadian, Mahdi Nasiri, B. Minaei-Bidgoli, “Clustering Based Multi-Objective Rule Mining using Genetic Algorithm”, *International Journal of Digital Content Technology and its Applications*, Volume 4, No.1, 2010.
13. H. R. Qodmanan, M. Nasiri, and B. Minaei-Bidgoli, “Multi-objective association rule mining with genetic algorithm without specifying minimum support and minimum confidence,” *Expert Syst. Appl.*, vol. 38, no. 1, pp. 288–298, Jan. 2011.
14. B. Alatas, E. Akin, and A. Karci, “MODENAR: Multi-objective differential evolution algorithm for mining numeric association rules,” *Appl. Soft Comput.*, vol. 8, no. 1, pp. 646–656, Jan. 2008.
15. P. Lenca, P. Meyer, B. Vaillant, and S. Lallich, “On selecting interestingness measures for association rules: User oriented description and multiple criteria decision aid,” *Eur. J. Oper. Res.*, vol. 184, no. 2, pp. 610–626, 2008.
16. D. Martín, A. Rosete, J. Alcalá-Fdez, and F. Herrera, “A multi-objective evolutionary algorithm for mining quantitative association rules,” in *Proc. 11th Int. Conf. ISDA*, 2011, pp. 1397–1402.
17. K.Y. Fung, C.K. Kwong, K.W.M. Siu, K.M. Yu, “A multi-objective genetic algorithm approach to rule mining for affective product design”, *Expert Systems with Applications*, vol.39, pp. 7411–7419, 2012.
18. B. Minaei-Bidgoli, R. Barmaki, M. Nasiri, “Mining numerical association rules via multi-objective genetic algorithms”, *Information Sciences*, vol.233, pp. 15–24, 2013.
19. D. Martín, A. Rosete, J. Alcalá-Fdez, F. Herrera, “QAR-CIP-NSGA-II: A new multi-objective evolutionary algorithm to mine quantitative association rules”, *Information Sciences*, vol. 258, pp.1–28, 2014.
20. M.M.Ballesteros, I.A.N-Chamorro, J.C. Riquelme “Discovering gene association networks by multi-objective evolutionary quantitative association rules”, *Journal of Computer and System Sciences*, vol. 80 (2014), pp. 118–136.
21. M.Almasi, M.S. Abadeh, “Rare-PEARs: A new multi objective evolutionary algorithm to mine rare and non-redundant quantitative association rules,” *Knowledge-Based Systems*, vol. 89, pp.366–384, 2015.
22. M. Kaya and R. Alhajj, “Facilitating fuzzy association rules mining by using multi objective genetic algorithms for automated clustering,” in *Proc. 3rd IEEE ICDM*, pp. 561–564, 2003.
23. M. Kaya and R. Alhajj, “Integrating multi-objective genetic algorithms into clustering for fuzzy association rules mining,” in *Proc. 4th IEEE ICDM*, pp. 431–434, 2004.
24. Mehmet Kaya , “Multi-objective genetic algorithm based approaches for mining optimized fuzzy association rules”, *Soft Computing*, vol.10, pp. 578–586, 2005.
25. R. Alhajj and M. Kaya, “Multi-objective genetic algorithms based automated clustering for fuzzy association rules mining,” *J. Intell. Inf. Syst.*, vol. 31, no. 3, pp. 243–264, 2008.
26. C.-H. Chen, T.-P. Hong, V. S. Tseng, and L.-C. Chen, “A multi-objective genetic-fuzzy mining algorithm,” in *Proc. IEEE Int. Conf. GRC*, 2008, pp. 115–120.
27. S. G. Matthews, M. A. Gongora, and A. A. Hopgood, “Evolving temporal fuzzy association rules from quantitative data with a multiobjective evolutionary algorithm,” in *Proc. Int. Conf. HAIS—Vol. Part I*, 2011, pp. 198–205.

A Study on the Structural Hole of Patent Applicant Network in R&D Management

Iori Nakaoka

*Dept. of Business Administration, National Institute of Technology, Ube College,
2-14-1 Tokiwadai, Ube City, Yamaguchi Pref., 755-8555, Japan
nakaoka@ube-k.ac.jp*

Yousin Park

*Dept. of Business Administration, Prefectural University of Hiroshima,
1-1-71 Ujina-Higashi, Minami-ku, Hiroshima City, Hiroshima Pref., 734-8558, Japan
ecventure@pu-hiroshima.ac.jp*

Yunju Chen

*Faculty of Economics, Shiga University,
1-1-1, Banba, Hikone City, Shiga Pref., 522-8522, Japan
yun-chen@biwako.shiga-u.ac.jp*

Abstract

The arrangement of R&D staff refers to the issue of the linkage between structural holes in a network. In order to examine the linkages between multiple R&D projects in a company, we use the patent information as the index of R&D capability and examine our propositions by social network analysis. In this paper we focus on top-shared companies in Japanese cosmetic industry, and suppose that these companies keep their market shares due to their smoothly changes of business fields to cope with the threat of new comers from other industries. The analysis in this paper include: 1) calculate the betweenness centrality, and create heat maps to visualize the change of the betweenness centrality, 2) examine the structural hole.

Keywords: patent analysis, social network analysis, heat maps, Japanese cosmetic industry, structural hole

1. Introduction

The development of new products is needed for a company to sustain its competitive advantage, while the results of development process are affected by the management of R&D organization. The arrangement of R&D staff refers to the issue of the linkage between structural holes in a network [1]. By using the patent data as the index of R&D capability, the R&D network structures can be visualized and analyzed by social network analysis. In Japan, one of the industries that face strong competitions due to numbers of new entries

is cosmetic industry. Although new entries never stop, top-shared companies keep their market shares in the industry. We suppose that if there is any feature in these companies' R&D management, and the features of R&D management contribute these companies to keep their growth.

In this paper, we focus on four top-shared companies in Japanese cosmetic industry to examine their R&D

In this paper, we focus on four top-shared companies in Japanese cosmetic industry to examine their R&D strategies, as well as the change of core researchers in their R&D projects by social network analysis, based on

the patent data. The analysis include: 1) calculate the betweenness centrality, and create heat-maps to visualize the change of the betweenness centrality, 2) examine the structure hole. The results of these analyses will be discussed to find out the reason why these companies can cope with the new entries.

2. Background

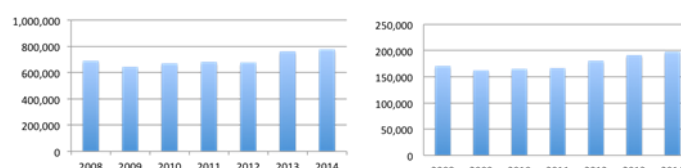
2.1 Structural hole and patent analysis

A structural hole is a relationship of non-redundancy between two contacts. The hole is a buffer, like an insulator in an electric circuit. As a result of the hole between them, the two contacts provide network benefits that are in some degree additive rather than overlapping [2]. Brokerage across the structural holes between groups provides a vision of options otherwise unseen, which is the mechanism by which brokerage becomes social capital.

Patent documents are an ample source of technical and commercial knowledge. The patent is one of the indicators of capacity for technological development. There are some researches aimed at visualizing and analyzing patents, or proposing efficient text-mining approaches for creating patent maps. However, there are few researches focusing on R&D management strategies based on text-mining analysis of patents. Therefore, this paper describes the features of Japanese cosmetic companies' R&D management based on the patent analysis.

2.2 The overview of cosmetic industry

Although the expansion of market scale benefits the Japanese cosmetic manufacturers to keep their growth, the mature of cosmetic market and customer slow down their speed of growth. The total sales of the industry have kept flat since the beginning of 2000, however, new comers from other industries have entered one after another after 2000. There are 12 large new comers into cosmetic industry and their entries concentrated on 2006-2009. The shares of sales of top 5 companies in 2014 were: Shiseido 37.9%, Kao 28.4%, Pola Holdings 9.5%, Kose 9.5%, Mandom 3.4%. The top 5 shared companies occupied the 80% of the total sales of the cosmetic market. Figure 1 shows the sales of Shiseido and Pola from 2008-2014. Their sales kept growing even after 2009, which the new entries most concentrated.



(a) Shiseido
(b) Pola
Figure 1 Total sales of each company

3. Methodology and data

In the following sections, the trends of R&D project management strategies of Japanese cosmetic companies are analyzed. In order to examine target companies' R&D strategies and the change of core researchers in their R&D projects, we visualize their patent information in 3 steps: the number calculation of patent publications, text mining, and social network analysis. Then diagrams are created by these analyses.

In Japan, patent documents are archived in J-PlatPat, and are browsed and retrieved ubiquitously. All patents are classified according to each three classification codes, IPC (International Patent Classification), FI (File Index) and F-term (File Forming Term). Both of FI and F-term are classification codes under IPC. Especially, F-term is given to every patent from F-term list based on the technical items indicated in patent documents. Thus, almost every patent has multi-F-term codes. Table 1 is most frequently used F-terms in cosmetic industry. Based on these F-term related to cosmetic, patents related to cosmetic published by each company are extracted and collected from the patent information.

Table1 F-term list of cosmetics patents

F-term	Contents
4C083AA	NATURAL INGREDIENTS AND INGREDIENTS WITH UNKNOWN STRUCTURES AND COMPOSITIONS
4C083AB	INORGANIC INGREDIENTS
4C083AC	ORGANIC INGREDIENTS CHARACTERIZED BY ELEMENTS
4C083AD	ORGANIC INGREDIENTS CHARACTERIZED BY STRUCTURES
4C083BB	FUNCTION SPECIFIC INGREDIENTS
4C083CC	KINDS OF PRODUCTS
4C083DD	FORMS OF PRODUCTS
4C083EE	EFFECTS
4C083FF	METHODS, DEVICES FOR MANUFACTURE

4. Analysis

4.1 An approach based on the number of patent publications

As our first approach, the numbers of patent publications associated with cosmetics in each of the companies are shown in Figure 2.

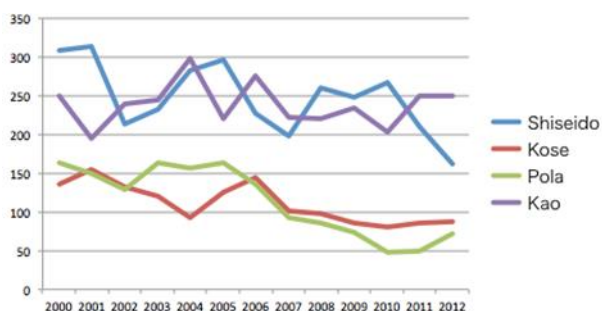


Figure 2 The number of patents of each companies

Every company obtains related patents to a certain extent and the number of patents of all of them kept on decreasing during the years. Shiseido and Kao obtain more than 200 patents every year although the rates of R&D spending and net sales fell. However, we can consider that R&D of Shiseido is efficiently because the rate of R&D spending and net sales of Shiseido is lower than Kao.

4.2 An approach by the text mining

We use the correspondence analysis based on text mining to disclose the technical trends and features based on typical words associated with cosmetic. Result of the analysis of Shiseido is Figure 3(a), and result of another cosmetic company Pola is Figure 3(b). The reference data in the analysis is the numbers of each their patent document in each year, including to cosmetic noun. These figures are based on dates of patent publication, and patents are applied to products in the companies. Figure 3(a) shows that there is low R&D continuity in Shiseido. Therefore it is considered that Shiseido changed its contents of technology depend on the year. On the other hand, Pola has developed similar technology continuously because the results almost outputted around the same place over all of the period in Figure 3(b).

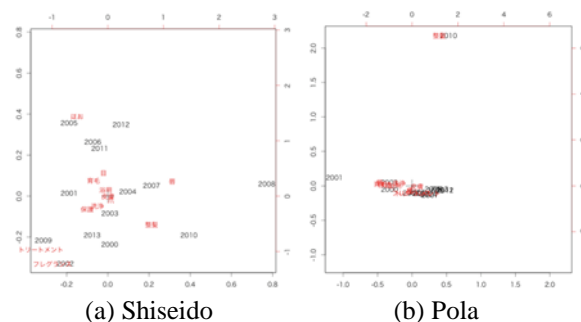


Figure 3 Results of correspondence analysis

4.3 An approach by the social network analysis

4.3.1. R&D network

We disclose the R&D project structures of the target companies by the social network analysis in this section.

The results are outputted as heat maps. Figure 4 (a) and (b) are the R&D networks that show Shiseido and Pola's personnel engaged in R&D (nodes) and linkages of joint patent applicants (edge). In addition, Figure 4 (c) and (d) are the heat maps that visualized the percentage of major R & D networks occupied in the entire networks. The vertical axis in the figure shows top 10 networks ranked by network size, and the scores mean the percentage of personnel belonging to the top 10 networks. When the color is dark, it means that the percentage of personnel belonging to the network is high. We can consider that Shiseido has adopted the overconcentration organization which emphasizes on cooperation because the percentage of the person who belongs to the biggest network in all of the years is high. On the other hand, other companies such as Pola and so on have adopted decentralized organization which differentiated by each function.

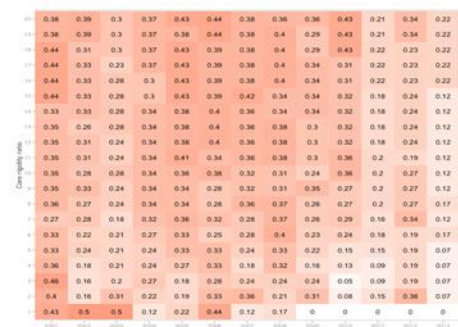
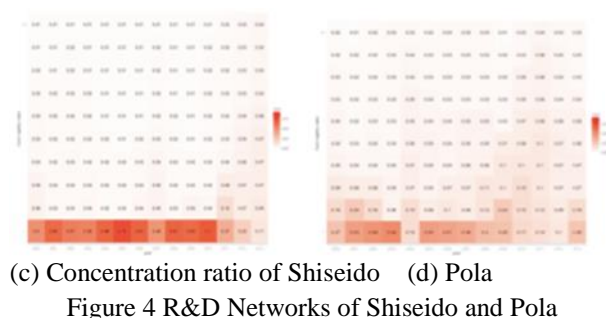
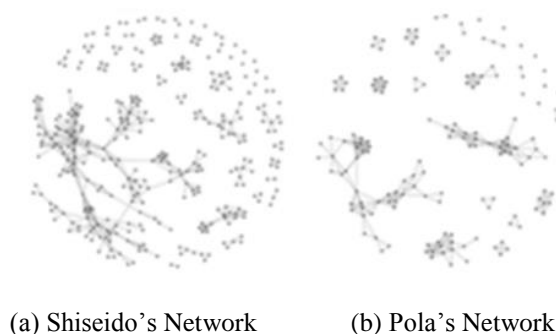


Figure 5 The Degree of core rigidity of Shiseido

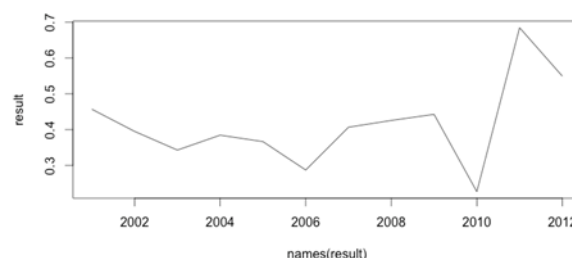


Figure 6 The change of R&D area that core structural hole personnel involved in

4.3.2. Structural hole resource of R&D

The structural hole means the gap between social groups. Since personnel who connect organizations play the role as the structural hole serves to relay the information, we use betweenness centrality to visualize the change of the core structural holes connection personnel in this paper. Betweenness Centrality is one of the well-known indices that Freeman proposed in the social network analysis [3].

In addition, we focus on the change of R&D area that structural holes connection core personnel involved in to express how the structural holes personnel develop new technologies. As one of the example, the core rigidity of human resource and the change of R&D area the structural holes personnel involved in Shiseido are shown in Figure 5 and 6. There is no significant change in Shiseido's core rigidity degree. However, it was found that the core rigidity degree somewhat reduced in recent years while new entrant company increased. In addition, structural hole personnel were found to involve in various areas at a constant level from area of the previous year.

5. Conclusions

There is a thesis that innovation has exploitation and exploration type [4]. From these results, the innovation type of Shiseido's R&D strategy is an "exploration type", and the innovation type of other companies (Pola and so on) of R&D strategy is an "exploitation type". As further works, the patent data of the other country and the other companies should be carefully examined. We would like to modify our approach into more sophisticated one and to build up a more reliable theoretical background.

References

1. R. S. Burt, Structural Holes and Good Ideas, *American Journal of Sociology*, Vol. 110 (2004), pp. 349-399.
2. R. S. Burt, *Structural holes: The social structure of competition* (Harvard University Press, Cambridge, MA, 1992).
3. L. C. Freeman, Centrality in Social Networks Conceptual Clarification, *Social Networks*, vol.1 (1978-1979), pp.215-239.
4. D. A. Levinthal, and J. G. March, The myopia of learning, *Strategic Management Journal*, vol.14 (1993), pp.95-112.

The TCE-RBV Framework for Information Systems Outsourcing: Empirical Testing using Survey Data in Japan

Seigo Matsuno*

Dept. of Business Administration, National Institute of Technology, Ube College, Ube, Yamaguchi 755-8555, Japan

Tsutomu Ito

Hino Motors, Ltd., Hino, Tokyo 191-0003, Japan

Yasuo Uchida

Dept. of Business Administration, National Institute of Technology, Ube College, Ube, Yamaguchi 755-8555, Japan

Yoshiki Mikami

Graduate School of Engineering, Nagaoka University of Technology, Nagaoka, Niigata 940-2137, Japan

Takao Ito

Graduate School of Engineering, Hiroshima University, Higashi-Hiroshima, Hiroshima 739-8527, Japan

**Corresponding author, E-mail: matsuno@ube-k.ac.jp*

Tel: +81-836-35-4016, Fax: +81-836-35-4016

Abstract

This paper investigates the factors that influence the motives of make-or-buy decisions on information systems from the viewpoints of Transaction cost economics (TCE) and the resource-based view (RBV). Using our original questionnaire survey data carried out in 2007 targeting Japanese firms, we analyze the relationships between the recognition related to the role of their information systems and the pattern of their make-or-buy decisions. As a result, we make it clear that there are two cases in which TCE-motive and RBV-motive are complement or contradict each other. And in latter case, TCE-motive tends to dominate over RBV-motive. Finally, the implications for theory and practice are discussed.

Keywords: Information systems outsourcing, Make-or-buy decisions, Transaction Cost Economics, Resource-based View

1. Introduction

Up to now, two influential perspectives of outsourcing, that is, Transaction cost economics (TCE) and the resource-based view (RBV) have been both making a valuable contribution to understanding and explaining the complexities of outsourcing. However, the discussion has treated TCE and RBV as independent

approaches to the outsourcing decisions. This paper investigates the factors that influence the motives of make-or-buy decisions on information systems (IS) from the viewpoints of TCE and the RBV.

This paper is organized as follows. In Section 2, we briefly review some previous arguments of the IS outsourcing. After reviewing the relevant literature on the IS outsourcing, we analyze the relationships

between the recognition related to the role of their information systems and the pattern of their make-or-buy decisions. The TCE-RBV framework is tested empirically by using our original questionnaire survey data targeting Japanese firms in Section 3. In Section 4, we discuss the implications derived from the results of the statistical testing. Finally, in Section 5 we conclude by a summary of this paper.

2. Literature review on IS outsourcing

2.1. Transaction-based perspective

TCE posits that organizations prefer insourcing when the market costs are higher than internal governance costs [1]. Markets generally lead to smaller production costs, because of economies of scale obtained by suppliers and/or vendors. However, markets lead to higher transaction costs arising from three principal attributes of transactions: asset specificity, uncertainty, and frequency [2].

Asset specificity for the IS outsourcing has two aspects; for business of a client company supported by the developed information systems, and for technologies which external vendors utilize. If the business that a client company outsources is unusual, external vendors have to be familiar with the business so that the asset specificity will occur and increase on mainly human resources. Similarly, if technology used by external vendors is very specific, it will be difficult to use the information systems for other purposes on the client company. Due to the investment to these unusual assets, the transaction costs would increase.

Hence, if it is necessary to reduce the risk of opportunism resulted from asset specificity and to restrict the increase of transaction costs, insourcing or quasi-outsourcing would be selected.

2.2. Resource-based perspective

The RBV of the firm posits that organizations prefer insourcing when a resource or capability is strategic so as to enable them to sustain competitive advantage [3]. It builds upon four properties of a strategic resource: economic value, rareness, imperfect imitability, and non-substitutability. The RBV is important to the study of the IS outsourcing, as superior performance achieved

in the IS activities related to external vendors would explain why such activities are performed internally.

Thus understanding of managerial resources as an advantage for the company is called “core competencies” in general today. Prahalad and Hamel (1990) defined the core competence as “a combination of technologies and production skills which is based on the company’s infinite product lines” [4]. This concept is understood more broadly today and is recognized as their own resources and abilities, which are hard to be imitated and implemented by other companies, as a source of the company’s sustainable competitive advantage.

From the viewpoint of the RBV, competitive advantage of organizations can only be achieved through a focus on core competencies, the management of organizations have chosen to concentrate on what an organization does better than anyone else while outsourcing the rest.

2.3. TCE-RBV Framework

The large number of studies of the IS outsourcing was published in the past [5]. Especially, in the previous study on the two patterns of the IS outsourcing, some focus on factors of the influence on its selection. For instance, Barthelemy and Geyer (2005) classify the factors of the influence on the choice of either conventional outsourcing or quasi-outsourcing into internal and external factors [6]. They focus on testing some hypotheses which are suggested based on the TCE approach, but they do not refer to the RBV arguments.

The TCE and the RBV approach are treated as independent argument so far, but each theoretical perspective alone cannot fully describe the phenomena of the IS outsourcing. Then there is a growing bodies of research on the recognition that the TCE and the RBV are complementary one another [7].

McIvor (2009) integrated the TCE and RBV perspectives into a framework specifically assessing the outsourcing decisions [8]. The TCE dimension of this framework focuses upon the potential for opportunism in any outsourcing decision. The RBV dimension focuses upon a firm’s resource position against potential suppliers or competitors. This conceptual framework (see Fig. 1) suggests that for an activity in which the firm has a weak resource position or capability, and the potential for opportunism is low, outsourcing is the best

option. In the opposite case, where a firm enjoys strong resource position and potential for opportunism is high, insourcing is the best answer. This framework implies not only complementary but also contradictory prescriptions of the RBV and TCE in outsourcing decisions due to the inherent conflicts between the two theories [9].

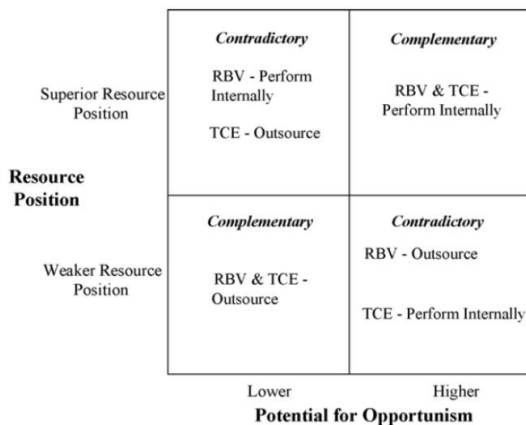


Fig. 1. The TCE-RBV Framework. (Adapted from McIvor, 2009.)

3. Data and Method

3.1. Data collection

We conducted a mail questionnaire survey from July to September 2007 with the research objective of investigating “the current state and issues in IS outsourcing and inter-firm collaboration”. Since ordinarily the implementation of IS outsourcing is likely to be affected by a firm size, we targeted Japanese firms with 500 or more employees in this survey. The number of valid response rate obtained from randomly sampled firms was 25.9%, but detailed results are omitted here.

3.2. Constructs variables and operationalization

In this study, it is postulated that both ‘TCE-motive’ attaching importance to the logic of TCE and ‘RBV-motive’ attaching importance to the logic of RBV affect make-or-buy decision making on information systems. And we assume that these two constructs consist of each four question items shown in Table 1. Each score (6-point scale) obtained directly from each question item is regarded as an interval scale.

Table 1. Status of the recognition related to the roles of ICT and information systems

Construct	Items
TCE-motive ($\alpha = 0.73$)	<ol style="list-style-type: none"> 1. Even if the company's own information systems are outsourced, it isn't expected to reduce the cost concerning them. 2. When the company's own information systems are outsourced, it isn't expected to accumulate skills and know-how concerning them. 3. When the company's own information systems are outsourced, there is a risk that it would be dependent excessively on a specific vendor. 4. When the company's own information systems are outsourced, it isn't possible to correspond to internal users' needs rapidly.
RBV-motive ($\alpha = 0.80$)	<ol style="list-style-type: none"> 1. ICT is very important to reduce the cost of the company's products and services. 2. ICT is very important to improve the quality of the company's products and services. 3. ICT is closely related to and operated integrally with the execution of the company's core business. 4. ICT is an important infrastructure which supports the execution of the company's core business.

Note: Each item is measured by 6-point scale. 1 = It does not apply at all. 6 = It applies fully.

Here, we omit exploratory factor analysis process for examining the validity of the assumed constructs variables and use the value obtained by dividing the total of the values of the items pertaining to each construct variable by the number of items. The reliability of the measurements was calculated using the Cronbach's α .

Then, we classified sample data into 4 groups based on the average value of each construct variable. For example, LOSR (Lower potential for Opportunism and Superior Resource position) group means that the average value of TCE-motive is lower than the average value of the whole and the average value of RBV-motive is higher than the average value of the whole.

On the contrary, HOWR (Higher potential for Opportunism and Weaker Resource position) group means that the average value of TCE-motive is higher and the average value of RBV-motive is lower than each average value of the whole.

4. Analysis and discussion

We conducted a chi-squared test between the 4 groups mentioned above and the IS sourcing pattern (insourcing or outsourcing). Such a contingency table is shown in Table 2. The result was significant ($\chi^2(3) = 11.96$, $p = 0.01$, Cramer's $V = 0.26$, $power = 0.84$) and therefore the two variables are not independent. The evaluation of effect size was medium degree and power of the test was a desirable level sufficiently.

In Table 3, from the multiple comparison testing among 4 groups (adjusted p -value is based on Benjamini and Hochberg, 1995) [10], we found out the significant difference between each of HOSR–LOSR, HOSR–LOWR, LOSR–HOWR, LOWR–HOWR ($\chi^2(1) = 4.92$, $p = 0.05$; $\chi^2(1) = 4.55$, $p = 0.05$; $\chi^2(1) = 5.34$, $p = 0.05$; $\chi^2(1) = 5.00$, $p = 0.05$, respectively).

Table 2. Contingency table of the relation between the 4 groups and the IS sourcing pattern

	Outsourcing	Insourcing
HOSR	28 (0.47)	31 (0.53)
LOSR	32 (0.71)	13 (0.29)
LOWR	31 (0.70)	13 (0.30)
HOWR	14 (0.42)	19 (0.58)

Note: The numerical value in each parenthesis is the relative frequency in each line.

Table 3. Multiple comparison test among 4 groups

	χ^2	df	$adj. p$
HOSR – LOSR	4.92	1	0.05
HOSR – LOWR	4.55	1	0.05
HOSR – HOWR	0.06	1	0.97
LOSR – LOWR	0.00	1	1.00
LOSR – HOWR	5.34	1	0.05
LOWR – HOWR	5.00	1	0.05

In light of the above analysis, the percentage of IS insourcing is high by HOSR group, and the percentage of IS outsourcing is high by LOWR group conversely. This means that TCE-motive and RBV-motive are

complement mutually. On the other hand, the percentage of IS outsourcing is high by LOSR group, and the percentage of IS insourcing is high by HOWR group. Therefore, when TCE-motive and RBV-motive contradict each other, TCE-motive tends to relatively dominate over RBV-motive.

5. Concluding remarks

This paper investigates the factors that influence the motives of make-or-buy decisions on information systems from the viewpoints of TCE and the RBV. We empirically test the TCE-RBV framework by using our original questionnaire survey data targeting Japanese firms. As a result, we made it clear that there were two cases in which TCE-motive and RBV-motive were complement or contradict each other. And in latter case, TCE-motive tends to dominate over RBV-motive.

References

1. R. Coase, The nature of the firm, *Economica*, **4**(16) (1937), 386–405.
2. O. Williamson, *Markets and Hierarchy: Analysis and Antitrust Implications* (Free Press, 1975).
3. J. Barney, Firm resources and sustained competitive advantage, *J. Management*, **17**(1) (1991), 99–120.
4. C. Prahalad and G. Hamel, The core competence of the corporation, *Harvard Business Review*, **68**(3) (1990), 79–91.
5. S. Matsuno, T. Ito, and Z. Xia, Determinants of information systems outsourcing: An empirical investigation in Japan, *Artificial Life and Robotics*, **14**(3) (2009), 337–341.
6. J. Barthelemy and D. Geyer, An empirical investigation of IT outsourcing versus quasi-outsourcing in France and Germany, *Information & Management*, **42**(4) (2005), 533–542.
7. O. Williamson, Strategy research: Governance and competence perspectives, *Strategic Management J.*, **20** (1999), 1087–1108.
8. R. McIvor, How the transaction cost and resource-based theories of the firm inform outsourcing evaluation, *J. Operations Management*, **27**(1) (2009), 45–63.
9. B. Brewer, C. Wallin, and B. Ashenbaum, Outsourcing the procurement function: Do actions and results align with theory?, *J. Purchasing & Supply Management*, **20** (2014), 186–194.
10. Y. Benjamini and Y. Hochberg, Controlling the false discovery rate: a practical and powerful approach to multiple testing. *J. Royal. Statistical. Society. Ser. B*, **57**(1) (1995), 289–300.

Momentum and Its Implications in Corporate Management

Tsutomu Ito*, Takao Ito, Katsuhiko Takahashi, Katsumi Morikawa
*Graduate School of Engineering, Hiroshima University, 1-4-1 Kagamiyama
Higashi-Hiroshima, Hiroshima 739-8527, Japan
fw.eldorado.500cuin@gmail.com*

Rajiv Mehta
*School of Management, New Jersey Institute of Technology University Height
Newark, NJ 07102-1982 USA
mehta@njit.edu*

Sakamoto Makoto
*Faculty of Engineering University of Miyazaki 1-1, Gakuenkibanadai-nishi
Miyazaki, 889-2192 JAPAN
sakamoto@cs.miyazaki-u.ac.jp*

Abstract

The basis of corporate strategy stems from two seminal books: The Art of War, and On War written by Sun Tzu in the late sixth century BC and Carl von Clausewitz in 1827, respectively. In contrasting these two theses with current strategic theories, discussions on momentum, an important concept, have been sparse, although in the context of current management strategies the pivotal nature of momentum recently has been operationalized and discussed in research on marketing, and finance. The current manuscript reviews the literature associated with corporate strategy, and proposes a new approach of acceleration to measure momentum based on limited cycle theory. Thus, this research manuscript makes a contribution to extant thought by: 1) Defining momentum, 2) Discussing the nature of the relationship between momentum to its external environment, and company scale, 3) Ascertaining the momentum period, and 4) Proposing a four-cell model composed of momentum and company scale for judging a firm's position. Additionally, the relationship between momentum and the impact of 2007-2008 financial crises is addressed. Based on the findings, the study limitations are identified and directions for further research are suggested.

Keywords: Momentum, velocity, limit cycle theory, four cell model, strategy

1. Introduction

The basis of corporate strategy stems from two seminal books: The Art of War, and On War written by Sun Tzu in the late sixth century BC and Carl von Clausewitz in 1827, respectively. In comparing these two books, especially the Art of War, with extant strategic theories,

discussions on momentum, an important concept, have been sparse, although in the context of current management strategies, the pivotal nature of momentum recently has been operationalized and discussed in research on marketing, and finance. This paper reviews the literature associated with corporate strategy to propose a new approach of acceleration for measuring

© The 2016 International Conference on Artificial Life and Robotics (ICAROB 2016), Jan. 29-31, Okinawa Convention Center, Okinawa, Japan

momentum based on limited cycle theory. This research also attempts to shed light on the relationship between sales revenue and momentum, and offers an explanation why the business cycle in Japan's automobile industry changed to a four-year period. Furthermore, the paper also develops a four cell model comprising momentum and firm scale as an effective approach for improving corporate performance.

This paper is structured as follows. Section 2 reviews the literature focusing on the momentum and corporate management. In section 3, the paper explicates the calculation process of momentum and data collection. Section 4 discusses our findings and managerial implications based upon our calculation. The study limitations are identified and directions for further research are proffered in Section 5.

2. The Main Text

Momentum is a term to express power, force and speed of organizational movement. The original description of momentum appears in *Art of War* written by famous strategist Sun Tzu. Indicating the importance of momentum at the beginning of his book, Sun Tzu famously asserts: It is important to "look for advantages when applying my principles and you will gather sufficient force to take on unforeseen situations. Force is tilting the balance of power to your side by gathering advantages" to win any battle [1, 01.11-01.12]. He continued to explain the meaning of momentum in chapter five as force. In this context, he asserts "the rush of torrential waters tossing boulders illustrates force. The strike of a bird of prey breaking the body of its target illustrates timing. Therefore, the force of those skilled in warfare is overwhelming and their timing precise. Their force is like a drawn crossbow and their timing is like the release of the trigger" [1, 05.08-05.10]. Furthermore, in analyzing the relationship between the momentum and war, Sun Tzu, posits "Those skilled in warfare seek victory through force and do not require too much from individuals. Therefore, they are able to select the right men and exploit force. One who exploits force commands men into battle like rolling logs and boulders. Logs and boulders are still when on flat ground, but roll when on steep ground. Square shapes are still, but round shapes roll. Therefore, those skilled in warfare use force by making the troops in battle like boulders rolling down a steep mountain. This is force" [1, 05.16-05.18].

© The 2016 International Conference on Artificial Life and Robotics (ICAROB 2016), Jan. 29-31, Okinawa Convention Center, Okinawa, Japan

It is widely acknowledged that military strategy forms the basis of corporate strategy. But in the strategic management literature, surprisingly there is no theoretical description nor application of momentum, which plays an important role in the performance of business activities. An on-line browse of the term "strategy momentum" (in Japanese) yielded approximately 932,000 hits which suggest that it obviously is an important concept in corporate strategy. Momentum expresses a force or speed of movement. In this paper, momentum is defined as a force or impetus of firms to maintain firm's development durability in certain period. Why is momentum becoming more and more important? A possible explanation is that inherent uncertainty is in-built within the dynamic, high-speed global economy. With the high rate of innovation, the speed of decision-making has become a condition for successful performance.

In 1995, as a new method applying business to U.S. army logistics, velocity management focused on improving the speed and accuracy with which materials and information flow from providers to users. Meanwhile, velocity management is an emergent scientific field that conflates army operations and business together to reflect the new realities of the global environment. Mourier observed that velocity management is decision making at speeds consistent with today's competitive environment and technology [2].

It is noteworthy that momentum has been the subject of study in finance and marketing. Momentum in stock and securities is used to illustrate that their price is more likely to keep moving in the same direction than to change directions. In technical analysis, momentum is considered as an oscillator and is used to help identify trend lines. It is the empirically observed tendency for rising asset prices to rise further, and falling prices to keep falling. One of the important achievements in finance is that stocks with strong past performance continue to outperform stocks with poor past performance in the next period with an average excess return of about 1% per month [3].

However, to our best knowledge, this is the first work that shows how to calculate momentum using velocity for corporate strategy. The basic reasons why we have to calculate momentum using limit cycle theory because the global economy is becoming increasingly uncertain and most of the corporate behaviors are non-linear. This body

of thought is important as it will help increase our understanding and provide guidance that strategic management practitioners can use to increase organizational performance. Thus, this study addresses the paucity in the strategic management literature and makes a contribution to the field by being the first, initial, investigation that illustrates how to measure momentum using velocity, and its observed importance for corporate strategy.

3. Measurement and Data Collection

Previous studies have showed that chaos, which is generally described as a disorder state, is driven by deterministic nonlinear processes, such as hydraulic flow and astronomical phenomena. Findings in physics and biology have discovered some examples of chaos. For example, Tsuda et al, found a chaotic pulsation in a finger's capillary vessels in normal subjects and psychiatric patients, as well as cardiac chaos [4].

Additional research illustrated that chaotic movement is not only applicable in physics and biology, but also in sociology and management science. For instance, Priesmeyer and Baik proposed a new method to discover the pattern of chaos in 1989. They noticed that organization have characteristics limit cycle like the human heart. They indicated "Company data tend to adhere to an attractor as they collect their quarterly sales and drive their quarterly profits. One can almost hear the organizational heartbeat pounding out 'Quarter 1, Quarter 2, Quarter 3, Quarter 4'" [5]. Furthermore, Ito and Sakamoto shed light on the nature of the relationship between economic development and the velocity history of the typical companies in Japan [6].

Because most of the behaviors of the firms are nonlinear, momentum should be calculated based on complex systems theory. In this paper, momentum is conceptualized as a force that composed of sales and profit movement, and is calculated based upon limit cycle theory because of its non-linear movement.

In order to calculate and assess the impact of momentum on corporate performance, data were collected from 35 selected companies, including 10 car makers and 25 parts suppliers. In order to understand the impacts of the Lehman shock on momentum, the data includes sales and profit from 2003 to 2013.

4. Discussions and Analysis

The t in Momentum equation may vary depending on different analysis proposed. For instance, one-year momentum is calculated when t is equal to 1, and two-year momentum is calculated when t is equal to 2. To understand the movement of the momentum within a short period, one-year momentum is calculated as below.

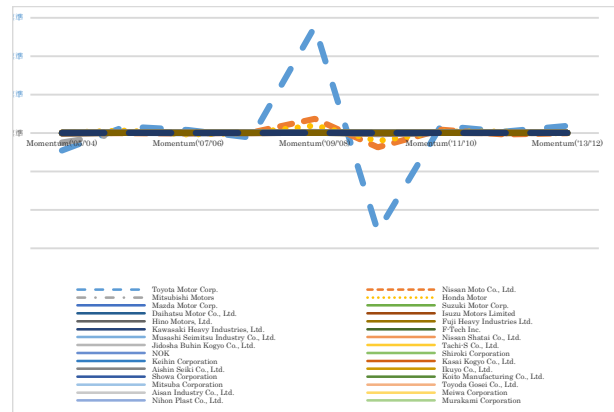


Fig. 1. One-year momentum of each firm (2005-2013).

All momentum looks very stable except the period from 2007 to 2010. As a well-known fact, 2007-2008 financial crisis resulted from subprime lending practices. The prospects of Japan's economy are unpredictable and the sales of new decreased. The unstable momentum could be considered as a reaction of the financial crisis. Therefore, two conclusions are made based on observing Fig. 1. First, momentum is very sensitive to external changes. Another important fact is that momentum of Toyota increased in 2008, decreased in 2009, and recovered in 2010. Other car makers, such as Nissan and Mitsubishi, reacted similarly. Second, the financial crisis had an impact over three years on the Japanese car market. In other words, momentum could be considered as an effective index to calculate the environmental changes. Next, the multiple year momentum was calculated, which is illustrated in Fig. 2.

In Fig. 2, Toyota is seen to have the biggest value for momentum over 9-years. The second is Honda, and the least is Mitsubishi. As time t becomes longer, momentum of a big scale company grows larger. The third conclusion is that the reaction is apparently pronounced if the scale of the company is large.

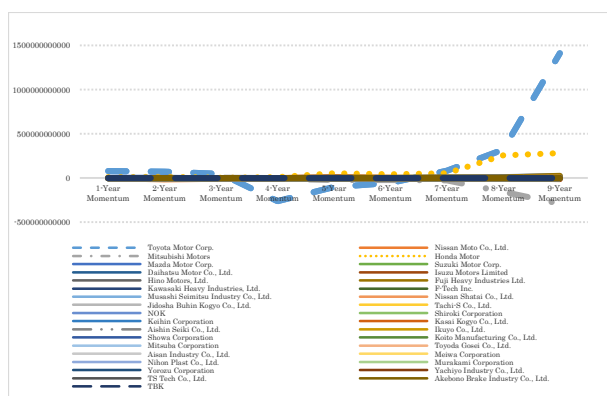


Fig. 2. 1-9 year Momentum of each firm (2005-2013).

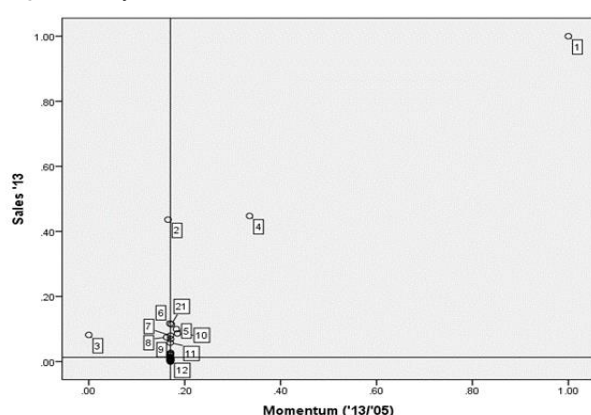


Fig. 3. A four-cell model of momentum ('13/'05) and Sales '13

Based on the results, it is also possible to identify successful companies as well as firms with impaired performance using momentum measurements. Based on the findings, momentum is influenced by the external environment, company scales, and corporate performance. Thus a four-cell model is proposed in this paper. Comprising of momentum and scale should be effective. The four-cell model of momentum ('13/'05) and sales'13 is illustrated in Fig. 3.

The reference line of x axis and y axis are the median of momentum and sales '13 respectively in Fig. 3. The firms located in the 1st quadrant and the 3rd quadrant are good firms and poorly performing firms, respectively, because they have appropriate relationship between momentum and sales'13. The firm is called developing company with high development potential if it is located in 4th quadrant, while the firm is called problem child if it is located in 2nd quadrant. A firm moving from 3rd quadrant

to 2nd or 4th quadrant, or further from 2nd and 4th to 1st quadrant would be considered positive signs. All the companies are divided into four different groups. Our next conclusion is that the four-cell model is appropriate to judge a firm's position

5. Conclusions

This paper proposed a new approach for using momentum based on the limit cycle theory after reviewing the relevant literature. The relationship between momentum and its external changes, momentum and company scale were analyzed over various momentum periods. Furthermore, the four-cell model composed of momentum and company sales confirmed that it is effective for judging firm's position. Additionally, the impact of the financial crisis was also considered.

Sales and profit, as indices of corporate performance, is insufficient. Additional indices, such as aggregate market value and ROI (return on investment), should be investigated. What's more, in the future these models should be tested using data drawn from other settings, such as, information technology, the ship-building industry for comparative research as well as replicating the current findings.

References

1. Sun Tzu's The Art Of War, Translated by the Sonshi Group, <https://www.sonshi.com/original-the-art-of-war-translation-not-giles.html>, Retrieved July 30, 2015
2. Pierre Mourier, (2001), Velocity management: - creating organizational instinct, Strategy & Leadership, Vol. 29 Issue 2, pp.24 - 28
3. Chakrabarti Gagari (2015) Time-series momentum trading strategies in the global stock market, Business, <http://www.thefreelibrary.com/Time-series+momentum+trading+strategies+in+the+global+stock+market.-a0423234977>, Retrieved October 22, 2015
4. Tsuda I., Tahara T., and Iwanaga H. (1992) Chaotic Pulsation in Human Capillary Vessels and its Dependence on Mental and Physical Conditions, International Journal of Bifurcation and Chaos, Vol.2, No.2, pp.313-324, World Scientific Publishing Company.
5. Priesmeyer H. R., Kibok Baik (1989) Discovering the Patterns of Chaos, Planning Review, pp.14-21 and pp.46-47, November/December 1989
6. Ito T. and Sakamoto M. (2007) A Consideration on Limit Cycle Theory, The papers of Technical Meetings on Information Systems, IS-07-10 ~ 15, pp. 19-23, The Institute of Electrical Engineers of Japan (Japanese Edition)

A Method for Secure Communication Using a Discrete Wavelet Transform for Sound Data

Yuji Tsuda¹, Kouhei Nishimura², Haruka Oyaizu³, Yasunari Yoshitomi², Taro Asada², and Masayoshi Tabuse²

1: Software Service, Inc.

Nishi-Miyahara, Yodogawa-Ku, Osaka 532-0004, Japan

2: Graduate School of Life and Environmental Sciences, Kyoto Prefectural University,

1-5 Nakaragi-cho, Shimogamo, Sakyo-ku, Kyoto 606-8522, Japan

E-mail: {yoshitomi, tabuse}@kpu.ac.jp, t_asada@mei.kpu.ac.jp}

http://www2.kpu.ac.jp/ningen/infosys/English_index.html

3: NHK Media Technology, Inc.

Kamiyama-cho, Shibuya-ku, Tokyo 150-0047, Japan

Abstract

We developed a method for secure communication using a discrete wavelet transform. Two users must have one piece of music before communicating each other. The music and the original sound data are transformed into a code using the scaling coefficients obtained from a discrete wavelet transform. The user can produce the sound similar to the original sound using an inverse discrete wavelet transform with the code made from the music, the information on the difference between these two codes.

Keywords: Secure communication, Sound data processing, Wavelet transform, Coding.

1. Introduction

Recently, some kinds of frauds have been critical issues. Especially, elder persons tend to be targets of fraud using a telephone. The fraud pretends to be a grandchild of the elder person in talking through the telephone, and appeals the elder person to send money, for example, through a bank budget account. When the elder person takes the fraud for a grandchild, the fraud can get money. Even if the voice of fraud is not similar to that of the grandchild, the elder person might send money to the fraud. This is because the fraud skillfully appeals a serious monetary trouble such as a traffic accident to the elder person who cherishes a real grandchild.

In the present study, we propose a method for secure communication using a discrete wavelet transform (DWT). The method can be used for the

Internet protocol (IP) telephone, and has a potential for stopping frauds using a telephone.

2. Wavelet Transform

In this section, we briefly explain the DWT, according to the references.¹

The original sound data $s_k^{(0)}$, which is used as the level-0 wavelet decomposition coefficient sequence, where k denotes the element number in the data, are decomposed into the elements of multi-resolution representation (MRR) and the elements of multi-resolution analysis (MRA) by repeatedly applying the DWT. The wavelet decomposition coefficient sequence $s_k^{(j)}$ at level j is decomposed into two wavelet decomposition coefficient sequences at level $j+1$ by using (1) and (2):

$$s_k^{(j+1)} = \sum_n \overline{p_{n-2k}} s_n^{(j)} \quad (1)$$

$$w_k^{(j+1)} = \sum_n \overline{q_{n-2k}} s_n^{(j)}, \quad (2)$$

where p_k and q_k denote the scaling and wavelet sequences, respectively, and $w_k^{(j+1)}$ denotes the development coefficient at level $j+1$. The development coefficients at level J are obtained using (1) and (2) iteratively from $j=0$ to $j=J-1$. Fig. 1 shows the process of multi-resolution analysis by DWT.

In the present study, we use the Daubechies wavelet for the DWT, according to the reference.² As a result, we obtain the following relation between p_k and

$$q_k = (-1)^k p_{1-k} \quad (3)$$

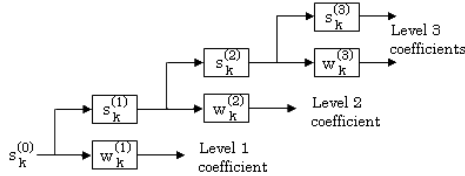


Fig. 1. Multi-resolution analysis by the DWT.¹

3. Proposed Method

3.1. Coding

3.1.1. Phenomenon exploited in coding algorithm for sound data

It is known that the histogram of the wavelet coefficients of each domain of the MRR sequences has a distribution which is centered at approximately 0 when the DWT is performed on sound data.¹ In the present study, we have found that the histogram of the scaling coefficients of each domain of the MRA sequences also has a distribution which is centered at approximately 0 when the DWT is performed on sound data. Exploiting this phenomenon, we developed a secure communication method using sound data.

3.1.2. Parameter setting

As with the digital watermark (DW) techniques for images^{2, 3} and digital sound⁴, we set the following coding parameters.

The values of $Th(minus)$ and $Th(plus)$ in Fig.2 are chosen such that the non-positive scaling coefficients (S_m in total frequency) are equally divided into two

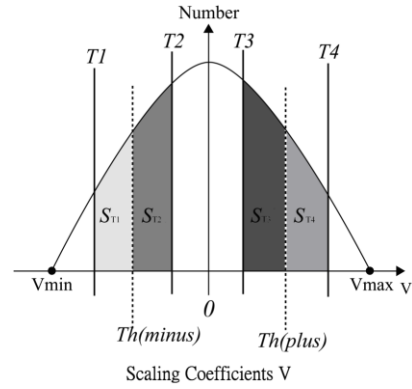


Fig. 2. Schematic diagram of the histogram of MRA scaling coefficients.

groups by $Th(minus)$, and the positive scaling coefficients (S_p in total frequency) are equally divided into two groups by $Th(plus)$. Next, the values of T_1 , T_2 , T_3 , and T_4 , which are the parameters for controlling the authentication precision, are chosen to satisfy the following conditions:

- 1) $T_1 < Th(minus) < T_2 < 0 < T_3 < Th(plus) < T_4$.
- 2) The value of S_{T1} , which is the number of scaling coefficients in $(T_1, Th(minus))$, is equal to S_{T2} , which is the number of scaling coefficients in $[Th(minus), T_2)$, i.e., $S_{T1} = S_{T2}$.
- 3) The value of S_{T3} , the number of scaling coefficients in $(T_3, Th(plus)]$, is equal to S_{T4} , the number of scaling coefficients in $(Th(plus), T_4)$, i.e., $S_{T3} = S_{T4}$.
- 4) $S_{T1} / S_m = S_{T3} / S_p$.

In the present study, the values of both S_{T1} / S_m and S_{T3} / S_p are set to 0.3, which was determined experimentally.

3.1.3. Coding

To prepare the coding of sound data, the procedure separates the scaling coefficients V of an MRA sequence into five sets (hereinafter referred to as G_0 , G_1 , G_2 , G_3 , and G_4), as shown in Fig. 3, by using the following criteria:

- $G_0 = \{V \mid V \in V^{SC}, V \leq T_1\}$,
- $G_1 = \{V \mid V \in V^{SC}, T_1 < V < T_2\}$,
- $G_2 = \{V \mid V \in V^{SC}, T_2 \leq V \leq T_3\}$,
- $G_3 = \{V \mid V \in V^{SC}, T_3 < V < T_4\}$,
- $G_4 = \{V \mid V \in V^{SC}, T_4 \leq V\}$,

where V^{sc} is the set of scaling coefficients in the sound data file.

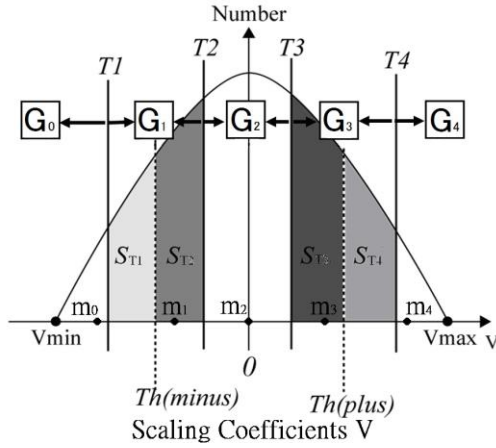


Fig. 3. Schematic diagram for demonstrating scaling coefficient selection in coding sound data.

The scaling coefficients of an MRA sequence are coded according to the following rules, in which V_i denotes one of scaling coefficients:

- When $V_i \in G_0$, symbol c_i is set to be 0.
- When $V_i \in G_1$, symbol c_i is set to be 1.
- When $V_i \in G_2$, symbol c_i is set to be 2.
- When $V_i \in G_3$, symbol c_i is set to be 3.
- When $V_i \in G_4$, symbol c_i is set to be 4.

Then, the representative value for each set is set as its average value (m_0, m_1, m_2, m_3, m_4), respectively. For sound data formation, we use a code C (hereinafter referred to as an original code), which is the sequence of c_i , and m_j defined above.

3.2. Sound data formation using code replacement

The scaling coefficient sequence for sound data A is expressed by

$$S(A)_k = \{x_1, x_2, x_3, \dots, x_k\},$$

where k is the number of scaling coefficient of A . Then, a sequence

$$C(A)_k = \{X_1, X_2, X_3, \dots, X_k\}$$

is given, where $X_i (\in \{0, 1, 2, 3, 4\})$ is the index showing one of five sets of scaling coefficients to which x_i belongs.

Next, the sound data A' is defined as having the scaling coefficient sequence $S(A')_k$ and the value of

zero for all wavelet coefficient values at every level. $S(A')_k$ is obtained as:

$$S(A')_k = \{a_1, a_2, a_3, \dots, a_k\},$$

where $a_i (\in \{m_0^A, m_1^A, m_2^A, m_3^A, m_4^A\})$ is an average at the range of scaling coefficients of A , which is indicated by $X_i (\in \{0, 1, 2, 3, 4\})$ obtained from A .

Then, the sound data B'_A is defined as having the scaling coefficient sequence $S(B'_A)_k$ and the value of zero for all wavelet coefficient values at every level. $S(B'_A)_k$ is obtained as:

$$S(B'_A)_k = \{b_{A,1}, b_{A,2}, b_{A,3}, \dots, b_{A,k}\},$$

where $b_{A,i} (\in \{m_0^B, m_1^B, m_2^B, m_3^B, m_4^B\})$ is an average at the range of scaling coefficients of B , which is indicated by $X_i (\in \{0, 1, 2, 3, 4\})$ obtained from A .

$S(B'_A)_k$ is obtained by replacing Y_i to X_i when $Y_i \neq X_i$, followed by replacing b_i to $b_{A,i}$, where b_i is an average at the range of scaling coefficients of B , which is indicated by Y_i . Therefore, $C(B'_A)_k = C(A)_k$. As a result, B'_A is expected to be similar to A .

3.3. Data for communication

A sequence $D1(B'_A)_n$ is defined as:

$$D1(B'_A)_n = \{z_1, z_2, \dots, z_n\},$$

where n is the number is the total number of the cases of $Y_i \neq X_i$, and $z_p = \lfloor y_i \rfloor \bmod 256$, in which the integer p is increased from 1 to n one by one when $Y_i \neq X_i$ happens. Here, $\lfloor x \rfloor$ is the maximum integer that is not bigger than x . Then, a sequence $D2(B'_A)_n$ is defined as:

$$D2(B'_A)_n = \{Z_1, Z_2, \dots, Z_n\},$$

where n is the number is the total number of the cases of $Y_i \neq X_i$, and $Z_p = X_i$, in which the integer p is increased from 1 to n one by one when $Y_i \neq X_i$ happens.

In the communication between two users, both a sender and a receiver have B as a secret key, and the sender sends $D1(B'_A)_n$ and $D2(B'_A)_n$ to the receiver. Then, using the processing described in the section 3.4, the receiver makes B'_A -like sound data named by B''_A , which is expected to be similar to A .

3.4. Sound data composition

The scaling coefficient sequence for sound data B is expressed by

$$S(B)_k = \{y_1, y_2, y_3, \dots, y_k\},$$

where k is the number of scaling coefficient of B . Then, a sequence

$$C(B)_k = \{Y_1, Y_2, Y_3, \dots, Y_k\}$$

is given, where $Y_i (\in \{0, 1, 2, 3, 4\})$ is the index showing one of five sets of scaling coefficients to which a scaling coefficient y_i of B belongs. $S(B')_k$ is obtained as:

$$S(B')_k = \{b_1, b_2, b_3, \dots, b_k\},$$

where $b_i (\in \{m_0^B, m_1^B, m_2^B, m_3^B, m_4^B\})$ is an average at the range of scaling coefficients of B , which is indicated by $Y_i (\in \{0, 1, 2, 3, 4\})$ obtained from B .

A sequence $D3(B)_k$ is defined as:

$$D3(B)_k = \{z_{B,1}, z_{B,2}, \dots, z_{B,k}\},$$

where k is the number of scaling coefficient of B , and $z_{B,q} = \lfloor y_q \rfloor \bmod 256$. B''_A is composed as follows;

$S(B''_A)_k$ is composed from $S(B')_k$ by replacing b_q to $m_{z_{B,q}}^B$ when $z_{B,q} = z_p$ happens from $p=1$ to n ; then, the sound data B''_A is composed by IDWT using the scaling coefficient sequence $S(B''_A)_k$ and the value of zero for all wavelet coefficient values at every level. The receiver makes B''_A using $D1(B'_A)_n$ and $D2(B'_A)_n$, which are made with both A and B and are sent by the sender, in addition to B which the receiver has beforehand. B''_A is expected to be similar to A .

3.5. Communication of sound data having arbitrary length

In general, the amount of recording time of A is not the same as that of B . We use B having a unit recording time such as one second. Then, we apply the proposed method described in the above sections to A every unit time of recording time of A . When the recording time of A cannot be divisible by the unit time, additional scaling coefficients needed for application of the proposed method are set as 0.

4. Numerical Experiment

We applied the proposed method to several voice sounds as A using as B the music of (1) 'Classical', (2) 'Hip-hop' having one second of recording time each. The music is clipped out from the database⁵. In all cases of the experiment, B''_A was audible and similar to

A . However, B''_A had the noise mainly of low frequency. After erasing the low frequency noise, the sound became more audible and the tone of voice was changed as if the speaker had been a different person. In the next target, we try to develop a method for decreasing the noise with keeping the tone of voice of the speaker.

5. Conclusion

We developed a method for secure communication using a discrete wavelet transform for sound data. In this method, two users must have one piece of music, which has a length of one second and plays a role of secret key, before communicating each other. The music is beforehand transformed into a code using the scaling coefficients obtained from a discrete wavelet transform. The sound data are transformed into another code using the same method as that for the music. The information on the difference between these two codes is sent from one user to the other. The user who receives the information can produce the sound similar to the original sound using an inverse discrete wavelet transform with the code made from the music, the information on the difference between these two codes, and values of zero for all wavelet coefficients. The voice produced by the proposed method was audible.

References

1. Y. Yoshitomi, T. Asada, Y. Kinugawa, and M. Tabuse, An authentication method for digital audio using a discrete wavelet transform, *J. Inf. Sec.* **2**(2) (2011) 59-68.
2. D. Inoue and Y. Yoshitomi, Watermarking using wavelet transform and genetic algorithm for realizing high tolerance to image compression, *J. IIEEJ*, **38**(2) (2009) 136-144.
3. M. Shino, Y. Choi, and K. Aizawa, Wavelet domain digital watermarking based on threshold-variable decision, Technical Report of IEICE, DSP2000-86, **100**(325) (2000) 29-34. (in Japanese)
4. S. Murata, Y. Yoshitomi, and H. Ishii, Audio watermarking using wavelet transform and genetic algorithm for realizing high tolerance to MP3 compression, *J. Inf. Sec.* **2**(3) (2011) 99-112.
5. M. Goto, H. Hashiguchi, T. Nishimura and R. Oka, RWC music database: database of copyright-cleared musical pieces and instrument sounds for research purposes, *Trans. IPSJ*, **45**(3) (2004) 728-738.

An Authentication Method Using a Discrete Wavelet Transform for a Recaptured Video

Ren Fujii, Yasunari Yoshitomi, Taro Asada, and Masayoshi Tabuse

Graduate School of Life and Environmental Sciences, Kyoto Prefectural University,

1-5 Nakaragi-cho, Shimogamo, Sakyo-ku, Kyoto 606-8522, Japan

E-mail: { r_fujii, t_asada }@mei.kpu.ac.jp, { yoshitomi, tabuse }@kpu.ac.jp

http://www2.kpu.ac.jp/ningen/infsys/English_index.html

Abstract

Recently, several digital watermarking techniques have been proposed for protecting the copyright of moving image files by hiding data in the frequency domain. In the present study, we applied our method for authenticating a moving image, which uses a discrete wavelet transform for a static image and a method for selecting several frames from a moving image, to a recaptured video. In contrast to digital watermarking, no additional information is inserted into the original moving image by the proposed method.

Keywords: Authentication, Moving image, Copyright protection, Recaptured video, Wavelet transform

1. Introduction

Digital watermarking is a promising method for protecting the copyright of digital data. Several studies have developed methods in which a digital watermark (DW) can be extracted from data, even after compression, and the quality of the digital data remains high after the DW has been embedded. However, a there is usually a tradeoff between these two properties. For a useful DW, any distortion it introduces must be imperceptible, and it must be robust to signal processing methods, such as compression or attempts to delete it. Both the processing rate and the complexity of DWs have adversely affected their performance.

In order to overcome these performance issues, we developed alternative authentication methods for digital audio¹ and static images.² These methods use a discrete wavelet transform (DWT), and in contrast to digital watermarking, our method for static images² does not insert additional information into the original digital

data. The authentication is based on features extracted by a DWT and a characteristic code.

In the present study, we will review our method³ for authenticating a digital moving image; it is a combination of our previously proposed method² for static images and a proposed method³ for selecting several frames from a moving image. As in our method² for static images, no additional information is inserted into the original moving image, and it is authenticated by features extracted by a DWT and a characteristic code. We present the results of an experiment in which we evaluated the ability of our proposed authentication method³ to recapture a moving image. We will describe this method³ and present the results of the experiment in the following sections.

2. Observed Phenomenon Underpins the Authentication Method

It has been observed that when a DWT is applied to a natural image, in the histogram of the wavelet

coefficients of the MRRs, the center of the distribution is very close to zero.⁴ We exploited this phenomenon in order to develop an authentication method for a static image.²

3. Authentication Ratio

We set the authentication parameters as discussed below.²

In Fig. 1, $Th'(\text{minus})$ was chosen so that it divides the nonpositive wavelet coefficients (S'_m in total frequency) into two equal groups, and $Th'(\text{plus})$ was chosen so that it divides the positive wavelet coefficients (S'_p in total frequency) into two equal groups. Next, the values of the parameters $T1' - T4'$, which control the precision of the authentication precision, were chosen such that the following conditions were satisfied:

- 1) $T1' < Th'(\text{minus}) < T2' < 0 < T3' < Th'(\text{plus}) < T4'$.
- 2) The value of S'_{T1} , the number of wavelet coefficients in $(T1', Th'(\text{minus}))$, is equal to S'_{T2} , the number of wavelet coefficients in $[Th'(\text{minus}), T2']$, i.e., $S'_{T1} = S'_{T2}$.
- 3) The value of S'_{T3} , the number of wavelet coefficients in $(T3', Th'(\text{plus}))$, is equal to S'_{T4} , the number of wavelet coefficients in $(Th'(\text{plus}), T4')$, i.e., $S'_{T3} = S'_{T4}$.
- 4) $S'_{T1}/S'_m = S'_{T3}/S'_p$.

In the present study, the value of both S'_{T1}/S'_m and S'_{T3}/S'_p is set to 0.25, which is the same setting used for creating the code for the original image file². When preparing the authentication codes, the wavelet coefficients V' for each MRR sequence are divided into three sets (hereinafter referred to as F, G, and H), as shown in Fig. 1; these sets are defined as follows:

- $F = \{V' | V' \in V'^{AC}, V' < Th'(\text{minus})\}$
- $G = \{V' | V' \in V'^{AC}, Th'(\text{minus}) \leq V' \leq Th'(\text{plus})\}$
- $H = \{V' | V' \in V'^{AC}, Th'(\text{plus}) < V'\}$,

where V'^{AC} is the set of wavelet coefficients from the target image file that is used to create the authentication code.

The wavelet coefficients V'_i are then classified according to the following rules with the flags f_i used in creating the original code C :

When $f_i = 1$ and $V'_i \in G$, b'_i is set to 0.

When $f_i = 1$ and $V'_i \in (F \cup H)$, b'_i is set to 1.

When $f_i = 0$, b'_i is set to 0.5.

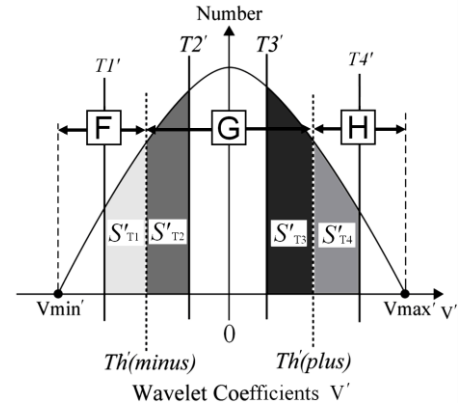


Fig. 1. Three sets (F, G, and H) of MRR wavelet coefficients used for authentication.¹

Note that the value 0.5 can be chosen arbitrarily, since the value of b_i that is the bit for creating the code for the original image file² does not influence the method's performance. Finally, this sequence of b'_i values is used to form the authentication code C' .

The authentication ratio AR (%) is defined as follows:

$$AR = \frac{100 \sum_{i=1}^N f_i (1 - |b_i - b'_i|)}{\sum_{i=1}^N f_i}, \quad (1)$$

where N is the number of wavelet coefficients chosen to create the authentication code for the original image file.² As can be seen in equation (1), neither b_i nor b'_i influence the value of AR when $f_i = 0$, which occurs when the corresponding V_i that is the wavelet coefficient of the original image is not selected for coding in the original image file.²

To use the proposed method, we need to store the flags f_i and the original code C for each copyrighted file that we want to protect. When calculating (1) in order to authenticate an image file, we do not use the original image file; instead, we use the flags f_i and the code C for that file.²

4. Authentication of a Moving Image

We applied our proposed authentication method³ to a recaptured digital moving image. We explain the proposed method³ in this section.

4.1. Authentication code

We obtained 10 codes for each moving image segment, each of which had.

Step 1: Let N_{total} be the total number of frames in the moving image. Calculate frame No. k_B , where k_B is the smallest integer not less than $0.1 \times N_{total}$, and calculate frame No. k_E , where k_E is the largest integer not greater than $0.9 \times N_{total}$.

Step 2: Output the images of frames No. k_B and k_B+1 as BMP files. For each pixel, evaluate the difference between the grayscale level in frame No. k_B and that in frame No. k_B+1 . Calculate the total sum $S[1]$ of squares of these differences. Store the grayscale levels of frame No. k_B+1 in array A_1 . Set the initial conditions as $C[1] := k_B + 1$, $count := 1$, and $k := k_B + 2$.

Step 3: If $k = k_E + 2$, go to Step 8. Otherwise, go to Step 4.

Step 4: Overwrite the image of frame No. k onto that of frame No. $k_B - 2$ in the BMP file. Store the grayscale levels of frame No. k in array B . For each pixel, evaluate the difference between the grayscale level in frame No. $k - 1$ and that in frame No. k . Calculate the total sum T of squares of these differences. Update the value of k to $k := k + 1$.

Step 5: If $count < 10$, update the value of $count$ to $count := count + 1$, and go to Step 6. Otherwise, go to Step 7.

Step 6: Overwrite the array A_{count} with B , i.e., $A_{count} := B$. Set $S[count] := T$, and $C[count] := k - 1$. Go to Step 4.

Step 7: Calculate $l = \arg \max_{i=1,2,\dots,10} S[i]$. If $S[l] > T$,

overwrite the array A_l with B , i.e., $A_l := B$. Set

$S[l] := T$, and set $C[l] := k - 1$. If $k = k_E + 1$, go to Step 8. Otherwise, go to Step 4.

Step 8: Output the arrays $A_i (i = 1, 2, \dots, 10)$ as BMP files. Obtain the codes and flags used for the authentication codes by using the method described in Ref. 2. Output the codes, the flags, $C[i] (i = 1, 2, \dots, 10)$, and $S[i] (i = 1, 2, \dots, 10)$.

4.2. Authentication

We used the method described in Section 4.1 to select frames from moving images. The codes and the flags for the selected frames were obtained using the methods described in Ref. 2. For a given test moving image and a given moving image in the database, the authentication ratio of the test moving image to the moving image in the database is defined as the largest authentication ratio of any selected frame in the test moving image to any selected frame in the moving image in the database.

This is determined for each moving image in the database, and the one with the highest authentication ratio is selected as the assumed original image.

5. Experiment

We evaluated the performance of the proposed method by conducting a computer experiment. In this section, we present the results.

5.1. Method

The experiment was performed in the following computational environment: Dell OptiPlex 3020; CPU: Intel Core i5-4570 3.2 GHz; 4.0 GB memory; OS: Microsoft Windows 7 Professional. The development language was Microsoft Visual C++ 6.0.

The experiment proceeded as follows. We obtained 77 moving image segments, provided as MPEG-1 files, from MUS-CLE-VCD-2007.⁵ These were converted from RGB components into YCrCb components, and for each of these segments, we obtained ten codes for Y components. We numbered the segments in the order in which they were recorded and then divided them into 11 groups of 7 members each. We then chose the six segments (Nos. 24, 45, 27, 21, 93, and 91) that recorded the middle amount of time in each group that had the shortest to the sixth shortest recording time among 11 groups. Nos. 24 and 45 were monochrome, and so we replaced them with the two segments that had the most similar recording times, Nos. 34 and 100, respectively. These six segments were displayed on a liquid crystal television screen of Panasonic VIERA TH-19C305, and the moving images were recaptured by a digital video camera (Sony Handy-cam HDR-CX7); they were then saved as MPEG-2 files, followed by cutting useless margin and being saved as MPEG-4 files. Divide all frames into 10 groups for each file by the time from the beginning, and pick up 10 frames per a group by our previously proposed method³ except the first and last groups in the sense of time from the beginning. This resulted in 80 frames for each recaptured moving image, and these were used for authentication of the 77 segments.

We used FFmpeg⁶ to output a BMP file for each segment; 24 bits were used for the grayscale level and the image consisted of 256×256 pixels. For the DWT, we used Daubechies wavelets. Based on the results of preliminary experiments, we used the LH components obtained from the DWT up to level 4.²

Several consecutive frames in which most pixels are black (or most are white) are sometimes inserted into a moving image, because they can be useful for scene transitions. A frame in such a series is neither representative nor unique to that moving image, and if it is selected to be coded, it could damage the ability of the code to authenticate that moving image. Therefore, we used only frames in which the average grayscale level for the Y component was in the range of 5 to 250 (the full range is 0 to 255).

5.2. Results and discussion

Table 1 shows some examples of the authentication ratios obtained in the experiment. In the six moving image segments (Nos. 34, 100, 27, 21, 93, and 91), the average authentication ratio was in the range 71.6% to 74.3% when the recaptured segment was from a different section of the original moving image, but it was in the range of 91.7% to 97.0% when the recaptured segment was from the same segment; see Table.1. When authenticating the recaptured segment No. 93 against the codes of the original segment No. 17, the authentication ratio was 90.1%. This unusually high authentication ratio was caused by a pair of similar structures, which can be seen in the frames shown in Fig. 2. An example of authentication by the proposed method is shown in Fig. 3.

Table 1. Authentication ratios for recaptured moving images.

	Original file No. for recaptured moving image					
	100	34	27	21	93	91
Average for others	73.9	73.1	74.3	73.5	71.6	72.4
For corresponding raw file	95.5	94.7	96.2	97.0	94.7	91.7
Maximum for others	87.1	82.6	86.4	84.8	90.1	88.6
Recording time (min:sec)	00:30	03:20	06:58	11:32	14:50	19:50

(%)

6. Conclusion

We applied our proposed authentication method³ to a recaptured digital moving image in order to evaluate the ability of the method to recapture a moving image. In contrast to digital watermarking, in the proposed method, no additional information is inserted into the original moving image. The experimental results show that the proposed authentication method performs well.

© The 2016 International Conference on Artificial Life and Robotics (ICAROB 2016), Jan. 29-31, Okinawa Convention Center, Okinawa, Japan

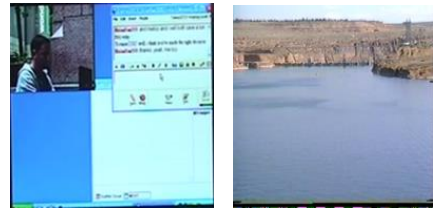


Fig. 2. Left: recaptured frame of moving image segment No. 93; right: frame of moving image segment No. 17 in the database.

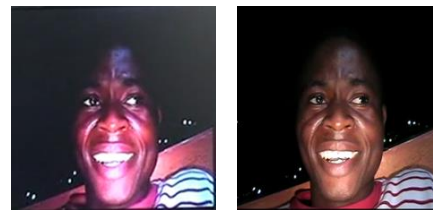


Fig. 3. Left: recaptured frame of moving image segment No. 27; right: frame in the database with an authentication ratio of 96.2% with segment No. 27.

References

1. Y.Yoshitomi, T.Asada, Y.Kinugawa, and M.Tabuse, An authentication method for digital audio using a discrete wavelet transform, *J. Inf. Sec.* **2**(2) (2011) 59-68.
2. T. Asada, Y. Yoshitomi, and M. Tabuse, A verification method for a digital image file using a discrete wavelet transform, *J. IEEEJ*, **39**(6) (2010) 1088-1094. (in Japanese)
3. R. Fujii, Y. Yoshitomi, T. Asada, and M. Tabuse, Authentication method using a discrete wavelet transform for a digital moving image, *J. Inf. Sec.* to be published.
4. M. Shino, Y. Choi, and K. Aizawa, Wavelet domain digital watermarking based on threshold-variable decision, *Technical Report of IEICE*, DSP2000-86, **100**(325) (2000) 29-34. (in Japanese)
5. MUSCLE-VCD-2007, <http://www.rocq.inria.fr/imedia/civrbench/index.html> Accessed 9 September 2015.
6. FFmpeg, <http://ffmpeg.org/> Accessed 9 September 2015.

A System for Facial Expression Analysis of a Person While Using Video Phone

Taro Asada, Yasunari Yoshitomi, Ryota Kato, and Masayoshi Tabuse
*Graduate School of Life and Environmental Sciences, Kyoto Prefectural University,
1-5 Nakaragi-cho, Shimogamo, Sakyo-ku, Kyoto 606-8522, Japan
E-mail: {t_asada, r_kato}@mei.kpu.ac.jp, {yoshitomi, tabuse}@kpu.ac.jp*

Jin Narumoto
*Graduate School of Medical Science, Kyoto Prefectural University of Medicine,
Kajii-cho, Kawaramachi-Hirokoji, Kamigyo-ku, Kyoto 602-8566, Japan
E-mail: jnaru@koto.kpu-m.ac.jp*

Abstract

We developed a method for analyzing the facial expressions of a person having a conversation on a videophone. This was implemented on a wireless local area network, consisting of two personal computers and a router; the subject and the operator are placed in front of each computer. The module contains a function for determining the reference frame and for locally searching for the mouth area in the image to determine the most appropriate position for each frame.

Keywords: Facial expression analysis, Movement analysis, Mouth area, OpenCV, and Skype.

1. Introduction

In Japan, the average age of the population has been increasing, and this trend is expected to continue. Along with this, the number of older people with dementia and/or depression living in rural areas is increasing very rapidly. Due to a mismatch between the number of patients and the number of healthcare professionals, it is difficult to provide adequate psychological assessment and support for all patients.

To improve the quality of life (QOL) of elderly people living in a care facility or at home, we have developed a method for analyzing the facial expressions of a person who is having a conversation with another person on a videophone.^{1,2} The video is analyzed using image-processing software (OpenCV)³ and a previously proposed feature parameter (*facial expression intensity*) that is based on the mouth area.^{1,2}

In the present study, exploiting our reported researches^{1, 2}, we developed a system for facial expression analysis of a person while using video phone.

2. Proposed System and Method

2.1. System overview and outline of the method

The platform includes Skype⁴ for the videophone, and conversations are recorded for the analysis of facial expressions. In the recorded data, the size of the faces are standardized, and the data are analyzed by using OpenCV and the proposed feature parameters for facial expressions, as outlined below. The Y component obtained from each frame in the dynamic image is used for analyzing the facial expressions. The proposed method consists of (1) the size of the lower part of the face is standardized; (2) the mouth area is extracted; (3)

the facial expression intensity is measured; (4) the reference frame is selected; (5) the best position for mouth area in the frame is determined; (6) utterances are evaluated; and (7) the feature parameter for facial expression strength is calculated. In the following subsections, (2), (3), (4), (5) and (7) are explained in detail. On the details for (1) and (6), see Refs 1-2.

The structure of the proposed system is shown in Fig.1. We developed a wireless local area network, consisting of two personal computers (PCs) and one router, in which the subject is placed in front of a PC with a module for analyzing facial expressions, and the subject converses via videophone with the module operator, who is placed in front of the other PC.



Fig. 1. Structure of the proposed system.

2.2. Extraction of the mouth area

Next, by using OpenCV, the mouth area is extracted as a rectangular shape.¹ The mouth area is selected because it is where the difference between neutral and happy facial expressions is most distinct. An example of a face image and the extracted image of the mouth area is shown in Fig. 2.

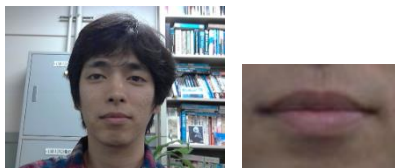


Fig. 2. Whole-face image (left), extracted image of the mouth area (right).

2.3. Measurement of facial expression intensity

For the Y component of the selected frame, the feature vector for the facial expression is extracted for the

mouth area; this is performed by using a 2D-DCT for each section of 8×8 pixels.

As the feature parameters for expressing facial expression, we selected 15 low-frequency components from the 2D-DCT coefficients; this did not include the direct current component. Next, we obtained the mean of the absolute value of each of these components in the area of the mouth. In total, we obtained 15 values as elements of the feature vector. The facial expression intensity is defined as the norm of the difference vector, which is a vector of the difference between the feature vector for the neutral facial expression and that for the observed expression, and it can be used to analyze changes in facial expression.

The candidate of facial expression intensity defined as the norm of the difference vector between two feature vectors is used for selection of the reference frame as described in the section 2.4.

2.4. Selection of the reference frame

We propose a method for automatically selecting the reference frame to be used for measuring the facial expression intensity; this can be used for a moving image in which the initial facial expression is neutral and there is no utterance. The existence of an utterance is determined by a method that we proposed in a previous paper.^{1, 2} The frame prior to any utterance is used as the target in following procedure.

We calculated the sum of the norms of the difference vectors for the feature vector calculated for each of the candidates for the reference frame, and we designated the one for which this sum was minimized as the reference frame. The facial expression intensity is then obtained as the norm of the vector of the differences between the feature vector and the feature vector of the reference frame.

2.5. Correction of position of mouth area

There is no guarantee that the center of the extracted mouth area will remain in a suitable and constant position by eyes, and in fact, we observed that it did vary. This change in position could affect the evaluated facial expression intensity. Therefore, we propose a way to decrease the influence on the facial expression intensity due to changes in the location of the mouth area.

After using OpenCV to extract the mouth area, the best position of the mouth area under the condition on the shift of the area is found by deciding each shift-value for the area in the range of -3 to 3 pixels in each of the horizontal and vertical directions, in order to give the smallest value of facial expression intensity for the frame.

2.6. Feature parameter for facial expression strength

In diagnosing a patient having dementia and/or depression, it might be useful for healthcare professionals to evaluate the strength of facial expressions by using a simple measure.¹ Moreover, it might be more advantageous for a diagnosis of dementia and/or depression to separately evaluate the strength of the facial expression as a speaker and a listener.¹ Therefore, we measure the feature parameter for facial expression strength as the average of facial expression intensity as a speaker and a listener¹, if necessary.

3. Experiments

3.1. Experimental environment

The experiment was performed in the following computational environment: the PC set in front of subject A was a Dell Vostro 3350; CPU: Intel Core i7-2620M 2.7 GHz; 4.0 GB memory; OS: Microsoft Windows 7 Professional. The development language was Microsoft Visual C++ 2008 Express Edition.

Three males (subject A in his 30s, subject B in his 20s, and subject C in his 40s; C is a psychiatrist) participated in addition to an operator. Each experiment consisted of a two-way videophone conversation that lasted from 27 to 36 seconds. Experiment 1 was a conversation between subject A in Tokyo and subject B in Kyoto, and it was conducted using Skype. Experiment 2 took place face-to-face as an interview to subject A by subject C. We saved the visual and audio information as AVI files, and these were then used for measuring the feature parameters of the facial expressions. The size of the image frame was 640×480 pixels, and the size of the standardized lower part of the face image was set to 240×96 pixels.

3.2. Results and discussion

Fig. 3 shows the mouth area of subject A at the beginning of each experiment.

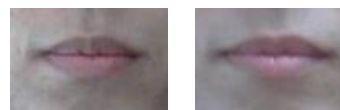


Fig. 3. The mouth area of subject A at the beginning of Experiment 1 (left), and at the beginning of Experiment 2 (right).

The facial expression intensity for subject A was recorded during both experiments. In Experiment 1, the timing of utterances was 11.4 seconds. During his utterances in Experiment 1, there were four local peaks in the facial expression intensity of subject A. These occurred at approximately 3, 6, 15, and 21 seconds after the starting point (see Fig. 4). During the times when subject A was not making utterances during Experiment 1, there were five local peaks in his facial expression intensity; these were at approximately 3, 7, 11, 13, and 23 seconds after the starting point (see Fig. 5); characteristic images of the face and mouth area are shown in Fig.5. In Experiment 2, the timing of utterances was 12.4 seconds; there were four local peaks in the facial expression intensity for subject A; these were at approximately 14, 16, 23, and 26 seconds after the starting point (see Fig. 6). In both Experiments 1 and 2, the images of the face and mouth areas at the characteristic timing points show that the proposed method can quantitatively determine the facial expression (see Figs. 5 and 6).

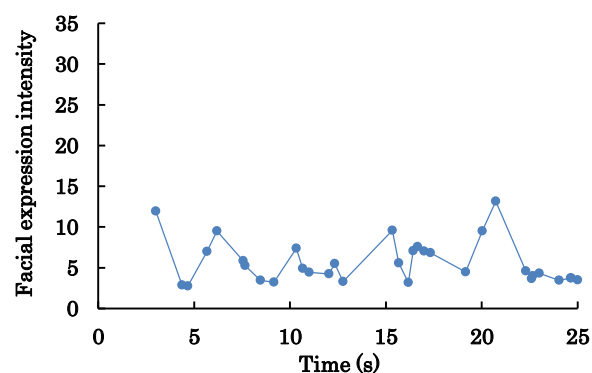


Fig. 4. Changes in the facial expression intensity for subject A at times of utterance during Experiment 1.

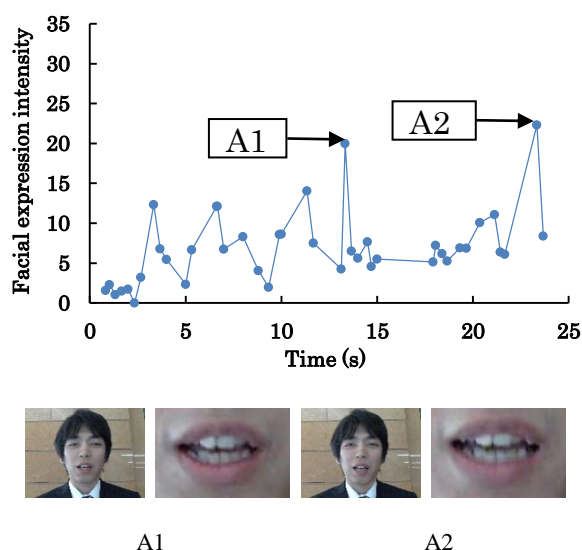


Fig. 5. Changes in the facial expression intensity for subject A at times of no utterance during Experiment 1 (upper graph). Whole-face images and mouth images are shown for two moments, A1 and A2, which are indicated on the graph (lower images).

The feature parameters for the facial expression intensity are shown in Table 1. Note that the intensity tended to be greater during face-to-face conversation than during a videophone conversation.

The processing time for analyzing the facial expressions using the proposed system was 126 s for Experiment 1 and 135 s for Experiment 2.

Table 1. Feature parameter for facial expressions of subject A.

Experiment	Utterance	Feature parameter
1	with	5.65
	without	6.96
2	with & without	10.67

4. Conclusion

We developed a wireless local area network system, consisting of two PCs and one router, which includes a module for analyzing the facial expressions of a subject engaged in a two-way videophone conversation.

The results show the usefulness of the proposed method. As an area of future work, we intend to develop a related method for estimating the mental state and/or recognition ability of a patient.

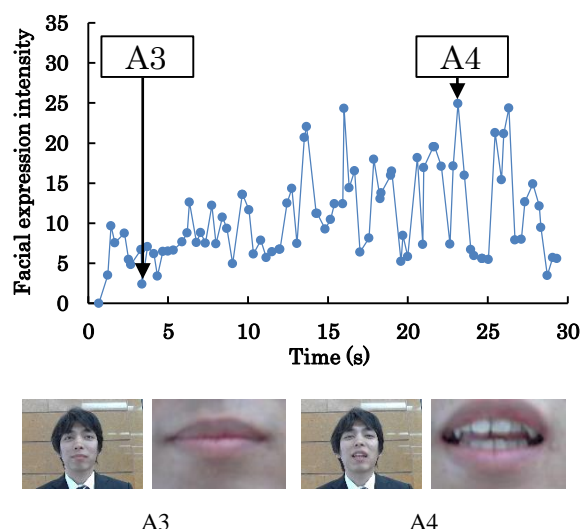


Fig. 6. Changes in the facial expression intensity for subject A during Experiment 2 (upper graph). Whole-face images and mouth images are shown for two moments, A3 and A4, which are indicated on the graph (lower images).

Acknowledgements

This research was supported by COI STREAM of the Ministry of Education, Culture, Sports, Science, and Technology of Japan.

References

1. T. Asada, Y. Yoshitomi, R. Kato, M. Tabuse, and J. Narumoto, Quantitative evaluation of facial expressions and movements of persons while using video phone, *J. Robotics, Networking and Artif. Life* **2**(2) (2015) 111-114.
2. T. Asada, Y. Yoshitomi, R. Kato, M. Tabuse and J. Narumoto, Analysis of facial expressions robust against small imperfections in mouth-part area extraction from face-images of persons while using video phone (in Japanese), in *Proc. of Human Interface Symposium 2015* (Japan, Hakodate, 2015), pp.187-190.
3. Open CV, <http://opencv.org/> Accessed 1 December 2015.
4. Skype Web page, <http://www.skype.com/> Accessed 5 November 2015.

Emotion Recognition of a Speaker Using Facial Expression Intensity of Thermal Image and Utterance Time

Yuuki Oka

*NTT DATA Financial Solutions Corp.
Kandanishikicho, Chiyoda-ku, Tokyo 101-0054, Japan*

Yasunari Yoshitomi, Taro Asada, and Masayoshi Tabuse

*Graduate School of Life and Environmental Sciences, Kyoto Prefectural University,
1-5 Nakaragi-cho, Shimogamo, Sakyo-ku, Kyoto 606-8522, Japan
E-mail: {yoshitomi, tabuse}@kpu.ac.jp, t_asada@mei.kpu.ac.jp
http://www2.kpu.ac.jp/ningen/infsys/English_index.html*

Abstract

Herein, we propose a method for recognizing human emotions that utilizes the standardized mean value of facial expression intensity obtained from a thermal image and the standardized mean value of the time at utterance. In this study, the emotions of one subject could be discerned with 76.5% accuracy when speaking 23 kinds of utterances while intentionally displaying the five emotions of “anger,” “happiness,” “neutrality,” “sadness,” and “surprise.”

Keywords: Emotion recognition, Mouth and jaw area, Thermal image, Utterance judgment.

1. Introduction

This research is intended to facilitate the development of robots that can perceive human feelings and mental states. While various mechanisms for recognizing human feelings from facial expressions have received considerable attention in the field of computer vision research in recent years, the results achieved to date fall far short of human capabilities. This is due to the limited accuracy of facial expression recognition, which is influenced by inevitable gray level changes that result from local variations in lighting, shade, reflection, and darkness.

To avoid this problem and to facilitate the development of a robust facial expression recognition method that would be applicable to widely varied

lighting conditions, we use imagery obtained from infrared rays to describe the thermal distribution of a subject's face.¹⁻³ The timing used by a robot when attempting to recognize facial expressions is also important because the required processing can be time-consuming. Accordingly, we adopted utterances as the key for expressing human feelings because humans tend to speak aloud when expressing their feelings.^{2, 3}

In the present study, using 23 different utterance combinations based on the first and last vowels in each utterance, we investigated the performance of our previously proposed method⁴ of recognizing emotions by utilizing facial expression intensity⁵ and the utterance time.

2. Evaluation Method

The proposed method consists of (1) mouth and jaw area extraction, (2) facial expression intensity measurement, (3) utterance judgment, and (4) calculation of feature parameters for facial expression and voice.⁴

2.1. Extraction of mouth and jaw areas

Six facial areas extracted at 0.1 frames per second via the thermal image processing reported in our previous study³ are used in the processing of dynamic thermal imagery, as shown in Fig. 1. The mouth and jaw area was selected because facial expression differences between neutrality and happiness are most distinctive in this area.⁵ Fig. 2 shows thermal image examples of whole face and the mouth and jaw areas.

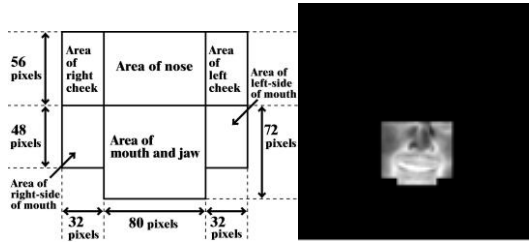


Fig. 1. Blocks for extracting partial face areas (left), and the thermal image after partial face extraction (right).²



Fig. 2. Thermal face (left) and mouth and jaw area imagery (right).⁵

2.2. Measurement of facial expression intensity

For the extracted frames, the expression feature vectors in the mouth and jaw area are extracted by applying a two-dimensional discrete cosine transform (2D-DCT) for each 8×8 pixel domain.⁵ To accomplish this, we begin by selecting 15 low-frequency components of the 2D-DCT coefficients, excluding the direct current component, as the facial expression feature parameters.⁵

Next, we obtain the mean of the absolute value for each 2D-DCT coefficient component in the mouth and jaw area.⁵ A total of 15 values are obtained and used as feature vector elements. Facial expression intensity, which is defined as the norm of the differences between the neutral facial expression feature and the observed expression vectors, can then be used for analyzing facial expression changes.⁵

2.3. Utterance judgment

After sample collection, the sound data are smoothed to erase noise. Then, all sampled data that fall within $[\bar{x}_s - 14\sigma_s, \bar{x}_s + 14\sigma_s]$, where \bar{x}_s and σ_s express the average and the standard deviation of the sound data value, respectively, for one second under the no utterance condition, are considered to be the range for no utterance.⁵ When at least one sampled datum has a value outside $[\bar{x}_s - 14\sigma_s, \bar{x}_s + 14\sigma_s]$, our system judges that the sound data contains an utterance.⁵

2.4. Feature parameters

In our proposed method,⁴ two parameters are used as feature vector elements. One is the mean of the standardized facial expression intensity at the time of each utterance and for 0.3 s before and after the utterance, while the other is the standardized time at each utterance. The standardization used for creating feature parameters is expressed by Eq. (1).

$$x_{i,j}^* = \frac{x_{i,j} - \bar{x}_i}{\sigma_i}, \quad (1)$$

where $x_{i,j}^*$, $x_{i,j}$, \bar{x}_i , and σ_i express the standardized feature parameter, the measured feature parameter, the average, and the standard deviations of the measured feature parameters of the training data, respectively, and i, j denote the number (1 or 2) of the feature parameter and number (1, 2, ..., m) of the utterance, respectively. Then, using the Ward method, clustering is performed separately for the training and test data to determine major and minor clusters for each class of the emotions in the feature vector space. Next, to recognize emotions from the test data, the center-of-gravity coordinates of the major cluster for each emotion class of the training and test data is used.

3. Experiments

3.1. Conditions

Thermal imagery produced by a TVS-700 thermal video system (Nippon Avionics, Tokyo, Japan) and sounds captured by an ECM-23F5 Electret condenser microphone (Sony, Tokyo, Japan), as amplified by an AT-PMX5P mixer (Audio-Technica, Tokyo, Japan), were transformed into a digital signal via an ADV-300 analog/digital (A/D) converter (Thomson Canopus, Kobe, Japan).

The converted signals were input into an Optiplex 780 personal computer (PC) (DELL, Round Rock, TX) equipped with an E8400 3.00 GHz Core 2 Duo central processing unit (CPU) (Intel, Santa Clara, CA) and 3.21

GB of main memory, as well as a 1394-PCI3/DV6 IEEE1394 interface board (I-O Data Device, Ishikawa, Japan).

As for software, the PC was equipped with the Windows 7 Professional operating system (OS), while Visual C++ 6.0, and Visual C++ 2008 Express Edition, (Microsoft, Redmond, WA) were used as the programming languages.

To generate a thermal image that would allow the face area of a subject to be easily extracted, 256 gray levels were set to cover the detectable temperature range of our experimental device setup. The visual and audio information was saved in the PC as a Type 2 digital video-audio video interleave (DV-AVI) file, in which the video frame had a spatial resolution of 720×480 pixels and 8-bit gray levels, while 48 kHz and 16-bit level sound was saved in a stereo pulse-code modulation (PCM) format.

Subject A, a male wearing eyeglasses, deliberately performed each of the emotions of “anger,” “happiness,” “neutrality,” “sadness,” and “surprise,” while speaking the semantically neutral utterance of each of the Japanese first names listed in Table 1. However, all utterances of the Japanese first name “taro” (the first and last vowels of which are /a/ and /o/) and “tsubasa” (the first and last vowels of which are /u/ and /a/) were excluded because they had been used in the previous study.⁴

Table 1. Japanese first names used in the experiment.

		First vowel				
		a	i	u	e	o
Last vowel	a	ayaka	shinnya	-	keita	tomoya
	i	kazuki	hikari	yuki	megumi	koji
	u	takeru	shigeru	fuyu	megu	noboru
	e	kaede	misae	yusuke	keisuke	kozue
	o	-	hiroko	yuto	keiko	tomoko

In this study’s experiment, Subject A intentionally maintained a front view in the AVI files, which were saved as both training and test data. In total, 15 training data and 15 test data samples were assembled. The AVI files were used for measuring the facial expression intensity. WAVform Audio format (WAV) files obtained from the AVI files were used for measuring the utterance times.

3.2. Results and discussion

Our results show that the subject’s emotion was reflected in his thermal face image even at 0.3 s before he began to speak.⁴ From a comparison with the data analyzed at the time of utterance, we found that the time series facial expression intensity differences for the five targeted emotions became more distinct when the analysis included the time range beginning 0.3 s before to the subject started to speak to 0.3 s after he finishing speaking.⁴

Table 2 shows the emotion recognition accuracy values obtained using our method. As can be seen in this table, the average emotion recognition accuracy was 76.5%, which was near 80% for “taro” and “tsubasa” used in the previous experiment.⁴ Table 3 shows the emotion recognition accuracy values for each utterance obtained using our method. The emotion recognition accuracy for each utterance was from 60% to 100%.

In the case of “sadness,” the accuracy was 100%, primarily because the utterance time was remarkably longer than for other utterances, which made it easy to distinguish. In contrast, the emotions of “anger,” and “surprise,” were confused with each other much more often, primarily because the utterance times when expressing these two emotions were quite similar. Fig. 3 shows two-dimensional center-of-gravity distributions for the dominant cluster of each emotion class for both the training and test data samples. When the nearest neighbor rule is used, it can be seen that emotion recognition accuracy was 100% and 60% for the utterance of “kaede” and “fuyu,” respectively.

Table 2. Emotion recognition accuracy.

	Input emotion				
	Angry	Happy	Neutral	Sad	Surprised
Recognized emotion	Angry	86.96	4.35		26.09
	Happy		56.51	13.04	8.7
	Neutral		26.09	82.61	8.7
	Sad		8.7	100	
	Surprised	13.04	4.35	4.35	56.51

(%)

Table 3. Emotion recognition accuracy for each utterance.

	Utterance	Input emotion					Accuracy (%)
		A	H	N	Sa	Su	
Recognized emotion for each utterance	ayaka	Su	H	Su	Sa	Su	60
	kazuki	A	Sa	N	Sa	Su	80
	takeru	Su	N	N	Sa	Su	60
	kaede	A	H	N	Sa	Su	100
	shinnya	A	N	N	Sa	A	60
	hikari	A	Sa	N	Sa	Su	80
	shigeru	A	H	N	Sa	A	80
	misae	A	N	N	Sa	Su	80
	hiroko	A	H	N	Sa	Su	100
	yuki	A	H	N	Sa	A	80
	fuyu	Su	H	N	Sa	A	60
	yusuke	A	H	H	Sa	Su	80
	yuto	A	Su	N	Sa	A	60
	keita	A	N	N	Sa	N	60
	megumi	A	H	H	Sa	A	60
	megu	A	H	N	Sa	Su	100
	keisuke	A	H	H	Sa	Su	80
	keiko	A	N	N	Sa	Su	80
	tomoya	A	N	N	Sa	Su	80
	koji	A	A	N	Sa	N	60
	noboru	A	H	N	Sa	H	80
	kozue	A	H	N	Sa	H	80
	tomoko	A	H	N	Sa	Su	100

A=Angry, H=Happy, N=Neutral, Sa=Sad, Su=Surprised

4. Conclusion

In a previous study, we proposed a method for recognizing human emotions. Using that method, the emotions of one subject were discernable with 76.5% accuracy in speaking each of 23 utterance types while intentionally exhibiting each of the five emotions of “anger,” “happiness,” “neutrality,” “sadness,” and “surprise.”

The recorded accuracy level was near 80% for “taro” and “tsubasa” in the previous experiment.⁴ These results show that the method is capable of producing good results.

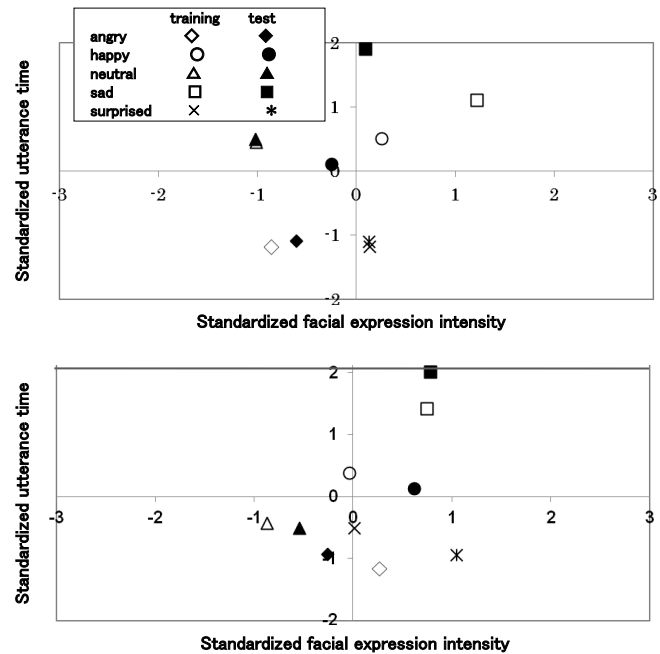


Fig. 3. Two-dimensional center-of-gravity distribution of major cluster of training and test data; upper: “kaede”, lower: “fuyu”.

Acknowledgements

The present study was partially supported by KAKENHI (22300077).

References

1. Y. Yoshitomi, N. Miyawaki, S. Tomita, and S. Kimura, Facial expression recognition using thermal image processing and neural network, in *Proc. 6th IEEE Int. Workshop on Robot and Human Communication*, (Japan, Sendai, 1997), pp. 380–385.
2. Y. Yoshitomi, T. Asada, K. Shimada, and M. Tabuse, Facial expression recognition of a speaker using vowel judgment and thermal image processing, *J. Artif. Life and Robotics* **16**(3) (2011) 318–323.
3. Y. Yoshitomi, M. Tabuse, and T. Asada, Facial expression recognition using thermal image processing, in *Image processing: methods, applications and challenges* ed. V. H. Carvalho (Nova Science Publisher, New York, 2012), pp. 57–85.
4. Y. Yoshitomi, T. Asada, R. Kato, M. Tabuse, Facial Expression Recognition Using Facial Expression Intensity Characteristics of Thermal Image, *J. Robotics, Networking and Artif. Life* **2**(1) (2015) 5–8.
5. Y. Yoshitomi, T. Asada, R. Kato, M. Tabuse, Method of facial expression analysis using video phone and thermal image, *J. Robotics, Networking and Artif. Life* **1**(1) (2014) 7–11.

Estimation of Learners' Subjective Difficulty in e-Learning Using Thermal Image Processing

Yuki Yoshimitsu and Masayoshi Tabuse

Graduate School of Life and Environmental Sciences, Kyoto Prefectural University

1-5 Hangi-cho, Shimogamo, Sakyo-ku, Kyoto 606-8522, Japan

E-mail: y_yoshimitsu@mei.kpu.ac.jp, tabuse@kpu.ac.jp

Abstract

In recent years, e-learning has been utilized as a learning system in many schools. In a conventional class, a teacher teaches learners face-to-face, so that a teacher observes facial expressions and posture change of learners and estimates learners' subjective difficulty of the lecture. On the other hand, e-learning is usually utilized in the self-study. A learner learns a teaching material using a computer by oneself, so that a teacher can't observe the state of the learner. It is difficult for a teacher to estimate learners' subjective difficulty. Therefore, we propose a learners' subjective difficulty estimation system. This system captures the face of a learner in e-learning with a thermal camera. It extracts the face region, measures the temperature changes of the nose region and the forehead region of the learner, and estimates the subjective difficulty of the learner based on the temperature changes.

Keywords: learners' subjective difficulty, thermal image, e-learning, temperature changes.

1. Introduction

In recent years, e-learning has been utilized as a learning system in many schools. In a conventional class, a teacher teaches learners face-to-face, so that a teacher observes facial expressions and posture change of learners and estimates learners' subjective difficulty of the lecture. On the other hand, e-learning is usually utilized in the self-study. A learner learns a teaching material using a computer by oneself, so that a teacher can't observe the state of the learner. It is difficult for a teacher to estimate learners' subjective difficulty. Therefore, we estimate a learners' subjective difficulty. Because the thermal image of the human face changes depending on a bloodstream change with the automatic nerve activity, the change of the thermal image of the human face, especially the nose region, reflect human physiological psychological conditions.¹

Our proposed system captures the face of a learner in e-learning with a thermal camera. It extracts the face region, measures the temperature changes of the nose

region and the forehead region of the learner, and estimates the subjective difficulty of the learner based on the temperature changes.

2. Thermal Image

Thermal image is obtained according to the Stefan-Boltzmann law which describes the power radiated from a black body in terms of its temperature, expressed as $W = \varepsilon \sigma T^4$, where ε is emissivity, σ is the Stefan-Boltzmann constant ($=5.6705 \times 10^{-12}$ W/cm²K⁴), and T is the temperature (K). For human skin, ε is estimated as 0.98 to 0.99.² The human face area is easily extracted from an image by using the value of 1 for ε when a range of skin temperatures is selected to produce a thermal image. Fig. 1 shows example of thermal image of a male. In our study thermal image is expressed in gray image with 256 gray levels where gray value 0 and 255 indicate temperatures beyond the setup minimum and maximum ones respectively.



Fig. 1. Thermal image of a male.

3. Extraction of face region

When the setup temperatures are chosen so that the human skin temperature might enter between the minimum temperature and the maximum temperature, the human region are expressed by gray values between 0 and 255 and the lower temperature background are expressed by 0. We first operate binary image processing to thermal image and obtain binary image, shown in Fig. 2. The human region has value 255 and the background has 0. We apply labeling to the binary image and have regions with more than 2000 pixels, shown in Fig. 3. Next we scan labeling image from $y = 0$ to $y = H$ (height of thermal image) for each x and when the coordinate (x, y) is in the labeling region, we set 1 on 2 dimensional array $M(x, y)$ from there to $y = H$. We scan labeling image from $x = 0$ to $x = W$ (width of thermal image) and from $x = W$ to $x = 0$ for each y . When the coordinate (x, y) is in the labeling region, we add 1 on $M(x, y)$ from there to right and from there to left, respectively, shown in Fig. 4.



Fig. 2. Binary image.

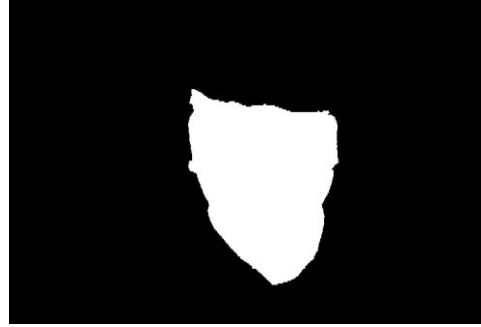


Fig. 3. Labeling.



Fig. 4. 2 dimensional array $M(x, y)$. White, light gray, gray and black colors indicate the area with the values of 3, 2, 1 and 0.

We operate the raster scan on $M(x, y)$ from $(0, 0)$ to (W, H) and find the top coordinate of the human region (x_{human}, y_{human}) where the value of $M(x, y)$ has 3. We measure the maximum width W_{max} of the human region from y_{human} to y-coordinate of the center of mass of the largest labeling region. From y_{human} to y-coordinate of the bottom of the largest labeling region we calculate the frequency distribution of the width of the region which have 2 or 3 and determine the width of the maximum frequency within $1.2W_{max}$ as the facial width W_{face} and x-coordinate of the left and right boundaries of the human region as left and right boundary of the face region x_{left} and x_{right} , respectively. We find y-coordinate of $0.8W_{face}$ width of the human region downward from y_{human} and the top y-coordinate of the face region y_{top} is $0.2W_{face}$ above from there. The bottom of the face region y_{bottom} is W_{face} downward from y_{top} , shown in Fig. 5. The upper left and the lower right coordinates of the face region are (x_{left}, y_{top}) and (x_{right}, y_{bottom}) . The height of face region is $H_{face} = W_{face}$.

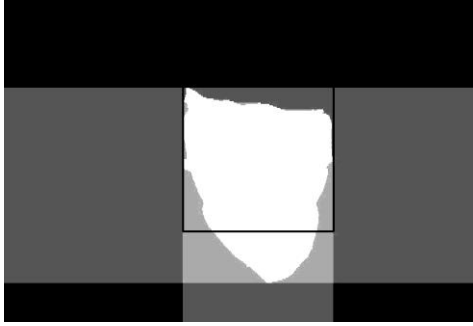


Fig. 5. Face region.

Finally we operate a rotation correction to the thermal image. We measure midpoints of the left and right boundaries of binary image in the face region from $y_{top} + 0.45H_{face}$ to $y_{top} + 0.75H_{face}$. We estimate a roll angle θ of the face using the least-square method (Fig. 6.) and rotate the thermal image by $-\theta$ around the center of the face region. We normalize the face region with the size of 400×400 pixels.

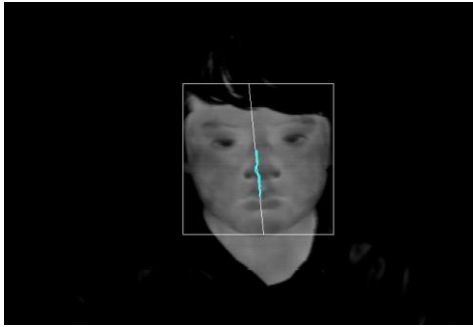


Fig. 6. Estimation of a roll angle.

4. Template matching, the nose and forehead regions

We utilize the template matching to detect the nose region correctly. We first click the tip of the nose and obtain a template. The size of a template is $H_{tmp} \times W_{tmp} = 140 \times 280$ pixels and the upper left coordinate is $(x_{click} - 0.5W_{tmp}, y_{click} - 0.85H_{tmp})$ where (x_{click}, y_{click}) is a coordinate of the tip of the nose in the face region. The nose region is $(x_{tmp} + 0.35W_{tmp}, y_{tmp} + 0.2H_{tmp})$ - $(x_{tmp} + 0.65W_{tmp}, y_{tmp} + H_{tmp})$ where (x_{tmp}, y_{tmp}) is the coordinate of the tip of the nose. The forehead region is $(x_{tmp} - 0.35W_{tmp}, y_{tmp} - 40)$ - $(x_{tmp} + 0.65W_{tmp}, y_{tmp})$, shown in Fig. 7.

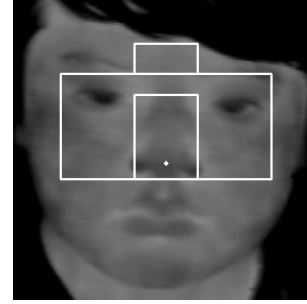


Fig. 7. Template, nose region and forehead region.

5. Experiments

5.1. Condition

The thermal image produced by the infrared thermal image camera (Nippon Avionics TVS-700) is output as a composite video signal, which is input to the PC (Dell Optiplex 9010, CPU: Intel Core i7-3770 3.4GHz, main memory: 8GB and OS: Microsoft Windows7 Professional 64bit) through the video capture device (I-O DATA GV-USB2/HQ). The thermal image is expressed in gray image with 256 gray levels and the setup minimum and maximum temperatures are 29°C and 39°C , respectively. The thermal image size is 704×480 pixels. We used Microsoft Visual C++ 2013 Express as a programming language and OpenCV 2.4.11 as image processing library. Subject A is a male in his 20s.

5.2. Mental workload

Subjects perform a mental calculation as a mental workload.^{1,3} Fig. 8 shows a mental calculation system which gives questions of mental calculation of double-, triple- or quadruple-digits. The system displays a number and the subject memorizes it and clicks the enter button. Then the system displays a different number, the subject adds it to the memorized number, input the answer and clicks the enter button. The system records the number of the answers, the number of the correct answers and answer time for each question.

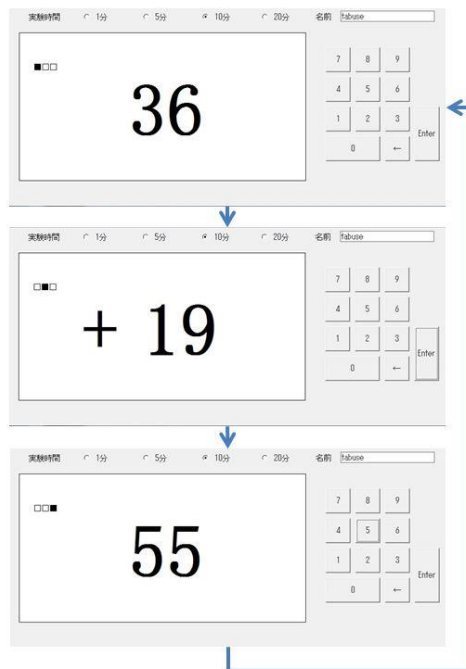


Fig. 8. Mental calculation system.

5.3. Results

The change of temperatures of the face region, the nose region and the forehead region of subject A with quadruple-digits mental calculation are shown in Fig. 9, 10, 11. Answer time for each question and time series variation of correct and incorrect answers are shown in Fig. 12, Fig. 13.

6. Conclusion

We measure the change of temperatures of the face region, the nose region and the forehead region of a subject while doing mental calculations.

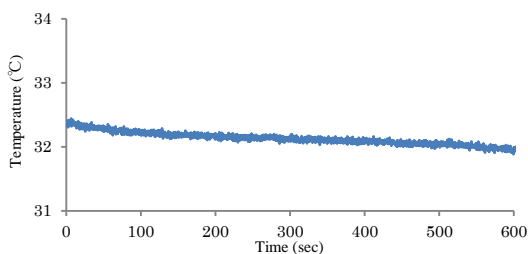


Fig. 9. Average temperature of the face region.

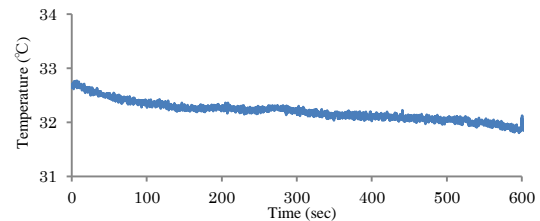


Fig. 10. Average temperature of the nose region.

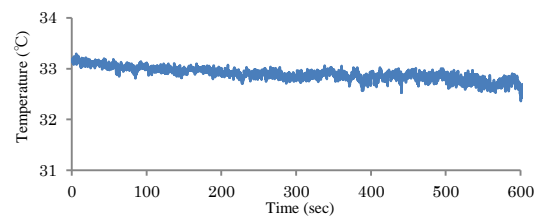


Fig. 11. Average temperature of the forehead region.

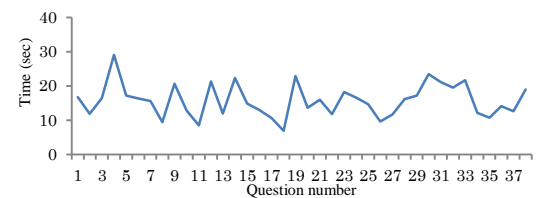


Fig. 12. Answer time.

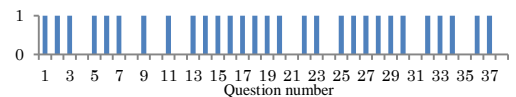


Fig. 13. Time series variation of correct and incorrect answers (1: correct answer, 0: incorrect answer).

References

1. T. Mizuno, S. Nomura, A. Nozawa, H. Asano and H. Ide, Evaluation of the effect of intermittent mental work-load by nasal skin temperature (in Japanese), IEICE J93-D(4) 535-543 (2010).
2. H. Kuno, *Infrared rays engineering* (in Japanese). (IEICE, Tokyo, 1994).
3. S. Kunimasa, K. Seo, H. Shimoda and H. Ishii, The inference method of cognitive working states while performing mental tasks based on performance-cognitive load model (in Japanese), The Transactions of Human Interface Society 17(4) 395-410 (2015).